M. Fukugita
T. Yanagida

Physics of Neutrinos
and Applications
to Astrophysics

Springer-Verlag Berlin Heidelberg GmbH

Texts and Monographs in Physics

Springer-Verlag Berlin Heidelberg GmbH

Physics and Astronomy ONLINE LIBRARY

Masataka Fukugita   Tsutomu Yanagida

Physics of Neutrinos

and Application to Astrophysics

With 111 Figures and 64 Tables

Springer

Professor Masataka Fukugita

University of Tokyo
Institute for Cosmic Ray Research
277-8582 Kashiwa, Chiba
Japan
e-mail: fukugita@icrr.u-tokyo.ac.jp

Professor Tsutomu Yanagida

University of Tokyo
Department of Physics
Graduate School of Science
7-3-1 Hongo, Bonkyo-ku
Tokyo 113-0033
Japan
e-mail: tsutomu@hep-th.phys.s.u-tokyo.ac.jp

Preface

This book aims to provide a survey of the current state of research in the physics of neutrinos, which has undergone dramatic development during the last decade, in a form accessible to the nonspecialist and the graduate student. The major issue during the last two decades has been the neutrino mass, whereas the interaction of neutrinos was well understood within the framework of the standard theory, which was established in the 1970s. In 1994, we published a textbook-format review article *"Physics of Neutrinos"* in *"Physics and Astrophysics of Neutrinos"*, in anticipation that the mass of the neutrino would be found in the near future. It was indeed found thanks to the Super-Kamiokande experiment four years after that book was written, and a flurry of activity followed in the phenomenology of the neutrino mass. From the theoretical point of view, the importance of this discovery stems from the fact that it probably indicates the presence of a new energy scale beyond the standard theory. At the same time, the formalism for massive neutrinos and the techniques to find the neutrino mass have now realistic importance and have become the subject of standard physics. On the other hand, experiment revealed that the pattern of the neutrino mass and mixing among generations appears in a way different from what has been speculated on the basis of existing theoretical models. For these reasons, we feel that it is timely to summarise the current state of our understanding – both success and failure – concerning the physics of neutrinos.

We expand the book to include a range of subjects so that it provides a global view of the physics where neutrinos play important roles, including astrophysics and cosmology. We detail formulae and numbers, with the hope that this book is useful as a handbook for researchers in this field. Emphasis is also given to the description of the principles of neutrino experiments. In early chapters, we discuss physical processes and physical effects that involve neutrinos. They are important subjects of neutrino physics in their own right, but also give a base for the exploration for the neutrino mass and its origins, both theoretically and experimentally, as we discuss in later chapters. As in the previous book, the mathematical formulation for massive neutrinos is one of the central subjects. We also discuss details concerning the evidence for finite masses of neutrinos.

VI   Preface

The reader will find a change between Chaps. 8 and 9. Chapters up to and including Chap. 8 summarise knowledge which is established or well understood, at least as a matter of principle. On the contrary, subjects discussed in Chap. 9 and further chapters are theories from workshops of theorists. It is possible that these ideas will be completely revised or abandoned some day as our understanding evolves. The problem is that we are not successful yet in understanding the mass pattern and mixing of the neutrino mass, although we have good reasoning as to why neutrinos have very small masses and how they are generated. Notwithstanding this, we decided to document these ideas to convey our struggle to understand the neutrino mass matrix, as we believe that even failed attempts will not be completely useless in the process of the development of understanding. This is in fact the prime reason why theorists are attracted to the neutrino mass.

Particular care has been taken so that this book serves graduate students who want to learn the physics of neutrinos and related topics. We start the description at an elementary level, which is readily accessible to graduate students who have finished an elementary course in quantum field theory. Knowledge of the Weinberg–Salam theory of electroweak unification is a cornerstone of this book, but it is not assumed; we start with a practical introduction to the electroweak theory. We do not assume knowledge other than that within a standard course in elementary physics, such as that given in Landau and Lifshitz's textbooks on physics. We supply introductory materials for advanced subjects, although we limit ourselves to those which are inevitable to understand the subject relevant to the physics of neutrinos. A general problem for students is the presence of a gap between textbooks and advanced research papers. We intend to fill this gap; we try to embark from elementary concepts and to show intermediate steps in calculations of fundamental equations often used in research papers without any derivations, as much as space permits.

We are indebted to many colleagues in completing this book. In particular, we would like to express our sincere thanks to Jiro Arafune (Tokyo, ICRR), John Bahcall (Princeton, IAS), Samoil Bilenky (Munich), Alexander Friedland (Princeton, IAS), Morihiro Honda (Tokyo, ICRR), Takaaki Kajita (Tokyo, ICRR), Masahiro Kawasaki (Tokyo, Hongo), Kuniharu Kubodera (South Carolina), Takahiro Kubota (Osaka), Masato Morita (Osaka, emeritus), Masayuki Nakahata (Tokyo, ICRR), Kazuhiko Nishijima (Tokyo/Kyoto, emeritus), Atsuto Suzuki (Tohoku), Hideyuki Suzuki (Tokyo Science University), Yoichiro Suzuki (Tokyo, ICRR), Gyo Takeda (Tohoku, emeritus), Morimitsu Tanimoto (Niigata), Toshiaki Tomoda (Aomori), Yoshio Yamaguchi (Tokyo, emeritus), and Motohiko Yoshimura (Tokyo, ICRR) for invaluable advice, comments, and help in various stages of writing.

Tokyo   *Masataka Fukugita*
January, 2003   *Tsutomu Yanagida*

Table of Contents

1 Historical Introduction

Ever since it was first proposed [1], the neutrino has played crucial roles from time to time in the advancement of our understanding of particle physics. The history around the neutrino and how it has contributed to the development of the particle theory are fascinating and instructive. In this book, however, we describe the material in a logical way, attaching little weight to the historical account. Therefore, we present in this chapter a brief historical account to partially compensate for this.

1.1 Neutrinos and the Law of Weak Interactions

The story dates back to Chadwick (1914) [2], who discovered the continuous spectrum of beta rays (in Ra B + C = ^{214}Pb + ^{214}Bi), which posed a difficult problem for theoretical interpretation.[1] The interpretation was divided into two: (i) it is attributed to a broadening of the spectrum due to secondary processes and some loss of energy in nuclei (Rutherford [7]; Meitner 1922 [8]), and (ii) it is of primary origin (Ellis 1922 [9]). The absolute calorimetry of heat generation by Ellis and Wooster (1927) [10] has shown that it agrees with the average energy of beta decay, but not with the maximum energy of beta rays, indicating that there is no loss of energy inside the nuclei: electrons of various energy are emitted directly from nuclei.

This leaves us with two possibilities: (i) energy conservation does not hold in the nucleus (Bohr [11]), or alternatively, (ii) a neutral and penetrating particle that carries missing energy is emitted together with electrons. This second view was conjectured by Pauli in a public letter to *"Gruppe der*

---

[1] The state that precedes the discovery of Chadwick was confusing. In early days the β spectrum was thought to be monoenergetic [3] like the α spectrum, and then to be a set of monoenergetic lines [4, 5]. The experiments those days used photographic plates to detect electrons which were let pass through a slit into a space where a magnetic field perpendicular to the β rays was applied, serving as a spectrometer [3]. It was not easy to recognise the continuum components with the photographic technique, while discrete lines, which originated from internal conversion of γ rays (the effect identified later by Ellis (1921) [6]), were easily detected. Chadwick (worked in Berlin with Geiger) used a counter technique to measure the electron flux.

Radioaktiven" at the *Gauvereins Tagung* in Tübingen written in December 1930 [1] as a *"verzweifelter Ausweg"* (*desperate wayout*) to save the energy conservation law in the nuclear beta-decay process. At the same time, this proposal was also intended to resolve the problem of wrong statistics for ^{14}N and ^{6}Li. At that time, the neutron was not yet known, and the nuclei were supposed to consist of protons and electrons (which were the only known elementary particles other than the photon), and hence ^{14}N, etc. turn out to be a fermion whereas molecular spectroscopy experiments indicated that it was a boson [12]. In his first proposal, Pauli considered the new neutral particle as a constituent of the nucleus bound by magnetic force, thus endowing it with roles of both neutrino and neutron in today's language. He discarded this idea, because of the empirical nuclear mass, in 1931 at the *American Physical Society* meeting in Pasadena [13,14].[2] The neutron which was discovered by Chadwick in 1932 [16], fully solved the problem of the nuclear structure [17].

According to Pauli's conjecture, this hypothetical particle is electrically neutral and has a mass much smaller ($0.01\ m_p$ at most) than the proton. The particle was supposed to have a spin of 1/2 and to respect the Pauli exclusion principle. He argued that this neutral particle has a finite, but small, magnetic moment no greater than $10^{-13}e$ cm (0.02 times the Bohr magneton) and a penetration power at least 10 times greater than that of the gamma ray. Pauli asked experimentalists participating in the conference in Tübingen whether such a particle could be experimentally viable. He received a positive response from Geiger [14].

Pauli had not published this idea since he considered the proposal too tentative to justify its appearance in published records [18]. In 1933, it was mentioned for the first time in Heisenberg's report to the *Septième Conseil de Physique* (Solvay Conference) in Brussels [19]. In the meantime, however, his idea spread through the community, and in particular greatly influenced Fermi [14,18]. At the *Convegno di Fisica Nucleare* in Rome, Fermi referred to the Pauli particle as a 'neutrino' to distinguish it from the newly discovered neutron, and this became the official name [18]. Towards the end of 1933, a theory of beta decay was published by Fermi in a form in which the interaction is written as a product of four spinor fields,

$$\mathcal{H} = g\bar{\psi}_p \Gamma \psi_n \bar{\psi}_e \Gamma \psi_\nu + \text{h.c.}, \qquad (1.1)$$

now called the four-Fermi interaction [20]. Here, the introduction of the neutron and neutrino was crucial, and the idea was clearly formulated that a neutron converts into a proton *creating* an electron and an (anti)neutrino (rather than liberating these particles from a nucleon – the more conventional view in those days). This specified the way the neutrino interacts with matter. Being aware of the various possible forms of the interaction Hamiltonian, Fermi took the vector form for the interaction in analogy with the second-

---

[2] See the analysis by Brown [15] for a different view.

order perturbation of quantum electrodynamics. This gave the Pauli conjecture a firm theoretical basis. Taking ψ as a quantised field, Fermi succeeded in explaining correctly the shape of the beta-ray spectrum. The Fermi theory is regarded as the earliest triumph of the theory of the quantum field [21]. He also discussed how to measure the mass of neutrinos from the end-point spectrum of beta decay, called today a Kurie plot, and then assumed that it is zero to explain an experiment with Ra E=^{210}Bi (see also Perrin [23] for an argument for the zero mass).

The Fermi theory gives the same electron spectrum for allowed decay whichever interaction form is. The selection rule derived from Fermi's vector interaction ($\Delta J = 0$, J being angular momentum; no parity change), however, turned out to be too selective to explain all known beta-decay processes. Gamow and Teller showed that another matrix $\langle \sigma \rangle$, derived from axial-vector or tensor interactions, which allows a transition obeying a different selection rule ($\Delta J = 0$ and ± 1; no parity change; $0 \to 0$ transition is forbidden, however), fits a wide class of beta decays known at that time (Gamow–Teller transitions) [24]. Beta decays induced by a nonrelativistic matrix element $\langle 1 \rangle$, as derived from the vector or scalar interaction, are called Fermi transitions.

In Fermi's theory, there are five types of interactions, 1 scalar (S), γ_μ vector (V), $\sigma_{\mu\nu}$ tensor (T), $\gamma_\mu \gamma_5$ axial vector (A), and γ_5 pseudoscalar (P) (or their linear combinations) [22]. The problem is what types are realised in weak interaction. Note that universality is the basic postulate behind this research (if the type depends on the beta-decay process, this question would not make sense). We observe a long and confusing history to determine the type of the interaction. The first important step came from Fierz who showed that the coexistence of S and V (or T and A) leads to extra energy dependence of the form $[1 + c(m_e/E_e)]$, which does not agree with the experimental shape of the beta ray spectrum [25]: the shape of most beta rays is described well by the simple statistical weight factor as predicted in the Fermi theory. This interference term was called the 'Fierz term.' Since it was known from the selection rule that both Fermi and Gamow–Teller types of transitions should exist, this meant that the allowed types are either (S,T), (S,A), (V,T), or (V,A), where P may or may not exist in any case, as P does not contribute to the transition in the leading order of nonrelativistic approximations.[3]

The distinction between 'allowed' and 'forbidden' was known before the Fermi theory from an empirical plot of lifetime versus the maximum energy of beta rays (Sargent 1933) [27]. Fermi attributed it correctly to orbital angular

---

[3] The path was in fact not so straight. Most beta decays studied in the early days were those derived from the uranium and thorium sequences, and they are mostly forbidden transitions. Therefore, the interpretation of the spectrum was not obvious. For instance, Konopinski and Uhlenbeck [26] introduced derivative interactions to account for spectral distortion for some beta rays. It is after many experiments with artificial radioactivity and in particular after clear understanding of forbidden transitions (see below) that this statement is firmly established.

momentum involved in the transition. We had to wait, however, for the work of the multipole expansion of the matrix elements for a clear comprehension of the forbidden transitions (Konopinski and Uhlenbeck 1941) [28]. The classification of beta transitions [29] underwent great advancement only after the introduction of the nuclear shell model by Jensen, Haxel, and Suess, and by Meyer (1949) [30]. In particular, it turned out from the shell model that those beta decays known earlier (especially those where $Z > 60$) are mostly forbidden transitions.

Many forbidden beta transitions have the same spectrum as that of the allowed transitions. An argument similar to Fierz' analysis was applied to the forbidden transitions that show the 'allowed spectrum,' i.e., those that exhibit a straight line in the Kurie plot. This showed that (V,T), (S,A) and (A,P) cannot coexist in the interaction, since this would lead to an extra energy dependence similar to the Fierz term. This restricts the interaction forms to either STP (or ST) or VA [31].

This dichotomy of the type also received theoretical support. If the energy of the process is high enough, $E_e \gg m_e$, the mass is irrelevant, and the weak interaction must show definite symmetry under a chiral transformation $\psi \to \gamma_5 \psi$ for both electron and neutrino. This requires that the Hamiltonian be either STP or VA [32].

The most 'decisive' reason for the choice of ST before 1956 was the angular correlation experiments of the electron and recoil nucleus for ^{6}He (GT only). The angular dependence agreed very well with the T interaction, excluding the A type (Rustad and Ruby; Allen and Jentschke) [33]. Extra support for the preference of STP came from the interpretation of the distorted spectrum of Ra E (^{210}Bi), which was ascribed to destructive interference between T and P [34]. Further evidence for ST is given by the Michel parameter ρ [35] of μ decay, i.e., when one writes the electron energy spectrum of μ decay as

$$d\Gamma/dE_e \propto 4 \left(\frac{E_e}{E_0}\right)^2 \left(3(1 - E_e/E_0) + \frac{2}{3}\rho(4E_e/E_0 - 3)\right), \qquad (1.2)$$

with E_e the electron energy and E_0 its maximum value. Here ρ must be 3/4 for the VA interaction, whereas early experiments were consistent with $\rho \approx 0$ [36]. It is difficult to find a result indicating VA in the literature around those times.

The breakthrough came from the interpretation of the experiment for a 'new particle', the kaon. The motivation was the so-called $\theta - \tau$ puzzle. There appear to be 'two particles,' θ and τ, degenerate in mass and lifetime; one of them decays into two pions and the other into three pions, both with S waves. The problem was whether they are two different particles with opposite parities and the same mass or the same particle but parity is broken. Lee and Yang published two papers (1956): shortly after their first paper proposing parity-doublet particles [37], the second paper followed, which propounded the possibility of parity violation [38], noting that there were no experiments ever carried out that directly set constraints on par-

ity violation in the weak interaction.[4] They noted that such effects can be measured only through a pseudoscalar formed from a product of observables, e.g., $\boldsymbol{p}_1 \times \boldsymbol{p}_2 \cdot \boldsymbol{p}_3$ or $\boldsymbol{\sigma} \cdot \boldsymbol{p}$, and proposed to measure the asymmetry of electron emission in beta decay from polarised ^{60}Co. This was immediately carried out by Wu and collaborators (1957) [42] with polarised cobalt employing the Rose–Gorter method for cerium magnesium/cobalt nitrate [43]; their results were decisive. They discovered a large asymmetry of beta rays with respect to the spin direction of the oriented nuclei, and such a correlation of spin with the beta-ray momentum can be understood only in terms of a violation of the parity invariance. Garwin, Lederman and Weinrich, and Friedman and Telegdi immediately confirmed parity violation by observing large asymmetry in the positron in the decay of a polarised μ^+ produced from a pion [44].

While parity violation was being established, the suggestion was made that neutrinos have two components, as expected if the neutrino is massless,[5] rather than four [45] (such a possibility was considered by Weyl as early as 1929 [46], but was considered inapplicable to nature because it violates parity [47]). This looked like the most natural way to understand the asymmetry seen in Wu et al.'s experiment, although the two-component theory itself did not solve the original $\theta - \tau$ puzzle. On the other hand, knowledge about the type of weak interaction was still controversial, or even more controversial than ever around the time of parity violation. The support for ST was still strong (especially that from ^{6}He), while new evidence appeared indicating the VA interaction. However, 1957 was the year the controversy starts converging towards a universal V–A theory . The first correct indication pointing to the vector interaction (in the Fermi transition) was obtained from the angular correlation of the electron and the neutrino in a ^{35}A recoil experiment (Herrmannsfeldt et al. 1957) [48]. It was also shown that the e^+ emitted in β^+ decay has positive helicity, supporting the V–A interaction [49] (see also [50]). The helicity of neutrino was then found to be negative (i.e., left-handed) by Goldhaber, Grodzins and Sunyar (1958) [47], who devised an exquisite experiment. They measured the circular polarisation of a photon emitted in the transition from the excited to the ground state (spin 0) of ^{152}Sm following electron capture of ^{152}Eu (spin 0). The neutrino helicity was determined from angular momentum conservation and momentum balance. Therefore, the weak interaction is V–A and the GT transition is determined to be axial-vector.

---

[4] In retrospect there had been very early experiments that observed longitudinal polarisation of electrons emitted in beta decay [39], but nobody, including the authors themselves, apparently had connected their results with parity violation. This was just not the right time (see [40]). Experimentally, the first reference to parity violation was made in [41] to explain $\Lambda \to p\pi^-$ decay, and the conclusion was postponed.

[5] The converse is not true; a two component formalism is possible for massive fields.

Marshak and Sudarshan [52], Feynman and Gell-Mann [53], and Sakurai [54] postulated the universal V–A weak interaction theory, in which all spinors in the Fermi theory should be $(1 - \gamma_5)\psi$ instead of ψ in (1.1). This eliminated all interactions other than V–A. The novel feature of the V–A theory is the conserved vector current: the strength of the vector coupling (Fermi transition) is not modified in the presence of strong interactions [53] (this was discovered earlier by Gershtein and Zel'dovich in 1955 [55]). On the other hand, the axial current is not conserved, and the strength is renormalised in the presence of strong interactions. At the time of these proposals, however, there were two important experiments that did not agree with the prediction of V–A: the tensor dominance of the electron–neutrino angular correlation in ^{6}He decay (cited above) and the absence of $\pi \to e\nu$ decay at the 1/10 level of the prediction of the V–A theory, $\Gamma(\pi \to e\nu)/\Gamma(\pi \to \mu\nu) = 1.2 \times 10^{-4}$ [56]. On the other hand, the Michel parameter had continuously increased from year to year, and it was already close to 0.75 in 1957 (see a review in [57], which summarised the 'time dependence' of the Michel parameter). The ratio of the couplings of the axial-vector to vector currents, and the relative sign of the two couplings were measured by studying asymmetry in the decay of the polarised neutron [58].

Gell-Mann further proposed a few tests for the conserved vector current hypothesis [59]: (i) universality of $0^+ \to 0^+$ nuclear beta decays, where only the vector current contributes; (ii) $\pi^+ \to \pi^0 + e^+ + \nu$, the rate of which is unambiguously predicted; and (iii) weak magnetism induced by the vector current where the magnetic moment should take the value observed in electromagnetic interactions with strong interaction corrections included. He emphasized the use of a ^{12}B, ^{12}C, ^{12}N triad for (iii) and also presented some indirect evidence for weak magnetism.

It took a few more years for the dust to settle. A new experiment with ^{6}He angular correlation now gave the axial-vector dominance rather than the tensor dominance [60], and new experiments searching for $\pi \to e\nu$ resulted in a branching ratio in agreement with the universal V–A theory [61]. Pion beta decay was also discovered as the theory predicts [62]. The Michel parameter reached 0.75 in 1959 [57], and the weak magnetism predicted by the conserved vector current hypothesis was confirmed by Lee, Mo and Wu [63]. Universality was apparently observed for $0^+ \to 0^+$ nuclear beta decays, but nuclear physicists were sceptical as to the validity of the isospin invariance for middle-heavy to heavy nuclei, because of their large neutron excess. It was only after the discovery of isobaric analogue states, which appeared as narrow resonances [64], that they were convinced of the validity of isospin symmetry for such nuclei. The V–A nature of weak interaction was thus fully established by the early 1960s.

Now, it was established that beta decay takes the form

$$\mathcal{H}_{\text{int}} = (1/\sqrt{2})G_{\text{F}}\bar{p}\gamma_\mu(1 - \lambda\gamma_5)n\bar{e}\gamma^\mu(1 - \gamma_5)\nu \ , \tag{1.3}$$

where G_F is the universal Fermi coupling constant. Feynman and Gell-Mann (1958) [53] introduced a concept of the weak current,

$$J_\mu = \bar{\psi}_e \gamma_\mu (1 - \gamma_5) \psi_\nu + \bar{\psi}_n \gamma_\mu (1 - \gamma_5) \psi_p \ , \tag{1.4}$$

and wrote the interaction Hamiltonian as a product of the current

$$\mathcal{H}_\mathrm{int} = \frac{G_\mathrm{F}}{\sqrt{2}} J_\mu^\dagger J_\mu \ . \tag{1.5}$$

Combined with the eightfold way (Gell-Mann 1961; Ne'eman 1991 [65]) and then with quarks (Gell-Mann 1964; Zweig 1964 [66]), together with the concept of partially conserved axial-vector current (Gell-Mann and Lévy 1960 [67]; Nambu 1960 [68]; Bernstein et al. 1960 [68]; Chou 1960 [68]) this current–current form of weak interaction achieved great success in describing varieties of weak interaction phenomena (Gell-Mann 1964 [69]); see [70] for a summary.

One of the theoretical significances of the V–A interaction was that it allowed a description of the interaction in terms of intermediate bosons. This is impossible with the ST interaction, since the tensor part, which is antisymmetric, cannot be mediated by either spin-one (unless there is derivative coupling, which does not agree with experiment) or spin-two particles. The establishment of the V–A interaction opened hope that one might construct a renormalisable theory for weak interaction. Another important implication was the fact that all fields entering this interaction Hamiltonian take $(1 - \gamma_5)\psi$, which implies that massless fields are essential in weak interaction. We had to await the Weinberg–Salam theory, however, for full understanding.

1.2 Detection of the Neutrino and the Discovery of Generations

Bethe and Peierls (1934) [71] were the first to estimate the cross section of a neutrino scattering off nucleons and demonstrated that it is very small ($\sigma < 10^{-44}\,\mathrm{cm}^2$ for a 2.3 MeV neutrino beam).[6] They concluded that "there is no practically possible way of observing the neutrino." Bethe (1935) [74] also calculated the cross section of a neutrino scattered off a charged particle via the magnetic dipole moment. Unfortunately, Pauli's limit on the magnetic moment was far too modest: as it turned out later, it is smaller than 10^{-9} Bohr magnetons, so that the cross section is at least 14 orders of magnitude smaller than would be expected from Pauli's limit. Experimentally, Nahmias (1935) [75] found by using 5 gr of radium that neutrinos do not

---

[6] Calculations based on the Fermi theory were made by Fierz (1936) [72] and by Tomonaga and Tamaki (1937) [73].

produce more than one ion pair per 3×10^5 km of path in air NTP, which corresponds to an upper limit of the cross section $< 10^{-31}$ cm^2. Crane (1939) also searched for $\nu + {}^{35}\text{Cl} \rightarrow {}^{35}\text{S} + e^-$ by using a 1-mC actinium source, and set a limit $< 10^{-30}$ cm^2 [76]. These numbers are more than 10 orders of magnitude larger than expected for neutrino reactions.

The situation changed when Fermi and collaborators completed a nuclear pile and successfully achieved chain nuclear reactions in 1942 [77]. About 6.1 neutrinos are ejected from a single fission of uranium ^{235}U [78], and so even Fermi's 2 kW nuclear reactor produces 4×10^{14} neutrinos per second. The use of a pile to search for the neutrino reaction had been the subject of conversation among physicists since the advent of the pile [79]. An explicit argument was made by Pontecorvo (1946) [80] (and later by Alvarez [81]), who suggested using a pile or hot uranium extracted from a pile as a neutrino source and proposed chemical separation of neutrino reaction products and counting collected atoms with a small counter. These authors emphasised the particular advantage of using ^{37}Cl. There was still the enormous technical problem of realising any experimental detection of neutrino-induced reactions: using a conventional counter placed near a pile, Fermi obtained only $\sigma < 10^{-31}$–10^{-32} cm^2 [82]. Construction of a huge detector, whose active mass is of the order of a ton, was needed.

In his 1933 publication, Pauli [19][7] suggested an experiment to examine the momentum balance in beta decay to detect the neutrino. Bethe and Peierls [71] also discussed this test. The first experiment carried out by Leipunski [84] was consistent with the existence of the neutrino, but the accuracy was not enough to conclude it. More definitive evidence was obtained by Crane and Halpern [85] for a missing agent that carries momentum. The correlation of the electron and recoil nucleus was measured by Jacobsen and Kofoed-Hansen and by Sherwin [86] for beta decay, but the clearest conclusion was derived from the experiment by Rodeback and Allen (1952) [87], who detected recoil nuclei in the electron capture of ^{37}A and found that both energy and momentum conservation are satisfied if a neutrino is emitted in the process. Although this is clear evidence for the existence of the neutrino by today's standard, it was not accepted as 'definitive confirmation' in those days, since conservation of energy was doubted.

A technical innovation for building a large detector followed the discovery of organic scintillators. In 1947, Broser and Kallmann [88] discovered that naphthalene emits scintillation when charged particles pass through it. Within a few years, it was found that the same is true of many kinds of liquids that contain aromatic compounds and that the scintillation yield is particularly high when two or more different compounds coexist [89]. These discoveries opened the possibility of building a large scintillation detector based on affordable cost and technology. Reines and Cowan [90] took this opportunity and constructed a 300-litre liquid scintillator. They used a toluene

---

[7] Earlier reference to this experiment is seen in his letter to Klein in 1931 [83].

solution of p-terphenyl (with an additional small amount of a wavelength shifter to match the scintillation spectrum with the photomultiplier response); cadmium propiponate was loaded as a neutron absorber. The target was hydrogen in the scintillator. The detector was exposed to the Hanford nuclear reactor. They used a delayed coincidence technique, identifying the reaction $\bar{\nu} + p \rightarrow e^+ + n$ by the promptly following signal of $e^+ e^- \rightarrow \gamma\gamma$ and the delayed signal of gamma rays from a neutron absorbed in cadmium. The first detection was reported in 1953 [91]. The reported value was 2 ± 1 times the prediction of the four-component neutrino theory. In time they also improved the detector: $(CdCl_2)$-loaded 200 litre of water was used as the target and two such tanks were sandwiched between three 1400-litre liquid scintillators consisting of a triethylbenzene solution of p-terphenyl. The more powerful (700 MW) Savannah River reactor was employed as the neutrino source. In their second report, the detection was secured (signal:background = 3:1) and the cross section was decreased by a factor of 2, which brought it in good agreement with the (four-component) theory [92]. During this time, the two-component theory was established. Eventually, they obtained a value by a factor of 2, in agreement with the two-component theory [93].

The experiment using ^{37}Cl was pursued by Davis (1955) [94]. This target is not sensitive to $\bar{\nu}$ (if $\nu \neq \bar{\nu}$), and he obtained only an upper bound. By 1960, the sensitivity went well beyond the value that is expected in standard theory if ν and $\bar{\nu}$ were identical [95]. His null result, therefore, was taken as indicating that ν and $\bar{\nu}$ are different particles (different helicities in a modern interpretation). This method later became the most important tool in the study of the neutrino flux from the Sun for over a quarter of a century, after the recognition that the reaction rate of $^3He(\alpha, \gamma)^7Be$ is a thousand times larger than was thought [96] and hence neutrinos from ^8B produced in the Sun would be significant (1958) [97].

With increasing activity at high-energy accelerators and the construction of more powerful accelerators (AGS at Brookhaven, CERN-PS, and others planned), Pontecorvo (1959) [98] and Schwartz (1960) [99] proposed experiments with high-energy neutrinos arising from pions. The first experiment was carried out by Danby et al. (1962) [100]. This is also the first use of a spark chamber, which was invented in 1959 by Fukui and Miyamoto [101] and developed rapidly around 1960–1961 [102]. This is another device that can be constructed for a large facility with reasonable cost and effort. Danby et al. used 10 one-ton modules and identified the charged particle tracks with stereographic photographs. The experiment showed that a neutrino produced in pion decay always produces a muon, and hence proved that it is not ν_e.

The two-neutrino was studied before its discovery; afterwards it motivated many important theoretical considerations. In 1935, Yukawa conjectured the existence of a 'meson' as an agent responsible for the nuclear force [103]. In 1947 Neddermeyer and Anderson [104] identified the cosmic ray particles that were long known to have strong penetrating power [105] as a new particle

with mass between that of the electron and that of the proton, and Yukawa tried to identify it with his meson [106]. It turned out, however, that the lifetime of the new 'meson' was too long and the interaction cross section was too small to be identified with Yukawa's meson [107]. Tanikawa, Sakata, and Inoue (1942) [108] proposed that the two particles are different and Yukawa's meson decays into 'm' and 'n' with 'm' identified with the charged particle found in cosmic rays and 'n' a light neutral particle, or alternatively decays into an electron and ν. In particular, Sakata and Inoue assumed that 'm' and 'n' are fermions and suggested the decay 'm'→ $e + \nu$+'n' where 'n' and ν are different particles. In 1947, Conversi, Pancini, and Piccioni [109] confirmed the leptonic nature of the muon ('m'), as its negative charged partner was not absorbed in matter as much as predicted by Tomonaga and Araki under the assumption that it was Yukawa's meson [110]. In the same year, the decay of Yukawa's particle (π meson) into a muon ('μ meson') was discovered in nuclear emulsion exposed to cosmic rays [111]. The studies that followed showed the decay of the muon, $\mu \rightarrow e + \bar{\nu}_e + \nu_\mu$, just as predicted by Sakata and Inoue [112].[8]

The intriguing fact was that the muon and the electron behave in the same way, as evidenced in μ captures compared with electron captures in nuclei [114] (see also [115, 116]), whereas the muon does not decay into an electron and a photon. The question then was whether the neutral particle appearing in the pion decay is the same as ν (ν_e). Although the majority seemed to favour only one neutrino for economy, there were some physicists, besides Sakata and Inoue, who considered that the two 'neutrinos' are probably different [117]. A reason is the absence of $\mu \rightarrow e + \gamma$ [118], which implied that the muon and the electron belong to different families [34], as do the two neutral particles [119, 120]. The two-neutrino hypothesis, however, was taken seriously only after Danby et al.'s discovery. It is interesting to note that the full four members of the first- and second-generation leptons were thus already in place in 1962, whereas one member (the charm quark) remained missing until 1974 for the hadron family and very few people suspected its presence.

Soon after the discovery of two-neutrinos, Katayama, Matumoto, Tanaka, and Yamada (1962) [121] and Maki, Nakagawa, and Sakata (1962) [122] considered the possibility of mixing between the two neutrinos. Their aim was to construct a theory of hadronic and leptonic weak interactions parallel with each other by assuming that the physical states are given by a 2×2 orthogonal transformation of ν_e and ν_μ, and likewise for hadrons with a conjecture concerning the existence of a new hadron (the charm in today's language) corresponding to ν_μ. Their work was motivated by the Sakata

---

[8] The work in Japan during the wartime had seldom been appreciated in the West, so it had been somewhat decoupled from the mainstream progress of particle theory. This two-meson theory is an example: it was rediscovered by Marshak and Bethe (1947) [113] after the discovery of $\pi \rightarrow \mu$ decay.

model (1956), in which p, n, and Λ are taken as the fundamental triplet that constitutes all hadrons [123] and by lepton–hadron symmetry [124, 125]. Katayama et al. and Maki et al. interpreted the leakage of the weak interaction in hadronic current to the strange quark sector discovered by Gell-Mann and Lévy (1960) [67] and later confirmed by a phenomenological analysis by Cabibbo (1963) [126] as a result of mixing of the states.[9] The fourth flavour was conjectured as a *hadron* partner of ν_μ in their work (see also Tarjanne and Teplitz 1963 [127]).

For the correct theory, these 'fundamental' baryons were yet to be replaced with quarks. The quark model was invented by Gell-Mann and Zweig in 1964 [66]. This was introduced as a realisation of the highly successful eightfold way or flavour SU(3) symmetry of hadrons. Thus p, n, and Λ of the Sakata model are replaced with u, d, and s with fractional charges. Maki, Hara, and Bjørken and Glashow (1964) [128] conjectured the existence of the fourth quark for lepton–quark symmetry. Glashow, Illiopoulos, and Maiani (1970) [129] then showed that one can avoid the strangeness-changing neutral current, which emerges in higher order perturbations, whereas experiment indicates the contrary, in the presence of the fourth quark and write the charged current as an orthogonal transformation, as done by Katayama et al. and Maki et al., so that flavour-changing neutral currents cancel between (u, d) and (c, s) (GIM mechanism). A later calculation showed that the mass of the fourth quark should be smaller than a few GeV for the cancellation mechanism to work [130].

This may have been taken as the first compelling reason for the existence of the charm quark. In those days, however, the prediction of the charm quark did not attract much attention. In the late 1960s, quarks were not yet fully accepted as fundamental particles for hadrons, due to the lack of understanding of quark confinement. There was strong pressure against introducing new hadrons which did not fit the eightfold way: the success of the eightfold way in hadron physics was overwhelming.

In 1971, Niu, Mikumo, and Maeda [131] discovered a candidate for the charm in the product produced by cosmic rays. Kobayashi and Maskawa (1972) were among a few people who took this event seriously; it was natural for them to extend the four-quark model into a model with six quarks [132]. The charm quark ($c\bar{c}$ bound state) was officially discovered in 1974 in e^+e^- pair production in p-Be collisions (Ting and collaborators [133]) and in an e^+e^- collider experiment (Richter and collaborators [134]) as a self-bound state ($c\bar{c}$) which is manifest as a surprisingly narrow resonance and is named J/ψ. Charmed mesons were discovered one year later [135]. This was followed by the discovery of the third-generation charged lepton by Perl and collaborators (1975) [136]. The discovery of a quark counter-part, Υ, was made within

---

[9] The same remark as in the previous footnote also applies here. This work had not been appreciated in the West.

2 years [137], but it took 25 more years to complete the particle family by direct detection of ν_τ [138].

The years 1972–75 were also a great time for strong interaction physics. The conceptual foundations were established for the quantum chromodynamics (QCD) of quarks and gluons, the theory for hadron dynamics. Following the discovery of the colour degree of freedom in hadrons (Fritzsch and Gell-Mann 1972 [139]; for earlier work see Greenberg 1964; Han and Nambu 1965 [140]; Bogolyubov, Struminsky and Tavkhelidze 1965 [141]; Miyamoto 1965 [142]) the asymptotic freedom of coloured gauge theory was discovered in 1973 (Gross and Wilczek; Politzer [143]). This was immediately applied [144, 145] to elucidation of the long-standing puzzle of strong interaction in which hadrons behave as an aggregate of free point-like particles in high-energy deep inelastic lepton–nucleon scattering [146], which was envisaged by Bjorken's scaling [147] and Feynman's parton model [148]. Quantum chromodynamics was soon taken as the most promising candidate for the fundamental theory of strong interaction. From the experimental point of view, even the most suspicious physicists would have been convinced of the existence of quarks after the discovery of two jets in e^+e^- collisions, whose angular distribution showed the spin-1/2 nature of the parent particles [149], together with successful spectroscopy of $c\bar{c}$ states such as the charmonium [150]. Wilson (1974) and Polyakov (1975) [151] invented the lattice regularisation of QCD, which made nonperturbative treatments of strong interaction possible. The most difficult question in QCD, as to why quarks are permanently confined, was answered in the strong coupling limit of the lattice regularised theory, although it had to wait for demonstration in Creutz' numerical work (1980) [152], which shows a smooth continuum limit of the lattice theory, before people were convinced that quark confinement was actually realised in QCD.

1.3 Search for Intermediate Bosons to the Unified Theory of Electroweak Interactions

The chief aims of the second-generation high-energy neutrino experiments were to study nucleon form factors [153, 154] and to search for intermediate bosons [155]. The detectors used for these experiments were spark chambers and bubble chambers, especially those filled with heavy liquids such as freon (CF_3Br) to increase the sensitivity to electromagnetic showers and to increase the target mass. A magnetic horn (called the "Horn of Plenty" in the early days) was invented by van der Meer [156] to intensify the neutrino beam. It was already used from the beginning in the second-generation experiments (1963) [157]. In parallel to accelerator experiments, the first detection of neutrinos of cosmic-ray origin was made deep underground in 1965 at Kolar Gold Field, India [158], and in a South African gold mine near Johannesburg [159]. As neutrino energy increases, the first goal was modified

to determine the structure functions of nucleons (i.e., the quark distribution functions of nucleons), and then to explore quantum chromodynamics by using neutrino scattering off nucleons in a deep inelastic region [160]. The quest for the intermediate bosons gradually transferred to high-energy proton–nucleus scattering (ultimately $p\bar{p}$ collision) with which higher energy is accessible [161]. It continued until W and Z were finally found in $\bar{p}p$ collisions in 1983 [162, 163] at the mass predicted by the Weinberg–Salam theory.

The need for intermediate bosons is quite old. Fermi [20] wrote his interaction Hamiltonian as a second-order perturbation in analogy with quantum electrodynamics. Yukawa, in his classic paper [103], suggested that the particle that induces a nuclear force may also mediate the weak interaction with a different coupling to leptons. Klein introduced a charged B field which mediates beta decay in addition to an A field of electromagnetic interaction, hoping to unify the two interactions (this work may be taken as a precursor to the Yang–Mills theory discovered later) [164].

In fact, the Fermi theory did not look like a fundamental interaction to many physicists despite its remarkable success for many years. Cross sections derived from the Fermi Hamiltonian blow up indefinitely as energy increases, as noted by Tomonaga and Tamaki [73] and by Heisenberg [165]. This problem was more clearly recognised when serious attention was paid to renormalisation of the field theory: the Fermi interaction, having field-dimension six, is not renormalisable. Serious attempts towards a renormalisable theory, however, had been hampered by the favour towards the ST-type of weak interactions, for which one cannot construct an intermediate boson theory.

The establishment of the V–A interaction led us to hope that one may construct a theory of intermediate bosons with vector particles. The first field-theoretic formulation of the weak interaction theory that includes the intermediate vector boson was presented by Schwinger (1957) [166] (see also Leite Lopes 1958 [167]), who tried to unify weak interaction with electromagnetic interaction. His theory contained an artificial disparity between the charged boson and the neutral boson (photon): the massive vector field was not renormalisable due to the appearance of field derivatives in the commutators of fields and currents and the appeerence of a $k^{\mu}k^{\nu}/M^2$ factor in the numerator of the propagator. An important step was taken by Glashow (1961) [168], who identified the correct algebraic structure [SU(2)×U(1)] of the vector boson family and mixing in electroweak interactions by adding one massive neutral vector boson to the vector boson triplet, which solved the problem of mass disparity. Although the theory of non-Abelian gauge fields had already appeared (Yang and Mills 1954 [169]; Utiyama 1956 [170]), Glashow did not refer to the gauge principle (which was employed later by Salam and Ward [171]). The problem of the gauge boson mass and the issue of renormalisability still remained unsolved.

The solution had to await the advent of the Higgs mechanism [172], the idea of spontaneous symmetry breaking [173] applied to gauge theories. In gauge theories the zero-mass boson, which should appear when symmetry is broken by a scalar field developing a vacuum expectation value, is absorbed into the longitudinal mode of the gauge field, giving the gauge field a mass. Weinberg [175] and Salam [176] constructed a theory based on the gauge principle with the SU(2)×U(1) group and incorporated the Higgs mechanism to generate gauge-boson mass. Although this is the correct theory of weak interactions, the theory received full attention only after 'tHooft's proof that the theory is renormalisable. By virtue of the self-coupling of gauge fields, commutators do not contain higher derivatives of fields. Furthermore, the current conservation was expected to hold even when symmetry was spontaneously broken, so that $k^\mu k^\nu/M^2$ terms should always decouple from the S matrix. The theory was thus supposed to be renormalisable, but a technical difficulty in the quantisation of non-Abelian gauge theory [177] hindered the proof of renormalisability until Faddeev and Popov (1967) [178] and de Witt (1967) [179] found a way out of this problem. They discovered a way to recover the unitarity of Feynman diagrams by expressing a fermion determinant in the path integral in terms of fictitious scalar fields that obey wrong statistics. The full internal consistency of the Weinberg–Salam theory as a field theory was shown in a proof of renormalisability by 'tHooft (1971) [180].

The remaining theoretical problem was how to incorporate hadrons into the theory, in particular the treatment of the strange quark, while avoiding the emergence of a strangeness-changing neutral current (note that this was before the discovery of the charm quark). This was solved by the adoption of the GIM scheme [181, 182]. Bouchiat et al. [182] also showed that anomaly is cancelled between quarks and leptons, so that the theory is fully consistent. This completed the theory of electromagnetic and weak interactions. On the experimental side, the pressing need was to discover the *strangeness-conserving* neutral current [183], a novel prediction of the Weinberg–Salam theory. The search was made for parity-violating effects in electromagnetic processes and for neutrino scattering via the neutral current. The correctness of the theory was evidenced by the discovery of neutral-current-induced neutrino interactions $\nu_\mu + e \to \nu_\mu + e$ and $\nu_\mu + N \to \nu_\mu +$ hadrons in a large heavy-liquid bubble chamber, *Gargamelle* ($6.2\,\mathrm{m}^3$, freon) (1973) [184]. The interferences between weak and electromagnetic interactions are detected just by the amount predicted by the theory of Weinberg and Salam in inelastic scattering of longitudinally polarised electrons on nucleons (1978) [185]. This excluded variant theories that were proposed after the Weinberg–Salam theory. The theory was firmly established by further explorations of neutrino-induced reactions and other parity-violating effects associated with the neutral current [186]. It was finally completed by the discovery of the W and Z (1983) [162, 163]. Today, the theory is tested to quite a high precision, including higher orders of perturbations of electroweak interactions; we know

that nature is extremely close to what the Weinberg–Salam theory predicts, which, on the other hand, is frustrating for those people looking for something beyond the standard theory.

1.4 The Neutrino-Mass Quest

As another line of the research, the quest for the neutrino mass has continued from Pauli's time to date. If the neutrino has a finite mass, many questions would open up concerning the properties of the neutrino. Whether it is of the Dirac type or of the Majorana type is the most fundamental question. In 1937, Majorana [187] proposed a self-conjugate neutrino: $\nu = \bar{\nu}$ except for helicity, and the helicity flip is caused by a mass term that violates lepton number. This mass term shows a marked contrast with the ordinary Dirac mass term, which conserves lepton number while flipping helicity. Generation mixing would also be an important issue, which would provide a hint for the understanding of the mass problem in particle physics, namely, what are the relations between the mass matrix of quarks and that of leptons. We must ask whether the massive neutrino is stable or not. CP violation in the lepton sector might be substantially different from what we have seen in the quark sector [188]. As will be seen below, all of these questions may be closely related to physics at very high energy, much higher than the scale the present experiments can directly explore.

The dominant part of the current experimental effort with neutrinos is concerned with the search for a finite neutrino mass. The most direct is the search for the electron neutrino mass in nuclear beta decay. According to the Fermi theory, the beta ray should have the spectrum

$$\rho(E_e)dE_e \propto p_e E_e (E_0 - E_e + m_\nu) \tag{1.6}$$
$$\times \sqrt{(E_0 - E_e)(E_0 - E_e + 2m_\nu)}F(Z, E_e)dE_e \;,$$

where E_0 is the maximum energy of the electron ($= \Delta E - m_\nu$ where ΔE is the difference between the energy levels) and $F(Z, E_e)$ is the Fermi function [20] correcting for the Coulomb force. This form can be used to determine neutrino mass. Or, as Kurie et al. (1936) [189] did, we can plot $K(E_e) = [\rho(E_e)/p_e E_e F(Z, E_e)]^{1/2}$ as a function of $E_0 - E_e$ and look for a deviation from a straight line $K(E_e) \propto E_0 - E_e$ (Kurie plot). The limit on the electron neutrino mass has been continuously improved during the 70 years (see Fig. 1.1). In the beginning, Pauli concluded that it is by no means larger than 0.01 times the proton mass [1]. Earlier searches for the neutrino mass were made by Lyman (1939) [190] and Haxby et al. (1940) [191], resulting in $0 \pm 0.2m_e$ and $0 \pm 0.1m_e$, respectively, using $^{13}\text{N} \rightarrow {}^{13}\text{C} + e^+ + \nu_e$. Konopinski (1947) [192] noted that $^{3}\text{H} \rightarrow {}^{3}\text{He} + e^- + \bar{\nu}_e$ has an unusually small Q value and concluded from existing experiments that $m_\nu < 10\,\text{keV}$. (Furthermore, he derived a finite neutrino mass to match the lifetime of ^{3}H with that of
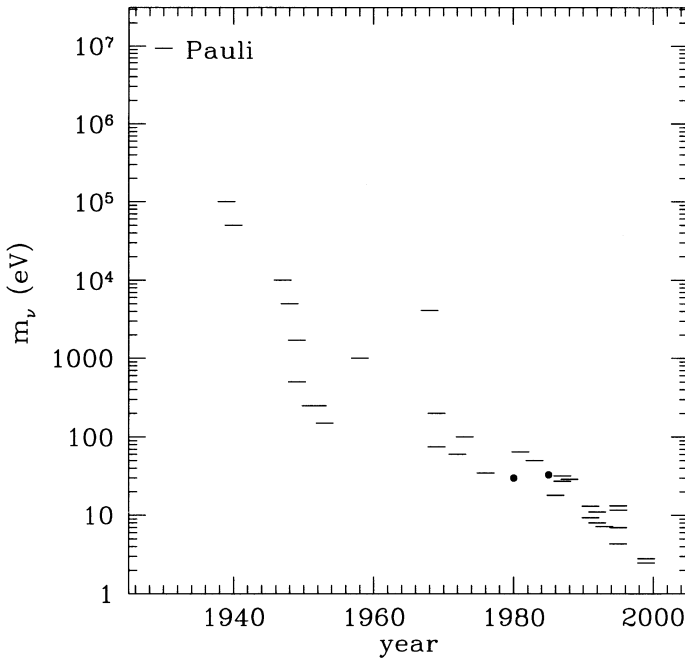
Fig. 1.1. Advancement of the empirical upper limit on the electron neutrino mass from the time of Pauli. The two points denoted by solid circles are 'finite' values reported from the ITEP experiment; see the text.

^{6}He from a phase-space-volume consideration. This was caused by too small a Q value of ^{3}H–^{3}He known at that time.) Taking advantage of this small Q value, Curran, Angus, and Cockcroft (1948) used this tritium beta decay to set a limit on the neutrino mass of $m_{\nu_e} < 1.8\,\text{keV}$ [193]. The work of Hanna and Pontecorvo (1949) followed to set a limit of $m_{\nu_e} < 0.5\,\text{keV}$ [194]. Since these reports, tritium has been used almost exclusively to study the electron neutrino mass. Modern spectrometer experiments were started by Hamilton et al. (1951), using electrostatic retardation [195], and by Langer and Moffat (1952), using a magnetic spectrometer [196]. The limit obtained by both groups, $< 250\,\text{eV}$, was the best limit until Bergkvist [197] obtained a new limit ($m_{\nu_e} < 60\,\text{eV}$) in 1971 with a very careful study. The experimental technique developed by Bergkvist has been followed in more modern experiments. In 1980 a surprise was encountered by the Moscow ITEP group (1980) [198] which reported a finite mass, $17\,\text{eV} < m_{\nu_e} < 40\,\text{eV}$. Several groups then initiated work to confirm or to refute the ITEP result; it took a decade to rule out conclusively a finite mass in this range. As a positive aspect, however, this erroneous result has had a great impact on research in cosmology.

The second means to explore neutrino mass is to search for neutrino-less double beta decays. The search for double beta decays also has a long history. Following a study by Goeppert–Mayer (1935) [199] for $(N, Z) \rightarrow (N, Z+2) + 2\bar{\nu} + 2e^-$, Furry (1939) [200] pointed out that neutrinoless double beta decays, $(N, Z) \rightarrow (N, Z+2) + 2e^-$, may take place if the neutrino is of the Majorana type, i.e., $\bar{\nu} = \nu$, so that $\bar{\nu}$ emitted virtually in beta decay of a neutron is absorbed by another neutron, which induces electron emission. The amplitude of neutrinoless double beta decays is proportional to the strength of lepton-number violation, i.e., the Majorana neutrino mass. Early searches for neutrinoless double beta decay are reviewed in [201]. There are two methods for detecting this process. The first is the geochemical method, in which one measures relative abundances of nuclei of $(N, Z + 2)$ and (N, Z). The most notable example is a measurement of the relative abundances of ^{128}Xe and ^{130}Xe derived from their tellurium parents, which could differentiate neutrinoless double beta decay from two-neutrino double beta decay [202]. The second method is the counter experiment to directly search for two-electron emission, the electron energy of which is monoenergetic when added. There were occasional positive reports for neutrinoless double beta decay close to the detection limit, but none survived further exploration. Interest in this process was revived with the advent of grand unification of strong and electroweak interactions, where neutrinos are likely to appear as the Majorana type. To date we have only upper limits, but they are now approaching a physically interesting value.

Pontecorvo (1957) [203] suggested that a neutrino may oscillate into its antiparticle in vacuum if lepton number is not conserved, just like $K^0 - \bar{K}^0$ oscillation proposed by Gell-Mann and Pais (1955) [204]. Maki et al. (1962) [122] suggested virtual transitions among different kinds of neutrinos. Oscillation as we understand it today was formulated by Gribov and Pontecorvo (1969) [205]. This may occur if some of the neutrinos are massive and if there is mixing between the different neutrinos. If the mass of neutrinos is significantly smaller than 1 eV, neutrino oscillation is the only feasible way to detect it. Early considerations of neutrino oscillation [205, 206] were concerned with the problem of the solar neutrino flux, which was smaller than expected [207]. We quote a review by Bilenky and Pontecorvo (1978) [208], which was written just before a flood of laboratory experiments. After 1980 there was persistent effort to search for neutrino oscillation by using a variety of neutrino beams, i.e., those from nuclear reactors or accelerators. All conventional experiments gave null results.

The only case in which neutrino oscillation has been positively suspected is with solar neutrinos. Davis and his collaborators began a large-scale experiment in 1967 to measure the neutrino flux arising from nuclear fusion in the Sun by using a chlorine detector [207] (see Bahcall and Davis [209] for

a historical account).[10] Since the first report in 1968, they have given fluxes consistently smaller than predicted in the standard solar model, in which the Sun is treated as a hydrodynamically supported gas sphere starting with a homogeneous elemental composition. The neutrino oscillation hypothesis, however, has been taken with reservations, partly because the explanation requires very large neutrino mixing (which looked unlikely from the experience with quark mixing) and a fine-tuned mass difference squared which just fits the distance between the Sun and Earth, but also because it seems possible that there are some unknown uncertainties in the solar dynamics that would affect the calculated solar neutrino flux: only a 5% error in the temperature at the centre of the Sun would have solved the problem. In 1986 Mikheyev and Smirnov [211] came up with the idea that electron neutrinos may be efficiently converted into muon neutrinos in matter via a resonance-like mechanism even when the intrinsic mixing angle is very small. When the diffractive phase in matter [212] cancels the phase from the mass difference, the oscillation effect is maximised. Furthermore, this mechanism does not require tuning the neutrino mass difference to the Sun–Earth distance. (This proposal received great publicity after a paper by Bethe [213].) At that moment, many particle physicists started to take the neutrino oscillation idea seriously as a solution to the long-standing solar neutrino problem. The excitement arises particularly from the fact that the presence of mass (provided that it is of a Majorana mass) would point to the first indication of the presence of a new energy scale beyond electroweak unification.

The conclusive evidence for the presence of neutrino oscillation, however, came from a different direction. In the early 1980s, several groups constructed massive detectors [214–218] to search for proton decays, which are a unique signature of grand unified theories of strong and electroweak interactions [219–221]. These apparatuses, placed deep underground, inevitably detect neutrinos from pions and muons produced by cosmic rays that interact with the atmosphere [222,158, 159] as background events (they are called atmospheric neutrinos). In particular, two groups, IMB (the Irvine-Michigan-BNL collaboration at the Morton salt mine in Minnesota) and Kamiokande (Kamioka Nucleon Decay Experiment at the Kamioka zinc mine) noticed a deficit in the muon neutrino flux relative to the electron neutrino flux compared with the calculation [223, 224]. This muon neutrino deficit is so large that it cannot be ascribed to statistical effects. The IMB group, who derived the ν_μ deficit from detecting the associated muon decay rate, however, took the conservative attitude that this deficit is probably ascribable to some unknown systematics [225]. On the other hand, the Kamiokande, relying upon its capability for clear $e\mu$ event separation, ventured to interpret it as a result of neutrino oscillation. The group further investigated this problem and found that the higher energy neutrino flux shows a nontrivial zenith-

---

[10] We refer the reader to the monograph by Bahcall for a detailed account of the solar neutrino problem up to 1994 [210].

angle dependence that can be explained by the neutrino oscillation hypothesis (1994) [226]. This has not convinced everybody yet, however, as the statistical confidence was not very high and, in addition, lower energy data did not show a clear signal for oscillation. The oscillation interpretation requires very large mixing between two-neutrinos, which did not look reasonable; so people were rather reluctant to take the evidence seriously. Finally, Super-Kamiokande (the enlarged facility of Kamiokande by 15 times in mass) has conclusively shown that every aspects of atmospheric neutrino data are consistent with neutrino oscillation between muon neutrinos and τ neutrinos with a mass difference squared of about $(0.05\,\text{eV})^2$, and, surprisingly, mixing is nearly maximal (1998) [227].

Taking advantage of their huge photomultipliers, the Kamiokande group demonstrated that a water Čerenkov detector can be used for solar neutrino detection by successfully decreasing the threshold energy of recoil electron detection to below 10 MeV [228]. This experiment, using νe elastic scattering[11], observed solar neutrinos of higher energy and showed suppression of the neutrino flux different from that observed in Davis et al.'s experiment. At this time, long-awaited solar neutrino experiments using gallium as targets [230] were started [231, 232]. This experiment is very sensitive to the lowest energy neutrinos which arise from $p + p$ nuclear reactions responsible for the dominant part of solar energy generation.[12] These gallium experiments resulted in yet different flux suppression factors. The neutrino oscillation hypothesis (either in vacuo or in matter) satisfactorily describes the different deficits of solar neutrino capture rates and leads to narrow ranges of allowed neutrino mixing parameters. The neutrino oscillation hypothesis was finally confirmed by the newest experiment of neutrino deuterium scattering [234] at the Sudbury Neutrino Observatory at statistics of $3.3\,\sigma$ by combining it with the Super-Kamiokande result (2001): the ^{8}B neutrino flux observed with the pure charged-current reaction on deuterium is smaller by about a factor of 2 than the flux that induces the neutral-current reactions obtained by subtracting the charged-current-induced reaction rate from the full neutrino electron scattering rate at Super-Kamiokande. The neutrino flux that induces the neutral-current reaction, thus estimated, agrees with the neutrino generation rate anticipated for the Sun [235].

1.5 The Interest in Neutrinos Today

We have seen that the advancement of particle physics has been inseparably connected with the understanding of neutrinos. The aspect of neutrino

---

[11] For an early attempt to measure νe elastic scattering, see Reines and Kropp (1964) [229]. The detector was too small to give a meaningful result.

[12] Sunyar and Goldhaber [233] were the first who discussed the detection of pp solar neutrinos. They proposed to use ^{87}Rb.

physics that is of interest today arises from the belief that the physics of
the neutrino might yet lead to new physics beyond the standard theory, if it
exists. There are a few points we should particularly emphasise.

The first is that we want to look for a more fundamental interaction that
leads to a low-energy effective theory for particle interactions as indicated
by a finite neutrino mass. The presence of an effective theory means that
we should have some energy scale on which new physics sets in. The classic
example is again the Fermi theory of the weak interaction described by (1.1).
As we mentioned earlier, the cross section of $\bar{\nu} + p \to e^+ + n$ scattering
violates the limit derived from unitarity if the incident laboratory energy
becomes larger than $1\,\mathrm{TeV}$. This means that the new physics sets in on an
energy scale at $\lesssim 1\,\mathrm{TeV}$. The Weinberg–Salam theory tells us that this scale
is $\approx 100\,\mathrm{GeV}$.

We find a similar situation with the neutrino mass. The mass of the
neutrino is very small compared with the mass of other particles. It is smaller
than others by at least a factor of 10^5. A reasonably convincing explanation
for a small neutrino mass is that the smallness is ascribed to a small lepton
number violation, i.e., the neutrino mass is controlled by a Majorana mass
term rather than by the Dirac mass term, which is responsible for the mass
of other particles.

If we try to describe the coupling which gives rise to the Majorana mass
term in terms of the fields that appear in the standard theory, we necessarily
have an interaction of the dimension greater than four,

$$\mathcal{L}_{\mathrm{mass}} = f\ \nu\nu\phi\phi\,, \tag{1.7}$$

where ϕ is Weinberg–Salam's Higgs doublet [236]. When ϕ develops a vacuum-
expectation value, this interaction yields a lepton-number-violating Majorana
mass term. In fact, most of the models for the neutrino mass take essentially
this form. In this expression the coupling constant f has the dimension
of $[\mathrm{mass}]^{-1}$; this interaction is regarded as an effective Lagrangian, just as
in (1.1), where G_{F} has the dimension of $[\mathrm{mass}]^{-2}$. If we consider $\nu\phi \to \nu\phi$
scattering, the cross section does not decrease as $(\mathrm{energy})^{-2}$ as required
by unitarity, but remains constant. If we require this to satisfy the S-wave
unitarity limit for energy smaller than the value corresponding to the Planck
mass $(m_{\mathrm{pl}} = 1.22 \times 10^{19}\,\mathrm{GeV})$, we must have $f < 2\pi/m_{\mathrm{pl}}$, that is, the neutrino
mass must be $< 3 \times 10^{-5}\,\mathrm{eV}$. If the neutrino has a mass larger than this limit,
there should be a new interaction below the Planck mass scale. This is the
most conservative argument.

We can suppose a more specific case. In most unification models lepton
number is broken on high-energy scales. This gives a large mass for neutrinos.
This is allowed if it concerns the right-handed neutrino. In such a situation,
a small mass is induced for the left-handed neutrino via Yukawa coupling that
connects right-handed to left-handed sectors. We expect a mass of the order
of $m_\nu \simeq m_{\mathrm{D}}^2/M_{\mathrm{R}}$, where M_{R} is the large right-handed neutrino mass and m_{D}

the Dirac mass from the Yukawa coupling, which would be in parallel with other charged particle masses. This is called the seesaw mechanism (Yanagida 1979; Gell-Mann, Ramond and Slansky 1979 [237]), and it may explain why the observed neutrino mass is so small. In other words, the neutrino mass indicates a mass scale where some unification takes place, but it may also allow us to explore the structure of unification. This is the prime reason why we are so interested in the neutrino-mass search.

If the neutrino is of the Dirac type, on the other hand, we do not find a compelling reason why the mass is so small. It just happened so. There would be no immediate new physics here.[13]

The second point is that the neutrino is the only particle that is free from interactions stronger than the weak interaction and that we may hope that the weaker interaction would be most apparent in the physics of neutrinos. For instance, the standard electroweak theory predicts that the magnetic moment of a neutrino is extremely small, of the order of 10^{-19} Bohr magnetons or less, whereas the current upper limit is only about 10^{-11} Bohr magnetons. If the magnetic moment were somewhere in the middle, it immediately means some new interaction, e.g., a hypothetical right-handed current, is acting.

Another modern interest in neutrinos arises from their significance in astrophysics and cosmology. Neutrinos are produced copiously in high-temperature and/or high-density environments and they often dominate the physics and control the astrophysical evolution of the system. The first example is its role in stars. In stars more evolved than the He-burning stage, cooling is dominated by neutrino emission and it controls the lifetime of such stars [239–242]. For example, Stothers [243] claimed the existence of νe interactions from the evolutionary timescale of helium- and carbon-burning stars and the cooling of white dwarfs prior to the detection of this interaction in laboratories [244]. The role of neutrinos is essential in the core collapse of type-II supernovae.

The role of neutrinos in the Sun is astrophysically insignificant, but it produces a very strong neutrino flux that can be observed on Earth. As we have seen, solar neutrino experiments have led us to serious considerations of the possibility of neutrino oscillation, for which we received no support from laboratory experiments.

Cosmology is another place where neutrinos play an important role.[14] Shortly after the seminal '$\alpha\beta\gamma$' paper (Alpher, Bethe, and Gamow 1948 [247]), Hayashi (1950) recognised the importance of the neutrino and weak interactions in the thermal history of the universe [248]. In a very hot universe, neutrinos were in equilibrium with other particles. This relic neutrino determined the neutron-to-proton ratio in the hot universe through beta-process

---

[13] There is a recent suggestion that a small Dirac mass of neutrinos may be explained within a higher-dimensional brane world [238]. The theory is still too premature to take it as a realistic possibility.

[14] We refer to a review by Dolgov and Zeldovich [245] and a monograph by Kolb and Turner [246].

equilibrium, and this determined the helium abundance [249–251]. This helium abundance is sensitive to temperature when the β equilibrium was frozen out, which in turn was controlled by the expansion rate that varies with the number of neutrino species. This limits the number of light neutrino species and hence, probably the number of families of particles.

The number density of neutrinos in the universe is about 100 per cubic centimetres today. If the neutrino had a mass of more than 0.2 eV, the total mass density of neutrino would exceed the mass density of baryons and if it is in excess of a few eV, they may even gravitationally dominate the universe [252, 253] and should have controlled the formation of cosmic structures [254]. In fact a limit on the mass of ν_μ and ν_τ, much stronger than obtained in laboratories, is derived from such a cosmological argument [252, 255]. This is why the ITEP result on neutrino mass has excited astrophysicists: the mass was just in the right range to govern structure formation in the universe. Motivated by this result, the role of weak interacting massive particles was worked out in detail, first with neutrinos [256], and then extended to more hypothetical weakly interacting massive particles, named cold dark matter (CDM) [257]. The structure formation model based on CDM is now taken as the standard, or at least the fiducial for studies of cosmogony (see Rees [258] for a brief overview). It is ironical that such studies would be at least delayed, if the ITEP result did not exist. As a separate cosmological issue, the physics of neutrinos may also be closely related to the creation of the baryon number in the universe through triangle anomaly [259, 260], if neutrinos are of the Majorana type [261].

In summary, the interest in neutrinos in relation to astrophysics and cosmology is threefold: (i) whether neutrinos serve to understand yet unsolved phenomena of astrophysics and cosmology, (ii) use neutrinos as a probe to explore the interior of optically thick objects, that are not accessible by optical means, and (iii) use astrophysical and cosmological environments as laboratories for particle physics.

Throughout this book, we use the natural unit $c = \hbar = 1$, but we occasionally put c or $\hbar$ to emphasise its role. We adopt the time-favoured metric for relativity $ds^2 = dt^2 - dx^2$. The unit for electromagnetisms is the Heaviside–Lorentz, i.e., $\alpha = e^2/4\pi \simeq 1/137$.

2 Standard Theory of Electroweak Interactions

2.1 Classical Theory of Weak Interactions

In the four-Fermi interaction the neutrino interacts with the electron via the V–A current of the form

$$\bar{e}\gamma_\mu(1 - \gamma_5)\nu \ . \tag{2.1}$$

In modern field theory, left- and right-handed fields are regarded as fundamental fields (this handedness is called chirality). They are given by

$$\psi_{\substack{L \\ R}} = \frac{1 \mp \gamma_5}{2}\psi \ , \tag{2.2}$$

where ψ is the conventional Dirac field and ψ_L and ψ_R are two-component fields called the Weyl fermions [46,45]. ψ_L and ψ_R are eigenstates of the chiral transformation [262,263,32] $\psi \to \gamma_5\psi$ with eigenvalues of -1 and $+1$, respectively. The weak current of form (2.1) is written as

$$\bar{\psi}_L\gamma_\mu\psi_L \ , \tag{2.3}$$

up to a factor 2 compared with (2.1). This means that the weak interaction is invariant under a chiral transformation, i.e., it conserves chirality. The mass term $m\bar{\psi}\psi$, on the other hand, flips the chirality; it is written as

$$m(\bar{\psi}_R\psi_L + \bar{\psi}_L\psi_R) \ . \tag{2.4}$$

The mass term alone breaks the chiral invariance of the weak interaction theory.

For leptons we take the fundamental fields for the first-generation particles as chirally projected fields e_L, ν_L, and e_R, where e_R does not appear in the V–A theory. Likewise for quarks, they are q_L and q_R with $q = u$ or d, and q_R does not appear in the V–A weak-interaction processes. Whether ν_R exists or not in nature is unknown because it decouples from the theory. The standard (massless neutrino) theory assumes that it does not exist.

The classical weak interaction Hamiltonian is given by

$$H_W = \frac{G_F}{\sqrt{2}}J_\mu^\dagger J_\mu \ , \tag{2.5}$$

where the current J_μ is

$$J_\mu = 2(\bar{\nu}_{\rm L} \gamma_\mu e_{\rm L}^- + \bar{u}_{\rm L} \gamma_\mu d_{\rm L}) \qquad (2.6)$$

and $G_{\rm F}$ is the Fermi coupling constant. The right-handed field does not appear in this Hamiltonian.

The interaction of the form given in (2.5) suggests that the weak interaction has an underlying SU(2) symmetry and that $e_{\rm L}$ and $\nu_{\rm L}$ ($u_{\rm L}$ and $d_{\rm L}$) form a doublet. The nonappearance of $e_{\rm R}$ leads us to suppose that it is a singlet of SU(2), i.e.,

$$\psi_{\rm L} = \begin{pmatrix} \nu_{\rm L} \\ e_{\rm L} \end{pmatrix} \ \ \mathbf{2} \ , \quad \psi_{\rm R} = e_{\rm R} \ \ \mathbf{1} \ . \qquad (2.7)$$

The first term of (2.6), for instance, is then written as

$$\bar{\psi}_{\rm L} \gamma_\mu \tau_+ \psi_{\rm L} \quad \left(\tau_+ = \frac{\tau_1 + i\tau_2}{2} \right) \ , \qquad (2.8)$$

where the Pauli matrices τ describe SU(2) (weak isospin) of the weak interaction,

$$\tau_1 = \begin{bmatrix} 0 & 1 \\ 1 & 0 \end{bmatrix}, \quad \tau_2 = \begin{bmatrix} 0 & -i \\ i & 0 \end{bmatrix}, \quad \tau_3 = \begin{bmatrix} 1 & 0 \\ 0 & -1 \end{bmatrix} \ . \qquad (2.9)$$

2.2 Weinberg–Salam Theory of Electroweak Interactions

2.2.1 SU(2) × U(1) Symmetry

We now sketch the Weinberg–Salam theory of electroweak interaction [175, 176], the fundamental theory that describes both weak and electromagnetic (em) interactions. The theory is taken as the prototype of the unified theories to which we often refer in this book. We review the theory only for its practical merit and defer the theoretical details to other textbooks (e.g., [264–266]).

In the Weinberg–Salam theory, the symmetry of the weak interaction is taken as a local (gauge) symmetry, like U(1) of the electromagnetic interaction. Therefore, the SU(2) quantum number is regarded as the charge of a particle. For instance, the neutrino $\nu_{\rm L}$ has a weak isospin charge, $T = 1/2$ and $T_3 = 1/2$, while it carries no electromagnetic charge; $e_{\rm R}$ has $T = 0$ and $T_3 = 0$.

The most general unitary transformation for $\psi_{\rm L}$ and $\psi_{\rm R}$ in (2.7) is U(2) × U(1):

$$\psi_{\rm L} \to U\psi_{\rm L} \ , \qquad \psi_{\rm R} \to V\psi_{\rm R} \ , \qquad (2.10)$$

where U is a unitary matrix of 2×2 and V is 1×1. This, however, includes the lepton-number phase transformation

$$\psi_L \to e^{i\alpha}\psi_L , \qquad \psi_R \to e^{i\alpha}\psi_R , \qquad (2.11)$$

which we would like to exclude from gauge symmetry.[1] Therefore, the most general desired symmetry is SU(2)$\times$ U(1); in fact, it turns out that this is the symmetry that correctly describes both electromagnetic and weak interactions at the same time. Let T_i ($i = 1, 2, 3$) be the three operators of SU(2), $T_i = \tau_i/2$. The operator Y defined by

$$Y = Q - T_3 \qquad (2.12)$$

commutes with T_i (Q represents the em charge operator) and gives the desired U(1) operator. This is a Nishijima–Gell-Mann relation. A consistent description is made if the U(1)$_Y$ charge $-1/2$ is assigned to ψ_L and -1 to ψ_R.

2.2.2 The Gauge Fields

The Weinberg–Salam theory is a theory of gauge fields [169, 170] that couple universally to weak charges of SU(2) (**T**) and U(1) (Y). Three gauge fields, $W_{1,2}$ and W_3, are associated with the generator of SU(2), and one gauge field B with U(1)$_Y$.

The gauge principle dictates that the gauge fields interact with matter fields ψ_L, ψ_R through the covariant derivative,

$$D_\mu = \partial_\mu + ig\mathbf{W}_\mu \mathbf{T} + ig' B_\mu Y . \qquad (2.13)$$

We use a vector notation $\mathbf{W} = (W^1, W^2, W^3)$ for the components in weak SU(2) isospin space. With the charge assignment for ψ_L and ψ_R discussed above,

$$\mathcal{L} = i\bar{\psi}_L \, \slashed{D}\psi_L + i\bar{\psi}_R \, \slashed{D}'\psi_R , \qquad (2.14)$$

where

$$D_\mu = \partial_\mu + ig\mathbf{W}_\mu \frac{\tau}{2} - i\frac{g'}{2}B_\mu , \qquad (2.15)$$

$$D'_\mu = \partial_\mu - ig' B_\mu \qquad (2.16)$$

from (2.13).

This uniquely determines the coupling of the gauge bosons to matter fields. At this level, all fields, including fermion fields, are massless because there are no interactions that break the chiral symmetry.

---

[1] We show later that lepton number cannot be gauged due to the presence of anomaly.

The covariant derivative means that $D_\mu\psi_L$ and $D'_\mu\psi_R$ transform just like ψ itself under a gauge transformation. The part concerning $g'B_\mu$ is Abelian and the same as we encounter in quantum electrodynamics. For the U(1) gauge transformation

$$\psi_L(x) \to \psi'_L(x) = e^{-i\xi(x)/2}\psi_L(x) \ , \tag{2.17}$$

an infinitesimal version is written,

$$\delta\psi_L(x) = -i\frac{\xi(x)}{2}\psi_L(x) \ . \tag{2.18}$$

$D_\mu\psi_L$ transforms as

$$\delta[D_\mu\psi_L(x)] = -i\frac{\xi(x)}{2}[D_\mu\psi_L(x)] \ , \tag{2.19}$$

if

$$\delta B_\mu(x) = -\frac{1}{g'}\partial_\mu\xi(x) \ . \tag{2.20}$$

Applying the covariant derivative twice, we find for $g = 0$,

$$[D_\mu, D_\nu]\psi_L = i\frac{g'}{2}B_{\mu\nu}\psi_L \ , \tag{2.21}$$

where

$$B_{\mu\nu} = \partial_\mu B_\nu - \partial_\nu B_\mu \ , \tag{2.22}$$

which is obviously invariant under the gauge transformation (2.20).

The non-Abelian character appears for the part concerning gW_μ. The gauge transformation is given by

$$\psi_L(x) \to \psi'_L(x) = U(\theta)\psi_L = e^{i\boldsymbol{\theta}\mathbf{T}}\psi_L(x) \ , \tag{2.23}$$

and its infinitesimal version is

$$\delta\psi_L(x) = i\boldsymbol{\theta}(x)\mathbf{T}\psi_L(x) \ . \tag{2.24}$$

Under (2.24), $D_\mu\psi$ transforms as

$$\delta[D_\mu\psi_L(x)] = i\boldsymbol{\theta}(x)\mathbf{T}[D_\mu\psi_L(x)] \ , \tag{2.25}$$

if

$$\delta\mathbf{W}_\mu(x) = -\frac{1}{g}\partial_\mu\boldsymbol{\theta}(x) + \mathbf{W}_\mu(x) \times \boldsymbol{\theta}(x). \tag{2.26}$$

The outer product $\mathbf{W}_\mu(x) \times \boldsymbol{\theta}(x)$ may also be written as $\epsilon_{\alpha\beta\gamma}W^\beta\theta^\gamma$. A covariant derivative for the gauge field can be constructed by applying D_μ

successively,

$$[D_\mu, D_\nu]\psi_{\mathrm{L}} = ig\mathbf{F}_{\mu\nu}\mathbf{T}\psi_{\mathrm{L}} \, , \tag{2.27}$$

where

$$\mathbf{F}_{\mu\nu} = \partial_\mu \mathbf{W}_\nu - \partial_\nu \mathbf{W}_\mu - g\mathbf{W}_\mu \times \mathbf{W}_\nu \, . \tag{2.28}$$

$F^\alpha_{\mu\nu}$ is the field strength that transforms like the adjoint representation $\mathbf{T}^{\mathrm{adj}}$

$$\delta\mathbf{F}^\alpha_{\mu\nu} = i\boldsymbol{\theta}(\mathbf{T}^{\mathrm{adj}})^{\alpha\beta}F^\beta_{\mu\nu} \, , \tag{2.29}$$

and $\mathbf{FF}$ is invariant under the gauge transformation.

The Lagrangian for the gauge field is thus constructed as

$$\mathcal{L} = -\frac{1}{4}\mathbf{F}_{\mu\nu}\mathbf{F}^{\mu\nu} - \frac{1}{4}B_{\mu\nu}B^{\mu\nu} \, . \tag{2.30}$$

The integral form of the gauge transformation (2.26) is

$$W_\mu \to W'_\mu : \quad \mathbf{T}\mathbf{W}'_\mu = U(\theta)\left[\mathbf{T}\mathbf{W}_\mu + \frac{i}{g}U^{-1}(\theta)\partial_\mu U(\theta)\right]U^{-1}(\theta) \, . \tag{2.31}$$

2.2.3 Spontaneous Symmetry Breaking and the Higgs Mechanism

In reality, SU(2) × U(1) symmetry must be broken since only the U(1)$_{\mathrm{em}}$ charge is conserved in nature. This is deeply related to the fact that only the photon is a massless gauge field.

There are generally two ways to break symmetry, explicitly and spontaneously. We must take the latter for gauge theory since otherwise symmetry breaking spoils the renormalisability of the entire theory. In order to break symmetry spontaneously, we introduce a scalar field ϕ. In principle, it may be in any representation other than the singlet of SU(2). The simplest choice is to take ϕ as a doublet, which agrees with experiment. The contribution from scalars with other representations, if any, must be small. We introduce

$$\phi = \begin{pmatrix} \phi^+ \\ \phi^0 \end{pmatrix} \quad \mathbf{2} \, , \ Y = +1/2 \tag{2.32}$$

and give a vacuum-expectation value to ϕ^0 to break SU(2) × U(1)$_Y$ down to U(1)$_{\mathrm{em}}$. The choice of Y is made to satisfy (2.12). Coupling to the gauge field is given by

$$(D_\mu\phi)^\dagger(D^\mu\phi) \, , \tag{2.33}$$

where D_μ is given by (2.13) with $\mathbf{T} = \boldsymbol{\tau}/2$ and $Y = +1/2$:

$$D_\mu = \partial_\mu + ig\frac{\boldsymbol{\tau}}{2}\mathbf{W}_\mu + i\frac{g'}{2}B_\mu \ . \tag{2.34}$$

We may assume a self-interaction of the scalar field (Higgs potential) with a negative mass squared,

$$V(\phi) = -\mu^2\phi^\dagger\phi + \lambda(\phi^\dagger\phi)^2 \ , \tag{2.35}$$

with $\mu^2 > 0$. The potential then takes a minimum where $\partial V/\partial\phi = 0$, i.e., at $\phi^\dagger\phi = \mu^2/2\lambda$. The vacuum is given by

$$\langle\phi\rangle = e^{i\boldsymbol{\zeta}(x)\boldsymbol{\tau}/2v} \begin{pmatrix} 0 \\ v/\sqrt{2} \end{pmatrix} \ , \tag{2.36}$$

where

$$v = \sqrt{\mu^2/\lambda} \ , \tag{2.37}$$

and $\boldsymbol{\zeta}$ are three real functions.

To save perturbation theory, we define

$$\phi = e^{i\boldsymbol{\zeta}(x)\boldsymbol{\tau}/2v} \begin{pmatrix} 0 \\ \frac{v+\phi'}{\sqrt{2}} \end{pmatrix} . \tag{2.38}$$

This is a map (ϕ^+, ϕ^0) onto $(\phi', \boldsymbol{\zeta})$, but $\boldsymbol{\zeta}$ does not appear in the potential V, i.e., the fields $\boldsymbol{\zeta}$ are massless Nambu–Goldstone bosons associated with broken SU(2) [173]. Only one scalar field ϕ' is massive: $m^2 = \partial^2 V/\partial\phi'^2 = 2\mu^2$.

Now, we apply a gauge transformation

$$\phi \to U\left[\boldsymbol{\Lambda}(x)\right]\phi = \begin{pmatrix} 0 \\ \frac{v+\phi'}{\sqrt{2}} \end{pmatrix} \ , \tag{2.39}$$

where

$$U\left[\boldsymbol{\Lambda}(x)\right] = e^{-i\boldsymbol{\Lambda}\boldsymbol{\tau}} \tag{2.40}$$

with

$$\boldsymbol{\Lambda}(x) = \frac{\boldsymbol{\zeta}(x)}{2v} \ . \tag{2.41}$$

At the same time the gauge field is subject to the transformation given in (2.31), where $\boldsymbol{\theta}$ is replaced by $\boldsymbol{\Lambda}$. The Lagrangian is invariant under this gauge transformation. We now write, after this gauge transformation (in the unitary gauge),

$$\phi^+ = 0, \qquad \phi^0 = \frac{v+\phi'}{\sqrt{2}} \ . \tag{2.42}$$

In gauge theory the zero-mass Nambu–Goldstone bosons are absorbed into gauge transformation, i.e., into the longitudinal mode of the gauge bosons to make them massive (Higgs mechanism), as shown in what follows [172]. The gauge taken here is called the *unitary gauge*. This is seen by calculating

$$
\begin{aligned}
(D_\mu\phi)^\dagger(D_\mu\phi) &= \left|\left(\partial_\mu + ig\frac{\tau}{2}\mathbf{W}_\mu + i\frac{g'}{2}B_\mu\right)\begin{pmatrix} 0 \\ \frac{v+\phi'}{\sqrt{2}} \end{pmatrix}\right|^2 \\
&= \frac{1}{2}(\partial_\mu\phi')^2 \\
&\quad + \frac{1}{8}\left[g^2(W_\mu^1 W^{1\mu} + W_\mu^2 W^{2\mu})\right. \\
&\qquad \left. + (-gW_\mu^3 + g'B_\mu)(-gW^{3\mu} + g'B^\mu)\right]v^2 \\
&\quad + O(\text{field}^3).
\end{aligned}
\tag{2.43}
$$

This shows that W^1, W^2 and the combination $-gW^3 + g'B$ become massive. Note that the cross term $(\partial_\mu\phi')W^\mu$ vanishes for real ϕ'. In fact, the unitary gauge means the gauge in which this cross term vanishes. We also see that only one scalar field is physical.

2.2.4 Gauge Boson Mixing

The Higgs ϕ^0 that develops a vacuum expectation is an SU(2) nonsinglet and has a nonzero U(1)$_Y$ charge but zero U(1)$_Q$ charge. Thus, it breaks SU(2)×U(1)$_Y$, but the U(1)$_Q$ charge,

$$
Q = T_3 + Y ,
\tag{2.44}
$$

remains unbroken. Therefore, the gauge field

$$
A_\mu \propto \frac{1}{g}W_\mu^3 + \frac{1}{g'}B_\mu ,
\tag{2.45}
$$

that couples to

$$
Q = \frac{1}{g}(gT_3) + \frac{1}{g'}(g'Y)
\tag{2.46}
$$

remains massless. The field orthogonal to (2.45),

$$
Z_\mu \propto \frac{1}{g'}W_\mu^3 - \frac{1}{g}B_\mu ,
\tag{2.47}
$$

becomes massive (as seen explicitly in (2.43) above). $(W^3, B) \to (A, Z)$ is an orthogonal transformation [168],

$$
\begin{pmatrix} A_\mu \\ Z_\mu \end{pmatrix} = \begin{pmatrix} \cos\theta_W & \sin\theta_W \\ -\sin\theta_W & \cos\theta_W \end{pmatrix}\begin{pmatrix} B_\mu \\ W_\mu^3 \end{pmatrix} ,
\tag{2.48}
$$

and the angle θ_{W} is called the Weinberg angle or the weak mixing angle,

$$\mathrm{tg}\ \theta_{\mathrm{W}} = \frac{g'}{g}\ , \tag{2.49}$$

from (2.45) and (2.47). Note that the combination for Z is exactly what appeared in the mass term with the Higgs mechanism (2.43) above. The weak mixing angle is not determined within the theory.

In terms of A_μ and Z_μ, (2.43) reads

$$(D_\mu\phi)^\dagger(D_\mu\phi) = \frac{1}{2}(\partial_\mu\phi')^2 + \left(\frac{g^2}{4}W_\mu^+W^{-\mu} + \frac{g^2+g'^2}{8}Z_\mu Z^\mu\right)v^2 + \cdots \tag{2.50}$$

after rewriting W^3 and B with Z and A, as well as $(W^1 \mp iW^2)/\sqrt{2}$ with $W^\pm$. This shows that the W_μ and Z_μ fields acquire masses of

$$m_W^2 = \frac{g^2v^2}{4} \tag{2.51a}$$

and

$$m_Z^2 = \frac{g^2+g'^2}{4}v^2\ , \tag{2.51b}$$

respectively, whereas the A_μ field (photon) remains massless. We note that the relation

$$\frac{m_W^2}{m_Z^2} = \frac{1}{1+(g'/g)^2} = \cos^2\theta_{\mathrm{W}} \tag{2.52}$$

is a consequence of ϕ being a doublet.

2.2.5 Fermion Mass

The doublet ϕ field also couples to leptons. The coupling pattern is unique and takes the form

$$\mathcal{L}_{\mathrm{Y}} = -f_e\overline{(\nu_e, e^-)_{\mathrm{L}}}\begin{pmatrix}\phi^+\\\phi^0\end{pmatrix}e_{\mathrm{R}}^- + \mathrm{h.c.} \tag{2.53}$$

This is called the Yukawa coupling.[2] The vacuum-expectation value of ϕ also breaks chiral symmetry (the ϕ field carries chirality -2), giving the electron a mass of

$$m_e = f_e\langle\phi^0\rangle = \frac{f_e v}{\sqrt{2}}\ . \tag{2.54}$$

---

[2] When we allow complex f_e, we usually write the coupling that appears in (2.53) as the complex conjugate f_e^*; see (2.74).

2.2.6 Introduction of Quarks

The introduction of quarks [181] is straightforward. We take

$$
\psi_{\mathrm{L}} = \begin{cases} \begin{pmatrix} u \\ d \end{pmatrix}_{\mathrm{L}} & \mathbf{2}, & Y = & 1/6 \\ u_{\mathrm{R}} & \mathbf{1}, & Y = & 2/3 \\ d_{\mathrm{R}} & \mathbf{1}, & Y = & -1/3 \end{cases} ,
\tag{2.55}
$$

so that (2.44) is satisfied. The Yukawa couplings read

$$
\mathcal{L}_{\mathrm{Y}} = -f_e \overline{(\nu_e, e^-)_{\mathrm{L}}} \begin{pmatrix} \phi^+ \\ \phi^0 \end{pmatrix} e_{\mathrm{R}}^-
$$
$$
- f_d \overline{(u, d)_{\mathrm{L}}} \begin{pmatrix} \phi^+ \\ \phi^0 \end{pmatrix} d_{\mathrm{R}} - f_u \overline{(u, d)_{\mathrm{L}}} \begin{pmatrix} \phi^{0*} \\ -\phi^- \end{pmatrix} u_{\mathrm{R}} + \mathrm{h.c.} , \tag{2.56}
$$

where ϕ and its conjugate

$$
\tilde{\phi} = i\tau_2 \phi^* \tag{2.57}
$$

give masses to the d and u quarks, respectively. This is the most economical choice; ϕ and $\tilde{\phi}$ may be two different Higgs doublets, as happens in some extended unified models.

2.2.7 Low-Energy Weak Interactions

The couplings of the A_μ, Z_μ, W_μ gauge fields to matter fields are given in (2.14)–(2.16). To study low-energy effective theory we write the operator

$$
\mathcal{O}_\mu = g\mathbf{T}\mathbf{W}_\mu + g'Y B_\mu \tag{2.58}
$$

in (2.14) explicitly in terms of A_μ, Z_μ, and $W_\mu^\pm = \frac{1}{\sqrt{2}}(W_\mu^1 \mp iW_\mu^2)$:

$$
\mathcal{O}_\mu = g\left[\sin\theta_{\mathrm{W}} Q A_\mu + \cos\theta_{\mathrm{W}}(T_3 - \mathrm{tg}^2\theta_{\mathrm{W}} Y)Z_\mu \right.
$$
$$
\left. + \frac{1}{\sqrt{2}}(T_1 - iT_2)W_\mu^- + \frac{1}{\sqrt{2}}(T_1 + iT_2)W_\mu^+ \right] . \tag{2.59}
$$

It is obvious that $g\sin\theta_{\mathrm{W}}$ can be identified with the electric charge e,

$$
e = g\sin\theta_{\mathrm{W}} . \tag{2.60}
$$

The Lagrangian describing the coupling to matter (2.14) is written

$$
\mathcal{L} = -\bar\psi_{\mathrm{L}} \,\not{\mathcal{O}}\psi_{\mathrm{L}} - \bar\psi_{\mathrm{R}} \,\not{\mathcal{O}}\psi_{\mathrm{R}} . \tag{2.61}
$$

The part where $W_\mu^\pm$ appear is

$$\mathcal{L}(W^\pm) = -\frac{g}{2\sqrt{2}}(J_\mu W^{+\mu} + J_\mu^\dagger W^{-\mu}) , \qquad (2.62)$$

where J_μ is the current of (2.6). Using this Lagrangian, one can calculate the effective Hamiltonian describing scattering of a lepton and a quark, e.g., $e_L^- + u_L \to \nu_L + d_L$ with the $W^\pm$ boson exchanged; it reads

$$-iH_W^{\text{eff}} = -ig^2 \frac{1}{2}(\overline{\nu_L}\gamma_\mu e_L)\frac{1}{m_W^2 - k^2}(\overline{d_L}\gamma^\mu u_L) , \qquad (2.63)$$

where k is the momentum transfer between leptons and quarks. When $|k^2| \ll m_W^2$, H_W^{eff} reduces to the four-Fermi interaction with the identification

$$\frac{G_F}{\sqrt{2}} = \frac{g^2}{8m_W^2}. \qquad (2.64)$$

The other part of (2.61) describes the electromagnetic and the weak neutral current (NC) interactions that contain A_μ and Z_μ:

$$\mathcal{L}(A, Z) = -g\bar{\psi}_L[\sin\theta_W Q A_\mu + \cos\theta_W(T_3 - \text{tg}^2\theta_W Y)Z_\mu]\psi_L$$
$$-g'\bar{\psi}_R Q[\cos\theta_W A_\mu - \sin\theta_W Z_\mu]\psi_R , \qquad (2.65)$$

$$= -eA^\mu J_\mu^{\text{em}} - \frac{g}{\cos\theta_W}\frac{1}{2}J_\mu^{NC}Z^\mu , \qquad (2.66)$$

with

$$J_\mu^{\text{em}} = Q\bar{\psi}\gamma_\mu\psi \qquad (2.67)$$

and

$$J_\mu^{NC} = 2\sum_{L,R}\bar{\psi}_{L,R}(T_3 - \sin^2\theta_W Q)\gamma_\mu\psi_{L,R} \qquad (2.68)$$

$$= 2\sum_i(g_{iL}\bar{\psi}_{Li}\gamma_\mu\psi_{Li} + g_{iR}\bar{\psi}_{Ri}\gamma_\mu\psi_{Ri}) , \qquad (2.69)$$

where $g_{iL,R}$ is given in Table 2.1 for convenience.

A procedure similar to (2.63) leads to an effective Hamiltonian which is valid at low energies; the weak interaction Hamiltonian is summarised as

$$H_W^{\text{eff}} = \frac{G_F}{\sqrt{2}}(J_\mu^\dagger J_\mu + \rho J_\mu^{NC}J_\mu^{NC}) , \qquad (2.70)$$

where the current is given in (2.6) and (2.69) and

$$\rho \equiv \frac{m_W^2}{m_Z^2\cos^2\theta_W} , \qquad (2.71)$$

which is unity due to (2.52). If there are several Higgs bosons ϕ_i with weak isospin $\mathbf{T}(\phi_i)$, ρ is given by

$$\rho = \frac{\sum_i[T(\phi_i)(T(\phi_i) + 1) - Y(\phi_i)^2]|\langle\phi_i\rangle|^2}{2\sum_i Y(\phi_i)^2|\langle\phi_i\rangle|^2} . \qquad (2.72)$$

2.2.8 Introduction of the Generations

So far we have discussed only the first generation of particles, $(\nu_e, e^-)_{\rm L}$, $e_{\rm R}^-$, $(u, d)_{\rm L}$, $u_{\rm R}$, and $d_{\rm R}$. There are, however, two additional generations in nature. It is easy to incorporate these three generations into the Weinberg–Salam theory. Let us denote the generation with superscripts $\alpha, \beta, \cdots$. The gauge coupling can be written in a form that is diagonal with respect to the generation:

$$i\bar{\psi}_{\rm L}^\alpha \not{D}\psi_{\rm L}^\alpha , \qquad i\bar{\psi}_{\rm R}^\alpha \not{D}\psi_{\rm R}^\alpha . \tag{2.73}$$

The Yukawa coupling that gives the matter field a mass is then

$$f^{\alpha\beta}\bar{\psi}_{\rm R}^\alpha\psi_{\rm L}^\beta\tilde{\phi} , \tag{2.74}$$

and the mass term is generally given by the matrix $M^{\alpha\beta}\bar{\psi}_{\rm R}^\alpha\psi_{\rm L}^\beta$ with nonvanishing off-diagonal elements ($M^{\alpha\beta} = f^{\alpha\beta}\langle\phi\rangle$). Allowing for complex Yukawa couplings, f defined here corresponds to the complex conjugate of that defined in (2.53) and (2.56). We note that there are three matrices corresponding to f_e, f_d, and f_u, as in (2.56).

The matrix M can be diagonalised by a biunitary transformation,

$$V^{-1}MW = \widetilde{M}, \tag{2.75}$$

where $\widetilde{M}$ stands for a diagonal matrix. This can be easily shown by applying the polar decomposition theorem, which states that one can write M as

$$M = HU \tag{2.76}$$

where H is a hermitian matrix and U a unitary matrix. Since H can be diagonalised by the unitary matrix V as

$$V^{-1}HV = \widetilde{M} , \tag{2.77}$$

we obtain (2.75) upon writing $U^{-1}V = W^{-1}$.

Table 2.1. Neutral-current couplings

	g_{iL}		g_{iR}
$e_{\rm L}$	$-\frac{1}{2} + \sin^2\theta_{\rm W}$	$e_{\rm R}$	$\sin^2\theta_{\rm W}$
$\nu_{\rm L}$	$+\frac{1}{2}$		
$u_{\rm L}$	$+\frac{1}{2} - \frac{2}{3}\sin^2\theta_{\rm W}$	$u_{\rm R}$	$-\frac{2}{3}\sin^2\theta_{\rm W}$
$d_{\rm L}$	$-\frac{1}{2} + \frac{1}{3}\sin^2\theta_{\rm W}$	$d_{\rm R}$	$\frac{1}{3}\sin^2\theta_{\rm W}$

The eigenstate of gauge coupling, i.e., the eigenstate of the weak interaction (we denote it with a prime) is given by the mass eigenstate as

$$\psi'_{\rm L} = W\psi_{\rm L} , \qquad \psi'_{\rm R} = V\psi_{\rm R} . \tag{2.78}$$

The weak current is then written with the mass eigenstates of the charge $2/3$ quark fields and the charge $-1/3$ quark fields as

$$
\begin{aligned}
J_\mu &\equiv \bar\psi'_{\rm L}(Q = 2/3)\gamma_\mu\psi'_{\rm L}(Q = -1/3)\\
&= \bar\psi_{\rm L}(Q = 2/3)U_q\gamma_\mu\psi_{\rm L}(Q = -1/3),
\end{aligned} \tag{2.79}
$$

where

$$U_q = W^\dagger(Q = 2/3) \; W(Q = -1/3) . \tag{2.80}$$

This matrix U_q is usually called the Cabibbo (when 2×2)[3] or the Kobayashi–Maskawa [132] matrix (when 3×3). In this book, we refer to it as the *quark mixing matrix*.

In this manipulation four transformation matrices $[V(Q = 2/3), V(Q = -1/3), W(Q = 2/3), W(Q = -1/3)]$ appear. We emphasise that only U_q is physical in the standard Weinberg–Salam theory. In order to demonstrate this, we note that the original Lagrangian (the kinetic and gauge parts) is invariant under three rotations with respect to the generation index:

$$\psi_{\rm L}^\alpha \to S_\psi^{\alpha\beta}\psi_{\rm L}^\beta \qquad \left[\psi_{\rm L} \equiv \binom{u}{d}_{\rm L}\right] , \tag{2.81}$$

$$d_{\rm R}^\alpha \to S_d^{\alpha\beta}d_{\rm R}^\beta , \tag{2.82}$$

$$u_{\rm R}^\alpha \to S_u^{\alpha\beta}u_{\rm R}^\beta . \tag{2.83}$$

We can therefore diagonalise the Yukawa term $f_d^{\alpha\beta}\bar\psi_{\rm R}^\alpha\phi d_{\rm L}^\beta$ using (2.81) and (2.82); this means that we can take $W(Q = -1/3) = V(Q = -1/3) = 1$ without any loss of generality. The freedom of rotation, (2.82) and (2.83), can further be used to choose V in (2.78) to be unity. This makes only $U_q = W^\dagger(Q = 2/3)$ physical. If there exist some new interactions that break invariance under (2.81)–(2.83), however, the relevant transformation matrices acquire physical meaning.

A feature to be noted is that a flavour-changing neutral current such as $\bar s d$ does not emerge because the transformation is orthogonal; the neutral current is always $\bar d d$ and $\bar s s$, etc.

---

[3] Gell-Mann and Lévy (1958) [67] introduced this mixing angle to keep universality of the weak interaction and showed that it describes K decays. Cabibbo (1963) [126] then carried out a more extensive analysis, showing that this mixing describes well the weak interaction phenomenology of K mesons and hyperons. The mixing matrix in an orthogonal matrix form (the GIM form) was first introduced by Katayama et al. (1962) [121] and Maki, Nakagawa, and Sakata (1962) [122], and later by GIM.

An $n \times n$ unitary matrix U_q generally has $n(n+1)/2$ phases. In (2.79), however, n phase degrees of freedom can be absorbed into the phase of $\bar{\psi}_{\mathrm{L}}(Q = 2/3)$, and additional $n-1$ phases into $\psi_{\mathrm{L}}(Q = 1/3)$. We are therefore left with $(n-1)(n-2)/2$ physical phases in the matrix. For $n = 3$, we have only one physical phase, which is supposed to give rise to CP violation [132].

The situation with the lepton sector is different. If all of the neutrino mass vanishes (or precisely degenerates), the unitary transformation for the neutrino $W(\nu)$ has no physical meaning. One can therefore always choose $W(\nu)$ so that it cancels $W(l)$, i.e., $U_l = W^\dagger(\nu)W(l) = 1$. Lepton mixing becomes physically meaningful when neutrinos have finite (and nondegenerate) masses. For massive neutrinos, the convention frequently adopted in recent literature is

$$U_\ell = W(\ell)^\dagger W(\nu) \,, \qquad (2.84)$$

rather than its conjugate. Extra phases may appear if the neutrinos are of the Majorana type (see Sect. 8.3).

2.3 Quantum Field Theory: The Renormalisable Gauge

The full Lagrangian for the Weinberg–Salam theory is obtained by collecting (2.30), (2.14), (2.43), (2.35), and (2.56). The Feynman rule is derived by quantising the fields in the Lagrangian. The propagators are obtained by inverting the parts that are quadratic in the fields. Namely, if the Fourier representation of the Lagrangian is written as $\phi(k)K(k)\phi(k)$, the propagator is given by $i\Delta(k) = -iK(k)^{-1}$. The vertices are obtained from any parts higher than quadratic in the field by removing fields and putting i: for $A_{ijk}\phi_i\phi_j\phi_k$, it is iA_{ijk}. There is, however, a complication in the gauge theory. The gauge must be fixed to allow the inversion of K. In the preceding section, we worked with the unitary gauge to clarify the physical structure of the theory. In this gauge, the gauge field propagator takes the form

$$\Delta_{\mu\nu}(k) = \frac{-g_{\mu\nu} + k_\mu k_\nu/m^2}{k^2 - m^2} \,, \qquad (2.85)$$

as obtained by inverting the quadratic part of the Lagrangian, the sum of (2.30) and (2.43). The problem is that this propagator behaves as $O(1)$ rather than $O(k^{-2})$ for large k. Hence the canonical power-counting rule does not apply and renormalisability becomes obscure. Hence, it is inconvenient to use this gauge for calculations of Feynman diagrams beyond the tree level.

Let us briefly discuss propagators in the renormalisable ξ gauge [267], a non-Abelian generalisation of the gauge introduced by Lee and Yang [268]. In this gauge the gauge field propagator has the asymptotic behaviour of $O(k^{-2})$ and the use of the power-counting rule is justified.

We write the Lagrangian of the scalar field,

$$\mathcal{L}_{\text{scalar}} = (D_\mu \phi)^\dagger (D^\mu \phi) - V(\phi) , \qquad (2.86)$$

where

$$\phi = \begin{pmatrix} \phi^+ \\ \frac{v}{\sqrt{2}} + \phi^0 \end{pmatrix} . \qquad (2.87)$$

To obtain the propagator of the gauge fields, we introduce the gauge fixing term

$$\mathcal{L}_{\text{gf}} = \frac{1}{2\xi} [f(A_\mu, \phi, v)]^2 \qquad (2.88)$$

such that the cross terms of the gauge fields (W_μ, B_μ) and $\partial \phi^i$ arising in $(D_\mu \phi)^\dagger (D^\mu \phi)$ are cancelled. The cross terms in (2.86) are

$$-i\frac{g}{2}\partial_\mu W^{\mu+}\phi^{+\dagger}v - i\frac{(g^2 + g'^2)^{1/2}}{2\sqrt{2}}\partial_\mu Z^\mu \phi^{0\dagger}v + \text{h.c.} \qquad (2.89)$$

Hence, we take

$$\mathcal{L}_{\text{gf}} = -\frac{1}{2\xi} \left[\left| \partial_\mu W^{\mu+} + i\xi \phi^+ \frac{g}{2} v \right|^2 + \left| \partial_\mu Z^\mu + i\xi \phi^0 \frac{(g^2 + g'^2)^{1/2}}{2\sqrt{2}} v \right|^2 \right] . \qquad (2.90)$$

The part quadratic in Z is thus

$$\mathcal{L}_{Z^2} = -\frac{1}{4}(\partial_\mu Z_\nu - \partial_\nu Z_\mu)(\partial^\mu Z^\nu - \partial^\nu Z^\mu) + \frac{1}{2}M_Z^2 Z_\mu Z^\mu - \frac{1}{2\xi}(\partial^\mu Z^\mu)^2 , \qquad (2.91)$$

or

$$Z_\mu K^{\mu\nu}(k) Z_\nu = \frac{1}{2} Z_\mu \left[g^{\mu\nu}(k^2 - m_Z^2) - \frac{\xi - 1}{\xi} k^\mu k^\nu \right] Z_\nu \qquad (2.92)$$

in the Fourier representation. The propagator is the inverse of $K^{\mu\nu}$ and then,

$$i\Delta_{\mu\nu}(k) = -i[K^{\mu\nu}(k)]^{-1} = i\frac{1}{k^2 - m_Z^2 + i\epsilon}\left[-g_{\mu\nu} - \frac{(\xi - 1)k_\mu k_\nu}{k^2 - \xi m_Z^2} \right] . \qquad (2.93)$$

We obtain the propagator for W in the same way with m_Z replaced by m_W. Here $\xi = 1$ is the Feynman gauge, $\xi = 0$ is the Landau gauge, and $\xi = \infty$ is the unitary gauge. Unless $\xi = \infty$, all propagators damp as $O(k^{-2})$, and the power-counting rule applies properly.

In deriving the full Feynman rule for the gauge part, we must reduce the functional space of the path integral by deleting the gauge degree of freedom with $\Pi\delta^{(m)}(\theta - f(w))$, where w is the physical part of W and Z and the dimension of θ is m. In (2.90) the gauge function $F = \partial_\mu W^{\mu+} + i\xi\phi^+\frac{g}{2}v$ is an implicit function of the gauge parameter θ; therefore, the δ function should be replaced by

$$\det \left\| \frac{\partial F}{\partial \theta} \right\| \Pi\delta^{(m)}\left(F^\alpha(W, Z) \right) , \qquad (2.94)$$

and this determinant in turn is represented by a functional integral over Grassmann fields with the action $\bar{\omega}[\frac{\partial F}{\partial \theta}]\omega$, as if they were fermion fields [178,179]. Here $\bar{\omega}$ and ω are called the Faddeev–Popov–De Witt ghost. By introducing the Faddeev–Popov–De Witt ghost, unitarity holds in the Feynman amplitudes.

The derivation of the Feynman rule is now straightforward, but we do not write it here, since we do not use it explicitly in this book; the radiative corrections we are going to present explicitly are all calculated with the unitary gauge, with which physical content is more transparent. The renormalisable ζ gauge is convenient when one deals with loops including gauge-boson self-couplings.

2.4 Consistency of the Quantum Field Theory: Anomaly Cancellation

2.4.1 Renormalisability

Two critical elements of the consistency of the quantum field theory are unitarity and renormalisability of the S matrix. As we have seen in the previous section, the introduction of the ghost field is the crucial step for unitarity. Field theory is renormalisable if infinities of the Feynman amplitudes are cancelled by adding counter terms, whose form agrees exactly with that contained in the original Lagrangian, respecting the underlying symmetry. This requirement is satisfied if the canonical power-counting rule holds and if the symmetry structure (the most important is gauge symmetry) is respected in the perturbation series. The latter is guaranteed by the conservation of currents, which is usually expressed in terms of the Ward identity. In such a case, infinity is absorbed into the coupling constant and the normalisation of the fields. For instance, in quantum electrodynamics (QED) electromagnetic current conservation is strictly respected in any orders of the perturbation series and guarantees that the divergence in the vertex $\bar{\psi}\,\slashed{A}\psi$ and that in the kinetic term $\bar{\psi}\,\slashed{\partial}\psi$ are equal, so that the form $\bar{\psi}(i\,\slashed{\partial} - e\,\slashed{A}\psi)$ is always respected in the divergent Feynman amplitude, provided that the divergence of e is removed separately. This amounts to a simple rescaling of the field definition in the original Lagrangian to remove the divergence.

The logic and calculation are substantially more complicated in non-Abelian gauge theory such as quantum chromodynamics, but it can be shown that the currents corresponding to gauge symmetry are all conserved by using dimensional regularisation, and renormalisability is shown in the same way [269, 270]. Unitarity is unbroken by virtue of current conservation. As with the Weinberg–Salam theory, further complication arises from the spontaneous breakdown of gauge symmetry and from the presence of both vector and axial-vector currents. Current conservation, however, is not spoiled by

the spontaneous breakdown of symmetry, and the former problem is solved by noting that the divergence cannot be simply absorbed by a simple field rescaling but we have for the Higgs potential

$$\lambda[Z(|\phi|^2 - v^2) - \Delta v^2]^2 \ , \qquad (2.95)$$

where Z and Δv^2 are both divergent. The change of v^2 is absorbed into rescaling of the mass of the Higgs field and hence does not cause any problems after all [271]. Unitarity also remains unbroken.

2.4.2 Triangle Anomaly

The presence of the vector and axial-vector currents, however, causes a subtle problem. For the renormalisability of the theory, both currents must be conserved, but this is not possible due to the presence of a phenomenon called the triangle anomaly [272, 273]. Fermion triangle diagrams are divergent, and a regulator is necessary to calculate them. There are no regulators, however, that respect chiral symmetry. It is possible to find a regulator that respects the vector current conservation, but such a regulator breaks axial-vector current conservation, and vice versa. Namely, current conservation is generally broken due to quantum fluctuations when the gauge fields couple with fermion fields. This does not cause a problem with QED, where only vector current conservation is associated with gauge symmetry, but it spoils the renormalisability of the electroweak theory.

The only way to maintain the renormalisability of the electroweak theory is to require that the fermion contributions to the triangle diagram are cancelled as a whole. This leads to a constraint on the quantum number of fermion fields such that for generators of the gauge group T_a,

$$\frac{1}{2} \sum_i \mathrm{Tr}[\{T_a(i), T_b(i)\} T_c(i)] = 0 \ , \qquad (2.96)$$

where i are fermions that couple to the gauge fields and the curly bracket means the anticommutator. We explain the anomaly problem and derive this condition in what follows, but readers who are not interested in the details of the calculations may skip the derivation up to (2.118).

Let us consider the three-point function defined by

$$\Gamma_{abc}^{\mu\nu\lambda} = \langle 0|T\{j_a^\mu j_b^\nu j_c^\lambda\}|0\rangle \ , \qquad (2.97)$$

where the fermion current is

$$j_a^\mu = \bar{\psi}_{\mathrm{L}} \gamma^\mu T_a \psi_{\mathrm{L}} \ , \qquad (2.98)$$

which couples to a gauge field A_μ^a as

$$\mathcal{L} = -gA_\mu^a \bar{\psi}_{\mathrm{L}} \gamma^\mu T_a \psi_{\mathrm{L}} \,. \tag{2.99}$$

In gauge theory this current is conserved: $\partial_\mu j_a^\mu = 0$. In what follows, we show that this conservation law is broken at the one-loop order. Let us now take a partial derivative of $\Gamma_{abc}^{\mu\nu\lambda}$,

$$
\begin{aligned}
\partial_\mu \Gamma_{abc}^{\mu\nu\lambda} &= \langle 0|T\{\partial_\mu j_a^\mu(x) j_b^\nu(y) j_c^\lambda(z)\}|0\rangle \\
&\quad +\delta(x^0 - y^0)\langle 0|T\{[j_a^0(x), j_b^\nu(y)] j_c^\lambda(z)\}|0\rangle \\
&\quad +\delta(x^0 - z^0)\langle 0|T\{j_b^\nu(y)[j_a^0(x), j_c^\lambda(z)]\}|0\rangle. \tag{2.100}
\end{aligned}
$$

With current conservation and algebra of currents,

$$[j_a^0(x), j_b^\nu(y)]_{x_0=y_0} = ic_{abc}j_c^\nu(y)\delta^3(x-y) \tag{2.101}$$

where c_{abc} is the structure constant that appears in

$$[T_a, T_b] = ic_{abc}T_c \,. \tag{2.102}$$

Then,

$$
\begin{aligned}
\partial_\mu \Gamma_{abc}^{\mu\nu\lambda}(x,y,z) &= ic_{abd}\delta^4(x-y)\langle 0|T\{j_d^\nu(y) j_c^\lambda(z)\}|0\rangle \\
&\quad +ic_{acd}\delta^4(x-z)\langle 0|T\{j_b^\nu(y) j_d^\lambda(z)\}|0\rangle. \tag{2.103}
\end{aligned}
$$

This is the Ward identity corresponding to conservation of currents.

We now examine the three-point function in one-loop perturbation theory. We compute the diagram depicted in Fig. 2.1 as

$$
\begin{aligned}
\Gamma_{abc}^{\mu\nu\lambda} &= \frac{-1}{(2\pi)^{12}} \int d^4k_1 d^4k_2 e^{-i(k_1+k_2)x} e^{+ik_1 y} e^{+ik_2 z} \\
&\quad \times \int d^4p \Bigg[\mathrm{Tr}(T_b T_c T_a)\mathrm{Tr}\left(\frac{i}{\not p}\gamma^\lambda \frac{i}{\not p + \not k_2}\gamma^\mu \frac{i}{\not p - \not k_1}\gamma^\nu \frac{1-\gamma_5}{2}\right) \\
&\quad +\mathrm{Tr}(T_c T_b T_a)\mathrm{Tr}\left(\frac{i}{\not p}\gamma^\nu \frac{i}{\not p + \not k_1}\gamma^\mu \frac{i}{\not p - \not k_2}\gamma^\lambda \frac{1-\gamma_5}{2}\right) \Bigg] \,. \tag{2.104}
\end{aligned}
$$
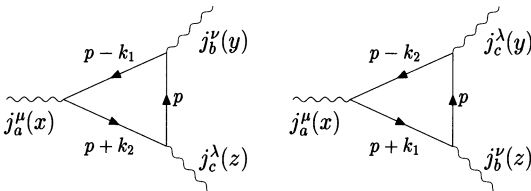
Fig. 2.1. Triangle diagrams that give anomaly.

We ignore here fermion masses that are unimportant for our argument. The derivative is

$$\partial_\mu \Gamma_{abc}^{\mu\nu\lambda} = \frac{i}{(2\pi)^{12}} \int d^4k_1 d^4k_2 e^{-i(k_1+k_2)x} e^{+ik_1 y} e^{+ik_2 z}$$

$$\times \int d^4p \left(\mathrm{Tr}(T_b T_c T_a) \mathrm{Tr}\left[\frac{1}{\not{p} - \not{k}_1} \gamma^\nu \frac{1}{\not{p}} \gamma^\lambda \frac{1}{\not{p} + \not{k}_2} (-i)(\not{k}_1 + \not{k}_2) \frac{1 - \gamma_5}{2} \right] \right.$$

$$\left. + \mathrm{Tr}(T_c T_b T_a) \mathrm{Tr}\left[\frac{1}{\not{p} - \not{k}_2} \gamma^\lambda \frac{1}{\not{p}} \gamma^\nu \frac{1}{\not{p} + \not{k}_1} (-i)(\not{k}_1 + \not{k}_2) \frac{1 - \gamma_5}{2} \right] \right).$$

$$(2.105)$$

Using

$$k_1 + k_2 = (p + k_2) - (p - k_1) \tag{2.106}$$

to cancel one of the denominator factors, we obtain

$$\partial_\mu \Gamma_{abc}^{\mu\nu\lambda} = \frac{1}{(2\pi)^{12}} \int d^4k_1 d^4k_2 e^{-i(k_1+k_2)x} e^{+ik_1 y} e^{+ik_2 z}$$

$$\times \int d^4p \left\{ \mathrm{Tr}(T_b T_c T_a) \left[\mathrm{Tr}\left(\frac{1}{\not{p} - \not{k}_1} \gamma^\nu \frac{1}{\not{p}} \gamma^\lambda \frac{1 - \gamma_5}{2} \right) \right. \right.$$

$$\left. - \mathrm{Tr}\left(\frac{1}{\not{p}} \gamma^\lambda \frac{1}{\not{p} + \not{k}_2} \gamma^\nu \frac{1 - \gamma_5}{2} \right) \right]$$

$$+ \mathrm{Tr}(T_c T_b T_a) \left[\mathrm{Tr}\left(\frac{1}{\not{p} - \not{k}_2} \gamma^\lambda \frac{1}{\not{p}} \gamma^\nu \frac{1 - \gamma_5}{2} \right) \right.$$

$$\left. \left. - \mathrm{Tr}\left(\frac{1}{\not{p}} \gamma^\nu \frac{1}{\not{p} + \not{k}_1} \gamma^\lambda \frac{1 - \gamma_5}{2} \right) \right] \right\}. \tag{2.107}$$

We decompose the trace of the product of Ts into symmetric and antisymmetric parts:

$$\mathrm{Tr}[T_b T_c T_a] = \frac{1}{2} \mathrm{Tr}[\{T_b, T_c\} T_a] + \frac{1}{2} \mathrm{Tr}[[T_b, T_c] T_a]$$

$$= d_{bca} + \frac{i}{4} c_{bca} . \tag{2.108}$$

The terms proportional to antisymmetric c_{abc} from the first and fourth terms of (2.107) are

$$\frac{i}{2} c_{abc} \frac{1}{(2\pi)^8} \delta^4(x - z) \int d^4k e^{-ik(x-y)} \int d^4p \mathrm{Tr}\left(\frac{1}{\not{p} - \not{k}} \gamma^\nu \frac{1}{\not{p}} \gamma^\lambda \frac{1 - \gamma_5}{2} \right),$$

$$(2.109)$$
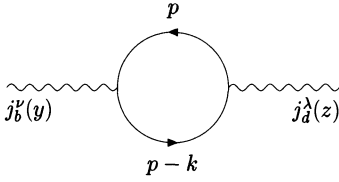
Fig. 2.2. One-loop diagram for the two-point function.

which is just the one-loop expression of the two-point function (Fig. 2.2)

$$\frac{i}{2}c_{abd}\delta^4(x-z)\langle 0|T[j_b^\nu(y)j_d^\lambda(z)]|0\rangle. \qquad (2.110)$$

Adding the similar contribution from the second and third terms, we find the Ward identity (2.103) for the antisymmetric component.

Now, we examine whether the component proportional to symmetric d_{abc} vanishes. We first consider the part that does not include γ_5. If we shift the integral variable p to $p+k_1$, the fourth term cancels against the first term. We see a similar cancellation between the second and third terms. It is a straightforward task to find the cancellation between the first and the fourth terms and also between the second and third terms by noting an antisymmetric tensor arising from $\text{Tr}\gamma^\mu\gamma^\nu\gamma^\lambda\gamma^\rho\gamma_5$.

This argument, however, is not correct because the integral is linearly divergent and it is not invariant under the shift of the integration variable as we did. Also, $\partial_\nu\Gamma_{abc}^{\mu\nu\lambda}$ and $\partial_\lambda\Gamma_{abc}^{\mu\nu\lambda}$ do not vanish. Let us consider the function $f(x)$, which behaves as $f \rightarrow$ constant, as $x \rightarrow \pm\infty$. It follows that

$$\Delta = \int_{-\infty}^{\infty} dx[f(x) - f(x+a)]$$

$$= \int_{-\infty}^{\infty} dx[a\ f'(x) + \frac{a^2}{2}f''(x) + ...]$$

$$= a[f(\infty) - f(-\infty)]\ , \qquad (2.111)$$

which is nonvanishing. Therefore care is necessary in calculating the integral. In view of this uncertainty, we shift the integration variable $p \rightarrow p+a$ in the first two terms (those proportional to $\text{Tr}[T_bT_cT_a]$), and $p \rightarrow p+b$ in the last two terms (those proportional to $\text{Tr}[T_cT_bT_a]$) in (2.107) [266]. We see that the sum of the first and the fourth and that of the second and the third cancel pairwise with the choice of $a = -b$, and vector current conservation is respected. For other choices of a and b, the integral does not vanish, and vector current conservation is violated.

Let us see what happens to the axial-vector part. For the sum of the first and the fourth terms of (2.107), the p integration is

$$\int d^4p \left\{ \mathrm{Tr} \left[\frac{1}{\not{p} - \not{k}_1 + \not{a}} \gamma^\nu \frac{1}{\not{p} + \not{a}} \gamma^\lambda (-\gamma_5/2) \right] \right.$$

$$\left. - \mathrm{Tr} \left[\frac{1}{\not{p} + \not{b}} \gamma^\nu \frac{1}{\not{p} + \not{k}_1 + \not{b}} \gamma^\lambda (-\gamma_5/2) \right] \right\}$$

$$= -\frac{1}{2} \int d^4p \, \mathrm{Tr}(\gamma^\mu \gamma^\nu \gamma^\rho \gamma^\lambda \gamma_5) \tag{2.112}$$

$$\times \left[\frac{(p + b + \delta)_\mu}{(p + b + \delta)^2} \frac{(p + b + k_1 + \delta)_\rho}{(p + b + k_1 + \delta)^2} - \frac{(p + b)_\mu}{(p + b)^2} \frac{(p + b + k_1)_\rho}{(p + b + k_1)^2} \right] ,$$

where $\delta = a - b - k_1$. A four-dimensional analogue to (2.111) is

$$\int d^4p [f(p + \delta) - f(p)] = \delta^\mu \int d^4p \frac{\partial f}{\partial p^\mu} + O(\delta^2)$$

$$= 2i\pi^2 \delta^\mu \lim_{R \to \infty} R_\mu R^2 f(R) . \tag{2.113}$$

After some algebra, (2.112) reads

$$-2\frac{\pi^2}{3} \epsilon^{\mu\nu\lambda\sigma} [(a - b)_\mu (k_1)_\lambda - (a - b)_\lambda (k_1)_\mu] . \tag{2.114}$$

With our choice of $a = -b$, the symmetric part, which is proportional to d_{abc} of $\partial\Gamma$, is

$$\partial_\mu \Gamma_{abc}^{\mu\nu\lambda}|_{\mathrm{sym}}$$

$$= -\frac{2\pi^2}{(2\pi)^{12}} d_{abc} \epsilon^{\mu\nu\lambda\sigma} \int d^4k_1 d^4k_2 e^{-i(k_1+k_2)x} e^{+ik_1y} e^{+ik_2z} a_\mu (k_1 + k_2)_\lambda .$$

$$\tag{2.115}$$

One may think that this vanishes if we take $a = 0$. We note, however, that

$$\partial_\nu \Gamma_{abc}^{\mu\nu\lambda}|_{\mathrm{sym}} \propto \epsilon^{\mu\nu\lambda\sigma} (k_2 + a)_\mu k_{1\lambda} , \tag{2.116}$$

$$\partial_\lambda \Gamma_{abc}^{\mu\nu\lambda}|_{\mathrm{sym}} \propto \epsilon^{\mu\nu\lambda\sigma} (-k_1 + a)_\mu k_{2\lambda} . \tag{2.117}$$

The choice $a = k_1 + k_2$ makes (2.115) and (2.117) vanishing, but leaves (2.116) nonvanishing. It is obvious that one cannot make anomaly equations for all three derivatives vanishing at the same time. The same holds true even if we relax the condition $a = -b$, which would make the ∂VVV vertex nonvanishing. This means that the conservation of the chiral current is broken by quantum fluctuations (anomaly). Nonconservation of the current makes the theory nonrenormalisable. To make the theory renormalisable, we must require that

$$\sum_i d_{abc}(i) = \frac{1}{2} \sum_i \mathrm{Tr}[\{T_a(i), T_b(i)\} T_c(i)] = 0 , \tag{2.118}$$

where i refers to fermions in the internal loop. This is the anomaly-free conditionimposed on gauge theory and plays a very important role in model building, as we explore later in this book.

We should make a remark about the relation between the logic we followed here [266] and that of the more conventional approach [272]. In the latter, one takes the vector current as always conserved: the derivative of the VVV vertex and that of the vector current in the VVA vertex vanishes. In fact this is possible, while $VV\partial A$ is anomalous.[4] We may follow this argument in our formalism: the condition that the antisymmetric part of the three-point function, including the derivative of the vector current, vanishes fixes a and b uniquely, leaving anomaly only for the divergence of the axial current. In chiral gauge theory, however, one cannot separate the vector and axial parts from the chiral currents.

2.4.3 Implications of Anomaly

With the assignment of $SU(2)_L$ and $U(1)_Y$ charges (2.7), (2.12), and (2.55), we can see that $SU(2)_L^2 \cdot U(1)_Y$ and $U(1)_Y^3$ anomalies are cancelled in the following way. For $SU(2)_L^2 \cdot U(1)_Y$, noting that only $a = b$ gives a finite trace for the $SU(2)_L$ part, the condition is

$$\sum_i Y_i = 3 \times \left(\frac{1}{6}\right) - \frac{1}{2} = 0 , \qquad (2.119)$$

where the two terms are $SU(2)$ doublets $(u, d)_L$ and $(\nu_e, e^-)_L$, and for $U(1)_Y^3$,

$$\sum_i Y_i^3 = 6 \times \left(\frac{1}{6}\right)^3 + 3 \times \left(-\frac{2}{3}\right)^3 + 3 \times \left(\frac{1}{3}\right)^3 + 2 \times \left(-\frac{1}{2}\right)^3 + (+1)^3 = 0 ,$$

$$(2.120)$$

where the summation is taken over all particles. The trace obviously cancels for $SU(2)_L^3$.

This means that anomaly cancels for the known fermion content, generation by generation, so that the theory is renormalisable [182]. This imposes a tight condition between leptons and quarks. The mass of the fermion does not enter the anomaly equation. Namely, heavy fermions, if any, would contribute to anomaly in the same way.

We note that anomaly is not cancelled if the triangle diagram involves other types of currents, such as baryonic and leptonic currents defined by

$$j_B^\mu = \frac{1}{3} \sum (\bar{q}_L \gamma^\mu q_L + \bar{u}_R \gamma^\mu u_R + \bar{d}_R \gamma^\mu d_R) \qquad (2.121)$$

---

[4] In QED it is sufficient if the conservation of the vector current is sustained, and this is realised by Pauli–Villars regularisation. So, if the axial-vector current is introduced as an external current, its conservation is broken by anomaly. This leads to a physical effect such as $\pi^0 \to 2\gamma$.
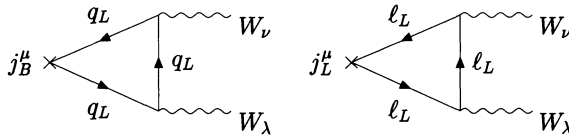
Fig. 2.3. Triangle diagrams for baryon and lepton currents

and

$$j_{\rm L}^\mu = \sum (\bar{\ell}_{\rm L} \gamma^\mu \ell_{\rm L} + \bar{e}_{\rm R} \gamma^\mu e_{\rm R}) , \qquad (2.122)$$

where the summations are made over families and colour (for the quarks). The diagram is given in Fig. 2.3. From the derivation given above, we can set a regulator so that derivatives of the two currents (those associated with gauge symmetry) vanish. This leaves the divergence of $j_{\rm L}^\mu$ or j_B^μ nonvanishing. This anomaly, however, is harmless to the theory. It means that neither baryon nor lepton number U(1) can be gauged, and the conservation of these U(1) may not be exact. This leads to an important physical implication, which will be discussed in Chap. 11. We remark that the combination $B - L$ is not anomaly-free, but it becomes anomaly-free if the right-handed neutrino exists (see Sect. 9.3.3).

2.5 Experimental Test

2.5.1 Electroweak Parameters

The Weinberg–Salam theory contains three fundamental parameters: g, g', and v. We represent these parameters in terms of $\alpha = e^2/4\pi$, $G_{\rm F}$, and $\sin^2 \theta_{\rm W}$. Here, α is the electromagnetic coupling defined on the mass shell (the Thomson scattering limit) and traditionally referred to as the fine-structure constant. The most accurate determination of α comes from the anomalous magnetic moment of electrons (eighth order perturbations; error 3.8 ppb). The α from quantum Hall effect and the ac Josephson effect reach an accuracy that can be compared (20 ppb and 14 ppb, respectively) [274]. The value from muonium ground-state hyperfine splitting has recently been improved and can also be compared with others (57 ppb). We take a value from the 1998 compilation of CODATA [274], which is also quoted by the Particle Data Group (PDG; RPP2000) [275]:[5]

$$\alpha^{-1} = 137.03599976(50) . \qquad (2.123)$$

---

[5] The most accurate values from the three methods are 137.03599958(52) from the electron anomalous magnetic moment, 137.0360030(27) from quantum Hall, and 137.0360084(33) from ac Josephson. The values from quantum Hall and ac Josephson differ from that from electron anomalous magnetic moment by 1 and 2 σ, respectively.

The Fermi coupling constant is defined by the muon decay constant, using

$$\Gamma(\mu \to e\nu\bar{\nu}) = \frac{G_\mu^2 m_\mu^5}{192\pi^3} f(m_e^2/m_\mu^2) \left[1 + \frac{\alpha}{2\pi}\left(\frac{25}{4} - \pi^2\right)\right]\left(1 + \frac{3}{5}\frac{m_\mu^2}{m_W^2}\right),$$
(2.124)

where

$$f(x) = 1 - 8x + 8x^3 - x^4 - 12x^2 \ln x \qquad (2.125)$$

is the electron mass correction to the phase-space volume factor. The definition of $G_F(= G_\mu)$ takes into account radiative corrections only for QED. The effect of the W boson propagator [276] is retained [277].

From $\tau_\mu = \Gamma_\mu^{-1} = 2.19703(4)$ μs and using $\alpha = \alpha(m_\mu) \simeq 1/136$,

$$G_F \equiv G_\mu = 1.16639(1) \times 10^{-5} \text{GeV}^{-2}. \qquad (2.126)$$

(In this book we adopt data from [275], unless otherwise explicitly quoted.) The weak mixing angle $\sin^2\theta_W$ is determined from a variety of neutral-current effects and the physics of the W and Z bosons.

The test of the Weinberg–Salam model is reduced to testing whether $\sin^2\theta_W$ is determined consistently from different effects. A prime determination of $\sin^2\theta_W$ comes from the gauge-boson masses. From (2.60) and (2.64),

$$m_W = \frac{(\pi\alpha/\sqrt{2}G_F)^{1/2}}{\sin\theta_W} \qquad (2.127)$$

and from (2.52),

$$m_Z = m_W/\cos\theta_W , \qquad (2.128)$$

or

$$\sin^2\theta_W = 1 - \frac{m_W^2}{m_Z^2} . \qquad (2.129)$$

The most precisely determined quantity is the Z mass. The average of experiments at the LEP (Large Electron Positron Collider) at CERN [278] yields $m_Z = 91.1882 \pm 0.0022$ GeV [275]. The error is only 24 ppm. If we use

$$\sin^2\theta_W = \frac{1}{2}\left[1 - \sqrt{1 - 4(A/m_Z)^2}\right] \qquad (2.130)$$

$[A = (\pi\alpha/\sqrt{2}G_F)^{1/2} = 37.2802$ GeV] obtained from (2.127) and (2.128), this m_Z gives $\sin^2\theta_W = 0.2121 \pm 0.0000$. The mass of W is less precise, but there are no significant discrepancies between the tevatron experiments (CDF and D0) [279] and the LEP experiments [280]. The average is $m_W = 80.419 \pm 0.056$ GeV [275]. Using (2.127), we obtain 0.2149 ± 0.0003. Alternatively, if we use (2.128), we get 0.2222 ± 0.0003. The values we derived differ by as much as 0.01. This is due to a neglect of radiative corrections. The

mixing angle we obtained here may also be compared with a value from low-energy neutral-current processes: for example, $R(\nu) = \sigma(\nu_\mu + N \to \nu_\mu + X)/\sigma(\nu_\mu + N \to \mu + X) = 0.3072 \pm 0.0032$ from the CDHS [281] yields $\sin^2\theta_W = 0.236 \pm 0.007$ ignoring radiative corrections (see Sect. 3.14). Other νN data (CHARM [282] and CCFR [283]) give consistent angles. We see later that the differences in $\sin^2\theta_W$ are removed if radiative corrections are taken into account.

2.5.2 Higher Order Perturbations

A full discussion of the radiative correction is much too involved to be presented here. The most important effects, however, are understood from the simple calculations we sketch in this section. Because the definitions of parameters $e, g, g', m_W, m_Z, v, \theta_W$ are renormalisation-scheme-dependent, we must first fix the scheme to give unambiguous meaning to the coupling constants. For α it is customary to take the value defined by Thomson scattering, and for G_F that by muon decay. The following two schemes are conceptually simple and are often used to define $\sin^2\theta_W$.

(i) $\overline{\text{MS}}$ (modified minimal subtraction) scheme [284]. The renormalised couplings g_r, g_r' are defined by subtracting $2/(4 - n) + \log 4\pi - \gamma_E$ from divergent g and g' (Euler constant $\gamma_E = 0.5772$), and the electroweak mixing angle is defined by

$$\sin^2\hat{\theta}_W(\mu) = \frac{g_r'^{\,2}(\mu)}{g_r^2(\mu) + g_r'^{\,2}(\mu)}. \tag{2.131}$$

This definition of $\sin^2\theta_W$ depends on the renormalisation point μ, where the couplings g and g' are defined; μ is usually chosen to be m_Z.[6]

(ii) On-shell scheme [286–288]. The weak mixing angle is defined by

$$\sin^2\theta_W = 1 - \frac{m_W^2}{m_Z^2}, \tag{2.132}$$

where the gauge-boson masses are their on-shell (physical) values.

Let us first discuss the radiative correction with scheme (i). The most important correction to (2.127) is QED correction to α. This correction is significant since α in this expression is defined at $\mu = m_Z$, far from $\mu = m_e$. Noting that the renormalised coupling constant $e(\mu)$ is related to the bare coupling constant e_0 as

$$e(\mu) = e_0\sqrt{Z_3} = e_0\left(1 - \frac{\alpha}{3\pi}\ln\frac{\Lambda}{\mu}\right), \tag{2.133}$$

---

[6] A more sophisticated modification is adopted in the recent version of the PDG summary [285]. Their values differ from the simple $\overline{\text{MS}}$ definition by 0.0002 in $\sin^2\hat{\theta}_W(\mu)$. We use the simple $\overline{\text{MS}}$ throughout this book.

where Λ is the cutoff; we can relate the two coupling constants defined at μ and μ' by

$$e(\mu) = e(\mu')\left(1 - \frac{\alpha}{3\pi}\ln\frac{\mu'}{\mu}\right) , \qquad (2.134)$$

and therefore,

$$\frac{1}{\alpha(m_Z)} = \frac{1}{\alpha} - \frac{1}{3\pi}\ln\left(\frac{m_Z}{m_e}\right)^2 , \qquad (2.135)$$

when the electron is the only charged particle.[7] Equation (2.134) is a renormalisation-group equation [289, 290] and is usually expressed as

$$\mu\frac{de}{d\mu} = \beta(e) , \qquad (2.136)$$

where $\beta = \frac{4}{3}\frac{e^3}{(4\pi)^2}$ is the Gell-Mann–Low or Callan–Symanzik beta function.

When all charged fermions of mass smaller than m_Z are taken into account,

$$\alpha(m_Z)^{-1} = \alpha^{-1} - \frac{1}{3\pi}\left[3\sum_{i=u,d,s,c,b} Q_i^2 \ln(m_Z/m_i)^2 + \sum_{i=e,\mu,\tau} \ln(m_Z/m_i)^2\right]$$

$$\simeq 128.4 . \qquad (2.137)$$

Here we have ignored the contribution from the top quark ($m_t \gg m_Z$) and W boson loops, which are small. A more precise value is obtained by integrating $\sigma(e^+e^- \to$ all hadrons) over energy for the hadronic part and also by taking into account the W loop. A careful evaluation including higher order contributions [291, 292] yields

$$\alpha(m_Z)^{-1} = 127.93 \pm 0.03 . \qquad (2.138)$$

This running α effect explains most ($\gtrsim 90\%$) of the disagreement between the electroweak mixing angles seen above.

The renormalisation literature adopts the expressions [284]

$$m_W = \frac{(\pi\alpha/\sqrt{2}G_{\mathrm{F}})^{1/2}}{\sin\hat\theta_{\mathrm{W}}(1 - \Delta\hat r_W)^{1/2}} \qquad (2.139)$$

and

$$m_Z = \frac{m_W}{(1 + \Delta\hat\rho)^{1/2}\cos\hat\theta_{\mathrm{W}}(\mu)} . \qquad (2.140)$$

---

[7] We note here that $\alpha(m_e)$ is defined with the $\overline{\mathrm{MS}}$ scheme at a renormalisation point $\mu = m_e$, and it agrees with the Thomson-scattering definition, which is defined for all particles on the mass shell.

Using the QED correction,

$$\frac{1}{(1 - \Delta \hat{r}_W)} \simeq \alpha(m_Z)/\alpha, \tag{2.141}$$

which gives $\Delta \hat{r}_W = 0.067$. This value is compared with those in Table 2.2, which are obtained by a full radiative correction calculation [293, 291].[8] Our simple calculation reproduces 93–96% of the full correction.

The other electroweak corrections are usually small, but there is an exception: the correction to (2.128), i.e., $\Delta \hat{\rho}$, becomes substantial if the top quark mass is large [294]. (In principle, this correction may also affect $\Delta \hat{r}_W$, but a calculation shows that the contribution is cancelled in the leading order [293].) The correction arises from the gauge-boson self-energy (mass correction). When the gauge-boson propagator is written as

$$\Delta_F(q^2) = \frac{-g_{\mu\nu}}{q^2 - M^2}, \tag{2.142}$$

the corrected propagator is given by

$$i\Delta'_F = i\Delta_F + i\Delta_F(i\Pi)i\Delta_F + ...$$

$$= i\frac{-g_{\mu\nu}}{q^2 - M^2 - \Pi(q^2)}, \tag{2.143}$$

with $\Pi_{\mu\nu} = g_{\mu\nu}\Pi$ the gauge-boson self-energy (Fig. 2.4),

$$i\Pi_{\mu\nu}(A, B, A', B', m, m') \tag{2.144}$$

$$= -\int \frac{d^4k}{(2\pi)^4} \frac{\gamma_\nu(A - B\gamma_5)(\slashed{k} + m)\gamma_\mu(A' - B'\gamma_5)[(\slashed{q} + \slashed{k}) + m']}{(k^2 - m^2 + i\epsilon)[(q + k)^2 - m'^2 + i\epsilon]},$$

where we write the first vertex as $\bar{\psi}\gamma_\mu(A - B\gamma_5)\psi$ and the second $\bar{\psi}\gamma_\mu(A' - B'\gamma_5)\psi$. Note that the mass shift $\delta m^2 = \Pi(0)$. It is sufficient for us to evaluate the integral at $q = 0$. Upon taking the trace of the gamma matrices and using the Feynman trick to combine the denominators, the integral reads
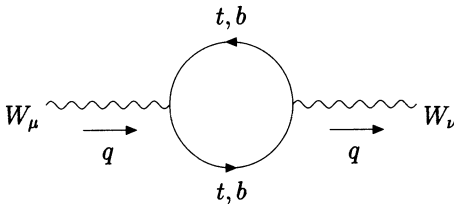
Fig. 2.4. Gauge-boson self-energy.

---

[8] The numbers in this table are obtained by interpolating the values given in [293] with respect to the Higgs mass.

$$i\Pi_{\mu\nu}(A, B, A', B', m, m') = -\int_0^1 dx \int \frac{d^4k}{(2\pi)^4} \frac{C(2k_\mu k_\nu - g_{\mu\nu}k^2) + Dg_{\mu\nu}}{(k^2 - \Delta^2 + i\epsilon)^2},$$

(2.145)

where

$$C = 4(AA' + BB'),$$
$$D = 4mm'(AA' - BB'),$$
$$\Delta = xm^2 + (1-x)m'^2.$$

Integrating the expression by extending the space–time dimension to n (n-dimensional regularisation [295]), we obtain

$$\Pi_{\mu\nu}(A, B, A', B', m, m')$$
$$= -\frac{1}{(4\pi)^2} \left\{ \left[\frac{1}{\varepsilon} - \gamma_E + \ln(4\pi) \right] \left(-C\frac{m^2 + m'^2}{2} + D \right) \right.$$
$$- D\left(\frac{m^2}{m^2 - m'^2} \ln m^2 - \frac{m'^2}{m^2 - m'^2} \ln m'^2 - 1 \right)$$
$$\left. + \frac{C}{2}\left(\frac{m^4}{m^2 - m'^2} \ln m^2 - \frac{m'^4}{m^2 - m'^2} \ln m'^2 - \frac{m^2 + m'^2}{2} \right) \right\},$$

(2.146)

where $\epsilon = (4 - n)/2$. Now, from the definition,

$$1 + \Delta\hat\rho = \frac{1}{\cos^2 \hat\theta_W(\mu)} \frac{(m_W^0)^2 + \delta m_W^2}{(m_Z^0)^2 + \delta m_Z^2}.$$

(2.147)

For the correction to the W mass, the internal loop including heavy quarks is given by $\bar bt$, and to the Z mass, it is $\bar bb$ and $\bar tt$. Using the coupling factors given in Table 2.1 (u for t and d for b), we obtain

$$\Delta\hat\rho = \frac{\delta m_W^2 - \cos^2 \hat\theta_W(\mu)\delta m_Z^2}{(m_W^0)^2}$$
$$= \frac{1}{m_W^2}\left\{ \Pi(1, 1, 1, 1, m_b, m_t) \right.$$
$$- \cos^2 \hat\theta_W\left[\Pi\left(1 - \frac{8}{3}\sin^2 \hat\theta_W, 1, 1 - \frac{8}{3}\sin^2 \hat\theta_W, 1, m_t, m_t \right) \right.$$
$$\left. \left. + \Pi\left(-1 + \frac{4}{3}\sin^2 \hat\theta_W, -1, -1 + \frac{4}{3}\sin^2 \hat\theta_W, -1, m_b, m_b \right) \right] \right\}$$
$$= \frac{3G_F}{8\pi^2\sqrt 2}\left(m_t^2 + m_b^2 - \frac{2m_t^2 m_b^2}{m_t^2 - m_b^2} \ln \frac{m_t^2}{m_b^2} \right).$$

(2.148)

The UV divergences cancel among contributions. For a large m_t,

$$\Delta\hat{\rho} \simeq \frac{3G_{\mathrm{F}}m_t^2}{8\sqrt{2}\pi^2} = 0.00960(m_t/175\,\mathrm{GeV})^2 \,, \tag{2.149}$$

which is a 1% correction of the ρ value. This is compared with accurate calculations [293] in Table 2.2.

Table 2.2. Renormalisation corrections $\Delta\hat{r}_W$ and Δr for $m_\phi = 250$ GeV.

m_t	$\Delta\hat{r}_W$	Δr	$\Delta\hat{\rho}$
100 GeV	0.0695	0.0608	0.0032
175 GeV	0.0717	0.0330	0.0121
200 GeV	0.0722	0.0222	0.0156

Let us discuss what happens with scheme (ii). With definition (2.132), the self-energy correction is now absorbed into $\sin^2\theta_W$, and a large m_t-dependent correction of (2.149) enters θ_W. From the definition of the ρ parameter, $(1 + \delta\hat{\rho})^{1/2}\cos\hat{\theta}_W(\mu) = \cos\theta_W$; therefore, $\sin\theta_W$ receives the correction $\sin\theta_W \to \sin\hat{\theta}_W\left(1 - \cot^2\hat{\theta}_W\delta\hat{\rho}\right)^{1/2}$, i.e., $\sin^2\hat{\theta}_W - \sin^2\theta_W \approx 0.0074$ for $m_t = 175$ GeV, which is compared with 0.0082 obtained by an accurate calculation. If we define

$$m_W = \frac{(\pi\alpha/\sqrt{2}G_{\mathrm{F}})^{1/2}}{\sin\theta_W(1 - \Delta r)^{1/2}}, \tag{2.150}$$

the correction factor Δr is

$$\Delta r \approx \Delta\hat{r}_W - \Delta\rho\cot^2\hat{\theta}$$

$$\approx 0.067 - 0.0096(m_t/175\,\mathrm{GeV})^2\cot^2\hat{\theta} \,. \tag{2.151}$$

This gives values close to Δr seen in Table 2.2. For example, we obtain $\Delta r = 0.024$ for $m_t = 200$ GeV, compared with 0.022. In this way, we can understand dominant parts (about >90–95%) in the radiative correction with QED corrections and the contribution of the top quark to the gauge-boson propagator. Beyond this level, an involved full one loop-calculation is necessary.

The Higgs scalar would also make a nonnegligible contribution to $\Delta\hat{r}_W$ and Δr if its mass is very large. The correction factor would be modified by the amount $\Delta\hat{r}_W = +0.12(\log_{10}m_\phi(\mathrm{GeV}) - 2.4)$ and $\Delta r = +0.95(\log_{10}m_\phi$ (GeV) $- 2.4)$ [293].

The phenomenology of neutral-current-induced processes, governed by (2.70), must be modified by taking into account process-dependent radiative

corrections. For (2.70), the NC interaction strength is multiplied by $(1+\Delta\rho_i)$, and $\sin^2\theta_W$ in (2.68) is replaced by $(1 + \Delta\kappa_i)\sin^2\theta_W$, where i is the process being considered.

The electroweak mixing angles obtained from the Z, W phenomenology and a few other examples of neutral-current effects are presented in Table 2.3[9] [275]. The most accurate phenomenological analyses are done with the Z boson. Various partial decay widths of Z, the axial-vector–vector interference term, and charge asymmetry with polarised beam collisions serve as the most high-precision tests for the standard model including radiative corrections. The accuracy of neutrino scattering processes or of atomic parity violation to measure the weak mixing angle is less by an order of magnitude.

The most convincing verification for the correctness of the electroweak theory, including the radiative correction, is the predictive power for the top-quark mass from the consistency test for electroweak interactions. Before the discovery of the top quark, a mass of 100–170 GeV was predicted (e.g., [296, 297]). With the advancement of e^+e^- collider experiments at LEP, the prediction of the t quark mass became 169^{+22}_{-27} GeV just before its discovery (1994) [298]. The top quark was discovered by CDF in 1995 [299]. The mass is 174.3 ± 5.1 GeV [300]. This is a dramatic confirmation of the standard model. Once the top mass is known, a similar argument applies to predicting the mass of the Higgs particle, though the theory is less sensitive to the Higgs mass (see Sect. 2.6.2 below).

The current determination of the electroweak mixing angle is [275, 301]

$$\sin^2\hat{\theta}_W(m_Z) = 0.2312 \pm 0.0002 \,, \tag{2.152}$$

$$\sin^2\theta_W = 0.2230 \pm 0.0002 \,. \tag{2.153}$$

Table 2.3. Weak mixing angle $\sin^2\theta_W$ derived from various experiments. We take $m_t = 174.3 \pm 5.1$ GeV and m_ϕ as a free parameter. $m_\phi = 98^{+57}_{-38}$ GeV is predicted as a result of the fit. "All data" means the average including processes that are not in this table.

	Tree	With one-loop corrections	
		$\overline{\text{MS}}$	On-shell
m_Z	0.2122(1)	0.2312(2)	0.2229(5)
m_W	0.2149(3)	0.2311(4)	0.2227(9)
$\nu N \to \nu X$	0.240(7)	0.234(2)	0.225(2)
$\nu_\mu e \to \nu_\mu e$	0.237(10)	0.229(8)	0.221(8)
All data		0.2312(2)	0.2230(4)

---

[9] The values in this table differ from those we derived in the text by no more than 0.001.

This is a subject that has been continuously updated. The progress of analyses are perhaps divided into three periods; before the discovery of W and Z [302], after their discovery [303], and after the advent of the LEP experiments [296, 297, 301].

2.5.3 Other Elementary Parameters in the Weinberg–Salam Theory

From the above results, we can calculate other elementary parameters that appear in the Weinberg–Salam theory. The two gauge couplings of the theory are $\alpha_2 \equiv g^2/4\pi \simeq 1/30$ and $\alpha_1 \equiv g'^2/4\pi \simeq 1/100$. For the vacuum-expectation value of the Higgs field, we have

$$v = 2^{-1/4}G_{\mathrm{F}}^{-1/2} \simeq 246\,\mathrm{GeV} \ . \tag{2.154}$$

The Yukawa couplings are given by $f_i \simeq 5.7 \times 10^{-6}(m_i/1\,\mathrm{MeV})$, where m_i is the relevant fermion mass. For $m_t = 174.3$ GeV, we find $f_t = 1.00$. The ϕ^4 coupling constant is related to the Higgs mass as $\lambda \simeq (1/19)(m_\phi^2/m_W^2)$.

2.6 The Problem with the Higgs Sector and the Search for the Higgs Particle

2.6.1 Theoretical Considerations on the Higgs Mass

The Higgs sector is the least understood part of the Weinberg–Salam theory. It may well be more complicated than the minimal version which we have described here, without modifying the predictions in the gauge sector. In turn, the Higgs sector would provide us with a number of interesting problems for particle physics, which may be taken to imply the presence of a new energy scale. In this section, we can give only a glimpse of the problem.

The only well-constrained aspect in the Higgs sector is that the Higgs particles that give masses to the gauge bosons are dominated by SU(2)$_\mathrm{L}$ doublet(s), as indicated by the ρ parameter of (2.71) which is so close to unity. If one removes radiative corrections, it is 0.998 ± 0.011 from the νN scattering R parameter (e.g., [281]).

The mass of the Higgs particle (or equivalently the ϕ^4 coupling in the minimal version of the model) is ill-constrained within the model. There are, however, a number of arguments that would point to a range of the Higgs mass that is not too arbitrary. The most popular guess is that it is in the range of 100 to a few hundred GeV.

There are two basic observations that lead to constraints on the Higgs mass. The first is that the self-coupling of the Higgs fields λ is proportional to the Higgs mass squared,

$$\lambda = m_\phi^2 / 2v^2, \tag{2.155}$$

and a large mass means a large coupling. Too large a coupling would make radiative corrections, for instance, to a weak boson mass so large that it would invalidate the agreement of the prediction of the Weinberg–Salam theory with experiment or lead to violation of unitarity for gauge-boson scattering. Another argument arises from the observation that radiative corrections would induce an effective potential of the form $\phi^4 \log \phi^2$ which, when added to the bare Lagrangian, might destabilise the vacuum which is necessary for the Higgs mechanism.

It was noted by Veltman [304] that the radiative correction to the W boson mass, when written as $M_W^2(1 + \delta)$, amounts to $\delta \approx \frac{g^2}{128\pi^2} \left(\frac{m_\phi}{m_W} \right)^2$ and that the correction exceeds 10% if $m_\phi > 600$ GeV.

Another consideration is about tree unitarity [305]. The $W_{\rm L}^+ + W_{\rm L}^- \rightarrow W_{\rm L}^+ + W_{\rm L}^-$ amplitude (L stands for longitudinally polarised) induced by a Higgs scalar exchange (Born diagram) is

$$T(W_{\rm L}^+ + W_{\rm L}^- \rightarrow W_{\rm L}^+ + W_{\rm L}^-) = -\sqrt{2}G_{\rm F} m_\phi^2 \left(\frac{s}{s - m_\phi^2} + \frac{t}{t - m_\phi^2} \right), \tag{2.156}$$

while the partial wave amplitude $a_J(s)$ of

$$T(s,t) = 16\pi \sum_J (2J + 1)a_J(s)P_J(\cos\theta) \tag{2.157}$$

should not exceed unity. The constraint $a_0 \leq 1$ gives

$$|a_0(W_{\rm L}^+ + W_{\rm L}^- \rightarrow W_{\rm L}^+ + W_{\rm L}^-)| \rightarrow \left| -\frac{G_{\rm F} m_\phi^2}{4\pi\sqrt{2}} \right| < 1 . \tag{2.158}$$

Simultaneous consideration of the $Z_{\rm L}Z_{\rm L}$, $\phi\phi$, and $Z_{\rm L}\phi$ channels makes the bound slightly stronger, $\lambda < 8\pi/3 \simeq 8.38$, or $m_\phi < 1$ TeV. This upper limit, however, corresponds to too large a coupling, and the validity of a perturbative argument is not clear.

One way to take account of higher orders of perturbation is to resort to a renormalisation group. The renormalisation group equation for λ is

$$\mu \frac{d\lambda}{d\mu} = \frac{24}{16\pi^2} \lambda^2 , \tag{2.159}$$

which means that λ develops as

$$\frac{1}{\lambda} = \frac{1}{\lambda_0} - \frac{3}{2\pi^2} \ln(\mu/\mu_0) . \tag{2.160}$$

λ increases as the energy scale, and eventually blows up to infinity at $\lambda_0 = (2\pi^2/3)[\ln(\mu/\mu_0)]^{-1}$ (this is called the Landau pole [306]). The increase of

λ with energy makes the upper limit even stronger; in order to avoid the Landau pole, λ_0 must be smaller than $6.58/\ln(\mu/\mu_0)$ where $\mu_0 = m_Z$. If we require that this blowup should not happen on an energy scale smaller than the Planck mass, λ_0 must be smaller than 0.17 or $m_\phi < 143$ GeV. If the theory should be validated to a grand unification energy scale $\sim 2 \times 10^{16}$ GeV, $m_\phi < 160$ GeV. This argument still resorts to a one-loop calculation but also ignores the contribution from fermion loops; we will discuss later how the argument is modified in the presence of the heavy top quark.

Attempts to go beyond perturbation are made using the lattice regularisation formalism. The argument uses the formal result that the ϕ^4 theory becomes trivial when the cutoff of the theory is brought to infinity [307]. To have a finite renormalised coupling constant, one needs to retain a finite cutoff, yet one must find the regions of coupling space where the effect of the cutoff scale is reasonably small for physical quantities. This condition is satisfied when λ, and hence the Higgs mass, is small [308, 309]. In the lattice theory, this is represented in the following way [309]. The renormalised coupling λ_r (subscript r refers to a renormalised quantity) vanishes in the continuum limit $a \to 0$ of the lattice spacing a, whereas the physical mass is kept fixed. Near $a = 0$, we can define a nontrivial interacting theory on the lattice, where physical quantities receive $\ln a$ corrections, and their coefficients are determined by nonperturbative (Monte Carlo) calculations. For this regime to be valid, the ratio $R = m_\phi/\langle \phi_r \rangle$ should be bounded for any choice of the parameters λ and μ in the bare Lagrangian. Monte Carlo calculations showed that $R \lesssim 2.6$, which means $\lambda_r = R^2/2 \lesssim 3.4$. Using the perturbation relation $\lambda_r \simeq (g^2/8)(m_\phi/m_W)$, which should be valid for small g, the bound on R means $m_\phi \lesssim 600$ GeV [310]. This estimate, too, ignores the effect of the heavy top quark. A realistic calculation must include the fermion degree of freedom, which, however, is hampered by the well-known difficulty of formulating chiral fermions on the lattice.

Another argument to constrain the Higgs mass comes from the observation that the Higgs potential receives a radiative correction of the form

$$V_1(\phi) = B\phi^4 \ln(\phi^2/\bar{\mu}^2) + ..., \tag{2.161}$$

where

$$B = \frac{1}{64\pi^2 v^4}\left[\frac{3}{4}m_\phi^4 + 3(2m_W^2 + m_Z^2) - 3\sum m_f^4\right], \tag{2.162}$$

and $\bar{\mu}$ in the logarithm is a renormalisation scale, at which the ϕ^4 coupling is defined so that $\partial^4(V + V_1)/\partial\phi^4 = 6\lambda_r$ [311]. For $B > 0$, the correction would disturb the Higgs vacuum if the Higgs mass is too small ($m_\phi < 6.8$ GeV) [312]. If $B < 0$, the large ϕ behaviour of the Higgs potential becomes negative, i.e., the potential becomes unbounded, destabilising the vacuum. A practically relevant condition is to avoid $B < 0$, which would arise from a negative fermion contribution from the heavy top quark [313]. As the top quark mass

becomes larger, λ must be large enough to overcome the negative contribution from the top quark, and it gives a lower bound on the Higgs mass. (In actual application, one should note that this perturbative expansion is made with respect to $\alpha \ln \phi$ rather than α and it is not applicable to a large ϕ. This is avoided by writing a renormalisation group equation for the potential [314].) The result of the analysis is summarised by the requirement that the running self-coupling λ is always positive [315] between the scale of the Weinberg–Salam theory and the cutoff. The renormalisation group equation for λ is

$$16\pi^2 \frac{d}{dt}\lambda(t) = 24\lambda^2(t) + 12\lambda(t)f_t^2 - 6f_t^4 , \qquad (2.163)$$

where f_t is the Yukawa coupling with m_t defined at the pole mass including QCD radiative corrections, and the running parameter $t = \ln \mu/\mu_0$. In this equation, the contributions from gauge bosons are omitted. For a small λ and a large f_t, the right-hand side is negative, which drives λ to negative; eventually, however, the λ^2 term overwhelms the equation and brings it positive and eventually to infinity (Landau pole). By requiring $\lambda > 0$ below the cutoff energy scale, which is taken as the Planck energy scale, it is found that (e.g., [316])

$$m_\phi > 135\,\mathrm{GeV} + 2.1(m_t - 174\,\mathrm{GeV}) . \qquad (2.164)$$

The upper limit from the absence of the Landau pole below the Planck mass is 200 GeV for $m_t = 174$ GeV [316].

There is an interesting possibility that nontrivial theory exists if the contribution of the Yukawa coupling cancels the Higgs coupling at the cutoff of infinity. The renormalisation group equation (2.163) is supplemented by

$$16\pi^2 \frac{d}{dt}f_t(t) = \frac{9}{2}f_t^3(t) - 8f_t(t)g_s^2(t) , \qquad (2.165)$$

$$16\pi^2 \frac{d}{dt}g_s(t) = -bg_s^3(t) , \qquad (2.166)$$

where g_s is the QCD gauge coupling constant and only the most important couplings are retained; b is the QCD beta function coefficient

$$b = (33 - 2N_f)/3 ,$$

and $b = 7$ for $N_f = 6$. Let us first consider the behaviour of f_t as $t \to \infty$. We want to require that Yukawa theory with f_t is also asymptotic-free, i.e., $f_t \to 0$ as $t \to \infty$. The condition can be derived by writing a renormalisation group equation for $\ln f_t(t)/g_s(t)$, combining the two equations:

$$16\pi^2 \frac{d}{dt}\ln(f_t/g_s) = \frac{9}{2}f_t^2(t) - g_s^2(t) . \qquad (2.167)$$

If we impose the condition $g_s^2(t) \geq (9/2)f_t^2(t)$, this ensures that the right-hand side of (2.167) is negative; hence $f_t(t) \leq g_s(t)$, while $g_s(t) \to 0$ as

$t \rightarrow \infty$. This leads to an upper limit on the top quark mass, $m_t < 220$ GeV. For the Higgs coupling, we see that $\lambda(t) \rightarrow 0$ holds only if $\lambda(0)$ satisfies $\lambda(0) = (1/2)h_t^4(0)/g_s^2(0)$. If $\lambda(0)$ is larger than this value, $\lambda(t)$ blows up as $t \rightarrow \infty$, and if smaller, $\lambda(t)$ becomes negative, causing instability of the vacuum. With $m_t = 174$ GeV and $\alpha_s(m_Z) = 0.117$, the conditions lead to a unique value $m_\phi = 203$ GeV. If the Higgs mass does not take this value, there should be a finite cutoff scale [317].

2.6.2 Empirical Limits on the Higgs Mass

Although the Higgs coupling to ordinary matter via the Yukawa interaction is very small, the coupling to gauge bosons takes the universal strength of g. Therefore, direct searches for Higgs particles have been made looking for $Z^0 \rightarrow \phi +$ "Z^0(virtual)," "Z^{0}" $\rightarrow \ell^+\ell^-$, $\bar{\nu}\nu$, $\gamma\gamma$, or hadrons. As the Higgs mass increases, a newly opened decay mode always dominates Higgs decays (see Fig. 1 of [318]). In an early phase of the LEP experiment, the Aleph group [319] (and subsequently other groups) excluded a Higgs particle in the mass range $0 \le m_\phi \le 41$GeV (95%CL) for the minimal version of the model. The significance of this result is exclusion of the simple possibility that spontaneous symmetry breaking is caused by radiative corrections, starting from a flat effective potential (Coleman–Weinberg mechanism), which predicts m_ϕ=9.7 GeV [311]. As the energy of the storage ring is upgraded to ≈ 200 GeV, improved limits are derived from $e^+ + e^- \rightarrow Z^0$(real) $+ \phi$. A recent lower limit is $m_\phi > 114.1$ GeV (95% CL) at $\sqrt{s} \le 202$ GeV [320]. (For light Higgs particle in the minimum supersymmetric model, the limit is > 91.0 GeV [321].) The most recent Higgs search reports "discovery" of the Higgs boson at $m_\phi = 114$ GeV at a 3σ level ($\sqrt{s} = 206 - 209$ GeV) [322]. Confirmation is obviously a pressing issue.

The information on Higgs mass can also be obtained from the analysis of radiative correction of electroweak interactions, just as was done for the mass of the top quark. The results of published analyses are summarised as $m_\phi = 150^{+170}_{-60}$ GeV [323]. The latest fit of PDG (see Table 2.3) predicts $m_\phi = 98^{+57}_{-38}$ GeV [301].

2.6.3 Theoretical Implications of a 'Small' Higgs Mass

Now let us discuss the 'problem' associated with a 'light' Higgs particle. The origin of the 'problem' is the observation that the self-energy correction to the Higgs mass is quadratically divergent, and we must add a counter term which is of the order of $\Lambda_{\rm cut}^2$, which may be $m_{\rm pl}^2$ or $m_{\rm GUT}^2$, to make the Higgs mass to be of the order of 100 GeV. If we take a conservative view, this is not a problem because the theory is renormalisable and only the value after renormalisation anyway makes physical sense. This seems unsatisfactory to some physicists, however, because the origin of a small Higgs mass is unexplained.

Historically, there are three views to explain the smallness of the Higgs mass. The first possibility from the past lesson is that the Higgs is a (pseudo) Nambu–Goldstone boson. This, however, is not acceptable because the coupling of the Higgs to fermions must be of the Yukawa type, whereas the low-energy theorem derived for the Nambu–Goldstone boson requires that the coupling be of the derivative type. The second possibility is that the Higgs scalar is not a fundamental particle, but a condensation $\langle \bar{\psi}\psi \rangle \neq 0$ plays the role of a Higgs scalar, i.e., the Higgs scalar is a composite particle [324]. There have been a number of attempts to construct such theories consistent with experiment, but none turns out to be successful [325]. In these models, one must introduce some extra gauge interactions (often called technicolour) that connect the composite Higgs made of $\bar{\psi}\psi$ with quarks and leptons to make them massive. The non-Abelian nature of the new gauge interactions then induces unwanted flavour-changing neutral currents. In addition, all proposed models are, it is now shown, inconsistent with the high precision electroweak tests we have seen above [326].

The third possibility, which is paid much attention, is that the loop diagram cancels between boson and fermion contributions and there is no quadratic divergence. This is realised by imposing supersymmetry [327]. Since we expect chiral symmetry for the Higgsino (fermion partner of the Higgs particle), the mass of the Higgs should be no more than the order of the supersymmetry-breaking scale. We return to this problem in Sect. 9.3.2. Here, we only note that most of the arguments given in Sect. 2.6.1 are invalidated in the presence of supersymmetry because of the cancellation in the loop diagrams. On the other hand, in the supersymmetric model, $\lambda = g^2$ holds, and the Higgs mass is related to the Z boson mass. There are two Higgs bosons, and the mass of the lighter one is constrained to be $\lesssim 120 - 140$ GeV after radiative corrections [328].

3 Applications of the Electroweak Theory

3.1 Physics with the Charged Current

The weak decay processes known from early times are all described by charged-current interactions. As given in (2.6), the charged current is the sum of leptonic and hadronic currents:

$$J_\mu = J_\mu^{(\ell)} + J_\mu^{(h)} , \tag{3.1}$$

where

$$J_\mu^{(\ell)} = \bar{\nu}_e \gamma_\mu (1 - \gamma_5) e^- + \bar{\nu}_\mu \gamma_\mu (1 - \gamma_5) \mu^- + \bar{\nu}_\tau \gamma_\mu (1 - \gamma_5) \tau^- \tag{3.2}$$

and

$$J_\mu^{(h)} = (\bar{u}, \bar{c}, \bar{t}) U_q \gamma_\mu (1 - \gamma_5) \begin{pmatrix} d \\ s \\ b \end{pmatrix} . \tag{3.3}$$

Here U_q is a 3×3 unitary (Kobayashi–Maskawa) matrix for quark mixing of the form,

$$U_q = \begin{bmatrix} U_{ud} & U_{us} & U_{ub} \\ U_{cd} & U_{cs} & U_{cb} \\ U_{td} & U_{ts} & U_{tb} \end{bmatrix} , \tag{3.4}$$

which receives constraints from unitarity

$$|U_{ud}|^2 + |U_{us}|^2 + |U_{ub}|^2 = 1 , \tag{3.5}$$

$$U_{ud} U_{cd}^* + U_{us} U_{cs}^* + U_{ub} U_{cb}^* = 0 , \tag{3.6}$$

$$U_{ud} U_{td}^* + U_{us} U_{ts}^* + U_{ub} U_{tb}^* = 0 , \tag{3.7}$$

and so on. If all neutrinos are massless, we can define gauge-coupling eigenstates of leptons as simultaneous mass eigenstates, so we do not need a mixing matrix. If they are massive, a similar matrix should be set for the leptonic current. This will be discussed in a greater detail in Chap. 8. At low energy charged-current-induced processes are described by the interaction Hamiltonian which is the product of the currents as in (2.70),

$$H_W^{\text{eff}} = \frac{G_F}{\sqrt{2}} J_\mu^\dagger J_\mu \ . \tag{3.8}$$

The term involved in (3.8) takes the form $\bar{\psi}^B \Gamma_\mu^a \psi^A \bar{\psi}^D \Gamma^{b\mu} \psi^C$. The fermion line flows as $A \to B$ and $C \to D$. The process may also be viewed as $A \to D$ and $C \to B$ since the interaction is also formally written as $\bar{\psi}^D \Gamma_\mu^c \psi^A \bar{\psi}^B \Gamma^{d\mu} \psi^C$ for the four-Fermi interaction, which takes the form of a contact-interaction vertex. This rearrangement is called the Fierz transformation [25]. To show this, we start from

$$\bar{\psi}_\alpha^B (\Gamma^a)_{\alpha\beta} \psi_\beta^A \bar{\psi}_\gamma^D (\Gamma^b)_{\gamma\delta} \psi_\delta^C = -(\Gamma^a)_{\alpha\beta}(\Gamma^b)_{\gamma\delta} \psi_\beta^A \bar{\psi}_\gamma^D \psi_\delta^C \bar{\psi}_\alpha^B \ , \tag{3.9}$$

where Lorentz summation indices are dropped. The spinor product $\psi_\beta^A \bar{\psi}_\gamma^D$ is written

$$\psi_\beta^A \bar{\psi}_\gamma^D = \sum_i c_i (H^i)_{\beta\gamma} \bar{\psi}^D H^i \psi^A \tag{3.10}$$

where the coefficients $c_1 = -1/4$, $c_{\gamma_\mu} = -1/4$, $c_{\gamma_\mu\gamma_5} = 1/4$, $c_{\gamma_5} = -1/4$, and $c_{\sigma_{\mu\nu}} = -1/8$, so that (3.9) is

$$-\sum_{ij} c_i c_j Tr(\Gamma^a H^i \Gamma^b H^j) \bar{\psi}^D H^i \psi^A \bar{\psi}^B H^j \psi^C. \tag{3.11}$$

Applying this to $\psi_L = \frac{1-\gamma_5}{2}\psi$ and $\Gamma^a = \Gamma^b = \gamma_\mu$, we see that the spinor product is nonvanishing only when $(H^i, H^j) = (\gamma_\mu, \gamma_\nu)$ or $(\gamma_\mu\gamma_5, \gamma_\nu\gamma_5)$. Using the coefficients c_i given above, we can show that

$$\bar{\psi}_L^B \gamma_\mu \psi_L^A \bar{\psi}_L^D \gamma^\mu \psi_L^C = \bar{\psi}_L^D \gamma_\mu \psi_L^A \bar{\psi}_L^B \gamma^\mu \psi_L^C \ . \tag{3.12}$$

The V–A theory is Fierz transformation invariant [329]. This result is nearly obvious (up to the sign) because all spinor products with an operator other than γ_μ ($\gamma_\mu\gamma_5$ is equivalent) vanish on the right-hand side if the spinors are left-handed projections.

3.2 Muon Decay

The simplest process is muon decay $\mu^- \to e^- \bar{\nu}_e \nu_\mu$, which is described by

$$H_W^{\text{eff}} = \frac{G_F}{\sqrt{2}} \bar{\nu}_\mu \gamma_\mu (1 - \gamma_5) \mu^- \overline{e^-} \gamma_\mu (1 - \gamma_5) \nu_e \ . \tag{3.13}$$

The decay rate is calculated as

$$\begin{aligned}
&\Gamma(\mu \to e\nu\bar{\nu}) \\
&= \frac{1}{2} \frac{1}{2m_\mu} \int \frac{d^3q}{(2\pi)^3 2q^0} \int \frac{d^3\ell}{(2\pi)^3 2\ell^0} \int \frac{d^3k}{(2\pi)^3 2k^0} (2\pi)^4 \delta^4(q + k + \ell - p)|T|^2 \ ,
\end{aligned} \tag{3.14}$$

where p, q, k and ℓ are momenta of μ, e^-, $\bar\nu_e$ and ν_μ, respectively, and T is the matrix element of $-iH_W^{\text{eff}}$ with the wave function normalisation factor removed. The spin averaged matrix element square is

$$|T|^2 = 128 G_{\text{F}}^2 (kq)(p\ell) , \tag{3.15}$$

if the electron mass is neglected. To obtain the energy spectrum of the emitted electron, it is convenient to use the formula

$$\int \frac{d^3\ell}{2\ell^0} \int \frac{d^3k}{2k^0} \delta^4(k+\ell-r) k^\alpha \ell^\beta = \frac{\pi}{24}(g^{\alpha\beta} r^2 - 2r^\alpha r^\beta) . \tag{3.16}$$

After integration, we obtain

$$\frac{d\Gamma}{dE_e} = \frac{G_{\text{F}}^2 m_\mu^2}{12\pi^3} E_e^2 \left(3 - 4\frac{E_e}{m_\mu}\right) , \tag{3.17}$$

where the range of $E_e (= q^0)$ is $0 \le E_e \le m_\mu/2$. The total decay rate is thus

$$\Gamma = \int_0^{m_\mu/2} \frac{d\Gamma}{dE_e} dE_e = \frac{G_{\text{F}}^2 m_\mu^5}{192\pi^3} . \tag{3.18}$$

When the electron mass is retained, the mass correction factor appears as in (2.125), which gives a -0.019% correction.

The energy spectrum of ν_μ takes the same form as that of the electron owing to the Fierz invariance for $\nu_\mu \leftrightarrow e^-$:

$$\frac{d\Gamma}{dE_{\nu_\mu}} = \frac{G_{\text{F}}^2 m_\mu^2}{12\pi^3} E_{\nu_\mu}^2 \left(3 - 4\frac{E_{\nu_\mu}}{m_\mu}\right) . \tag{3.19}$$

The $\bar\nu_e$ spectrum is obtained by integrating (3.14) over q and ℓ using a formula similar to (3.16),

$$\frac{d\Gamma}{dE_{\bar\nu_e}} = \frac{G_{\text{F}}^2 m_\mu^2}{12\pi^3} E_{\bar\nu_e}^2 \left(1 - 2\frac{E_{\bar\nu_e}}{m_\mu}\right) . \tag{3.20}$$

We note that the spectra of ν_μ and $\bar\nu_e$ are different: $\langle E_{\nu_\mu}\rangle = \frac{7}{20}m_\mu = 37.0$ MeV; $\langle E_{\bar\nu_e}\rangle = \frac{3}{10}m_\mu = 31.7$ MeV.

A muon produced from the decay of a pion $\pi^- \to \mu^- + \bar\nu_\mu$ is fully polarised and has helicity $+1/2$ in the rest frame of the pion. In the rest frame of the muon, the angular distribution of the neutrino (and the electron) from a polarised muon receives an extra contribution that depends on the direction of the muon spin. Equation (3.19) is modified to

$$\frac{d\Gamma}{dE_{\nu_\mu}} = \frac{G_{\text{F}}^2 m_\mu^2}{12\pi^3} E_{\nu_\mu}^2 \left[\left(3 - 4\frac{E_{\nu_\mu}}{m_\mu}\right) + \left(1 - 4\frac{E_{\nu_\mu}}{m_\mu}\right)\cos\Theta\right] , \tag{3.21}$$

where Θ is the angle between the muon spin and the direction of the neutrino (electron) considered (E_{ν_μ} is replaced by E_e for the electron spectrum). Similarly, (3.20) is modified to

$$\frac{d\Gamma}{dE_{\bar{\nu}_e}} = \frac{G_F^2 m_\mu^2}{12\pi^3} E_{\bar{\nu}_e}^2 \left(1 - 2\frac{E_{\bar{\nu}_e}}{m_\mu}\right)(1 + \cos\Theta) . \qquad (3.22)$$

For μ^+ from $\pi^+ \to \mu^+ \nu_\mu$, the sign of the $\cos\Theta$ terms is reversed.

Muon decay is used to determine the strength of weak interactions, and great accuracy is desired for the decay rate formula. $O(\alpha)$ radiative corrections are calculated by inserting a photon propagator into the muon and electron lines and between the two [330]. The calculation can be carried out conveniently after the Fierz transformation, so that the muon and the electron are on the same fermion line connected with a $\gamma_\mu(1-\gamma_5)$ vertex. The structure of the divergent part can easily be studied: the divergence arising from the vertex integral takes the form $\frac{\alpha}{2\pi^2}(\log\Lambda)\gamma_\mu(1-\gamma_5)$; this is cancelled against the wave function renormalisation of the two charged fermions just as happens with $Z_1 = Z_2$ in QED, despite the fact that the vector Ward identity is broken due to the difference in mass of the muon and electron. The mass renormalisation of charged leptons is done as in QED. Radiative correction of muon decay is thus ultraviolet finite. The sum of the diagrams for virtual photon emission, however, diverge in the infrared; we must add the real photon emission process $\mu^- \to e^- + \bar{\nu}_e + \nu_\mu + \gamma$ to cancel the divergence. The radiative correction, hence, depends on the treatment of real photon emission (the energy resolution of the detector). If the experiment is completely blind to photon emission, the radiative correction is obtained by integrating over all available photon energy. The calculation yields $(\alpha/2\pi)(25/4 - \pi^2) = -0.42\%$, as given in (2.124) of Chap. 2. A detailed description of the calculation is in [331]. Two-loop calculation (the analytic result) is now available [332].

3.3 Weak Decays Involving Hadrons: Classification

Weak decays involving hadrons are complicated by strong interactions in the matrix elements of the current (or its product). In the order of complication the weak processes are classified in terms of the hadronic matrix elements involved:

$$(1) \qquad \langle 0|J_\mu^{(h)}|h\rangle , \qquad (3.23)$$

$$(2) \qquad \langle h'|J_\mu^{(h)}|h\rangle , \qquad (3.24)$$

$$(3) \qquad \langle h'h''|J_\mu^{(h)}|h\rangle , \qquad (3.25)$$

$$(4) \qquad \langle h'|J_\mu^{(h)} J^{\mu\dagger(h)}|h\rangle , \qquad (3.26)$$

$$(5) \qquad \langle h'h''|J_\mu^{(h)} J^{\mu\dagger(h)}|h\rangle . \qquad (3.27)$$

We write $J_\mu^{(h)} = V_\mu - A_\mu$ with V_μ and A_μ the vector and axial-vector currents.

The matrix element of type (1) appears in leptonic decays of pseudoscalar mesons, $\pi \to \mu\bar{\nu}_\mu, e\bar{\nu}_e$, $K \to \mu\bar{\nu}_\mu$ $D \to \mu\bar{\nu}_\mu$, etc. The next simplest matrix element (2) is relevant to the semileptonic decay of hadrons, such as beta decays of nucleons and nuclei. There are also hyperon beta decays $\Lambda \to p + e^- + \bar{\nu}_e$, $\Sigma^- \to n + e^- + \bar{\nu}_e$, and beta decays of mesons $\pi^+ \to \pi^0 + e^+ + \nu_e$, $K^- \to \pi^0 + e^- + \bar{\nu}_e$ (often named $K_{\ell 3}$). $K^- \to K^0 + e^- + \bar{\nu}_e$ is unobserved simply due to its small decay rate. Neutrino scattering off the nucleon (inverse beta decay) also belongs to this category. (3) is the matrix element for $K_{\ell 4}$, $K^- \to \pi^+ + \pi^- + e^- + \bar{\nu}$, etc., which is complicated by $\pi - \pi$ final state interactions. The most important process described by (4) is $K^0 - \bar{K}^0$, $D^0 - \bar{D}^0$, and $B^0 - \bar{B}^0$ mixing, which are relevant to the physics of flavour-changing neutral current and CP violation. (5) is responsible for hadronic weak decays, such as two pion decays of kaons, and hyperon decays $\Lambda \to p + \pi^-$, $\Sigma^0 \to p + \pi^-$, etc. These hadronic decays are fully complicated by nonperturbative strong interactions, and the physics is not yet well understood. We do not touch on hadronic decays in this book.

In what follows we discuss several typical weak decay processes that are important within the scope of this book. For more extensive surveys we refer the reader to classical textbooks [334, 335]. Neutrino scattering will be discussed in Sects. 3.10–3.16.

Before discussing individual processes, let us mention the consequence of the conserved vector current (CVC) hypothesis [53], which plays a central role in the following discussion. We consider $q = (u, d)$ as an SU(2) doublet in isospin space and write the vector current as $V_+^\mu = V_1^\mu + iV_2^\mu$, where

$$V_i^\mu = \bar{q}\frac{\tau_i}{2}\gamma^\mu(1 - \gamma_5)q \qquad (3.28)$$

with τ_i Pauli matrices acting on isospin space. Conservation of the vector current $\partial_\mu V_i^\mu = 0$ means that the charge

$$T_i = \int d^3x V_i^0(x) \qquad (3.29)$$

is conserved and forms SU(2) algebra $[T_i, T_j] = i\epsilon_{ijk}T_k$. The electromagnetic current is written as $J_{\rm em}^\mu = V_3^\mu + V_Y^\mu$ where the operator Y in V_Y^μ (hypercharge current) behaves as an isoscalar under SU(2). This gives a commutator, for example,

$$[J_{\rm em}^\mu, T_+] = V_+^\mu , \qquad (3.30)$$

which fixes the normalisation of the hadronic matrix elements of the vector current at zero momentum transfer to specific values via, e.g., $\langle\pi^0|V_+^\mu|\pi^-\rangle = -\sqrt{2}\langle\pi^-|J_{\rm em}^\mu|\pi^-\rangle$, and $\langle p|V_+^\mu|n\rangle = \langle p|J_{\rm em}^\mu|p\rangle - \langle n|J_{\rm em}^\mu|n\rangle$. This enables us to determine the strengths of weak interactions from experiments.

Another remark concerns radiative corrections of the decay process involving hadrons. The diagrams for radiative corrections are divided into those

concerning only the lepton, only the hadron, and those bridging across the hadron and lepton. The radiative correction for hadrons is complicated by nonperturbative strong interaction physics. Only when the current is conserved and the matrix element is taken within the same isomultiplet, can one estimate this radiative correction almost model-independently [334, 336]. This applies to the vector-current-induced weak decay, $\pi^- \to \pi^0 + e^- + \bar{\nu}_e$, and the Fermi transition of nuclear β decay. Even if the current to the tree process is purely of the vector type, there appears an axial-vector-current process induced by radiative corrections in the diagram where the photonic correction bridges the lepton and hadron. This axial-current-induced process cannot be estimated in a model-independent way, but the model dependence is fairly modest, and the accuracy is controlled to some degree. We emphasise that radiative corrections are essential in estimating the $|U_{ud}|$ element, since the departure from unity is only 2.3%, comparable to the size of radiative corrections. The radiative correction of an axial-vector-induced weak process depends on the structure of the particle, and hence is model-dependent.

3.4 Leptonic Decays of Mesons

The matrix element of the axial-vector current for pion decay is written

$$\sqrt{2q^0}\langle 0|A^{\mu}_{\pi^+}|\pi^-\rangle = iq^{\mu}f_{\pi} , \qquad (3.31)$$

where $A^{\mu}_{\pi^+} = \bar{u}\gamma_{\mu}\gamma_5 d$ and q is four momentum of the pion. The decay rate of the pion is then,

$$\Gamma(\pi \to \mu + \bar{\nu}) = \frac{G_F^2}{8\pi}\cos^2\theta_c f_{\pi}^2 \frac{m_{\mu}^2(m_{\pi}^2 - m_{\mu}^2)^2}{m_{\pi}^3} , \qquad (3.32)$$

where $\cos\theta_c = |U_{ud}|$. Using $\Gamma(\pi \to \mu + \bar{\nu})^{-1} = 26.0$ ns and $|U_{ud}| = 0.974$ (see below), we find $f_{\pi} = 131$ MeV. We note that the matrix element of $\pi \to \mu + \bar{\nu}$ is proportional to the lepton mass. When the leptonic current $\bar{\mu}\gamma_{\mu}(1 - \gamma_5)\nu$ is multiplied by (3.31), $q^{\mu}\gamma_{\mu}$ turns out to be the leptonic mass by virtue of the Dirac equation. This leaves $\bar{\mu}(1 - \gamma_5)\nu$, which means that the antineutrino is right-handed and the muon is left-handed if chiral symmetry is exact. On the other hand, angular momentum conservation requires that the two particles go in opposite directions to have the same chirality. Therefore, the decay proceeds only through chiral symmetry violation by leptonic mass. This means that the decay into $e^-\bar{\nu}_e$ is strongly suppressed compared with decay into muons:

$$\frac{\Gamma(\pi \to e + \nu)}{\Gamma(\pi \to \mu + \nu)} = \frac{m_e^2}{m_{\mu}^2}\frac{(m_{\pi}^2 - m_e^2)^2}{(m_{\pi}^2 - m_{\mu}^2)^2} = 1.2834 \times 10^{-4}. \qquad (3.33)$$

With a -3.9% reduction due to the radiative correction [337], the ratio of the two modes inclusive of one photon emission is 1.233×10^{-4} in precise

agreement with experiment, $(1.230 \pm 0.004) \times 10^{-4}$, which is the average of the two comparable experiments [338]. This provides one of the best verifications for $e - \mu$ universality.

Theoretical calculations of the pion decay constant f_π require nonperturbative treatment of QCD. The current lattice QCD calculations yield f_π at 10% accuracy [339], but such calculations still resort to the "quenched approximation" where the reaction of the quark to the gluon field is ignored.

Similarly, we obtain the leptonic decay rate of charged kaons with the quark mixing angle $\cos\theta_c$ of (3.32) replaced by $|U_{us}| = \sin\theta_c$. The kaon decay constant is $f_K = 0.160$ for $\Gamma^{-1} = 19.5$ ns. $f_K/f_\pi = 1.22$ stands for breaking of flavour SU(3) symmetry realised by (u,d,s). The ratio of $K \to e + \nu$ to $K \to \mu + \nu$ is 2.6×10^{-5}.

These decays are the dominant source of neutrinos in accelerator experiments and in cosmic rays. The accelerator neutrino beam is thus dominated by muon neutrinos (the main source of electron neutrinos is from K_{e3}), unless the beam line is very long, which allows decay of muons. The average energy of the neutrino beam is $\langle E_\nu \rangle = (E_{\pi,K}/2)(1 - m_\mu^2/m_{\pi,K}^2)$ for a parent energy of $E_{\pi,K}$, so that higher energy neutrinos are dominated by K decays.

Note that the axial-vector current is not conserved. If we take a derivative of the axial-vector current,

$$q_\mu A^\mu_{\pi^+} = (m_u + m_d)(\bar{u}\gamma_5 d) \neq 0 \,, \tag{3.34}$$

unless chiral symmetry is exact. Equation (3.31) indicates that the derivative of the axial-vector current behaves as

$$\partial_\mu A^\mu_\pi(x) = f_\pi m_\pi^2 \phi_\pi(x) \tag{3.35}$$

in coordinate space. This relation is referred to as PCAC [67].

Leptonic decays of heavy D and B mesons are described by f_D and f_B with similar formulae. These decay constants are phenomenologically important in heavy quark physics. Because of very small branching fractions, however, the empirical estimate of decay constants is not easy. We have now some data for f_D but those for f_B are not available yet. For phenomenology, values are often used from lattice QCD calculations with the aid of various heavy quark formalisms [340].

3.5 Semileptonic Decays of Mesons

Only the vector current contributes to beta decays of mesons, $\pi^- \to \pi^0 + e^- + \bar{\nu}$, and $K^- \to \pi^0 + e^- + \bar{\nu}$. The matrix element of pion beta decay is given by

$$\langle \pi^0(p')|V_\mu|\pi^-(p)\rangle = (2\pi)^{-3}(2p'^0 2p^0)^{-1/2}[f_+(q^2)(p+p')_\mu + f_-(q^2)(p-p')_\mu] \,, \tag{3.36}$$

where $q = p' - p$.

In pion decay isospin violation is small and the vector current is nearly conserved, $\partial_\mu V^{\mu'} = 0$, which leads to

$$f_-(q^2) = 0 \,. \tag{3.37}$$

The momentum transfer q is small, so that $f_+(q^2)$ is replaced with $f_+(0)$, which is determined to the $\sqrt{2}$ from CVC, as seen above. The decay rate is calculated as

$$\Gamma(\pi^- \to \pi^0 + e^- \bar\nu) = \frac{G_F^2}{30\pi^3} |U_{ud}|^2 (m_{\pi^-} - m_{\pi^0})^5 \,, \tag{3.38}$$

if m_e is ignored. With m_e retained, the mass correction factor is $f(x) = \sqrt{(1-x^2)}(1 - \frac{9}{3}x^2 + 4x^4) + \frac{15}{2}x^4 \ln(1 + \sqrt{1+x^2}/x) = 0.942$ where $x = m_e/(m_{\pi^-} - m_{\pi^0})$; this yields $\Gamma(\pi^- \to \pi^0 + e^- + \bar\nu)/\Gamma(\pi^- \to \mu + \bar\nu) = 1.057 \times 10^{-8}$ in agreement with experiment: $1.025 \pm 0.034 \times 10^{-8}$. The model-dependence in the radiative correction is modest, and one may use this process to estimate $|U_{ud}|$, but the accuracy is currently limited by the statistics of experiment due to a small branching ratio.

Kaon beta decay is the process of prime importance for deriving $|U_{us}|$. The crucial issue is reliable calculation of $f_+(0)$. In a first approximation, $f_+(0)$ is determined by extending algebra of the vector current to flavour SU(3). Although SU(3) symmetry is largely broken, the effect on the vector-current process appears only in the second order of symmetry breaking by virtue of the Ademollo–Gatto theorem [341]. For precise determination of $|U_{us}|$, however, we need to estimate $f_+(0)$ more accurately. The method currently adopted (Leutwyler and Roos [342]) is to expand $f_+(0) = f_0 + f_1 m_q + f_2 m_q^2 + \ldots$ in powers of quark mass. The leading term is obviously $f_0 = 1$ from SU(3) symmetry. f_1 and f_2 are calculated by using chiral perturbation theory. Leutwyler and Roos obtained $f^{K^0 \to \pi^-}(0) = 0.961 \pm 0.008$.

The calculation of the decay rate is similar to π beta decay but is a bit more complicated. We must consider the q^2 dependence of the form factor and a nonvanishing f_- component (a second-order effect). For the form factors, we assume

$$f_\pm(q) = f_\pm(0)\left(1 - \frac{q^2}{M_\pm^2}\right) \,, \tag{3.39}$$

where $M_\pm$ are parameters of the mass dimension that are directly estimated from the lepton spectrum. Using experimental decay rates, Leutwyler and Roos obtained $|U_{us}| \simeq 0.2188 \pm 0.003$ for $K^0 \to \pi^-$ decay. Here, the errors from experiment and a theoretical estimate for f_+ are about even. The value from $K^+ \to \pi^0$ is 0.2248 ± 0.003 which is larger by 2.8%. It is noted that π^0 is mixed with η in the presence of isospin breaking, and it modifies $f_+^{K^+ \to \pi^0}$ by a few percent in the first-order coefficient f_0: $f_+^{K^+ \to \pi^0}/f_+^{K^0 \to \pi^-} = 1.022$. This removes the disparity in the two values beyond the statistical error of

experiment (1%). By averaging the two values, they obtained

$$|U_{us}| = 0.2196 \pm 0.0023 , \qquad (3.40)$$

which is the best current value for this matrix element.

3.6 Theory of Nuclear Beta Decays

3.6.1 Fermi Theory

Nuclear beta decays have been one of the major subjects of nuclear physics for many years. There are many complications as well as rich physics concerning nuclear structure. It is beyond the scope of this book to review such theories, and we must defer the discussion to standard textbooks of nuclear beta decays, e.g., Morita [343] and Blin-Stoyle [344]; here we must content ourselves with introductory aspects.

For elementary beta decay $n \to p + e^- + \bar{\nu}_e$, the most general matrix element for the nucleon is written

$$\langle N(p')|V_\mu|N(p)\rangle = \bar{u}(p')\left(\gamma_\mu F_{\mathrm{V}} + \frac{1}{2m_N}i\sigma_{\mu\nu}q^\nu F_W + \frac{1}{m_N}q^\nu F_{\mathrm{S}}\right)u(p), \quad (3.41)$$

$$\langle N(p')|A_\mu|N(p)\rangle = \bar{u}(p')\left(\gamma_\mu\gamma_5 F_{\mathrm{A}} + \frac{1}{2m_N}i\gamma_5\sigma_{\mu\nu}q^\nu F_{\mathrm{PT}} + \frac{1}{m_N}\gamma_5 q_\mu F_{\mathrm{P}}\right)u(p) ,$$

Here F_{S} vanishes by virtue of CVC, and F_{PT} should also vanish in the presence of isospin symmetry (second-class current). The pseudoscalar term (F_{P}) is multiplied by m_e^2 for beta decay matrix elements and hence is negligible. This leaves three form factors. When the momentum transfer between the two nucleons is small, we may drop the weak magnetism (tensor) term F_W that accompanies q and approximate the vector and axial-vector form factors with two constants: $F_{\mathrm{V}}(0) = g_V = 1$ and $F_{\mathrm{A}}(0) = g_A$; the former again is a consequence of the CVC. We remark that $F_W(0)$ is also fixed by CVC: $F_W(0) = \mu_p^a - \mu_n^a$, where $\mu_p^a = \mu_p - 1$ and $\mu_n^a = \mu_n$ are anomalous magnetic moments of the proton and neutron in units of the nuclear magneton $\mu_N = e/2m_N$. The effect of F_W (weak magnetism) was tested through the size of asymmetry in the energy spectrum of $\beta^\pm$ decay of ^{12}N$\to^{12}$C and ^{12}B$\to^{12}$C [63].

The ordinary treatment of beta decays uses

$$\langle N(p')|V_\mu - A_\mu|N(p)\rangle = \bar{u}(p')\gamma_\mu(1 - g_A\gamma_5)u(p) . \qquad (3.42)$$

We may therefore work with the effective Hamiltonian,

$$H = \frac{G_{\mathrm{V}}}{\sqrt{2}}\bar{e}\gamma^\mu(1 - \gamma_5)\nu \, \bar{p}\gamma_\mu(1 - g_A\gamma_5)n , \qquad (3.43)$$

where $G_{\mathrm{V}} = G_{\mathrm{F}}|U_{ud}| = G_{\mathrm{F}}\cos\theta_c$.

Using the nonrelativistic reduction (Pauli reduction) for the nucleon part, we obtain the matrix element squared:

$$\frac{1}{2}|T|^2 = \frac{G_V^2}{2} 8 E_e E_\nu \left[(1 + \beta \cos\theta) + 3g_A^2 \left(1 - \frac{\beta}{3} \cos\theta \right) \right], \qquad (3.44)$$

where E_e and E_ν are the electron and neutrino energies, $\beta = p_e/E_e$ is the velocity, θ is the angle between e and $\bar{\nu}_e$, and the factor $4m_N^2$ is removed to make the expression agree with conventional nonrelativistic normalisation. The decay rate is given by

$$\begin{aligned}\Gamma &= \int \frac{d^3p_e}{2E_e(2\pi)^3} \frac{d^3p_\nu}{2E_\nu(2\pi)^3} (2\pi)\delta(E_0 - E_e - E_\nu)\frac{1}{2}|T|^2 \\ &= \frac{G_F^2}{2\pi^3}|U_{ud}|^2 \int_{m_e}^{E_0} dE_e E_e p_e E_\nu p_\nu \, [1 + 3g_A^2] , \end{aligned} \qquad (3.45)$$

where $E_0 = Q + m_e$ with $Q = m_n - (m_p + m_e)$.

Nuclear beta decay generally includes the nuclear matrix elements

$$\langle f|\chi_p^\dagger \chi_n|i\rangle = \langle 1 \rangle$$
$$\langle f|\chi_p^\dagger \boldsymbol{\sigma} \chi_n|i\rangle = \langle \boldsymbol{\sigma} \rangle \qquad (3.46)$$

in the vector and the axial-vector parts, respectively (NB: $\langle 1 \rangle = 1$, and $\langle \boldsymbol{\sigma} \rangle^2 = 3$ for nucleons). These matrix elements are referred to as the Fermi and Gamow–Teller (GT) matrix elements. Instead of (3.45),

$$\Gamma = \frac{G_V^2}{2\pi^3} \int_{m_e}^{E_0} dE_e E_e p_e E_\nu p_\nu \, [\langle 1 \rangle^2 + g_A^2 \langle \boldsymbol{\sigma} \rangle^2] F(E_e, Z), \qquad (3.47)$$

where we insert the Fermi function $F(E_e, Z)$ correcting for Coulomb attraction between the electron and nucleus with charge Z (see below).

Writing

$$f(E_0, Z) = \int_1^{w_0} w\sqrt{w^2 - 1}(w_0 - w)^2 \, F(w, Z)dw \qquad (3.48)$$

for $m_\nu = 0$ ($w_0 = E_0/m_e$), we obtain

$$\Gamma = \frac{G_V^2}{2\pi^3} m_e^5 \, f(E_0)[\langle 1 \rangle^2 + g_A^2 \langle \boldsymbol{\sigma} \rangle^2]. \qquad (3.49)$$

Using half-life, $t = \ln 2/\Gamma$,

$$|M_\beta|^2 \equiv \langle 1 \rangle^2 + g_A^2 \langle \boldsymbol{\sigma} \rangle^2 = \frac{2\pi^3 \ln 2}{(ft)m_e^5 G_V^2} = 6291.7\,\mathrm{s}/(ft), \qquad (3.50)$$

where the numerical value does not include any corrections and $\cos\theta_c = 0.974$ is used. This equation states that the size of the nuclear matrix element is represented by the ft (or $\log ft$) values.

From (3.47) the electron spectrum (for $m_\nu = 0$) is

$$\frac{d\Gamma}{dE_e} \propto E_e \sqrt{E_e^2 - m_e^2} (E_0 - E_e)^2 F(E_e, Z), \qquad (3.51)$$

and the neutrino spectrum is

$$\frac{d\Gamma}{dE_\nu} \propto E_\nu^2 (E_0 - E_\nu) \sqrt{(E_0 - E_\nu)^2 - m_e^2} . F(E_e, Z) . \qquad (3.52)$$

When m_e and the Fermi function are ignored, the shape is

$$d\Gamma/dx \simeq x^2 (1 - x)^2, \qquad (3.53)$$

where $x = E_\nu / E_0$.

The Fermi function for Coulomb distortion.   The electron wave function of the beta ray is distorted by Coulomb interaction with the final state nucleus. The outgoing wave function (normalised to $e^{i\mathbf{p}\mathbf{r}}$ at infinity) for an attractive Coulomb field is

$$\psi_p^{(+)}(\mathbf{r}) = e^{\pi\eta/2} \Gamma(1 - i\eta) e^{i\mathbf{p}\mathbf{r}} F(i\eta, 1; i(pr - \mathbf{p}\mathbf{r})) , \qquad (3.54)$$

where $F(a, b; x)$ is the confluent hypergeometric function and $\eta = Z\alpha m_e/p$. The action of the Coulomb field on the motion of a particle near the origin is given by $\psi_p^{(+)}(0)$. Compared with the plane wave $\psi_p = e^{i\mathbf{p}\mathbf{r}}$, we obtain[1] the enhancement

$$F(E, Z) = \frac{|\psi_p^{(+)}(0)|^2}{|\psi_p(0)|^2} = \frac{2\pi\eta}{1 - e^{-2\pi\eta}} , \qquad (3.55)$$

where we have used $\Gamma(1 + i\eta)\Gamma(1 - i\eta) = \pi\eta / \sinh(\pi\eta)$. For repulsion (for β^+ decay),

$$F(E, Z) \simeq \frac{2\pi\eta}{e^{2\pi\eta} - 1} . \qquad (3.56)$$

A more accurate treatment can be done by using the solution of the Dirac equation in the Coulomb field and comparing it with the plane wave at the nuclear surface [20]. After some calculation (see e.g., [343] for a derivation),

$$F(E, Z) = \frac{1 + \gamma}{2} 4(2pR)^{2\gamma - 2} e^{\pi\eta} \frac{|\Gamma(\gamma + i\eta)|^2}{[\Gamma(2\gamma + 1)]^2} , \qquad (3.57)$$

---

[1] This treatment is invalid for relativistic wave functions, which are singular at the origin. More appropriately, the Fermi function is given by the wave functions at the nuclear radius rather than at the origin.

where $\gamma = \sqrt{1 - \alpha^2 Z^2}$ and

$$\eta = \alpha Z E / p. \tag{3.58}$$

When $\gamma \approx 1$, this Fermi function reduces to (3.55) [or (3.56)] where η is substituted by (3.58).[2]

Radiative corrections.   Radiative corrections to beta decay[3] are given by Feynman diagrams shown in Fig. 3.1. These corrections are divergent within QED and become convergent with the Weinberg–Salam theory [346]. Sirlin divided the corrections into the 'outer part', which does not depend on the details of strong interaction and the short-distance behaviour of the weak interaction, and the rest, which is called the 'inner part' [347] (see also [336]). Writing the nucleon vertex of the beta decay as $W_\nu(p_2, p_1)$ with p_1 and p_2 the neutron and proton momenta, the outer part is defined by the QED correction that is written as an overall multiplicative factor on the decay width, irrespective of the details of W. This includes a part of the vertex correction (Fig. 3.1a), the self-energies of the electron and proton (Fig. 3.1b,c), and the bremsstrahlung (Fig. 3.1d,e). The vertex correction is give by

$$M^{(a)} = \frac{G_V}{\sqrt{2}} i e^2 \int \frac{d^4 k}{(2\pi)^4} \frac{1}{(\ell - k)^2 - m_e^2} \frac{1}{(p_2 + k)^2 - m_p^2} \frac{1}{k^2 - \lambda^2}$$
$$\bar{u}_e(\ell)\gamma^\mu[(\slashed{\ell} - \slashed{k}) + m_e]\gamma^\nu(1 - \gamma_5)v_\nu(\ell')$$
$$\bar{u}_p(p_2)\gamma_\mu[(\slashed{p}_2 + \slashed{k}) + m_p]W_\nu(p_2 + k, p_1)u_n(p_1), \tag{3.59}$$

where ℓ is the electron momentum, k is the photon momentum, and λ is the photon mass that serves as a regulator for the IR divergence. The division

p e^- $\bar{\nu}_e$

n

(a)   (b)   (c)   (d)   (e)
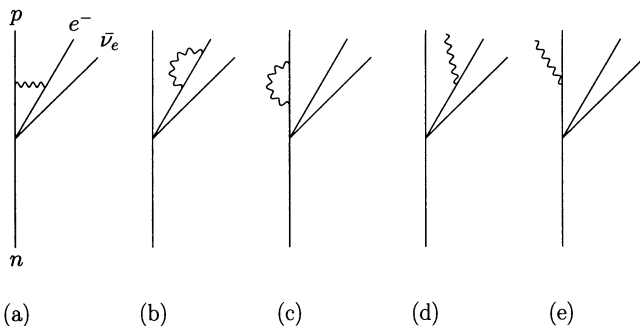
Fig. 3.1.   Feynman diagrams for QED radiative corrections to beta decay.

---

[2] For more accurate correction factors using a numerical solution of the Dirac equation for finite nuclei, see [345].

[3] The authors thank T. Kubota for discussion.

is made by writing the vertex as $W_\nu(p_2 + k, p_1) = W_\nu(p_2, p_1) + [W_\nu(p_2 + k, p_1) - W_\nu(p_2, p_1)]$, where the first term is identified as the outer part and the terms in the square bracket as the inner part.

Writing the correction factor as $1 + \delta_{\text{out}}^{(a,b,c)} + \delta_{\text{out}}^{(d,e)}$, the contribution from diagrams (a)–(c) is given by

$$\delta_{\text{out}}^{(a,b,c)} = \frac{e^2}{8\pi^2} \left[1 + \ln\left(\frac{\Lambda^2}{m_e^2}\right) - \frac{2}{\beta} \text{th}^{-1}\beta \ln\left(\frac{m_e^2}{\lambda^2}\right) + \frac{2}{\beta} L\left(\frac{2\beta}{1+\beta}\right) \right. \quad (3.60)$$
$$\left. - \frac{2}{\beta}(\text{th}^{-1}\beta)^2 + 2\beta\text{th}^{-1}\beta \right] + 2\left(Z_2(e)^{1/2} - 1 + Z_2(p)^{1/2} - 1 \right),$$

where Λ is a momentum cutoff, Z_2 is the renormalisation constant for the electron and proton, and $L(x)$ is dilogarithm (Spence function) defined below. The UV divergence of the vertex part (the second term) is cancelled by the wave function renormalisation of the electron and proton. The expression involves an infrared divergence, which is cancelled when the contribution from the bremsstrahlung

$$\delta_{\text{out}}^{(d,e)} = \frac{e^2}{8\pi^2} \left[2 + \left(\frac{4}{\beta}\text{th}^{-1}\beta - 4 \right)\left(\ln\frac{2(E_0 - E)}{\lambda} - \frac{3}{2} \right) \right.$$
$$+ \frac{4}{3}\frac{E_0 - E}{E}\left(\frac{1}{\beta}\text{th}^{-1}\beta - 1 \right) + \frac{1}{6}\frac{(E_0 - E)^2}{E^2}\frac{1}{\beta}\text{th}^{-1}\beta$$
$$\left. + \frac{2}{\beta}\text{th}^{-1}\beta - \frac{2}{\beta}(\text{th}^{-1}\beta)^2 + \frac{2}{\beta}L\left(\frac{2\beta}{1+\beta}\right) \right] \quad (3.61)$$

is added. Here we have integrated over all available photon energy.

The inner part of the QED correction (a part of (3.59)), which depends on the structure of W, is UV divergent (it is IR convergent), and this divergence is cancelled after the inclusion of the full electroweak radiative corrections. Sirlin [347] showed that only the outer part depends on E and E_0, thus depending on the beta decay process, whereas the inner part amounts to the modification of the coupling strengths when the terms of order of $\alpha(E/m_p)\ln(E/m_p)$ are neglected. We write the radiative corrections by replacing $|M_\beta|^2$ with

$$\left[\langle 1 \rangle^2 \left(1 + \frac{\alpha}{\pi}C \right) + g_A^2 \langle \sigma \rangle^2 \left(1 + \frac{\alpha}{\pi}D \right) \right] \left[1 + \frac{\alpha}{2\pi}g(E, E_0) \right], \quad (3.62)$$

where $(\alpha/\pi)C$ and $(\alpha/\pi)D$ are the inner part which is often denoted as δ_{in}. Adding (3.60) and (3.61), the outer part $\delta_{\text{out}} = (\alpha/2\pi)g(E, E_0)$ is given by[4]

---

[4] If we use the conventional Z_2 factor

$$Z_2 = 1 - \frac{e^2}{16\pi^2}\left(\ln\frac{\Lambda^2}{m^2} + \frac{9}{2} - 2\ln\frac{m^2}{\lambda^2} \right),$$

we obtain a constant $-3/2$, instead of $-3/4$. Sirlin defined the proton self-energy correction in a different way.

$$g(E, E_0) = 3 \ln\left(\frac{m_p}{m_e}\right) - \frac{3}{4} + \frac{4}{\beta} L\left(\frac{2\beta}{1+\beta}\right)$$
$$+ 4(\text{th}^{-1}\beta/\beta - 1)\left[\frac{E_0 - E}{3E} - \frac{3}{2} + \ln\frac{2(E_0 - E)}{m_e}\right]$$
$$+ \frac{1}{\beta}\text{th}^{-1}\beta\left[2(1 + \beta^2) + \frac{(E_0 - E)^2}{6E^2} - 4\text{th}^{-1}\beta\right], \quad (3.63)$$

where

$$L(x) = \int_0^x \frac{dt}{t}\ln(1 - t). \quad (3.64)$$

After taking average over the electron spectrum, one finds

$$\bar{g} \approx 3\ln\frac{m_p}{2E_0} + \frac{81}{10} - \frac{4\pi^2}{3}, \quad (3.65)$$

which is an asymptotic formula for $E_0 \gg m_e$ and $F = 1$ [333].

The same expression also applies to β^+ decay. Although the Feynman diagrams involved in β^+ decay appear quite different, the Feynman integral is identical with that for the β^- decay up to the sign of the four-momentum of the proton. This leaves (3.63) unchanged.

In the Weinberg–Salam theory, the UV cutoff is automatically given by the gauge-boson mass, and the correction for the Fermi matrix element is [348]

$$\delta_{\text{in}} = \frac{\alpha}{\pi}C \simeq \frac{\alpha}{2\pi}\left(4\ln\frac{M_Z}{m_p} + \ln\frac{m_p}{m_A} + 2c_A\right) \quad (3.66)$$
$$\simeq 0.0234 \pm 0.0008, \quad (3.67)$$

where the last two terms arise from corrections for the axial-vector current (induced by radiative corrections), and $m_A \approx 1 \pm 0.6$ GeV is an effective infrared cutoff parameter of the loop integral. The constant c_A is a long-distance correction that depends on the nuclear structure. Marciano and Sirlin [348] estimated it for free nucleons to give $c_A \simeq 0.798g_A(\mu_p + \mu_n)/\mu_N = 0.885$. Shell model calculations give values close to this free nucleon model, 0.881 ± 0.030 [349]. Note that m_p does not appear in the final result of $\delta_{\text{in}} + \delta_{\text{out}}$.

When the inner correction (3.67) is included, the coefficient of (3.50) becomes 6147 s. It has also been noted that there is a process-dependent constant correction arising from the axial-vector–current-induced process involving two nucleons [350] c_{NS}, and it is included in the outer part as $[g(E, E_0) + 2c_{\text{NS}}]$; c_{NS} is calculated in [350, 349].

Accurate calculations are not available for D (see [336] for discussion), but it is not essential for most cases because the GT matrix element is not known to such accuracy that radiative corrections matter (except for free neutron beta decay). We note that the sign of the radiative correction for beta decay is opposite to that for muon decay, and the former [typically $+(3 - 4)\%$] is larger than the latter (-0.4%) by an order of magnitude.

Analysis of neutron beta decay.   When an accurate evaluation is necessary for the Fermi transition, the integral of f in (3.48) is replaced by

$$f(E_0, Z) = \int_1^{w_0} w\sqrt{w^2 - 1}(w_0 - w)^2 F(w, Z)C(w)dw , \qquad (3.68)$$

with C the spectral shape factor, which takes account of (i) the screening effect of atomic electrons, (ii) the dependence of the nuclear matrix element on E_e, and (iii) the correction from second-forbidden matrix elements.

Let us now discuss neutron decay in some detail [351]. Ignoring the Fermi function, integration of (3.48) gives

$$f(E_0) = (w_0^2 - 1)^{1/2} \left(\frac{1}{30}w_0^4 - \frac{3}{20}w_0^2 - \frac{2}{15} \right)$$
$$+ \frac{w_0}{4} \ln |w_0 + (w_0^2 - 1)^{1/2}|. \qquad (3.69)$$

The proton neutron mass difference is

$$\Delta = m_n - m_p = 1.2933318 \, \text{MeV}, \qquad (3.70)$$

and the electron end-point energy is $E_0 = (m_n^2 - m_e^2 - m_p^2)/2m_n$, or $w_0 = \Delta/m_e - [(\Delta/m_e)^2 - 1](m_e/2m_n)$, including a nucleon recoil correction, so that $f(E_0) = 1.62989$. From (3.50),

$$|U_{ud}|^2 = \frac{2\pi^3}{\tau_n m_e^5 G_F^2 f(E_0)[1 + 3(g_A/g_V)^2]} = \frac{5283.2 \, \text{s}}{\tau_n[1 + 3(g_A/g_V)^2]} . \qquad (3.71)$$

The Coulomb corrections increases $f(E_0)$ by $+0.05603$ and the outer radiative correction amounts to $+0.02542$. The next important correction is the effect of nucleon recoil on the phase space [352], which is $+0.00282$. Wilkinson [351] examined other small terms in detail and found an extra correction of $+0.00066$. Altogether, we have $f(E_0) = 1.71483$. Including the inner radiative correction of (3.67), we find $f(E_0) = 1.75495$, and thus

$$|U_{ud}|^2 = \frac{4906.7 \pm 5 \, \text{s}}{\tau_n[1 + 3(g_A/g_V)^2]} , \qquad (3.72)$$

where the inner radiative correction for the axial-vector part is set equal to that for the vector part, following Marciano [353]. The error, which is largely from the inner radiative correction, is also borrowed from [353].

Using the current value of the decay rate

$$\tau_n = 886.7 \pm 1.9 \, \text{s} , \qquad (3.73)$$

and

$$g_A = 1.2670 \pm 0.0035 , \qquad (3.74)$$

we obtain

$$|U_{ud}| = 0.9754 \pm 0.0030 . \qquad (3.75)$$

3.6.2 Classification of Nuclear Beta Decays

For a nucleus with A nucleons, Z protons, and N neutrons ($A = Z + N$), the matrix element of (3.46) is replaced with

$$\langle 1 \rangle = \langle \Psi_f(1, 2, ..., A)| \sum_{k=1}^{A} \tau_+^{(k)} |\Psi_i(1, 2, ..., A) \rangle \, ,$$

$$\langle \boldsymbol{\sigma}_i \rangle = \langle \Psi_f(1, 2, ..., A)| \sum_{k=1}^{A} \tau_+^{(k)} \boldsymbol{\sigma}_i^{(k)} |\Psi_i(1, 2, ..., A) \rangle \, , \qquad (3.76)$$

where we insert the isospin raising operator $\tau_+ = \tau_1 + i\tau_2$ for β^- decay. The matrix element squares (summed over spins) are often denoted as $B(F)$ and $B(GT)$. It is convenient to introduce reduced matrix elements since we are not usually interested in magnetic quantum numbers and the matrix element with a different quantum number is related to each other by the Wigner–Eckart theorem. We define the reduced matrix element for an operator $T_{\lambda\lambda_z}$ of the spherical tensor of rank λ with the third component λ_z by

$$\langle J_f M_f | T_{\lambda\lambda_z} | J_i M_i \rangle = \frac{1}{\sqrt{2J_f + 1}} (J_i M_i \lambda \lambda_z | J_f M_f) \langle J_f \| T_\lambda \| J_i \rangle \, , \qquad (3.77)$$

where $(J_i M_i \lambda \mu | J_f M_f)$ is the Clebsch–Gordan coefficient and the double stripes mean the reduced matrix element that does not depend on magnetic quantum numbers. The transition probability is the sum over M_f and λ_z, so that

$$\sum_{M_f, \lambda_z} |\langle J_f M_i | T_{\lambda\lambda_z} | J_i M_i \rangle|^2$$

$$= \frac{1}{2J_i + 1} \frac{1}{2J_f + 1} \sum_{M_i, M_f, \lambda_z} |(J_i M_i \lambda \lambda_z | J_f M_f)|^2 |\langle J_f \| T_\lambda \| J_i \rangle|^2$$

$$= \frac{1}{2J_i + 1} |\langle J_f \| T_\lambda \| J_i \rangle|^2 \, , \qquad (3.78)$$

using the orthogonality relation for the Clebsch–Gordan coefficients. Therefore,

$$B(F) = |\langle 1 \rangle|^2 = |\langle J_f T_f \| \sum_{k=1}^{A} \tau_+^{(k)} \| J_i T_i \rangle (2J_i + 1)^{-1/2}|^2 \, ,$$

$$B(GT) = |\langle \boldsymbol{\sigma} \rangle|^2 = |\langle J_f T_f \| \sum_{k=1}^{A} \boldsymbol{\sigma}^{(k)} \tau_+^{(k)} \| J_i T_i \rangle (2J_i + 1)^{-1/2}|^2 \, . \qquad (3.79)$$

The Fermi matrix element is particularly simple since the operator is simply the total isospin operator T_+. Therefore, the matrix element is nonvanishing only for $\Delta T = 0$, $\Delta J = 0$, and no parity change. For $|\Psi_i\rangle = |J, T, T_3\rangle$

and $|\Psi_f\rangle = |J, T, T_3 + 1\rangle$,

$$\langle 1 \rangle = \sqrt{(T - T_3)(T + T_3 + 1)} \, . \tag{3.80}$$

For the mirror transition ($A = $ odd, $|N - Z| = 1$), $T = 1/2$, and $\langle 1 \rangle^2 = 1$; for the $0^+ \rightarrow 0^+$ transition, which occurs only among $T = 1$ triplets, $\langle 1 \rangle^2 = 2$. When the Fermi transition is allowed, beta decay is called superallowed. With $\langle 1 \rangle^2 \geq 1$, $ft \leq 6000$ ($\log ft \leq 3.8$). The fastest decays are ^{6}He and ^{18}Ne, for which $ft \simeq 800$.

The Gamow–Teller matrix element [24] $\langle \boldsymbol{\sigma} \rangle$ is nonvanishing if $\Delta T = 0$, ± 1, $\Delta J = 0$, ± 1, and parity is conserved ($J = 0 \rightarrow J = 0$ is forbidden, however). Such a transition is called 'allowed.' A typical $\log ft$ is around 5, but it may vary from 4 to 9. The GT transition element depends on the details of the nuclear structure, and the calculation has been a major subject in nuclear physics for many years.

Beta decay with vanishing Fermi and GT elements is called a forbidden transition; the spatial structure of the nuclear part then becomes relevant. The spatial integral of the nonrelativistic Hamiltonian should be replaced by [20]

$$\int d^3 x \langle f | \chi^\dagger(\mathbf{x}) O \chi(\mathbf{x}) | i \rangle e^{i\mathbf{k}\mathbf{x}} \, , \tag{3.81}$$

where the exponential comes from plane waves of the two outgoing leptons and $\mathbf{k}$ is the sum of lepton momenta. Multipole expansion of $e^{i\mathbf{k}\mathbf{x}}$ gives a systematic classification of forbidden transitions [28]. The term involving $\mathbf{x}$ is called first-forbidden transitions, which are subject to the selection rule $\Delta J = 0, \pm 1, \pm 2$, and a unit parity change. The relevant operators are

$$\int \mathbf{x} \, , \qquad \int \boldsymbol{\sigma} \cdot \mathbf{x} \, , \qquad \int \boldsymbol{\sigma} \times \mathbf{x} \, , \qquad \int B_{ij} \, , \tag{3.82}$$

where $B_{ij} = x_i \sigma_j - x_j \sigma_i - (2/3)\delta_{ij}\boldsymbol{\sigma} \cdot \mathbf{x}$. There is another class of first-forbidden transitions induced by nonvanishing small components of the Dirac spinors in the nonrelativistic reduction. The operators are

$$\int \gamma_5 \, , \qquad \int \boldsymbol{\alpha} \, . \tag{3.83}$$

The matrix elements involving $O(x^2)$, $O(p^2)$, or $O(xp)$ (p is the momenta of nucleons) give second-forbidden transitions. We do not discuss forbidden transitions further, since they are not important to us.

3.6.3 Electron Capture

A process closely related to beta decay is electron capture, in which an electron in a low atomic orbit is captured by a nucleus with the emission of a neutrino: $e^- + (A, Z) \rightarrow (A, Z - 1) + \nu$. This process was predicted by

Yukawa and Sakata as a consequence of the Fermi theory [354] and was discovered by Alvarez for ^{67}Ga [355]. This is the process that takes place in proton-rich nuclei (relative to the nuclear valley) together with β^+ decay, whereas ordinary β^- decay occurs in neutron-rich nuclei. The importance of this process in our context is that this is inverse to neutrino capture. Unstable nuclei formed by low-energy neutrino reactions necessarily undergo this electron capture back to original nuclei, and therefore are used to identify neutrino capture.

It is appropriate to discuss briefly the Q value and mass differences involved in various neutrino processes. The mass of a nucleus is usually represented by the neutral atomic mass, the sum of masses of a nucleus and atomic electrons, denoted here as $M(A, Z)$ [356]. The maximum kinetic energy release in β^- decay of $(A, Z - 1) \rightarrow (A, Z)$ is therefore $\Delta M = M(A, Z-1) - M(A, Z)$ (ignoring the electron binding energy), where $M(A, Z)$ includes the mass of a newly produced electron. For electron capture, the maximum kinetic energy release is also $\Delta M = M(A, Z+1) - M(A, Z)$ which accounts for annihilation of electron mass. This ΔM is exactly the threshold energy of the neutrino capture reaction. In β^+ decay, a positron is produced, and the final nucleus has one excess electron; so the maximum kinetic energy release is $\Delta M = M(A, Z + 1) - [M(A, Z) + 2m_e]$. If the mass difference of the atoms $(A, Z + 1)$ and (A, Z) is less than $2m_e$, electron capture is the only allowed beta process for proton-rich nuclei. We write ΔM as exothermic energy Q.

The electron capture rate for a nucleus with (A, Z) is given by

$$\Gamma = N|\Psi(0)|^2 G_V^2 \int \frac{4\pi q^2 dq}{(2\pi)^3} (2\pi)\delta(Q - E_\nu - E_X)\frac{1}{2}|M_\beta|^2 , \qquad (3.84)$$

where $\Psi(x)$ is the wave function of the orbital electrons, N is the number of electrons in the relevant shell, and E_X is the binding energy of the shell. For the K orbit, $\Psi_{n=1,\ell=0} = \pi^{-1/2}(Z/a_0)^{3/2} \exp(-Zr/a_0)$ with the Bohr radius $a_0 = (m_e \alpha)^{-1}$ for the hydrogen-like wave function of charge Z. The matrix element M_β in (3.84) is the same as that for the β^- decay of (3.50). It then follows that

$$\Gamma = \frac{G_V^2}{\pi^2}(Q - E_X)^2 (m_e \alpha Z)^3 |M_\beta|^2 , \qquad (3.85)$$

where N is set equal to 2. The emitted neutrino is monoenergetic with energy equal to $E_\nu = Q - E_X$.

As is clear from (3.84), capture takes place only from $\ell = 0$ states. (NB: For a relativistic wave function, it takes place from both $s_{1/2}$ and $p_{1/2}$, although the latter is suppressed.) Since $|\Psi(0)_{nl}|^2 = \delta_{\ell 0}|\Psi(0)_{10}|^2/n^3$, the ratio of captures from the L and K orbits is

$$\frac{\Gamma_K}{\Gamma_L} = \frac{1}{8}\frac{(Q - E_L)^2}{(Q - E_K)^2}, \qquad (3.86)$$

where E_K and E_L are binding energies for the K and L orbits.

It is interesting to compare the electron capture rate with the β^+ decay rate. When $Q \gg m_e$ the β^+ decay rate, which is given by the same expression as (3.49), is [see (3.69)],

$$\Gamma(\beta^+) \simeq \frac{G_V^2}{2\pi^3} \frac{Q^5}{30} |M_\beta|^2 \,. \tag{3.87}$$

Therefore,

$$\frac{\Gamma_K}{\Gamma_{\beta^+}} \simeq 60\pi \left(\frac{m_e}{Q}\alpha Z\right)^3 , \tag{3.88}$$

which means that β^+ decay dominates if kinematically allowed.

There are some secondary processes associated with electron capture. Electron capture creates a hole in a lower electron orbit, and an electron at a higher orbit undergoes a transition to fill the hole. This either produces X rays or leads to associated emission of another electron (Auger electron). For K-shell electron capture, the X ray is called a K X ray and its energy, when the transition takes place from the L orbit (i.e., K_α), is given by

$$E_{K_\alpha(i)} = E_K - E_{L_i}, \tag{3.89}$$

where L_i is the ith L shell, sometimes named $i =$ I, II, III, etc., in order of decreasing binding energies.[5] E_K, E_L etc. are tabulated in [358] (see also [359]). Vacancies in the K shell are sometimes filled by an electron fell from a higher orbit, say the X shell, and the liberated energy is used to emit a second electron from another orbit, say the Y shell. This process is called the KXY Auger transition. For instance, when one of the L shell electrons is emitted while one of them undergoes a transition to the K orbit, the energy of an Auger electron is

$$E_{KLL} = (E_K - E_{L_i}) - E_{L_j}^{(i)} \tag{3.90}$$

where $E_{L_j}^{(i)}$ is the binding energy of an L shell with the L_i orbit having a hole and is approximated as $E_{L_j}^{(i)}(Z) \approx E_{L_j}(Z + \Delta Z)$, where ΔZ is somewhat smaller than unity. The table cited above can be used to calculate the energy of Auger electrons fairly accurately. The fractional yield of K X rays (called fluorescence yield) depends on the charge of the nucleus as

$$f_{K_X}/(1 - f_{K_X}) = (-a + bZ - cZ^3) , \tag{3.91}$$

where $a \simeq 4 - 6 \times 10^{-2}$, $b \simeq 3 \times 10^{-2}$, and $c \simeq 1 \times 10^{-6}$. The relative yield of KL_iL_j Auger transitions $(i, j =$ I,II,III) is given in [359]. In ^{37}Cl or ^{71}Ga solar neutrino experiments, K X rays and KLL Auger electrons are dominant signatures for counting the number of captured neutrinos. Examples of the binding energy are given in Table 3.1.

---

[5] The transitions are sometimes named K_{α_1}=K$-$L$_{III}$, K_{α_2}=K$-$L$_{II}$, K_{β_1}=K$-$M$_{III}$, K_{β_2}=K$-$N$_{III}$, according to Siegbahn [357].

Table 3.1. Binding energies of K, L, and M shells in units of keV.

	$E(K)$	$E(L_I)$	$E(L_{II})$	$E(L_{III})$	$E(M_I)$	$E(M_{II,III})$
Cl	2.822	0.270	0.202	0.200	0.018	0.007
Ga	10.367	1.194	1.043	1.020	0.136	0.087

3.6.4 $0^+ \rightarrow 0^+$ Transitions

Superallowed transitions where the GT transition is forbidden are particularly simple and important. By virtue of vector-current conservation, the matrix element is not corrected by strong interaction physics: it is independent of nuclear structure and can then be used to estimate the precise strength of beta decay G_V, and hence $|U_{ud}|$. This takes place for the transition from a $J = 0$ state to another $J = 0$ state. All known $0^+ \rightarrow 0^+$ transitions are $T = 1$ triplets, and therefore $\langle 1 \rangle^2 = 2$ with the nominal ft value $ft \approx 3146$ s from (3.50). The measured transitions are β^+ decays: ^{10}C, ^{14}O, ^{26m}Al, ^{34}Cl, ^{38m}K, ^{42}Sc, ^{46}V, ^{50}Mn, and ^{54}Co, where alminium and potassium are isomeric states, whose ground states are $J^P = 5^+$ and 3^+, respectively. With an exception of ^{10}C, β^+ decay is the predominant decay mode of the ground state ($> 99\%$). The ft values are obtained after correcting for the electron capture mode (with a calculation), which is of the order of 0.1%.

We have already discussed spectral distortion by Coulomb interactions and radiative corrections. In addition, we must take account of other nuclear corrections in (3.68). This is the most difficult part for the $0^+ \rightarrow 0^+$ transitions because they depend explicitly on nuclear structure. The correction arises from two effects: (i) binding of protons is weaker than that of neutrons, leading to the tail of a radial wave function for protons that extends more to the outer part and hence reducing the matrix element, and (ii) configuration mixing in the nuclear shell varies from member to member within the same isomultiplet.

One usually writes this effect by replacing ft with

$$(ft)' = ft(1 + \delta_{\text{out}})(1 - \Delta_c) , \qquad (3.92)$$

where outer radiative corrections are $\delta_{\text{out}} = (\alpha/2\pi)[\langle g(E, E_0) \rangle + 2C_{\text{NS}}] + \delta_2$ with δ_2 a higher order correction of $O(Z\alpha^2)$, which is nonnegligible. Towner and Hardy [360] concluded that higher order radiative corrections of the two groups [361, 362], which appear to disagree, are consistent with one another if a finite-size nuclear charge distribution is taken into account. The leading correction of δ_{out} decreases from 1.5% (^{10}C) to 0.8% (^{54}Co), and higher order corrections of $Z\alpha^2$ increase from 0.2% to 0.5%. Including one photon correction to two nucleons c_{NS}, the total amount of the outer radiative corrections remains nearly constant at 1.3–1.5% for varying nuclei.

The estimate of Δ_c depends on authors, especially for heavy nuclei. Towner and collaborators [363, 360] estimated that it varies from 0.18% for ^{10}C to 0.61% for ^{54}Co. Ormand and Brown [364] gave similar values, but they are smaller by 10−30%. Barker's estimate [365] is consistent with Towner et al.'s for ^{10}C, but his Δ_c decreases for heavier nuclei, contrary to the trend Towner et al. showed. For ^{54}Co, Barker's correction is 0.05%, compared to Towner et al.'s value of 0.61%.

The most recent compilation of $(ft)'$ by Towner and Hardy [360] indicates no systematic variation with Z (using Δ_c of their own or of Ormand and Brown's), and yields an average value

$$(ft)' = 3072.3 \pm 0.9 \, \text{s} \,, \tag{3.93}$$

where only random errors are included. With (3.50),

$$|U_{ud}|^2 = \frac{\pi^3 \ln 2 / m_e^5}{(ft)' G_\mu^2 (1 + \delta_{\text{in}})}$$
$$= \frac{2984.4 \pm 0.1 \, \text{s}}{(ft)'(1 + \delta_{\text{in}})} \,, \tag{3.94}$$

and using the inner radiative correction δ_{in} of (3.67), we obtain

$$|U_{ud}| = 0.9742 \pm 0.0005. \tag{3.95}$$

The dominant sources of errors are those arising from Δ_c (usually taken as 0.02%) and inner radiative corrections for the axial-vector part (0.04%). If one would adopt Barker's Δ_c, $|U_{ud}|$ would become 0.16% smaller, which is three times the error quoted in (3.95). It is difficult to assign a reliable value to the error dominated by such systematics. To reduce the error, one should perhaps focus on $0^+ \to 0^+$ decay of light elements, ^{10}C, and ^{14}O, i.e., p shell nuclei, for which corrections are consistent among different calculations.

3.6.5 Nuclear Structure and Gamow–Teller Matrix Elements

In order to find the wave function that is needed to evaluate GT matrix elements, we must, in principle, solve the Schrödinger equation:

$$H|\Psi(1, 2, ..., A)\rangle = E|\Psi(1, 2, ..., A)\rangle \,, \tag{3.96}$$

with H the summation of kinetic energy and two-body nucleon–nucleon potential energy,

$$H = \sum_{i=1}^{A} K_i + \sum_{i,j=1}^{A} V_{ij}. \tag{3.97}$$

For a many nucleon system, this is practically impossible, but also our knowledge of the two-body potential is not accurate. A number of approximations and truncations are made to handle the problem.

In the first approximation, nuclei are represented by a shell structure, just like atoms which have shell structures with closures at $Z = 2, 8, 18, ...$ corresponding to $n = 1, 2, 3, ...$ energy levels [30] (for nuclear shell model textbooks, see [366]). This empirical rule implies that the nucleus is treated as an assembly of independent nucleons moving in the average potential well, i.e., treated as a one-body problem. If the nuclear potential is close to harmonic, the major shell closure occurs at $N = 2$ ($1s$), 8 ($1s + 1p$), 20 ($1s + 1p + 1d + 2s$), 40 ($1s + ... + 1f + 2p$), etc. Because of the deviation of the potential from the harmonic and the presence of the strong spin-orbit force, however, the grouping is disturbed for higher levels. The grouping that is close to the reality is: $1s_{1/2}$; $1p_{3/2}$, $1p_{1/2}$; $1d_{5/2}$, $2s_{1/2}$, $1d_{3/2}$; $1f_{7/2}$; $2p_{3/2}$, $1f_{5/2}$, $2p_{1/2}$, $1g_{9/2}$; ..., where semicolons mean the closure of major shells. Therefore, the cumulative numbers of states are $N = 2, 8, 20, 28, 50...$, which are called "magic numbers" of nuclei. The shells are called s, p, sd, fp shells, etc. The first three shell closures agree with the harmonic potential case. Note that higher $j = \ell + s$ states have lower energy for given ℓ and s, and that the spin-orbit force is so strong that the $1f_{7/2}$ level is significantly lowered, lying in the middle of the sd and fp shells. Also $1g_{9/2}$ lies close to the fp shell levels. This grouping applies to the proton and the neutron separately; ^{4}He, ^{16}O, and ^{40}Ca form a closed shell. Beyond ^{40}Ca, ^{48}Ca has a closed shell and is stable, but the double magic nucleus ^{56}Ni is β unstable. The ground states of closed shell nuclei have spin-parity $j^P = 0^+$.

Nuclei in the immediate vicinity of a closed shell are expected to be described by a single particle (or hole) configuration as a good approximation. The properties of those nuclei are described by one valence nucleon (hole) in a specific shell. For example, ^{5}He or ^{5}Li (which are unstable nuclei though) are described by a single particle configuration of the neutron or proton in the $1p_{3/2}$ state. This predicts that the ground states of these nuclei have $j^P = 3/2^-$. In the same way, ^{15}N and ^{15}O are described by $(1p_{1/2})^{-1}$ (power -1 means a hole configuration), and hence $j^P = 1/2^-$ is predicted. The prediction of magnetic moments of these nuclei is straightforward and is known to agree with experiment with reasonable accuracy. A similar argument applies to the calculation of a GT matrix element for the transition between mirror nuclei in neighbours of a closed shell; the matrix element is obtained by angular momentum algebra. From (3.76), the GT matrix element for a multinucleon system is given by

$$|\langle f|\boldsymbol{\sigma}|i\rangle|^2 = \sum_{M_f} \sum_m | \int \psi_{J_f, M_f : T_f, T_{3f}} \sum_k \tau_+^{(k)} \sigma_m^{(k)} \psi_{J_i, M_i : T_i, T_{3i}} |^2 . \qquad (3.98)$$

For mirror nuclei, $J_f = J_i = J$, $T_f = T_i = 1/2$. One may also assume that $M_i = J$. With the aid of the Wigner–Eckart theorem to relate the σ_- matrix element with that of σ_z,

$$|\langle f|\boldsymbol{\sigma}|i\rangle|^2 = \frac{J+1}{J} | \int \psi_{J,J} \sum_k \sigma_z^{(k)} \psi_{J,J} |^2 . \qquad (3.99)$$

For a single particle ($k = 1$) configuration,

$$\psi_{J,M} = \sum_{M,\sigma} (\ell, m, 1/2, \sigma | J, M) Y_{\ell,m}(\theta, \phi) \chi_\sigma \ , \qquad (3.100)$$

so that

$$(\psi^\dagger_{J,M}, \sigma_z \psi_{J,M}) = \pm 2M/(2\ell + 1) \ , \qquad (3.101)$$

where $\pm$ refer to $L = \ell \pm 1/2$. The isospin part is trivial (unity). With some algebra for the Clebsch–Gordan coefficients, a single particle GT transition matrix element is given by

$$\begin{aligned} |\langle f|\sigma|i\rangle|^2 &= \tfrac{J+1}{J} \quad \text{for } J_i = J_f = \ell + 1/2 \ , \\ &= \tfrac{J}{J+1} \quad \text{for } J_i = J_f = \ell - 1/2 \ . \end{aligned} \qquad (3.102)$$

Examples of single particle GT matrix elements are compared with experiments in Table 3.2.

The calculation is significantly complicated for nuclei with more than one valence particle. To handle such cases, we form the jj coupled wave function of two particle states:

$$\psi_{j,\mu} = \sum_{m_1 m_2} (j_1 m_1 j_2 m_2 | j\mu) \psi_{j_1 m_1} \psi_{j_2 m_2} \ , \qquad (3.103)$$

and consider two-body interaction energy $\langle \psi_{j,\mu'} | V | \psi_{j,\mu} \rangle$ (V is supposed to be scalar) as a residual of the one-body potential. We then diagonalise the matrix to obtain the energy and the wave function. The form of interaction is generally not well known, so a method conventionally used by shell model physicists is to take the two-body interaction matrix elements as free parameters and find parameters that fit the relevant nuclear spectra best [367]. Angular momentum algebra including Fermi statistics constraints for such a calculation is also quite involved. Shell model physicists prefer to use the

Table 3.2. One-particle transition calculation of GT elements for mirror nuclei in neighbours of the closed shell.

Process	$(J^P, I)_i \to (J^P, I)_f \beta^\pm$	Valence	ft	$B(\text{GT})_{\text{expt}}$	$B(\text{GT})_{\text{sp}}$
$n \to p$	$(1/2^+, 1/2) \to (1/2^+, 1/2)\beta^-$	$s_{1/2}$	1057	3	3
$^3\text{H} \to {}^3\text{He}$	$(1/2^+, 1/2) \to (1/2^+, 1/2)\beta^-$	$s_{1/2}^{-1}$	1143	2.929	3
$^{15}\text{O} \to {}^{15}\text{N}$	$(1/2^-, 1/2) \to (1/2^-, 1/2)\beta^+$	$p_{1/2}^{-1}$	4260	0.30	1/3
$^{17}\text{F} \to {}^{17}\text{O}$	$(5/2^+, 1/2) \to (5/2^+, 1/2)\beta^+$	$d_{5/2}$	2195	1.16	7/5
$^{39}\text{Ca} \to {}^{39}\text{K}$	$(3/2^+, 1/2) \to (3/2^+, 1/2)\beta^+$	$d_{3/2}^{-1}$	3875	0.39	3/5
$^{41}\text{Sc} \to {}^{41}\text{Ca}$	$(7/2^-, 1/2) \to (7/2^-, 1/2)\beta^+$	$f_{7/2}$	2540	0.92	9/7

creation–annihilation operator formalism with $a^\dagger_{jm}$ and a_{jm} to handle the antisymmetrisation of the nucleus as well as angular momentum algebra. For instance, the angular momentum operator $J_+ = \sum_k j^{(k)}$ is written

$$J_+ = \sum_{jm} \sqrt{(j-m)(j+m+1)} a^\dagger_{jm+1} a_{jm} \, , \qquad (3.104)$$

etc., and the construction of angular momenta $(j,m) \times (j'm') \to (J,M)$ is performed as $[a^\dagger_{jm} \times a^\dagger_{j'm'}]^{JM}$, etc. Representative wave functions popularly used are those of Cohen and Kurath for the p shell [368], and of Brown and Wildenthal for the sd shell [369]. For fp shell calculations, see [370] and references therein.

For example, the p shell model treats the nucleus with N and Z between 2 and 8, up to ^{16}O. The possible two-particle states are $(p_{3/2})^2_0$, $(p_{1/2})^2_0$, $(p_{3/2}p_{1/2})_1$, $(p_{3/2})^2_2$, $(p_{3/2}p_{1/2})_2$ for $T = 1$, and $(p_{3/2})^2_1$, $(p_{3/2}p_{1/2})_1$, $(p_{1/2})^2_1$, $(p_{3/2}p_{1/2})_2$, and $(p_{3/2})^2_3$ for $T = 0$, where the subscripts are J and the superscripts are the multiplicity. The $T = 0$ interaction is characterised by eight matrix elements (five diagonal and three off-diagonal), and likewise for $T = 1$. The shell model wave function is obtained by diagonalising these matrices.

Using the shell model wave function, GT matrix elements are calculated as the sum of the matrix elements over all single-particle orbits denoted as j:

$$\langle f|\tau^+\sigma|i\rangle = \sqrt{(2J_f+1)(2J_i+1)} \sum_{jj'} D_{jj'} \langle j'\|\sigma\|j\rangle \, , \qquad (3.105)$$

where $D_{jj'}$ is the one-body transition density calculated with the model wave function, as

$$D_{jj'} = \frac{\langle f\|[a^\dagger_j \times \tilde{a}_{j'}]^{\Delta J \Delta T}\|i\rangle}{[(2\Delta J + 1)(2\Delta T + 1)]^{1/2}} \, , \qquad (3.106)$$

where the triple-striped matrix elements mean doubly reduced with respect to both spin and isospin.

Extensive studies of the GT elements have been made for the p shell by Wilkinson [371] and by Brown, Wildenthal, and their collaborators [372,373]. A comparison is shown for 61 beta decays for $A \leq 16$ (up to p-shell nuclei) in Fig. 3.2, where the abscissa is the reduced matrix element $M_{\mathrm{GT}} = [(2J_i + 1)g^2_A B(\mathrm{GT})]^{1/2}$ derived from experiment and the ordinate is shell model predictions [372]. The identical regression and lines for $\sqrt{2}$ deviations (i.e., factor of 2 deviations in the decay widths) are also indicated. Example numbers are presented in Table 3.3. Calculations using the Cohen–Kurath wave functions agree well with those using Wildenthal's wave functions which are presented in the figure. Although we see the trend that the shell model reproduces experiments semiquantitatively, there are considerable scatters; the predictions often are off from experiments by a factor of several to occasionally more than 10. This is more often seen with nuclei away from the
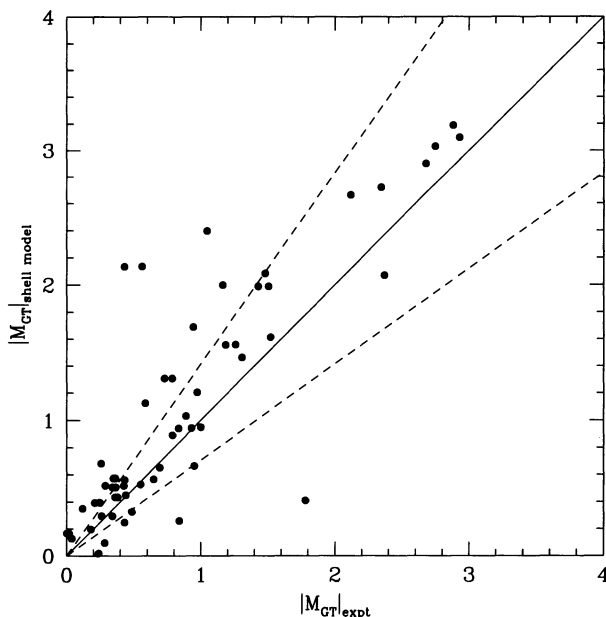
Fig. 3.2. Calculation of GT matrix elements with the shell model, compared with experiment for p shell nuclei [372]. The lines indicate the identical regression and factor of 2 deviations in the decay rate.

stable valley (e.g., ^{11}Li, ^{11}Be) and transitions involving excited states.[6] There is a general trend for the model to overestimate the rate. This means that better agreement may be obtained if one reduces g_A from the free neutron value to a value around unity. This is called the quenching effect. The origin is usually ascribed to nuclear correlations outside of the valence major shell and Δ isobar admixtures in the nuclear states [369, 375, 376].

For the sd shell, agreement with experiment scatters more wildly. It is difficult to calculate the GT matrix elements between specific states within a factor of 2, even with a 'good wave function' [369] (e.g., see Table 3.9 below). It is also known that the predicted GT elements depend significantly on specific wave functions [377]. The shell-model calculation for the sd shell nuclei may be good only to the extent to predict global qualitative characteristics but cannot be used for quantitative prediction, unless extra empirical constraints are introduced. The situation is obviously worse for the fp shell, for which full diagonalisation is already a tedious task and drastic truncations of model space are usually employed.

---

[6] A particularly drastic failure is seen with ^{14}C$\rightarrow^{14}$N, for which the predicted decay rate is 10 000 times faster than experiment. This is ascribed to tensor-force induced configuration mixing, which leads to nearly a perfect cancellation between the two transition amplitudes [374].

Table 3.3. Examples of beta decay (GT transitions) for light nuclei.[a]

Process	$(J^P,I)_i \to (J^P,I)_f$	$T_{1/2}$(sec)	Q (MeV)	$\log f$	$\log ft$	Expt.	$|M_{GT}|^b$ shell	EOM
$n(\beta^-)p$	$(1/2^+,1/2) \to (1/2^+,1/2)$	616.6	0.7823	0.234	3.024	3.100	3.096	—
^{3}H$(\beta^-)^3$He	$(1/2^+,1/2) \to (1/2^+,1/2)$	3.887E+8	0.0186	-5.533	3.058	2.929	3.096	3.096
^{6}He$(\beta^-)^6$Li	$(0^+,1) \to (1^+,0)$	0.8067	3.508	3.003	2.910	2.748	3.031	2.630
^{7}Be(EC)^{7}Li	$(3/2^-,1/2) \to (3/2^-,1/2)$	4.604E+6	0.862	-3.410	3.300	2.882	3.187	2.747
	$(3/2^-,1/2) \to (1/2^-,1/2,0.478)$			-4.112	3.534	2.678	2.901	2.493
^{8}He$(\beta^-)^8$Li	$(0^+,2) \to (1^+,1,0.981)$	0.111	10.654	5.045	4.166	0.647	0.566	0.506
^{8}B$(\beta^+)^8$Be	$(2^+,1) \to (2^+,0,3.12)$	0.770	16.004	~5.38		0.364	0.507	0.456
	$(2^+,1) \to (2^+,0,16.8)$			~2.00		5.9	4.32	3.69
^{10}C$(\beta^+)^{10}$B	$(0^+,1) \to (1^+,0,0.718)$	19.29	3.648	1.757	3.048	2.344	2.721	2.284
^{11}C$(\beta^+)^{11}$B	$(3/2^-,1/2) \to (3/2^-,1/2)$	1223	1.982	0.512	3.598	1.480	2.084	1.783
^{12}B$(\beta^-)^{12}$C	$(1^+,1) \to (0^+,0)$	0.0202	13.369	5.748	4.071	1.258	1.558	1.284
	$(1^+,1) \to (2^+,0,4.439)$			4.912	5.11	0.379	0.434	0.400
^{12}N$(\beta^+)^{12}$C	$(1^+,1) \to (0^+,0)$	0.011	17.338	6.053	4.118	1.184	1.558	1.284
^{13}B$(\beta^-)^{13}$C	$(3/2^-,3/2) \to (1/2^-,1/2)$	0.0174	13.437	5.759	4.034	1.506	1.989	1.626
^{13}N$(\beta^+)^{13}$C	$(1/2^-,1/2) \to (1/2^-,1/2)$	597.9	2.220	0.895	3.671	0.788	0.891	0.778
^{14}C$(\beta^-)^{14}$N	$(0^+,1) \to (1^+,0)$	1.81E+11	0.156	-2.208	9.049	0.002	0.167	0.183
^{15}C$(\beta^-)^{15}$N	$(1/2^+,3/2) \to (1/2^+,1/2,5.299)$	2.449	9.772	3.526	4.114	0.972	1.206	0.990
^{15}O$(\beta^+)^{15}$N	$(1/2^-,1/2) \to (1/2^-,1/2)$	122.2	2.754	1.557	3.644	0.889	1.032	0.889

[a] This table is an excerpt from Chou et al. [372].
[b] $|M_{GT}|$ is the reduced matrix element multiplied by g_A: $|M_{GT}| = \sqrt{(2J_i+1)}\, g_A^2\, B(\text{GT})$.

In general, the shell model would give a better description if sufficiently many shells are included in the calculation, which, however, makes the dimension of the model space explosively large for nuclei in the middle of two closed shells. For practical feasibility, we must truncate the shell at some minimal level. The effect of core excitation (core polarisation) is often important. Also missing in this formalism is the effect which is not included in the basic Hamiltonian, such as the weak current that couples to pion exchange between nucleons (called exchange current) [378]. One way devised to include core polarisation (and also the exchange current) effectively is the 'effective operator method' (EOM) [375, 376, 379]. In this method one finds an effective operator O_{eff} such that its expectation value with the truncated shell-model wave function Ψ' mimics the expectation value of the true GT operator $O = \tau\sigma$ with full shell-model wave functions, by extending operator space but with shell-model space fixed. The practical implementation of this formalism for calculating GT matrix elements is made by the replacement of

$$g_{\mathrm{A}} \langle j' \| \boldsymbol{\sigma} \| j \rangle \to \langle j' \| g_{\mathrm{A}}^{\mathrm{eff}} \boldsymbol{\sigma} + g_{\ell}^{\mathrm{eff}} \boldsymbol{\ell} + g_{p}^{\mathrm{eff}} [Y_2 \times \boldsymbol{\sigma}]^{(1)} \| j \rangle \qquad (3.107)$$

in (3.105), keeping $D_{jj'}$ fixed; the three coefficients are determined so that $B(\mathrm{GT})$ calculated with the effective operators would optimally reproduce the chosen set of empirical $B(\mathrm{GT})$.

One advantage of this effective operator approach is that one can understand the quenching effect of g_{A}. By truncating the shell-model space, Towner [375] obtained $g_{\mathrm{A}}^{\mathrm{eff}} \simeq 0.81$, $g_{\ell}^{\mathrm{eff}} = 0.01$, and $g_{p}^{\mathrm{eff}} = 0.05$. This approach somewhat improves the agreement of the shell model prediction with experiment (see Fig. 3.3, compared with Fig. 3.2) [372]. Little improvement, however, is seen for those matrix elements that are predicted far off from experiment. Only 64% of 61 beta decay rates for p shells are predicted within a factor of 2. There are many transitions where the prediction fails badly. The parameters that Chou et al. [372] obtained for the p shell nuclei are $g_{\mathrm{A}}^{\mathrm{eff}} \simeq 0.82$, $g_{\ell}^{\mathrm{eff}} < 0.02$, and $g_{\mathrm{p}}^{\mathrm{eff}} < 0.02$, which are not far from Towner's model calculations. Brown and Wildenthal found a very similar set of parameters from beta decays for the sd shell [369]. However, Adelberger et al. [380] studied the case for $^{37}\mathrm{Ca} \to ^{37}\mathrm{K}$ and claimed that the quenching effect indicated by Brown and Wildenthal is not visible. Brown replied that the issue depends on the wave functions used [377].

Yet, the shell model is the best nuclear model with some predictive power. Unfortunately, one cannot take literally the GT element result from a shell model calculation when one needs a result with an error less than by a factor of 2. Practically, the most important problem is that there are no ways to know in advance where it fails.

As we will see in Sect. 3.13, knowledge of GT elements is crucial for solar neutrino detection. We need neutrino capture cross sections with an error typically smaller than 10%; calculations with 50% error will be of no use. For such a purpose, one must find a way to estimate the GT element empirically
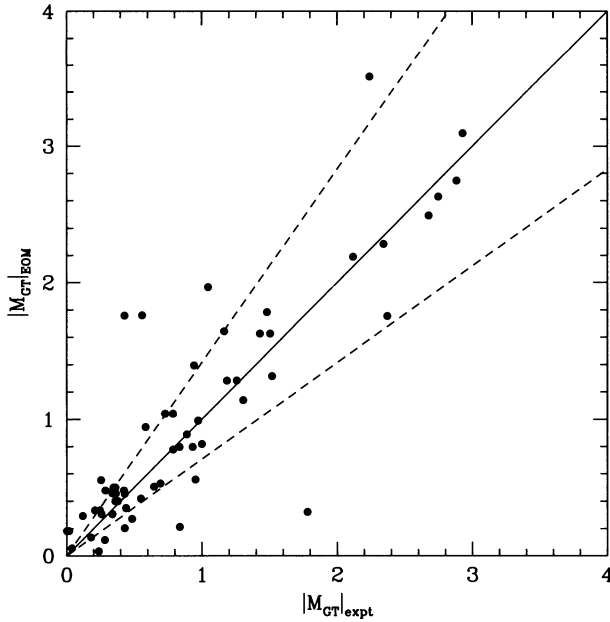
Fig. 3.3. Calculation of GT matrix elements by the effective operator method, as compared with experiment for p shell nuclei [372]. The lines indicate the identical regression and factor of 2 deviations in the decay rate.

without resorting to explicit shell model calculations, or to find reactions where the Fermi transition dominates and uncertainties in the GT element are not very important.

3.7 Hyperon Beta Decay

The formalism for hyperon beta decays ($\Sigma^- \rightarrow \Lambda e\bar{\nu}$, $ne\bar{\nu}$, $\Lambda \rightarrow pe\bar{\nu}$, $\Xi^- \rightarrow \Lambda e\bar{\nu}$, $\Xi^- \rightarrow \Sigma^0 e\bar{\nu}$ etc) is similar to that for nucleon beta decays. The basic form factors are the same as given in (3.42), where F_{PT} is nonvanishing as SU(3) symmetry is broken. An approximation similar to (3.42) may also apply, but for a more accurate treatment one retains the term F_W and occasionally F_{PT}. The q dependence is also often retained assuming dipole form factors.

The strength of the current couplings depends on the process due to different quark wave functions in hyperons. The conventional approximation starts by assuming that u, d, and s quarks form flavour SU(3) symmetry and classifies hyperons as an octet of SU(3). The current obtained by extending $\tau/2$ to $\lambda/2$ (Gell-Mann's SU(3) matrices) is also a member of an octet. The coupling is unique for the vector current, but two different couplings are

allowed for the axial-vector current, symmetric (called D type) and antisymmetric (F type) with respect to the two octets. Hyperon decays (including nucleon decay) are described by D, F and the ratio of the quark mixing angles $|U_{us}|/|U_{ud}|$.

Hyperon beta decay is significantly modified by SU(3) symmetry breaking for the axial-vector couplings, for which the Ademollo–Gatto theorem [341] does not hold. Although fits with the parameters, $D/(F + D)$ and $|U_{us}|/|U_{ud}|$, give reasonable solutions, the detail of quark mixing parameters depends on the model of SU(3) symmetry breaking. There is also a systematic discrepancy in the fit among decay modes. Donoghue et al. [381] obtained $|U_{us}| = 0.220 \pm 0.003$, but the value from $\Xi^- \to \Lambda^0 e\bar\nu / \Lambda \to pe\bar\nu$, for instance, is smaller than experiment by more than 2σ, implying a significant error in the symmetry-breaking model. Flores-Mendieta et al. [382] discussed this point, showing that $|U_{us}|$ may take a value between 0.215 and 0.243, much beyond the formal error of the fit. It seems that hyperon beta decay is not a suitable place to obtain an accurate value of $|U_{us}|$.

3.8 Determination of Quark Mixing Angles

Quark mixing angles are determined by comparing G_μ from μ decay with the strength of semileptonic weak interactions of hadrons. We have already discussed the determination of $|U_{ud}|$ (3.95) and $|U_{us}|$ (3.40), which are the most accurate values among all elements. In this section we discuss other matrix elements.

U_{ub} is a very small quantity. The *Review of Particle Physics* (RPP) [275] adopts

$$|U_{ub}| = 0.0036 \pm 0.0009 , \qquad (3.108)$$

from $|U_{ub}/U_{cb}| = 0.090 \pm 0.025$ and $|U_{cb}|$ discussed below. The ratio $|U_{ub}/U_{cb}|$ is obtained by comparing inclusive decay $b \to u\ell\bar\nu$ with $b \to c\ell\bar\nu$, using the information on the lepton energy spectrum. Inclusive decays are not complicated by hadron form factors and are generically the same as that for $\mu \to e\bar\nu_e\nu_\mu$. In practice, however, the spectrum in the high-energy electron end-point region, which is crucial for extracting $b \to u\ell\bar\nu$, is distorted by soft hadronic decays and hence is significantly model-dependent [383]. The U_{ub} element is alternatively estimated from exclusive semileptonic decays $B^0 \to \pi^- \ell^+ \nu$ and $B^0 \to \rho^- \ell^+ \nu$, yielding $(2.2 - 4.0) \times 10^{-3}$ depending on the theoretical model used [384]. This is consistent with (3.108).

The matrix elements that are relevant to the charm quark (the second row) are not as accurately estimated as those for the u quark. The estimate of $|U_{cd}|$ uses opposite charge dimuon production in deep inelastic ν_μ (or $\bar\nu_\mu$) scattering through charm production from d quarks. Neutrino scattering yields μ^-, and the decay of the positively charged charm yields μ^+. The event

rate is proportional to $\sigma(\nu_\mu + N \rightarrow \mu^- + c + ...)|U_{cd}|^2 Br(D \rightarrow \mu^+ + ...)\eta$, where the muon production cross section is given by (3.209) of Sect. 3.14 and η represents the suppression of charm production due to slow scaling, which is estimated empirically from the data (see discussion at the end of Sect. 3.14). With the average of CDHS and CCFR experiments $|U_{cd}|^2 Br = (0.49 \pm 0.05) \times 10^{-2}$ and using $Br = 0.099 \pm 0.012$, one gets $|U_{cd}| = 0.224 \pm 0.016$ [385, 386].

$|U_{cs}|$ can, in principle, be derived from D meson decay $D \rightarrow \bar{K}e^+\nu_e$, or from neutrino production of the charm from strange sea quarks in nucleons. Neither method, however, gives a result accurate enough to find a departure from $|U_{cs}| = 1$. D_{e3} decay is proportional to $|U_{cs}|^2|f_+(0)^D|^2$, but a sufficiently accurate value is not available for the form factor. For neutrino production of the charm quark, one needs an assumption about strange quark density in the nucleon sea. The branching fraction to $W \rightarrow c\bar{s}$ jets gives $|U_{cs}| = 0.94 \pm 0.30 \pm 0.13$ [387]. The value quoted in RPP is $|U_{cs}| = 1.04 \pm 0.16$, which says only that this matrix element is the dominating component in the second row. More useful information on $|U_{cs}|$ is derived from the unitarity constraint (3.6).

U_{cb} is estimated from both exclusive and inclusive decays of the B meson into the $\overline{D}$ meson. The most accurate result is derived from $B \rightarrow \overline{D}\ell^+\nu_e$ and $B \rightarrow \overline{D}^*\ell^+\nu_e$, where the heavy quark effective theory [388] allows a reasonably accurate treatment of the matrix element for $B \rightarrow \overline{D}$, assuming that both b and c quarks are heavy. The use of modern data gives $|U_{cb}| = 0.0387 \pm 0.0021$. Combining it with the value from inclusive decay $b \rightarrow c + \ell^- + \bar{\nu}_e$, the best current value is $|U_{cb}| = 0.0395 \pm 0.0017$ [389].

For the third row involving the t quark, the only available piece of information is from $t \rightarrow b\ell^+\nu_e$ that $t \rightarrow b$ dominates over others, $|U_{tb}|^2 / \sum_i |U_{ti}|^2 = 0.99 \pm 0.29$ [390].

The resulting matrix elements are

$$U_q = \begin{pmatrix} 0.9742 \pm 0.0005 & 0.2196 \pm 0.0023 & 0.0036 \pm 0.0009 \\ 0.224 \pm 0.016 & 1.04 \pm 0.16 & 0.0387 \pm 0.0021 \\ ... & ... & 0.99 \pm 0.15 \end{pmatrix} \quad (3.109)$$

An interesting issue is the test of the universality of weak interactions for leptons and hadrons. This is translated to the test of unitarity in our context. A precise test can be made only for the first row; from (3.109), we obtain

$$|U_{ud}|^2 + |U_{us}|^2 + |U_{ub}|^2 = 0.9969 \pm 0.0020 \,. \quad (3.110)$$

The deviation from unitarity is not significant, only at a 1.5 standard deviation level. We note that the errors of $|U_{ud}|$ and $|U_{us}|$ contribute by the same amount. $|U_{ub}|$ hardly contributes to the sum, and so does its error. The test for the unitarity constraint does not say much about the possible existence of the fourth generation, unless mixing with the first generation happens to be unexpectedly large.

The quark mixing matrix for practical use is determined by assuming three generations and imposing the unitarity constraint. A modern determination in RPP reads

$$U_q = \begin{pmatrix} 0.9742 - 0.9757 & 0.219 - 0.226 & 0.002 - 0.005 \\ 0.219 - 0.225 & 0.9734 - 0.9749 & 0.037 - 0.043 \\ 0.004 - 0.014 & 0.035 - 0.043 & 0.9990 - 0.9993 \end{pmatrix} . \quad (3.111)$$

A few different parametrisations have been used for the 3×3 matrix in the literature. Kobayashi and Maskawa [132] parametrised it as

$$U_q = \begin{pmatrix} 1 & 0 & 0 \\ 0 & \cos\theta_2 & -\sin\theta_2 \\ 0 & \sin\theta_2 & \cos\theta_2 \end{pmatrix} \begin{pmatrix} \cos\theta_1 & -\sin\theta_1 & 0 \\ \sin\theta_1 & \cos\theta_1 & 0 \\ 0 & 0 & 1 \end{pmatrix}$$

$$\times \begin{pmatrix} 1 & & \\ & 1 & \\ & & -e^{i\delta} \end{pmatrix} \begin{pmatrix} 1 & 0 & 0 \\ 0 & \cos\theta_3 & \sin\theta_3 \\ 0 & -\sin\theta_3 & \cos\theta_3 \end{pmatrix} \quad (3.112)$$

$$= \begin{pmatrix} c_1 & -s_1 c_3 & -s_1 s_3 \\ s_1 c_2 & c_1 c_2 c_3 - s_2 s_3 e^{i\delta} & c_1 c_2 s_3 + s_2 c_3 e^{i\delta} \\ s_1 s_2 & c_1 s_2 c_3 + c_2 s_3 e^{i\delta} & c_1 s_2 s_3 - c_2 c_3 e^{i\delta} \end{pmatrix},$$

where $c_i = \cos\theta_i$ and $s_i = \sin\theta_i$.

In modern literature, the following representation [391] is frequently used:

$$U_q = \begin{pmatrix} 1 & 0 & 0 \\ 0 & \cos\theta_{23} & \sin\theta_{23} \\ 0 & -\sin\theta_{23} & \cos\theta_{23} \end{pmatrix} \begin{pmatrix} \cos\theta_{13} & 0 & \sin\theta_{13}e^{-i\delta} \\ 0 & 1 & 0 \\ -\sin\theta_{13}e^{i\delta} & 0 & \cos\theta_{13} \end{pmatrix}$$

$$\times \begin{pmatrix} \cos\theta_{12} & \sin\theta_{12} & 0 \\ -\sin\theta_{12} & \cos\theta_{12} & 0 \\ 0 & 0 & 1 \end{pmatrix} \quad (3.113)$$

$$= \begin{pmatrix} c_{12}c_{13} & s_{12}c_{13} & s_{13}e^{-i\delta} \\ -s_{12}c_{23} - c_{12}s_{23}s_{13}e^{i\delta} & c_{12}c_{23} - s_{12}s_{23}s_{13}e^{i\delta} & s_{23}c_{13} \\ s_{12}s_{23} - c_{12}c_{23}s_{13}e^{i\delta} & -s_{23}c_{12} - s_{12}c_{23}s_{13}e^{i\delta} & c_{23}c_{13} \end{pmatrix}.$$

The advantage of this parametrisation is that the phase always appears with s_3 multiplied, which is a small number $\sim 10^{-3}$. Therefore, small CP violation is automatically built in, irrespective of the value of δ.

It is shown that the product $U_{ik}U_{jl}U_{il}^*U_{jk}^*$, where (i,j) and (k,l) take (1,2), (2,3), or (3,1) independently, is invariant under rephasing of the matrix elements, and that the physical quantities that are relevant to CP violation are proportional to the imaginary part of this product [392, 393]

$$J = \text{Im}(U_{ik}U_{jl}U_{il}^*U_{jk}^*) . \quad (3.114)$$

The J factors constructed from nine combinations of (i, j, k, l) are identical up to the sign by virtue of unitarity. For the representation of (3.113), $J = \pm c_{12}c_{13}^2 c_{23}s_{12}s_{23}s_{13}\sin\delta$. It is also shown that the necessary and sufficient condition of CP violation is

$$J \prod_{i<j}(m_{u_j}^2 - m_{u_i}^2)(m_{d_j}^2 - m_{d_i}^2) \neq 0 \,, \tag{3.115}$$

where (u_1, u_2, u_3) stand for (u, c, t) and (d_1, d_2, d_3) for (d, s, b) [392,394].

Since $s_{13} \sim 10^{-3}$ and $s_{23} \sim 10^{-2}$, c_{13} and c_{23} are virtually unity, so that we may approximate $s_{12} = |U_{us}|$, $s_{13} = |U_{ub}|$, $s_{23} = |U_{cb}|$, and $c_{12} = |U_{ud}|$. We note that

$$U_{td} = U_{us}U_{cb} - U_{ud}U_{ub}e^{i\delta} \,, \tag{3.116}$$

where all U's on the right-hand side are real. Therefore, δ is written only in terms of the real matrix elements as

$$\cos\delta = \frac{1}{2U_{us}U_{cb}U_{ud}U_{ub}}[-|U_{td}|^2 + (U_{us}U_{cb})^2 + (U_{ud}U_{ub})^2] \,. \tag{3.117}$$

The orthogonality relation between row 1 and row 3,

$$U_{ud}U_{ub}^* + U_{cd}U_{cb}^* + U_{td}U_{tb}^* = 0 \,, \tag{3.118}$$

defines a triangle on a complex plane. By noting that $s_{12} \sim O(0.1)$, $s_{23} \sim O(0.01)$, and $s_{13} \sim O(0.001)$ are hierarchical, one may parametrise these angles as $s_{12} = \lambda$, $s_{23} = A\lambda^2$, and $s_{13}e^{i\delta} = A\lambda^3(\rho - i\eta)$ [395]. Then an apex of the triangle is $\rho + i\eta$ with the other apices at $(0, 0)$ and $(1, 1)$ (see Fig. 3.4).

The leptonic counterpart of unitarity for the quark mixing matrix is $e - \mu - \tau$ universality, irrespective of whether or not neutrinos have a finite mass because neutrinos are not measured. Writing the effective coupling constants for the $\ell\bar{\nu}W(Z)$ vertex, which refer to $\ell = e, \mu$ and τ, as $g^{(e)}, g^{(\mu)}, g^{(\tau)}$, i.e.,
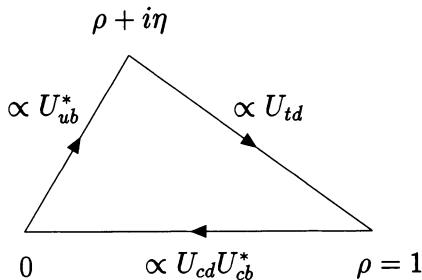
Fig. 3.4. Rescaled unitarity triangle of the Kobayashi–Maskawa matrix.

<div align="center">**Table 3.4.** $e-\mu-\tau$ universality tests.</div>

	$[g^{(e)}/g^{(\mu)}]^2$		$[g^{(\tau)}/g^{(e)}]^2$
$\frac{\pi\to e\nu}{\pi\to\mu\nu}$	0.998 ± 0.004		
$\frac{\tau\to e\nu_e\nu_\tau}{\tau\to\mu\nu_\mu\nu_\tau}$	0.997 ± 0.005		
$\frac{W\to e\nu}{W\to\mu\nu}$	1.016 ± 0.033	$\frac{W\to\tau\nu}{W\to e\nu}$	0.979 ± 0.044
$\frac{\tau\to\pi\nu_\tau}{\pi\to e\nu_e}$			1.062 ± 0.016
$\frac{\tau\to e\nu\bar\nu}{\mu\to e\nu\bar\nu}$			0.996 ± 0.006
$\frac{Z\to ee}{Z\to\mu\mu}$	1.000 ± 0.003	$\frac{Z\to\tau\tau}{Z\to ee}$	1.003 ± 0.004

($G_\mu \propto g^{(e)}g^{(\mu)}$, etc.), we list a number of tests in Table 3.4.[7] It shows that universality is verified within 0.3–0.4% for the ratio $[g^{(e)}/g^{(\mu)}]^2$ and within 0.4–0.6% for $[g^{(\tau)}/g^{(\mu,e)}]^2$.

The validity of universality means that one cannot bring hypothetical particles that couple to leptons or quarks into the model: such particles, if any, should have very large masses or very weak couplings to matter fields. See Sect. 10.3 for examples of applications.

3.9 Number of Generations

All species of neutrinos are equally produced in some high-energy reactions, and such experiments give information concerning the number of generations.

The most definitive constraint is derived from the total width of Z^0. Z^0 decays into e^+e^-, $\mu^+\mu^-$, $\tau^+\tau^-$, $q\bar q$ ($\bar q = u,d,s,c,b$) and $\nu\bar\nu$'s, with the partial width to $\nu\bar\nu$ in particular,

$$\Gamma_{\nu\bar\nu} = \frac{1}{12\pi}\frac{G_{\rm F}}{\sqrt2}M_Z^3 N_\nu \simeq 0.181 N_\nu \text{ GeV} \tag{3.119}$$

for the neutral-current coupling given in (2.66) of Chap. 2. The partial width of Z^0 for invisible decays measured with LEP experiments yields

$$N_\nu = 2.994 \pm 0.012 . \tag{3.120}$$

The result gives the number of neutrino species but also means that any hypothetical particles that carry $SU(2)_L$ and/or $U(1)_Y$ charge with a mass

---

[7] In the table we use $\Gamma(W \to \tau\nu)/\Gamma(W \to \mu\nu) = 1 - 3m_\tau^2/m_W^2$ and $\Gamma(Z \to \bar\tau\tau)/\Gamma(Z \to \bar\mu\mu) = [(1 - 6m_\tau^2/m_Z^2) + (1 - 4\sin^2\theta_W)^2]/[1 + (1 - 4\sin^2\theta_W)^2]$ to correct for the mass effect.

smaller than $\approx m_Z/2$ are excluded. A typical example is triplet majorons which will be discussed in Sect. 6.8.

A constraint can also be inferred from neutrino counting experiments with $e^+e^- \to \nu\bar{\nu}+\gamma$ [396]. This process might, in principle, give a constraint independent of that from Z^0 decay, for instance, when there exist light right-handed neutrinos and scalar particles that couple to $\nu_R\nu_L$, although such a scenario receives stronger constraints from other phenomenology. The LEP experiments, which yield $N_\nu = 3.00 \pm 0.06$, however, were carried out at the Z^0 pole, and hence do not give any information independent of the Z^0 invisible width.

Before these laboratory limits became available, $N_\nu \lesssim 4$ was inferred from the argument on primordial nucleosynthesis for light elements. The constraint is derived from the fact that extra neutrino species increase the expansion rate of the early universe and thus increase the decoupling temperature of β equilibrium $(n + \nu_e \rightleftarrows p + e^-$ etc); this increases the neutron fraction and thus the ^{4}He abundance. The limit is derived from the consistency of the calculated light element abundance with observations. More details will be discussed in Sect. 4.6.2.

3.10 Neutrino–Lepton Scattering

The part of (2.70) relevant to $\nu_\ell e^-$ scattering is

$$H_W^{\text{eff}} = \frac{G_F}{\sqrt{2}}\left\{[\bar{e}\gamma_\mu(1-\gamma_5)\nu_e][\bar{\nu}_e\gamma^\mu(1-\gamma_5)e]\right.$$
$$\left. + 2\rho\left[\bar{\nu}_\ell\gamma_\mu\frac{1}{2}(1-\gamma_5)\nu_\ell\right][\bar{e}\gamma^\mu(g_V - g_A\gamma_5)e]\right\}, \qquad (3.121)$$

where $g_V = g_L + g_R = -1/2 + 2\sin^2\theta_W$, $g_A = g_L - g_R = -1/2$, and $\rho = 1$. The first term is absent for $\nu_\mu e^-$ scattering. After the Fierz rearrangement of the first term,

$$H_W^{\text{eff}} = \frac{G_F}{\sqrt{2}}[\bar{\nu}_\ell\gamma_\mu(1-\gamma_5)\nu_\ell][\bar{e}\gamma^\mu(c_V - c_A\gamma_5)e], \qquad (3.122)$$

where

$$
\begin{array}{ccc}
 & \nu_e e^- & \nu_\mu e^- \\
c_V = & \rho g_V + 1 & \rho g_V, \\
c_A = & \rho g_A + 1 & \rho g_A.
\end{array}
\qquad (3.123)
$$

The matrix element squared is

$$\frac{1}{2}|-iH_W^{\text{eff}}|^2 = 16G_F^2\left[c_L^2(s - m_e^2)^2 + c_R^2(u - m_e^2)^2 + c_Lc_Rm_e^2t\right], \qquad (3.124)$$

where $s = (p_\nu + p_e)^2$, $t = (p_\nu - p'_\nu)^2$, and $u = (p_e - p'_\nu)^2$ are the Lorentz invariant Mandelstam variables, which in the laboratory-frame are written

$$\begin{aligned}
s &= m_e^2 + 2m_e E_\nu \\
u &= m_e^2 - 2m_e E'_\nu \\
t &= m_e(E'_\nu - E_\nu) \,,
\end{aligned}$$

(3.125)

with the primed variables referring to the final state, and the coefficients

$$\begin{aligned}
c_L = \frac{c_V + c_A}{2} &= g_L + 1 \quad \text{(for} \quad \nu_e) \\
&= g_L \quad\quad\ \text{(for} \quad \nu_\mu) \\
c_R = \frac{c_V - c_A}{2} &= g_R \,.
\end{aligned}$$

(3.126)

Using

$$\int \frac{d^3 p'_\nu}{(2\pi)^3 2E'_\nu} \frac{d^3 p'_e}{(2\pi)^3 2E'_e} (2\pi)^4 \delta^4(p_e + p_\nu - p'_e - p'_\nu) = \frac{1}{8\pi} \int \frac{dE'_e}{E_\nu} \,,$$

(3.127)

the cross section in the laboratory-frame variables is

$$\frac{d\sigma}{dE'_e} = \frac{1}{32\pi} \frac{1}{m_e E_\nu^2} \frac{1}{2} | - iH_W^{\text{eff}}|^2 \,.$$

(3.128)

which reads [397]

$$\frac{d\sigma}{dT'_e} = \frac{2G_F^2 m_e}{\pi} \left[c_L^2 + c_R^2 \left(\frac{E'_\nu}{E_\nu}\right)^2 - c_L c_R \frac{m_e}{E_\nu} \frac{E_\nu - E'_\nu}{E_\nu} \right] \,,$$

(3.129)

where T'_e is the recoil electron kinetic energy

$$T'_e = E'_e - m_e = E_\nu - E'_\nu.$$

(3.130)

One often uses the inelasticity parameter

$$y = T'_e/E_\nu = (E_\nu - E'_\nu)/E_\nu,$$

(3.131)

$(0 \le y \le 1)$ and writes,

$$\sigma = \frac{2G_F^2 m_e E_\nu}{\pi} \int_0^1 dy \left[c_L^2 + c_R^2(1-y)^2 - c_L c_R \frac{m_e}{E_\nu} y \right] \,.$$

(3.132)

The total cross section is

$$\sigma = \frac{2G_F^2 m_e E_\nu}{\pi} \left[c_L^2 + \frac{1}{3} c_R^2 - \frac{1}{2} c_L c_R \frac{m_e}{E_\nu} \right] \,.$$

(3.133)

Table 3.5. Coefficients that appear in neutrino–lepton scattering.

	c_{L}	c_{R}	$c_{\mathrm{L}}^2 + \frac{1}{3}c_{\mathrm{R}}^2$	$\frac{1}{2}c_{\mathrm{L}}c_{\mathrm{R}}$
$\nu_e e^-$	$1/2 + \sin^2\theta_W$	$\sin^2\theta_W$	0.5525	0.0845
$\bar{\nu}_e e^-$	$\sin^2\theta_W$	$1/2 + \sin^2\theta_W$	0.2317	0.0845
$\nu_\mu e^-$	$-1/2 + \sin^2\theta_W$	$\sin^2\theta_W$	0.0901	0.0311
$\bar{\nu}_\mu e^-$	$\sin^2\theta_W$	$-1/2 + \sin^2\theta_W$	0.0775	0.0311

For $\bar{\nu}_{e(\mu)}\, e$ scattering, c_{L} and c_{R} are interchanged. For convenience, $c_{\mathrm{L}}, c_{\mathrm{R}}$ are tabulated in Table 3.5. With $\sin^2\theta_W = 0.2312$ ($\overline{\mathrm{MS}}$, a hat symbol is omitted), νe scattering cross sections are

$$\sigma(\nu_e e^- \to \nu_e e^-) = 0.952 \times 10^{-43}(E_\nu/10\,\mathrm{MeV})\,\mathrm{cm}^2 , \qquad (3.134)$$
$$\sigma(\bar{\nu}_e e^- \to \bar{\nu}_e e^-) = 0.399 \times 10^{-43}(E_\nu/10\,\mathrm{MeV})\,\mathrm{cm}^2 , \qquad (3.135)$$
$$\sigma(\nu_\mu e^- \to \nu_\mu e^-) = 0.155 \times 10^{-43}(E_\nu/10\,\mathrm{MeV})\,\mathrm{cm}^2 , \qquad (3.136)$$
$$\sigma(\bar{\nu}_\mu e^- \to \bar{\nu}_\mu e^-) = 0.134 \times 10^{-43}(E_\nu/10\,\mathrm{MeV})\,\mathrm{cm}^2 , \qquad (3.137)$$

when the third term of (3.133) is ignored ($E_\nu \gg m_e$).

The recoil electron has a nearly flat energy spectrum with respect to T'_e (see Fig. 3.5). Table 3.6 shows a fraction of the neutrino reaction rate when the recoil electron energy is restricted to $T'_e \geq T'_{th}$ for neutrinos from a $^8\mathrm{B}$ beta decay source ($E_\nu \leq 15\,\mathrm{MeV}$) using the spectrum measured by Ortiz
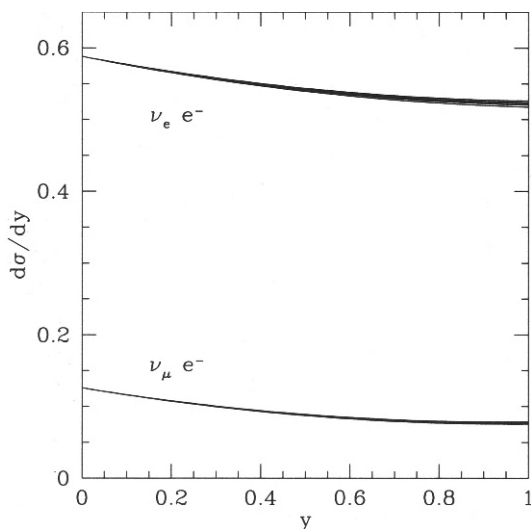
Fig. 3.5. Differential cross section of $\nu_e e^-$ and $\nu_\mu e^-$ scattering for $E = 5\text{–}10\,\mathrm{MeV}$. The curve is moving upwards (downwards) slightly with the energy of neutrinos for $\nu_e e$ ($\nu_\mu e$) scattering.

Table 3.6. Neutrino electron scattering for ^{8}B solar neutrinos. Detection fractions are shown for the given threshold energy for recoil electrons. Radiative corrections are not taken into account.

T'_{th} (MeV)	$\nu_e e$	$\nu_\mu e$	$\sigma(\nu_e e)/\sigma(\nu_\mu e)$
4	42.9%	38.2%	6.64
4.5	37.0%	32.7%	6.69
5	31.6%	27.8%	6.72
5.5	26.7%	23.3%	6.77
6	22.2%	19.2%	6.83
6.5	18.2%	15.6%	6.89
7	14.6%	12.5%	6.90
7.5	11.5%	9.8%	6.93
8	8.9%	7.6%	6.92
10	2.4%	2.0%	7.02
$\sigma_{tot}(\text{cm}^2)$	6.39×10^{-44}	1.08×10^{-44}	5.91

et al. [398]. The detectable fraction is $\approx 30\%$, if the recoil electron energy threshold is set at 5 MeV.

Two types of radiative corrections, those due to purely QED [399] and those characteristic of electroweak theory [400–404], can be handled separately. The QED correction amounts to multiplying the c_L^2, c_R^2 and $c_L c_R$ terms of (3.132) by the correction functions $[1 + \frac{\alpha}{\pi} f_i(s,y)]$ $(i = -, +, +-)$,

$$\sigma = \frac{2G_F^2 m_e E_\nu}{\pi} \int_0^1 dy \Big\{ c_L{}^2[1 + (\alpha/\pi)f_-] + c_R{}^2(1-y)^2[1 + (\alpha/\pi)f_+]$$
$$-c_L c_R[1 + (\alpha/\pi)f_{+-}]\frac{m_e}{E_\nu}y \Big\} \tag{3.138}$$

The analytic form of f_+ and f_- is given for $E_\nu \gg m_e$ as [403][8]

$$f_-(s,y) = -\frac{2}{3}\ln(s/m_e^2) + \ln(s/m_e^2)\left[\ln(1-y) - \frac{1}{2}\ln y + \frac{1}{2}y + \frac{1}{4}\right]$$
$$+\frac{1}{2}\left[L(y) + \frac{1}{6}\pi^2\right] - \frac{1}{2}\ln^2\frac{1-y}{y} + y\ln y$$
$$-\left(\frac{23}{12} + \frac{1}{2}y\right)\ln(1-y) - \frac{47}{36} - \frac{11}{12}y + \frac{1}{24}y^2 , \tag{3.139}$$

---

[8] The $c_L c_R$ interference term is small for $E_\nu \gg 1$ MeV, so f_{+-} is not important.

$$(1-y)^2 f_+(s,y) = -\frac{2}{3}(1-y)^2 \ln(s/m_e^2) + \ln(s/m_e^2)\left[\left(y(1-y) - \frac{1}{2}\right)\ln y\right.$$

$$+ (1-y)^2 \ln(1-y) - \frac{1}{2}(1-y)\Big]$$

$$+ \left[\ln^2 y - \frac{1}{6}\pi^2 - L(y)\right]\left[y(1-y) - \frac{1}{2}\right]$$

$$+ (1-y)^2 \ln(1-y)\left[\ln y - \frac{1}{2}\ln(1-y)\right] \qquad (3.140)$$

$$+ \ln y \left[-\frac{3}{4} + \frac{1}{2}y + y^2\right]$$

$$+ \frac{1}{3}(1-y)\ln(1-y)\left[-\frac{7}{2} + 5y\right] - \frac{1}{72}(1-y)(31 - 49y) ,$$

where $L(y)$ is defined by (3.64) and $s = 2m_e E_\nu$. Approximate expressions for f_+, f_- and f_{+-} including the electron mass effect are given in [404]. The effect of electron mass is negligible for $E_\nu > 1$ MeV.

The correction takes a simple expression for the total cross section for $E_\nu > 1$ MeV. The two coefficients c_L^2 and c_R^2 are modified as

$$\sigma = \frac{2G_F^2 m_e E_\nu}{\pi}\left\{\left[1 + \frac{\alpha}{\pi}F_-(s)\right]c_L^2 + \frac{1}{3}\left[1 + \frac{\alpha}{\pi}F_+(s)\right]c_R^2\right\} , \qquad (3.141)$$

with

$$F_- = -\frac{2}{3}\ln(s/m_e^2) - \frac{1}{6}\left(\pi^2 - \frac{19}{4}\right) ,$$

$$F_+ = F_- + 1 . \qquad (3.142)$$

$\ln(s/m_e^2)$ stands for mass singularity for the incoming state, implying that the correction is increasingly important at high energies. Note that mass singularities arising from the outgoing state that appears in in (3.139) and (3.140) are cancelled by summation of the final states [405].

The nonphotonic radiative correction of the electroweak theory is absorbed into changes of the coupling constants appearing in the effective Hamiltonian,

$$H_W^{\mathrm{eff}} = \frac{G_F}{\sqrt{2}}\rho^{(\nu,\ell)}[\bar{\nu}\gamma_\mu(1-\gamma_5)\nu]\{\bar{e}\gamma^\mu[c_V'(q^2) - c_A'(q^2)\gamma_5]e\} , \qquad (3.143)$$

where $\rho^{(\nu,\ell)} = 1$ for the charged-current-induced part[9], but it receives a correction for the neutral-current induced part as $\rho^{(\nu,\ell)} = 1.0126 \pm 0.0016$ [404]. The two coefficients, c_V' and c_A', are obtained in the $\overline{\mathrm{MS}}$ scheme by replacing

---

[9] The corrections are identical with those for μ decay, and hence the effects are absorbed into G_F. See [403].

$$\sin^2\theta_W \longrightarrow \kappa^{(\nu,\ell)}(q^2)\sin^2\hat\theta_W , \qquad (3.144)$$

where

$$\kappa^{(\nu_e,e)} = 0.9791 + 0.0097I(T'_e) \pm 0.0025 ,$$
$$\kappa^{(\nu_\mu,e)} = 0.9970 - 0.0004I(T'_e) \pm 0.0025 ; \qquad (3.145)$$

the integral I is

$$I(T'_e) = \frac{1}{6}\left[\frac{1}{3} + (3 - x^2)\left(\frac{1}{2}x\ln\frac{x+1}{x-1} - 1\right)\right] , \qquad (3.146)$$

with $x = (1 + 2m_e/T'_e)^{1/2}$. Analytic expressions for $\rho^{(\nu,\ell)}$ are given in (3b)–(3d), and $\kappa^{(\nu,\ell)}$ in (5a)–(5e) of [403].

By combining the two corrections,

$$\sigma = \frac{2G_F^2 m_e E_\nu}{\pi}\int_0^1 dy\Big\{c_L'^2[1 + (\alpha/\pi)f_-] + c_R'^2(1 - y)^2[1 + (\alpha/\pi)f_+]$$

$$-c_L'c_R'[1 + (\alpha/\pi)f_{+-}]\frac{m_e}{E_\nu}y\Big\} , \qquad (3.148)$$

where

$$c_L' = \rho^{(\nu,\ell)}[-1/2 + \kappa^{(\nu_\mu,e)}(q^2)\sin^2\theta_W] ,$$
$$c_R' = \rho^{(\nu,\ell)}\kappa^{(\nu_\mu,e)}(q^2)\sin^2\theta_W \qquad (3.149)$$

for $\nu_\mu e$ scattering and

$$c_L' = \rho^{(\nu,\ell)}[-1/2 + \kappa^{(\nu_e,e)}(q^2)\sin^2\theta_W] + 1 ,$$
$$c_R' = \rho^{(\nu,\ell)}\kappa^{(\nu_e,e)}(q^2)\sin^2\theta_W \qquad (3.150)$$

for $\nu_e e$ scattering ($\rho^{(\nu,\ell)}$ does not depend on ν_e or ν_μ).

For low-energy (5–10 MeV) neutrinos (with $T'_e > T'_{th} = 5$ MeV cutoff) the correction to the total cross section is -0.7% (QED)$+2.8\%$(weak) $= +2.1\%$ for $\nu_\mu e$ scattering and $-0.7 - 2.0\% = -2.7\%$ for $\nu_e e$ scattering. Hence, for example, $\sigma(\nu_e e)/\sigma(\nu_\mu e)$ in Table 3.6 will be ≈ 6.78 for $T'_{th} = 5$ MeV. The reason for small QED corrections is ascribed to the UV convergence of the radiative correction, the same as that for muon decay. A larger electroweak correction reflects the cutoff with vector bosons, at which the tree values are defined. The correction for the differential and total cross section are explicitly worked out in [401–404]. This is nonnegligible in precision solar neutrino experiments achieved today.

3.11 Neutrino–Nucleon Scattering

Neutrino–nucleon (nucleus) scattering (often referred to as quasi-elastic neutrino–nucleon scattering), $\bar\nu p \to e^+ n$ and $\nu n \to e^- p$, is historically called inverse beta decay [71]. Using (3.44) the cross section is written

$$\sigma = \frac{1}{2E_\nu} \int \frac{d^3 p_e}{2E_e (2\pi)^3} (2\pi)\delta(E_\nu - E_e \pm \Delta)\frac{1}{2}|T|^2, \qquad (3.151)$$

with $\Delta = m_n - m_p$, i.e.,

$$\sigma(\bar\nu_e p \to e^+ n) = \sigma(\nu_e n \to e^- p)$$

$$= \frac{G_F^2 E_e p_e}{\pi}|U_{ud}|^2 \left(1 + 3g_A^2\right) \qquad (3.152)$$

$$\simeq 9.30 \times 10^{-42} \left(\frac{E_\nu}{10\,\text{MeV}}\right)^2 \text{cm}^2, \qquad (3.153)$$

where the mass difference between the proton and the neutron is neglected and $g_A = 1.267$ and $\cos\theta_c = |U_{ud}| = 0.974$ are used in the last expression. The differential cross section is almost flat; $d\sigma/d\theta \propto 1 - 0.104\cos\theta$, where θ is the scattering angle of the recoil electron, as can be seen from (3.44); see also (3.172) below.

When we include $O(E_\nu/m_N)$ corrections, $(1 + 3g_A^2)$ in (3.152) becomes

$$1 + 3g_A^2 - \frac{E_\nu}{m_N}\left[(1 \pm g_A)^2 \pm 2g_A(\mu_p^a - \mu_n^a)\right], \qquad (3.154)$$

where $\pm$ refer to $\bar\nu_e p \to e^+ n$ (upper sign) and $\nu_e n \to e^- p$ (lower sign); $E_\nu \gg m_e$, $\Delta(\Delta = m_n - m_p)$ are assumed. This gives a few % correction for 5–10 MeV neutrinos. Note also that the energy of the recoil electron is smaller than that of the incident neutrino by the amount of

$$E_\nu - E_e \simeq \Delta + \frac{1}{m_p}\left[\frac{\Delta^2 - m_e^2}{2} + E_e(E_e + \Delta)\right] \qquad (3.155)$$

for $\bar\nu_e p \to e^+ n$ (for $\nu_e n \to e^- p$, the replacement, $\Delta \to -\Delta$ and $m_n \to m_p$, is made). This correction is important in estimating E_ν when the neutrino beam has a spectrum that falls off rapidly [406]. Radiative corrections also give a few % corrections, as calculated in [406, 407]. The problem of the uncertainty in the correction to the axial-vector-current-induced reaction is circumvented by using empirical neutron beta decay rate.

For energy $E_\nu \gtrsim 30$–50 MeV the structure of nucleons must be taken into account. Using the form factors defined by (3.42), the quasi-elastic scattering cross section is calculated [153, 154, 408, 409] to give

$$\frac{d\sigma}{d|q^2|}\begin{bmatrix} \nu_e + n \to p + e^- \\ \bar\nu_e + p \to n + e^+ \end{bmatrix}$$

$$= \frac{G_F^2}{4\pi}\cos^2\theta_c\left[A(q^2)\frac{m_N^2}{2E_\nu^2} \pm B(q^2)\frac{(s-u)}{2E_\nu^2} + C(q^2)\frac{(s-u)^2}{2m_N^2 E_\nu^2}\right], \qquad (3.156)$$

where the functions A, B and C are given by

$$A = \frac{m_\ell^2 - q^2}{4m_N^2} \left\{ \left(4 - \frac{q^2}{m_N^2} \right) F_A^2 - \left(4 + \frac{q^2}{m_N^2} \right) F_V^2 - \frac{q^2}{4m_N^2} \left(4 + \frac{q^2}{m_N^2} \right) F_W^2 \right.$$
$$- \frac{4q^2 F_V F_W}{m_N^2} - \frac{m_\ell^2}{m_N^2} \left[(F_V + F_W)^2 + (F_A + 2F_P)^2 \right.$$
$$\left. \left. - \left(4 - \frac{q^2}{m_N^2} \right) F_P^2 \right] \right\} , \tag{3.157}$$

$$B = -\frac{q^2}{m_N^2} F_A (F_V + F_W) , \tag{3.158}$$

$$C = \frac{1}{4} \left(F_A^2 + F_V^2 - \frac{q^2}{4m_N^2} F_W^2 \right) , \tag{3.159}$$

and

$$s - u = 4m_N E_\nu + q^2 - m_\ell^2 .$$

Here $q = p' - p$, and the form factors F_V, F_W, F_A and F_P are assumed to be real functions. The four-momentum transfer $q^2 = t$ is written using the electron recoil angle θ (lab system) with respect to the incident neutrino direction:

$$\cos\theta = \frac{(s - m_\nu^2 - m_N^2)(s + t - m_\nu^2 - m_N^2) + 2m_N^2(t - m_\nu^2 - m_\ell^2)}{\sqrt{K(s, m_\nu^2, m_N^2) K(u, m_\ell^2, m_N^2)}}, \tag{3.160}$$

with

$$K(x, y, z) = x^2 + y^2 + z^2 - 2xy - 2yz - 2zx, \tag{3.161}$$

where $m_\nu^2 = 0$ is retained for the symmetry of the expression.

For ν_e and ν_μ scattering the terms proportional to the lepton mass squared are all ignored, and we obtain

$$\frac{d\sigma}{d|q^2|} \left(\begin{matrix} \nu_e + n \to p + e^- \\ \bar{\nu}_e + p \to n + e^+ \end{matrix} \right)$$
$$= \frac{G_F^2}{4\pi} \cos^2\theta_c \left\{ (F_V + F_W \pm F_A)^2 + (F_V + F_W \mp F_A)^2 \left(1 + \frac{q^2}{2E_\nu m_N} \right)^2 \right.$$
$$+ \left[F_A^2 - (F_V + F_W)^2 \right] \frac{(-q^2)}{2E_\nu^2}$$
$$\left. + \left[F_W^2 \frac{(-q^2 + 4m_N^2)}{4m_N^2} - 2(F_V + F_W)F_W \right] \left[2 + \frac{q^2(m_N + 2E_\nu)}{2E_\nu^2 m_N} \right] \right\} , \tag{3.162}$$

where

$$\cos\theta = 1 + \frac{m_N q^2}{E_\nu(2m_N E_\nu + q^2)} \ . \tag{3.163}$$

From conservation of the vector current,

$$F_{V,W}(q^2) = F_{V,W}^{(p)}(q^2) - F_{V,W}^{(n)}(q^2) \ , \tag{3.164}$$

and $F_V(0) = 1$, $F_W(0) = (\mu_p^a - \mu_n^a)/\mu_N$, where $(\mu_p^a - \mu_n^a)/\mu_N = 3.706$ is the isovector combination of the proton and neutron anomalous magnetic moments in units of the nuclear magneton.

The parametrisation of the q^2 dependence, taken conventionally, is

$$F_V(q^2) = \left(1 - \frac{q^2}{m_V^2}\right)^{-2} \ ,$$

$$F_W(q^2) \propto F_V(q^2) \ ,$$

$$F_A(0) = (g_A/g_V)\left(1 - \frac{q^2}{m_A^2}\right)^{-2} \ , \tag{3.165}$$

where the scales of the dipole form factors are $m_V = 0.84$ GeV from electron scattering off protons [410] and $m_A = 1.05 \pm 0.05$ GeV from $\nu_\mu p \rightarrow \mu^- n$
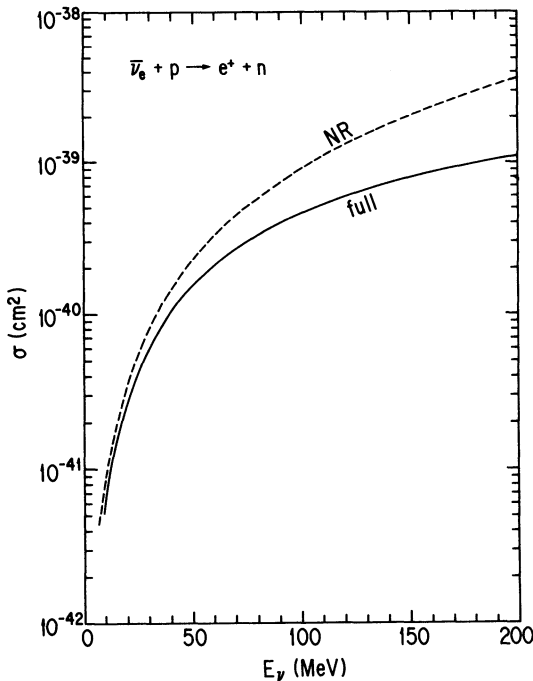
Fig. 3.6. Cross section of $\bar{\nu}_e + p \rightarrow e^+ + n$ calculated from the full expression (3.162). The nonrelativistic expression (NR) is also plotted for comparison.
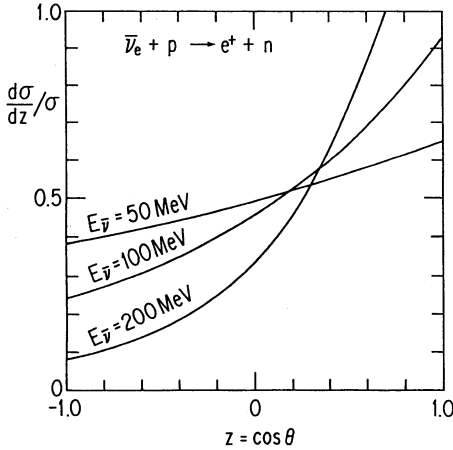
Fig. 3.7. Normalised differential cross section of $\bar{\nu}_e + p \to e^+ + n$. θ is the angle between the incident neutrino and the recoil electron.

scattering [411]. The total and differential cross sections are shown for $\bar{\nu}_e + p \to n + e^+$ in Figs. 3.6 and 3.7. The forward peak develops as E_ν increases, e.g., $\sigma(0°)/\sigma(180°) = 1.7$ at $E_\nu = 50\,\text{MeV}$ and 3.7 at $E_\nu = 100\,\text{MeV}$ for $\bar{\nu}_e + p \to e^+ + n$.

For the neutral-current interaction the effective Hamiltonian is

$$H_{\text{eff}} = \frac{G_F}{\sqrt{2}} \left[\bar{\nu}\gamma^\mu \left(1 - \gamma_5\right) \nu\right] \left\{ \bar{N} \left[(g_V \gamma_\mu + g_A \gamma_\mu \gamma_5) \frac{\tau_3}{2} - 2\sin\theta_W Q g_V \gamma_\mu\right] N \right\} ,$$

(3.166)

where $N = p$ or n. The cross section for $\overset{(-)}{\nu} p \to \overset{(-)}{\nu} p$ and $\overset{(-)}{\nu} n \to \overset{(-)}{\nu} n$ can then be obtained by replacing the form factors in (3.162) as

$$F_{V,W} \longrightarrow \pm\frac{1}{2} F_{V,W} - \sin^2\theta_W F_{V,W}^{(p \text{ or } n)} ,$$

$$F_A \longrightarrow \pm\frac{1}{2} F_A .$$

(3.167)

For experiments, we refer to [412]. The axial-vector form factor derived is $m_A = 1.06 \pm 0.05$ GeV consistent with the value from charged-current reactions.

Above the neutrino energy of 0.15 GeV, the threshold opens for pion production. Pion production becomes important at $> 0.34\,\text{GeV}$, when $\Delta_{33}(1232)$ is produced. Above 1 GeV multipion production dominates the neutrino–nucleon reactions. We discuss inelastic scattering in Sects. 3.13 and 3.14.

3.12 Neutrino–Nucleus Scattering

3.12.1 General Considerations

Neutrino–nucleus scattering is of practical importance since nuclei are often used as targets for detecting low-energy neutrinos. The advantage of using

a nuclear target lies in the fact that the reaction is selective, thus efficiently reducing the background. For very low energy neutrinos, $E_\nu \lesssim 5\,\text{MeV}$, this is the only method actually used to date for neutrino detection.[10]

For the low-energy neutrino reaction of $\nu_e + (A, Z) \to e^- + (A, Z + 1)$, only superallowed and allowed transitions contribute significantly, and the cross section is given by

$$\sigma = \frac{G_F^2}{\pi} \cos^2 \theta_c \sum_i |M_{\nu i}|^2 \, E_e \, (E_e^2 - m_e^2)^{1/2} F(Z + 1, E_e) \,, \qquad (3.168)$$

where

$$|M_{\nu i}|^2 = \langle 1 \rangle_i^2 + g_A^2 \langle \sigma \rangle_i^2 \qquad (3.169)$$

and the summation i is taken over the nuclear levels under consideration. This matrix element is the same as that for beta decays that appear in (3.50) up to the spin weight factors in the final state summation:

$$|M_\nu|^2 = |M_\beta|^2 \frac{(2J_B + 1)}{(2J_A + 1)} \qquad (3.170)$$

for the pair $B \to A + \bar{\nu} + e^-$ and $\nu + A \to e^- + B$. For $\nu_e + n \to p + e^-$, $\langle 1 \rangle^2 = 1$ and $\langle \vec{\sigma} \rangle^2 = 3$, and we recover (3.152).

We show examples of rough estimates of the reaction cross section in Table 3.7. They are much smaller than that expected for a free neutron times the number of neutrons in the nuclei and are often even smaller than that for a single neutron.[11] The differential cross section has an angular dependence of

Table 3.7. Neutrino (ν_e) captures in nuclei. The threshold energy for E_ν and cross section (for $E_\nu \sim 35\,\text{MeV}$) are shown.

		n	^{2}H	^{12}C	^{16}O	^{37}Cl	^{56}Fe
E_{th}	(MeV)	-0.78	1.44	17.34	15.43	0.814	4.57
σ	($\times 10^{-41}\text{cm}^2$)	11.4	5.9	1.50^a	0.64	8.3	28
σ/neutron	($\times 10^{-42}\text{cm}^2$)	114	59	2.5	0.80	4.2	9.3
Ref.		—	[413]	[414]	[415]	[416]	[417]

^{a}With the aid of experimental information.

[10] For antineutrinos, the background can be efficiently reduced by a coincidence technique using produced neutrons, and hence other methods can be successfully used.

[11] ^{18}O is an exceptional case; the neutrino cross section of ^{18}O is close to $2 \times \sigma(\nu n)$.

$$\frac{d\sigma}{d\theta} \propto 1 + \alpha\cos\theta\,, \tag{3.171}$$

where θ is the angle between the incident neutrino and the outgoing electron and α is

$$\alpha = \frac{\langle 1\rangle^2 - \frac{1}{3}g_A^2\langle\sigma\rangle^2}{\langle 1\rangle^2 + g_A^2\langle\sigma\rangle^2}\,, \tag{3.172}$$

as can be seen from (3.44). When a number of nuclear levels contribute, this α is summed over individual states with the weight of partial cross sections.

For neutrino–nucleus scattering, the ground state to ground state transition is calculated from the ft value of the relevant electron capture process (or β decay), as

$$\sigma = \frac{2\pi^2\log 2}{(ft)m_e^5}E_e p_e F(Z,E_e)\left(\frac{2J_B+1}{2J_A+1}\right) \tag{3.173}$$

from (3.50) and (3.168). For the transition to excited states, the Fermi transition $\langle 1\rangle^2$ is reliably calculated to an accuracy up to isospin violation. A reliable estimate is generally difficult for the Gamow–Teller (GT) matrix element. There are, however, a few exceptional cases. The best known example is neutrino capture on ^{37}Cl; the GT matrix elements for ^{37}Cl $\to$ ^{37}A can be estimated from β decay of the mirror process ^{37}Ca $\to$ ^{37}K $+\beta^+$ (see Fig. 3.8) [420], [418,419,421].
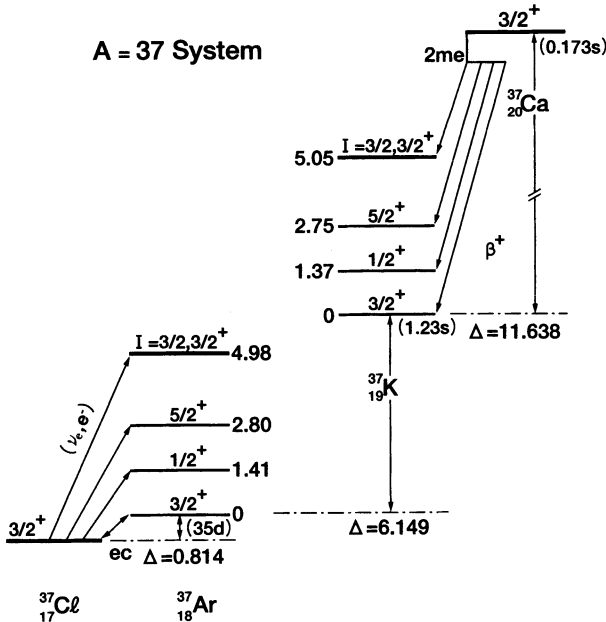
Fig. 3.8. $A = 37$ $^{37}_{17}$Cl–$^{37}_{18}$A–$^{37}_{19}$K–$^{37}_{20}$Ca system. Energy levels and the Q value Δ are in units of MeV. Levels denoted by thick lines are the $I = 3/2$ isobaric analogue states.

Table 3.8. GT matrix elements from the (pn) reaction compared with those from beta decay.

Nucleus	J_I	J_f	E_f	$B(GT)_\beta$	$B(GT)_{(p,n)}$	Ref.
^{13}C	$1/2^-$	$1/2^-$	gs	0.20	0.39	[427]
^{14}C	0^+	1^+	3.95	3.18	2.82	[427]
^{15}N	$1/2^-$	$1/2^-$	gs	0.26	0.54	[427]
^{17}O	$5/2^+$	$5/2^+$	gs	1.08	0.99	[427]
^{18}O	0^+	1^+	gs	3.18	3.54	[427]
^{19}F	$1/2^+$	$1/2^+$	gs	1.65	2.13	[427]
^{26}Mg	0^+	1^+	1.06	1.14	1.14	[427]
^{32}S	0^+	1^+	gs	0.0021	0.014	[428]
^{39}K	$3/2^+$	$3/2^+$	gs	0.27	0.39	[427]
^{39}K	$3/2^+$	$1/2^+$	2.47	0.00017	0.017	[428]

We have already discussed the accuracy of the GT element calculation using the shell model for p shell nuclei, as the most elementary case. The rms accuracy is a factor of 2 for level to level for low-lying levels. It is also likely that the accuracy deteriorates for higher excitations, for which higher shells contribute more importantly. The difficulty obviously increases as we go to the sd shell for $8 \leq N, Z \leq 20$. An example is shown in Table 3.9 below. The shell model calculation may be good only to the extent of predicting global characteristics and cannot be used for quantitative prediction.

Donnelly and Walecka [422] developed the approach in which single particle matrix elements of transition operators are evaluated empirically by electron scattering and/or electromagnetic decays. With sufficient experimental information, this should decrease the uncertainties and errors of the shell model calculation. It would be particularly powerful when we cannot apply other methods. The study so far is limited to $A = 12, 16$ [422, 423] and 11 nuclei [424].

Another general method often used to estimate GT matrix elements is to use an approximate proportionality between the GT matrix element and the (p, n) reaction cross section in the forward direction, as empirically found by Goodman et al. [425]. Ever since, much effort has been invested in this work, e.g., [426, 427]. The proportionality of the two reactions implies the validity of the direct reaction in (p, n) scattering that a spin–isospin flip strong interaction takes place in a single step to the nucleus, as happens in a meson exchange. Complications with strong interactions are treated with a distorted wave Born approximation (DWBA) for which the calculated cross section is proportional to the free GT value. The GT strength can be extracted as

$$B(GT) = [\sigma(0°)_{expt}/\sigma_{DWBA}(0°)]B(GT, free), \qquad (3.174)$$

Table **3.9.** Comparison of the Gamow–Teller matrix elements $g_A^2 \langle\boldsymbol{\sigma}\rangle^2$ for $^{37}\text{Cl}(\nu_e, e^-)\,^{37}$A.

^{37}Cl level (keV)	^{37}K level (keV)	J^P	^{37}Ca → ^{37}K β^+ Sextro et al. [420]	^{37}Ca → ^{37}K β García et al. [421]	^{37}Ca → ^{37}K β Trinder et al. [434]	sd shell[a] [369]
0	0	$3/2^+$	0.0493	0.0483	0.048(2)	0.072
1410	1371	$1/2^+$	0.0510	0.074(10)	0.013(1)	0.034
2796	2750	$5/2^+$	0.0833	0.067(4)	0.102(3)	0.273
3170	3239	$(5/2)^{+b}$	—	0.004(1)	0.087(4)	0.058
3602	3622	$3/2^+$	0.0907	0.075	0.073(2)	0.157
?	3840	?	0.118	0.094(5)	0.093(3)	$\times^c$
?	4191	?	—	0.002(1)	—	$\times^c$
?	4413	?	0.0464	0.043	—	$\times^c$
?	4495	$1/2^+$	0.0894	0.060	—	0.356
?	4665	?	0.0561	—	—	$\times^c$
?	5016	?	0.1186	0.064(64)	—	$\times^c$
4980	5051	$3/2^+$	3.083*	3.10(10)*	—	3.119*
?	5120	$1/2^+$	0.414	0.47(2)	—	$\times^c$
5130	5320	$3/2^+$	0.0868	0.048(3)	—	0.131

*The Fermi transition contribution is included.

[a] $g_A^{\text{eff}} = 1$ is used.

[b] Spin-parity assignment according to the shell model.

[c] Levels that do not appear in the sd shell model.

where $B(\text{GT, free})$ is the GT strength for the free nucleon [426]. In Table 3.8, a comparison is presented between the beta decay GT matrix element and the GT element deduced from the (p, n) reaction [427,428]. Reasonable agreement (within a factor of 2) is seen between the two values, at least for the transition with a large B(GT) value. The discrepancy, however, can be by a factor of $\gtrsim 10$ for small GT elements. Detailed tests are made mostly for light nuclei; it is unclear whether the agreement at this level holds for heavy nuclei, which are more important from the viewpoint of applications. A greater discrepancy has been known for this proportionality for the excited levels of the $^{37}\text{Cl} - ^{37}\text{A}$ transition, but the agreement improves significantly in newer experiments (as discussed below). A complication that enters the proportionality argument is the presence of $S = 1, L = 2$ ($J = 1$) operators ($\sim [Y^{(2)} \times \sigma]^{J=1}$) that may contribute to the (p, n) reaction in addition to the GT operator and significantly modify some GT elements estimated from (p, n) scattering [429, 428] (NB: The inclusion of this term hardly improves the disagreement seen for weak GT matrix elements in Table 3.8). This (p, n) method is also extended to $(^3\text{H}, ^3\text{He})$ [430]. The advantage is a fine energy resolution attained with ^3H compared with neutron detection. The disadvantage is an extra complication due to nuclear effects of the projectile.

In the following, we discuss several specific cases of interest: $\nu_e {}^{37}\text{Cl} \rightarrow e^- {}^{37}\text{A}, \nu_e {}^{71}\text{Ga} \rightarrow e^- {}^{71}\text{Ge}, \nu_e {}^{12}\text{C} \rightarrow e^- {}^{12}\text{N}$, and $\nu + d \rightarrow p + p + e^-, p + n + \nu$. For other candidate targets for low-energy neutrino detection, a reliable estimate of the neutrino capture cross section is far more difficult. For a systematic estimate of the neutrino capture cross sections relevant to solar neutrinos, see [431].

To represent solar neutrino captures, the *solar neutrino unit* (SNU) [432], 1 SNU=10^{-36} captures per target atom per second, is frequently used.

3.12.2 Examples of Specific Reactions

(i) $\nu_e {}^{37}\text{Cl} \rightarrow e^- \; {}^{37}\text{A}$.   This classic example of a low-energy neutrino target ($Q = 0.814$ MeV) [80,81,94,207] is a fortunate case for which reliable estimates of the low-energy neutrino capture cross section can be made for two reasons: (1) a large fraction of the cross section is due to the Fermi transition to the $3/2^+$ isobaric analogue state at 4.98 MeV ($\langle 1 \rangle^2 = 3$) [433], and (2) the other GT elements can be inferred from the mirror process $^{37}\text{Ca} \rightarrow ^{37} \text{K} + e^+ + \nu$ [418–421].

Various estimates are available for the GT matrix element, and this process also serves as a reference to assess the accuracy of those methods. The level scheme of $A = 37$ nuclei is shown in Fig. 3.8. GT strengths are compared in Tables 3.9 and 3.10 for low-lying ($E < 5.15$ MeV) states. Table 3.9 compiles GT elements estimated from $^{37}\text{Ca} \rightarrow ^{37} \text{K} + e^+ + \nu$, and compares them with a shell model calculation. Table 3.10 shows GT elements from (p, n) reactions. The shell model calculation is recapitulated as a reference. Figure 3.9 presents GT elements integrated over the 2-MeV energy interval, including states up to

Table 3.10. Comparison of the Gamow–Teller matrix elements $g_A^2 \langle\sigma\rangle^2$ for $^{37}\mathrm{Cl}(\nu_e, e^-)^{37}\mathrm{A}$.

^{37}Cl level (keV)	^{37}K level (keV)	J^P	(pn) Rapaport et al. [435]	(pn) Wells et al. [436]	(sd) shell[a] [369]
0	0	$3/2^+$	0.034		0.072
1410	1371	$1/2^+$	≤ 0.009	0.014(4)	0.034
2796	2750	$5/2^+$		0.077(10)	0.273
3170	3239	$(5/2)^{+b}$	0.23	0.136(15)	0.058
3605	3622	$(3/2)^{+b}$		0.075	0.157
?	3840	?			$\times^c$
?	4191	?			$\times^c$
?	4413	?			$\times^c$
?	4495	$1/2^+$	0		0.356
?	4665	?			$\times^c$
?	5016	?			$\times^c$
4980	5051	$3/2^+$	3.08		3.119
?	5120	$1/2^+$			$\times^c$
5130	5320	$3/2^+$			0.131

[a] $g_A^{\mathrm{eff}} = 1$ is used.
[b] Spin-parity assignment according to the shell model.
[c] Levels that do not appear in the sd shell model.
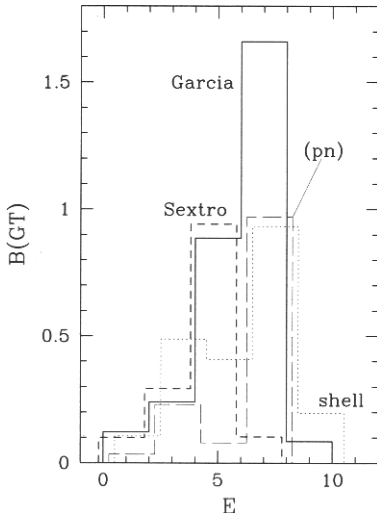
Fig. 3.9. GT strengths integrated over the 2-MeV energy interval for $^{37}\mathrm{Cl}\to^{37}\mathrm{A}$ transitions. The data from Sextro et al. [420], García et al. [421], (pn) data from Rapaport et al. [435], and an (sd) shell model calculation are shown.

8.8 MeV, which is a one-particle unbound threshold $(n+{}^{36}\text{Cl})$ [the α particle threshold opens at a lower energy (6.4 MeV), but this channel is practically negligible due to a high Coulomb barrier].

Columns 4 and 5 of Table 3.9 are GT elements from ${}^{37}\text{Ca} \rightarrow {}^{37}\text{K} + e^+ + \nu$, where ${}^{37}\text{K}$ is identified by its decay into ${}^{36}\text{Ar}$ with delayed proton emission. The experiments of Sextro et al. [420] and García et al. [421] measured the spectrum of this delayed proton for the ${}^{37}\text{K}$ states higher than the first excited state which lies below the one-particle unbound threshold of ${}^{37}\text{K}$. The GT strength to the first excited state is inferred by subtracting from the total decay width of ${}^{37}\text{Ca}$ the integrated GT (and Fermi) strengths to the one-particle unbound excited states and the GT strength to the ground state (gs). Even this relatively direct determination of the GT elements offers a number of subtle problems.

Reasonable agreement is seen between the results of Sextro et al. and García et al. for $E\lesssim5$ MeV, including the first excited state. For higher energy excitations, however, a large discrepancy is seen between the two. Sextro et al. reports basically zero GT strengths above 6.5 MeV: García et al.'s estimate gives very large (even larger than those for levels below 6 MeV) GT strengths. The latter agrees with that predicted in a shell model [437] and also inferred from the (pn) reaction. The missing GT strength of Sextro et al. is ascribed to their presumption that all ${}^{37}\text{K}$ levels above the one-particle threshold decays into $p+{}^{36}\text{A}(\text{gs}, 0^+)$. If the decay to ${}^{36}\text{A}(2^+, 1.97\,\text{MeV})$ is taken into account, as done by García et al., one recovers the strong GT strengths for high-lying levels predicted in the shell model. More recently, Trinder et al. [434] (Column 6 of Table 3.9 reported that γ emission is more important than proton emission for some excited ${}^{37}\text{K}$ states. García et al. estimated $\Gamma_\gamma/\Gamma_p = 1/100$ for the second excited level at 2750 keV and assumed that γ decays are negligible for all levels. Trinder et al., however, observed a ratio $\approx 1/2$ for the 2750-keV level. They also found that the γ decay width is 20 times that for p decay for the third excited level, which means that the GT strength to $5/2^+(3170)$ is underestimated by a factor of 20 by García et al. This revision improves the agreement of the GT strengths from ${}^{37}\text{Ca}$ beta decay and (pn) reactions, for which an order of magnitude discrepancy existed before the experiment of Trinder et al. They also give generally larger strengths for other states and hence resulted in a much smaller GT strength (by a factor of 4–6) for the first excited state, which brings its GT value in good agreement with that inferred from the (pn) reaction.

The (pn) experiment was carried out by Rapaport et al. [435] (see Column 4 of Table 3.10 and more recently by Wells et al. [436] (Column 5). The level to level agreement between the GT from ${}^{37}\text{Ca}$ β decays and that from (pn) is better than 50% at least for the first four levels with the new data [Wells et al.'s for (p,n) data and Trinder et al.'s for ${}^{37}\text{Ca}$ β decay data]. The large discrepancy (often by more than one order of magnitude) seen in the earlier data (Rapaport et al. vs. Sextro et al. or García et al.) is mostly

ascribed to the incompleteness of both experiments. A large discrepancy still visible between the two is too small GT's from (pn) in the 5-MeV region. One may suspect it as a result of oversubtraction of the Fermi strength in the (pn) experiment [437]. The resolution of Rapaport et al.'s (pn) experiment is not sufficient to make a detailed level to level comparison. We must wait for a high resolution (pn) experiment at higher levels before drawing conclusions about the accuracy of the GT strengths from the (pn) experiment.

The shell model result quoted in the tables uses the wave functions of Brown and Wildenthal [369] with a quenched axial-vector coupling constant $g_A = 1$. The integrated GT strengths are rather close to the value estimated from ^{37}Ca, though the shape is appreciably tilted (see Fig. 3.9). For level to level, the agreement with experimentally deduced matrix elements is by a factor of 2–3. An interesting feature of the shell model is that very strong GT strengths above 6.5 MeV *were* correctly predicted. Whether quenching is necessary is a matter of debate ([369] versus [380]), depending on the nuclear model used [377].

Notwithstanding significant changes from Sextro et al. to García et al. and then to Trinder et al., the neutrino capture cross section for solar neutrinos has changed little. This is largely because about 65% of the expected capture cross section is given by the Fermi transition to $A(3/2^+, E = 4.98\,\text{MeV})$, and the integrated GT strengths between 1.4 and 5 MeV are similar among the various estimates.[12] For higher energy neutrinos, such as those from stopped muon decays, however, the GT strengths of García et al. give a significantly larger cross section compared with that calculated with Sextro et al.'s data. The cross section for low-energy neutrinos is presented in Fig. 3.10 with various GT matrix elements. The numerical values from Bahcall et al. [398] which use the assessment of Aufderheide et al. [438] are given in Table 3.11 for low-energy neutrinos. Table 3.12 compares various estimates of integrated values for ν_e from stopped μ^+.[13]

(ii) $\nu_e\,^{71}\text{Ga} \rightarrow e^-\,^{71}\text{Ge}$.   The important solar neutrino target ^{71}Ga [230] offers another example from which one can estimate the solar neutrino capture rate with good accuracy. ^{71}Ga $(3/2^-, \text{gs}) \rightarrow\,^{71}$Ge $(1/2^-, \text{gs})$ has a sufficiently low threshold $(Q = 0.2327\,\text{MeV})$ [441] to detect the most copious pp solar neutrinos $(E_{\text{max}} = 0.42\,\text{MeV})$, yet the first excited state $(5/2^-, 0.175\,\text{MeV})$

---

[12] This is due to a somewhat tricky, but lucky situation. The cross section for the neutrino flux other than ^{8}B neutrinos is solely determined by the GT(gs), which is well determined. For the ^{8}B neutrino capture cross section a large change from García et al.'s B(GT) to Trinder et al.'s B(GT) is mostly a redistribution of the GT strengths at low-lying levels. It is fortunate that the first excited level of ^{37}A is located above the maximum energies of all solar neutrino fluxes other than ^{8}B neutrinos and that the GT strength to the first excited state is estimated by subtraction from the total decay rate, which is well constrained.

[13] The calculation of Kuramoto et al. takes into account the large GT strengths for $E > 5$ MeV levels, as expected from the (pn) experiment.
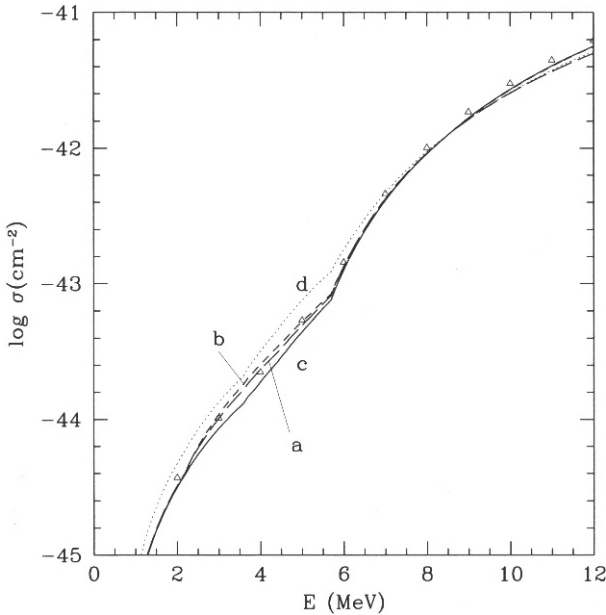
Fig. 3.10. Neutrino capture cross sections for ^{37}Cl. The four curves are based on the GT elements of (a) Sextro et al., (b) García et al., (c) Trinder et al. with higher excitations using García et al.'s, and (d) the Brown–Wildenthal sd shell model with $g_A = 1$. The triangles are the estimates of Bahcall et al. [398] quoted in Table 3.11.

Table 3.11. Cross sections for ^{37}Cl(ν_e, e^-) ^{37}A and for ^{71}Ga(ν_e, e^-) ^{71}Ge at low energies (in units of 10^{-42}cm^2, taken from [398, 445].

E_ν	$\sigma(^{37}$Cl$)$	E_ν	$\sigma(^{71}$Ge$)$	E_ν	$\sigma(^{71}$Ge$)$
1	5.21×10^{-4}	0.24	1.31×10^{-3}	4	0.213
2	3.70×10^{-3}	0.25	1.36×10^{-3}	5	0.438
3	1.02×10^{-2}	0.275	1.50×10^{-3}	6	0.843
4	2.23×10^{-2}	0.3	1.66×10^{-3}	7	1.53
5	5.38×10^{-2}	0.35	2.02×10^{-3}	8	2.58
6	0.144	0.4	2.41×10^{-3}	9	3.97
7	0.462	0.45	2.86×10^{-3}	10	5.71
8	1.01	0.5	3.31×10^{-3}	11	7.78
9	1.85	0.6	4.30×10^{-3}	12	10.2
10	3.00	0.7	5.40×10^{-3}	13	12.9
11	4.45	0.8	6.85×10^{-3}	14	15.9
12	6.21	0.9	8.28×10^{-3}	15	19.1
13	8.27	1.0	9.83×10^{-3}	16	22.6
14	10.6	1.2	1.44×10^{-2}	18	30.4
15	13.3	1.4	1.92×10^{-2}	20	39.0
16	16.2	1.6	2.55×10^{-2}	30	87.9
18	22.8	1.75	3.06×10^{-2}		
20	30.5	2.0	3.97×10^{-2}		
30	82.0	3.0	9.91×10^{-2}		

Table 3.12. Cross sections for $^{37}\text{Cl}(\nu_e, e^-)\,^{37}\text{A}$ for ν_e from stopped muons. Units are in cm^2.

Bahcall–Ulrich [439]	Donnelly–Haxton [440]	Kuramoto et al. [416]
7.2×10^{-41a} 7.6×10^{-41b}	9.9×10^{-41}	$(9.4 \pm 1.4) \times 10^{-41}$

^{a}without/ ^{b}with forbidden corrections.

Table 3.13. Solar neutrino capture rate on ^{71}Ga in units of SNU. Flux is taken from Bahcall et al. (BP2000) [442].

	$pp\nu$	other ν's	Sum
Ground state	69.7	43.1	112.8
Excited states	0.0	15.1	15.1
Sum	69.7	58.2	128
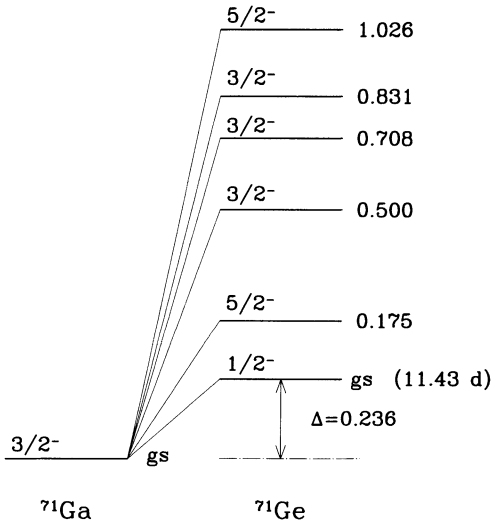
Fig. 3.11. Energy levels of the ^{71}Ga–^{71}Ge system.

lies at an energy that is so high that pp neutrinos contribute very little. As a result, 87% of the neutrino capture takes place through ground-to-ground transition (see Table 3.13). For the rest, uncertainties in GT matrix elements could change the capture rate by as much as a factor of 2 or more. However, the uncertainty in the total capture rate still remains small.

In Fig. 3.11, we show a few low-lying levels of ^{71}Ge. The GT strength for the ground($3/2^-$) to ground($1/2^-$) transition is well known from the electron capture rate [$B(\text{GT}) = 0.087 \pm 0.001$] [443]. The estimate varies

for excited levels. Table 3.14 gives a compilation of estimates for the two lowest excited states. The first row is the values inferred from systematics of the $3/2^- \rightarrow 5/2^-$ transitions in neighbouring nuclei [431]. A criticism on this is the presence of the example that largely violates "systematics": ^{73}Ga$(3/2^-) \rightarrow^{73}$ Ge$(1/2^-)$ is suppressed by 50 times compared to the ground–ground transition of ^{71}Ge$(3/2^-) \rightarrow^{71}$ Ga$(1/2^-)$ [428]. The next three lines are estimates from (p,n) scattering [429, 431], and the third presents Haxton's limit when the $S = 1, L = 2$ term is included. The fifth line is the value extracted from the reaction ^{3}He $+^{71}$ Ga $\rightarrow^3$ H $+^{71}$ Ge [430]. The next two lines are theoretical calculations [446, 447], which largely disagree with each other. The last line (bold-faced) gives a limit from the GALLEX ^{51}Cr experiment [448], which we discuss in what follows.

The gallium solar-neutrino experiment groups carried out cross section calibration experiments using a very strong artificial radioactive source of ^{51}Cr (see Sect. 4.8.5 for more discussion). The ^{51}Cr source produces two monoenergetic neutrino lines from electron capture, one to the ground state of ^{51}V ($E_\nu \simeq 746$ keV, 90%), and the other to its $5/2^-$ excited state ($E_\nu \simeq 431$ keV, 10%) (more precisely speaking each line further splits into two lines corresponding to K and L captures). The first component of neutrinos excites the two lowest excited Ge levels in addition to the ground state, whereas the second allows only the transition to the ground state. Therefore, a constraint, when normalised to the ground-to-ground GT strength, is given on the combination

$$R = \left[1 + 0.667 \frac{B(\mathrm{GT}, 5/2^-, 0.175)}{B(\mathrm{GT}, \mathrm{gs})} + 0.218 \frac{B(\mathrm{GT}, 3/2^-, 0.500)}{B(\mathrm{GT}, \mathrm{gs})} \right] . \quad (3.175)$$

The two experiments give $R = 0.98 \pm 0.08$ (GALLEX [448]) and $R = 1.00^{+0.13}_{-0.12}$ (SAGE [449]), which indicate that the data are consistent with the ground-to-ground transition alone, meaning that the GT strengths to excited states are significantly smaller, assuming that there is no unknown normalisation error in the experiments. The limits on the GT strengths obtained from the GALLEX result is given in the last line of Table 3.14. The limit is consistent with the results from the (p, n) reaction, but only the upper limits can be deduced. This result leaves an uncertainty up to 8% for ^{7}Be solar neutrino capture (34 SNU).

The capture cross section for ^{8}B neutrinos is much more uncertain because many higher levels contribute. The (p, n) studies indicate that there are a number of strong GT levels that are as large as $B(\mathrm{GT})/B(\mathrm{GT}, \mathrm{gs}) = $ 3–5 (at > 4 MeV). In Bahcall's estimate using the (pn) data, the integrated GT amounts to $36.3B(\mathrm{GT}, \mathrm{gs})$, giving $\sigma(^8\mathrm{B}) = 2.40 \times 10^{-42}$cm^2 or 12.1 SNU (12% is due to the ground-to-ground transition) [445]. Ejiri et al. [430] estimate it from ^{3}H $+^{71}$ Ga $\rightarrow^3$ H $+^{71}$ Ge with the result that $\sum B(\mathrm{GT}) = (42.8 \pm 1.3)B(\mathrm{GT}, \mathrm{gs})$, and gives $\sigma(^8\mathrm{B}) = 2.26 \times 10^{-42}$cm^2 (11.4 SNU). Bahcall's estimate of the low-energy cross section is given in Table 3.11.

Table 3.14. The strength of GT matrix elements for excited levels of ^{71}Ge.

Authors	$B(5/2^-)/B(gs)$	$B(1/2^-)/B(gs)$	Methods
Bahcall et al. [431]	< 0.046		Systematics
Krofcheck et al. [444]	< 0.005	0.011 ± 0.002	(p, n)
Bahcall [445]	< 0.056	0.146	(p, n)
Hata and Haxton [428]	< 0.087	< 0.057	(p, n), w/$L = 2$ operator
Ejiri et al. [430]	0.055 ± 0.019	0.233 ± 0.024	$(^3\mathrm{H}, ^3\mathrm{He})$
Mathews et al. [446]	0.23	0.014	Theory
Grotz et al. [447]	0.001	0.86	Theory
Anselmann et al. [448]	**<0.06**	**<0.28**	GALLEX ^{51}Cr

3.12.3 Nuclear Excitation with the Neutral Current

The neutral current induces nuclear excitation $\nu A \to \nu A^*$. Such excitation can be measured by counting γ rays emitted in the transition back to the ground state [450–453,424,454]. This offers the interesting possibility of measuring neutral-current-induced neutrino reactions at low energy. This experiment is of particular interest for neutrino physics because the neutral-current-induced reactions are not affected by neutrino oscillation, the most plausible explanation for the solar neutrino problem.

Since the isoscalar axial-vector current does not cause nuclear excitation, we consider only the isovector axial-vector current part of (2.70). The effective interaction is given by

$$H_{\mathrm{eff}} \simeq \frac{G_{\mathrm{F}}}{2\sqrt{2}} g_A \boldsymbol{\sigma} \tau_3 [\bar{\nu}\gamma(1 - \gamma_5)\nu] \ . \tag{3.176}$$

The cross section is then

$$\sigma = \frac{G_{\mathrm{F}}^2}{\pi} \sum_i |M_i|^2 (E_\nu - E_i)^2 \ , \tag{3.177}$$

where

$$|M_i|^2 = |\frac{1}{2}\langle \boldsymbol{\sigma}\tau_z \rangle|^2 \ . \tag{3.178}$$

This matrix element is often estimated from the $ep \to e'p$ reaction or from the magnetic dipole transition, as in the Donnelly–Walecka formalism.

Special considerations have been given to nuclear excitation of ^{6}Li : $1^+ \to 0^+$ (3.162 MeV) [451, 452]; ^{11}B : $3/2^- \to 1/2^+$(2.11MeV), $5/2^-$ (4.45 MeV), $3/2^+$(5.02 MeV) [424] (see Fig. 3.12); ^{12}C : $0^+ \to 1^+$ (15.1 MeV) [414, 451–453, 455], and ^{13}C : $1/2^- \to 3/2^-$(3.68 MeV), $1/2^-$(8.86 MeV), $3/2^-$(9.90 MeV) [454]. ^{11}B has been proposed as a promising target for solar-neutrino detection [424]. The 1^+ level of ^{12}C is too high for solar neutrinos, but it is a good candidate for detecting neutral-current-induced neutrino reactions from a stellar collapse [174]. The special interest in carbon is that

^{11}B – ^{11}C System
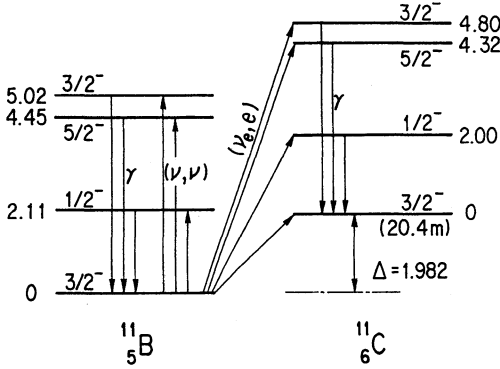
Fig. 3.12. $^{11}_5$B–$^{11}_6$C mirror system.

it is a major ingredient of organic scintillators, which are used for low-energy neutrino detection. The neutral-current reaction has already been measured with ^{12}C using the neutrino beam from stopped muons (see Sect. 3.12.4). Natural carbon contains 1.1% ^{13}C and could be used to detect solar neutrinos [454].

3.12.4 Neutrino Reactions off Carbon

The uniqueness of ^{12}C is that the GT transition of ^{12}C(0^+, gs) to the triad 1^+ states ^{12}N(1^+, gs), ^{12}C(1^+, 15.1 MeV), and ^{12}B(1^+, gs) can be calculated in a model-independent manner. On the experimental side, carbon is the only nuclear target (along with deuterium) for which a laboratory experiment is available, that allows a test of the calculation. For earlier theoretical work with ^{12}C we refer to [456, 457].

The 1^+ states are the famous triad that was used for the decisive test of weak magnetism to verify the CVC hypothesis [63]. We may treat the nucleus as an elementary particle with given quantum numbers and express the matrix elements in terms of the form factors allowed by the transformation properties of the current and the nuclear states. This treatment should be sufficiently good for low-energy reactions. Insofar as the nuclear form factors are well constrained by experimental data, we can make a model-independent prediction of the neutrino reactions.

The matrix elements for the vector and axial-vector currents for the neutral current reactions are written:

$$\langle ^{12}\mathrm{C}(1^+); p'|V^3_\mu(0)|^{12}\mathrm{C}(0^+); p\rangle = \frac{1}{\sqrt{2}} \frac{\epsilon_{\mu\nu\lambda\sigma} q^\nu P^\lambda \varepsilon^\sigma}{2M} F_\mathrm{M}(q^2)\,, \qquad (3.179)$$

$$\langle ^{12}\mathrm{C}(1^+); p'\,|A^3_\mu(0)|\,^{12}\mathrm{C}(0^+); p\rangle$$

$$= \frac{1}{\sqrt{2}} \left[\varepsilon_\mu F_A(q^2) + q_\mu(\varepsilon\cdot q)\frac{F_\mathrm{P}(q^2)}{m_\pi^2} + P_\mu(\varepsilon\cdot q)\frac{F_T(q^2)}{2M}\right],$$

$$(3.180)$$

where $q = p'-p$, $P = (p+p')/2$, $M = M(^{12}C)$ and ε is the polarisation vector for a spin 1 nucleus. An application of the Wigner–Eckart theorem allows us to represent the $\langle ^{12}N(1^+); p'|(V, A)^+_\mu(0)|^{12}C(0^+); p\rangle$ elements by exactly the same expression with the factor $1/\sqrt{2}$ removed. For electron production, one can ignore the F_P term which contributes with a factor of lepton mass squared.

The form factors at zero momentum transfer can be evaluated from beta and gamma decays of the triad: $F_M(0)$ from $^{12}C^*(1^+, 15.1\,\mathrm{MeV}) \to$ $^{12}C^*(\mathrm{gs}) + \gamma$ with the aid of CVC $[\Gamma_\gamma = (2/3)\alpha F^2_M E^3_\gamma]$; F_A (and a small contribution from F_T) from the ft values for $^{12}N^*(1^+, \mathrm{gs}) \to^{12} C^*(\mathrm{gs}) + \beta^+$ and $^{12}B^*(1^+, \mathrm{gs}) \to^{12} C^*(\mathrm{gs})+\beta^-$; the ratio F_T/F_A from angular correlations of the same beta decays. We obtain $F_A(0) = 0.711 \pm 0.024$, $F_T(0)/F_A(0) = 0.0020 \pm 0.0002$, and $F_M(0) = (1.516 \pm 0.016) \times 10^{-3}\,\mathrm{MeV}^{-1}$.

The q^2 dependence becomes important as energy increases. The q^2 dependence of F_M is obtained from inelastic electron scattering $e +^{12} C \to$ $e +^{12} C^*(1^+, 15.1\,\mathrm{MeV})$. With a parametrisation motivated by the nuclear model that includes spin-orbit coupling,

$$F_M(|q|^2) = F_M(0) \left[1 - \frac{1-\rho}{6}(b|q|)^2\right]^2 \exp\left[-\frac{1}{2}(b|q|)^2\right] , \qquad (3.181)$$

where $b = 1.88 \pm 0.5$ fm, and $\rho = 0.23(1 \pm 0.1)$ [458].[14] For the axial-vector form factor, the relation $F_A(q^2)/F_A(0) = F_M(q^2)/F_M(0)$ holds within 10% accuracy up to $q^2 \simeq (120\,\mathrm{MeV})^2$, as indicated from muon capture of ^{12}C [461].

If we ignore a contribution from the tensor (2% at 15 MeV), the cross section is given by

$$\sigma = \frac{3G^2_F}{2\pi}F^2_A E'^2_\nu I , \qquad (3.182)$$

with

$$I = \frac{1}{2}\int_{-1}^{1} dz f(|q|^2)\left\{ \left(1 - \frac{z}{3}\right) \pm \frac{4}{3}(E_\nu + E'_\nu)(1 - 2\sin^2\theta_W)(1 - z)\frac{F_M}{F_A}\right.$$
$$\left. +\frac{2}{3}\left[E'_\nu + E_\nu(1 - z^2) + (1 - z)q^2\right](1 - 2\sin^2\theta_W)^2 \left(\frac{F_M}{F_A}\right)^2\right\}$$

$$(3.183)$$

for the neutral-current-induced reaction, where the upper (lower) sign refers to the neutrino (antineutrino) reaction and scattering angle θ is represented

---

[14] For more recent electron scattering data, see [459]. As a later verification, q^2 dependence of F_A from νC scattering is roughly described by $b \approx 2.0 \pm 0.8$ fm [460].

by $z = \cos\theta$. E_ν and $E'_\nu = E_\nu - \Delta M$ ($\Delta M = 15.1$ MeV) refer to energies of the incident and final-state neutrinos. The cross section for the charged-current reaction is obtained by replacing the factors E'^2_ν with $E'_e p'_e$ and E'_ν with E'_e, setting $\sin^2\theta_W = 0$, and multiplying the expression by a factor of 2 times $\cos^2\theta_c$.

This calculation, sometimes called 'elementary particle treatment' (EPT), was carried out in [414] up to $E_\nu = 100$ MeV. The error comes mostly from uncertainties in the input data and isospin violation and is estimated to be 12% at ≈ 100 MeV. The result was confirmed by other calculations [462, 455]. The latter authors and the authors of [463] extended the calculation to higher energies, 135 MeV for $\sigma(\nu_e^{12}\mathrm{C} \to e^{12}\mathrm{N})$ and 160(250) MeV for $\sigma(\nu_\mu^{12}\mathrm{C} \to \mu^{12}\mathrm{N})$. These calculations are not directly constrained (most importantly due to the lack of $F_A(q^2)$ for a large q^2), but the agreement with experiment is still reasonable, as we discuss below. The cross section for ν_e increases to $E_\nu \simeq 100$ MeV, and then remains constant at higher energies. Table 3.15 gives cross sections up to 50 MeV, taken from [414] [the calculation includes the tensor component omitted in (3.183)]. We summarise in Table 3.16 the prediction of charged- and neutral-current-induced reactions for neutrinos from stopped muon decays.

There are also a number of calculations of these processes with a variety of shell-model-like approaches. The problem with the nuclear shell calculation is that the ground state of $^{12}\mathrm{C}$ is not described well by the lowest energy $(p_{3/2})^4$ configuration but mixes largely with $(p_{1/2})^2(p_{3/2})^2$. The calculation yields generically a cross section larger than experiment by a factor of ≈ 4. Donnelly [423] and Donnelly and Peccei [453] used the shell model whose

Table 3.15. Cross section of neutrino $^{12}\mathrm{C}$ reactions (in units of $10^{-42}\mathrm{cm}^2$), taken from [414].

E_ν (MeV)	$^{12}\mathrm{C}(\nu_e, e^-)^{12}\mathrm{N}$	$^{12}\mathrm{C}(\bar{\nu}_e, e^+)^{12}\mathrm{B}$	$^{12}\mathrm{C}(\nu, \nu)^{12}\mathrm{C}^*$	$^{12}\mathrm{C}(\bar{\nu}, \bar{\nu})^{12}\mathrm{C}^*$
E_{th}	17.34 MeV	13.37 MeV	15.11 MeV	15.11 MeV
16	—	0.086	0.010	0.0095
18	0.036	0.327	0.106	0.099
20	0.287	0.711	0.302	0.279
22	0.772	1.23	0.599	0.547
24	1.49	1.87	0.994	0.896
26	2.44	2.62	1.49	1.32
28	3.62	3.48	2.07	1.82
30	5.03	4.42	2.74	2.38
35	9.47	7.10	4.78	4.03
40	15.1	10.1	7.26	5.95
45	21.8	13.2	10.1	8.03
50	29.2	16.4	13.1	10.2

Table 3.16. Cross section of $\nu+\ ^{12}$C reactions (in units of 10^{-42}cm^2) for the neutrino beam from stopped muons.

Authors	Method	$\langle^{12}\mathrm{C}(\nu_e,e^-)^{12}\mathrm{N}\rangle$ stopped μ	$\langle^{12}\mathrm{C}(\nu_e,\nu_e)^{12}\mathrm{C}$ $+^{12}\mathrm{C}(\bar{\nu}_\mu,\bar{\nu}_\mu)^{12}\mathrm{C}\rangle$ stopped μ
Donnelly [423]	Shell model	12[a]	
Donnelly-Peccei [453]	Shell model		3.6+3.6=7.2
Fukugita et al. [414]	EPT	9.2	4.5+5.4=9.9
Minz/Pourkaviani [455, 462]	EPT	9.0	4.9+5.8=10.7
Kolbe et al. [465]	RPA	9.3	4.7+5.9=10.6
Engel et al. [463]	Shell model	9.1	9.8
Auerbach et al. [466]	RPA	7.1–10.1	
Hayes and Towner [467]	Shell model	8–35	
Allen/Krakauer et al. [464]	Expt.	$10.5 \pm 1.0 \pm 1.0$	
KARMEN [468]	Expt.	$9.4 \pm 0.5 \pm 0.8$	$11 \pm 0.85 \pm 1.0$
LSND [470]	Expt.	$9.1 \pm 0.4 \pm 0.9$	

[a]9.4 is quoted in [464].

single particle matrix elements are rescaled to fit electromagnetic decays. Kolbe et al. [465, 463] introduced an empirical reduction factor of 4 to fit the beta decay process in their random phase approximation (RPA) calculations that are applied to nuclear excitations including continuum levels (called continuum RPA) [471]. This reduction factor is 2.7 times larger than the value that is deduced for beta decays of general p shell nuclei. After this reduction, the predicted cross section agrees well with that from EPT up to ≈ 150 MeV. Auerbach et al. [466] indicated that this reduction is explained by considering the pairing correlation in the framework of RPA, but Vogel [472] claims the contrary. A large shell-model space calculation ($\leq 4\hbar\omega$) was done by Hayes and Towner [467]. The prediction varies depending on the treatments. The results of these calculations are also quoted in Table 3.16. For reviews, see [473, 472].

The experiment was carried out by three groups: two groups at LAMPF (ANL-Irvine-LANL Collaboration [464] and LSND [470]) and one group (KARMEN) at ISIS [468] of the Rutherford Laboratory. The first group of the LAMPF experiments used neutrinos from stopped μ^+. The KARMEN experiment used neutrino beams from the beam dump with monoenergetic $\nu_\mu = 29.8$ MeV from stopped π^+, and ν_e and $\bar{\nu}_\mu$ from stopped μ^+ up to 52.8 MeV. The LSND group used neutrino beams from π^+ decaying in flight in addition to those from stopped μ^+. The detector (=target) was liquid or plastic scintillators in all experiments. The resulting cross sections are given in Table 3.16. The three experiments verify the EPT predictions (and also the others that agree with EPT) within a $\approx 10\%$ error of the experiments.

Table 3.17. Cross section of $\nu +$ ^{12}C reactions (in units of 10^{-42}cm^2) (continued).

Authors	Method	$\langle^{12}\text{C}(\nu_\mu,\nu_\mu)^{12}\text{C}\rangle$ stopped π	$\langle^{12}\text{C}(\nu_\mu,\mu^-)^{12}\text{N}\rangle$ π decay in flight
Donnelly-Peccei [453]	Shell model	2.7	
Fukugita et al. [414]	EPT	2.7	
Minz/Pourkaviani [455, 462]	EPT	2.7	
Engel et al. [463]	EPT		62.9
Kolbe et al. [465]	RPA	2.8	64−75
Engel et al. [463]	Shell model		63.5
Auerbach et al. [466]	RPA		39−50
Hayes and Towner [467]	Shell model		70−240
KARMEN [469]	Expt.	$3.2 \pm 0.5 \pm 0.4$	
LSND [470]	Expt.		$66 \pm 10 \pm 10$

In Table 3.17 neutral-current-induced nuclear excitation is shown. The measurements were made only for the sum of (ν_e, ν_e) plus $(\bar\nu_\mu, \bar\nu_\mu)$. The two components can be separated if experiments are carried out with oppositely charged stopped muons because the difference in the spectra between ν_e and ν_μ from decayed muons leads to $\approx$30% difference in averaged cross sections.

The experiment also measured the cross section to excited states and showed that the ground-to-ground transition is the dominant (65%) component. Krakauer et al. [464] found that $\langle\sigma(^{12}\text{C}(\nu_e,e^-)^{12}\text{N}^*)\rangle$ is $5.4 \pm 1.9 \times 10^{-42}$cm^2, KARMEN [468] obtained $5.7 \pm 0.8 \times 10^{-42}$cm^2, and LSND [470] $6.1 \pm 1.4 \times 10^{-42}$cm^2. The theoretical calculation is model-dependent, but it is encouraging to see that the RPA calculation of Kolbe et al. [465] gives 6.3×10^{-42}cm^2, in agreement with the experiment (with an empirical quenching factor of 4, however). LSND additionally measured $\sigma(^{12}\text{C}(\nu_\mu,\mu^-)^{12}\text{N(gs)}) = 66 \pm 14 \times 10^{-42}$cm^2 for ν_μ beams arising from pion decays in flight (E = 123–280 MeV with $\langle E\rangle$ =156 MeV). An EPT calculation requires some extrapolations of the form factors and also a poorly unconstrained F_P, but it gives a cross section in good agreement with the experiment [463]. The value is also given in Table 3.17.

Note that transitions to the $A = 12$ triad are only the case where EPT can be applied. For other nuclei, sufficient empirical information is not available to constrain the form factors. Another remark concerns the difference between ^{12}C and ^{16}O. In the former case, the ground-to-ground transition is of allowed type and has a large GT matrix element. Thus the cross section increases as $(E - E_{\text{th}})^2$ from the threshold. For ^{16}O(0^+) the ground-to-ground transitions [to ^{16}F(0^-), E_{th} = 15.42 MeV; ^{16}N(2^-), E_{th} = 10.42 MeV] is forbidden. GT transitions take place only to excited states, the 3.76, 4.65, and 6.23 MeV levels for ^{16}F; and the 3.36, 4.32, and 5.24 MeV levels for ^{16}N. So the

effective threshold energy is higher than the real threshold by 5 MeV or so. For ν_e interaction on a natural oxygen target, $^{18}O \rightarrow ^{18}F$, for which the ground-to-ground transition is allowed with $E_{th} = 1.66$ MeV, dominates at low energies below 20 MeV, in spite of a very small natural abundance of ^{18}O (0.204%). Calculations are carried out using the shell model in [415, 474].

3.12.5 Neutrino Reactions off Deuterium

Deuterium offers the case for which one can calculate the neutrino reaction cross section with good accuracy [475–478]. This is due to the fact that deuterium is a two-body system and the Schrödinger equation can be solved with good accuracy given the empirically determined nuclear force and also to the fact that nucleon–nucleon scattering is not very sensitive to the details of the short range nuclear force [479]. An advantage of deuterium as a low energy neutrino detector [234]is that the cross section of $\nu + d \rightarrow e^- + p + p$ is much larger than that of $\nu + e$ elastic scattering, so that the detector size can be made small. It would give us information different from that obtained from neutrino electron scattering because the deuterium reaction is sensitive only to the charged current: the difference in the estimated fluxes from the two reactions is taken as the contribution of the neutral-current-induced-reaction to electron scattering. Furthermore, a deuterium target offers the promising possibility of detecting directly the neutral-current interaction through the dissociation process $\nu + d \rightarrow \nu + p + n$ by identifying the neutron using the characteristic γ ray arising from its subsequent absorption into deuterium, e.g., $n + d \rightarrow ^3He + \gamma$ (6.25MeV) or that from capture on some heavier nuclei doped into the detector as neutron absorbers.

The low-energy two-proton final state is in $^1S_0$. So the transition from the deuteron $^3S_1$ takes place via the Gamow–Teller matrix element. The reaction cross section for $\nu + d \rightarrow e^- + p + p$ is given by

$$\sigma = \int dE_N d\Omega_e \frac{1}{4\pi^4} E_e p_e m_p p \, G_V^2 F(E_e, 2) g_A^2 \left(1 - \frac{1}{3}\cos\theta\right) |J|^2 , \quad (3.184)$$

where $p = |\mathbf{p_1} - \mathbf{p_2}|/2$ is the relative momentum of the two protons, $E_N = p^2/2m_p$, and

$$J = \int dr \frac{F_0(pr)}{p} u_d(r) , \quad (3.185)$$

where $u_d(r)$ is the radial wave function of a deuteron and F_0 is the wave function of the two-proton scattering state $(r = |\mathbf{x_1} - \mathbf{x_2}|)$.[15] The factor $1/3$ in the angular dependence is that of the pure Gamow–Teller transition; see (3.172). The neutral-current-induced dissociation cross section, $\sigma(\nu + d \rightarrow$

---

[15] Our definition of the radial wave function of F_0 differs from that adopted in [480] by a factor of $(4\pi)^{1/2}$, which comes from the spherical harmonics.

$\nu + p + n$), is given by the same expression as (3.184) with the replacement $G_V^2 \to G_F^2/2$.

Early calculations used effective range approximations to evaluate the integral J [475]. Modern calculations resort to the explicit use of wave functions obtained from a phenomenological nuclear potential with an impulse approximation. More elaborate estimates use the expression in terms of the reduced matrix elements of higher multipole operators and take account of higher partial waves of the final nucleons [481]. Modern work includes computations of Kubodera and collaborators [480,473] and of Haxton and collaborators [482, 483].[16] Both groups calculated the cross section up to ∼160–170 MeV. An appreciable disagreement between the two groups in their early publications was resolved in their later versions. The review of Kubodera and Nozawa [473] gives an annotation as to the origin of the discrepancies and the resolution.

The remaining discrepancy between the two calculations is 5% (see Fig. 3.14 below), and it was ascribed to the pion exchange current, which was included in that of Nozawa et al. [473] but not in Ying et al. [483]. It is shown that higher partial waves are not very important up to $E_\nu \sim 100$ MeV. The size of a p wave is comparable to that of an s wave only at 160 MeV. The d wave contribution is still one-fifth that of an s wave even at this energy.[17]

More recently, Nakamura et al. [413] updated the calculations of [473] and carried out a detailed comparison with other calculations. Their results are shown in Fig. 3.13. For convenience we reproduced their numerical results for cross sections up to 50 MeV in Table 3.18. The result of [413] differs from that of [473] up to 5% at high energies (see Fig. 3.14), and this is primarily caused by the updated choice of the mass scale of the axial-vector form factor. They showed that the results depend little ($< 1\%$) on the choice of the adopted phenomenological nuclear potential [485]. It was also demonstrated that the result agrees with that of Ying et al. to within 1% if the exchange current is switched off and the same form factors are used in calculating them.

The size of the effect of the meson exchange current is still a matter of debate. Nakamura et al. estimated it from a fit to the M1 transition amplitude of $n+p \to \gamma+d$, and the size in $\nu+d$ reaction to be about 5%, which increases to 8% at higher energies. Carlson et al. [486] used the tritium β decay rate to estimate the meson exchange current effect. With their estimate, the contribution to the νd reaction is about 2%, and 5% at higher energies. Unless more

---

[16] See also Butler and Chen [484], who used nucleon–nucleon effective field theory to calculate νd cross sections. In their calculation, however, there is one free parameter (an isovector axial two-body matrix element), and the results agree with those of either Kubodera et al. or Haxton et al. depending on the choice of this parameter. The calculation is limited to a low-energy region < 20 MeV.

[17] This contrasts with the earlier conclusion of Ying et al. [482], which is ascribed to an error in their computer code [473, 483].
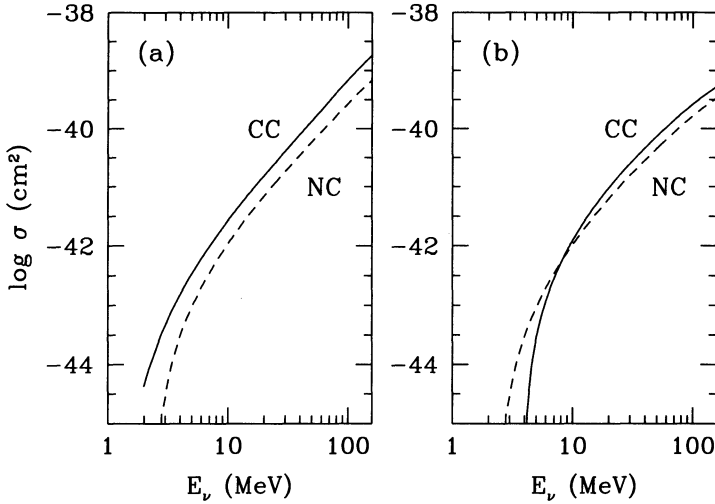
Fig. 3.13. Neutrino reaction cross sections on deuterium (**a**) $\nu_e + d \rightarrow e^- + p + p$ (*solid curve*) and $\nu + d \rightarrow \nu + p + n$ (*dashed curve*); (**b**) $\bar{\nu}_e + d \rightarrow e^+ + n + n$ (*solid curve*) and $\bar{\nu} + d \rightarrow \bar{\nu} + p + n$ (*dashed curve*). Data are taken from calculations of [413].

systematic studies are done, the size of the exchange current remains a main uncertainty of the $\nu + d$ reaction cross-section calculations. We may assign a 3% error to the state-of-the-art calculation of the absolute value of the cross section for low-energy neutrinos up to 50 MeV. This uncertainty, however, mostly cancels if one takes the ratio of charged- to neutral-current cross sections. The uncertainty in the ratio is smaller than 0.3% at low energies. The uncertainty seems to increase for $E_\nu > 100$ MeV.

A recent experiment [487] confirms the calculations (see Table 3.19), but the error (10−20%) is not small enough to differentiate the details of the calculations. Note that recent solar neutrino experiments with deuterium targets require the accuracy of the calculation better than a few percent.

The size of radiative corrections one expects is about the same order of magnitude as the uncertainty of the nuclear calculations. For pioneering work on radiative correction, see Towner [488]. He assumed that the inner radiative correction of the axial-vector part is equal to that of the vector part which is calculable. For the correction of the neutral-current-induced reaction, his renormalisation scheme is obscure.

3.12.6 Neutrino–Nucleus Reactions at Middle–High Energies

Estimation of the cross section for $E_\nu \gtrsim 50$ MeV is much more difficult because many higher excitations contribute but also forbidden transitions start to contribute significantly. Furthermore, one has to retain the terms involving $O(E_\nu/M)$ and higher orders in calculating the matrix elements. Yet, such

a calculation is of practical importance for detecting neutrinos of astrophysical or cosmic-ray origin. A straightforward method is the summation of contributions from individual levels, but when inclusive reactions become more important, there are other useful approaches: (i) a closure approximation using a sum rule [417, 489] and (ii) a Fermi gas model [490–494]. In the closure approximation, we replace the summation

$$\sum_f [E_\nu - (E_f - E_i)]^2 |\langle f|M|i\rangle|^2 \quad \rightarrow \quad [E_\nu - \langle \Delta E_{fi}\rangle]^2 \langle i|M^* M|i\rangle \;, \quad (3.186)$$

where $\langle \Delta E_{fi}\rangle$ is the average of the excitation energy $E_f - E_i$. This approximation is expected to be good for $E_\nu \gg E_f - E_i$. Pauli blocking is taken into account in evaluating the $M^* M$ matrix element. In the Fermi gas model, the reaction is assumed to take place through quasi-free scattering of nucleons contained in the noninteracting Fermi gas.

Here we consider three examples which are of experimental importance: $^{37}Cl(\nu_e, e^-)^{37}A$, $^{16}O(\nu_\ell, \ell)X$, and $^{12}C(\nu_\ell, \ell)X$. Chlorine detectors measure only argon final states. For this reaction, contributions from excited states are
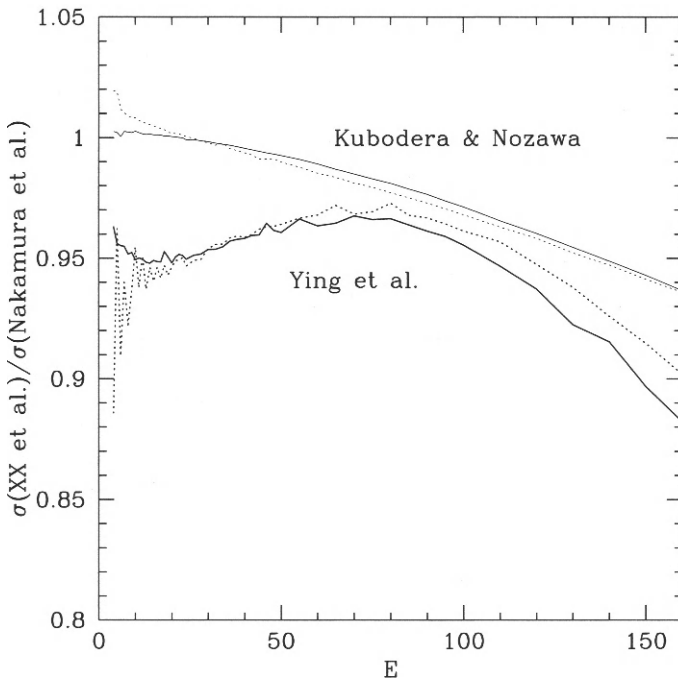
Fig. 3.14. Difference in cross sections among different calculations. The curves compare the ratios of the cross sections of Ying et al. [483] (*thick curves*) and Kubodera & Nozawa [473] (*thin curves*) to those of Nakamura et al. [413]. The *solid lines* are for $\nu_e + d \rightarrow e^- + p + p$ and the *dashed lines* for $\nu + d \rightarrow \nu + p + n$.

Table 3.18. Cross section of the neutrino reactions on deuterium (in units of 10^{-42}cm^2), taken from [413].

E_ν (MeV)	$\nu_e + d \to$ $e^- + p + p$	$\nu + d \to$ $\nu + p + n$	$\bar{\nu}_e + d \to$ $e^+ + n + n$	$\bar{\nu} + d \to$ $\bar{\nu} + p + p$
2.0	0.0036	—	—	—
3.0	0.0464	0.00336	—	0.00332
4.0	1.547	0.0306	—	0.0301
5.0	0.342	0.0947	0.0280	0.0927
6.0	0.617	0.201	0.118	0.196
7.0	0.984	0.353	0.279	0.342
8.0	1.450	0.553	0.518	0.532
9.0	2.016	0.802	0.835	0.767
10.0	2.686	1.100	1.233	1.047
12.0	4.349	1.851	2.270	1.741
14.0	6.456	2.811	3.626	2.614
16.0	9.024	3.984	5.295	3.663
18.0	12.07	5.374	7.268	4.886
20.0	15.61	6.984	9.539	6.279
25.0	26.71	11.99	16.46	10.49
30.0	41.21	18.45	25.07	15.70
35.0	59.34	26.40	35.25	21.86
40.0	81.30	35.88	46.89	28.93
45.0	107.3	46.92	59.88	36.86
50.0	137.4	59.54	74.13	45.59

explicitly added to the neutron emission threshold of 8.8 MeV using B(GT) obtained from ^{37}Ca$\to^{37}$K+β^+ with the aid of the information from the (pn) reaction and the shell model [416]. The calculation is made for neutrino energies up to $E_\nu = 300$ MeV. The authors note that uncertainties in the calculation rapidly increase from $E_\nu \simeq 80$ MeV due to the increase of contributions from poorly constrained forbidden transitions, which exceed those from allowed GT transitions for $E_\nu \gtrsim 100$ MeV. Below 70 MeV the allowed transition dominates, and the calculation is reasonably constrained.

Table 3.19. Deuterium reaction cross sections for antineutrinos from a reactor.

	$\sigma(\bar{\nu} + d \to e^+ + n + n)$	$\sigma(\bar{\nu} + d \to \bar{\nu}^+ + p + n)$
Calc. [473]	10.02×10^{-45} cm^2	6.02×10^{-45} cm^2
Expt. [487]	$9.83 \pm 2.04 \times 10^{-45}$ cm^2	$6.08 \pm 0.77 \times 10^{-45}$ cm^2
Ratio	0.97 ± 0.21	1.01 ± 0.13
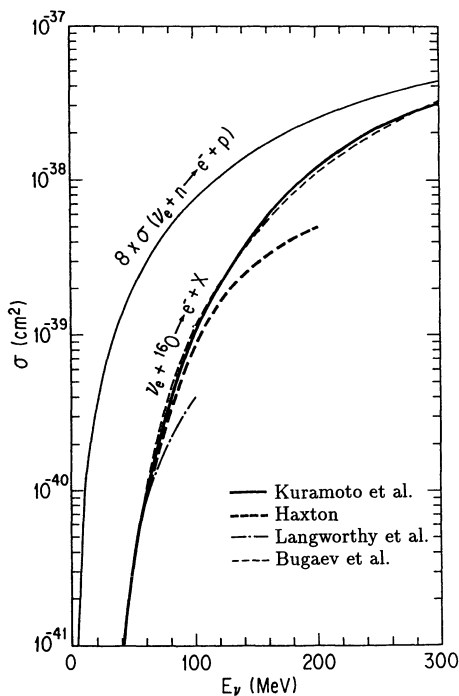
Fig. 3.15. Neutrino reaction cross sections on ^{16}O (inclusive reactions). The calculations of Langworthy [474] and Haxton [415] use the shell model, and those of Bugaev et al. [491] and Kuramoto et al. [416] adopt a Fermi gas model. $8 \times \sigma(\nu_e + n \to e^- + p)$ is also plotted for comparison.

Oxygen is an essential constitutent of water Čerenkov detectors, and many considerations have been made to date. Examples of calculations are shown in Fig. 3.15 for the inclusive reaction $\nu_e +^{16} O \to e^- + X$. Langworthy et al. [474] and Haxton [415] made explicit summations of excited levels using the shell model. In particular, the latter author takes all levels of ^{16}F states up to $2\hbar w(1\hbar w)$ excitations for positive (negative) parity states. The bending of the cross section as energy increases, compared with other curves, however, indicates that the number of states is still insufficient to describe scattering in an $E_\nu \sim 100$-MeV region: the result seems to be valid only up to 70 MeV. Bugaev et al. [491] and Kuramoto et al. [416] used the (relativistic) Fermi gas model. The two cross sections agree with each other and smoothly continue to the shell-model calculation at low energy (see [416] for detailed discussion). The Super-Kamiokande group [493] used the Fermi gas model for the event simulation; the resulting cross section agrees well with the calculations of [491,416]. Singh and Oset [494] also carried out a relativistic Fermi gas model calculation. Their prediction is close to other Fermi gas results at high energies but significantly lower at low energies. All Fermi gas results approach $8 \times \sigma(\nu_e + n \to e + p)$ at high energies, as the Fermi blocking effect becomes unimportant. We do not depict closure approximation calculations. These calculations [489,495] give cross sections significantly higher than the Fermi gas model as energy increases (by a factor of 2 at 300 MeV). They

even exceed $8 \times \sigma(\nu_e + n \to e + p)$ at high energies (typically for $E_\nu > 200$ MeV), implying that this approach overestimates the coherent nuclear effect, which is typical of giant resonances. This effect becomes conspicuous when the energy is higher than the giant resonance energy. RPA (continuum RPA) gives a result very similar to the Fermi gas model for high energies [413]. The cross section used by the Super-Kamiokande group is given in Table 3.20 [493].

The treatment is similar for $^{12}C(\nu_\ell, \ell)X$. For this reaction an experiment is available for both $\ell = e$ (neutrinos from stopped muons) and $\ell = \mu$ (neutrinos from decays of π in flight). The average energy for the former is low, but it is 156 MeV for the latter. The RPA calculation gives a correct cross section for the low-energy $^{12}C(\nu_e, e)X$ reaction, as we discussed above, but gives the $^{12}C(\nu_\mu, \mu)X$ cross section of 19×10^{-40}cm^2, which is larger by a factor of 2 [496] than the experiment, $11.3 \pm 0.3 \pm 1.8 \times 10^{-40}$cm^2 [470]. The same is true with a prediction of the Fermi gas model. A large space shell-model calculation [467] gives a similar result. There are a few a posteriori attempts which could reduce this cross section by nearly a factor of 2, bringing the result in agreement with experiment [497,466]. It is, however, not clear whether the assumptions used in these models are justified.

This disagreement in $^{12}C(\nu_\mu, \mu)X$ cross section is alarming because a similar effect may happen for $^{12}O(\nu_\mu, \mu)X$, which plays a major role in atmospheric neutrino detection. It is, however, possible that the discrepancy of a factor of 2 takes place only for ^{12}C, which is far from a closed shell; we might expect good behaviour for ^{16}O, a typical closed shell.

Table 3.20. Neutrino ^{16}O cross sections used in the event simulation of the Super-Kamiokande group (in units of 10^{-40} cm^2).

E_ν (MeV)	$\sigma(\nu_e, e^-)$	$\sigma(\bar{\nu}_e, e^+)$	$\sigma(\nu, \nu)$	$\sigma(\bar{\nu}, \bar{\nu})$	$\sigma(\nu_\mu, \mu^-)$	$\sigma(\bar{\nu}_\mu, \mu^+)$
40	0.12	0.064	0.045	0.028		
60	0.26	0.14	0.10	0.060		
80	0.54	0.25	0.21	0.11		
100	1.22	0.48	0.47	0.21		
120	1.90	0.72	0.73	0.31	0.13	0.055
140	3.16	1.04	1.21	0.45	1.03	0.39
160	4.60	1.39	1.76	0.61	2.21	0.84
180	6.22	1.76	2.38	0.77	3.58	1.28
200	8.34	2.17	3.19	0.95	5.53	1.75
220	10.5	2.58	4.00	1.13	7.47	2.22
240	12.5	3.02	4.79	1.32	9.65	2.70
260	14.6	3.45	5.58	1.51	11.9	3.17
280	16.6	3.89	6.36	1.70	14.1	3.64
300	18.5	4.32	7.09	1.88	16.1	4.10

3.13 Single Pion Production

Pion production becomes important as the energy of an incident neutrino increases. The charged-current interaction gives rise to $\nu N \to \mu^- N\pi$ and $\bar{\nu} N \to \mu^+ N\pi$. The final $N\pi$ system may be decomposed into $I = 1/2$ and $3/2$ states; one may write the single pion production as

$$A(\nu N \to \mu^- N\pi) = \sum_{I_s = 1/2, 3/2} c_{I_s} A_{I_s} \qquad (3.187)$$

with c_{I_s} the Clebsch–Gordan coefficients for the πN channel. Specifically, $\nu n \to \mu^- p\pi^+$ receives a contribution only from $A_{3/2}$.

The proper evaluation of these amplitudes requires a full nonperturbative treatment of the πN system, which is not possible. The phenomenological approach picks up only empirically important contributions to this process. The $I = 3/2$ amplitude is dominated by isobar $\Delta_{33}(1232)$ production, $\nu N \to \mu^- \Delta_{33}$ followed by $\Delta_{33} \to \pi N$ [498–501]. The scattering matrix element is written

$$T = \frac{G_V}{\sqrt{2}} \langle \Delta^\lambda | V_\mu - A_\mu | N \rangle \bar{\nu}(k') \gamma^\mu (1 - \gamma_5) \ell(k) . \qquad (3.188)$$

To see the form of the vector form factors, we inspect an effective Lagrangian for the $N\Delta$ vertex of the vector field tensor $F^{\mu\nu}$

$$\mathcal{H}_{\text{eff}} = i \frac{C_3^V}{m_N} \bar{\Delta}_\nu \gamma_5 \gamma_\mu N F^{\mu\nu} + \frac{C_4^V}{m_N^2} (\partial_\mu \bar{\Delta}_\nu) \gamma_5 N F^{\mu\nu} + \frac{C_5^V}{m_N^2} \bar{\Delta}_\nu \gamma_5 (\partial_\mu N) F^{\mu\nu} . \qquad (3.189)$$

The $N\Delta$-transition vector form factor is thus parametrised as

$$\langle \Delta(p'') | V_\mu | N(p) \rangle = U_\rho(p'') \left\{ \left[(-qg^{\rho\mu} + q^\rho \gamma^\mu) \frac{C_3^V}{m_N} + (-qp'' g^{\rho\mu} + q^\rho p''^\mu) \frac{C_4^V}{m_N^2} \right. \right.$$
$$\left. \left. + (-qpg^{\rho\mu} + q^\rho p^\mu) \frac{C_5^V}{m_N^2} \right] \gamma_5 \right\} u(p) , \qquad (3.190)$$

where $p'' = p + q$ and conservation of the vector current is assumed. The axial-vector form factor is simple:

$$\langle \Delta(p'') | A_\mu | N(p) \rangle = U_\rho(p'') C_5^A u(p). \qquad (3.191)$$

Using the PCAC relation applied to Lehmann–Symanzik–Zimmermann (LSZ)'s reduction of $\langle \Delta | \pi N \rangle$, $C_5^A(0) = g_{\pi N\Delta} f_\pi / m_\pi$, where $g_{\pi N\Delta}$ is the $\pi N\Delta$ coupling constant defined by

$$\mathcal{H}_{\text{int}} = \frac{g_{\pi N\Delta}}{m_\pi} \bar{N} \Delta_{i\mu} \partial^\mu \pi_i + \text{h.c.} , \qquad (3.192)$$

and $g_{\pi N\Delta} = 2.1$ from the decay width of Δ.

The cross section is calculated as

$$\frac{d\sigma}{dt} = \frac{1}{2\pi} \frac{m_N m_\Delta}{(s - m_N^2)^2} H_{\mu\nu}^\lambda L^{\mu\nu} \, , \tag{3.193}$$

where $t = (k - k')^2$,

$$H_{\mu\nu} = \frac{1}{2} G_V^2 \langle \Delta^\lambda | V_\mu - A_\mu | N \rangle \langle \Delta^\lambda | V_\nu - A_\nu | N \rangle^* \, , \tag{3.194}$$

and

$$L^{\mu\nu} = k^\mu k'^\nu + k^\nu k'^\mu - (k \cdot k') g^{\mu\nu} - \epsilon^{\mu\nu\sigma\rho} k_\sigma k'_\rho \, . \tag{3.195}$$

The vector form factors are multiplied by the mass difference $m_N - m_\Delta$ or its power. This means that the axial-vector contribution dominates, and we obtain

$$\frac{d\sigma}{dt} \simeq \frac{G_V^2}{12\pi} \frac{s - m_\Delta^2}{s - m_N^2} \left(\frac{m_\Delta + m_N}{m_\Delta} \right)^2 |C_5^A(t)|^2 \, . \tag{3.196}$$

Using $C_5^A(0) = 2.0$, we obtain the differential cross section in the forward direction as $d\sigma/dt|_{t=0} \simeq 1.2 \times 10^{-39}$ cm^{2}GeV^{-2} in agreement with $\nu p \to \mu^- p \pi^+$ experiments for $m_{p\pi} < 1.4$ GeV [502, 503]. To estimate the total cross section, we need an assumption concerning the t dependence of the form factor. If we take the dipole form with the effective axial-vector mass scale m_A, integration for a large s yields

$$\sigma = \frac{G_V^2}{36\pi} |C_5^A(0)|^2 \left(\frac{m_A}{m_N} \right)^2 \left[(m_\Delta + m_N)^2 + m_A^2/2 \right] \, . \tag{3.197}$$

If we take $m_A = 0.8$ GeV consistent with the differential cross-section data, the asymptotic (large s) total cross section is $\sim 4 \times 10^{-38}$ cm^2, which is consistent with the $\nu p \to \mu^- p \pi^+$ experiment for $m_{p\pi} < 1.4$ GeV [502–505] (see Fig. 3.16).

For a more detailed calculation, we need to consider off-shell Δ, which can be done by considering the amplitude

$$A_\Delta = \frac{G_F}{\sqrt{2}} \cos\theta_C J_\mu^{(\ell)} \frac{g_{\pi N\Delta}}{m_\pi} \bar{u}(p') q'^\nu i \frac{1}{(p+q)^2 - m_\Delta^2} U_\nu(p+q) \tag{3.198}$$

$$\times \langle \Delta(p+q) | V_\mu - A_\mu | N(p) \rangle \, , \tag{3.199}$$

where p and p' are momenta of the incoming and outgoing nucleons and q' is the momentum of the outgoing pion; $[(p+q)^2 - m_\Delta^2]^{-1} U_\nu(p+q) \langle \Delta(p+q)|$ in this expression is in fact off shell, and the wave function together with $[(p+q)^2 - m_\Delta^2]^{-1}$ should be replaced with the propagator for the spin 3/2
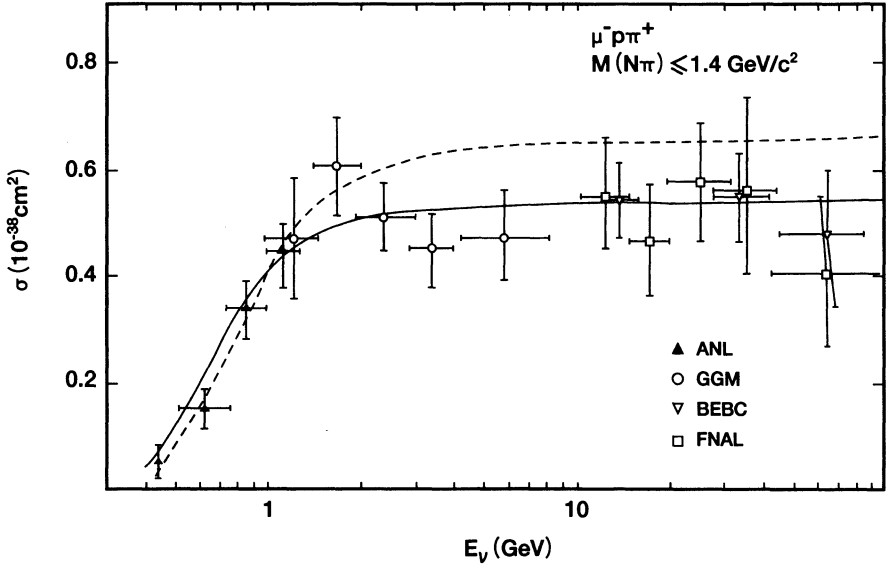
Fig. 3.16. Cross section of $\nu p \to \mu^- p\pi^+$ as a function of the energy of the neutrino for the final hadron invariant mass of $M(N\pi) \leq 1.4$ GeV. The *solid curve* is the prediction of Fogli and Narduli [501], and the *dashed* is that of Rhein and Sehgal [508], compared with data taken from BEBC [502], FNAL [503], ANL [504], and Gargamelle (GGM) [505].

Rarita–Schwinger field of Δ,

$$\Delta_{\mu\nu}(p) = \frac{U_\mu(p)\bar{U}_\nu(p)}{p^2 - m_\Delta^2}$$

$$= \frac{1}{p^2 - m_\Delta^2}\left[\left(g_{\mu\nu} - \frac{p_\mu p_\nu}{m_\Delta^2}\right) - \frac{1}{3}\left(g_{\mu\rho} - \frac{p_\mu p_\rho}{m_\Delta^2}\right)\left(g_{\nu\lambda} - \frac{p_\nu p_\lambda}{m_\Delta^2}\right)\gamma^\rho\gamma^\lambda\right].$$

$$(3.200)$$

We must retain vector form factors, which are interrelated as $C_4^V(0) = (m_N/m_\Delta)C_3^V(0)$, and $C_5^V(0) = 0$ from the knowledge of Δ photoproduction that is dominated by a magnetic dipole transition. The magnitude of these form factors is fixed by an electroproduction experiment to give $C_3^V(0) = 2.07$.

Most uncertain in the calculation is the momentum dependence of the form factors. Fogli and Narduli [501] assume a soft form factor $\exp(-a\sqrt{q^2})$ for the vector part [506] and a dipole form for the axial-vector part [507].

As one goes to a larger invariant mass of $N\pi$, the $I = 1/2$ channel also becomes important. Examples of conspicuous nucleon resonances are $D_{13}(1520)$, $D_{15}(1670)$ and $F_{15}(1688)$. Fogli and Narduli considered only resonances with $m_{N\pi} < 1.6$ GeV and take account of $P_{11}(1440)$, $D_{13}(1520)$, and $S_{11}(1535)$, in

addition to the nucleon Born term. The nucleon Born term is given by

$$A_N = \frac{G_\mathrm{F}}{\sqrt{2}} cos\theta_C J_\mu^{(\ell)} g_{NN\pi} \bar{u}(p')\gamma_5 \frac{i}{(p+q)^2 - m_N^2} u(p+q)$$

$$\times \langle N(p+q)|V_\mu - A_\mu|N(p)\rangle \,, \tag{3.201}$$

for which the parametrisation of the form factors was already discussed in Sect. 3.11. An appropriate modification is needed for higher spin resonances. Rhein and Sehgal [508] summed all resonances up to $m_{N\pi} < 2$ GeV (in both I=1/2 and 3/2 channels), using quark model predictions for the coupling parameters. They found that the calculated pion production cross section for the $I = 1/2$ channel is smaller than experiment, and added incoherently the contribution from an arbitrary constant scattering matrix element to fit the data.

Fogli and Narduli considered, in addition, contributions from pion exchange in the crossed channel (t-channel) and nucleon exchange in the other crossed channel (u-channel), which both behave as a smooth background in the s channel. The difference in the cross sections between the two authors [501, 508] is about 20%.

The calculation of the total cross section by Fogli and Narduli is shown in Fig. 3.16 together with experimental data (with a hydrogen target) [502–505]. We note that the nuclear effect is ignored in these calculations, although the experiments are often done with nuclear targets. The calculation is parallel for the $\bar{\nu}$ induced reaction, but the sign of the VA interference term of the leptonic part is reversed.

The calculation of neutral-current-induced pion production was done in an analogous way by modifying the vector and axial-vector couplings to $g_V = 1-2\sin^2\theta_W$ and $g_A = 1$, except that we must add the contribution from the isoscalar current [509]. The isoscalar current is purely of the vector type, and the relevant form factors can be estimated from the electroproduction of pions. See [510] for nuclear effect considerations.

3.14 Deep-Inelastic Neutrino Scattering off Nucleons

In high-energy neutrino scattering, the nucleon fragments into multihadrons, which experimentalists do not explicitly identify in most cases. The outgoing lepton is observed, and its momentum distribution gives information on the structure of hadrons, i.e., how the quarks are distributed in hadrons in momentum space. This is called inclusive experiments.

For kinematics when a large momentum transfer is involved, the inclusive process is described by a parton model of Feynman, where nucleons are pictured as an assembly of quarks and scattering is written as an incoherent sum of scattering off these quarks [511]. Asymptotic freedom of QCD justifies

this description but also enables us to calculate perturbative corrections [145]. The outgoing quarks are supposed to fragment into multihadrons.

Let us consider process $\nu_\mu + p \to \mu^- +$ hadrons, where only the final muon is measured. We consider the laboratory frame where the initial proton is at rest with four momentum $p_\mu = (m_N, \mathbf{0})$ and the initial neutrino has four momentum $k_\mu = (E, \mathbf{k})$. The momentum of the final muon is $k'_\mu = (E', \mathbf{k'})$. We write the scattering angle between the final muon and incident neutrino as θ. We write this process as an incoherent sum of neutrino quark elastic scattering, $\nu + d \to \mu^- + u$ and $\nu + \bar{u} \to \mu^- + \bar{d}$, where the antiquark is the sea component from virtual $q\bar{q}$ pair production in the nucleon.

In the parton model we assume that each quark carries a fraction x of proton four-momentum, i.e.,

$$p_{\text{quark}} = x p_{\text{proton}} . \tag{3.202}$$

Therefore, for large E, the Mandelstam variables $s \simeq 2m_N E$ and $u \simeq -2m_N E'$ are multiplied by x. $t = (k' - k)^2 = q^2$ is not modified. The cross section of neutrino quark scattering is given by (3.162) with $F_V = F_A = 1$ and $F_W = F_P = 0$ (i.e., the quark has no structure). For neutrino antiquark scattering, we reverse the sign of F_A, i.e., $F_A = -1$, and interchange s and u. We write

$$\frac{d\sigma}{dq^2} = \int du \frac{d\sigma}{dtdu} x\delta(t + xs + xu) , \tag{3.203}$$

where the argument of the δ function is the identity $t + xs + xu = \Sigma m_q^2 = 0$, and therefore the δ function means $x = -t/(s+u)$; hence x is identified with Bjorken's scaling variable $x = -q^2/2m_N\nu$ [147] with $\nu = (qp)/M = E - E'$.

The cross section is thus

$$\left(\frac{d^2\sigma}{dtdu}\right)_{\nu d \to \mu^- u} = \frac{G_F^2}{\pi} |U_{ud}|^2 x\delta(t + xs + xu) , \tag{3.204}$$

and

$$\left(\frac{d^2\sigma}{dtdu}\right)_{\nu\bar{u} \to \mu^- \bar{d}} = \frac{G_F^2}{\pi} |U_{ud}|^2 x(1-y)^2\delta(t + xs + xu) , \tag{3.205}$$

where y is defined in the same way as in (3.131), i.e., $y = (E - E')/E$.

The inelastic scattering cross section of a neutrino off a proton is written by summing up the neutrino quark cross sections with the weight of the quark distribution function $d(x)$ and $\bar{u}(x)$, which represent the probabilities that a d and a $\bar{u}$ quark have the momentum fraction x in the proton:

$$\left(\frac{d^2\sigma}{dtdu}\right)_{\nu p \to \mu^- X} = \frac{G_F^2}{\pi} |U_{ud}|^2 \int dx \left[xd(x) + x(1-y)^2\bar{u}(x)\right] \frac{1}{s+u}\delta(x - \zeta) , \tag{3.206}$$

where $\zeta = -t/(s+u)$, and the quark distribution function is normalised as

$$\int_0^1 [u(x) - \bar{u}(x)]dx = 2, \qquad \int_0^1 [d(x) - \bar{d}(x)]dx = 1 \qquad (3.207)$$

for the proton. After x integration, we change the variables (t,u) back into (x,y) and write the cross section in the form

$$\left(\frac{d^2\sigma}{dxdy}\right)_{\nu p \to \mu^- X} = \frac{2G_F^2 m_N E}{\pi}|U_{ud}|^2 \left[xd(x) + x(1-y)^2\bar{u}(x)\right] . \qquad (3.208)$$

For practical reasons, experimentalists prefer to use a nuclear target, which is nearly an equal mixture of protons and neutrons. For such isoscalar targets N,

$$\left(\frac{d^2\sigma}{dxdy}\right)_{\nu N \to \mu^- X} = \frac{2G_F^2 m_N E}{\pi}|U_{ud}|^2 \left[xq(x) + x(1-y)^2\bar{q}(x)\right] , \qquad (3.209)$$

where the quark distribution functions are

$$q(x) = \frac{u(x) + d(x)}{2} , \qquad (3.210)$$

$$\bar{q}(x) = \frac{\bar{u}(x) + \bar{d}(x)}{2}. \qquad (3.211)$$

The total inclusive cross section reads

$$\sigma(\nu N \to \mu^- X) = \frac{G_F^2 s}{\pi}|U_{ud}|^2 \int_0^1 dx \left[xq(x) + \frac{x}{3}\bar{q}(x)\right]. \qquad (3.212)$$

The quark distribution functions are not strictly constant but receive perturbative QCD $\ln(q/\Lambda)^2$ corrections, which are most readily treated by using the Altarelli–Parisi evolution equation [512]. The quark distribution functions for practical use are given in [513–516].

Note that the region $2m_\nu E_\nu y(1-x) \le W_c^2 - m_N^2$ overlaps that of one-pion production, where W_c is the upper limit of the invariant mass set for the $N\pi$ system in one-pion production. If one uses a deep-inelastic scattering cross section to describe the total muon production cross section together with quasi-elastic scattering and one-pion production, the integration is to be made excluding this region to avoid double counting.

The $\bar{\nu}q$ cross section is the same as that of $\nu\bar{q}$ scattering, and the $\bar{\nu}N$ cross section is given by interchanging $q(x)$ and $\bar{q}(x)$ in (3.209) and (3.212). The ratio of the charged-current reactions induced by ν and $\bar{\nu}$ is then given by

$$r = \frac{\sigma(\bar{\nu}N \to \mu^+ + X)}{\sigma(\nu N \to \mu^- + X)} = \frac{1/3 + \xi}{1 + \xi/3} , \qquad (3.213)$$

where

$$\xi = \frac{\int dx x \bar{q}(x)}{\int dx x q(x)}. \qquad (3.214)$$

The ratio r is $1/3$ if the antiquark component is ignored. Experiment shows that the neutrino–nucleon scattering total cross section increases linearly with E_ν, as predicted, and $\sigma_{\text{total}}/E_\nu = (0.677 \pm 0.014) \times 10^{-38}\ \text{cm}^2\,\text{GeV}^{-1}$ for ν_μ and $(0.334 \pm 0.008) \times 10^{-38}\ \text{cm}^2\,\text{GeV}^{-1}$ for $\bar{\nu}_\mu$ for $10 \leq E_\nu < 350$ GeV [517]. This means that $r = 0.493 \pm 0.016$ indicating $\xi = 0.191 \pm 0.024$. The first moment of the quark distribution function is

$$\int_0^1 dx x q(x) = 0.212, \qquad \int_0^1 dx x \bar{q}(x) = 0.041. \qquad (3.215)$$

Parallel calculation yields the neutral-current cross section,

$$\left(\frac{d^2\sigma}{dx dy}\right)_{\nu N \to \nu X} = \frac{G_F^2 s}{4\pi} \rho \left[x q_1(x) + x(1-y)^2 \bar{q}_1(x)\right] , \qquad (3.216)$$

where $q_1(x)$ and $\bar{q}_1(x)$ are

$$q_1(x) = 4[g_L^2(u) + g_L^2(d)]q(x) + 4[g_R^2(u) + g_R^2(d)]\bar{q}(x) , \qquad (3.217)$$

and

$$\bar{q}_1(x) = 4[g_L^2(u) + g_L^2(d)]\bar{q}(x) + 4[g_R^2(u) + g_R^2(d)]q(x) , \qquad (3.218)$$

with the couplings given in Table 2.1.

The ratio of the neutral- to charged-current-induced neutrino (antineutrino) reactions is given by

$$R(\nu N) = \frac{\sigma^{NC}(\nu N \to \nu + X)}{\sigma^{CC}(\nu N \to \mu + X)}$$
$$= [1/2 - \sin^2 \theta_W + 5/9(1+r)\sin^4 \theta_W]\rho , \qquad (3.219)$$
$$R(\bar{\nu} N) = \frac{\sigma^{NC}(\nu N \to \nu + X)}{\sigma^{CC}(\nu N \to \mu + X)}$$
$$= [1/2 - \sin^2 \theta_W + 5/9(1 + 1/r)\sin^4 \theta_W]\rho. \qquad (3.220)$$

These expressions are used to derive $\sin^2 \theta_W$ from deep-inelastic neutrino scattering. For instance, the CHARM experiment [282][18] gives $R(\nu N) = 0.3093 \pm 0.0031$, and $r = 0.456 \pm 0.011$ after applying a cut for total hadron

---

[18] This r somewhat differs from the value derived from the high-energy neutrino–nucleon reaction cross section cited above. This is due to an effective lower hadron energy with which the sea quark contribution diminishes. For low-energy neutrinos we expect $r \sim 1/3$ (no sea quark contribution).

energy $E_h > 4$ GeV. Solving (3.219) for $\sin^2\theta_W$, we obtain $\sin^2\theta_W \simeq 0.236$.[19] To obtain a more accurate value, the following corrections must be made [281,518]:

(1) nonisoscalar target (-0.0090),
(2) strange quark pairs in nuclei $(+0.0046)$,
(3) charm quark pairs in nuclei $(+0.0005)$,
(4) mass effects on charm production $(+0.0110)$, and
(5) $O(\alpha)$ radiative corrections (on-shell scheme) [518] (-0.009).

After these corrections, one obtains $\sin^2\theta_W = 0.234$ $(\overline{\text{MS}})$, which is close to the value presented in Table 2.3 of Sect. 2.5.

Deep inelastic scattering of neutrinos off nucleons provided important information on the structure of nucleons and allowed us to verify the validity of QCD in the perturbative regime [520].

We can calculate the heavy flavour production in a similar manner. In this case, one may use a phenomenological prescription [519] to treat the heavy mass effect by replacing the scaling variable

$$x \to \xi = x \left[1 + \frac{m_c^2}{(-q^2)} \right] , \qquad (3.221)$$

say, for charm production, and multiply the integrand (3.209) by a suppression factor $(1 - m_c^2/2m_N E_\nu \xi)$, together with appropriate replacement of the quark mixing matrix element, $|U_{ud}| \to |U_{cd}|$. This expression was used to determine $|U_{cd}|$ in Sect. 3.8.

3.15 Ultra-High-Energy Neutrino–Nucleon Scattering

There is increasing interest in neutrino scattering with energy much higher than is accessible with accelerators, say, $E_\nu \gg 10^5$ GeV, to detect ultra-high-energy neutrinos from astrophysical sources. The formulae we derived should hold for such high-energy scattering with a few modifications [521].

The momentum transfer q^2 varies across a wide range, and q^2 dependence (scaling violation) should properly be considered for the quark distribution functions $q(x,q^2)$ and $\bar{q}(x,q^2)$. For $E_\nu \gg 10^5$ GeV, a perturbative QCD correction of $\alpha_s \log q^2/\Lambda^2$ becomes unity, and the next leading log correction should also be included.

Heavy quarks (s,c,b,t) in the nucleon sea become more important inside the nucleus, as high momentum gluon exchanges produce more massive quarks and antiquarks.

---

[19] If we adopt the CDHS experiment with the same E_h cut, $R(\nu N) = 0.3167$, and $r = 0.453$, which results in $\sin^2\theta_W \simeq 0.224$, and hence 0.222 after the corrections.

The W boson exchange can no longer be treated as a point interaction, and the weak boson propagator must be recovered in the cross section formula, as

$$G_{\mathrm{F}}^2 \to G_{\mathrm{F}}^2 \frac{1}{(1 - q^2/m_W^2)^2} = G_{\mathrm{F}}^2 \frac{1}{(1 - 2m_N E_\nu xy/m_W^2)^2} \, . \qquad (3.222)$$

At energies $E_\nu \gg 10^5\,\mathrm{GeV}$, the weak-boson propagator gives a weight to a small q^2 region, $-q^2 = -t = 2m_N E_\nu xy \lesssim m_W^2$. This means that an important contribution to the x integral comes from the region around $x \lesssim m_W^2/(2m_N E_\nu \langle y \rangle)$. For the sea quarks show more singular behaviours near $x \simeq 0$ compared with valence quarks, the former contributions dominate when $E_\nu > 10^6\,\mathrm{GeV}$. Experiments at HERA [522] enable us to estimate the quark distribution functions at small x, typically for $10^{-5} < x < 10^{-2}$. Two estimates of the cross sections of ultra-high-energy neutrino–nucleon scattering give a consistent result [523,524]. For example, Gandhi et al. [524] use

$$x q_{sea}(x) \to x^{-0.332} \qquad (3.223)$$

and give

$$\sigma_{CC}(\nu N) \simeq 2.69 \times 10^{-36} \mathrm{cm}^2 \left(\frac{E_\nu}{1\,\mathrm{GeV}} \right)^{0.402} , \qquad (3.224)$$

$$\sigma_{NC}(\nu N) \simeq 1.06 \times 10^{-36} \mathrm{cm}^2 \left(\frac{E_\nu}{1\,\mathrm{GeV}} \right)^{0.408} , \qquad (3.225)$$

$$\sigma_{CC}(\bar{\nu} N) \simeq 2.53 \times 10^{-36} \mathrm{cm}^2 \left(\frac{E_{\bar{\nu}}}{1\,\mathrm{GeV}} \right)^{0.404} , \qquad (3.226)$$

$$\sigma_{NC}(\bar{\nu} N) \simeq 0.98 \times 10^{-36} \mathrm{cm}^2 \left(\frac{E_{\bar{\nu}}}{1\,\mathrm{GeV}} \right)^{0.410} , \qquad (3.227)$$

for neutrino scattering off an isoscalar nuclear target for $E_\nu \simeq 10^6 - 10^{12}\,\mathrm{GeV}$. The difference between the neutrino and antineutrino cross sections is small, consistent with the sea quark dominance.

3.16 Coherent Nuclear Scattering

The vector part of the neutral current induces coherent scattering of neutrinos off nuclei. For a nucleus with charge Z and atomic number A (neutron number is $N = A - Z$),

$$g_V^p = g_L^p + g_R^p = 2(g_L^u + g_R^u) + (g_L^d + g_R^d) = \frac{1}{2} - 2\sin^2\theta_W,$$

$$g_V^n = g_L^n + g_R^n = (g_L^u + g_R^u) + 2(g_L^d + g_R^d) = -\frac{1}{2} \, , \qquad (3.228)$$

i.e., scattering is described by the effective Hamiltonian with $g_V = (\frac{1}{2} - 2\sin^2\theta_W)Z - \frac{1}{2}N$. With the matrix element given by

$$\langle A(p')|V_\mu|A(p)\rangle = \frac{1}{(2\pi)^3}\frac{1}{\sqrt{2E'2E}}(p+p')_\mu\, g_V f(q^2)\,, \qquad (3.229)$$

where

$$f(q^2) = A\, e^{-bq^2}\,, \qquad b = \frac{1}{6}\langle r^2\rangle\,, \qquad (3.230)$$

the cross section is

$$\frac{d\sigma}{dq^2} = \frac{G_F^2}{2\pi}\left[\left(\frac{1}{2} - 2\sin^2\theta_W\right)Z - \frac{N}{2}\right]^2 e^{-2bq^2}\left(1 - q^2\frac{2m_A E_\nu + m_A^2}{4m_A^2 E_\nu}\right)\,, \qquad (3.231)$$

where $q = p' - p$ and $m_A = A\, m_N$. For small q,

$$\frac{d\sigma}{d\cos\theta} = \frac{G_F^2}{2\pi}\left[\left(\frac{1}{2} - 2\sin^2\theta_W\right)Z - \frac{N}{2}\right]^2 E_\nu^2(1 + \cos\theta)\,. \qquad (3.232)$$

Note that the coefficient of Z nearly vanishes and the cross section is proportional to the neutron number. For an isoscalar target $Z = N = A/2$, the total cross section is

$$\sigma \simeq 1.68 \times 10^{-42}\sin^4\theta_W A^2\left(\frac{E_\nu}{10\,\mathrm{MeV}}\right)^2 \mathrm{cm}^2\,. \qquad (3.233)$$

For $E_\nu \simeq 10\,\mathrm{MeV}$ and $A = 56(\mathrm{Fe})$, $\sigma = 2.8 \times 10^{-40}\mathrm{cm}^2$ corresponds to the mean free path $\lambda = 330\,\mathrm{m}/(\rho/10^{13}\,\mathrm{g\ cm^{-3}})$. This is compared with $\lambda = 3.8 \times 10^4\,\mathrm{m}/(\rho/10^{13}\,\mathrm{g\ cm^{-3}})$ for νe scattering. This provides a mechanism for a neutrino trap in the core of protoneutron stars after supernova core collapse and plays an important role in supernova explosions [525] (see Sect. 4.5). The large cross section of (3.233) is one of the basic principles of cryogenic detection of low-energy neutrinos [526] (and of Dirac neutrino–like dark matter particles in the Galactic halo [527]).

3.17 Refractive Effects

Neutrinos propagating through matter are refracted due to their interaction with it [212]. If the interaction gives extra energy V, the energy (E)–momentum (k') relation is

$$E = \sqrt{k'^2 + m^2} + V\,. \qquad (3.234)$$

The refractive index n is defined by

$$\Psi = \exp(i\, n\, \mathbf{kx} - iEt) , \qquad (3.235)$$

where k and E satisfy the dispersion relation in vacuo, $k^2 + m^2 = E^2$. Since k' is identified with nk,

$$(nk)^2 + m^2 = E^2 - 2EV , \qquad (3.236)$$

i.e.,

$$n = 1 - \frac{EV}{k^2} . \qquad (3.237)$$

For interaction of the form (3.122),

$$V = \sqrt{2}G_{\mathrm{F}}c_V n_e \qquad (3.238)$$

$$\begin{aligned} &= \pm\sqrt{2}G_{\mathrm{F}}(+1/2 + 2\sin^2\theta_W)n_e , &&\text{for } \nu_e \\ & \pm\sqrt{2}G_{\mathrm{F}}(-1/2 + 2\sin^2\theta_W)n_e , &&\text{for } \nu_\mu \text{ and } \nu_\tau \end{aligned} \qquad (3.239)$$

with n_e the electron density when matter is at rest (note that only the $\mu = 0$ component contributes, i.e. $\langle \bar{e}\gamma_\mu e \rangle = \langle e^\dagger e \rangle = n_e\delta_{\mu 0}$; also note that $\bar{\nu}_e\gamma^0(1 - \gamma_5)\nu_e = 2\nu_{e_L}^\dagger\nu_{e_L}$). The $\pm$ sign in front refers to $\nu(+)$ and $\bar{\nu}(-)$. Although the deviation of n from unity is very small, $\Delta n \sim 7.6 \times 10^{-19}(\rho/100\,\mathrm{g\,cm^{-3}})(E/10\,\mathrm{MeV})^{-1}$, this has an important effect on neutrino propagation if the neutrino has a small mass.

Similarly, for interactions with protons and neutrons, we obtain from Table 2.1 for c_V,

$$V = \pm\sqrt{2}G_{\mathrm{F}}(1/2 - 2\sin^2\theta_W)n_p \mp \sqrt{2}G_{\mathrm{F}}(1/2)n_n , \qquad (3.240)$$

where the $\pm$ and $\mp$ signs refer to ν(upper) and $\bar{\nu}$(lower) for all three neutrinos.

For electrically neutral matter ($n_e = n_p$) with nuclei having (A, Z),

$$V = 2^{-1/2}G_{\mathrm{F}}(3Z - A)n_A , \qquad \text{for } \nu_e, \qquad (3.241)$$

and

$$V = 2^{-1/2}G_{\mathrm{F}}(Z - A)n_A , \qquad \text{for } \nu_\mu, \nu_\tau. \qquad (3.242)$$

In the environment where neutrinos are copiously present (such as the supernova core), neutrino–neutrino interactions must be added, which for ν_e amount to

$$V = 2^{-1/2}G_{\mathrm{F}}(4n_{\nu_e} + 2n_{\nu_\mu} + 2n_{\nu_\tau}), \qquad (3.243)$$

where an extra factor of 2 for ν_e accounts for the statistics of identical particles.

An interesting application of the refractive effect is calculation of the force acting on a macroscopic body when neutrino flux passes through. Simple consideration gives a force

$$F = S\phi_\nu k_\nu |n - 1| \,, \tag{3.244}$$

where

$$n - 1 = \frac{V}{m_\nu v_\nu^2} \,, \tag{3.245}$$

which is of the order of 10^{-8} for $m_\nu \approx 20$ eV and $v_\nu \approx 300$ km s^{-1}. The force $F \approx 2.5 \times 10^{-15}$ dyne for $S \approx 1$ m^2 is only a few orders of magnitude smaller than the force measured in the Eötvos–Dicke experiment [528], lending us hope of measuring the cosmic neutrino background radiation of 1.9 K [529]. In reality, however, the force first order in G_F, i.e., $(1 - n)\nabla\rho_\nu(x)$ vanishes for isotropic neutrino distribution, and the net force acting on a body is of the order of $(1 - n)^2\phi_\nu \propto G_F^2$, which is 4×10^{-23} dyne, too small to motivate any realistic considerations [530] (see [531] for a somewhat more optimistic view).

The phase of the neutrino wave function induced by the coherent effect discussed above rotates by 2π when it propagates, typically $2\pi/V \sim 1.6 \times 10^9$ cm$(\rho/1\text{gH})^{-1}$ (gH stands for gramme hydrogen equivalent). This is a first-order effect in G_F and is greatly shorter than the interaction length for the low-energy neutrino $l \sim 1/\sigma(\nu_e e \to \nu_e e)n_e \sim 1.8 \times 10^{19}$ cm $(E/10\,\text{MeV})^{-1}(\rho/1\text{gH})^{-1}$. The most dramatic effect happens when neutrinos are massive and the phase from the mass is cancelled by the refractive phase (see Sect. 8.6).

The refractive effect in a high-temperature background, such as in the early universe, and higher order effects are considered in [532–535].

3.18 Flavour-Changing Neutral Current

Flavour-changing neutral current weak interactions are strongly suppressed compared with charged-current processes. Typical examples are

$$\frac{\Gamma(K_L^0 \to \mu^+\mu^-)}{\Gamma(K^+ \to \mu^+\nu)} = 2.7 \times 10^{-9} \,, \tag{3.246}$$

$$\frac{\Gamma(K^+ \to \pi^+\nu\bar{\nu})}{\Gamma(K^+ \to \pi^0 e^+\nu)} = 3.1 \times 10^{-9} \,. \tag{3.247}$$

The small size of the $K_L^0 - K_S^0$ mass difference is another notable example. The electroweak theory we discussed in the last chapter is the model by which the strong suppression of flavour-changing neutral current is naturally

explained. If one tries to extend the standard model, the suppression may be lifted, and experiment gives a strong constraint on the model. Therefore, the channels associated with flavour-changing neutral current can be used to test nonstandard interactions that often appear in higher unified models, as we shall discuss later in this book.

It would be instructive to see how the suppression of the flavour-changing neutral current takes place in the standard model. The lowest order diagram that would induce flavour-changing effects is the exchange of the Z boson. The coupling of the Z boson to quarks takes the form

$$\bar{q}T_3qZ \simeq (\bar{u}_L u_L - \bar{d}'_L d'_L)Z + (\bar{c}_L c_L - \bar{s}'_L s'_L)Z + ... \qquad (3.248)$$

where only weak-isospin dependence is shown and only the first two generations are retained with the prime denoting the unmixed (weak eigenstate of the) quark fields. It is clear that this form is invariant under the unitary transformation of quark fields s' and d'. The Z boson does not induce any flavour-changing effect. If, however, the c quark were not present and s were isosinglet, the second term is absent in (3.248) and the flavour-changing effect emerges upon quark mixing $d = d' \cos\theta_c + s' \sin\theta_c$.

From this argument, it is clear that the condition of flavour conservation of the Z boson requires that all quark fields of the same charge and helicity belong to the same $\mathrm{SU}(2)_\mathrm{L}$ representation of the weak isospin [536]. Photons and gluons conserve flavour, so that their radiative corrections do not induce flavour-changing neutral current of the order of $G_\mathrm{F}\alpha$ or $G_\mathrm{F}\alpha_s$.

On the other hand, weak charged currents induced by $W^\pm$ are, in principle, flavour-changing and hence higher order effects would induce flavour-changing neutral currents. A typical example is given in Fig. 3.17. For simplicity, if we restrict our consideration to two generations, the internal quark lines connected to the d and $\bar{s}$ quarks are u and c quarks with couplings $g\cos\theta_c \sin\theta_c$ and $g(-)\sin\theta_c \cos\theta_c$, respectively. If the masses of the two quarks were equal, the two contributions exactly cancel, and there is no net flavour-changing neutral-current effect. This cancellation would not take place if the c quark were absent. This was in fact the situation before the discovery of the charm quark in 1974. Enforcing the cancellation of the strangeness-changing neutral current in the higher order correction, Glashow,
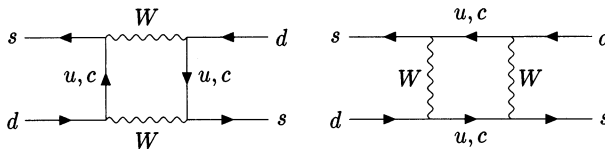
Fig. 3.17. Diagrams inducing flavour-changing neutral current: $K^0 - \bar{K}^0$ mixing.

Illiopoulos, and Maiani [129] gave a raison d'être for the existence of the charm quark (this is called the GIM mechanism).

For three generations, cancellation is ensured by the orthogonality relation $\sum_i U_{is}^* U_{id} = 0$. In reality quark masses are different, which leaves a residual contribution of the order of $G_F^2(m_c^2 - m_u^2)$. However, there is no contribution of the order of $G_F^2 m_W^2$ which would arise from loop momentum much larger than the quark mass.

There is yet another possible contribution from scalar particles. In the standard theory, Higgs couplings to quarks are obviously diagonal, and there is no flavour-changing effect. If there is more than one set of Higgs doublets, however, this is not trivial. In general, mass diagonalisation does not diagonalise the couplings at the same time, which causes flavour-changing interactions [536]. We need some mechanism to ensure that masses and couplings are simultaneously diagonalised to suppress flavour-changing effects. This is realised in a two Higgs model with Peccei–Quinn symmetry and 'minimal' supersymmetric models. In extended models, some scalar particles may also appear that would couple to the flavour-changing neutral current. For a general review of flavour-changing neutral-current effects, we refer to [537].

$K^0 - \bar{K}^0$ **mixing.** The degeneracy of K^0 and $\bar{K}^0$ masses is lifted if there is an interaction that communicates the $s\bar{d}$ and $d\bar{s}$ states, a typical action of the flavour-changing neutral current. There is an associated problem that the $\Delta S = 2$ interaction has a complex phase and induces CP violation. We discuss here $K^0 - \bar{K}^0$ mixing, ignoring a small CP violation effect.

There are two diagrams for the $\Delta S = 2$ process, as given in Fig. 3.17. Both diagrams give the same contribution in the limit of the small external momenta. A simple calculation yields the effective Hamiltonian [130]:

$$H_{\text{eff}}(\Delta S = 2) \simeq \sin^2 \theta_C \cos^2 \theta_C \frac{G_F^2}{16\pi^2}(m_c^2 - m_u^2)\bar{d}\gamma^\mu(1 - \gamma_5)s\,\bar{d}\gamma^\mu(1 - \gamma_5)s \,,$$

$$(3.249)$$

for m_u, $m_c \ll m_W$.

For three generations with m_t larger than m_W, (3.249) is replaced by a more accurate expression [538],

$$H_{\text{eff}}(\Delta S = 2) = \frac{G_F^2 m_W^2}{16\pi^2}I\bar{d}\gamma^\mu(1 - \gamma_5)s\,\bar{d}\gamma^\mu(1 - \gamma_5)s, \qquad (3.250)$$

with

$$I = \lambda_c^2 S(x_c) + \lambda_t^2 S(x_t) + 2\lambda_c\lambda_t S(x_c, x_t) \,, \qquad (3.251)$$

where $x_i = m_i^2/m_W^2$, $\lambda_i = U_{id}U_{is}^*$, and m_u is set equal to zero. The integrals are

$$S(x) = \frac{4x - 11x^2 + x^3}{4(1-x)^2} - \frac{3x^3 \ln x}{2(1-x)^3} \,, \qquad (3.252)$$

and

$$S(x_c, x_t) = x_c \left[\ln \frac{x_t}{x_c} - \frac{3x_t}{4(1-x_t)} - \frac{3x_t^2 \ln x_t}{4(1-x_t)^2} \right], \qquad (3.253)$$

where $m_c \ll m_t$ is assumed in the second expression.

Generically, K^0 and $\bar{K}^0$ masses are degenerate. So even a minuscule interaction between K^0 and $\bar{K}^0$ gives rise to 45° mixing. We write the eigenstate

$$|K_L^0\rangle = \frac{|K^0\rangle + |\bar{K}^0\rangle}{\sqrt{2}} \,, \quad |K_S^0\rangle = \frac{|K^0\rangle - |\bar{K}^0\rangle}{\sqrt{2}} \,. \qquad (3.254)$$

The mass difference between the two states is then given by

$$\Delta M = 2\langle K^0 | H_{\text{eff}}(\Delta S = 2) | \bar{K}^0 \rangle \,. \qquad (3.255)$$

To estimate $K^0 - \bar{K}^0$ mixing, we must evaluate the hadronic matrix element of the four-quark operator. We write

$$\langle K^0 | \bar{d}\gamma^\mu (1 - \gamma_5)s \bar{d}\gamma^\mu (1 - \gamma_5)s | \bar{K}^0 \rangle \simeq \frac{8}{3} f_K^2 m_K^2 B_K. \qquad (3.256)$$

The factors in front of B_K are those obtained by inserting the vacuum state between all possible pairs of quark fields in the intermediate state; $B_K = 1$ if this approximation (vacuum saturation) is valid. We must carry out a nonperturbative calculation to evaluate B_K. This quantity is well converged within lattice QCD calculations, albeit with the quench approximation [539]. The best current value is $B_K = 0.82 \pm 0.07$.[20] Neglecting the small effect from a t quark loop,

$$\Delta M \sim \left(\frac{m_c}{1.4 \text{GeV}} \right)^2 \times 0.82 \times 2.4 \times 10^{-6} \text{eV}. \qquad (3.257)$$

This estimate ignores long distance contributions, which require a model-dependent argument [540].

---

[20] This value is based on quenched lattice QCD calculations. There are some discrepancies depending on the actions used. With the Kogut–Susskind quark action, the best value is $B_K(\mu = 2\text{GeV}) = 0.625 \pm 0.030$, and with domain wall quarks, it is 0.575 ± 0.020. Here we adopt $B_K(\mu = 2\text{GeV}) = 0.61 \pm 0.05$, and perturbatively converted it into the renormalisation invariant B_K for three light flavours of quarks.

When K^0 or $\bar{K}^0$ is produced in strong interactions, only K_L^0 survives in the beam line when the length is more than a metre. When the K_L beam traverses matter, the K^0 and $\bar{K}^0$ components of K_L^0 interact differently with matter, resulting in a modification of the relative phase between the K^0 and $\bar{K}^0$, which is observed as regeneration of K_S^0. By measuring the regenerated K_S^0 flux as a function of matter thickness, one can determine the regeneration length in terms of the oscillation length which is related to the mass difference ΔM. In this way, one can measure a tiny mass difference between K_L^0 and K_S^0 quite accurately. The current value is

$$\Delta M = (3.489 \pm 0.008) \times 10^{-6}\text{eV}. \qquad (3.258)$$

Comparison of this value with the prediction (3.257) tells us that m_c is of the order of ≈ 2 GeV. This is the logic that led to the prediction of the charm quark mass before its discovery [130].

Let us now examine the constraint on the flavour-changing coupling of a non-conventional scalar particle. We write

$$\mathcal{L} = g_{12}\bar{s}_L d_R \Phi + \text{h.c.} \qquad (3.259)$$

This scalar particle induces a $s\bar{d} - d\bar{s}$ transition, which reads, when expressed in units of the strength of the two W boson contributions,

$$\frac{A(\Phi \text{ exchange})}{A(\text{two W box})} = \left(\frac{10^{14}(\text{GeV})^2}{m_\Phi^2}\right) g_{12}g_{21}^* . \qquad (3.260)$$

If we require that this ratio be smaller than unity, we obtain

$$\frac{g_{12}g_{21}^*}{m_\Phi^2} < 1 \times 10^{-14}(\text{GeV})^{-2}. \qquad (3.261)$$

Constraint on scalar couplings from other processes. Constraints can be derived on the coupling of scalar particles that would induce flavour-changing neutral-current effects in a similar way. We consider CP violation and $K_L \to \bar{\ell}\ell$ ($\ell = e$ or μ). We may obtain a limit from the condition that the effect induced by scalar particles does not exceed the standard model contribution. The constraints obtained in this way are presented in Table 3.21, where g_{ij} is the scalar coupling to quarks defined in a way similar to (3.260) and f_{ij} is that to leptons defined by

$$\mathcal{L} = f_{ij}\bar{\ell}_{Li}e_{Rj}\Phi + \text{h.c.} \qquad (3.262)$$

Note that the scalar particle does not contribute to $K^+ \to \pi^+\nu\nu$ decay.

We may repeat the same argument for the B mesons: $B^0 - \bar{B}^0$ and $B_s^0 - \bar{B}_s^0$ mass differences, and $B^0 \to \bar{\ell}\ell$. The derived constraints are given in Table 3.21.

Table 3.21. Constraints on scalar particle couplings from flavour-changing neutral-current processes, represented as coefficients of $(4m_\Phi^2)^{-1} = 10^{-12}\,\text{GeV}^{-2}$.^{a}

$\Delta M_{K_L-K_S}$	ϵ(CP violation)	$K_L \to \mu^+\mu^-$	$K_L \to e^+e^-$	$K_L \to \mu^\pm e^\mp$
$\|g_{12}g_{21}\|$	$\text{Im}[g_{12}g_{21}^*]$	$\|(g_{12}+g_{21})f_{22}\|$	$\|(g_{12}+g_{21})f_{11}\|$	$\|(g_{12}+g_{21})/\sqrt{2}\|(\|f_{12}\|^2 + \|f_{21}\|^2)^{1/2}$
$< 10^{-2}$	$< 2\times 10^{-5}$	< 0.1	$< 5\times 10^{-4}$	$< 0.1^{(*)}$
$\Delta M_{B_0-\bar B_0}$		$B_0 \to \mu^+\mu^-$	$B_0 \to e^+e^-$	$B_0 \to \mu^\pm e^\mp$
$\|g_{13}g_{31}\|$		$(\|g_{13}\|^2+\|g_{31}\|^2)^{1/2}\|f_{22}\|$	$(\|g_{13}\|^2+\|g_{31}\|^2)^{1/2}\|f_{11}\|$	$(\|g_{13}\|^2+\|g_{31}\|^2)^{1/2}\|f_{12}\|$
< 60		< 1	5×10^{-3}	$1\times 10^{3(*)}$
$\Delta M_{B_s-\bar B_s}$		$B_s \to \mu^+\mu^-$	$B_s \to e^+e^-$	$B_s \to \mu^\pm e^\mp$
$\|g_{23}g_{32}\|$		$(\|g_{23}\|^2+\|g_{32}\|^2)^{1/2}\|f_{22}\|$	$(\|g_{23}\|^2+\|g_{32}\|^2)^{1/2}\|f_{11}\|$	$(\|g_{23}\|^2+\|g_{32}\|^2)^{1/2}\|f_{12}\|$
$< 6\times 10^2$		< 10	5×10^{-2}	$1.2\times 10^{3(*)}$

^{a}The 'limits' are obtained by the condition that the contribution of a hypothetical scalar particle exchanges is smaller than that from the standard model. For $e\mu$ decay [denoted by (*)], the limits are derived from experiment because the standard model contribution vanishes.

4 Neutrino Sources and Detection

4.1 Reactor Neutrinos

Fission of nuclear materials (^{235}U, ^{238}U, ^{239}Pu, ^{241}Pu, etc.) results in two neutron-rich nuclei [541], which undergo consecutive β^- decays with an antineutrino emitted in each step. About two to three neutrons are emitted at the same time. The mass number distribution of the fission products depends on the parent nuclear material and on the energy of the incident neutron.

The distribution of fission products of ^{235}U generally shows two broad peaks at around $A = 135-145$ (dominantly Br, Kr, Zr) and $90-100$ (dominantly Ba, Cs, Xe, I, Te). For fission of Pu, the two peaks get a little closer. Large varieties of neutronrich nuclei are produced in fission, and many hundreds of beta decay processes are involved. A representative decay chain is ^{95}Zr$\rightarrow^{92}$Nb$\rightarrow^{92}$Mo, on one hand, and ^{138}I$\rightarrow^{138}$Xe$\rightarrow^{138}$Cs $\rightarrow^{138}$Ba, on the other hand. These pair decays involve emission of five antineutrinos. The average number of neutrinos emitted in fission of ^{235}U is 6.1, and for ^{239}Pu it is 5.6, as estimated from the chemical abundance of the final product.

The energy released is 201.7 ± 0.6 MeV for ^{235}U, 205.0 ± 0.9 MeV for ^{238}U, 210.0 ± 0.9 MeV for ^{239}Pu, and 212.4 ± 1.0 MeV for ^{241}Pu per fission [542]. So a 1-MW (thermal power) reactor produces 2×10^{17} antineutrinos per second, which would provide an excellent source for neutrino experiments. The typical power of reactors used for neutrino experiments is a few GW. The planned long-baseline experiment at Kamioka (KamLAND) [543] aims to measure neutrinos from many power stations located within $100-250$ km with a total of 70 GW thermal power, giving 2×10^6 cm^{-2}s^{-1}, which is comparable to the ^{8}B solar neutrino flux.

In reactors 90% of the energy is usually generated from ^{235}U and ^{239}Pu, but the composition changes with time. In the Gösgen reactor 69% comes from ^{235}U, 21% from ^{239}Pu, 7% from ^{238}U, and 3% from ^{241}Pu when fresh fuel is installed. The fraction of Pu, especially of ^{241}Pu, increases with time by breeding. After 11 months of operation, the above fractions change to 47% : 38% : 7% : 8% (see Fig. 4.1) [544]. ^{236}U, ^{240}Pu, and ^{242}Pu are also nuclear material, but their contributions are less than 0.1%.

The neutrino spectrum is calculated by superposition of the neutrino spectra of individual beta decays. A calculation has been made in [545].
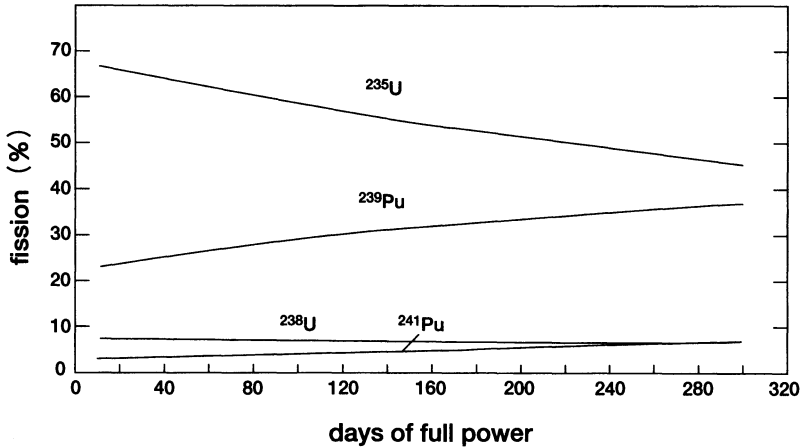
Fig. 4.1. Time dependence of the composition of nuclear fuel in the Gösgen reactor.

The spectrum is also inferred empirically from laboratory experiments using thin uranium or plutonium foils as targets for thermal neutron irradiation [546,547]. The electron spectrum is approximated by some 30 important beta processes, and the neutrino spectrum is obtained by the inversion:

$$N_\nu(E_\nu) = \sum_i f(E_{i0} - E_e; E_{i0}) \,, \qquad (4.1)$$

for

$$N_e(E_e) = \sum_i f(E_e; E_{i0}) \,, \qquad (4.2)$$

where $f(x) \approx x^2(1-x)^2 F(Z,x)$ with $x = E_e/E_{i0}$, E_{i0} is the end point energy of assumed nucleides i, and $F(Z,x)$ is the Fermi function for the Coulomb correction. The authors of [546, 547] claim that the error from the inversion of the neutrino spectrum is less than 1%. They also infer that total systematic errors are 3–4%.[1] Such measurements are available for ^{235}U [546], ^{239}Pu, and ^{241}Pu [547]. Fission of ^{238}U takes place only with a fast neutron [549], and experiments with thermal neutrons do not apply to this case. For ^{238}U, the calculation of [545] (available only for $E_\nu < 8$ MeV) is usually adopted by modifying the normalisation. (The calculation for the first three processes agrees with experiment up to the normalisation.) Figure 4.2 shows the neutrino spectrum for the first three fission processes represented by neutrino numbers per MeV per fission. The spectrum of ^{239}Pu falls off significantly faster than that of ^{235}U; so it is essential to know the composition of nuclear fuel at the instant of experiments. Reactor neutrinos

---

[1] A direct verification using the neutrino flux from the Bugey reactor did not decrease this error due to a 5% systematic error caused by the energy scale uncertainty [548].
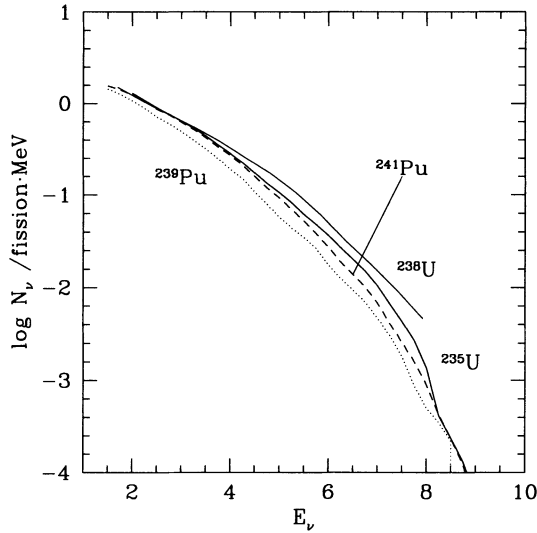
Fig. 4.2. Neutrino spectra from fission of ^{235}U, ^{239}Pu, ^{241}Pu (measured), and ^{238}U (calculated).

are usually detected with $\bar{\nu}_e + p \to e^+ + n$, and hence the detection threshold is $E_{\text{th}} = [(m_n + m_e)^2 - m_p^2]/2m_p = 1.806\,\text{MeV}$. The reactor antineutrino flux above this threshold is about one-fourth of the total flux.

4.2 Accelerator Neutrinos

Accelerator neutrinos come mostly from decays of π and K mesons. The decays $\pi^+ \to \mu^+ \nu_\mu$ (branching ratio $\approx 100\%$) and $K^+ \to \mu^+ \nu_\mu$ (63.5%) are the main sources, and therefore ν_μ's dominate the beam. The neutrino spectrum consists mostly of two components, the low-energy peak which is due to pion decay and the high-energy contribution from K decays. The contamination of ν_e comes mostly from $K^+ \to \pi^0 e^+ \nu_e$ (4.8%), unless the beam energy is so high that many τ's are produced; the contribution from $\pi^+ \to e^+ \nu_e$ (1.2×10^{-4}) and muon decay is usually small. The ν_e flux is suppressed by $\approx 10^{-3}$ at around the lower energy peak, but only by 1/30 at higher energies. This is a limiting factor for $\nu_\mu - \nu_e$ oscillation experiments. One advantage of the low-energy neutrino beam for neutrino physics is that contamination of ν_e can be reduced.

Neutrino production usually uses a Be (or Al) target 2–5 cm long. The target is chosen to be several interaction-lengths long, but as short as possible to permit the secondaries to escape before they interact with the target material. The calculation of neutrino flux is straightforward once the produced particles in p-Be collision are known as a function of the momentum (p)
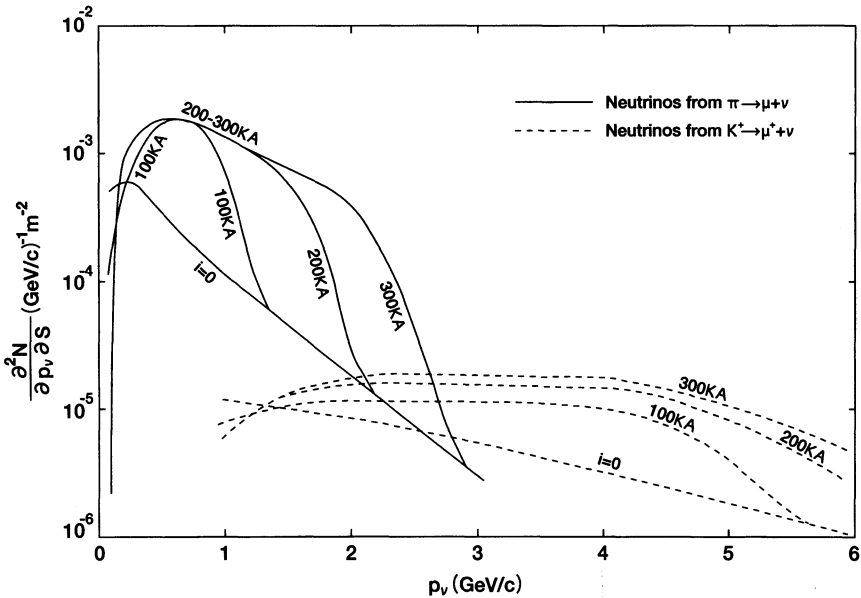
Fig. 4.3. Expected neutrino flux per proton for different excitatory currents of a neutrino horn. After [555].

and angle (θ) of the secondary particle (for typical data, see [550, 551]). The Sanford–Wang formula [552] for the differential yield of a proton beam is often used for this purpose:

$$\frac{d^2\sigma}{d\theta dp} = c_1 p^{c_2} \left(1 - \frac{p}{p_i}\right) \exp\left[-\frac{c_3 p^{c_4}}{p_i^{c_5}} - c_6 \theta(p - c_7 p_i \cos^{c_8} \theta)\right] , \qquad (4.3)$$

where c_k (k =1–8) are fitting parameters that depend on π or K. The beam momentum is p_i. The factor in the first parenthesis ensures that the cross section vanishes in the kinematic limit. The property that renders this formula useful in applications is approximate scaling for $\theta p_i = \theta' p_i'$ (see also [553]), where the primed are quantities with a different beam energy. The typical precision of this formula is claimed to be 10% for a beam energy of 10−50 GeV.[2]

Almost all accelerator neutrino experiments use van der Meer's magnetic horn to enhance the neutrino beam from early days [156, 555]. The average production angle of particles produced in the laboratory is greater than their average decay angle, and a substantial gain is obtained in the flux by focusing the produced particles before they decay. The horn has a conical

---

[2] A typical set of parameters is $c_1 = 196$ mb $(\text{GeV})^{-1}\text{str}^{-1}$, $c_2 = 1.08$, $c_3 = 2.15$, $c_4 = 2.31$, $c_5 = 1.98$, $c_6 = 5.73$ and $c_8 = 24.1$ for a 12.4-GeV/c proton [554]. (The authors use $p_i - (1 \text{ GeV})$ instead of p_i in the denominator of the first parenthesis.)
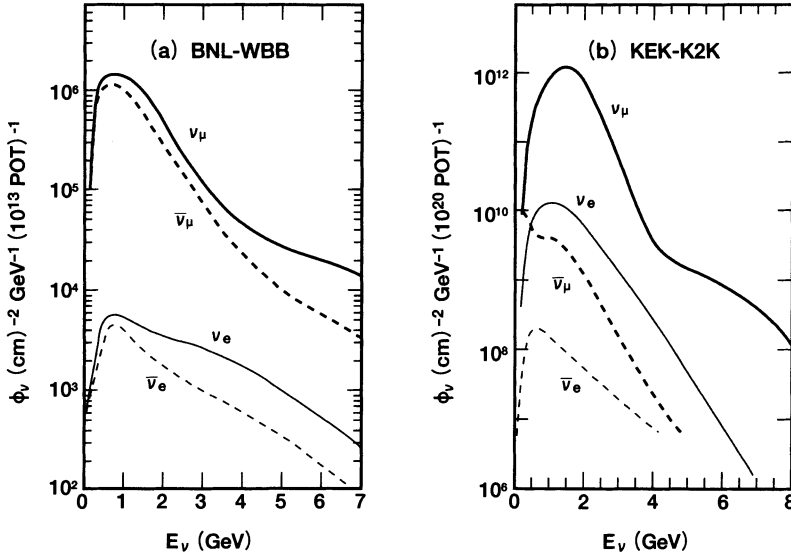
Fig. 4.4. (a) Neutrino flux in the Brookhaven AGS wide-band neutrino beam produced from 28.3-GeV protons on a sapphire (Al_2O_3) target with two horns ($12\,kV \times 250\,kA$) which enhance alternatively the neutrino or antineutrino flux. The curve shows the flux at the detector located 110 m away from the second horn with 10^{13} protons incident on target (POT). Data taken from [551]. (b) Neutrino flux produced by the KEK 12 GeV PS, used for the K2K long baseline neutrino oscillation experiment at Kamioka. The curve shows the flux at the front detector, which is located at a distance of 300 m from the second horn (operated at 250 kA) which focuses only positively charged particles. 10^{20} POT are the goal number of accumulated protons in the K2K experiment. Data taken from [558].

structure with a high electric current of several hundred kA flowing along the horn that produces a toroidal magnetic field. This focuses particles with one charge; those with the opposite charge are defocused and absorbed in the surrounding shield. The device differs from the lens system in that the horn accepts particles of widely varying momenta, not only those with different emission angles. The high electric currents needed for the horn limit its use only with a pulse of short durations; so it is used with a fast extracted beam of a short duty cycle (a few μs). The efficiency of the horn is exemplified in Fig. 4.3 from early calculations [555]. The use of the horn is particularly effective for a high-energy beam and is crucial for long-baseline experiments.

The dominant neutrino component is that from $\pi \to \mu\nu$. Near the forward direction, the energy of neutrinos with decay angle θ_ν is

$$E_\nu = \frac{m_\pi^2 - m_\mu^2}{2m_\pi} \frac{m_\pi}{E_\pi - p_\pi \cos\theta_\nu} \simeq \frac{m_\pi^2 - m_\mu^2}{m_\pi^2 + p_\pi^2 \theta_\nu^2} p_\pi \,, \qquad (4.4)$$

i.e., $E_\nu = 0.42 p_\pi$ for $\theta_\nu = 0$. Replacing π with K, we see that the energy of a neutrino from $K \to \mu\nu$ is 2.3 times higher than that from π decay. The neutrino flux from a pion at the distance L is

$$\phi_\nu \simeq \frac{1}{4\pi L^2} \left(\frac{m_\pi}{E_\pi - p_\pi \cos\theta_\nu} \right)^2 \simeq \frac{1}{4\pi L^2} \left[\frac{2E_\pi/m_\pi}{1 + \theta_\nu^2 (E_\pi/m_\pi)^2} \right]^2 . \qquad (4.5)$$

One may calculate the neutrino flux by combining (4.3) with (4.5). For accurate estimates, most neutrino experiments use elaborate Monte Carlo simulations. The energy of the peak of the neutrino flux is about 1/10 the proton beam energy, and the second peak appears at an energy twice higher. We refer the reader to [556, 557, 551] for literature that emphasises neutrino beam calculation. An example of the neutrino flux used for accelerator experiments is shown in Fig. 4.4.

4.3 Atmospheric Neutrinos

Neutrinos are produced from decays of π and μ that are produced by interactions of cosmic-ray protons with the atmosphere. Markov advocated the experimental feasibility of atmospheric neutrino detection in 1960 [222]. Since then, many calculations have been made for atmospheric neutrino flux [559] (see also [560, 561]). Atmospheric neutrinos were first detected in 1965 [158, 159]. Modern calculations include [562–572]. Several representative calculations are compared, and the origin of the discrepancies is discussed in [573, 574].

The calculation of neutrino flux consists of the following steps: estimates of (i) the primary cosmic-ray flux at the top of the atmosphere for all directions at the location of the detector, (ii) propagations and interactions of cosmic rays in the air to produce mesons, and (iii) decay of mesons and muons while propagating through the air and Earth. For high-energy neutrinos the production of muons from ν_μ in Earth is also the subject of studies.

Primary cosmic-ray flux. The cosmic-ray flux at the top of the atmosphere differs from that of interstellar space due to two effects: (i) modulations due to the solar wind, which decelerates cosmic rays; and (ii) a cutoff of low-energy cosmic rays due to geomagnetic fields. The first effect is correlated with solar activity and is largely time-dependent. The second effect depends on the geomagnetic latitude of the experimental site, but also is modestly time-dependent.

Much work has been done to measure the energy spectrum and composition at the top of atmosphere using balloons or satellites.[3] The early standard of the proton and helium spectrum is that of Ormes and Webber (1–10 GeV),

---

[3] There are several ways to represent the cosmic-ray energy of nuclei. The expression most relevant to our considerations here is kinetic energy per nucleon. The

continued to a higher energy by Ryan et al. (50−1000 GeV) [575], and the gap was filled by Webber et al. [576]. It shows a smooth spectrum

$$dN/dE_k \sim E_k^\alpha \tag{4.6}$$

with $\alpha \approx -2.75$ for a wide energy range except for a very low energy region. The observations of Seo et al. (LEAP) [577], however, resulted in a proton flux that is 1.6 times lower than the flux given by Webber et al. in the 5−100 GeV range. For $\lesssim 100$ GeV, a number of observations have been made in the last 5 years. Five experiments were published after 1999, MASS [578], CAPRICE [579], IMAX [580], BESS [581] and AMS [582]. These experiments gave fluxes that roughly agree with LEAP, but the MASS and IMAX's fluxes are even lower than LEAP by 15−20%. The two latest observations (BESS and AMS) agree very well with each other and give fluxes in good agreement with LEAP for $E_k < 10$ GeV (higher by 10% for the $E_k = 10-100$ GeV region.) They are 15% higher than the fluxes of MASS, IMAX (for $E_k = 1-100$ GeV), and CAPRICE for $E_k > 10$ GeV. With these two latest high statistics experiments, we consider that the proton flux problem is settled within a $\lesssim 10\%$ error up to ≈ 100 GeV, which is relevant to ~ 10-GeV neutrinos (they give 'confined neutrino events' in the detector). For the energy region of $100-10^4$ GeV, the only available data are those of Ryan et al. [575]. Their flux does not match the modern lower energy measurements by 50% in a 100-GeV energy region. Above 10^4 GeV, data are available only from air showers (Yangbajing array) [583] or nuclear emulsions [584–586]. The data show a gross continuity with the Ryan spectrum at the lower energy end, but errors are large. We note that all realistic neutrino flux calculations published to date and used in analyses of atmospheric neutrino experiments are those using cosmic-ray fluxes prior to modern measurements. So, the absolute flux predictions bear a significant uncertainty.

For a crude estimate, one may use

$$dN_p/dE_k \sim 1.2 \times 10^4 E_k^{-2.7} \text{m}^{-2} \text{s}^{-1} \text{sr}^{-1} \text{GeV}^{-1} \tag{4.7}$$

for the 5−100 GeV region (E_k in GeV units) after applying solar modulation (see below).[4] This curve is shown in Fig. 4.5 together with the BESS and AMS data.

The helium flux is measured together with the proton flux. The helium flux also differs among the authors. CAPRICE and IMAX gave He fluxes 50% lower than that of Webber et al. The fluxes from BESS and AMS [587], however, are substantially higher than those of CAPRICE and IMAX, but

---

way specific to cosmic-ray physics is an expression with *rigidity pc/Ze* where p is momentum and Z is the charge of nuclei, given in units of GV. Particles with the same rigidity follow identical paths in a given magnetic field.

[4] The power law is supposed to be valid down to ≈ 10 MeV, below which cosmic rays suffer significant ionisation loss from the interstellar medium.
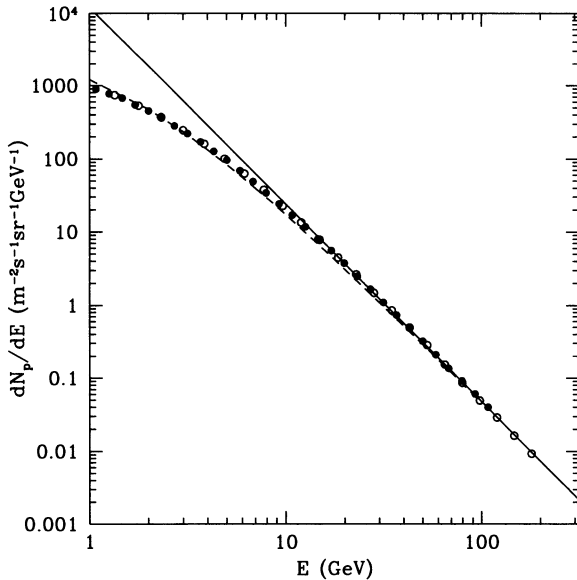
Fig. 4.5. Cosmic-ray proton flux measured by BESS (*solid circles*) and AMS (*open circles*). The *solid curve* represents (4.7). The *dashed curve* that closely matches the data points is the same spectrum but modulated by the solar wind according to the Gleeson–Axford formula (4.9) with $\phi = 750\,\mathrm{MeV}$.

lower than Webber et al.'s flux by only 10–15%. Taking the AMS and BESS results, the ratio He/H$\simeq$ 0.06 in numbers for $\gtrsim$10 GeV. This ratio increases to 0.1 at 100 GeV.

The next abundant elements are the CNO group. At 10 GeV/nucleon the ratio H: He: CNO is roughly 0.94:0.06:0.003 [588, 589]. The CNO abundance shows a slow increase with energy; at 10^4 GeV/nucleon, the ratio to hydrogen increases by a factor of 2 [586]. See Agrawal et al. [564] for a compilation of the fluxes. The iron abundance Fe/H$\simeq$ 0.00018 at 10 GeV, but the increase with energy is faster. It amounts to a factor of 3 between 10 and 1000 GeV [584, 586]. It is an interesting unsettled problem whether the iron group elements dominate the cosmic ray at 10^6 GeV, the so-called 'knee' region.

The contributions of heavy cosmic rays to neutrino flux are not negligible, especially to $\nu_e/\bar{\nu}_e$ ratio which depends strongly on the ratio of π^-/π^+ production. Helium bears 80% of the neutron flux, the CNO group contributes 15%, and the iron group 5%. The difference in cosmic-ray composition and cosmic abundance is primarily due to the efficiency of acceleration, which is affected by the first ionisation potential.

The solar wind decelerates cosmic rays. The effect is usually described by the diffusion–convection model, with which the observed spectrum i is given

in terms of the interstellar spectrum i_0 as

$$i(p,r,t) = i_0(p) \exp \left[- \int_{r_\oplus}^{r_{\text{lim}}} \frac{V(t)}{D(p,r',t)} dr' \right] ,$$ (4.8)

where $r_\oplus$ and r_{lim} are the distances of Earth (1 AU) and the boundary of the solar wind (33−43 AU) from the Sun, respectively, $V(t)$ is the (time-dependent) velocity of the solar wind ($\approx 430\,\text{km s}^{-1}$), and D is the diffusion coefficient [590, 591]. This effect becomes maximum at the solar maximum. The proton flux at 1 GeV in the solar minimum is twice as large as that in the solar maximum. The effect is reduced to $< 10\%$ at 10 GeV. A convenient parametrisation often taken in the literature is a spherically symmetric model by Gleeson and Axford [591]:

$$i(E,r,t) = \frac{E^2 - E_0^2}{(E+\Phi)^2 - E_0^2} i_0(E + \Phi, \infty) ,$$ (4.9)

where

$$\Phi = |Z| e \phi$$ (4.10)

with

$$\phi(t) = \int_{r_\oplus}^{r_{\text{lim}}} \frac{V(t)}{3k_1} dr .$$ (4.11)

Here, E represents the total energy, and $E_0 = m_p$ is the rest mass. The diffusion coefficient is written with a separable form as $D = k_1(r)\mathcal{R}\beta$ where $\mathcal{R}$ is the rigidity and β is the velocity of the particle. Empirically, ϕ is of the order of 500−1000 MeV. This reproduces the empirical spectrum very well, assuming that the interstellar spectrum obeys the power low (see Fig. 4.5 for an example). For more elaborate expressions, see [592, 593].

Low-energy cosmic rays do not reach Earth due to the dipolar magnetic field, which acts as a shield. An approximate cutoff momentum for the dipolar geomagnetic field is given by Störmer's formula [594],

$$p_c = p_0 \frac{\cos^4 \lambda}{[1 + (1 - \cos^3 \lambda \sin \theta \sin \phi)^{1/2}]^2} ,$$ (4.12)

where $p_0 = eR_\oplus B/c \simeq 59$ (GeV/c) (B is the magnetic field at the magnetic equator; $R_\oplus$ is the radius of the Earth), λ is the magnetic latitude, θ is the zenith angle, and ϕ is the azimuth measured clockwise from magnetic north. For a nucleus, the momentum is replaced with the rigidity. A calculation was carried out to take account of higher multipole components [595] of the geomagnetic field [596, 597]. The result does not differ much from Störmer's cutoff at a low geomagnetic latitude, but the difference amounts to 30% at high latitudes. The azimuthal dependence is often averaged in applications.

The actual cutoff effect is more complicated. Accurate calculations use back-tracking of negatively charged test particles (antiprotons) emitted from a specific site on Earth to see whether the particles go out of Earth under the
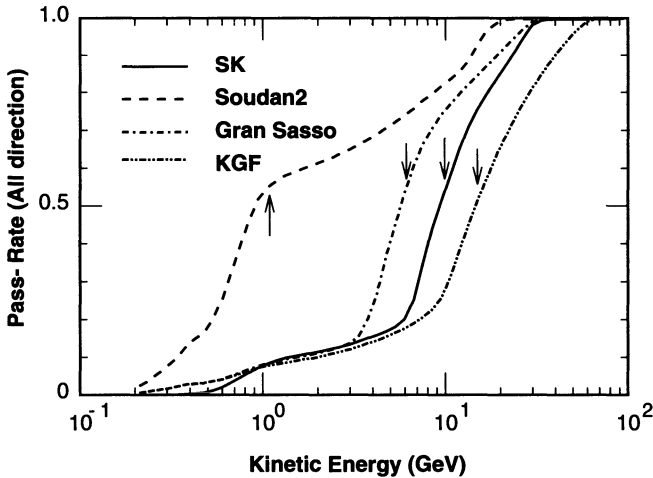
Fig. 4.6. Path rates for cosmic rays at various sites of neutrino experiments: Super-Kamiokande (SK), Gran Sasso, Soudan mine, and Kolar Gold Field (KGF). The arrows show the calculated geomagnetic cutoffs.

terrestrial magnetic field expressed as a multipole expansion [574]. Examples of the pass rate as a function of rigidity are shown in Fig. 4.6 [574]. It is seen that the effective rigidity–cutoff approximation overestimates the neutrino flux between 0.4 to 1 GeV by 10% [573].

Interactions of cosmic rays with air.   Cosmic rays interact with nuclei in the atmosphere and produce hadrons. A complication is the competition of decays with interactions and energy loss while propagating through the atmosphere. To obtain a rough idea of the propagation of cosmic rays, let us start with a gross overview.

Roughly speaking, the vertical density profile of the atmosphere is exponential,

$$\rho(h) = \rho_0 \exp(-h/h_0) \qquad (4.13)$$

where h is the altitude from the surface of Earth, $h_0 = 6.42\,\text{km}$ is the scale height, and $\rho_0 = 1.225 \times 10^{-3}\,\text{g\,cm}^{-3}$ is the density at Earth's surface. The actual distribution, however, deviates appreciably from this exponential form, and accurate calculations should use an atmosphere model, an example of which is given in [598].[5] Figure 4.7 shows a model atmosphere of [598] which is compared to an exponential form, where the normalisation is increased to $\rho_0 \simeq 1.61 \times 10^{-3}\,\text{g\,cm}^{-3}$ to adjust to the actual column density. The atmosphere consists of 78.1% N_2, 20.9% O_2, 0.9% Ar, 0.03% CO_2, and 0.002% Ne by volume. The composition is almost uniform up to 85 km (homosphere).

---

[5] The atmospheric density profile also depends on the location and the season. This would affect the neutrino flux by a few percent.
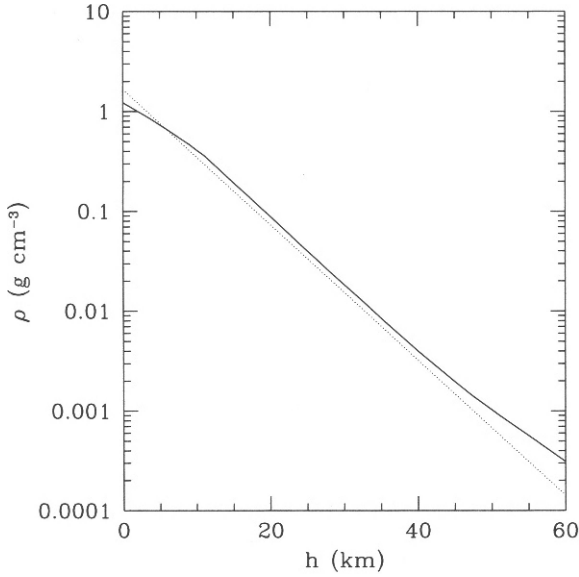
Fig. 4.7. Density of the atmosphere as a function of altitude. The *solid curve* shows the model atmosphere of [598], and the *dashed curve* represents the simple exponential law (4.13) with $\rho_0 = 1.61 \times 10^{-3}\,\mathrm{g\,cm^{-3}}$.

Let us consider a proton cosmic ray of $10-20\,$GeV energy. The inelastic cross section of pA scattering is about $(40\,\mathrm{mb})A^{2/3}$. This means that the mean free path is $\lambda \approx 40A^{-1/3}\,\mathrm{g\,cm^{-2}}$. Distribution (4.13) means that the first interaction takes place at an altitude around $15\,$km. A 5-GeV charged pion produced in this interaction travels about $c\tau_\pi(E_\pi/m_\pi) \approx 300\,$m, or $3.6\,\mathrm{g\,cm^{-2}}$ before decay. The amount of atmosphere traversed is small compared to the interaction length of pions, which is about $160\,\mathrm{g\,cm^{-2}}$, so most pions decay. The ionisation energy loss of pions is also negligible, $\Delta E \approx 2\,\mathrm{MeV/g\,cm^{-2}} \cdot 3.6\,\mathrm{g\,cm^{-2}} = 7\,$MeV. A 2.5-GeV muon from a pion would run for $25\,$km, i.e., reach the surface of the Earth. Such a muon, however, undergoes an ionisation energy loss of $2\,$GeV. The decay and energy loss compete for muons. When a muon hits Earth, it loses energy quickly and stops. Then, it is either absorbed into a nucleus (μ^-) or decays.

Considering the energy loss, parent muons of sub-GeV neutrinos have $E \lesssim 3\,$GeV, and most muons decay before reaching the surface of Earth. So the ratio of the fluxes of muon neutrinos to electron neutrinos is 2:1, and the zenith-angle distribution is approximately flat because the increases in the solid angle and the distance cancel as the zenith angle varies. On the other hand, parent muons that produce multi-GeV neutrinos ($E_\mu > 5\,$GeV) coming from the zenith and its antipodes would not have enough path length to decay, whereas those from oblique directions mostly decay (the path length is given by $\ell = -R_\oplus|\cos\zeta| + (R_\oplus\cos\zeta)^2 + h^2 + 2R_\oplus h]^{1/2}$ where ζ is the

zenith angle, and h is the thickness of the atmosphere). This makes both ν_e and ν_μ distributions peak at $\zeta = 90°$ (the horizontal direction) for multi-GeV neutrinos. For the zenith direction the flux ratio of ν_e to ν_μ decreases from one-half as energy increases. For an order of magnitude estimate of the ν_μ flux, one may use the flux given in (4.7) by replacing $E \to 5E$, i.e.,

$$\phi_{\nu_\mu} \sim 1.2 \times 10^4 (5E)^{-2.7}\,\mathrm{m}^{-2}\mathrm{s}^{-1}\mathrm{sr}^{-1}\mathrm{GeV}^{-1} \tag{4.14}$$

for 0.5–10 GeV neutrinos.

For more accurate treatments the master equation that governs the propagation of cosmic ray particles is

$$\frac{\partial I_i(E, x, \theta)}{\partial x} = -\mu_i(E)I_i(E, x, \theta) - \frac{m_i}{E\tau_i\rho(x)}I_i(E, x, \theta)$$
$$+ \sum_j \int dE' d\theta' \mu_j(E') S_{ji}(E', \theta, E, \theta) I_j(E', x, \theta') , \tag{4.15}$$

where I_i is the flux of cosmic rays of particle $i = $ nucleus, p, π, etc., at the position x measured in units of the amount of materials traversed $(\mathrm{g\,cm}^{-2})$ from the top of the atmosphere, with zenith angle θ and energy E; m_i and τ_i are mass and decay lifetime; μ_i is the absorption coefficient of particle i; ρ is the density of the atmosphere; and S_{ji} is the probability of particle production from $j \to i$. The first term represents a loss of flux by absorption (interactions), the second term is the loss by decay, and the third term is the production of the particle considered. Here, we ignore the energy loss term, which is important only for the propagation of muons, for which we write

$$\frac{\partial I_\mu(E, x, \theta)}{\partial x} = -\frac{m_i}{E\tau_i\rho(x)}I_\mu(E, x, \theta) + S_\mu(E, x, \theta)$$
$$+ \frac{\partial}{\partial E}[B(E)I_\mu(E, x, \theta)] , \tag{4.16}$$

where S_μ is the muon source function and

$$B(E) = dE/dx \simeq (a + bE) \tag{4.17}$$

is the energy loss rate, where $a \simeq 2.2\,\mathrm{MeV}/(\mathrm{g\,cm}^{-2})$ is the ionisation energy loss (see (4.238)) and the second term is the sum of the energy losses by bremsstrahlung (fee-free radiation), e^+e^- pair creation, and nuclear interaction [599], $b = b_{\mathrm{brems}} + b_{\mathrm{pair}} + b_{\mathrm{nucl}}$. The cross section of bremsstrahlung is of the order of $\sigma(k_\gamma)dk_\gamma \sim Z^2\alpha(m_e/m_\mu)^2 r_e^2 dk_\gamma/k_\gamma$ where $r_e = \alpha/m_e$ and k_γ is the momentum of the emitted photon; hence $dE_\mu/dx \sim E_\mu\sigma \sim Z^2\alpha^3 m_\mu^{-2}$ up to logarithmic factors[6] The cross section of e^+e^- pair creation via virtual photon emission receives one more power of α, but it does not depend on the

---

6 We write $b_{\mathrm{brems}} = X_0^{-1}$ where x_0 is called the radiation length. b_{brems} is given for the completely screened medium as

mass of the projectile, i.e., $\sigma dk \sim Z^2 \alpha^2 r_e^2 dk/k$, where k is the momentum of the virtual photon. The actual expression is fairly complicated; see [600]. The energy transfer, however, is suppressed by the factor of m_e/m_μ, so that $dE_\mu/dx \sim E(m_e/m_\mu)\sigma \sim Z^2 \alpha^2 m_\mu^{-1} m_e^{-1}$. Therefore, the two contributions are on the same order. The energy loss due to the nuclear reaction is also known to be on the same order. Detailed calculations [601] show that $b_{\text{pair}} > b_{\text{brems}} > b_{\text{nucl}}$ and $b = (3.0 - 3.5) \times 10^{-6}\,\text{g cm}^{-2}$ for $E_\mu \sim 1 - 10^3$ TeV in the air (or in the water). The bE term becomes more important than the a term only for $E \gtrsim 1$ TeV.

Russian groups developed a semianalytic method to solve these equations [566, 567]. More direct and practically simpler is to resort to a Monte Carlo simulation, as adopted in [563, 565].

For simplicity, most calculations employ a one-dimensional approximation, in which the direction of the neutrino is the same as that of the primary protons, $\theta' = \theta$ in (4.15). Note that this is not quite justified because the average transverse momentum of a pion from hadronic interaction is 300 MeV, which can be comparable to the lowest neutrino energy of interest ($E_\nu > 200$ MeV). Calculations with a one-dimensional approximation, however, give results that do not differ much from three-dimensional calculations for the flux (within uncertainties of other origins), except that three dimensional calculations enhance the neutrino flux close to the horizontal direction for $E_\nu \lesssim 1$ GeV due to a conspicuous increase in the acceptance angle near the horizontal direction [572]; see [602] for a comparison of the 1D and 3D calculations.

The calculation of the interaction of a cosmic ray with a nucleus requires experimental knowledge of hadronic interactions of a proton (or nucleus) on a nucleus. Experimental data available from accelerator experiments, which are appropriate for estimating neutrino beams for accelerator experiments, however, are not sufficient to calculate atmospheric neutrino flux. The main reason is that the acceptance angle of accelerator counter experiments is limited to milli-radian solid angles relative to the beam direction, and hence data with a small $x = E_\pi/E_N$, typically $x < 0.15$, are entirely lacking. One has to resort to extrapolations and/or the use of nuclear emulsion or bubble chamber data that are not quite suitable for extracting inclusive reaction data at high precision.

$$b_{\text{brems}} = \frac{4Z(Z+1)\alpha^3 n_A}{m_\mu^2} \ln(183/Z^{1/3}),$$

i.e.,

$$X_0 = 3.07 \times 10^7 \frac{A}{Z(Z+1)} \left(\ln 183/Z^{1/3}\right)^{-1} \text{g cm}^{-2},$$

where n_A is the density of the atom with atomic number and weight (A, Z) that constitutes the medium. For a fully ionised plasma, the ln factor is replaced with $\ln(2E/m_\mu)$.
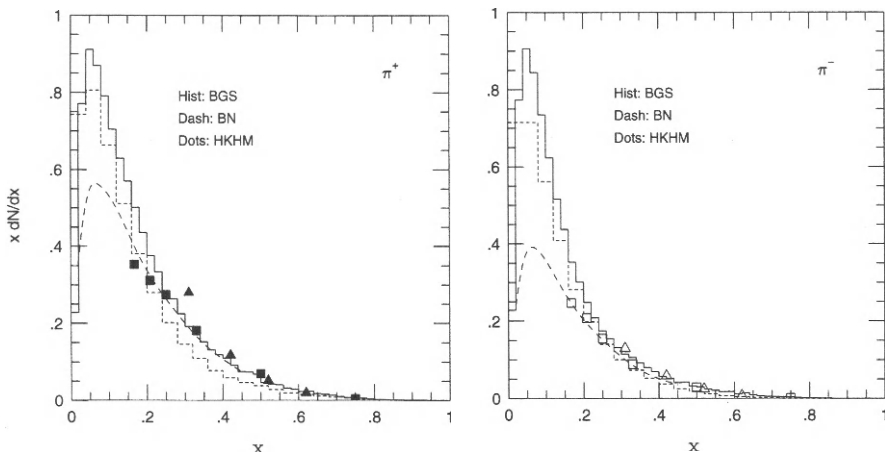
Fig. 4.8. Momentum distributions of $\pi^{\pm}$ in p–Be collisions. The distributions used in atmospheric neutrino calculations are compared with data. After [573].

Realistic atmospheric neutrino flux calculations use a parametrised data set [563, 566] or semiempirical hadron jet Monte Carlo programmes [565] (see Table 4.1 below). Hadron production cross sections were assessed in [573]. It was concluded that the treatment of hadron production for small x, where experimental constraints are lacking, is the most important source of the discrepancy in the resulting neutrino flux (see Fig. 4.8).

Modern calculations take into account all decay processes with branching ratios typically larger than 1%. The contribution of kaons to the neutrino flux in $< 10\,\text{GeV}$ range is less than 10%. The muon from π decay is completely polarised in the rest frame. The polarisation remains at about 30% in the laboratory system. This makes ν_e from μ^+ to have a higher energy compared to the unpolarised case, and hence it increases $(\nu_e + \bar{\nu}_e)/(\nu_\mu + \bar{\nu}_\mu)$ [603].

For the purpose of illustrating calculations, let us present a quantitative but crude approach [569] (see also [570]). If we replace the decay length and the absorption length with their mean values, the ν_μ flux from $\pi \to \mu\nu_\mu$ is written

$$\frac{dF_\nu}{dE_\nu d\Omega} = N \int dh \int dE_\pi \int dy \frac{d\Gamma_\nu(E_\pi, E_\nu)}{dE_\nu} D_\pi(E_\pi) R_\pi(E_\pi, h, y) \frac{d^2 J_\pi(E_\pi, y)}{dE_\pi dy} \,,$$

(4.18)

where $d\Gamma_\nu(E_\pi, E_\nu)/dE_\nu$ is the neutrino spectrum from the decay of pions; $D_\pi(E_\pi) = \tau_\pi^{-1}(m_\pi/E_\pi)$ is the decay rate of a pion; $R_\pi(E_\pi, h, y)$ is the probability that a pion of energy E_π produced at height y survives at altitude h, where it decays; the last factor is the pion energy spectrum at the altitude y, as given by

$$\frac{d^2 J_\pi(E_\pi, y)}{dE_\pi dy} = \sigma_{\text{inel}} N_L \rho(y) \int_{\max[E_\pi, E_c(\theta)]}^{\infty} \frac{d\Gamma_\pi(E_\pi, E_p)}{dE_\pi} \frac{d^2 J_p(E_p, y, \Omega)}{dE_p dy} dE_p \,.$$

(4.19)

Here, $d^2 J_p(E_p, y, \Omega)/dE_p dy$ is the energy spectrum of the primary proton at altitude y, and $d\Gamma_\pi(E_\pi, E_p)/dE_\pi$ is the pion production energy spectrum, which may be approximated as

$$\frac{d\Gamma_\pi(x)}{dx} \approx \frac{(1-x)^3}{x} , \tag{4.20}$$

where $x =$ (momentum of pion)/(momentum of proton) in the laboratory system; $N_L = 6.02 \times 10^{23}$ g^{-1} is the Loschmidt (Avogadro) number. When expression (4.18) is integrated over solid angle Ω, the geomagnetic effect should be taken into account. For more accurate calculations, the experimental data should be used directly to evaluate $d\Gamma_\pi(x)/dx$, for which the data are lacking for $x < 0.15$, however, as mentioned above. The lower end of the integral E_c in (4.19) is the geomagnetic cutoff, or else the pion production threshold is taken.

For the neutrino (ν_e and $\bar{\nu}_\mu$) flux from muon decay, we make the following replacement in (4.18):

$$\frac{d\Gamma_\nu(E_\pi, E_\nu)}{dE_\nu} \to \int dz \int dE_\mu \frac{d\Gamma_\nu(E_\mu, E_\nu)}{dE_\nu} D_\mu(E_\mu) R_\mu(E_\mu, z, h)$$

$$\times \frac{d\Gamma_\mu(E'_\mu, E_\pi)}{dE'_\mu}\Big|_{E'_\mu = E_\mu + \Delta E_\mu(z,h)} , \tag{4.21}$$

where $\Delta E_\mu(z, h) = 2.2\,\mathrm{MeV\,g\,cm^{-2}}\rho(z)$ is the ionisation energy loss of a muon. The factor $d\Gamma_\nu(E_\mu, E_\nu)/dE_\nu$ should include the effect of polarisation.
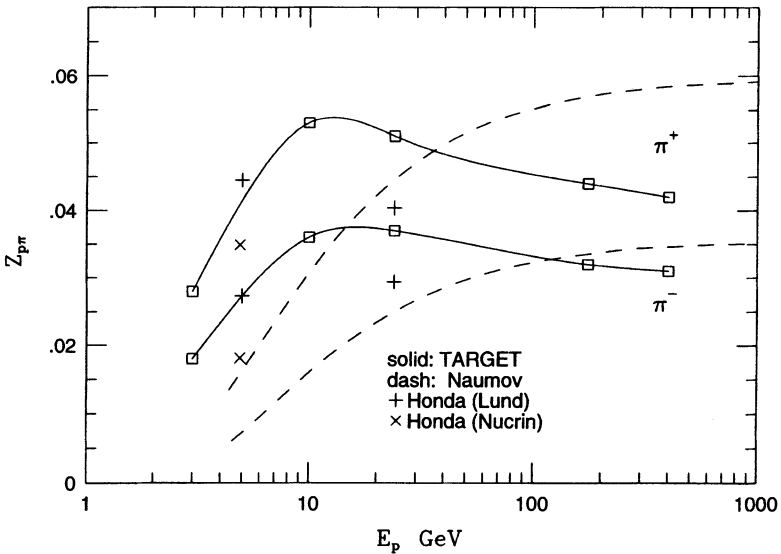
Fig. 4.9. Comparison of the pion production function $Z(p \to \pi)$ in (4.22) for p–Be collisions.

The most uncertain factor in (4.18) is the pion production spectrum $d\Gamma_\pi$, which enters the integral roughly with the form

$$Z(p \to \pi) = \int_0^1 dx \, x^{1.7} \frac{d\Gamma(x)}{dx} \ . \tag{4.22}$$

Gaisser et al. [573] depicted $Z(p \to \pi)$ (see Fig. 4.9) for the three representative neutrino flux calculations, Barr et al. (BGS) [563], Honda et al. (HKKM) [565], and Bugaev and Naumov (BN) [566]. This uncertainty can be removed only after accelerator experiments for the production of particles for small x regions with nuclear targets.
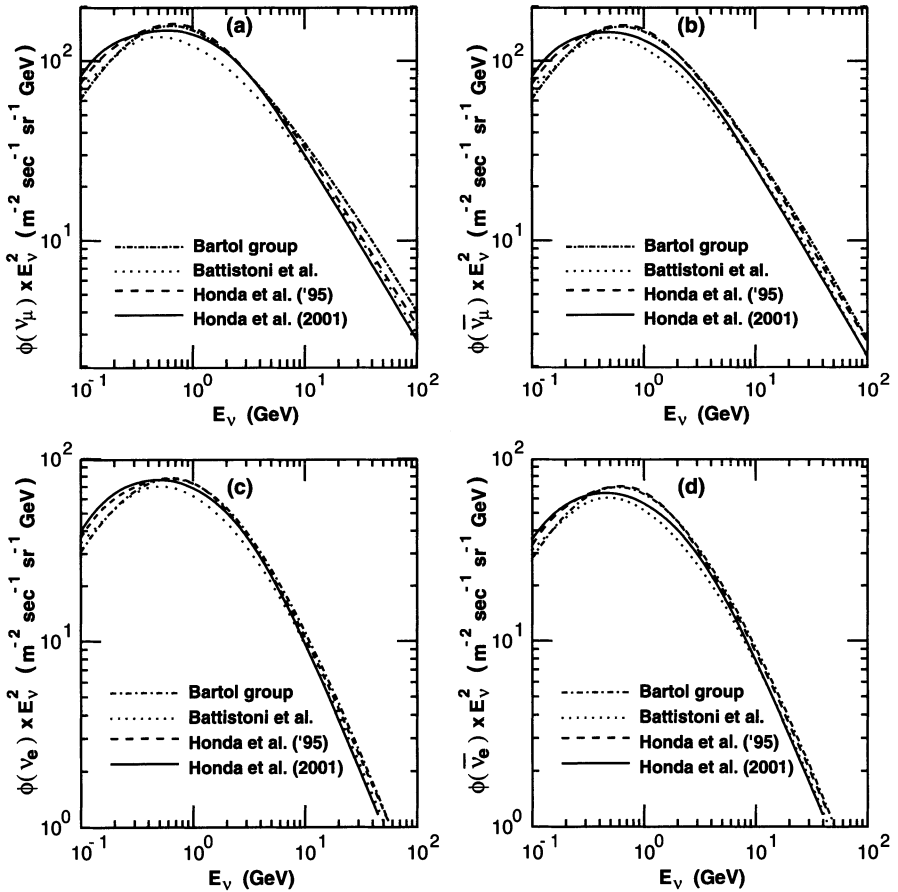
Fig. 4.10. Comparison of the atmospheric neutrino fluxes of BGS [563]/AGLS [564] (Bartol group), Battistoni et al. [572], HKKM [565] (Honda et al. 1995), and Honda et al. 2001 [610]: **(a)** ν_μ flux, **(b)** $\bar{\nu}_\mu$ flux, **(c)** ν_e flux, and **(d)** $\bar{\nu}_e$ flux.

Table 4.1. Calculations of atmospheric neutrino flux.

Authors	Geomag cutoff	Propagation	Hadronic int	Energy range
HKKM [565]	Ray trace [604]	Monte Carlo [604]	NUCLIN [605] and FRITIOF [606]	30 MeV $-$ 3 GeV
			idem+COSMOS [604]	$1 - 10^3$ GeV
BGS [563]	Cutoff [596]	Monte Carlo	Database: TARGET [607]	60 MeV $-$ 3 GeV
AGLS [564]	Cutoff [564]	Monte Carlo	Database: TARGET [607]	$1 - 10^4$ GeV
BN [566]	Cutoff [597]	Semianalytic	Parametrised database [608]	30 MeV $-$ 3 GeV
Battistoni [572]	Ray trace	Monte Carlo [609]	in FLUKA package [609]	60 MeV $-$ 3 GeV
Honda01 [610]	Ray trace [604]	Monte Carlo [604]	DPMJET3 [611]	30 MeV $- 10^3$ GeV

Neutrino flux results. Representative examples of the atmospheric neutrino calculations are listed in Table 4.1. The top four, which are often cited in the experimental work as the reference, were made before 1996, i.e., before accurate measurements of the cosmic-ray proton and helium flux became available. This affects the absolute flux and also the neutrino to antineutrino flux ratio through a change of the He/H ratio. There are, however, no updates in other experimental data that would modify the flux ratio of ν_e to ν_μ. The low-energy calculations ($E < 3$ GeV) are primarily for 'confined events,' and high-energy calculations are for 'through muons.'

In Fig. 4.10 and 4.11 we present neutrino fluxes of four calculations, HKKM, BGS, Battistoni et al. and a newer calculation by Honda et al. [610] for the Kamiokande site. The panels (a)–(d) of Fig. 4.10 show the absolute fluxes for each species and panels (a)–(c) of Fig. 4.11 give the ratios $\bar{\nu}_\mu/\nu_\mu$.
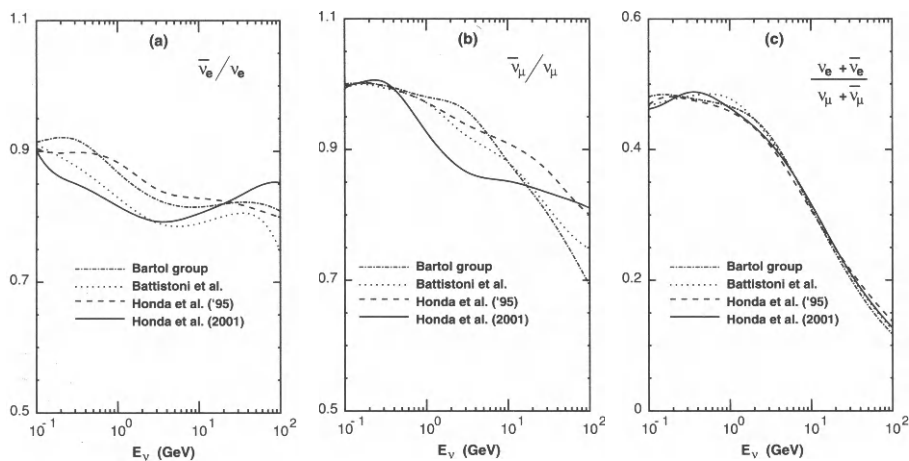
4.4 Neutrinos from Stars

4.4.1 Theory of Stars: Fundamental Equations

The stationally burning star[7] is taken as a sphere of gas which is in hydrostatic equilibrium under gravitational compression and the force from the pressure gradient, i.e.,

$$\frac{dP}{dr} = -\frac{Gm(r)\rho}{r^2} , \qquad (4.23)$$

where $m(r)$ is the mass within the radius r and ρ is the density, i.e.,

$$\frac{dm(r)}{dr} = 4\pi r^2 \rho . \qquad (4.24)$$

One more equation is energy conservation:

$$\frac{dL(r)}{dr} = 4\pi r^2 \rho(\varepsilon_n - \varepsilon_\nu) - T\frac{\partial S}{\partial t} , \qquad (4.25)$$

where $L(r)$ is the luminosity from a sphere of radius r; ε_n and ε_ν are, respectively, nuclear energy production and energy loss due to neutrino emission from the shell at r, and S is stellar entropy per mass. This entropy term can be neglected for stars in hydrostatic equilibrium.

The set of the three dynamic equations governs the physics of stars when they are supplemented by a few physics ingredients: one of them is the equation of state:

$$P = P(T, \rho) . \qquad (4.26)$$

In hot stellar interiors, the gas is close to an ideal state, and (4.26) is

$$P = nkT , \qquad (4.27)$$

where n is the number density of free particles, the sum over free electrons n_e and ions n_i,

$$n = n_e + n_i = \left[\left(X + \frac{Y}{2} + \frac{Z}{2}\right) + \left(X + \frac{Y}{4} + \frac{Z}{A_{\text{eff}}}\right)\right]\frac{\rho}{m_{\text{H}}} , \qquad (4.28)$$

where X, Y, and Z are the mass fractions of hydrogen, helium, and elements heavier than lithium ($X + Y + Z = 1$; effective mass number $A_{\text{eff}} \gg 1$) and m_{H} is hydrogen mass. It is usually expressed using the mean molecular

---

[7] We must limit ourselves only to the most elementary aspects here. We refer readers to standard textbooks: Chandrasekhar [612], Schwarzshild [613], Hayashi, Hoshi, and Sugimoto [614], Clayton [615], Cox & Giuli [616], and for a more modern text book, e.g., Kippenhahn and Weigert [617].

weight μ:

$$n = \frac{1}{\mu}\frac{\rho}{m_H} \,, \qquad (4.29)$$

with

$$\frac{1}{\mu} \simeq 2X + \frac{3}{4}Y + \frac{1}{2}Z \,. \qquad (4.30)$$

For high-density stars the equation of state is given by degenerate electron Fermi gas; in the nonrelativistic (NR) limit,

$$P = \left(\frac{9\pi^4}{125 m_e^3 \mu_e^5 m_N^5}\rho^5\right)^{1/3} = K_1\left(\frac{\rho}{\mu_e}\right)^{5/3} \,, \qquad (4.31)$$

where the combination $\rho/\mu_e m_N = n_e$ with

$$\mu_e^{-1} = X + Y/2 + Z/2 \qquad (4.32)$$

is the first curly bracket of (4.28) and $K_1 = 1.00 \times 10^6$ cgs. Comparing the pressure of (4.27) with (4.31), we take the state as nondegenerate if

$$\frac{\rho}{\mu_e} < 2.36 \times 10^{-8} T^{3/2}(\text{K}) \,. \qquad (4.33)$$

In the centre of the Sun ($T \simeq 1.5 \times 10^7\,\text{K}$, $\rho \simeq 150\,\text{g cm}^{-3}$, $\mu \simeq 1.38$), this condition is satisfied with an allowance of one order of magnitude.

In the extreme relativistic (ER) limit,

$$P = \left(\frac{3\pi^2}{64 m_N^4 \mu_e^4 \rho^4}\right)^{1/3} = K_2\left(\frac{\rho}{\mu_e}\right)^{4/3} \,, \qquad (4.34)$$

where $K_2 = 1.24 \times 10^{15}$ cgs. Since the Fermi momentum in units of electron mass is $p_F/m_e = 1.01 \times 10^{-2}(\rho/\mu_e)^{1/3}$, the transition from NR to ER takes place at $\rho \approx 10^6\,\text{g cm}^{-3}$.

One more equation we need is that for radiative transport [8]:

$$L(r) = -4\pi r^2 \frac{c}{3\kappa\rho}\frac{d}{dr}(aT^4) \,, \qquad (4.35)$$

where $a = (\pi^2/15)(k^4/c^3\hbar^3) = 7.56 \times 10^{-15}\,\text{erg cm}^{-3}\text{deg}^{-4}$ is the radiation density constant and κ is the quantity called opacity, which is an inverse of the mean free path of the photon per unit mass, i.e.,

$$\kappa = \langle \sigma n_e\rangle \frac{1}{\rho} \,. \qquad (4.36)$$

---

[8] We do not derive this important equation here. We refer the reader to [612] (pp. 198–213), [613] (pp. 37–42), or [618] (pp. 579–586).
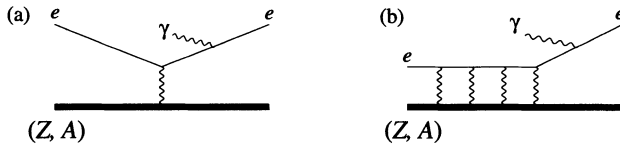
Fig. 4.12. Bremsstrahlung (free-free scattering) and photoionisation (bound-free scattering).

The opacity is calculated given atomic processes of emission and absorption of light. If Thomson scattering dominates the atomic process, as happens at high temperature, $\sigma = \sigma_T = (8\pi/3)(\alpha^2/m_e^2)$, and

$$\kappa = 0.20(1 + X) \text{ cm}^2/\text{g} . \tag{4.37}$$

In most parts of the interior of the Sun, free-free scattering (bremsstrahlung, see Fig. 4.12a) is one of the two major sources of opacity: it is approximately calculated to give

$$\kappa_{ff} = 3.7 \times 10^{22} \langle g_{ff} \rangle (1 + X) \frac{\rho}{T^{3.5}} \text{ cm}^2/\text{g} \tag{4.38}$$

in cgs units, where $\langle g_{ff} \rangle$ is a quantity of order unity (Gaunt factor).[9] This is called the Kramers opacity [619]. We see that the free-free opacity dominates over Thomson scattering if

$$\rho > 17 \langle g_{ff} \rangle^{-1} T_7^{3.5} \tag{4.39}$$

with T_7 the temperature in units of 10^7 K. This is satisfied in the solar interior.

An equally important source of the opacity in the solar interior is the bound-free process (photoionisation, or photoelectric effect, Fig. 4.12b) and its inverse process (recombination). With a rather crude approximation,

$$\kappa_{ff} = 4.4 \times 10^{25} \frac{\langle g_{bf} \rangle}{t} Z(1 + X) \frac{\rho}{T^{3.5}} \text{ cm}^2/\text{g} , \tag{4.40}$$

where $\langle g_{bf} \rangle/t$ is a quantity of order 0.1–1 (g is the Gaunt factor and t is Eddington's guillotine factor for absorption edges). The bound-free opacity also takes the same form as the free-free opacity, and this simple expression is called the Kramers opacity together with (4.38) given above. The bound-free opacity is more important than the free-free opacity for stars with solar metallicity ($Z \approx 0.02$). (See Fig. 4.16 below for a sample plot.)

---

[9] The cross section depends generally on the frequency of photons. In the opacity this dependence is averaged with the weight of the strength of the radiation field, as it appears in the equation of radiation transport (Rosseland mean).

Where the temperature is low, radiative transport is not efficient, and convection starts to take over energy transport.[10]This happens for the Sun in the outer layer ($r > 0.7R_\odot$). The convective region increases as the mass of the star decreases: a star with $M < 0.4M_\odot$ is completely convective. For neutrino physics, however, the physics of convection plays only a minor role; so we do not discuss this important subject further.

We explain here some standard notations and a few of the most elementary quantities that frequently appear in stellar astrophysics. The physical quantities for the Sun are most often taken as units of astrophysical quantities and are referred to by the symbol $\odot$. Examples are mass $M_\odot = 1.99 \times 10^{33}$ g, luminosity $L_\odot = 3.84 \times 10^{33}$ erg s^{-1}, radius $R_\odot = 6.96 \times 10^{10}$ cm, and heavy element abundance $Z_\odot \simeq 0.017$. We often use such as T_7 to denote temperature T in units of 10^7 K. We refer to Allen's *Astrophysical Quantities* [620] for the standard reference for numbers that appear in astrophysics.

4.4.2 Theory of Stars: Simple Solutions

Among the three dynamic equations (4.23)–(4.25), the first two determine the most fundamental properties of stars, and first-order understanding of stars can be had by solving these two equations by assuming a simple equation of state:

$$P = K\rho^\Gamma , \quad \Gamma = 1 + \frac{1}{n} , \tag{4.41}$$

which is called the polytropic equation of state [621] (n is called the polytropic index). Writing

$$\rho = \rho_c \theta^n , \tag{4.42}$$

$$r = a\,\xi , \tag{4.43}$$

(4.23) and (4.24) are combined to give

$$\frac{1}{\xi^2} \frac{d}{d\xi} \xi^2 \frac{d\theta}{d\xi} = -\theta^n , \tag{4.44}$$

where a is set equal to

$$a = \left[(n+1) \frac{K\rho_c^{\frac{1}{n}-1}}{4\pi G} \right]^{1/2} . \tag{4.45}$$

---

[10] The condition for convective instability is obtained by the following consideration. Suppose that an element at a distance r from the centre of the star is adiabatically brought to $r + \Delta r$. If the decrement of the density of this element is larger than that of the environment the buoyancy brings the element further and convection takes place. Namely the condition for convection is $|d\rho/dr|_{\text{adiabatic}} \Delta r > |d\rho/dr|_{\text{star}} \Delta r$, or $|dT/dr|_{\text{adiabatic}} < |dT/dr|_{\text{star}}$. This is called the Schwarzschild condition.

This is the Lane–Emden equation. The boundary conditions are

$$\theta(0) = 1 , \quad \theta'(0) = 0 .$$ (4.46)

The first condition means that ρ_c is the central density, and the second follows from $dP/dr|_{r=0} = -(4\pi/3)Gr\rho_c^2 = 0$ at the centre. The solution of $\theta(\xi)$ is monotonically decreasing with ξ: for $n < 5$, it crosses zero at a finite value of ξ_1. $\theta(\xi_1) = 0$ means $P = \rho = 0$ at ξ_1, i.e., the surface of the star. For $n = 5$, θ vanishes at $\xi = \infty$. From (4.41) and (4.43),

$$(P/P_c) = (\rho/\rho_c)\theta .$$ (4.47)

This means that θ represents the temperature (normalised to unity at the centre) for an ideal gas.

Table 4.2. Solutions of the Lane–Emden equation.

n	ξ_1	$-\xi_1^2 \frac{d\theta}{d\xi}\|_{\xi_1}$	$\rho_c/\langle\rho\rangle$
0	2.4495	4.8988	1
1	3.1416	3.1416	3.2899
1.5	3.6538	2.7141	5.9907
3	6.8969	2.0182	54.1825
3.25	8.0189	1.9498	88.153
5	∞	1.7321	∞

The Lane–Emden equation is solved analytically for $n = 0, 1$ and 5, or otherwise, it is solved by numerical integration. We are particularly interested in two quantities of the solution, ξ_1 and $[-\theta'(\xi_1)]$ (see Table 4.2), for the following reason. We can calculate the radius of the star as

$$R = a\xi_1,$$ (4.48)

and the mass

$$M = \int_0^R 4\pi r^2 \rho dr = 4\pi a^3 \rho_c \int_0^{\xi_1} d\xi \xi^2 \theta^n$$ (4.49)

$$= 4\pi a^3 \rho_c \xi_1^2 [-\theta'(\xi_1)] ,$$ (4.50)

where the Lane–Emden equation is used and integration is carried out by parts from the first to the second line. By deleting a from M and R, we obtain the mean density $\bar{\rho} = M/(4\pi R^3/3)$ as

$$\frac{\bar{\rho}}{\rho_c} = 3[-\theta'(\xi_1)]/\xi_1.$$ (4.51)

Also,

$$P_c = \frac{GM^2}{4\pi R^4} \frac{1}{(n+1)[-\theta'(\xi_1)]^2}$$

$$\simeq 3.29 \times 10^{17} (M/M_\odot)^2 (R/R_\odot)^{-4} \frac{1}{(n+1)[-\theta'(\xi_1)]^2} \text{ erg cm}^{-3}. (4.52)$$

The effective polytrope n of a main sequence star like the Sun is close to 3.25. This can be seen from

$$\frac{\frac{dP}{dr}}{\frac{dT}{dr}} = + \frac{GM\rho}{r^2} \frac{16\pi r^2 a c T^3}{3\kappa \rho L} \propto \frac{T^3}{\kappa} \frac{GM}{L}, \tag{4.53}$$

where (4.23) is used for dP/dr and dT/dr is derived from (4.35). For the Kramers opacity $\kappa \sim \rho T^{-3.5}$, we find $dP/dT \sim \rho^{-1} T^{6.5} \sim P^{-1} T^{7.5}$, which is integrated to give $P \sim T^{4.25}$, i.e., $n = 3.25$. The effective polytrope of the Sun, as calculated by

$$\frac{d\log P}{d\log T} = n_\text{eff} + 1 , \tag{4.54}$$

is close to this value, especially when averaged from the centre to the bottom of the convective layer.

With $n = 3.25$, it is found that $\xi_1 = 8.01894$ and $-\xi_1^2 \theta'(\xi_1) = 1.94980$ [612], so that we find $\rho_c(\odot) = 124 \text{ g cm}^{-3}$ for $\bar\rho = 1.4 \text{ g cm}^{-3}$ in fair agreement within 20% with the accurate solar model value 152 g cm^{-3}. From (4.47), with the aid of

$$T_c = \frac{P_c}{\rho_c} \frac{\mu}{(k/m_H)} , \tag{4.55}$$

we find $T_c(\odot) = 1.38 \times 10^7$ K, which also agrees within 15% with an accurate model calculation of 1.58×10^7 K.

Let us show how luminosity varies with stellar mass. As an order of magnitude argument, from (4.23), (4.27), and $R \sim (M/\rho)^{1/3}$, we obtain $T/\mu \sim G\rho^{1/3} M^{2/3}$ or

$$\frac{\rho}{T^3} \sim \frac{1}{G^3 \mu^3 M^2} . \tag{4.56}$$

The equation of radiative transport (4.35) is

$$L \sim \frac{RT^4}{\kappa\rho} \tag{4.57}$$

$$\sim \frac{G^4 M^3 \mu^4}{\kappa} , \tag{4.58}$$

when T is deleted using (4.56). The temperature of stars with $M > 2M_\odot$ is sufficiently high that Thomson scattering dominates opacity. In this case, $\kappa \sim$ constant, and $L \propto M^3$, which agrees with the observation. For stars with $M < 2M_\odot$, the Kramers opacity applies. If we approximate it as

$\kappa \sim \rho/T^3$, (4.56) means $\kappa \sim 1/M^2$, and we obtain $L \propto M^5$, which is compared with the empirical $M^{4.75}$ dependence. For low mass stars where convection dominates, one can show that $L \propto M^{1.68}$. Note that the luminosity is determined irrespective of nuclear reactions in the first-order argument.

4.4.3 Nuclear Reactions in Stars and Neutrino Emission: Formalism

The nuclear reaction rate of two particles 1 and 2 with number densities n_1 and n_2 in a thermal bath is given [622, 623] by averaging the reaction rate $\sigma v_{\rm rel}$ over the Maxwell–Boltzmann distribution of two reacting particles:

$$r = n_1 n_2 \langle \sigma v_{\rm rel} \rangle \tag{4.59}$$

$$= n_1 n_2 \int \frac{d^3 p_1}{(2\pi)^3} \frac{d^3 p_2}{(2\pi)^3} \left(\frac{2\pi}{m_1 kT}\right)^{3/2} e^{-\frac{p_1^2}{2m_1 kT}} \left(\frac{2\pi}{m_2 kT}\right)^{3/2} e^{-\frac{p_2^2}{2m_2 kT}} \sigma v_{\rm rel} . \tag{4.60}$$

The factor $n_1 n_2$ is replaced with $n^2/2$ if 1 and 2 are identical particles. We take $k = 1$ hereafter. Using new variables $p_1 + p_2 = P$ and $p_1/m_1 - p_2/m_2 = p/m_r$ ($1/m_r = 1/m_1 + 1/m_2$), (4.60) simplifies to

$$r = 4\pi n_1 n_2 \left(\frac{1}{2\pi m_r T}\right)^{3/2} \int dp\, p^2 (p/m_r) \sigma e^{-\frac{p^2}{2m_r T}} \tag{4.61}$$

$$= n_1 n_2 \frac{4}{(2\pi m_r)^{1/2}} T^{-3/2} \int_0^\infty dE\, E \sigma(E) e^{-E/T} . \tag{4.62}$$

When resonances do not exist in the reaction we usually parametrise

$$\sigma(E) = \frac{S(E)}{E} \exp\left(-\frac{2\pi Z_1 Z_2 \alpha}{\hbar v_{\rm rel}}\right) , \tag{4.63}$$

where $1/E$ takes account of the low-energy cross section $\sigma \sim \pi \lambda^2$ with $\lambda \sim \hbar/p$ the de Broglie length and the exponential is Gamow's penetration factor for the Coulomb barriers for two nuclei with charges $Z_1 e$ and $Z_2 e$. $S(E)$ is then approximately constant. This factor leads to strong suppression of low-energy reactions, in contrast to the Boltzmann factor which highly suppresses the integral for $E > T$. The contribution to the integral arises from the region where the two suppression factors balance (Gamow peak). Inserting (4.63) into (4.62), we write the integral as

$$\int dE\, S(E) e^{-f(E)} , \tag{4.64}$$

where

$$f(E) = \frac{E}{T} + \left(\frac{2m_N A}{E}\right)^{1/2} \pi Z_1 Z_2 \alpha , \tag{4.65}$$

and the integral is evaluated using the saddle point method by writing $f(E) = f(E_0) + \left(\frac{E-E_0}{\Delta E}\right)^2$ with $E_0 = (bT/2)^{2/3}$, $b = \pi Z_1 Z_2 \alpha \sqrt{2m_N A} = 31.40 Z_1 Z_2 A^{1/2}$ (keV)$^{1/2}$, and $(\Delta E)^2 = (4/3)E_0 T$ with $A = A_1 A_2/(A_1 + A_2)$ the harmonic mean of atomic numbers of the two nuclei,[11] i.e.,

$$E_0 = 1.223(Z_1^2 Z_2^2 A T_6^2)^{1/3} \text{ keV} . \tag{4.66}$$

The reaction rate is written as

$$r = n_1 n_2 \frac{S(E_0)}{T^{2/3}} \gamma e^{-\beta/T^{1/3}} , \tag{4.67}$$

where

$$\gamma = \frac{2^{7/3} \pi^{1/3}}{3^{1/2}} \left(\frac{\alpha}{m_N}\right)^{1/3} \left(\frac{Z_1 Z_2}{A}\right)^{1/3} , \tag{4.68}$$

$$\beta = \frac{3}{4^{1/3}} (2\pi^2 Z_1^2 Z_2^2 \alpha^2 m_N A)^{1/3} . \tag{4.69}$$

Or

$$r = 2.80 \times 10^{-16} n_1 n_2 \frac{S(E_0)}{T_7^{2/3}} \left(\frac{Z_1 Z_2}{A}\right)^{1/3} \exp\left[-\frac{19.77(Z_1^2 Z_2^2 A)^{1/3}}{T_7^{1/3}}\right] \text{ cm}^{-3} \text{ s}^{-1} , \tag{4.70}$$

where $S(E)$ is measured in units of keV·barn.

The S factor is often represented by an expansion

$$S(E) = S(0) + E \left.\frac{dS}{dE}\right|_{E=0} . \tag{4.71}$$

Retaining the contribution from the next order term proportional to kT/E_0 in the integral around the saddle point, we may rewrite the resulting expression in the form of (4.70) using the effective S factor [624],

$$S_{\text{eff}}(E_0) = S(0) + \frac{5}{12}\frac{T}{E_0} + \frac{S'(0)}{S(0)}\left[E_0 + \frac{35}{36}T\right] . \tag{4.72}$$

In the plasma free electrons that cluster around positive ions reduce the Coulomb force, thus increasing nuclear reaction rates [625, 626]. In the weak screening limit we may apply Debye–Hückel theory, in which the potential near the nucleus of charge $Z_1 e$ is written

$$\phi_1 = \frac{e}{4\pi}\frac{Z_1}{r} e^{-r/r_D} \simeq \frac{e}{4\pi} Z_1 \left(\frac{1}{r} - \frac{1}{r_D}\right) \tag{4.73}$$

---

[11] We ignore the binding energy and take the proton mass as mass units. More accurately, we should use atomic units m_A, for which $m_H = 1.0079 m_A$, and correct for electron mass.

with the Debye screening length

$$r_D = \left(\frac{4\pi n \alpha \chi}{T} \right)^{-1/2} , \tag{4.74}$$

where $n = \rho/m_{\mathrm{H}}$ and $\chi = \sum_i Z_i(Z_i+1)X_i/A_i$. The two terms in χ arise from the effect of nuclei and electrons, the latter of which diminishes if the medium is strongly electron degenerate. For the Sun the electron degeneracy is not strong, and the degeneracy effect is taken into account by multiplying the second term with 0.92 [626]. The potential shift $\Delta\phi_1 = -eZ_1/4\pi r_D$ increases the probability that the charge $Z_2 e$ comes close to $Z_1 e$ by the Boltzmann factor,

$$f = \exp(-eZ_2\Delta\phi_1/kT) = \exp\left(\frac{Z_1 Z_2 \alpha}{T r_D} \right) . \tag{4.75}$$

The nuclear reaction rate, hence, increases by this factor [625, 626].[12]

The energy generation rate ε that appears in (4.25) is given by

$$\varepsilon = n_1 n_2 \langle \sigma v \rangle (Q - Q_\nu)/\rho = r(Q - Q_\nu)/\rho \tag{4.76}$$

where Q is the Q value of the reaction and Q_ν the neutrino energy loss. The luminosity of a star is given by

$$L = \int_0^R dr 4\pi r^2 \varepsilon(r) . \tag{4.77}$$

4.4.4 Nuclear Reactions in the Sun and Solar Neutrinos

The initiating reaction is the weak interaction process [632, 633]

$$p + p \rightarrow d + e^+ + \nu_e + 0.420\mathrm{MeV} , \tag{4.78}$$

where e^+ combines with an ambient electron and produces energy of 1.022 MeV, which is added to (4.78). This very slow process controls the lifetime of stars. This reaction is viewed as beta decay of a zero-energy unbound

---

[12] This approximation applies only to the case $|eZ_2\Delta\phi_1/kT| < 1$, and hence does not apply to the reaction at a short distance. Many attempts have been made to derive a general screening formulae [627–629]. Most of them deal with a strong plasma where electrons are degenerate. Some authors then try to apply the formula to the case of the Sun by using an interpolation formula that connects strong and weak plasmas. Such an interpolation, however, does not give a correct formula since the electron degeneracy itself is weak, but only the potential becomes large in the vicinity of a nucleus. Gruzinov and Bahcall [629] show that the departure from the Debye–Hückel approximation is not large in the Sun. There was also confusion as to whether the screening factor in the exponent should be multiplied by 3/2 [630]. This is due to a misconception concerning the nature of Coulomb interactions in the plasma [631].

diproton (^{2}He) in the $^1S_0$ state to $d + e^+ + \nu_e$ where the deuteron is in the $^3S_1$ state. Hence, the decay rate is given by the GT transition, and according to (3.49):

$$\Gamma = \frac{G_V^2}{2\pi^3} m_e^5 f(w_0) 3g_A^2 | \int \psi_{pp}^* \psi_d d^3x |^2 , \qquad (4.79)$$

where ψ_d is the wave function for the ground state of the deuteron and ψ_{pp} is the wave function of two protons normalised per unit density at infinity ($\sim e^{ikx}$), with which the scattering rate is correctly accounted for [633,634]. Considering the prefactor of the wave functions, the integral is often represented as $\int \psi_{pp}^* \psi_d d^3x = \gamma^{-3/2}(8\pi C)^{1/2}\Lambda$, where $\gamma = \sqrt{M_N \Delta_d} \simeq (4.31 \text{ fm})^{-1}$ ($\Delta_d = 2.22 \text{ MeV}$ is the binding energy of the deuteron) is the size of the deuteron, $C = 2\pi\eta/(e^{2\pi\eta} - 1)$ is the Coulomb barrier factor which comes from the asymptotic behaviour of the Coulomb wave function $\phi \simeq C^{1/2}[G_0(kr) + \cot\delta F_0(kr)]$ of two protons with F and G nonsingular and singular wave functions. The normalised end point energy $w_0 = (2m_p - m_d - m_e)/m_e = (2m_H - m_{2H} - 2m_e)/m_e$ and hence $f(w_0) = 0.144$.

Noting $\sigma = \Gamma/v_{\text{rel}}$ and using (4.63), we obtain

$$S(0) = \frac{6}{\pi} G_V^2 m_e^5 m_p \alpha \frac{\Lambda^2}{\gamma^3} g_A^2 f(w_0) . \qquad (4.80)$$

Salpeter [634] (see also [635]) gave $\Lambda^2 = 6.82(1\pm0.05)$, which differs little from the value obtained from a simple effective-range description of pp scattering. This calculation has been updated in [636,637], with the modern result $\Lambda^2 = 6.92(1 + 0.001)$ which is well within Salpeter's error range. This gives the S factor $S(0) = 4.00\left(1^{+0.025}_{-0.015}\right) \times 10^{-22}$ keV·barn. Using (4.67) we obtain

$$r_{pp} = 7.06 \times 10^{-37} n_H^2 T_7^{-2/3} \exp(-15.69 T_7^{-1/3}) \text{ cm}^{-3}\text{s}^{-1}. \qquad (4.81)$$

The lifetime of protons in the core of the Sun r/n_H is then

$$t^{-1} = r/n_H \sim (1.2 \times 10^{10}\text{yr})^{-1} \qquad (4.82)$$

for $T = 1.5 \times 10^7$ K, $\rho = 150 \text{ g cm}^{-3}$ and $X = 0.5$. Bethe and Critchfield (1938) showed that this gives the correct lifetime of a star, and the correct energy production rate $\epsilon \approx 30 \text{ erg g}^{-1}$. This continuous energy production halts the star from collapse, which otherwise takes place with the Kelvin time scale, i.e. (thermal energy)/(luminosity)$\approx 10^7$ yr.

The energy of the Gamow peak is 6 keV. This reaction has the temperature dependence $r \propto T^n$ with $n = d\ln r/d\ln T \simeq 3.9$ at $T \approx 1.5 \times 10^7$ K, which is roughly equal to the increase in luminosity with central temperature. This process emits neutrinos, called pp neutrinos. The shape of the beta decay spectrum with the end point of 420 keV is somewhat distorted toward higher energy due to the Coulomb correction, and the mean energy is 265 keV.

This *pp* reaction is followed by

$$d + p \to {}^3\text{He} + \gamma + 5.494 \text{ MeV}, \qquad (4.83)$$

$$^3\text{He} + {}^3\text{He} \to {}^4\text{He} + p + p + 12.860 \text{ MeV}. \qquad (4.84)$$
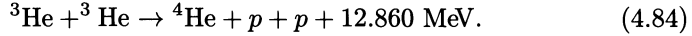
These two reactions are very fast, and complete the cycle $4p + 2e^- \to {}^4\text{He} + 26.731$ MeV. This is called the *pp*-I chain. Among the liberated $\Delta_\alpha = 26.73$ MeV, $0.265 \times 2 = 0.53$ MeV (2%) is lost by neutrinos. If this cycle dominates the nuclear reactions in the Sun, we expect the neutrino flux on Earth,

$$\phi_\nu = \frac{2L_\odot}{\Delta_\alpha - 2\langle E_\nu \rangle} \frac{1}{4\pi d^2} \qquad (4.85)$$

$$= \frac{3.84 \times 10^{33} \text{ erg s}^{-1}}{(26.73 - 0.53) \text{ MeV}} \frac{2}{4\pi (1.50 \times 10^{13} \text{ cm})^2} = 6.5 \times 10^{10} \text{ cm}^{-1}\text{s}^{-1}, \qquad (4.86)$$

which differs from accurate calculations by only 10%.

Reaction (4.78) is supplemented by

$$p + e^- + p \to d + \nu + 1.442 \text{ MeV} \qquad (4.87)$$
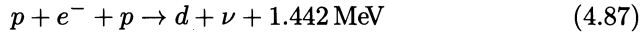
in a high-density environment. For the Sun the fraction of this *pep* process is 0.4%. The neutrino flux is monoenergetic at 1.442 MeV.

There is a side chain, called the *pp*-II chain. ^3He reacts not only with ^3He but also with preexisting or produced ^4He at a somewhat suppressed rate:

$$^3\text{He} + {}^4\text{He} \to {}^7\text{Be} + \gamma + 1.586 \text{ MeV}. \qquad (4.88)$$
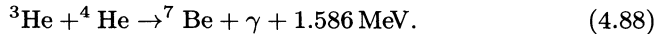
The branching fraction of this reaction is 15%. This is followed by electron capture

$$^7\text{Be} + e^- \to {}^7\text{Li} + \nu_e + 0.862 \text{ MeV}, \qquad (4.89)$$

and terminated with

$$^7\text{Li} + p \to {}^4\text{He} + {}^4\text{He} + 17.347 \text{ MeV}. \qquad (4.90)$$
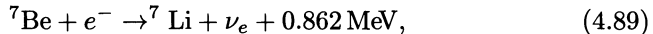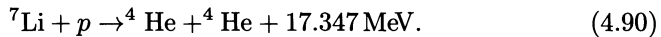
Electron capture of $^7\text{Be}(3/2^-, \text{gs})(e^-, \nu)^7\text{Li}$ produces two monoenergetic neutrino lines at 0.862 MeV (90%) in the transition to $(3/2^-, \text{gs})$ and 0.384 MeV (10%) to $(1/2^-, 0.478)$, which are referred to as ^7Be solar neutrinos. This side chain reduces the *pp* neutrino flux (4.86) estimated from the luminosity approximately by 7.5%, which brings to $6.0 \times 10^{10} \text{ cm}^{-2}\text{s}^{-1}$, and produces the ^7Be neutrino flux $5 \times 10^9 \text{ cm}^{-2}\text{s}^{-1}$. These crude estimates agree with the accurate calculation with a few % errors. This electron capture reaction rate is obtained by replacing $N|\Psi(0)|^2 q^2$ in (3.84) with the integration over the distribution function of a Fermi gas,

$$\frac{2}{(2\pi)^3} \int d^3 p_e \frac{(E_e + Q)^2}{e^{(E_e - \mu)/T} + 1} F(E_e, Z), \qquad (4.91)$$

where the chemical potential μ is determined by the electron density n_e. Approximating the Fermi distribution with the Boltzmann distribution, and from (3.55), $F(E_e, Z) \approx 2\pi Z \alpha m/p$ for $kT \ll m_e, Q$, the capture rate is calculated to be

$$\Gamma = G_V^2 \alpha Z n_e \left(\frac{2m_e}{\pi T} \right)^{1/2} q_\nu^2 |M_\beta|^2 \,, \tag{4.92}$$

where q_ν is the energy of emitted neutrinos. By comparing this with (3.85), we obtain $\Gamma = (2m_e/\pi T)^{1/2}\pi^2 n_e/m_e^3(\alpha Z)^2 \tau_{\text{atomic}}^{-1} = 5.3 \times 10^{-9} T_6^{-1/2} \mu_e^{-1} \,\text{s}^{-1}$, where $\tau_{\text{atomic}} = 4.60 \times 10^6\,\text{s}$ (Table 3.3) is the lifetime of atomic ^{7}Be [638]. From a more detailed calculation, which includes electron capture from the bound state [639], a reaction-rate compilation paper [640] quotes

$$\Gamma = 5.60 \times 10^{-9}(\rho/\mu_e)T_6^{-1/2}[1 + 0.004(T_6 - 16)]\,\text{s}^{-1} \,. \tag{4.93}$$

A similar calculation [640] yields for the $p + e^- + p$ reaction (4.87),

$$\Gamma_{pep} = 5.51 \times 10^{-5}\rho(1 + X)T_6^{-1/2}(1 + 0.02T_6)r_{pp}$$

where r_{pp} is given in (4.81).

The ^{7}Be produced in (4.88) is almost always destroyed by electron capture, but may react with a proton to produce ^{8}B (the pp-III chain) with a small probability (0.02%):

$$^7\text{Be} + p \rightarrow {}^8\text{B} + \gamma + 0.137\,\text{MeV}, \tag{4.94}$$
$$^8\text{B} \rightarrow {}^8\text{Be}^*(2^+, 2.94\,\text{MeV}) + e^+ + \nu_e + 15.04\,\text{MeV}, \tag{4.95}$$
$$^8\text{Be}^* \rightarrow {}^4\text{He} + {}^4\text{He} + 3.03\,\text{MeV}. \tag{4.96}$$
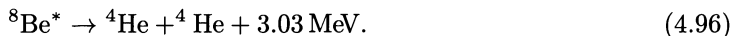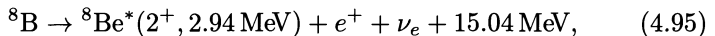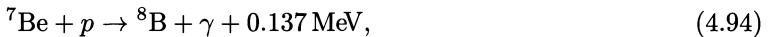
This pp-III chain is energetically unimportant and plays no role in the evolution of the Sun but is important from the viewpoint of neutrino physics, because the chain involves emission of a neutrino with a maximum energy of 15 MeV. The energy difference between ^{8}B and ^{8}Be is 17.979 MeV, but the spin-parity of ^{8}B is 2^+ and that of the ground state of ^{8}Be (2α unstable) is 0^+; so beta decay takes place dominantly to an excited 2^+ (2.94 MeV) level of ^{8}Be (97%),[13] and 2α decay immediately follows from the excited level. Thus the 2^+ level is broad; the beta decay spectrum is smeared by this width (see Fig. 4.13). The ^{8}B neutrino spectrum is estimated from the empirical beta ray spectrum measured near the end point [398]. In the pp-III chain, 28% of the nuclear energy is lost by neutrino emission.

When the temperature is high enough to sustain abundance equilibrium, the total energy liberated by the pp chain is expressed approximately by [617]

$$\varepsilon_{pp} = 2.38 \times 10^6 \psi \rho X^2 T_6^{-2/3} e^{-33.80/T_6^{1/3}}$$
$$\times \left(1 + 0.0123 T_6^{1/3} + 0.0109 T_6^{2/3} + 0.0009 T_6 \right) \,\text{erg}\,\text{s}^{-1}\text{g}^{-1} \,, \tag{4.97}$$

---

[13] 3% goes to a higher 2^+ level at 16.63 MeV.

${}^8\text{B}(\beta^+){}^8\text{Be}(2\alpha)$ decay
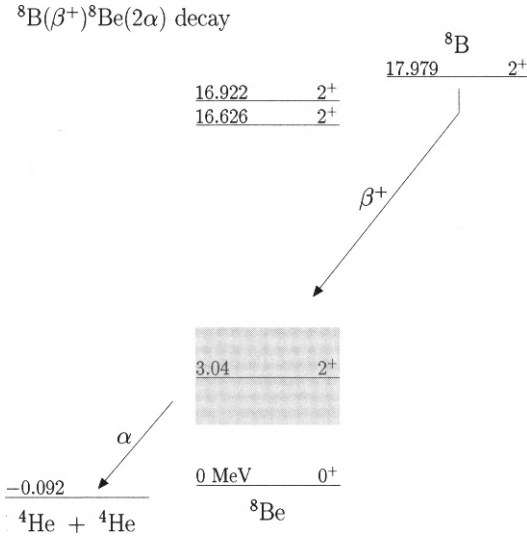
Fig. 4.13. Beta decay of ^{8}B.

where ψ is a slowly varying function of the temperature and chemical abundance; when the pp-I chain dominates ($T \lesssim 1.3 \times 10^7$ K), $\psi \simeq 1$, and it increases to 2 for $T \approx 2 \times 10^7$ K, where pp-II dominates, and approaches 1.5 when pp-III dominates at $T > 3 \times 10^7$ K [641, 617]. For the Sun, $\psi \simeq 1.4$ for $X = 0.5$. For stars with a solar heavy element abundance, the energy generation from the CNO cycle dominates over that of the pp chains before pp-II dominates. pp-II and pp-III become important only for metal-poor, population II stars.

Another slow process that could be significant from the viewpoint of neutrino physics is the *hep* reaction:

$$ {}^3\text{He} + p \to {}^4\text{He} + e^+ + \nu_e + 18.77\,\text{MeV} . \tag{4.98} $$
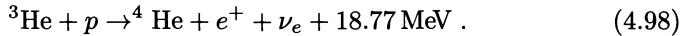
The branching to this process is estimated to be as small as 2×10^{-7}, but *hep* neutrinos ($\langle E_\nu \rangle = 9.625\,\text{MeV}$) could be detected by the present neutrino detector facilities. There is also a counterpart,

$$ {}^3\text{He} + e^- + p \to {}^4\text{He} + \nu_e + 19.795\,\text{MeV} , \tag{4.99} $$
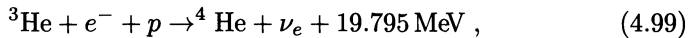
which emits quite a high-energy monoenergetic neutrino, but it is perhaps too slow to be detected.

von Weizsäcker [642] and Bethe [643] found that there is another process that could be more efficient for energy production in the presence of heavy elements. In this process ^{12}C acts as a catalyst to synthesise four protons into helium:

$$ {}^{12}\text{C}(p,\gamma){}^{13}\text{N}(,e^+\nu){}^{13}\text{C}(p,\gamma){}^{14}\text{N}(p,\gamma){}^{15}\text{O}(,e^+\nu){}^{15}\text{N}(p,\alpha){}^{12}\text{C} , \tag{4.100} $$

and there is a subchain

$$...^{15}\mathrm{N}(p,\gamma)^{16}\mathrm{O}(p,\gamma)^{17}\mathrm{F}(,e^+\nu)^{17}\mathrm{O}(p,\alpha)^{14}\mathrm{N}...\,,\qquad(4.101)$$
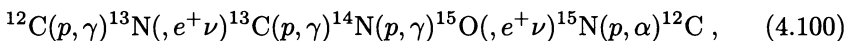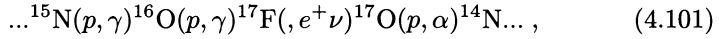
that replaces the last part of (4.100). This is called the CNO cycle. Medium-energy neutrinos are produced in positron beta decays,

$$^{13}\mathrm{N} \to\, ^{13}\mathrm{C} + e^+ + \nu \quad (E_{\nu,\mathrm{max}} = 1.199\,\mathrm{MeV})\,,\qquad(4.102)$$
$$^{15}\mathrm{O} \to\, ^{15}\mathrm{N} + e^+ + \nu \quad (E_{\nu,\mathrm{max}} = 1.732\,\mathrm{MeV})\,,\qquad(4.103)$$
$$^{17}\mathrm{F} \to\, ^{17}\mathrm{O} + e^+ + \nu \quad (E_{\nu,\mathrm{max}} = 1.740\,\mathrm{MeV})\,.\qquad(4.104)$$
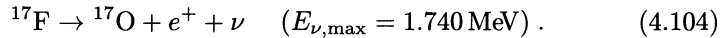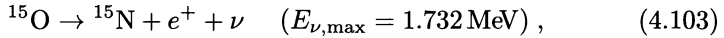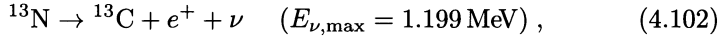
Energy generation is given approximately by

$$\varepsilon_{\mathrm{CNO}} = 8.67 \times 10^{27} \rho X Z_{\mathrm{CNO}} T_6^{-2/3} e^{-152.28/T_6^{1/3}}$$
$$\times \left(1 + 0.0027 T_6^{1/3} - 0.00778 T_6^{2/3} - 0.00015 T_6\right)\,\mathrm{erg\,s^{-1}g^{-1}}\,.$$
$$(4.105)$$

Figure 4.14 shows that energy production by the CNO cycle becomes larger than that of the pp chain above $T = 1.8 \times 10^7$ K for the solar composition with $Z = 0.017$ and $Z_{\mathrm{CNO}}/Z = 0.66$. In the Sun, the CNO cycle produces only 1.6% of the energy production, but from the neutrino physics viewpoint, it is more important than the energetics implies.

The energy spectrum of the neutrinos produced in the nuclear reactions in the Sun is summarised in Fig. 4.15 [210].

The energy of particles involved in astrophysical nuclear reactions is low, and nuclear reaction rates are extremely slow due to Coulomb barriers. For most reactions, the experimental reaction rates are obtained at some higher energies (nevertheless, such experiments are quite difficult),[14] and astrophysically relevant cross sections are estimated by extrapolations to zero energy. The effort invested during a half-century is summarized by Fowler and collaborators [645, 646]. The initiating pp reaction is far too slow to be measured in laboratories. The most recent compilations of reaction rates are given from the Seattle workshop in 1998 by Adelberger et al. [640][15] and by Angulo et al. [648] under the auspices of the European Commission's Human Capital and Mobility programme. In Table 4.3 we list Q values, Gamow peak energies, astrophysical S factors [$S(0)$ and the derivative $S'(0)$], and approximate reaction lifetimes in the Sun, mostly from Adelberger et al.

---

[14] In addition to very small cross sections, the target must be very thin to minimise the energy loss. So foils or gas jet targets are usually used. The estimate of target thickness is not too easy for the latter. Electron screening causes additional complications.

[15] In a recent paper, Dar and Shaviv [647] considered the possibility of unconventional reaction rates for the reactions of the pp chain. Adelberger et al. discussed how these unconventional values would arise. The arguments by both authors are instructive.
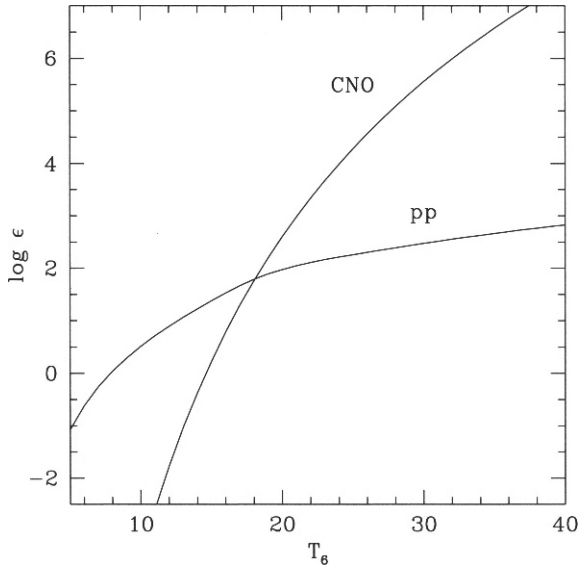
Fig. 4.14. Energy production rates of the *pp* chain and the CNO cycle as a function of temperature. Solar heavy-element abundance is assumed.
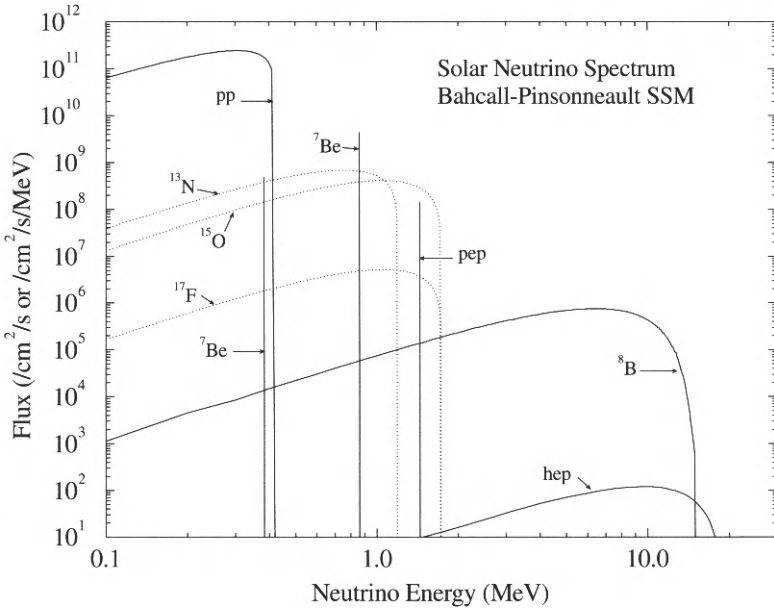
Fig. 4.15. Solar neutrino spectrum expected at Earth. Continuous spectra are represented in units of $\mathrm{cm}^{-2}\mathrm{s}^{-1}\,\mathrm{MeV}^{-1}$, and the monoenergetic spectra are in $\mathrm{cm}^{-2}\mathrm{s}^{-1}$. After [644].

Table 4.3. Nuclear reactions in the pp chain.

process	Q (MeV)	Gamow peak (keV)	$S(0)$ keV·barn	$\partial S/\partial E\vert_{E=0}$ barn	lifetime (yr)
S_{11} ^{1}H$(p,e^+\nu)^2$H	1.442	6.0	$4.00\left(1^{+0.025}_{-0.015}\right)\times 10^{-22a}$	4.52×10^{-24b}	10^{10}
S_{12} ^{2}H$(p,\gamma)^3$He	5.494	6.6	2.5×10^{-4b}	7.9×10^{-6b}	10^{-8}
S_{33} ^{3}He$(^3$He$,2p)^4$He	12.860	22	$(5.40\pm 0.05)\times 10^{3a}$	-4.1 ± 0.5^a	10^5
S_{34} ^{3}He$(\alpha,\gamma)^7$Be	1.586	23	0.53 ± 0.05^a	-0.00030^a	10^6
S'_{17} ^{7}Li$(p,\alpha)^4$He	17.347	15	$52(1\pm 0.5)^b$	0	10^{-5}
S_{17} ^{7}Be$(p,\gamma)^8$B	0.137	18	$19^{+4\times 10^{-2}}_{-2}{}^a$		10^2
S_{14} ^{3}He$(p,e^+\nu)^4$He	19.795	11.1	2.3×10^{-20a}		10^{12}

The energy of the Gamow peak is for $T_7 = 1.5$.

^{a} Taken from Adelberger et al. [640].

^{b} Taken from Bahcall [210].

A recent experiment to measure the ^{3}He$(^3$He$,2p)^4$He reaction rate already reached the energy of the Gamow peak, $E_0 \approx 22$ keV [649]. There seem to be no significant discrepancies among experiments for this reaction.[16] For the ^{3}He$(\alpha,\gamma)^7$Be rate, the energy dependence is smooth down to $E \simeq 100$ keV. Estimates of the low energy cross section assume that this smooth behaviour persists, as expected in direct capture with E1 transition from the S and D waves [651].[17] There is a discrepancy in normalisation by 30% (peak–valley) among experiments. A 15% discrepancy exists between the two experimental methods.[18] The mean value depends on how the data are weighted (see [640] vs. [647]): Adelberger et al. give 5.4 ± 0.4 MeV·barn, whereas Angulo et al. give 5.18 MeV·barn.

There is a well-known discrepancy (about 33%) among the existing experiments for ^{7}Be$(p,\gamma)^8$B. The data of Kavanagh et al. [652] and Parker [653] agree with each other and give the reaction rate $S(0) \simeq 24.5 \pm 2$ eV·barn, systematically higher than those of Filippone et al. [654] and Vaughn et al. [655] ($S(0) \simeq 18.5 \pm 2$ eV·barn). Adelberger et al. [640] adopted only the Filippone et al. data, excluding the other three:[19] $S(0) = 19^{+4}_{-2}$ eV·barn.

---

[16] For attempts of microscopic calculations see [650].

[17] The direct capture is in the sense that the reaction does not follow from the formation of a compound state.

[18] The detections of γ yield $S(0) = 0.507 \pm 0.016$ (mean) and those of ^{7}Be activity give $S(0) = 0.572 \pm 0.026$ (mean). Adelberger et al. adopted a mean of the two.

[19] Adelberger et al. set the criterion that they "consider only those experiments that were described in sufficient detail that allow assessment of the reliability of the error assignments." This criterion was not met by the three experiments cited here, and they are excluded from the average. They also excluded the data obtained by Coulomb dissociation for the reason that "the validity of the technique is yet to be demonstrated."

Angulo et al. give 21 ± 2 eV·barn. Two recent experiments of [656,657] favour the lower value, whereas another experiment [658] presents a value somewhat higher ($S(0) \simeq 20.3$ eV·barn). There are also several experiments using Coulomb dissociation of ^{8}B. The results favour the lower value [659,660]. The assessment by Adelberger et al. is supported by the recent experiments, and the discrepancy seems to be resolved. To obtain an astrophysically relevant S factor, however, we still need to extrapolate from 100 keV to 18 keV, assuming smooth behaviour towards low energies, which is anticipated in a direct-capture process (E1 transition from the S and D waves of p^7Be) [661].

The $^3\mathrm{He}(p, e^+\nu)^4$He rate is the most uncertain. This value is entirely theoretical, and it has large model-dependent uncertainties arising from significant cancellation among the matrix elements involved, unlike the pp reaction. Adelberger et al. adopted the result of Schiavilla et al. [662], but the latter authors' more recent calculation gives a value larger by a factor of 4 [663].

4.4.5 Accurate Modelling of the Sun

The treatment we have shown of stars is very crude. More accurate treatment can be done only by numerically integrating the set of equations consistently including the energy equation and the radiative and/or convective transport. We also need to formulate the surface boundary conditions more accurately. In our rough treatment we take $P = 0$ and $\rho = 0$ as the surface (the zero boundary condition). Physical boundary conditions take the surface ($r = R$) as a photosphere at an optical depth of 2/3, from which the bulk of the radiation is emitted:

$$\tau = \int_R^\infty \kappa \rho dr = 2/3 \ . \qquad (4.106)$$

The temperature of the surface is given by $T_R = T_{\mathrm{eff}}$ where the effective temperature is defined by

$$L = 4\pi R^2 \sigma_{\mathrm{SB}} T_{\mathrm{eff}}^4 \ , \qquad (4.107)$$

with $\sigma_{\mathrm{SB}} = \pi^4/15$ the Stefan–Boltzmann constant, which is 5.67×10^{-5} erg cm^{-2}s^{-1}K^{-4}. Using (4.23), the integral of (4.106) is written as

$$P(R) = \frac{GM}{R^2} \frac{2}{3} \frac{1}{\langle \kappa \rangle} \ , \qquad (4.108)$$

where $\langle \kappa \rangle$ is the mass weighted mean over the stellar atmosphere for $r > R$. The most commonly used integration scheme for the stellar equations is the relaxation method developed by Heyney et al. [664] (it is also explained in [617]). This method is particularly appropriate when there are two sets of boundary conditions (at the centre and the surface). Solution starts with an approximate answer and is gradually made accurate by iteration.
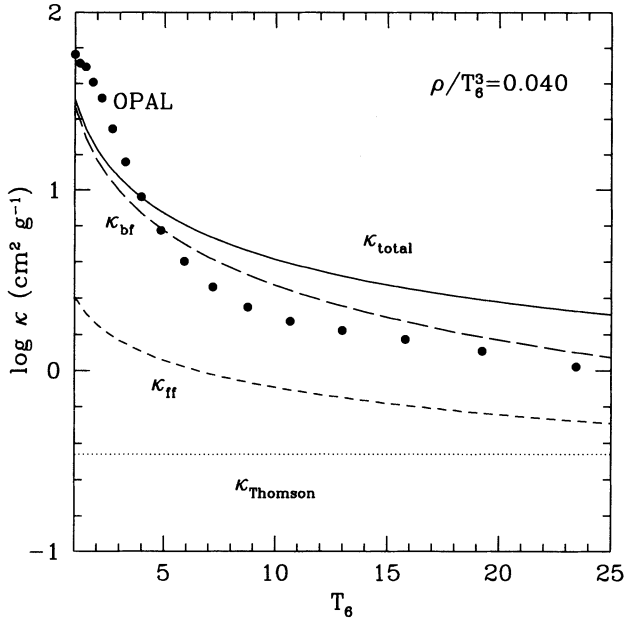
Fig. 4.16. Representative examples of opacity from the OPAL library. We take $X = 0.73$, $Z = 0.0195$, and $\rho/T_6^3 = 0.040$. The curves show the Kramers opacities discussed in Sect. 4.4.1 for the same parameter set and opacity from Thomson scattering. We assume $g_{ff} = 1$ and $g_{bf}/t = 1$.

For an accurate treatment the knowledge of opacity is important. The most commonly used in the past was the Los Alamos Astrophysical Library [665], but it was superseded by the opacity library prepared by the Lawrence Livermore Laboratory group (OPAL library) [666] (see Fig. 4.16 for a representative sample). The OPAL opacity has solved a number of detailed problems in stellar physics, indicating a clear advantage over the old one. The heavy element abundance and composition directly affect opacity. The solar value is taken to be the standard of the heavy element abundance. The estimate of solar abundance is compiled in [667,668]. A recent spectroscopic estimate of heavy element abundance is mostly consistent with that from meteorites (CI 1 chondrites) [668] except for a few elements.[20] The most conspicuous disagreement is seen for ^{7}Li, for which the photospheric value is $1/160$ the meteoritic value. The total heavy element abundance

---

[20] CI 1 chondrites (carbonaceous chondrites of the Ivuna type and petrological type 1) undergo aqueous alteration, but are considered to represent best the primordial composition of the Sun. While C3 chondrites undergo metamorphism least, they show volatile depletions. The classification of meteorites is after [669].

is $Z/X = 0.0230$ which compares to 0.0235 from helioseismology [670].[21]
The equation of state takes account for the effect of mild electron degen-
eracy, screening, and exchange effects, and ionisation equilibrium at lower
temperature [674]. The calculation for the Sun starts with a homogeneous
composition at $t = 0$, and follows the evolution for the age of the Sun[22]
$t_\odot = 4.57(1 \pm 0.004)\,\mathrm{Gyr}$. The luminosity of the Sun is in principle an output
of the calculation, but for the purpose of accurate modelling of the Sun
the present-day luminosity $L_\odot = 3.842(1 \pm 0.004)\,\mathrm{erg\,s^{-1}}$ [676] is used as
a constraint on the model.

   In most stellar evolution calculations the heavy element abundance in the
stellar interior has usually been assumed to be the same as that observed
at the photosphere. In modern calculations for the Sun, however, the effect
of helium and heavy element diffusion is taken into account [677–681]. With
diffusion the initial value $[Z/X]_{\mathrm{init}} = 0.0266$ is 15% higher than the surface
value observed today (0.0230). This also makes Z_{core} today 5% larger than
Z_{init} [644]. The importance of diffusion effects for accurate modelling of the
Sun is indicated by helioseismology, as we mention below.

   Bahcall and collaborators have pursued the accuracy of the solar model
for 40 years [209,682]. It is remarkable that the predicted solar neutrino flux
(also the capture rate with ^{37}Cl) changes little from Bahcall, Bahcall and
Shaviv's calculation in 1968 [683] to the most updated one in 2000 [644]
in spite of many improvements in the stellar code, nuclear reaction rates,
treatments of opacity, and others. Their state-of-the-art model BP2000 [644]
is the most elaborate model of the Sun within the standard assumptions
for stars [such models are referred to as the standard solar model (SSM)].
There are also several other groups who have attempted accurate modelling
of the Sun. Those in the last decade include [678, 684–690]. Bahcall and
Pinsonneault [691], who compared a number of available models, concluded
that different results arise mostly from different input parameters and that
all calculations give the consistent results at a 2% level for solar neutrino
fluxes, if input physical parameters are standardised.

Helioseismology.   An impressive verification of the solar model is given by
helioseismology, which has undergone significant progress in the last decade.
It has been known that the solar surface oscillates at an approximate period

---

[21] The iron abundance is often taken as a measure of heavy element abundance.
The modern estimates for iron abundance in the solar photosphere, however,
are in dispute at the level of 40−50%; the values vary from $\log N(\mathrm{Fe})/N(\mathrm{H}) =$
7.48 ± 0.05 [671] to 7.64 ± 0.03 [672], whereas Grevesse and Sauval [668] took it as
7.50 ± 0.05 from meteoritic abundance. See [673] for a discussion. BP2000 [644]
assigned a 6% error to Z/X.

[22] The most accurate estimate is obtained from ^{207}Pb-^{206}Pb dating (using ^{204}Pb
as a normalisation) for chondrites, especially for calcium-aluminium inclusions
(refractory inclusions) which are supposed to have condensed at the highest
temperature. See Wasserburg in [675].

of 5 minutes.[23] This is identified as the superposition of the characteristic oscillations of the Sun with pressure for the restoring force (p-mode oscillation). The characteristic frequency is determined by the time required for sound to travel from the centre of the Sun to the surface:

$$\nu_0 = \left[2 \int_0^{R_\odot} \frac{dr}{c_s} \right]^{-1} \tag{4.109}$$

with c_s the sound velocity $c_s = \sqrt{\gamma_{\text{ad}} P / \rho} \propto \sqrt{T/\mu}$ (adiabatic index $\gamma_{\text{ad}} = d \ln P / d \ln \rho|_{\text{adiabatic}}$). Namely, helioseismological frequencies are dominantly controlled by the combination of temperature and mean molecular weight. With the harmonic expansion, the frequency of p-mode oscillation for $n \gg \ell$ is given by [700],

$$\nu_{n\ell} \simeq \nu_0 \left[n + \frac{1}{2}\ell + u_{n\ell} \right] , \tag{4.110}$$

where $u_{n\ell}$ is a slowly varying function of n and ℓ. The difference in eigenfrequencies is

$$\Delta \nu_{n\ell} = \nu_{n\ell} - \nu_{n-1\,\ell} \simeq \nu_0 . \tag{4.111}$$

This quantity is largely controlled by the solar surface where c_s is small (NB: $c_s \approx 500\,\text{km}\,\text{s}^{-1}$ in the centre of the Sun, decreasing to $120\,\text{km}\,\text{s}^{-1}$ at $r = 0.9 R_\odot$). There is another difference, called the small-spacing difference,

$$\delta \nu_{n\ell} = \nu_{n\ell} - \nu_{n-1\,\ell+2} \tag{4.112}$$

$$\simeq -\frac{(4\ell + 6)}{4\pi^2} \frac{\nu_0}{\nu_{n\ell}} \int_0^{R_\odot} \frac{dc_s}{dr} \frac{dr}{r}, \tag{4.113}$$

which is sensitive to physical conditions in the stellar core [690, 700]. Both $\Delta \nu_{n\ell}$ and $\delta \nu_{n\ell}$ decrease with the age of the sun due mainly to the increase of the helium abundance in the stellar core. These quantities, for which

---

[23] In 1962 Leighton, Noyes and Simon [692] discovered that the solar surface is covered with vertically oscillating element everywhere with the period of approximately 5 minutes. This oscillation was identified by Ulrich (1970) [693] with standing acoustic waves (p-mode) trapped in a layer below the photosphere [694]. In 1975 a high resolution observation resolved the power of the 5 minutes oscillation into several discrete ridges in the wavenumber frequency plane (i.e., for a given wavenumber only certain periods will cause a standing wave in the solar cavity) [695], which agree with theoretical calculations of the p-mode oscillation [693, 696]. Helioseismology became an importnat probe for the deep interior of the sun particularly after the observation of global oscillations (i.e., low ℓ modes) and their identification as acoustic modes [697, 698]. For reviews of helioseismology see [699].

uncertainties associated with modelling of outer layers are substantially cancelled, can be used to test solar models, and give a powerful diagnostic as great accuracy has been achieved for $\nu_{n\ell}$ in modern seismological observations [701]. Elsworth et al. [702] used ν_{n0} and ν_{n1} to show that standard solar models fit helioseismology and remove the need to introduce nonstandard cores, which were devised to explain the solar neutrino problem. With the improvement of seismological data Guenther & Demarque [690], and Bahcall et al. [703] showed that standard solar models give a consistency among age, heavy element abundance and p-mode frequency difference only when helium and heavy element diffusions are taken into account. They also excluded classes of nonstandard solar models. The most elaborate test was made in BP2000, in which both frequency differences show a good agreement with observations for $t_\odot \simeq 4.57\,\mathrm{Gyr}$ (see Table 4.4), which at the same time shows that models with a nonstandard solar core are excluded [644].

Table 4.4. Differences of the p-mode helioseismological frequencies: a comparison of the model (BP2000) with the data. The numbers are in units of μHz. The bracket means averages of $n = 10-22$. For $\langle \Delta_{n\ell} \rangle$ an extra average of $\ell = 1-3$ is taken. After [644].

	$\langle \Delta_{n\ell} \rangle$	$\langle \delta_{n0} \rangle$	$\langle \delta_{n1} \rangle$
BiSON+LOWL	135.33	10.51	17.81
GOLF	135.12	10.46	17.75
GOLF2	134.84	10.22	17.18
GONG	134.86	10.04	18.24
MDI	134.95	10.14	17.64
BP2000 ($t = 0$)	170.57	19.65	31.34
BP2000 ($t = 4.034$ Gyr)	140.16	11.67	19.68
BP2000 ($t = 4.570$ Gyr)	*136.10*	*10.57*	*17.97*
BP2000 ($t = 5.017$ Gyr)	132.87	9.92	16.95

Another way to compare models with observations is to carry out inversions of frequencies to obtain the sound speed [704–706]. This is an application of the technique that has been used in geophysics and meteorological science [707]. This sound velocity [701,708] can be directly compared with the solar model predictions [644,703,709]. The advantage of this method is that one can clearly see the region where the two disagree. The BP 2000 model with helium and heavy element diffusions show an impressive agreement between the model and the data of no worse than 0.1% for most regions, and of 0.3% beneath the convective zone. The increase in discrepancies below the convective zone is common to standard solar models; see [710] for discussion.

Solar models. Accurate models of the Sun are used to predict solar neutrino fluxes. In Table 4.5 we present several representative results for solar

Table **4.5.** Prediction of solar neutrino fluxes on Earth.

Neutrino flux $(cm^{-2}s^{-1})$	$E_{\nu,\max}$ (MeV)	(1) BP2000 [644]	(2) BP95 [675]	(3) BU88 [711]	(4) Saclay 93 [684]	(5) Yale 97 [690]
pp (10^{10})	0.265	5.95 (1± 0.01)	5.91 (1± 0.01)	6.0 (1± 0.02)	6.03	5.95
pep (10^8)	1.442*	1.40 (1± 0.015)	1.40 ($1^{+0.01}_{-0.02}$)	1.4 (1± 0.05)	1.39	1.40
^{7}Be (10^9)	0.862+0.384*	4.77 (1± 0.10)	5.15 ($1^{+0.06}_{-0.07}$)	4.7 (1± 0.15)	4.34	4.94
^{8}B (10^6)	15	5.05 ($1^{+0.20}_{-0.16}$)	6.62 ($1^{+0.14}_{-0.17}$)	5.8 (1± 0.37)	4.43	5.96
^{13}N (10^8)	1.199	5.48 ($1^{+0.21}_{-0.17}$)	6.18 ($1^{+0.17}_{-0.20}$)	6.1 (1± 0.50)	3.83	5.64
^{15}O (10^8)	1.732	4.80 ($1^{+0.25}_{-0.19}$)	5.45 ($1^{+0.19}_{-0.22}$)	5.2 (1± 0.58)	3.18	4.89
^{17}F (10^6)		5.63 (1±0.25)	6.48 ($1^{+0.15}_{-0.19}$)	5.2 (1± 0.48)	—	5.92
hep (10^3)	18.77*	9.3	1.21	7.6	—	1.22
^{37}Cl (SNU)		7.6 $^{+1.3}_{-1.1}$	9.3 $^{+1.2}_{-1.4}$	7.9 ± 2.6	6.36	8.35
^{71}Ga (SNU)		128 $^{+9}_{-7}$	137 $^{+8}_{-7}$	132 $^{+20}_{-17}$	122.5	133

Table **4.6.** Prediction of physical properties at the centre of the Sun.

Authors	(1) BP2000	(2) BP95	(3) BU88	(4) Saclay 1993	(5) Sackman 1990
T_c (10^7K)	1.5696	1.583	1.56	1.54	1.543
ρ_c (g cm^{-3})	152.7	155.9	148	147	146.4
X_c	0.3397	0.3333	0.3411	—	0.3629

neutrino fluxes from recent calculations.[24] The first three are taken from Bahcall et al. (BP2000 [644], BP95 [675], BU88 [711]), and the last two are from other groups [684,690]. In this book, we adopt (1) as the reference solar model. In Table 4.6 we also present several physical parameters at the centre of the sun for the same models. Figure 4.17 shows the profile of temperature and density as a function of the radius from BP2000. The density profile shows good exponential behaviour except near the centre, where the increase towards the centre is slower than exponential. Table 4.7 gives logarithmic partial derivatives $\partial \phi_{\nu,i}/\partial X_j$ with respect to the input parameters [711] and to the central temperature [712]. The former is convenient for understanding how solar neutrino fluxes depend on uncertain nuclear reaction rates, and the latter is useful for obtaining physical insights concerning the changes in neutrino fluxes when some given conditions are modified. This table verifies

---

[24] Using revised nuclear reaction rates (^{3}He-^{3}He, pp) and a revised heavy-element abundance, Bahcall et al. (1968) [683] gave $\phi_\nu(^8$B$) = 4.7 \times 10^6 \, cm^{-2}s^{-1}$ and 7.5 ± 3 SNU for captures on ^{37}Cl. Since then these values have changed little.
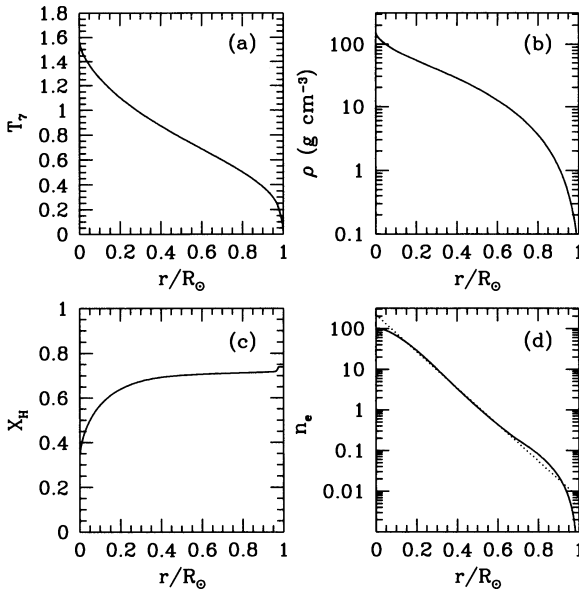
Fig. 4.17. Physical properties of the Sun in the standard solar model (BP2000): (a) temperature (in units of 10^7 K); (b) density; (c) hydrogen fraction; (d) electron density (in units of the Loschmidt number). All curves are plotted as functions of the fractional radius. In (d), an exponential profile $n_e = 250 \exp(-10.5r/R_\odot)$ is shown for comparison.

that the uncertainty in S_{17} directly propagates to that of the ^{8}B solar neutrino flux, and the change of S_{34} modifies both ^{8}B and ^{7}Be fluxes. The pp neutrino flux is proportional to $L^{0.7}$ rather than L. The most important source of uncertainty for the ^{8}B neutrino flux ($+20\%$, -17%) comes from S_{17}, but the uncertainties from S_{34} and Z/X (8% each) are also nonnegligble.

Table 4.7. The dependence of solar neutrino flux on nuclear reaction rates and other parameters.

Neutrino	S_{11}	S_{33}	S_{34}	S_{17}	$L_\odot$	Z/X	$t_\odot$	T_c
pp	$+0.14$	$+0.03$	-0.06	$-$	$+0.73$	-0.08	-0.07	-1.1 ± 0.1
pep	-0.17	$+0.05$	-0.09	$-$	$+0.87$	-0.17	$+0.00$	-2.4 ± 0.9
^{7}Be	-0.97	-0.43	$+0.86$	$-$	$+3.40$	$+0.58$	$+0.69$	10 ± 2
^{8}B	-2.59	-0.40	$+0.81$	1.0	$+6.76$	$+1.27$	$+1.28$	24 ± 5
^{13}N	-2.53	$+0.02$	-0.05	$-$	$+5.16$	$+1.86$	$+1.01$	24.4 ± 0.2
^{15}O	-2.93	$+0.02$	-0.05	$-$	$+5.94$	$+2.03$	$+1.27$	27.1 ± 0.1
^{17}F	-2.94	$+0.02$	-0.05	$-$	$+6.25$	$+2.09$	$+1.29$	27.8 ± 0.1
hep	-0.08	-0.45	-0.08	$-$	$+0.12$	-0.22	-0.11	

Table 4.8. Physical properties of main sequence stars at zero age for solar composition.

$M/M_\odot$	$\log(L/L_\odot)$	$\log T_{\text{eff}}$	$\log(R/R_\odot)$	$\log T_c(\text{K})$	$\log \rho_c(\text{g cm}^{-3})$
100	6.07	4.72	1.13	7.63	0.21
50	5.51	4.66	0.96	7.60	0.39
20	4.56	4.53	0.76	7.54	0.66
10	3.67	4.39	0.58	7.49	0.95
5	2.65	4.22	0.41	7.42	1.32
2	1.17	3.97	0.18	7.32	1.82
1	−0.15	3.73	−0.01	7.14	1.94
0.7	−0.85	3.65	−0.20	7.04	1.94
0.5	−1.43	3.58	−0.36	6.95	1.93
1 (BP2000)	−0.17	3.75	−0.061	—	—

Finally, let us note that the depletion of ^{7}Li in the solar photosphere, as mentioned above, is an important unsolved problem. The temperature in the convective layer is too low to destroy the lithium, and the diffusion is not efficient enough to transport the lithium. Such depletion is seen not only in the Sun, but also in other old main sequence stars with a solar mass. For a recent attempt to account for the depletion of ^{7}Li, see [688, 710].

There are many calculations for main sequence stars with varying stellar masses. The majority of them are concerned only with the physical properties of outer layers and the locus of the main sequence in the Hertzsprung–Russell diagram (in the $T_{\text{eff}} - L$ plane). The authors of these calculations often do not refer to any physical properties concerning stellar cores. Astronomers are not too much interested in the stellar core! In Table 4.8, as an example, we give the calculation by Ezer and Cameron [713] for the physical properties of main sequence stars at zero age (called zero age main sequence, ZAMS).[25] The last row shows the corresponding number of BP2000 [644] for comparison. Note that the Sun, as of today (4.6 Gyr after birth) is mildly, but significantly evolved from ZAMS: the luminosity is 40% greater, and the central temperature is 13% higher than the ZAMS values. The ^{8}B neutrino flux is strongly affected. Bahcall et al. [644] calculated that it has increased by a factor of 40 in 4.6 Gyr. The zero age main sequence stars form a well-defined track in the plane of luminosity versus effective temperature.

4.4.6 Solar Neutrino Problem

Whether the neutrino flux expected in Table 4.5 is actually observed is an important verification of our understanding of the Sun. Davis and collaborators

---

[25] For a newer calculation, see [714], which gives physical states for the range 0.8–10$M_\odot$. Since the difference between [713] and [714] is small, we quote the former calculation, which covers a wide mass range.

started an experiment detecting solar neutrinos in 1967 using a chlorine target, which he had already used to search for the interaction of (anti)neutrinos from nuclear reactors. In 1968 they [207] reported 3 SNU as an upper limit, in contrast to 7.5 SNU from a solar model [683]. They eventually observed a signal somewhat below this limit [715]. The observed neutrino capture rates were smaller than expected, and this situation has persisted for many years. There are many proposals to 'explain' this deficit in the solar neutrino capture rate [209, 210, 716]. They range from suspicions concerning the recollection rate of argon gas in the chlorine tank (one must collect some 10 atoms in a tank containing 615 tons of liquid) and those concerning the assumptions of the standard solar model, to speculations invoking nonstandard intrinsic particle physics properties of neutrinos. The instrumental concerns raised were refuted in early days [715]. Astrophysical explanations and particle physics explanations, however, could not be discriminated. A temperature at the centre of the Sun that is only slightly lower (5%) than that in the standard model can reduce the flux to the observed level. Many proposals were made to do this by introducing nonstandard assumptions, say, a rapidly rotating core, precipitation of iron from the gas to reduce the opacity, a mixed-up core, and others. They are all difficult to refute, if not very likely.[26] Therefore, people do not find a strong reason to ascribe the problem to an unknown neutrino property.[27] The atmosphere changed when Mikheyev and Smirnov (1985) discovered a mechanism [211] which may completely convert ν_e into ν_μ in matter even with a very small mixing angle. This is perfectly consistent with the idea that particle physicists had and seemed the most natural solution to the solar neutrino problem. (We discuss this in detail in Chap. 8). Particle physicists have then started to take the solar neutrino problem seriously.

New light was shed when the Kamiokande reported the observation of solar neutrinos (1989) [717] using a water Čerenkov detector, which was originally constructed to search for proton decays [718]. This experiment detects only a high energy tail of ^{8}B neutrinos. The report showed that the flux is smaller than the standard solar model prediction by a factor of 2. This looked roughly consistent with what Davis and collaborators found, but scrutiny showed that the result has a more profound implication. The suppression of the flux observed with the chlorine detector, which is also sensitive to lower energy neutrinos, is stronger than that observed at the Kamiokande. This means that lower energy neutrinos such as ^{7}Be and *pep* neutrinos are more strongly suppressed than the ^{8}B neutrino flux, which

---

[26] With the progress in helioseismology, one can now exclude most nonstandard solar models, as discussed in the preceding section.

[27] The only particle physics solution that looked reasonable without introducing something unorthodox was the neutrino oscillation hypothesis. To explain the solar neutrino problem, however, very large mixing was necessary, which looked unnatural in those days.

is most sensitive to the temperature of the Sun. Because all astrophysical solutions reduce the temperature of the Sun at the centre, and hereby reduce the ^{8}B neutrino flux while reducing the ^{7}Be neutrino flux only little, the observed suppression pattern is not consistent with astrophysical solutions. The solution to the solar neutrino problem should be ascribed to a particle physics property of the neutrino [719].

The third solar neutrino experiment uses gallium as a target; it is sensitive to the lowest energy solar neutrinos from the pp reaction. The result, reported in 1992 by the Gallex collaboration [232], showed that only 65% $(83 \pm 20 \, \text{SNU})$ of the expected capture rates were recorded.[28] This implied that pp neutrinos are suppressed only mildly. This result was soon confirmed by the SAGE collaboration [720]. The results of the gallium experiments are completely consistent with the idea of neutrino conversion in matter, and the three experiments altogether narrow the allowed range of the mass (mass squared difference) and mixing parameters of ν_e and ν_μ (ν_τ). When the bulk of the manuscript of this book was completed, the Sudbury Neutrino Observatory (SNO) group [235] reported the pure charged-current reaction rate for ^{8}B neutrinos using deuterium as a target. From a comparison with neutrino–electron scattering rates observed at Super-Kamiokande, which include neutral-current-induced reactions, the neutrino oscillation hypothesis was confirmed at a 3.3σ confidence level.[29] The results also support the correctness of the standard solar model.

Table 4.9 summarises the current experimental status. A detailed discussion of neutrino oscillation is given in Chap. 8.

Table 4.9. Summary of solar neutrino experiment.

Experiment	Target	Flux/capture rate	Ratio to SSM value[a]
Homestake [721]	$\nu_e + {}^{37}\text{Cl} \rightarrow e^- + {}^{37}\text{Ar}$	$2.56 \pm 0.16 \pm 0.16$ SNU	0.337 ± 0.030
Kamiokande [722]	$\nu e^- \rightarrow \nu e^-$	$2.80 \pm 0.19 \pm 0.33 \times 10^6 \text{ cm}^{-2}\text{s}^{-1}$	0.554 ± 0.075
Super-Kamiokande [723]	$\nu e^- \rightarrow \nu e^-$	$2.32 \pm 0.03 {}^{+0.08}_{-0.07} \times 10^6 \text{ cm}^{-2}\text{s}^{-1}$	0.459 ± 0.017
	$\nu e^- \rightarrow \nu e^-$ ($hep\,\nu$)	$< 40 \times 10^3 \text{ cm}^{-2}\text{s}^{-1}$	< 4.3
Gallex+GNO-I [724]	$\nu_e + {}^{71}\text{Ga} \rightarrow e^- + {}^{71}\text{Ge}$	$74.1 \pm 5.4 {}^{+4.0}_{-4.2}$ SNU	0.578 ± 0.053
SAGE [725]	$\nu_e + {}^{71}\text{Ga} \rightarrow e^- + {}^{71}\text{Ge}$	$70.8 {}^{+5.3}_{-5.2} {}^{+3.7}_{-3.2}$ SNU	0.589 ± 0.061
SNO [235]	$\nu_e + d \rightarrow e^- + p + p$	$1.75 \pm 0.07 {}^{+0.13}_{-0.12} \times 10^6 \text{ cm}^{-2}\text{s}^{-1}$	0.347 ± 0.029
	$\nu e^- \rightarrow \nu e^-$	$2.39 \pm 0.34 {}^{+0.16}_{-0.14} \times 10^6 \text{ cm}^{-2}\text{s}^{-1}$	0.473 ± 0.074

[a] BP(2000) is adopted for the SSM values. The errors for the ratio to SSM include both statistical and systematical in quadrature but do not include those of the SSM.

[28] SAGE was the first to report the gallium results [231]. The result was consistent with no detection ($20 \pm 35 \, \text{SNU}$). They gave results consistent with GALLEX from their second report.

[29] After the completion of the manuscript of this book we learned a new result from SNO, which conclusively demonstrated neutrino oscillation and the correctness of the standard solar model. See *Note add in Proof* (p. 517) in the end of this book.

4.4.7 Neutrino Energy Losses

Neutrinos are copiously produced in scattering processes in a high-temperature and/or a high-density environment. The neutrinos produced rarely interact with matter, unless the density of stars exceeds $\rho \approx 10^{12}\,\mathrm{g\,cm^{-3}}$, and carry the nuclear energy produced in the core away from the star. The energy drain from neutrino emission can be much faster than that from photon emission in stars with hot or dense cores. In such circumstances, the production of neutrinos changes the evolution of stars. The importance of neutrino emission via the bremsstrahlung process in the late stage of stellar evolution was pointed out by Gamow and Schönberg (1940) [239] and by Pontecorvo (1959) [240].

Figure 4.18 shows the four diagrams of neutrino production in stars: (i) photo-neutrino production [726], (ii) pair neutrino production [242, 727], (iii) plasmon decay [728], and (iv) bremsstrahlung of neutrino production [241, 729]. The importance of each process depends on the temperature and density of stars. Many calculations have been made with the four Fermi (CVC) theory and more recently with the Weinberg–Salam theory. An early summary within the Fermi theory was given by Beaudet, Petrosian, and Salpeter [730]. Calculations with the Weinberg–Salam theory were carried out in [731]. The most modern calculation was given by Itoh et al. [732].

For simplicity of expressions, we discuss here calculations for some limiting cases. In the nonrelativistic (NR) limit, photoproduction of the neutrino pair is calculated as

$$\sigma_{\text{photo}-\nu} = \frac{4\alpha}{35\pi^2} G_F^2 \frac{E_\gamma^4}{m_e^2} \xi_1 \,, \tag{4.114}$$

$$= 1.17 \times 10^{-48} \left(\frac{E_\gamma}{m_e}\right)^4 \xi_1 \,\mathrm{cm}^2 \,, \tag{4.115}$$
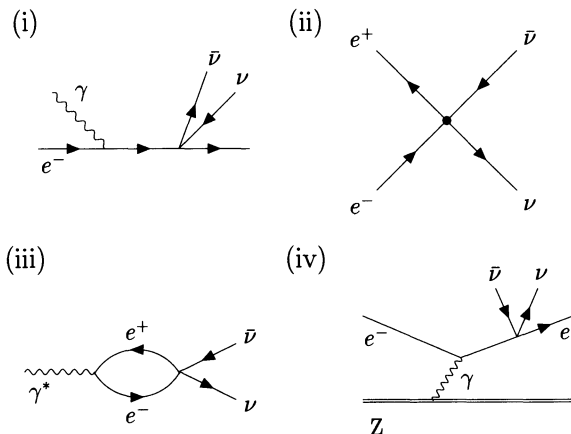
Fig. 4.18. Diagrams for neutrino production in stars.

where E_γ is the energy of the incident photon and

$$\xi_1 = \sum_{\nu_e, \nu_\mu, \nu_\tau} \frac{1}{6}(|c_V|^2 + 5|c_A|^2) = \frac{3}{4} - \frac{1}{3}\sin^2\theta_W + 2\sin^4\theta_W = 0.780 \quad (4.116)$$

is the factor for the ratio of the Weinberg–Salam theory to the V–A theory. The energy loss rate is given by

$$\varepsilon_\nu = \int E_{\nu+\bar{\nu}} \sigma v \mathcal{N}_\gamma \mathcal{N}_{e^-} d^3 p_{e^-} d^3 p_\gamma \quad (4.117)$$

where

$$\mathcal{N}_{e^\mp} = \frac{2}{(2\pi)^3} \frac{1}{e^{(E \mp \mu)/T} + 1} \quad (4.118)$$

and

$$\mathcal{N}_\gamma = \frac{2}{(2\pi)^3} e^{-E/T} \ . \quad (4.119)$$

Here, $\mathcal{N}_{e^\mp}$ is constrained by

$$n_+ - n_- = \int d^3 p_{e^\pm} (\mathcal{N}_{e^-} - \mathcal{N}_{e^+}) = n_e = N_L \frac{\rho}{\mu_e} \ , \quad (4.120)$$

and $\mathcal{N}_{e^+} = 0$ unless $T >$ a few $\times 10^9$ K ($N_L = 6.02 \times 10^{23}$ g^{-1} is the Loschmidt number).

For NR and nondegenerate material, we obtain

$$\varepsilon_\nu = \frac{576}{\pi^4} \frac{G_F^2 \alpha}{\mu_e} N_L \frac{T^8}{m_e^2} \xi_1 = 1.00 \frac{1}{\mu_e} T_8^8 \xi_1 \ \text{erg g}^{-1}\text{s}^{-1} \ . \quad (4.121)$$

This process dominates in a low-density and a low-temperature environment. It is clear that for temperature $T < 10^8$ K this is negligible compared to nuclear energy production (see Fig. 4.14). The process affects stellar evolution only for helium-burning stars or those in stationary heavy-element burning.

For temperature higher than 10^9 K, the electron becomes relativistic, and pair creation (ii) dominates neutrino emission. The $e^+ e^- \to \nu\bar{\nu}$ cross section at low energy is given by[30]

$$\sigma_{\text{pair}-\nu} = \frac{1}{\beta} \frac{1}{\pi} G_F^2 m_e^2 \xi_2 \ , \quad (4.122)$$

$$= 4.40 \times 10^{-45} \beta^{-1} \xi_2 \ \text{cm}^2 \ , \quad (4.123)$$

where β is the relative velocity of an electron and a positron in units of the velocity of light, and ξ is the ratio of the Weinberg–Salam theory value to

---

[30] The matrix element is given by (3.124) with an appropriate replacement of the variables and the statistical weight factor.

that of the V–A theory,

$$\xi_2 = \sum_{\nu_e, \nu_\mu, \nu_\tau} |c_V|^2 = \frac{3}{4} - 2\sin^2\theta_W + 12\sin^4\theta_W = 0.929. \qquad (4.124)$$

The energy loss rate is obtained by integrating over electron and positron distributions.

In the nondegenerate, NR limit

$$\varepsilon_\nu = 2m_e\sigma\beta\frac{n_+n_-}{\rho} = \frac{G_F^2 m_e^6}{\pi^4}\frac{T^3}{\rho}\xi_2 e^{-2m_e/T}$$

$$= \frac{5.04 \times 10^{15}}{\rho}T_8^3 e^{-\frac{118.6}{T_8}}\xi_2 \text{ erg g}^{-1}\text{s}^{-1}, \qquad (4.125)$$

where $n_+n_- = \left(\frac{1}{\pi^2}\int_0^\infty e^{-E/T}p^2 dp\right)^2$ for a nondegenerate Fermi gas is used. This process is very efficient if the temperature exceeds the electron–positron threshold. Pair neutrinos are the dominant cooling agent in type II super-novae.

In a high-density environment, dominant neutrino emission is due to plasmon decay. In a finite-density environment, the photon obeys the dispersion relation,

$$\omega = k^2 + \omega_p^2, \qquad (4.126)$$

with the plasma frequency

$$\omega_p^2 = \frac{4\pi\alpha}{\sqrt{m_e^2 + p_F^2}}n_e, \qquad (4.127)$$

where $p_F = (3\pi^2 n_e)^{1/3}$ is the electron Fermi momentum. Equation (4.127) is written as

$$\frac{\hbar\omega_p}{kT} = \frac{3.344}{\left[1 + 1.017(\rho_6/\mu_e)^{2/3}\right]^{1/4}}\frac{(\rho_6/\mu_e)^{1/2}}{T_8}. \qquad (4.128)$$

The photon behaves as a particle of mass ω_p and it decays into a neutrino–antineutrino pair via the e^+e^- virtual state. The energy loss due to plasmon decay is calculated as

$$\varepsilon_\nu = \frac{G_F^4}{\alpha\rho}\frac{\zeta(3)}{24\pi^4}\omega_p^6 T^3\xi_2$$

$$= \frac{7.22 \times 10^{21}}{\rho}\left(\frac{\omega_p}{m_e}\right)^9\left(\frac{\omega_p}{T}\right)^{-3}\xi_2 \text{ erg g}^{-1}\text{s}^{-1}, \quad \text{for} \quad \frac{\hbar\omega_p}{kT} \ll 1, \quad (4.129)$$

and

$$\varepsilon_\nu = \frac{G_F^2}{\alpha\rho}\frac{(2\pi)^{1/2}}{96\pi^4}\omega_p^{15/2}T^{3/2}\xi_2 e^{-\omega_p/T}$$

$$= \frac{3.77 \times 10^{21}}{\rho}\left(\frac{\omega_p}{m_e}\right)^9\left(\frac{\omega_p}{T}\right)^{-1.5}e^{-\frac{\omega_p}{T}}\xi_2 \text{ erg g}^{-1}\text{s}^{-1} \quad \text{for} \quad \frac{\hbar\omega_p}{kT} \gg 1, \qquad (4.130)$$

for the transverse mode (the contribution of the longitudinal mode is small). In an environment with an even higher density, bremsstrahlung becomes more important. The energy loss rate is given by

$$\varepsilon_\nu = 0.76\frac{Z^2}{A}T_8^6\xi_3 \text{ erg g}^{-1}\text{s}^{-1} \tag{4.131}$$

in the high-density limit, where

$$\xi_3 = \sum_{\nu_e,\nu_\mu,\nu_\tau} \frac{1}{2}(|c_V|^2 + |c_A|^2) = \frac{3}{4} - \sin^2\theta_W + 6\sin^4\theta_W = 0.84. \tag{4.132}$$

This bremsstrahlung is important in cooling of neutron stars from their crusts.

The formulae for general cases are given by numerical tables or analytic fitting formulae [732]. Figure 4.19 shows the importance of each process in a given (ρ, T) environment, taking a helium core as an example (after [732]). The neutrino luminosity is given by

$$L_\nu = \int dr 4\pi r^2 \varepsilon_\nu \tag{4.133}$$

if $\rho \lesssim 10^{11}$ g cm^{-3}. Neutrino energy loss is sensitive to temperature, but the relevant nuclear reactions are even more sensitive to temperature. So, neutrino cooling causes a slight increase in temperature which compensates
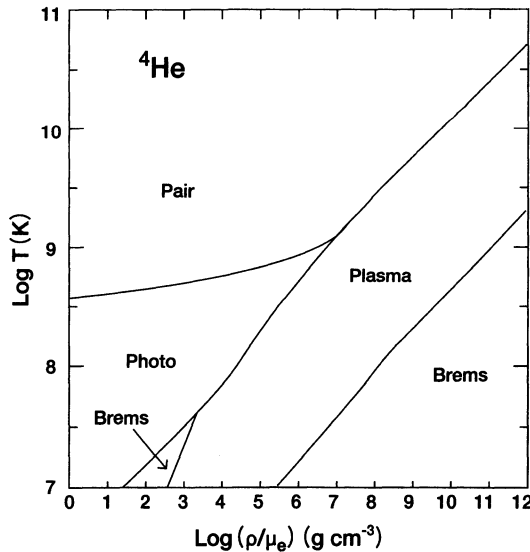
Fig. 4.19. Dominant process of neutrino energy losses for given T and ρ. A helium core is assumed. After Itoh et al. [732].

for the energy loss due to neutrino emission. This changes stellar dynamics very little but promotes the speed of evolution by an increased rate of nuclear fuel consumption for the amount of neutrino energy loss.

Gamow and Schönberg [239] considered a cycle of the process

$$(Z, A) + e^- \rightarrow (Z - 1, A) + \nu_e \qquad (4.134)$$

$$(Z - 1, A) \rightarrow (Z, A) + e^- + \nu_e \qquad (4.135)$$
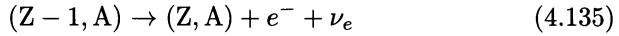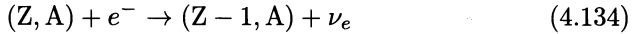
and named it the Urca process.[31] For this process to take place in an efficient way, however, a number of special conditions must be satisfied, and after all, this Urca process turns out to be inefficient in stars. There is, however, a related process which is considered dominant in neutron star cooling. In neutron stars all fermions are degenerate. The processes, $n \rightarrow p + e^- + \bar{\nu}_e$ and $e^- + p \rightarrow n + \nu_e$, are blocked by energy-momentum conservation in a degenerate Fermi gas because both Fermi momentum and the energy of protons and electrons are much smaller than those of neutrons. If there is a bystander, however, energy momentum conservation can be satisfied, and an Urca-like process takes place:

$$n + n \rightarrow n + p + e^- + \bar{\nu}_e , \qquad e^- + n + p \rightarrow n + n + \nu_e , \qquad (4.136)$$
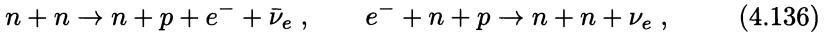
which is called a modified Urca process [733]. This is an important cooling mechanism for a hot neutron star.

Another important process similar to the modified Urca is neutrino pair bremsstrahlung, $N + N \rightarrow N + N + \nu + \bar{\nu}$ [734]. The importance of this process in stellar collapse, especially for low-energy ν_μ, ν_τ production, is emphasised in [735].

4.4.8 Evolution from the Main Sequence

When hydrogen is consumed in the centre of stars, a helium core forms; the absence of energy generation in the core causes a decrease in pressure to support the stellar mass, inducing a contraction of the core. Hydrogen is still burning outside the He core (H shell burning). The decrease in pressure at the boundary of the core causes the outer envelope to expand greatly to balance the equilibrium around the core surface. As a result, the temperature of the surface drops. This results in a huge jump in the density of stars across the core surface. This state is called a red giant. The red giant has a small, dense, and isothermal core and a large, low-density envelope.

This rapid evolution takes place when $\approx 12\%$ of hydrogen is consumed. The age of main sequence stars is then

$$t_{\rm MS} \sim (M/L) \Delta X \ \epsilon({\rm He}) \qquad (4.137)$$

$$\sim 1.2 \times 10^{10} \, {\rm yr} (M/M_\odot)^{-3.75} , \quad \text{for } M < 2M_\odot \text{ stars} , \quad (4.138)$$

---

[31] After the fate of gamblers' money in the playrooms of the Casino da Urca in Rio de Janeiro.

where the empirical $L \sim M^{4.75}$ law is used, $\Delta X = 12\%$, and $\epsilon(\text{He}) = \Delta_\alpha/M(\text{He}) = 0.0071c^2$, which is $6.4 \times 10^{18}\,\text{erg}\,\text{g}^{-1}$. For a higher mass star, $L \simeq M^3$, and hence $t_{\text{MS}} \sim M^{-2}$.

For example, for the fate of the Sun, a numerical calculation [736] shows that the luminosity doubles in 5.5 Gyr. The radius increases by a factor of 10 in 7.5 Gyr from now, and the radius at maximum expansion amounts to $200\,R_\odot$ (0.9 AU) within 100 Myr in the red giant phase. The sun shrinks to $\sim 10R_\odot$ after helium ignition and stays at this radius for another 100 Myr, but it expands again when helium is exhausted and the radius reaches $\sim 1000R_\odot$ (asymptotic giant phase).

The evolution of stars after the main sequence is qualitatively well understood, but substantial uncertainties remain in quantitative predictions. For reviews, see [737]. A typical calculation for the evolutionary track of the core is shown in Fig. 4.20, taken from Paczyński's work [738]. The model assumes 0.8, 1.5, 3, 5, 7, and $15M_\odot$. As core contraction continues, the core temperature T_c increases. When T_c reaches $\approx 10^8$ K, helium is ignited, and $3\alpha \rightarrow^{12}\text{C}$ takes place. The energy generation rate is given by [617]

$$\varepsilon_{3\alpha} = 5.09 \times 10^{11} \rho^2 Y^3 T_8^{-3} e^{-44.027/T_8} \ . \tag{4.139}$$

The physics of stars is different depending upon whether helium ignition takes place where the electron is degenerate or nondegenerate [see (4.33)], as indicated by the *dash-dotted curve* in Fig. 4.20. The former takes place for stars of $M < 2.5M_\odot$. In such a star, the pressure is sustained by electron degeneracy, and the increase in temperature promoted by He ignition does not induce a decrease in pressure. The absence of negative feedback leads to abrupt burning of helium, which is called *helium flash*. The critical helium core mass of the flash is $M_c = 0.46M_\odot$ with neutrino energy loss. Just before the helium flash, the density of the core is about $10^{5.5}\,\text{g}\,\text{cm}^{-3}$ and temperature is $10^{7.8}$ K which depend little on the initial stellar mass. The neutrino energy loss, which comes predominantly from plasmon decay, amounts to $\approx 5\,\text{erg}/\text{g}$ (this is a fairly large effect in the absence of nuclear energy generation in the core) and increases the critical mass by $0.03M_\odot$. A calculation shows that the luminosity of the tip of the red giant L_{tip} (the star with the maximum luminosity of the red giant branch) and that of a helium-burning star after the flash L_{He} both depend on the core mass M_c and hence on neutrino cooling. The difference $L_{\text{tip}} - L_{\text{He}}$ still depends on M_c, and the change of $0.03M_\odot$ increases it by 20% (0.2 magnitude).[32] The detection of this effect may be marginal, when one considers uncertainties in chemical abundance determinations and in model

---

[32] Sweigart and Gross [739] give absolute magnitudes of the tip of the giant branch and the horizontal branch (helium burning for metal-poor stars) as

$$M_{\text{tip}}(\text{mag}) = -3.54 + 0.9(Y - 0.25) - 0.23(\lg Z/Z_\odot + 1.3) - 11.3M_c/M_\odot \ ,$$

$$M_{\text{HR}}(\text{mag}) = +0.59 - 3.5(Y - 0.25) + 0.16(\lg Z/Z_\odot + 1.3) - 7.3M_c/M_\odot \ ,$$
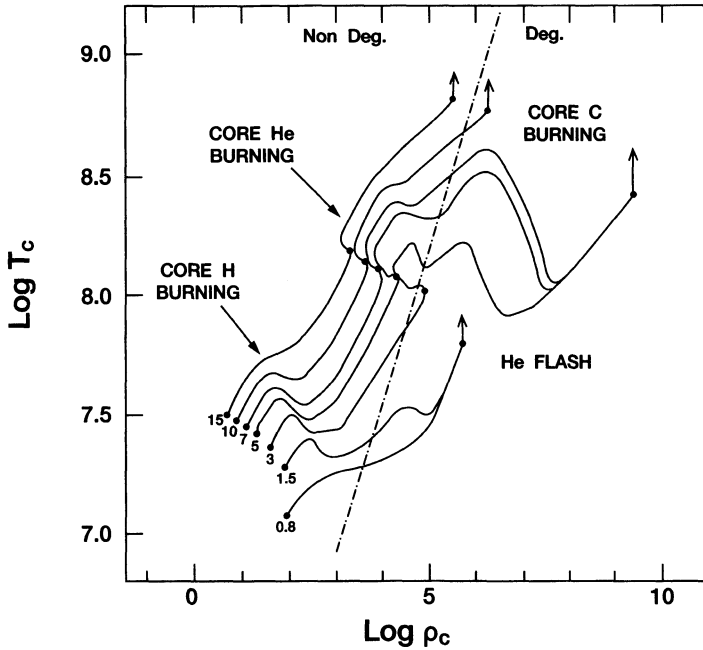
Fig. 4.20. Evolution of the core of 0.8, 1.5, 3, 5, 7, 10, and $15M_\odot$ mass stars. The upper terminating points are carbon ignition. The *dash-dotted line* separates the degenerate and the nondegenerate regions of the Fermi gas. After Paczyński [738].

calculations. (If the loss were three times more, say, the effect could be observed. Raffelt [740] used this argument to constrain the magnetic moment of neutrinos.)

The flash continues until the temperature is high enough to dissolve electron degeneracy. The liberated energy, however, is not large enough to be observed directly from the outside. After the flash, the star enters into a stable He-burning phase for about 10^8 years. The onset of helium burning changes the physical properties of the surface and moves the position rapidly in the Herzsprung–Russell (HR) diagram. These stars stay at nearly the same position until helium is exhausted about 2×10^8 year after the helium flash. These stars are observed as a blue horizontal branch (HB; including RR Lyr variables) if the heavy element abundance is low, or if not, as a red clump (a clump at an effective temperature of 4800 K) in the HR diagram. A conspicuous feature is that the positions in the HR diagram depend very little on the initial stellar mass (at least for $1-2.3M_\odot$) and the time after the flash. This gives an interesting standard candle for estimating distance of

___

where M on the left-hand side is the V band absolute magnitude, which is related to luminosity as $M - 4.83\text{mag} = 2.5\log(L_V/L_{V\odot})$. We expect $\approx 20\%$ error in the coefficients.

stars. In this phase, stars have double energy sources, 90−80% from H-shell burning, and 10−20% from the He core. A calculation [741] for red clump stars shows that the temperature of the core is about 1.1×10^8 K and the density is $3 \times 10^4 \,\mathrm{g\,cm^{-3}}$ for the star mass range $\approx 1.5-2M_\odot$ (core mass $\sim 0.5M_\odot$) and for a duration of 150 Myr. The neutrino energy loss is still small ($\approx 0.03\%$ of total luminosity), but if neutrinos had a magnetic moment just below the laboratory limit, this would affect the evolution considerably. The limit is derived typically from [742]

$$\varepsilon < 40 \,\mathrm{erg\,g^{-1}s^{-1}} , \quad \text{for } T = 1.1 \times 10^8 \,\mathrm{K} , \quad \rho = 10^{4.5} \,\mathrm{g} , \qquad (4.140)$$

where ε is the excess energy loss, and this value corresponds to the mean energy generation rate in the He core in the stationary burning phase (15−20% of $\approx 50L_\odot$). In the presence of such excess energy loss, the core temperature increases slightly to compensate for the energy loss, which shortens the lifetime of the He-burning phase by a factor of 2. Raffelt [743] claims that the limit can be derived even for $\epsilon < 10 \,\mathrm{erg\,g^{-1}s^{-1}}$. The conditions for limits from HB stars are similar.

If ignition takes place where electrons are not degenerate, as happens in a massive star of $M > 2.5M_\odot$, the increase in temperature causes an increase in pressure, leading to expansion that results in a drop in temperature; negative feedback stabilises helium burning. The temperature is then regulated, and stationary helium burning continues. The lifetime depends on the mass of stars, which determines the core temperature and hence the energy generation rate. In the He-burning phase carbon captures an alpha, forming oxygen, and then oxygen captures an alpha, forming ^{20}Ne. When neon forms, helium is nearly exhausted in the core.

When helium is exhausted in the core, helium-shell burning takes place, and the outer region expands again (asymptotic giant branch). During this time the helium core contracts, and the core temperature rises; carbon is ignited at $T \sim 10^9$ K. The rise in temperature of stars with $M < 3M_\odot$, however, is not high enough to ignite carbon, so they die into carbon (or carbon–oxygen) white dwarfs. For stars with $3M_\odot < M < 8M_\odot$, carbon ignition takes place in the degenerate region, which causes carbon flash. The energy liberated by carbon flash, is large enough to disrupt stars. It is, however, not clear whether this actually happens in isolated stars. In the red giant phase the star rapidly loses the bulk of its mass from the very low-density envelope, so that ignition is unlikely to happen. (Such ignition happens at least in binary stars where mass transfer takes a dominant role. This is considered to be a type Ia supernova [744].)

For stars with mass $M > 8M_\odot$, carbon ignition takes place in a nondegenerate region, synthesising ^{20}Ne and ^{23}Na. These products turn mostly into ^{28}Si by capturing p, n, and α. Oxygen burning produces ^{28}Si, ^{31}P, ^{31}S, and ^{32}S. The burning is stable, and the star becomes a red supergiant. A hydrogen envelope is retained.

When carbon burning starts, neutrino energy loss becomes very important. A calculation for a $15M_\odot$ star [745] shows that at carbon ignition the energy loss due to neutrinos is even with that from photons, and the carbon-burning phase lasts for 6.3×10^3 yr. At neon ignition, neutrino luminosity is far larger, $L_\nu/L_\gamma = 1.8 \times 10^3$, and the duration is 7 yr. At Si ignition $L_\nu/L_\gamma = 9.2 \times 10^5$ with a duration of 6 days. Such stable burning results in an onion-skin shell structure with these layers from the outside: H+He; ^{4}He; ^{12}C+^{16}O; ^{16}O+^{20}Ne+^{24}Mg; ^{16}O+^{24}Mg+^{28}Si; ^{32}S+^{28}Si. This is a progenitor of core collapse, which is identified as a type II supernova. This late stages of stellar evolution and supernovae are the origin of heavy element abundance, as discussed in detail by Burbidge, Burbidge, Fowler, and Hoyle [746] and by Cameron [747].

Late stages of massive stars are dominated by neutrino energy loss. It may appear that such stars are suitable for testing neutrino cooling. In practice, however, calculations of evolved massive stars have many uncertainties due, for example, to mixing of elements by convection or instabilities across layers, chemical composition of the core, and mass loss by stellar winds; definitive predictions are difficult.[33]

The importance of neutrinos in the late stages of stellar evolution is clear. Nevertheless, it is not obvious how to observe their effect. One can construct a model where the neutrino energy loss is consistent with observations, but in many cases it is also possible to make models that fit observations equally well without neutrinos within the uncertainties of astrophysics in evolved stars. It is necessary from the viewpoint of neutrino physics to look for the place where neutrino emission causes an observable effect beyond the uncertainties of astrophysics.[34]

4.4.9 White Dwarfs

The white dwarf supports itself against gravity by the pressure of degenerate electrons [749]. The equation of state of the degenerate Fermi gas obeys the

---

[33] A historical example is tests for neutrino energy loss for $h + \chi$ Persei, whose stars have masses of about $15M_\odot$. Hayashi et al. [614] compared the number of red population (which is supposed to correspond to the C-burning stage) and that of the blue population (He-burning stage) and concluded from the presence of red populations that the neutrino energy loss rate, which makes the evolution of carbon burning very short, must be $<1/100$ of the Fermi theory prediction (this was before Reines et al. observed neutrino electron scattering using a reactor). The problem here whether helium burning takes place while stars are blue or red has a significant uncertainty. Stothers reconsidered this problem and concluded that the statistics of such heavy stars are consistent with the energy loss predicted by the Fermi theory [748]. In fact, he obtained a limit that the cooling rate must be larger than 0.01 times the Fermi theory prediction. In view of uncertainties in stellar calculation, this is not a firm limit either.

[34] We refer the reader to a monograph by Raffelt on this subject [743].

$\Gamma = 5/3$ ($n = 3/2$) polytrope in the NR limit and the $\Gamma = 4/3$ ($n = 3$) polytrope in the ER limit, as seen in (4.31) and (4.34). For small mass white dwarfs, $\rho \lesssim 10^6 \, \mathrm{g \, cm^{-3}}$, and the NR equation of state applies. Using (4.31) and the solutions given in Table 4.2 we obtain the radius and mass of a white dwarf:

$$R = 1.122 \times 10^4 (\rho_c/10^6 \, \mathrm{g \, cm^{-3}})^{-1/6} (\mu_e/2)^{-5/6} \, \mathrm{km} \, ,$$

$$M = 0.4964 (\rho_c/10^6 \, \mathrm{g \, cm^{-3}})^{-1/2} (\mu_e/2)^{-5/2} M_\odot \tag{4.141}$$

$$= 0.7011 (R/10^4 \, \mathrm{km})^{-3} (\mu_e/2)^{-5} M_\odot \, . \tag{4.142}$$

For a large mass white dwarf, using the ER equation of state (4.34), we obtain

$$R = 3.447 \times 10^4 \rho_{c,6}^{-1/6} (\mu_e/2)^{-2/3} \, \mathrm{km} \, ,$$

$$M = 1.44 (\mu_e/2)^{-2} M_\odot \tag{4.143}$$

$$\equiv M_{\mathrm{Ch}} \, . \tag{4.144}$$

In the ER limit ($\rho \to \infty$), $M \to M_{\mathrm{Ch}}$. The mass of a white dwarf cannot exceed M_{Ch} which is the Chandrasekhar mass [750]. A more accurate treatment is given by Chandrasekhar [612].

The luminosity of white dwarfs is estimated as follows [751,613]. The radiative transport near the surface is given by (4.53) with equation of state (4.27), so that by deleting ρ,

$$P dP = \left(\frac{4ac}{3} \frac{4\pi GM}{\kappa_0 L} \frac{k}{\mu m_N} \right) T^{7.5} dT \, , \tag{4.145}$$

where we assume the Kramers opacity $\kappa = \kappa_0 \rho T^{-3.5}$. Solving this equation with the boundary condition $P = 0$ at $T = 0$ (surface) and with the aid of the equation of state for an ideal gas, we obtain

$$\rho = \left(\frac{8ac}{25.5} \frac{4\pi GM}{\kappa_0 L} \frac{\mu m_N}{k} \right)^{1/2} T^{3.25} \, . \tag{4.146}$$

This approximation is invalid when (4.31) equals (4.27), i.e., $\rho > 2.4 \times 10^{-8} \mu_e T^{3/2} \, \mathrm{g \, cm^{-3}}$, which is not far from the surface. With this ρ, we obtain from (4.146)

$$L = (5.7 \times 10^5 \mathrm{erg \, s^{-1}})(\mu/\mu_e^2) \frac{1}{Z(1+X)} \frac{M}{M_\odot} T^{3.5}$$

$$= 2 \times 10^6 \mathrm{erg \, s^{-1}} (M/M_\odot) T^{3.5} \tag{4.147}$$

for $X = 0$, $Y = 0.9$ and $Z = 0.1$ ($\mu \sim 2$ and $\mu_e \sim 1.4$), and we adopt $\langle g \rangle / t \simeq 0.1$ in (4.69). This means $L \sim (10^{-2} - 10^{-5}) L_\odot$ for $T \sim 10^6 - 10^7$ K, which is consistent with observations.

The evolution of luminosity is given by

$$-\frac{dU}{dt} = L \, , \tag{4.148}$$

where $U = (M/Am_N)(3kT/2)$ (A is the effective mass number), and $L = cMT^{3.5}$, as given by (4.147). Integration of (4.148) yields

$$\frac{3}{5}\frac{k}{Am_N}\left(T^{-5/2} - T_i^{-5/2}\right) = c(t - t_i) \, , \tag{4.149}$$

where the subscript i means the initial value. For $T_i \gg T$ we obtain Mestel's cooling law [751]

$$L = M(K[t - t_i])^{-7/5} \tag{4.150}$$

with $K = (3k/5AM_N)c^{-2/7}$. This means $t - t_i \sim 10^9$ yr for $L \sim 10^{-3}L_\odot$, the typical luminosity of old white dwarfs.

Neutrino cooling due to plasmon decay dominates over photon cooling for hot white dwarfs, such as $\log(L/L_\odot) \gtrsim -0.5$ or $T \gtrsim 10^{7.8}$ K. We expect that the cooling law deviates from (4.150).

Observationally, the cooling curve is tested by studying the luminosity function of white dwarfs (i.e., the number of white dwarfs as a function of luminosity). If white dwarfs are produced at a constant rate, the number of white dwarfs per log unit luminosity $\phi(L)d\log L$ is

$$\phi(L) \propto \left[\frac{d\log L}{d\tau}\right]^{-1} \, , \tag{4.151}$$

i.e.,

$$\log \phi(L) = (5/7)\log L \, . \tag{4.152}$$

A more detailed calculation is given in [752]. Neutrino cooling would disturb this distribution. The effect may be barely visible for hotter white dwarfs, but it is difficult to conclude that it is due to the poor statistics of such stars [618]. Stothers [243] derived from the statistics of white dwarfs that the interaction strength of νe coupling should not be larger than $\approx 10 G_F$. If neutrino cooling takes place 100 times faster than predicted in the Fermi theory, it seems that white dwarfs cool too fast.

4.5 Neutrinos from Type II Supernovae

4.5.1 Stellar Core Collapse: Type II Supernovae

A type II supernova (SN II) is identified with the collapse of the iron core of massive evolved stars at the ends of their thermal life [753]. A star more

massive than $\approx 8M_\odot$[35] can ignite silicon at the temperature $T \simeq 3.4 \times 10^9$ K. This final stage lasts for a few days, and the iron core grows. When the iron core exceeds the Chandrasekhar mass ($M_{\mathrm{Ch}} \simeq 1.4M_\odot$ with the number of electrons per nucleon $Y_e \approx 0.4$), gravitational collapse starts and the photodisintegration $^{56}\mathrm{Fe}\rightarrow 13\,^4\mathrm{He}+4n-124.4$ MeV further promotes the collapse. A type II SN is supposed to leave a neutron star [753] (or a black hole if the core mass is large).

The energy released by a type II SN leaving a neutron star is estimated to be

$$\Delta E = \left(-G\frac{M^2}{R}\right)_{\mathrm{GS\ core}} - \left(-G\frac{M^2}{R}\right)_{\mathrm{NS}}, \qquad (4.153)$$

where GS and NS refer to a giant star and neutron star, and the first term is negligible. Numerically,

$$\Delta E = 2.7 \times 10^{53}\mathrm{erg} \left(\frac{M}{M_\odot}\right)^2 \left(\frac{R}{10\,\mathrm{km}}\right)^{-1}. \qquad (4.154)$$

On the other hand, the energy used for photodisintegration is considerably less than $1.4M_\odot \times 6 \times 10^{23} \times 3.2\,\mathrm{MeV} \approx 6 \times 10^{51}$ erg, and the kinetic energy of explosion is of the order of $E_{\mathrm{kin}} = \frac{1}{2}M_{\mathrm{ej}}v^2 \approx 1 \times 10^{51}$ erg for the ejecta mass of $M_{\mathrm{ej}} \approx 10M_\odot$ and $v \approx 2000\,\mathrm{km\,s^{-1}}$. Optical energy is much smaller than this value. Gravitational waves may carry away energy at most by 0.1% of the core mass ($\lesssim 2 \times 10^{51}$ erg), but the dominant part of the energy ($\gtrsim 99\%$) is carried away by neutrino emission.

To find the neutrino flux at the time of explosion, one has to carry out an involved hydrodynamic calculation with neutrino transport. The gross characteristics, however, may be seen from simple considerations. The core density is $> 10^{13}\,\mathrm{g\,cm^{-3}}$, so the core is opaque to neutrino transport. One may then estimate the effective temperature using the radiation law,

$$T_{\mathrm{eff}} = \left[\frac{\Delta E/\tau}{4\pi\sigma R_{\mathrm{eff}}^2} \frac{1}{(7/8)g_\nu}\right]^{1/4}, \qquad (4.155)$$

where σ is the Stefan–Boltzmann constant, $g_\nu/2$ the number of neutrino species, and $R \approx$ several times $10\,\mathrm{km}$. The cooling time τ is of the order of $5-10\,\mathrm{sec}$, as we shall see below. We then find the effective temperature $T_{\mathrm{eff}} \approx 3\,\mathrm{MeV}$ and the average neutrino energy $\varepsilon_\nu = 3.15T_{\mathrm{eff}} \approx 10\,\mathrm{MeV}$. The total neutrino flux is estimated as

$$\Phi_\nu = \frac{\Delta E}{\varepsilon_\nu} \approx 2 \times 10^{58}. \qquad (4.156)$$

---

[35] There is a considerable uncertainty in this threshold mass. The current thought varies from 6 [754] to $11M_\odot$ [755].

Therefore, if a SN occurs at the centre of the Galaxy ($d \simeq 10$ kpc), the expected neutrino flux on Earth is

$$\phi_\nu = \Phi_\nu / 4\pi d^2 \approx 1.6 \times 10^{12} \, \text{cm}^{-2} \, . \tag{4.157}$$

Corresponding to this number, we expect roughly 170 $\bar\nu p \to e^+ n$ events and 8 $\nu_e e^- \to \nu_e e^-$ events in a 1000-ton water detector. The cooling time is given by the neutrino diffusion time

$$\tau_d \approx (4\sigma\lambda)^{-1} R^2 C_v T^{-3} \approx 5\text{--}10 \, \text{s} \tag{4.158}$$

with λ the neutrino mean free path, C_v the specific heat, and R the core radius.

On 23 February 1987, 7:35UT, a supernova SN1987A emerged in the Large Magellanic Cloud at $d \approx 50$ kpc [756]. This supernova was the closest and brightest since the one discovered by Kepler in 1604 in Ophiuchus ($d \approx 5$ kpc). Searches for the neutrino burst associated with this supernova were made by several groups; the Kamiokande collaboration discovered 11 events of neutrino burst which identified the time of the core collapse [757], and with the aid of Kamiokande timing information the IMB group found 8 events [758]. The number of events, the energy of neutrinos, and the duration of the burst roughly agree with those expected from the theoretical consideration given here [759]. For a documentation of the defection of neutrinos from SN1987A, we refer the reader to the article by Koshiba [760]. Searches for a pulsar in the remnant of SN1987A yielded evidence of emission with modulation of a 2.14-ms period in optical and near infrared observations, but it still awaits confirmation [761].

Neutrinos are a dominant carrier of the energy liberated in SNe and also play an important dynamical role in the explosion because the core of SNe is opaque to neutrinos (Colgate and White) [762].[36] The neutral-current cross section of (3.233) gives opacity (see (4.36)) $\kappa \approx 3.0 \times 10^{-18}(E_\nu/10\,\text{MeV})^2$ cm^2 g^{-1}, which means a mean free path $\lambda = 1/\kappa\rho \approx 35$ km for $E_\nu \approx 10$ MeV and $\rho \approx 10^{11}$ g cm^{-3}.

Theory of stellar core collapse. The theory of stellar core collapse is quite an involved subject. We must content ourselves here with only a rough sketch of the idea, which looks reasonable. Interested readers should refer to review articles [764–767]. The bottom line is that there are no consistent models that lead to successful explosion.[37]

---

[36] An early study with more accurate neutrino transport was done by Arnett [763].

[37] Let us quote from Arnett [765]: "The question of how a star collapses and gives rise to a supernova has been one of the most frustrating to the discerning astrophysicists. For three decades there has been a progression of ideas which were each proclaimed to be *the* solution to the problem. The failure rate may have equaled this impressive rate of production."

As contraction proceeds in massive stars, the core density increases, and the larger electron Fermi pressure drives electron capture on iron ($Q = 3.695$ MeV, i.e., the threshold density of the Fermi gas for electron capture is $\rho/\mu_e = 0.53 \times 10^9$ g cm^{-3}). In the state just before core collapse starts, $\rho_c \approx 10^9 - 10^{10}$ g cm^{-3}, $T_c \approx 0.7$ MeV, and the radius of sphere that encircles the Chandrasekhar mass is ≈ 3000 km. When collapse starts, free protons are produced through photodisintegration of iron and the subsequent process ^{4}He$\rightarrow 2p + 2n - 28.30$ MeV, and electron capture is further promoted because electron capture on free protons has a much larger cross section. Electron capture decreases the number of electrons per nucleon (Y_e) and hence reduces M_{Ch}, thus further promoting the collapse. Protons consumed in electron capture are replenished from heavy nuclei. This process produces a large amount of neutrinos, whose luminosity amounts to 10^{52} erg s^{-1}. The core material becomes opaque to neutrinos if $R \gtrsim 10\lambda$ [762]. It soon happens that the neutrino diffusion time becomes longer than the dynamical time, and neutrinos thus produced are trapped in the core. A region of density $\rho > 10^{11}$ g cm^{-3} forms a neutrino sphere with a radius of the order of 70 km by the time of the bounce [768] [the neutrino sphere is defined by a condition similar to (4.106)]. This neutrino trapping increases the Fermi pressure of the neutrino and then suppresses a drastic increase in electron capture [769]. The timescale of the collapse is represented approximately as $t \sim 25\rho_{11}^{-0.7}$ ms, so that this process takes place in 25 ms.

The processes described above altogether result in a sudden drop in supporting pressure. The inner region of the iron core ($r \leq 40$ km) collapses homologously $v(r) \propto -r$, and the core density increases, while preserving its profile [770]. When the core density exceeds the nuclear density $\rho_{\text{nucl}} = 3 \times 10^{14}$ g cm^{-3}, the increase in matter pressure becomes sufficient to halt the collapse [771]. The outer core free-falls at supersonic velocity onto the inner core and undergoes a bounce on the stiff inner core, generating a shock wave propagating outwards [772,771]. The stiff part (inner core) remains unshocked. The sonic point is $\rho \sim 10^{14}$ g cm^{-3} at $R \sim 20$ km. Electron neutrinos in the neutrino sphere remain confined until the shock reaches the neutrino sphere; once it reaches, matter is heated to $T \sim 10$ MeV, and protons and neutrons are liberated, which drastically increases electron capture on protons; neutrinos are emitted copiously, giving rise to an initial ν_e burst (deleptonisation burst) on a timescale of the order of 10 ms [773]. The energy liberated in this burst is of the order of a few times 10^{51} erg.

After this initial deleptonisation burst, the neutrino sphere heated by the shock emits almost blackbody neutrino radiation mostly arising from pair neutrino creation (i.e., an equal number of all species of neutrinos and antineutrinos). In this stage, a steady state is established between the flow of neutrinos from the inner to the outer core and those radiated from the neutrino sphere ($t \lesssim 1$ s). A protoneutron star is formed, and its dynamics nearly decouples from explosion, besides the effect on delayed neutrino heating. The

protoneutron star consists of a dense core and a mantle that is shrinking, and it continues to cool by emitting neutrino blackbody radiation on the neutrino diffusion timescale [768,774]. It has been pointed out that this neutrino wind may be responsible for the r-process formation of heavy elements near the surface of a protoneutron star [775],[38] in place of the traditional idea that the r-process is driven by neutron flux [746].

A large-scale hydrodynamic calculation is necessary to find the shock propagation and the neutrino transport with general relativity taken into account [776–780].[39] The PDE (partial differential equation) solver is quite involved even for spherically symmetric models. The solver must be prepared for a very short timescale of less than milliseconds for shock generation and propagation, and integration over several seconds is necessary to get physics. Different groups use different input physics (progenitor stellar mass and profiles, equation of state, etc.). This makes it difficult to compare not only the results of calculations but also the reliability of the numerical integration scheme (see [782,783] for comparisons of neutrino transport). The gross characteristics obtained from these calculations are: a deleptonisation burst of ν_e emerges shortly after the onset of collapse; in the later phase the luminosity of ν_e is about the same as that of other species of neutrinos, $\bar{\nu}_e$, as well as ν_μ, ν_τ and their antiparticles; the energies of neutrinos show the ordering $\langle E_{\nu_e} \rangle < \langle E_{\bar{\nu}_e} \rangle < \langle E_{\nu_{\mu\tau}} \rangle$, where $\nu_{\mu\tau}$ includes ν_μ, ν_τ, and their antiparticles. This first inequality is understood by the fact that $\nu_e(n,p)e^-$ has a larger opacity than $\bar{\nu}_e(p,n)e^+$ since n is more abundant than p, and the neutrino sphere of $\bar{\nu}$ is located deeper (and then hotter) than that of ν_e. The neutrino sphere of $\nu_{\mu\tau}$ is located still deeper since $\nu_{\mu\tau}$ interacts with (p,n) only via the neutral current. Most authors give $\langle E_{\nu_e} \rangle \sim 10-15\,\text{MeV}$, $\langle E_{\bar{\nu}_e} \rangle \sim 12-18\,\text{MeV}$, and $\langle E_{\nu_{\mu\tau}} \rangle \sim 20-25\,\text{MeV}$, but the details depend significantly on the authors (see Table 4.10). The neutrino energy distribution shows a peak narrower than the Fermi distribution of a zero chemical potential. For low energies a smaller neutrino cross section results in a smaller neutrino sphere, which leads to a smaller flux due to a smaller radiation area. For high energies the neutrino sphere extends to a cool region, and the flux is reduced. The

---

[38] The r-process in this case starts from $A \approx 100$ elements that are produced by α process nucleosynthesis, rather than from iron formed in the e-process.

[39] The most commonly usd is the multigroup flux limited diffusion (MGFLD) scheme to truncate the full Boltzmann equation [777] (the original scheme was developed for photon transport by Castor [781]). This is based on a diffusion approximation with a flux limiter for free-streaming and uses variables with their angle dependence integrated out. An alternative approach is to use Monte Carlo calculation [778]. A full Boltzmann equation solver is also developed [779]. Some authors compared the results of the different schemes [782] and claimed that the MGFLD calculation would underestimate the neutrino density in the free-streaming regime, and hence the heating rate in a outer core region, which is relevant to shock retrieval (this arises from neglect of the correct angular distribution in neutrino transport).

Table 4.10. Neutrino energies (MeV) from supernova calculations.

Calculation		$\langle E_{\nu_e} \rangle$	$\langle E_{\bar{\nu}_e} \rangle$	$\langle E_{\nu_{\mu\tau}} \rangle$
Dalhead-Wilson [784]	at 1 s	12.5	16	24
Yamada et al. [783]	model W1	12.7	16.1	24.2
Burrows et al. [785]	model BM	9	12	22
Bruenn et al. [799]	model S15s7b, at 1 s	16−21*	19−24*	21−28*

Note: (*) rms energy (approximately 10% higher than the mean).

distribution is effectively described by a modified Fermi distribution ('pinched form')

$$f = \frac{1}{D} \frac{1}{e^{+(E_\nu/T - \eta)} + 1} \,, \tag{4.159}$$

with $\eta = 1$–5 and D the dilution factor [786, 787][40]. Figure 4.21 shows the time profile of the neutrino flux of Wilson and Dalhed's calculation, taken from Totani et al. [784], as an example.[41]

An important question for the numerical work is whether the star really explodes. This is a highly nontrivial problem: the shock stalls before reaching the surface of the iron core due to a severe energy loss by photo-disintegration of iron and by neutrino emission. Two scenarios considered for possibly successful explosion are (i) sufficiently strong prompt explosion by an initial shock wave (the explosion takes place within $< 0.1\,\mathrm{s}$) [789, 790] and (ii) delayed explosion due to neutrino deposition in the outer core that promotes the shock [791, 792]. This takes place in $\approx 0.5\,\mathrm{s}$. The calculation of [789] using a soft equation of state appeared to be promising for the first scenario, but the inclusion of more accurate neutrino transport revealed that the energy loss by neutrinos was too great, and explosion failed [793, 794]. The soft equation of state also encounters the problem that one cannot have neutron stars of $M \approx 1.4 M_\odot$ [795]. More authors have taken the delayed explosion scenario as more realistic, but further studies have shown that energy deposition is not sufficiently large to retrieve the shock; one probably needs neutrino flux significantly stronger than simple models yield. Wilson and Mayle [796] succeeded in delayed explosion but with the assumption of efficient convection in the core. Recent effort has been directed to the hydrodynamic issue of convection in the core [797] and in an outer region where the shock wave sweeps [798]. The results, however, are contradictory among different authors on both aspects; opposite conclusions were obtained

---

[40] Some authors give a negative η for $\bar{\nu}_e$ ($t > 3\,\mathrm{s}$) and $\nu_{\mu\tau}$ and ascribe the reason to the scattering effect of the neutrino flux by 'atmosphere' in the outer region of the neutrino sphere [767, 788].

[41] The explosion in this model was achieved by increasing the neutrino flux assuming convection in the protoneutron star (yet to be justified). This is the only model to claim to have successfully generated an explosion.
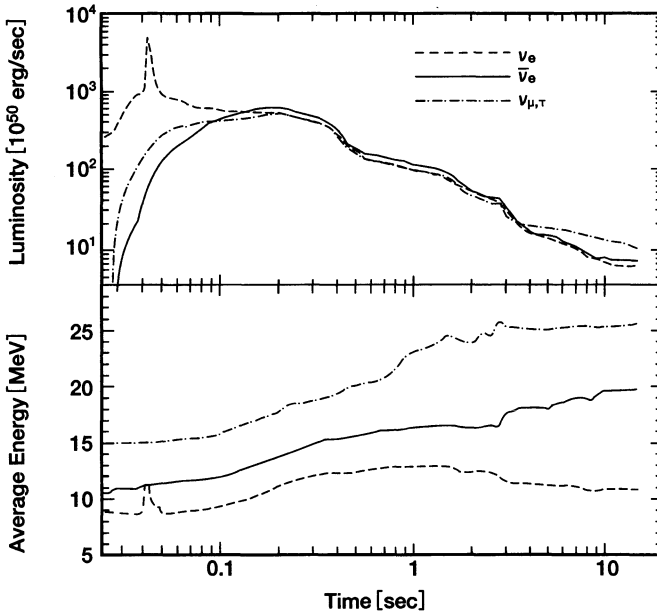
Fig. 4.21. Typical neutrino fluxes form a stellar core collapse, as calculated by Wilson and collaborators. The upper panel shows the luminosity, and lower panel shows the mean energy. $\nu_{\mu,\tau}$ stands for each of ν_μ, ν_τ and their antiparticles. After Totani et al. [784].

as to the importance of convection. The conclusion we can draw now is that the problem is subtle and a more accurate hydrodynamic treatment and an accurate neutrino transport scheme are needed in a coupled way to solve it. There are no self-consistent models that realise a successful supernova explosion in the state-of-the-art numerical work [799].

There have been many arguments to obtain constraints on neutrino properties or exotic particles from SN1987A. Most of them invoke the argument that extra energy loss must be nominally smaller than neutrino energy loss, or else the energy loss makes explosion unlikely. Since we have no successful models of supernova explosion, we cannot take these arguments too seriously. We should understand these arguments in the way that the energetics of a supernova would be affected if such an extra energy loss occurs. We cannot obtain any constraints on particle physics unless successful models of supernovae are realised for some ranges of input parameters and such a parameter range is shown to disappear due to extra energy loss. For this reason, we ignore the constraints on the magnetic moment of neutrinos or something else derived from supernova SN1987A.

Neutrino energy of SN1987A.   A number of authors estimated the neutrino spectrum from the neutrino events observed at Kamiokande and
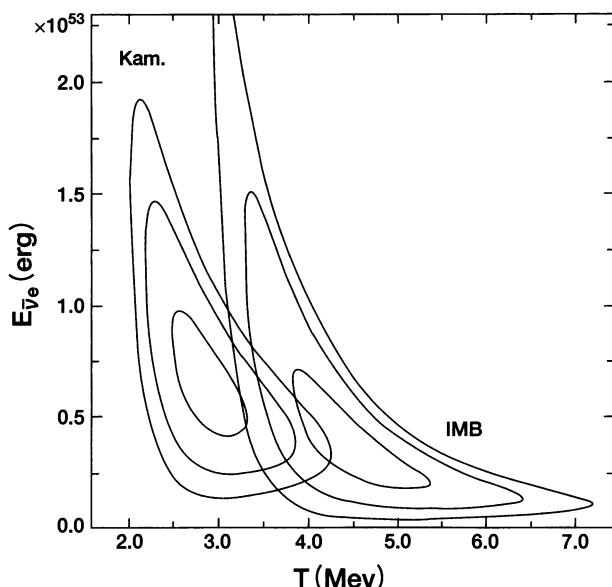
Fig. 4.22. Estimates of the temperature and the luminosity of neutrinos from SN1987A. The three contours indicate 68, 95, and 99% confidence levels outwards. After Janka and Hillebrandt [786].

IMB [786, 800]. The Kamiokande events (11 events with fiducial 2140 tons, >50% efficiency for $E > 8.5\,\mathrm{MeV}$) are described well by the Fermi distribution of $T = 2.8 \pm 0.5\,\mathrm{MeV}$ ($\eta < 2$), whereas the IMB events (8 events with fiducial 6800 tons, >50% efficiency for $> 27\,\mathrm{MeV}$) give a higher temperature, $4.5 \pm 0.5\,\mathrm{MeV}$ ($\eta < 4$). The two estimates overlap only at $2\,\sigma$ (Fig. 4.22). We return to this problem in Sect. 8.9.

Neutron star cooling. A few weeks after a supernova explosion, a hot neutron star cools to $10^9\,\mathrm{K}$ and becomes transparent to neutrinos. Neutrino emission continues to dominate cooling until the temperature drops to $10^8\,\mathrm{K}$, i.e., for a period of the order of 10^5 years [801, 802]. The dominant neutrino emission mechanism is the modified Urca process, which gives $L_\nu \approx 5.3 \times 10^{39}\,\mathrm{erg\,s^{-1}}(M/M_\odot)(\rho/\rho_{\mathrm{nucl}})^{-1/3}T_9^8$ [803]. Also important is bremsstrahlung emission from the crust, $L_\nu \approx 5 \times 10^{39}\,\mathrm{erg\,s^{-1}}(M_{\mathrm{crust}}/M_\odot)$ $(\rho/\rho_{\mathrm{nucl}})^{-1/3}T_9^6$ [804] A milder temperature dependence of the latter process means that the bremsstrahlung dominates at lower temperatures, say, for a period of $10^{3.5}-10^5\,\mathrm{yr}$, after which X-ray emission dominates. Neutrino cooling depends much on the nuclear equation of state and also on many unknown factors, possible superfluidity of nucleons, pion condensation, and free quark states with or without strange quarks, and so on. One could, in principle, explore the physics of matter in the ultra-high-density interior via neutrino cooling. Comparisons of predicted and observed cooling curves have

revealed a number of problems in both observation and theory; see reviews of [805].

4.5.2 Supernova Rate and Relic Neutrinos

Supernova rate. Historical supernovae in the Milky Way are summarised in Table 4.5.2 [620]. Six SNe are recorded after 1000 AD. This gives a SN rate of $1/(170\,\text{yr})$. If we consider obscuration due to interstellar dust in the Galactic plane that makes only $\approx 1/6$ of Galactic SN visible, their rate would be $1/(28\,\text{yr})$. Tammann estimated the frequency of supernovae in the Milky Way as $1/((20\text{–}50)\,\text{yr})$ [808]. This rate is multiplied by ≈ 0.4 for type II SNe, and hence the SN II rate is $\approx 1/80\,\text{yr}$. Pulsar counting suggests $1/(70\,\text{yr})$ [809] for SNe II.

Table 4.11. Historical supernovae in the Milky Way after 1000 AD^a.

Optical	Remnant	Year	Distance (kpc)	m_{pg}(mag)	M_{pg}(mag)	Type
Lup-Cen	G327.6+14.6	1006	1.8	?		Ia
Tau	Crab Nebula	1054	2	-3.5	-17	II
Cas	3C58	1181	3	< 0		?
Cas (Tycho)	G120.1+1.4	1572	2.4	-4	-18.5	Ia
Oph (Kepler)	G4.5+6.8	1604	3–6	-3	$-(18.5 - 20)$	Ia
unobserved	Cas A	1671±1	3.4	faint		II

^{a}This Table is constructed from Stephenson and Green [806]. Absolute magnitudes are calculated by assuming Galactic extinction $A_{\text{pg}} \simeq 1.0$ mag kpc^{-1} [$E(B - V) = 0.25$ mag kpc^{-1}]. For a catalogue of SN remnants, see [807].

A number of statistical estimates have been made for the extragalactic SN rate. The results [810–812] are listed in Table 4.12 in units of h^2 per $10^{10} L_B(\odot)$ per 100 yr.[42] The results imply that the Galactic rate of SNe II (plus SNe Ib/c, which are ascribed to stellar collapse) is $1/(30\,\text{yr})-1/(90\,\text{yr})$,[43] in gross agreement with historical SN rates. The rate of SNe Ia is significantly lower, roughly $1/(300\,\text{yr})$.

---

[42] h is the Hubble constant in units of $100\,\text{km}\,\text{s}^{-1}\text{Mpc}^{-1}$; see Sect. 4.6.3 below. E and S stand for elliptical and spiral galaxies, and 0, a, .., d means the progression of the disc component and spiral arms classified according to the Hubble sequence (morphological types) [813]. The average takes account of the morphological fractions of E–S0, S0a–Sb, and Sbc–Sd as 0.32:0.28:0.34 (0.06 is ascribed to Im). Cappellaro et al. [812] give the SN rate for S0a–Sb combined; the separation into S0a–Sa and Sab–Sb is taken from [814].

[43] $L_B(\text{MW}) = 1.6 \times 10^{10} L_{B\odot}$ and $h = 0.7$ are used. The Milky Way is supposed to be classified into Sbc.

Table 4.12. Extragalactic supernova rate. The numbers are in units of h^2 per $10^{10}L_B(\odot)\cdot 100$ yr.

Morphological type	E–S0	S0a–Sa	Sab–Sb	Sbc–Sd	Average
Type II (Ib/c)					
v.d. Bergh & McClure [810]	0	0	2.03 (0.43)	1.07 (0.36)	0.65 (0.18)
Tammann et al. [811]	0	0.16 (0.04)	1.36 (0.28)	3.92 (0.76)	1.55 (0.30)
Cappellaro et al. [812]	0	0.28 (0.28)	0.96 (0.16)	1.56 (0.28)	0.73 (0.15)
Type Ia					
v.d. Bergh & McClure [810]	0.25	0.57	0.30	0.18	0.26
Tammann et al. [811]	1.00	0.48	0.48	0.48	0.62
Cappellaro et al. [812]	0.27	0.44	0.32	0.43	0.33

Supernova relic neutrinos There are relic neutrinos from SNe II that occurred in the past, and they may be detected as a diffuse neutrino background [815, 816]. If SNe II occurred at a constant rate during the history of galaxies, the total energy density of antineutrinos (which are easier to detect than neutrinos) would be

$$\rho_{\bar{\nu}} = \int_0^{t_0} n_{SN}(t')L_{\bar{\nu}_e}\left[\frac{a(t')}{a(t_0)}\right]^4 dt' \,, \tag{4.160}$$

where $L_{\bar{\nu}_e}$ is the $\bar{\nu}_e$ luminosity and the supernova density is

$$n_{SN}(t') = n_{SN}(t_0)\left[\frac{a(t_0)}{a(t')}\right]^3 \tag{4.161}$$

with $a(t)$ the scale factor of the universe (see (4.164) below). Then (4.160) can easily be integrated in the Einstein–de Sitter universe [for which $a(t)\sim t^{2/3}$] to give

$$\rho_{\bar{\nu}_e} = \frac{3}{5}n(t_0)_{SN}L_{\bar{\nu}_e}t_0 \,, \tag{4.162}$$

where 3/5 is the redshift factor for the mean energy of neutrinos [816]. For $L_{\bar{\nu}_e}\sim 0.5\times 10^{53}$ erg, $n_{SN}\sim 1.1h^2$ yr$^{-1}(10^{10}L_\odot)^{-1}$, and the local luminosity density $\mathcal{L}\sim 2.4\times 10^8 hL_\odot$ (Mpc)$^{-3}$, we obtain

$$\phi_{\bar{\nu}_e}\sim 2.5 \text{ cm}^{-2}\text{s}^{-1} \,, \tag{4.163}$$

where the mean neutrino energy of local supernovae is assumed to be 10 MeV and the Hubble constant in units of $100\,\text{km s}^{-1}\text{Mpc}^{-1}$ is $h\sim 0.7$. This gives 0.02 events/yr in a 1-kton water detector.

A number of calculations [817] have been carried out since [815, 816]. Later works [818, 819] have incorporated the effect of galaxy evolution, the understanding of which has undergone rapid development recently [820]. The

results of relic neutrino calculations vary by two orders of magnitudes depending on authors, mostly caused by uncertainties in estimating the SN rate and its time history. The work of [819] uses the evolution of an heavy element abundance as indicator of galaxy evolution with the justification that both heavy elements and SNe II result from massive stars. The authors presented a flux significantly ($\lesssim$10 times) larger than (4.163). The model given in [821] uses empirical star formation rates and empirical constraints on the neutrino spectrum inferred from the observation of neutrinos from SN1987A.

The experimental problem is the large background from reactor antineutrinos and solar neutrinos at lower energies and from atmospheric neutrinos at higher energies. This leaves $\approx$20$-$35 MeV as an optimum window. In this window, we also expect the background of electrons from decays of low energy muons that are produced in $\nu_\mu N$ interactions while their energies are so low that they are invisible in the water Čerenkov detector [822, 823]. The upper limit on the relic neutrino flux obtained at Kamiokande was $\phi_{\bar{\nu}_e} < 226 \, \text{cm}^{-2} \, \text{s}^{-1}$ in the energy interval from 19 to 35 MeV [822]. Since the electron spectrum from muon decay is precisely known, however, one can subtract the background. The Super-Kamiokande group has successfully subtracted electrons from muon decays and obtained < 2.0 event per year per 22.5 kton in the window of 18 to 50 MeV (with 3.5 years of operation) [824]. With uncertainties of the neutrino flux model and the star formation rate, a reasonable event rate we expect is 0.4$-$2.5 events/yr [821]. The current data already give a meaningful constraint on the star formation rate (see Fig. 4.23(a)). Neutrino events for 18$-$50 MeV is dominated by local ($z < 0.25$) SNe, but those for a lower energy region, 12$-$18 MeV say, are more sensitive to SNe at $z = 0.25-0.5$ (see Fig. 4.23(b)). The total flux that includes low-energy neutrinos which cannot be detected is a more uncertain quantity, since it receives a large contribution from high redshift SNe.

4.6 Neutrinos in Cosmology

4.6.1 Elements of Cosmology

The starting assumption concerning the universe is that it is homogeneous and isotropic.[44] Such space is uniquely described by the Robertson–Walker metric

$$ds^2 = dt^2 - a^2(t) \left(\frac{dr^2}{1 - kr^2} + r^2 d\Omega^2 \right) , \qquad (4.164)$$

where $a(t)$ is the scale factor and the curvature k takes 0 or ± 1. The physical length is given by $x = a(t)r$, and r is called the comoving coordinate, in which the distance between two particles remains constant unless a force acts on

---

[44] For standard text books of cosmology, see Weinberg [825] and Peebles [826].
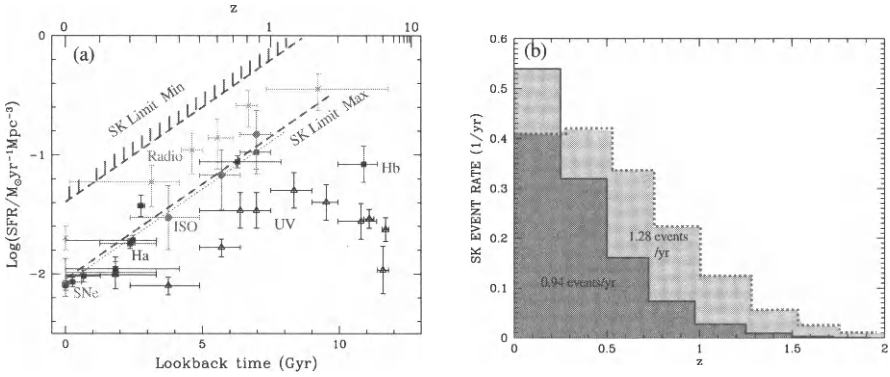
Fig. 4.23. (a) Star formation rate as a function of the lookback time inferred from $H\alpha$/UV/near infrared/radio indicators [820] and that from supernova rate (denoted as SNe) [810–812], compared with the 90% constraint from Super-Kamiokande. The two lines (denoted as SK Limit) correspond to a minimum (i.e. a conservative) and a maximum upper limit allowed by the uncertainty of the neutrino flux model. The *dotted line* is a fiducial curve for the star formation rate inferred from $H\alpha$ line widths. (b) Expected neutrino events partitioned according to the redshift of supernovae. The *solid (dotted)* histogram corresponds to the energy window of $18-50$ MeV ($12-18$ MeV). Figures are taken from [821].

them. When the scale factor grows, $\dot{x} = (\dot{a}/a)x$, and

$$H = \frac{\dot{a}}{a} \tag{4.165}$$

is the expansion rate of the universe; its present value is called the Hubble constant.

The physical contents of the universe determine the evolution of $a(t)$. The Einstein equation applied to the Robertson–Walker metric gives

$$\left(\frac{\dot{a}}{a}\right)^2 + \frac{k}{a^2} - \frac{\Lambda}{3} = \frac{8\pi G}{3}\rho \,, \tag{4.166}$$

$$2\frac{\ddot{a}}{a} + \left(\frac{\dot{a}}{a}\right)^2 + \frac{k}{a^2} - \Lambda = -8\pi G p \,, \tag{4.167}$$

where ρ and p are energy density and pressure; Λ is the cosmological constant or $\rho_v = \Lambda/8\pi G$ is taken as the vacuum energy. From the two equations (Friedmann–Lemaître equations), we obtain

$$\frac{1}{2}\dot{a}^2 = \frac{4\pi}{3}G\rho a^2 - \frac{k}{2} + \frac{\Lambda}{6}a^2 \,, \tag{4.168}$$

which is equivalent to Newton's equation of motion for the unit mass placed on a sphere of radius a if $\Lambda = 0$. The other equation reads

$$\frac{d}{dt}(a^3 \rho) + p\frac{d}{dt}a^3 = 0 \,, \tag{4.169}$$

which is the equation of continuity. This means that the energy density in the radiation-dominated universe (RD) with $p = \rho/3$ behaves as $\rho \propto a^{-4}$ and in the matter-dominated universe (MD) with $p = 0$ behaves as $\rho \propto a^{-3}$.

Equations (4.166) and (4.167) may also be represented as

$$\Omega + \lambda + K = 1 \,, \tag{4.170}$$

and

$$q = \frac{\Omega}{2} - \lambda \,, \tag{4.171}$$

where

$$\Omega = \rho/\rho_c \,, \quad q = -\ddot{a}\,a/\dot{a}^2 \,, \quad \lambda = \Lambda/3H^2 \,, \quad K = k/a^2 H^2 \,, \tag{4.172}$$

and

$$\rho_c = 3H^2/8\pi G \,. \tag{4.173}$$

We denote the present-day values with suffix 0.

4.6.2 Radiation-Dominated Universe and the Thermal History

At a sufficiently high temperature, all particles behave as relativistic particles, i.e., as radiation.[45] In the massless limit the energy density of bosons is

$$\rho = \frac{2}{(2\pi)^3} \int d^3p \frac{p}{e^{E/T} - 1} = \frac{\pi^2}{15}T^4 \,, \tag{4.174}$$

for particles with two spin states, and for left- (or right-)handed fermions,

$$\rho = \frac{2}{(2\pi)^3} \int d^3p \frac{p}{e^{E/T} + 1} = \frac{7}{8}\frac{\pi^2}{15}T^4 \,, \tag{4.175}$$

including particles and antiparticles. Writing the number of the species of relativistic particles N_{B} (boson) and N_{F} (fermion), the total energy density is

$$\rho = \frac{\pi^2}{15}T^4 g_* \,, \tag{4.176}$$

where

$$g_* = N_{\mathrm{B}} + \frac{7}{8}N_{\mathrm{F}} \tag{4.177}$$

---

[45] We refer the reader to a textbook by Kolb and Turner for a detailed discussion of the early universe, especially of the interface between cosmology and particle physics [246].

is 29/8 for $T \lesssim 1\,\mathrm{MeV}$ (photons and three neutrinos are relativistic),[46] 43/8 for $1\,\mathrm{MeV} \lesssim T \lesssim 100\,\mathrm{MeV}$, 30.9 for $150\,\mathrm{MeV} \lesssim T \lesssim 1\,\mathrm{GeV}$ where quarks and gluons are free particles, and so on. Note that this degree of freedom does not depend on whether neutrinos are Majorana (Weyl) or Dirac, unless the neutrinos are as heavy as a few MeV or more: the degree of right-handed neutrinos, even if they are light, is suppressed by the helicity factor of $(m_\nu/T)^2$, unless interactions are present that are relevant to right-handed neutrinos; hence, it contributes very little to g_*.

Noting that $a \propto T^{-1}$ from $\rho \propto a^{-4}$ and $\rho \propto T^4$, the equation of motion (4.168) is

$$-\frac{\dot{T}}{T} = \frac{\dot{a}}{a} = \left(\frac{8\pi^3}{45}Gg_*\right)^{1/2}T^2 \,, \tag{4.178}$$

ignoring the curvature and cosmological constant terms. After integration,

$$t = \left(\frac{45}{32\pi^3 g_*}\right)^{1/2}\frac{m_{\mathrm{pl}}}{T^2}$$
$$= \frac{1.71}{T(\mathrm{MeV})^2}\frac{1}{\sqrt{g_*}}\,\mathrm{s}\,, \tag{4.179}$$

where $G = 1/m_{\mathrm{pl}}^2$. The scale factor grows as $a \propto t^{1/2}$. Note that $T \to \infty$, as $t \to 0$, which is the singularity of the Big Bang [827].

For later convenience, let us give the number density of relativistic particles corresponding to (4.174) and (4.175):

$$n_\gamma = \frac{2\zeta(3)}{\pi^2}T^3 \,, \quad n_{\nu+\bar{\nu}} = \frac{3}{4}\frac{2\zeta(3)}{\pi^2}T^3 \,, \tag{4.180}$$

where the ζ function $\zeta(3) = 1.20206$.

At high temperature, reaction rates among particles mediated by effective interactions (interactions with dimensional coupling) are much higher than expansion rates, and particles are in thermal equilibrium. For neutrinos, the most important reaction that persists to the lowest energy is $\bar{\nu}\nu \rightleftharpoons e^+e^-$. The evolution of the neutrino number density is described by the Boltzmann equation [828]:

$$\frac{dn_\nu}{dt} + 3\frac{\dot{a}}{a}n_\nu = -\langle\sigma(\bar{\nu}\nu \to e^+e^-)v\,[n_\nu^2 - (n_\nu^{\mathrm{eq}})^2]\rangle \,. \tag{4.181}$$

The reaction is in equilibrium if

$$\langle\sigma(\bar{\nu}\nu \to e^+e^-)vn_\nu^2\rangle \gg \frac{\dot{a}}{a}n_\nu \,. \tag{4.182}$$

---

[46] Actually this number is smaller because the neutrino temperature is lower by $(11/4)^{1/3}$ due to reheating: $g_* = 1.682$ with T measured in the photon temperature. See the text below.

The cross section is given by $\sigma v = (4G_F^2/3\pi)\xi(p_1 \cdot p_2)^2/E_1 E_2$, where (p_1, E_1) and (p_2, E_2) are the energy and momentum of the two incident particles and ξ is

$$\xi = 1/4 + \sin^2 \theta_W + 2\sin^4 \theta_W \,, \quad \text{for } \bar{\nu}_e \nu_e \,,$$
$$\xi = 1/4 - \sin^2 \theta_W + 2\sin^4 \theta_W \,. \quad \text{for } \bar{\nu}_{\mu(\tau)} \nu_{\mu(\tau)} \,. \tag{4.183}$$

Integration over the Fermi–Dirac distribution of neutrinos gives

$$\Gamma = \langle \sigma v n_\nu^2 \rangle = \frac{49\pi^4}{32400} \xi \frac{G_F^2}{\pi} T^8 \,. \tag{4.184}$$

Equating this with $(\dot{a}/a)n_\nu = (1/2)(1/t)n_\nu$, where t is given by (4.179) and n_ν by half that given in (4.180), yields the temperature $T \simeq 2.4$ and $3.7\,\text{MeV}$ for ν_e and ν_μ, respectively. Below this temperature, neutrinos behave as free particles, except for occasional interaction with nucleons, whose cross section is significantly larger. This is called decoupling of neutrinos from thermal equilibrium. A more precise decoupling effect is studied by integrating the Boltzmann equation numerically (we must include $\nu e \rightarrow \nu e$ scattering). After decoupling the Fermi distribution is preserved with the 'temperature'[47] simply redshifting as $T \propto a^{-1}$. Equation (4.180) is justified insofar as the mass of the neutrino is smaller than the decoupling temperature. For the opposite case, see appendix of Chap. 5.

When the universe cools to $T \lesssim 1$ MeV, $\gamma\gamma \rightarrow e^+ e^-$ becomes suppressed due to the Boltzmann factor $\exp(-2m_e/T)$, and existing $e^+ e^-$ annihilate into photons, which reheats photons. This takes place adiabatically, and hence entropy is conserved. Specific entropy $s \propto g_* T^3$, so

$$\left(1 + 2\frac{7}{8}\right) T_i^3 = T_f^3 \,, \tag{4.185}$$

before and after the annihilation, where initial temperature T_i is identified with that felt by neutrinos T_ν, and T_f with that felt by photons T_γ, i.e.,

$$T_\gamma = \left(\frac{11}{4}\right)^{1/3} T_\nu \,. \tag{4.186}$$

We do not expect any appreciable energy injection into photon gas after this epoch. Photons obey the Planck distribution, and the energy redshifts as $\sim a(t)$, as the universe expands. The observation of the cosmic microwave background (CMB) tells us that

$$T_0 = 2.728 \pm 0.004 \text{ K} \tag{4.187}$$

---

[47] This T does not have meaning as a real temperature since particles are not in thermal equilibrium any longer. We call this temperature simply because the distribution function still obeys the Fermi (Bose) function. So this would be more appropriately called a 'pseudotemperature.'

today [829]. This means that the neutrino temperature is $T_0 = 1.947\,\mathrm{K}$. Using the Fermi distribution, the number density of neutrinos per species today is, from (4.180),

$$n_{\nu+\bar{\nu}} = 112\ \mathrm{cm}^{-3} \qquad (4.188)$$

for $m_\nu \ll 1\,\mathrm{MeV}$.

Note that reheating due to e^+e^- annihilation leads to hotter electrons and positrons in the epoch $0.5 \lesssim T \lesssim 1\,\mathrm{MeV}$, and this causes some distortion of the neutrino spectrum, in particular on the high-energy side, where interactions of neutrinos with electrons are stronger [830]. The fractional distortion of the ν_e spectrum is $\delta f_\nu / f_\nu \approx 3 \times 10^{-4}(E/T)(11E/4T - 3)$.

Primordial nucleosynthesis. Even after decoupling from the thermal bath, neutrinos are not completely free above $T \approx 0.8\,\mathrm{MeV}$. They are still in strong thermal contact with protons and neutrons because the neutrino reaction cross section off the nucleon is larger than that for leptons. The reactions are
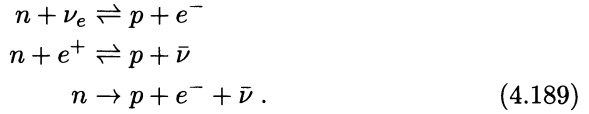
$$n + \nu_e \rightleftharpoons p + e^-$$
$$n + e^+ \rightleftharpoons p + \bar{\nu}$$
$$n \rightarrow p + e^- + \bar{\nu}\,. \qquad (4.189)$$

For the first reactions, the rate is given by

$$\Gamma(n + \nu_e \to p + e^-) = G_V^2\, \frac{1 + 3g_A^2}{2\pi^3}$$
$$\times \int dp_\nu\, p_e E_e p_\nu^2\, \frac{1}{e^{E_\nu/T_\nu} + 1}\left(1 - \frac{1}{e^{E_e/T_e} + 1}\right),$$
$$\Gamma(p + e^- \to n + \nu_e) = G_V^2\, \frac{1 + 3g_A^2}{2\pi^3}$$
$$\times \int dp_e\, E_\nu^2 p_e^2\, \frac{1}{e^{E_e/T_e} + 1}\left(1 - \frac{1}{e^{E_\nu/T_\nu} + 1}\right),$$
$$(4.190)$$

and for the second,

$$\Gamma(n + e^+ \to p + \bar{\nu}) = G_V^2\, \frac{1 + 3g_A^2}{2\pi^3}$$
$$\times \int dp_e\, E_\nu^2 p_e^2\, \frac{1}{e^{E_e/T_e} + 1}\left(1 - \frac{1}{e^{E_\nu/T_\nu} + 1}\right),$$
$$\Gamma(p + \bar{\nu} \to n + e^+) = G_V^2\, \frac{1 + 3g_A^2}{2\pi^3}$$
$$\times \int dp_\nu\, p_e E_e p_\nu^2\, \frac{1}{e^{E_\nu/T_\nu} + 1}\left(1 - \frac{1}{e^{E_e/T_e} + 1}\right),$$
$$(4.191)$$

where the factor $G_V^2(1+3g_A^2)/2\pi^3$ may be replaced with $[\tau_n m_e^5 f(E_0)]^{-1}$ with τ_n the neutron lifetime and and $f(E_0) = 1.7549$ [see (3.67)]. The relation between $T_e(=T_\gamma)$ and T_ν is given by an equation similar to (4.186) but with the electron mass retained:

$$\left(\frac{T_\gamma}{T_\nu}\right)^3 = 1 + \frac{45}{2\pi^4}\frac{1}{T_\gamma^4}\int_0^\infty dp$$

$$\times\, p^2\left[\sqrt{m_e^2+p^2}+\frac{1}{3}\frac{p^2}{\sqrt{m_e^2+p^2}}\right]\frac{1}{\exp(\sqrt{m_e^2+p^2}/T_\gamma)+1}\,. \quad (4.192)$$

The neutron fraction X_n changes with time as

$$-\frac{dX_n}{dt} = \Gamma(n\to p)X_n - \Gamma(p\to n)(1-X_n)\,, \quad (4.193)$$

where $\Gamma(n\to p) = \Gamma(n+\nu_e\to p+e^-)+\Gamma(n+e^+\to p+\bar\nu)$, etc. When the reaction proceeds slowly,

$$X_n = \frac{\Gamma(p\to n)}{\Gamma(p\to n)+\Gamma(n\to p)}\,. \quad (4.194)$$

For an approximate calculation, the Fermi blocking factors in the brackets of (4.190) and (4.191) are taken as unity, and the Fermi distribution is replaced by the Boltzmann factor. The rates of the two reactions of (4.193) differ only by the suppression factor due to the proton neutron mass difference (detailed balance). Hence,

$$\frac{\Gamma(p\to n)}{\Gamma(n\to p)} \simeq e^{-\Delta/T}\,, \quad (4.195)$$

where $\Delta = m_n - m_p = 1.293\,\text{MeV}$. The Boltzmann equation was numerically integrated by Alpher, Follin, and Hermann (1953) [831] after Hayashi [248] noted that the n/p ratio should be determined by weak interactions, and by Peebles [832] just after the discovery of the cosmic 3-K radiation [833]. A qualitative argument can be made by comparing the reaction rate of the beta process with the expansion rate. The cross section of the beta process is given in (3.152); so by integrating over the neutrino distribution,

$$2\langle n_\nu\sigma v\rangle = 45\zeta(5)\frac{G_V^2(1+3g_A^2)}{\pi^3}T^5\,. \quad (4.196)$$

Equating this to $\dot a/a$ in (4.178) yields $T_\beta = 0.73\,\text{MeV}$. If we represent the result of numerical integration[48] in terms of the effective temperature to give the correct n/p ratio, it is $T_\beta = 0.794\,\text{MeV}$. This means that $X_n = 0.164$ when neutron decay is ignored, and 0.131 at $t = 200\,\text{s}$ (at which nucleosynthesis takes place) allowing for decay.

---

[48] For a semianalytic treatment, see [834].

When the temperature drops to 0.1 MeV, photodisintegration $\gamma + d \rightarrow p + n$ (binding energy $\sim 2\,\text{MeV}$) is hindered, and deuterium forms by $p + n \rightarrow \gamma + d$. After deuterium is produced, the synthesis up to ^4He is fast. If the universe would not have expanded, all neutrons that survive decay are captured in ^4He, which has the largest binding energy. In reality, the expansion of the universe leaves a small amount (10^{-5}) of neutrons in deuterium and ^3He [835]. If nearly all neutrons are captured in ^4He, the mass fraction of helium is

$$Y = \frac{2N_n}{N_p + N_n} = 2X_n ,\qquad (4.197)$$

where $X_n = 0.131$, and so we obtain $Y = 0.26$. Actually neutron decay during the epoch of nucleosynthesis is not negligible, and Y is a gradually increasing function of the baryon density, which enters the calculation in the form

$$\eta = n_B / n_\gamma .\qquad (4.198)$$

Deuterium is fragile and sensitive to baryon abundance $(\text{D/H} \propto \eta^{-1.6})$. The gap of stable nuclei at $A = 5$ makes lithium production very small (10^{-10}). Another gap at $A = 8$ makes heavier elements virtually absent. For $A \leq 4$, this primordial nucleosynthesis is only the origin of a large amount of helium [836] and a small amount of fragile deuterium [837]. Figure 4.24 shows a calculation of the primordial abundance of light elements up to ^7Li.

An important test is to see whether observations of the primordial elemental abundance lead to a convergent value of η. Calculations have been continuously updated with improved input parameters and compared with newer observations [838, 839] (the standard computer code is given by Wagoner [840]). The agreement of the observed abundance of D, ^3He, ^4He, and ^7Li with the prediction has been taken as evidence for the great success of the Big Bang hypothesis. At a detailed level, however, the status of the observational determination of primordial elemental abundances is still confusing. Some of the most important determinations disagree with each other by more than quoted errors. We have two values for primordial helium abundance, the traditionally accepted value $Y = 0.234 \pm 0.002$ [841, 842], and a new value from Izotov and Thuan [843], $Y = 0.245 \pm 0.002$. The two values are 5.5σ away, indicating that systematic errors are underestimated. Helium abundance is estimated from the strengths of the recombination lines of neutral helium observed in metal-deficient dwarf galaxies (extragalactic HII regions) [844]. It seems that the raw spectroscopic data are mutually consistent [841, 843]. The difference arises from the use of different calculations for the helium recombination rate, different rates of collisional excitation, and different treatments of corrections of underlying stellar absorption.[49]

---

[49] We note that different recombination lines $[3d^1 \rightarrow 2p^1(\lambda 6678), 4d^3 \rightarrow 2p^3(\lambda 4471), 3d^3 \rightarrow 2p^3(\lambda 5875)]$ give answers that differ by more than the quoted error; these results are usually averaged, and $1/\sqrt{N}$ statistics is applied [843].
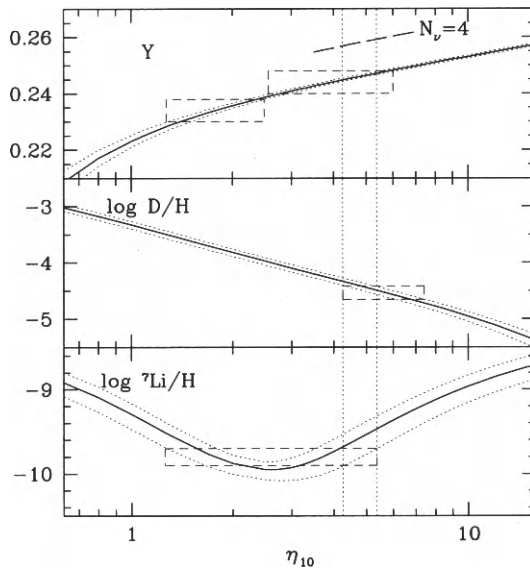
Fig. 4.24. Calculation of the light element abundance from primordial nucleosynthesis as a function of the baryon to photon ratio η in units of 10^{-10}: (a) helium abundance Y_p (mass fraction), (b) deuterium to hydrogen ratio in numbers, and (c) ^{7}Li to hydrogen ratio by numbers. The boxed regions show observations. The curves are taken from Olive et al. [848]. For observational data, see the text.

The modern observation of deuterium abundance uses quasar's deuterium absorption lines caused by high redshift intervening clouds (called Lyman limit systems).[50] Such observations for five clouds yield a deuterium to hydrogen ratio of D/H= $(3.0 \pm 0.4) \times 10^{-5}$ by numbers [845], and those for the two others give a high deuterium abundance of 2×10^{-4} [846]. Low deuterium abundance is usually preferred for the reason that the accidental coincidence of a hydrogen absorption line of a different cloud with the position of the deuterium line would mimic a large deuterium abundance. Another reason is that high deuterium abundance seems to be difficult to reconcile with the Galactic deuterium abundance, which is D/H= 2×10^{-5}: it seems difficult to destroy deuterium by a factor of 10 [847].

Olive et al. [848] quote two solutions for the 2σ range: the high baryon option $\eta = (4.5-6.0) \times 10^{-10}$ with high helium and low deuterium abundance and the low baryon option $\eta = 1-2 \times 10^{-10}$ with high deuterium and low helium abundance. In a review presented by PDG, Olive [849] takes the region that contains both solutions as allowed. A powerful diagnostic is recently given from high-resolution CMB anisotropy experiments (see below) [850]. The rather low height of the second acoustic peak is understood only by

---

[50] Hydrogen clouds of column density $3 \times 10^{17} < N_{H\,I} < 2 \times 10^{20}$ cm^{-2} are opaque to ionising radiation and are called Lyman limit systems.

high baryon abundance [850, 851]; it excludes the low baryon option. An analysis of the most recent data from the Boomerang experiment gives $\eta = (5.7\pm0.8) \times 10^{-10}$ [852]. In this book, therefore, we take only the high baryon option, although the quoted error may underestimate the systematics. In particle physics contexts the ratio of the baryon density to the specific entropy $s = 7.040n_\gamma$ is often used because this quantity is unchanged through the adiabatic evolution of the universe:

$$kn_B/s = (6.4-8.6) \times 10^{-11} , \qquad (4.199)$$

corresponding to the high baryon solution.

The change in relativistic degrees of freedom modifies the expansion rate of the universe, and hence the n/p freeze-out temperature. More relativistic degrees of freedom (say, one additional neutrino species) causes earlier decoupling and a larger n/p ratio, resulting in a larger helium abundance [836,835,853]. The increase in helium abundance by additional neutrino species, δN_ν, is estimated as

$$\delta Y = \frac{\partial T_\beta}{\partial g_*} \frac{\partial X_n}{\partial T_\beta} \frac{\partial Y}{\partial X_n} \frac{7}{8} \delta N_\nu = 0.012\delta N_\nu , \qquad (4.200)$$

from (4.196), (4.178), (4.195) and (4.197). Taking the 2σ range of the high baryon solution, the allowed number of extra 'neutrino' species is

$$\delta N_\nu \leq 0.25 . \qquad (4.201)$$

(If we would allow the low baryon option at the same time, the limit becomes 1.3, which is adopted in [849].)

The same argument applies to any light particles that decouple earlier than the epoch of the n/p freeze-out [854]. Let us suppose a light particle that decouples when the relativistic degree of freedom is g_{*X}. The number density is diluted due to successive reheating by the epoch of the n/p freeze-out by the factor of $(g_{*1}/g_{*X})^{4/3}$ with $g_{*1} = 43/8$. Table 4.13 shows g_{*X} and the equivalent number of neutrino species at the n/p freeze-out when one extra species of chirally projected fermions (say, right-handed neutrinos) decouples at the relevant temperature. Taking the allowed extra light fermion species as 0.25, Table 4.13 shows, for example, that one or two extra 'neutrino' species is allowed if it decouples above the QCD phase transition. We have seen that the decoupling temperature $T_d \propto G_F^{-2/3} \propto M_W^{4/3}$. For a new gauge interaction and an associated particle X, if any, the same rule applies. $T_d > T_{QCD} \approx 150\,\mathrm{GeV}$ means that the scale relevant to the X particle (say, W_R boson of the right-handed interaction) must be heavier than 1.5 TeV. To allow three species of 'neutrinos', $T_d > 2\,\mathrm{GeV}$ is needed, which means an interaction scale (W_R) of $> 10\,\mathrm{TeV}$.

Table 4.13. Relativistic degrees of freedom (taking the photon as unity) and the effective number of additional 'neutrinos' at the epoch of n/p freeze-out for a light 'neutrino' decoupled in the relevant epoch.

	$\gamma + \nu$	e	μ	π	T_{QCD}	c, τ	b	$W + Z$	t
g_*	1.682	43/8	57/8	69/8	247/8	303/8	345/8	381/8	423/8
ΔN_ν		1	0.69	0.53	0.097	0.074	0.062	0.055	0.047

Thermal history after the 'first three minutes'. The photon number becomes fixed when the temperature cools to $\approx 1\,\mathrm{keV}$, at which free-free scattering and double Compton scattering that change photon numbers decouple. When extra energy is injected into the hot plasma (e.g., this applies to the photonic decay of unstable relic particles) earlier than this epoch, this increases the temperature of CMB. There will be no change in the spectroscopic feature of the CMB. The effect is absorbed into a downward shift of η estimated from nucleosynthesis arguments.

Compton scattering decouples only at $\approx 100\,\mathrm{K}$ if free electrons exist. Thermal contact of photons with matter (electrons but also protons via Coulomb interactions), however, decouples at $T \simeq 4000\,\mathrm{K}$, when electrons recombine to form neutral hydrogen [855]. Since then, photons stream freely. What we observe with the CMB is these photons last scattered off matter in this epoch. Thus the fluctuations in matter density in this epoch are imprinted in the CMB.

From $T \approx 1\,\mathrm{keV}$ to hydrogen recombination, the number of photons is conserved even if energy injection takes place. The energy injected into plasma works to distort the Planck distribution. If the injection happens in an early epoch ($T \gtrsim$ a few eV), Compton scattering is fast and brings the distribution into equilibrium described by the Bose–Einstein distribution with nonzero chemical potential $\mu \sim 1.4\Delta E/E_{\mathrm{CMB}}$, where ΔE is the injected energy. The observation tells us that $\mu < 1.3 \times 10^{-4}$ (95% CL) [829]. Later energy injection causes the blackbody spectrum to shift to the higher energy side (Sunyaev–Zeldovich effect) [856]. The observational limit on the energy injection is $\Delta E/E_{\mathrm{CMB}} < 5 \times 10^{-5}$ (95% CL) [829].

4.6.3 Universe in the Matter-Dominated Epoch

The present universe is dominated by matter (and vacuum energy). We write the matter density today as

$$\rho_0 = \Omega_0 \rho_{\mathrm{crit}} , \tag{4.202}$$

with

$$\rho_{\rm crit} = \rho_{c,0} = \frac{3H_0^2}{8\pi G}$$
$$= 1.879 \times 10^{-29} h^2 \,{\rm g\,cm^{-3}} = 10.54 h^2 \,{\rm keV\,cm^{-3}} , \quad (4.203)$$

[see (4.173)], where we use h to denote the Hubble constant in units of $100\,{\rm km\,s^{-1}Mpc^{-1}}$. This is compared to the photon energy density

$$\rho_{\gamma,0} = \frac{\pi^2}{15} T_0^4 = 0.262 \,{\rm eV\,cm^{-3}} \qquad (4.204)$$

with T_0 of (4.187). Including neutrinos, the radiation energy density is $\rho_{\rm rad} = [1 + (7/8)\cdot 3\cdot(4/11)^{4/3}]\rho_{\gamma,0}$, if ν is massless.

The epoch t of the universe is represented by redshift z, defined by

$$\frac{a_0}{a(t)} = 1 + z . \qquad (4.205)$$

Photons of wavelength $\lambda_{\rm emit}$ emitted in epoch $a(z)$ (*i.e.*, from the object which is $d = cz/H_0$ away from an observer) undergo redshift $z + 1 = \lambda_{\rm obs}/\lambda_{\rm emit}$, when viewed by an observer in the present epoch. Because the radiation energy density increases as $\rho \sim (1+z)^4$ and the matter density as $\rho \sim (1+z)^3$ towards the past, the two cross at

$$1 + z_{\rm eq} = 2.45 \times 10^4 \Omega_0 h^2 , \qquad (4.206)$$
$$T_{\rm eq} = 6.68 \Omega_0 h^2 \,{\rm eV} . \qquad (4.207)$$

Structure formation in the universe. The important feature of the matter-dominated epoch is that density perturbations grow to form cosmic structure by self-gravity.[51]

The formation of structure basically reads as follows. In some early epoch, density fluctuations are generated adiabatically. The most promising idea ascribes the origin to quantum fluctuations of Hawking radiation in the de Sitter phase of inflation [859–861], and these fluctuations are frozen into classical fluctuations in the inflation era [862]. The fluctuations are close to Gaussian noise, and their spectrum is represented as

$$P(k) \propto \langle |\delta_k|^2 \rangle \sim k^n , \qquad (4.208)$$

where n is close to unity. This noise is amplified by self-gravity in an expanding universe [863]. Fluctuations grow as the scale factor according to Newtonian theory when the universe is matter dominated and the scale considered (i.e., $\lambda = 2\pi/k$) is within the horizon. Superhorizon-scale fluctuations also grow as $\propto a^2$ in the radition dominated epoch and $\propto a$ in the matter

---

[51] We must be content with a brief sketch of this subject. For a fuller account, we refer to [857,858].

dominated epoch[52]. Due to the fact that the growth of subhorizon-scale fluctuations is halted in the radiation dominated epoch, the perturbation spectrum is modified as

$$P(k, z) = Ak^n T(k)(1 + z)^{-1}. \qquad (4.209)$$

Here $T(k)$ is the transfer function that depends on the matter content of the universe and $(1+z)^{-1}$ is the growth rate in the Einstein-de Sitter universe[53], which is a good approximation until the curvature or the cosmological constant becomes effective at low redshifts.

The transfer function $T(k) \sim 1$ for small k. For the universe dominated by cold dark matter (CDM)[54], it behaves as $\sim k^{-4}$ for large k and the transition takes place at around $k \simeq k_{eq} \simeq 2\pi/ct_{eq}$, where

$$ct_{eq} = 6.5(\Omega h)^{-1} h^{-1} \, \text{Mpc} , \qquad (4.210)$$

is the horizon scale at matter-radiation equality; see (4.207) [865]. An example of the transfer function [257, 826] is

$$T(k) = \frac{1}{(1 + a_1 k + a_2 k^2)^2} , \qquad (4.211)$$

where $a_1 \approx 8/\Omega_0 h^2$ and $a_2 \approx 4.7/(\Omega_0 h^2)^2$; see also [865,866] (Note that these coefficients scale as $\Gamma \approx \Omega_0 h$ with comoving k measured in units of $h \, \text{Mpc}^{-1}$.) Hence, the universe acts as a low-pass gravitational amplifier of cosmic noise. Empirically, the amplitude of the fluctuations that enter the horizon, $\Delta_k^2 = (k^3/2\pi^2)P(k) \propto k^3|\delta_k|_H^2 \sim k^{n-1}$, is nearly constant ($n \simeq 1$) [867] and is of the order of $\Delta_{k=H_0} \approx 10^{-5}$. The small-scale fluctuations become non-linear at $z \simeq 10-20$; the first objects form from high peaks of rare Gaussian fluctuations. As time passes, lower peaks and larger scale fluctuations enter the nonlinear regime and eventually form gravitationally bound systems that

---

[52] Note that fluctuations of a superhorizon scale do not have a definite physical meaning, because δ_k is gauge dependent. The growth here is in the gauge with which the Poisson equation holds between the gauge independent potential Φ and δ_k as in Newtonian theory.

[53] The universe with $\Omega = 1$ and a vanishing cosmological constant is called an Einstein–de Sitter universe.

[54] Dark matter that does not have thermal motion is called cold dark matter. Massive neutrinos with mass $m_\nu \ll 1 \, \text{MeV}$ decouple while they are relativistic and are classified as hot dark matter. These particles remember thermal history. If their mass is much heavier than $1 \, \text{MeV}$, they decouple after they became nonrelativistic (see the Appendix of Chap. 5). These particles are classified as cold dark matter. They do not have thermal motion in the early universe. These two classes of dark matter lead to distinctly different scenarios for cosmic structure formation. We now know that a universe dominated by hot dark matter disagrees with observations. The dark matter between the two is called 'warm.' This classification of dark matter is due to Bond [864].

decouple from the expansion of the universe. We call this state 'collapsed.' In the present epoch $(z = 0)$, objects larger than $\sim 8h^{-1}$ Mpc are still in the linear regime.

The fluctuations are characterised by a single function of the power spectrum $P(k)$ scaled to today, and the normalisation is represented by rms mass fluctuations within spheres of radius of $8h^{-1}$ Mpc:

$$\sigma_8 = \langle (\delta M/M)^2 \rangle^{1/2}|_{R=8h^{-1}\text{Mpc}} \tag{4.212}$$

$$= \frac{1}{(2\pi)^3} \int_0^\infty 4\pi k^2 dk P(k) W(kR) , \tag{4.213}$$

where $W(x) = (3j_1(x)/x)^2$ is the window function. $P(k)$ is measured by galaxy clustering [868][55] or the abundance of galaxy clusters [869] at low redshifts. The cluster abundance at $z \approx 0$ yields

$$\sigma_8 \approx 0.5\Omega^{-0.5} . \tag{4.214}$$

The fluctuations (adiabatic fluctuations) in the recombination epoch $(z \sim 1000)$ are imprinted on the CMB [870–873]. They are conveniently represented by multipoles of the temperature field as

$$\langle (\Delta T/T)^2 \rangle = \sum_\ell \frac{2\ell + 1}{4\pi} C_\ell . \tag{4.215}$$

The fluctuations at low ℓ (i.e. very large scale) is dominated by those of the gravitational potential at the last scattering surface (Sachs–Wolfe effect) [874], and are given approximately for $n = 1$,

$$C_\ell \approx A \frac{\Omega^{1.54}}{2\pi} H_0^4 \int_0^\infty \frac{j_\ell^2(kr)}{k} dk \tag{4.216}$$

$$= \frac{\Omega^{1.54}}{4\pi} \frac{H_0^4}{\ell(\ell + 1)} A , \tag{4.217}$$

where $r \simeq 2/H_0$ is the distance to the last scattering surface of CMB. Thus the fluctuations at low redshift and those at $z \approx 1000$ are tied. The coefficient A derived from the quadrupole component of CMB $Q = (5/4\pi)^{1/2}C_2^{1/2}T_0 \simeq 18 \pm 1.6\,\mu$K measured by the COBE satellite [875] (see also [876]) corresponds to $\sigma_8 \approx 1$, and thus matches the amplitude from galaxy clustering if Ω_0 is 0.2–0.4.

It was a great moment for cosmology that the COBE satellite discovered the fluctuations which were supposed to be present in the CMB [877]. The magnitude of fluctuations are exactly of the order we have anticipated from

---

[55] There is an uncertainty of a multiplicative factor as to what extent galaxies trace the actual mass distribution, called biasing. The estimate from the cluster abundance is free from this uncertainty.
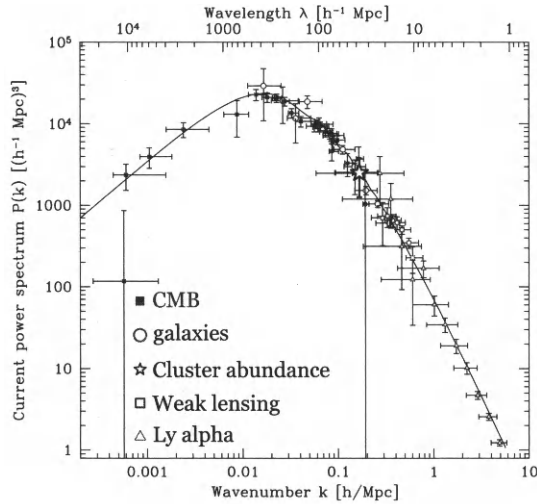
Fig. 4.25. Power spectrum of cosmological density fluctuations. Solid points are estimates from CMB fluctuations with the aid of the CDM model, and open points are low redshift clustering observations. The solid curve shows the prediction of the CDM model with a flat spectrum ($n = 1$) and cosmological parameters $H_0 = 70$ km s^{-1}Mpc^{-1}, $\Omega_0 = 0.29$, $\lambda_0 = 0.71$, and $\sigma_8 = 0.815$. After [882]

large scale clustering of galaxies using the model based on cold dark matter (CDM) dominance. The spectral index is close to unity ($n \simeq 1$), which is also expected from inflation. Analyses showed that the the power spectrum estimated from large scale galaxy clustering closely matches that derived from the CMB (COBE) when correctly scaled by the factor of $\approx 10^5$ (in amplitude) predicted in the CDM model [878, 879]. This has brought us the confidence that we are working with the correct theory of cosmic structure formation even if CDM is yet to be discovered. It is emphasised that the CDM hypothesis plays a crucial role: without CDM this matching is impossible. This statement was strengthened by recent high angular-scale observations of the CMB [850, 852, 880], which revealed a multipeak structure in the harmonics (C_ℓ) distribution. The observation is reproduced excellently by the CDM model with adiabatic perturbations [850, 852, 880, 881]. We know no other models that reproduce it.

The power spectrum scaled to zero redshift is constructed from various observations as shown in Fig. 4.25 [882]. Open points show low redshift clustering observations. In addition to galaxy clustering [868], the data from weak lensing (cosmic shear) [883] and Lyman alpha clouds [884] for small scale clustering are presented. The asterisk indicates the normalisation estimated from the cluster abundance. Solid points are estimates from CMB fluctuations with the aid of the CDM structure formation model. The solid curve is the

prediction of the CDM model with a flat spectrum ($n = 1$) and cosmological parameters $H_0 = 70$ km s^{-1}Mpc^{-1}, $\Omega_0 = 0.29$, $\lambda_0 = 0.71$, and $\sigma_8 = 0.815$.

Whether the collapsed object forms a brightly shining single entity (galaxy) or an assembly of galaxies depends on the cooling timescale (t_{cool}) compared to the dynamical timescale of the object, $t_{\mathrm{dyn}} \sim (G\rho)^{-1/2}$ [885]. For $t_{\mathrm{cool}} < t_{\mathrm{dyn}}$, the object cools and shrinks by dissipation, and stars form, shining as a (proto)galaxy. Otherwise, the object remains a virialised cloud and is observed as a group or a cluster of galaxies. In the latter case, only gravity works efficiently, so that the system is sufficiently simple to test gravitational clustering theory [857]. Galaxy formation is very complicated due to the action of the cooling process, which eventually leads to star formation, and also to feedback effects from UV radiation and supernova winds from stars. With the COBE normalisation, we expect that the first galaxies form at around $z \sim 10$. The period between $z \sim 1000$ and the epoch of first galaxy formation constitutes a dark age in cosmological history. Observationally, the highest redshift securely measured is $z = 6.3$ for a quasar [886]. How galaxies formed and evolved are the most important arena for astrophysical cosmologists today, both theoretically and observationally, but we do not discuss them further.

Cosmological parameters.[56]   The Hubble constant is now reasonably well determined. The best value [888] is

$$H_0 = (72 \pm 8) \times \begin{matrix} 1.15 \\ 0.95 \end{matrix} \, \mathrm{km\,s}^{-1}\,\mathrm{Mpc}^{-1} \, , \qquad (4.218)$$

where we have attached the error by a factor of $0.95 - 1.15$ due to the uncertainty in the distance to the LMC.[57]

Many observations indicate that mass density of the universe is significantly smaller than unity. The most likely value is

$$\Omega_0 = 0.3 \pm 0.15 \, . \qquad (4.219)$$

The cosmological constant has been an anathema to physicists for long, although the necessity has occasionally been suggested. The most recent revival in the 1990s was hinted at by the number count of galaxies as a function of magnitude [889] and by the shape of $P(k)$ [892]. A decade of studies has

---

[56] We present only the results of an analysis. We refer the reader to [887] for the basic materials that led to the present assessment and the original literature.

[57] The HST Key Project team for the Hubble constant concluded that $H_0 = 72 \pm 3 \pm 7\,\mathrm{km\,s}^{-1}\,\mathrm{Mpc}^{-1}$ in their final report [888], assigning a 5% error to the uncertainty in the LMC distance, which gives the zero point of their work. The central value and the error they adopted, however, are simply based on a "decision by majority" among many different estimates which vary wildly from 42 to 55 kpc. We do not know the origin of the systematics of the LMC distance and which distance is more reliable, so we leave the wide range of errors as it is.
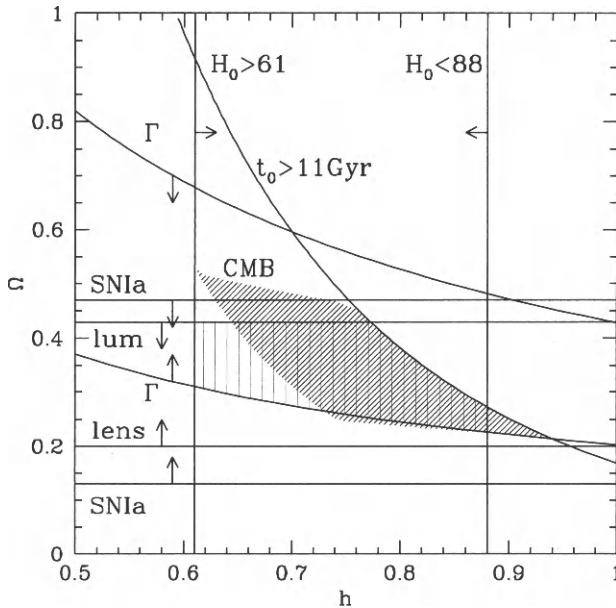
Fig. 4.26. Concordance of a global cosmological parameters in a flat Universe TBR.

revealed that we cannot avoid a nonzero cosmological constant (see [890] for the passage to the present conclusion). The brightness–distance relation of type Ia supernovae has indicated the presence of the cosmological constant in a significant excess of matter density [891]. High-resolution CMB experiments unambiguously show that the universe's curvature is close to flat [850], as already indicated by earlier experiments. The crucial information is the position of the first peak in the ℓ space. The recent analysis gives

$$\lambda_0 = (1 - \Omega_0)\ ^{+0.08}_{-0.04}\ . \tag{4.220}$$

For low matter density, this means that the presence of the cosmological constant is compelling. A nonzero cosmological constant is also required for precise matching of the CMB multipole with the power inferred from large-scale clustering of galaxies. The concordance of cosmological parameters from various observations is shown in Fig. 4.26 for flat universes. We cannot draw a consistent picture if $\lambda_0 = 0$.

The dominant part of mass comes from dark matter. Table 4.14 gives a summary as to where we need dark matter; see [894,895] for details. Massive neutrinos *cannot be* the principal component of the dark matter, as we discuss in Sect. 5.3.

The baryon mass density is given by

$$\Omega_b = 0.00367(\eta/10^{-10})h^{-2}\ . \tag{4.221}$$

Table 4.14. Evidence for the presence of dark matter.

Item		Observation	Assumption	Refs.	ν as dark matter?
Cluster M/L		$M/L = (250-400)h$			$m_\nu > 2\,\text{eV}$
	M	Velocity dispersion	Well-virialised	[896]	
	M	X-ray emission	Hydrostatic equil.	[897]	
	M	Gravitational lensing		[898]	
CMB fluctuations	σ_8	$\sigma_8(\text{COBE}) = \sigma_8(\text{clusters})$	Clustering theory	[878]	$\sum m_{\nu_i} < 2-4\,\text{eV}$
	C_ℓ	Harmonics distribution	Clustering theory	[881]	$\sum m_{\nu_i} < 2-4\,\text{eV}$
$\Omega_b < \Omega_0$		$\Omega_0/\Omega_b = 5-10$			$\sum m_{\nu_i} > 10\,\text{eV}$
	Ω_b	Primordial nucleosynthesis			
	Ω_b	Local baryon abundance		[893]	
	Ω_0	Many methods (Fig. 4.26)			
Milky Way M/L		$M/L \simeq 70$ at $r = 100\,\text{kpc}$			$m_\nu > 30\,\text{eV}$
	M	Satellite galaxy motion	Stationary state	[899]	
	M	Magellanic stream	Model fit	[900]	
	M	M31+MW kinematics	Bound system	[901]	
Normal galaxies M/L		$M/L = (100-250)h$			$m_\nu > 30\,\text{eV}$
	M	Satellite galaxy motion	Bound system	[902]	
	M	Gravit. lensing shear field		[903]	
	$M(r)$	Flat rotation curve[a]	Simplest interpret.	[904]	
Normal galaxies		Disc stability	Theor. argument	[906]	$m_\nu > 30\,\text{eV}$
Dwarf sph M/L					$m_\nu > 500\,\text{eV}$
	M	Velocity dispersion[b]	Nonatmospheric	[907]	

[a] This flat rotational curve itself cannot be taken as compelling evidence for dark matter. Although its simplest interpretation is to assume the presence of an isothermal dark matter halo, the flat rotational curve can also be reproduced by a disc plus a bulge component alone for most galaxies [905].

[b] M/L is not universal. The evidence comes from Draco and Ursa Major. Some dwarf spheroidals do not show evidence for dark matter.

For $\eta = (4.5-6.0) \times 10^{-10}$ and $h = 0.7$, we find that $\Omega_b = 0.045$, roughly a factor of 5 smaller than the total mass density. This gap is filled by cold dark matter. The baryon density locked up in stars is about $\Omega_b = 0.003-0.005$, one-tenth the total baryon density. A similar amount of baryons is in the hot gas and is observable with X rays, but most baryons reside in warm gas, which is hard to detect [893]. Massive neutrinos contribute to Ω_0 by

$$\Omega_\nu = 0.0107h^{-2}m_\nu(\text{eV}) . \qquad (4.222)$$

It is interesting to note that the universe is filled predominantly with invisible components: 70% vacuum energy, 25% dark matter, and 4% baryons that escape detection; only 1% is visible. We emphasise that modern successful cosmological theories assume (i) the presence of a cosmological constant, (ii) the presence of cold dark matter, and (iii) inflation as a mechanism to generate density fluctuations.

4.7 Geophysical Neutrinos

Earth generates heat at a rate of $\approx 40\,\mathrm{TW}$ (4×10^{20} erg/s), which gives a value of $6.7\times10^{-8}\,\mathrm{erg\,s^{-1}g^{-1}}$ when divided by the mass of Earth, 5.97×10^{29} g. In the conventional view, this heat is ascribed to the radioactivity of uranium, thorium, and potassium contained in the crust. The decay chains of ^{238}U and ^{232}Th are shown in Table 4.15. An estimate of the heat from radioactivity is given in Table 4.16 [908]. This accounts for 60% of the total heat. The next important entry is ^{87}Rb, but its contribution is less than 1%.

Antineutrinos are emitted in the decay process. The possibility of detecting such antineutrinos was discussed by Eder (1966), just after the proposal of a solar neutrino experiment [909], and then by a few authors [816,910–912]. The neutrino flux can be calculated as

$$
\begin{aligned}
F_\nu &= \frac{1}{4\pi}\int r^2 dr\, d\Omega \,\frac{1}{(R_\oplus - r\cos\theta)^2 + (r\sin\theta)^2} f_\nu(r) \\
&= \frac{1}{2R_\oplus}\int_0^{R_\oplus} r\, dr \ln\frac{1+r/R}{1-r/R} f_\nu(r) ,
\end{aligned}
\tag{4.223}
$$

Table 4.15. Naturally occurring radioactive decay series.

Isotope	Name	$\tau_{1/2}$	$E_\beta^{\max}$ (MeV)	Isotope	Name	$\tau_{1/2}$	$E_\beta^{\max}$ (MeV)
^{238}U	UI	$4.47\cdot10^9$ y		^{232}Th	Th	$1.41\cdot10^{10}$ y	
$\alpha\downarrow$				$\alpha\downarrow$			
^{234}Th	UX$_1$	24.1 d		^{228}Ra	MsTh$_1$	5.76 y	
$\beta\downarrow$			0.18	$\beta\downarrow$			0.05
^{234m}Pa	UX$_2$	1.175 m		^{228}Ac	MsTh$_2$	6.13 h	
^{234}Pa	UZ	6.75 h		$\beta\downarrow$			2.14
$\beta\downarrow$			2.29	^{228}Th	RdTh	1.913 y	
^{234}U	UII	$2.45\cdot10^5$ y		$\alpha\downarrow$			
$\alpha\downarrow$				^{224}Ra	ThX	3.66 d	
^{230}Th	Io	$8.0\cdot10^4$ y		$\alpha\downarrow$			
$\alpha\downarrow$				^{220}Rn	Tn	55.6 s	
^{226}Ra	Ra	$1.60\cdot10^3$ y		$\alpha\downarrow$			
$\alpha\downarrow$				^{216}Po	ThA	0.15 s	
^{222}Rn	Rn	3.824 d		$\alpha\downarrow$			
$\alpha\downarrow$				^{212}Pb	ThB	10.64 h	
^{218}Po	RaA	3.05 m		$\beta\downarrow$			0.57
$\alpha\downarrow$				^{212}Bi	ThC	60.60 m	
^{214}Pb	RaB	26.8 m		$\beta\downarrow$			2.25
$\beta\downarrow$			1.02	^{212}Po	ThC$'$	0.30 μs	
^{214}Bi	RaC	19.7 m		$\alpha\downarrow$			
$\beta\downarrow$			3.27	^{208}Pb	ThD	Stable	
^{214}Po	RaC$'$	0.164 ms					
$\alpha\downarrow$							
^{210}Pb	RaD	22.3 y					
$\beta\downarrow$			0.06				
^{210}Bi	RaE	5.01 d					
$\beta\downarrow$			1.16				
^{210}Po	RaF	138.4 d					
$\alpha\downarrow$							
^{206}Pb	RaG	Stable					

For ^{212}Bi (ThC), a branch: $\alpha\searrow$ ^{208}Tl ThC$''$ 3.05 m, $\beta\swarrow$ 1.79

Table 4.16. Radioactive elements as the source of terrestrial heat.

Element	Heat production	Mean abundance	Terr. heat
K	$3.6 \times 10^{-5}\,\mathrm{erg\,s^{-1}g^{-1}}$	$170\,\mathrm{ppm}$	$3.7\,\mathrm{TW}$
U	$0.97\,\mathrm{erg\,s^{-1}g^{-1}}$	$18 \times 10^{-3}\,\mathrm{ppm}$	$10.4\,\mathrm{TW}$
Th	$0.27\,\mathrm{erg\,s^{-1}g^{-1}}$	$65 \times 10^{-3}\,\mathrm{ppm}$	$10.5\,\mathrm{TW}$
Sum			$24.6\,\mathrm{TW}$

if the radioactive elements are spherically distributed [815]. Here, $f_\nu(r)$ is the neutrino source function per unit volume at radius r from the centre of Earth. Usually, we consider that all of these elements are in the crust, so that the integration is done for a thin crust whose thickness is of the order of 30 km.

The energy spectrum is calculated by adding all beta decay spectra for elements in the decay chain. The abundance N_k of elements k is governed by

$$\dot{N}_1 = -\lambda_1 N_1 \,,$$
$$\dot{N}_2 = -\lambda_2 N_2 + \lambda_1 N_1 \,,$$
$$\cdots \qquad\qquad , \qquad\qquad (4.224)$$

which is integrated to give

$$N_k/N_{k-1} = \lambda_{k-1}/\lambda_k \,, \qquad\qquad (4.225)$$

where λ_k is the decay rate and $t \gg \lambda_k^{-1}$ ($k \neq 1$) is assumed (radiation equilibrium). The neutrino source function is

$$f_\nu = \sum_{i,k} N_k B(i;k)\phi(i,k;E) \,, \qquad\qquad (4.226)$$

where i is the decay channel, ϕ is the neutrino spectrum, and B is the branching fraction. The highest energy neutrino comes from ^{214}Bi (Ra C) ($E_\mathrm{max} = 3.271\,\mathrm{MeV}$) in the ^{238}U chain. ^{212}Bi ($E_\mathrm{max} = 2.246\,\mathrm{MeV}$), ^{228}Ac ($E_\mathrm{max} = 2.078\,\mathrm{MeV}$), both in the ^{232}Th chain, and ^{234}Pa ($E_\mathrm{max} = 2.29\,\mathrm{MeV}$) in the ^{238}U chain follow. There are many decay channels that produce $\approx$1-MeV antineutrinos. ^{40}K produces 1.5-MeV neutrinos (EC) in addition to 1.3-MeV antineutrinos. Antineutrinos from superheavy elements, as discussed here, show a spectrum largely skewed toward the high-energy end due to a large correction of the Fermi function of electron emission. This gives a unique feature for geological neutrinos. These antineutrinos are superposed on reactor antineutrinos as shown in Fig. 4.27, which is taken from Raghavan et al. [913].

The authors of [913] take the radiogenic heat from uranium and thorium as 16 TW [914], 5 TW smaller than given in our budget table. In fact, the estimates of both total heat and crustal abundance of radioactive elements

have substantial uncertainties, and it is not quite clear yet whether the discrepancy in the energy budget (40 TW versus 20−25 TW) is serious. The total potassium abundance is also uncertain; it may be dissolved in the mantle, and the core in bulk. The detection of antineutrinos from Ra C would verify the uranium abundance, which will be the first step in verifying the conventional energetics model discussed here. Using the KamLAND detector, one expects ≈50 events a year, while 700 events are expected from reactor neutrinos
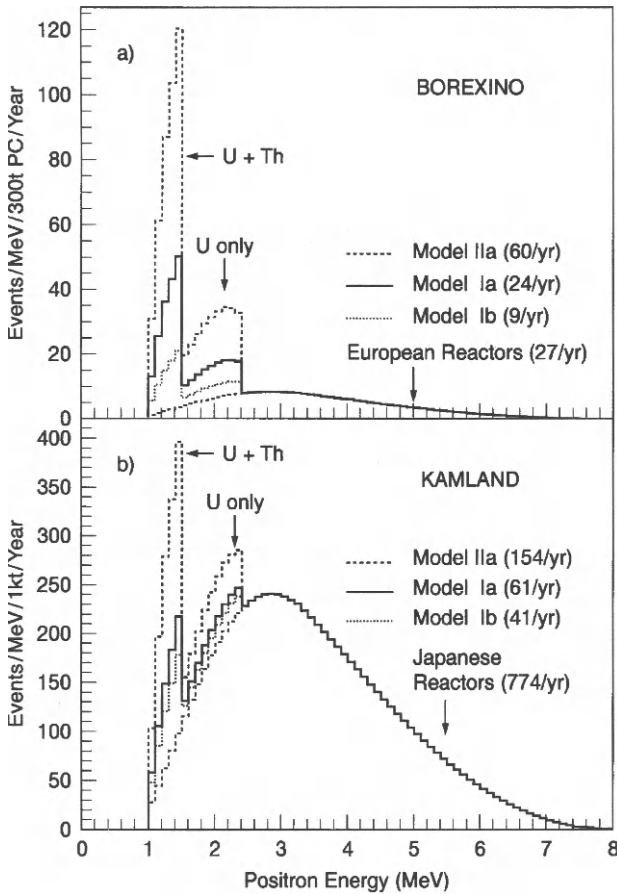
Fig. 4.27. Antineutrino spectrum from ^{238}U and ^{232}Th deposited in Earth's crust, expected in Borexino and KamLAND neutrino detectors. The three curves show different models: Ia and Ib correspond to two different models with the estimated crustal abundance of U/Th [914]; II assumes a full 40 TW ascribed to U/Th radioactivity. Model a employs an estimated distribution of crustal U/Th [914], and b assumes a uniform distribution in the crust. After [913].

(the KamLAND site is much noisier than the Borexino site). Nevertheless, geophysical antineutrinos would produce visible signals within one year of the operation.

4.8 Detection of Low-Energy Neutrinos

4.8.1 Overview of Neutrino Detectors

The detection of neutrinos requires massive detectors. Detection of low-energy neutrinos is particularly difficult because of small cross sections and a small energy deposit, whereas a large background is expected from cosmic rays, cosmic-ray-induced particles, and natural radioactivity. The cross section of $10^{-41}\,\mathrm{cm^2}$ ($\bar{\nu}p$ at $10\,\mathrm{MeV}$) corresponds to a mean free path of $1.7 \times 10^{17}\,\mathrm{g\,cm^{-2}}$. Bethe and Peierls (1934) [71], who estimated the neutrino-induced reaction (called inverse beta decay) for the first time, concluded that "there is no practically possible way of observing the neutrinos." In fact, one needs at least $100\,\mathrm{kg}$ to $1000\,\mathrm{ton}$ of target material to have one event a day of low-energy neutrino reactions for a neutrino flux of $10^{8\pm1}\,\mathrm{cm^{-2}s^{-1}}$. Nevertheless, the progress in detector technology was so great that it was possible to detect the neutrino by the mid-1950s. Reines and Cowan (1953) [91, 93] succeeded in detecting electron antineutrinos from a nuclear reactor, thus directly confirming the existence of the neutrino. This became possible by the invention of organic scintillators [88, 89], which made the construction of a massive detector feasible at an affordable cost. Reines and Cowan used a 300-litre scintillator (at that time it was a huge detector; the detector was upgraded to hold 1400 litres in their 1956 experiment) consisting predominantly of triethylbenzene (TEB) with an admixture of a small amount of fluor and a wavelength shifter. Efficient background reduction is achieved by delayed coincidence of positron signals with γ rays which are emitted upon absorption of a neutron into cadmium (which has a large neutron capture cross section) doped in the detector. In parallel, an experiment using a ^{37}Cl target, first proposed by Pontecorvo (1946) [80] and studied further by Alvarez (1949) [81], was initiated by Davis to detect reactor (anti)neutrinos. The experiment uses radiochemistry, extracting neutrino-induced radioactive argon produced in a large tank ($3900\,\ell$) filled with carbon tetrachloride ($\mathrm{CCl_4}$), and collecting it in a small vessel for radioactivity counting [94]. This was a precursor of the solar neutrino experiment, which used a much larger tank deep underground at the Homestake gold mine (using $\mathrm{C_2Cl_4}$) [207]. This experiment motivated Kuzmin (1966) [230] to propose another radiochemical experiment using ^{71}Ga to detect yet lower energy pp solar neutrinos. It took 25 years to yield the first result. In the meantime spark chamber technology was invented [101]. This also allowed constructing massive detectors at modest cost and soon led to the discovery of muon neutrinos using a high-energy accelerator neutrino beam [100]. Spark chamber technology since then

has been used not only for neutrino experiments but also for many other experiments. This counter technique, however, cannot be applied to low-energy neutrino detection because the energy deposit is too small. Another line of development is driven by successful reduction of the background events in a massive water Čerenkov detector to observe the feeble light from recoil electrons of $\nu e \to \nu e$ scattering by the Kamiokande group [228]. This opens the possibility of constructing a multikiloton detector at modest cost.

Since these pioneering experiments, continuous advancement has been made in low-energy neutrino detection techniques, and successively larger detectors have been constructed. There is, however, no drastic change in the basic principles. The detection either observes recoil electrons of $\nu_e e \to \nu_e e$ or those produced in neutrino captures in a nucleus using scintillation or Čerenkov light, or counts the yield of nuclei produced in neutrino reactions. These two types of detection are often referred to as 'real time detection' and 'radiochemical detection.' We show in Table 4.17 a summary of major detectors for low-energy neutrino experiments that are currently operating or under construction. The original Reines–Cowan apparatus is included for comparison.

4.8.2 Detection of Electrons: Čerenkov Light

The energy spectrum of a recoil electron from νe scattering is

$$\frac{dN}{dT} = N_e \int dE_\nu \phi_\nu(E_\nu) \frac{d\sigma(E_\nu)}{dT} \; , \qquad (4.227)$$

where $d\sigma/dT$ is given in (3.129). For neutrino captures on nuclei, the energy of an electron is simply determined by the incident neutrino energy,

$$E_e = E_\nu - Q \; . \qquad (4.228)$$

There are two different principles used for electron detection: Čerenkov radiation and scintillation. In this section we discuss Čerenkov radiation [925].

When a charged particle moves in a dielectric medium, the speed of light is no longer "light velocity," and energy-momentum conservation is satisfied for the process $e \to e + \gamma$. Let us write (p, E) and (p', E') for the initial and the final electron energy momenta and k and ω for the photon wavenumber and energy, where $k = n\omega$ with n the refractivity (=dielectric constant squared). The energy conservation is

$$E = \sqrt{m_e^2 + (\mathbf{p} - \mathbf{k})^2} + \omega$$
$$\simeq E - \frac{pk}{E} \cos\theta + \omega \; , \qquad (4.229)$$

where

$$\cos\theta = 1/n\beta \; , \qquad (4.230)$$

Table 4.17. Major detectors for low-energy neutrino experiments.

Experiment	Depth (mwe)	Detector	Reaction	Main source	Active volume	Event/day[a]
Kamiokande [915]	2700	H_2O Č	νe, $\nu(p,O)$	Solar ν, > 7.5 MeV, atmospheric ν	3000 ton	0.29
Super-Kamiokande [916]	2700	H_2O Č	νe, $\nu(p,O)$	Solar ν, > 5 MeV, atmospheric ν	50,000 ton	14, 8.3
SNO [917]	6010	D_2O Č	νd	Solar ν CC/NC	1000 ton	
IMB [918]	1570	H_2O Č	$\nu(p,O)$	atmospheric ν	8000 ton	
Borexino [919]	3600	PC, sci	νe	Solar ν ^{7}Be	300 ton	46 (SSM)
KamLAND I [543]	2700	Dodecane+PC, sci	$\bar{\nu}p$	Reactor $\bar{\nu}$, > 1.8 MeV	1000 ton	~ 1
II			νe	Solar ν ^{7}Be		200 (SSM)
Homestake [721]	4200	C_2Cl_4, RC	$\nu^{37}Cl$	Solar ν ^{7}Be+^{8}B	615 ton	0.48
Gallex/GNO [920]	3600	$GaCl_3$, RC	$\nu^{71}Ga$	Solar ν pp+^{7}Be+^{8}B	30.3 ton (Ga)	1.5
SAGE [231,725]	4715	Metallic Ga, RC	$\nu^{71}Ga$	Solar ν pp+^{7}Be+^{8}B	30 ton	1.5
Reines et al. [93]		TEB(+Cd), sci	$\bar{\nu}p$	Reactor $\bar{\nu}$, > 1.8 MeV	300 ℓ	
Gösgen [544]		MO, sci+MWPC	$\bar{\nu}p$	Reactor $\bar{\nu}$, > 1.8 MeV	377 ℓ	24–76
LSND [921]		MO, sci	$\bar{\nu}p$,^{12}C	Stopped muon	167 ton	
KARMEN [922]		MO+PC, sci	$\bar{\nu}p$,^{12}C	Stopped muon	65000 ℓ	
CHOOZ [923]		MO(+Gd), sci	$\bar{\nu}p$	Reactor $\bar{\nu}$, > 1.8 MeV	5 ton	25
Palo Verde [924]		MO+PC(+Gd), sci	$\bar{\nu}p$	Reactor $\bar{\nu}$, > 1.8 MeV	11 ton	85

[a] Event rates are given per fiducial volume rather than active volume of the detector.
Acronyms of detectors: Kamiokande = Kamioka Nucleon Decay Experiment; SNO = Sudbury Neutrino Observatory; IMB=Irvine-Michigan-Brookhaven collaboration, KamLAND = Kamioka Liquid Scintillator AntiNeutrino Detector; GNO = Gallium Neutrino Observatory; SAGE = Soviet-American Gallium Experiment; LSND = Liquid Scintillator Neutrino Detector; KARMEN = Karlsruhe-Rutherford Medium Energy Neutrino Experiment.
Other abbreviations: PC=pseudocumene; MO=mineral oil (paraffinic oil); Č=Čerenkov detector; sci=scintillation detector; MWPC=multiwire proportional counter; RC=radiochemical experiment; TEB=triethylbenzene; SSM=standard solar model prediction.

θ is the angle between the initial electron and the emitted photon, and β is the velocity of the electron. As a particle moves, these emitted photons form a wavefront with the half-angle θ with respect to the direction of electron motion. The radiation is distributed over the surface of a cone. The condition (threshold) for radiation is $\beta > 1/n$.

The calculation of this photon emission is elementary. The Lagrangian of the electromagnetic field in dielectric media is given by

$$\mathcal{L} = \frac{\varepsilon}{2}\mathbf{E}^2 - \frac{1}{2\mu}\mathbf{H}^2 \,, \tag{4.231}$$

with $\mu = 1$ and $\varepsilon\mu = n^2$. The matrix element is

$$S = \int d^4x \langle p', (k\omega)|ie\bar{\psi}\gamma_\mu A^\mu \psi|p\rangle \,, \tag{4.232}$$

where we must use

$$A_\mu = n^{-1}\sum_k \frac{1}{\sqrt{2\omega_k V}} a_k e^{-ikx} + \text{h.c.} \tag{4.233}$$

with n^{-1} in front to satisfy the correct canonical commutation relation $[A, \pi] = i\delta^3(x - x')$ or $[A, \dot{A}] = in^{-2}\delta^3(x - x')$. The electron field ψ is the usual plane wave expansion with box normalisation. The transition rate per unit length x is

$$\begin{aligned}
\frac{d\Gamma}{dx} &= \frac{|S|^2}{vT} \\
&= \frac{e^2}{n^2v}\frac{1}{2E}\int \frac{d^3p'}{(2E')(2\pi)^3}\frac{d^3k'}{(2\omega)(2\pi)^3}(2\pi)^4\delta^4(p - p' - k')|\bar{u}'\gamma^\mu u \, \epsilon_\mu|^2 \\
&= \alpha\int d\omega[1 - \cos^2\theta(\omega)] \,.
\end{aligned} \tag{4.234}$$

Here $T \to \infty$ is the time for the transition. Therefore, the energy loss rate due to Čerenkov radiation is

$$-dE/dx = \alpha\omega\left(1 - \frac{1}{n^2\beta^2}\right)d\omega \,. \tag{4.235}$$

The natural cutoff for a short wavelength is the plasma frequency $\omega_p = (4\pi n_e\alpha/m_e)^{1/2}$, where the dielectric constant $\varepsilon(\omega) = 1 - \omega_p/\omega$ vanishes; but in practice, photons useful for detection are those that do not receive too strong Rayleigh scattering or absorption and fall in the sensitivity range of photomultiplier tubes (PMT), which usually extends from $3000-3500\,\text{Å}$ to

4500−5000 Å.[58] With the effective quantum efficiency $q(\omega)$ (including the light collection efficiency) and the path length L, the number of photoelectrons observed in a detector is

$$N_{\text{p.e.}} = \alpha L \langle \sin^2 \theta \rangle \int d\omega q(\omega) e^{-\ell/\lambda(\omega)}$$

$$= 370 (\text{eV} \cdot \text{cm})^{-1} L(\text{cm}) \langle \sin^2 \theta \rangle \int d\omega q(\omega) e^{-\ell/\lambda(\omega)} , \quad (4.236)$$

where $\lambda(\omega)$ is the attenuation length in the medium ($\approx 50\,\text{m}$ [926] for water at 4000 Å) and ℓ is the length to the detector. The typical quantum efficiency of bialkali cathodes (Sb–Rb–Cs) is 30% at maximum, so that $\int d\omega q(\omega) \approx 0.28\,\text{eV}$ (see Fig. 4.28), assuming a 100% photon collection efficiency. For a water detector the plasma frequency is 21 eV, but transparency rapidly diminishes below 3000 Å due to Rayleigh scattering which increases as $\sim \lambda^{-4}$. The refraction index of water $n \simeq 1.33$ varies little in the UV to optical region that concerns us. The emission angle is $\theta = 41°$ in the high-energy limit. It differs little for the electron energy of interest to us. An electron produces a ring across PMTs installed on the wall of the apparatus. For a 10 MeV electron in water $N_{\text{p.e.}} \approx 370 \times 4.5(E_e/10\,\text{MeV}) \times 0.43 \times 0.28 \times 0.2 \times 0.82 \simeq 3.3 E_e(\text{MeV})$, where we assume 20% coverage of PMT's (Kamiokande), and a length of 10 m from the track to the detector. An empirical value of the Kamiokande detector is $N_{\text{p.e.}} \simeq 3 E_e$ (MeV) [915].

The photon energy emitted in the wavelength range that is useful to Čerenkov light detection is about 1 keV per 1 cm path length. Efficiency, as defined by the ratio to the loss energy of the incident particle, which is about 2 MeV per gramme, is 5×10^{-4}. Most of the Čerenkov photon energy resides in the far UV region and is lost by scattering or absorption in the material.

The Kamiokande group demonstrated that one can decrease the detection threshold for electrons from $\nu e \to \nu e$ scattering from a point neutrino source to 7.5 MeV and thus can detect ^{8}B solar neutrinos with a water Čerenkov detector [228]. An important element here was a large fraction of PMT coverage using a large format (50-cm aperture) PMT specifically designed for Kamiokande [928]. The detector became ready for solar neutrino detection in February 1987, and the detection of neutrinos from supernova SN1987A

---

[58] Ordinary photomultipliers use bialkali (Cs–K–Sb or Cs–Rb–Sb) or trialkali (Na–K–Cs–Sb) cathodes, and the sensitivity extends to 3000 Å. The transmission of glass (e.g., borosilicate BK7 glass), however, sharply drops short of 3500 Å. To enhance transmission shortwards, one needs to use ultraviolet transparent glass UBK7, or quartz, which are more expensive. Modern photomultipliers attain high sensitivity to 2000 Å with Cs–Te cathodes and CaF_2 or MgF_2 as the window material. We note, however, that the extension of the gain into the ultraviolet is not worth much (it could even be worse) because such UV photons are dominated by scattered light that diffuses both positional and energy information.
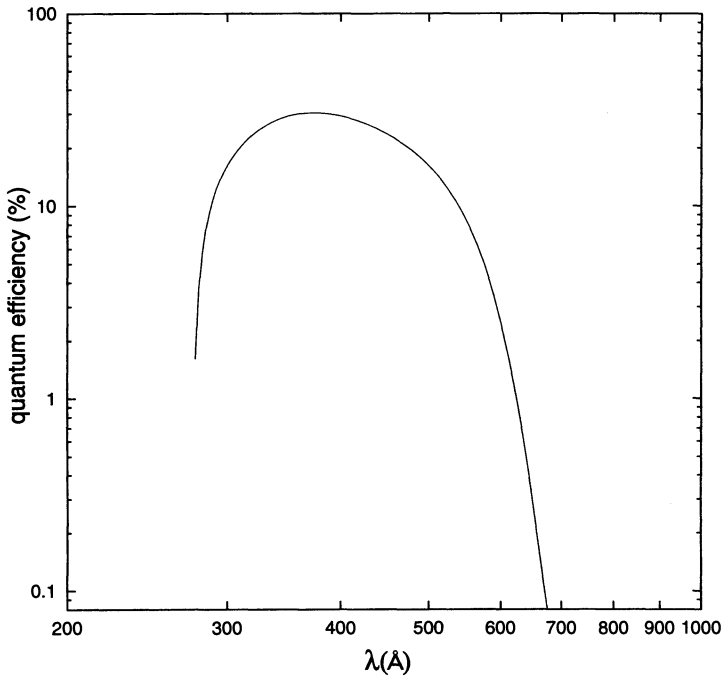
Fig. 4.28. Quantum efficiency of typical photomultipliers. The example is a Type 400K bialkali cathode of Hamamatsu Photonics with borosilicate glass windows [927].

was a wonderful gift [757]. The successor, Super-Kamiokande, was designed to decrease the detection threshold to 5 MeV by increasing the PMT covering density by a factor of 2 and also to decrease systematic errors arising from energy calibration and uncertainties of the energy and angular resolutions. The aim is to measure the energy spectrum of ^{8}B neutrinos, as well as to increase the event rate for a highly precise determination of neutrino flux.

The water Čerenkov detector observes electrons and also muons if $E_\mu > 160$ MeV $(T_\mu > 55$ MeV). The pattern of rings are distinctively different between electrons and muons. The ring produced by an electron exhibits a more diffuse pattern due to multiple Coulomb scattering that affects electrons more strongly, and electromagnetic showers. They are distinguished by evaluating relative likelihoods computed for events over relevant PMT's, provided that the coverage of PMT's is sufficiently large. Kamiokande's Monte Carlo calculation showed that the two cases are virtually non-overlapping in the likelihood plane, and achieved 98% discrimination between the two particles [929]. This was a crucial element in discovering neutrino oscillation in atmospheric neutrinos.

The detector of IMB was similar in concept, but the detection threshold was 20 MeV. A more recent apparatus at SNO is equipped with 1000 tons of heavy water [234, 235]. The aim is to detect Čerenkov light from electrons produced in $\nu_e + d \to e^+ + n + n$ in addition to those from νe scattering. The requirement for background noise reduction is stronger than for the Kamiokande since the electron produced in νd scattering has a mild angular dependence. The detection threshold is 6.5 MeV. The advantage is a large cross section of the neutrino–deuterium cross section, and a unique feature is that $\nu_e + d \to e^+ + n + n$ measures purely charged-current-induced neutrino reactions for ^{8}B solar neutrinos. Another important aim of the heavy water detector is to measure the neutral-current reaction $\nu + d \to \nu + p + n$ by detecting a γ ray of 6.25 MeV (mostly via Compton scattering and partly conversion into an e^+e^- pair) emitted by $n + d \to \gamma + ^3$ H. The neutron capture efficiency is 25%. This will be enhanced to 45% by dissolving 2.5 tons of NaCl as a neutron absorber and detecting 8.6-MeV γ rays from $n+^{35}$Cl.

The energy resolution of the water Čerenkov detector primarily depends on the total number of photoelectrons; with 20% coverage of the detector surface using 950 50-cmϕ PMTs, Kamiokande achieved [915]

$$\frac{\sigma(E)}{E} \approx \frac{0.63}{\sqrt{E}} \tag{4.237}$$

for $E \lesssim 12$ MeV, where energy is in units of MeV. The square root reflects the nature of photon statistics. The density of photomultipliers in the Super-Kamiokande is twice as high (40% coverage of the surface with 11000 PMTs), so that the resolution is $\approx 0.46/\sqrt{E}$, a factor of $\sqrt{2}$ increase, compared to the Kamiokande [930].

The energy calibration constitutes an important part of low-energy neutrino detection. The Super-Kamiokande uses an electron linear accelerator specifically for this purpose and supplements it with artificial radioactivity (6.13 MeV γ) generated by $n +^{16}$ O $\to p +^{16}$ N using a neutron generator of $d + t \to$ He $+ n$ (this radioactive source is used for calibration for upward going electrons). They have achieved a systematic error smaller than $< 0.64\%$, which results in a 1.5% error in the final neutrino flux [931]. The energy resolution was also measured to within 2.5% accuracy. SNO uses artificial ^{16}N, $p + t \to^3$ He $+ \gamma$ (19.8 MeV) and ^{8}Li (14 MeV β) for energy calibration.

4.8.3 Detection of Electrons: Scintillation

When a charged particle passes through matter, a wake of excited atoms (molecules) is produced by the pulsed electric field generated by the charged particle. This leads to an energy loss of charged particles moving through matter, as described by the Bethe–Bloch formula [932, 933],

$$-\frac{dE}{dx} = \frac{4\pi Z^2 \alpha^2 n_e}{\beta^2 m_e} \left[\ln \frac{2\beta^2 m_e}{\bar{I}(1-\beta^2)} - \beta^2 \right] , \tag{4.238}$$

where dE is the energy loss while a charged particle travels the distance dx, β is the velocity of a charged particle, n_e is the electron number density of matter, $\overline{I} \approx 13.5Z$ eV is the mean ionisation energy,[59] and m_e is electron mass. An elementary derivation of this formula basically due to Bohr [935], in a classical approximation, is given in the textbook by Fermi [936], pp. 27–30. For electrons, we must consider the exchange interaction, and the energy loss is given by [937]

$$-\frac{dE}{dx} = \frac{2\pi\alpha^2 n_e}{\beta^2 m_e}\left[\ln\frac{\beta^2 m_e T_e}{2\overline{I}^2(1-\beta^2)} - (2\sqrt{1-\beta^2}-1+\beta^2)\ln 2 + 1 - \beta^2\right],$$
$$(4.239)$$

where T_e is the kinetic energy of the electron. The energy loss for an electron is smaller than (4.238) by only a few percent. The curves for electrons and muons are presented in Fig. 4.29.[60] This shows that the energy loss is about $\rho dE/dx = 2$–$3\,\mathrm{MeV/g\,cm^2}$ for a wide range of energy of a moving particle. It increases only slowly towards high energies.[61]
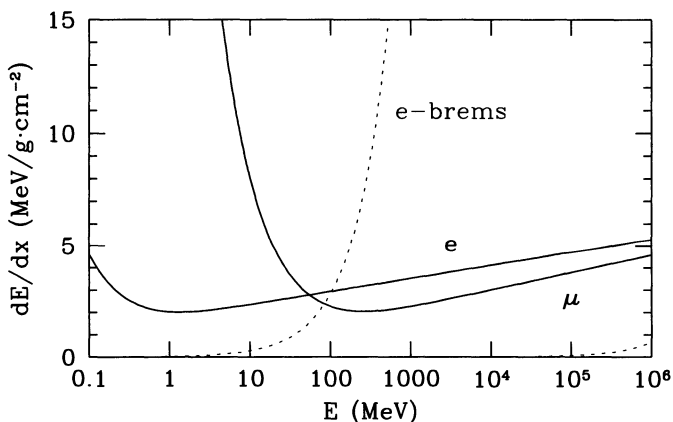
Fig. 4.29. Ionisation energy losses for an electron and a muon in water, (4.238) and (4.239). The density effect is not included. The energy loss of an electron by bremsstrahlung is shown for comparison (*dotted curve*).

---

[59] $\overline{I}$ is the mean ionisation potential of the atom, taking into account that there are electrons at many different energy levels in the atoms of the material which are ejected by a moving charged particle. It is a difficult task to calculate this $\overline{I}$, and an empirical value is used. See [934].

[60] The figure is drawn by a straightforward evaluation of the formulae given here. More accurately, the formulae receive a density correction, which suppresses the ionisation rate from increasing logarithmically at very high energies [938].

[61] Another important energy loss is due to bremsstrahlung, which is proportional to E/X_0 with X_0 the radiation length. For the electron the ionisation loss dominates for $E < 80\,\mathrm{MeV}$, and for the muon $E < 1\,\mathrm{TeV}$. [See footnote after (4.17).]

In some materials, a part of this energy is used to reemit photons. If these photons are not absorbed by the material itself, these photons can be detected as a signal of a charged particle. This is called scintillation. Typical examples of such materials are NaI, ZnS, CsI, and many organic materials that contain aromatic rings. Noble-gas liquids such as Ar, Ne, Xe emit scintillation in the far UV region.

Although solid materials (inorganic crystals and plastic) are used for high-energy particle detectors, liquid scintillators, with which one can construct massive detectors relatively easily, are particularly important in neutrino detection. The scintillating material, which is rich in protons, itself is used as a neutrino target. We briefly describe the principle and applications of the liquid scintillator, and refer to [939, 940] for details.

A typical liquid scintillator uses two aromatic materials, the solvent and the solute. The solvent itself emits light, but the light yield is usually small due to self-absorption. The yield is largely enhanced if another material (fluor) is added [89]. The mechanism of scintillation in organic material is as follows: (1) the lost energy of a moving particle is used to excite or ionise molecules of the material (solvent) around the particle; (2) this energy is transferred to other molecules in the solvent; (3) the transfer occasionally takes place between a molecule in the solvent and a solute molecule; and (4) fluorescent light is emitted by the transition from an excited state to the ground state of a solute molecule.

A typical solvent is a material that contains many π bonds, which are rather unstable and transfer energy efficiently from one molecule to another. (The excitation of σ electrons undergoes mainly thermal dissipation.) π electrons exist abundantly in unsaturated chemical bonds, which are numerous in aromatic compounds. There are a number of energy transfer mechanisms; the most important are dipole–dipole interaction and the formation of intermediate states (excimers). When a solute molecule is excited, emission of fluorescent light takes place in the electronic transition of excited molecules in $1-10$ ns. Almost all known fluorescent light emission results from the singlet–singlet transition between the first excited and the ground states. (The transition of a triplet to a singlet is much slower ($> 10^{-4}$ s), categorised as phosphorescence.) The spectrum appears as a 'continuum' due to the presence of many vibrational and rotational states. Fluorescence frequently occurs in unsaturated compounds with π electron bonds.

It is important that the emitted light is not reabsorbed by the solvent (colour quenching). Although most solvent used in a scintillator is itself an emitter of fluorescent light, a large fraction of the emitted light is immediately absorbed by solvent molecules and does not work as a scintillator. It is also important to find a solvent for which the energy loss from energy transfer (chemical quenching) between molecules is small. Oxygen is highly electron accepting and gives a large chemical quenching effect, so that one needs to reduce the amount of oxygen dissolved in the solvent. It is also practi-
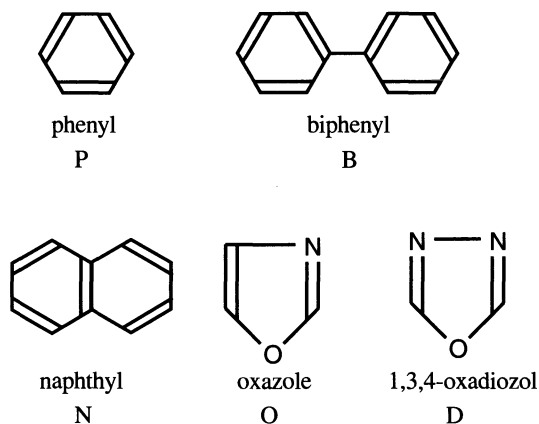
Fig. 4.30. Radicals that appear in scintillator chemistry: P, B, N, O, and D.

cally important to match the emitted spectrum with the sensitivity of the photomultiplier. When the emission spectrum does not match the detector sensitivity, a wavelength shifter is added as a second solute. For a discussion of light propagation from a practical point of view, see [943].

The most commonly used solvents are benzene, toluene (=methylbenzene), xylene (= 1,2 dimethylbenzene), and pseudocumene (1-2-4 trimethylbenzene; C_9H_{12}). Solutes (fluors) are often somewhat more unusual chemical compounds. The name of the compound is customarily represented by an abbreviation for the radical: P (phenyl), B (biphenyl), N (naphthyl), O (oxazone), and D (1,3,4-oxadiazole); the chemical structures are given in Fig. 4.30 (see also Fig. 4.31 for typical examples). One of the most popular fluors is PPO, which is readily soluble in benzene, toluene, or xylene. Figure 4.32 shows the emission and absorption spectra of PPO. The separation of the two spectra is called the Stokes shift. Other frequently used solutes include butyl-PBD, bis-MSB, etc. The Reines and Cowan experiment used triethylbenzene as a solvent and p-terphenyl as the first solute (fluor) with a small amount of POPOP as the second solute (wavelength shifter). p-terphenyl is not popular any more because of low solubility. Borexino uses a pseudocumene solution of PPO (1.5 g/ℓ). KamLAND uses dodecane $CH_3(CH_2)_{10}CH_3$ (80%) as the base of the scintillator to reduce the flashing temperature, with a 20% admixture of pseudocumene. PPO at 1.5 g/ℓ is added as a fluor. It was found that with this cocktail a light yield of 70% of pure pseudocumene + PPO, which is about the yield of anthracene, is sustained for electrons.

Examples of scintillation efficiency (= Σ(photon energy)/ (particle energy)) are given in Table 4.18. A typical value for an efficient scintillator is 3−5%, which is 100 times the value of Čerenkov light detection.

PPO $C_{15}H_{11}NO$

POPOP $C_{24}H_{16}N_2O_2$

CH3

CH3

1,2,4-trimethylbenzene
= pseudocumene

C_9H_{12}

CH3
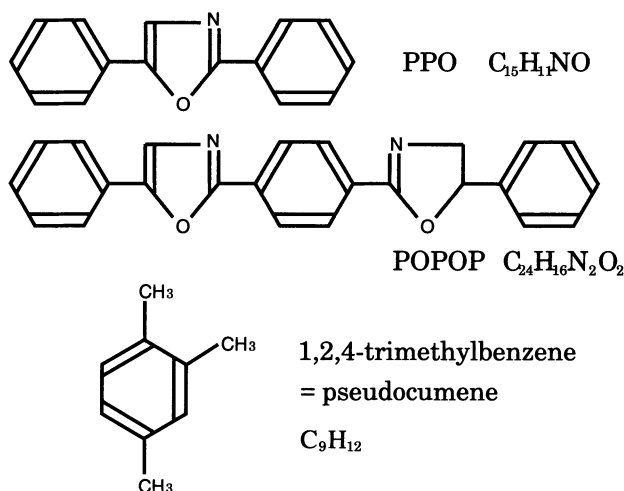
Fig. 4.31. Chemical structures of PPO, POPOP, and pseudocumene.
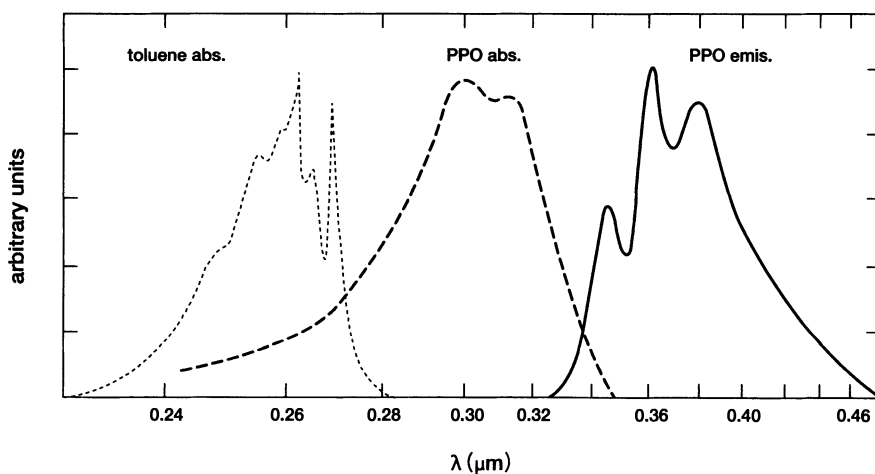
Fig. 4.32. Emission and absorption spectra of PPO (*thick curves*) and the absorption spectrum of toluene. Data are taken from [940].

The light yield (luminescence) is a nonlinear function of the energy loss of an incident particle,

$$\frac{d\mathcal{L}}{dx} = \mathcal{L}_0 \frac{\frac{dE}{dx}}{1 + k_b \frac{dE}{dx}} , \qquad (4.240)$$

where k_b is called Birk's constant which is determined empirically by energy calibration.

Table 4.18. Efficiency of scintillation.

Scintillator	Efficiency
Crystal anthracene	0.040
Toluene + PPO +POPOP	0.052
Benzene + p-terphenyl	0.042
Pseudocumene + PPO	0.040
Dodecane (80%) + Pseudocumene (20%) + PPO	0.027

A typical energy resolution is

$$\frac{\sigma(E)}{E} = \frac{0.10}{\sqrt{E}} \tag{4.241}$$

at around 1 MeV, with a 32% coverage of the detector surface at Kam-LAND [543].[62] About an order of magnitude improvement compared to (4.237) is due to the photon yield which is 100 times that of Čerenkov light.

Čerenkov versus scintillation counter. Scintillation photons are characterised by a high yield. This makes it possible to detect very low energy neutrino reactions. This advantage, however, is partly offset by the problem of background radioactivity. The great advantage of Čerenkov radiation is the directionality of photons along the charged particle path. For a source from a given direction (e.g., solar neutrino), this reduces the background enormously, but also gives us the confidence that we are actually observing the neutrino from the source. Furthermore, the Čerenkov detector is insensitive to low-energy alpha particles, which are abundantly produced in natural radioactive materials. Čerenkov detectors are preferable when one wants to detect higher energy (> 5 MeV) electrons for which the photon yield is sufficiently large. On the other hand, the projects that attempt to detect sub-MeV neutrinos should resort to scintillators. To take advantage of scintillation, particular effort is necessary to reduce the background.

A different, but practically important factor, is that water is much cheaper than scintillating material and is easy to handle, so that one can construct a much larger apparatus for water Čerenkov detectors.

All experiments detecting reactor antineutrinos ($\langle E_\nu \rangle \sim 3$ MeV) use scintillation detectors. The event rate is sufficiently high and the background noise can be efficiently rejected by the delayed coincidence without difficult efforts to reduce natural radioactivity in the material. The KamLAND project [543], whose prime aim is to detect antineutrinos from reactors located far away, also belongs to this class. More difficult efforts are required for Borexino [919] and the second phase of the KamLAND, both of which aim to detect sub-MeV (in particular ^{7}Be) solar neutrinos.

---

[62] A recent report from KamLAND shows that $\sigma(E)/E = 0.05/\sqrt{E}$ was achieved.

4.8.4 Background to Electron Detection

The reduction of background events is a key issue in low-energy electron detection. One major source of the background is cosmic-ray muons and radioactive nuclei induced by cosmic rays. Muon tracks are easily triggered out, but at the cost of dead time. In water detectors, muons cause fragmentation of oxygen or produce pions that interact with oxygen to produce radioactive nuclei. Secondary neutrons also cause nuclear spallation. Examples of cosmogenic radioactive nucleides are ^{12}B ($t_{1/2}$=20.4 ms), ^{12}N ($t_{1/2}$=11 ms), ^{8}B ($t_{1/2}$=0.77 ms), ^{8}Li ($t_{1/2}$=0.84 ms), and ^{11}Be ($t_{1/2}$=13.8 s). In addition, a stopped muon captured by oxygen produces ^{16}N ($t_{1/2} = 7.13$ s). The lifetimes of these unstable nuclei are short enough that the effect can be rejected by spatial and temporal coincidence (veto) with muon tracks. There are more abundantly produced nuclei, ^{15}O ($t_{1/2} = 122.1$ s), ^{14}O ($t_{1/2}$=70.6 s), ^{13}N ($t_{1/2}$=9.96 m), etc., but the energy of their beta rays is low and they do not give a background to the Čerenkov detector. Typical cross sections of abundantly produced nuclei are of the order of 10 to several 100 μbarns for 100-GeV muons, and increases with energy as E^α with $\alpha \approx 0.7 \pm 0.2$. Examples of the cross section are given in Table 4.19 [941].

Table 4.19. Production cross sections (in units of μbarn) of radioactive nuclei off ^{12}C with the high energy muon beam. After [941].

E_μ (GeV)	^{11}C	^{7}Be	^{10}C	^{6}He	^{8}B	^{9}C	^{8}Li	^{11}Be
100	576 ± 45	127 ± 13	77.4 ± 4.9	10.15 ± 1.0	4.16 ± 0.81	—	2.93 ± 0.80	< 1.22
190	905 ± 58	230 ± 23	115.4 ± 14.6	16.02 ± 1.60	7.13 ± 1.46	4.83 ± 1.51	4.02 ± 1.46	< 2.34

For organic scintillators, carbon is bombarded to give ^{11}C ($t_{1/2} = 20.38$ m), ^{10}C ($t_{1/2} = 19.20$ s), ^{7}Be ($t_{1/2} = 53.3$ d), etc. The lifetime of ^{10}C is short enough that the contribution can be vetoed by coincidence, but ^{11}C and ^{7}Be are important sources of the background that limits the performance of low-energy neutrino detection. In particular the detection of $1-2$-MeV neutrinos is severely limited by cosmogenic ^{11}C. Cosmogenic backgrounds are estimated in [941, 942] for Borexino and KamLAND.

To reduce the cosmic-ray muon background, experiments searching for rare events are carried out deep underground. Figure 4.33 shows the muon flux as a function of the depth below the surface. The curve is represented by

$$I_\mu(x) = I_0(x/h)^{-\alpha} \exp(-x/h) \,, \tag{4.242}$$
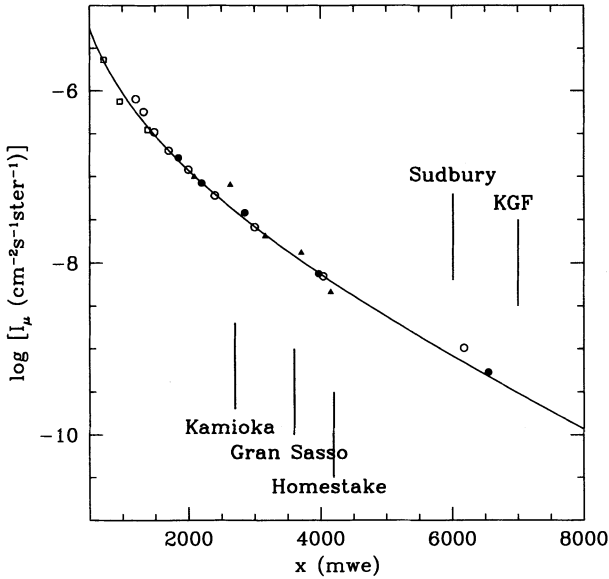
Fig. 4.33. Vertical cosmic-ray muon flux as a function of the depth in units of metre water equivalent. The data are taken from [944, 946–948] (*open squares, solid triangles, open circles*, and *solid circles*, respectively). The curve shows (4.242). The depths of five experimental sites (Kamioka, Gran Sasso, Homestake, Sudbury, and Kolar Gold Field) are indicated.

where x is the depth in $\mathrm{g\,cm^{-2}}$, $I_0 = 0.89 \times 10^{-6}\,\mathrm{cm^{-2}\,s^{-1}\,sr^{-1}}$, $h = 1.45 \times 10^5\,\mathrm{g\,cm^{-2}}$, and $\alpha = 2$ [944]. This fitting formula[63] describes data well for $x \gtrsim 10^5\,\mathrm{g\,cm^{-2}}$ (= 1000 mwe). The muon flux at ground level, $\approx 0.8 \times 10^{-2}\,\mathrm{cm^{-2}\,s^{-1}\,sr^{-1}}$ [950], is reduced to $4 \times 10^{-8}\,\mathrm{cm^{-2}\,s^{-1}\,sr^{-1}}$ at a depth of 1000 m underground (2700 mwe; the depth of the Kamiokande detector). A further reduction by a factor of 10 is achieved at 4000 mwe (the depth of the Gran Sasso Laboratory).

One must also reject neutrons and γ rays from surrounding rocks. These neutral particles are produced in rocks by (α, n) reaction from uranium and thorium or from spontaneous fission of $^{238}\mathrm{U}$, in addition to cosmic-ray-induced reactions. The rejection is efficiently done by a water shield, i.e., by setting a fiducial volume cut against the outer part of the water detector or by preparing an outer tank filled with water around the detector. The event rate as a function of the distance from the wall can be used as an indicator of this background. Kamiokande used only 680 tons out of a 3000-ton active

---

[63] Given the muon flux of the form $I(0) = A(E/E_0)^{-\gamma}$ at ground level, it is easy to obtain the theoretical depth dependence $I(x) = [a(bE_0)^{-1}(e^{bx} - 1)]^{-\gamma}$ by integrating the energy loss equation (4.17) [945]. This formula fits the data well with $A = (5.04 \pm 0.13)\,\mathrm{cm^{-2}\,s^{-1}\,sr^{-1}}$, $b = (2.94 \pm 0.09) \times 10^{-6}\,\mathrm{cm^2\,g^{-1}}$, and $\gamma = 2.78$ ($E_0 = 1\,\mathrm{GeV}$) [944]; see also [949].

volume, and Super-Kamiokande uses 22,500 tons out of an active volume of 50,000 tons for the analysis. SNO installed a sphere of a 1000-ton active volume in a tank of 7000 tons of water: a further cut reduces the fiducial volume to 770 tons.

After rejecting the cosmic-ray-induced background and neutral particles from rocks, we are left with the background from radioactivity in the target material, air, the vessel, and the photomultipliers. The main agents are ^{238}U, ^{232}Th, ^{40}K, ^{14}C, ^{85}Kr, and ^{222}Rn. The unit convenient to denote the noise is Bq $(= 1$ disintegration per second),[64] which translates to the following amounts of impurities:

$$
\begin{aligned}
^{238}\text{U} \quad & 10^{-12}\text{gU/g} = 12.4 \text{ Bq/kton} , \\
^{232}\text{Th} \quad & 10^{-12}\text{gTh/g} = 4.04 \text{ Bq/kton} , \\
\text{K(natural)} \quad & 10^{-12}\text{gK/g} = 31 \text{ mBq/kton} , \\
^{14}\text{C} \quad & 10^{-18}\text{g}^{14}\text{C/g} = 278 \text{ Bq/kton} .
\end{aligned}
\tag{4.243}
$$

This background becomes rapidly more serious as one goes to a lower energy. For a Čerenkov detector, the problem is relatively easily handled. The prime origin of the background is beta rays of 3.26-MeV ^{214}Bi (Ra C) derived from ^{226}Ra and ^{222}Rn or its progenitor ^{238}U. Spontaneous fission of ^{238}U also yields prompt γ rays that sum up to 8 MeV. Although the detection threshold is usually set higher than beta rays from Ra C, events are occasionally detected as statistical effects due to the finite energy resolution of the detector. In the Kamiokande experiment, uranium is efficiently reduced to 1/50 using chelate resin (CR-55), i.e., to the level of 10 Bq/kton, and radium is also reduced to a similar level by an ion exchanger. Radon contained in the air (in the Kamioka mine, its concentration is 100 times higher than in ordinary air due to granite-rich rock) is suppressed by a vacuum degasification system to the level of 500 Bq/kton [915], and at Super-Kamiokande to 1.4 Bq/kton with the further aid of an air purification system [951]. Yet, radon is the most important background that prevents a further decrease in the detection threshold. Note that the level of radioactivity is still quite high compared with the ^{8}B solar neutrino event rate, which is 7×10^{-6} event per s·kton, but the sharp directionality of Čerenkov radiation is efficiently used to reduce the background. When such directional information cannot be used very efficiently, as in the experiment detecting neutrino scattering off deuterium at SNO, the requirement for radio-impurity becomes much stronger [235, 917]. The removal of radioactivity to the ppq level (ppq=10^{-15} g/g) is needed for neutral-current detection. Table 4.20 shows the level of radio-impurity in respective experiments.

The requirement for radio-impurity reduction is particularly severe for scintillation detectors for lower energy neutrinos. At 1 MeV all radioactivity from ^{238}U and ^{232}Th (and ^{226}Ra), not only beta and gamma rays but also

---

[64] This is equivalent to 27 pCi.

Table 4.20. Natural radioactivity in the counter. The units are Bq/kton (g/g)

	^{238}U	^{232}Th	^{222}Rn
Kamiokande [915, 951]	9	—	500
Super-Kamiokande [931, 951]	< 0.12 ($< 1 \times 10^{-14}$)	0.08 ($< 2 \times 10^{-14}$)	1.4
SNO [235]	0.07 (5×10^{-15})	0.007 (1.7×10^{-15})	0.04
Borexino [952]	0.004 (4×10^{-16})	0.0018 (4×10^{-16})	0.004
KamLAND* [953]	< 0.008 ($< 6.4 \times 10^{-16}$)	< 0.0007 ($< 1.6 \times 10^{-16}$)	—

This purity is achived only with N_2 bubbling and circulation of the material through water.

alpha rays, generates scintillation, contributing to the background.[65] For the detection of ^{7}Be solar neutrinos of 0.861 MeV, the event rate for the SSM is 3×10^{-3} per s·kton. Therefore, one must suppress the radioactivity of scintillating material to at least a level of 1×10^{-3} Bq per kton, which means contamination of U at 0.3 ppq and Th at 0.9 ppq, a requirement 1000 times higher than that for the water Čerenkov detector. It is known that high purity hydrocarbon can be produced by a synthetic method that gives the raw material a contamination of about 100 ppq. Radon is efficiently removed by circulating nitrogen through the detector (this also serves to remove oxygen, which causes chemical quenching). Uranium and thorium in organic (nonpolar) liquid are removed efficiently by circulation through water (which is polar). Further reduction of U and Th can be achieved by distillation. One must also remove ^{85}Kr which comes from air.

The advancement made by the Borexino [952] and KamLAND [953] is impressive. The results from both collaborations demonstrate that one can reduce the uranium and thorium contaminants to the level that is required to measure the ^{7}Be solar neutrino flux. A difficult problem one encounters in purifying material to this level is measuring the impurity at such a low concentration. Borexino used counting itself in a small facility (CTF), water assay system (for radon), and neutron activation. KamLAND used counting (spectroscopy) in the full size detector and neutron activation; only upper limits were obtained.

At lower energies, the background from cosmogenic ^{14}C contained in hydrocarbons becomes serious. In spite of low beta ray energy ($E_{max} = 0.154$ MeV), the beta ray statistically contributes to counting due to the finite energy resolution of the detector, and the low-energy detection threshold is practically limited by the ^{14}C background. The Borexino group studied this in detail and showed that $< 1 \times 10^{-18}$ is needed to set the detector threshold to 0.25 MeV. Fortunately, petroleum is buried deep underground for many years, so the amount of ^{14}C in petroleum derivatives is very small: the Borexino measurement gave $1.9 \pm 0.1 \times 10^{-18}$ [954].

---

[65] Some reduction of the background from α particles can be made by using different pulse shapes.
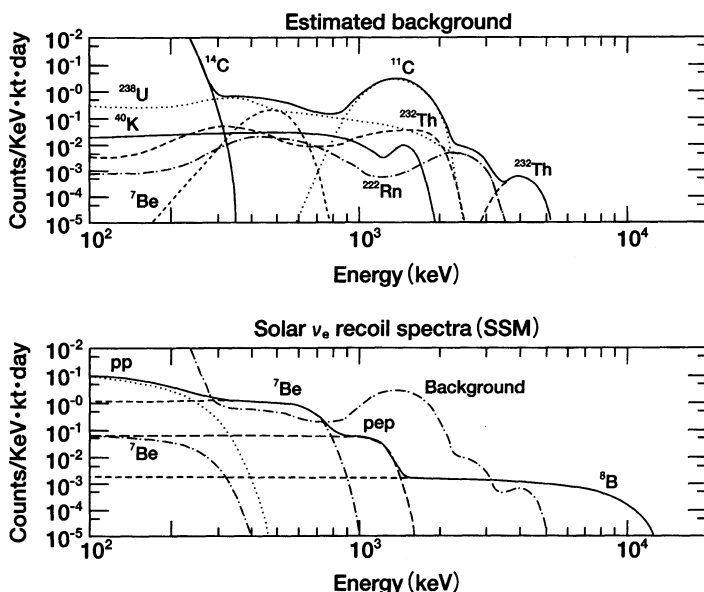
Fig. 4.34. (a) Composition of the background noise expected in the KamLAND scintillator. (b) Comparison of the standard solar model prediction of the neutrino electron scattering rate with the background. For assumed impurity abundances and detector resolution, see the text. After [543].

In Fig. 4.34(a) we show the composition of the background from radio-impurity and cosmogenic radioactivity expected in the second phase of the KamLAND experiment. The assumed impurity is 0.1 ppq for U and Th, 10^{-18} g/g for ^{40}K and ^{14}C, 1700 atoms/day for the cosmogenic production of ^{11}C, and 400 atoms/day for ^{7}Be. The assumed energy resolution is $\Delta E/E = 0.10/\sqrt{E}$. Figure 4.34(b) compares the standard solar model prediction of neutrino capture rates with the background noise. This figure shows the difficulty of detecting *pep* and CNO neutrinos due to the background from ^{11}C.

The ultimate source of noise is the photomultiplier itself. It arises from thermal noise (at room temperature) and from radioactivity from U, Th, and ^{40}K contained in the glass. The read noise of SK PMT is 3 kHz, which is mostly of thermal origin. The contribution from ^{40}K in potassium-free glass (0.13% concentration of potassium) is estimated to be 0.4 kHz [930].

4.8.5 Radiochemical Detection

Radiochemical experiments have been used for 40 years for low-energy neutrino detection. Neutrino captures on specific nuclei form radioisotopes, and these isotopes are chemically collected for counting. The great advantage of

this method is that it is quite insensitive to the background, and the chemistry to collect produced atoms is well established. This has been and still is the only way to detect sub-MeV neutrinos at this time.

The first experiment uses $\nu_e + {}^{37}\text{Cl} \rightarrow e^- + {}^{37}\text{Ar}$ in a tank filled with 615 tons of tetrachloroethylene (perchloroethylene) C_2Cl_4, which contains 2.17×10^{30} ${}^{37}\text{Cl}$ atoms. The experiment has been carried out at Homestake Mine, South Dakota, at 1480 m underground since 1967 [207, 715]. The experimental procedures are as follows [721]:

1. Before starting each exposure, 0.2 cm^3 of either ${}^{36}\text{Ar}$ or ${}^{38}\text{Ar}$ is added to serve as a carrier for the ensuing run.
2. The tank is exposed to neutrino flux for about 30−50 days.
3. After exposure, the argon in the tank is removed by circulating 1 tank volume He gas for 20 hours.
4. The gas is sent to a condenser at $-40°C$, which freezes out most of the tetrachloroethylene vapours, and to a laminar differential pressure gas flow meter (which measures the He gas). It is then sent to molecular sieve traps at room temperature, which remove residual tetrachloroethylene gas.
5. The gas is sent to a charcoal trap cooled to liquid N_2 temperature to adsorb argon. The helium gas flows back to the tank. At this stage, 95% of argon is collected.
6. Argon is extracted from a heated charcoal trap to a line where it is purified. Active gases are removed by exposing the sample to titanium metal powder heated to 900°C, and other gases (most importantly ${}^{85}\text{Kr}$ and ${}^{222}\text{Rn}$) are removed by gas chromatography with a charcoal column. It is then loaded into a small (0.3−0.5 cm^3) proportional counter along with tritium-free methane, which serves as a counting gas.
7. The carrier yield is determined by mass spectroscopy.

The counting is done for KLL Auger electrons (81.5%; total energy 2.823 keV) and K X rays (8.7%) for the electron capture process of ${}^{37}\text{Ar}$ back to ${}^{37}\text{Cl}$ with $t_{1/2} = 35.02$ day.

The most important source of nonsolar production of ${}^{37}\text{Ar}$ is photonuclear interactions of energetic muons with nuclei to produce protons and the subsequent ${}^{37}\text{Cl}(p, n){}^{37}\text{Ar}$ reaction. Based on a ${}^{37}\text{Ar}$ production experiment at a shallow depth, Clevelend et al. [721] estimated, with the aid of an empirical extrapolation formula, the production rate to be 0.047±0.013 atoms day^{-1}, which is a tenth of the solar neutrino capture rate of 0.48 atoms day^{-1}. The contributions from other sources are smaller at least by an order of magnitude.

Another radiochemical experiment that used $\nu_e + {}^{71}\text{Ga} \rightarrow e^- + {}^{71}\text{Ge}$ was proposed by Kuzmin [230]. The unique feature of the gallium experiment is that it is sensitive to pp solar neutrinos. The experiment was carried out by

two groups, the Gallex at Gran Sasso Laboratory[66] and the SAGE at Baksan Neutrino Observatory. The Gallex experiment used 104 tons of a $GaCl_3$–HCl solution containing 30 tons of gallium (1.04×10^{29} ^{71}Ga atoms), and SAGE used 55 tons of metallic gallium (1.89×10^{29} ^{71}Ga atoms). The procedure of the Gallex experiment is as follows [920]:

1. At the beginning of a new exposure, 1 mg Ge carrier (^{70}Ge, ^{72}Ge ^{74}Ge, ^{76}Ge) is added to the $GaCl_3$–HCl solution. (NB: radioactive ^{68}Ge must be removed from the tank before the experiment.)
2. The tank is exposed for 2 to 3 weeks.
3. The tank is purged with 1900 m^3 of N_2–gas for 12−20 hours. Germanium is removed from the solution as volatile germanium chloride, $GeCl_4$.
4. The gas stream is passed through water scrubbers where $GeCl_4$ is absorbed. At the end of this process, germanium is contained in a volume of 30 ℓ in the first scrubber. A series of smaller columns concentrates the germanium in a volume of 1 ℓ of water. The final concentration step is an extraction into CCl_4 and back-extraction into 50 $m\ell$ of tritium-free water.
5. $GeCl_4$ is converted into germane, GeH_4, by the reducing reagent sodium borohydride ($NaBH_4$), and GeH_4 is dried and purified by gas chromatography. Its volume is measured to determine the overall yield.
6. GeH_4 gas is put together with Xe gas in a small proportional counter (active volume is 1 cm^3). The mean chemical yield in the state of the art is 99%.

The proportional counter detects Auger and X-ray emission in K (87.6%; 1.2 keV) and L(10.3%; 10.4 keV) electron captures of ^{71}Ge back to ^{71}Ga ($t_{1/2} = 11.43$ day).

As in the chlorine experiment, the most important source of the background is $^{71}Ga(p, n)^{71}Ge$; the proton is produced in the tank from (α, p) and (n, p) reactions and from cosmic-ray muon interactions. This cosmic-ray-induced background event rate is estimated to be 2.8 ± 0.6 SNU from an experiment exposing a small gallium detector to the muon beam [955]. The neutron-induced event rate is estimated to be 0.15 ± 0.10 SNU. The two contributions altogether are 1/20 the solar neutrino signal.

The SAGE experiment uses metallic gallium liquid at just above the melting point (29.8°C). The extraction procedure is as follows [725]:

1. 700 µg of natural Ge carrier is added in the form of a Ga–Ge alloy and thoroughly stirred to maintain uniformity.
2. Exposure is typically for 4 weeks.
3. A weak acidic solution (HCl) is added to the gallium tank in the presence of an oxidising agent (H_2O_2) to extract Ge into the aqueous phase. The

---

[66] The Gallex experiment is now named Gallium Neutrino Observatory (GNO). At present, only the electronics is upgraded compared to Gallex.

HCl is cooled to $-15°$C and the water to $-4°$C to minimise the heating of this violently exothermic chemical reaction.

4. The mixture is intensively stirred, and Ga metal and the solution form fine globules. Germanium dissolved in gallium migrates to the surface of the globules.
5. The extraction is ended by adding 7N HCl and further stirring.
6. The extracted solution is siphoned away from the tank. Germanium is concentrated by vacuum evaporation in a glass aparatus. HCl is added to the solution and argon gas purge is applied, which sweeps germanium as $GeCl_4$ from its acid solution into water.
7. A solvent extraction procedure is used first to extract the germanium into CCl_4 and then to back-extract it into tritium-free water. The final product is in a $100\,cm^3$ volume.
8. Germane is synthesised with $NaBH_4$ in the presence of dilute $NaOH$ in a small flask heated to $70°$C in a sealed He flow system. Thus formed GeH_4 is purified by gas chromatography, and the purified sample is introduced into a proportional counter. The extraction efficiency is about 80%.

Both K and L peaks are measured for electron capture of ^{71}Ge.

Calibration experiments. For radiochemical experiments, it is highly desirable to demonstrate that all procedures actually work as designed, partly because the experiment uses complicated chemistry (although the procedures are chemically justified) and partly because cross sections of excited states are uncertain. The most straightforward check is to expose the detector to an artificial neutrino source with a known activity level and appropriate energy. Both Gallex and SAGE carried out this ambitious experiment.

The original idea of using an artificial radioactive source to measure the efficiency of solar neutrino detection is due to Alvarez, who proposed a ^{65}Zn source [956]. Raghavan proposed using ^{51}Cr for low-energy neutrino detectors [957], and Haxton proposed ^{37}Ar [958].

Gallex prepared a 62.5-PBq ^{51}Cr source by irradiating $36\,kg$ of enriched chromium (50% of ^{50}Cr, compared to the 4.35% natural abundance) with a neutron beam at the Siloé reactor in Grenoble for 24 days [959]. ^{51}Cr decays to ^{51}V with electron capture with a half-life of $27.706 \pm 0.007\,days$. The Q value is $751\,keV$, and the neutrino spectrum consists of $751\,keV$ (9%), $746\,keV$ (81%), $431\,keV$ (1%) and $426\,keV$ (9%) monoenergetic lines. The decay emitting a 430-keV neutrino is associated with γ radiation of $320\,keV$, which can be easily shielded. The level of radioactivity is measured using calorimetry, an ionisation chamber, high-resolution gamma ray spectroscopy, and neutron activation to measure the ^{51}V abundance. The measured values agree within errors, which vary from 1.3 to 5% depending on the method used [448]. The result of neutrino calibration experiments shows the ratio of (experiment)/(expected)=0.97 ± 0.11 [959], where the neu-

trino capture cross section $5.9 \times 10^{-45} \, \text{cm}^{-2}$ of Bahcall and Ulrich [711] is assumed.

A comparable experiment was also carried out for SAGE [449]. A 19.1-PBq source of ^{51}Cr was prepared using 513 g chromium, enriched to 93% for ^{50}Cr, by irradiation at the BN-350 fast neutron reactor in Aktau (Kazakhstan) for 115 days. The activity level was measured by calorimetry with a 1% error. A 13-ton gallium detector was exposed to this source, with the result (experiment)/(expected)=0.95±0.12.

These measurements demonstrated the reliability of gallium solar neutrino experiments. The small capture rates for solar neutrinos are ascribed to the solar neutrino flux deficit.

Other radiochemical experiments. There are several other targets proposed for radiochemical experiments. The candidates include ^{81}Br$(\nu, e)^{81}$Kr ($E_{\text{th}} = 0.570 \, \text{keV}$) [960] and ^{127}I$(\nu, e)^{127}$Xe ($E_{\text{th}} = 0.789 \, \text{keV}$) [961], for which chemistry is similar to that for ^{37}Cl, and experiments can be done by replacing the chlorine with the relevant chemicals (say, $C_2H_2Br_2$ and $C_2H_2I_2$). The merit of these new experiments is larger cross sections, especially a larger capture rate for ^{7}B neutrinos with ^{81}Br. The important problem to be solved is uncertainty in the capture cross sections. Unless we can estimate them with a 10−20% error, the experiment will not give very useful information. Another difficulty with the ^{81}B experiment is the long lifetime of ^{81}Kr ($t_{1/2} = 2 \times 10^5 \, \text{yr}$), which prevents us from using the standard counting technique (see [960]). Other candidate targets are ^{7}Li [962] and ^{9}F. For ^{7}Li we can accurately estimate the capture cross sections for the first two levels, which are relevant to ^{7}Be neutrinos. The chemistry may not be too difficult. The problem is how to identify Auger electrons of 50 eV. An estimate of capture cross sections for various targets is given in Table 4.21 together with those for ^{37}Cl and ^{71}Ga. For more discussion about these targets, see Bahcall [210].

Table 4.21. Estimated neutrino capture rates (in units of SNU). The estimates are taken from [210] and for ^{127}I from [961].

	Nat. abund.	*pp*	*pep*	^{7}Be	^{8}B	CNO	*hep*	Total
^{37}Cl	24.23%	0	0.2	1.1	6.1	0.4	0.03	7.9
^{71}Ga	39.9%	70.8	3.0	34.3	14.0	10.0	0.06	132
^{81}Br	49.31%	0	1.1	8.6	15.3	1.8	0.07	27.8
^{127}I	100%	0	1.2	9.6	44	2.8		58
^{7}Li	92.5%	0	9.2	4.5	22.5	15.5	0.06	51.8
^{115}In	95.7%	468	8.1	116	14.4	32.3	0.05	639

4.8.6 Other Types of Experiments

A class of experiments we have not mentioned so far is *geochemical experiments*. One could measure the number of atoms produced in solar neutrinos accumulated in a rock during a geological timescale. Geochemical experiments have successfully given the lifetime of two-neutrino double beta decays. The detection of solar neutrinos is more demanding (the accumulated number of atoms is $\sim 10^{-6}$ times smaller) but does not seem impossible. The targets considered are ^{98}Mo$(\nu, e)^{98}$Tc [963], ^{205}Tl$(\nu, e)^{205}$Pb [964], and ^{7}Li$(\nu, e)^7$Be [965]. In particular, much effort was invested to measure the ^{98}Tc concentration in molybdenite ore [966]. An interesting feature of this reaction is that ^{98}Tc itself is unstable and has a lifetime of 2×10^6 yr, so the ^{98}Tc yield would tell us about the solar neutrino flux for a well-determined period, which otherwise has geological uncertainty. The expected physics was discussed in [967]. Unfortunately, the experiment ceased without producing a result. A preliminary study was done for ^{205}Tl [968]. The general difficulties common to geochemical experiments are that one must make sure that the rocks have not metamorphosed, and one needs a reliable estimate of nonsolar neutrino-induced production of the relevant element by cosmic rays and natural radioactivities, in addition to the difficulty common to most targets that accurate estimates are not available for solar neutrino capture cross sections.

There are several experiments proposed for real-time solar neutrino detection using nuclear targets. The first is to use ^{115}In [969]. The advantage of this target is a very large capture rate, especially for *pp* solar neutrinos: the estimated capture rate exceeds 600 SNU. Much effort was invested to study the feasibility of this target, mostly using liquid or plastic scintillators with a significant amount of indium doped, or using InP as a semiconductor detector [970]. An inherent difficulty is that ^{115}In itself is unstable and has a lifetime of $t_{1/2} = 4.4 \times 10^{14}$ yr that produces a large background. Solar neutrino capture from ^{115}In(gs, $9/2^+$) to ^{115}Sn(613 keV, $7/2^+$) gives a recoil signal of e^- and two cascade gammas, a 100.7-keV γ ray for the transition to the ($3/2^+$, 497.3 keV) level and a 497.3-keV γ to the $1/2^+$ ground state. The triple coincidence technique can be applied, but the background from β decay (triple forbidden, 486 keV) is still too heavy unless the detector is segmented into a large number of cells. The current conclusion is that the detection of *pp* neutrinos is difficult, although the detection of the ^{7}Be neutrino may not be impossible.

Another proposed experiment (ICARUS: Imaging Counter and Rare Underground Signals) for real-time neutrino detection uses ^{40}Ar ($E_{\text{th}} = 1.505$ MeV), which serves as material for a time projection chamber. The detector identifies each track and energy with good resolution by forming a three-dimensional electronic image of drifting electrons in a homogeneous electric field onto a readout plane, where the charge is recorded [971]. This is a technique frequently used for high-energy experiments. The neutrino

reaction is dominated by the transition to the isobaric analogue state of ^{40}K at 4.38 MeV, for which the Fermi transition dominates and the reaction cross section is known with good accuracy. This detector is also useful for a long-baseline accelerator experiment. A unique feature of this detector is that one can identify the charge of recoil leptons if a magnetic field is applied. This can be used to explore CP violation.

There are also several candidate targets for pp neutrino detection recently proposed. They include ^{176}Yb, ^{160}Gd, ^{82}Se [972], and ^{100}Mo [973]. In these experiment, the excited level is identified. Therefore, the problem of uncertainties in the capture cross section can be avoided, in principle, if one measures the transition by exposing the detector to the neutrino beam from a stopped muon channel or those from a strong artificial radioactive source.

Yet a new type of experiment is considered using a low-temperature technique. The principle is to use the very small specific heat of materials (e.g., Si, Ge, etc.) at a low temperature to detect the heat generated by the recoil energy of electrons or nuclei. The most ambitious is the proposal by Drukier and Stodolsky [974], which uses superconducting grains to detect recoil energy as small as 10 eV. Their goal is to detect neutral-current-induced coherent scattering off nuclei, which have a large cross section, $\sigma \simeq 0.42 \times 10^{-44} N^2 (E/1\,\text{MeV})^2\,\text{cm}^2$ [see (3.232)]. The recoil energy $E_{\text{recoil}} = \mathbf{q}^2/2AM_N$, where $\mathbf{q}$ is the three momentum transfer and A is the atomic number. When integrated over the cross section,

$$\langle E_{\text{recoil}} \rangle = \frac{1}{3} \frac{q_m^2}{2AM_N}$$
$$= \frac{0.71}{A} \frac{q_m}{2AM_N}\,\text{keV}\,, \qquad (4.244)$$

where $q_m = 2E_\nu$ is the maximum value of $\mathbf{q}$. For $E_\nu = 1.44$ MeV, $E_{\text{recoil}} = 20$ eV, which would heat a germanium granule of a radius of 4.5 μm (coated with 0.5 μm of gallium) by 10 mK at an operating temperature of 50 mK. Granules are held in a magnetic field, whose strength is so adjusted that a small temperature increase will flip them into a normal state. So the 10 mK increase induces the transition of superconducting gallium to a normal state, and the signal is picked up with a SQUID. Drukier and Stodolsky estimated 1.3 events per 100 kg of granule for solar neutrinos if the radius of the granule is 2.3 μm.

Cabrera et al. [975] proposed using crystalline silicon cooled to 1−10 mK. The Debye temperature of silicon is high, $\Theta = 636$ K, so that the specific heat $C_V = 1.9 \times 10^{10}(T/\Theta)^3$ erg/mol·K is very small in the mK regime: a 100-keV recoil energy of an electron heats 1 kg of silicon by 1 mK, which can be detected with a thermal sensor, e.g., a tungsten superconducting film, installed on the crystal [976]. The signal is picked up by a SQUID. The detection threshold, however, is of the order of 100 keV for the recoil energy. So this technique can be used for νe scattering for pp solar neutrinos, and

νA coherent scattering only for ^{8}B solar neutrinos. The size of the detector should be $\gtrsim 1\text{--}10$ tons.

Lanou et al. [977, 978] considered the use of superfluid helium, in which the electron recoil energy of νe scattering is partly used to excite rotons. Rotons travel ballistically through helium and produce heat at the surface, which can be detected by a silicon wafer. For $E_{\text{recoil}} = 200$ keV, the number of rotons is of the order of 10^8, which heat a $200\,\text{cm}^2$ wafer $250\,\mu$m thick by $2.6\,$mK at $T = 20\,$mK. The estimated size of the detector is 10 tons for pp neutrinos.

The low temperature detector has an application to detect dark matter particles. The technique, however, is still premature, and it is reserved as a future possibility.

Towards the definitive solution of the solar neutrino problem. Whatever techniques one would use, what is necessary for future experiments is high statistics, comparable to or more than those that Super-Kamiokande and SNO achieved, and real time detection. Accurate estimates of reaction cross sections are also an important requisite, although experiments without accurate cross sections would not be completely useless for studying time variations.

If our present understanding of the solar neutrino problem is on the right track, the two decisive experiments are a long-baseline reactor neutrino flux measurement (KamLAND) and ^{7}Be solar neutrino experiments (Borexino, KamLAND II). The most likely solution predicts a deficit of antineutrino flux from reactors. Another allowed solution suggests a large day–night variation of ^{7}Be solar neutrino flux. Yet two other solutions, though less likely, lead to either a deficit or a seasonal variation of ^{7}Be solar neutrino flux. Therefore, all possibilities in our minds can be uniquely discriminated by these two experiments. Expensive experiments to measure pp neutrinos in real time would not be compelling, unless the two experiments result in a surprise. More details are discussed in Sect. 8.8.

4.9 Other Astrophysical Sources of Neutrinos

4.9.1 Neutrino from Dark Matter Annihilation

The Galactic halo is dominated by cold dark matter. The flat rotation curve of particles orbiting in the Galactic disc (stars, neutral hydrogen atoms), i.e., the circular velocity $v_c =$const independent of the radius r, means that the gravitational mass of the Galaxy $M \propto r$.[67] This persists to $r \approx 200$ kpc,

---

[67] The simplest interpretation for the flat rotational curve is to assume isothermal dark haloes. The evidence for haloes, however, is not quite compelling from the rotational curve itself for the majority of galaxies since observations do not

which is about the virial radius of the Milky Way. On the other hand, the distribution of visible matter is limited to within $< 20\,\mathrm{kpc}$. The mass to light (observed in the blue optical band) ratio increases with r and $M/L_B \simeq 100 M_\odot/L_{B\odot}$ at $r = 200\,\mathrm{kpc}$ [894]. Assuming that $M/L_B = 100 - 200$ is universal to galaxies,[68] the mass density calculated as $\rho = \mathcal{L}_B \langle M/L_B \rangle$ using the luminosity density $\mathcal{L}_B = 2.4 \pm 0.4 \times 10^8 L_\odot\,\mathrm{Mpc}^{-3}$ is about $(0.1\text{--}0.2)\rho_{\mathrm{crit}}$, which is half the total matter density we have discussed in Sect. 4.6.3 (the other half is likely to be in a small structure). This implies that the halo is dominated by cold dark matter. The dark matter mass density in solar neighbourhood is inferred to be $\approx 0.3\,\mathrm{GeV\,cm}^{-3}$.

When such dark matter particles hit the Sun, they would be captured and eventually sink to the core of the Sun [979, 980]. Dark matter particle, X, will then interact with its antiparticle and annihilate. This will produce energetic $(E_\nu \lesssim m_X/2)$ neutrinos, which could be detected on Earth [981]. The estimate of the neutrino flux consists of calculations of (i) the trapping rate Γ_T of X particles, which is roughly $\Gamma_T = \pi R_\odot^2 n_X v (R_c/R_\odot)$, where n_X is the density of X particles in the halo, $v = \sqrt{2}v_c$[69] is the rms velocity of the X particle, and the last factor $(R_c/R_\odot)$ is the gravitational enhancement factor for a slowly moving X where $R_c = 2GM_\odot/v^2$ (for more details, see [980][70]); (ii) the equilibrium condition $\Gamma_T = \Gamma_A$, where $\Gamma_A = (4\pi/3)R_\odot^3 n_{X\odot}^2 \langle \sigma v \rangle_A\, w$ is the annihilation rate ($w = \int dV n_{X\odot}^2(r)/V n_{X\odot}^2$ is a density weighting factor) (this condition determines the density of an X particle in the Sun); and (iii) the neutrino flux, which is obtained as $\phi_\nu = \nu \Gamma_T/4\pi d^2$, where ν is the average number of neutrinos produced per annihilation event. The neutrino flux generally decreases as $\sim M_X^{-1}$, but too light an X $(m_X \lesssim 6\,\mathrm{GeV})$ would not be captured by the Sun [980, 983]. Calculations for a ≈ 10-GeV dark particle mass give a neutrino flux of the order of $0.1\text{--}1\,\mathrm{cm}^{-2}\mathrm{s}^{-1}$, which is comparable to atmospheric neutrino flux [984, 985]. In particular, the case of supersymmetric dark matter is studied in detail [986]. Experimental limits are obtained from upward through-going muons for which the background is minimised [987–991]. The strongest limit obtained from the Super-Kamiokande, $\phi_\mu \lesssim 1 \times 10^{-14}\,\mathrm{cm}^{-2}\mathrm{s}^{-1}$, is significantly smaller than the muon flux of the atmospheric origin, $\langle \phi_\mu \rangle \approx 2 \times 10^{-13}\,\mathrm{cm}^{-2}\mathrm{s}^{-1}\mathrm{sr}^{-1}$ (averaged over the solid angle) [991]. This leads to meaningful constraints on the particle-physics nature of dark matter for $M_X = 30$ to a few hundreds GeV.

---

extend much in the radius $(r < 10\text{--}20\,\mathrm{kpc})$, and the curve can be fitted with a disc and a bulge without assuming haloes [905].

[68] This is justified by the detection of the shear induced by galaxies in weak lensing observations [903].

[69] This holds for the isothermal distribution. We consider that the distribution of dark matter in the halo is close to isothermal.

[70] It is pointed out that some fraction of dark matter particles is bound in solar orbit and does not interact with the Sun or Earth [982].

4.9.2 Ultra-High-Energy Neutrinos

It was found that some astrophysical sources emit TeV γ rays. The sources include supernova remnants (including pulsars) in the Milky Way and active galactic nuclei. Examples of the former are the Crab nebula [992], the Vela pulsar region [993],[71] and a supernova remnant SN1006 (SNR RXJ1713.7-3946) [995]. For the latter, we know Mrk 421 [996] and Mrk501 [997], which are both BL Lac objects.[72] These observations indicate particle acceleration to super-TeV energies. The mechanisms of high-energy γ emission are [998] (i) neutral pion production in high-energy pp collisions; (ii) the collision of high-energy protons with ambient photons to produce neutral pions; (iii) inverse Compton scattering of high-energy electrons off a microwave background or infrared photons; and (iv) synchrotron radiation of electrons, though it requires very strong magnetic fields. For (i) the typical energy of γ rays is about one-tenth that of protons. For (ii) the threshold of pion production is $4\epsilon_\gamma E_p + m_p^2 > (m_N + m_\pi)^2$, where ϵ_γ is the energy of ambient photons. The average energy of photons produced in inverse Compton scattering (iii) is $k_\gamma = (4/3)(E_e/m_e)^2 \varepsilon_\gamma$, where ε_γ [see (16.69) of Ginzburg's monograph [998]] is the energy of target photons. For CMB photons, $k_\gamma = 0.14(E_e/\text{TeV})^2$ GeV. The energy of photons produced in synchrotron radiation typically is $k_\gamma = 0.44(E_e/m_e)^2(eB/m_e)$ [see idem (5.40a)], which reads $2 \times 10^{-5}(E_e/\text{TeV})^2(B/\text{Gauss})$ GeV. Only with $B > 10^5$ Gauss, does synchrotron radiation give energetic photons comparable to those from the inverse Compton process. If (i) and/or (ii) are a dominant process, the decay of charged pions and muons produces very high-energy neutrino fluxes whose energy is comparable to that of gamma rays [999].

The neutrino flux observed on Earth, dN_ν/dE, is related to the source luminosity $\mathcal{L}$ as

$$\int E \frac{dN_\nu}{dE} dE = \frac{1}{4\pi d^2} \eta_\nu \mathcal{L} , \qquad (4.245)$$

where d is the distance to the source and η_ν is the neutrino energy fraction. If we assume the spectral shape $dN_\nu/dE \sim E^{-2}$, we obtain

$$\begin{aligned}
\frac{dN_\nu}{dE} &= \frac{1}{4\pi d^2} E^{-2} \eta_\nu \mathcal{L} \left[\ln(E_{\max}/E_{\min})\right]^{-1} \\
&= 5 \times 10^{-12} (d/10\,\text{kpc})^{-2} (E/1\,\text{TeV})^{-2} (\mathcal{L}/10^{37}\,\text{erg}\,\text{s}^{-1}) \quad (4.246) \\
&\times (\eta_\nu/0.1)[\ln(E_{\max}/m_p)/10]^{-1}\,\text{cm}^{-2}\text{s}^{-1}\text{TeV}^{-1} . \qquad (4.247)
\end{aligned}$$

The detectors currently operating (Lake Baikal [948] and the AMANDA experiment [944, 1000]) are not large enough; a $\gtrsim$1-km^3 detector would be

---

[71] A doubt has been cast on the detection of γ rays from Vela [994].

[72] BL Lac objects are active galactic nuclei characterised by rapid variability, a nonthermal, featureless optical spectrum, and strong radio emission. A BL Lac object is usually supposed to be an active galactic nucleus as viewed from the direction of jets associated with the accretion disc.

needed to detect such neutrinos, or at least will set a meaningful bound, which would give us a hint to understand the nature of the acceleration mechanism for high-energy cosmic rays. The flux of (4.247) with the optimistic default parameters shown in parentheses gives one event a year for a 1-km^3 detector for 1-TeV neutrinos.

We do not discuss very high energy neutrinos further. We only quote several references that discuss sources and fluxes of very high energy neutrinos [1001, 1002].

5 Properties of the Neutrino

5.1 Electromagnetic Properties

5.1.1 Electromagnetic Form Factors

We define electromagnetic form factors by

$$\langle \nu(p', \lambda') | J_\mu^{\text{em}} | \nu(p, \lambda) \rangle = \bar{\nu}(p', \lambda') \{ \gamma_\mu F_1(q^2) - \gamma_\mu \gamma_5 G_1(q^2)$$
$$+ \sigma_{\mu\nu} q^\nu [F_2(q^2) - \gamma_5 G_2(q^2)] \} \nu(p, \lambda) , \quad (5.1)$$

with $q = p' - p$. F_1 and G_1 are charge form factors, and F_2 and G_2 are magnetic and electric dipole form factors, respectively. For the left-handed neutrino (5.1) reduces to

$$\langle \nu'_L | J_\mu^{\text{em}} | \nu_L \rangle = \bar{\nu}_L \gamma_\mu [F_1(q^2) + G_1(q^2)] \nu_L , \quad (5.2)$$

where $F_1(0) + G_1(0)$ is the charge. For the right-handed neutrino the charge is $F_1(0) - G_1(0)$. A two-component (Weyl or Majorana) neutrino cannot have a magnetic or an electric dipole moment.[1]

If we rewrite (5.2) with the Majorana field χ [see (6.19) of Sect. 6.3],

$$\langle \chi | J_\mu^{\text{em}} | \chi \rangle = -\frac{1}{2}(F_1 + G_1) \bar{\chi} \gamma_\mu \gamma_5 \chi . \quad (5.3)$$

The divergence is
$$\langle \chi | \partial^\mu J_\mu^{\text{em}} | \chi \rangle = -(F_1 + G_1) m_\chi . \quad (5.4)$$

---

[1] This is trivial, but it can be easily verified in the following way [see (6.19) of Sect. 6.3]. Let us write

$$\mathcal{L} = \bar{\chi} \sigma_{\nu\mu} (f + g\gamma_5) \chi .$$

Rewriting this in terms of $\chi^c = C\bar{\chi}^T$,

$$\mathcal{L} = -\bar{\chi}^c \sigma_{\mu\nu} (f + g\gamma_5) \chi^c$$
$$= -\bar{\chi} \sigma_{\mu\nu} (f + g\gamma_5) \chi ,$$

where the Majorana property $\chi^c = \chi$ is used in the last step. This proves that the dipole form factors f and g vanish.

The electromagnetic current is not conserved unless $m_\chi = 0$ or $F_1 + G_1 = 0$. Only a neutral fermion ($F_1 + G_1 = 0$) can have a finite Majorana mass (a Majorana particle is by definition a completely neutral particle).

We refer the reader to the classical article by Bernstein, Ruderman, and Feinberg [1003] for a survey of the electromagnetic properties of the neutrino.

5.1.2 Electric Charge

Whether strict charge neutrality can be derived from the standard theory is an intriguing question. Let us define the charge in units of the charge of the gauge particle or equivalently, of the Higgs particle. At a simple level, the prediction of the theory is only $Q_\nu - Q_e = 1$. $Q_\nu[= F_1(0) + G_2(0)] = 0$ is set by choosing $Y = -1/2$ for $\psi_L = (\nu, e^-)_L$ by hand. (If the neutrino has a Majorana mass, obviously $Q_\nu = 0$.)

When one looks into the full internal consistency of the theory, a stronger condition is obtained on the neutrino charge. The requirement is that the theory is free from any triangular anomaly [272]; the triangle diagram should be cancelled among all fermions contained in the theory. The contributions from fermions other than neutrinos cancel between their left- and right-handed components, but, if the left-handed neutrinos would have a finite charge, there appears an axial-vector current contribution to the three-photon diagram [1004]. The strict charge neutrality is derived from the $\gamma - \gamma - \gamma$ diagram that vanishes[2], i.e.,

$$Q^3_{\nu\,\mathrm{em}} = 0 \ . \tag{5.5}$$

If there exists, however, a right-handed partner of the neutrino, the $\gamma - \gamma - \gamma$ diagram vanishes due to the cancellation between ν_L and ν_R, and the charge of the left-handed neutrino becomes free. We show below that the neutrino (and also the neutron) may have a charge, but $Q_n + Q_\nu = Q_p + Q_{e^-} = 0$ should strictly hold based on the more general anomaly-free conditions within the standard theory.

To study the structure of anomaly-free conditions, let us start with (2.96) of Sect. 2.4:

$$\sum_i \mathrm{Tr}[T_a^i \{T_b^i, T_c^i\}] = 0 \ , \tag{5.6}$$

where T_a^i is the coupling matrix of the gauge field A_μ^a and i refers to fermions. We assign the U(1) hypercharge Y of the lepton and quark fields as A (ℓ_L), B (e_R), C (q_L), D (u_R) and E (d_R). By requiring that cancellation of the

---

[2] If one allows a parity violation in the electromagnetic interaction, the neutrino can have a nonvanishing electric charge, $Q_{\nu\,\mathrm{em}} = \epsilon$. In this case, however, $\langle\phi\rangle \neq 0$ breaks the electric charge conservation and gives rise to a finite photon mass [1005]. The present upper limit on the photon mass, $m_\gamma < 10^{-25}$ eV [1006], implies $Q_{\nu\,\mathrm{em}} = 10^{-26}$ [1005].

gauge anomalies takes place within one family, we obtain

$$2C = D + E \text{ for the } [\text{SU}(3)]^2 \cdot \text{U}(1) \quad \text{anomaly},$$
$$3C + A = 0 \text{ for the } [\text{SU}(2)]^2 \cdot \text{U}(1) \quad \text{anomaly}, \quad (5.7)$$
$$2A^3 + 6C^3 = B^3 + 3(D^3 + E^3) \text{ for the } [\text{U}(1)]^3 \quad \text{anomaly}.$$

Other combinations, such as $[\text{SU}(2)]^3$, automatically vanish by a trace operation.

This does not uniquely fix hypercharges $A, \ldots, E$. There are two paths to charge quantisation. If we require that all fermions, except for the neutrino, acquire masses through the Yukawa coupling to ϕ (we assume that the U(1) hypercharge of ϕ is F), as in (2.32),

$$A - B - F = 0,$$
$$C - E - F = 0,$$
$$C - D + F = 0. \quad (5.8)$$

Note that the first equation of (5.7) is not independent of (5.8). Without loss of generality we choose $F = 1$ for the normalisation of the hypercharge. Now (5.7) and (5.8) have a unique solution:

$$A = -1,$$
$$B = -2,$$
$$C = 1/3,$$
$$D = 4/3,$$
$$E = -2/3, \quad (5.9)$$

in agreement with the $\text{U}(1)_Y$ charge assignment of the standard electroweak theory. This means that electromagnetic charges are quantised, and in particular, $Q_\nu = 0$.[3]

We now discuss the anomaly-free condition when the right-handed neutrino ν_R is introduced. We take the U(1) hypercharge $Y = G$ for ν_R. The last equation of (5.7) is modified as

$$2A^3 + 6C^3 = B^3 + 3(E^3 + D^3) + G^3, \quad (5.10)$$

---

[3] We may derive the charge quantisation without assuming Higgs coupling to fermions if we impose the condition of the cancellation of the gravitational anomaly. The graviton couples to all particles with equal weight, and the [graviton]$^2 \cdot$U(1) anomaly cancellation gives $\sum Y = 0$, i.e.,

$$2A + 6C = B + 3(D + E).$$

This allows three discrete sets of solutions, and one of them agrees with (5.9). The two other solutions ($D = -E$ and $D = -E/2$) are unphysical.

which, when combined with the other equations of (5.7) and (5.8), gives

$$G = -3C + F \, . \tag{5.11}$$

This means that we lose the quantisation of electromagnetic charges.

If we write the charge of neutrino as $G = \varepsilon$, we obtain

$$
\begin{aligned}
A &= -1 + \varepsilon \, , \\
B &= -2 + \varepsilon \, , \\
C &= (1 - \varepsilon)/3 \, , \\
D &= (4 - \varepsilon)/3 \, , \\
E &= -(2 + \varepsilon)/3 \, ,
\end{aligned}
\tag{5.12}
$$

which leads to the condition

$$Q_n + Q_\nu = Q_p + Q_e = 0 \, . \tag{5.13}$$

This guarantees the neutrality of the hydrogen atom. Inspection of (5.12) shows that ϵ corresponds to a $B - L$ charge, and the combination that appears in (5.12) is $Y' = Y + B - L$. This means that introduction of the $B - L$ U(1) gauge field does not lead to any new constraints.

In summary,

$$
\begin{aligned}
Q_e &= -1 + \epsilon \, , \\
Q_{\nu_L} &= Q_{\nu_R} = \epsilon \, , \\
Q_u &= 2/3 - \epsilon/3 \, , \\
Q_d &= -1/3 - \epsilon/3 \, .
\end{aligned}
\tag{5.14}
$$

This means that

$$Q(\text{proton}) = 1 - \epsilon \, , \qquad Q(\text{neutron}) = -\epsilon \, . \tag{5.15}$$

These conditions are derived only in the presence of the Higgs coupling to fermions (5.8). The gravitational anomaly-free condition does not give an independent relation. Only when we extend the group to $\text{SU}(2)_L \times \text{SU}(2)_R \times \text{U}(1)$, is the electric charge quantised, and $Q_\nu = 0$ results.[4]

The experimental limit on Q_ν is

$$|Q_\nu| \le (0.5 \pm 2.9) \times 10^{-21} \qquad (68\% \text{ CL}) \, . \tag{5.16}$$

---

[4] We assign the U(1) charge ($B - L$ quantum number) a to q_L, b to q_R, c to ℓ_L, and d to ℓ_R. Then the anomaly-free condition from $\text{SU}(3)^2\text{U}(1)$ leads to $a = b$, $\text{SU}(2)_L^2\text{U}(1)$ to $c + 3a = 0$, $\text{SU}(2)_R^2\text{U}(1)$ to $d + 3b = 0$, and $\text{U}(1)^3$ to $6a^3 + 2c^3 = 6b^3 + 2d^3$. (The other conditions are not independent.) This has a unique solution: $a = b$, and $c = d = 3a$. This is precisely the desired charge quantisation. In this derivation, we do not need to refer to the Yukawa coupling to the Higgs scalar.

This is obtained by assuming charge conservation in $n \to p + e^- + \bar{\nu}_e$ with the combined use of the measurement $|Q_p + Q_{e^-}| = 0.9 \pm 2.7 \times 10^{-21}$ (from an acoustic technique by applying an alternating electric field to SF_6 gas in a cavity) [1007] and $Q_n = (-0.4 \pm 1.1) \times 10^{-21}$ (68% CL) from a null result from the deflection of a cold neutron beam in a strong electric field [1008]. The astrophysical limit derived for the charge is $|Q_\nu| < 2 \times 10^{-15}$ from SN1987A [1009].

5.1.3 Magnetic and Electric Dipole Moments

The Dirac neutrino may have a magnetic dipole moment, $\mu = F_2(0) \neq 0$. In the Weinberg–Salam theory with ν_R, it is induced by radiative corrections and is calculated as [1010, 1011] (see also [1012])

$$\mu_{\nu_i} = \frac{3eG_F}{8\sqrt{2}\pi^2} m_{\nu_i} = 3 \times 10^{-19} \mu_B \left(\frac{m_\nu}{1\,\mathrm{eV}}\right) , \tag{5.17}$$

where μ_B is the Bohr magneton,

$$\mu_B = e/2m_e = 5.788 \times 10^{-9}\,\mathrm{eV} \cdot \mathrm{Gauss}^{-1} = 1.93 \times 10^{-11} e\,\mathrm{cm}. \tag{5.18}$$

A Dirac neutrino has a finite magnetic moment if $m_\nu \neq 0$. In a more general context, the magnetic moment is not necessarily proportional to the neutrino mass, and even a massless neutrino may have a finite magnetic moment. This subject is discussed fully in Chap. 10.

A particle with a finite magnetic moment scatters off electrons with a cross section [74] of

$$\frac{d\sigma}{dE'_e} = \pi \left(\frac{\alpha^2}{m_e}\right) \mu_\nu^2 \left(\frac{1}{E'_e - m_e} - \frac{1}{E_\nu}\right) \tag{5.19}$$

with a recoil electron energy of E'_e or

$$\sigma \simeq \pi \left(\frac{\alpha}{m_e}\right)^2 \mu_\nu^2 \log(q_{\max}^2 / q_{\min}^2) , \tag{5.20}$$

where $q_{\max}^2$ and $q_{\min}^2$ are cutoffs ($q_{\min}^2 \gg m_e^2$) of momentum squared at high- and low-momentum transfers. With this scattering, ν_L flips to ν_R.

In the original proposal for the neutrino, Pauli set the limit that μ_{ν_e} must be smaller than $0.02\mu_B$ based on the absence of interactions with matter (yet he wanted to have a finite value, as we have seen earlier) [1]. The detection of the neutrino interaction [93] immediately improved the limit to $\mu_{\nu_e} < 1 \times 10^{-9}\mu_B$ [1013]. Derbin [1014] reviewed the reactor data [244, 1015], and concluded from recoil electron energy distributions that

$$\mu_{\nu_e} < 1.8 \times 10^{-10}\mu_B \tag{5.21}$$

at 90% CL (see also [1016]). A modern stopped muon experiment resulted in $\mu_{\nu_e} < 10.8 \times 10^{-10}\mu_B$ [1017]. Note that a better limit is obtained more

easily from a lower energy neutrino beam since the weak interaction cross section increases as E_ν, whereas (5.20) remains constant. This explains why the stopped muon experiment does not improve the limit obtained by Cowan and Reines [1013] 40 years ago. For ν_μ stopped (π^+, μ^+) experiments [1017] (see also [1018, 1019]) give

$$\mu_{\nu_\mu} < 7.4 \times 10^{-10} \mu_{\rm B} \ . \tag{5.22}$$

The laboratory limit on μ_{ν_τ} is

$$\mu_{\nu_\tau} < 3 \times 10^{-6} \mu_{\rm B} \ , \tag{5.23}$$

derived from $e^+ e^- \to \nu \bar{\nu} \gamma$ [1020–1022]. There is also a limit from a search for $\nu_\tau e^- \to \nu_\tau e^-$ in a bubble chamber (CERN-BEBC) in the beam dump experiment, where ν_τ is supposed to come from D_s^0 meson [1023], $\mu_{\nu_\tau} <$ $5.4 \times 10^{-7} \mu_{\rm B}$. This limit assumes that the D_s^0 meson production cross section is 0.1 times that of a D^0 meson.

A stronger limit is derived from the constraint against excess stellar cooling. As discussed in Sect. 4.4.7, a photon that has acquired a mass of the plasma frequency in the stellar interior decays into a neutrino pair through virtual $e^+ e^-$ pair production. The presence of a finite magnetic moment would enhance this effect and deprive the stellar core of nuclear energy, resulting in excess cooling, which would promote evolution of the star [1003, 1024–1026]. The energy loss rate via magnetic moment is given by

$$\varepsilon_{\nu\text{mag mom}} = \frac{\alpha \zeta(3)}{12\pi^2} \frac{m_e^5}{\rho} \left(\frac{\mu}{\mu_{\rm B}}\right)^2 \left(\frac{\omega_p}{m_e}\right)^7 \left(\frac{\omega_p}{kT}\right)^{-3} \ , \tag{5.24}$$

where ω_p is defined in (4.127). An application of the condition (4.140) gives a limit $\mu_{\nu_i} < 1 \times 10^{-11} \mu_{\rm B}$ [742] on the largest of the magnetic moments of neutrinos from the number count of He-burning stars (red clump) in open clusters. This argument is not too sensitive to model details because the essential input is only the temperature of the stellar core at helium burning and the number count of He-burning stars. Blinnikov [1027] derived $\mu_{\nu_i} <$ $0.5 \times 10^{-11} \mu_{\rm B}$ from the luminosity function of cooling white dwarfs, using an argument similar to that by Stothers [243]. This argument is also robust since the structure of white dwarfs is simple. A stronger bound of $\mu_{\nu_i} <$ $0.3 \times 10^{-11} \mu_{\rm B}$ was inferred by Raffelt [740] from an estimate of the effect on the critical mass for a helium flash, which affects the difference in luminosities of the tip of the red giant branch and the horizontal branch stars. We may take

$$\mu(\nu_i) < (0.3 - 1) \times 10^{-11} \mu_{\rm B} \tag{5.25}$$

as a limit from astrophysics. Stronger limits are inferred from the cooling argument for supernova SN1987A [1028], but we do not take them for the reasons we discussed in Sect. 4.5.1. The limit from neutron-star cooling is weak [1029].

A similar, but slightly weaker limit is derived from cosmological considerations. In the high-temperature environment of the early universe, electrons are abundant and ν_L scatters off electrons, turning into ν_R (depolarisation). If this process takes place fast while ν_L is in equilibrium ($T \gtrsim 4$ MeV), it produces ν_R as abundantly as ν_L and increases the expansion rate of the universe; hence helium abundance increases excessively. This effect was first noticed in [1030] ($\mu_\nu \leq 1.5 \times 10^{-11}\mu_B$ is derived), but proper treatment of the infrared cutoff by Debye screening makes the limit weaken to $\mu_\nu \leq 5.2 \times 10^{-11}\mu_B$ [1027]. A more accurate treatment of the plasma effect on depolarisation was developed in [1031]; it gives $\mu_\nu \leq 6.2 \times 10^{-11}\mu_B$.

The Dirac neutrino may also have an electric dipole moment if both parity and CP are broken, but it always vanishes when $m_\nu = 0$, because the phase of the wave function can be rotated away so that CP is effectively unbroken. For $m_\nu \neq 0$, the neutrino may have an electric dipole moment. Since νe scattering experiments are done using neutrino beams with an energy much larger than the possible neutrino mass, neutrinos essentially behave as left-handed, and neutrinos scattering off electrons via an electric dipole moment and that via a magnetic dipole moment yield an identical result. Therefore, the limits on the magnetic moment are interpreted as those on the electric dipole moment. Using conventional units, the experimental limit (5.21) is reexpressed as

$$ed \leq 3 \times 10^{-21} e \text{ cm.} \tag{5.26}$$

5.1.4 Charge Radius

The charge radius is defined by

$$\langle r^2 \rangle = 6 \frac{\partial}{\partial q^2} f(q^2)\Big|_{q^2=0} , \tag{5.27}$$

where $f(q^2) = F_1(q^2) + G_1(q^2)$ and $f(0) = 0$. The neutrino may generally have a finite $\langle r^2 \rangle$. The charge density of the neutrino is not positive definite and $\langle r^2 \rangle$ can be negative.

The calculation of the charge radius in the standard model has a confusing history [1032]; if one calculates only vertex corrections, they are not gauge invariant and are generally divergent, and therefore physically meaningless. Finally, Degrassi et al. [1033] identified $\langle r^2 \rangle$ as that measured in experiments with a target-independent part of the radiative correction for neutrinos scattering off leptons or hadrons. This physical (gauge-independent) $\langle r^2 \rangle$ contains not only radiative corrections of the $\nu\bar{\nu}\gamma$ vertex but also terms arising from box diagrams. The calculated $\langle r^2 \rangle$ is sensitive to the top quark mass, and the result given in Table I of [1026] may be represented as

$$\begin{aligned}
\langle r^2 \rangle_{\nu_e} &= [+0.51 + 0.40(m_{t174}^2 - 1)] \times (10^{-16}\text{cm})^2 , \\
\langle r^2 \rangle_{\nu_\mu} &= [+0.82 + 0.40(m_{t174}^2 - 1)] \times (10^{-16}\text{cm})^2 , \\
\langle r^2 \rangle_{\nu_\tau} &= [+0.99 + 0.40(m_{t174}^2 - 1)] \times (10^{-16}\text{cm})^2
\end{aligned} \tag{5.28}$$

at an accuracy of 10%, where $m_{t174} = m_t/174\,\mathrm{GeV}$, and the on-shell scheme of Sect. 2.5.2 is used for renormalisation.

The effect of the $\langle r^2 \rangle$ term on νe elastic scattering is obviously absorbed into a shift of the vector coupling of the Z^0 exchange $g_V = g_L + g_R$ as $g_V + 2\delta$, where

$$2\delta = \frac{\sqrt{2}\pi\alpha}{3G_F}\langle r^2 \rangle = 2.38 \times 10^{30}\,\mathrm{cm}^{-2}\langle r^2 \rangle\,, \tag{5.29}$$

or $\sin^2 \theta_W \to \sin^2 \theta_W + \delta$. Within the standard theory this is included in one-loop radiative corrections.

For $\sin^2 \theta_W = 0.2230$ derived from Z physics (on-shell scheme), the $\nu_\mu e \to \nu_\mu e$ experiment by Ahrens et al. [1019][5] gives

$$-5.3 \times 10^{-32} < \quad \langle r^2 \rangle_{\nu_\mu} \quad < 1.3 \times 10^{-32}\,\mathrm{cm}^2\,. \tag{5.30}$$

If we use the data of the CHARM II collaboration [1018], we find

$$-0.77 \times 10^{-32} < \quad \langle r^2 \rangle_{\nu_\mu} < 2.5 \times 10^{-32}\,\mathrm{cm}^2\,. \tag{5.31}$$

For ν_e the LAMPF experiment [1017] yields

$$-5.0 \times 10^{-32} < \quad \langle r^2 \rangle_{\nu_e} \quad < 10.2 \times 10^{-32}\,\mathrm{cm}^2\,. \tag{5.32}$$

The experimental limit is consistent with the prediction of (5.28). The consistency would be violated if $\sin^2 \theta_W$ were > 0.226, or m_t were larger than 210 GeV.

The prediction of the standard theory is of the order that the next generation experiment can detect, in contrast to the case with the magnetic dipole moment where an ample gap exists between the empirical limit and the one-loop prediction of the standard model.

5.2 Limit on the Mass of Neutrinos

While the neutrino has been traditionally supposed to be massless, no exact symmetry is known that forbids neutrinos from having a finite mass. (It should be remembered that gauge symmetry forbids the photon from having a finite mass [1034].) Searches for the neutrino mass have been made for many years, and the existence of a finite mass was finally confirmed in the last few years using an indirect method. We defer the task of describing this indirect determination to Chap. 8. Here, we discuss only results from direct searches for the neutrino mass.

---

[5] Ahrens et al. [1019] remarked that their earlier publication contained errors in their formula. Their corrected formula, however, still contains errors of a factor $\sqrt{2}$. Here, these errors are corrected to derive (5.30).

Table 5.1. Atomic and molecular corrections for tritium beta decays. P_0 is the probability of remaining in the ground state, and $\overline{\Delta E}$ is the average energy of excitations.

	T (atomic) [1035]	HT (molecular) [1037]	CH$_3$T [1042]	[1043]	CH$_3$–CHT–CH$_3$ [1043]	Valine [1042]
P_0	0.7023	0.5769	0.6122	0.607 ~ 0.623	0.598	0.6122
$\overline{\Delta E}$(eV)	27.21	29.27	30.30	—	—	30.12

The direct laboratory limits on the neutrino masses are summarised as follows:

$$m_{\nu_e} < 2.5\,\text{eV} \qquad (95\%\ \text{CL})\,, \tag{5.33}$$

$$m_{\nu_\mu} < 170\,\text{keV} \qquad (90\%\ \text{CL})\,, \tag{5.34}$$

$$m_{\nu_\tau} < 18\,\text{MeV} \qquad (95\%\ \text{CL})\,. \tag{5.35}$$

The modern ν_e mass measurements use exclusively the decay of tritium $^3\text{H} \rightarrow {}^3\text{He} + \bar{\nu}_e + e^-$, which has a small Q value, $Q = 18.6\,\text{keV}$, and look for a rounding of the electron spectrum at the end point in the Kurie plot. For allowed or superallowed β transitions, the transition matrix element is constant and the transition rate Γ is determined solely by the phase-space volume factor,

$$d\Gamma \propto d^3p_e d^3p_\nu \delta(E_e + E_\nu - E_0) \propto E_e p_e E_\nu p_\nu dE_e\ . \tag{5.36}$$

For the massless neutrino the shape factor of the electron spectrum is defined by

$$S(E_e) \equiv \frac{d\Gamma(E_e)/dE_e}{E_e p_e F(E_e, Z)} \propto (E_0 - E_e)^2\ , \tag{5.37}$$

where $E_0(= Q - m_\nu)$ is the maximum energy of the electron and $F(E_e, Z)$ is the Fermi function. With a finite mass, the shape factor is modified to

$$S(E_e) \propto (E_0 - E_e + m_\nu)[(E_0 - E_e)(E_0 - E_e + 2m_\nu)]^{1/2}$$
$$= (Q - E_e)[(Q - E_e)^2 - m_\nu^2]^{1/2}\ . \tag{5.38}$$

In practice, this spectrum is rounded by the finite resolution of the spectrometer, the energy loss at the tritium source, and the final state excitation. Radiative corrections change the end-point spectrum very little.

In exploring the neutrino mass, the fact must be taken into account that β decay excites the helium atom and/or surrounding atoms [197]. For a free tritium atom, for instance, the shape factor is replaced by

$$S(E_e) = \sum_{n=1}^{\infty} P_{nS} S_{nS}(m_\nu; E_{nS}) + \int_0^\infty dE_\alpha P_\alpha(E_\alpha) S_\alpha(m_\nu : E_\alpha), \quad (5.39)$$

where P_{nS} (P_α) is the probability that the nS state (the continuum state) is excited and $S_{nS(\alpha)}$ is given by (5.38) with $E_0 \to E_0 - E_{nS(\alpha)}$. For a free hydrogen atom,

$$P_{nS} = |\langle Z = 2, nS | Z = 1, 1S \rangle|^2, \quad (5.40)$$

in the impulse approximation, and is calculated as

$$P_{nS} = \frac{512 n^5 (n-2)^{2(n-2)}}{(n+2)^{2(n+2)}}, \quad (5.41)$$

which gives $P_{1S} = 70.2\%, P_{2S} = 25\%, P_{3S} = 1.27\%, ..., P_{\text{cont}} = 2.6\%$ with mean excitation energy $\overline{\Delta E} = 27.21$ eV, including excitation to the continuum [1035, 1036]. Elaborate calculations have been carried out for a T_2 molecule [1037–1040]. It is shown that P_{1S} is smaller (58%) than that for atomic tritium. The effect of the crystal is considered in [1041]. Higher excitation, it is shown, is more important than for gaseous T_2; the effect is nonnegligible when one explores a $m_{\nu_e} < 10$ eV range.

For convenience in making a strong tritium source in a thin film, it is often embedded in organic molecules. The correction for surrounding molecules, especially for the shake-off process (ionisation), is substantially more complicated. Calculations for molecules were made in [1042–1044] using the wave function obtained by the molecular orbital method. It is claimed that the results are sufficiently accurate to extract the mass of the electron neutrino at the necessary level. The most important parameters that control $S(E_e)$ are the probability of the ground state and the mean excitation energy, which are given in Table 5.1.

The spectral shape (5.37) means that the statistics requirement becomes more demanding as one approaches the end point to measure a smaller m_{ν_e}. This requires a strong tritium source. The experimentally crucial elements are proper knowledge of the response function of the detector, with which the electron spectrum is convoluted, and the electron energy loss function at the source. The latter problem is minimised by making the source as thin as possible, but this reduces the intensity of the source. High resolution and an intense source are also contradictory requirements on the spectrometer.

For precision electron spectroscopy, a $\pi\sqrt{2}$ magnetic spectrometer (which uses the principle that an electron beam focuses at an angle of $\pi\sqrt{2}$ under the $B \propto 1/\sqrt{r}$ magnetic field) has been the traditional apparatus (e.g., [197, 1045]). The spectrometer is built without any magnetic materials to avoid

hysteresis effects and disturbances so that the magnetic field distribution is accurately controlled; the magnetic field from Earth is also screened. Some recent experiments use a (magnetic material free) toroidal magnetic field spectrometer, called the Tretyakov type spectrometer [1046]. The principle is proposed in [1047]: electrons emitted in the radial direction, perpendicular to the magnetic field, focus at every $180°$ turn under a magnetic field of $1/r$ distribution. The advantage of the toroidal spectrometer is large solid angle acceptance from the source. There is also a new type of spectrometer using electrostatic retardation. The magnetic field forms a 'bottle' with necks at the two ends, and the electron beam emitted from one neck is transported along the magnetic field lines. In the middle, a negative electrostatic potential is applied to filter out electrons whose energy is lower than a given threshold. Electrons that pass through the filter are then reaccelerated to the other end and focused by the guiding magnetic field for detection [1048]. (For a more detailed discussion on detectors, see [1049].)

Recent ν_e mass experiments are summarised in Table 5.2. Note that all experiments (with the exception of ITEP, which gave a positive neutrino mass) resulted in a negative m_ν^2 for their best fits. It is also to be noted that the shape factor given by (5.38) does not fit the data quite well for the electron spectrum in a wide range and some groups introduce a shape correction factor $[1 + \alpha_n(E_0 - E_e)^n]$ $(n = 1, 2)$ into (5.38) for better fitting, which, however, should introduce further systematic errors since the origin of this distortion is not understood. The best current upper limit on ν_e is 2.5 eV, obtained by the Troitsk and Mainz groups, but a reservation should be made for possible systematic effects that are not understood.

Table 5.2. Summary of ν_e mass experiments using tritium β decay.

Group [ref.]	Source	Detector	Corrections	Fit of m_ν^2 (eV^2)	m_ν limit (eV) (at 95% CL)
ITEP (1980-1987) [198, 1050]	Valin $C_5H_9T_2NO_2$	Tret.	[1042]	$+970 \pm 50 \pm 160$	$17 < m_\nu < 40$
Los Alamos (1987) [1051]	T_2 gas	Tret.	[1038]	-57^{+453}_{-118}	< 27
Zürich (1990) [1052]	Octadecyl-trichlorosilane	Tret.	CH_3T [1044]	$-24 \pm 48 \pm 61$	< 11
INS (1991) [1045]	Cd icosanoate $(C_{20}H_{32}T_8O_2)_2Cd$	$\pi\sqrt{2}$	[1042]	$-65 \pm 85 \pm 65$	< 13
Los Alamos (1991) [1053]	T_2 gas	Tret.	[1037–1039]	$-147 \pm 68 \pm 41$	< 9.3
Mainz (1992) [1054]	Frozen T_2 (2.8K)	ES	[1041]	$-39 \pm 34 \pm 15$	< 7.2
LLNL (1995) [1055]	T_2 gas	Tret.	[1037]	-130 ± 20	< 7
Troitsk (1999) [1056]	T_2 gas	ES	[1040]	$-1.9 \pm 3.4 \pm 2.2$	< 2.5
Mainz (1999) [1057]	T_2 gas	ES	[1041]	$-3.7 \pm 5.3 \pm 2.1$	< 2.8

A few methods have been proposed to use electron capture to measure electron neutrino mass. The first is the use [1058] of internal bremsstrahlung electron capture (IBEC) $(Z, A) + e^- \rightarrow (Z-1, A) + \nu_e + \gamma$ [1059]. The photon (X ray) emitted in the internal conversion has an end-point spectrum of the form of (5.38) where E_e is replaced by the photon energy k_γ (the prefactor $E_e p_e$ is replaced by k_γ). De Rújula has shown that the IBEC rate, which is otherwise too small, receives a resonance-like enhancement if k_γ is close to the energy of the characteristic X rays. As a promising candidate, he has proposed ^{163}Ho, which has the smallest Q value ($\simeq 2.5$ keV) among the known electron capture nuclei. This Q value is so small that K and L captures ($E_K \simeq 54$ keV, and $E_L \simeq 8$–9 keV) are forbidden, and the M orbit ($E_M \simeq 2$ keV) is the lowest in which the electron can be captured; therefore, the neutrino energy is as small as 500 eV, appropriate for finite neutrino mass detection.

The second method is to use relative electron capture rates. When the neutrino is massive, the q^2 factor in (3.84) is replaced by qE_ν, and captures from the orbits close to the Q value could differentiate the neutrino mass by comparing the capture rates from $3s_{1/2}$, $3p_{1/2}$ and $4s_{1/2}$ [1060].

Several groups carried out experiments and derived limits on the neutrino mass of the order of a few hundred eV [1061–1063] using ^{163}Ho. However, the derived Q values differ among the experiments by as much as 150 eV, which makes it difficult for us to take seriously the derived mass limits. The general problems are too small an IBEC capture rate close to the end point for the first method and uncertainties in the atomic physics of ^{163}Dy.[6]

The limit on the ν_μ mass is obtained from the two-body kinematics of $\pi^+ \rightarrow \mu^+ + \nu_\mu$ decay. The most precise measurement of the muon momentum is that by Assamagan et al. [1065] using stopped π^+. When combined with a precision measurement of pion mass (using X rays from the $4f$–$3d$ transition in pionic ^{24}Mg) [1066] and muon mass, the measured muon momentum yields the best fit for the kinematics with $m_{\nu_\mu}^2 = -0.016 \pm 0.023$ (MeV)^2, or a limit $m_{\nu_\mu} < 0.17$ MeV at a 90% CL. The error budget of the measurement is shown in Table 5.3. The precision of muon momentum has increased by an order of magnitude during the last decade, and it is now comparable to that of pion mass. Note that pion mass from the $4f$–$3d$ transition suffers from an ambiguity concerning the electronic configurations in the K orbit, whether it is occupied by either one and two or zero and one electrons (the data are consistent with their being composed of two peaks). Accordingly, Jeckelmann et al. [1066] give two solutions, but one of their solutions gives too small a pion mass to be consistent with the muon momentum measurement and is discarded. Even with the other solution, $m_{\nu_\mu}^2$ is still negative, as we quoted, indicating that the true pion mass would be larger than that obtained from

---

[6] In this connection, we refer to the measurement of the bound-state β^- decay from ^{163}Dy with stripped electrons to ^{163}Ho, which also offers a method of measuring the neutrino mass [1064].

Table 5.3. Error budget for ν_μ mass measurements.

Year	$\Delta p_\mu / p_\mu$	$\Delta m_\pi / m_\pi$	$\Delta m_\mu / m_\mu$	m_{ν_μ} limit
1986	28 ppm [1067]	3.8 ppm [1068]	0.32 ppm [275]	< 0.27 MeV [1067]
1996	3.7 ppm [1065]	2.5 ppm^a [1066]	0.32 ppm [275]	< 0.17 MeV [1065]

^{a} Systematic errors are not included (see text).

the pionic atom measurement. Reduction of systematic errors is necessary for pion mass measurement to improve the limit on m_{ν_μ}.

There is another type of experiment measuring p_π and p_μ for pion decay in flight [1069]. The advantage is that the uncertainty in m_π enters the result as a minor factor. The limit from this method is $m_{\nu_\mu} < 0.50$ MeV at a 90% CL.

The best limit on the ν_τ mass is derived from the invariant mass distribution of 3π and 5π systems in $\tau \to 3(5)\pi + \nu_\tau$. Using the maximum likelihood analysis, the Aleph group [1070] obtained $m_{\nu_\tau} < 18.2$ MeV at a 95% CL(see also [1071]). The OPAL group tried to obtain a limit from the distribution of the missing energy using the double three-charged-particle decay mode of τ in $Z^0 \to \tau^+\tau^-$. They obtained $m_{\nu_\tau} < 35.3$ MeV [1072].

We have discussed direct limits on the neutrino mass, but those on ν_μ and ν_τ are unrealistically weak. In Chap. 8 we shall see that mass difference squares of three neutrinos are no more than 0.004 eV^2. Combined with the direct limit on ν_e mass, the realistic limits on the masses of three neutrinos are

$$m_{\nu_e}, \; m_{\nu_\mu}, \; m_{\nu_\tau} < 2.5 \, \text{eV} \,, \tag{5.42}$$

and at least one neutrino has a mass more than ≈ 0.04 eV.

In the past, many interesting possibilities have been discussed for moderately massive neutrinos. Now they are all no more than of academic interest.

5.3 Neutrino Mass: Cosmological and Astrophysical Considerations

A strong and robust limit is derived on the neutrino mass from a cosmological argument [252, 255]. In the early universe neutrinos were in equilibrium with other radiation, and the number density is prescribed by the Fermi distribution. The density today should be $\simeq 110$ cm^{-3} per neutrino species, as we have seen in Chap. 4 [see (4.188)]. Massive neutrinos contribute to the mass

density of the universe by the amount of $m_\nu n_{\nu+\bar{\nu}}$. By requiring that this does not exceed the critical density of the universe (4.203), $\rho_{\text{crit}} = 10.54h^2 \text{ keV}$,

$$m_\nu n_{\nu+\bar{\nu}} < \rho_{\text{crit}}, \tag{5.43}$$

one obtains

$$\sum_i m_{\nu_i} \lesssim 96h^2 \text{ eV} , \tag{5.44}$$

if the neutrinos are stable on the cosmological timescale. The constraint becomes stronger by a factor of 3 if we use the observed mass density of the universe (see Sect. 4.5.1). These limits are stronger by several orders of magnitude than the laboratory limits for ν_μ and ν_τ, thus leading us to believe that the masses of all three neutrinos are very small. Limit (5.44) is the least model-dependent cosmological limit. We cannot evade it insofar as we accept the Big Bang. The only escape is to suppose that the neutrino has already decayed. Within the standard theory, however, the lifetime of neutrinos ($m_\nu \lesssim 1 \text{ MeV}$) should be longer than the age of the universe.

We now know that masses of neutrinos are all smaller than a few eV, and thus satisfy limit (5.44). The neutrino contributes to the cosmological mass density by the amount of

$$0.0008 \lesssim \Omega_\nu \lesssim 0.16 . \tag{5.45}$$

The number density of the cosmic neutrino is so great that it would easily dominate the universe, if the mass of the neutrino is of the order of 10 eV [252–255]. A number of important considerations have been made on this possibility. The first is whether massive neutrinos could be dark matter of the universe, in particular, whether it would be the major component of the Galactic halo. Neutrinos are fermions, so there is a phase-space limit as to the density of neutrinos. The Liouville theorem states that the phase-space density decreases only as the system relaxes. Assuming the isothermal distribution in gravitationally clustered objects (like haloes), the phase-space number density of neutrinos is given by the Maxwellian distribution,

$$n_\nu(\mathbf{x}, \mathbf{p}) = \rho_\nu \frac{1}{m_\nu^4} \frac{1}{(2\pi\sigma^2)^{2/3}} \exp(-\mathbf{v}^2/2\sigma^2) , \tag{5.46}$$

where $\mathbf{v} = \mathbf{p}/m$ and σ is the line of site value of the virial velocity determined by gravitational clustering. Requiring that the largest of this density does not exceed that of the Fermi distribution, two per unit phase-space volume, we have

$$\rho_\nu \frac{1}{m_\nu^4} \frac{1}{(2\pi\sigma^2)^{2/3}} < \frac{2}{(2\pi)^3} . \tag{5.47}$$

The virial equilibrium is

$$m_\nu \frac{G \left(\frac{4\pi}{3} R^3 \rho_\nu \right)}{R} = 2m_\nu \frac{1}{2} \langle v^2 \rangle , \tag{5.48}$$

where $\langle v^2 \rangle = 3\sigma^2$ and R is the size of the bound object. From these two conditions we obtain [1073]

$$m_\nu > (100 \, \text{eV}) \left(\frac{100 \, \text{km s}^{-1}}{\sigma} \right)^{1/4} \left(\frac{1 \, \text{kpc}}{R} \right)^{1/2}. \qquad (5.49)$$

This means that $m_\nu > 20 \, \text{eV}$ if neutrinos are dark matter of the Galactic halo ($R \sim 20 \, \text{kpc}$, $\sigma \sim 300 \, \text{km s}^{-1}$). For cluster cores ($R \sim 500 \, \text{kpc}$, $\sigma \sim 1000 \, \text{km s}^{-1}$), the limit is $> 2.5 \, \text{eV}$.

If the universe is gravitationally dominated by neutrinos, they control the formation of cosmic structure [256]. The important feature of neutrinos as dark matter is that the neutrinos stream while they are relativistic and smear out perturbations smaller than the free streaming scale. The streaming scale is $\ell \sim ct \sim c m_{\text{pl}}/m_\nu^2$ where $t \sim m_{\text{pl}}/T^2$ is the cosmic time when the neutrino becomes nonrelativistic ($T \sim m_\nu$). Therefore, the mass in the sphere encircled by this length scale is $M \sim m_\nu^4 \ell^3 \sim m_{\text{pl}}^3/m_\nu^2 \sim 10^{15} M_\odot (m_\nu/30 \, \text{eV})^{-2}$ [256]. To make cluster size objects, $m_\nu > 30 \, \text{eV}$ is necessary. Zeldovich [1074] proposed the scenario that clusters form first with light neutrinos, and then galaxies form by a dissipative collapse of clusters. This possibility, however, is ruled out by now because *no nonlinear structure* forms in this scenario by the present epoch if the adiabatic perturbation spectrum is normalised to the COBE observation.[7]

Even if neutrinos do not dominate the universe, massive neutrinos would affect the formation of the cosmic structure if the mass density from neutrinos is $\gtrsim 10\%$ of the cosmic matter density. This, it was once thought, saves the problem of the deficiency in large-scale power of the cosmic density perturbations in the Einstein–de Sitter universe [1075]. The advance in observations, however, has shown that the matter density of the universe is smaller than unity. A low-density universe automatically solves the problem of the deficiency in large-scale power [892], and light mass neutrinos are rather unwelcome. Figure 5.1 shows the effect of massive neutrinos on the power spectrum of cosmic perturbations for a universe with $\Omega_0 = 0.3$ and $\lambda_0 = 0.7$: massive neutrinos reduce the power on the small scale and the power is affected significantly even by 1-eV(summation over three species) neutrinos [1076]. The normalisation of the left-wing of the curve is fixed by fluctuations imprinted on the CMB, as measured by the COBE satellite [1077]. The power spectrum on the small scale is explored by galaxy clustering (see Sect. 4.6.3). Such analyses have some uncertainties in the normalisation, but the most ambiguity-free determination of the normalisation of the power spectrum is provided by cluster abundance [1078]. The two normalisations on large and small scales constrain the contribution from the neutrino and hence, its mass. This generally leads to $\sum_i m_{\nu_i} < 2.7 - 4.5 \, \text{eV}$ [1079–1082].

---

[7] It was suspected that the formation of clusters may be too slow, even if one takes a rather large fluctuation spectrum. The observation of COBE set the normalisation of the spectrum and made this statement definitive.
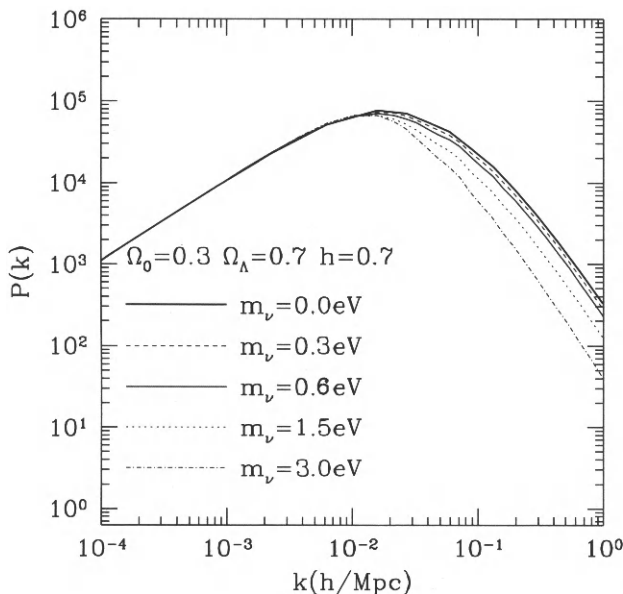
Fig. 5.1. Effects of massive neutrinos on the power spectrum of cosmological perturbations. The neutrino mass indicated stands for the sum over three neutrinos. The spectrum is normalised on a large scale by the CMB data.

See also [1083], which derived a comparable limit (2.2 eV) on the neutrino mass from $P(k)$ alone with $n = 1$ and $\Omega_0 < 0.5$ assumed (with the same assumptions the cluster abundance and the COBE result lead to a limit of 2.7 eV [1081]). The ambiguity in this argument is that the intrinsic tilting of the spectrum [n of (4.208)] would give a similar effect, and blue tilting ($n > 1$, i.e., more power on small scales) might prepare the condition that is compensated for by neutrinos to give an acceptable power spectrum, thus evading the constraint on neutrino mass. The new generation experiments on CMB fluctuations [850], when combined with baryon abundance from nucleosynthesis, however, constrain the tilting parameter, so that the above argument is validated. $\sum_i m_{\nu_i} < 4$ eV was derived in [1082] from such a consideration[8] (see also [1080]).

Finally, we mention the attempts to set a limit on m_{ν_e} based on the duration of the neutrino burst at the time of supernova SN1987A [1084]. The presence of mass delays the arrival time of the neutrinos by the amount $\Delta t = \frac{1}{2}(m/E_\nu)^2(\ell/c)$. Since E takes a thermal distribution, the propagation causes a spread of the neutrino burst of the order of Δt, while this spread should be shorter than the duration of the observed burst. The limit derived varies from $\lesssim 6$ eV to $\lesssim 30$ eV; stronger limits are more model-dependent.

---

[8] Whether one neutrino has 4 eV or it is shared by three neutrinos makes no difference in this argument.

Appendix: Cosmological Limits on the Mass of Heavy 'Neutrinos'

In connexion with cosmological constraints on neutrino mass, it is interesting to consider the case for heavy 'neutrinos' [1085]. Although we now know that all neutrinos are light, the case has wide application to weakly interacting massive particles (WIMP), which are candidates for dark matter in the universe. If the mass of neutrinos is more than a few MeV, neutrinos are nonrelativistic when they decouple from the thermal bath, and the number density is reduced by a factor of $\sim \exp(-2m_\nu/T)$. This Boltzmann factor also pushes up the decoupling temperature. These massive particles do not annihilate completely even in the presence of particle–antiparticle symmetry, and a small but cosmologically significant amount may be left over [828].

The number density of neutrinos obeys (4.188). Writing $n_\nu = T^3 f$ and $n_\nu^{eq} = T^3 f_{eq}$ and using the variable $x = m/T$, we rewrite (4.188) with the aid of (4.181):

$$\frac{df}{dx} = -\langle \sigma v \rangle \frac{m_\nu}{Ax^2}(f^2 - f_{eq}^2) , \qquad (5.50)$$

where $A = (8\pi^3 G g_*/45)^{1/2}$ and

$$f_{eq}(x) = \frac{2}{(2\pi)^3} \int d^3u \frac{1}{e^{\sqrt{x^2+u^2}} + 1} , \qquad (5.51)$$

with $u = p/T$. For the annihilation cross section of pair neutrinos $\langle \sigma v \rangle \sim \sigma_0 x^{-n}$, we obtain

$$\frac{df}{dx} = -\lambda x^{-n-2}(f^2 - f_{eq}^2) , \qquad (5.52)$$

with $\lambda = \sigma_0 m_\nu/A$. This equation can be numerically integrated with the initial condition $f = f_{eq}$ at $x = 0$ ($T \to \infty$) to obtain $f(x)$. To get an approximate solution [1086,246], we suppose that $x_d = m_\nu/T_d$ is the decoupling temperature and write $\delta f = f - f_{eq}$. Equation (5.52) is

$$(\delta f)' + f_{eq}' = -\lambda x^{-n-2}(\delta f)(\delta f + 2f_{eq}) . \qquad (5.53)$$

For $T \ll T_d$ ($x \ll x_d$), $f_{eq} \approx 0$, so that

$$(\delta f)' = -\lambda x^{-n-2}(\delta f)^2 . \qquad (5.54)$$

Integration from $x = x_d$ to ∞, noting that $\delta f(x_d) \gg \delta f(\infty)$, gives

$$f(\infty) \simeq \delta f(\infty) = \frac{n+1}{\lambda} x_d^{n+1} . \qquad (5.55)$$

Then,

$$f(\infty) \simeq \frac{\sqrt{g_*}(n+1)}{\langle \sigma v \rangle m_\nu m_{pl}} x_d \sqrt{\frac{8\pi^3}{45}} . \qquad (5.56)$$

Here, $x_d \approx 15 + 3\ln(m_\nu/1\,\text{GeV})$ is obtained by numerical integration. Thus the heavy neutrino abundance at $T \to 0$ depends only on its mass and annihilation cross section: a weaker interaction leads to a larger abundance.

For heavy Dirac neutrinos, we find

$$\langle \sigma v \rangle \simeq K \frac{G_F^2 m_\nu^2}{2\pi} \,, \tag{5.57}$$

with $K \approx 5$, so that $f(\infty) \approx 2.7 \times 10^{-8}\sqrt{g_*}$. From

$$n_{\nu 0} = f(\infty)T_{\nu 0}^3 \simeq 570 f(\infty)\ \text{cm}^3 \,, \tag{5.58}$$

the relic neutrino abundance varies as $\sim m_\nu^{-3}$, and the condition $m_\nu n_{\nu 0} < \rho_{\text{crit}}$ gives [1085] (see also [1087, 1088]),

$$m_\nu \gtrsim 2h^{-1}\,\text{GeV}. \tag{5.59}$$

For the Majorana neutrino the limit is $\gtrsim 5h^{-1}\text{GeV}$ instead [1089].

If the neutrino has a mass just above the critical value, it can be *cold* dark matter of the universe (neutrinos are nonrelativistic at the time of decoupling). The candidate particle cannot be the neutrino but may be some other weakly interacting massive particles; the most promising candidate is the lightest supersymmetric particle (LSP) [1090, 1091]. A calculation similar to that sketched here applies to LSP; see [1092].

Massive neutrinos may decay. If they decay into electromagnetically interacting particles, the constraints are very strong from cosmology (see Sect. 10.5.2), but decay into weakly interacting particles receives only weak constraints. The argument that cosmological energy density must be smaller than the critical value leads to

$$m_\nu n_{\nu+\bar{\nu}}\left(\frac{\tau_\nu}{t_0}\right)^{1/2} \leq \rho_{\text{crit}} \,, \tag{5.60}$$

where $n_{\nu+\bar{\nu}}$ is the cosmic neutrino mass density and t_0 is the age of the universe. For neutinos that are not too heavy ($m_\nu < 1\,\text{MeV}$), using (4.188),

$$m_\nu^2 \tau_\nu \lesssim 3.8 \times 10^{21}h^4\,\text{s eV}^2 \,, \tag{5.61}$$

where the age of the universe is taken to be 14 Gyr.[9] For heavy neutrinos ($m_\nu > 10\,\text{MeV}$), $n_{\nu+\bar{\nu}}$ must be replaced by (5.58) [1087, 1093].

---

[9] This limit, however, is conservative; to have successful cosmic structural formation, the universe must have been matter-dominated essentially all the time after hydrogen recombination at least at the redshift $z \simeq 1500$, or even earlier.

6 Massive Neutrinos

6.1 Massive Neutrinos – Overview

The mass term connects a left-handed field to its right-handed partner, i.e., it is the term that flips the chirality of a particle. There are two possible mass terms, the Dirac mass term,

$$m(\bar{\psi}_R \psi_L + \text{h.c.}) \,, \tag{6.1}$$

and the Majorana mass term,

$$M(\overline{\psi^c_L} \psi_L + \text{h.c.}) \,, \tag{6.2}$$

where $\psi^c = C\gamma^0\psi^*$ is the charge-conjugated field of ψ and $\psi^c_L \equiv (\psi_L)^c = \frac{(1+\gamma_5)}{2}\psi^c$ has right-handed chirality. The former is the term $m\bar{\psi}\psi$ that gives a mass to quarks and charged leptons. The latter obviously violates lepton-number conservation by two units and makes a particle and its antiparticle indistinguishable. (The classical experiment by Davis [94], who showed that $\bar{\nu} + {}^{37}\text{Cl} \rightarrow {}^{37}\text{A} + e^-$ does not take place, is interpreted as a virtue of the right-handed helicity of $\bar{\nu}$; this test does not preclude the possibility of the Majorana neutrino.) As discussed in Sect. 5.1, a Majorana mass term is allowed only for the neutrino. When neutrinos have a Majorana mass term, they are generally called "Majorana neutrinos." This terminology is not quite accurate and a more precise definition is given in this chapter.

The Majorana field is originally a name given to a completely neutral fermion field, which can be constructed from a Dirac field by imposing the reality condition (Majorana condition) [187]. With this condition the spinor component is reduced from four to two. Another familiar representation of the two-component filed is the Weyl field [47], defined by the chirality projection of the Dirac field, $\chi_\pm = \frac{1\pm\gamma_5}{2}\psi$ (equivalently the Dirac field is given by two Weyl fields). It is shown that the Majorana field is a unitary equivalent to the Weyl field. If there exists only one Weyl field χ, the Majorana mass would be the only mass allowed for the field; this necessarily breaks lepton number. If there are two Weyl fields, $\chi^{(1)}$ and $\chi^{(2)}$, there may exist a mass term that conserves lepton number defined by $L = L^{(1)} - L^{(2)}$, where $L^{(i)}$ refers to $\chi^{(i)}$. In particular, if $\chi^{(2)}_L = \chi^{(1)c}_L$, the mass is called the Dirac mass.

This implies that there are two ways to extend the standard electroweak theory to incorporate massive neutrinos. If there exists ν_R in addition to ν_L, one can construct a Dirac mass term and treat the neutrino mass in parallel with the mass term for other charged particles. If only the ν_L exists, the Majorana mass is the only possible form to give the neutrino a finite mass. Within the Weinberg–Salam theory, however, the Majorana mass term is necessarily nonrenormalisable and is taken as an effective interaction [236] that arises from more fundamental interactions at a higher energy scale. In turn, this would explain why the mass of the neutrino is so small compared with the masses of other charged particles.

In fact, the problem of understanding the smallness of the mass of neutrinos is one of the central issues of neutrino physics. We mention here three examples. The simplest is the so-called seesaw mechanism [237], in which the right-handed neutrino ν_R has a large Majorana mass M and the left-handed neutrino ν_L is given a mass through leakage of the order of $\sim (m/M)$, with m the Dirac mass which causes mixing between ν_L and ν_R and is probably of the order of the other charged particle mass. Such a mechanism plays a crucial role in grand unification, which would require that the neutrino Dirac mass and the charge $-2/3$ quark mass be related. In the second example, the small neutrino mass is ascribed to small violation of lepton number induced by a scalar particle χ that couples to $\bar{\psi}^c \psi$ and develops a small vacuum-expectation value [1094]. Although this is conceptually a simple model, the prototype model is already excluded by experiment. The third example is a model in which a small mass is generated by a radiative correction of scalar particles that violate lepton number in the Higgs potential [1095]. These examples all require the neutrino to be of the Majorana type.

It is not easy to find a natural reason for a very small mass if the neutrino is of the Dirac type. The smallness of mass is ascribed to a small Yukawa coupling; there is no obvious new physics inferred from the neutrino mass.[1]

The feature of the Majorana field, that the particle is not distinguishable from the antiparticle, makes the quantisation somewhat nontrivial. The discussion concerning quantisation is essential to calculate the process involving Majorana fields. This problem is fully discussed in the next chapter. The phenomenological consequences of massive neutrinos are discussed in Chap. 8.

6.2 Dirac Matrices

To show the features that are characteristic of the Dirac, Weyl, and Majorana fields, it is convenient to introduce different Dirac matrix representations that are related to each other by unitary transformations. We adopt the convention

---

[1] There is recent speculation that a geometrical separation of ν_R from l_L and ϕ in higher dimensional space-time may explain an extremely small Yukawa coupling $f_\nu \ll 1$ [238].

$$\{\gamma^{\mu}, \gamma^{\nu}\} = 2g^{\mu\nu} \,,$$
$$g^{\mu\nu} = \text{diag}(1, -1, -1, -1) \,. \tag{6.3}$$

For the Dirac field: This is the representation most conventionally taken in the literature (Pauli–Dirac representation):

$$\gamma^0 = \begin{pmatrix} 1 & 0 \\ 0 & -1 \end{pmatrix}, \quad \gamma^i = \begin{pmatrix} 0 & \sigma^i \\ -\sigma^i & 0 \end{pmatrix},$$
$$\gamma^5 = i\gamma^0\gamma^1\gamma^2\gamma^3 = \begin{pmatrix} 0 & 1 \\ 1 & 0 \end{pmatrix},$$
$$\sigma^{\mu\nu} = \frac{i}{2}[\gamma^{\mu}, \gamma^{\nu}] \,, \tag{6.4}$$

where all elements stand for 2×2 matrices and σ^i is the Pauli matrix.
For the Weyl field: We take

$$\gamma^0 = \begin{pmatrix} 0 & -1 \\ -1 & 0 \end{pmatrix}, \quad \gamma^i = \begin{pmatrix} 0 & \sigma^i \\ -\sigma^i & 0 \end{pmatrix},$$
$$\gamma^5 = \begin{pmatrix} 1 & 0 \\ 0 & -1 \end{pmatrix}, \tag{6.5}$$

so that

$$\frac{1 + \gamma_5}{2} = \begin{pmatrix} 1 & 0 \\ 0 & 0 \end{pmatrix}, \quad \frac{1 - \gamma_5}{2} = \begin{pmatrix} 0 & 0 \\ 0 & 1 \end{pmatrix} \tag{6.6}$$

are projections to the upper (right-handed) and lower (left-handed) components, respectively. These matrices are related to (6.4) by a unitary transformation:

$$\gamma_{\mu}(\text{Weyl}) = \frac{1}{\sqrt{2}}(1 - \gamma_5\gamma_0)\gamma_{\mu}\frac{1}{\sqrt{2}}(1 + \gamma_5\gamma_0) \,, \tag{6.7}$$

where the γ's on the right-hand side are those of (6.4).
For the Majorana field: Because the field is real in nature, it is convenient to adopt the representation

$$\text{Re}[\gamma^{\mu}] = 0 \,, \tag{6.8}$$

so that all components of the Dirac equation are also real. The representation is expressed [187] as

$$\gamma^0 = \begin{pmatrix} 0 & \sigma_2 \\ \sigma_2 & 0 \end{pmatrix}, \gamma^1 = -i\begin{pmatrix} \sigma_3 & 0 \\ 0 & \sigma_3 \end{pmatrix}, \gamma^2 = \begin{pmatrix} 0 & \sigma^2 \\ -\sigma_2 & 0 \end{pmatrix}, \gamma^3 = i\begin{pmatrix} \sigma_1 & 0 \\ 0 & \sigma_1 \end{pmatrix},$$
$$\gamma^5 = \begin{pmatrix} 0 & \sigma_1 \\ \sigma_1 & 0 \end{pmatrix}. \tag{6.9}$$

The unitary transformation between (6.9) and (6.5) is given by

$$\gamma_{\mu}(\text{Majorana}) = \frac{1}{\sqrt{2}}(1 - \gamma_2)\gamma_{\mu}\frac{1}{\sqrt{2}}(1 + \gamma_2) \,. \tag{6.10}$$

6.3 Massless Neutrinos

We define here the Weyl and Majorana fields and show their equivalence. A more formal argument will be found in Sect. 7.2. We now work with the Weyl representation. The two-component Weyl spinors are defined by

$$\psi_L \equiv \frac{1-\gamma_5}{2}\psi = \begin{pmatrix} 0 \\ \eta \end{pmatrix} \tag{6.11}$$

and

$$\psi_R \equiv \frac{1+\gamma_5}{2}\psi = \begin{pmatrix} \xi \\ 0 \end{pmatrix} , \tag{6.12}$$

where ψ is the Dirac spinor

$$\psi = \begin{pmatrix} \xi \\ \eta \end{pmatrix} . \tag{6.13}$$

Charge conjugation is defined by

$$\psi^c = \mathcal{C}^\dagger \psi \mathcal{C} = C\bar{\psi}^T . \tag{6.14}$$

With the choice of $C = i\gamma^2\gamma^0$,

$$\psi^c = i\gamma^2\psi^* . \tag{6.15}$$

Then, charge conjugation of ψ_L and ψ_R is

$$(\psi_L)^c = \begin{pmatrix} i\sigma_2\eta^* \\ 0 \end{pmatrix} = \frac{1+\gamma_5}{2}\begin{pmatrix} i\sigma_2\eta^* \\ 0 \end{pmatrix} , \tag{6.16}$$

$$(\psi_R)^c = \begin{pmatrix} 0 \\ -i\sigma_2\xi^* \end{pmatrix} = \frac{1-\gamma_5}{2}\begin{pmatrix} 0 \\ -i\sigma_2\xi^* \end{pmatrix} .$$

The kinetic term is written

$$\mathcal{L} = i\bar{\psi}_R \,\partial\!\!\!/\,\psi_R + i\bar{\psi}_L \,\partial\!\!\!/\,\psi_L . \tag{6.17}$$

The Majorana field is defined by the Majorana condition that

$$\chi^c = \pm\chi \tag{6.18}$$

imposed on a four-component spinor χ. Let us define the two fields by [1096]

$$\chi \equiv \psi_L + \psi_L^c , \tag{6.19}$$

$$\omega \equiv \psi_R - \psi_R^c . \tag{6.20}$$

These fields obviously satisfy the Majorana condition, and are taken as Majorana fields. Conversely,

$$\frac{1-\gamma_5}{2}\chi = \psi_L \,, \quad \frac{1+\gamma_5}{2}\chi = \psi_L^c \,,$$

$$\frac{1-\gamma_5}{2}\omega = -\psi_R^c \,, \quad \frac{1+\gamma_5}{2}\omega = \psi_R \,. \tag{6.21}$$

Substituting (6.19) and (6.20) into (6.17), the kinetic term is written

$$\mathcal{L} = \frac{i}{2}(\bar{\chi}\,\partial\!\!\!/\chi + \bar{\omega}\,\partial\!\!\!/\omega) \,; \tag{6.22}$$

the two terms correspond to left- and right-handed fields.

The advantage of (6.17) over (6.22) is that introducing gauge coupling is simply done by replacing ∂ with $D = \partial - igT^a A^a$ in (6.17); the procedure appears to be more complicated with the kinetic term (6.22), unless the representation of the gauge group is real.

6.4 Massive Majorana Neutrinos

The Lagrangian with a mass term for the Majorana field is given by

$$\mathcal{L} = \frac{i}{2}\bar{\chi}\,\partial\!\!\!/\chi - \frac{1}{2}m\bar{\chi}\chi \,, \tag{6.23}$$

by omitting the term for the ω field in (6.22). We assume here that m is real. As a generalisation of (6.19), if we define

$$\chi = (e^{i\alpha}\psi_L + e^{i\beta}\psi_L^c) \,, \tag{6.24}$$

χ satisfies the Majorana condition in an extended sense,

$$\chi^c = e^{-i(\alpha+\beta)}\chi \,. \tag{6.25}$$

With (6.24), (6.23) reads

$$\mathcal{L}' = i\bar{\psi}_L\,\partial\!\!\!/\psi_L - \frac{m}{2}\left[e^{-i(\alpha-\beta)}\bar{\psi}_L\psi_L^c + e^{i(\alpha-\beta)}\bar{\psi}_L^c\psi_L\right] \,. \tag{6.26}$$

Writing

$$M = me^{i(\alpha-\beta)} \,, \tag{6.27}$$

we obtain

$$\mathcal{L}' = i\bar{\psi}_L\,\partial\!\!\!/\psi_L - \frac{M}{2}\bar{\psi}_L^c\psi_L + \text{h.c.} \tag{6.28}$$

Here, the mass M is complex, but its phase can be absorbed into the phase of the ψ_L field. (The phase in (6.24) accounts for the phase of ψ_L.) The second term obviously breaks lepton number carried by the ψ_L field.

6.5 Massive Dirac Neutrinos

If there are two Weyl fields $\psi_L^{(1)}$ and $\psi_L^{(2)}$, we can construct a mass term as

$$\mathcal{L} = -\frac{m_{ij}}{2}\overline{\psi_L^{(i)c}}\psi_L^{(j)} + \text{h.c.} , \tag{6.29}$$

as a generalisation of (6.28). If $m_{ii} = 0$, the 'lepton number' $L_i - L_j$ is conserved. Hence, if we define two fields ψ_L and ψ_R by

$$\psi_L = \psi_L^{(i)} , \quad \psi_R = [\psi_L^{(j)}]^c , \tag{6.30}$$

(6.29) gives a conventional Dirac mass term,

$$\mathcal{L}_{\text{mass}} = -m\bar{\psi}\psi = -m(\bar{\psi}_L\psi_R + \bar{\psi}_R\psi_L) \tag{6.31}$$

for the Dirac field,

$$\psi = \begin{pmatrix} \psi_R \\ \psi_L \end{pmatrix} . \tag{6.32}$$

The kinetic term is given by

$$\mathcal{L}_{\text{kin}} = i\bar{\psi}\,\partial\!\!\!/\,\psi = i(\bar{\psi}_L\,\partial\!\!\!/\,\psi_L + \bar{\psi}_R\,\partial\!\!\!/\,\psi_R) . \tag{6.33}$$

If we assign $\psi_L^{(i)}$ and $\psi_L^{(j)c}$ to fields with different flavours (e.g., $\psi_L^{(1)} = \nu_{eL}$, $\psi_L^{(2)} = \nu_{\mu L}$), we have a Dirac mass term which is off-diagonal in the flavour degrees of freedom. This possibility was originally discussed by Zeldovich, Konopinski, and Mahmoud [1097], and re-presented in a modern form by Wolfenstein [1098]. This is often called a pseudo-Dirac mass term.

6.6 Massive Neutrinos in the Weinberg–Salam Theory

From the argument given above, we can introduce a Dirac mass term if ν_R exists in addition to ν_L, i.e.,

$$\mathcal{L}_{\text{mass}} = m\overline{\nu_R}\nu_L , \tag{6.34}$$

which is induced by giving the Higgs field ϕ^0 in (2.32) a vacuum-expectation value through the Yukawa coupling,

$$\mathcal{L}_{\text{mass}} = f_\nu\overline{\nu_R}\phi l_L . \tag{6.35}$$

One can take this term on an equal footing, as done for the other mass terms in (2.56).

If there is no ν_R, however, the Majorana mass term is the only mass term that gives the neutrino mass. Since $\overline{\nu_L^c}\nu_L$ is an SU(2) triplet, the simplest

possible mass term has the form

$$\mathcal{L} = \frac{1}{2} G \bar{l}_L^c l_L \frac{\phi\phi}{M} \,, \tag{6.36}$$

and the neutrino mass is given by $m_\nu = G\langle\phi_0^2\rangle/M$. This Lagrangian is non-renormalisable, and M is an effective mass. The form in (6.36) gives a hint as to how the smallness of the neutrino mass is realised, i.e., $m_\nu \to 0$ as $M \to \infty$. On the contrary, for the Dirac mass term (6.35), we must impose that $f_\nu \ll f_e$ by many orders of magnitude.

Let us consider $\nu_L \phi \to \nu_L^c \phi$ scattering with interaction (6.36). The cross section is calculated as

$$\sigma = \frac{2}{\pi} \frac{G^2}{4M^2} \,. \tag{6.37}$$

On the other hand, the cross section for the ℓth partial wave is bounded by unitarity as

$$\sigma_\ell \leq \frac{4\pi(2\ell+1)}{2} \frac{1}{k^2} \,. \tag{6.38}$$

Since the scattering process considered takes place with an s-wave, we must have

$$\frac{2}{\pi} \left(\frac{G}{2M} \right)^2 \leq \frac{8\pi}{s} \,. \tag{6.39}$$

The requirement that this holds for $s = m_{\text{pl}}^2$ leads to $G/M \leq 2\pi/m_{\text{pl}}$, or

$$m_\nu < 1.5 \times 10^{-5}\,\text{eV} \,, \tag{6.40}$$

for $\langle\phi\rangle = 250/\sqrt{2}\,\text{GeV}$. If m_ν does not satisfy (6.40), there must be a new physical scale smaller than the Planck mass.

6.7 Seesaw Mechanism

The seesaw mechanism [237] is perhaps the simplest model that leads to an effective interaction of form (6.36) within a renormalisable class of interactions. Let us assume that the mass term is given by

$$\mathcal{L} = f \overline{\nu_R} \nu_L \langle\phi^0\rangle + \frac{M}{2} \overline{\nu_R^c} \nu_R + \text{h.c.} \tag{6.41}$$

Then, the diagram shown in Fig. 6.1, when the heavy field $(M \gg \langle\phi\rangle)$ is integrated out, yields

$$\mathcal{L}_{\text{eff}} = \frac{f^2}{2M} \phi^0 \phi^0 \overline{\nu_L^c} \nu_L \,, \tag{6.42}$$
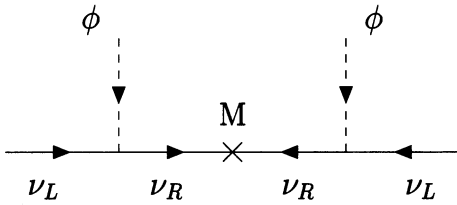
Fig. 6.1. Seesaw mechanism that gives the left-handed neutrino a small Majorana mass.

the same form as in (6.36). Equivalently, this is obtained by diagonalising the mass matrix,

$$\begin{matrix} & \nu_L \quad \nu_R \\ \begin{pmatrix} 0 & m \\ m & M \end{pmatrix} & \begin{matrix} \nu_L \\ \nu_R \end{matrix} \, , \end{matrix} \tag{6.43}$$

where two rows (columns) refer to left- and right-handed neutrinos and the Dirac mass $m = f\langle\phi\rangle$ in (6.41) induces mixing between the two sectors. Then,

$$m_{\nu_L} \simeq \frac{m^2}{M} \tag{6.44}$$

in agreement with (6.42). Note that we have reversed the sign of m_{ν_L} using the degree of freedom for the phase factor (6.27). The attractive feature of this model is that the smallness of the neutrino mass can be understood in terms of a large-mass scale M, which often appears in higher unification theories.

An alternative idea to give an effective form of (6.36) is to introduce an SU(2) triplet scalar particle χ [1099], whose mass is sufficiently large $(M_\chi \gtrsim 45\,\mathrm{GeV})$ that it is not visible in the decay of Z^0. It works to suppress lepton number violation, which takes place at the coupling of χ to $\overline{l_L^c}l_L\chi$ for low-energy phenomena. A possible mechanism giving rise to the effective term (6.36) is, therefore, to consider the process depicted in Fig. 6.2 which is induced from the Lagrangian

$$\mathcal{L} = \frac{1}{2}h\overline{l_L^c}l_L\chi + \lambda M\phi\phi\chi + M^2|\chi|^2 \ + \ \mathrm{h.c.} \tag{6.45}$$
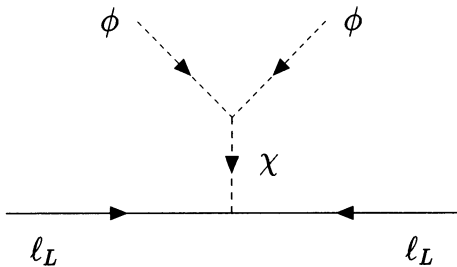
Fig. 6.2. Seesaw mechanism without a heavy fermion.

In fact, integration of the χ field in this diagram leads to

$$\mathcal{L}_{\text{eff}} = \frac{h\lambda}{2M}\phi\phi\bar{l}_L^c l_L \,, \tag{6.46}$$

in agreement with (6.36).

6.8 Majoron Model

We can think of a model where neutrino mass is generated by spontaneous symmetry breaking of lepton number. It appears possible in (6.45) that the SU(2) triplet scalar field χ that couples to $\bar{l}_L^c l_L$ would directly induce a Majorana mass if it develops a vacuum-expectation value $\langle\chi\rangle = w/\sqrt{2}$, which violates lepton number, without introducing a vertex explicitly violating it. The value of w must be tiny so that it does not conflict with our empirical knowledge of very small neutrino mass and other approximate lepton-number conservation. Namely, the smallness of the neutrino mass is understood as small lepton-number violation.

In this model, spontaneous breakdown of lepton number produces a massless Nambu–Goldstone boson which is referred to as the Majoron $M(x)$ [1094]. This model necessarily contains one additional light neutral scalar particle χ^0 whose mass is of the order of the vacuum-expectation value $\langle\chi\rangle = w/\sqrt{2}$ [1100]. Both Majoron and χ^0, which are components of the SU(2) triplet χ, couple to the Z^0 boson. Therefore, this model is completely excluded by LEP experiments on the Z^0 decay width.

Some authors, however, have suggested a way to circumvent this problem by introducing an additional singlet (complex) scalar field σ [1101]. To see the essential point of this idea, let us consider the Higgs potential for the Weinberg–Salam doublet $\phi(x)$ and the singlet scalar $\sigma(x)$. The potential for the $\sigma(x)$ field is invariant under the SU(2)×U(1) gauge transformation as well as a global phase rotation, which we identify with lepton number U(1). The minimal potential is

$$V = \lambda_1(\sigma\sigma^\dagger)^2 + \lambda_2(\phi_i\phi_i^\dagger)^2 - \mu_1^2\sigma\sigma^\dagger - \mu_2^2\phi_i\phi_i^\dagger \,, \tag{6.47}$$

where $\lambda_{1,2} > 0$ and $\mu_{1,2}^2 > 0$. For the vacuum

$$\langle\phi\rangle = v/\sqrt{2} \,, \quad \langle\sigma\rangle = w_0/\sqrt{2} \,, \tag{6.48}$$

with

$$v = \sqrt{\frac{\mu_1^2}{\lambda_1}} = 2^{-3/4}G_F^{1/2} \,, \quad w_0 = \sqrt{\frac{\mu_2^2}{\lambda_2}} \,. \tag{6.49}$$

The massless Majoron field $M_0(x)$ is defined as

$$\sigma = \frac{(\eta + w_0)}{\sqrt{2}}e^{iM_0/w_0} \,, \tag{6.50}$$

where η is a massive real field.
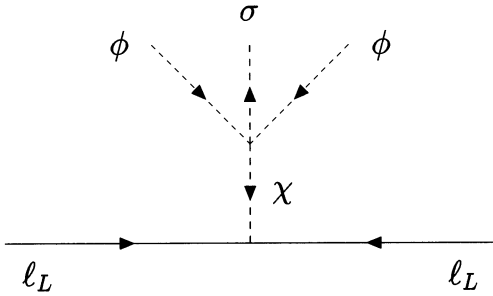
Fig. 6.3. Diagram for the triplet-singlet Majoron model.

We introduce an $SU(2)$ triplet χ_{ij} which couples to $\phi_i^\dagger \phi_j^\dagger$ and σ with a four-field coupling constant $f \ll 1$. The minimal potential for χ is

$$V_\chi = \mu_\chi^2 \chi_{ij} \chi_{ij}^\dagger - (f\sigma\chi_{ij}\phi_i^\dagger \phi_j^\dagger + \text{h.c.}) , \tag{6.51}$$

so that the χ field acquires a vacuum-expectation value

$$\langle \chi_{22} \rangle = w/\sqrt{2} , \quad w = \frac{fw_0}{2}\frac{v^2}{\mu_\chi^2} . \tag{6.52}$$

The χ field couples to $\bar{\psi}^c \psi$ as in (6.45), and hence the neutrinos acquire Majorana mass

$$m_\nu = \frac{h}{\sqrt{2}}w . \tag{6.53}$$

This mechanism is schematically shown in Fig. 6.3. A small neutrino mass results if hfw_0 is small [we take μ to be naturally of the electroweak scale $\mu_\chi^2 \sim O(v^2)$].

When ϕ and σ develop vacuum-expectation values, the quartic coupling in (6.51) gives mass to the field $M_0/w_0 + M_\chi/w$, where M_χ is defined as

$$\chi_{22} = \frac{(\chi + w)}{\sqrt{2}}e^{iM_\chi/w} . \tag{6.54}$$

A field orthogonal to this combination $M_0/w - M_\chi/w_0$ remains massless; hence it is identified with the Majoron field $M(x)$, i.e., the Majoron field is dominantly an SU(2) singlet with a small admixture of a triplet,

$$M \simeq M_0 + \frac{w}{w_0}M_\chi . \tag{6.55}$$

A light scalar field $\sigma^0(x)$ appears in addition to the massless Majoron $M(x)$, as in the original Majoron model. The triplet component of the light scalar σ^0, however, is also suppressed by the factor w/w_0, so that the contribution to the Z^0 width from $Z^0 \to M + \sigma^0$ is suppressed by $(w/w_0)^4$. In terms of the equivalent number of neutrino flavours [1101], the additional

decay width for Z^0 decay is

$$\delta N_\nu = 2 \left(\frac{w}{w_0} \right)^4 . \tag{6.56}$$

This can be consistent with experiment for a sufficiently small f, provided that the mass of triplet χ_{ab} is heavier than the Z^0 mass.

6.9 Neutrino Mass Induced by Radiative Corrections

The mass term for neutrinos, $\bar{\nu}^c \nu \phi^2$, in (6.36) may be induced from radiative corrections if a scalar field that breaks lepton number is introduced in the Higgs potential (Zee model) [1095]. As an example, let us suppose h^- which transforms as $(\mathbf{1}, -1)$ under $SU(2) \times U(1)_Y$. The Yukawa coupling of h^- is

$$\mathcal{L}_{\text{Yukawa}} = \kappa^{ab} \epsilon_{ij} (\overline{l^a_{Li}})^c l^b_{Lj} h^\dagger + \text{h.c.}, \tag{6.57}$$

where indices i, j refer to $SU(2)_L$ and a, b to generation, and

$$\kappa^{ab} = -\kappa^{ba} \tag{6.58}$$

from the Fermi statistics. If there exist two (or more) Higgs doublets, we have a cubic coupling term of the form

$$\mathcal{L}_{\phi \phi h} = \lambda_{\alpha\beta} \epsilon_{ij} \phi^\alpha_i \phi^\beta_j h + \text{h.c.}, \tag{6.59}$$

where

$$\lambda_{\alpha\beta} = -\lambda_{\beta\alpha} , \tag{6.60}$$

with $\alpha, \beta = 1, 2$.

Combining (6.57) and (6.59), lepton number is broken by two units, and a Majorana mass term $m_{ab} (\overline{\nu^a_L}) \nu^b_L$ is induced from the diagram of Fig. 6.4, where

$$m_{ab} = \kappa^{ab} (m_b^2 - m_a^2) \frac{\lambda_{12} v_2}{v_1} F(m_h^2, m_\phi^2) , \tag{6.61}$$

with

$$F(x, y) = \frac{1}{16\pi^2} \frac{1}{x - y} \log \frac{x}{y} , \tag{6.62}$$

(m_a is the charged lepton mass of generation a, and v_α is the vacuum-expectation value of ϕ^α_0). The $\phi^0 \phi^- h^-$ coupling induces mixing between ϕ^- and h^-, and we define m_h and m_ϕ as masses of the physical charged scalar particles after mixing [1102].

If λ is of the order of charged Higgs mass, m_ϕ, and if $m_h \gg m_\phi$, we obtain

$$m_{ab} \sim \frac{1}{16\pi^2} \kappa^{ab} m_\phi \frac{m_b^2 - m_a^2}{m_h^2} , \tag{6.63}$$

for $v_1 \sim v_2 \sim v$. We see that a small neutrino mass arises from $m_{a,b}^2 / m_h^2 \ll 1$ and a small coupling factor $\kappa / 16\pi^2$.
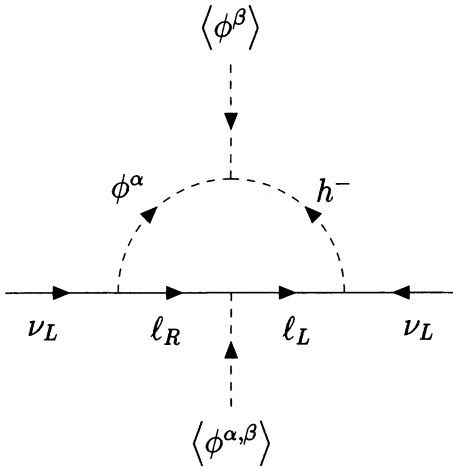
Fig. 6.4. One-loop radiative correction giving rise to a neutrino mass (Majorana mass). h^- is an $SU(2)_L$-singlet charged scalar particle.

6.10 Models for Dirac Neutrinos

For Dirac neutrinos, the small mass is usually assumed without reasons, i.e., an extremely small Yukawa coupling constant of the order of $< 10^{-12}$ is assumed for the Higgs doublet that couples to neutrinos. In this section we show two classes of models that would explain such a small Yukawa coupling constant. One class of models ascribes it to the seesaw mechanism, and the other to a result from D-brane theories.

Seesaw mechanism for Dirac neutrinos
We consider a specific model employing chiral U(1) symmetry. Suppose that $q_L, \bar{u}_R, \bar{d}_R, \ell_L$, and $\bar{e}_R$ have U(1) charge $Q = 1$. We assume a charge of -1 for $\overline{\nu}_R$. If we have two Higgs doublets ϕ_1 and ϕ_2 that have $Q = -2$, the possible Yukawa couplings are

$$f_1 \bar{u}_R q_L \phi_1 \;+\; f_2 \bar{d}_R q_L \phi_2 \;+\; f_3 \bar{e}_R \ell_L \phi_2 + \text{h.c.} \qquad (6.64)$$

The above U(1) charge assignment for ν_R does not allow the neutrino to have a Dirac mass term.

We now introduce a pair of heavy singlet fermions $\overline{N}_R$ and N_L with the U(1) charge of $+1$ and -1, respectively, and assume the Dirac mass term,

$$M \overline{N}_R N_L + \text{h.c.} \qquad (6.65)$$

We may also have the coupling,

$$g \overline{N}_R \ell_L \phi_1 \;. \qquad (6.66)$$

We introduce a Higgs χ with a U(1) charge of $+2$ to break the U(1) symmetry. We then have a Yukawa coupling of the form

$$\mathcal{L} = h \overline{\nu}_R N_L \chi \;. \qquad (6.67)$$

Since there are no $\bar{\nu}_R\bar{\nu}_R\chi$ or $N_L N_L \chi$ terms, $\langle\chi\rangle \neq 0$ does not break lepton number. The full Dirac mass matrix for $\nu_{L,R}$ and $N_{L,R}$ is given by

$$(\bar{\nu}_R \ \overline{N}_R) \begin{pmatrix} 0 & h\langle\chi\rangle \\ g\langle\phi_1\rangle & M \end{pmatrix} \begin{pmatrix} \nu_L \\ N_L \end{pmatrix} . \tag{6.68}$$

By diagonalising this matrix, we obtain a light Dirac neutrino mass,

$$m_\nu^D \simeq hg\frac{\langle\chi\rangle\langle\phi_1\rangle}{M} . \tag{6.69}$$

If we take $M \simeq m_{pl} = 10^{19}$ GeV and $\langle\chi\rangle \simeq 10^{10}$ GeV,

$$m_\nu^D \simeq 10^{-9} hg\langle\phi_1\rangle \sim 10^{-9}(hg/f)m_\ell , \tag{6.70}$$

where m_ℓ is the mass of the charged lepton. The U(1) symmetry discussed here might be identified with $U(1)_{PQ}$ in Sect. 9.9. The possibility of the seesaw mechanism for the Dirac neutrino was first discussed in [1103] in the context of a superstring 'inspired' model.

D-brane explanation

In the context of higher dimensional theory, there is speculation that the real world is realised as a boundary of a higher dimensional manifold [1104]. Arkani-Hamed et al. [1105] invoked this idea to solve the hierarchy problem. Let us suppose that the fundamental theory is described in (4+1)-dimensional space, and our real world is on a $(3+1)$-dimensional boundary (3-brane).

The Einstein–Hilbert action of gravity in five-dimensional space-time is given by

$$\mathcal{S} = M_*^3 \int \int_0^L \sqrt{-g^{(5)}}\mathcal{R}d^4xdy , \tag{6.71}$$

where M_* is the gravitational scale in five-dimensional space-time and $g^{(5)}$ and $\mathcal{R}$ are the metric and the scalar curvature. The fifth dimension is assumed to be compactified to space of radius L. We assume that the metric in the fifth dimension is orthogonal to those for four-dimensional space:

$$d^2s = g_{\mu\nu}dx^\mu dx^\nu - dy^2 , \tag{6.72}$$

where g is the metric in four-dimensional space-time. The integration over dy leads to the action in four-dimensional space

$$\mathcal{S}_4 = M_*^3 L \int \sqrt{-g_4}\mathcal{R}_4 d^4x . \tag{6.73}$$

The coefficient in front of the integral must be the true gravitational scale, m_{pl}, so that

$$m_{\text{pl}}^2 = M_*^3 L . \tag{6.74}$$

The Planck scale in four-dimensional space-time appears to be an effective scale induced from the 'fundamental scale' of the theory M_*. We would obtain

the correct value of m_{pl} even if M_* is as small as 1 TeV if the compactification size L is sufficiently large. The weakness of gravity is a result of a large compactification scale (submillimetre scale) in the fifth dimension.

In this theory, all gauge-interacting fields reside on three-brane localised at $y = 0$. The right-handed neutrino, however, does not couple to gauge interactions, and it may reside on five-dimensional bulk, rather than three-brane [238]. The action involving the neutrino is then,

$$\mathcal{S} = M_* \int \int_0^L \sqrt{-g_5}\bar{\nu}_R\partial\!\!\!/\nu_R d^4xdy + \int \int_0^L \sqrt{-g_5}f\bar{\nu}_R\ell_L\phi\delta(y = 0)d^4xdy + \text{h.c.}$$

(6.75)

Integration over the fifth coordinate yields the action in four dimensions as

$$\mathcal{S}_4 = M_* L \int \sqrt{-g_4}\bar{\nu}_R\partial\!\!\!/\nu_R d^4x + \int \sqrt{-g_4}f\bar{\nu}_R\ell_L\phi d^4x + \text{h.c.} \qquad (6.76)$$

We renormalise the wave function of ν_R by multiplying $1/\sqrt{M_*L}$, so that it has a canonical kinetic term. The Yukawa coupling then is suppressed by $1/\sqrt{M_*L} = M_*/m_{\mathrm{Pl}}$. For $f = 1$ and $M_* \simeq 1\,\text{TeV}$, we obtain the effective Yukawa coupling $f_{\mathrm{eff}} \simeq 10^{-16}$ or a neutrino (Dirac) mass of $\simeq 10^{-5}$ eV.

6.11 Pontecorvo's Neutrino Oscillation

If the neutrino is a four-component Dirac fermion and if it has a Majorana mass in addition to the lepton-number conserving Dirac mass, a neutrino may oscillate into an antineutrino. This is neutrino oscillation first noticed by Pontecorvo [203] in analogy with $K^0 - \bar{K}^0$ oscillation. This oscillation turns ν_L into $(\nu_R)^c$, and helicity is conserved.

Let us explain how this happens in our formalism. The Lagrangian of the neutrino mass in our situation is

$$\mathcal{L}_{\mathrm{mass}} = \frac{1}{2}(\overline{\nu^c}_L m_L\nu_L + \overline{\nu^c}_R m_R\nu_R) + \bar{\nu}_R m_D\nu_L + \text{h.c.} , \qquad (6.77)$$

where m_D is the Dirac mass and $m_{R,L}$ are Majorana masses. In the basis of $(\nu_L, \overline{\nu^c}_R)$, the mass matrix is

$$\begin{pmatrix} m_L & m_D \\ m_D & m_R^* \end{pmatrix} . \qquad (6.78)$$

In the presence of off-diagonal components, a neutrino of the weak interaction eigenstate turns into another while propagating. A neutrino ν_L, after a time interval of t, is given by

$$|\nu_L\rangle_t = \cos\theta e^{-E'_L t}|\nu'_L\rangle + \sin\theta e^{-E'_R t}|\nu'^c_R\rangle , \qquad (6.79)$$

where $|\nu'_L\rangle$ and $|\nu'^c_R\rangle$ are mass eigenstates obtained by diagonalising the mass matrix of (6.78) as

$$
\begin{pmatrix} \nu_L \\ \nu^c_R \end{pmatrix} = \begin{pmatrix} \cos\theta & \sin\theta \\ -\sin\theta & \cos\theta \end{pmatrix} \begin{pmatrix} \nu'_L \\ \nu'^c_R \end{pmatrix} , \tag{6.80}
$$

and $E'_i = \sqrt{p^2 + m'^2_i}$ $(i = L, R)$ with mass defined by

$$
\mathcal{L}_{\text{mass}} = \frac{1}{2} \left(\overline{\nu'^c}_L m'_L \nu'_L + \overline{\nu'^c}_R m'_R \nu'_R \right) + \text{h.c.} , \tag{6.81}
$$

where

$$
\begin{pmatrix} m'_L & \\ & m'^*_R \end{pmatrix} = \begin{pmatrix} \cos\theta & -\sin\theta \\ \sin\theta & \cos\theta \end{pmatrix} \begin{pmatrix} m_L & m^T_D \\ m_D & m^*_R \end{pmatrix} \begin{pmatrix} \cos\theta & \sin\theta \\ -\sin\theta & \cos\theta \end{pmatrix} . \tag{6.82}
$$

We assume that all mass parameters are real, for simplicity.

With (6.79) the transition amplitudes of $|\nu_L\rangle$ to $|\nu_L\rangle$ and $|\nu^c_L\rangle$ are

$$
\langle \nu_L | \nu_L \rangle_t = \cos^2\theta e^{-iE'_L t} + \sin^2\theta e^{-iE'_R t} , \tag{6.83}
$$

and

$$
\langle \nu^c_R | \nu_L \rangle_t = \sin\theta\cos\theta \left(-e^{-iE'_L t} + e^{-iE'_R t} \right) . \tag{6.84}
$$

For $p = |\mathbf{p}| \gg m_i$, we expand $E'_i = \sqrt{p^2 + m^2_i} \simeq p + m^2_i/2p \simeq p + m^2_i/2E$ and write (6.83) and (6.84) as

$$
\langle \nu_L | \nu_L \rangle_t \simeq e^{-i\left(p + \frac{m'^2}{2E}\right)} \left(\cos^2\theta + \sin^2\theta e^{-i\frac{\Delta m^2}{2E}t} \right) \tag{6.85}
$$

and

$$
\langle \nu^c_R | \nu_L \rangle_t \simeq e^{-i\left(p + \frac{m'^2}{2E}\right)} \sin\theta\cos\theta \left(-1 + e^{-i\frac{\Delta m^2}{2E}t} \right) , \tag{6.86}
$$

where $\Delta m^2 \equiv m'^2_R - m'^2_L$ and $m'^2 = (m'^2_L + m'^2_R)/2$.

The probabilities of finding ν_L and ν^c_R at a distance L from the source of ν_L are given by

$$
P(\nu_L \rightarrow \nu_L) = 1 - (\sin 2\theta)^2 \left(\sin \frac{\Delta m^2 L}{4E} \right)^2 \tag{6.87}
$$

and

$$
P(\nu_L \rightarrow \nu^c_R) = (\sin 2\theta)^2 \left(\sin \frac{\Delta m^2 L}{4E} \right)^2 . \tag{6.88}
$$

Since ν^c_R is a gauge singlet, it does not interact with a detector, leading to an effective reduction of the neutrino flux at the detector. This effect vanishes only when $m_R = m_L = 0$ or one of m_L and m_R is infinity.

7 Quantisation of the Majorana Field

7.1 Necessity of Quantisation

Proper formulation of quantisation is essential for developing quantum field theory with Majorana neutrinos. This is not so obvious a problem because there exists a constraint that identifies a particle with an antiparticle. Because of this constraint that makes the field real, the Majorana field has both positive- and negative-frequency parts. In order to define the energy eigenstate separating the positive-frequency part from the other, quantisation plays a crucial role.

   In this chapter we develop a quantum field theory of Majorana particles following Case [1106]. We first provide a full proof for the unitary equivalence of the Majorana and the Weyl fields, a subject we have already discussed in Chap. 6 in a less formalistic manner. We then discuss quantisation of the massive Weyl field. This makes the procedure of quantisation easier than that in the presence of constraints but also is appropriate in the context of the Weinberg–Salam theory, where fields are always projected onto a definite chirality. A few elementary examples are given for calculating Feynman diagrams involving Majorana fields. Examples include neutrinoless double beta decay, which is practically the most important application that involves a propagator of the Majorana field.

7.2 Unitary Equivalence of the Majorana and the Weyl Fields

We start with the four-component Dirac spinor $\psi(x)$, which is defined by the transformation property under the Lorentz group, as

$$\psi(x) \rightarrow \psi'(x') = D(\alpha)\psi(x) \equiv \exp\left(-\frac{\alpha_{\mu\nu}}{2}\sigma^{\mu\nu}\right)\psi , \qquad (7.1)$$

$$x'^{\mu} = \Lambda^{\mu}_{\ \nu}x^{\nu} , \qquad (7.2)$$

where $\alpha_{\mu\nu}$ are six real parameters corresponding to the Lorentz transformation $\Lambda^{\mu}_{\ \nu}$ and $\sigma^{\mu\nu}$ in the spinor representation $D(\alpha)$ are defined by the commutator of the Dirac γ matrices (6.4), which satisfy Clifford algebra (6.3).

If we take the Weyl representation of the γ matrices (6.5), we can show straightforwardly that $D(\alpha)$ is reduced into 2×2 diagonal matrices,

$$
D(\alpha) = \begin{bmatrix} \exp[-i(\frac{i}{2}\alpha_{0i}\sigma_i + \frac{\alpha_{ij}}{2}\epsilon_{ijk}\sigma_k)] & 0 \\ 0 & \exp[-i(-\frac{i}{2}\alpha_{0i}\sigma_i + \frac{\alpha_{ij}}{2}\epsilon_{ijk}\sigma_k)] \end{bmatrix} .
$$
(7.3)

There are two convenient ways to decompose a four-component Dirac spinor into two irreducible representations of the Lorentz group. One of them is decomposition into two Weyl spinors,

$$
\psi = \psi_L + \psi_R = \begin{pmatrix} \xi \\ \eta \end{pmatrix} ,
$$
(7.4)

where ψ_L and ψ_R are defined in (6.11) and (6.12). From (7.3) it is obvious that η and ξ form independent irreducible vector spaces and transform under the Lorentz group as

$$
\eta(x) \to \eta'(x') = M\eta(x) = \exp\left[-i\left(\frac{\alpha_{ij}}{2}\epsilon_{ijk}\sigma_k - i\frac{\alpha_{0j}}{2}\sigma_j\right)\right]\eta(x) ,
$$
(7.5)

$$
\xi(x) \to \xi'(x') = \tilde{M}\xi(x) = \exp\left[-i\left(\frac{\alpha_{ij}}{2}\epsilon_{ijk}\sigma_k + \frac{\alpha_{0j}}{2}\sigma_j\right)\right]\xi(x) .
$$
(7.6)

Here M and $\tilde{M}$ satisfy

$$
\det M = \det \tilde{M} = 1 ,
$$
(7.7)

and are thus independent two-dimensional representations of SL(2,C). This proves that the Weyl representation of the Lorentz group is a 2×2 irreducible representation of SL(2,C) [47].

Another reduction of the Dirac spinor is given by [187]

$$
\chi_{\pm} = \frac{\psi \pm \psi^c}{\sqrt{2}} ,
$$
(7.8)

where ψ^c is the charge conjugation of ψ defined by (6.14). Because ψ^c has the same transformation property as that for ψ under the Lorentz group, $\chi_{\pm}$ are also Lorentz spinors. $\chi_{\pm}$ obviously satisfy

$$
\chi_{\pm}^c = \pm\chi_{\pm} .
$$
(7.9)

These $\chi_{\pm}$ are the fields that were introduced by Majorana. By taking the Majorana representation of γ matrices (6.9), it is readily shown that $\chi_{\pm}$ are four-component real fields. In what follows, we show that these $\chi_{\pm}$ and (χ, ω) defined in (6.19)–(6.21) are unitary equivalent [263, 1096, 1107–1111].

Let us now construct a unitary operator U that connects the Majorana spinor with a Weyl spinor,

$$U\chi_+ U^{-1} = \psi_L + \psi_L^c \equiv \chi \,,$$
$$U\chi_- U^{-1} = \psi_R - \psi_R^c \equiv \omega \,, \qquad (7.10)$$

or equivalently,

$$U^{-1}\psi_L U = \frac{1-\gamma_5}{2}\chi_+ \,, \quad U^{-1}\psi_R U = \frac{1+\gamma_5}{2}\chi_- \,,$$
$$U^{-1}\psi_L^c U = \frac{1+\gamma_5}{2}\chi_+ \,, \quad U^{-1}\psi_R^c U = -\frac{1-\gamma_5}{2}\chi_- \,, \qquad (7.11)$$

so that the two sets of spinors are unitary equivalent.

To construct U, we first expand the Dirac field $\psi(x)$ in terms of wave functions $u_r(\mathbf{p})$ and $v_r(\mathbf{p})$ of a massless fermion as

$$\psi(x) = \frac{1}{(2\pi)^{3/2}} \sum_{r=1}^{2} \int d^3p \left[a_r(\mathbf{p})u_r(\mathbf{p})e^{ipx} + b_r^\dagger(\mathbf{p})v_r(\mathbf{p})e^{-ipx}\right] \,, \qquad (7.12)$$

where u and v satisfy

$$\not{p}u_r(\mathbf{p}) = 0, \quad v_r(\mathbf{p}) = Cu_r^*(\mathbf{p}) \,, \qquad (7.13)$$

$$\gamma_5 u_1(\mathbf{p}) = u_1(\mathbf{p}), \quad \gamma_5 u_2(\mathbf{p}) = -u_2(\mathbf{p}) \,. \qquad (7.14)$$

The ψ_L, ψ_L^c, ψ_R, ψ_R^c, and $\chi_\pm$ fields are expanded similarly:

$$\psi_R(x) = \frac{1}{(2\pi)^{3/2}} \int d^3p \left[a_1(\mathbf{p})u_1(\mathbf{p})e^{ipx} + b_2^\dagger(\mathbf{p})v_2(\mathbf{p})e^{-ipx}\right] \,, \qquad (7.15)$$

$$\psi_R^c(x) = \frac{1}{(2\pi)^{3/2}} \int d^3p \left[b_2(\mathbf{p})u_2(\mathbf{p})e^{ipx} + a_1^\dagger(\mathbf{p})v_1(\mathbf{p})e^{-ipx}\right] \,, \qquad (7.16)$$

$$\psi_L(x) = \frac{1}{(2\pi)^{3/2}} \int d^3p \left[a_2(\mathbf{p})u_2(\mathbf{p})e^{ipx} + b_1^\dagger(\mathbf{p})v_1(\mathbf{p})e^{-ipx}\right] \,, \qquad (7.17)$$

$$\psi_L^c(x) = \frac{1}{(2\pi)^{3/2}} \int d^3p \left[b_1(\mathbf{p})u_1(\mathbf{p})e^{ipx} + a_2^\dagger(\mathbf{p})v_2(\mathbf{p})e^{-ipx}\right] \,, \qquad (7.18)$$

$$\chi_+(x) = \frac{1}{(2\pi)^{3/2}} \sum_{r=1}^{2} \int d^3p \frac{1}{\sqrt{2}}\{[a_r(\mathbf{p}) + b_r(\mathbf{p})]u_r(\mathbf{p})e^{ipx}$$
$$+[a_r^\dagger(\mathbf{p}) + b_r^\dagger(\mathbf{p})]v_r(\mathbf{p})e^{-ipx}\} \,, \qquad (7.19)$$

$$\chi_-(x) = \frac{1}{(2\pi)^{3/2}} \sum_{r=1}^{2} \int d^3p \frac{1}{\sqrt{2}}\{[a_r(\mathbf{p}) - b_r(\mathbf{p})]v_r(\mathbf{p})e^{ipx}$$
$$+[-a_r^\dagger(\mathbf{p}) + b_r^\dagger(\mathbf{p})]v_r(\mathbf{p})e^{-ipx}\} \,. \qquad (7.20)$$

Let us write U in the form

$$U = e^{\theta(b^\dagger a - a^\dagger b)} \,. \qquad (7.21)$$

For a real θ, U satisfies $U^{-1} = U^\dagger$.

Now,

$$U^{-1}aU = e^{-\theta(b^\dagger a - a^\dagger b)} a\, e^{\theta(b^\dagger a - a^\dagger b)}$$

$$= a + \theta[(b^\dagger a - a^\dagger b), a]$$

$$+ \frac{\theta^2}{2!}\left[(b^\dagger a - a^\dagger b), [(b^\dagger a - a^\dagger b), a]\right]$$

$$+ \dots$$

$$= a\cos\theta + b\sin\theta\,, \tag{7.22}$$

where $[(b^\dagger a - a^\dagger b), a] = b$ is used from the second to the third line. Similarly,

$$U^{-1}bU = a\cos\theta - b\sin\theta\,. \tag{7.23}$$

With the choice of $\theta = \pi/4$, i.e.,

$$U = \exp\left[\frac{\pi}{4}(b_1^\dagger a_1 - a_1^\dagger b_1 - b_2^\dagger a_2 + a_2^\dagger b_2)\right]\,, \tag{7.24}$$

we obtain

$$\frac{1}{\sqrt{2}}[a_1(\mathbf{p}) + b_1(\mathbf{p})] = U^{-1}a_1(\mathbf{p})U\,,$$

$$\frac{1}{\sqrt{2}}[b_2(\mathbf{p}) + a_2(\mathbf{p})] = U^{-1}b_2(\mathbf{p})U\,,$$

$$\frac{1}{\sqrt{2}}[a_2(\mathbf{p}) - b_2(\mathbf{p})] = U^{-1}a_2(\mathbf{p})U\,,$$

$$\frac{1}{\sqrt{2}}[b_1(\mathbf{p}) - a_1(\mathbf{p})] = U^{-1}b_1(\mathbf{p})U\,, \tag{7.25}$$

which is equivalent to (7.10), i.e., our end [1111]. We note that U is unitary only in the four-component Dirac spinor space. If one applies it to the Dirac spinor ψ,

$$U^\dagger \psi U = \frac{1}{\sqrt{2}}(\psi - \gamma_5 \psi^c). \tag{7.26}$$

This is the Pauli–Gürsey transformation [1108, 1109].

7.3 Quantisation of Majorana Fermions

Let us consider the Lagrangian for the free massive Weyl field $\psi_L(x)$,

$$\mathcal{L} = \bar{\psi}_L i\partial\!\!\!/\psi_L - \frac{1}{2}m\bar{\psi}_L^c\psi_L + \text{h.c}\,. \tag{7.27}$$

This Lagrangian is written in terms of the Weyl spinor field η of (6.11) as

$$\mathcal{L} = i\eta^\dagger(\sigma^\mu\partial_\mu)\eta - \frac{i}{2}m\eta^T\sigma_2\eta + \frac{i}{2}m\eta^\dagger\sigma_2\eta^* , \tag{7.28}$$

where

$$\sigma^\mu \equiv (1, -\sigma_i) . \tag{7.29}$$

We also introduce

$$\tilde{\sigma}^\mu = (1, \sigma_i) \tag{7.30}$$

for later convenience [1112]. Equation (7.28) is invariant under the SL(2,C) transformation of (7.5). The Euler–Lagrange equation of motion is derived with the aid of the variational principle as

$$\sigma^\mu\partial_\mu\eta + m\sigma_2\eta^* = 0 , \tag{7.31}$$

$$\tilde{\sigma}^\mu\sigma_2\partial_\mu\eta^* - m\eta = 0 . \tag{7.32}$$

Multiplying $\tilde{\sigma}^\mu\partial_\mu$ on the left of (7.31), we obtain

$$(\partial_0^2 - \nabla^2 + m^2)\eta = 0 . \tag{7.33}$$

Procedures of quantisation are now standard. We can carry out quantisation by imposing the equal-time anticommutation relations on $\eta(x)$ and its canonical conjugate field $\pi(x)$,

$$\{\eta(\mathbf{x}, t), \pi(\mathbf{x}', t)\} = i\delta(\mathbf{x} - \mathbf{x}') ,$$
$$\{\eta(\mathbf{x}, t), \eta(\mathbf{x}', t)\} = \{\eta^*(\mathbf{x}, t), \eta^*(\mathbf{x}', t)\} = 0 . \tag{7.34}$$

We expand $\eta(x)$ as

$$\eta(x) = \frac{1}{(2\pi)^{3/2}} \int d^3p \sqrt{\frac{p_0 + |\mathbf{p}|}{2p_0}} \{[a_-(\mathbf{p})\beta(\mathbf{p}) + b_+(\mathbf{p})\alpha(\mathbf{p})]e^{-ipx}$$
$$+[c_-(\mathbf{p})\beta(\mathbf{p}) + d_+(\mathbf{p})\alpha(\mathbf{p})]e^{ipx}\} , \tag{7.35}$$

$$\eta^*(x) = \frac{1}{(2\pi)^{3/2}} \int d^3p \sqrt{\frac{p_0 + |\mathbf{p}|}{2p_0}} \{[c_-^\dagger(\mathbf{p})\beta^*(\mathbf{p}) + d_+^\dagger(\mathbf{p})\alpha^*(\mathbf{p})]e^{-ipx}$$
$$+[a_-^\dagger(\mathbf{p})\beta^*(\mathbf{p}) + b_+^\dagger(\mathbf{p})\alpha^*(\mathbf{p})]e^{ipx}\} , \tag{7.36}$$

where $\alpha(\mathbf{p})$ and $\beta(\mathbf{p})$ are helicity eigenspinors that satisfy

$$\sigma\mathbf{p}\alpha(\mathbf{p}) = |\mathbf{p}|\alpha(\mathbf{p}) ,$$
$$\sigma\mathbf{p}\beta(\mathbf{p}) = -|\mathbf{p}|\beta(\mathbf{p}) , \tag{7.37}$$

and the orthonormal condition,

$$\alpha^\dagger(\mathbf{p})\alpha(\mathbf{p}) = \beta^\dagger(\mathbf{p})\beta(\mathbf{p}) = 1 , \tag{7.38}$$
$$\alpha^\dagger(\mathbf{p})\beta(\mathbf{p}) = \beta^\dagger(\mathbf{p})\alpha(\mathbf{p}) = 0 . \tag{7.39}$$

We take the convention for their relative phase that

$$\sigma_2 \alpha^*(\mathbf{p}) = +i\beta(\mathbf{p}) ,$$
$$\sigma_2 \beta^*(\mathbf{p}) = -i\alpha(\mathbf{p}) . \tag{7.40}$$

The equations of motion (7.31) and (7.32) determine the relation between the expansion coefficients,

$$d_+ = \frac{m}{p_0 + |p|} a_-^\dagger ,$$
$$b_+ = -\frac{m}{p_0 + |p|} c_-^\dagger , \tag{7.41}$$

leaving two independent coefficients (operators) a_- and c_-. Upon writing $c_-^\dagger \rightarrow a_+$, $\eta(x)$ is written

$$\eta(x) = \frac{1}{(2\pi)^{3/2}} \int d^3p \sqrt{\frac{p_0 + |\mathbf{p}|}{2p_0}} \left\{ \left[a_-(\mathbf{p})\beta(\mathbf{p}) - \frac{m}{p_0 + |\mathbf{p}|} a_+(\mathbf{p})\alpha(\mathbf{p}) \right] e^{-ipx} \right.$$
$$\left. + \left[a_+^\dagger(\mathbf{p})\beta(\mathbf{p}) + \frac{m}{p_0 + |\mathbf{p}|} a_-^\dagger(\mathbf{p})\alpha(\mathbf{p}) \right] e^{ipx} \right\} . \tag{7.42}$$

The anticommutation relations of (7.34) yield

$$\{a_\pm(\mathbf{p}), a_\pm^\dagger(\mathbf{p}')\} = \delta(\mathbf{p} - \mathbf{p}') ,$$
$$\text{or otherwise} = 0 . \tag{7.43}$$

The stress energy-momentum tensor is defined by

$$T^{\mu\nu} = \frac{\partial \mathcal{L}}{\partial(\partial_\mu \eta)} \frac{\partial \eta}{\partial x^\nu} - g^{\mu\nu} \mathcal{L}$$
$$= i\eta^\dagger \sigma^\mu \partial^\nu \eta - g^{\mu\nu} \mathcal{L} . \tag{7.44}$$

With the aid of the equations of motion (7.31) and (7.32), the energy-momentum four-vector

$$P^\mu \equiv \int d^3x \, T^{0\mu} , \tag{7.45}$$

is given by

$$P^\mu = \int d^3x \left[i\eta^* \partial^\mu \eta - g^{0\mu} \frac{i}{2} \partial_0 (\eta^* \eta) \right] , \tag{7.46}$$

or

$$E = \frac{i}{2} \int d^3x \left(\eta^\dagger \frac{\partial \eta}{\partial t} - \frac{\partial \eta^\dagger}{\partial t} \eta \right) , \tag{7.47}$$

$$\mathbf{P} = -\frac{i}{2} \int d^3x \, [\eta^\dagger \boldsymbol{\nabla} \eta - (\boldsymbol{\nabla} \eta^\dagger)\eta] . \tag{7.48}$$

In terms of the expansion coefficients, they are written

$$E = \int d^3p \; p_0 \; [a_-^\dagger(\mathbf{p})a_-(\mathbf{p}) + a_+^\dagger(\mathbf{p})a_+(\mathbf{p})] \;, \qquad (7.49)$$

$$\mathbf{P} = \int d^3p \; \mathbf{p} \; [a_-^\dagger(\mathbf{p})a_-(\mathbf{p}) + a_+^\dagger(\mathbf{p})a_+(\mathbf{p})] \;, \qquad (7.50)$$

where the zero-point energy is omitted. This allows the interpretation that $a_\pm^\dagger(\mathbf{p})$ and $a_\pm(\mathbf{p})$ are, respectively, the creation and annihilation operators of a particle with a definite energy and a momentum, p_0 and $\mathbf{p}$. The Hilbert space can be constructed in the standard manner by operating $a_\pm^\dagger$ onto the vacuum $|0\rangle$. We note that $\eta(x)$ contains creation operators for helicity $+$ states and annihilation operators for helicity $-$ states. This interpretation, however, holds only when $m = 0$, and becomes meaningless for $m \neq 0$ because helicity is not a conserved quantity in the presence of a mass term.

We conclude this section by calculating the Feynman propagator for the free massive Weyl spinor field $\eta(x)$. Using the properties satisfied by the spinors $\alpha(\mathbf{p})$ and $\beta(\mathbf{p})$,

$$\beta_a\beta_b^* = \frac{1}{2|\mathbf{p}|} \; (|\mathbf{p}| - \sigma_i p_i)_{ab} \;,$$

$$\alpha_a\alpha_b^* = \frac{1}{2|\mathbf{p}|} \; (|\mathbf{p}| + \sigma_i p_i)_{ab} \;, \qquad (7.51)$$

we have

$$\{\eta_a(x), \; \eta_b^*\} = i(\tilde{\sigma}^\mu\partial_\mu)_{ab}D(x - x') \;, \qquad (7.52)$$

and

$$\{\eta_a(x), \; \eta_b(x')\} = im(\sigma_2)_{ab}D(x - x') \qquad (7.53)$$

with $D(x)$ defined by

$$D(x) = \frac{1}{(2\pi)^3} \int \frac{d^3p}{2p_0} \; (e^{ipx} - e^{-ipx}) \;. \qquad (7.54)$$

The Feynman propagators are defined by

$$\langle 0|T[\eta(x)\eta^\dagger(x)]\,|0\rangle = \theta(x_0 - x_0')\langle 0|\eta(x)\eta^\dagger(x')|0\rangle$$
$$+ \theta(x_0' - x_0)\langle 0|\eta^\dagger(x')\eta(x)|0\rangle \;, \qquad (7.55)$$

$$\langle 0|T[\eta(x)\eta^T(x)]\,|0\rangle = \theta(x_0 - x_0')\langle 0|\eta(x)\eta^T(x')|0\rangle$$
$$+ \theta(x_0' - x_0)\langle 0|\eta(x')\eta^T(x)|0\rangle \;. \qquad (7.56)$$

With the aid of the formula

$$\theta(x_0) = \frac{1}{2\pi i} \int \frac{d\lambda}{\lambda - i\varepsilon} \; e^{i\lambda x_0} \;, \qquad (7.57)$$

we obtain

$$\langle 0|T[\eta(x)\eta^\dagger(x')]\,|0\rangle = \frac{1}{(2\pi)^4}\int d^4p\,\frac{\tilde\sigma^\mu p_\mu}{p^2-m^2}\,e^{-ip(x-x')} \tag{7.58}$$

and

$$\langle 0|T[\eta(x)\eta^T(x')]\,|0\rangle = \frac{1}{(2\pi)^4}\int d^4p\,\frac{im\sigma_2}{p^2-m^2}\,e^{-ip(x-x')}\,. \tag{7.59}$$

The nonvanishing right-hand side of (7.59) indicates that lepton-number conservation is violated by the mass (Majorana mass) term.

7.4 Simple Derivation of Feynman Propagators

The Feynman propagators of (7.58) and (7.59) can be readily obtained from the reality condition. By adding the source term $\bar J_R\psi_L + \bar\psi_L J_R$ to the Lagrangian (7.27), we write the path integral

$$Z[J] = \int d\psi_L d\bar\psi_L e^{-i\int d^4x \mathcal{L}_J}\,, \tag{7.60}$$

where $\mathcal{L}_J$ is written in the form

$$\mathcal{L}_J = \frac{1}{2}(\bar\Phi O\Phi + \bar J\Phi + \bar\Phi J) \tag{7.61}$$

with

$$\Phi = \psi_L + \psi_L^c\,, \tag{7.62}$$
$$J = J_R + J_R^c\,, \tag{7.63}$$

and

$$O = i\partial\!\!\!/ - m\,. \tag{7.64}$$

Integration of (7.60) over the ψ_L and $\bar\psi_L$ fields yields

$$Z[J] = e^{i\int d^4x(-\frac{1}{2}\bar J O^{-1}J)}\,. \tag{7.65}$$

With the self-conjugate condition $J^c = J$, J is written in the Weyl representation

$$J = \begin{pmatrix} j \\ -i\sigma_2 j^* \end{pmatrix}\,. \tag{7.66}$$

Using (7.66), we have

$$\bar{J}_R \not{p} J_R = j^\dagger p_\mu \tilde{\sigma}^\mu j \,,$$
$$\bar{J}_R^c m J_R = -im j^T \sigma_2 j \,, \tag{7.67}$$

so that the integrand of (7.65) reads

$$-\frac{1}{2}\bar{J}O^{-1}J = -\frac{1}{2}\bar{J}\frac{\not{p}+m}{p^2-m^2}J$$

$$= -j^\dagger \left[\frac{1}{(2\pi)^4}\int d^4p \, \frac{p_\mu \tilde{\sigma}^\mu}{p^2-m^2} \, e^{-ipx}\right] j$$

$$-\frac{1}{2}j^T \left[\frac{1}{(2\pi)^4}\int d^4p \, \frac{-im\sigma_2}{p^2-m^2} \, e^{-ipx}\right] j$$

$$+\text{h.c.}, \tag{7.68}$$

where the expressions in the square brackets are the Feynman propagators in agreement with (7.58) and (7.59).

7.5 Simple Examples of Applications

As examples, we show elementary calculations for two processes involving Majorana particles, the decay of a Majorana neutrino N into e_L^- and a scalar particle φ and the annihilation process $N + N \to e^+ + e^-$.

7.5.1 $N \to e_L^- + \varphi^{(+)}$

Let us suppose that the interaction Lagrangian is given by

$$\mathcal{L}_{\text{int}} = g(\bar{e}_L N_L^c \varphi^\dagger + \bar{N}_L^c e_L \varphi) \,. \tag{7.69}$$

Using the Weyl spinors, η for N_L and ζ for e_L^-, (7.69) is written

$$\mathcal{L}_{\text{int}} = ig(\zeta^* \sigma_2 \eta^* \varphi^\dagger - \eta \sigma_2 \zeta \varphi) \,. \tag{7.70}$$

Assigning the momentum as in Fig. 7.1, we calculate

$$\langle q, \, k \,|\, i\mathcal{L}_{\text{int}} \,|\, p\rangle = -g\int d^4x \langle k|\varphi^\dagger|0\rangle \langle q|\xi^*|0\rangle \sigma_2 \langle 0|\eta^*|p\rangle \,. \tag{7.71}$$
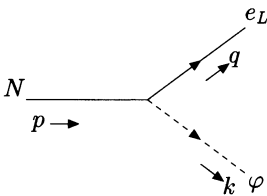
Fig. 7.1. Feynman diagram for the decay of a Majorana particle: $N \to e_L^+ + \varphi$. Momentum flows are represented by p, q, and k.

For notational convenience, we write (7.42) in the form

$$\eta(x) = \frac{1}{(2\pi)^{3/2}} \sum_s \int d^3p \sqrt{\frac{p_0 + |\mathbf{p}|}{2p_0}} \left[a_s(\mathbf{p}) U^{(s)}(\mathbf{p}) e^{-ipx} \right.$$

$$\left. + a_s^\dagger(\mathbf{p}) V^{(s)}(\mathbf{p}) e^{+ipx} \right] , \tag{7.72}$$

$$\eta^*(x) = \frac{1}{(2\pi)^{3/2}} \sum_s \int d^3p \sqrt{\frac{p_0 + |\mathbf{p}|}{2p_0}} \left[a_s^\dagger(\mathbf{p}) U^{(s)*}(\mathbf{p}) e^{+ipx} \right.$$

$$\left. + a_s(\mathbf{p}) V^{(s)*}(\mathbf{p}) e^{-ipx} \right] , \tag{7.73}$$

where

$$U^{(-)}(\mathbf{p}) = \beta(\mathbf{p}) , \quad U^{(+)}(\mathbf{p}) = -\frac{M_N}{p_0 + |\mathbf{p}|} \alpha(\mathbf{p}) ,$$

$$V^{(-)}(\mathbf{p}) = \frac{M_N}{p_0 + |\mathbf{p}|} \alpha(\mathbf{p}) , \quad V^{(+)}(\mathbf{p}) = \beta(p) . \tag{7.74}$$

The scattering amplitude (7.71) is then

$$\langle q, k | i\mathcal{L}_{\text{int}} | p \rangle$$

$$= -(2\pi)^4 \delta^4(p - k - q) g \frac{1}{\sqrt{2k_0}} \sqrt{\frac{p_0 + |\mathbf{p}|}{2p_0}} \sqrt{\frac{q_0 + |\mathbf{q}|}{2q_0}} u_e^{(s)*}(\mathbf{q}) \sigma_2 V^{(s')*}(\mathbf{p}) . \tag{7.75}$$

Using

$$\frac{1}{2} \sum_{s,s'} |u_e^{(s)*}(\mathbf{q}) \sigma_2 V^{(s')*}(\mathbf{p})|^2 = \frac{1}{2} T_r(\sigma_2 V^* V \sigma_2 u_e u_e^*) = \frac{1}{2} \frac{2(pq)}{(p_0 + |\mathbf{p}|)(q_0 + |\mathbf{q}|)} , \tag{7.76}$$

we obtain the decay rate

$$\Gamma(N \rightarrow e^- + \varphi^+) = \int \frac{d^3q}{(2\pi)^3} \frac{d^3k}{(2\pi)^3} (2\pi)^4 (p - q - k) \frac{g^2}{2k_0}$$

$$\times \frac{p_0 + |\mathbf{p}|}{2p_0} \frac{q_0 + |\mathbf{q}|}{2q_0} \frac{1}{2} \sum_{ss'} |U^* \sigma_2 V^*|^2$$

$$= \frac{1}{(2\pi)^2} \int d^3q \, d^3k \, \delta(p - q - k) \frac{(pq)}{2p_0 2q_0} \frac{1}{2k_0}$$

$$= \frac{g^2}{32\pi} M_N , \tag{7.77}$$

where we have assumed $m_e = 0$ and $m_\varphi = 0$, for simplicity. Similarly,

$$\Gamma(N \to e^+ + \varphi^-) = \frac{g^2}{32\pi} M_N . \tag{7.78}$$

Then,

$$\Gamma_{\text{total}}(N) = \frac{g^2}{16\pi} M_N . \tag{7.79}$$

In case when N is a Dirac fermion,

$$\mathcal{L}_{\text{int}} = g(\bar{e}_L N_R \varphi^\dagger + \bar{N}_R e_L \varphi) , \tag{7.80}$$

instead of (7.69). Therefore, $N \to e_L^- + \varphi^+$ is allowed, but $N \to e_L^+ + \varphi^-$ is forbidden. A standard calculation gives

$$\Gamma_{\text{total}}(N) = \frac{g^2}{32\pi} M_N , \tag{7.81}$$

which is half the rate for the Majorana case.

7.5.2 $N + N \to e_L^- + e_L^+$

Let us consider the interaction Lagrangian,

$$\mathcal{L}_{\text{int}} = g(\bar{e}_L N_R \varphi^\dagger + \overline{N}_R \, e_L \, \varphi). \tag{7.82}$$

Instead of N_L^c in (7.69), we use N_R to define the Majorana field, $N = N_R - N_R^c$. The annihilation process of the Majorana N_R, $N + N \to e_L^- + e_L^+$, is given by the φ exchange. With $m_\varphi \gg m_N, m_e$, the effective Lagrangian is

$$\mathcal{L}_{\text{eff}} = \frac{g^2}{m_\varphi^2} (\overline{N}_R e_L)(\bar{e}_L N_R)$$

$$= -\frac{g^2}{2m_\varphi^2} (\overline{N}_R \gamma_\mu N_R)(\bar{e}_L \gamma_\mu e_L) . \tag{7.83}$$

Substitution of the Weyl spinors ξ for N_R and ζ for e_L^- yields

$$\mathcal{L}_{\text{eff}} = -\frac{g^2}{2m_\varphi^2} (\xi^* \tilde{\sigma}_\mu \xi)(\zeta^* \sigma_\mu \zeta) , \tag{7.84}$$

where σ_μ and $\tilde{\sigma}_\mu$ are given in (7.29) and (7.30). With the momentum assignment given in Fig. 7.2, we calculate

$$\langle p', q' | i\mathcal{L}_{\text{eff}} | p, q \rangle = +i \frac{g^2}{2m_\varphi^2} \int dx \langle p', q' | \zeta^*(x) \sigma_\mu \zeta(x) | 0 \rangle \langle 0 | \xi^*(x) \tilde{\sigma}_\mu \xi(x) | p, q \rangle . \tag{7.85}$$
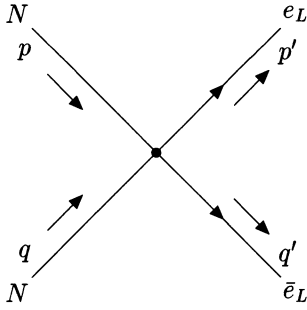
Fig. 7.2. Feynman diagram for scattering of two Majorana particles: $N + N \to e_L^- + e_L^+$.

The Weyl spinors, $\xi(x)$ and $\xi^*(x)$, are expanded similarly to (7.72) and (7.73) with

$$U^{(+)}(\mathbf{p}) = \alpha(\mathbf{p}) , \qquad U^{(-)}(\mathbf{p}) = -\frac{M_N}{p_0 + |\mathbf{p}|}\beta(\mathbf{p}) ,$$

$$V^{(+)}(\mathbf{p}) = \frac{M_N}{p_0 + |\mathbf{p}|}\beta(\mathbf{p}), \qquad V^{(-)}(\mathbf{p}) = \alpha(\mathbf{p}) , \tag{7.86}$$

instead of (7.74). The scattering amplitude (7.85) is then

$$\langle p', q' | s | p, q \rangle = i\frac{g^2}{2m_\varphi^2}\frac{1}{(2\pi)^2}\delta^{(4)}(p + q - p' - q')\sqrt{\frac{p_0 + |\mathbf{p}|}{2p_0}}\sqrt{\frac{q_0 + |\mathbf{q}|}{2q_0}}$$

$$\times \sqrt{\frac{p'_0 + |\mathbf{p'}|}{2p'_0}}\sqrt{\frac{q'_0 + |\mathbf{q'}|}{2q'_0}}\,[u_e^*(\mathbf{p'})\sigma_\mu v_e(\mathbf{q'})]$$

$$\times \left[V^{*(s)}(\mathbf{p})\tilde{\sigma}_\mu U^{(s')}(\mathbf{q}) + V^{*(s')}(\mathbf{q})\tilde{\sigma}_\mu U^{(s)}(\mathbf{p})\right] . \tag{7.87}$$

It is now straightforward to obtain the annihilation cross section σ,

$$\sigma = \frac{1}{(2\pi)^2}\frac{1}{v_{\rm rel}}\left(\frac{g^4}{4m_\varphi^4}\right)\int d^3p'd^3q'\delta^{(4)}(p + q - p' - q')$$

$$\times \frac{1}{2}\frac{p_0 + |\mathbf{p}|}{2p_0}\frac{q_0 + |\mathbf{q}|}{2q_0}\frac{2p'q'}{2q'_0 2p'_0}\frac{2}{(q_0 + |\mathbf{q}|)(p_0 + |\mathbf{p}|)}\left(qp + \frac{\mathbf{q}\cdot\mathbf{p}}{|\mathbf{q}||\mathbf{p}|}M_N^2\right)$$

$$\simeq \left(\frac{g^2}{4m_\varphi^4}\right)\frac{M_N^2}{8\pi}\beta , \tag{7.88}$$

with $\beta = |\mathbf{p}|/m$ ($m_e = 0$ is assumed). In this calculation we used

$$\frac{1}{4}\sum_{s,s'}|V^{*(s')}(\mathbf{q})\tilde{\sigma}_\mu U^{(s)}(\mathbf{p})|^2 = \frac{1}{4}\frac{2qp}{(q_0 + |\mathbf{q}|)(p_0 + |\mathbf{p}|)} ,$$

$$\frac{1}{4}\sum_{s,s'}\left[V^{*(s)}(\mathbf{p})\tilde{\sigma}_\mu U^{(s')}(\mathbf{q})V^{(s')}(\mathbf{q})\tilde{\sigma}^\mu U^{*(s)}(\mathbf{p})\right]$$

$$= \frac{1}{4}\frac{2\mathbf{q}\cdot\mathbf{p}}{qp}\frac{1}{q_0 + |\mathbf{q}|}\frac{1}{p_0 + |\mathbf{p}|}M_N^2 . \tag{7.89}$$

We note that the annihilation cross section σ is proportional to β. The $\overline{N}_R \gamma_\mu N_R$ part in (7.83) is written in terms of the Majorana field N:

$$\overline{N}_R \gamma_\mu N_R \to \frac{1}{2} \overline{N} \gamma_\mu \gamma_5 N .$$

This means that N has only an axial-vector coupling, and the annihilation process near the threshold is thus dominated by the p-wave [1113]. This significantly suppresses the low-energy cross section compared with the annihilation of Dirac fermions, $f + \bar{f} \to e^+ + e^-$, which proceeds with the s-wave.

7.6 Double Beta Decay

A conspicuous consequence of propagator (7.59) of the Majorana neutrino is that it induces neutrinoless double beta decay ${}^A_Z\square \to {}^A_{Z+2}\square + e^- + e^-$ ($0\nu2\beta$ in brevity), shown in Fig. 7.3 [200]. Because of a strong pairing force between like nucleons, it occasionally happens in middle-heavy to heavy nuclei that even-even nuclei have large binding energies and ordinary β decay ${}^A_Z\square \to {}^A_{Z+1}\square + e^- + \bar{\nu}_e$ is energetically forbidden, which leaves double beta decay as the only allowed decay mode (see Fig. 7.4). There is also another double beta-decay mode ${}^A_Z\square \to {}^A_{Z+2}\square + e^- + e^- + \bar{\nu}_e + \bar{\nu}_e$ ($2\nu2\beta$ in short), which takes place irrespective of whether the neutrino is of the Dirac or the Majorana type; it is simply a very slow process [199]. Here, we are mostly concerned with double beta decay of the first type ($0\nu2\beta$), but we also discuss briefly the latter. As the published date of the original literature [199,200] shows, this is an old subject and much work has been done during many years (see [1114] for a review of the early work). More recently, interest has been revived from the point of view that the neutrino naturally appears as a Majorana particle in grand unified theories of particle interactions (e.g., [1115]). The detail of the theory of double beta decay is a rather involved subject, and we must defer the discussion to dedicated review articles [1116–1121]. Here, we confine ourselves only to an elementary account.
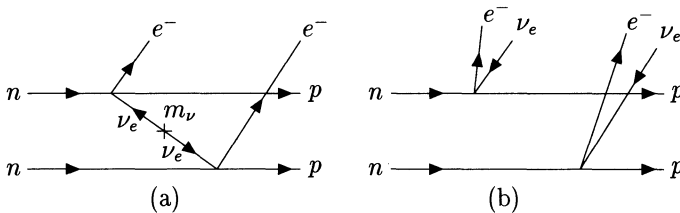
Fig. 7.3. Feynman diagrams giving rise to (**a**) neutrinoless double beta decay, and (**b**) two neutrino double beta decay. In the first diagram the cross (m_ν) stands for the Majorana mass of the neutrino.
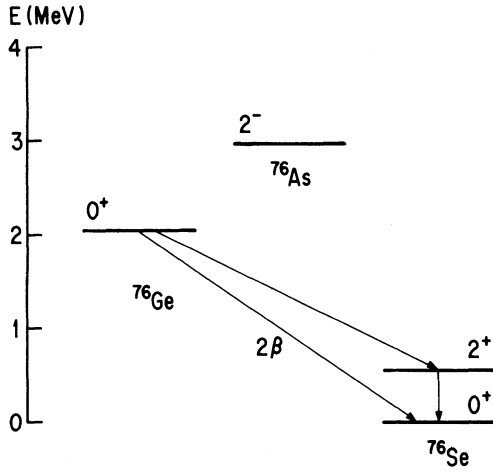
E (MeV)

7.6.1 0ν2β Decay Rate

The 0ν2β amplitude shown in Fig. 7.3a is calculated in the following manner [1114–1118, 1122, 1123]. With the charged-current Hamiltonian (2.5), the effective operator for 0ν2β decay is

$$H_{\text{eff}} = (\sqrt{2}G_F \cos\theta_c)^2 (\bar{e}_L \gamma_\mu \nu_L)(-\overline{\nu_L^c}\gamma_\nu e_L^c)$$
$$\times [\bar{p}\gamma^\mu(1 - g_A\gamma_5)n][\bar{p}\gamma^\nu(1 - g_A\gamma_5)n]. \tag{7.90}$$

For the $\nu_L\overline{\nu_L^c}$ contraction, we obtain from (7.59),

$$\langle T[\psi_\nu(x)\overline{\psi_\nu^c}(y)]\rangle = \frac{1}{(2\pi)^4}\int d^4k \frac{m_\nu}{k^2 - m_\nu^2}e^{-ik(x-y)} . \tag{7.91}$$

In the static approximation for the nucleon currents, the 0ν2β amplitude reads

$$M = -2G_F^2\cos^2\theta_c \int \frac{d^4k_\nu}{(2\pi)^4}\bar{u}(p_1)\gamma_\mu \frac{m_\nu}{k_\nu^2 - m_\nu^2}\frac{1 - \gamma_5}{2}\gamma_\nu v(p_2)e^{i\mathbf{k}_\nu\mathbf{r}}$$
$$\times\langle N_1'|J^\mu|N_1\rangle\langle N_2'|J^\nu|N_2\rangle 2\pi\delta(k^0 - E_{1i} + E_{1n} + \epsilon_1)$$
$$= -2G_F^2\cos^2\theta_c L_{\mu\nu}H^{\mu\nu} , \tag{7.92}$$

where L and H refer to the leptonic and hadronic parts, $\mathbf{r}$ is the relative distance of the two nucleons N_1 and N_2, and k_ν is the neutrino four-momentum [energy variables other than k^0 (neutrino energy) in the delta function are defined below]. The leptonic part is

$$L_{\mu\nu} = \int \frac{d^3k_\nu}{(2\pi)^3}\bar{u}(p_1)\gamma_\mu\gamma_\nu\frac{1 + \gamma_5}{2}v(p_2)\frac{m_\nu}{k_\nu^2 - m_\nu^2}e^{i\mathbf{k}_\nu\mathbf{r}} , \tag{7.93}$$

where $1/(k_\nu^2 - m_\nu^2)$ is written

$$
\frac{1}{k_\nu^2 - m_\nu^2} = \frac{1}{2\epsilon_\nu} \frac{1}{(E_{1i} - E_{1n} - \epsilon_1)^2 - \epsilon_\nu^2}
$$

$$
= \frac{-1}{2\epsilon_\nu} \left(\frac{1}{E_{1i} - E_{1n} - \epsilon_1 - \epsilon_\nu} + \frac{1}{E_{2i} - E_{2n} - \epsilon_2 - \epsilon_\nu} \right). \quad (7.94)
$$

Here, E_{1i} and E_{2i} are the energies of the two nucleons in the initial state, E_{1n} and E_{2n} are those in the intermediate state, ϵ_1 and ϵ_2 are those of the emitted two electrons $(1,2)$, and $\epsilon_\nu = \sqrt{m_\nu^2 + \mathbf{k}_\nu^2}$. We used in (7.94) the energy conservation $E_{1i} + E_{2i} = E_{1n} + E_{2n} + \epsilon_1 + \epsilon_2$. The two terms in (7.94) correspond to the diagrams emitting electron 1 first and electron 2 first. For the practically most important $0^+ \to 0^+$ transitions, two electrons are emitted in the s-wave. For this case it is sufficient to retain only $g_{\mu\nu}$ of $\gamma_\mu\gamma_\nu = g_{\mu\nu} + \frac{1}{2}[\gamma_\mu, \gamma_\nu]$ in the numerator. Writing $E_{1i} + E_{2i} = E_i$ and $E_{1n} + E_{2n} = E_n$ in (7.94), we obtain

$$
L_{\mu\nu} = g_{\mu\nu} m_\nu \bar{u}(p_1) \frac{1 + \gamma_5}{2} v(p_2) \int \frac{d^3 k}{(2\pi)^3} \sum_\kappa \frac{-1}{2\epsilon_\nu} \frac{1}{E_i - E_n - \epsilon_\kappa - \epsilon_\nu} e^{i\mathbf{k}_\nu \cdot \mathbf{r}},
$$
$$(7.95)$$

and after squaring $L_{\mu\nu}$,

$$
|M|^2 = 4 G_F^4 \cos^4 \theta_c H_\mu^\mu H_\rho^\rho m_\nu^2 2(p_1 p_2) \left[\frac{1}{4\pi} F(r) \right]^2, \quad (7.96)
$$

where

$$
F(r) = \frac{1}{4\pi^2} \sum_{\kappa=1}^{2} \int d^3 k_\nu \frac{e^{i\mathbf{k}_\nu r}}{(-\epsilon_\nu)(E_i - E_n - \epsilon_\kappa - \epsilon_\nu)} \quad (7.97)
$$

and

$$
H_\mu^\mu = \langle f | \tau_+(1) \tau_+(2)(1 - g_A^2 \boldsymbol{\sigma}(1) \boldsymbol{\sigma}(2)) | i \rangle, \quad (7.98)
$$

using the nonrelativistic expansion for the nuclear matrix elements; p_1 and p_2 are the momenta of the two electrons.

The decay rate is given by

$$
\Gamma = \frac{1}{2} \int \frac{d^3 p_1}{2\epsilon_1 (2\pi)^3} \int \frac{d^3 p_2}{2\epsilon_2 (2\pi)^3} (2\pi) \delta(\epsilon_1 + \epsilon_2 - Q) |M|^2
$$

$$
= \frac{G_F^4 \cos^4 \theta_c}{64\pi^5} \int d\epsilon_1 d\cos\theta \; p_1 p_2 (\epsilon_1 \epsilon_2 - \mathbf{p}_1 \mathbf{p}_2) m_\nu^2
$$

$$
\times \left| \langle f | \tau_+(1) \tau_+(2) [1 - g_A^2 \boldsymbol{\sigma}(1) \boldsymbol{\sigma}(2)] F(r) | i \rangle \right|^2. \quad (7.99)
$$

When we consider a nucleus, we must sum over all nucleons in the nuclei, $(1,2) \rightarrow \Sigma(i,j)$. In (7.97) we should also sum over the intermediate excited states n as

$$\sum_n \frac{|n\rangle \langle n|}{E_i - E_n - \epsilon_\kappa - \epsilon_\nu}. \qquad (7.100)$$

Here, a closure approximation is commonly used to evaluate the matrix element by replacing E_n with its average $\langle E_n \rangle$. Namely, (7.100) is approximated as

$$\frac{1}{E_i - \langle E_n \rangle - \epsilon_\kappa - \epsilon_\nu}. \qquad (7.101)$$

For $0\nu2\beta$ decay this is supposed to be a good approximation because the neutrino energy in the virtual state is much greater than the typical energy of the relevant nuclear levels (see below). This process takes place only for $|f\rangle = |0^+\rangle$ when $|i\rangle = |0^+\rangle$ (the initial states of the nuclei that concern us all have 0^+).[1]

Finally, the differential rate is written

$$\frac{d\Gamma}{d\cos\theta d\epsilon_1} = \frac{G_F^4 \cos^4\theta_c}{16\pi^5} \epsilon_1 \epsilon_2 p_1 p_2 \left(1 - \frac{\mathbf{p}_1}{\epsilon_1} \frac{\mathbf{p}_2}{\epsilon_2} \right) m_\nu^2$$
$$\times \left| \left\langle 0_f^+ \left\| \frac{1}{2}\tau_+(i)\tau_+(j)[1 - g_A^2 \boldsymbol{\sigma}(i)\boldsymbol{\sigma}(j)]F(r_{ij}) \right\| 0_i^+ \right\rangle \right|^2 , \quad (7.102)$$

where

$$F(r) = \frac{1}{4\pi^2} \sum_{k=1}^{2} \int d^3 k_\nu \frac{e^{i\mathbf{k}_\nu \mathbf{r}}}{(-\epsilon_\nu)(E_i - \langle E_n \rangle - \epsilon_k - \epsilon_\nu)} . \qquad (7.103)$$

Since typical neutrino momentum is of the order of

$$\langle k_\nu \rangle \sim \frac{1}{\langle r_{ij} \rangle} \sim 100 \, \text{MeV} \qquad (7.104)$$

for $\langle r_{ij} \rangle \sim 2\text{fm}$, we expect $\epsilon_\nu \gg |\langle E_n \rangle + \epsilon_k - E_i| \approx 10 \, \text{MeV}$. Equation (7.103) then simplifies to

$$F(r) = \frac{1}{2\pi^2} \int d^3 k_\nu \frac{e^{i\mathbf{k}_\nu \mathbf{r}}}{\epsilon_\nu^2}$$
$$= \frac{e^{-m_\nu r}}{r}. \qquad (7.105)$$

---

[1] 1^+ and 2^+ final states can be excited only when the right-handed current exists. For neutrino mass induced double beta decay, $0^+ \rightarrow 2^+$ takes place only when the nucleon recoil is taken into account; see [1124].

If $m_\nu \ll \langle k_\nu \rangle \sim (2\text{fm})^{-1} \simeq 100\,\text{MeV}$,

$$F(r) \simeq 1/r \,, \qquad (7.106)$$

i.e., the matrix element becomes independent of the neutrino mass, and m_ν is factored out from the amplitude. If the energy denominator $\langle E_n \rangle + \epsilon_k - E_i \equiv \Delta$ is retained, (7.103) is

$$F(r) \simeq \frac{2}{\pi r}[\sin(r \cdot \Delta)\text{ci}(r \cdot \Delta) - \cos(r \cdot \Delta)\text{si}(r \cdot \Delta)] \,, \qquad (7.107)$$

where

$$\text{si}(x) = -\int_x^\infty dt \frac{\sin t}{t}, \quad \text{ci}(x) = -\int_x^\infty dt \frac{\cos t}{t}. \qquad (7.108)$$

The nuclear matrix element has often been evaluated using (7.107) rather than (7.106).

The differential rate (7.102) is integrated to give

$$\Gamma = (G_F \cos\theta)^4 G_{0\nu} \left(\frac{m_\nu}{m_e}\right)^2 \left|\left\langle 0_f^+ \left\|\frac{1}{2}\Sigma\tau_\pm(i)\tau_\pm(j)[1 - g_A^2\boldsymbol{\sigma}(i)\boldsymbol{\sigma}(j)]F(r_{ij})\right\| 0_i^+ \right\rangle\right|^2 \,, \qquad (7.109)$$

where

$$\begin{aligned} G_{0\nu} &= \frac{m_e^2}{8\pi^5} \int_{m_e}^{T_0 + m_e} p_1 p_2 \epsilon_1 \epsilon_2 d\epsilon_1 \\ &= \frac{m_e^7}{8\pi^5}\left(\frac{t_0^5}{30} + \frac{t_0^4}{3} + \frac{4}{3}t_0^3 + 2t_0^2 + t_0\right) \end{aligned} \qquad (7.110)$$

with $t_0 = T_0/m_e$, the maximum kinetic energy of the electron normalised by its mass. A correction for the Coulomb distortion of the wave function $F(\epsilon_1, Z)F(\epsilon_2, Z)$ must be inserted into the integrand of (7.110) for practical use. A relativistic treatment of the Coulomb correction is needed for such heavy nuclei that often appear in double beta decay [1125]. The Coulomb correction enhances the decay rate, e.g., by a factor of ~ 5 for tellurium, which is larger than the nonrelativistic correction by a factor of 2–3. The sum of the electron energies is monoenergetic.

7.6.2 $2\nu 2\beta$ Decay

This process is not of direct interest in this chapter, but we include it in our discussion since it is parallel to $0\nu 2\beta$ decay both experimentally and theoretically. Nuclear levels that appear in the summation of the matrix element involved in $2\nu 2\beta$ decay are different from those for $0\nu 2\beta$, and the former does not give direct information on the matrix element for $0\nu 2\beta$ decay. However, it may serve at least as a diagnostic for the nuclear model used to calculate $0\nu 2\beta$ matrix elements.

The calculation for the $2\nu2\beta$ decay rate is straightforward [1126], and the decay rate for $0^+ \rightarrow 0^+$ is

$$d\Gamma = \frac{(G_F\cos\theta)^4}{16\pi^2}p_1^2p_2^2dp_1\,dp_2\,k_1^2k_2^2dk_1\,dk_2$$
$$\times \sum_n \Big[(K^2 + L^2 - KL)\langle f|\tau^+|n\rangle\langle n|\tau^+|i\rangle$$
$$+ \frac{g_A^4}{3}(K^2 + L^2 + KL)\langle f|\tau^+\boldsymbol{\sigma}|n\rangle\langle n|\tau^+\boldsymbol{\sigma}|i\rangle$$
$$- g_A^2 KL\,\mathrm{Re}(\langle f|\tau^+|n\rangle\langle n|\tau^+\boldsymbol{\sigma}|i\rangle + \langle f|\tau^+\boldsymbol{\sigma}|n\rangle\langle n|\tau^+|i\rangle)\Big] , \quad (7.111)$$

where

$$K = \frac{1}{E_i - \epsilon_1 - k_1 - E_n} + \frac{1}{E_i - \epsilon_2 - k_2 - E_n} ,$$
$$L = \frac{1}{E_i - \epsilon_1 - k_2 - E_n} + \frac{1}{E_i - \epsilon_2 - k_1 - E_n} , \quad (7.112)$$

and k_i are the neutrino momenta. For the case that concerns us, the Fermi-type transition contributes only through mixing of high-lying 0^+ isobaric analogue states, so that it is generally very small; it is sufficient to retain only Gamow–Teller matrix elements. The intermediate states are, therefore, limited to 1^+. The final state can be 0^+, 1^+, and 2^+. The decay rate formula for 1^+ and 2^+ final states includes the factor $(K - L)^2$ [1122], which strongly suppresses the process (typically $\ll 1/100$), since $K \approx L$ in the first approximation (for ^{76}Ge, say, the suppression is $1/800$). Another suppression comes from the sharp Q dependence of the decay rate for a smaller Q value for 2^+ states. We do not need to consider 1^+ final states, for they are not low-lying.

Typical nuclear excitation energy via the Gamow–Teller matrix element is about $E_n - E_i \approx$ several MeV, which is larger than the lepton energy involved in double beta decay, $\approx$1 MeV. So we approximate the K and L factors as

$$K = \frac{1}{\frac{E_i+E_f}{2} - E_n}\left(\frac{E_i + E_f}{2} - \langle E_n\rangle\right)\langle K\rangle,$$
$$L = \frac{1}{\frac{E_i+E_f}{2} - E_n}\left(\frac{E_i + E_f}{2} - \langle E_n\rangle\right)\langle L\rangle, \quad (7.113)$$

where $\langle E_n\rangle$ is the mean energy of intermediate nuclear states (the total released energy is $W_0 = Q_{\beta\beta} + 2m_e = E_i - E_f$). Using this approximation, the decay rate is written

$$\Gamma = (G_F\cos\theta)^4 g_A^4 G_{2\nu}|M^{2\nu}|^2 , \quad (7.114)$$

with

$$M^{2\nu} = \sum_n \frac{\langle J_f^P\|\tau^+\sigma\|1_n^+\rangle\langle 1_n^+\|\tau^+\sigma\|0_i^+\rangle}{\frac{E_i+E_f}{2} - E_n} , \quad (7.115)$$

and the phase-space volume integrated, including the energy denominators,

$$G_{2\nu} = \frac{1}{24\pi^7} \int_{m_e}^{W_0 - m_e} p_1 \epsilon_1 d\epsilon_1 \int_{m_e}^{W_0 - \epsilon_1} p_2 \epsilon_2 d\epsilon_2$$

$$\times \int_{m_e}^{W_0 - \epsilon_1 - \epsilon_2} k_1^2 k_2^2 dk_1 (K^2 + L^2 + KL)$$

$$\approx \frac{m_e^{11}}{1800\pi^7} \int_0^{T_0/m_e} dt \, t \, (t_0 - t)^5 (t^4 + 10 \, t^3 + 40 \, t^2 + 60 \, t + 30),$$

$$(7.116)$$

where the Fermi functions $F(\epsilon_1, Z) F(\epsilon_2, Z)$ must be inserted in the integrand for actual evaluations; see the comment after (7.110); $t = T/m_e$ is the sum of the kinetic energy of the two electrons, and t_0 its maximum. The electron energy spectrum is shown in Fig. 7.5, together with that of $0\nu 2\beta$ decay.
    Earlier authors further used a closure approximation in (7.115) that

$$M^{2\nu} \approx \frac{\langle J_f^P \| \tau^+ \sigma \tau^+ \sigma \| 0_i^+ \rangle}{\frac{E_i + E_f}{2} - \langle E_n \rangle} . \qquad (7.117)$$

The empirical suppression of $2\nu 2\beta$ decay, however, indicates that this is a poor approximation and an explicit summation is necessary in (7.115).
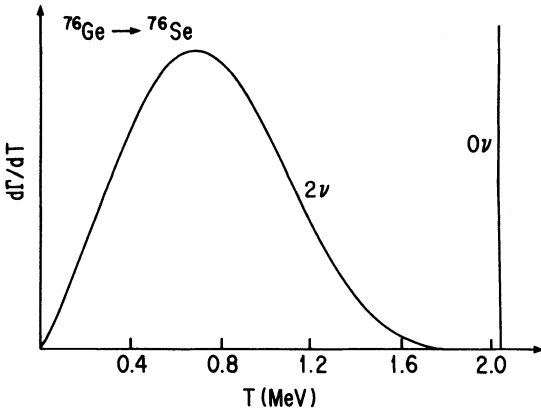
Fig. 7.5. Kinetic energy spectrum of the two electrons emitted from the double beta decay of ^{76}Ge. T is the sum of the kinetic energies of the two electrons.

7.6.3 Nuclear Matrix Elements

Haxton and Stephenson (HS) [1116] listed 35 candidates for $\beta^- \beta^-$ and 6 candidates for $\beta^+ \beta^+$. We list in Table 7.1 those $(\beta^- \beta^-)$ that have received attention in modern experiments. Those dropped from the list are ^{46}Ca, ^{70}Zn, ^{80}Se, ^{86}Kr, ^{94}Zr, ^{98}Mo, ^{104}Ru, ^{110}Pd, ^{114}Cd, ^{122}Sn, ^{124}Sn, ^{134}Xe, ^{142}Ce, ^{146,148}Nd, ^{154}Sm, ^{170}Er, ^{176}Yb, ^{186}W, ^{192}Os, ^{198}Pt, ^{204}Hg, and ^{232}Th for

Table 7.1. Examples of $\beta\beta$ decay candidates and the experimental results.

Transition	Q value (MeV)	Natural. abund. (%)	$T_{1/2}(2\nu2\beta)$ (yr)	$T_{1/2}(0\nu2\beta)^a$ (yr)
^{48}Ca $\rightarrow$ ^{48}Ti	4.271	0.187	$4.3^{+2.4}_{-1.1} \pm 1.4 \times 10^{19}$ [1127]	$> 9.5 \times 10^{21}$ (76%) [1128]
^{76}Ge $\rightarrow$ ^{76}Se	2.040	7.8	$1.77 \pm 0.01^{+0.13}_{-0.11} \times 10^{21}$ [1129]	$> 1.6 \times 10^{25}$ (90%) [1130]
			$0.92^{+0.07}_{-0.04} \times 10^{21}$ [1131]	
			$1.12^{+0.48}_{-0.26} \times 10^{21}$ [1132]	
			$0.9 \pm 0.1 \times 10^{21}$ [1133]	
^{82}Se $\rightarrow$ ^{82}Kr	2.995	9.2	$1.08^{+0.26}_{-0.06} \times 10^{20}$ [1134]	$> 2.7 \times 10^{22}$ (68%) [1134]
^{96}Zr $\rightarrow$ ^{96}Mo	3.350	2.8	$2.1^{+0.8}_{-0.4} \pm 0.2 \times 10^{19}$ [1135]	$> 1.0 \times 10^{21}$ [1135]
^{100}Mo $\rightarrow$ ^{100}Ru	3.034	9.6	$7.6^{+2.2}_{-1.4} \times 10^{18}$ [1136]	$> 5.2 \times 10^{22}$ (68%) [1137]
			$6.82^{+0.38}_{-0.53} \pm 0.68 \times 10^{18}$ [1138]	
			$9.5 \pm 0.4 \pm 0.9 \times 10^{18}$ [1139]	
^{100}Mo $\rightarrow$ ^{100}Ru(0^{+*})	1.904	9.6	$6.1^{+1.8}_{-1.1} \times 10^{20}$ [1140]	
^{116}Cd $\rightarrow$ ^{116}Sn	2.802	7.5	$3.75 \pm 0.35 \pm 0.21 \times 10^{19}$ [1141]	$> 2.9 \times 10^{22}$ (90%) [1142]
			$2.6^{+0.9}_{-0.5} \times 10^{19}$ [1143]	
^{128}Te $\rightarrow$ ^{128}Xe	0.868	31.7	$7.7 \pm 0.4 \times 10^{24}$ [1144]	$> 1.7 \times 10^{22}$ [1145]
^{130}Te $\rightarrow$ ^{130}Xe	2.533	34.5	$2.7 \pm 0.1 \times 10^{21}$ [1144]	$> 5.6 \times 10^{22}$ [1145]
			$2.6 \pm 0.3 \times 10^{21}$ [1146]	
			$(0.8 \pm 0.1 \times 10^{21})$ [1147]	
^{136}Xe $\rightarrow$ ^{136}Ba	2.479	8.9	$> 3.6 \times 10^{20}$ [1148]	$> 4.4 \times 10^{23}$ (90%) [1148]
^{150}Nd $\rightarrow$ ^{150}Sm	3.367	5.6	$0.68 \pm 0.04 \pm 0.68 \times 10^{19}$ [1138]	$> 1.2 \times 10^{21}$ (90%) [1138]
			$1.7^{+1.0}_{-0.5} \pm 0.35 \times 10^{19}$ [1149]	
^{160}Gd $\rightarrow$ ^{160}Dy	1.730	21.8		$> 0.3 \times 10^{21}$ [1150]
^{238}U $\rightarrow$ ^{238}Pu	1.146	99.3	$2.0 \pm 0.6 \times 10^{21}$ [1151]	

^{a}Only the best limit is quoted for $0\nu2\beta$ half-lives.

$\beta^-\beta^-$, and ^{78}Kr, ^{96}Ru, ^{106}Cd, ^{124}Xe, ^{130}Ba, and ^{136}Ce for $\beta^+\beta^+$. In addition, ^{92}Mo$(\beta^-\beta^-)$ was also studied experimentally [1152]. The final states of these nuclei often have 0^+ states more than one below the energy level of the parents. The branching to different 0^+ states is useful for testing nuclear model calculations. Among the nuclei in this list, ^{46}Ca and ^{48}Ca undergo ordinary beta decay, but their lifetimes (yet undetected) are expected to be as long as $2\nu2\beta$ decay or even longer because of a very small Q value.

The problem in extracting the physical result from double beta decay is the evaluation of nuclear matrix elements. It is difficult to infer the error of the calculations, and usually one would blindly hope that the scatter among different calculations would stand for uncertainties.

The lightest candidate for double beta decay experiments is ^{48}Ca (^{46}Ca is the lightest, but its natural abundance is very small). All others are nuclei with $A > 70$, such as ^{76}Ge, ^{82}Se, ^{100}Mo, ^{128}Te, ^{130}Te, and ^{136}Xe. It is only ^{48}Ca that can be handled by a shell model with reasonable effort without heavy truncations of model space. Even for ^{48}Ca, we need the fp shell

$\{2p_{1/2}, 2p_{3/2}, 1f_{5/2}, 1f_{7/2}\}$ wave functions in addition to the double magic ^{40}Ca core, and it already requires quite large model space (maximum dimension to be handled is 6.3×10^5) for the full $0\hbar\omega$ model for the intermediate and final states, for which neutrons and protons coexist in the valence shell. Therefore, most calculations restrict model space with various truncations for ^{48}Ti and intermediate ^{48}Sc [1116,1153,1154] (for earlier calculations see references cited in [1116]). HS gave 2.9×10^{19} yr, and Zhao et al. [1153] gave 1.9×10^{19} yr, as compared with the experimental value of $4.3^{+2.4}_{-1.1} \pm 1.4 \times 10^{19}$ yr [1127]. Caurier et al. [1155] and Ogawa and Horie [1156] carried out a full $0\hbar\omega$ calculation. The former authors obtained $T_{1/2} = 3.7 \times 10^{19}$ yr, and the latter gave 3.2×10^{19} yr for $g_A = 1$.[2] The mutual agreement between the two calculations and also with the experimental value is very good. The results of HS and Zhao et al. are not too far away from the $0\hbar\omega$ full shell calculations, indicating that the truncations are probably not too bad for $A = 48$.

For heavier nuclei such as ^{76}Ge and ^{82}Se, we usually need a heavy truncation of model space. The approximation used in HS is to decouple proton and neutron shells [1157]. The proton and neutron shells are diagonalised independently, and (pn) interactions are then introduced to allow mixing of the configurations. There are also ad hoc omissions of some orbits, although the validity of such approximations is not clear. A number of truncation schemes or effective treatments were devised in the literature [1158–1165]; the most popular among them is the quasi-particle random phase approximation which we shall discuss in what follows. Another approach [1166] uses a Monte Carlo technique to diagonalise the Hamiltonian in the time-discretised path-integral formulation [1167]. A large-space (10^8 dimensional) shell-model calculation was recently pioneered by Caurier et al. [1168]. We give a list of calculations of matrix elements in Table 7.2.

Quasi-particle random phase approximation (QRPA) [1158, 1160, 1162, 1163, 1165]. The most popular effective model for heavy nuclei is a random phase approximation [1178] applied to quasi-particles of the pn mode [1179][3] to describe excitation of an even-even to an odd-odd nucleus. The 0^+ state of an even-even nucleus is taken as a (pn)-phonon vacuum and an excited state (odd-odd nucleus) is represented as a single (pn)-phonon state.

One starts the formalism with the BCS state to incorporate the strong pairing correlation between two protons (and separately between two neutrons) in the 0^+ ground state. For pp pairing, for example, we consider a Bogoliubov transformation,

$$c^{\dagger}_{pjm} = u_{pj}a^{\dagger}_{pjm} + v_{pj}\tilde{a}_{pjm} \,, \qquad (7.118)$$

---

[2] Whether one adopts $g_A = 1$ or 1.27 is an uncertainty. Here, we normalise the result of Ogawa and Horie using $g_A = 1$; see the discussion in Sect. 3.6.5.

[3] This formalism was developed to calculate the GT matrix element of middle to heavy nuclei.

Table 7.2. Nuclear matrix element calculations.

Authors	Modes	Nuclei	Method
Haxton and Stephenson (1984) [1116]	$0\nu, 2\nu$	^{48}Ca $A > 70$	Shell model, truncated Shell model: (pn) weak coupling
Zhao et al. (1990) [1153]	2ν	^{48}Ca	Shell model, truncated
Ogawa and Horie (1990) [1156]	2ν	^{48}Ca	Shell model, full $0\hbar\omega$
Caurier et al. (1990) [1155]	2ν	^{48}Ca	Shell model, full $0\hbar\omega$
Retamosa et al. (1995) [1169]	0ν	^{48}Ca	Shell model, full $0\hbar\omega$
Radha et al. (1996) [1166]	2ν	^{48}Ca, ^{76}Ge	Shell model Monte Carlo
Grotz and Klapdor (1985–1986) [1162]	$0\nu, 2\nu$	$A > 70$	QRPA, $g_{pp} = 0$
Vogel and Fisher (1985) [1163]	2ν	$A > 70$	QRPA, $g_{pp} = 0$
Civitarese et al. (1987) [1165]	$0\nu, 2\nu$	$A > 70$	QRPA, $g_{pp} = 0$
Engel et al. (EVZ, 1988) [1170]	$0\nu, 2\nu$	$A > 70$	QRPA
Engel et al. (1989) [1171]	$0\nu, 2\nu$	$A > 70$	Seniority-based shell truncation
Staudt et al. (1990) [1172]	$0\nu, 2\nu$	$A > 70$	QRPA
Tomoda (1991) [1119]	0ν	$A > 70$	QRPA
Hirsch, Castaños et al. (1995) [1173]	$0\nu, 2\nu$	$A > 150$	Pseudo SU(3) [1174]
Caurier et al. (1996) [1168]	$0\nu, 2\nu$	$A = 76, 82, 136$	$O(10^8)$ dimensional shell model
Simkovic et al. (1997) [1175]	0ν	$A > 70$	QRPA ("renormalised")
Stoica and Klapdor (2001) [1176]	0ν	$A > 70$	QRPA [1177]

where $a^\dagger$ is the creation operator for a physical proton in the considered shell-model orbit that has angular momentum (jm) and the tilde denotes time reversal, i.e., backward propagation. The BCS state is defined by

$$c_{pjm}|0\rangle_{\text{BCS}} = 0. \qquad (7.119)$$

The coefficients u and v represent the amplitudes of a hole and a filled state and are determined by minimising the 0^+ ground state matrix element of the effective Hamiltonian for pp interactions,

$$H_p = \sum(T + V)a^\dagger_{pjm}a_{pjm} + \sum V' a^\dagger_{pj_1 m_1} a^\dagger_{pj_2 m_2} a_{pj_3 m_3} a_{pj_4 m_4} , \qquad (7.120)$$

(T is the kinetic part, and V and V' are the one- and two-body potentials) as

$$\delta\langle\text{gnd} : J = 0^+|H_p|\text{gnd} : J = 0^+\rangle_{\text{BCS}} = 0 . \qquad (7.121)$$

The constraint is imposed that $u^2 + v^2 = 1$ for each orbit, and the expectation value of the total number of protons is Z. The same procedure is followed for the neutron system independently.

We define a quasi-particle corresponding to a (pn) phonon by

$$Q(J)^\dagger = \sum_{pn} \left(\alpha_J [c_p^\dagger \times c_n^\dagger]^J + \beta_J [\tilde{c}_p \times \tilde{c}_n]^J \right) , \qquad (7.122)$$

and the 'QRPA vacuum' by

$$Q|0\rangle_{\mathrm{QRPA}} = 0. \qquad (7.123)$$

The vacuum is written as $|0\rangle_{\mathrm{QRPA}} = |0\rangle_{\mathrm{BCS}} + \kappa c_p^\dagger c_n^\dagger c_p^\dagger c_n^\dagger |0\rangle_{\mathrm{BCS}} + \cdots$. Writing the Hamiltonian of full nuclear interactions with c and $c^\dagger$, we truncate the commutator as (RPA),

$$\langle 0| \, [c_p c_n, ([H, Q_J^\dagger] - \omega Q_J^\dagger)] \, |0\rangle = 0 ,$$
$$\langle 0| \, [c_p^\dagger c_n^\dagger, ([H, Q_J^\dagger] - \omega Q_J^\dagger)] \, |0\rangle = 0 , \qquad (7.124)$$

for any p, n states. Here $|0\rangle$ is usually approximated as $|0\rangle_{\mathrm{BCS}}$. This gives the QRPA equation,

$$\begin{pmatrix} A & B \\ -B & -A \end{pmatrix} \begin{pmatrix} \alpha \\ \beta \end{pmatrix} = \omega \begin{pmatrix} \alpha \\ \beta \end{pmatrix} , \qquad (7.125)$$

which determines the forward and backward amplitudes, α_J and β_J, in (7.122). The submatrix A contains one- and two-body parts, and B consists only of two-body parts. For double-beta decay calculations it is essential to retain both particle–hole interaction $\langle p'n'^{-1}|V'|pn^{-1}\rangle$ and particle–particle interaction $\langle p'n'|V'|pn\rangle$ for the two-body matrix elements. This contrasts with β^- decay, where only particle–hole interaction is important (see [1180], however). In early QRPA calculations for $\beta^-\beta^-$ decay, particle–particle interaction was ignored. It turned out that this leads to a gross overestimate of the $2\nu2\beta$ matrix elements, resulting in lifetimes of ^{82}Se and ^{128,130}Te much shorter than experimental values. Vogel and Zirnbauer [1181] noticed that particle–particle interaction is important and the $2\nu2\beta$ matrix element is very sensitive to the strength of $\langle p'n'|V|pn\rangle$ for the $S = 1$ and $T = 0$ state.[4]

---

[4] In (7.126) and (7.127) below, the GT operator is contracted against a pn^{-1} operator of $Q(1^+)$. In β^- decay only (7.126) is relevant, and the term $u_p v_n \alpha_{pn}^j$ dominates [note that the Fermi energy for the neutron is larger than that for the proton, so that u_p (creation of a proton particle) and v_n (creation of a neutron hole) take values of the order of unity; on the other hand, v_p and u_n are small; also note that forward amplitude α is larger than backward amplitude β]. In double beta decay, however, another term (7.127), whose conjugate is relevant to β^+ decay, is multiplied on (7.126). In (7.127) the two terms are small and can be

We assume that the 0^+ ground state of the even-even nucleus is given by the QRPA vacuum and the odd-odd $J = 1^+$ state is constructed by operating $Q(1^+)$. The $0^+ \to 1^+$ and $1^+ \to 0^+$ matrix elements are calculated as

$$\langle 1_j^+ \| \tau^+ \sigma \| 0_i^+ \rangle = \langle 0 \| Q(1^+) \tau^+ \sigma \, \| 0 \rangle_{\text{QRPA}}$$
$$= \sum_{pn} \langle p \| \tau^+ \sigma \| n \rangle (u_p v_n \alpha_{pn}^j + v_p u_n \beta_{pn}^j) \,, \qquad (7.126)$$

$$\langle 0_f^+ \| \tau^+ \sigma \| 1_j^+ \rangle = \sum_{pn} \langle p \| \tau^+ \sigma \| n \rangle (v_p^* u_n^* \alpha_{pn}^{j*} + u_p^* v_n^* \beta_{pn}^{j*}) \,. \qquad (7.127)$$

Note that QRPA equations are solved separately for both initial and final states, and an overlap is taken between the two 1^+ states. One usually takes 10–15 shell model orbits to compute matrix elements.

By parametrising the matrix element with a short-range approximation $\langle p'n'|V|pn \rangle = g_{pp} \delta(r)$, it is shown that the $2\nu 2\beta$ matrix element changes sign at some g_{pp} that is close to the value obtained by fitting β^+ decay strengths (see footnote above). Therefore, the $2\nu 2\beta$ decay rate is very sensitive to the choice of the strength of the particle–particle interaction, and it can be very small. Tomoda et al. [1119, 1165] gave up predicting $2\nu 2\beta$ matrix elements. The authors of this book believe that this is the correct attitude. Notwithstanding, we uncritically present in Table 7.3 the predictions for $2\nu 2\beta$ decay made by a number of authors [1170–1172, 1175]. Assessment of the reliability of such calculations is difficult.

There is a belief among nuclear physicists that calculations of the $0\nu 2\beta$ matrix element are more reliable than those for $2\nu 2\beta$ because this subtle cancellation does not take place for the $0\nu 2\beta$ matrix element. (The contribution of g_{pp} is still sizable in reducing the matrix element for $0\nu 2\beta$.) The estimated matrix element squares still differ sometimes by 10–100 among different calculations (e.g., compare [1170] with [1172] or [1119]); see Table 7.4 below. In particular, a large-space shell model calculation [1168, 1169] gives a matrix element square 10 times smaller than typical QRPA calculations [1119, 1172].

The nuclear levels that are important for $0\nu 2\beta$ are $\approx 10\,\text{MeV}$, which are higher than those for the $2\nu 2\beta$ process ($E \sim$ a few MeV). Therefore, even if the latter is checked against experiment, it does not verify the reliability of the former. Some authors use tests of conservation laws or sum rules as criteria to judge the reliability of a model. They are certainly more satisfied, but it is not clear how the failure of conservation laws propagates into the calculation of matrix elements; on the other hand, it is unclear whether the models that satisfy the conservation law necessarily give better results. QRPA is a drastic truncation of shell model space. We should remember that the

of the same order. In this situation, the inclusion of particle–particle interaction largely affects the B term of (7.125), and enhances backward amplitude β. This strongly affects (7.127); the two terms may nearly cancel each other for particle–particle interaction of a strength that is close to the value inferred from β^+ decay. For full arguments on this point, see [1181, 1119].

original application of QRPA to beta decays of heavy nuclei (^{58}Ni to ^{142}Nd) gave decay lifetime in agreement with experiment no better than one order of magnitude [1179]. Griffiths and Vogel [1180] discussed that QRPA cannot reproduce simultaneously all experimental quantities for the $A = 100$ system, ^{100}Tc(1^+) $\rightarrow$ β^- ^{100}Ru($0^+, 0^{+*}$(1.13) MeV) and ^{100}Mo$\rightarrow$ $\beta^-\beta^-$ ^{100}Ru(0^+, gs). This is a vital test for the QRPA calculation of the double beta-decay matrix elements for ^{100}Mo. For a more detailed discussion of nuclear calculations, see [1119].

Table 7.3. Nuclear model calculations for $2\nu2\beta$ decays. The last column shows experimental results. The numbers are in units of 10^{20} yr.

Nuclei	HS84 [1116]	Caurier90,96 [1155, 1168]	EVZ88 [1170]	Staudt et al. 90 [1172]	Expt.
^{48}Ca	0.29	0.37			0.43
^{76}Ge	4.1		13–1.5	29	9–18
^{82}Se	0.26	0.80	1.2–0.27	1.2	1.1
^{100}Mo			0.060	0.011:	0.07–0.09
^{116}Cd			0.63		0.3–0.4
^{128}Te	880		5500–920	26300	77000
^{130}Te	0.17		2.2–0.46	18.4	26
^{136}Xe		16.7	8.2–2.0	46.4	
^{150}Nd				0.074	0.07–0.17

7.6.4 Experimental Techniques

Direct counting method [1182].   Double beta decay is a very slow process, and the rejection of the overwhelming background is crucial. The background ultimately comes from natural radioactivity from impurities in the materials used in the source, counter, and shielding, even if the apparatus is set up deep under the ground. Since the electron energy of double beta decay is ≈ 1 MeV, all radioactive contaminants of material have to be reduced. For example, the material must be purified to the level of 1 part per billion or less for U and Th chain isotopes. Along with the reduction of contaminants, there are two ways to enhance low-rate signals: one way is to identify the vertex of two-electron production, and the other is to make the energy resolution of the detector very high. The former is achieved with the time projection chamber (TPC), which has tracking capability [1134, 1138, 1148, 1149]. The first laboratory detection of $2\nu2\beta$ decays was made using a TPC for ^{82}Se, where a selenium plate is sandwiched between two chambers. The limitation of this method was that the source must be sufficiently thin (e.g., 7 mg (cm)$^{-2}$ in [1134]) to avoid disturbance of the track by scattering at the source. Using

xenon, the source acts as the detector, and the target mass can be increased to a few kg [1148], although xenon is an expensive material.

The most notable example of the second method is the germanium experiment that takes advantage of very high energy resolution ($\Delta E \approx 2$–$3\,\mathrm{keV}$) of germanium as a counter [1183–1185,1131]. The particular advantage is for detection of $0\nu2\beta$ decay for which the electron spectrum, when coadded, is monoenergetic at 2040 keV. With the resolution of germanium, one can reject 2021- and 2053-keV gamma rays from ^{214}Bi (Ra C) generated in the decay chain of ^{238}U. One can also take advantage of the technique that enables us to purify the material highly against radioactive impurities. The recent experiment of the Heidelberg-Moscow group [1129, 1130] uses p-type HPGe with ^{76}Ge enriched to 86%, compared to the natural abundance of 7.8%; the active mass is as large as 11 kg (installed at the Gran Sasso Underground Laboratory). Their work gives the best current lower limit on the $0\nu2\beta$ lifetime for ^{76}Ge, which surpassed the limit given by the LBL-UCSB group [1184], the long-standing record holder of the limit.

Geochemical method.   The first evidence for $2\nu2\beta$ decay was given by a geochemical experiment, initiated by Inghram and Reynolds [1186] (see also [1187, 1188]). The technique uses the fact that a noble gas is strongly depleted in minerals at the time of crystallisation. A tiny amount of radiogenic mass, accumulated over a geophysical timescale, can be measured by mass spectroscopy. The application has been primarily to Te, whose daughter is Xe, and to Se, which decays into Kr. The crucial points regarding this method are (i) whether one can know the geological time during which the daughter element has been accumulated, (ii) the rock has not metamorphosed, and (iii) the rock had been placed deep enough so that the daughter nuclei were not significantly produced by cosmic rays. For ^{82}Se geologically measured half-lives [1146, 1189, 1190] (including those using a meteorite) show good mutual agreement and agree with the more modern laboratory value [1134]. There was a discrepancy between the two earlier geological measurements for ^{128}Te and ^{130}Te [1146, 1189], but this was resolved by a more modern geological measurement [1144]. For an application of the geochemical method to nongaseous daughter products, see [1191].

^{128}Te/^{130}Te ratio: No energy information is available from geochemical detection, and one cannot generally distinguish $0\nu2\beta$ from $2\nu2\beta$. The ratio of ^{128}Xe/^{130}Xe in a mineral, however, provides us with a unique indicator to infer the importance of the $0\nu2\beta$ process relative to the $2\nu2\beta$ process, and hence, the value of m_ν without knowing the decay modes explicitly [202]. Because of the small Q value of ^{128}Te $\to$ ^{128}Xe (0.87 MeV), $2\nu2\beta$ decay, which involves a four-body phase-space volume, is strongly suppressed, whereas the suppression is not that much for $0\nu2\beta$. By simply accounting for the difference in the phase-space volume, we expect $T_{1/2}^{2\nu}(^{128}\mathrm{Te})/T_{1/2}^{2\nu}(^{130}\mathrm{Te}) = 5700$, whereas $T_{1/2}^{0\nu}(^{128}\mathrm{Te})/T_{1/2}^{0\nu}(^{130}\mathrm{Te}) = 24.5$. It is expected that much of

the experimental uncertainty in geological measurements, as well as part of the uncertainties in nuclear physics calculations, cancels in the ratio of the two isotopes. If $T_{1/2}(^{128}\mathrm{Te})/T_{1/2}(^{130}\mathrm{Te})$ were substantially smaller than a thousand, it would indicate a finite neutrino mass (see [1115]).

Table 7.4 presents a compilation of the predicted ratios from various nuclear physics calculations. They should be compared with the experiment of Bernatowicz et al. [1144], which gives $T_{1/2}(^{128}\mathrm{Te})/T_{1/2}(^{130}\mathrm{Te}) \approx 3000 \pm 200$, just consistent with an older lower limit of Kirsten et al. [1146], $T_{1/2}(^{128}\mathrm{Te})/T_{1/2}(^{130}\mathrm{Te}) > 3040$ (at 95% CL). This is smaller than the ratio of phase-space volumes for pure $2\nu2\beta$ decay but is consistent with nuclear model calculations, which vary by a factor of 2–3. With nuclear physics uncertainties we can say that $0\nu2\beta$ may compete with $2\nu2\beta$ for $^{128}\mathrm{Te}$ if $m_\nu \gtrsim 2$ eV (see Tables 7.3 and 7.5), and may modify the lifetime ratio significantly. Therefore, we can conclude that there is no evidence for a finite neutrino mass at least in excess of $\gtrsim 2$ eV. This is an example of the wonderful results that are obtained from geochemistry.

Table 7.4. $T_{1/2}(^{128}\mathrm{Te})/T_{1/2}(^{130}\mathrm{Te})$: predictions for $2\nu0\beta$ and $0\nu2\beta$ decays by various authors. Experiments indicate $T_{1/2}(^{128}\mathrm{Te})/T_{1/2}(^{130}\mathrm{Te}) \approx 3000$ [1144].

	$T_{1/2}^{2\nu}(^{128}\mathrm{Te})/T_{1/2}^{2\nu}(^{130}\mathrm{Te})$	$T_{1/2}^{0\nu}(^{128}\mathrm{Te})/T_{1/2}^{0\nu}(^{130}\mathrm{Te})$
Phase space	5685	24.5
Haxton-Stephenson (1984) [1116]	5180	25
Engel et al. (1988) [1170]	2500–2000	19.2
Tomoda (1991) [1119]		18.1
Engel et al. (1989) [1171]	2290	16.4
Staudt et al. (1990) [1172]	1430	15.9
Simkovic et al. (1997) [1175]		18.7

Radiochemical method. Some of the daughter isotopes of double beta decay are radioactive and are rare enough that only double beta decay produces those elements. Radioactivity allows counting to measure double beta decay products that are accumulated for 10–30 years or so. The advantage over the geochemical method is that this method is free from uncertainties concerning the age of the sample. Positive evidence was derived for the double beta decay of $^{238}\mathrm{U} \rightarrow ^{238}\mathrm{Pu}$ ($T_{1/2} = 88$ year) using 33 year old uranyl nitrate [1151]. Other candidates for radiochemical experiments are $^{232}\mathrm{Th} \rightarrow ^{232}\mathrm{U}$ ($T_{1/2} = 72$ year) and $^{244}\mathrm{Pu} \rightarrow ^{244}\mathrm{Cm}$ ($T_{1/2} = 18$ year).

7.6.5 Limit on the Majorana Neutrino Mass

An uncritical compilation of nuclear matrix element calculations for $0\nu2\beta$ decay is given in Table 7.5, where the numbers shown are half-lives for an

Table 7.5. Nuclear model calculations for $0\nu2\beta$ decays, assuming the Majorana neutrino mass $m_\nu = 1$ eV. Experimental lower limits are also quoted. The numbers are in units of 10^{24}yr.

Nuclei	HS84 [1116]	Tomoda91 [1119]	EVZ88 [1170]	Staudt90 [1172]	Simkovich97 [1175]	Engel89 [1171]	Caurier96 [1168, 1169]	Expt.
^{48}Ca	3.2						10.0	> 0.43
^{76}Ge	1.7	2.2	27-140	2.3	9.5	9.2	18.5	>16
^{82}Se	0.58	4.7	11-45	0.60		7.3	2.4	>0.027
^{100}Mo		0.26	1.9	1.27:	0.25			>0.052
^{116}Cd				0.49				
^{128}Te	3.9	9.8	25	7.8	8.8	18		
^{130}Te	0.16	0.54	1.3	0.49	0.47	1.1		>0.0325
^{136}Xe		1.4	6.3	2.2			12.1	>0.34
^{150}Nd		0.045		0.034				>0.0012

Table 7.6. Upper limits on the Majorana neutrino mass in eV units

Nuclei	HS84 [1116]	Tomoda91 [1119]	EVZ88 [1170]	Staudt90 [1172]	Simkovic97 [1175]	Caurier96 [1168, 1169]	Engel89 [1171]
^{48}Ca	2.7					8.4	
^{76}Ge	**0.33**	**0.37**	**1.3–3.0**	**0.38**	**0.77**	**1.1**	**0.9**
^{82}Se	4.6	0.61	20–40	4.7		9.4	16
^{100}Mo		2.2	6.0	4.9	2.2		
^{130}Te	2.2	4.1	6.3	3.9	3.8	5.8	
^{136}Xe		2.0	4.3	2.5		6.0	
^{150}Nd		6.1		5.3			

assumed Majorana neutrino mass of 1eV. The empirical lower limits on half-lives are given in the last column. Limits on the neutrino mass are presented in Table 7.6 using various nuclear calculations. The best limit on the Majorana neutrino mass comes from the ^{76}Ge result, $T_{1/2} > 1.6 \times 10^{25}$ yr (90% CL) [1129] (bold-faced numbers in Table 7.6). Most calculations yield a limit of

$$m_\nu < 0.3 - 0.8 \, \text{eV}, \tag{7.128}$$

but a large-space shell model calculation by Caurier et al. [1168] gives

$$m_\nu < 1.1 \, \text{eV}. \tag{7.129}$$

The limit derived using the matrix element by Engel et al. [1170] is even weaker by a factor up to 3. The limits on m_ν from other processes are weaker by a factor of 5–10. We take $m_\nu < 1$ eV as the current limit on the Majorana mass for $\tau > 1.6 \times 10^{25}$ yr.

In the presence of generation mixing, m_ν discussed above is not the Majorana mass of the electron neutrino alone but receives leakage contributions from other neutrinos, as $\pm m_{\nu_\mu} \sin^2\theta_{\nu_e\nu_\mu} \pm m_{\nu_\tau}\sin^2\theta_{\nu_e\nu_\tau}$. In this sense, the

effective mass inferred from double beta decays is often denoted as $\langle m_\nu \rangle$. See Sect.8.10.2 for more details concerning this point.

7.6.6 Several Remarks Concerning Double Beta Decay

(i) If 0ν beta decay is controlled by a heavy Majorana particle such that $M_\nu \gtrsim 1$ MeV, (7.107) should be modified (the neutrino mass cannot be factored out), and also the resulting limit on neutrino mass [1192]. For even heavier neutrinos, $m_\nu \gtrsim 1$ GeV, the effect of the nucleon size becomes important [1123]. For $m_\nu \to \infty$, $F(r)$ is calculated as [1116]

$$F(r) \sim \frac{1}{48} \frac{1}{r} \left(\frac{M_A}{m_\nu} \right)^2 e^{-M_A r} [(M_A r)^3 + 3(M_A r)^2 + 3(M_A r)] , \qquad (7.130)$$

rather than (7.105), where a dipole form factor $\sim 1/(1 - k_\nu^2/M_A^2)^2$ is assumed for the nucleon weak vertex.

(ii) In addition to the diagrams shown in Fig. 7.3 (two nucleon mechanism), there are other diagrams that cause double beta decay through isobar excitation in nuclei [1193] or through the exchange current (Fig. 7.6) [202]. It is shown, however, that isobar excitation does not contribute to $0^+ \to 0^+$ transition [1125] (see also [1115]), insofar as nucleon recoil is ignored [1119]. The exchange current effect is negligible $(< 1\%)$, unless $0\nu 2\beta$ decay is directly controlled by a heavy Majorana neutrino [1194].

(iii) In relation to two positron-emission double beta decay, we expect processes of capture of one or two atomic electrons [1195].

(iv) If right-handed symmetry exists at high energy, the contribution of the right-handed current is expected at low energies from the exchange of the right-handed weak boson W_R. In this case, 0ν double beta decay takes place even if $m_\nu = 0$ [1196]. The Feynman diagrams that give rise to $0\nu 2\beta$ decay
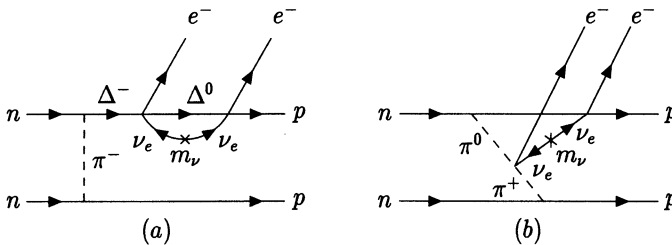
Fig. 7.6. (a) Neutrinoless double beta decay induced by the Δ (1232) excitation. (b) Neutrinoless double beta decay induced by the pion exchange current.
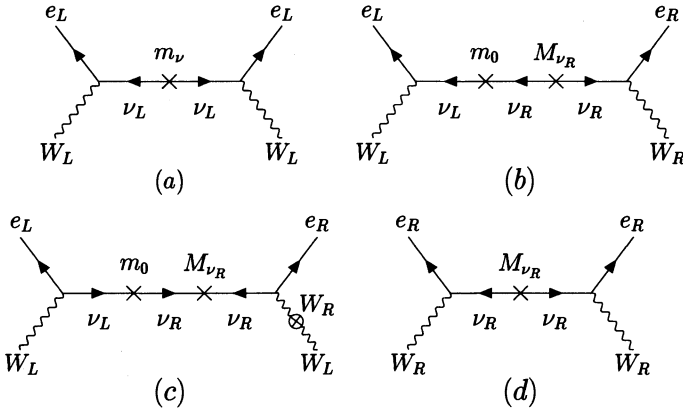
Fig. 7.7. Feynman diagrams leading to neutrinoless double beta decay in the presence of right-handed current. The nucleon part that couples to W bosons is omitted in the figure. (**a**) is the standard process, and (**b**)–(**d**) are those with right-handed current. See text for the explanation.

are depicted in Fig. 7.7. The corresponding amplitudes are

$$(\text{a}) \sim G_F^2 \frac{m_\nu}{k_\nu} \,, \tag{7.131}$$

$$(\text{b}) \sim G_F \frac{g^2}{m_{W_R}^2} \frac{m_D M_{\nu_R}}{M_{\nu_R}^2} \sim G_F^2 \gamma^2 \xi \,, \tag{7.132}$$

$$(\text{c}) \sim G_F^2 \frac{m_D M_{\nu_R}}{M_{\nu_R}^2} \sim G_F^2 \epsilon \xi \,, \tag{7.133}$$

$$(\text{d}) \sim \left(\frac{g^2}{m_{W_R}^2} \right)^2 \frac{f}{M_{\nu_R}} \sim G_F^2 \gamma^4 f / M_{\nu_R} \,, \tag{7.134}$$

where $\gamma \equiv m_{W_1}/m_{W_2} \simeq m_{W_L}/m_{W_R}$, ε is the W_R component in the mass eigenstate W_1, which is

$$W_1 = W_L + \varepsilon W_R \,,$$

$$W_2 = -\varepsilon W_L + W_R \,. \tag{7.135}$$

M_{ν_R} is the Majorana mass of ν_R, $\xi = m_D/M_{\nu_R}$, and $f \simeq 0.35\,\text{GeV}$ [1197] is an effective correction factor for the heavy neutrino exchange. (a) is the standard $0\nu2\beta$ process, but is added in Fig. 7.7 for completeness. Note that $\xi m_D = m_\nu$, and hence (b) and (c) vanish if $m_\nu = 0$. Namely, the constraint on the right-handed coupling is not independent of that on the neutrino mass. On the other hand, (d) does not vanish in the $m_\nu = 0$ limit. The processes involving the right-handed current are generally summarised

by the effective interaction,

$$H_{\text{eff}} = \frac{G_F \cos\theta_c}{\sqrt{2}} [J_L^{(\ell)\dagger} J_L^{(h)} + \eta_{LR} J_L^{(\ell)\dagger} J_R^{(h)} + \eta_{RL} J_R^{(\ell)\dagger} J_L^{(h)} + \eta_{RR} J_R^{(\ell)\dagger} J_R^{(h)}],$$

$$(7.136)$$

where η_{LR}, η_{RL}, and η_{RR} are given by amplitudes (b)–(d) of (7.132)–(7.134) if we use the left–right symmetric model. The corresponding formula for the double beta decay rate was first given in [1114] and in a modern notation using (7.136) in [1198]. The interference term from the left- and right-handed currents gives rise to $0^+ \rightarrow 2^+$ and $0^+ \rightarrow 1^+$ $0\nu2\beta$ decays, together with $0^+ \rightarrow 0^+$ decays; the spin changing processes will thus be a unique signature for the presence of right-handed current [1198]. The present limits are $\eta_{LR} < 0.2 - 2 \times 10^{-7}$ and $\eta_{RR} < 2 \times 10^{-6}$. The combined limits on m_{W_R} and m_ν are discussed in [1199].

(v) $0\nu2\beta$ emission may take place with the association of majoron emission (triplet-singlet majoron [1200]; see Sect. 6.8). The matrix element is basically the same as that for $0\nu2\beta$ emission, but the phase space is integrated over three bodies, which makes the electron spectrum continuous with the peak of the spectrum higher than that for $2\nu2\beta$ decay.

(vi) $0\nu2\beta$ processes induced by SUSY particle exchanges are occasionally discussed in the literature [1201]. Such processes, however, occur only when R parity is broken, which usually induces a number of unwanted effects (fast proton decay, etc.).

8 Generation Mixing of Neutrinos

8.1 Generation Mixing – the Case of Dirac Neutrinos

Let us generalise the mass term (6.34) so as to incorporate generation,

$$\mathcal{L}_{\text{mass}} = -\bar{\nu}_R^\alpha m_{\alpha\beta} \nu_L^\beta + \text{h.c.} , \tag{8.1}$$

where $\nu^\alpha = (\nu^e, \nu^\mu, \nu^\tau)$ are the eigenstates of the weak interaction specified by

$$\mathcal{L}_{\text{int}} = \frac{g}{\sqrt{2}} W_\mu^+ \left(\bar{\nu}_L^e \gamma^\mu e_L + \bar{\nu}_L^\mu \gamma^\mu \mu_L + \bar{\nu}_L^\tau \gamma^\mu \tau_L \right) + \text{h.c.} \tag{8.2}$$

Taking a basis in which the charged lepton mass term is diagonal, we further diagonalise the neutrino mass term by

$$\nu_L^\alpha = U_{\alpha i} \nu_L^{'i}, \tag{8.3}$$

$$\nu_R^\alpha = V_{\alpha i} \nu_R^{'i} , \tag{8.4}$$

i.e.,

$$\mathcal{L}_{\text{mass}} = -\bar{\nu}_R^{'i} V_{i\alpha}^\dagger m_{\alpha\beta} U_{\beta j} \nu_L^{'j} + \text{h.c.}$$
$$= -\bar{\nu}_R^{'i} m_i \nu_L^{'i} + \text{h.c.}, \tag{8.5}$$

so,

$$V^\dagger m U = m_{\text{diag}} . \tag{8.6}$$

Here, without loss of generality, we choose the phases of $\nu_{L,R}^{'i}$ so that m_i is real and semipositive definite. Using the basis of the mass eigenstate $\nu^{'i}$ of (8.3), we rewrite the interaction Lagrangian (8.2) as

$$\mathcal{L}_{\text{int}} = \frac{g}{\sqrt{2}} W_\mu^+ (\bar{\nu}^{'1}, \bar{\nu}^{'2}, \bar{\nu}^{'3})_L U^\dagger \gamma_\mu \begin{pmatrix} e \\ \mu \\ \tau \end{pmatrix}_L + \text{h.c.} , \tag{8.7}$$

where $U^\dagger$ is the 'CKM matrix' for leptons, which we refer to the lepton mixing matrix [121, 122].[1] We note that neutrinos which appear most often

---

[1] Katayama et al. [121] considered maximal mixing between the two neutrinos. A general 2×2 matrix is considered by Maki et al. [122]

in laboratory experiments are the eigenstate of the weak interaction, ν^α. The mass eigenstate of the neutrinos ν'^i appears only in a neutrino mass experiment. (This is in contrast to quarks, for which we usually deal with the mass eigenstate.)

If neutrinos have finite masses, the lepton numbers (e-, μ- number, etc.) are not conserved separately within the standard electroweak theory, unless the off-diagonal elements of the mass matrix vanish. The effect of the lepton-number violation caused by generation mixing, however, is greatly suppressed in the charged lepton sector, because such amplitudes should necessarily involve a small neutrino mass. For instance, $l_\alpha \to l_\beta \gamma$ is given by [1202]

$$\Gamma(l_\alpha \to l_\beta \gamma) = \frac{1}{2}\alpha G_F^2 \left(\frac{1}{32\pi^2}\right)^2 m_{l_\alpha}^5 \left|\sum_i U_{\alpha i}^* U_{\beta i} \frac{m_{\nu_i}^2}{M_W^2}\right|^2 . \tag{8.8}$$

The branching ratio is thus

$$B(l_\alpha \to l_\beta \gamma) = (3\alpha/32\pi) \left|\sum_i U_{\alpha i}^* U_{\beta i} (m_{\nu_i}^2/M_W^2)\right|^2 \lesssim 2 \times 10^{-46}, \tag{8.9}$$

with the upper-limit value of the ν_τ mass $m_{\nu_e} = 2.5\,\mathrm{eV}$ in (5.42) The experimental limit is far too large:

$$B(\mu \to e\gamma) < 1.2 \times 10^{-11} ,$$
$$B(\tau \to e\gamma) < 2.7 \times 10^{-6} ,$$
$$B(\tau \to \mu\gamma) < 1.1 \times 10^{-6} . \tag{8.10}$$

We expect similar suppression for $\mu \to ee\bar{e}$ [1202]:

$$B(\mu \to ee\bar{e}) = \frac{3\alpha^2}{16\pi^2} \left|\sum_i U_{\mu i}^* U_{ei} \frac{m_{\nu_i}^2}{M_W^2} \ln \frac{m_{\nu_i}^2}{M_W^2}\right|^2 \lesssim 2 \times 10^{-45} , \tag{8.11}$$

which is compared with experiment,

$$B(\mu \to ee\bar{e}) < 1.0 \times 10^{-12} . \tag{8.12}$$

The laboratory limits on flavour-changing leptonic decays do not give any constraints on lepton-number violation arising from generation mixing.

In the presence of generation mixing, a heavier neutrino may also decay into a light one by emitting a photon or two light neutrinos. The lifetime of radiative decay in the standard model is estimated as (see Chap. 10)

$$\tau(\nu_i \to \nu_j + \gamma) > 2 \times 10^{34} \mathrm{\ yr} \left(\frac{m_{\nu_i}}{2.5\mathrm{\ eV}}\right)^{-5} . \tag{8.13}$$

Three-neutrino decays are even slower. Thus, all neutrinos are practically stable.

8.2 Generation Mixing – the Case of Majorana Neutrinos

The mass term for Majorana neutrinos is written

$$\mathcal{L}_{\text{mass}} = -\frac{1}{2}\nu_L^{\alpha T}C^{-1}m_{\alpha\beta}\nu_L^\beta + \text{h.c.} \tag{8.14}$$

Taking again the basis in which the charged lepton-mass term is diagonal, we diagonalise this mass term by

$$\nu_L^\alpha = U_{\alpha i}\nu_L^{\prime i}, \tag{8.15}$$

so that

$$\begin{aligned}\mathcal{L}_{\text{mass}} &= -\frac{1}{2}\nu_L^{\prime i}C^{-1}U_{i\alpha}m_{\alpha\beta}U_{\beta j}\nu_L^{\prime j} + \text{h.c.}\\ &= -\frac{1}{2}\nu_L^{\prime i}C^{-1}m_i\nu_L^{\prime i} + \text{h.c.},\end{aligned} \tag{8.16}$$

i.e.,

$$U^T m U = m_{\text{diag}} , \tag{8.17}$$

or

$$m = U^* m_{\text{diag}} U^\dagger . \tag{8.18}$$

If the elements of the mass matrix (8.14) are real, $\mathcal{L}_{\text{mass}}$ is CP invariant, and the Majorana neutrinos can be classified by the CP property. This was first pointed out by Yang and Tiomno (1950) [1203] and rediscovered by Wolfenstein [1098]. The unitary matrix U of (8.15) becomes an orthogonal matrix O, and (8.17) reads

$$O_{k\alpha}^T m_{\alpha\beta} O_{\beta\ell} = \eta_k m_k \delta_{k\ell}, \tag{8.19}$$

where m_k is real positive and $\eta_k = +1$ or -1. Defining a Majorana field by

$$\chi_k = \sum_\alpha O_{k\alpha}\nu_L^\alpha + \eta_k O_{k\alpha}(\nu_L^\alpha)^c \tag{8.20}$$

with $\overline{(\nu_L^\alpha)^c} = \nu_L^{\alpha T}C^{-1}$, we can write

$$\mathcal{L}_{\text{mass}} = \sum m_k \overline{\chi_k}\chi_k . \tag{8.21}$$

This χ_k is nominally the eigenstate of C because

$$C\chi_k C^{-1} = \eta_k \chi_k . \tag{8.22}$$

As the neutrino interaction does not respect charge-conjugation invariance, however, the eigenstate of C is not physically a useful concept. Now let us

discuss the relation between χ_k and the CP eigenstate. Under parity transformation,

$$P\chi_k P^{-1} = \xi_P \gamma^0 \chi_k \ . \tag{8.23}$$

Then,

$$(CP)\chi_k(CP)^{-1} = \xi_P \eta_k \gamma^0 \chi_k \ . \tag{8.24}$$

We take $\xi_P = +1$ by convention. χ_k is not an eigenstate of CP, but the relative sign of η_k is still meaningful because the interaction Lagrangian is invariant under CP transformation.

For example, consider a tensor-type transition between two Majorana neutrinos χ_1 and χ_2 (see Sect. 6.5 for details). If $\eta_1/\eta_2 = +1$, only the term $\bar{\chi}_1 \gamma_5 \sigma_{\mu\nu} \chi_2$ is allowed. If $\eta_1/\eta_2 = -1$, the allowed term is $\bar{\chi}_1 \sigma_{\mu\nu} \chi_2$ instead. The two terms coexist if CP is violated [1204].

Pseudo-Dirac neutrinos. If the Majorana mass matrix m_{ij} takes the form

$$m_{ij} = \begin{pmatrix} 0 & * \\ * & 0 \end{pmatrix}, \tag{8.25}$$

there are two neutrinos with $\eta = +1$ and $\eta = -1$ that are degenerate in mass. The relative lepton number of ν_1 and ν_2 is conserved, and thus, the set of (ν_1, ν_2) is called a pseudo-Dirac neutrino [1098] (see also the argument at the end of Sect. 6.5).

8.3 Phases of Mixing Matrices

The 3×3 mixing matrix U in (8.3) can be represented by

$$U = e^{i\alpha} e^{i\beta\lambda_3} e^{i\gamma\lambda_8} u e^{i\beta'\lambda_3} e^{i\gamma'\lambda_8}, \tag{8.26}$$

where λ_3 and λ_8 are Gell-Mann's λ matrices for the SU(3) group and u stands for the conventional Kobayashi–Maskawa (KM) representation of a 3×3 matrix with four parameters. For the case of Dirac neutrinos the phases β' and γ' are absorbed into phase rotation of the wave function of ν', which is always multiplied on U from the right [see (8.3)]. Then,

$$U = e^{i\alpha} e^{i\beta\lambda_3} e^{i\gamma\lambda_8} u \ . \tag{8.27}$$

The interaction Lagrangian (8.7) is written

$$\mathcal{L}_{\text{int}} = \frac{g}{\sqrt{2}} W_\mu^\dagger (\bar{\nu}'^1 \bar{\nu}'^2 \bar{\nu}'^3) u^\dagger e^{-i\gamma\lambda_8} e^{-i\beta\lambda_3} e^{-i\alpha} \gamma_\mu \begin{pmatrix} e \\ \mu \\ \tau \end{pmatrix} . \tag{8.28}$$

The three phases α, β, γ are now absorbed into the phases of the charged leptons, and we are left with

$$\mathcal{L}_{\text{int}} = \frac{g}{\sqrt{2}} W_\mu^\dagger \bar{\nu}' u^\dagger \gamma_\mu \ell + \text{h.c.}, \tag{8.29}$$

where $\ell = (e, \mu, \tau)^T$. Only the phases of a matrix which cannot be factored out as in (8.26) are physical and would give rise to CP violation. For n flavours, the number of such physical phases is easily calculated as

$$n^2 - \frac{n(n-1)}{2} - (n-1) - n = \frac{(n-1)(n-2)}{2} \tag{8.30}$$

for an $n \times n$ matrix. The last two terms on the left-hand side correspond to phases which we factored out and hence absorbed into the wave function.

For the Majorana neutrino, the two phases β' and γ' cannot be absorbed into the wave function of ν' because the mass term takes the form $\nu'^T U^T m U \nu'$, where the same U appears twice, rather than $V^\dagger$ and U for the Dirac case. The other three phases α, β, and γ are absorbed into the charged-lepton wave function, as in (8.28), in the weak-interaction Lagrangian. Therefore, we are left with

$$\mathcal{L}_{\text{int}} = \frac{g}{\sqrt{2}} W_\mu^\dagger \bar{\nu}_L' e^{-i\beta'\lambda_3} e^{-i\gamma'\lambda_8} u^\dagger \gamma_\mu \ell + \text{h.c.} \tag{8.31}$$

instead of (8.29). The number of physical phases for n generation is

$$n^2 - \frac{n(n-1)}{2} - n = \frac{n(n-1)}{2} , \tag{8.32}$$

i.e., we may see effects of CP violation even for $n = 2$ for Majorana neutrinos [1205–1207].

If one absorbs the phase in (8.31) into the neutrino wave function as $\nu_L'' = e^{i\gamma'\lambda_8} e^{i\beta'\lambda_3} \nu_L'$, the phase appears in the mass matrix,

$$\mathcal{L}_{\text{mass}} = -\frac{1}{2} \overline{\nu_L''^c} e^{-i\gamma'\lambda_8} e^{-i\beta'\lambda_3} m_{\text{diag}} e^{-i\beta'\lambda_3} e^{-i\gamma'\lambda_8} \nu_L'' . \tag{8.33}$$

This means that the effect of CP violation arising from this extra Majorana phase always appears together with the neutrino mass, and hence the effect is suppressed by $(m_\nu/E)^2$ [1208] with E the energy of the neutrino.

Let us exemplify the above argument more explicitly for $n = 2$. The neutrino mass term,

$$\mathcal{L}_{\nu\,\text{mass}} = \bar{\nu}_L^c \begin{pmatrix} m_{11} & m_{12} \\ m_{21} & m_{22} \end{pmatrix} \nu_L + \text{h.c.} , \tag{8.34}$$

has six parameters $(m_{12} = m_{21})$. We may write (8.26) as

$$U = e^{i\alpha} e^{i\beta\tau_3} \begin{pmatrix} \cos\theta & \sin\theta \\ -\sin\theta & \cos\theta \end{pmatrix} e^{i\beta'\tau_3}. \tag{8.35}$$

The diagonalisation of the mass matrix is now

$$U^* \begin{pmatrix} m_1 & \\ & m_2 \end{pmatrix} U^\dagger = \begin{pmatrix} m_{11} & m_{12} \\ m_{21} & m_{22} \end{pmatrix}, \tag{8.36}$$

corresponding to (8.15)–(8.18). We note that $m_1, m_2, \alpha, \beta, \theta, \beta'$ are determined by the six parameters of m_{ij}. With (8.35), (8.36) reads

$$e^{-2i\alpha} e^{-i\beta\tau_3} \begin{pmatrix} \cos\theta & \sin\theta \\ -\sin\theta & \cos\theta \end{pmatrix} \begin{pmatrix} m_1 e^{-2i\beta'} & 0 \\ 0 & m_2 e^{2i\beta'} \end{pmatrix} \begin{pmatrix} \cos\theta & -\sin\theta \\ \sin\theta & \cos\theta \end{pmatrix} e^{-i\beta\tau_3}$$

$$= \begin{pmatrix} m_{11} & m_{12} \\ m_{21} & m_{22} \end{pmatrix}. \tag{8.37}$$

The weak current is now

$$\begin{aligned} J_\mu &= \bar\ell_L \gamma_\mu \nu_L \\ &= \bar\ell_L \gamma_\mu U \nu'_L \\ &= \bar\ell_L \gamma_\mu e^{i\alpha} e^{i\beta\tau_3} \begin{pmatrix} \cos\theta & \sin\theta \\ -\sin\theta & \cos\theta \end{pmatrix} e^{i\beta'\tau_3} \nu'_L. \end{aligned} \tag{8.38}$$

The two phases α and β are absorbed into the phase of $\bar\ell_L$ upon the redefinition

$$\bar\ell'_L = \bar\ell_L e^{i\alpha} e^{i\beta\tau_3}. \tag{8.39}$$

On the other hand, β' cannot be absorbed into the phase of ν'_L, and remains physical. If we define

$$\nu''_L = e^{i\beta'\tau_3} \nu'_L, \tag{8.40}$$

then,

$$\mathcal{L}_{\nu\ \text{mass}} = \overline{\nu''_L} \begin{pmatrix} m_1\ e^{-2i\beta'} & \\ & m_2\ e^{2i\beta'} \end{pmatrix} \nu''_L. \tag{8.41}$$

The phase β' generally causes CP violation.

There are a few special cases in which CP is not violated. If $\beta' = 0$ or $\beta' = \pi/2$, the mass terms are real, and CP is conserved. In this case, the relative CP, as discussed in (8.24), is $+1$. The other case is $\beta' = \pi/4$, for which

$$\begin{pmatrix} m_1\ e^{-2i\alpha - \frac{\pi}{2}i} & 0 \\ 0 & m_2\ e^{-2i\alpha + \frac{\pi}{2}i} \end{pmatrix} = \begin{pmatrix} -m_1 & 0 \\ 0 & m_2 \end{pmatrix}, \tag{8.42}$$

using the freedom to choose α. This corresponds to a relative CP of -1.

The pseudo-Dirac neutrino (8.25) is written

$$U^\dagger m U = U^\dagger \begin{pmatrix} 0 & m_{12} \\ m_{21} & 0 \end{pmatrix} U = \begin{pmatrix} -m_1 & 0 \\ 0 & m_1 \end{pmatrix}, \tag{8.43}$$

which is a special case of $\beta' = \pi/4$.

8.4 Neutrino Oscillation in Vacuum

8.4.1 Formulation

In the presence of off-diagonal components of the neutrino mass matrix, a neutrino of the weak interaction eigenstate may change into another kind while propagating through vacuum [122, 205]. A neutrino of the generation α, after a time interval of t, is given by

$$|\nu^\alpha\rangle_t = \sum_i U_{\alpha i} e^{-iE_i t} |\nu'^i\rangle , \tag{8.44}$$

and the transition amplitude to the state $|\nu^\beta\rangle$ is

$$\langle \nu^\beta | \nu^\alpha \rangle_t = \sum U_{\alpha i} (U^\dagger)_{i\beta} e^{-iE_i t}. \tag{8.45}$$

For $p = |\mathbf{p}| \gg m_i$, we expand $E_i = \sqrt{p^2 + m_i^2} \simeq p + m_i^2/2p \simeq p + m_i^2/2E$. Using (8.3) we write (8.44) as

$$|\nu^\alpha\rangle_t \simeq e^{-ipt} U \begin{bmatrix} e^{-im_1^2 t/2E} & & \\ & e^{-im_2^2 t/2E} & \\ & & \ddots \end{bmatrix} U^\dagger |\nu^\beta\rangle$$

$$= e^{-ipt} U \begin{bmatrix} 1 - i\frac{m_1^2}{2E}t + \cdots & & \\ & 1 - i\frac{m_2^2}{2E} + \cdots & \\ & & \ddots \end{bmatrix} U^\dagger |\nu^\beta\rangle . \tag{8.46}$$

Since

$$U^\dagger m^\dagger m U = m_{\text{diag}}^2 = \begin{pmatrix} m_1^2 & & 0 \\ & m_2^2 & \\ 0 & & \ddots \end{pmatrix}, \tag{8.47}$$

we may write

$$|\nu^\alpha\rangle_t \simeq e^{-ipt} [e^{-i\frac{m^\dagger m}{2E}t}]_{\alpha\beta} |\nu^\beta\rangle, \tag{8.48}$$

i.e., $|\nu^\alpha\rangle_t$ is a solution of the Schrödinger equation,

$$i\frac{d}{dt}|\nu^\alpha\rangle_t \simeq \frac{m^\dagger m}{2E}|\nu^\alpha\rangle , \tag{8.49}$$

up to the phase factor e^{-ipt}.

If we restrict ourselves to mixing between the two generations, we can generally parametrise U as

$$U = \begin{pmatrix} e^{i\alpha} & \\ & e^{-i\alpha} \end{pmatrix} \begin{pmatrix} \cos\theta & \sin\theta \\ -\sin\theta & \cos\theta \end{pmatrix} \begin{pmatrix} e^{i\beta} & \\ & e^{-i\beta} \end{pmatrix} , \tag{8.50}$$

where the phase factor $e^{i\tau_3\beta}$ does not appear in $\langle\nu^\beta|\nu^\alpha\rangle_t$ and $e^{i\tau_3\alpha}$ can be absorbed into the wave functions of $|\nu^\alpha\rangle_t$. We may then take

$$U = \begin{pmatrix} \cos\theta & \sin\theta \\ -\sin\theta & \cos\theta \end{pmatrix} \tag{8.51}$$

without loss of generality. The situation does not differ between the Dirac and the Majorana cases because the mass matrix related to neutrino oscillation is always $m^\dagger m = Um_{\text{diag}}^2 U^\dagger$ [1209], as in (8.47), and not $m^T m$. With (8.51),

$$m^\dagger m = Um_{\text{diag}}^2 U^\dagger = \begin{bmatrix} m_1^2\cos^2\theta + m_2^2\sin^2\theta & \frac{1}{2}(m_2^2 - m_1^2)\sin 2\theta \\ \frac{1}{2}(m_2^2 - m_1^2)\sin 2\theta & m_1^2\sin^2\theta + m_2^2\cos^2\theta \end{bmatrix}$$

$$= \frac{m_1^2 + m_2^2}{2} + \frac{\Delta m^2}{2}\begin{pmatrix} -\cos 2\theta & \sin 2\theta \\ \sin 2\theta & \cos 2\theta \end{pmatrix} , \tag{8.52}$$

where $\Delta m^2 = m_2^2 - m_1^2$. Hence, (8.48) becomes

$$|\nu^\alpha\rangle_t = e^{-i(p+\frac{m_1^2+m_2^2}{4E})t}\left[e^{-i\frac{\Delta m^2}{4E}\tau^a r^a\, t}\right]_{\alpha\beta}|\nu^\beta\rangle \tag{8.53}$$

with $r^a = (\sin 2\theta, 0, -\cos 2\theta)$, so that

$$|\nu^\alpha\rangle_t = \begin{pmatrix} \cos\frac{\Delta m^2}{4E}t - i\sin\frac{\Delta m^2}{4E}t\cos 2\theta & -i\sin\frac{\Delta m^2}{4E}t\sin 2\theta \\ -i\sin\frac{\Delta m^2}{4E}t\sin 2\theta & \cos\frac{\Delta m^2}{4E}t + i\sin\frac{\Delta m^2}{4E}t\cos 2\theta \end{pmatrix}|\nu^\beta\rangle , \tag{8.54}$$

omitting the unimportant common phase factors. The transition from $|\nu^e\rangle = (1,0)^T$ to $|\nu^e\rangle_t$ is then

$$\langle\nu^e|\nu^e\rangle_t = \cos\frac{\Delta m^2}{4E}t - i\sin\frac{\Delta m^2}{4E}t\cos 2\theta , \tag{8.55}$$

and its transition probability reads

$$P_{\nu_e \to \nu_e} = |\langle\nu^e|\nu^e\rangle_t|^2$$

$$= 1 - \sin^2 2\theta \sin^2\frac{\Delta m^2}{4E}t. \tag{8.56}$$

This shows oscillation of the neutrino beam propagating through a vacuum as formulated by Gribov and Pontecorvo [205]. For $\nu_e \to \nu_\mu, \nu_\mu = (0,1)^T$, and we have

$$P_{\nu_e \to \nu_\mu} = |\langle \nu^\mu | \nu^e \rangle|^2$$

$$= \sin^2 2\theta \sin^2 \frac{\Delta m^2}{4E} t, \tag{8.57}$$

and the same expression also for $\nu_\mu \to \nu_e, \bar{\nu}_e \to \bar{\nu}_\mu, \bar{\nu}_\mu \to \bar{\nu}_e$. We call l_0, which satisfies

$$\frac{\Delta m^2}{4E}(\ell_0/c) = \pi \tag{8.58}$$

($c = 1$, light velocity), the oscillation length. If we observe the neutrino flux at a distance $L(= ct)$ from the source, we find from (8.56),

$$P_{\nu_e \to \nu_e} = 1 - \sin^2 2\theta \sin^2 \left(\pi \frac{L}{\ell_0} \right) . \tag{8.59}$$

For $L \gg \ell_0$ or

$$\Delta m^2 \gg 4\pi E/L = \Delta m^2_{\min}, \tag{8.60}$$

the second sine factor oscillates rapidly, so that

$$P_{\nu_e \to \nu_e} = 1 - \frac{1}{2} \sin^2 2\theta, \tag{8.61}$$

which stands for a reduction of the ν_e flux averaged over a sufficiently long time. (In practice, this averaging is caused by the momentum spread of the neutrino beam.) This is often called 'time-averaged oscillation,' but it does not represent an actual oscillation phenomenon any longer; P measures merely neutrino mixing (see the next subsection). When (8.60) is satisfied, we generally expect that

$$P_{\nu_e \to \nu_e} \geq 1/2. \tag{8.62}$$

For N generations, (8.56) is modified to

$$P_{\nu_e \to \nu_e} = 1 - \sum_{i,j} 4 \, | \, U_{ei} \, |^2 | \, U_{ej} \, |^2 \sin^2 \frac{\Delta m^2_{ij}}{4E} t, \tag{8.63}$$

and then

$$P_{\nu_e \to \nu_e} \geq 1/N, \tag{8.64}$$

when $\Delta m^2_{ij} \gg 4\pi E/\ell_0$ for all (i,j) pairs.

We emphasize again that the same argument applies to both Dirac [1210] and Majorana [205] neutrinos; hence, the experiment does not distinguish between the two cases.

8.4.2 Neutrino Oscillation and the Uncertainty Principle

If the energy and the momentum of neutrino are measured sufficiently accurately so that the error δm_ν of $m_\nu = \sqrt{E_\nu^2 - p_\nu^2}$ is smaller than the mass difference of two neutrinos, the transition into the other neutrino state cannot take place. This means that neutrino oscillation disappears if both π and μ momenta are measured with extreme precision in a neutrino oscillation experiment using $\pi \to \mu\nu$ decays. Although this statement sounds paradoxical in view of what we have argued, this "puzzle" is resolved if one considers the uncertainty principle of quantum mechanics. In fact, if the momentum is measured with extreme precision, the information concerning the position, as to where neutrinos are produced, will be lost.

To keep the error of $m_\nu^2 (= \delta m^2)$ smaller than Δm^2, one must measure p_ν with a precision of δp_ν that satisfies

$$\Delta m^2 \gg \delta m^2 = (\partial m_\nu^2 / \partial p_\nu) \delta p_\nu = 2 p_\nu \delta p_\nu. \qquad (8.65)$$

This means that the position becomes undetermined to the order of $\delta x \delta p_\nu > \hbar$ (we take $\hbar = 1$), i.e.,

$$\delta x > \frac{2 p_\nu}{\Delta m^2} = \frac{1}{2\pi} \ell_0. \qquad (8.66)$$

The positional precision is lost, at least to the order of the oscillation length, and the oscillation pattern is erased by this uncertainty. The result then reduces to time-averaged oscillation (8.61), where the deviation of $P_{\nu_e \to \nu_e}$ from unity is a consequence of the fact that either of the mass eigenstates chosen by the observation is the sum of the two weak eigenstates, i.e.,

$$P_{\nu_e \to \nu_e} = \cos^4 \theta + \sin^4 \theta, \qquad (8.67)$$

where the first term is a contribution from virtual intermediate state ν_1, the second is that from ν_2, and they are added incoherently. The probability (8.67), of course, agrees with (8.61).

A similar effect is seen in the following situation: if the neutrino beam is localised at the origin, the neutrino clouds corresponding to the two different mass eigenstates move with different velocities and will be separated by an amount of $(\Delta v)ct \approx (\Delta m^2 / E^2)ct$ after time t. If this separation is larger than the neutrino coherence length, the two clouds no longer overlap, and hence do not interfere. This means that neutrino oscillation eventually disappears and that $P_{\nu_e \to \nu_e}$ reduces to (8.61) [1211]. The condition for oscillation can also be obtained by applying the uncertainty principle.

This situation is clearly understood in the formulation using the wave packet [1212, 1213], from which quantum mechanical conditions for the interference of neutrino waves are derived. In practical applications, however, the momentum spread of the neutrino beam is much larger than that prescribed by the quantum mechanical limit. So the condition amounts to whether

such a spread destroys the interference of neutrino waves. In this situation, a formalism using decomposition into energy eigenstates, as proposed in [1214, 1215], suffices. In what follows, we present two formulations and clarify their relation.

Wave-packet formalism for neutrino oscillation. We write a normalised wave packet for the mass eigenstate as [1212, 1213]

$$\psi_i(x,t) = \frac{1}{\sqrt{2\pi}\sigma_x} \exp\left[i\left(\overline{p_i}x - \overline{E_i}t\right) - \frac{(x - v_it)^2}{4\sigma_x^2} \right], \qquad (8.68)$$

where $\overline{p_i}$ is the mean momentum, $\overline{E_i} = \sqrt{\overline{p_i}^2 + m_i^2}$, v_i is the group velocity $v_i = \partial\overline{E_i}/\partial\overline{p_i} = \overline{p_i}/\overline{E_i}$, and σ_x is the Gaussian width in coordinate space. In momentum space, (8.68) is written

$$\psi_i(p) = \frac{1}{\sqrt{2\pi}\sigma_p} \exp\left[-\frac{(p - \overline{p_i})^2}{4\sigma_p^2} \right], \qquad (8.69)$$

where σ_p satisfies

$$\sigma_x\sigma_p = 1/2. \qquad (8.70)$$

Let us consider the two-neutrino case and a neutrino of flavour α created at $x = t = 0$ in the weak interaction process. The probability of finding a neutrino of flavour β at x and t is given by

$$P_{\alpha\to\beta}(x,t) = \left| \sum_i U_{\beta i}^*\psi_i(x,t)U_{\alpha i} \right|^2. \qquad (8.71)$$

Using (8.35) for U, we obtain for $\alpha = \nu_e$, $\beta = \nu_\mu$,

$$
\begin{aligned}
P_{\nu_e\to\nu_\mu} &= \frac{1}{2\pi} \frac{1}{\sigma_x^2} \sum_{i,j} U_{\mu i}^* U_{ei} U_{\mu j} U_{ej}^* \ \exp[i(\overline{p_i} - \overline{p_j})x - i(\overline{E_i} - \overline{E_j})t] \\
&\quad \times \exp\left[-\frac{(x - v_it)^2}{4\sigma_x^2} - \frac{(x - v_jt)^2}{4\sigma_x^2} \right] \\
&= \frac{1}{2\pi\sigma_x^2} 2\sin^2\theta\cos^2\theta\{1 - \cos[(\overline{p_i} - \overline{p_j})x - (\overline{E_i} - \overline{E_j})t]\} \\
&\quad \times \exp\left[-\frac{(x - v_it)^2}{4\sigma_x^2} - \frac{(x - v_jt)^2}{4\sigma_x^2} \right].
\end{aligned}
\qquad (8.72)
$$

Integrating over t, taking the relativistic limit, and using (8.70), (8.72) becomes

$$
\begin{aligned}
P_{\nu_e\to\nu_\mu} &= 2\sin^2\theta\cos^2\theta\left\{ 1 - \cos\left(\frac{\Delta m^2}{2\overline{p}}x\right) \right. \\
&\quad \left. \times \exp\left[-\frac{x^2}{8\sigma_x^2}\left(\frac{\Delta m^2}{2\overline{p}^2}\right)^2 - (1 + \kappa)\frac{(\Delta m^2)^2}{32\sigma_p^2\overline{p}^2} \right] \right\},
\end{aligned}
\qquad (8.73)
$$

where

$$\kappa = \frac{\overline{p_1}^2 - \overline{p_2}^2}{\Delta m^2}. \tag{8.74}$$

The second factor in the exponential ensures energy conservation within the uncertainty of σ_p [1216]. When the exponential factor is close to unity, we recover neutrino oscillation as given in (8.57),

$$P_{\nu_e \to \nu_\mu}(x) \simeq \frac{1}{2} \sin^2 2\theta \left[1 - \cos\left(\frac{\Delta m^2}{2\overline{p}} x\right) \right] = \sin^2 2\theta \sin^2\left(\frac{\Delta m^2}{4E} t\right). \tag{8.75}$$

For this to happen, we need two conditions:

$$\sigma_p \gg \Delta m^2/\overline{p}, \tag{8.76}$$

and

$$\frac{x^2}{8\sigma_x^2} \left(\frac{\Delta m^2}{2\overline{p}^2}\right)^2 \ll 1. \tag{8.77}$$

The first condition is that the momentum should not be determined too precisely, so that it allows the transition to a different mass state [see (8.65)]. The second condition reads

$$x \ll \frac{\sigma_x}{\Delta m^2/2\overline{p}^2} \simeq \frac{\sigma_x}{|v_1 - v_2|}, \tag{8.78}$$

which means that the wave packets corresponding to the two mass states are not separated by more than the packet size. Using (8.70) the condition is also written

$$\frac{\sigma_p}{\overline{p}} \ll 2\sqrt{2} \frac{\overline{p}}{x \Delta m^2}, \tag{8.79}$$

or

$$\frac{\delta E}{\overline{E}} \ll \frac{\ell_0}{x}, \tag{8.80}$$

where ℓ_0 is given by (8.58), dropping an unimportant $O(1)$ quantity.

In practice, the energy spread δE of the neutrino beam is much larger than that prescribed by the quantum mechanical condition, but we still need to satisfy (8.80) so that the interference is not destroyed. Namely, the quantum mechanical condition of (8.76) is trivially satisfied with a large allowance factor, and what practically matters is only (8.80).

When either of the two conditions, (8.76) and (8.80), is not satisfied, the exponential function gives a damping factor in (8.73), and we obtain

$$P_{\nu_e \to \nu_\mu} = 2 \sin^2 \theta \cos^2 \theta, \tag{8.81}$$

in agreement with the formula for time-averaged oscillation (8.67), the incoherent sum of $\nu_e \to \nu_1' \to \nu_\mu$ and $\nu_e \to \nu_2' \to \nu_\mu$.

The formalism using energy eigenstates. The neutrinos emitted from a source may take a wave function with a complicated wave packet that depends on the detailed dynamics of the neutrino production process. Particularly unclear is the question of the decoherence length of neutrino waves (the size of the wave packet in coordinate space). In a realistic case where an oscillation experiment is carried out, the size of the source is small compared with the oscillation length and the distance to the detector; neutrinos are emitted *continuously* from an approximate point source. With this stationary condition, one can circumvent the problem concerning the form of the wave packet and the decoherence length.

The neutrino beam which is stationarily produced from a point source is expanded in energy eigenstates as [1214]

$$|\nu_\alpha(x, t)\rangle = \int g(E)dE e^{-iEt} \sum_{j=1}^{3} U_{\alpha j} e^{ip_j x} |\nu_j\rangle, \tag{8.82}$$

where $|\nu_j\rangle$ denote the mass eigenstates. The spectral function $g(E)$ is determined by the production process.

We assume that the neutrino just produced ($x = 0$) is in a pure weak interaction eigenstate at any time and suppose that it is ν_e. The wave function at $x = 0$ is subject to the constraint [1215]

$$\sum_{j=1}^{3} U_{ej}\langle\nu_\mu|\nu_j\rangle = \sum_{j=1}^{3} U_{ej}\langle\nu_\tau|\nu_j\rangle = 0. \tag{8.83}$$

The wave function $|\nu_\alpha(0, t)\rangle$ describes a pure ν_e state at $x = 0$ for each individual energy component. The momentum p_j is determined by the energy E and the neutrino mass m_j.

The propagation of the energy eigenstates in free space is completely determined by classical trajectories. Flavour mixing at the detector is given by (8.82) with the detector coordinate x. For two-neutrino oscillation, the relative phase of the neutrino wave functions of ν_1 and ν_2 at distance x is

$$\delta\phi(x) = (p_1 - p_2)x = \frac{\Delta m^2}{2p}x. \tag{8.84}$$

$\delta\phi(x)$ is common to all energy eigenstates, and it coincides with the phase difference obtained in the previous section. This justifies the analysis of neutrino oscillation in which the behaviour of a single energy eigenstate is examined by assuming plane waves.

Note that the coherence between the two waves disappears if the phase shift $\delta\phi(x)$ varies by more than 2π across the energy width δE. Thus, the observability of neutrino oscillation is [1215]

$$\frac{\delta E}{E} < \frac{\ell_0}{x}, \tag{8.85}$$

which agrees with (8.80). At very large x, the wave packet separates into two packets since states with different masses have different velocities. The classical separation s is given by

$$s = \frac{\delta p}{p} x = \frac{\Delta m^2}{2p^2} x. \tag{8.86}$$

The condition $s \ll \sigma_x$ is equivalent to (8.78). There is no interference if the two wave packets are separated by more than the width of each packet [1211, 1212]. This formalism is perfectly valid for practical purposes. Note that, rigorously speaking, neutrinos are not produced at the point source at $x = 0$, or otherwise the neutrino momentum diverges. This problem was handled in the wave-packet formalism.

Examination of experimentally relevant cases. In laboratory experiments the condition that neutrino oscillation can actually be observed is, from (8.60) and (8.80),

$$\frac{2\pi E}{L} \lesssim \Delta m^2 \lesssim \frac{2\pi E}{L} \left(\frac{\delta E}{E} \right)^{-1}, \tag{8.87}$$

where δE is the energy (momentum) spread of the beam, which is usually $(\delta E/E)^{-1} \sim 1 - 3$. Condition (8.78) is $\Delta m^2 \lesssim (2\pi E/L)(E\sigma_x/\pi)$, where the coherence length for $\pi \to \mu\nu$ is $\sigma_x \sim \tau_\pi c$, and thus $E\sigma_x/\pi \sim 10^{16}(E/1\,\text{GeV})$. Hence we do not need to consider (8.78). For such neutrino oscillation experiments, real oscillation is visible only when $2\pi E/L \approx \Delta m^2$. For $2\pi E/L \ll \Delta m^2$, average oscillation takes place.

An interesting case for which the energy spread is much smaller the beam energy is ^{7}Be solar neutrinos [1211]. The full width half maximum of ^{7}Be solar neutrinos is $1.6\,\text{keV}$ [1217], and therefore $(\delta E/E)^{-1} \approx 800$. The condition for oscillation is therefore,

$$0.7 \times 10^{-11}\,\text{eV}^2 \lesssim \Delta m^2 \lesssim 6 \times 10^{-9}\,\text{eV}^2. \tag{8.88}$$

8.4.3 $\nu_L \to \nu_R^c$ Oscillation

As discussed in Sect. 6.11, a left-handed neutrino, ν_L, may oscillate into ν_R^c which has the same helicity as ν_L [203]. This process may be experimentally relevant, only if the mass of right-handed neutrino is as small as that of the left-handed neutrino. It is straightforward to incorporate the family degree of freedom into (6.81). The Lagrangian for the neutrino mass is now

$$\mathcal{L}_{\text{mass}} = \frac{1}{2}(\overline{\nu^c}_{\alpha L} m_{\alpha\beta}^L \nu_{\beta L} + \overline{\nu^c}_{\alpha R} m_{\alpha\beta}^R \nu_{\beta R})$$
$$+ \overline{\nu}_{\alpha R} m_{\alpha\beta} \nu_{\beta L} + \text{h.c.} \tag{8.89}$$

Here, α and β represent family indices ($\alpha, \beta = 1 - N$), and both m^{L} and m^{R} are symmetric with respect to α and β due to Fermi statistics. The weak eigenstates ($\nu_L^\alpha, \nu_R^{c\alpha}$) are related to the mass eigenstates (ν_L^i, ν_R^{ci}) by four $N \times N$ matrices $U^{(a)}(a = 1 - 4)$, as

$$\begin{pmatrix} \nu_{\alpha L} \\ \nu_{\alpha R}^c \end{pmatrix} = \begin{pmatrix} U^{(1)} & U^{(2)} \\ U^{(3)} & U^{(4)} \end{pmatrix} \begin{pmatrix} \nu_{iL} \\ \nu_{iR}^c \end{pmatrix}, \qquad (\alpha, i = 1 - N). \qquad (8.90)$$

Using the mass eigenstates, (8.89) reads

$$\mathcal{L}_{\mathrm{mass}} = \frac{1}{2}(\overline{\nu^c}_{iL} m^L_{\mathrm{diag}i} \nu_{iL} + \overline{\nu^c}_{iR} m^R_{\mathrm{diag}i} \nu_{iR}) + \mathrm{h.c.} \qquad (8.91)$$

The diagonalised mass matrix is given by

$$\begin{pmatrix} m^L_{\mathrm{diag}} & \\ & m^{\dagger R}_{\mathrm{diag}} \end{pmatrix} = \begin{pmatrix} U^{(1)T} & U^{(3)T} \\ U^{(2)T} & U^{(4)T} \end{pmatrix} \begin{pmatrix} m^L & m^T \\ m & m^{R\dagger} \end{pmatrix} \begin{pmatrix} U^{(1)} & U^{(2)} \\ U^{(3)} & U^{(4)} \end{pmatrix}, \qquad (8.92)$$

where $U^{(i)}$ satisfy the unitarity condition,

$$U \equiv \begin{pmatrix} U^{(1)} & U^{(2)} \\ U^{(3)} & U^{(4)} \end{pmatrix},$$

$$U^\dagger U = UU^\dagger = \mathbf{1}. \qquad (8.93)$$

If both m_{1L} and m_{1R} are small enough ($< 1\,\mathrm{eV}$, say) and $m_1^L \neq m_1^R$, $\nu_{\alpha L} \to \nu_{\beta R}^c$ oscillation, as well as $\nu_{\alpha L} \to \nu_{\beta L}$ oscillation, takes place. The probability of finding $\nu_{\beta L}$ at a distance L from a source of $\nu_{\alpha L}$ is given by solving (8.49) for a general 6×6 matrix of m.

The $\nu_{\alpha R}$ does not interact with detectors, and hence is the so-called *sterile neutrino*. Therefore, unlike in neutrino mixing among different flavours, neutral-current-induced reactions are also affected [1218, 1219]. In particular, for the single family, the ratio of charged- to neutral-current-induced reactions is unchanged. We briefly discuss the oscillation pattern including ν_R later in this chapter, but we should remark that this possibility looks rather unnatural. We find no sensible models that would give a reason for such a small m^{R}.

8.5 Experimental Test for Neutrino Oscillation

8.5.1 Survey

The detection of $P_{\nu_e \to \nu_e} \neq 1$ or $P_{\nu_e \to \nu_\mu} \neq 0$ provides important information on a small neutrino mass which otherwise would be too small to detect

directly. In physical units the oscillation length given by (8.58) is

$$\ell_0 = 4\pi E/\Delta m^2 = 2.48 \times 10^2 \, \text{cm} \frac{E/\text{MeV}}{\Delta m^2/\text{eV}^2} \ . \tag{8.94}$$

To observe oscillation, we may need $L \gtrsim \ell_0/2$. This may be realised by making either the beam line length L long enough or the neutrino energy small enough to match the mass difference squared. A neutrino beam from an accelerator can explore down to $\sqrt{\Delta m^2} \gtrsim 1.2 \, \text{eV} \, (E/1 \, \text{GeV})^{1/2} (L/1 \, \text{km})^{-1/2} \epsilon^{1/2}$, where ϵ is the sensitivity for neutrino detection. For example, ϵ can be $10^{-2} - 10^{-3}$ for ν_e detection in the ν_μ beam (i.e., appearance experiments, $\nu_\mu \rightarrow \nu_e$), but it is of the order of 0.1 for disappearance experiments. In typical reactor neutrino experiments ($\bar{\nu}_e$ disappearance experiments, $\bar{\nu}_e \not\rightarrow \bar{\nu}_e$), one may explore the neutrino mass difference to $\sqrt{\Delta m^2} \gtrsim 0.05 \, \text{eV} \, (E/3 \, \text{MeV})^{1/2} \, (L/50 \, \text{m})^{1/2}$. To explore a mass difference of the order of $10^{-2} \, \text{eV}$, we need more than 250 km for accelerator experiments, or 1 km for experiments using nuclear reactors. One way to investigate such a small mass difference is to use atmospheric neutrinos [1220,1221] and to compare the detected flux with calculations or to compare fluxes produced at both sides of Earth ($L \sim 10^4 \, \text{km}$). With a typical energy of 1 GeV, one can detect effects down to $\sqrt{\Delta m^2} \gtrsim 0.01 \, \text{eV}$ [1222,1223]. Even a smaller neutrino mass difference would be relevant to astrophysical neutrinos.

The suggestion that neutrino oscillation may be a realistic possibility was first made by Pontecorvo [1224,205] in relation to the early solar neutrino experiment of Davis and collaborators [207], which indicated that the observed solar neutrino flux was smaller than theoretical calculations. The possibility of neutrino oscillation in various experiments was occasionally explored [1225], but more systematic searches began in the late 1970s, first by looking at existing data [1210,1226] and then by using accelerator and reactor neutrino beams [1227–1229]. In particuler, Reines et al. [1228] reported 'evidence' for oscillation of reactor neutrinos. This was followed by a flurry of experimental activities to search for oscillation in the 1980s [1230]. By that time, the search for neutrino oscillation was strongly motivated by both experiment and theory. On the experimental side, the Moscow group [198] reported positive evidence for the electron neutrino mass from tritium decay, and on the theory side, the motivation was given by the grand unification (e.g., [1231]) and cosmic dark matter. The solar neutrino problem continued to be a driving force [1232–1236]. The effort of searching for neutrino oscillation with an accelerator and reactors has continued to the present [1237–1244]. No positive evidence has been reported, except for the report from the LSND collaboration at LAMPF [1241] (see [1242], however). The parameter region where LSND claims oscillation, however, is nearly excluded by negative results from a comparable experiment of the KARMEN collaboration [1243] (a negative result from Bugey [1244] further narrowed the region), although there still remains a narrow region allowed at a 90% CL. As we discuss later in this

chapter, this positive evidence, if confirmed, would bring us a challenging problem in theoretically interpretating the neutrino oscillation pattern.

Figures 8.1 and 8.2 show a summary of the constraint on neutrino oscillation for $\nu_\mu - \nu_e$ [1237,544,1241,1243,1244] and for the transition involving ν_τ [1238–1240] from conventional accelerator and reactor experiments. The boundaries roughly consist of two segments: a vertical line corresponding to $\sin^2 2\theta \simeq 2\epsilon$ for $\Delta m^2 > 4E/L$ and an oblique line segment corresponding to $\sin^2 2\theta[(\Delta m^2/4E)L]^2 \approx \epsilon$ for $\Delta m^2 \sim 4E/L$. With $\nu_\mu \rightarrow \nu_e$ appearance experiments, one can explore oscillation to $\epsilon = P_{\nu_\mu \rightarrow \nu_e} > 10^{-3}$, the limitation set by contamination of ν_e from K decays (and τ decays) [1237]. In disappearance experiments, ϵ cannot be much smaller than 0.1, which is determined by uncertainties in the estimate of neutrino flux. Therefore, $\nu_\mu \rightarrow \nu_\tau$ appearance experiments [1239,1240] give a limit far stronger than disappearance experiments $(\nu_\mu \not\rightarrow \nu_\mu)$ [1238] for ν_τ.

The convincing evidence for neutrino oscillation came from the atmospheric neutrino experiments of Kamiokande and Super-Kamiokande, which reached a Δm^2 range substantially smaller than that explored by laboratory experiments [226, 227]. This motivated reactor experiments using a longer distance from the reactor to the detector [1245,924]. The null result, which does not contradict atmospheric experiments, placed a significant constraint on the neutrino mass matrix. The Kamiokande results also promoted long-
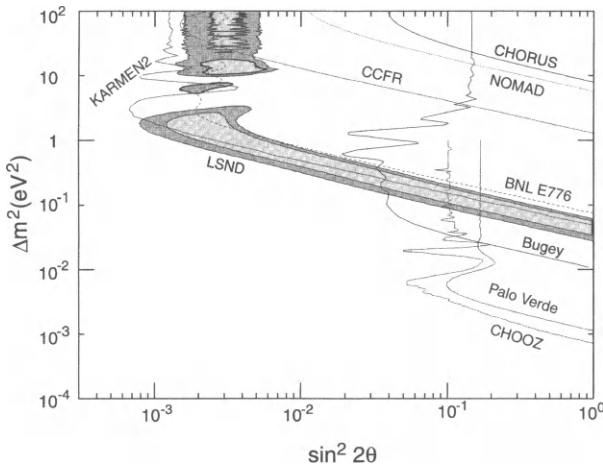
Fig. 8.1. Limits on neutrino oscillation involving ν_e. The data include $\nu_\mu - \nu_e$ (or $\bar\nu_\mu - \bar\nu_e$) oscillation from BNL E776 (Borodovsky et al. [1237]); CCFR (Romosan et al. [1237]); NOMAD (Astier et al. [1240]); CHORUS (Eskut et al. [1240]); KARMEN (Eitel [1243]); $\bar\nu_e$ disappearance experiments of Bugey (Achkar et al. [1244]); CHOOZ (Apollonio et al., [1245]); and Palo Verde (Boehm et al. [924]). All limits are at a 90% confidence level. The data shown by shading is a region (thin shade: 90% and thick shade: 99% CL) allowed by LSND (Aguilar et al. [1241]). The figure is taken from [1246].
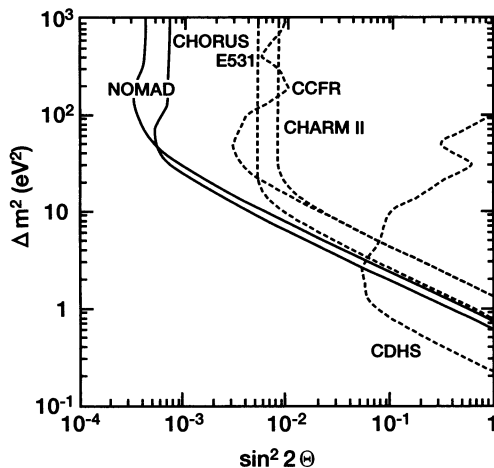
Fig. 8.2. Limit on oscillation for $\nu_\mu - \nu_\tau$. The data are taken from CDHSW (Dydak et al. [1238]); CCFR (McFarland et al.), CHARM (Gruwé et al.), Fermilab E531 (Ushida et al.) [1239]; NOMAD (Astier et al.); and CHORUS (Eskut et al.) [1240]. All limits are at a 90% confidence level.

baseline accelerator experiments (with $L \sim 250$ km); the first result points towards confirmation of the atmospheric neutrino results [1248].

Neutrino oscillation has been suspected for solar neutrinos for many years, and accumulating evidence has indicated that neutrino oscillation gives a consistent explanation for all solar neutrino experiments. It is, however, from the most recent experiment [235] that we can conclude that neutrino oscillation is actually the solution to the solar neutrino problem. Here, a matter effect (which we discuss in Sect. 8.6) plays an important role.

In what follows, we discuss the key experiments for neutrino oscillation, but limit ourselves to oscillation in vacuo. We note that neutrino oscillation takes place from a weak eigenstate to a weak eigenstate (not necessarily a pure state), but not to a mass eigenstate. Mass eigenstates appear only in the intermediate state.[1] This is clear from the fact that oscillation takes place via $m^\dagger m$ (see (8.49)) [1209].

8.5.2 Atmospheric Neutrino Oscillation Experiments

Atmospheric neutrinos were first detected in the Kolar Gold Field (India) at a great depth of 7000 mwe [158] and at the East Rand Propriety gold mine

---

[1] In what follows, we see that ν_μ and ν_τ are nearly maximally mixed. Oscillation of solar neutrinos from ν_e to other neutrinos takes place via the lower mass eigenstate made of ν_μ and ν_τ. So in practice, the final state of solar neutrino oscillation is rather close to the mass eigenstate of the $\nu_\mu - \nu_\tau$ sector. The difference is that the $\nu_e - \nu_\mu$ sector is not diagonalised.

near Johannesburg (South Africa) at 8800 mwe [159]. At these depths, the number of events induced by the vertical muon flux is comparable to that of expected neutrino events. Some deficit in the atmospheric muon neutrino flux has been known from the early days of these underground neutrino experiments [1249] (expt./theory $= 0.62 \pm 0.16$ in the Johannesburg experiment). Reines was the first who referred to the possibility of neutrino oscillation [1250] but admitted that the evidence was no more than suggestive because of low statistics and anticipated uncertainties in the flux calculation.

It was during runs to search for proton decay that experimentalists realised more seriously that muons produced by atmospheric neutrinos are fewer than expected [223, 224]. With a more careful study the Kamiokande collaboration [1251] concluded that the ν_μ flux is substantially smaller than the ν_e flux which nearly agrees with the expectation. Considering the fact that calculations of the ν_μ/ν_e ratio[2] are more reliable than those for the fluxes themselves (see Fig. 4.11 (c)), the Kamiokande authors used the double ratio $R = [(\nu_\mu + \bar{\nu}_\mu)/(\nu_e + \bar{\nu}_e)]_{\rm obs}/[(\nu_\mu + \bar{\nu}_\mu)/(\nu_e + \bar{\nu}_e)_{\rm calc}] = 0.60 \pm 0.09 \neq 1$ as an indicator and claimed that this deficit would be accounted for by neutrino oscillation, likely to be between ν_μ and ν_τ with $\Delta m^2_{\nu_\mu \nu_\tau} \gtrsim 10^{-3}$ eV^2. The IMB group [225] also found a similar ν_μ deficit (0.54 ± 0.05 for the same flux ratio) compared to simulations, but the authors were more conservative in interpreting it as the result of neutrino oscillation; they tended to ascribe the deficit to some unknown detector systematics.

General doubt concerned problems of the efficiency of μ/e separation (which the Kamiokande group claimed was very good, the error was $\sim$2% by virtue of the large coverage of the detector wall with large-size photomultipliers)[3] and the detection efficiency of the ν_μ event (in the Kamiokande, it was about 90%). Yet unknown systematics of the detector were also suspected. Furthermore, no anomaly was detected at IMB and Baksan for the upward through-going muon flux ($E_\nu \gtrsim 100$ GeV) and for upward-going muons that

---

[2] The atmospheric-neutrino event simulation of the Kamiokande is described in [493]. It takes account of quasi-elastic (and elastic) neutrino proton scattering [with formulae (3.162) and (3.167); $M_A = 1.01$ GeV is assumed], one-pion production (using the model of Fogli and Nardulli [501]) and multiple pion production using the deep-inelastic scattering formalism (see Sect. 3.14) with pion multiplicity simulated assuming the Koba–Nielsen–Olsen scaling [1252] and mean multiplicity normalised to $\langle n_\pi \rangle = 0.09 + 1.83 \ln M^2_{\rm pions}$. The interaction model is tested against the ANL experiment of [1253]. Neutrino oxygen scattering is calculated using the relativistic Fermi gas model, as tabulated in Table 3.20 in Chap. 3. In later analyses the Fogli–Nardulli model for one-pion production is replaced by the Rhein–Sehgal model [508], and the nucleon structure functions are allowed to evolve in q^2. The latest simulation includes $(m_\ell/m_N)^2$ terms in (3.156) to handle τ particle production [1254].

[3] The early IMB analysis [223] used μ decay in the detector as a signal for ν_μ and considered the rate of neutrino events that are associated with μ decays, rather than relying on the showering vs. nonshowering character.

stop in the detector ($E_\nu \approx 10\,\mathrm{GeV}$); both set significant constraints on the oscillation scenario indicated by the Kamiokande collaboration. In fact, the best-fit parameter region seemed to be excluded [1255, 1256]. In addition, the Nusex [1257], Frejus [1258], and Baksan [1256] experiments claimed no anomalies in the muon neutrino flux, albeit with fewer statistics and poorer μ/e separation. During that time, the Kamiokande group demonstrated that the water Čerenkov detector, as used at Kamioka, worked as designed, with an accelerator beam test [929] and confirmed that the neutron background is sufficiently small [1259]. An important step was the discovery of the zenith-angle dependence in the ν_μ/ν_e ratio (at about three standard deviations) in a careful follow-up analysis of higher energy ('multi-GeV') neutrino events, which indicate a characteristic of neutrino oscillation in the atmospheric neutrino [226].
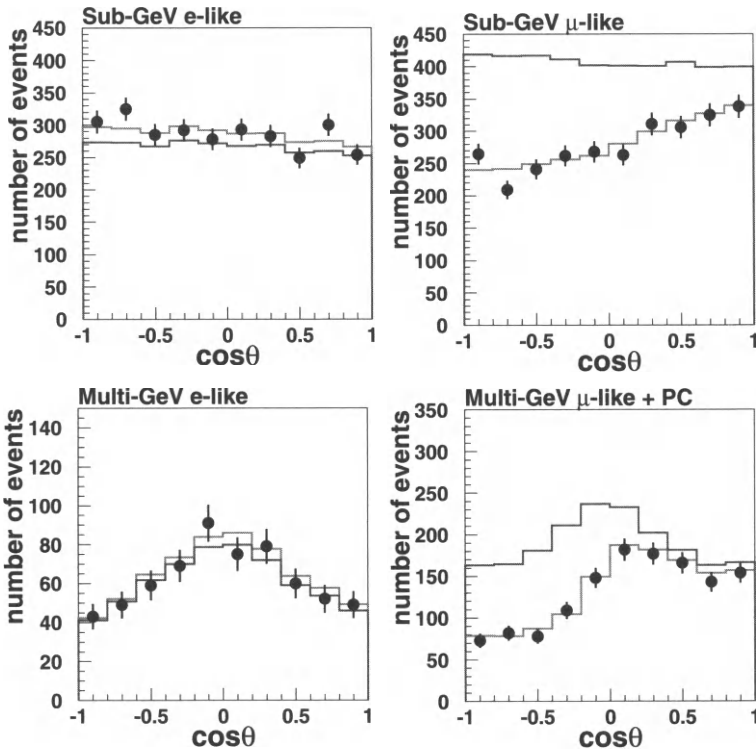
Fig. 8.3. Zenith-angle distributions of the electron- (*left column*) and muon-like (*right column*) events accumulated for 3 years in the Super-Kamiokande detector. The data are divided into sub- (*upper row*) and multi-GeV (*lower row*) events. The histograms with black lines show the Monte Carlo simulation without neutrino oscillation, and the grey lines are with neutrino oscillation with the parameters $\Delta m^2 \simeq 2.2 \times 10^{-3}\,(\mathrm{eV})^2$ and $\sin^2 2\theta \simeq 1$. After [1260].
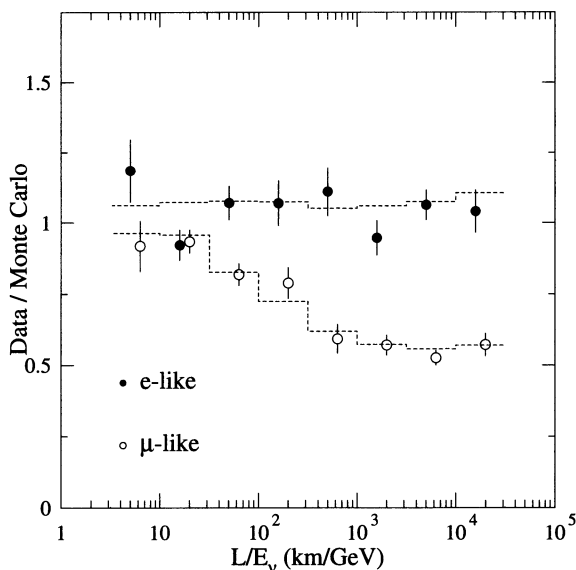
Fig. 8.4. Ratio of the observed to expected events for e- and μ-like events as a function of L/E_ν. The *dotted curves* show a Monte Carlo calculation using the neutrino oscillation parameters given in Fig. 8.3. After [1260].

The compelling evidence for neutrino oscillation was given by the Super-Kamiokande (SK) experiment [227]. It showed that the zenith-angle distribution of the muon neutrino flux significantly deviated from the calculation, whereas the electron neutrino flux did not show any anomaly: the muon neutrino flux from the opposite side of Earth is suppressed relative to that from above. Figure 8.3 shows the zenith-angle (θ) dependence of e- and μ-like events produced in the SK detector, compared with the expected distributions, taken from the latest report of SK [1260]. (The events are divided into sub-GeV and multi-GeV events. Confined events are plotted, except for multi-GeV μ-like events for which partially confined events are coadded.) The histogram expected for μ-like events without neutrino oscillation (black curves)[4] largely deviates from the observed distribution, but nearly a perfect fit is obtained for both sub-GeV and multi-GeV events if oscillation is taken into account with the assumed parameters, $\Delta m^2 \simeq 2.2 \times 10^{-3}$ (eV)^2 and the maximal mixing angle $\sin^2 2\theta = 1$ (grey curves). In Fig. 8.4 the ratios of observed to expected events are plotted as a function of the path length divided by energy, L/E_ν, which is directly converted to the value of the neutrino mass difference squared. The histogram shows the fit with the above parameter. An important test for possible detector systematics is that the up–down asymmetry of recoil muons disappears for lower energies, implying

---

[4] The peak at $\cos\theta = 0$ seen for multi-GeV events was explained in Sect. 4.3.

that the detector sensitivity is spatially homogeneous and the zenith-angle dependence is unlikely to be due to an artefact of the detector. (NB: the directionality of recoil muons towards the direction of the neutrino beam develops as energy increases; see Sect. 4.8). It was concluded that oscillation takes place between ν_μ and ν_τ; oscillation between ν_μ and ν_e does not fit the data. The allowed region for the neutrino mixing parameters is given in Fig. 8.5.
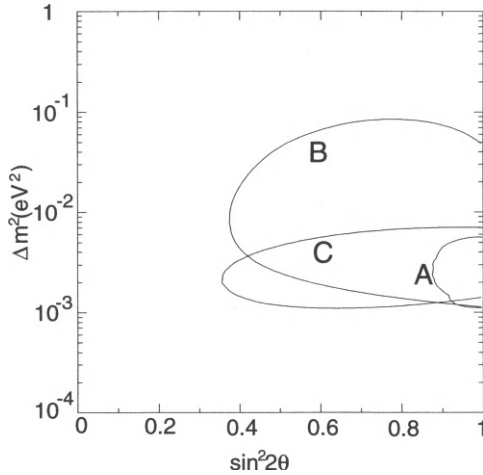
Fig. 8.5. Neutrino oscillation $(\nu_\mu - \nu_\tau)$ parameters obtained in the Super-Kamiokande experiment: (A) confined (and partially confined) events; (B) upward through-going muons; (C) upward stopped muons. All contours are at a 90% confidence level. After [1260].
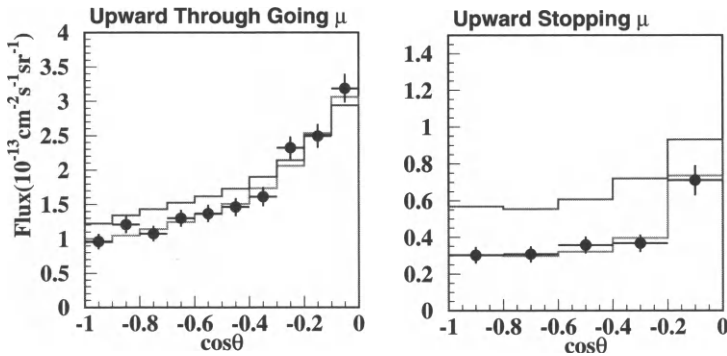
Fig. 8.6. Zenith-angle distributions of upward through-going muons and upward stopping muons detected at Super-Kamiokande. *Black* and *grey lines* indicate expectations without and with neutrino oscillation. From [1260].

A further analysis of Super-Kamiokande for upward through-going muons showed that the zenith-angle dependence is inconsistent with no-oscillation (see Fig.8.6), but a good fit is obtained in the presence of neutrino oscillation, and the parameters are consistent with those derived from the confined neutrino event analysis (see Fig. 8.5) [1261]. Moreover, they have shown that the ratio of stopped muon events to through-going muon events, both induced by upward-going muon neutrinos, $0.22 \pm 0.02(\text{stat}) \pm 0.01(\text{sys})$, is significantly smaller than 0.37 ± 0.05 which is expected with no-oscillation models [1262] (Fig.8.6). The oscillation parameters derived from stopped muons also agree with those from the others (Fig. 8.5). The best parameters obtained at the 90% confidence level from the latest SK report are [1260]

$$\Delta m^2_{\nu_\mu \nu_\tau} = (1.7 - 3.7) \times 10^{-3} \ (\text{eV})^2,$$
$$\sin^2 2\theta_{\nu_\mu \nu_\tau} = 0.9 - 1. \tag{8.95}$$

Their additional analysis [1263] showed that neutral-current interactions take place independently of the zenith-angle, indicating that the matter effects of Earth act for the initial (ν_μ) and final neutrinos (ν_τ) in the same way, contrary to oscillation into sterile neutrinos (see the next section). Hence, the sterile neutrino is disfavoured as the oscillation partner (at 2.4 sigma). The angular dependence of through-going neutrinos is better fitted in the presence of the matter effect of Earth, which also disfavours oscillation into sterile neutrinos (at 2.9 sigma). The combined analysis excludes sterile neutrinos as an oscillation partner at a 99% confidence level [1263].

The MACRO experiment [1264] reported that the zenith-angle dependence of upward through-going muons is inconsistent with no-oscillation. Their derived parameters are consistent with those given by SK.[5] The Soudan-2 experiment (using tracking calorimeters in massive iron modules) separated e- and μ-like events with 'tracks' and 'showers.' The oscillation parameters derived from the deficit in muon neutrino flux are consistent with the SK results, although they are not very well determined [1265]. Figure 8.7 compares the oscillation parameters from Kamiokande, SK, and MACRO, together with the limits on $\nu_e - \nu_\tau$ oscillation discussed in the next subsection.[6]

In Table 8.1, a brief history of the confirmation of atmospheric neutrino oscillation is summarised. We refer to a dedicated review article [1271] for a more detailed discussion. Note that the atmospheric neutrino experiment

---

[5] The Feldman–Cousins statistics that the MACRO group used, however, gave unusually small errors compared to that expected from the number of events they actually observed. So we remove their results from the comparison figure, Fig. 8.7.

[6] The only data with reasonable statistics which are only marginally consistent with the parameter region derived from SK are results from Kamiokande [1266,1251]. The 90% contour of the Kamiokande overlaps (8.95) just at its upper edge. The SK group ascribes it to a statistical effect.

Table 8.1. Atmospheric neutrino oscillation – brief history.

Expt.	Indicator	Result[a]	Interpretation
Johannesburg 1978 [1249]	ν_μ flux	0.62 ± 0.16	Poss. oscil., but evidence too premature [1250]
IMB 1986 [223]	ν_μ flux	0.76 ± 0.09	No interpretation
Kamiokande 1988 [224]	ν_μ flux	0.59 ± 0.07	Unable to explain with systematics
Nusex 1989 [1257]	ν_μ/ν_e	No anomaly	
Frejus 1990 [1258]	ν_μ/ν_e	No anomaly	$\Delta m^2 > 4 \times 10^{-3}$ (eV)^2 excluded
IMB 1991-2 [225]	ν_μ decay fraction	$0.71 \pm 0.06 \pm 0.07$	Systematics errors (?)
Baksan 1991 [1256]		No anomaly	$\Delta m^2 > 1 \times 10^{-4}$ (eV)^2 excluded
Baksan 1991 [1256]	Up-going μ flux	No anomaly	$\Delta m^2 > 3 \times 10^{-4}$ (eV)^2 excluded
Kamiokande 1992 [1251]	ν_μ/ν_e	$0.60 \pm 0.07 \pm 0.05$	Oscil. interp. given: $\Delta m^2 \approx 8 \times 10^{-3}$ (eV)^2
IMB 1992 [1255]	Up-going μ, stop./through	No anomaly	$\Delta m^2 = 2 \times 10^{-4} - 2 \times 10^{-2}$ excluded
Kamiokande 1994 [226]	ν_μ/ν_e: ζ dep. (multi GeV)	Tilted	Consistent with oscil., $\Delta m^2 \approx 10^{-2}$ (eV)^2
Frejus 1995 [1267]	Up-going μ flux	No anomaly	
IMB 1997 [1268]	ν_μ/ν_e (multi GeV)	No anomaly	
Soudan 2: 1997 [1269]	ν_μ/ν_e	$0.72 \pm 0.19 \pm 0.06$	
Super-Kam 1998 [1270]	ν_μ/ν_e	$0.61 \pm 0.03 \pm 0.05$	
Super-Kam 1998 [227]	ν_e, ν_μ: ζ dep	Tilted	Evidence for oscil., $\Delta m^2 \approx 2.2 \times 10^{-3}$ (eV)^2
Super-Kam 1998 [1261]	Up-going (through) μ, ζ dep.	Tilted	Consistent with oscil., $\Delta m^2 \approx 6 \times 10^{-3}$ (eV)^2
MACRO 1998 [1264]	Up-going μ ζ dep.	Tilted	Consistent with oscil.,
Soudan-2: 1999 [1269]	ν_μ/ν_e	0.64 ± 0.11	No interpretation
Super-Kam 1999 [1262]	Up-going μ, stop./through	$0.59 \pm 0.06 \pm 0.08$	Oscillation: $\Delta m^2 \approx 3 \times 10^{-3}$ (eV)^2

a Numbers are ratios of the observed to the expected without neutrino oscillation. Two errors are statistical and systematic; theoretical errors are included in the second numbers when available.

measures

$$P(\nu_\mu \to \nu_\mu) = P(\bar{\nu}_\mu \to \bar{\nu}_\mu) = 1 - 4(1 - |U_{\mu 3}|^2)|U_{\mu 3}|^2 \sin^2\left(\frac{\Delta m^2}{2E}t\right) \ , \quad (8.96)$$

when written in mixing matrix elements, i.e., it measures $|U_{\mu 3}|$. The search for τ particles produced from ν_μ is being carried out at SK.

8.5.3 Reactor Experiments with an Extended Baseline

A group working at the Chooz reactor (Ardennes, France; 8.5 GW thermal power) installed the detector sufficiently far from the reactor ($L \simeq 1$ km, $\langle E_\nu \rangle = 3$ MeV), so that the explored range covers the neutrino oscillation parameters derived from the atmospheric neutrino experiment [1245]. This disappearance experiment measures $|U_{e3}|$ as

$$P(\bar{\nu}_e \to \bar{\nu}_e) = 1 - 4(1 - |U_{e3}|^2)|U_{e3}|^2 \sin^2\left(\frac{\Delta m^2}{2E}t\right) \ . \quad (8.97)$$

The result was negative, setting a limit $\sin^2\theta < 0.1$ at the 90% CL (see Fig. 8.7) for $\Delta m^2 \approx 10^{-3}$ (eV)^2. This means that $\bar{\nu}_e$ does not oscillate into
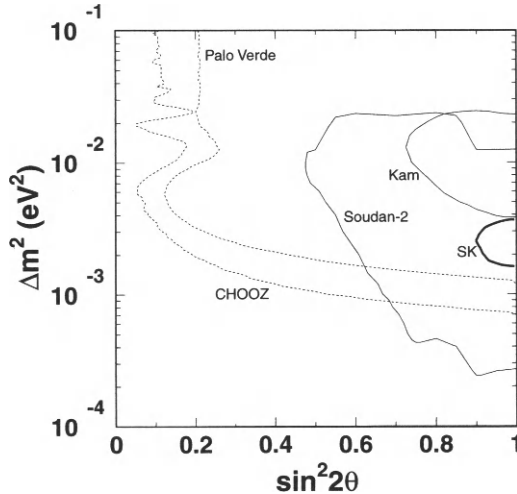
Fig. 8.7. Neutrino oscillation parameters for τ neutrinos. The data plotted (*solid curves*) are the regions allowed for $\nu_\mu - \nu_\tau$ oscillation from SK [1260], Kamiokande [1266], and Soudan-2 [1269]. We also plot with *dotted curves* the regions forbidden for $\nu_e - \nu_\tau$ from CHOOZ [1245] and Palo Verde [924] (*inside the contours*). All contours are at a 90% confidence level.

$\bar{\nu}_\mu$ or $\bar{\nu}_\tau$ at a large probability.[7] A similar result was obtained from the Palo Verde (Arizona) long-baseline reactor experiment ($L \simeq 0.75 - 0.89$ km, 11.6 GW thermal power), although the derived limit ($\sin^2\theta < 0.3$) is somewhat weaker [924].

8.5.4 Long-Baseline Accelerator Experiments

The first long-baseline accelerator experiment is being carried out using the muon neutrino beam ($\langle E_\nu \rangle \sim 1.3$ GeV; 98.2% ν_μ) produced from an aluminium target bombarded by a 12-GeV proton beam at KEK (Tsukuba), pointed at the Super-Kamiokande detector, which is located 250 km away (the K2K experiment) [1247]. The beam is fast-extracted protons (spill of 1.1 µs) every 2.2 s (approximately 6×10^{12} protons). The π^-'s produced are focused by two neutrino horns. Accurate timing information is used to reduce the background efficiently. The neutrino flux multiplied by interaction cross sections is measured at a front detector of 1 kton water, which has a design similar to the Kamiokande detector, located 280 m from the target on the site of KEK. The accuracy of the beam alignment is better than 0.1 mrad, and the neutrino spectrum is nearly constant across 4 mrad.

The first report [1248] gave 28 detected events compared with 38 expected events at the state of 2.3×10^{19} protons on the target. This is a 2σ effect, but the best-fit parameter $\Delta m^2 \simeq 3 \times 10^{-3}$ agrees with the atmospheric neutrino result.

8.5.5 Neutrino Oscillation in Solar Neutrinos

The three types of solar neutrino experiments (^{37}Cl, water Čerenkov, ^{71}Ga [721, 723–725]) showed that the neutrino fluxes are reduced in all experiments, compared to the standard solar model prediction, but the reduction factors are not uniform (see Table 4.9). Because the flux is reduced to <50% in the ^{37}Cl and water Čerenkov experiments, the effect cannot be explained simply with average oscillation between two neutrinos, which occurs when the mass difference squared is much larger than $2\pi E/d = 0.7 \times 10^{-10}$eV^2($E/8$ MeV) ($d = 1.5 \times 10^{13}$ cm is the Sun–Earth distance). The pp neutrino flux is less strongly suppressed than the higher energy ^{8}B neutrino flux, so the average oscillation scenario among three neutrinos does not work either.

An interesting possibility was a more accidentally-looking case that one of the neutrino mass differences takes a value just so that the oscillation length (or its integer multiple) coincides with the Sun–Earth distance (the so-called just-so scenario) [1232]–[1235]. If this happens, the ν_e flux reduction

---

[7] Here we assume $\Delta m_{21}^2 \ll \Delta m_{31}^2$. If Δm_{21}^2 could be as large as 5×10^{-4} (eV)^2, as allowed in the LMA solution for the solar neutrino problem at 99% CL (see below), the limit presented here is somewhat disturbed via the effect of $\bar{\nu}_e \rightarrow \bar{\nu}_2 \rightarrow \bar{\nu}_\tau$.

depends strongly on the neutrino energy, and the neutrino capture rates can fall below one-third, even if oscillation takes place between two neutrinos. The reduction factor also wildly varies with neutrino energy. Mass differences giving the same $\Delta m^2 d/4E$ with modulo π are also solutions, insofar as the modulo factor is not too large. (We may label the solutions as VAC_n with n the modulo counted as $n = 0, 1, 2...$). It appears that one can tune the mixing parameters to fit the experiment. Detailed calculations showed that the solutions that explain the flux reduction factors in the three experiments are located in many narrow strips of constant Δm^2 in a region of large $\sin^2 2\theta$ [1234–1236, 1272–1274]. The region allowed by the flux measurements was around

$$\Delta m^2 = (0.6 - 1.2), \ (2.5 - 3), \ \text{and} \ 5 \times 10^{-10} \, \text{eV}^2,$$
$$\sin^2 2\theta = 0.7 - 1.0. \tag{8.98}$$

Theoretical interest in the VAC solution was that $m_\nu \approx (\Delta m^2)^{1/2}$ is close to the unitarity limit for Majorana neutrinos (6.40).

Such neutrino oscillation in vacuo generically produces a wildly energy dependent flux reduction pattern (see Fig. 8.13 below), and this energy dependence persists to higher energies of $> 5\,\text{MeV}$, which can be tested by the Super-Kamiokande experiment. The observation indicates that the recoil electron energy spectrum does not show any distortion from 5 to $14\,\text{MeV}$ beyond a 10% level [1275,723]. This excludes all parameter regions at least at a 95% confidence level, as shown by detailed likelihood analyses [1272–1274].[8] Modern analyses show that low n solutions of (8.98) (which are 'just-so'-like solutions) allowed in earlier analysis are excluded at a $> 99\%$ confidence level [1273] (see also [1272] and [1274]).[9]

Notwithstanding, let us mention the possibility of seeing unique evidence characteristic of neutrino oscillation in vacuo. The 'just-so' type scenario is sensitive to the distance from Earth to the Sun. So one expects a semiannual variation of the monoenergetic ^{7}Be neutrino capture rate related to the eccentricity of Earth's orbit, which varies by 3.4%, in a much amplified form that does not necessarily vary according to the inverse square of the distance. The oscillation phenomenon persists up to $\Delta m^2 \sim 6 \times 10^{-9} \, \text{eV}^2$ for ^{7}Be neutrinos [e.g., [1276]; see (8.88)]; for $\Delta m^2 \sim 1 \times 10^{-10} \, eV^2$, we would expect a 40% semiannual variation in the ^{7}Be flux and hence a 6% variation in the neutrino capture rate in a ^{37}Cl detector or a 12% variation in a ^{71}Ga detector [1232–1236]. The statistics of the existing experiments, however, do not allow a conclusion about this effect.

---

[8] Only the highest Δm^2 solution of (8.98) remains at a 99% confidence level of the data.

[9] These authors adopt somewhat different conditions and inputs. For instance, [1274] allows the presence of sterile neutrinos, so that the allowed region is slightly wider, or else their analysis agrees with [1273] at good accuracy. The constraint from the CHOOZ experiment is included in [1273].

Note that the final state relevant to oscillation of solar neutrinos is

$$|\nu\rangle \simeq [U^\dagger]_{2\mu}|\nu_\mu\rangle + [U^\dagger]_{2\tau}|\nu_\tau\rangle \qquad (8.99)$$

in the approximation that $U_{e3} \simeq 0$.

8.6 Neutrino Oscillation in Matter

8.6.1 Neutrino Conversion

When neutrinos propagate through matter, ν_e and ν_μ(or ν_τ) feel different potentials because ν_e interacts with electrons via both neutral and charged currents, whereas $\nu_\mu(\nu_\tau)$ interacts only via the neutral current (see Fig. 8.8) [212]. This induces a coherent effect in which maximal conversion of ν_e into ν_μ takes place even for a small intrinsic mixing angle, when the phase arising from the potential difference between the two neutrinos cancels the phase caused by the mass difference, as pointed out by Mikheyev and Smirnov [211].[10] For this reason, this mechanism (Mikheyev–Smirnov–Wolfenstein; MSW mechanism) has been supposed to be the most attractive solution to the solar-neutrino problem, as promulgated by Bethe [213]. Accumulating evidence for years indicates that this is most likely to be the solution, but it is with a large intrinsic mixing angle unlike the original idea.

In the presence of the effective interaction,

$$H_{\text{eff}} = \frac{G_F}{\sqrt{2}} \; \bar{\nu}_e\gamma_\mu(1 - \gamma_5)\nu_e \; \bar{e}\gamma_\mu(1 - \gamma_5)e \;, \qquad (8.100)$$

the electron neutrino energy in (8.44) receives an extra contribution of $\sqrt{2}G_F n_e$, where n_e is the electron number density in matter. [This is $V(\nu_e, e) - V(\nu_\mu, e)$ in (3.239).][11] Therefore, the time evolution of the neutrino wave function is given by

$$i\frac{d}{dt}\begin{pmatrix}\nu_e \\ \nu_\mu\end{pmatrix} = \begin{pmatrix} -\frac{\Delta m^2}{4E}\cos2\theta + \sqrt{2}G_F n_e & \frac{\Delta m^2}{4E}\sin2\theta \\ \frac{\Delta m^2}{4E}\sin2\theta & \frac{\Delta m^2}{4E}\cos2\theta \end{pmatrix}\begin{pmatrix}\nu_e \\ \nu_\mu\end{pmatrix} \qquad (8.101)$$

instead of (8.49) and (8.52).

----

[10] This effect was also noted, though less explicitly, by Barger et al. [1277] for atmospheric neutrinos propagating through Earth. Unfortunately, its importance in the solar neutrino problem was dismissed in their work.

[11] The original paper by Mikheyev and Smirnov [211] contained an error in the sign of the $\sqrt{2}G_F n_e$ term of (8.101). This error was corrected in the paper by Bethe [213].
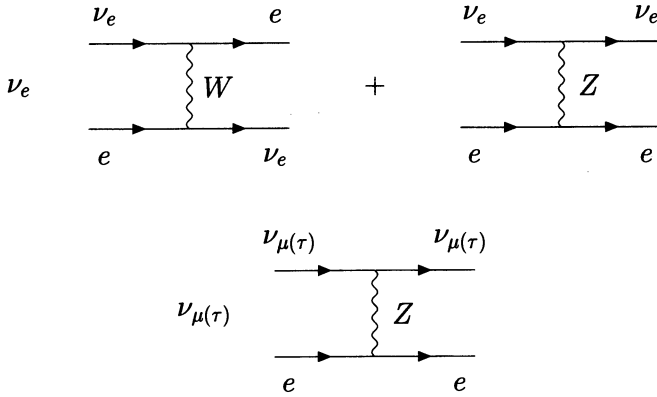
Fig. 8.8. Coherent scattering of ν_e and $\nu_\mu(\nu_\tau)$ in matter.

It is obvious that (8.101) is valid for both Dirac and Majorana cases because only the left-handed neutrino interacts with matter and the theory is not concerned with whether the right-handed counterpart is a neutrino (the Dirac case) or an antineutrino (the Majorana case) (e.g., ref. [1278]).

We diagonalise the Hamiltonian of (8.101) by

$$\begin{pmatrix} \nu_e \\ \nu_\mu \end{pmatrix} = U \begin{pmatrix} \tilde{\nu}_1 \\ \tilde{\nu}_2 \end{pmatrix} = \begin{pmatrix} \cos\tilde{\theta} & \sin\tilde{\theta} \\ -\sin\tilde{\theta} & \cos\tilde{\theta} \end{pmatrix} \begin{pmatrix} \tilde{\nu}_1 \\ \tilde{\nu}_2 \end{pmatrix}, \tag{8.102}$$

where $\tilde{\nu}$ is the energy eigenstate in matter and $\tilde{\theta}$ is given by

$$\cos2\tilde{\theta} = \frac{-A/\Delta m^2 + \cos2\theta}{\sqrt{(A/\Delta m^2 - \cos2\theta)^2 + \sin^2 2\theta}} \tag{8.103}$$

and

$$\sin2\tilde{\theta} = \frac{\sin2\theta}{\sqrt{(A/\Delta m^2 - \cos2\theta)^2 + \sin^2 2\theta}} \tag{8.104}$$

with

$$A = 2\sqrt{2}EG_F n_e \ . \tag{8.105}$$

The energy eigenvalues are

$$\tilde{m}^2_{\frac{1}{2}} = \frac{A}{2} \mp \frac{1}{2}\sqrt{(A - \Delta m^2 \cos2\theta)^2 + (\Delta m^2)^2 \sin^2 2\theta} \ . \tag{8.106}$$

We plot $\tilde{m}^2$ and $\tilde{\theta}$ as a function of n_e in Fig. 8.9.

This is a well-known level-crossing phenomenon of the two-level problem of quantum mechanics, and its importance in the solar neutrino problem was first realised by Mikheyev and Smirnov [211] (see also Bethe [213]). The level
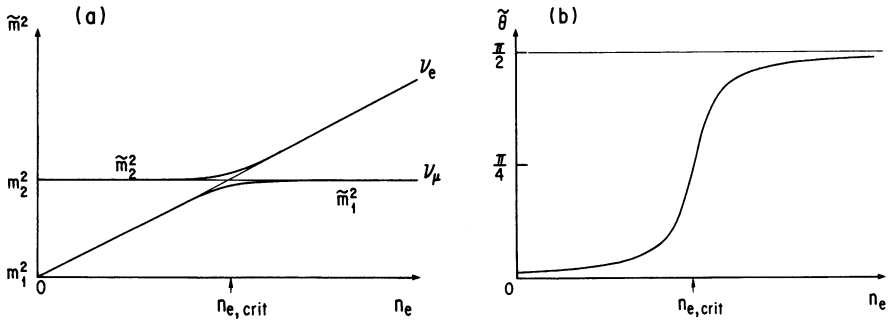
Fig. 8.9. (a) Effective neutrino mass squared in the medium with electron density n_e. $n_{e,crit}$ is the crossing point defined by (8.107). This figure corresponds to $\sin^2 2\theta = 0.01$. (b) Mixing angle $\tilde{\theta}$ in the medium as a function of n_e, corresponding to the case shown in (a).

crossing ("resonance") occurs at $A/\Delta m^2 = \cos 2\theta$, i.e.,

$$n_e = n_{e,\text{crit}} \equiv \frac{1}{2\sqrt{2}G_F} \frac{\Delta m^2}{E} \cos 2\theta \quad . \tag{8.107}$$

As can be seen in Fig. 8.9, if $n_e \ll n_{e,\text{crit}}$, $\tilde{\theta} \simeq \theta$, and neutrinos oscillate with a mixing length in matter of $l_0 = 4\pi E/\Delta m^2$, as in vacuo. For $n_e \gg n_{e,\text{crit}}$, $\tilde{\theta}$ approaches $\pi/2$. The mixing length in matter,

$$\tilde{l} = \frac{4\pi E}{\tilde{m}_2^2 - \tilde{m}_1^2} = \frac{4\pi E}{\Delta m^2} \frac{1}{[(A/\Delta m^2 - \cos 2\theta)^2 + \sin^2 2\theta]^{1/2}} \quad , \tag{8.108}$$

is much shorter than l_0 for large n_e. At $n_e = n_{e,\text{crit}}$, two neutrinos mix maximally, i.e., $\tilde{\theta} = \pi/4$.

If ν_e is produced in the region $n_e > n_{e,\text{crit}}$ and propagates into the region $n_e < n_{e,\text{crit}}$, the state follows the upper branch given in Fig. 8.9; then, ν_e fully converts into ν_μ, provided that the density gradient, $d(\ln n_e)/dr$, is sufficiently small that neutrino conversion occurs adiabatically. This adiabatic condition may be written

$$(\text{energy gap}) \times (\text{transition time}) \gg \hbar \quad , \tag{8.109}$$

where the energy gap $\delta E = (\tilde{m}_+^2 - \tilde{m}_-^2)_{\min}/2E$ is

$$\delta E = \frac{1}{2E} (\Delta m^2) \sin 2\theta \tag{8.110}$$

from (8.106). The transition time in the level-crossing region is

$$\delta t = \delta r/c = \left(\frac{1}{n_e} \frac{dn_e}{dr} \right)^{-1} \frac{\delta n_e}{n_e}$$

$$= \left(\frac{1}{n_e} \frac{dn_e}{dr} \right)^{-1} \frac{\delta A}{A} \quad . \tag{8.111}$$

Since 'resonance' occurs at $A = \Delta m^2 \cos 2\theta$ and its width is $\delta A \sim \Delta m^2 \sin 2\theta$ from (8.104), we find that (8.109) is written[12]

$$\frac{1}{n_e}\frac{dn_e}{dr} \ll \frac{\Delta m^2}{2E}\frac{\sin^2 2\theta}{\cos 2\theta} \quad . \tag{8.112}$$

The probability for $\nu_e \to \nu_e$ is easily calculated in a manner similar to (8.67) by averaging the time-varying part, i.e.,

$$P_{\nu_e \to \nu_e} = \sin^2 \theta \sin^2 \tilde{\theta} + \cos^2 \theta \cos^2 \tilde{\theta}$$
$$= \frac{1}{2}(1 + \cos 2\theta \cos 2\tilde{\theta}), \tag{8.113}$$

where $\tilde{\theta}$ is the mixing angle at the initial point.

If the adiabatic condition (8.112) is not satisfied, the state of the upper branch undergoes a transition to the lower branch while passing through the crossing point with a probability given by [1281, 1282]

$$P_{\mathrm{f}} = \exp\left(-\frac{\pi}{2}\gamma\right), \tag{8.114}$$

where

$$\gamma = \frac{\Delta m^2 \sin^2 2\theta}{2E\cos 2\theta(1/n_e)(dn_e/dr)} \tag{8.115}$$

is the ratio of the right-hand side to the left-hand side of inequality (8.112). This is a straightforward application of the well-known Landau–Zener formula for level crossings [1283], and its derivation is recapitulated in Sect. 8.6.3. Note that the appearance of the $\cos 2\theta$ factor, which vanishes at $\theta = \pi/4$, is an artefact of a logarithmic derivative of the matter density; $n_e = \Delta m^2 \cos 2\theta/2\sqrt{2}G_F E$ cancels the cosine factor.

Using this P_{f} we write the probability for $\nu_e \to \nu_e$ for a general case [1281]:

$$P_{\nu_e \to \nu_e} = (\sin^2 \theta \sin^2 \tilde{\theta} + \cos^2 \theta \cos^2 \tilde{\theta})(1 - P_f)$$
$$+ (\sin^2 \theta \cos^2 \tilde{\theta} + \cos^2 \theta \sin^2 \tilde{\theta})P_f$$
$$= \frac{1}{2} + \left(\frac{1}{2} - P_{\mathrm{f}}\right)\cos 2\theta \cos 2\tilde{\theta}. \tag{8.116}$$

For $n_e \to \infty$, $\cos 2\tilde{\theta} \to -1$, and this reduces to

$$P_{\nu_e \to \nu_e} = \sin^2\theta + \cos 2\theta \, P_{\mathrm{f}} \quad . \tag{8.117}$$

---

[12] This agrees with the condition derived in [1279] $[D^{-1}d\tilde{\theta}/dr]_{\tilde{\theta}=\pi/4} \ll 1$, where $D = (\Delta m^2/4E)[(A/\Delta m^2 - \cos 2\theta)^2 + \sin^2 2\theta]^{1/2}$. It is shown that this condition [and also (8.112)] is modified to $(\cos\theta)^{-1}[D^{-1}d\tilde{\theta}/dr]_{\tilde{\theta}=\pi/4+\theta/2} \ll 1$, when $\theta \gtrsim \pi/4$ [1280]. For the realistic large mixing angle solution of the solar neutrino problem (see below), the modified condition gives $\Delta m^2/E$ about 1.5 times the value derived from (8.112).

Note here that the neutrinos emergent from the Sun are in the eigenstate of mass, irrespective of whether or not conversion takes place, unless the mass difference is very small. This is clear from the fact that $\nu_e = \tilde{\nu}_2$ for a high-density region; the state follows the branch all the way adiabatically, or does so before and after a flip in the resonance region, and the two branches continue smoothly to ν_2 or ν_1 at the surface of the Sun. These neutrinos emergent from the Sun hence do not undergo further oscillation in vacuo. [The same also applies to $\bar{\nu}$ ($\bar{\nu}$ from stars never oscillates, if the level crossing takes place for ν), although this is irrelevant to solar neutrinos.] The exception is when the neutrino mass difference is so small that the resonance condition is satisfied only close to the surface of the Sun; when the oscillation length becomes longer than the distance between the resonance position and the surface, neutrinos do not fall into mass eigenstates. In this case, oscillation in vacuo may take place, as in the "just-so" scenario.

In summary, complete conversion of ν_e to ν_2 takes place in the Sun when two conditions are satisfied [211]: (i) in the centre of the Sun, $n_e > n_{e,\text{crit}}$ [see (8.107)], which leads to $\Delta m^2 \lesssim \text{const}$ (resonance condition); and (ii) $\Delta m^2 \sin^2 2\theta \gtrsim \text{const}$, as derived from (8.112) (when θ is not too close to 45°) (adiabatic condition). In addition, (8.117) shows that $P_{\nu_e \to \nu_e} = 1/2$ at $\sin^2 2\theta = 1$ ($\gamma = \infty$) independent of Δm^2 and energy [1281]. This means that the $P_{\nu_e \to \nu_e} = \text{const}$ ($\lesssim 1/2$) forms approximately a rectangular triangle (which we refer to as the MSW triangle) in the ($\Delta m^2, \sin^2 2\theta$) plane (see Fig. 8.10).

Let us remark here concerning the spectroscopic characteristics of neutrino conversion. The conversion is generally neutrino-energy dependent. The high-energy component that satisfies (8.107) is sharply cut off by conversion into ν_μ or ν_τ (it is called adiabatic conversion) across a narrow region: $\delta E/E (\sim \delta \Delta m^2 / \Delta m^2) \sim \sin \theta$. On the other hand, the energy dependence of (8.112) indicates that the lower energy component is suppressed across the $\Delta m^2 \sin 2\theta \sim \text{const}$ line. The energy dependence appears in the expo-
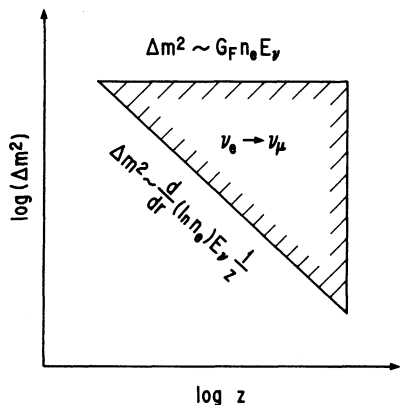
Fig. 8.10. Schematic figure of the MSW triangle. The abscissa is the logarithm of $z = \sin^2 2\theta / \cos 2\theta$. Complete conversion of $\nu_e \to \nu_\mu$ takes place inside the triangle.
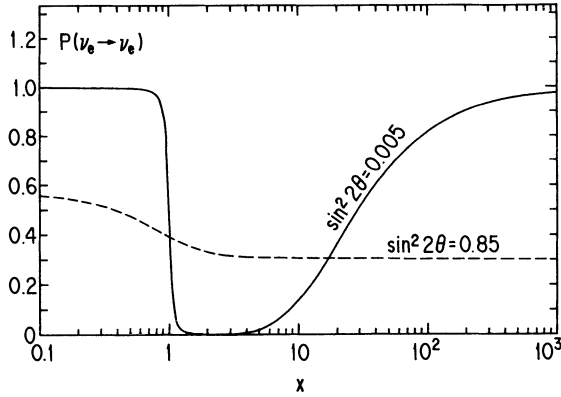
Fig. 8.11. MSW filter function $P(\nu_e \to \nu_e)$ as a function of $x = 2(E/\Delta m^2)\sqrt{2}G_F n_e = (E/1\,\mathrm{MeV})(1.52 \times 10^{-5}\,\mathrm{eV^2}/\Delta m^2)^{-1}$ ($\rho = 100\,\mathrm{g\,H\,cm^{-3}}$ is adopted). The two curves show a small- (*solid curve*, $\sin^2 2\theta = 0.005$) and a large-angle case (*dashed curve*, $\sin^2 2\theta = 0.85$). The parameters correspond to the two solutions, LMA and SMA, described in the text below. The Landau–Zener formula is adopted to calculate these curves.

nential function and is not very sharp. For the vertical branch, the reduction of the ν_e flux is approximately energy-independent; the flux reduction is simply $\sim \sin^2 \theta$. In Fig. 8.11, we show $P(\nu_e \to \nu_e)$ calculated from (8.114) and (8.116) with two typical choices of parameters: (A) $\sin^2 2\theta = 0.01$ and (B) $\sin^2 2\theta = 0.85$. For other parameters we take $\rho_c = 100\,\mathrm{g\,H/cm^3}$ and $d(\ln n_e)/dR = 10.5/R_\odot$. The horizontal axis,

$$x \equiv \frac{5.4 \times 10^{-6}\mathrm{eV^2}}{\Delta m^2}\left(\frac{E}{1\,\mathrm{MeV}}\right)\,, \tag{8.118}$$

corresponds to going down along a line of constant $\sin^2 2\theta$ in Fig. 8.10; the region of $P < 1$ corresponds to the inside of the triangle. [$x \simeq 1$ is the resonance condition (8.107).] The features discussed above are apparent in this example.

The cases for three generations are discussed in [1284]. For reviews of the MSW effect, see [1285, 1286].

8.6.2 Derivation of the Transition Probability

Let us first discuss the propagation of neutrinos in more detail and derive formula (8.116) in a more formalistic manner [1281]. We assume that ν_e is produced at t_i, passes through the resonance at t_r, and is detected at $t_f \to \infty$ in vacuum. At $t = t_i$,

$$\psi_{\nu_e}(t_i) = \cos\tilde\theta\,|\tilde\nu_1,\ t_i\rangle + \sin\tilde\theta\,|\tilde\nu_2,\ t_i\rangle\,, \tag{8.119}$$

according to (8.102). At $t = t_r - \epsilon$,

$$\psi(t_r - \epsilon) = \cos\tilde{\theta}\; e^{i\int_{t_i}^{t_r} \varepsilon_1 dt}\; |\nu_1,\; t_r\rangle + \sin\tilde{\theta}\; e^{i\int_{t_i}^{t_r} \varepsilon_2 dt}\; |\nu_2,\; t_r\rangle\;, \qquad (8.120)$$

where $\varepsilon_{1,2} = \tilde{m}_{1,2}^2/2E$. At $t \simeq t_r$, a flip to the other state may take place, and the state is written

$$\begin{aligned} |\tilde{\nu}_1\rangle &\to \alpha|\tilde{\nu}_1\rangle + \beta|\tilde{\nu}_2\rangle \\ |\tilde{\nu}_2\rangle &\to -\beta^*|\tilde{\nu}_1\rangle + \alpha^*|\tilde{\nu}_2\rangle \end{aligned} \qquad (8.121)$$

with $|\alpha|^2 + |\beta|^2 = 1$. Hence, after the resonance point,

$$\begin{aligned} \psi(t_r + \epsilon) &= \cos\tilde{\theta}e^{i\int_{t_i}^{t_r} \varepsilon_1 dt}[\alpha\;|\tilde{\nu}_1,\; t_r\rangle\; + \beta\;|\tilde{\nu}_2,\; t_r\rangle\;] \\ &\quad + \sin\tilde{\theta}e^{i\int_{t_i}^{t_r} \varepsilon_2 dt}[-\beta^*|\tilde{\nu}_1,\; t_r\rangle\; + \alpha^*|\tilde{\nu}_2,\; t_r\rangle\;] \\ &\equiv A(0;t_r)\;|\tilde{\nu}_1,\; t_r\rangle + B(0;t_r)\;|\tilde{\nu}_2,\; t_r\rangle\;. \end{aligned} \qquad (8.122)$$

For $t > t_r$, it propagates as

$$\psi(t) = A(0;t_r)e^{i\int_{t_r}^{t} \varepsilon_1 dt}|\tilde{\nu}_1,\; t\rangle + B(0;t_r)e^{i\int_{t_r}^{t} \varepsilon_2 dt}|\tilde{\nu}_2,\; t\rangle\;. \qquad (8.123)$$

At $t_f = \infty$,

$$\begin{aligned} \psi(\infty) &= A(0;t_r)e^{i\int_{t_r}^{\infty} \varepsilon_1 dt}(\cos\theta\;|\nu_e\rangle - \sin\theta\;|\nu_\mu\rangle) \\ &\quad + B(0;t_r)e^{i\int_{t_r}^{\infty} \varepsilon_2 dt}(\sin\theta\;|\nu_e\rangle + \cos\theta\;|\nu_\mu\rangle)\;, \end{aligned} \qquad (8.124)$$

where $|\tilde{\nu}_i,\; \infty\rangle = |\nu_i\rangle$ and $|\nu_i\rangle = U^\dagger|\nu^\alpha\rangle$ are used. Then,

$$\langle\nu_e|\psi(\infty)\rangle = A(0;t_r)\;\cos\theta\;e^{i\int_{t_r}^{\infty} \varepsilon_1 dt} + B(0;t_r)\;\sin\theta\;e^{i\int_{t_r}^{\infty} \varepsilon_2 dt} \qquad (8.125)$$

and

$$\begin{aligned} P_{\nu_e\to\nu_e} &= |A|^2\cos^2\theta + |B|^2\sin^2\theta \\ &\quad + 2|AB|\;\cos\theta\sin\theta\cos\left[\int_{t_r}^{\infty}(\varepsilon_1 - \varepsilon_2)dt + \Omega\right] \end{aligned} \qquad (8.126)$$

with $\Omega = \arg A^*B$. The last term vanishes if we take an average over the detector position (or the beam energy spread). Inserting expressions for $A(0;t_r)$ and $B(0;t_r)$ [see (8.122)], we obtain

$$\begin{aligned} \langle P_{\nu_e\to\nu_e}\rangle_\infty &= |A|^2\cos^2\theta + |B|^2\sin^2\theta \\ &= \frac{1}{2} + \frac{1}{2}(|\alpha|^2 - |\beta|^2)\cos2\tilde{\theta}\cos2\theta \\ &\quad -|\alpha\beta|\;\sin2\tilde{\theta}\cos2\theta\cos[\int_0^{t_r}(\varepsilon_1 - \varepsilon_2)dt + \omega]\;, \end{aligned} \qquad (8.127)$$

where $\omega = \arg \alpha^* \beta$. The last term also vanishes if we take an average over the position of neutrino production. Identifying

$$|\beta|^2 = P_{\mathrm{f}} ,\qquad (8.128)$$

we obtain (8.116), i.e.,

$$\langle P_{\nu_e \to \nu_e} \rangle_{i,\ \infty} = \frac{1}{2} + \left(\frac{1}{2} - P_{\mathrm{f}} \right) \cos 2\theta \cos 2\tilde{\theta} \ . \qquad (8.129)$$

In particular, for $n_e \to \infty$ $(\cos 2\tilde{\theta} \to -1)$,

$$\langle P_{\nu_e \to \nu_e} \rangle_{i,\ \infty} = \sin^2\theta + P_{\mathrm{f}} \cos 2\theta \ , \qquad (8.130)$$

in agreement with (8.117).

8.6.3 Derivation of the Landau–Zener Formula

We recapitulate the derivation of P_{f} following Zener [1283]. Let us write (8.101) in the form

$$H\psi = \begin{pmatrix} \epsilon_1 & \epsilon_{12} \\ \epsilon_{12} & \epsilon_2 \end{pmatrix} \psi, \qquad (8.131)$$

where

$$\begin{aligned}
\epsilon_1 &= [a(t) - \cos 2\theta]\Delta m^2/4E \ , \\
\epsilon_2 &= \cos 2\theta\, \Delta m^2/4E \ , \\
\epsilon_{12} &= \sin 2\theta\, \Delta m^2/4E \ ,
\end{aligned} \qquad (8.132)$$

ignoring unimportant constant terms. Here, $a(t) = \sqrt{2}G_F n_e(t)$ is taken as a function of time. Taking an orthonormal basis (c_1, c_2), the Schrödinger equation $(H - i\partial/\partial t)\psi = 0$ is written

$$\left(H - i\frac{d}{dt} \right) [c_1(t)e^{-i\int \epsilon_1 dt} + c_2(t)e^{-i\int \epsilon_2 dt}] = 0. \qquad (8.133)$$

Using (8.131), (8.133) becomes

$$\begin{aligned}
i\frac{dc_1}{dt} &= \epsilon_{12} e^{-i\int(\epsilon_2-\epsilon_1)dt} c_2 \ , \\
i\frac{dc_2}{dt} &= \epsilon_{12} e^{-i\int(\epsilon_1-\epsilon_2)dt} c_1 \ .
\end{aligned} \qquad (8.134)$$

The boundary condition is that ψ is in the eigenstate of $|\nu_e\rangle = |c_1\rangle$, i.e., on the upper branch in Fig. 8.6 at $t \to \infty$ $(n_e \to \infty)$,

$$\begin{aligned}
|c_1(-\infty)| &= 1 \ , \\
c_2(-\infty) &= 0 \ .
\end{aligned} \qquad (8.135)$$

The problem is to find the probability that ψ jumps from the upper to the lower branch in the resonance region, i.e., that ψ is in the state $|\nu_e\rangle = |c_1\rangle$ at $t \to +\infty$,

$$P = |c_1(\infty)|^2 = 1 - |c_2(\infty)|^2. \tag{8.136}$$

We now eliminate c_1 from (8.134),

$$\frac{d^2 c_2}{dt^2} + \left[i(\epsilon_1 - \epsilon_2) - \frac{\dot{\epsilon}_{12}}{\epsilon_{12}} \right] \frac{dc_2}{dt} + \epsilon_{12}^2 c_2 = 0. \tag{8.137}$$

We assume that $n_e(t)$ varies linearly in t in the resonance region, which is taken as $t = 0$:

$$n_e(t) = n_e^0 + \dot{n}_e^0 t, \tag{8.138}$$

where n_e^0 satisfies the resonance condition, $\sqrt{2} G_F n_e^0 = (\Delta m^2 / 2E) \cos 2\theta$. Writing

$$\epsilon_1 - \epsilon_2 = \sqrt{2} G_F \dot{n}_e^0 t \equiv \alpha t, \tag{8.139}$$

and putting

$$c_2(t) = e^{-\frac{i}{2} \int (\epsilon_2 - \epsilon_1) dt} U(t), \tag{8.140}$$

(8.137) reads

$$\frac{d^2 U}{dt^2} + \left[\epsilon_{12}^2 - \frac{i}{2} \alpha + \frac{1}{4} (\alpha t)^2 \right] U = 0. \tag{8.141}$$

Upon changing variables,

$$z = \sqrt{\alpha} \, e^{-i\pi/4} t \tag{8.142}$$

and

$$n = i\epsilon_{12}^2 / \alpha \, , \tag{8.143}$$

(8.141) becomes the Weber equation [1287],

$$\frac{d^2 U}{dz^2} + \left(n + \frac{1}{2} - \frac{z^2}{4} \right) U = 0 \, . \tag{8.144}$$

The solution is called the Weber function, $D_{-n-1}(\pm iz)$. Because $D_{-n-1}(iz)$ behaves asymptotically, $D_{-n-1}(iz) \to 0$ as $z \to \infty e^{-\frac{3}{4}\pi i}$ or $\infty e^{-\frac{\pi}{4} i}$,

$$U = A_+ D_{-n-1}(-iz) \tag{8.145}$$

satisfies the required boundary condition, $c_2 \sim U \to 0$, as $t \to -\infty$. Here, A_+ is the normalisation factor that is determined by $|c_1(-\infty)| = 1$. Using the second equation of (8.134) and the asymptotic behaviour of $D_{-n-1}(iRe^{-\pi i/4})$ as $R \to \infty$,

$$R_{-n-1}(iRe^{-\pi i/4}) \sim e^{-\frac{\pi}{4}(n+1)i} e^{-iR^2/4} R^{-n-1}, \tag{8.146}$$

we have

$$c_1(\infty) = \frac{\sqrt{\alpha}}{\epsilon_{12}} A_+ e^{-\frac{\pi}{4}\nu} e^{-\frac{3}{4}\pi i - i\nu \ln(-\sqrt{\alpha}t)}. \tag{8.147}$$

The normalisation condition is then given by

$$|A_+| = \sqrt{\nu} e^{-\frac{\pi}{4}\nu}, \tag{8.148}$$

where

$$\nu = -in = \epsilon_{12}^2/\alpha. \tag{8.149}$$

For $t \to +\infty$, we pick up the leading term of the asymptotic expansion of $D_{-n-1}(iRe^{3\pi i/4})$ as $R \to \infty$,

$$D_{-n-1}(iRe^{3\pi i/4}) \sim \frac{\sqrt{2\pi}}{\Gamma(n+1)} e^{\frac{\pi}{4}in} e^{iR^2/4} R^n + e^{\frac{3}{4}\pi i(n+1)} e^{-iR^2/4} R^{-n-1}. \tag{8.150}$$

Then,

$$\begin{aligned} |c_2(\infty)|^2 &= \nu e^{-\frac{\pi}{2}\nu} \frac{\sqrt{2\pi}}{[\Gamma(i\nu+1)\Gamma(-i\nu+1)]^{1/2}} e^{-\frac{\pi}{2}\nu} \\ &= 2\sinh(\pi\nu) e^{-\pi\nu} \\ &= 1 - e^{-2\pi\nu}, \end{aligned} \tag{8.151}$$

where

$$\nu = \frac{1}{4} \frac{\Delta m^2}{2E} \frac{\sin^2 2\theta}{\cos 2\theta} \frac{1}{d\ln n_e/dr} \equiv \frac{1}{4}\gamma \tag{8.152}$$

from (8.132), (8.139), (8.143) and the resonance condition. Therefore, we obtain

$$P_{\mathrm{f}} = \exp\left(-\frac{\pi}{2}\gamma\right),$$

the desired result (8.114). The Landau–Zener formula applies when the variation in density is linear in r and is accurate unless the mixing angle is close to $\pi/4$, which corresponds to zero matter density. Practically, however, this gives quite an accurate result for most of the cases relevant to the solar neutrino problem.

A number of different derivations have been discussed in the literature. The analytic solution is known for the exponential density distribution $n_e \propto \exp(-r/r_0)$ [1288, 1289], for which

$$P_f = \frac{e^{\gamma'} \cos^2 \theta - 1}{e^{\gamma'} - 1} \tag{8.153}$$

where $\gamma' = \pi r_0 \Delta m^2/E$. This formula is applicable for any value of θ. The analytic solution is also known for the $n_e \propto 1/r$ profile [1290], etc.; see [1286] for a review. It is shown that these classes of models are written using a hypergeometric differential equation [1291]; see also [1280].

8.6.4 Slab Model

It would be instructive to consider the case in which $\sin\theta$ is small as a typical example of a nonadiabatic neutrino conversion [1292]. In this case, neutrino conversion takes place in a very narrow region around the position of resonance; outside this region, a neutrino propagates without oscillation since $\sin 2\tilde{\theta}$ is also very small, as seen in (8.104).

Writing the energy matrix of (8.101) in the form

$$\begin{pmatrix} A & B \\ B & C \end{pmatrix} \tag{8.154}$$

and eliminating the ν_μ component, (8.101) is written in the form

$$\ddot{P} - i(A - C)\dot{P} + B^2 P^2 = 0, \tag{8.155}$$

where $P(t)$ is defined by

$$\nu_e(t) = P(t) \exp\left[-i \int_0^t A(t')dt'\right]. \tag{8.156}$$

Here, we assume that ν_e is created at $t = 0$. The probability of finding ν_e at time t is given by

$$P(\nu_e \to \nu_e; t) = |P(t)|^2. \tag{8.157}$$

Inside the resonance region $(A = C)$, $P(t)$ obeys

$$\ddot{P} + B^2 P = 0. \tag{8.158}$$

Assuming $P = e^{i\alpha}$ when ν_e enters the resonance region, we find

$$P(t) = e^{i\alpha} \cos[B(t - t_0 + \delta t_0)], \quad t_0 - \delta t_0 \le t \le t_0 + \delta t_0, \tag{8.159}$$

where t_0 corresponds to the time when the neutrino arrives at the position of the resonance and $2\delta t_0$ is the time interval for a neutrino propagating through the resonance region. The time interval $\delta t_0 = \delta R_0$ was calculated in (8.111) as $[n_e/(dn_e/dr)]\mathrm{tg}2\theta$. The probability of finding ν_e at $t(> t_0 + \delta t_0)$ is then

$$P(\nu_e \to \nu_e;\ t > t_0) = \cos^2(2B\delta t_0)$$
$$= \cos^2\gamma, \tag{8.160}$$

where γ was defined by (8.115). We note that the distance $2\delta r_0$ across which maximal mixing $\sin^2 2\tilde{\theta} = 1$ occurs is assumed to be small compared with the oscillation length at the resonance point. This condition is

$$2\delta r_0 \ll \tilde{\ell}_{\mathrm{osc}} \equiv \frac{4\pi E}{\Delta m^2 \sin 2\theta} = \frac{\pi}{B}, \tag{8.161}$$

i.e.,

$$\frac{\Delta m^2}{2E}\frac{\sin^2 2\theta}{\cos 2\theta}\left(\frac{n_e}{dn_e/dr}\right)_{\text{res}} \equiv \gamma \ll \pi. \qquad (8.162)$$

Equation (8.160) is compared with the result of the Landau–Zener approximation (for $\sin^2\theta \sim 0$) (8.114), i.e., $P \simeq \exp(-\pi\gamma/2)$. We see that (8.160) agrees with (8.114) within 30%, as long as $0 \le \gamma \lesssim 1.2$, or equivalently, $1 \ge P_f \gtrsim 0.15$.

8.6.5 The MSW Effect in the Solar-Neutrino Problem

The MSW effect was proposed to solve the solar-neutrino problem. The density at the centre of the Sun is equivalent to $\rho_c \simeq 100\,\text{g}\,\text{H}\,\text{cm}^{-3}$ for electrons. The radial profile of the electron density is close to exponential and is described well for $0.1 \lesssim R/R_\odot \lesssim 0.9$ (see Fig. 4.17d) by

$$\rho_e(R) \approx 250 \exp[-10.5(R/R_\odot)] \text{ g cm}^{-3} . \qquad (8.163)$$

Numerically, the resonance condition (8.107) is

$$\Delta m^2 = 1.52 \times 10^{-5}\text{eV}^2(E/1\,\text{MeV})(\rho/100\,\text{g H cm}^{-3})\frac{1}{\cos 2\theta}. \qquad (8.164)$$

The adiabatic condition (8.112) is

$$\Delta m^2 \sin^2 2\theta > 5.7 \times 10^{-10}\text{ eV}^2(E/1\,\text{MeV})\cos 2\theta\left(\frac{d\ln\rho}{dr}\right)R_\odot. \qquad (8.165)$$

Hence, the MSW effect would affect the propagation of neutrinos produced in the core of the Sun if $\Delta m^2 \lesssim 1.5 \times 10^{-4}\,\text{eV}^2$ (for $E \lesssim 10$ MeV) and $\Delta m^2 \sin^2 2\theta \gtrsim 2 \times 10^{-9}\,\text{eV}^2$ for $E \gtrsim 0.3$ MeV (the region can be wider when θ is close to $45°$). The experiments indicate that ν_e produced in the Sun are only partially converted into a combination of ν_μ and ν_τ [see (8.99)]: the parameters $(\Delta m^2, \sin^2 2\theta)$ should be located near the boundaries of the MSW triangle. The attractive feature of this explanation *was* that a large suppression of neutrino captures results even from a reasonably small mixing angle between two neutrinos and that it does not require particular fine-tuning of the parameters (the former reason, which has made this solution very attractive, is no longer important!). It can naturally explain the energy-dependent suppression pattern observed in the three experiments by appropriately choosing the mixing parameters. For its attractiveness, a large number of detailed analyses have been made with increasingly accurate and elaborate input data, more elaborate statistical methods, and also with different emphases [211, 213, 1281, 1282, 1292–1295, 1272–1274]. The calculations have generally yielded a well-convergent answer, which does not depend much on the method or approximations used.

Semirealistic calculations using the Landau–Zener (LZ) formula give a reasonably accurate approximation for neutrino propagation in the Sun. The

iso-SNU contours in the $\Delta m^2 - \sin^2 2\theta$ plane obtained with the LZ formula agree well with those obtained by numerically integrating (8.101), within a few percent for $\sin^2 2\theta \lesssim 0.5$.

To explain the mechanism how the oscillation parameters are determined by the three experiments (^{37}Cl, water Č, and ^{71}Ga), we present in Fig. 8.12 one such semirealistic calculation for the data as of 1992, just after the first report from GALLEX [232]. In the region encircled by two thick curves, the ν_e flux is consistent with the Homestake ^{37}Cl experiment (capture rate was 29±3% times the predicted source flux) for the 90% CL The position of the horizontal branch agrees with (8.164) for $E \simeq 8$ MeV, the average energy of ^{8}B neutrinos. A wiggle along the oblique branch is caused by the MSW effect acting on ^{7}Be neutrinos at Δm^2 by a factor of 10 smaller than the main horizontal branch. The oblique line agrees with (8.165), and the vertical line represents a 30% ν_e survival, slightly inward of the 50% conversion line which is $\sin^2 2\theta = 1$.

The dashed curves are the 90% confidence contour from Kamiokande that measures $\nu e^- \rightarrow \nu e^-$ reactions with the recoil electron energy threshold of 7.5 MeV. The Kamiokande analysis includes the energy spectrum and the day–night effect. Note that $\nu e^- \rightarrow \nu e^-$ receives a contribution from the neutral-current-induced reaction, whose cross section is about 1/7.0 the charged-current reaction rate (see Table 3.6) and is not affected by neutrino oscillation. The (incomplete) horizontal branch lies slightly above that for
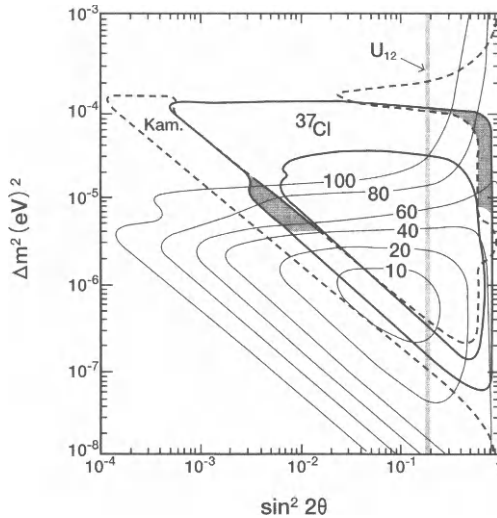
Fig. 8.12. 'MSW triangles' for the ^{37}Cl and water Čerenkov (Kam) experiments allowed at a 90% confidence level in the early 1990s. Iso-SNU contours are drawn for neutrino captures on ^{71}Ga. The two shaded regions are selected from the first report from the Gallex experiment. The quark mixing angle U_{12} is shown for comparison.

the ^{37}Cl experiment due to the fact that Kamiokande measures only a higher energy component of ^{8}B neutrinos. The displacement of the oblique line outwards compared with the ^{37}Cl contour is a result of lesser suppression in the Kamiokande flux measurement (36±7% after subtracting a 14% neutral-current contribution) [915]. The incomplete horizontal branch means that the central part is excluded by the neutrino energy spectrum, for which Kamiokande does not see any evidence of distortion above its threshold of 7.5 MeV (discussed in more detail below). We also see an excluded sector along the horizontal branch, which results from the absence of the day–night effect, as we discuss in the next section. When the constraint from Kamiokande is overlaid on that from Homestake, the solution on the horizontal branch is ruled out: the solution must be along the oblique branch (a nonadiabatic solution) below the ^{7}Be wiggle or along the vertical branch (vacuum-like oscillation).

Contours of capture rates on ^{71}Ga are displayed by thin curves. The horizontal branch of, say, 40 SNU (a one-third survival fraction), is located at Δm^2 that is 25 times smaller than the horizontal branch of the ^{37}Cl contour. By virtue of this large shift, iso-SNU contours of gallium capture rates grossly cross with those from the two other experiments. As a consequence, the solution can be determined allowing for discrete ambiguities if ^{71}Ga capture rates are measured. When the first report of GALLEX, 83±21 SNU, became available [232], two solutions were left, one on the oblique branch at $\sin^2 2\theta = 0.003 - 0.012$, $\Delta m^2 = (0.3 - 1) \times 10^{-5}$ eV^2, and the other on the vertical branch at $\sin^2 2\theta = 0.6 - 0.9$, $\Delta m^2 = (0.4 - 3) \times 10^{-5}$ eV^2. These two solutions, characterised by small and large mixing angles, are named 'small-mixing angle solution' (SMA) and 'large-mixing angle solution' (LMA) [1296]. There is one more possible solution, albeit of low probability, at the lower corner of the triangle, which is called 'LOW solution' (low mass, low probability) [1296]. These solutions changed little for the decade, despite much improvement in the input data, solar models, and calculational methods, until recent reports on the detailed neutrino spectrum and on the deuterium scattering measurement became available in the year 2001.[13]

---

[13] Let us remark a subtle difference between the Kamiokande and Super-Kamiokande data. In an earlier stage SMA seemed somewhat more favoured than LMA based on the data from Kamiokande, which indicated that the flux reduction measured by νe scattering is less than that for the chlorine experiment (this was particularly so with the result from Kamiokande III, the last phase of the Kamiokande experiment). This means that intermediate-energy neutrinos are more strongly reduced in agreement with SMA. Super-Kamiokande gives a larger (by 20%) reduction factor for high-energy ^{8}B neutrino flux (see Table 4.9). When the expected neutral-current contribution is subtracted, the flux reduction factor (0.31±0.02) is consistent with that of the chlorine experiment (0.34±0.03). This change has made the semienergy-independent flux reduction expected from LMA more favoured than that from SMA.

None of the mixing angles of the three solutions agrees with those for the quark mixing angle, whichever is U_{12} or U_{13}. As we shall see in the next chapter, this excludes the natural prediction from SO(10) grand unification, the only theoretically motivated prediction concerning the mixing angle known to date.

The notable feature of MSW neutrino conversion is that it gives a characteristic energy dependence in the neutrino conversion rate. The SMA shows strongly energy-dependent suppression: the ^{8}B neutrino flux is significantly reduced (by a factor of ≈ 2), and the ^{7}Be neutrino flux is even more strongly reduced (to <20%), whereas pp neutrinos receive little modification, as one can easily guess from the positions of the triangles. To make this explicit, we show in Figs. 8.13 and 8.14 the 'filter function' $P(\nu_e \to \nu_e)$ and the suppression pattern for typical parameter sets. The energy spectrum measured at Kamiokande ($E > 7.5$ MeV), though it was consistent with no energy variation, was not sufficient to rule out the SMA. This was later achieved by the SK experiment which attained a lower threshold at 5.5 MeV and much higher statistics. Although the energy dependence becomes somewhat modest on the left edge of the SMA region, the entire SMA region was excluded at $\gtrsim$95% confidence level. The suppression patterns for LMA and LOW are similar: all ν_e fluxes other than pp neutrinos are nearly uniformly reduced (it is like that expected with the averaged neutrino oscillation in vacuo, but the pp neutrino flux is less reduced).

In Fig. 8.13 we added the filter function for VAC. The figure shows that it is highly energy-dependent, but also is wildly Δm^2-dependent.
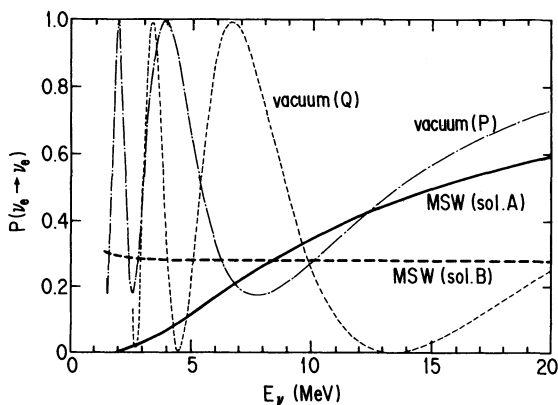
Fig. 8.13. Figure 29: Energy dependence of the filter function $P(\nu_e \to \nu_e)$ for the two MSW solutions (A: $\sin^2 2\theta = 0.008$, $\Delta m^2 = 5 \times 10^{-6}$ [SMA]; B: $\sin^2 2\theta = 0.8$, $\Delta m^2 = 1 \times 10^{-5}$ [LMA]) and for two choices of parameters for long-wavelength neutrino oscillation in vacuo: P: $\sin^2 2\theta = 0.83$, $\Delta m^2 = 6.4 \times 10^{-11}$; Q: $\sin^2 2\theta = 1.0$, $\Delta m^2 = 1.1 \times 10^{-10}$. The figure is taken from [1234].
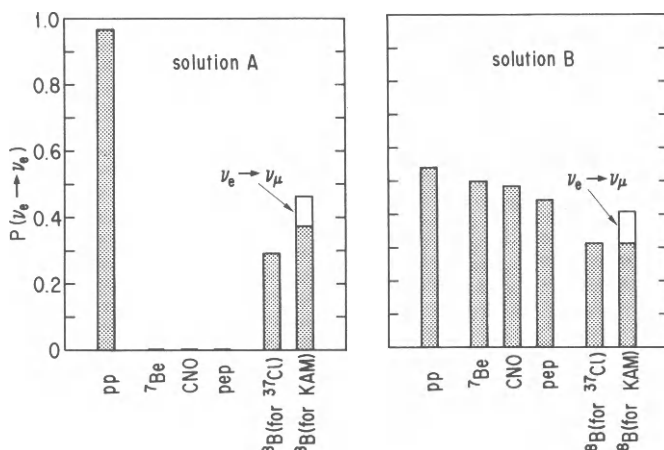
Fig. 8.14. Suppression patterns (filter functions, $P(\nu_e \to \nu_e)$) of each solar neutrino component for the two MSW solutions A and B (see Fig. 8.13). The contribution from ν_μ for the water Čerenkov detector, $P(\nu_e \to \nu_\mu) \times (1/7)$, is indicated by histograms without shading.

8.7 The Effect of Earth on Neutrino Propagation

The MSW effect may also take place for a neutrino propagating through Earth. In a certain range of neutrino parameters, the Earth effect flips ν_2 (ν_μ and ν_τ), converted from ν_e in the Sun, partially back to ν_e. Solar neutrinos propagate through Earth only during the night, and this conversion is observed as a day–night effect [1297]. The effect of Earth also takes place for atmospheric neutrinos [1277] and for a long-baseline neutrino experiment.

For Earth the resonance condition is satisfied if

$$\Delta m^2 \approx 0.8 \times 10^{-6} \, \text{eV}^2 (\rho Y_e \text{g cm}^{-3})(E/10\,\text{MeV}) \sec 2\theta \ , \qquad (8.166)$$

with $\rho = 3.5 - 13\,\text{g cm}^{-3}$ [1298] and the electron yield $Y_e = 1/2$ (the electron number per atomic number). The neutrino oscillation length on the resonance (see (8.108)) $\tilde{\ell}|_{\text{res}} = (4\pi E/\Delta m^2)(\sin 2\theta)^{-1} \simeq 2.5 \times 10^9 \, \text{cm}(\Delta m^2/10^{-6}\,\text{eV})^{-1}$ $(E/10\,\text{MeV}) \, (\sin 2\theta)^{-1}$ is comparable to the diameter of Earth $(1.3 \times 10^9 \, \text{cm})$; therefore, the effect is cut at

$$\tilde{\ell}|_{\text{res}} = \frac{4\pi E}{\Delta m^2} \frac{1}{\sin 2\theta} < 2\pi R_\oplus. \qquad (8.167)$$

We expect significant conversion in the region sandwiched by conditions (8.166) with $\rho \simeq 13\,\text{g cm}^{-3}$ and (8.167). Note that the slope of (8.167) on the $\Delta m^2 - \sin^2 2\theta$ plane is half that of the adiabatic condition (8.112).

Many calculations have been carried out for the day–night effect [1297]. In Fig. 8.15 we show the result of a numerical computation of the ^{8}B solar ν
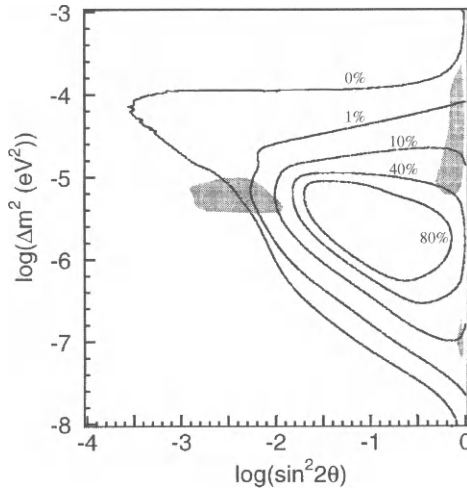
Fig. 8.15. Contours of the constant diurnal asymmetry $r = [(\text{night})-(\text{day})]/$ $[(\text{night})+(\text{day})]$ for ^{8}B solar neutrinos expected at Super-Kamiokande. Shaded regions are the three solutions, SMA, LMA, and LOW, but without imposing the constraints from the day–night effect and the spectrum.

flux [1299]. The contours represent the day–night asymmetry

$$r = 2[(\text{night flux}) - (\text{day flux})]/[(\text{night flux}) + (\text{day flux})] \,, \qquad (8.168)$$

which is equivalent to the conversion fraction for small r. The three solutions, LMA, SMA, and LOW, are also indicated in the figure. The current SK experiment gives [723]

$$r = 0.033 \pm 0.022 \pm 0.013 \,. \qquad (8.169)$$

The three solutions are located in the region where the day–night effect is small: only the bottom part of the LMA is cut by the 'absence' of the day–night effect.

Atmospheric neutrinos are, in principle, affected by Earth. For propagation of ν_μ, however, only the neutral current contributes, and the effect is the same for ν_μ and ν_τ, so that there is no net effect for $\nu_\mu - \nu_\tau$ oscillation. The situation is different if we consider $\nu_\mu \rightarrow \nu_s$ (sterile neutrino) oscillation since any interaction is absent for sterile neutrinos; the effect of neutral current on ν_μ becomes visible. For neutral-current interactions, the contributions from protons and electrons cancel, as seen in (3.242), leaving only neutrons as the source. Therefore, ρY_e in (8.166) is replaced by ρY_n. For the neutrino energy of 100 GeV, condition (8.166) matches $\Delta m^2_{\mu-\tau} \simeq 3 \times 10^{-3}$ and $\cos 2\theta \simeq 0.1$. The matter effect works to suppress $\nu_\mu - \nu_s$ oscillation for neutrinos that traverse Earth. The SK group compared zenith-angle dependences of $\nu_\mu - \nu_\tau$ oscillation and $\nu_\mu - \nu_s$ oscillation (see Fig. 8.14) [1263]. The difference is
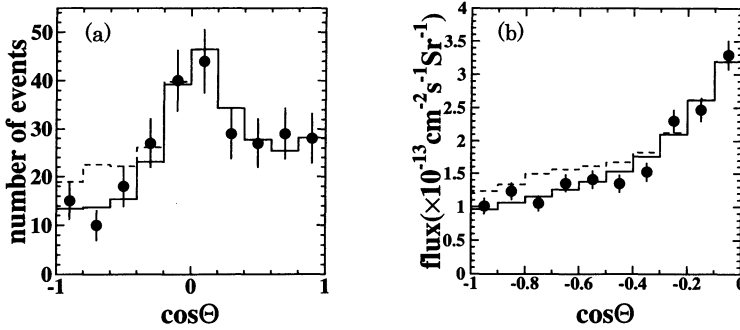
Fig. 8.16. Earth effect on atmospheric neutrinos observed at Super-Kamiokande. The figures show the zenith-angle distributions of (**a**) higher energy μ-like events (partially confined events) and (**b**) upward through-going muons. The *solid* histograms are expectations for $\nu_\mu - \nu_\tau$ oscillation where the Earth effect cancels; *dashed* show $\nu_\mu - \nu_s$ oscillation for which the Earth effect becomes apparent.

most clearly visible for upward through-going muons ($E_\nu \sim 100$ GeV), and the data disfavour oscillation into ν_s at 2.9σ. The effect is also visible in partially contained μ-like events ($E_\nu \sim 20$ GeV), which also disfavours $\nu_\mu - \nu_s$ oscillation at 2.3σ. Even at a lower energy, a preference for $\nu_\mu - \nu_\tau$ to $\nu_\mu - \nu_s$ is observed at 2.4σ when the sample is selected for multiring events to enrich neutral-current events. The combined analysis rejects oscillation into sterile neutrinos at a 99% confidence level.

The Earth effect may also be detected in high precision long-baseline neutrino oscillation experiments to be done in the future. The effect is small since the distance going through Earth is small, but this would give an effect competing with that of possible CP violation: matter acts as external fields and gives an effect similar to that of CP violation. This is discussed in Sect. 8.11.1 below.

Formalism. Although a rough feature of the Earth effect can be understood by (8.166) and (8.167), it may be useful to develop an approximate method for solving neutrino propagation through Earth analytically. We assume a constant density for Earth. Let us write the initial condition at the surface of Earth by a mixture of $|\nu_e >$ and $|\nu_\mu >$, i.e.,

$$\psi(0) = \alpha\psi_1(0) + \beta\psi_2(0) \quad (\alpha^2 + \beta^2 = 1), \tag{8.170}$$

where

$$\psi_1(0) = |\nu_e >= \begin{pmatrix} 1 \\ 0 \end{pmatrix},$$

$$\psi_2(0) = |\nu_\mu >= \begin{pmatrix} 0 \\ 1 \end{pmatrix}. \tag{8.171}$$

If we write

$$\begin{pmatrix} c_e \\ c_\mu \end{pmatrix} \equiv \exp\left[+i\int_0^t \sqrt{2}G_F n_e dt\right] \begin{pmatrix} \nu_e \\ \nu_\mu \end{pmatrix}, \tag{8.172}$$

the Schrödinger equation (8.101) is

$$i\frac{d}{dt}\begin{pmatrix} c_e \\ c_\mu \end{pmatrix} = [A\sigma_3 + B\sigma_1]\begin{pmatrix} c_e \\ c_\mu \end{pmatrix}, \tag{8.173}$$

with

$$A = \frac{1}{2}\left(\sqrt{2}G_F n_e - \frac{\Delta m^2}{2E}\cos 2\theta\right),$$

$$B = \frac{\Delta m^2}{4E}\sin 2\theta.$$

It is easy to solve this equation for $n_e = \text{const.}$ If we impose the boundary conditions $c_e(0) = 1$ and $c_\mu(0) = 0$, the solution is

$$c_e(t_f) = \cos\left(\frac{\pi t_f}{\tilde{\ell}}\right) - i\left(\frac{\tilde{\ell}}{\ell_0}\right)\sin\left(\frac{\pi t_f}{\tilde{\ell}}\right)\left(\frac{\ell_0}{\ell_N} - \cos 2\theta\right),$$

$$c_\mu(t_f) = -i\left(\frac{\tilde{\ell}}{\ell_0}\right)\sin\left(\frac{\pi t_f}{\tilde{\ell}}\right)\sin 2\theta, \tag{8.174}$$

where t_f is the epoch when the neutrino comes out of Earth; ℓ_0 and $\tilde{\ell}$ are the oscillation lengths in vacuum and in matter, defined by (8.58) and (8.108), respectively, and

$$\ell_N \equiv \frac{\sqrt{2}\pi}{n_e G_F}. \tag{8.175}$$

We note that if one solution is given by $\psi = (c_e, c_\mu)^T$, another solution that is orthogonal to ψ is given by $(-c_\mu^*, c_e^*)^T$. This is seen by taking the complex conjugate of (8.173),

$$-i\frac{d}{dt}\begin{pmatrix} c_e^* \\ c_\mu^* \end{pmatrix} = (A\sigma_3 + B\sigma_1)\begin{pmatrix} c_e^* \\ c_\mu^* \end{pmatrix}, \tag{8.176}$$

and by multiplying σ_2 from the left, i.e.,

$$+i\frac{d}{dt}\begin{pmatrix} -c_\mu^* \\ c_e^* \end{pmatrix} = (A\sigma_3 + B\sigma_1)\begin{pmatrix} -c_\mu^* \\ c_e^* \end{pmatrix}, \tag{8.177}$$

which has the same form as (8.173). We then take the two solutions to be ψ_1 and ψ_2.

The probability of finding ν_e after propagating through Earth is

$$
\begin{aligned}
P_{\nu_e} &= |\alpha\langle\nu_e|\psi_1\rangle|^2 + |\beta\langle\nu_e|\psi_2\rangle|^2 \\
&\quad + \alpha\beta^*\langle\nu_e|\psi_1\rangle\langle\nu_e|\psi_2\rangle^* + \alpha^*\beta\langle\nu_e|\psi_1\rangle^*\langle\nu_e|\psi_2\rangle \\
&= |\alpha|^2|c_e(t_f)|^2 + |\beta|^2|c_\mu(t_f)|^2 - \alpha\beta^* c_e(t_f)c_\mu(t_f) - \alpha^*\beta c_e^*(t_f)c_\mu^*(t_f).
\end{aligned}
\tag{8.178}
$$

The neutrino incident on Earth is generally written as

$$
\psi = \exp(iE_1 t + \phi)\cos\alpha|\nu_1\rangle + \exp(iE_2 t)\sin\alpha|\nu_2\rangle.
\tag{8.179}
$$

In the parameter region that concerns us, however, solar neutrinos that leave the Sun are almost in the mass eigenstate $|\nu_2\rangle$. For this case,

$$
\begin{aligned}
\alpha &= +\sin\theta\exp(iE_2 t), \\
\beta &= +\cos\theta\exp(iE_2 t).
\end{aligned}
\tag{8.180}
$$

Substitution of (8.174) into (8.178) yields

$$
\begin{aligned}
P_{\nu_e} &= \sin^2\theta\,|c_e(t_f)|^2 + \cos^2\theta|c_\mu(t_f)|^2 \\
&\quad - \sin\theta\cos\theta[c_e(t_f)c_\mu(t_f) + \text{h.c.}].
\end{aligned}
\tag{8.181}
$$

When the resonance condition is approximately satisfied, we have

$$
c_e(t_f) \simeq \cos\left(\frac{\sin 2\theta}{\ell_0}\pi t_f\right), \qquad c_\mu(t_f) = \sin\left(\frac{\sin 2\theta}{\ell_0}\pi t_f\right),
\tag{8.182}
$$

and then

$$
P_{\nu_e} = \frac{1}{2} + \frac{1}{2}\cos 2\theta\cos\left(\frac{2\sin 2\theta}{\ell_0}\pi t_f\right).
\tag{8.183}
$$

This yields the condition we have given in (8.167). The contour of the conversion probability is obtained by plotting (8.181).

Matter effect for more than two layers.   Earth consists of several layers of different densities. The density of the crust (about $10\,\text{km}$ thick) is about $3\,\text{g cm}^{-3}$. Beneath the crust, the density of the mantle gradually increases to $5.5\,\text{g cm}^{-3}$, and then it jumps to $10\,\text{g cm}^{-3}$ at the surface of the core, about $3500\,\text{km}$ from the centre of Earth. At the centre the density is about $13\,\text{g cm}^{-3}$. There are a number of models proposed for the density profile [1298] based on seismological data, and they agree with each other, except for some differences in the inner core (see [1300] for a comparison of models).

   When the matter consists of two layers of different densities, there appears a 'resonant enhancement' mechanism for neutrino conversion [1301]. In reality, the effect is small (a few percent at most) as it is smeared out by

the spread of neutrino energies, but let us briefly discuss the mechanism for theoretical interest.

We assume that Earth consists of two layers of constant densities, ρ' and ρ'' with electron yields, Y'_e and Y''_e, and calculate the probability of the $\nu_\mu \to \nu_e$ transition, $P_{\nu_\mu \to \nu_e}$.

The time evolution of the neutrino states in a single layer is given by solving (8.173),

$$\begin{bmatrix} c(t)_e \\ c(t)_\mu \end{bmatrix} = \left(\cos\phi - i\sigma_i\Theta^i_{\mathrm{m}}\sin\phi\right) \begin{bmatrix} c(0)_e \\ c(0)_\mu \end{bmatrix} \tag{8.184}$$

with

$$\phi = \frac{1}{2}\Delta E t \tag{8.185}$$

and

$$\Theta^1_m = \sin2\theta_{\mathrm{m}}, \quad \Theta^2_m = 0, \quad \Theta^3_m = -\cos2\theta_{\mathrm{m}}. \tag{8.186}$$

Here, θ_m is the mixing angle in matter defined in (8.106), (8.107) and $\Delta E = 2\pi/\tilde{\ell}$ with $\tilde{\ell}$ the oscillation length in matter defined in (8.111). We then get

$$P_{\mu \to e} = |\sin2\theta_{\mathrm{m}}\sin\phi|^2. \tag{8.187}$$

The maximal transition occurs when $\Delta E t = \pi(2k+1)$, where k is an integer.

For two constant-density layers, the time evolution is given by

$$\begin{bmatrix} c(t)_e \\ c(t)_\mu \end{bmatrix} = \left(\cos\phi'' - i\sigma_i\Theta''^i_{\mathrm{m}}\sin\phi''\right)\left(\cos\phi' - i\sigma_i\Theta'^i_{\mathrm{m}}\sin\phi'\right) \begin{bmatrix} c(0)_e \\ c(0)_\mu \end{bmatrix} \tag{8.188}$$

with

$$\phi' = \frac{1}{2}\Delta E't', \quad \phi'' = \frac{1}{2}\Delta E''t'' \tag{8.189}$$

and

$$\begin{aligned} \Theta'^1_m &= \sin2\theta'_{\mathrm{m}}, \quad \Theta'^2_m = 0, \quad \Theta'^3_m = -\cos2\theta'_{\mathrm{m}}, \\ \Theta''^1_m &= \sin2\theta''_{\mathrm{m}}, \quad \Theta''^2_m = 0, \quad \Theta''^3_m = -\cos2\theta'_{\mathrm{m}}, \end{aligned} \tag{8.190}$$

where θ'_m and θ''_m are the mixing angles in the first and second layers and E' and E'' are written with the oscillation lengths in the two layers as before; t' and t'' are the time intervals of neutrinos passing through the first and second

layers. We see by simple algebra that the transition probability becomes maximal

$$P^{\max}_{\nu_\mu \to \nu_e} = |\sin(2\theta''_m - 2\theta'_m)|^2 \tag{8.191}$$

when $\Delta E't' = \pi(2k'+1)$ and $\Delta E''t'' = \pi(2k''+1)$.

An extension to the more realistic case of three constant-density layers is straightforward. When the first and third layers correspond to the mantle and the second to the core, we obtain by a simple calculation the transition probability for $\nu_\mu \to \nu_e$ as [1301]

$$P^{\max}_{\nu_\mu \to \nu_e} = |\sin(2\theta''_m - 4\theta'_m)|^2. \tag{8.192}$$

We see that $P_{\nu_\mu \to \nu_e} \simeq O(1)$ even outside the MSW resonance region.

8.8 Solar Neutrino Analysis: Latest Results

Two recent experiments significantly advanced the solutions of the solar neutrino problem. One of them is information on the precise energy spectrum for the ^{8}B neutrino flux from SK. The observation does not show any spectral distortion from 5.5 to 13 MeV [1302,723]. In addition, statistics became higher for the absence of the the day–night effect. These results both act to exclude an inner region of the MSW triangle. The analysis by the SK group excluded SMA (and VAC) at 2σ (95% CL), leaving LMA as the only solution allowed at $< 90\%$ confidence [1272].

The other is a report from the SNO experiment which measures $\nu_e + d \to e^- + p + p$ for ^{8}B neutrinos for the same energy region as the SK measures [235]. The result shows that the neutrino flux inferred from the $\nu_e + d \to e^- + p + p$ reaction rate is smaller than that derived from $\nu + e \to \nu + e$ at SK at 3.3σ. This difference is ascribed to the neutral-current-induced interaction of neutrino electron scattering, which is unaffected by oscillation. From the difference the SNO authors inferred that the source ν_e flux is $\phi(^8\text{B}) = (5.44 \pm 0.99) \times 10^6$ cm^{-2} s^{-1}, which is in good agreement with the prediction of the standard solar model, see Table 4.5. This is the first active evidence that shows the action of neutrino oscillation. The result combined with the other flux measurements leaves a relatively inner part (with respect to the triangle) of the solutions as favoured parameters, which for SMA is opposite to the result from the SK spectral analysis. The combined constraints thus exclude SMA at more than 3σ (99.73% CL). The LMA solution is unaffected by the SNO results.

Figure 8.17 shows the allowed region in $\Delta m^2 - \text{tg}^2\theta$ plane taken from Fogli et al.'s analysis [1273] before and after the two pieces of data we discussed become available. We take $\sin^2\theta$ as the abscissa rather than $\sin^2 2\theta$, allowing for $\theta > 45°$, since the region that is interesting to us includes the
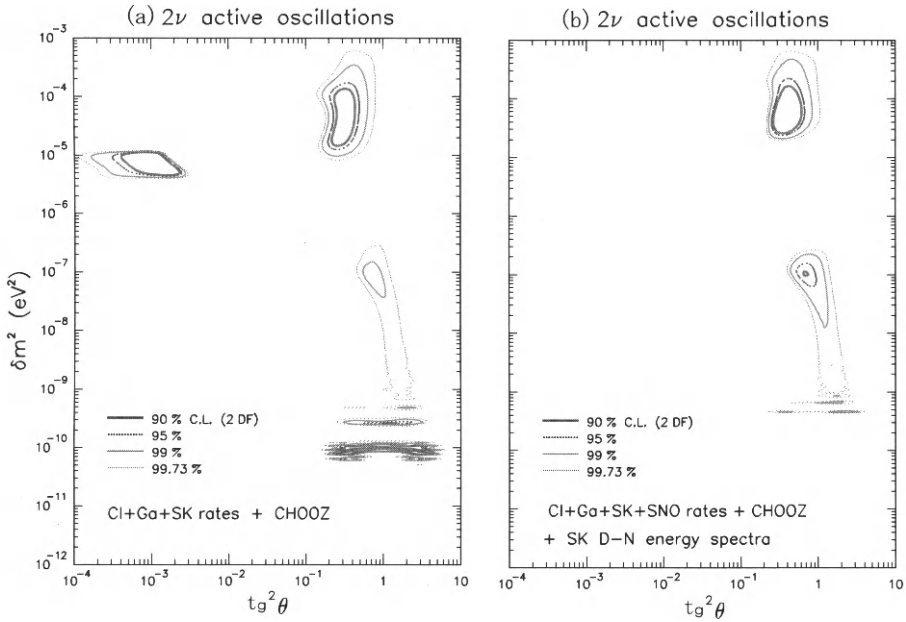
Fig. 8.17. Neutrino mixing parameters allowed by solar neutrino experiments: (a) the constraints derived using only neutrino reaction rates with ^{37}Cl, SK, and ^{71}Ga (with weak constraints from the CHOOZ experiment); (b) full analysis including the day and night spectra from SK and the SNO rates. After [1273].

nearly maximal mixing case. We usually implicitly assume $m_{\nu_1} < m_{\nu_2}$, but $\theta > 45°$ means that $m_{\nu_1} > m_{\nu_2}$, where ν_1 and ν_2 are neutrinos that smoothly continue to ν_e and ν_μ, respectively, for $\theta \to 0$. Table 8.2 demonstrates how the favoured parameter ranges are selected with new experiments, taking the analysis of Fogli et al. In the first column only the capture rate information from ^{37}Cl, SK, and ^{71}Ga experiments is taken. In the second column, full day and night spectral information from SK is included in addition. The numbers in the third column correspond to the state-of-the-art full analysis using all available information, including the SNO results. In sum the best favoured from the current experiments is LMA. The LOW solution is also viable (in fact it became more favoured than ever), but marginally at 90%: the allowed parameter region at 90% is close to a point. The VAC solution (large n) is excluded to the 99% confidence level of the experiment. SMA and low n VAC (='just-so') are excluded at more than 3σ. Another possibility is the parameters that are located between LOW and VAC (called quasi-VAC), $\Delta m^2 > 5 \times 10^{10}$ eV^2, where oscillation in vacuo is affected by matter effects [1303]: they are allowed, however, at only 3σ (99.73% confidence). The mixing parameters of LMA are (at 90%)

$$\sin^2 2\theta = 0.77 - 0.84, \quad \Delta m^2 = (2.6 - 16) \times 10^{-5} \text{ eV}^2, \qquad (8.193)$$

Table 8.2. Neutrino oscillation solutions of the solar neutrino problem. Numbers are taken from figures of [1273].

Solution	Rate only (before SNO)	Rate (w/o SNO) + SK day-night spectra	Full data (with SNO rate)
SMA	<90%	99%	Out
LMA	<90%	<90%	<90%
LOW	99%	95%	90%
Quasi-VAC	99.73%	99%	99.73%
VAC (large n)	90%	99%	99%
VAC (just-so)	Out	99.73%	Out

and for LOW,

$$\sin^2 2\theta \simeq 0.84, \ \Delta m^2 \simeq 1.1 \times 10^{-7} \, \text{eV}^2. \tag{8.194}$$

Note that maximal mixing $\sin^2 2\theta = 1$ is allowed only at 3σ for LMA and 2σ for LOW. $m_{\nu_1} > m_{\nu_2}$ is allowed only for VAC beyond 2σ of the experiment.

Ongoing and future experiments. All evidence we gathered indicates that neutrino oscillation is the solution of the long-standing solar neutrino problem, and we are now left with only two solutions as the most likely possibilities. Let us discuss what we can learn from on-going experiments and those being prepared, and what should be done to determine the solution uniquely.

The first to mention is the further experiment at Sudbury. It aims to observe not only charged-current reactions, but also neutral-current reactions via $\nu + d \rightarrow \nu + p + n$. It is an important proof that this direct measurement of the neutral current yields the flux which agrees with that inferred from the difference of $\nu + d \rightarrow e + p + p$ and $\nu + e \rightarrow \nu + e$.

We note that some of important pieces of information to distinguish among oscillation solutions to date come from null results (day–night effect, spectral distortion). What we really want to see is the unique feature that characterises each solution. The LMA solution would be actively verified by the KamLAND experiment [543], which is a 1000-ton liquid scintillator for observing, first of all, antineutrinos from nuclear power plants. The Kamioka experimental site is about 100–250 km away from the area where many nuclear power stations are situated, i.e., $\langle L/E \rangle \sim 5 \times 10^{-5} \, (\text{eV})^2$ which is just ideal for testing the oscillation of $\bar{\nu}_e$ in vacuo for the parameters of LMA. It is hoped that systematic errors will be no more than a few percent and that the experiment for two years of operation will accurately pin down the oscillation parameters. There is no sensitivity, however, for SMA or LOW in this experiment.

372   8 Generation Mixing of Neutrinos
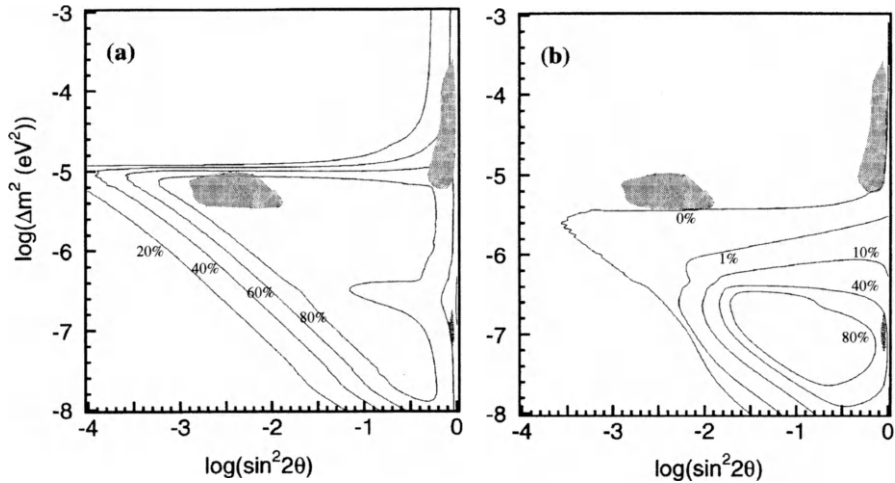
Fig. 8.18. (a) Reduction fraction for ^{7}Be solar neutrino flux due to the MSW effect. (b) Day–night asymmetry for ^{7}Be solar neutrino flux. The contours are for $r = 80\%, 40\%, 10\%, 1\%$, and 0%. Shaded regions are the three solutions, SMA, LMA, and LOW, but without imposing the constraints from the day–night effect and the spectrum.

SMA is strongly disfavoured by the current data, but if it were a real solution for some reason, the best signal is the suppression of the ^{7}Be flux to $<20\%$ of the predicted value (see Figure 8.18a).[5] The data will be obtained from Borexino, a 300-ton liquid scintillator aiming to detect low energy νe scattering constructed at the Gran Sasso Underground Laboratory [919],[6] or the second phase of KamLAND.

The LOW solution is actively explored by the day–night effect for ^{7}Be neutrino flux. For the region of the LOW solution we expect $> 40\%$ variation between night and day observations (see Figure 8.18b). Borexino and Kam-LAND are real-time detectors, so that this test can be carried out, once they detect ^{7}Be neutrinos. We consider that the VAC solution is ruled out. If it were the solution, however, it gives rise to a substantial seasonal effect in the ^{7}Be neutino flux, as we discussed in Sect. 8.5.4.

Insofar as we are on the right track, we may not need measurements of pp neutrinos, which are more demanding than those of ^{7}Be neutrinos, at least for the purpose of neutrino physics. These experiments would have vital

---

[5] In the low Δm^2 region of the LMA solution, the ^{7}Be neutrino flux becomes $>20\%$ of the solar model value, but this is the region that is already excluded by the absence of the day–night effect in the SK experiment.

[6] Borexino is not suitable for the reactor antineutrino experiment to test the LMA solution. The reactors are too far (~ 700 km) from the Gran Sasso Laboratory. Even if this experiment is carried out, the Δm^2 range that can be explored is in the region that is already excluded by the absence of the day–night asymmetry in SK.

importance only when some of the experiments discussed above would result in a surprise. The indicators we discussed here are summarised in Table 8.3, where crosses stand for active indicators for each solution.

Table 8.3. Capability of various types of neutrino experiments to give unique signatures for the four solutions of the solar neutrino problem.

	LMA	SMA	LOW	VAC
KamLAND/reactor $\bar{\nu}_e$	X			
^{7}Be flux		X		
^{7}Be seasonal				X
^{7}Be day/night			X	
pp day/night			X	

8.9 Other Applications of the MSW Effect

Supernova Neutrinos.   Supernova neutrinos arise dominantly from pair creation. So, almost equally abundant ν_e and ν_μ (and ν_τ) interchange or undergo mixing under the matter effect. This generally modifies the energy spectrum of neutrinos since the effective temperatures of ν_μ and ν_τ are higher. Oscillations, however, do not affect supernova dynamics because the level crossing for ν happens only in the outer layer of the star, which has little to do with supernova, and the state inside the core (ν or $\bar{\nu}$) hardly mixes with other states. The MSW effect may be seen only in the emergent neutrino flux.

Walker and Schramm considered that antineutrino fluxes are unchanged, whereas neutrino fluxes are modified due to interchange of flavours (assuming $m_{\nu_e} < m_{\nu_\mu} < m_{\nu_\tau}$) [1304]. However, this is not quite so for large mixing angles. Antineutrinos emergent from the surface of stars are always in the mass eigenstate. This means that the energy of $\bar{\nu}_e$ becomes higher if the neutrino mixing is large because the fraction of $\sin^2 \theta$ in the $\bar{\nu}_2$ flux is $\bar{\nu}_e$, as discussed by Wolfenstein [1305] (a similar effect is expected for a small mixing angle if neutrino mass shows inverted hierarchy [1306]). Smirnov, Spergel, and Bahcall [1307] carried out a detailed analysis and claimed that large mixing between ν_e and ν_μ is excluded for $10^{-7} < \Delta m^2 < 10^{-4}$ (eV)^2 because the energy of ν_e becomes too high compared with the observation of neutrinos from SN1987A [757,758]. This analysis, however, depends upon the reliability of the calculated source neutrino spectrum, but also ignored the Earth effect. The Earth effect must be taken into account for large mixing, as pointed out earlier in [1308] (see also [1306]). In fact, Jegerlehner et al. [1309]

showed that the effect pointed out by Smirnov et al. is diminished if the Earth effect is taken into account (still assuming that the representative SN neutrino spectrum is correct). We hardly have any limits on the mixing parameters from the observation of SN1987A. Lunardini and Smirnov [1310] considered the possibility that the difference in the neutrino spectra of SN1987A observed at Kamiokande [757] and IMB [758] (see Fig. 4.22) may be ascribed to different Earth effects at the two sites. This makes the agreement of the two temperatures somewhat better but does not solve the problem completely.

Neutrinos from the initial dileptonisation burst consist entirely of ν_e, for which we would expect a large effect [1311]. We expect half the neutrinos to convert into the combination of ν_μ and ν_e under large mixing. With the LMA solution, however, the converted ν_μ and ν_τ largely flip back to ν_e by the Earth effect. The detection of a dileptonisation burst would show that it consists of ν_e, ν_μ and ν_τ if a supernova takes place on the day side, but of increasing ν_e if it happens on the other side of Earth. The observation of both charged and neutral current reactions is crucial for this test.

Neutrinos in the early Universe. The MSW resonance effect works only for ν_e but not for $\bar{\nu}_e$ (or vice versa if $\theta > 45°$), so it may create asymmetry in the abundance of ν_e and $\bar{\nu}_e$. This would disturb the standard calculation of nucleosynthesis [1312]. Langacker et al. [1313] claimed that such asymmetry is created, but it is very small (since the initial lepton and baryon asymmetry is very small) and hence its effect on nucleosynthesis is negligible. Enqvist et al. [1314] showed that asymmetry itself is not created if the finite-temperature effect is properly taken into account. In a hot plasma, the electron neutrino feels the potential [533, 1314],

$$V_e \simeq \sqrt{2} G_F n_\gamma(T) \left(\delta N - \gamma \frac{T^2}{m_W^2} \right) , \qquad (8.195)$$

where $n_\gamma(T)$ is the number density of photons, δN is the particle asymmetry normalised by the photon number $\delta N_i = (N_i - N_{\bar{i}})/N_\gamma$,

$$\delta N = (1/2 + 2\sin^2 \theta_W)\delta N_e + (1/2 - 2\sin^2 \theta_W)\delta N_p$$

$$-\frac{1}{2}\delta N_n + 2\delta N_{\nu_e} + \delta N_{\nu_\mu} + \delta N_{\nu_\tau} \qquad (8.196)$$

from (3.239)–(3.242), and $\gamma = 4(1 + \frac{1}{2}\cos^2\theta_W)[7\zeta(4)/2\zeta(3)]^2 \simeq 55$. For $\delta N \sim 10^{-10}$ and $T \sim 1$ MeV, the T^2 term, which acts on ν and $\bar{\nu}$ in the same way, dominates over the δN term. So the MSW effect is irrelevant in the early universe.

The situation is different if there would be a sterile neutrino ν_s that mixes with ordinary neutrinos. Meaningful constraints are derived on mass and mixing from the nucleosynthesis argument. The production rate of ν_s is given by

$$\Gamma_{\nu_s} \simeq \sin^2 2\theta_0 \sin^2 \left(\frac{1}{2}\Delta_0 t \right) \Gamma_{\nu_e}, \qquad (8.197)$$

where we consider mixing between ν_s and ν_e with mixing angle θ_0 in vacuo and Γ_{ν_e} is the production rate of ν_e given in (4.184) with $\zeta = 25/4 + 5\sin^2\theta_W + 10\sin^4\theta_W$ taking account of $\bar{\nu}_i\nu_i \rightarrow \bar{\nu}_e\nu_e$ scattering during which $\nu_e \rightarrow \nu_s$ takes place. The oscillation factor is controlled by $\Delta_0 = \Delta m^2/2\langle E\rangle$ with $\langle E\rangle = 3.15T$ for the Fermi distribution; hence, $\Delta_0^{-1} \simeq 4 \times 10^{-9}(T/\text{MeV})(\Delta m^2/\text{eV}^2)^{-1}$ s is sufficiently fast at $T \sim 1\,\text{M\,eV}$ ($t \sim 1\,\text{s}$), and the oscillation factor is replaced by $1/2$. The production of ν_s must be sufficiently small below the QCD phase transition $T_{\text{QCD}} \simeq 150$ MeV (see Sect. 4.6.2),

$$\frac{\Gamma_{\nu_s}}{H} < 1 \quad \text{at } T_{\text{QCD}}, \tag{8.198}$$

where H is the expansion rate of the universe (4.178). This condition leads to

$$\sin^2 2\theta_0 < 10^{-6}. \tag{8.199}$$

This seems to exclude the entire parameter region relevant to explaining the LSND experiment in addition to atmospheric and solar neutrino oscillations (see Sect 8.10.1), but this naive argument is not correct since it ignores thermal plasma effects that suppress the transition to ν_s [1315]. With potential (8.195), the effective mixing angle θ_m is

$$\sin 2\theta_m = \left(\frac{\Delta_0}{\Delta_m}\right)\sin 2\theta_0, \tag{8.200}$$

where

$$\Delta_m = (\Delta_0^2 + V_e^2 - 2\Delta_0 V_e\cos 2\theta_0)^{1/2}, \tag{8.201}$$

and the production rate is modified to

$$\Gamma_{\nu_s} = \sin^2 2\theta_m\sin^2\left(\frac{1}{2}\Delta_m t\right)\Gamma_{\nu_e}. \tag{8.202}$$

For positive $\Delta m^2 = m_{\nu_s}^2 - m_{\nu_e}^2$, $\Delta_0/\Delta_m < 1$, and the oscillation factor is replaced by $1/2$, so that

$$\frac{\Gamma_{\nu_s}}{H} = \frac{1}{2}\sin^2 2\theta_0\left(\frac{\Delta_0}{\Delta_m}\right)^2\frac{\Gamma_{\nu_e}}{H}. \tag{8.203}$$

The condition $\Gamma_{\nu_s}/H < 1$ at $T < T_{\text{QCD}}$ leads to [1315]

$$\Delta m^2\sin^4 2\theta_0 < 4 \times 10^{-4}\text{eV}^2. \tag{8.204}$$

This is valid for $m_{\nu_s} < 10^4$ eV, or otherwise the thermal effect becomes negligible, and we go back to (8.199) for 10^4 eV $< m_{\nu_s} < 1$ MeV. For negative Δm^2, the constraint is stronger due to the MSW resonance effect [1316]. The result of numerical analysis is written roughly

$$\Delta m^2 \sin^2 2\theta_0 < 10^{-8} \text{ eV}^2 , \tag{8.205}$$

for $\nu_s-\nu_e$ mixing. For $\nu_s-\nu_{\mu,\tau}$ mixing, the constraint is $< 10^{-5}$ eV^2.

When these constraints are applied to the four-neutrino mixing scheme $(\nu_e, \nu_\mu, \nu_\tau, \nu_s)$ (see the next section), all cases with $m_{\nu_s} < m_{\nu_i}$ ($i = e, \mu$, or τ) are excluded.

Let us remark on the right-handed neutrino as dark matter in the universe. The abundance of light right-handed neutrinos is calculated as $\Gamma_s t$, that is (8.203), for $n_{\nu_s} < n_{\nu_e}$, where n_{ν_e} is given by (4.180). We find that

$$\frac{n_{\nu_s}}{n_\nu} \simeq 5 \times 10^4 \sin^2 2\theta_0 \left(\frac{m_{\nu_s}}{1\,\text{keV}}\right). \tag{8.206}$$

(For large θ the abundance is saturated at the equilibrium value $n_{\nu_s} = n_{\nu_e}$.) With this dilution factor, the cosmological mass density limit (5.43) reads

$$\sin^2 2\theta_0 < 10^{-8} \left(\frac{m_{\nu_s}}{1\text{keV}}\right) < 2 \times 10^7 h^2. \tag{8.207}$$

If $(\sin^2 2\theta_0, m_{\nu_s})$ take values that just satisfy this limit, the right-handed neutrino becomes dark matter. For the reason that the number density is between hot and cold dark matter, and also the Jeans scale (free streaming scale) is between the two (see Sect. 4.6.3), it is called *warm dark matter* [864]. Cosmological interest in view of the small-scale structure formation is discussed in [1317]. The decay of right-handed neutrinos is slow [1318]:

$$\tau(\nu_s \to \nu_\tau + \nu_i + \bar{\nu}_i) = \frac{1}{3}\tau_\mu (m_\mu/m_{\nu_\tau})^5 (\sin\theta_0 \cos\theta_0)^{-2} \tag{8.208}$$
$$= 2.4 \times 10^{20}\text{s}(m_{\nu_\tau}/1\,\text{keV})^{-5}(\sin 2\theta_0)^{-2} ,$$

so that the limit for a decaying particle (5.60) does not apply to this case, irrespective of $\sin^2 2\theta_0$, unless $m_\nu > 10$ MeV. [7]

---

[7] For $m_\nu > 1$ MeV an e^+e^- decay channel opens, which disturbs primordial nucleosynthesis. So the lifetime of a right-handed particle must be shorter than 1 s to avoid unwanted effects.

8.10 Neutrino Oscillation: Summary

8.10.1 Present Status

We conclude that the evidence for neutrino oscillation is compelling by now. The atmospheric neutrino experiment shows that oscillation takes place between ν_μ and ν_τ with nearly maximal mixing and mass difference squared $|\Delta m_{23}^2| = |m_3^2 - m_2^2| = (1.7 - 3.7) \times 10^{-3}$ eV^2. The experiment does not tell us the sign of Δm_{23}^2. The direct evidence of solar neutrino oscillation is at 3.3σ, and matter-enhanced neutrino oscillation explains all experiments consistently. Large mixing takes place between ν_e and a combination of ν_μ and ν_τ given in (8.99). Two solutions, LMA and LOW, are possible at a $< 90\%$ confidence level of experiment, albeit the probability of LOW is significantly lower. The mass difference of LMA is $\Delta m^2 = (2.6 - 16) \times 10^{-5}$ eV^2, and the mixing angle $\sin^2 2\theta = 0.77 - 0.84$. The allowed region does not reach maximal mixing at a 99% confidence level of experiment. This means that $\Delta m_{12}^2 = m_2^2 - m_1^2 > 0$. For LOW, $\Delta m_{12}^2 \simeq 1.1 \times 10^{-7}$ eV^2, and $\sin^2 2\theta \simeq 0.84$; the solution includes $\theta > 45°$ if $> 2\sigma$ is allowed. An interesting constraint is derived from the null result of the CHOOZ experiment, which indicates that $|U_{e3}|$ is small.

We have two possibilities for mass level schemes, as shown in Fig. 8.19, ignoring low-probability possibility of $\theta > 45°$. The first is a more natural

$$
\begin{array}{cccc}
\text{———} \; \nu_3 & \qquad & \text{———} \; \nu_2 \\
& & \text{———} \; \nu_1 \\
\text{———} \; \nu_2 & & \\
\\
\\
\text{———} \; \nu_1 & & \text{———} \; \nu_3
\end{array}
$$
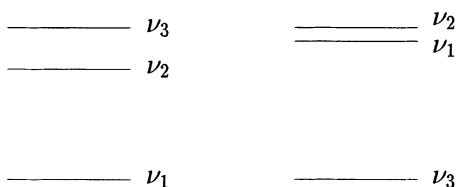
Fig. 8.19. Two possibilities for the neutrino mass level scheme. The levels 2 and 3 may be interchanged if $\theta_{23} > 45°$.

scheme, $m_{\nu_1} < m_{\nu_2} < m_{\nu_3}$ (scheme A), whereas the order is partially reversed for the second, $m_{\nu_3} < m_{\nu_1} < m_{\nu_2}$, which requires that ν_1 and ν_2 are nearly degenerate (scheme B). Oscillation does not tell us about the baseline of the neutrino mass. We may add some constant smaller than 2.5 eV (1 eV if Majorana), keeping the mass difference squared at the same values. We may refer to the extreme case, $m_{\nu_1} \simeq m_{\nu_2} \simeq m_{\nu_3}$, as degenerate neutrinos, and the case of negligible baseline mass as hierarchical neutrinos. We show in Table 8.4 the ratio of m_{ν_3}/m_{ν_2} for hierarchical neutrinos (we include SMA and VAC for comparison). From Table 8.4 we see that $m_{\nu_3}/m_{\nu_2} \sim (m_\tau/m_\mu)^{0.22-0.47}$ for LMA, or $\sim (m_\tau/m_\mu)^{0.90-0.97}$ for LOW.

The most surprising aspect is the nearly maximal mixing angles among neutrinos. This is not only quite different from what we know about quarks,

Table 8.4. Ratios of m_{ν_3}/m_{ν_2} for the four possible solutions of the solar neutrino problem. Boldfaced letters denote favoured solutions. The hierarchical neutrino mass is assumed.

	LMA	SMA	**LOW**	VAC
m_{ν_3}/m_{ν_2}	**3.3–12**	$10-27$	**125–180**	$1850-7900$

but also requires a nontrivial theoretical effort to understand it, unless the three neutrinos are nearly degenerate in mass.

Once $|U_{e2}|$, $|U_{\mu3}|$, and $|U_{e3}|$ are known, it is possible to determine the modulus of all 3×3 matrix elements. Even with the present data, we obtain [1319]

$$U_\ell = \begin{bmatrix} 0.74-0.90 & 0.45-0.65 & <0.16 \\ 0.22-0.61 & 0.56-0.77 & 0.57-1/\sqrt{2} \\ 0.14-0.55 & 0.36-0.68 & 1/\sqrt{2}-0.82 \end{bmatrix}, \tag{8.209}$$

if LMA is chosen (in our convention, the first row corresponds to U_{e1}, U_{e2}, U_{e3}). The undetermined phase is varied from 0 to 2π, and only the modulus is shown for the element. This matrix assumes $m_{\nu_2} < m_{\nu_3}$. For the opposite, the (2,3) and (3,3) elements are reversed. For LOW we have a similar, but more well-determined matrix:

$$U_\ell = \begin{bmatrix} 0.71-0.79 & 0.61-0.71 & <0.16 \\ 0.34-0.65 & 0.42-0.70 & 0.57-1/\sqrt{2} \\ 0.25-0.58 & 0.32-0.63 & 1/\sqrt{2}-0.82 \end{bmatrix}. \tag{8.210}$$

We remark that the phase of CP violation is given by

$$\cos\phi = \frac{1}{2|U_{e1}||U_{e2}||U_{e3}||U_{\mu3}||U_{\tau3}|} \tag{8.211}$$
$$\times [(1-|U_{e3}|^2)^2|U_{\mu1}|^2 - |U_{e2}|^2|U_{\tau3}|^2 - |U_{e1}|^2|U_{e3}|^2|U_{\mu3}|^2]$$

in terms of the modulus of the matrix element.

Sterile neutrinos?   If neutrino oscillation claimed by the LSND collaboration were real, the neutrino mixing pattern would be substantially more complicated than that presented here. Combining the LSND allowed region with negative results from KARMEN and Bugey, the mass range still allowed is 0.3–1 $(eV)^2$ with a mixing angle in a very narrow range. This mass difference squared is much larger than that derived from atmospheric or solar neutrino experiments, and there is no room to accommodate it in the three–neutrino scheme. The way discussed in literature is to introduce one more

'neutrino', which is sterile to any neutrino detectors (say, a light right-handed neutrino) [1320]. A scrutiny shows two possible mixing patterns. One is the so called '3+1 scheme" in which three ordinary neutrinos have mass difference squared that are relevant to atmospheric and solar neutrino oscillations and a sterile neutrino has mass 1 eV higher (or lower) than the others. The other is the '2+2 scheme,' where the sterile neutrino has a mass close to the electron neutrino mass and μ and τ neutrinos have masses 1 eV above (or below) the other two [1321–1323]. In the 3+1 scheme, the LSND effect is explained by a two–step transition from ν_μ to ν_e via ν_s. This is a θ^2 effect that requires both mixing angles to be reasonably large. From the beginning, this possibility was nearly ruled out [1321] by the constraints from the Bugey reactor experiment (ν_e disappearance) [1244] and the CDHSW experiment (ν_μ disappearance) [1238]. This conclusion was further confirmed by [1324,1325]. In the 2+2 scheme, solar neutrinos oscillate between ν_e and ν_s, whereas the LSND effect is explained by the $\nu_e - \nu_\mu$ mass difference. The 2+2 scheme has survived until recently (provided that $m_{\nu_e} \sim m_{\nu_s} > m_{\nu_\mu} \sim m_{\nu_\tau}$),[8] but it was disfavoured at the 95% confidence level by the latest SK analysis [1272]. More recently, the SNO experiment, which tells us that the partner of ν_e is predominantly an ordinary neutrino, excludes this scheme to a >95% confidence level (for LOW and VAC-like solutions). Therefore, we have no viable oscillation scheme consistent with the LSND effect. We shall not discuss neutrino mixing models involving the sterile neutrino further in this book.

8.10.2 Future Neutrino Experiments

Provided that LMA is the correct solution of the solar neutrino problem, $|U_{e2}|$, $|U_{\mu3}|$, Δm_{12}^2 and $|\Delta m_{23}^2|$ will be more precisely determined by ongoing and planned experiments (KamLAND, K2K and similar long-baseline experiments). What must be measured, in addition, are $|U_{e3}|$ and the sign of Δm_{23}^2 (or sign of Δm_{13}^2). Another undetermined parameter is the phase of the 3×3 matrix that is relevant to CP violation in the lepton sector, which we discuss in the next section.

For it is difficult to push forward reactor neutrino experiments much, we may think of using long-baseline accelerator experiments to determine $|U_{e3}|$ via $\nu_\mu \to \nu_e$. For a baseline length $2\pi E/\Delta m_{23}^2 < L < 2\pi E/\Delta m_{12}^2$, only ν_3 contributes to the intermediate state, and hence

$$P(\nu_\mu \to \nu_e) = 4|U_{\mu3}|^2 |U_{e3}|^2 \sin^2 \left(\frac{\Delta m_{23}^2}{4E} L \right) , \qquad (8.212)$$

where $|U_{\mu3}| \sim O(1)$. For such experiments it is essential to reduce ν_e contamination in the ν_μ beam as much as we can. Richter [1326] stressed the

---

[8] See Sect. 8.9 above.

advantage of using a low-energy ($E_\nu \lesssim 1$ GeV) beam to reduce the ν_e background.[9] (It is also important to reject the background from π^0.) A quantitative estimate given in [1327, 1328] shows that $\sin^2 2\theta > 0.01 - 0.03$ can be reached for $|U_{e3}|$ with a strong proton beam facility of megawatt power, e.g., JHF (295-km baseline) and MINOS (730-km baseline) [1329] (compared to 5 kW of the KEK proton synchrotron for K2K). The sign of Δm_{13}^2 can also be determined, if $\sin^2 2\theta$ is reasonably large, say $\gtrsim 0.01$, by comparing ν_μ and $\bar\nu_\mu$ induced reactions using the Earth effect in long-baseline experiments [1330, 1331,1327], although we may need a $\gtrsim 1000$-km baseline to see it (see an estimate given in the next section).

The important question concerning the neutrino mass is whether the neutrino is of the Majorana or the Dirac type. Using the mass matrices and mass levels discussed above, we can infer that the effective (Majorana) mass that appears in double beta decay is

$$
\begin{aligned}
\langle m_{\nu_e} \rangle &< 0.0053 \text{ eV} \qquad &\text{for LMA} \\
&< 0.0016 \text{ eV} \qquad &\text{for LOW}
\end{aligned} \tag{8.213}
$$

for hierarchical neutrinos of scheme A. It might be possible to detect $\langle m_{\nu_e} \rangle$ if it takes a value close to the upper limit, but generally it is difficult to detect such a small mass. The degenerate Majorana neutrino scheme or 'inverted' hierarchy, scheme B, gives $\langle m_{\nu_e} \rangle \gg 0.05$ eV, unless accidental cancellation takes place. Hence, such a scheme can either be verified or falsified in the next generation double beta-decay experiments.

8.11 CP Violation

8.11.1 CP Violation in Neutrino Oscillation

The transition amplitude from $|\nu^\alpha\rangle$ to $|\nu^\beta\rangle$ after time interval t is given by

$$
\langle \nu^\beta | \nu^\alpha \rangle_t = \sum_i U_{\alpha i} \, e^{i \frac{m_i^2}{2E} t} U_{i\beta}^\dagger \tag{8.214}
$$

[see (8.46)]. Hence,

$$
\begin{aligned}
P_{\alpha \to \beta} &= |\langle \nu^\beta | \nu^\alpha \rangle_t|^2 \\
&= \sum_{i,j} U_{\alpha i} U_{\beta i}^* U_{\alpha j}^* U_{\beta j} \, e^{i \frac{m_i^2 - m_j^2}{2E} t} \\
&= \sum_{i,j} |U_{\alpha i} U_{\beta i} U_{\alpha j} U_{\beta j}| \, e^{i\phi_{\alpha\beta ij}} (e^{i\Delta_{ij} t} - 1) + \delta_{\alpha\beta},
\end{aligned} \tag{8.215}
$$

---

[9] He argued that an E^{-2} factor from the argument of the oscillation function offsets the gain of E^3 (E^2 from beam focusing; see (4.5) and E from the cross section) for high-energy beams, leaving the net gain increasing only as E.

where
$$\phi_{\alpha\beta ij} = \arg\left(U_{\alpha i}U_{\beta i}^* U_{\alpha j}^* U_{\beta j}\right), \tag{8.216}$$

and $\Delta_{ij} = (m_i^2 - m_j^2)/2E$. Because $\phi_{\alpha\beta ij} = -\phi_{\alpha\beta ji}$,

$$P_{\alpha\to\beta} = \delta_{\alpha\beta} + 2\sum_{j>i}|U_{\alpha i}U_{\beta i}U_{\alpha j}U_{\beta j}|\left[\cos(\Delta_{ij}t + \phi_{\alpha\beta ij}) - \cos\phi_{\alpha\beta ij}\right]. \tag{8.217}$$

Using expression (8.26) for U, $\phi_{\alpha\beta ij}$ is written [1219]

$$\phi_{\alpha\beta ij} = \arg\left(u_{\alpha i}u_{\beta i}^* u_{\alpha j}^* u_{\beta j}\right) \ . \tag{8.218}$$

We note that phases α, β, γ, β', γ' all cancel in this combination. This is another demonstration that the properties of neutrino oscillation do not depend on whether neutrinos are of the Dirac or Majorana type.

It is easy to show that
$$P_{\alpha\to\beta} = P_{\bar\beta\to\bar\alpha}. \tag{8.219}$$

This is a consequence of CPT invariance [1332], which always holds in local field theory. This relation is shown by noting that

$$\langle\nu_\beta|\nu_\alpha\rangle_t = U_{\alpha i}\,e^{i\frac{m_i^2}{2E}t}U_{i\beta}^\dagger$$
$$= \exp\left(i\,\frac{1}{2E}\,U_{\alpha i}m_i^2 U_{i\beta}^\dagger\right) = \left[\exp i\frac{m^\dagger m}{2E}\,t\right]_{\alpha\beta} \tag{8.220}$$

and similarly that

$$\langle\bar\nu_\beta|\bar\nu_\alpha\rangle_t = U_{\alpha i}^* e^{i\frac{m_i^2}{2E}t}U_{i\beta}^T = \left[\exp i\frac{m^\dagger m}{2E}t\right]_{\alpha\beta}^T \ . \tag{8.221}$$

Hence,
$$\langle\bar\nu_\alpha|\bar\nu_\beta\rangle_t = \langle\nu_\beta|\nu_\alpha\rangle_t \ . \tag{8.222}$$

If CP invariance holds, we should have [1332]

$$\langle\nu_\beta|\nu_\alpha\rangle_t = \langle\bar\nu_\beta|\bar\nu_\alpha\rangle_t = \langle\nu_\alpha|\nu_\beta\rangle_t \ , \tag{8.223}$$

i.e.,
$$P_{\alpha\to\beta} = P_{\bar\alpha\to\bar\beta} = P_{\beta\to\alpha} \ . \tag{8.224}$$

In terms of the mass matrix, this condition is represented by

$$(m^\dagger m)^T = m^\dagger m \ , \tag{8.225}$$

as is obvious from (8.220) and (8.221).

By inspecting (8.217), we see that (8.224) is satisfied if $\phi_{\alpha\beta ij} = 0$. Equation (8.218) shows that CP violation in neutrino oscillation may take place only when $N \geq 3$ through the phase appearing in the 3×3 matrix; other phases, such as those characteristic of Majorana neutrinos, do not contribute to CP violation in neutrino oscillation. Furthermore, it is easy to show that CP violation does not take place if $m_{\nu_e} = m_{\nu_\mu} = 0$; the CP-violation effect is suppressed to the order of $m_{\nu_\mu}^2 L/2E$. Taking $i = 1$ for ν_τ, the arguments of (8.220) and (8.221) are $U_{\alpha 1} U_{\beta 1}^* m_{\nu_\tau}^2 / 2E$ and $U_{\alpha 1}^* U_{\beta 1} m_{\nu_\tau}^2 / 2E$, respectively. If we take the conventional KM representation of a 3×3 matrix, the $(i, 1)$ elements are $(\cos\theta_1, \sin\theta_1\cos\theta_2, \sin\theta_1\sin\theta_2)$ for $i = 1, 2, 3$, which do not contain a complex phase. This proves that $\langle \nu_\beta | \nu_\alpha \rangle_t = \langle \bar\nu_\beta | \bar\nu_\alpha \rangle_t$, i.e., CP invariance. This subject is detailed in the review of [1333].

Exploration of CP violation

The CP and T violating parts are equal in vacuo and are given by

$$\Delta P = P_{\nu_\alpha \to \nu_\beta} - P_{\bar\nu_\alpha \to \bar\nu_\beta} \tag{8.226}$$
$$= P_{\nu_\alpha \to \nu_\beta} - P_{\nu_\beta \to \nu_\alpha} \tag{8.227}$$
$$= -4(\mathrm{Im}\, U_{\beta 1} U_{\beta 2}^* U_{\alpha 1}^* U_{\alpha 2})(\sin \Delta_{21} L + \sin \Delta_{32} L + \sin \Delta_{13} L)$$
$$= 4Jf, \tag{8.228}$$

where $\Delta_{ij} = (m_i^2 - m_j^2)/2E$ and L is the distance from the neutrino source to the detector [1334]. J, as defined by (3.114) [392, 393], and f are given by

$$J = -\mathrm{Im}\, U_{\beta 1} U_{\beta 2}^* U_{\alpha 1}^* U_{\alpha 2}, \tag{8.229}$$
$$f = \sin \Delta_{21} L + \sin \Delta_{32} L + \sin \Delta_{13} L$$
$$= -4 \sin \frac{\Delta_{21} L}{2} \sin \frac{\Delta_{32} L}{2} \sin \frac{\Delta_{13} L}{2}. \tag{8.230}$$

The size of ΔP is proportional to J times the product of the sine of the three mass differences. The effect is proportional to E^{-3} rather than E^{-2} for small $\Delta_{ij} L$. There is hope that this effect will be visible in long-baseline neutrino oscillation experiments if $|U_{e3}|$ and J are not too small, as explored in the recent literature [1335, 1336, 1330, 1337]. Note that ΔP does not depend on the choice of α and β.

In practical application, CP violation experiments (with $\nu_\mu \to \nu_e$ versus $\bar\nu_\mu \to \bar\nu_e$) differ from T violation experiments, $(\nu_\mu \to \nu_e$ versus $\nu_e \to \nu_\mu)$ because of the matter effect which acts as the external field that breaks CP [1339]. For long-baseline experiments electron neutrinos propagate through matter, and the matter effect may compete with intrinsic CP violation [1330]. For $\rho \simeq 3$ g cm^{-3} and 1 GeV beam energy, (8.166) gives an effective $\Delta m^2 \approx 2 \times 10^{-4}$ (eV)^2, which is not too small compared to $\Delta m_{13}^2 \approx 2 \times 10^{-3}$ (eV)^2, i.e., the matter effect competes with or is more important than the CP-violating effect.

On the other hand, for propagation of antineutrinos (as described by $A \to -A$ in (8.105) and $U \to U^*$), the matter effect acts to increase the mass difference. Hence, we have a disparity in pair neutrino propagation, and it contributes to the CP indicator even in the absence of intrinsic CP violation. The matter effect is written [1330]

$$\Delta P_{\nu_\mu \to \nu_e} = P_{\nu_\mu \to \nu_e} - P_{\bar{\nu}_\mu \to \bar{\nu}_e} \tag{8.231}$$

$$= |U_{e3}U_{\mu 3}|^2 \left(1 - 2|U_{e3}|^2\right) \frac{4A}{E} \left(\frac{4}{\Delta_{31}^2} \sin^2 \frac{\Delta_{31}L}{2} - \frac{L}{E} \sin \frac{\Delta_{31}L}{2}\right) .$$

This effective CP-violating effect of Earth is attributed to CP asymmetry of the material that constitutes Earth.

One can separate intrinsic CP violation from the matter effect using the fact that the matter effect controlled by $A \propto E$ increases linearly in E_ν, whereas Δm_{ij}^2 does not depend on energy [see (8.105)]. Namely, ΔP has a linearly increasing oscillation envelope against L/E_ν, while the matter effect is constant for L/E_ν. This means that the intrinsic CP-violating effect becomes dominant for large L/E_ν [1330]. Pair reactions for T-violation experiments, on the other hand, receive the same matter effect, and the net effect cancels as long as the matter density profile is symmetric for the replacement of the neutrino source and the detector.

To see how large the expected effect is, let us take $L \simeq 250$ km and $E \sim 1$ GeV, which are the parameters for the KEK–Kamiokande long-baseline experiment (K2K). From (8.228) intrinsic CP violation $\Delta P \equiv P_{\nu_\alpha \to \nu_\beta} - P_{\bar{\nu}_\alpha \to \bar{\nu}_\beta}$ is proportional to f, which is roughly given by

$$f \simeq 2\Delta_{12} L \sin^2 \frac{\Delta_{31}L}{2}, \tag{8.232}$$

if $\Delta_{31} \simeq \Delta_{32}$ and $\Delta_{21} \ll 1$. Taking LMA for solar neutrino oscillation, we assume that $\Delta m_{32}^2 \simeq \Delta m_{31}^2 \simeq 2.5 \times 10^{-3}$ eV^2 and $\Delta m_{21}^2 \simeq 7 \times 10^{-5}$ eV^2. For these parameters,

$$\Delta_{32}L \simeq \Delta_{31}L \approx 1.6, \quad \Delta_{21}L \simeq 4.4 \times 10^{-2}, \tag{8.233}$$

i.e., $f \simeq 0.044$. The J factor can be expressed as [1319]

$$J = \frac{1}{4} \frac{\sqrt{\sin^2 2\theta_{\mathrm{sol}}} \sqrt{\sin^2 2\theta_{\mathrm{atm}}} |U_{e3}|}{1 - |U_{e3}|^2} \sin \phi , \tag{8.234}$$

where θ_{sol} is the mixing angle that is relevant to solar neutrino oscillation and θ_{atm} is that for atmospheric neutrino oscillation. We obtain $J \leq 0.04 \sin \phi$ where ϕ is the phase (this is compared to the maximum value $J = 1/(6\sqrt{3}) = 0.096$ [1336]). For the maximal CP-violation phase, $\phi = 90°$, ΔP is at most

0.7%. The effect is further smeared out by integrating over the neutrino energy spread. To detect CP violation, we need one order of magnitude larger L/E, i.e., $L/E \gtrsim 1000$ km/GeV, a > 1000 km baseline, and/or a lower neutrino energy of $\lesssim 100$ MeV. The detection of CP violation is difficult but perhaps not entirely hopeless *if* $|U_{e3}|$ is not too small, say $|U_{e3}| > 0.05$. (For the LOW solution, detection is hopeless.) The feasibility is discussed in detail in [1338, 1340, 1326, 1327], where the use of a low-energy narrowband neutrino beam is emphasized.

8.11.2 CP-Violation Characteristic of the Majorana Phase

The CP-violating phases β', γ' characteristic of the Majorana neutrino appear only in the effect associated with the neutrino mass term. Let us define the quantity [1341]

$$\psi_{\alpha\beta ij} = m_i m_j U_{\alpha i} U_{\beta j}^* (U_{\alpha j} U_{\beta i}^*)^* \ .$$ (8.235)

It is easily shown that $\psi_{\alpha\beta ij}$ is invariant under the redefinition of phases of neutrino wave functions. This combination appears when the process involves the Majorana phase.   /

As an example of CP-violation effects due to the Majorana phase, we consider the decay $\mu \to e \nu_i \nu_j$. There are two Feynman diagrams that contribute to this decay, as shown in Fig. 8.20, because the neutrino and the antineutrino are identical. The interference of the two diagrams leads to a term proportional to

$$\sum_{i,j} (U^\dagger)_{j\mu} m_j (U^\dagger)_{je} \times U_{ei} m_i U_{\mu i} = \sum_{i,j} m_i m_j (U_{ei} U_{\mu j}^*)(U_{ej} U_{\mu i}^*)^*$$

$$= \sum_{i,j} \psi_{e\mu ij} \ .$$ (8.236)

The imaginary part of (8.236) gives rise to CP-violating effects. This CP-violating term, however, is suppressed by a factor of $m_1 m_2 / m_\mu^2 < O(10^{-16})$, compared with the CP-conserving part of $\mu \to e \nu_i \nu_j$ decay.
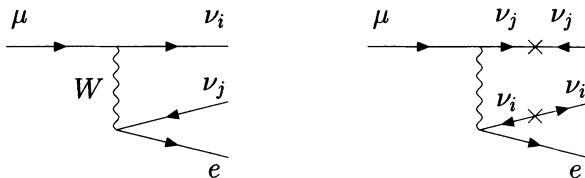
Fig. 8.20. Feynman diagrams for decay $\mu \to e + \nu_i + \bar{\nu}_j$. The cross in the second diagram stands for Majorana mass insertion.

$|\Delta L| = 2$ processes may also include the Majorana phase β' and γ'. The probability is proportional to

$$\zeta = \left| \sum_i m_i U_{\alpha i} U_{\beta i} \right|^2 , \qquad (8.237)$$

which is invariant under the phase transformation of neutrinos. Although the quantity ζ is real and has nothing to do with CP-violating phenomena, it depends on the Majorana phases β' and γ' [1207]. A well-known example of this kind is neutrinoless double β decay. This process measures the average neutrino mass

$$\langle m_{\nu_e} \rangle = \left| \sum_i m_i U_{ei} U_{ei} \right| . \qquad (8.238)$$

To see the dependence on the Majorana phase, we consider the two-family case. Using a representation of U in (8.50), we obtain

$$\langle m_{\nu_e} \rangle = |m_1 \cos^2 \theta e^{2i\beta} + m_2 \sin^2 \theta e^{-2i\beta}| . \qquad (8.239)$$

If $\beta' = \pi/4$ (relative CP=-1), the two contributions interfere destructively in the double β-decay amplitude, and it may happen that $\langle m_{\nu_e} \rangle < m_1$, where m_1 is the mass measured, for instance, in tritium beta decay. For the more special case, $m_1 = m_2$ and $\theta = \beta' = \frac{\pi}{4}$, $\langle m_{\nu_e} \rangle$ vanishes and hence double β decay does not take place [1098, 1207]. This is the case for the pseudo-Dirac neutrino.

For the CP-conserving case, (8.239) is generalised for N generations to

$$\langle m_{\nu_e} \rangle = \sum_i m_i \eta_i |U_{ei}|^2 , \qquad (8.240)$$

where η_i denotes the relative CP of the ith Majorana neutrino [see (8.24)].

9 Models for Massive Neutrinos

9.1 Beyond the Standard Model

Although the standard theory based on SU(3) and SU(2)×U(1) gauge symmetry (often called 'standard model') is highly successful, it is perhaps not the end of the story. There are too many (≥ 18) free parameters in the theory: we have three gauge couplings, nine Yukawa couplings that give matter fields masses, four parameters that specify the KM matrix, and at least two for the Higgs sector. There also exist too many particles that seem to be independent: there are 15 particles in one generation (counting left- and right-handed as independent); only a few of them such as $(\nu, e^-)_{\mathrm{L}}$ and $(u, d)_{\mathrm{L}}$ are unified as isodoublets. This family of 15 members appears three times. There are additional fundamental questions: why electromagnetic charges of quarks are integer multiples of $1/3$? More generally, why electromagnetic charges are quantised that way? (Note that the argument given in Sect. 5.1.2 gives only a partial answer.) Why the fundamental Lagrangian does not contain the term that violates CP invariance at a strong interaction level? Is global symmetry, such as baryon number, ultimately conserved? Is there more symmetry acting for particle physics? In particular, are there any correspondences between bosons and fermions? What is the role of gravity in particle physics?

Studies in particle physics from the late 1970s focused on answering these problems. No models are entirely successful, but there are many proposals that potentially solve a number of them and also look natural or promising. These proposals at least give us directions to studying the problems, and for this purpose the physics of neutrinos would serve as a useful probe. This is our prime interest in neutrinos today.

The most naturally looking idea beyond the standard model is that the three gauge groups are the low-energy manifestation of larger gauge groups [219, 220]. The prime attraction of this idea is that the three forces are different manifestations of one force split by symmetry breaking at some high energies (this is called grand unified theory, or GUT for short) [1342]. It enables us to describe the three gauge coupling constants in terms of one and to explain why we have quarks and leptons. In such a model, the charge quantisation problem is automatically solved. A particular possibility is that all particles are manifestations of a single irreducible representation of a unifying group. It naturally happens that the very light mass of neutrinos is a manifestation

of a very high energy unifying scale involved in the unification. This is why it is often said that neutrino mass searches explore a high-energy frontier.

The minimal group of the GUT is SU(5) [220]. All particles are classified into the two lowest irreducible representations **5*** and **10**. One may add **1** if the neutrino is massive. To unify the three coupling constants, the unification scale must be as high as 10^{15} GeV [1342]. This unification uniquely predicts the value of the weak mixing angle $\sin^2 \theta_W$. The classification of particles into **5*** and **10** automatically solves the charge quantisation problem like the quantisation of the third isospin component of pions and kaons in SU(2) multiplets. The number of the Yukawa coupling constants is also reduced since unification of quarks and leptons into two multiplets gives rise to some relations among masses of quarks and leptons such as $m_b = m_\tau$, $m_s = m_\mu$, and $m_d = m_e$ at the unification energy scale. The novel prediction of this unification is instability of protons.

This SU(5) unification had looked very promising, but the explorations since it was proposed proved that it is not as successful as was hoped. The theoretical problem is the coexistence of two vastly different energy scales that would induce very large radiative corrections for light scalar particles, for they are generically quadratically divergent (hierarchy problem). The experimental problem is more direct: with the advancement of low-energy coupling constant determinations, it was shown that the three coupling constants do not coincide on one scale, as required by unification. A more generic problem is that proton decay is unobserved, at least much slower than predicted. There are two directions to cure the problems: one is to extend the group to SO(10), and the other is to introduce supersymmetry.

In SO(10) unification [1343, 1344], symmetry breaking takes place more than once to bring it into SU(3)×SU(2)×U(1), so that the three couplings do not need to meet at one energy scale, but the mismatch of the unification scales represents the presence of two symmetry-breaking scales. The three advantages of SO(10) over SU(5) are that (i) matter fields are all included in one irreducible representation **16**, which is a fundamental spinor of SO(10); (ii) anomaly cancellation is generic because SO(10) is a real group; and (iii) neutrinos appear as massive particles. The lifetime of proton decay can be longer. The disadvantage is that the symmetry-breaking schemes are no longer unique, and predictive power is lost for the electroweak mixing angle. It might also be counted as a 'disadvantage' that the mass relation between quarks and leptons gets stronger than in SU(5). This would be welcome news in the sense that a relation is predictive between the quark- and lepton-mixing angles. The bad news is that the simplest prediction does not agree with the empirical neutrino mixing pattern. This may not be fatal, however, since there is still much freedom in the Higgs sector. Whether a quark–lepton mass matrix can be obtained compatibly with experiment is one of the major problems concerning neutrino physics today. The hierarchy problem remains unsolved in this extension of unification.

The alternative to SO(10) is to introduce supersymmetry (SUSY) into SU(5) unification [1345]. Attempts to understand fermions and bosons within unitary multiplets are old, but earlier ones were not successful due to Coleman–Mandula's no-go theorem [1346] which states that no conserved Lorentz tensors exist other than scalars, four-momenta, and angular momenta. This was avoided by introducing supercharges that obey anticommutation relations rather than commutation relations [1347]. This enabled us to set successfully super-Poincaré algebra of four-momenta, angular momenta, and supercharges [1348, 1349]. Introduction of supersymmetry doubles matter fields, which contribute to the renormalisation of the coupling constant through loop corrections, and bring the running of the three coupling constants in agreement at just one scale [1345]. The $\sin^2 \theta_W$ predicted this way agrees excellently with experiment. Because of the shift of the unification scale, proton decay mediated by gauge bosons becomes sufficiently slow. In this scheme all of the generic structure of SU(5) is retained. Another advantage is that Higgs particles do not receive large self-energy because of the cancellation of loop corrections between bosons and fermions [327]. Hence, once the potential is tuned, Higgs masses remain stable to radiative corrections. The immediate prediction is the presence of a large number of superparticles in a 100-GeV to 1-TeV region, which can be explored through experiment in the not too distant future. Such particles would provide us with a promising candidate for cold dark matter of the Universe [1350], which could also be subjected to experimental search. There is, however, a generic test that would falsify the theory. SUSY SU(5) predicts the process that causes fast proton decay via so-called dimension-five operators [1351]. The experimental lower limit for $p \rightarrow K^+ + \nu$ decay already seems to contradict, at least, the minimal version of SUSY SU(5) GUT. In the neutrino context, there is no compelling reason to introduce right-handed neutrinos into SUSY SU(5) GUT, and hence neutrinos remain naturally massless. One might consider, however, SU(5) of SU(5)×U(1), which is a subgroup of SO(10).[1] This requires the presence of right-handed neutrinos that cancel gauge anomaly arising from the $U(1)^3$ triangle diagram.

There are yet untouched problems in the above discussion: the presence of family, unification with gravity, and the strong CP problem. The first problem may naturally be considered along the line of extension of the unification idea. We may consider family (horizontal) gauge symmetry and unify it with the GUT gauge group. SU(5+N), SO(10+4N), E$_7$, and E$_8$ have been considered as candidates. These attempts, however, have turned out to be unsuccessful because the model always requires the quark–lepton families to be vector-like which is not compatible with our world [1352]. Should one want gauged family symmetry, one should not unify it with GUT but leave it outside the GUT frame.

---

[1] If we consider the SUSY extension of SO(10), the path of symmetry breaking must be SO(10)→SU(5)×U(1) to satisfy low-energy phenomenology.

We may, in principle, think of horizontal symmetry, such as $SU(N_F)$ ($N_F = 3$) independent of unification of forces, to understand generations. With $SU(3)$ the presence of a right-handed neutrino is obligatory to cancel anomaly. The problem is that one must break this symmetry in an intricate way to account for the masses and mixings of quarks and leptons, which show empirically quite a complicated pattern. This is a tough requirement, and no successful attempt is known. Strong restrictions of non-Abelian symmetry are relaxed if one takes $U(1)$ symmetry for family, assuming different $U(1)$ charges for different generations [1353]. Horizontal symmetry may not necessarily be local, though there is some preference for local in view of quantum gravity effects (briefly discussed below).

The other direction in the attempt at unification is to consider SUSY as gauge symmetry [1354]. This enables us to treat gravity within the theory. One advantage of supergravity theories is that one can (fine-)tune the theory so that the unwanted cosmological constant vanishes, whereas in SUSY theories, breaking of SUSY necessarily produces an unacceptably large positive cosmological constant.[2] On the other hand, supergravity theories do not solve the problem of the nonrenormalisability of gravity, i.e., they do not successfully unify gravity. To solve this problem one has to work with superstring. If superstring is the correct theory of particle unification, supergravity theory is regarded as 'low-energy' effective theory. Supergravity theory itself shows little predictive power, unless a correct path is found for the reduction from superstring. We do not touch on superstring theory in this book, since the current theory gives no insights for low energy physics.

The strong CP problem seems a bit off from the line of unification and may need some explanation. In QCD Lagrangian, there is no reason to exclude a term of the form [1355]

$$\mathcal{L} = \frac{\theta}{64\pi^2} \epsilon_{\mu\nu\rho\sigma} F^{\mu\nu} F^{\rho\sigma} , \tag{9.1}$$

where $F^{\mu\nu}$ is the field tensor of the gluon field. This operator, taking the form of $\mathbf{E} \cdot \mathbf{H}$, is odd under time inversion and, equivalently, CP reflection. This term can be rewritten as a total divergence of the current, and hence it does not contribute to physics within perturbation theory. In the presence of nontrivial topological excitations, like instantons [1356],[3] however, it gives rise to CP violation in the strong interaction [259]. Empirically observed very small CP violation means $|\theta| < 10^{-10}$.

---

[2] In supergravity theory the potential term has not only $|F|^2$ but also minus the superpotential squared, such that $V = (|F|^2 - 24\pi/m_{\text{pl}}^2|W|^2)\exp(8\pi K/m_{\text{pl}}^2)$, where notations are defined in Sect. 9.3.2. One can make V vanishing by tuning parameters.

[3] The action of instantons is visible in the large mass of the η' meson [259, 1357]. It is demonstrated in lattice QCD that nontrivial topological-charge gauge configurations are responsible for the large mass of η' [1358].

We have no reasons to suppress this θ term. The only mechanism known until now to solve this problem is to impose global U(1) symmetry, referred to as Peccei–Quinn (PQ) symmetry [1359]. The pseudo-Nambu–Goldstone boson, called axion, arising from spontaneous breakdown of PQ symmetry [1360], could render the θ parameter to vanish dynamically [1361], even in the presence of CP violation in weak interactions. Astrophysical and cosmological considerations require this U(1) symmetry-breaking scale $\simeq 10^9$–10^{13} GeV. The PQ mechanism itself has nothing directly related to neutrino masses, but one can think of a scenario where the right-handed neutrino acquires a Majorana mass when PQ symmetry is broken.

While PQ symmetry is one example of the necessity for global symmetry, there is the general issue whether global symmetry can exist in nature. The argument is that global symmetry is all broken at the Planck scale via the worm hole effect of quantum gravity which communicates one patch of spacetime with others, whereas the flow of quantum numbers of global symmetry is not conserved across the worm hole [1362]. If this is true, it would invalidate the PQ mechanism. Global symmetry corresponding to baryon and lepton number should also be broken in the same way. Then, the following implication results for the mechanism that gives the neutrino mass. In the standard model the neutrino is protected from having a Majorana mass by global lepton-number conservation. If it is broken at the Planck scale, operators arise that induce a Majorana neutrino mass; their lowest dimensional operator is $(1/m_{\rm pl})\ell\ell\phi\phi$ [1209]. This induces a neutrino mass of the order of 10^{-5} eV. To give some neutrino a mass of the order of $> 10^{-2}$ eV, as indicated by experiment, we must consider L or B–L necessarily as gauge symmetry, which is intact under the effect of worm holes. An important reservation for this argument is that we know little about quantum gravity and we do not know whether this 'hand-waving' argument, although it looks reasonable, is really valid in nature. Therefore, we do not take this quantum gravity argument as compelling in this book.

9.2 Classification of Models for Neutrino Mass

It is a widely accepted view that some physical reasons exist for the smallness of the neutrino mass. Reasonable mechanisms are known if the neutrino is of the Majorana type, as we have seen in Chap. 6. Two classes of models we know are (i) those in which the seesaw mechanism works and (ii) those in which the neutrino mass is induced by radiative corrections. The first class of models assumes the presence of the right-handed neutrino and ascribes the smallness of neutrino mass to the large mass of the right-handed neutrino. In the second, the right-handed neutrino is unnecessary; a small mass is understood by small factors that appear in the radiative correction. The problem is how these mechanisms can be embedded in the unified model of particle interactions.

The seesaw mechanism can be naturally incorporated in unified theo-
ries [237]. The problem can be considered in the following steps. Is there
any reason that requires the presence of the right-handed neutrino? What
is the mechanism that gives the right-handed neutrino a large mass? Does
the neutrino mass result from low-energy phenomenology consistent with
experiment? And finally, can we understand the mass and mixing pattern
inferred from experiment?

We may classify existing models as

		Symmetry	Energy scale
(1)	$U(1)_{B-L}$	Local	$> 1000\,\mathrm{GeV}$
(2)	Left–right symmetry	Local	$> 1000\,\mathrm{GeV}$
(3)	$SO(10)$ model	Local	10^9–$10^{14}\,\mathrm{GeV}$
(4)	Horizontal symmetry	Local	$> 10^6\,\mathrm{GeV}$
(5)	Horizontal symmetry	Global	$> 10^{10}\,\mathrm{GeV}$
(6)	Peccei–Quinn symmetry	Global	10^{10}–$10^{12}\,\mathrm{GeV}$
(7)	Lepton number	Global	no bound

(1)–(3) are the class of models where symmetry protecting the right-handed
neutrino from having a mass at high energies is associated with vertical
(gauge-interaction or unifying) symmetry. In all models of this class, the key
role is borne by the symmetry of the $B-L$ quantum number, and the right-
handed neutrino acquires mass when $U(1)_{B-L}$ symmetry is broken while
leaving $SU(3) \times SU(2) \times U(1)_Y$ of the standard model. In a bottom-up picture,
the key role of $U(1)_{B-L}$ symmetry is understood in the following way: in
low-energy phenomenology, the only conserved charges other than those that
appear in the standard model are baryon and lepton numbers. When we
take these two symmetries as gauged (local), the current associated with
either symmetry has gauge anomaly. This anomaly can be cancelled only if
the $B-L$ combination is taken and *only if the right-handed neutrino exists*
(see Sect. 2.4.3). Therefore, the $U(1)$ symmetry that is contained in higher
unifying gauge theory is necessarily $U(1)_{B-L}$, and $B-L$ gauge symmetry
requires right-handed neutrinos. The scale of this $U(1)$ symmetry breaking
receives strong constraints if it takes place together with breaking of other
non-Abelian symmetry. In a view of unified theory, unifying the right-handed
neutrino requires the minimal rank of the unification group to be 5, one
rank higher than needed for the standard model particles, and the neutrino
acquires mass when this rank drops to rank 4.

It is, in principle, possible to consider a non-Abelian group to protect
the right-handed neutrino from having mass. In this case the group must
be independent of unification of gauge groups, for which the constraint is
much stronger. Model (4) offers an example where the protecting symmetry
is horizontal $SU(3)$.

In the preceding chapter, we concluded that the lower limit for the heav-
iest neutrino mass is $\approx 0.04\,\mathrm{eV}$. By requiring that the Yukawa coupling
constant for the Dirac mass be smaller than unity, the upper limit on right-

handed neutrino mass is 10^{15} GeV from the seesaw formula. Therefore, there must be a new energy scale below the Planck mass, and this scale agrees with what is often inferred from other phenomenology. For SO(10) this upper limit agrees with the unification scale.

The lower limit on the right-handed neutrino mass may be $\approx 10^{11}$ GeV, taking τ mass as the Dirac mass, if left-handed neutrino masses are hierarchical. We may also think of the case where the three neutrinos have nearly degenerate masses. These masses cannot exceed 1 eV significantly. The three independent arguments are (i) a limit on ν_e from the tritium experiment (Chap. 5), (ii) a limit from double beta decay (Chap. 7), and (iii) a limit from cosmic structure formation (Chap. 5). For this case, the lower limit on the right-handed neutrino mass is 4×10^9 GeV. Therefore, we can take the range 10^9–10^{15} as allowed for right-handed neutrinos.

One may use global symmetry as protecting symmetry (provided that the argument for the effect of worm holes does not need to be respected). The absence of the requirement for anomaly cancellation makes the model flexible. We have no compelling reason to have a right-handed neutrino, nor internal constraints on the scale. Nevertheless, an interesting feature is that breaking of global symmetry induces a Nambu–Goldstone boson and the requirement that its coupling to matter be sufficiently weak requires symmetry-breaking scale higher than $> 10^{9-10}$ GeV, which is a natural scale for a right-handed neutrino. Peccei–Quinn symmetry [model (6)] and horizontal symmetry [model (7)] are among global symmetries that are physically motivated.

The MSW solution of solar neutrino problems also leads to the scale of right-handed neutrino mass similar to the range we inferred from atmospheric neutrino experiments. The understanding of the mass pattern, however, is a much more difficult problem. There are no predictions of the mass relation among the three generation neutrinos which we can claim to be natural. The mass formula $m_{\nu_e} : m_{\nu_\mu} : m_{\nu_\tau} = m_e^2 : m_\mu^2 : m_\tau^2$ or $m_u^2 : m_c^2 : m_t^2$, often mentioned in the literature, is obtained only when one assumes $M_{\nu_e \mathrm{R}} = M_{\nu_\mu \mathrm{R}} = M_{\nu_\tau \mathrm{R}}$, which is almost equivalent to assuming the left-handed neutrino masses themselves as they are. Even an inverted hierarchy $m_{\nu_e} > m_{\nu_\mu} > m_{\nu_\tau}$ is not so unnatural.

For the neutrino mixing angle, only SO(10) gives some 'natural' prediction, which is $U(\text{quark}) = U(\text{lepton})$. This relation is not satisfied empirically both by atmospheric and solar neutrino experiments, whichever solution we take (see Chap. 8). The theoretical work in the state of the art at best shows that one can construct a model consistent with experiment; it is far from the prediction. The most difficult to understand is nearly maximal mixing angles.

As an alternative route, one may look in heuristic ways for the mass matrix that gives an empirically acceptable mass-mixing pattern and look for some underlying symmetry that governs the mass matrix, forgetting about vertical unification of particles for a while. Maximal mixings are un-

derstood most naturally when three neutrinos have originally a degenerate mass.

The idea of radiative corrections to give the neutrino a small mass is realised by introducing a scalar particle (with a mass of the order of the electroweak energy scale) that breaks lepton number in the Higgs potential. A left-handed neutrino mass is induced by a radiative correction from a scalar particle loop, and the neutrino mass is typically $m_\nu \sim f^2 m_\ell$, where f is the Yukawa coupling and m_ℓ is the charged lepton mass. This model requires some new physics only at the electroweak energy scale. This idea, however, does not make the problem of the neutrino mass spectrum easier. Some ad hoc prescriptions are needed to make the mass matrix consistent with experiment.

In the case of the Dirac neutrino, there are no generic reasons to explain the small neutrino mass because the Yukawa couplings to the Higgs particle are all given parameters of the theory. One must assume a large disparity typically by $\gtrsim 10^{10}$ between the Yukawa couplings for charged leptons and neutrinos. (An exceptional case is the model where neutrino mass is assumed to vanish by imposing some symmetry; see Sect. 6.10.) This seems to be unnatural, but it does not conflict with any known principles. This view, however, encounters difficulty once one attempts to understand the particle mass spectrum within grand unification, where quarks and leptons are treated on an equal footing. This is one of the important reasons why theorists generally prefer the Majorana neutrino to the Dirac neutrino as a more natural possibility. Some authors discuss the theory of extra dimensions to explain a small neutrino mass (see Chap. 6). Such a theory and needed assumptions, while interesting, are still highly speculative, and we cannot discuss it at the same level as other models based on more conventional ideas.

9.3 Grand Unification: Introduction

9.3.1 SU(5) GUT

Let us explain the elements of grand unification by taking as an example the prototype GUT with SU(5) [220]. SU(5) is the minimal semisimple gauge group that unifies the three gauge groups, SU(3)× SU(2)$_L$ × U(1)$_Y$ of the standard model. The 24 gauge fields $A_\mu^a(x)$ ($a = 1$–24) form an adjoint representation of SU(5). The covariant derivative is defined by

$$D_\mu = \partial_\mu + ig_5 A_\mu^a T^a, \tag{9.2}$$

where T^a is the generator of SU(5) Lie algebra ($a = 1$–24),

$$[T^a, T^b] = if_{abc} T^c \tag{9.3}$$

with f_{abc} the structure constant of SU(5) and g_5 the gauge coupling constant. We take T^a $(a = 1\text{–}8)$ so that they form SU(3) Lie algebra. The gluon fields G_μ^a $(a = 1\text{–}8)$ of colour SU(3) are then taken to associate with them and are defined by

$$G_\mu^a = \frac{\text{Tr}(\bar{A}_\mu T^a)}{|T|^2}, \tag{9.4}$$

where $\bar{A} \equiv A^a T^a$ and $|T|$ is defined by

$$\text{Tr}(T^a T^b) = |T|^2 \delta_{ab}. \tag{9.5}$$

The weak boson fields of SU(2) are

$$W_\mu^1 = \frac{\text{Tr}(\bar{A}_\mu T^{22})}{|T|^2}, \quad W_\mu^2 = \frac{\text{Tr}(\bar{A}_\mu T^{23})}{|T|^2}, \tag{9.6}$$

and

$$W_\mu^3 = \frac{\text{Tr}(\bar{A}_\mu I^3)}{|T||I^3|}. \tag{9.7}$$

Here, I^3 is defined by

$$I^3 = -i \left[T^{22}, T^{23} \right], \tag{9.8}$$

and I^3 is written using two of the Cartan subalgebra elements $(T^3, T^8, T^{15}, T^{24})$,

$$I^3 = \sqrt{\frac{5}{8}} T^{24} - \sqrt{\frac{3}{8}} T^{15}. \tag{9.9}$$

The gauge field of U(1)$_Y$ is given by

$$B_\mu = \frac{\text{Tr}(\bar{A}Y)}{|T||Y|}, \tag{9.10}$$

where hypercharge Y is determined as an operator orthogonal to I^3:

$$Y = \kappa \left(\sqrt{\frac{3}{8}} T^{24} + \sqrt{\frac{5}{8}} T^{15} \right). \tag{9.11}$$

The normalization factor κ is fixed as $\kappa = -2\sqrt{\frac{5}{3}}$, so that the lepton doublet has $Y = -1$ (we will see below that the lepton doublet belongs to the 5^* representation). The electromagnetic gauge field A_μ is given by

$$A_\mu = \frac{\text{Tr}(\bar{A}Q)}{|T||Q|}, \tag{9.12}$$

$$= \frac{\text{Tr}\left[\bar{A}(I^3 + \frac{1}{2}Y) \right]}{|T||Q|}, \tag{9.13}$$

$$= \frac{1}{2} \frac{|Y|}{|Q|} B_\mu + \frac{|I^3|}{|Q|} W_\mu^3. \tag{9.14}$$

Thus, we find the weak mixing angle

$$\mathrm{tg}\theta_W = 2\frac{|I^3|}{|Y|} = \sqrt{\frac{3}{5}}, \tag{9.15}$$

or

$$\sin^2\theta_W = \frac{3}{8}. \tag{9.16}$$

For the fundamental representation, the generator T^a is given by the 5×5 extension of the 3×3 Gell–Mann matrix $\frac{1}{2}\lambda^a_{ij}$, and the gauge fields are written by a 5×5 matrix as

$$T^a A^a_\mu = \frac{1}{2}\lambda^a\, A^a_\mu = \frac{1}{2}\begin{pmatrix} \lambda^b G^b_\mu - \frac{2}{3}\sqrt{\frac{3}{5}}B_\mu & X_\mu \\ X^\dagger_\mu & \lambda^c W^c_\mu + \sqrt{\frac{3}{5}}B_\mu \end{pmatrix}, \tag{9.17}$$

with $a = 1$–24, $b = 1$–8, and $c = 1$–3. Here, X_μ is the new gauge field of SU(5) transforming $(\mathbf{3},\mathbf{2})$ under SU(3)$\times$ SU(2). By inserting (9.17) into (9.2), we easily see the relations among the three gauge coupling constants g_3, g_2, and g' of the standard-model gauge interactions in terms of the SU(5) gauge coupling constant g_5 as

$$g_3 = g_2 = g_5, \qquad g' = \sqrt{\frac{3}{5}}g_5. \tag{9.18}$$

It is obvious that the weak mixing angle

$$\sin^2\theta_W = \frac{g_1^2}{g'^2 + g_2^2} = \frac{3}{8}, \tag{9.19}$$

in agreement with (9.16).

SU(5) is supposed to be broken down to the standard-model gauge group by vacuum condensation of a Higgs scalar $\Sigma(\mathbf{24})$ of an adjoint representation. The vacuum-expectation value should be invariant under SU(3), SU(2) and conserve U(1)$_Y$ charge, i.e.,

$$\langle\Sigma(\mathbf{24})\rangle = \begin{pmatrix} 2/3 & & & & \\ & 2/3 & & & \\ & & 2/3 & & \\ & & & -1 & \\ & & & & -1 \end{pmatrix} V. \tag{9.20}$$

The gauge boson X_μ of (9.17) then acquires mass:

$$m_X = \frac{5\sqrt{2}}{3}g_5 V \ . \tag{9.21}$$

The quarks and leptons in the standard model are embedded into $\mathbf{5^*}$ and $\mathbf{10}$ representations:

$$f(\mathbf{5^*})_{\mathrm{L}} = \begin{bmatrix} d^c \\ e \\ -\nu \end{bmatrix}_{\mathrm{L}}, \qquad (9.22)$$

and

$$f(\mathbf{10})_{\mathrm{L}} = \left[\begin{pmatrix} u \\ d \end{pmatrix}, u^c, e^c \right]_{\mathrm{L}}. \qquad (9.23)$$

More explicitly, $f(\mathbf{10})_{\mathrm{L}}$ is written

$$f(\mathbf{10})_{\mathrm{L}} = \frac{1}{\sqrt{2}} \begin{pmatrix} 0 & u_3^c & -u_2^c & u_1 & d_1 \\ -u_3^c & 0 & u_1^c & u_2 & d_2 \\ u_2^c & -u_1^c & 0 & u_3 & d_3 \\ -u_1 & -u_2 & -u_3 & 0 & e^c \\ -d_1 & -d_2 & -d_3 & -e^c & 0 \end{pmatrix}_{\mathrm{L}}. \qquad (9.24)$$

The exchange of X gauge bosons (often referred to as leptoquark bosons) induces proton decay via the effective interaction of dimension six, written as

$$\mathcal{L}_{\mathrm{d}=6} = \frac{g_5^2}{m_X^2} \epsilon_{\alpha\beta\gamma} \left[\left(d_R^\alpha u_R^\beta \right) (u_L^\gamma e_L) + (1 + |U_{ud}|^2) \left(d_L^\alpha u_L^\beta \right) (u_R^\gamma e_R) \right]. \qquad (9.25)$$

The decay rate is given by

$$\Gamma(p \to \pi^0 e^+) = \left(\frac{g_5^2 A_R}{m_X^2} \right)^2 [1 + (1 + |U_{ud}|^2)^2] \frac{1}{4\pi^2} \int \frac{d^3 q'}{2q_0'}$$
$$\times \int \frac{d^3 k'}{2k_0'} |W(k - q')|^2 \frac{k'k}{2m_p} \delta^4(k - k' - q'), \qquad (9.26)$$

where $W(k - q')$ is the form factor of the $p \to \pi$ matrix element,

$$\langle \pi(q) | (d_R u_R) u_L | p(k) \rangle = \frac{1 - \gamma_5}{2} W(q - k) u_p(k), \qquad (9.27)$$

and k, k' and q' are four momenta of proton, positron, and pion, respectively; g_5 is the universal gauge coupling at the GUT scale, $g_5^2/4\pi \simeq 1/40$, and the factor $A_R \simeq 3.6$ represents the renormalization effect for the operators, $(d_R^\alpha u_R^\beta)(u_L^\gamma e_L)$ and $(d_L^\alpha u_L^\beta)(u_R^\gamma e_R)$. This matrix element was calculated with quenched lattice QCD [1363], which indicates that the momentum dependence of the hadron matrix element is weak and $W \simeq -0.15\,\mathrm{GeV}^2$, so that

$$\tau(p \to \pi^0 e^+) \simeq 1.5 \times 10^{31} \times \left(\frac{m_X}{10^{15}\,\mathrm{GeV}} \right)^4 \left(\frac{0.15\,\mathrm{GeV}^2}{|W|} \right)^2 \mathrm{yr}. \qquad (9.28)$$

The proton decay rate formula has traditionally been represented by the $|p\rangle \rightarrow |0\rangle$ transition amplitude with the aid of PCAC, which requires extrapolation of the pion energy-momentum to zero, and the matrix element is parametrised as

$$\alpha \Psi_p(\mathbf{k}) \equiv \epsilon_{\alpha\beta\gamma} \langle 0|(d_R^\alpha u_R^\beta)u_L^\gamma|p(\mathbf{k})\rangle \ . \tag{9.29}$$

There are many estimates using varieties of quark models, which result in a wide range, $\alpha = 0.003\text{--}0.03\,(\text{GeV})^3$ [1364]. The above lattice value, if represented effectively by this parametrisation, gives $\alpha \simeq 0.015\,\text{GeV}^3$.

The standard-model Higgs boson doublet H_f belongs to $\mathbf{5}$, and hence is accompanied with a coloured partner H_c (triplet) as

$$H(\mathbf{5}) = \begin{bmatrix} H_c \\ H_f \end{bmatrix} . \tag{9.30}$$

This Higgs $H(\mathbf{5})$ couples to fermions through the Yukawa coupling,

$$\mathcal{L}_{\text{Yukawa}} = \sqrt{2}f^{ij}f(\mathbf{10}_i^{\alpha\beta})_L f(\mathbf{5}^*{}_{\alpha j})_L H^*{}_\beta + \frac{1}{4}h^{ij}\epsilon_{\alpha\beta\gamma\delta\epsilon}f(\mathbf{10}_i^{\alpha\beta})_L f(\mathbf{10}_j^{\gamma\delta})_L H^\epsilon, \tag{9.31}$$

where $i, j = 1, 2, 3$ refer to families and $\alpha, \beta, \gamma...$ represent SU(5) indices. This yields, when written in components, the GUT mass relation for the quark–lepton mass, $m_e = m_d$, $m_\mu = m_s$, and $m_\tau = m_b$. The last relation turns out to be successful when one takes into account the renormalization effect [1365], but the first two are largely violated. We remark that a nonrenormalisable interaction,

$$\delta\mathcal{L}_{\text{Yukawa}} = \frac{g_{ij}}{m_{\text{pl}}}f(\mathbf{5}^*{}_i)_L f(\mathbf{10}_j)_L \Sigma(\mathbf{24})H^*(\mathbf{5}^*), \tag{9.32}$$

may disturb the GUT mass relation for the first and the second generations if $g_{ij} \simeq O(1)$, while such a contribution is negligible for the third generation.

The exchange of the coloured Higgs H_c induces operators for proton decay and hence its mass must be as large as the GUT scale to suppress it. On the other hand, the Higgs doublet H_f should have mass of the order of $100\,\text{GeV}$. This huge disparity can be realized, in principle, by introducing a coupling to $\Sigma(\mathbf{24})$, in addition to the SU(5) invariant mass, as

$$\mathcal{L} = \kappa H^*\Sigma H + M^2 H^* H. \tag{9.33}$$

We obtain mass splitting between H_f and H_c after SU(5) breaking as

$$m_{H_c}^2 = M^2 + \frac{2\kappa}{3}V, \qquad m_{H_f}^2 = M^2 - \kappa V. \tag{9.34}$$

The required mass spectrum is realised if $\kappa V \simeq M^2$. This requires, however, not only fine-tuning, but also stability to radiative corrections, which are quadratically divergent with the cutoff. Nevertheless, this is still logically consistent with the idea of renormalisation theory, and we may assume that the renormalised physical masses satisfy the requirement after all quantum corrections.

The two basic tests for this minimal SU(5) grand-unification model are the lifetime of proton decay and the weak mixing angle. We first need to estimate the GUT scale M_{G}. It is determined by using the renormalisation group equation,

$$\mu \frac{d\alpha_i}{d\mu} = -2b_i\alpha_i^2, \tag{9.35}$$

where μ is the energy scale of renormalisation and b_i are one-loop beta function coefficients. The requirement that the three couplings associated with SU(3), SU(2), and U(1) agree on one scale M_{G} leads to a unique prediction for the renormalisation of $\sin^2\theta_W$ [1342]. In the following argument, we assume Higgs particles of the minimal extent needed to break symmetries.

Integrating (9.35), the evolution of the three running coupling constants $\alpha_3(\mu)$, $\alpha_2(\mu)$ and $\alpha_1(\mu)$ from $\mu = M_{\mathrm{G}}$ to m_{Z^0} is given by

$$\alpha_i^{-1}(\mu) = \alpha_i^{-1}(M_{\mathrm{G}}) - 2b_i\log(M_{\mathrm{G}}/\mu) , \tag{9.36}$$

with

$$b_3 = \frac{1}{4\pi}\left(11 - \frac{4}{3}N_{\mathrm{f}}\right),$$

$$b_2 = \frac{1}{4\pi}\left(\frac{22}{3} - \frac{4}{3}N_{\mathrm{f}} - \frac{1}{6}N_H\right),$$

$$b_1 = -\frac{1}{4\pi}\left(\frac{4}{3}N_{\mathrm{f}} + \frac{1}{10}N_H\right), \tag{9.37}$$

where $N_H = 1$ is the number of Higgs doublets. We note that g_1 associated with U(1) in SU(5) is related to g' of U(1)$_Y$ by

$$g_1 = (5/3)^{1/2}g', \tag{9.38}$$

as shown in (9.18). By requiring unification, $\alpha_3(M_{\mathrm{G}}) = \alpha_2(M_{\mathrm{G}}) = \alpha_1(M_{\mathrm{G}})$ (this gives $\sin^2\theta_W \equiv g'^2/(g^2 + g'^2) = 3/8$ at $\mu = M_{\mathrm{G}}$), we obtain

$$\log\left(\frac{M_{\mathrm{G}}}{\mu}\right) = \frac{\alpha_{\mathrm{em}}^{-1}(\mu) - (\frac{8}{3})\alpha_3^{-1}(\mu)}{2[(\frac{8}{3})b_3 - b_2 - \frac{5}{3}b_1]}, \tag{9.39}$$

which gives

$$\sin^2\theta_W(\mu) = \frac{b_3 - b_2 + \frac{5}{3}(b_2 - b_1)\dfrac{\alpha_{\mathrm{em}}(\mu)}{\alpha_3(\mu)}}{\frac{8}{3}b_3 - b_2 - \frac{5}{3}b_1}. \tag{9.40}$$

These expressions are independent of N_f. Adopting the $\overline{\text{MS}}$ scheme, we obtain

$$M_G = 1.08 \, ^{+0.19}_{-0.17} \times 10^{15} \, \text{GeV}, \tag{9.41}$$

$$\sin^2 \theta_W(m_Z) = 0.2095 \, ^{+0.0007}_{-0.0006}, \tag{9.42}$$

with the use of the low-energy parameters $\alpha(m_Z)$ of (2.138) and

$$\alpha_3(m_Z) = 0.1185 \pm 0.0020 \tag{9.43}$$

for the QCD coupling constant [275]. The predictions are appreciably modified if we include two-loop corrections [1366],

$$M_G = 0.610 \, ^{+0.11}_{-0.097} \times 10^{15} \, \text{GeV}, \tag{9.44}$$

$$\sin^2 \theta_W(m_Z) = 0.213 \, ^{+0.0007}_{-0.0006}. \tag{9.45}$$

We see that the weak mixing angle (9.42) is significantly smaller than the experimental value 0.2312 ± 0.0002 [see (2.152); we omit a hat symbol here], now at 100σ! (e.g. [1367]). Furthermore, by equating M_G with m_X in (9.28), we obtain $\tau(p \to \pi^0 e^+) \simeq 1.9 \times 10^{30 \pm 0.8} \, \text{yr}$ for $|W| \simeq 0.15 \, \text{GeV}^2$. By 1985 the minimal version of the SU(5) model was ruled out due to the null result $\tau(p \to e^+ \pi^0) > 3 \times 10^{32} \, \text{yr}$ at the 90% CL (see, e.g. [1368]). The current lower limit is $> 1.6 \times 10^{33} \, \text{yr}$ at the 90% CL [1369], far off from the prediction.

The disagreement of the electroweak mixing angle is often represented in the following way. From the low-energy parameters $\alpha(m_Z)$ [(2.138)], $\sin^2 \theta_W(m_Z)$ [(2.152)] we may write with the aid of (2.131) and (9.38),

$$\alpha_1^{-1}(m_Z) = 59.98 \pm 0.04 \;, \tag{9.46}$$

and

$$\alpha_2^{-1}(m_Z) = 29.57 \pm 0.03 \;. \tag{9.47}$$

We may look at the evolution of the three running couplings, $\alpha_1, \alpha_2, \alpha_3$, as shown in Fig. 9.1, which indicates that they do not match on a single unification energy scale [1370], i.e., inconsistency of unification.

The concept of running coupling also applies to quark and lepton masses. The evolution of the mass ratio, m_{d_i}/m_{e_i} for generation i is given by

$$\frac{\partial}{\partial \ln \mu} \ln \frac{m_{d_i}(\mu)}{m_{e_i}(\mu)} = \frac{2}{\pi} \alpha_3(\mu) - \frac{1}{2\pi} \alpha_1(\mu), \tag{9.48}$$

at the one-loop level [1365] with $\alpha_3(\mu)$ and $\alpha_1(\mu)$ given by (9.36). Integration with the GUT boundary condition $m_{d_i}(M_G) = m_{e_i}(M_G)$ leads to
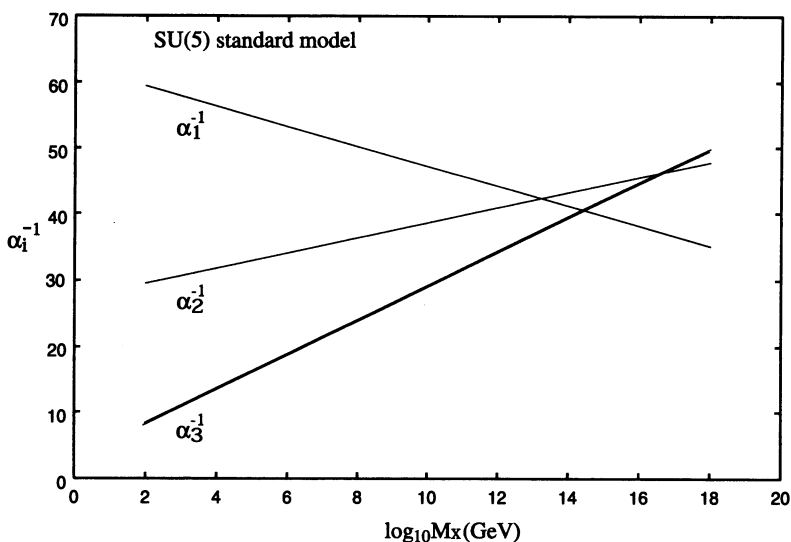
Fig. 9.1. Matching the three running couplings in the SU(5) grand unification model using the three low-energy parameters, α_1, α_2, and α_3, as input. The thick width of the curve for α_3^{-1} stands for the error range. The errors for α_1^{-1} and α_2^{-1} are smaller than the line widths. Two-loop calculations are included.

$$\ln\frac{m_{d_i}(\mu)}{m_{e_i}(\mu)} \simeq \frac{4}{11-4/3N_{\mathrm{f}}}\ln\frac{\alpha_3(\mu)}{\alpha_3(M_{\mathrm{G}})} + \frac{3}{4N_{\mathrm{f}}}\ln\frac{\alpha_1(\mu)}{\alpha_1(M_{\mathrm{G}})}. \qquad (9.49)$$

For $N_{\mathrm{f}} = 3$ we obtain

$$\frac{m_{d_i}(\mu)}{m_{e_i}(\mu)} \simeq \left[\frac{\alpha_3(\mu)}{\alpha_3(M_{\mathrm{G}})}\right]^{\frac{4}{7}} \times \left[\frac{\alpha_1(\mu)}{\alpha_1(M_{\mathrm{G}})}\right]^{\frac{1}{4}}. \qquad (9.50)$$

We may define the quark masses as $m_i(\mu) = \mu$. The bottom quark mass is probably large enough to justify a perturbative calculation. We obtain for $m_\tau = 1.8\,\mathrm{GeV}$,

$$m_b \sim 6\,\mathrm{GeV}, \qquad (9.51)$$

where $\alpha_3(10\,\mathrm{GeV}) \simeq 0.23$, $\alpha_1(10\,\mathrm{GeV}) \simeq 0.016$ and $\alpha_3(M_{\mathrm{G}}) \simeq 0.022$ are used. We show in Table 9.1 the quark and lepton masses at the unification scale calculated including two-loop corrections for the standard SU(5) GUT [1374,1371].[4] The GUT relation for the first and the second generations derived in the same way, however, does not agree with experiment.

---

[4] The unification scale does not meet at one point with non-SUSY GUT. Nevertheless, we assume that the unification scale is 10^{15} GeV. Only one Higgs multiplet is assumed, in addition to three families of quarks and leptons.

Table 9.1. Lepton and quark masses (in GeV units) at the physical scale and at the GUT energy scale [1371].

model	e	μ	τ	u	c	t	d	s	b
Physical scale[a]	0.511×10^{-3}	0.106	1.78	0.0025	1.25	174	0.0044	0.088	4.25
SU(5) GUT[b]	0.486×10^{-3}	0.103	1.74	0.00057	0.26	84	0.0010	0.020	1.10
SO(10) GUT[c]	0.460×10^{-3}	0.097	1.65	0.00055	0.25	82	0.0010	0.019	1.10
SUSY SU(5) GUT[d]	0.353×10^{-3}	0.073	1.25	0.00055	0.25	101	0.00073	0.014	1.03

a With lattice QCD estimate for $(m_u+m_d)/2 \simeq 3.44\,\mathrm{MeV}$ and $m_s \simeq 88\,\mathrm{MeV}$ at $\mu = 2\,\mathrm{GeV}$ [1372]; $m_u/m_d = 0.57$ is the current algebra value [1373].
b With an assumed unification scale of $2 \times 10^{15}\,\mathrm{GeV}$ for non-SUSY GUT.
c With the intermediate Pati–Salam group.
d With $\mathrm{tg}\beta_\mathrm{H} \simeq 20$.

The final comment concerns the SU(5) monopole that appears when SU(5) is broken to its subgroup [1375]. The problem is that such monopoles were created in the early universe by about one per volume of the horizon scale when the universe cooled passing through the symmetry-breaking temperature. The *comoving scale* corresponding to the horizon at GUT energy is about 10 cm, so that we have one monopole for every $1000\,\mathrm{cm}^{-3}$. Since the mass of GUT monopoles is of the order of $M_\mathrm{G}/\alpha_\mathrm{G}$, this leads to a gross overdensity of the universe by a factor of 10^{19}. The actual relic monopole abundance is much smaller than this value due to monopole–antimonopole annihilation, but it still largely exceeds the critical density by a factor of 10^{13} [1376]. We usually suppose that these monopoles are diluted by cosmological inflation [1377], or else, GUT scenario is invalidated.

9.3.2 SUSY SU(5) GUT

The supersymmetric (SUSY)-theory ($\mathcal{N} = 1$ SUSY)[5] extension is made by preparing for each particle i a chiral superfield Φ_i that contains a boson φ_i and a left-handed chiral fermion ψ_i as

$$\Phi_i = \varphi_i + \epsilon_{\alpha\beta}\theta_\alpha\psi_{\beta i} + \epsilon_{\alpha\beta}\theta_\alpha\theta_\beta F_i, \qquad (9.52)$$

where F_i is an auxiliary F field and θ is the anticommuting Grassmann coordinate. The Lagrangian $\mathcal{L}$ is written

$$\mathcal{L} = \int d^4\theta K(\Phi_i, \Phi_i^\dagger) + \int d^2\theta W(\Phi_i) + \mathrm{h.c.} \qquad (9.53)$$

---

[5] See textbooks [1378, 1379] for details.

In renormalizable theory we should take

$$K(\Phi_i, \Phi_i^\dagger) = \Phi_i^\dagger \Phi_i, \qquad (9.54)$$

which yields the kinetic term,

$$\mathcal{L}_K = \partial_\mu \varphi_i^\dagger \partial^\mu \varphi_i + \bar\psi_i \partial \psi_i + F_i^\dagger F_i, \qquad (9.55)$$

upon integration over θ. The superpotential W is a holomorphic function of Φ_i:

$$W(\Phi_i) = \kappa \Phi_i + m_{ij}\Phi_i \Phi_j + g_{ijk}\Phi_i \Phi_j \Phi_k. \qquad (9.56)$$

The potential is given by

$$V = F_i^\dagger F_i = \left| \frac{\partial W(\varphi_i)}{\partial \varphi_i} \right|^2. \qquad (9.57)$$

The gauge fields are contained in the superfields $\mathcal{W}_\alpha$ as

$$\mathcal{W}_\alpha^a = \lambda_\alpha^a + \left[D^a \delta_\alpha^\beta - \frac{i}{2}(\sigma^\mu \bar\sigma^\nu)_\alpha^\beta F_{\mu\nu}^a \right]\theta_\beta + \epsilon_{\gamma\delta}\theta_\gamma \theta_\delta \sigma_{\alpha\beta}^\mu D_\mu (\lambda^{aC})^\beta. \qquad (9.58)$$

Here, λ_α^a are fermion partners of gauge fields called gauginos, D^a are auxiliary D fields, $F_{\mu\nu}^a$ are field tensors of the gauge fields, and D_μ are the covariant derivatives defined as in Chap. 2. The matrices σ and $\bar\sigma$ are defined in (7.29) and (7.30); λ^C is the charge-conjugate field of λ. The Lagrangian for the gauge fields is written

$$\mathcal{L} = \int d^2\theta \epsilon_{\alpha\beta} \mathcal{W}_\alpha \mathcal{W}_\beta + \text{h.c.} \qquad (9.59)$$

This yields the kinetic term,

$$\mathcal{L} = \frac{1}{4} F^{a\mu\nu} F_{\mu\nu}^a + \bar\lambda^a \gamma^\mu D_\mu \lambda^a + D^2. \qquad (9.60)$$

It is straightforward to extend the standard model to a supersymmetric version by replacing all standard-model fields by superfields [1380]. There is, however, one new field to be included. We need a pair of Higgs chiral multiplets H and $\bar H$ to cancel gauge anomaly, i.e., we need two SU(2)-doublet Higgs bosons [1380]. Two Higgs multiplets are also necessary to give masses to up- and down-type quarks because the superpotential is a holomorphic function of chiral superfields Φ_i, which forbids us to use H^*, as in the standard theory.

The SUSY extension of the SU(5) GUT is also straightforward [1381]. The pair of Higgs multiplets is embedded in a pair of Higgs chiral superfields $H(\mathbf{5})$ and $\bar{H}(\mathbf{5^*})$, and in addition, we introduce a chiral superfield $\Sigma(\mathbf{24})$ whose scalar component has a vacuum-expectation value (9.20). This is the minimal version, often called *minimal SUSY SU(5) GUT*. With the superpotential,

$$W = M_\mathrm{H}\bar{H}H + \lambda\bar{H}\Sigma H , \qquad (9.61)$$

the scalar mass is given by

$$m_{\mathrm{H_c}} = M_\mathrm{H} + \frac{2}{3}\lambda V, \qquad m_{\mathrm{H_f}} = M_\mathrm{H} - \lambda V. \qquad (9.62)$$

As in ordinary GUT, we need fine-tuning ($M_\mathrm{H} \simeq \lambda V$) of the parameters M_H and λ to obtain the doublet Higgs at the electroweak scale. The advantage, however, is that the bare parameters in the superpotential do not receive quantum corrections in the SUSY limit due to cancellation between fermion and boson loops [1382]. The correction remains logarithmic in the presence of SUSY breaking. Thus, the small mass of the Higgs doublet is stable to radiative corrections and remains on the electroweak scale as long as the SUSY-breaking scale m_SUSY is of the order of the electroweak scale. We must assume $m_\mathrm{SUSY} \simeq 100\,\mathrm{GeV}$–$1\,\mathrm{TeV}$.

The quarks and leptons are embedded in chiral superfields $\Phi(\mathbf{5^*})$ and $\Psi(\mathbf{10})$ where fermion components are all left-handed. Thus, each quark and lepton is always accompanied with a boson partner, called a scalar quark (squark) and a scalar lepton (slepton). Similarly, all gauge fields are embedded in vector superfields, and they have fermion partners called gauginos. These SUSY particles are supposed to have masses of the order of the SUSY-breaking scale m_SUSY.

SUSY is supposed to be spontaneously broken by an F term condensation of some gauge singlet field Z which does not directly couple to the standard-model fields. The field Z induces the SUSY-breaking effect in the standard-model fields through nonrenormalisable effective operators [1383]

$$\mathcal{L} = \int d^4\theta \frac{h}{m_\mathrm{pl}^2} Z^\dagger Z \Phi_\mathrm{quark}^\dagger \Phi_\mathrm{quark} + \cdots + \int d^2\theta \frac{k}{m_\mathrm{pl}} Z\epsilon_{\alpha\beta}\mathcal{W}_\alpha\mathcal{W}_\beta + \mathrm{h.c.} \quad (9.63)$$

These interactions generate soft SUSY-breaking masses for squarks, sleptons, and gauginos as

$$m_\mathrm{squark}^2 = \frac{h}{m_\mathrm{pl}^2}|F_Z|^2, \quad \cdots, \quad m_\lambda = \frac{k}{m_\mathrm{pl}}|F_Z|. \qquad (9.64)$$

We assume that the SUSY breaking scale is $|F_Z| \simeq (10^{11}\,\mathrm{GeV})^2$, so that we obtain the effective SUSY-breaking scale for the SUSY partners as of the order of

$100\,\mathrm{GeV}-1\,\mathrm{TeV}$. If we extend the present model to supergravity, the gravitino (the fermion partner of the graviton) acquires mass of $|F_Z|/(\sqrt{3/8\pi}m_{\mathrm{pl}})$, which is the same order as masses of squarks and sleptons.

If SUSY particles (e.g., squarks, sleptons and gauginos) exist, they contribute to the coefficients of beta functions above their thresholds by the amount [1345]

$$\Delta b_3 = \frac{1}{4\pi}\left(-2 - \frac{2}{3}N_{\mathrm{f}}\right),$$

$$\Delta b_2 = \frac{1}{4\pi}\left(-\frac{4}{3} - \frac{2}{3}N_{\mathrm{f}} - \frac{1}{3}N_{\mathrm{H}}\right),$$

$$\Delta b_1 = \frac{1}{4\pi}\left(-\frac{2}{3}N_{\mathrm{f}} - \frac{1}{5}N_{\mathrm{H}}\right), \qquad (9.65)$$

where $N_{\mathrm{H}} = 2$ for the minimal SUSY GUT. With these modifications, the evolution of $\alpha_3(\mu)$ somewhat slows down relative to $\alpha_2(\mu)$ and $\alpha_1(\mu)$, and the three gauge couplings α_3, α_2, and α_1 meet on a single energy scale, which is higher than that for the SU(5) GUT. With empirical α_3 and α_{em}, we obtain $M_{\mathrm{G}} = 2.19^{+0.44}_{-0.37} \times 10^{16}\,\mathrm{GeV}$ and $\sin^2\theta_W = 0.2308 \pm 0.0006$ from (9.39) and (9.40). With two-loop corrections [1384],

$$\sin^2\theta_W(m_Z) = 0.2273 \pm 0.0006, \qquad (9.66)$$

$$M_{\mathrm{G}} = 2.97^{+0.60}_{-0.50} \times 10^{16}\,\mathrm{GeV}. \qquad (9.67)$$

This weak mixing angle shows very good agreement with experiment (2.152) [1370], and this is taken as evidence supporting the presence of supersymmetry. The unification scale is substantially higher than that of the conventional SU(5) model. Nucleon decay induced by the gauge-boson exchange via the conventional dimension-six operators is much slower, of the order of $\tau = 10^{36\pm1}$ yr.

In Fig. 9.2 the evolution of the three gauge couplings is shown using the experimentally determined low-energy coupling constants, $\alpha_3, \alpha_{\mathrm{em}}, \sin^2\theta_W$ as input. Here, all SUSY particles are assumed to have a common mass of $m_{\mathrm{SUSY}} = m_{Z^0}/2$. The agreement of the three couplings would not be spoiled insofar as $50\,\mathrm{GeV} \lesssim m_{\mathrm{SUSY}} \lesssim 10\,\mathrm{TeV}$.

The Yukawa couplings of Higgs multiplets are given by

$$W = \sqrt{2}f^{ij}\Psi_i^{\alpha\beta}\Phi_{\alpha j}\bar{H}_\beta + \frac{1}{4}h^{ij}\epsilon_{\alpha\beta\gamma\delta\epsilon}\Psi_i^{\alpha\beta}\Psi_j^{\gamma\delta}H^\epsilon, \qquad (9.68)$$

where $i, j = 1, 2, 3$ refer to families, and $\alpha, \beta, \gamma\dots$ represent SU(5) indices. The chiral superfields $\Phi(\mathbf{5}^*)$ and $\Psi(\mathbf{10})$ are given by the same form as (9.22) and (9.24), respectively. We now count how many physical parameters are involved in the Yukawa interaction. The complex Yukawa couplings f^{ij} have
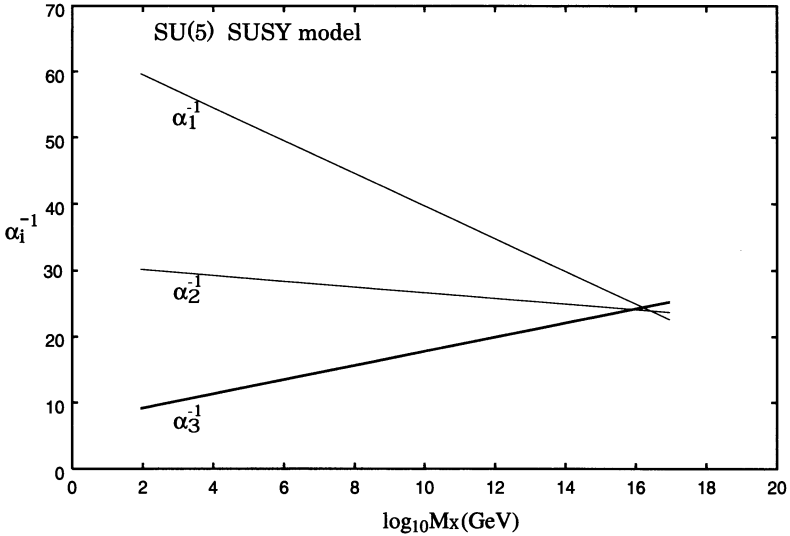
Fig. 9.2. Matching the three running couplings in the minimal SUSY SU(5) model (two-loop result). The masses of SUSY particles are all assumed to be $m_Z/2$.

$6{\times}2$, and a symmetric matrix h^{ij} contains $9{\times}2$. The freedom for the field redefinition of Φ_i and Ψ_i is U(3)$\times$U(3). Thus, the physical degree of freedom is $(6+9) \times 2 - 9 \times 2 = 3 + 3 + 4 + 2$, where the two 3's stand for the mass eigenvalues of up- and down-type quarks, 4 for the quark mixing matrix elements, and 2 for additional phases. We take a basis where h^{ij} is diagonal

$$h^{ij} = h^i e^{i\varphi_i} \delta^{ij}. \tag{9.69}$$

Then, f^{ij} is given by

$$f^{ij} = V_{ij}^* f^j, \tag{9.70}$$

where V_{ij} is the mixing matrix. Among the three phases φ_i, only two are independent; so we take

$$\varphi_u + \varphi_c + \varphi_t = 0. \tag{9.71}$$

The Yukawa couplings of Higgs to matter multiplets are given in terms of mass eigenstates $u_i, d_i, u_i^c, d_i^c, \nu_i, e_i, e_i^c$ as

$$W = f_i e_i^c \ell_i \bar{H}_{\mathrm{f}} + V_{ij}^* f^j q_i d_j^c \bar{H}_{\mathrm{f}} + h^i q_i u_i^c H_{\mathrm{f}}$$

$$+ V_{ij}^* f^j q_i \ell_j \bar{H}_{\mathrm{c}} + e^{-i\varphi_i} V_{ij}^* f^j u_i^c d_j^c \bar{H}_{\mathrm{c}}$$

$$+ \frac{1}{2} h^i e^{i\varphi_i} q_i q_i H_{\mathrm{c}} + h^i V_{ij} u_i^c e_j^c H_{\mathrm{c}}, \tag{9.72}$$

where

$$\ell_i = \begin{pmatrix} \nu_i \\ e_i \end{pmatrix},$$

$$q_i = \begin{pmatrix} u_i \\ V_{ij}d_j \end{pmatrix}. \tag{9.73}$$

This interaction gives quark and lepton masses. In particular, the mass ratio of top and bottom quarks is given by

$$\frac{m_t}{m_b} = \frac{h_t}{f_b} \mathrm{tg}\beta_{\mathrm{H}}, \tag{9.74}$$

where $\mathrm{tg}\beta_{\mathrm{H}} \equiv \langle H_{\mathrm{f}} \rangle / \langle \bar{H}_{\mathrm{f}} \rangle$.

In addition, we have dangerous baryon-number-violating Yukawa couplings,

$$W = k_{ijk} \Phi_{\alpha i} \Phi_{\beta j} \Psi_k^{\alpha\beta}, \tag{9.75}$$

which causes proton decay that is too fast. We suppress this operator by imposing an R parity (also called matter parity),

$$\Phi_{\alpha i} \to -\Phi_{\alpha i}, \qquad \Psi_i^{\alpha\beta} \to -\Psi_i^{\alpha\beta}. \tag{9.76}$$

Because of this matter parity, the lightest SUSY particle (LSP) is stable, and it may be an interesting candidate [1350] for the dark matter in the Universe.

The exchange of the coloured Higgs H_c and $\bar{H}_c$ induces a new class of operators (called dimension-five operators) that cause nucleon decay [1351]. The relevant operators are written

$$W_{\mathrm{d}=5} = \frac{1}{2m_{\mathrm{H_c}}} h^i e^{i\varphi_i} V_{kl}^* f^l (q_i q_i)(q_k \ell_l) + \frac{1}{m_{\mathrm{H_c}}} h^i V_{ij} e^{-i\varphi_k} V_{kl}^* f^l (u_i^c e_j^c)(u_k^c d_l^c), \tag{9.77}$$

with the contraction of SU(5) indices

$$(q_i q_i)(q_k \ell_l) = \epsilon_{\alpha,\beta,\gamma} (u_i^\alpha d_i'^\beta - d_i'^\alpha u_i^\beta)(u_k^\gamma e_l - d_k'^\gamma \nu_l),$$

$$(u_i^c e_j^c)(u_k^c d_l^c) = \epsilon^{\alpha,\beta,\gamma} u_{\alpha i}^c e_j^c u_{\beta k}^c d_{\gamma l}^c, \tag{9.78}$$

where α, β, γ are colour SU(3) indices and d_i' is defined by

$$d_i' = V_{ij} d_j. \tag{9.79}$$

Total antisymmetry in colour indices requires that the operators are flavour non-diagonal (i.e. $i \neq k$). Thus, dominant decay modes involve strangeness, like $n, p \to K\bar{\nu}$ [1385].

The dimension-five operators are converted into the standard form of dimension-six four-fermi operators at the SUSY-breaking scale by exchanges mainly of the charged wino $\tilde{w}^{\pm}$ (the fermion partner of $W^{\pm}$). The resulting four-Fermi operators are

$$\mathcal{L}'_{\text{d}=6} \simeq \frac{\alpha_2}{\pi} \frac{1}{m_{\text{H}_c} m_{\tilde{w}}} h^i e^{i\varphi_i} V^*_{jk} f^k \epsilon_{\alpha,\beta,\gamma} \times \left[(u^\alpha_i d'^\beta_i)(d'^\gamma_j \nu_k) \right.$$
$$\left. + (d'_i u^\beta_i)(u^\gamma_j e_k) + (d'^\alpha_i \nu_k)(d'^\beta_i u^\gamma_j) + (u^\alpha_i d'^\beta_j)(u^\gamma)_i e_k \right] . \quad (9.80)$$

We see that the main modes $n, p \to K\bar{\nu}$ come from the terms with $(i, j, k) = (c, u, s)$ and (t, u, s). The nucleon lifetime [1386] is

$$\tau(p \to K^+ \bar{\nu}) \quad (9.81)$$

$$\simeq 1.3 \times 10^{32} \left[\frac{0.014\,\text{GeV}^3}{\beta} \sin^2 \beta_{\text{H}} \frac{m_{\text{H}_c}}{10^{17}\,\text{GeV}} \left(\frac{m_{\tilde{f}}}{1\,\text{TeV}} \right)^2 \frac{200\,\text{GeV}}{m_{\tilde{w}}} \right]^2 \text{yr},$$

$$\tau(n \to K^0 \bar{\nu}) \quad (9.82)$$

$$\simeq 7.2 \times 10^{31} \left[\frac{0.014\,\text{GeV}^3}{\beta} \sin^2 \beta_{\text{H}} \frac{m_{\text{H}_c}}{10^{17}\,\text{GeV}} \left(\frac{m_{\tilde{f}}}{1\,\text{TeV}} \right)^2 \frac{200\,\text{GeV}}{m_{\tilde{w}}} \right]^2 \text{yr},$$

using the conventional definition of the matrix element reduced to $\langle 0|O|p\rangle$,

$$\beta \Psi_p(\mathbf{k}) \equiv \epsilon_{\alpha,\beta,\gamma} \langle 0|(d^\alpha_L u^\beta_L) u^\gamma_L |p, \mathbf{k}\rangle ; \quad (9.83)$$

$m_{\tilde{f}}$ denotes the mass of scalar leptons and quarks. These decay rate formulae assume that subtle cancellation does not happen among the terms[6]. In lattice QCD calculations the hadronic matrix element involved in $p \to K$ decays is estimated without resorting to $\langle 0|O|p\rangle$. Taking (9.83), however, as a convention, the result of lattice calculations [1363] corresponds to $\beta \simeq 0.014\,(\text{GeV})^3$. The limit on nucleon lifetime is [1390, 1391]

$$\tau(p \to K^+ \bar{\nu}) > 6.7 \times 10^{32} \text{yr}, \quad (9.84)$$

$$\tau(n \to K^0 \bar{\nu}) > 0.86 \times 10^{32} \text{yr}. \quad (9.85)$$

From the limit on $p \to K^+ \bar{\nu}$ decay we are led to coloured Higgs mass $m_{\text{H}_c} > 2 \times 10^{17}\,\text{GeV}$ [1388] for $m_{\tilde{f}} \lesssim 1\,\text{TeV}$ and $m_{\tilde{w}} \gtrsim 200\,\text{GeV}$. On the other hand, a renormalisation group analysis of running couplings [1392] shows that coupling unification is sustained only when $3.5 \times 10^{14} \lesssim M_{H_c} < 3.6 \times 10^{15}\,\text{GeV}$ (at a 90% confidence level) [1393]. This large disparity in m_{H_c} is counted as a difficulty of the minimal SUSY SU(5).

---

[6] It was argued that the $K\bar{\nu}_\mu$ decay mode may be suppressed if relative phases between Yukawa couplings of coloured Higgs interaction take specific values [1387]. Goto and Nihei [1388], however, showed that such cancellation does not take place and the $K\bar{\nu}$ decay rates vary little against the variation of the phase (and also of $\text{tg}\beta_H$) if the $K\bar{\nu}_\tau$ decay mode [1389] is included.

9.3.3 Introduction of $B-L$ and Massive Neutrinos

The natural way to discuss neutrino mass in the framework of SU(5) or SUSY SU(5) is to introduce extra U(1) symmetry. The anomaly-free conditions for $U(1)^3$ and $U(1)\cdot SU(5)^2$ triangle diagrams lead us to the unique assignment of U(1) charges $+1$, -3, and $+5$ for **10**, **5***, and **1**, where **1** represents the right-handed neutrino $(\nu_R)^c$ that is introduced to fulfill the anomaly-free conditions. This U(1) symmetry is called fiveness [we write it as $U(1)_5$] and agrees with U(1) of SU(5)$\times$U(1) contained as a subgroup in SO(10). When $U(1)_5$ is broken, the right-handed neutrino acquires mass. Breaking of $U(1)_5$ is independent of breaking of SU(5); so there is no constraint on the symmetry breaking scale from low-energy phenomenology. The simplest grand unification in which ν_R is automatically incorporated and a prediction is given for the neutrino mass is that with SO(10), but constraints are tight in this scheme. With SU(5), one may use the fact that in the SU(5)$\times$U(1) model, **10**, **5***, and **1** are independent, unlike in SO(10) where they belong to the same multiplet, as a freedom for model construction. This freedom may be used to construct a neutrino mass matrix consistent with experiment.

If one breaks SU(5)$\times U(1)_5$ down to the standard-theory gauge group but keeps an additional U(1), one ends up uniquely with SU(3)$\times$SU(2)$\times U(1)_Y \times U(1)_{B-L}$ where fiveness and a diagonal component of SU(5) are rearranged into $U(1)_Y$ and $U(1)_{B-L}$. Namely, $B-L$ is given by a linear combination of fiveness Y_5 and hypercharge Y:

$$B - L = \frac{1}{5}Y_5 + \frac{2}{5}Y. \tag{9.86}$$

$B-L$ gauge symmetry in the standard model is free from anomaly if right-handed neutrinos exist, and hence it is a key ingredient for predicting the existence of right-handed neutrinos. The neutrino mass is determined by the $B-L$ breaking scale. See Sect. 6.6 in this connection.

As an alternative path, this $B-L$ symmetry is naturally introduced into the left–right symmetric model: if SU(2)$_\mathrm{L}\times$SU(2)$_\mathrm{R}\times$U(1) breaks down to SU(2)$_L\times$U(1)$_Y$, the former U(1) must be $U(1)_{B-L}$. The ubiquity of the appearance of $U(1)_{B-L}$ in unified theories is due to the fact that it is the unique, anomaly-free U(1) gauge group other than the standard theory groups.

9.3.4 Constraints on U(1) Symmetry Breaking: Cosmic String Formation

U(1) symmetry breaking may receive a cosmological constraint from cosmic strings. Cosmic strings are created in an early universe when U(1) symmetry is broken [1394] (see [1395] for a review). If its energy scale is very high, strings may be sufficiently diluted by cosmological inflation together with monopoles. If U(1) symmetry breaking takes place below the inflation energy

scale, strings are not diluted but are still likely to be cosmologically harmless. Suppose a cosmic string that extends as the scale factor $a(t)$ as the universe expands. Its energy density decreases as $\rho_{\text{string}} \propto v^2 \times a/a^3$, where v is the U(1) breaking scale. The energy density of the cosmic string then decreases as t^{-1} and dominates the universe at later times since the radiation energy density decreases as $a^{-4} \sim t^{-2}$. A long string, however, produces many small loops which disappear emitting radiation or breaks up due to intercommutation [1396]. The cosmic strings rapidly lose energy through those effects and follow the scaling law that the number ξ of cosmic strings per horizon volume is constant in time; the length is about the size of horizon $\ell \sim ct$ [1396]. Thus, the energy density of cosmic strings at time t is

$$\rho_{\text{string}} \simeq \xi \frac{v^2 t}{t^3} , \tag{9.87}$$

where $\xi \sim 10$ is found by computer simulations [1397]. When divided by the radiation energy density

$$\rho_{\text{rad}} = \frac{3}{32\pi} \frac{m_{\text{pl}}^2}{t^2}, \tag{9.88}$$

obtained from (4.176) and (4.179), we find

$$\frac{\rho_{\text{string}}}{\rho_{\text{rad}}} \simeq \frac{32\pi\xi}{3} \frac{v^2}{m_{\text{pl}}^2}, \tag{9.89}$$

which is constant in time, fixed by the value when cosmic strings formed.

The cosmic strings induce $O(1)$ density fluctuations ($\delta\rho_{\text{string}}/\rho_{\text{string}} \simeq 1$) which are imprinted in the cosmic microwave background. The behaviour of C_ℓ (see (4.215) for the definition) for cosmic string perturbations, however, does not agree with observations.[7] So the contribution from strings must be much smaller (typically 1/10) than the CDM density-perturbation amplitude, which is 10^{-5}, i.e.,

$$\frac{\rho_{\text{string}}}{\rho_{\text{rad}}} < 0.1 \times 10^{-5}, \tag{9.90}$$

leading to a constraint $v < 10^{15}$ GeV.[8]

9.4 Left–Right Symmetry Model

The prototype model in which the seesaw mechanism [237] is naturally embedded is the left–right symmetric model [1400, 1401]. This model is one

---

[7] Cosmic fluctuations from strings are dominated by velocity perturbations and produce a single broad peak for C_ℓ [1398]. Therefore, the observed acoustic peaks [850, 852] are not produced.

[8] CMB is fixed after the universe enters the matter-dominated regime, and this constraint receives a small correction for the matter-dominated epoch. The order of magnitude will not change, however [1399].

of the simplest extensions of the Weinberg–Salam theory incorporating the right-handed neutrino. This model appears in various grand unified models.

Suppose that there is $SU(2)_L \times SU(2)_R \times U(1)$ gauge symmetry and that fermions belong to

$$\ell_L \equiv \begin{pmatrix} \nu \\ e \end{pmatrix}_L, \quad (\mathbf{2}, \mathbf{1}, -1);$$

$$\ell_R \equiv \begin{pmatrix} \nu \\ e \end{pmatrix}_R, \quad (\mathbf{1}, \mathbf{2}, -1);$$

$$q_L \equiv \begin{pmatrix} u \\ d \end{pmatrix}_L, \quad (\mathbf{2}, \mathbf{1}, 1/3);$$

$$q_R \equiv \begin{pmatrix} u \\ d \end{pmatrix}_R, \quad (\mathbf{1}, \mathbf{2}, 1/3), \tag{9.91}$$

where the representations refer to $[SU(2)_L, SU(2)_R, U(1)]$. This is a straightforward extension of Weinberg–Salam's assignment of (2.7) and (2.55). The assignment of U(1) charges is unique to give correct Y hypercharges after symmetry breaking [see (9.97) below]. The values of U(1) charges assigned to quarks and leptons show that this U(1) symmetry is the B–L number.

We introduce two Higgs scalars, ξ and ϕ, which break

$$SU(2)_L \times SU(2)_R \times U(1) \to SU(2)_L \times U(1)_Y \quad \text{with } \langle \xi \rangle \neq 0, \tag{9.92}$$

and

$$SU(2)_L \times U(1)_Y \to U(1)_{\text{em}} \quad \text{with } \langle \phi \rangle \neq 0. \tag{9.93}$$

We assume that ξ belongs to a triplet representation of $SU(2)_R$, i.e., $(\mathbf{1}, \mathbf{3}, +2)$ [1401]. The doublet Higgs ϕ should give masses to fermions, and we must take it as $(\mathbf{2}, \mathbf{2}^*, 0)$. This ϕ transforms as

$$\phi \to u_L \, \phi \, u_R^\dagger \tag{9.94}$$

under an $SU(2)_L \times SU(2)_R$ transformation. We represent ξ in a 2×2 matrix form,

$$\xi \equiv \frac{1}{\sqrt{2}} \tau_i \xi_i, \tag{9.95}$$

so that ξ transforms under $SU(2)_R$ as

$$\xi \to u_R \, \xi \, u_R^\dagger . \tag{9.96}$$

Symmetry breaking of (9.92) is specified by $U(1)_Y$ charge defined by

$$Y = I_R^3 + \frac{I}{2}, \tag{9.97}$$

where I_R^3 is the third component of $SU(2)_R$ and I is the U(1) charge. The $U(1)_Y$ charge content of ξ is (ξ^{++}, ξ^+, ξ^0). This can be seen by applying a $U(1)_Y$ rotation; under the rotation, ξ transforms as

$$
\begin{aligned}
\xi \to e^{-i\epsilon}\, e^{-i\epsilon\frac{\tau_3}{2}}\, \xi\, e^{+i\epsilon\frac{\tau_3}{2}} \\
= \xi - i\epsilon \left(\xi + \left[\frac{\tau_3}{2}, \xi\right]\right) + \cdots \\
= \xi - i\frac{\epsilon}{2}\begin{bmatrix} \xi_3/\sqrt{2} & 2(\xi_1 + i\xi_2)/\sqrt{2} \\ 0 & \xi_3/\sqrt{2} \end{bmatrix} + \cdots .
\end{aligned}
\tag{9.98}
$$

Therefore, the $U(1)_Y$ charge content of ξ is

$$
\xi = \begin{pmatrix} \xi^+/\sqrt{2} & \xi^{++} \\ \xi^0 & \xi^+/\sqrt{2} \end{pmatrix}.
\tag{9.99}
$$

The electromagnetic charge is given by

$$
Q_{\text{em}} = I_L^3 + Y = I_L^3 + I_R^3 + \frac{I}{2}.
\tag{9.100}
$$

For the SU(2) singlet ξ, the $U(1)_Y$ charge and the electromagnetic charge are the same. When ξ^0 develops a vacuum-expectation value V,

$$
\langle\xi\rangle = \begin{pmatrix} 0 & 0 \\ V & 0 \end{pmatrix},
\tag{9.101}
$$

$SU(2)_L \times SU(2)_R \times U(1)$ is broken to $SU(2)_L \times U(1)_Y$.

The electromagnetic charge assignment of ϕ is obvious:

$$
\phi = \begin{pmatrix} \phi_1^0 & \phi_1^+ \\ \phi_2^- & \phi_2^0 \end{pmatrix}.
\tag{9.102}
$$

If ϕ develops a vacuum-expectation value,

$$
\langle\phi\rangle = \begin{pmatrix} v_1 & 0 \\ 0 & v_2 \end{pmatrix},
\tag{9.103}
$$

$SU(2)_Y \times U(1)$ breaks down to $U(1)_{\text{em}}$, where $v_1^2 + v_2^2 = v^2/2$. We now discuss the Yukawa interaction, which may be written in the form

$$
\mathcal{L} = g\bar{\ell}_R\phi\ell_L + g'\bar{\ell}_R\tilde{\phi}\ell_L + f\bar{q}_R\phi q_L + f'\bar{q}_R\tilde{\phi}q_L + h\tilde{\bar{\ell}}_R^c\xi\ell_R + \text{h.c.},
\tag{9.104}
$$

where

$$
\tilde{\phi} \equiv \tau_2\phi^*\tau_2 = \begin{pmatrix} \phi_2^{0*} & -\phi_2^+ \\ -\phi_2^- & \phi_1^{0*} \end{pmatrix}
\tag{9.105}
$$

$$
\tilde{\ell}_R^c \equiv \overline{\ell_R^c}\, i\tau_2 = (\overline{e^c}, -\overline{\nu^c})_R.
\tag{9.106}
$$

The nonzero vacuum-expectation value $\langle \xi \rangle \neq 0$ induces a Majorana mass of ν_R,

$$
\begin{aligned}
\mathcal{L}^M_{\text{mass}} &= -h(\overline{e^c}, -\overline{\nu^c})_R \begin{pmatrix} 0 & 0 \\ V & 0 \end{pmatrix} \begin{pmatrix} \nu \\ e \end{pmatrix}_R + \text{h.c.} \\
&= hV(\overline{\nu^c_R}\nu_R + \text{h.c.}) \ .
\end{aligned}
\tag{9.107}
$$

Because of (9.103) the neutrino has a Dirac mass of the form

$$
\begin{aligned}
\mathcal{L}^D_{\text{mass}} &= gv_1 \overline{\nu}_R \nu_L + g'v_2^* \overline{\nu}_R \nu_L + \text{h.c.} \\
&= (gv_1 + g'v_2^*)\overline{\nu}_R \nu_L + \text{h.c.}
\end{aligned}
\tag{9.108}
$$

In sum, the mass term which refers to neutrinos is

$$
\mathcal{L}_{\text{mass}} = \frac{1}{2}(\overline{\nu^c_R} \ \ \overline{\nu}_L) \begin{pmatrix} A & B \\ B & 0 \end{pmatrix} \begin{pmatrix} \nu_R \\ \nu_L \end{pmatrix} + \text{h.c.} \ ,
\tag{9.109}
$$

with

$$
\begin{aligned}
A &= 2hV \\
B &= (gv_1 + g'v_2^*).
\end{aligned}
\tag{9.110}
$$

Writing

$$
\begin{aligned}
N &= \nu_R + \nu^c_R \\
\nu &= \nu_L + \nu^c_L \ ,
\end{aligned}
\tag{9.111}
$$

$$
\mathcal{L}_{\text{mass}} = \frac{1}{2}(\overline{N} \ \overline{\nu}) \begin{pmatrix} A & B \\ B & 0 \end{pmatrix} \begin{pmatrix} N \\ \nu \end{pmatrix},
\tag{9.112}
$$

where $N^c = N$ and $\nu^c = \nu$. The diagonalisation with

$$
\begin{aligned}
\nu' &= \nu \cos\theta + N \sin\theta \ , \\
N' &= -\nu \sin\theta + N \cos\theta
\end{aligned}
\tag{9.113}
$$

yields, when $A \gg B$ ($V \gg v_1, v_2$),

$$
\begin{aligned}
m_{N'} &\simeq A \\
m_{\nu'} &\simeq -B^2/A \ ,
\end{aligned}
\tag{9.114}
$$

and the mixing angle $\text{tg}2\theta = 2B/A$, in agreement with (6.44). The minus sign in $m_{\nu'}$ is absorbed into the phase of the wave function.

9.5 Left–Right Symmetry in SO(10)

The simplest grand unification with ν_R automatically included is the SO(10) model [1343, 1344]. All left-handed fermions are incorporated in the spinor representation of **16**:

$$\mathbf{16}_L = \left[\begin{pmatrix} \nu \\ e \end{pmatrix}, \begin{pmatrix} u \\ d \end{pmatrix}, \begin{pmatrix} \nu^c \\ e^c \end{pmatrix}, \begin{pmatrix} u^c \\ d^c \end{pmatrix} \right]_L . \tag{9.115}$$

This representation contains ν_L^c, i.e., the antiparticle of the right-handed neutrino. A desirable feature is that the model is automatically anomaly-free [1402].

SO(10) unification includes left–right symmetry, and the scale of left–right symmetry breaking is determined by low-energy phenomenology, thus having predictive power for the neutrino mass. There are many ways to break SO(10) down to SU(3)×SU(2)×U(1). We defer a full description of the model construction and its phenomenology to the following sections, with further mathematical details given in the Appendix (irreducible representations of SO(10) are summarised in Tables 9.2 and 9.3 [1403]). In this section we confine ourselves to the case

$$\mathrm{SO}(10) \to \mathrm{SU}(3) \times \mathrm{SU}(2)_L \times \mathrm{SU}(2)_R \times \mathrm{U}(1)_{B-L} \to \mathrm{SU}(3) \times \mathrm{SU}(2)_L \times \mathrm{U}(1)_Y$$

and discuss only the aspect related to the neutrino mass. In order to break SO(10) to SU(3) × SU(2)$_L$×SU(2)$_R$× U(1), we introduce an adjoint Higgs H of **45**. Further symmetry breaking to SU(3)×SU(2)$_L$×U(1)$_Y$ is caused by **126**, which includes $\xi(\mathbf{1}, \mathbf{3}, 2)$ of the previous section, and to SU(3)× U(1)$_{\mathrm{em}}$ by a vector **10**, which includes $\phi(\mathbf{2}, \mathbf{2}^*, 0)$.

The Yukawa interaction is written

$$\mathcal{L}_{\mathrm{Yukawa}} = \frac{g}{2} f(\mathbf{16})_L \cdot f(\mathbf{16})_L \cdot H(\mathbf{10}) + \frac{h}{2} f(\mathbf{16})_L \cdot f(\mathbf{16})_L \cdot H(\mathbf{126}) + \text{h.c.} \tag{9.116}$$

Table 9.2. Irreducible representations (IR) of SO(10).

Dimensionality	IR	Indices
10	Vector	Γ_μ
16	Spinor	ψ
45	Adjoint	$\Sigma_{\mu\nu}$
54	Symmetric second-rank tensor	$\Gamma_{\{\mu\nu\}}$
120	Antisymmetric third-rank tensor	$\Gamma_{[\mu\nu\lambda]}$
126	Antisymmetric fifth-rank tensor	$\Gamma_{[\mu\nu\lambda\rho\sigma]}$
210	Antisymmetric fourth-rank tensor	$\Gamma_{[\mu\nu\lambda\kappa]}$

Table 9.3. SU(5) and SU(2)$_L$×SU(2)$_R$×SU(4) contents of SO(10) IR's.

SO(10)	SU(5)	SU(2)$_L$×SU(2)$_R$× SU(4)
10	5+5*	(2,2,1)+(1,1,6)
16	1+5*+10	(2,1,4)+(1,2,4*)
45	1+10+10*+24	(3,1,1)+(1,3,1)+(1,1,15)+(2,2,6)
54	15+15*+24	(1,1,1)+(3,3,1) +(1,1,20)+(2,2,6)
126	1+5*+10+15*+45+50*	(1,1,6)+(3,1,10*)+(1,3,10)+(2,2,15)
210	1+5+5*+10+10*+24	(1,1,1)+(1,1,15)+(2,2,6)+(3,1,15)
	+40+40*+75	+(1,3,15)+ (2,2,10)+(2,2,10*)

The first term gives Dirac masses to the fermions. The Lagrangian of this part reads [see (A18)]

$$\mathcal{L}^{(10)}_{\text{Yukawa}} = \frac{g}{2}\overline{\psi^c_L}\ \beta\Gamma_\mu\psi_L\phi^\mu + \text{h.c.}, \qquad (9.117)$$

where ψ_L is a spinor in the **16** representation and ϕ^μ is a vector of **10**. The Γ^μ matrices ($\mu = 1$–10) of SO(10) satisfy Clifford algebra,

$$\{\Gamma_\mu, \Gamma_\nu\} = 2\delta_{\mu\nu}, \qquad (9.118)$$

and the charge conjugation matrix β is written

$$\beta = \Gamma_2\Gamma_4\Gamma_5\Gamma_8\Gamma_9. \qquad (9.119)$$

Noting that ϕ is a real field and consulting with the explicit representation given in the Appendix [see (A14)], (9.117) is

$$\mathcal{L}^{(10)}_{\text{Yukawa}} = g(\overline{u}_R u_L + \overline{\nu}_R \nu_L)(\phi^9 - i\phi^{10}) + g^*(\overline{d}_L d_R + \overline{e}_L e_R)(\phi^9 - i\phi^{10}) + \cdots. \qquad (9.120)$$

The quarks and leptons acquire masses when ϕ develops a vacuum-expectation value,

$$\langle\phi^\mu\rangle = \begin{bmatrix} 0 \\ 0 \\ \vdots \\ v \end{bmatrix} \begin{matrix} 1 \\ 2 \\ \vdots \\ 10 \end{matrix}. \qquad (9.121)$$

This, however, leads to the mass relation

$$m_u = m_\nu^D = m_d = m_e , \qquad (9.122)$$

which is not consistent with experiment. To leave the freedom which makes the prediction consistent with experiment, we need two **10**'s [1404] which

have the vacuum-expectation values

$$\langle \phi^{10} \rangle = v_1, \quad \langle \phi'^9 - i\phi'^{10} \rangle = v_2, \tag{9.123}$$

with v_1 and v_2 real numbers, or

$$\langle \phi^\mu \rangle = \begin{bmatrix} 0 \\ 0 \\ \vdots \\ v_1 \end{bmatrix}, \quad \langle \phi'^\mu \rangle = \begin{bmatrix} 0 \\ 0 \\ \vdots \\ \text{Re } v_2 \\ \text{Im } v_2 \end{bmatrix}, \tag{9.124}$$

so that

$$m_u = m_\nu^D = gv_1 + g'v_2$$
$$m_d = m_e = gv_1 + g'v_2^*. \tag{9.125}$$

This mass formula does not change even if we introduce more **10**'s. The right-handed neutrino acquires a Majorana mass when $SU(2)_R$ [and at the same time $U(1)_{B-L}$] is broken by $\langle H(\mathbf{126}) \rangle \neq 0$. The Yukawa term in (9.116) gives

$$M_{\nu_R} = h\langle H(\mathbf{126}) \rangle. \tag{9.126}$$

With the seesaw mechanism, we have

$$m_\nu = m_{\nu D}^2 / M_{\nu_R}$$
$$= m_u^2 / M_{\nu_R} , \tag{9.127}$$

or

$$m_\nu = m_{\nu D}^T \, M_{\nu_R}^{-1} m_{\nu D}$$
$$= m_u^T \, M_{\nu_R}^{-1} m_u ; \tag{9.128}$$

writing the mass in a matrix form taking the generation into account.

Now, we discuss the structure of the quark and lepton mixing angles and show that they are approximately equal:

$$U_{\text{lepton}} \simeq U_{\text{q}}, \tag{9.129}$$

i.e.,

$$\theta_{e\mu} \simeq \theta_{ds}, \quad \theta_{e\tau} \simeq \theta_{db} , \cdots . \tag{9.130}$$

If we take the basis in which m_u is diagonal, m_d and m_ℓ are expressed as

$$m_d = m_\ell = V^\dagger \begin{pmatrix} m_e & & \\ & m_\mu & \\ & & m_\tau \end{pmatrix} U \tag{9.131}$$

with two unitary matrices V and U.[9] Because the mass matrices for charge $-$ $1/3$ quarks and charged leptons are given by a vector $\mathbf{10}$, they are symmetric, i.e., $m_d^T = m_d$ and $m_\ell^T = m_\ell$, and, hence $V^\dagger$ can be identified with U^T. A unitary matrix is generally expressed as

$$U = K U_q^{-1} L \, , \qquad (9.132)$$

where K and L are the diagonal (phase) matrix and U_q is the Kobayashi–Maskawa matrix. Since L is absorbed into the phase of the state [see (8.28)], we write

$$m_d = m_e = U_q^{-1T} K \begin{pmatrix} m_e & & 0 \\ & m_\mu & \\ 0 & & m_\tau \end{pmatrix} K U_q^{-1}. \qquad (9.133)$$

The rotations that apply to d- and charged leptons are the same, so our next task is to show that the neutrino mass matrix is approximately diagonal. The neutrino mass matrix is

$$m_\nu = \begin{pmatrix} m_u & & 0 \\ & m_c & \\ 0 & & m_t \end{pmatrix} M_{\nu R}^{-1} \begin{pmatrix} m_u & & 0 \\ & m_c & \\ 0 & & m_t \end{pmatrix}. \qquad (9.134)$$

Because of the strong hierarchy $m_u \ll m_c \ll m_t$, the mass matrix takes the form

$$m_\nu = \begin{pmatrix} a & b & c \\ b & A & B \\ c & B & C \end{pmatrix} , \qquad (9.135)$$

where $a \sim O(m_u^2)$, $A \sim O(m_c^2)$, $b \sim O(m_c^2)$, etc. Diagonalisation of the (1,2) or (1,3) sector gives the mixing angle of the order of m_u/m_c or m_u/m_t, which are small. The same is true for the (2,3) sector. If we diagonalise the 2×2 submatrix of the (2,3) sector, the mixing angle is of the order of m_c/m_t. This means that the neutrino mass matrix is diagonal in the limit of $m_u/m_c \to 0$ and $m_c/m_t \to 0$, unless the matrix elements of $M_{\nu R}$ have strong hierarchy that compensates for hierarchy in the quark mass matrix. Then, an extra mixing angle which enters in the ν mass matrix is small, and we expect (9.129) to hold with good accuracy [1405].

If the right-handed neutrino mass matrix has hierarchical matrix elements such as $M_1/M_2 \sim M_2/M_3 \sim O(\varepsilon)$, (9.129) receives a correction of $O[(m_c/m_t)\varepsilon^{-1/2}]$. So (9.129) is completely disturbed if $\varepsilon \sim O[(m_c/m_t)^2]$. In other words, this is the condition that we can modify the prediction of quark and lepton mixings.

The generation dependence of the neutrino mass depends explicitly of the assumption on the spectrum of $M_{\nu R}$. It is often assumed to have the simplest form $M_{\nu R} = M \cdot \mathbf{1}$ ($\mathbf{1}$ is the unit matrix). With this assumption, we have

$$m_{\nu_e} : m_{\nu_\mu} : m_{\nu_\tau} = m_u^2 : m_c^2 : m_t^2 \, . \qquad (9.136)$$

---

[9] Note that the neutrino mixing matrix is given by $U = U_{\text{lepton}}^\dagger U_\nu$, where $U_\nu = 1$.

We note that the fermion masses receive large radiative corrections [1365], and relations (9.122) and (9.136) hold only at the unification scale. The up, charm, and top quark masses defined at the renormalisation point $\mu=2\,\text{GeV}$, m_c and m_t (physical scales), respectively, are related to the values at the unification scale M_G as given in Table 9.1 [1406]. We equate these quark masses with neutrino's Dirac masses at M_G, so that

$$\frac{m_{\nu_e D}(M_\text{G})}{m_u(2\,\text{GeV})} \simeq 0.22 \ , \tag{9.137}$$

$$\frac{m_{\nu_\mu D}(M_\text{G})}{m_c(m_c)} \simeq 0.20 \ , \tag{9.138}$$

$$\frac{m_{\nu_\tau D}(M_\text{G})}{m_t(m_t)} \simeq 0.47 \ . \tag{9.139}$$

Relation (9.136) then gives

$$m_{\nu_e} : \ m_{\nu_\mu} : \ m_{\nu_\tau} = 4.8 \times 10^{-6} : \ 1 \ : \ 1.1 \times 10^5 \ . \tag{9.140}$$

Note that radiative corrections to neutrino's Dirac masses are small since the mass of ν_R is very large. (The effective mass term $\nu_L \nu_L^c / M_{\nu_R}$ receives radiative corrections from the wave function renormalisation of ν_L, but we absorb it into M_{ν_R}.)

This mass relation is not supported by experiment whichever solution we adopt (see Table 8.4), indicating the presence of significant hierarchy in the right-handed neutrino mass matrix elements, if SO(10) is the correct theory.

In this connexion, we estimate the mass of the third-generation right-handed neutrino as

$$M_{\nu_R} \simeq 1.3 \times 10^{14}\,\text{GeV} \tag{9.141}$$

from $m_{\nu_3} \simeq m_t^2(M_\text{G})/M_{\nu_R}$ using the top quark mass at the GUT scale $m_t(M_\text{G}) \simeq 82\,\text{GeV}$ (see Table 9.1) and empirical value $m_{\nu_3} \simeq 5 \times 10^{-2}\,\text{eV}$.

The relations (9.129) and (9.130) do not receive QCD radiative corrections at the one-loop level since they cancel in the mass ratios.

Variant mass matrices. The prediction of the mass matrix obtained above can be relaxed by assuming a mixture of Higgs' **10 + 126** to give fermions masses. This makes the mixing angles fairly arbitrary. A specific model was proposed that **126** Higgs scalars are introduced so that they couple only to the (2,2) component of the fermion mass matrix, whereas others are given masses by **16** [1407]. In this case, we have the mass relations [1408],

$$m_d \simeq 3m_e$$

$$m_s \simeq \frac{1}{3}m_\mu$$

$$m_b \simeq m_\tau, \tag{9.142}$$

which fit the empirical mass pattern better. The mixing angles are [1407]

$$\theta_{e\mu} \simeq \frac{1}{3}\theta_{ds}$$
$$\theta_{\mu\tau} \simeq \theta_{sb}$$
$$\theta_{\tau e} \simeq \theta_{bd}. \tag{9.143}$$

Unfortunately, these mixing angles do not agree with experimental values.

Another way to get rid of the prediction of (9.136) and (9.130) is to suppose a strong hierarchy of the order of $O((m_u/m_c)^2, (m_c/m_t)^2)$ [1409] for the right-handed Majorana mass matrix. Consider, for instance, a mass matrix,

$$M_{\nu_R} = \begin{pmatrix} \epsilon^6 & \epsilon^5 & \epsilon^3 \\ \epsilon^5 & \epsilon^4 & \epsilon^2 \\ \epsilon^3 & \epsilon^2 & 1 \end{pmatrix} M_R, \tag{9.144}$$

with

$$\epsilon \simeq O\left(\sqrt{\frac{m_c}{m_t}}, \sqrt{\frac{m_u}{m_c}}\right). \tag{9.145}$$

From (9.134), we obtain

$$m_\nu = \begin{pmatrix} \epsilon^2 & \epsilon & \epsilon \\ \epsilon & 1 & 1 \\ \epsilon & 1 & 1 \end{pmatrix} \left(\frac{m_t^2}{M_R}\right). \tag{9.146}$$

Notice that ϵ or 1 shows only the order of magnitude, and four 1's are not exactly equal. This matrix gives large mixing between ν_μ and ν_τ, and the two corresponding eigenvalues are $O(1)$ and $O(\delta)$, where $\delta < O(1)$. Empirically, $\delta \sim 0.3$ if LMA is the solution of the solar neutrino problem. In this case, δ is of the same order as ϵ, and the matrix may cause large mixing between ν_μ and ν_e consistent with LMA. We see that the same matrix appears in Sect. 9.10.1 below. Unfortunately, we do not see any principles that lead to (9.144) in the basis where the up-type quark mass matrix is diagonal. We need a conspiracy between the Dirac mass and the Majorana mass for right-handed neutrinos. An example of such a correlated mass hierarchy is found in [1410]. The only thing we can show here is that the construction of a mass matrix compatible with experiment is not impossible. A number of models are proposed in the framework of SO(10) [1407, 1411].

Let us sketch one example [1412]. The idea is to add to the Yukawa coupling that gives fermions masses effective (nonrenormalisable) interactions at the Planck scale. Since $U_\ell \simeq U_q$ is the result of the symmetric nature of the Yukawa couplings of **10**'s, the action of the Higgs $\Sigma(\mathbf{45})$ that couple to $\mathbf{16_L}$ through

$$\delta\mathcal{L}_{\text{Yukawa}} = \frac{f}{2m_{\text{pl}}} f(\mathbf{16})_L \cdot f(\mathbf{16})_L \cdot \Sigma(\mathbf{45}) \cdot H(\mathbf{10})$$

$$+ \frac{f'}{2m_{\text{pl}}} f(\mathbf{16})_L \cdot f(\mathbf{16})_L \cdot \Sigma(\mathbf{45}) \cdot H(\mathbf{10'}) + \text{h.c.} , \tag{9.147}$$

in addition to (9.116), would modify the mass matrix structure. The modification could be $O(1)$ for the first and second families because $\langle\Sigma(\mathbf{45})\rangle/m_{\mathrm{pl}} \simeq 10^{-2}$. Babu et al. [1412] take $\langle\Sigma(\mathbf{45})\rangle \propto (B-L)$, so that the above interaction produces antisymmetric mass matrices for quarks and leptons, and show that one can construct mass matrices consistent with experiment. The actual construction, however, contains more ad hoc assumptions.

Neutrino mass without 126. The renormalisable Yukawa coupling is not the only mechanism that gives quarks and leptons masses. Effective couplings may arise from higher order interactions at the GUT scale or at the Planck scale. Such interactions generally have a dimension larger than four and have a prefactor M_{G}^{-1} or m_{pl}^{-1}; hence their contributions are usually suppressed at low energies. When the expectation value of the scalar particle is as large as the GUT energy scale, however, the mass factor does not give too strong a suppression.

Suppose that intermediate symmetry is broken by a Higgs scalar $\Phi(\mathbf{16})$ instead of $\xi(\mathbf{126})$. The right-handed neutrino remains massless at the tree level because $\Phi(\mathbf{16})$ has no Yukawa coupling to fermions. We expect, however, the Majorana masses of the right-handed neutrino induced by the two-loop diagram depicted in Fig. 9.3 [1413], which gives

$$M_{\nu_R} \sim \frac{\alpha_{\mathrm{G}}^2}{\pi^2}(g\tilde{g} + g\tilde{g}')\frac{\langle\Phi(\mathbf{16})\rangle^2}{M_{\mathrm{G}}}, \qquad (9.148)$$

where $\tilde{g}$ and $\tilde{g}'$ are trilinear couplings defined by

$$\mathcal{L} = \tilde{g}M_{\mathrm{G}}\Phi(\mathbf{16})\Phi(\mathbf{16})\phi(\mathbf{10}) + \tilde{g}'M_{\mathrm{G}}\Phi(\mathbf{16})\Phi(\mathbf{16})\phi(\mathbf{10}') . \qquad (9.149)$$

In (9.148) g and g' are Yukawa couplings of $\phi(\mathbf{10}), \phi(\mathbf{10}')$ to the matter fields [see (9.125)]. Since g and g' are proportional to m_u and m_d, it is likely that the masses of light neutrinos are proportional to a single power of the u quark mass. However, if we take $\langle\Phi(\mathbf{16})\rangle \simeq M_{\mathrm{G}} \approx 10^{16}$ GeV, we have $M_{\nu_R} \approx 10^{12}$ GeV [1413], which would be masked by another contribution from effective interactions at the Planck scale.
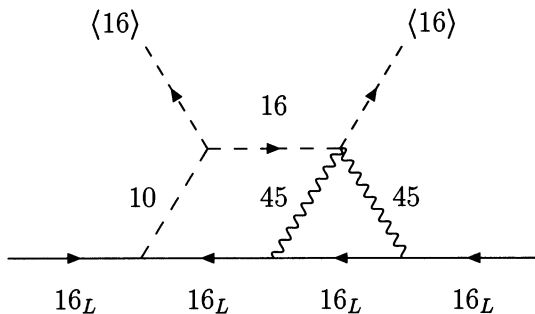
Fig. 9.3. Radiative correction involving a vacuum-expectation value of **16**, giving the right-handed neutrino a Majorana mass.

Interactions on the Planck scale may also give a similar effective coupling, unless it is forbidden by some symmetry principle. We expect

$$\frac{f}{2m_{\rm pl}} f(\mathbf{16})_L f(\mathbf{16})_L \Phi^*(\mathbf{16})\Phi^*(\mathbf{16}). \qquad (9.150)$$

This gives

$$M_{\nu_R} \simeq f \frac{\langle \Phi^*(\mathbf{16}) \rangle^2}{m_{pl}}. \qquad (9.151)$$

For $\langle \Phi \rangle \simeq 3 \times 10^{16}\,\mathrm{GeV}$ and $f \simeq 1$, we obtain

$$M_{\nu_R} \simeq 10^{14}\,\mathrm{GeV}, \qquad (9.152)$$

which gives $m_\nu \simeq 0.1\,\mathrm{eV}$ for the Dirac mass of $100\,\mathrm{GeV}$ [i.e., the Yukawa coupling is $O(1)$]. The idea of effective interactions of the form $\langle \Phi(\mathbf{16}) \rangle^2 / m_{\rm pl}$ is extensively developed in the next section.

A phenomenological difficulty with this simple model is the degeneracy of up- and down-type quarks. There is an attempt to lift the degeneracy by introducing fermions of **10** that mix with the ordinary **16** [1414].

9.6 General Discussion of SO(10) Grand Unification

9.6.1 Symmetry-Breaking Pattern and the Neutrino Mass

There are many ways to break SO(10) down to $G_0 = \mathrm{SU}(3) \times \mathrm{SU}(2) \times \mathrm{U}(1)$ (e.g., see [1415]). Here, we restrict our consideration to those cases in which symmetry is broken to G_0 in one or two steps:

    (i) $\mathrm{SO}(10) \xrightarrow{M_{\rm G}} G_0$

    (ii) $\mathrm{SO}(10) \xrightarrow{M_{\rm G}} \mathrm{SU}(5) \xrightarrow{M_{\rm I}} G_0$

    (iii) $\mathrm{SO}(10) \longrightarrow \mathrm{SU}(5) \times \mathrm{U}(1) \longrightarrow G_0$

    (iv) $\mathrm{SO}(10) \longrightarrow \mathrm{SU}(4) \times \mathrm{SU}(2)_L \times \mathrm{SU}(2)_R \longrightarrow G_0$

    (v) $\mathrm{SO}(10) \longrightarrow \mathrm{SU}(4) \times \mathrm{SU}(2)_L \times \mathrm{U}(1) \longrightarrow G_0$

    (vi) $\mathrm{SO}(10) \longrightarrow \mathrm{SU}(3) \times \mathrm{SU}(2)_L \times \mathrm{SU}(2)_R \times \mathrm{U}(1) \longrightarrow G_0$

    (vii) $\mathrm{SO}(10) \longrightarrow \mathrm{SU}(3) \times \mathrm{SU}(2)_L \times \mathrm{U}(1)_R \times \mathrm{U}(1) \longrightarrow G_0$ (9.153)

In (i) and (ii), SO(10) (rank=5) is reduced to rank 4 symmetry at the GUT scale $M_{\rm G}$. In the remainder, rank 5 is maintained at $M_{\rm G}$ and reduces to rank-4 symmetry at the intermediate scale M_I. In general, ν_R acquires a mass when

Table 9.4. Breaking SO(10) GUT and Higgs particles.

Intermediate symmetry G_I	Higgs: SO(10) $\to G_I$	Higgs: $G_I \to G_0$	Higgs: $G_0 \to$ U(1)$_{\mathrm{em}}$
SU(5)	**16** or **126**	**45,54** or **210**	**10**
SU(5) $\times$ U(1)	**45**	**126** $\oplus$45	**10**
		or **16**$\oplus$45	**10**
SU(4) $\times$ SU(2)$_L\times$ SU(2)$_R$	**54** or **210**	**16** or **126**	**10**
SU(4) $\times$ SU(2)$_L\times$ U(1)$_R$	**45**	**16** or **126**	**10**
SU(3) $\times$ SU(2)$_L\times$ SU(2)$_R\times$ U(1)$_{B-L}$	**45**	**16** or **126**	**10**
SU(3) $\times$ SU(2)$_L\times$ U(1)$_R\times$ U(1)	**45**	**16** or **126**	**10**

the symmetry is reduced to rank 4; ν_R becomes massive at $M = M_{\mathrm{G}}$ in (i) and (ii) and at $M = M_I$ in (iii)–(vii).

There exist so many choices of the Higgs scalars to cause symmetry breaking of (9.153). We consider only cases with Higgs particles of low dimensionalities. Note that (i) is regarded as a special case $M_I = M_{\mathrm{G}}$ of the others. The Higgs particles needed to cause symmetry breaking of (9.153) are summarised in Table 9.4. We discuss possible consequences for the neutrino mass in the following:

Case (ii). The first symmetry breaking around the grand-unified mass scale is caused by either **16** or **126**. If $\langle$**126**$\rangle \neq 0$ breaks the symmetry, the mass of ν_R is expected to be of the order of M_{G} because the SU(2)$_R$ triplet ξ is contained in **126** and ν_R obtains a Majorana mass of the order of M_I through $\langle$**126**$\rangle \neq 0$. We expect a somewhat different scenario if $\langle$**16**$\rangle \neq 0$ breaks SO(10) symmetry: **16** does not couple to ν_R, so, it does not acquire a Majorana mass. However, we may have an effective interaction, such as

$$\frac{f}{2m_{\mathrm{pl}}}\nu_R\nu_R\langle\mathbf{16}^*\rangle\langle\mathbf{16}^*\rangle \qquad (9.154)$$

from the physics at the Planck mass scale, which leads to a Majorana mass of ν_R of the order of $M_{\mathrm{G}}^2/m_{\mathrm{pl}}$. Breaking SU(5) to SU(3) $\times$ SU(2) $\times$ U(1) is caused by **24** of SU(5), i.e. $\langle$**45**$\rangle \neq 0$, $\langle$**54**$\rangle \neq 0$ or $\langle$**210**$\rangle \neq 0$ in terms of the SO(10) language.

Case (iii). The first breaking is caused by $\langle$**45**$\rangle \neq 0$. We need two Higgs' **126** $\oplus$ **45** or **16** $\oplus$ **45** to break the intermediate symmetry. In the former case ν_R receives a mass of the order of M_I. In the latter case the Majorana mass is perhaps of the order of M_I^2/m_{pl}.

Case (iv). The first breaking is caused by **54** or **210**, and the second by **16** or **126**. The argument for the ν_R mass is the same.

Case (v)–(vii). SO(10) is broken by **45**, and the intermediate symmetry by **16** or **126**. The argument for the ν_R mass is also the same.

In all cases, SU(3) × SU(2)$_L$× U(1) is broken to SU(3) × U(1)$_{em}$ by a Higgs of **10**, which contains an SU(2) doublet needed in the Weinberg–Salam theory. With one **10**, however, we are led to an undesirable relation, $m_u = m_d = m_e$, as noted in the previous section. To relax this relation, we need two or more **10**'s. The relation still holds that

$$m_d = m_e, \quad m_u = m_\nu (\text{Dirac}) . \tag{9.155}$$

The argument for the left-handed neutrino mass and its generation mixing is the same as we described in (9.127)–(9.136) above.

9.6.2 Prediction of the Mass Scale

The unification mass scales M_G and M_I can be predicted from low-energy coupling constants with the use of the renormalisation group equation, as discussed for SU(5) GUT. The same argument applies to the determination of M_G in (i) and M_I in (ii) and (iii). In (ii) and (iii), M_G remains undetermined by low-energy physics. In what follows we discuss for other cases of symmetry breaking how this gives us insight into the right-handed neutrino mass.

Case (iv) Pati–Salam symmetry SU(4) × SU(2)$_L$× SU(2)$_R$ [219] appears on the intermediate mass scale. Evolution of the three running couplings $\alpha_i(\mu)$, which associate with SU(4), SU(2)$_L$, and SU(2)$_R$, from $\mu = M_G$ to M_I obeys

$$\alpha_i^{-1}(\mu) = \alpha_G^{-1} - 2b_i \, \log(M_G/\mu) , \tag{9.156}$$

where

$$b_4 = \frac{1}{4\pi}\left(\frac{44}{3} - \frac{4}{3}N_f\right) + b_4(H),$$

$$b_{2L} = \frac{1}{4\pi}\left(\frac{22}{3} - \frac{4}{3}N_f\right) + b_{2L}(H),$$

$$b_{2R} = \frac{1}{4\pi}\left(\frac{22}{3} - \frac{4}{3}N_f\right) + b_{2R}(H) \tag{9.157}$$

and $b_i(H)$ is the contribution from Higgs particles that depend further on the model. To calculate $b_i(H)$, we may consider two models discussed above:

(a) $\chi(\mathbf{16})$ and $\phi(\mathbf{10})$. The SU(4), SU(2)$_L$, and SU(2)$_R$ contents of χ and ϕ are

$$\chi_L = (\mathbf{4, \, 2, \, 1}),$$
$$\chi_R = (\mathbf{4, \, 1, \, 2}),$$
$$\phi = (\mathbf{1, \, 2, \, 2^*}). \tag{9.158}$$

Thus, we have

$$b_4(H) = \frac{1}{4\pi}\left(-\frac{2}{3}\right), \quad b_{2L}(H) = \frac{1}{4\pi}(-1), \quad b_{2R}(H) = \frac{1}{4\pi}(-1). \quad (9.159)$$

(b) $\xi(\mathbf{126})$ and $\phi(\mathbf{10})$. In this case,

$$\xi_L = (\mathbf{10},\ \mathbf{3},\ \mathbf{1}),$$
$$\xi_R = (\mathbf{10},\ \mathbf{1},\ \mathbf{3}),$$
$$\phi = (\mathbf{1},\ \mathbf{2},\ \mathbf{2}^*). \quad (9.160)$$

This gives

$$b_4(H) = \frac{1}{4\pi}(-6), \quad b_{2L}(H) = \frac{1}{4\pi}(-7), \quad b_{2R}(H) = \frac{1}{4\pi}(-7). \quad (9.161)$$

For the energy scale from $\mu = M_I$ to M_W, the Weinberg–Salam doublet in $\phi(\mathbf{10})$ is the only Higgs particle that contributes to the beta function. The doublet has the SU(3), SU(2)$_L$, and U(1) content,

$$\phi = (\mathbf{1},\ \mathbf{2},\ 1/2)\ . \quad (9.162)$$

The evolution of the couplings for SU(3), SU(2)$_L$, and U(1) is governed by

$$\alpha_i^{-1}(\mu) = \alpha_i^{-1}(M_I) - 2b_i\ \log(M_I/\mu), \quad (9.163)$$

with

$$b_3 = \frac{1}{4\pi}\left(\frac{33}{3} - \frac{4}{3}N_{\mathrm{f}}\right),$$
$$b_2 = \frac{1}{4\pi}\left(\frac{22}{3} - \frac{4}{3}N_{\mathrm{f}} - \frac{1}{6}\right),$$
$$b_1 = \frac{-1}{4\pi}\left(\frac{4}{3}N_{\mathrm{f}} + \frac{1}{10}\right). \quad (9.164)$$

We then impose a matching condition on (9.156) and (9.163) at $\mu = M_I$ that

$$\alpha_3^{-1}(M_I) = \alpha_4^{-1}(M_I),$$
$$\alpha_2^{-1}(M_I) = \alpha_{2L}^{-1}(M_I),$$
$$\alpha_1^{-1}(M_I) = \frac{1}{5}[2\alpha_4^{-1}(M_I) + 3\alpha_{2R}^{-1}(M_I)]. \quad (9.165)$$

With the low-energy parameters of (9.46), (9.47), and (9.43), we obtain for (a),

$$M_{\mathrm{G}} = 10^{15.4}\text{–}10^{15.6}\ \mathrm{GeV},$$
$$M_I = 10^{14.0}\ \mathrm{GeV}, \quad (9.166)$$

and for (b),

$$M_G = 10^{15.3}\text{--}10^{15.5}\,\text{GeV},$$
$$M_I = 10^{14.0}\,\text{GeV} \tag{9.167}$$

(see Fig. 9.4a). For the ν_R Majorana mass, we then find

$$M_{\nu_R} \simeq f M_I^2/m_{\rm pl} \simeq 10^9 f\,\text{GeV} \tag{9.168}$$

for (a), and

$$M_{\nu_R} \simeq M_I \simeq 10^{14} h\,\text{GeV} \tag{9.169}$$

for (b), where f and h are coupling constants defined in (9.151) and (9.126).

Case (v). Similar to case (iv), we have two models depending upon whether intermediate symmetry SU(4) $\times$ SU(2)$_L$ $\times$ U(1)$_R$ is broken either by (a) **16** or (b) **126**. The beta function coefficient for α_{1R} is now

$$b_{1R} = \frac{1}{4\pi}\left(-\frac{4}{3}N_f\right) + b_{1R}(H). \tag{9.170}$$

The coefficients b_4 and b_{2L} are the same as in (9.157) up to $b_i(H)$.
(a) $\chi(\mathbf{16})$ and $\phi(\mathbf{10})$ are

$$\chi = (\mathbf{4},\ \mathbf{1},\ -1/2)$$
$$\phi = (\mathbf{1},\ \mathbf{2},\ -1/2), \tag{9.171}$$

where the last number is the U(1)$_R$ charge. The contribution to the Higgs loop is

$$b_4(H) = \frac{1}{4\pi}\left(-\frac{1}{6}\right),\quad b_{2L}(H) = \frac{1}{4\pi}\left(-\frac{1}{6}\right),\quad b_{1R}(H) = \frac{1}{4\pi}\left(-\frac{1}{2}\right). \tag{9.172}$$
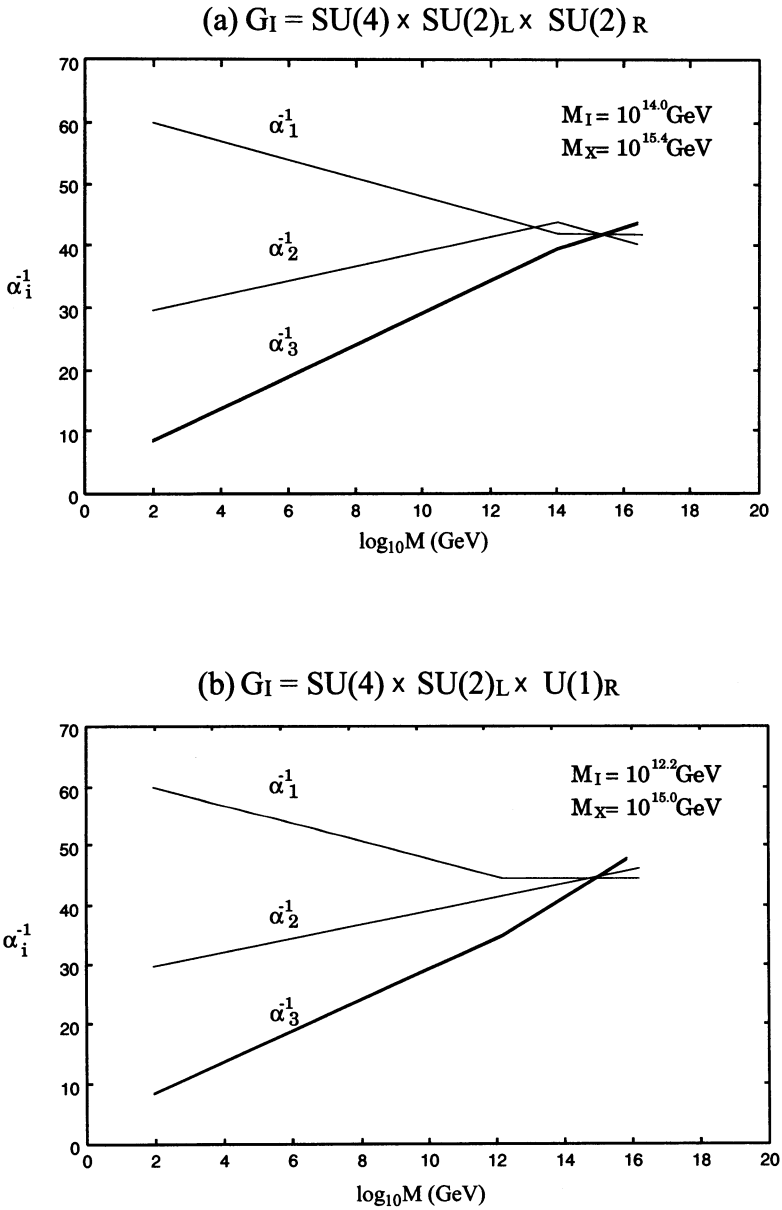
(b) $\xi(\mathbf{126})$ and $\phi(\mathbf{10})$ are

$$\xi = (\mathbf{10},\ \mathbf{1},\ -1),$$
$$\phi = (\mathbf{1},\ \mathbf{2},\ 1/2). \tag{9.173}$$

Then,

$$b_4(H) = \frac{1}{4\pi}(-1),\quad b_{2L}(H) = \frac{1}{4\pi}\left(-\frac{1}{6}\right),\quad b_{1R}(H) = \frac{1}{4\pi}\left(-\frac{7}{3}\right). \tag{9.174}$$

Evolution from M_I to M_W is the same as in (iv). With the matching condition

$$\alpha_3^{-1} = \alpha_4^{-1},\ \alpha_3^{-1} = \alpha_2^{-1},\ \alpha_1^{-1} = \frac{1}{5}(2\alpha_4^{-1} + 3\alpha_{1R}^{-1}) \tag{9.175}$$

(a) $G_I = SU(4) \times SU(2)_L \times SU(2)_R$

(b) $G_I = SU(4) \times SU(2)_L \times U(1)_R$

Fig. 9.4. Matching the three coupling constants in the SO(10) grand unification model. Examples are shown for intermediate symmetry (**a**) SU(4) $\times$ SU(2)$_L$ $\times$ SU(2)$_R$ and (**b**) SU(4) $\times$ SU(2)$_L$ $\times$ U(1)$_R$. The figures show one-loop calculations.

at $\mu = M_I$, we obtain (Fig. 9.4b)

$$
\begin{aligned}
(a) \quad M_G &= 10^{15.0}\text{--}10^{15.1} \text{ GeV}, \\
M_I &= 10^{12.8}\text{--}10^{12.9} \text{ GeV}, \\
(b) \quad M_G &= 10^{15.0}\text{--}10^{15.1} \text{ GeV}, \\
M_I &= 10^{12.1}\text{--}10^{12.2} \text{ GeV}.
\end{aligned}
$$

(9.176)

(9.177)

We see that M_I is substantially smaller than that in (iv). This gives the ν_R mass

$$
\begin{aligned}
(a) \quad M_{\nu_R} &\simeq 4 \times 10^6 f \text{ GeV} \\
(b) \quad M_{\nu_R} &\simeq 10^{12} h \text{ GeV}.
\end{aligned}
$$

(9.178)

(9.179)

Case (vi). Intermediate symmetry is $\mathrm{SU}(3) \times \mathrm{SU}(2)_L \times \mathrm{SU}(2)_R \times \mathrm{U}(1)_{B-L}$. The renormalisation group coefficients are

$$
b_3 = \frac{1}{4\pi}\left(\frac{33}{3} - \frac{4}{3}N_F\right),
$$

$$
b_{2L} = b_{2R} = \frac{1}{4\pi}\left(\frac{22}{3} - \frac{4}{3}N_F\right) + b_{2L,R}(H),
$$

$$
b_{B-L} = \frac{1}{4\pi}\left(-\frac{4}{3}N_F\right) + b_{R-L}(H).
$$

(9.180)

For the Higgs content, again we have two cases:
(a) $\chi(\mathbf{16})$ and $\phi(\mathbf{10})$.

$$
\begin{aligned}
\chi_L &= (\mathbf{1},\ \mathbf{2},\ \mathbf{1},\ \mathbf{1}) \quad \in \chi(\mathbf{16}), \\
\chi_R &= (\mathbf{1},\ \mathbf{1},\ \mathbf{2},\ \mathbf{1}) \quad \in \chi(\mathbf{16}), \\
\phi &= (\mathbf{1},\ \mathbf{2},\ \mathbf{2^*},\ \mathbf{0}) \quad \in \phi(\mathbf{10}),
\end{aligned}
$$

(9.181)

yielding

$$
b_3(H) = 0, \quad b_{2L,R}(H) = \frac{1}{4\pi}\left(-\frac{1}{2}\right), \quad b_{B-L}(H) = \frac{1}{4\pi}\left(-\frac{1}{2}\right).
$$

(9.182)

(b) $\xi(\mathbf{126})$ and $\phi(\mathbf{10})$.

$$
\begin{aligned}
\xi_L &= (\mathbf{1},\ \mathbf{3},\ \mathbf{1},\ +2) \quad \in \xi(\mathbf{126}), \\
\xi_R &= (\mathbf{1},\ \mathbf{1},\ \mathbf{3},\ +2) \quad \in \xi(\mathbf{126}), \\
\phi &= (\mathbf{1},\ \mathbf{2},\ \mathbf{2^*},\ \mathbf{0}) \quad \in \xi(\mathbf{10}).
\end{aligned}
$$

(9.183)

For $b_i(H)$,

$$
b_3(H) = 0, \ b_{2L,R}(H) = \frac{1}{4\pi}(-1), \ b_{B-L}(H) = \frac{1}{4\pi}(-3).
$$

(9.184)

Imposing the matching condition,

$$\alpha_3^{-1} = \alpha_3^{-1}, \ \alpha_{2L}^{-1} = \alpha_{2R}^{-1}, \ \alpha_1^{-1} = \frac{1}{5}(2\alpha_{B-L}^{-1} + 3\alpha_{2R}^{-1}), \tag{9.185}$$

we obtain from (9.156) and (9.180) for $M_I \le \mu \le M_G$ and (9.163) and (9.164) for $M_W \le \mu \le M_I$,

$$
\begin{aligned}
(a) \ \ M_G &= 10^{16.4}\text{--}10^{16.6} \text{ GeV}, \\
M_I &= 10^{11.1}\text{--}10^{11.4} \text{ GeV} \tag{9.186} \\
(b) \ \ M_G &= 10^{15.8}\text{--}10^{16.0} \text{ GeV}, \\
M_I &= 10^{10.6}\text{--}10^{10.9} \text{ GeV}. \tag{9.187}
\end{aligned}
$$

Hence,

$$
\begin{aligned}
(a) \ \ M_{\nu_R} &= 3 \times 10^3 f \text{ GeV} \tag{9.188} \\
(b) \ \ M_{\nu_R} &= 6 \times 10^{10} h \text{ GeV}. \tag{9.189}
\end{aligned}
$$

Case (vii). With intermediate symmetry $SU(3) \times SU(2)_L \times U(1)_R \times U(1)$, $\sin^2 \theta_W$ is smaller than the value predicted by SU(5) grand unification because the gauge coupling for $U(1)_Y$ is always smaller than those for the two U(1)'s. This is excluded by experiment.

9.6.3 Phenomenology with SO(10) GUT

The two difficulties with the minimal SU(5) GUT can be avoided in SO(10). The correct weak mixing angle can be derived by assuming a reasonable intermediate energy scale M_I. The unification scale M_G is significantly higher than that with SU(5), which makes the lifetime of nucleon decay consistent with the experimental limit [1416–1418] (see also [1419]).

There is another constraint on the SO(10) model. The Dirac masses of neutrinos are equal to the masses of up-type quarks, and hence the Majorana mass of the right-handed neutrino of the third family is $M_{\nu_R} \simeq 10^{14}$ GeV [see (9.141)]. This means that M_I should be larger than 10^{14} GeV, which selects uniquely a symmetry-breaking pattern (iv). The other schemes predict intermediate scales too low to explain the neutrino mass.

Precise prediction of $\sin^2 \theta_W$, M_G, and M_I, however, is generally difficult with SO(10) GUT, even if we fix the symmetry-breaking pattern. The reason is that there are a large number of scalar bosons with masses of the order of the unification scales. These particles may naturally lie above or below the unification scales by an order of magnitude or so, and these scalar particles contribute to the beta function differently. Although the threshold effect from a single scalar boson is small, the contribution from hundreds of such bosons in SO(10) causes large uncertainties in low-energy predictions [1418, 1420].

Indeed, the uncertainties are estimated to be as large as four orders of magnitude in nucleon lifetime and ± 0.06 in $\sin^2 \theta_W$ [1420], assuming that the scalar bosons lie at energies that are $10^{\pm 1}$ times the symmetry-breaking scale.

There is, however, a special case. These threshold uncertainties cancel for the intermediate symmetry group, $\mathrm{SU(4)} \times \mathrm{SU(2)}_L \times \mathrm{SU(2)}_R \times P$ [1421], with P parity (Z_2) symmetry for the interchange of $\mathrm{SU(2)}_L$ and $\mathrm{SU(2)}_R$ [1422]. This is the case of (iv), where we have assumed Higgs particles in a symmetric way.[10] Furthermore, the two-loop renormalization effect is small for the prediction of M_I [1423], whereas M_G is raised by a factor of 2 by the two-loop effect. We thus obtain

$$M_{\mathrm{G}} = 10^{15.6}\text{–}10^{15.8} \ \mathrm{GeV},$$
$$M_I = 10^{14.0} \ \mathrm{GeV}. \tag{9.190}$$

This M_I leads to a neutrino mass spectrum,

$$m_{\nu_e} = 3.0 \times 10^{-12} \ \mathrm{eV} \cdot h_e^{-1},$$
$$m_{\nu_\mu} = 6.3 \times 10^{-7} \ \mathrm{eV} \cdot h_\mu^{-1},$$
$$m_{\nu_\tau} = 6.7 \times 10^{-2} \ \mathrm{eV} \cdot h_\tau^{-1}, \tag{9.191}$$

where h_i are the Yukawa couplings for $\mathbf{16} \cdot \mathbf{16} \cdot \mathbf{126}$ for ith generation right-handed neutrinos. The ν_τ mass appears in the range marginally consistent with experiment (for $h_\tau \lesssim 1$) [1424,1423]. We expect $h_\mu, h_\tau \ll 1$, so, this symmetry-breaking pattern is a viable scheme.

If one of the pair Higgs (say, χ_L) has a mass much higher than the other, or there is no manifest left–right symmetry for the Higgs sector of model (iv), a cancellation of threshold corrections does not occur, and uncertainties become substantial [1425,1423]. For example, the case is considered for Higgs multiplets of $\mathbf{210}$, $\mathbf{126}$, and $\mathbf{10}$ with a further assumption that a submultiplet of $\mathbf{126}$, $\Delta(\mathbf{10}, \mathbf{1}, \mathbf{3})$, and $\phi(\mathbf{1}, \mathbf{2}, \mathbf{2}^*)$ of $\mathbf{10}$ lie near the intermediate scale $M_I \times 10^{\pm 1}$ and other components of these multiplets are around M_G. A submultiplet $\varphi(\mathbf{1}, \mathbf{2})$ of $\phi(\mathbf{1}, \mathbf{2}, \mathbf{2}^*)$ is taken to have a mass of the order of the electroweak energy scale. With the two-loop renormalisation effect [1426] taken into account [1423],

$$M_{\mathrm{G}} = 10^{15.8 \pm 0.2 {}^{+0.8}_{-0.7}} \ \mathrm{GeV},$$
$$M_I = 10^{11.5 \pm 0.03 {}^{+2.8}_{-1.5}} \ \mathrm{GeV}, \tag{9.192}$$

where the first errors are from the uncertainty in the low-energy parameters and the second are due to the threshold effect of Higgs particles. This gives

---

[10] The Higgs masses of χ_L and χ_R (or ξ_L and ξ_R) may differ by an order of magnitude or so, but the effect is small since the threshold effects are not so sensitive to the mass of the Higgs scalars.

a proton decay lifetime of $\tau_p \simeq 1.6 \times 10^{35 \pm 0.9 \, ^{+3.2}_{-2.8}}$ years and a neutrino mass spectrum of

$$m_{\nu_e} = (1 \times 10^{-12} \text{--} 3 \times 10^{-8}) \, \text{eV} \cdot h_e^{-1},$$
$$m_{\nu_\mu} = (3 \times 10^{-7} \text{--} 7 \times 10^{-3}) \, \text{eV} \cdot h_\mu^{-1},$$
$$m_{\nu_\tau} = (3 \times 10^{-2} \text{--} 7 \times 10^2) \, \text{eV} \cdot h_\tau^{-1}. \tag{9.193}$$

The range for the ν_τ mass includes the value inferred from experiment [1424,1423].

Another interesting symmetry-breaking chain is (vi) SO(10) → SU(3) × SU(2)$_L$ × SU(2)$_R$ × U(1). For the Higgs scalar multiplets **45**, **54**, **126**, and **10**, a similar analysis [1423] yields

$$M_{\text{G}} = 10^{15.8 \pm 0.25 \pm 0.2} \, \text{GeV},$$
$$M_I = 10^{9 \pm 0.18 \, ^{+0.3}_{-0.0}} \, \text{GeV}, \tag{9.194}$$

which predicts the proton lifetime to be $1.6 \times 10^{35 \pm 1 \pm 0.8}$ years. The neutrino masses are

$$m_{\nu_e} = (2 \times 10^{-7} \text{--} 1 \times 10^{-6}) \, \text{eV} \, h_e^{-1},$$
$$m_{\nu_\mu} = (2 \times 10^{-2} \text{--} 1 \times 10^{-1}) \, \text{eV} \, h_\mu^{-1},$$
$$m_{\nu_\tau} = (2 \times 10^3 \text{--} 1 \times 10^4) \, \text{eV} \, h_\tau^{-1}. \tag{9.195}$$

This mass spectrum is not consistent with experiment. Thus, we may conclude that case (iv), i.e., via an intermediate Pati–Salam gauge group is the only viable SO(10) symmetry-breaking scheme within the non-SUSY models.

9.7 Model with Horizontal Gauge Symmetry

We may consider horizontal gauge symmetry as an origin to give a mass to a neutrino. For three generations natural symmetry is either SO(3) or SU(3). In the former, the three families of quarks and leptons are assigned as **3**'s. The gauge theory is anomaly-free as it is; we find no reason to introduce right-handed neutrinos. However, SO(3) leads to degenerate quark masses in the zeroth order and is not favoured in view of the empirical mass pattern. If horizontal symmetry is SU(3), we need right-handed neutrinos to cancel anomaly [1427]. In what follows we consider the gauge group SU(2)$_L$ × U(1) × SU(3)$_H$, where H means horizontal.

We assume that q_L and ℓ_L belong to $(\mathbf{2}, \mathbf{3})$ of SU(2)$_L$ × SU(3)$_\text{H}$ and u_R, d_R, e_R, to $(\mathbf{1}, \mathbf{3})$. It is obvious from the mismatch of left–right symmetry for the neutrino that this model has gauge anomaly regarding SU(3)$_\text{H}$. This anomaly can be canceled if one adds $\nu_R(\mathbf{1}, \mathbf{3})$.

To explore the energy scale of this model, let us specify the Higgs sector. The simplest choice may be

$$\phi = (\mathbf{2}, \mathbf{8} + \mathbf{1}),$$
$$\chi = (\mathbf{1}, \mathbf{6}). \tag{9.196}$$

Two $(\mathbf{8}+\mathbf{1})$ ϕ's are necessary to give the correct mass to quarks and leptons. The horizontal gauge fields $S_\mu^i (i = 1\text{–}8)$ acquire their masses by $\langle \chi \rangle \neq 0$.

The exchange of S_μ^i gives rise to flavour-changing neutral currents, and one has to assume that $\langle \chi \rangle \gg \langle \phi \rangle$ in order to suppress unwanted effects. The most stringent limit is derived from the $K_L^0 - K_S^0$ mass difference, leading to $\langle \chi \rangle / \langle \phi \rangle \gtrsim 10^5$ [1428]. Therefore, the right-handed neutrino mass induced by

$$\mathcal{L} = \frac{h}{2} \nu_R^T \nu_R \chi + \text{h.c.} \tag{9.197}$$

is

$$M_{\nu_R} \gtrsim h \langle \chi \rangle \gtrsim h \times 10^7 \text{ GeV}. \tag{9.198}$$

If we take $m_D = m_\ell$ and $\langle \chi \rangle = V \delta_{ij}$, we find

$$m_{\nu_e} \lesssim h^{-1} \times 3 \times 10^{-5} \text{ eV},$$
$$m_{\nu_\mu} \lesssim h^{-1} \times 1 \text{ eV},$$
$$m_{\nu_\tau} \lesssim h^{-1} \times 300 \text{ eV}. \tag{9.199}$$

A potentially interesting possibility was that the mechanism that gives the neutrino a mass can be observed as a flavour-changing neutrino current effect. Empirical ν_μ and ν_τ neutrino masses, however, are much smaller than the limits from this model, implying that the symmetry-breaking scale must be much higher than the limit set by the absence of the flavour-changing neutrino current.

9.8 Seesaw Mechanism with Global Symmetry

9.8.1 Model with U(1) Symmetry

It is possible to identify the symmetry that protects the right-handed neutrino from having a mass with some global symmetry proposed in other contexts. For instance, we may take Peccei–Quinn (PQ) U(1) [1359]. We usually assign the PQ charge as

$$q_L = \begin{pmatrix} u \\ d \end{pmatrix}_L \quad 1 \quad \begin{matrix} u_R & -1 \\ d_R & -1 \end{matrix},$$
$$\ell_L = \begin{pmatrix} \nu \\ e \end{pmatrix}_L \quad 1 \quad e_R \quad -1. \tag{9.200}$$

We may add the right-handed neutrino

$$\nu_R \quad -1. \tag{9.201}$$

If we introduce a Higgs χ with a PQ charge of $+2$ to break PQ symmetry, we have a Yukawa coupling of the form

$$\mathcal{L}_Y = \frac{h}{2}\overline{\nu_R^c}\nu_R\chi. \tag{9.202}$$

Thus, ν_R acquires the mass

$$M_{\nu_R} = h\langle\chi\rangle \tag{9.203}$$

as χ develops a vacuum-expectation value. This model has predictive power for the neutrino mass: the vacuum-expectation value of χ is constrained to lie between 10^9 and 10^{12} GeV from astrophysical and cosmological arguments (see Sect. 9.9.3); therefore,

$$M_{\nu_R} \simeq h \times (10^9\text{–}10^{12})\,\text{GeV}. \tag{9.204}$$

This value is close to that empirically required if the neutrino Yukawa couplings are identified with those for charged leptons. In practice, however, there are some subtleties in constructing a model; they will be discussed in Sect. 9.9.

If U(1) symmetry is identified with that of lepton number, the model is essentially the singlet Majoron model [1429]. In this case, we have no bound on the symmetry-breaking scale since Majoron (NG boson) coupling to matter is extremely suppressed [1430].

9.8.2 Model with Family Symmetry

Family (horizontal) symmetry [1431, 1432] $\mathrm{SU}(3)_F$ may also be used as protecting symmetry. We take the assignment

$$q_L = \begin{pmatrix} u \\ d \end{pmatrix}_L \quad \mathbf{3} \qquad \begin{matrix} u_R \ \mathbf{3} \text{ or } \mathbf{3}^* \\ d_R \ \mathbf{3} \text{ or } \mathbf{3}^* \end{matrix},$$

$$\ell_L = \begin{pmatrix} \nu \\ e^- \end{pmatrix}_L \quad \mathbf{3} \qquad \begin{matrix} \nu_R \ \mathbf{3} \text{ or } \mathbf{3}^* \\ e_R \ \mathbf{3} \text{ or } \mathbf{3}^* \end{matrix}. \tag{9.205}$$

The Majorana mass term $M\nu_R\nu_R$ is forbidden by $\mathrm{SU}(3)_F$. To break $\mathrm{SU}(3)_F$ symmetry completely, we should prepare Higgs particles of (i) one $\mathbf{6}$, (ii) two $\mathbf{8}$'s, or (iii) two $\mathbf{3}^*(\mathbf{3})$'s. In case (i) or (iii) the Higgs particle gives ν_R a Majorana mass. If we introduce χ ($\mathbf{6}$ or $\mathbf{6}^*$) to break family symmetry, a Majorana mass arises from $h\nu_R^i\nu_R^j\chi_{ij}$,

$$[M_{\nu_R}]_{ij} = h\langle\chi\rangle_{ij}. \tag{9.206}$$

The case of symmetry breaking by triplet Higgs' (iii) leads to a qualitatively different scenario [1433], which will be discussed separately in Sect. 9.8.3. The Dirac mass is given by two $SU(2)_L$ doublet Higgs', either $(\mathbf{1}, \mathbf{2}) \oplus (\mathbf{8}, \mathbf{2})$ or $(\mathbf{6}, \mathbf{2}) \oplus (\mathbf{6}, \mathbf{2})$ of $(SU(3)_F, SU(2)_L)$. Two Higgs' are necessary to give the correct fermion mass spectrum.

A specific feature with the choice $(\mathbf{6}, \mathbf{2}) \oplus (\mathbf{6}, \mathbf{2})$ is that it leads to $U_q \simeq U_{\text{lepton}}$. These two Higgs' have $Y = 1/2$ and $Y = -1/2$, respectively, so the Yukawa couplings are

$$\mathcal{L} = f_d \bar{q}_L \phi_1 d_R + f_u \bar{q}_L \phi_2 u_R$$
$$+ f_e \bar{\ell}_L \phi_1 e_R + f_\nu \bar{\ell}_L \phi_2 \nu_R + \text{h.c.} \qquad (9.207)$$

Both d-type quarks and leptons acquire masses from the same Higgs $\langle \phi_1 \rangle$, and u-type quarks and neutrinos (Dirac mass) from $\langle \phi_2 \rangle$, so that quark and lepton mass matrices are simultaneously diagonalised.

Complete symmetry breaking produces 8 Nambu–Goldstone bosons (φ), which are called familons [1432]. Such bosons couple to flavour-changing neutral currents as

$$\mathcal{L} = \frac{1}{F_{e\mu}} \bar{e} \gamma^\mu (a + b \gamma_5) \mu \partial_\mu \varphi + \frac{1}{F_{ds}} \bar{d} \gamma^\mu (a' + b' \gamma_5) s \partial_\mu \varphi + ... + \text{h.c.}$$
$$(|a|^2 + |b|^2 = |a'|^2 + |b'|^2 = 1), \qquad (9.208)$$

which causes μ or K to decay

$$\mu \to e + \varphi , \qquad (9.209)$$
$$K \to \pi + \varphi , \qquad (9.210)$$

where F_{ij} is related to the symmetry-breaking scale $\langle \chi \rangle$. For instance, if the family symmetry is broken by $\langle \chi(\mathbf{6})_{ij} \rangle = V_i \delta_{ij}$, $F_{e\mu} \simeq F_{ds} \simeq V_2$, and $F_{\mu\tau} \simeq F_{sb} \simeq V_3$ for $V_1 < V_2 < V_3$. The coupling of φ to quarks and leptons is suppressed by $1/F_{ij}$ due to the Goldstone theorem; the existence of such zero mass particles is thus harmless, provided that v_{ij} is sufficiently large. The decay rates are given by

$$\Gamma(\mu^+ \to e^+ + \varphi) = m_\mu^3 (|a^2| + |b^2|)/16\pi F_{e\mu}^2 , \qquad (9.211)$$
$$\Gamma(K^+ \to \pi^+ + \varphi) = m_K^3 |a'|^2 /16\pi F_{ds}^2 . \qquad (9.212)$$

From the experimental limits [1434, 1435],

$$Br(\mu^+ \to e^+ + \varphi) < 2.6 \times 10^{-6}, \qquad (9.213)$$
$$Br(K^+ \to \pi^+ + \varphi) < 3 \times 10^{-10}, \qquad (9.214)$$

we obtain [1436, 1437]

$$F_{e\mu} > 5.5 \times 10^9 \text{ GeV} \qquad (9.215)$$
$$F_{ds} > 3.4 \times 10^{11} \delta \text{ GeV}, \qquad (9.216)$$

where $\delta = |a'|/(|a'|^2 + |b'|^2)^{1/2}$, which depends further on the details of the model. These lower limits roughly agree with the scale presumed for PQ symmetry breaking. For $M_{\nu_R} \gtrsim 10^{10}$ GeV, the mass of the left-handed neutrino is $m_{\nu_\tau} \simeq m_\tau{}^2/M_{\nu_R} \lesssim h^{-1} \times (0.1 \text{ eV})$ if the Dirac mass is taken to be the charged lepton mass. If the Dirac mass is identified with the quark mass, e.g., as in SO(10), then $m_{\nu_\tau} \lesssim h^{-1} \times (1 \text{ keV})$.

The presence of φ makes massive neutrinos unstable [1432]. For effective coupling of the form

$$\mathcal{L} = \frac{1}{F_{ij}} \overline{\nu_i} \gamma^\mu (A + B\gamma_5) \nu_j \partial_\mu \varphi, \ \ |A|^2 + |B|^2 = 1 \ , \qquad (9.217)$$

the decay rate of ν_j is given by

$$\begin{aligned} \Gamma &= m_{\nu_j}^3/16\pi F_{ij}^2 \\ &= (3.5 \times 10^{24} \text{ s})^{-1} (m_{\nu_j}/1 \text{ eV})^3 (v_{ij}/10^{10} \text{ GeV})^{-2}. \end{aligned} \qquad (9.218)$$

Thus, light neutrinos are practically stable even in the presence of φ.

9.8.3 Model for the Fourth-Generation Neutrino

If M_{ν_R} vanishes in (6.43) for one of the generations, say, the nth, the corresponding left-handed neutrino appears as a Dirac neutrino with $m_\nu = m$ [1433,1438]. Such a case is realised if family SU$(n)_F$ symmetry (either global or local) is broken by Higgs scalars in the fundamental representation [1433].

Let us assume that the left-handed leptons and quarks ℓ_L transform as the $\boldsymbol{n}$ representation of SU$(n)_F$ and the right-handed ν_R, e_R, u_R, and d_R as either $\boldsymbol{n}$ or $\boldsymbol{n}^*$ of SU$(n)_F$. (For local SU$(n)_F$, we must take $\boldsymbol{n}$ for the right-handed fermions to cancel gauge anomaly.) A complete breaking of SU$(n)_F$ is caused by $n-1$ Higgs scalars $\xi^{(a)}$ in the fundamental $\boldsymbol{n}$ representation of SU$(n)_F$ (they are assumed to be singlets of SU$(2)_L$). The vacuum-expectation values of $\xi^{(a)}(a = 1 \sim n - 1)$ can generally be written

$$\langle \xi^{(1)} \rangle = \begin{pmatrix} v_1^{(1)} \\ 0 \\ \vdots \\ 0 \end{pmatrix}, \ \dots, \ \langle \xi^{(n-1)} \rangle = \begin{pmatrix} v_1^{(n-1)} \\ \vdots \\ v_{n-1}^{(n-1)} \\ 0 \end{pmatrix}. \qquad (9.219)$$

The Higgs $\xi^{(a)}$ do not couple directly to ν_R, and hence it is natural to suppose effective interactions, the lowest dimensional form of which is written as

$$\frac{f_{ab}}{2M} (\xi_i^{(a)} \nu_R^i)(\xi_j^{(b)} \nu_R^j), \qquad (9.220)$$

where i and j denote the family indices and M is the effective mass scale. Thus, after $SU(n)_F$ breaking, ν_R acquires the Majorana mass term

$$M_{\nu_R} = \frac{f_{ab}}{M} \langle \xi^{(a)} \rangle \langle \xi^{(b)} \rangle \ . \tag{9.221}$$

This $n \times n$ matrix has vanishing matrix elements for either $i = n$ or $j = n$ and, therefore, one of the eigenvalues vanishes.

The Dirac mass terms for quarks and leptons are given by the Yukawa couplings of $SU(2)_L$ doublet Higgs scalars ϕ's which break $SU(2)_L \times U(1)$ to $U(1)_{em}$. The transformation property of ϕ under $SU(n)_F$ depends upon whether $\boldsymbol{n}$ or $\boldsymbol{n}^*$ is chosen for the right-handed fermions ψ_R. If ψ_R is taken as $\boldsymbol{n}$, we should prepare an $SU(n)_F$ adjoint ϕ^i_j and a singlet ϕ. The Yukawa couplings in the lepton sector are given by

$$\overline{e_R}^j (f_e^{(1)} \tilde{\phi}^i_j + f_e^{(2)} \tilde{\phi}\delta^i_j)\ell_{Li} + \overline{\nu_R}^j (f_\nu^{(1)}\phi^i_j + f_\nu^{(2)}\phi\delta^i_j)\ell_{Li} + \text{h.c.} \tag{9.222}$$

For $\psi_R = \boldsymbol{n}^*$, we need two $SU(n)_F$ symmetric $[n(n+1)/2]$ Higgs ϕ^{ij} and ϕ'^{ij}. The Yukawa couplings are

$$\overline{e}_{Ri}(f'_e \phi'^{ij})\ell_{Lj} + \overline{\nu}_{Ri}(f'_\nu \phi^{ij})\ell_{Lj} + \text{h.c.} \tag{9.223}$$

There is a significant difference in the symmetry structure of the Higgs sector between these two choices. For $\psi_R = \boldsymbol{n}^*$, unwanted $U(n)_F^\xi \times U(n)_F^\phi$ symmetry remains within the class of renormalisable interactions, where the two $U(n)_F$'s correspond to rotations of ξ^a_i and ϕ^{ij} (and ϕ'^{ij}) with respect to family indices. Since $U(n)_F^\phi$ is spontaneously broken by the condensation of ϕ^{ij} and ϕ'^{ij}, there appear n^2 Nambu–Goldstone bosons, which, however, are excluded by experiment because their coupling strengths are set by the weak scale. However, we may get rid of unwanted $U(n)_F^\phi$ symmetry by supposing an effective operator,

$$\frac{1}{M^2} \phi^{ij} \phi'^{k\ell} \xi_i^{(a)} \xi_j^{(b)} \xi_k^{(c)} \xi_\ell^{(d)}. \tag{9.224}$$

With this interaction the n^2 Nambu–Goldstone bosons acquire masses of the order of $\langle \xi \rangle^2 / M$, which is usually large.

For $\psi_R = \boldsymbol{n}$, on the other hand, unwanted $U(n)_F^\phi$ is broken by the renormalisable interaction,

$$\phi^i_j \phi^* \xi_i^{(a)} \xi_{(b)}^{*j}. \tag{9.225}$$

In either of the two models, the seesaw mechanism works only for the family $i = 1 \sim n - 1$ to give small Majorana masses to left-handed neutrinos,

$$m_\nu \simeq m_D M_{\nu_R}^{-1} m_D^T \ , \tag{9.226}$$

with

$$m_D = f_\nu^{(1)} \langle \phi_j^i \rangle + f_\nu^{(2)} \langle \phi \rangle \qquad \text{(for} \quad \psi_R = \boldsymbol{n}), \qquad (9.227)$$

or

$$m_D = f_\nu' \langle \phi^{ij} \rangle \qquad \text{(for} \quad \psi_R = \boldsymbol{n}^*) \,. \qquad (9.228)$$

For a neutrino of the nth generation, however, the seesaw mechanism does not work, and its mass is given by the Dirac mass of the nth generation ($n = 4$), which would be of the order of a few $\times$ 100 GeV, the mass supposed for the fourth-generation heavy lepton or quark, if it exists at all ("partially broken" seesaw mechanism).

If we suppose that family symmetry is broken at $\sim 10^{16}$ GeV and $M \sim m_{\text{pl}}$, we expect $M_{\nu_R} \sim 10^{14}$ GeV. If we take the Dirac masses of the neutrinos to be those of charge 2/3 quarks, we expect $m_{\nu_e} \sim 10^{-12}$ eV, $m_{\nu_\mu} \sim 10^{-6}$ eV and $m_{\nu_\tau} \sim 10^{-1}$ eV, while for the fourth generation, $m_{\nu_\sigma} \sim m_\sigma \gtrsim 100$ GeV.

9.9 Peccei–Quinn Symmetry and the Neutrino Mass

9.9.1 Strong CP Problem and Peccei–Quinn Symmetry

The presence of the anomaly and the instanton in SU(3) gauge theory leads us to suppose that the QCD vacuum has a nontrivial topological structure, with the true strong interaction Lagrangian

$$\mathcal{L} = \mathcal{L}_{\text{QCD}} + \frac{1}{32\pi^2} \theta F_{\mu\nu}^a \tilde{F}^{a\mu\nu}, \qquad (9.229)$$

where a stands for the colour index of the gluon field [1355,259] and $\tilde{F}^{\mu\nu} = \frac{1}{2}\varepsilon^{\mu\nu\rho\sigma} F_{\mu\nu}$. The second term is a total divergence of the axial-vector current and so it is omitted unless we consider topology. Diagonalisation of the quark mass matrix, $V^{-1} m_q U = m_q^{\text{diag}}$, is a chiral transformation that rotates the phase of the fermion fields by $\psi \to \exp(-\frac{i}{2}\gamma_5 \arg \det m_q)\psi$, which also contributes to θ. Hence θ is modified to

$$\theta_{\text{eff}} = \theta + \arg \det \| m_d m_u \|, \qquad (9.230)$$

taking into account both $Q = 2/3$ and $Q = -1/3$ quark matrices. Here, $\arg \det \| m_d m_u \|$ is δ of (3.113), which is of order unity (the determinant agrees with that of the quark mixing angle in the representation where m_d is diagonal). θ_{eff} labels the QCD vacuum, and the vacuum of any θ_{eff} must be equally acceptable.

On the other hand, the second term of (9.229) is $\propto \mathbf{E} \cdot \mathbf{H}$ that violates P and CP (P: $\mathbf{E} \to -\mathbf{E}, \mathbf{H} \to \mathbf{H}$, and CP: $\mathbf{E} \to \mathbf{E}, \mathbf{H} \to -\mathbf{H}$). Hence, θ_{eff} must be very small to make the theory consistent with experiment. The

parameter θ_{eff} is bounded by the absence of the electric dipole moment of the neutron $(d < 0.63 \times 10^{-25}e$ cm [1439]) as [1440]

$$|\theta_{\text{eff}}| < 10^{-10}. \tag{9.231}$$

This means a huge cancellation between θ and arg det$\| m_d m_u \|$. The reason for the smallness of θ_{eff} is unknown, and this is often referred to as the strong CP problem [259].

The best accepted solution of this problem is the model proposed by Peccei and Quinn [1359]. Consider the standard electroweak model extended to include two Higgs doublets ϕ_1 and ϕ_2, where ϕ_1 is supposed to give a mass to the electron and d quark and ϕ_2 to the u quark instead of ϕ_1^* [see (2.32)]. This extension allows us to have a new chiral U(1) symmetry. In parallel to (2.32), we write the Yukawa coupling

$$\mathcal{L}_Y = -f_e \bar{\ell}_L e_R \phi_1 - f_d \bar{q}_L d_R \phi_1 - f_u \bar{q}_L u_R \phi_2 + \text{h.c.} \tag{9.232}$$

This Lagrangian is invariant under the chiral rotation $\psi \rightarrow e^{i\alpha\gamma_5}\psi$, i.e.,

$$\ell_L \longrightarrow e^{-i\alpha}\ell_L, \quad e_R \longrightarrow e^{+i\alpha}e_R, \quad q_L \longrightarrow e^{-i\alpha}q_L,$$
$$u_R \longrightarrow e^{+i\alpha}u_R, \quad d_R \longrightarrow e^{+i\alpha}d_R,$$
$$\phi_1 \longrightarrow e^{-2i\alpha}\phi_1, \quad \phi_2 \longrightarrow e^{-2i\alpha}\phi_2. \tag{9.233}$$

This contrasts with the case with the minimal standard model where the third term of (9.232) violates invariance by $\phi^* \rightarrow e^{+2i\alpha}\phi^*$.

With this chiral rotation, the QCD Lagrangian transforms as

$$\delta \int d^4x \mathcal{L}_{\text{QCD}} = -2\alpha \frac{g^2}{32\pi^2} \int d^4x F_{\mu\nu}^a \widetilde{F}^{a\mu\nu}, \tag{9.234}$$

and the strong CP-violating term in (9.229) is now

$$\mathcal{L}_{\text{CP}} = \frac{g^2}{32\pi^2}(\theta_{\text{eff}} - 2\alpha)F_{\mu\nu}^a \widetilde{F}^{a\mu\nu}. \tag{9.235}$$

This means that the QCD vacuum angle θ_{eff} is physically meaningless and can be rotated away [1359].

U(1)$_{\text{PQ}}$, however, is broken, when ϕ_1 and ϕ_2 obtain vacuum-expectation values at the electroweak scale v. This gives rise to a Nambu–Goldstone (NG) boson, and the argument given above cannot be valid as it is. Furthermore, this U(1)$_{\text{PQ}}$ symmetry is explicitly broken by chiral anomaly at a QCD energy scale, as can be seen in (9.234). Hence, U(1)$_{\text{PQ}}$ remains only as approximate symmetry, and the NG boson acquires a small mass [1360] of the order of

$$m_A \sim \frac{f_\pi m_\pi}{v} \sim 100\,\text{keV}. \tag{9.236}$$

This pseudo-NG boson is called an axion [1360]. The mass and coupling property of the axion are prescribed by the Goldstone theorem. Axions are excluded by experiment [1441].

This undesirable feature can be avoided if $U(1)_{PQ}$ is broken at a scale much higher than v, so that the mass of the pseudo-NG boson is $m_A \sim f_\pi m_\pi / F_{PQ}$ [1442–1445]. For this purpose, one introduces an $SU(2)_L \times U(1)$ singlet Higgs χ, which carries $U(1)_{PQ}$ charge $+2$ and develops a vacuum-expectation value $V_{PQ} \gg v$. Here, the axion decay constant F_{PQ} is given by $F_{PQ} \simeq V_{PQ}/\sqrt{2}$. This χ transforms as

$$\chi \longrightarrow e^{+2i\alpha}\chi. \tag{9.237}$$

By virtue of the Goldstone theorem, this axion has a very small mass, and its coupling to matter is suppressed by m_f/F_{PQ} where m_f is mass of the fermion. This is the model of invisible axions [1442–1445].

We now return to the strong CP problem. The current of Peccei–Quinn symmetry has anomaly that contributes to the Lagrangian

$$\mathcal{L} = \frac{1}{32\pi^2} A(x) F^a_{\mu\nu} \widetilde{F}^{a\mu\nu}, \tag{9.238}$$

which should be added to (9.229). On the other hand, the axion acquires a mass term, through the QCD instanton effect, of the form [1446]

$$\mathcal{L}_{\text{mass}} = m_A^2 (A(x) + \bar{\theta}_{\text{eff}})^2, \tag{9.239}$$

so that the vacuum takes the expectation value

$$\langle A(x) \rangle = -\bar{\theta}_{\text{eff}}. \tag{9.240}$$

The anomaly term (9.229) plus (9.238) thus vanishes, restoring the CP invariance.

9.9.2 Model for the Neutrino Mass

Now, we introduce the right-handed neutrino [1447–1449], which transforms as

$$\nu_R \longrightarrow e^{+i\alpha}\nu_R. \tag{9.241}$$

The mass term that respects $U(1)_{PQ}$ is

$$\mathcal{L}_Y = -f_\nu \overline{\ell_L} \nu_R \phi_2 + \text{h.c.} \tag{9.242}$$

We may also have a mass term of the form

$$\mathcal{L} = \frac{h}{2} \overline{\nu_R^c} \nu_R \chi + \text{h.c.} \tag{9.243}$$

The introduction of ν_R changes the symmetry structure of the model. There are four U(1) symmetries, baryon number, lepton number U(1)$_L$, U(1)$_{\rm PQ}$, and U(1)$_Y$, of which the latter three are eventually broken. When χ develops a vacuum-expectation value, both U(1)$_L$ and U(1)$_{\rm PQ}$ appear to be broken. However, what is actually broken is a linear combination of the two U(1) symmetries; another U(1) remains unbroken. An analysis shows that the current corresponding to the remaining U(1) symmetry has anomaly; this U(1) is identified as a new PQ symmetry, meaning that the symmetry broken by $\langle\chi\rangle \neq 0$ corresponds to lepton number. This new PQ symmetry is broken only after the doublet ϕ_i develops a vacuum-expectation value. Accordingly, the mass of the axion is suppressed only as $f_\pi m_\pi / v^2$, contrary to our desire. This is essentially the case of the standard axion, which is already excluded by experiment.

To save the model, the authors of [1449] introduced an explicit symmetry-breaking term in the Higgs potential, so that lepton-number conservation is explicitly violated. They introduced a soft breaking term,[11]

$$\mathcal{L}_{\Delta L} = \lambda \phi_1 \phi_2 \chi + \text{h.c.} \tag{9.244}$$

Then, $\langle\chi\rangle \neq 0$ in (9.243) leads to U(1)$_{\rm PQ}$ violation, and the mass of the axion is given by $m_A \sim m_\pi f_\pi / \langle\chi\rangle$, as desired.

In this model, $\langle\chi\rangle \neq 0$ at the same time gives the right-handed neutrino a large Majorana mass,

$$M_{\nu_R} = h\langle\chi\rangle. \tag{9.245}$$

The argument of Sect. 9.8.1 now applies to this model. PQ symmetry, however, must be redefined in the presence of the symmetry-breaking term (9.244); i.e., under this U(1)$_{\rm PQ}$, the fermion fields should transform as

$$q_L \to e^{-i\alpha} q_L, \quad u_R \to e^{+i\alpha} u_R, \quad d_R \to e^{+i\alpha} d_R,$$
$$\ell_L \to \ell_L, \quad \nu_R \to e^{+2i\alpha} \nu_R, \quad e_R \to e^{+2i\alpha} e_R,$$
$$\phi_1 \to e^{-2i\alpha} \phi_2, \quad \phi_2 \to e^{-2i\alpha} \phi_2,$$
$$\chi \to e^{-4i\alpha} \chi \tag{9.246}$$

to make the Lagrangian invariant.

9.9.3 Astrophysical and Cosmological Constraints

A lower limit can be derived on the symmetry-breaking scale $F_{\rm PQ}$ from the argument for stellar evolution [1450, 1451]. If axions exist, they would be

---

[11] If one introduces a symmetry-breaking term of dimension four, $\mathcal{L}_{\Delta L} = g\phi_1\phi_2\chi\chi$, radiative corrections induce new quadratically divergent terms in the Higgs potential that destroy the desired hierarchy $\langle\chi\rangle \gg \langle\phi_i\rangle$. This problem is avoided by introducing a soft symmetry-breaking term since it does not give rise to a quadratic divergence; a hierarchy $\langle\chi\rangle \gg \langle\phi_i\rangle$, once satisfied at the tree level, also holds after radiative corrections, if $\lambda\langle\chi\rangle \lesssim \langle\phi_i\rangle^2$ is satisfied.
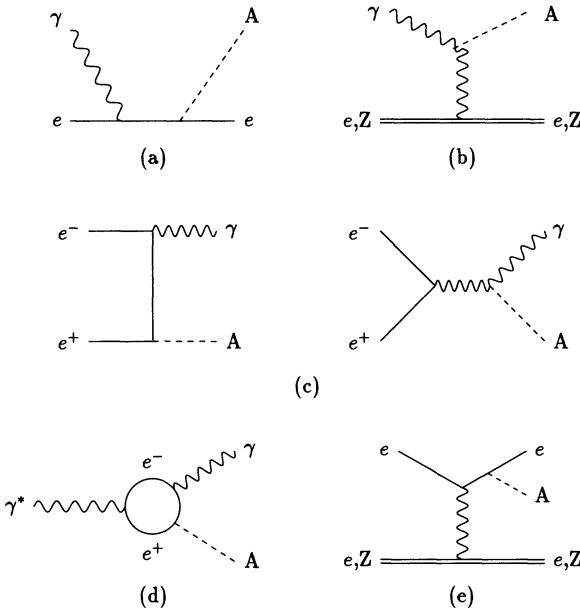
Fig. 9.5. Feynman diagrams for axion emission in stars. (**a**) Compton process; (**b**) Primakoff process; (**c**) e^+e^- pair annihilation; (**d**) plasmon decay; (**e**) bremsstrahlung axion emission.

copiously produced in the high-temperature environment of stellar plasma and would carry out stellar energy produced in nuclear reactions, like the neutrino production we have seen in Sect. 4.4. The limit is obtained in the same way as that on the neutrino magnetic moment discussed in Sect. 5.1.3.

The processes that are important in stars are analogous to neutrino production, as depicted in Fig. 9.5: Compton process $\gamma + e \rightarrow A + e$, Primakoff process $\gamma + \gamma_v$ (virtual) $\rightarrow A$, plasmon decay γ_ω (plasmon) $\rightarrow A + \gamma_{\omega'}(\omega' < \omega)$, e^+e^- pair annihilation $e^+e^- \rightarrow A + \gamma$, and bremsstrahlung $e + \text{nucleus} \rightarrow e + \text{nucleus} + A$. In helium-burning stars, the first three processes are important. Since the coupling of χ with a fermion is suppressed by m_f/F_{PQ}, all processes are suppressed by the factor F_{PQ}^{-2}. The detail of the coupling depends on axion models. For the model of [1443,1444], called the DFSZ axion,[12]

$$\mathcal{L}_{Ae\bar{e}} = i\frac{2}{1+x^2}\frac{m_e}{F_{PQ}}A\bar{e}\gamma_5 e \tag{9.247}$$

---

[12] There is a class of models [1442,1445], in which the axion does not couple to leptons (called hadronic or KSVZ axions). This model assumes the existence of heavy quarks that cancel the anomaly of the axion–gluon–gluon coupling arising from light quark loops. If the heavy quark is electric-charge neutral, the axion coupling to two photons is

$$\mathcal{L}_{A\gamma\gamma} = \frac{\alpha}{6\pi}\frac{4+z}{1+z}\frac{1}{F_{PQ}}A\epsilon^{\mu\nu\rho\sigma}F_{\mu\nu}F_{\rho\sigma} \ .$$

for the coupling to electrons, and

$$\mathcal{L}_{A\gamma\gamma} = \frac{2z}{1+z}\frac{\alpha}{\pi}\frac{1}{F_{\mathrm{PQ}}}A\epsilon^{\mu\nu\rho\sigma}F_{\mu\nu}F_{\rho\sigma} \qquad (9.248)$$

for two photons, where $x = \langle\phi_1\rangle/\langle\phi_2\rangle$ $(\langle\phi_1\rangle^2 + \langle\phi_2\rangle^2 = v^2)$ and $z = m_u/m_d \simeq 0.57$ [1373]. ($x = 1$ is assumed in the following analysis.)

When axion emissivity becomes of the order of the optical luminosity of stars, stellar evolution is affected (to derive a limit quantitatively, one should compare the change that would be caused by axion emission with observation; whether the change is detectable is the crucial point in deriving a constraint [1451]). The most reliable, yet stringent, limit is derived from a star in the helium-burning stage [1451]; it is[13]

$$F_{\mathrm{PQ}} > 2 \times 10^9 \,\mathrm{GeV}, \qquad (9.249)$$

where $x = 1$ is assumed. (Limits as strong as $F_{\mathrm{PQ}} > 10^9$–10^{11} are inferred from a consideration of supernova SN1987A [1452], but we do not take these limits literally since we have no consistent understanding of supernovae, as explained in Sect. 4.5.1.).[14]

An upper limit on $\langle\chi\rangle \simeq \sqrt{2}F_{\mathrm{PQ}}$ is derived from a cosmological consideration [1453]. When the PQ symmetry is broken, the axion field perhaps takes a random phase which varies from horizon to horizon. When the temperature decreases to the QCD scale, the axion field acquires a finite mass [1454], and it starts oscillating as the Hubble expansion timescale becomes longer than the oscillation frequency ($\sim m_A$). The oscillation is eventually damped by the viscous effect of the Hubble expansion and settles to the value of (9.240). This dynamics of the free axion field $\phi(x,t)$ $[= A(x,t)]$ is described by

$$\ddot{\phi} + 3\frac{\dot{a}}{a}\dot{\phi} + (m_A^2 - V/a^2)\phi = 0, \qquad (9.250)$$

where V is the Higgs potential and a is the scale factor of the Universe. This oscillating coherent field gives a mass density of

$$\rho = \frac{1}{2}m_A^2\phi^2 \approx 2 \times 10^{-30}\,\mathrm{gcm}^{-3}\Lambda_{200}^{-3/4}(F_{\mathrm{PQ}}/10^{12}\,\mathrm{GeV})^{7/6}, \qquad (9.251)$$

where Λ_{200} is the chiral phase-transition energy scale in units of $200\,\mathrm{MeV}$ [1455]. The constraint that oscillation is sufficiently damped and ρ then must

---

[13] The limit for the KSVZ axion is weaker by a factor of 3.

[14] Axion emission depends on the temperature with a high power $T^8 \sim T^{10}$. Therefore, the argument depends crucially on the core temperature, which is largely model-dependent. A slightly lower temperature deep inside the core greatly reduces axion emissivity.

be smaller than the critical density of the universe (4.203), gives an upper limit on F_{PQ} [1453],

$$F_{PQ} < 7 \times 10^{12}\,\text{GeV}\,h^{12/7}\Lambda_{200}^{9/14}. \tag{9.252}$$

When (9.252) is satisfied, the oscillation amplitude today corresponds to $\theta = \phi/F_{PQ} < 10^{-21}$, which is sufficiently small to satisfy (9.231).[15]

In this way, the symmetry-breaking scale F_{PQ} is constrained to a narrow range. Correspondingly, the mass of the axion is

$$10^{-5}\,\text{eV} < m_A < 10^{-3}\,\text{eV}, \tag{9.253}$$

where axion mass is related to F_{PQ} as

$$m_A = 10^{-5}\,\text{eV}\left(\frac{7 \times 10^{12}\,\text{GeV}}{F_{PQ}}\right). \tag{9.254}$$

If F_{PQ} takes a value slightly smaller than the cosmological limit, invisible axions would gravitationally dominate the universe. Invisible axions have never been in thermal equilibrium, so, they are cold and a candidate for cold dark matter. There are attempts to detect dark matter axions in laboratories using the Primakoff conversion of the axion to a microwave photon in a magnetic field [1457]. An intense magnetic field is applied to a low-temperature high-Q cavity with a tunable resonant frequency, and the cavity output power is monitored to search for a resonant signature while frequencies are scanned [1458].

9.9.4 Domain Wall Problem

In (9.235) we have seen that $U(1)_{PQ}$ is not symmetry of the full Lagrangian. In the presence of N_f families, (9.235) generalises to

$$\mathcal{L}_{\text{eff}} = \frac{1}{32\pi^2}(\theta_{\text{eff}} - 4\alpha N_f)F_{\mu\nu}^a \widetilde{F}^{a\mu\nu}. \tag{9.255}$$

Since θ_{eff} is an angle of mod 2π, the Lagrangian is invariant under

$$\alpha \to \alpha + \frac{2\pi}{4N_f}n \quad (n = \text{integer}), \tag{9.256}$$

---

[15] If $U(1)_{PQ}$ is embedded in a grand unifying group, symmetry breaking leaving $U(1)_{PQ}$ generates cosmic strings, and their decay produces copious axions. In such a case, the cosmological constraint is more stringent by an order of magnitude. The upper limit on the F_{PQ} scale is $\sim 10^{12}\,\text{GeV}$, but the details do not agree among authors [1456].

i.e., we still have Z_{4N_f} symmetry [1459]. The condensation of χ then causes spontaneous breakdown of this discrete symmetry, which gives rise to a domain wall problem.[16]

We can avoid this problem if we embed the Z_N discrete symmetry into the centre of some non-Abelian group [1460]; we then have a path which connects the Z_N vacua with a zero-energy gradient. For this to be realised, one has to extend the standard model. One of the simplest models is $SO(10) \times SU(3)_F$ [1461]. The matter field spinor $\mathbf{16}_L$ of $SO(10)$ is decomposed into $\psi_L(\mathbf{4}, \mathbf{2}, \mathbf{1})$ and $\bar{\psi}_L(\mathbf{4}^*, \mathbf{1}, \mathbf{2})$ under its maximal subgroup $SU(4) \times SU(2)_L \times SU(2)_R$. Under the transformation corresponding to the centre of $SU(4) \times SU(2)_L \times SU(2)_R$, these spinors transform as

$$\psi_L \to e^{-i\frac{2\pi}{2}\alpha} e^{-i\frac{2\pi}{4}\gamma} \psi_L \ ,$$
$$\bar{\psi}_L \to e^{-i\frac{2\pi}{2}\beta} e^{+i\frac{2\pi}{4}\gamma} \bar{\psi}_L \ . \tag{9.257}$$

Taking $\beta = \alpha + \gamma$, we see that both ψ_L and $\bar{\psi}_L$ transform under Z_4 as

$$\begin{pmatrix} \psi_L \\ \bar{\psi}_L \end{pmatrix} \to e^{-i\frac{2\pi}{4}\ell} \begin{pmatrix} \psi_L \\ \bar{\psi}_L \end{pmatrix} \tag{9.258}$$

with $\ell = 2\alpha + \gamma$. Therefore, under $SO(10) \times SU(3)_F$, $\mathbf{16}_L$ transforms as

$$\begin{pmatrix} \psi_L \\ \bar{\psi}_L \end{pmatrix} \to e^{-i\frac{2\pi}{4}\ell} e^{-i\frac{2\pi}{3}m} \begin{pmatrix} \psi_L \\ \bar{\psi}_L \end{pmatrix}$$
$$= e^{-i\frac{2\pi}{12}n} \begin{pmatrix} \psi_L \\ \bar{\psi}_L \end{pmatrix}, \tag{9.259}$$

where $n = 3\ell + 4m$. We take here the assignment that left-handed fermions belong to $\mathbf{3}$ of $SU(3)_F$ and right-handed fermions to $\mathbf{3}^*$, rather than $\mathbf{3}$. Transformation (9.259) is identified with the remaining Peccei–Quinn Z_{4N_f} symmetry for $N_f = 3$. The argument shows that starting with Peccei–Quinn $U(1)$ symmetry, we are led to $U(1)_{PQ} \times SU(3)_F \times SO(10)$ as the simplest possibility to make the model fully acceptable.

9.10 Heuristic Models for the Neutrino Mass Matrix

We have discussed a number of models where the existence of the neutrino is required by internal consistency. All models use the seesaw mechanism

---

[16] When discrete symmetry is broken in an early universe, walls are formed between two regions with different vacua. Such domain walls store very large energy, and it greatly exceeds the critical mass density of the universe, unless the symmetry-breaking energy scale is smaller than $< 100\,\mathrm{MeV}$ [1394].

to generate a light neutrino mass, and in most models, the right-handed neutrino mass is constrained by low-energy phenomenology up to the Yukawa coupling constant. This allows us to predict the order of magnitude of the neutrino mass, but the model is not sufficiently detailed to give the mass matrix. The only exception is SO(10) GUT, which predicts a mass matrix under reasonable assumptions for the Higgs sector, but the prediction is not consistent with experiment.

The task here is to speculate on a mass matrix that is consistent with experiment in heuristic ways. One common approach is to construct the mass matrix in parallel with that for quarks, or in a way to understand those of quarks and leptons at the same time. In this section we present examples of such attempts.

9.10.1 Model of Froggatt and Nielsen

The first model we describe uses global family U(1) symmetry proposed by Froggatt and Nielsen [1353]. The 'advantage' of U(1) symmetry is that one can take U(1) charge assignment arbitrarily and avoid strong constraints associated with non-Abelian symmetry such as $SU(3)_F$. We refer to this symmetry as $U(1)_{FN}$. Symmetry breaking is caused by the condensation of a scalar field Φ that carries $U(1)_{FN}$ charge -1. The Yukawa coupling of the Higgs particle ϕ to fermion fields is modified to

$$\mathcal{L} = h_{ij} \left(\frac{\langle \Phi \rangle}{m_{\mathrm{pl}}} \right)^{Q_i + Q_j} \psi_i \psi_j \phi , \tag{9.260}$$

where coupling constants h_{ij} are assumed to be $O(1)$ and Q_i are $U(1)_{FN}$ charges of fermion fields ψ_i. The $U(1)_{FN}$ charge of the Higgs scalar is assumed to vanish. For $\langle \Phi \rangle / m_{\mathrm{pl}} \equiv \epsilon \ll 1$, we can assign $U(1)_{FN}$ charges to the matter field in a way to give correct quark and lepton masses.

To be specific, we take SU(5) multiplets for the particle classification. Let us discuss the up-type quark mass matrix that is given by

$$\mathcal{L} = h_{ij} \left(\frac{\langle \phi \rangle}{M_{\mathrm{pl}}} \right)^{Q_i + Q_j} \mathbf{10}_i \mathbf{10}_j \phi(\mathbf{5}). \tag{9.261}$$

The empirical mass hierarchy,

$$m_t : m_c : m_u \simeq 1 : \epsilon^2 : \epsilon^4, \tag{9.262}$$

suggests $\epsilon \simeq 1/20$–$1/10$ and $U(1)_{FN}$ charges to be 2, 1, 0, for the first, second, and third families of $\mathbf{10}$'s. The down-type quark and charged-lepton mass matrices are given by

$$\mathcal{L} = f_{ij} \left(\frac{\langle \phi \rangle}{M_{\mathrm{pl}}} \right)^{Q_i + Q_j} \mathbf{10}_i \mathbf{5}^*_{\,j} \phi(\mathbf{5})^\dagger. \tag{9.263}$$

Table 9.5. U(1)$_{\rm FN}$ charge assignment for SU(5) multiplets. The subscript stands for generation.

	10_1	10_2	10_3	5_1^*	5_2^*	5_3^*	ν_{R1}	ν_{R2}	ν_{R3}
U(1)$_{\rm FN}$	2	1	0	2	1	1	α	β	γ

The empirical mass hierarchy

$$m_b : m_s : m_d \simeq m_\tau : m_\mu : m_e \simeq 1 : \epsilon : \epsilon^2, \tag{9.264}$$

suggests that the first, second, and third families of **5*** have U(1)$_{\rm FN}$ charges $a + 1, a, a$. To give the correct mass ratio between down- and up-quarks we take $a = 1$. The charge assignment is given in Table 9.5. It is not parallel between **10** and **5*** to adjust to the empirical mass pattern. It turns out below that this disparity explains large neutrino mixing between ν_μ and ν_τ [1462].

In the basis that the up-type quark mass matrix is diagonal, the mass matrices of quarks defined by

$$\mathcal{L}_{\rm mass} = \bar{\psi}_R M_\psi \psi_L \ , \tag{9.265}$$

are written

$$M_u = \begin{pmatrix} \epsilon^4 & & \\ & \epsilon^2 & \\ & & 1 \end{pmatrix} m_t, \tag{9.266}$$

and

$$M_d = \begin{pmatrix} \epsilon^3 & \epsilon^2 & \epsilon \\ \epsilon^2 & \epsilon & 1 \\ \epsilon^2 & \epsilon & 1 \end{pmatrix} m_b \ , \tag{9.267}$$

where all elements represent only orders of magnitude. These mass matrices give small mixing angles for quarks. Noting that $U = V_u^\dagger V_d$, where V^{-1} operates to the mass matrix from the left as $V^{-1}MW$, we have $U_{12} = [V_d]_{12} \simeq O(\epsilon)$, $U_{23} = [V_d]_{23} \simeq O(\epsilon)$, and $U_{13} = [V_d]_{13} \simeq O(\epsilon^2)$. This is acceptable if one takes account of $O(1)$ uncertainties in the matrix elements of (9.267).

The charged-lepton mass matrix is given by

$$M_\ell = (M_d)^T , \tag{9.268}$$

which causes large mixing in the (2,3) element of the lepton sector, $[V_\ell]_{23} \simeq O(1)$, whereas $[V_\ell]_{12} \simeq O(\epsilon)$, $[V_\ell]_{13} \simeq O(\epsilon)$. This is because **5*** that contains the lepton doublet ℓ_L has the same U(1)$_{\rm FN}$ charge for the second and third families. Notice that quark doublets q_L are in **10**'s, and hence each quark doublet has a different U(1)$_{\rm FN}$ charge, which results in mixing, at most, of the order of ϵ.

We introduce three right-handed neutrinos ν_{R_i} $(i = 1, 2, 3)$ and assign to them FN charges α, β, and γ. The Majorana mass matrix for the right-handed neutrinos is then given, in the basis where it is diagonal, by

$$M_{\nu_R} = \begin{pmatrix} \epsilon^{2\alpha} & & \\ & \epsilon^{2\beta} & \\ & & \epsilon^{2\gamma} \end{pmatrix} M_R. \tag{9.269}$$

The Dirac mass matrix of neutrinos is given by

$$m_{\nu D} = \begin{pmatrix} \epsilon^{1+\alpha} & \epsilon^{\alpha} & \epsilon^{\alpha} \\ \epsilon^{1+\beta} & \epsilon^{\beta} & \epsilon^{\beta} \\ \epsilon^{1+\gamma} & \epsilon^{\gamma} & \epsilon^{\gamma} \end{pmatrix} \epsilon \langle H \rangle. \tag{9.270}$$

Integration over the right-handed neutrinos leads to the neutrino mass matrix:

$$m_\nu = \begin{pmatrix} \epsilon^2 & \epsilon & \epsilon \\ \epsilon & 1 & 1 \\ \epsilon & 1 & 1 \end{pmatrix} \epsilon^2 \frac{\langle H \rangle^2}{M_R}, \tag{9.271}$$

independent of the FN charge assignment for right-handed neutrinos [1462]; the neutrino mass matrix is determined only by FN charges of the lepton doublets. We see that the mixing angle $[V_\nu]_{23}$ in the neutrino sector is also large. The lepton mixing matrix is given by

$$U_\nu = V_\ell^\dagger V_\nu. \tag{9.272}$$

Hence, the neutrino mixing angle, $[U_\nu]_{23}$, between ν_μ and ν_τ is of $O(1)$, unless accidental cancellation happens.

To see the other mixing angles, we diagonalise the 2×2 submatrix for the second and third generations, as

$$m_\nu = \begin{pmatrix} \epsilon^2 & \epsilon & \epsilon \\ \epsilon & \delta & 0 \\ \epsilon & 0 & 1 \end{pmatrix} m_{\nu 3} , \tag{9.273}$$

where δ is generally of the order of unity. The mixing angle θ_{12} is then given by

$$\tan 2\theta_{12} \simeq \frac{2\epsilon}{\delta}. \tag{9.274}$$

We need to tune δ to be $O(0.1)$ to make (9.273) consistent with the empirical neutrino mass pattern [1463]. We are then led to large mixing for ν_μ and ν_e. Note that U_{13} is always small, of the order ϵ. For further explorations, see [1464]. Models that generate the required small δ are discussed in [1465].

There is a proposal to assign the same FN charge to all $\mathbf{5}^*$'s [1466], with which bimaximal lepton mixing angles are obtained, but it seems difficult to explain the small U_{e3}.

A model with local $U(1)_{FN}$ symmetry is constructed by introducing a number of additional U(1) symmetries [1467]. This model, however, cannot explain the bi-maximal nature of the lepton mixing angles due to strong constraints from anomaly cancellation.

An FN type model based on non-Abelian (global) family symmetry is studied in [1468]. One needs many ad hoc assumptions to break family symmetry to obtain large mixing in the lepton sector while keeping small mixing in the quark sector.

9.10.2 Democratic Mass Matrix

Harari et al. [1469] considered another non-Abelian family symmetry to understand the empirical quark mass-mixing relation. In the zeroth-order approximation, the quark mass matrix seems to be dominated by the (3,3) matrix element, viz.,

$$m_q^0 = \frac{K}{3} \begin{pmatrix} 0\,0\,0 \\ 0\,0\,0 \\ 0\,0\,1 \end{pmatrix}. \qquad (9.275)$$

They have noted that this matrix is derived by treating three families of quarks on an equal footing, i.e., by imposing permutation symmetry S_3 among three families.

We start with the mass matrix,

$$m_q^0 = \frac{K_q}{3} \begin{pmatrix} 1\,1\,1 \\ 1\,1\,1 \\ 1\,1\,1 \end{pmatrix}, \qquad (9.276)$$

where q denotes up- or down-type quarks. The left-handed quark doublets q_L^i and the right-handed quark singlets u_R^i, d_R^i belong to $\mathbf{3} = \mathbf{2} + \mathbf{1}$ of the S_{3L} and S_{3R}, respectively. The state $|1\rangle + |2\rangle + |3\rangle$ is invariant under the permutation and corresponds to the unique massive state. The two other eigenvectors correspond to zero mass states. The hierarchy in the quark mass is understood as a result of $S_{3L} \times S_{3R}$ symmetry, and this matrix is given the name 'democratic' mass matrix. An elegant way to introduce symmetry breaking is to assume perturbations with a diagonal mass matrix [1470]

$$\delta m_q = \begin{pmatrix} \delta_1^q & 0 & 0 \\ 0 & \delta_2^q & 0 \\ 0 & 0 & \delta_3^q \end{pmatrix}. \qquad (9.277)$$

The matrix $m_q = m_q^0 + \delta m_q$ is diagonalised by the unitary matrix $U_q = AB_q$, where

$$A = \begin{pmatrix} 1/\sqrt{2} & 1/\sqrt{6} & 1/\sqrt{3} \\ -1/\sqrt{2} & 1/\sqrt{6} & 1/\sqrt{3} \\ 0 & -2/\sqrt{6} & 1/\sqrt{3} \end{pmatrix}, \qquad (9.278)$$

and

$$
B_q = \begin{pmatrix} \cos\theta^q & -\sin\theta^q & -\lambda_q\sin2\theta^q \\ \sin\theta^q & \cos\theta^q & -\lambda_q\cos2\theta^q \\ \lambda^q\sin3\theta^q & \lambda_q\cos3\theta^q & 1 \end{pmatrix} , \tag{9.279}
$$

with

$$
\mathrm{tg}2\theta^q \simeq \sqrt{3}\frac{\delta_2^q - \delta_1^q}{2\delta_3^q - \delta_2^q - \delta_1^q}, \tag{9.280}
$$

and

$$
\lambda_q \simeq \frac{1}{\sqrt{2}}\frac{1}{3K_q}\left[(2\delta_3^q - \delta_2^q - \delta_1^q)^2 + 3(\delta_2^q - \delta_1^q)^2\right]^{1/2} . \tag{9.281}
$$

It was shown [1470] that all quark masses and mixing angles $\theta^{\mathrm{quark}} = \theta^d - \theta^u$ are successfully given by choosing $\delta_1^q = -\delta_2^q$ ($q = u, d$) and adjusting the six parameters appropriately.

   This analysis can be extended to the lepton sector by assuming that the left-handed lepton doublets, ℓ_L^i, transform as $\mathbf{3} = \mathbf{2} + \mathbf{1}$ under S_{3L}, and right-handed charged leptons, e_R^i, also transform as $\mathbf{3} = \mathbf{2} + \mathbf{1}$ under S_{3R}. We then obtain a mass matrix similar to that for quarks. The mixing angle for the charged lepton sector is obtained by (9.278) and (9.279) with the angle θ^ℓ given by

$$
\sin\theta^\ell \simeq -\sqrt{m_e/m_\mu}. \tag{9.282}
$$

   The Majorana neutrino masses is given by the nonrenormalizable operator:

$$
\frac{1}{2M_R}\ell_{Li}\ell_{Lj}H^2. \tag{9.283}
$$

There are two invariants, $\mathbf{2_L} \times \mathbf{2_L}$ and $\mathbf{1_L} \times \mathbf{1_L}$, and hence we have two candidate matrices that are invariant under S_3,

$$
\begin{pmatrix} 1 & 0 & 0 \\ 0 & 1 & 0 \\ 0 & 0 & 1 \end{pmatrix}, \qquad \begin{pmatrix} 0 & 1 & 1 \\ 1 & 0 & 1 \\ 1 & 1 & 0 \end{pmatrix}. \tag{9.284}
$$

We choose the first form, which is clearly appropriate for describing degenerate neutrino masses [1471]. We introduce S_3 breaking perturbations in analogy with the quark and charged lepton sectors:

$$
\delta M_\nu = \begin{pmatrix} -\epsilon_\nu & 0 & 0 \\ 0 & \epsilon_\nu & 0 \\ 0 & 0 & \delta_\nu \end{pmatrix}. \tag{9.285}
$$

We then obtain the lepton mixing matrix, $U_\ell = (V_\ell)^\dagger V_\nu$,

$$
U_\ell \simeq \begin{pmatrix} 1/\sqrt{2} & -1/\sqrt{2} & 0 \\ 1/\sqrt{6} & 1/\sqrt{6} & -1/2\sqrt{6} \\ 1/\sqrt{3} & 1/\sqrt{3} & 1/\sqrt{3} \end{pmatrix}. \tag{9.286}
$$

This leads to nearly bimaximal neutrino oscillation [1471, 1472],

$$\sin^2 2\theta_{12} \simeq 1, \qquad \sin^2 2\theta_{23} \simeq 8/9, \tag{9.287}$$

and the vanishing U_{e3}. Though this solution roughly agrees with experiment, a closer look shows that $\sin^2 2\theta_{12} = 1$ is allowed only at 3σ for the LMA solution. Various extensions are studied to obtain the desired mixing angles [1473].

The mixing matrix of the form (9.286) was derived by Fritzsch and Xing [1474] by assuming that the zeroth-order term (9.276) vanishes for neutrinos for some reason and the neutrino mass term starts from the diagonal matrix of (9.285). In this model one must assume minuscule matrix elements for (9.285), i.e., the smallness of the neutrino mass is unexplained.

It is possible to accommodate this model in SU(5) grand unification. For the mass matrix of up-type quarks, $\mathbf{10} \times \mathbf{10}$ contains two invariant representations, and we need to choose their coefficients to give the democratic form (9.276). Therefore, the large mass hierarchy between the up-quark mass, as predicted in the democratic mass matrix, is not understood as a result of SU(5) symmetry but is an ad hoc requirement.

9.10.3 Models for Other Textures

The mass matrix m_ν for the three light neutrinos is given in seesaw models by

$$m_\nu = m_{\nu D}^T M_{\nu R}^{-1} m_{\nu D} \ , \tag{9.288}$$

with the Dirac mass matrix $m_{\nu D}$ and the Majorana mass matrix $M_{\nu R}$. The mass matrix for left-handed neutrino is, in principle, completely different from that for quarks, even if the Dirac mass matrix for neutrinos takes the same form as that for quarks. This allow us to account for large mixing for neutrinos. In the following we discuss a few examples.

Model with a Fritzsch type mass matrix

Fritzsch [1475] found that symmetric 3×3 matrices with only the $(1,2)[=(2,1)]$, $(2,3)[=(3,2)]$, and $(3,3)$ matrix elements describe the empirical quark mass mixing relation reasonably well. Consider a mass matrix

$$m_u = \begin{pmatrix} 0 & |a_u|e^{i\varphi_{12}} & 0 \\ |a_u|e^{i\varphi_{21}} & 0 & |b_u|e^{i\varphi_{23}} \\ 0 & |b_u|e^{i\varphi_{32}} & |c_u|e^{i\varphi_{33}} \end{pmatrix} \tag{9.289}$$

for the charge $2/3$ quarks and

$$m_d = \begin{pmatrix} 0 & |a_d|e^{i\varphi'_{12}} & 0 \\ |a_d|e^{i\varphi'_{21}} & 0 & |b_d|e^{i\varphi'_{23}} \\ 0 & |b_d|e^{i\varphi'_{32}} & |c_d|e^{i\varphi'_{33}} \end{pmatrix} \tag{9.290}$$

for the charge $-1/3$ quarks. For these mass matrices, the quark mixing matrix is given by [1470]

$$U = R_u^T \begin{pmatrix} 1 & & 0 \\ & e^{i\sigma} & \\ 0 & & e^{i\tau} \end{pmatrix} R_d, \qquad (9.291)$$

where R_u and R_d are the orthogonal matrices that diagonalise

$$m_u^* = \begin{pmatrix} 0 & |a_u| & 0 \\ |a_u| & 0 & |b_u| \\ 0 & |b_u| & |c_u| \end{pmatrix}, \quad m_d^* = \begin{pmatrix} 0 & |a_d| & 0 \\ |a_d| & 0 & |b_d| \\ 0 & |b_d| & |c_d| \end{pmatrix}, \qquad (9.292)$$

to the form,

$$R_u^T m_u^* R_u = \begin{pmatrix} m_u & & \\ & -m_c & \\ & & m_t \end{pmatrix}, \quad R_d^T m_d^* R_d = \begin{pmatrix} m_d & & \\ & -m_s & \\ & & m_b \end{pmatrix}. \qquad (9.293)$$

For $m_u \ll m_c \ll m_t$ and $m_d \ll m_s \ll m_b$, one obtains

$$U_{12} \simeq -\sqrt{\frac{m_d}{m_s}} + e^{i\sigma}\sqrt{\frac{m_u}{m_c}}, \quad U_{21} \simeq -\sqrt{\frac{m_u}{m_c}} + e^{i\sigma}\sqrt{\frac{m_d}{m_s}}$$

$$U_{23} \simeq e^{i\sigma}\sqrt{\frac{m_s}{m_b}} - e^{i\tau}\sqrt{\frac{m_c}{m_t}}, \quad U_{32} \simeq e^{i\sigma}\sqrt{\frac{m_c}{m_t}} - e^{i\tau}\sqrt{\frac{m_s}{m_b}}$$

$$U_{13} \simeq \sqrt{\frac{m_u}{m_c}} U_{23}, \qquad\qquad U_{31} \simeq \sqrt{\frac{m_d}{m_s}} U_{32}. \qquad (9.294)$$

It has been shown that $U_{12}(\simeq U_{21})$, $U_{23}(\simeq U_{32})$, U_{13}, and U_{31} can be within the range allowed by experiment, including CP phenomenology, with the choice of $\sigma \simeq \tau \simeq \pm\pi/2$, insofar as m_t in (9.294) is set to be $\lesssim 200\,\mathrm{GeV}$ [1476, 1477]. The empirical top mass $m_t \simeq 175\,\mathrm{GeV}$, however, gives $m_t(1\,\mathrm{GeV}) \simeq 330\,\mathrm{GeV}$, and the Fritzsch mass matrix, as it is, is not completely successful for the quark sector.

Now, we consider the Fritzsch matrix applied to the lepton sector [1478]:

$$m_{\nu D} = \begin{pmatrix} 0 & |A_\nu|e^{i\psi_{12}} & 0 \\ |A_\nu|e^{i\psi_{21}} & 0 & |B_\nu|e^{i\psi_{23}} \\ 0 & |B_\nu|e^{i\psi_{32}} & |C_\nu|e^{i\psi_{33}} \end{pmatrix}, \qquad (9.295)$$

$$m_e = \begin{pmatrix} 0 & |A_l|e^{i\psi'_{12}} & 0 \\ |A_l|e^{i\psi'_{21}} & 0 & |B_l|e^{i\psi'_{23}} \\ 0 & |B_l|e^{i\psi'_{32}} & |C_l|e^{i\psi'_{33}} \end{pmatrix}. \qquad (9.296)$$

The lepton mixing matrix may differ from the form given in (9.291) since extra phases may arise from the ν_R sector. The mass of the left-handed neutrino is given by (9.288). For simplicity, let us take M_{ν_R} proportional to the unit matrix in the basis where $m_{\nu D}$ is diagonal. In such a case, the mixing matrix is given by (9.291) with R_u and R_d replaced by $R_{\nu D}$ and R_e, defined similarly to (9.293) (we use η and ρ for leptons in place of σ and τ). This conclusion receives little modification for a reasonable variety of M_{ν_R}, insofar as the eigenvalues of $m_{\nu D}$ have a hierarchical structure $m_1 \ll m_2 \ll m_3$ (see the argument in Sect. 9.5). The argument may then be developed in a way parallel to the quark sector, with m_u, m_c, m_t replaced by the eigenvalues of $m_{\nu D}$, i.e., m_1, m_2, m_3, and m_d, m_s, m_b by m_e, m_μ, m_τ. The neutrino masses are given by

$$m_{\nu_1} = m_1^2/M_{\nu_R}, \; m_{\nu_2} = m_2^2/M_{\nu_R}, \; m_{\nu_3} = m_3^2/M_{\nu_R} \ . \tag{9.297}$$

For $m_e \ll m_\mu \ll m_\tau$ and $m_{\nu_1} \ll m_{\nu_2} \ll m_{\nu_3}$, we obtain

$$U_{21} = -\left(\frac{m_e}{m_\mu}\right)^{1/2} + e^{i\eta}\left(\frac{m_{\nu_1}}{m_{\nu_2}}\right)^{1/4}, \quad U_{12} = e^{i\eta}\left(\frac{m_e}{m_\mu}\right)^{1/2} - \left(\frac{m_{\nu_1}}{m_{\nu_2}}\right)^{1/4}$$

$$U_{32} = e^{i\eta}\left(\frac{m_\mu}{m_\tau}\right)^{1/2} - e^{i\rho}\left(\frac{m_{\nu_2}}{m_{\nu_3}}\right)^{1/4}, \quad U_{23} = -e^{i\rho}\left(\frac{m_\mu}{m_\tau}\right)^{1/2} + e^{i\eta}\left(\frac{m_{\nu_2}}{m_{\nu_3}}\right)^{1/4}$$

$$U_{31} = \left(\frac{m_{\nu_1}}{m_{\nu_2}}\right)^{1/4} U_{32} \ , \quad U_{13} = \left(\frac{m_e}{m_\mu}\right)^{1/2} U_{23} + \frac{m_{\nu_2}}{m_{\nu_3}}\left(\frac{\mu_{\nu_1}}{m_{\nu_3}}\right)^{1/2} \ . \tag{9.298}$$

The quartic-root nature of (9.298) makes the mixing angle generally large. With the empirical range of m_{ν_2}/m_{ν_3} (Table 8.4), this model gives $|U_{23}| = 0.3$–0.98. $|U_{12}|$ is consistent with experiment if $m_{\nu_e}/m_{\nu_\mu} = 0.02$–$0.27$, and $|U_{13}| = 0.02$–0.2 is predicted.

More about mass-matrix textures

Irrespective of the form for $m_{\nu D}$, any form of mass matrix is formally possible for left-handed neutrinos by assuming an appropriate M_{ν_R}. To obtain a mass matrix that gives large neutrino mixing, however, we generally need a specific, strong hierarchy in the matrix elements of M_{ν_R}, which correlates with the elements of $m_{\nu D}$ [1409]. To demonstrate this, suppose that the Dirac mass is diagonal $m_{\nu D} = \text{diag}(\epsilon^2, \epsilon, 1)m_D$ with $\epsilon \ll 1$, and write $M_{\nu_R}^{-1} = a_{ij}/M$. We have for (9.288),

$$m_\nu = \begin{pmatrix} \epsilon^4 a_{11} & \epsilon^3 a_{12} & \epsilon^2 a_{13} \\ \epsilon^3 a_{12} & \epsilon^2 a_{22} & \epsilon a_{23} \\ \epsilon^2 a_{13} & \epsilon a_{23} & a_{33} \end{pmatrix} \frac{m_D^2}{M} \ . \tag{9.299}$$

If all elements a_{ij} are of the same order of magnitude, off-diagonal elements are always smaller than diagonal ones by $O(\epsilon)$, and the mixing angle is $O(\epsilon)$. To obtain large mixing, the matrix elements of M_{ν_R} should have a large hierarchy that specifically cancels the hierarchy brought from the Dirac mass matrix. This means that the low-energy mass parameters in $m_{\nu D}$ and the high-energy mass parameters in M_{ν_R} have a conspiracy, while the origins of these mass matrices are generally unrelated. For special matrices that have some vanishing elements, we can avoid enforcing correlations of the magnitudes of the matrix elements, but we still have to require specifically correlated forms for $m_{\nu D}$ and M_{ν_R}.

Let us quote a few such examples proposed in the literature. The first example [1479] is

$$m_{\nu D} = \begin{pmatrix} x^2 y & 0 & 0 \\ 0 & x & x \\ 0 & -x^2 & 1 \end{pmatrix} m_D, \qquad M_{\nu_R} = \begin{pmatrix} 0 & 0 & 1 \\ 0 & 1 & 0 \\ 1 & 0 & 0 \end{pmatrix} M. \qquad (9.300)$$

We take $x \simeq 10^{-2}$ and $y \simeq 10^{-1}$ in analogy with the quark and lepton mass matrices. The seesaw formula leads to

$$m_\nu = \begin{pmatrix} 0 & x^4 y/A & x^4 y/A \\ x^4 y/A & x^2 & x^2 \\ x^4 y/A & x^2 & x^2 \end{pmatrix} \frac{m_D^2}{M}, \qquad (9.301)$$

which gives maximal mixing $\theta_{23} = \pi/4$ and nearly maximal mixing for θ_{12}. This model is modified in [1480].

Another example is [1481]

$$m_{\nu D} = \begin{pmatrix} 0 & 0 & x \\ 0 & x & 0 \\ x & 0 & 1 \end{pmatrix} m_D, \qquad M_{\nu_R} = \begin{pmatrix} M_1 & M_2 & 0 \\ M_2 & M_3 & 0 \\ 0 & 0 & M' \end{pmatrix}, \qquad (9.302)$$

with $m_D = m_t$ and $x = m_c/m_t$. This yields the mixing angle θ_{23} of the order of unity if $M_1 \sim M_2 \sim M_3$. The mixing angle θ_{12}, is predicted to be small.

We refer interested readers to [1482,1410] for more examples of mass matrices that give a large θ_{23}. In all models of this kind, however, the assumptions on the matrices are ad hoc, and it is unexplained why the two matrices simultaneously take the specific forms.

Frampton et al. [1483] discussed the texture of the general neutrino mass matrix. They showed that a matrix with more than two independent zeroes is not consistent with the empirical mass-mixing pattern and that there are seven (out of 15) empirically acceptable textures with two zeros. Further, it was shown that [1484] five textures among the seven can be realised by the see-saw mechanism by assuming appropriate textures for the Dirac and the right-handed Majorana mass matrices.

9.11 Neutrino Mass Matrix from Radiative Corrections

In Chap. 6 we discussed the model in which a small Majorana neutrino mass is induced from radiative corrections by a charged scalar particle h^- that breaks lepton number in the Higgs potential [1095]. The mass matrix is symmetric and off-diagonal:

$$m_\nu = \begin{pmatrix} 0 & m_{e\mu} & m_{e\tau} \\ m_{e\mu} & 0 & m_{\mu\tau} \\ m_{e\tau} & m_{\mu\tau} & 0 \end{pmatrix} , \tag{9.303}$$

with m_{ab} $(a, b = e, \mu, \tau)$ given explicitly in (6.63). This model has been further explored in [1485–1487].

The three parameters m_{ab} can be taken as real and positive without loss of generality by using phase rotations of the three neutrino fields. The traceless feature then translates to a condition for the eigenvalues m_1, m_2, m_3 [1102, 1487]:

$$m_1 + m_2 + m_3 = 0. \tag{9.304}$$

To obtain the empirical mass difference hierarchy

$$\delta m_{12}^2 \equiv |m_2^2 - m_1^2| \ll \delta m_{23}^2 \equiv |m_3^2 - m_2^2| \simeq |m_3^2 - m_1^2|, \tag{9.305}$$

there are two solutions that satisfy (9.304): (A) $m_1 \simeq -m_2$ and $m_3 \simeq 0$, and (B) $m_1 \simeq m_2$ and $m_3 \simeq -2m_2$.

Case (A) is realized by setting one of m_{ab} to vanish, as evident by considering the determinant of (9.303), which is equal to $m_1 m_2 m_3$. This leaves us with three possibilities: $m_{e\mu} = 0$, $m_{e\tau} = 0$, or $m_{\mu\tau} = 0$. Let us examine the pattern of neutrino oscillation for the three cases. As discussed in Chap. 8, neutrino oscillation is driven by $m_\nu m_\nu^\dagger$, which reads

$$m_\nu m_\nu^\dagger = \begin{pmatrix} m_{e\mu}^2 + m_{e\tau}^2 & m_{e\tau} m_{\mu\tau} & m_{e\mu} m_{\mu\tau} \\ m_{e\tau} m_{\mu\tau} & m_{e\mu}^2 + m_{\mu\tau}^2 & m_{e\mu} m_{e\tau} \\ m_{e\mu} m_{\mu\tau} & m_{e\mu} m_{e\tau} & m_{e\tau}^2 + m_{\mu\tau}^2 \end{pmatrix} . \tag{9.306}$$

With $m_{e\mu} = 0$, ν_μ oscillates predominantly into ν_e; hence this case is empirically disfavoured. With $m_{e\tau} = 0$, ν_μ does not oscillate, so that this is also excluded. The choice $m_{\mu\tau} = 0$ gives rise to the only viable possibility: the product of the neutrino mass matrix, $m_\nu m_\nu^\dagger$, is written

$$m_\nu m_\nu^\dagger = \begin{pmatrix} m_{e\mu}^2 + m_{e\tau}^2 & 0 & 0 \\ 0 & m_{e\mu}^2 & m_{e\mu} m_{e\tau} \\ 0 & m_{e\mu} m_{e\tau} & m_{e\tau}^2 \end{pmatrix} . \tag{9.307}$$

A large mixing angle θ_{23} is obtained if $m_{e\mu} \simeq m_{e\tau}$. Let us assume here $m_{e\mu} = m_{e\tau} \equiv m_0$ and introduce a small mass $m_{\mu\tau} \equiv \epsilon m_0$. After diagonali-

sation with respect to the second and third elements, (9.307) reads

$$m_\nu m_\nu^\dagger = \begin{pmatrix} 2 & \sqrt{2}\epsilon & 0 \\ \sqrt{2}\epsilon & 2+\epsilon^2 & 0 \\ 0 & 0 & \epsilon^2 \end{pmatrix} m_0. \qquad (9.308)$$

The mixing angle for the (1,2) sector is also large, consistent with bimaximal neutrino oscillation [1102, 1487].

Let us turn to case (B), which is realized when $m_{e\mu} \simeq m_{e\tau} \simeq m_{\mu\tau}$. Writing $m_{e\mu} = m_{e\tau} = m_{\mu\tau} \equiv m_0$,

$$m_\nu m_\nu^\dagger = \begin{pmatrix} 2 & 1 & 1 \\ 1 & 2 & 1 \\ 1 & 1 & 2 \end{pmatrix} m_0. \qquad (9.309)$$

This is the same matrix that appeared in the charged lepton mass matrix in the democratic texture model, though this time it appears in the neutrino sector. It is easy to see that the U_{13} is large [1102], which conflicts with the empirical evidence.

The radiatively induced neutrino mass scenario contains a neutrino mass matrix that can be compatible with bimaximal neutrino oscillation. For this to be realised, however, we need to have $m_{e\mu} \simeq m_{e\tau}$ and $m_{\mu\tau} \simeq 0$. The latter condition may be explained by imposing ad hoc symmetry such as $L_e - L_\mu - L_\tau$ conservation, but the former requires an accidental coincidence for the Yukawa couplings of h^- such that [1102]

$$\kappa_{e\mu} : \kappa_{e\tau} \simeq m_\tau : m_\mu. \qquad (9.310)$$

For an extension of the model in which radiatively induced neutrino mass appears at the two-loop level, see [1488]. The model cannot account for bimaximal mixing, however.

9.12 Brief Assessment of Models

We conclude with a brief and somewhat subjective assessment of the status of understanding of neutrino mass. We have a fairly convincing reason for the existence of right-handed neutrinos, provided that neutrinos are of the Majorana type. At low energies, the only candidate symmetry that can be gauged is B–L, and the associated current can be made anomaly-free only in the presence of ν_R. When B–L conservation is broken, the neutrino acquires mass. The small neutrino mass is ascribed to small violation of B–L at low energies. This implies that B–L may be broken on a high-energy scale. We can infer the energy scale of B–L violation from the mass of ν_τ. The estimate is model-dependent in the sense that the Dirac mass of neutrinos is unknown. If we take an SO(10) model, for example, we estimate that

the mass scale is 10^{14} GeV, which appears to be a natural unification scale inferred from low-energy phenomenology of gauge coupling constants. The empirical neutrino mass excludes symmetry-breaking patterns other than SO(10)→SU(4)×SU(2)$_L$×SU(2)$_R$.

So far, the SO(10) grand unified model appears to be successful. If we assume the simplest structure for the Higgs sector, however, we are led to the neutrino mass matrix, the mixing angles derived from which are identical to those for quarks. This does not agree with experiment which indicates that mixing angles among neutrinos are all large, close to maximal, in contrast to small mixing angles for quarks. This disagreement does not necessarily falsify SO(10), but once we relax the simplicity requirement for the Higgs sector, we have no principles to constrain it; therefore, the predictive power is lost.

In fact, what troubles model building for the neutrino mass matrix is the large mixing angles among three neutrinos. Most of the models that attempt to account for large mixing either start with degenerate mass or create some accidentally-looking degeneracy by correlating the Dirac mass with the Majorana mass with ad hoc assumptions imposed. A lot of proposals for mass matrices have been made in the last few years (some of which we reviewed in this chapter), but all attempts so far published lack strong physical motivation. The empirical fact that θ_{12} is large but not quite maximal (for LMA) makes model building even more difficult.

For further progress, we may pose two questions: (i) Are neutrinos (A) of the Dirac or (B) of the Majorana type, and (ii) Are masses of three neutrinos (α) generically hierarchical or (β) nearly degenerate? It seems likely that at least case (Bβ) can be verified or falsified with the next generation double beta decay experiment.

Appendix: Representation of SO(10) group

1. SO(N) group

The SO(N) group has $N(N-1)/2$ generators,

$$\Sigma_{ij} = -\Sigma_{ji} \quad (i,j = 1 - N) \, , \tag{A1}$$

which satisfy Lie algebra,

$$[\Sigma_{ij}, \Sigma_{\ell m}] = i\{\delta_{i\ell}\Sigma_{jm} + \delta_{jm}\Sigma_{i\ell} - \delta_{im}\Sigma_{j\ell} - \delta_{j\ell}\Sigma_{im}\} \, . \tag{A2}$$

2. Spinor representations of SO($N = 2n$)

The spinor representations of SO($2n$) are easily constructed by introducing γ matrices Γ_i ($i = 1 \sim 2n$) of SO($2n$), which satisfy Clifford algebra,

$$\{\Gamma_i, \Gamma_j\} = 2\delta_{ij} \, . \tag{A3}$$

These Γ_i are represented by $2^n \times 2^n$ matrices. The spinor representation of SO($2n$) Lie algebra is defined by

$$\Sigma_{ij} = \frac{1}{2i}[\Gamma_i, \Gamma_j] . \tag{A4}$$

The spinor field ξ, which consists of 2^n components, transforms under SO(10) as

$$\xi \rightarrow e^{i\omega_{k\ell}\Sigma_{k\ell}}\xi . \tag{A5}$$

For SO(N) with N even, there exists a chiral projection operator,

$$\Gamma_\chi \equiv -i\Gamma_1...\Gamma_{2n} . \tag{A6}$$

We define chiral spinor fields, ξ_+ and ξ_-, by

$$\xi_\pm \equiv \frac{1}{2}(1 \pm \Gamma_\chi)\xi, \tag{A7}$$

each of which has 2^{n-1} components. Because all Σ_{ij} commute with Γ_χ, the two spinors ξ_+ and ξ_- are independent and transform as

$$\xi_\pm \rightarrow e^{i\omega_{k\ell}\Sigma_{k\ell}}\xi_\pm . \tag{A8}$$

The Γ matrices of SO($2n$) can be constructed from those of SO($2n-2$) by induction as

$$\Gamma_i = \begin{pmatrix} 0 & -i\tilde{\Gamma}_i \\ i\tilde{\Gamma}_i & 0 \end{pmatrix} , \qquad i = 1 \sim 2n-2,$$

$$\Gamma_{2n-1} = \begin{pmatrix} 0 & -i\tau_3 \\ i\tau_3 & 0 \end{pmatrix} , \tag{A9}$$

$$\Gamma_{2n} = \begin{pmatrix} 0 & 1 \\ 1 & 0 \end{pmatrix} ,$$

where $\tilde{\Gamma}_i (i = 1 \sim 2n-2)$ are the Γ matrices of SO($2n-2$). The induction starts from $n = 1$ with $\Gamma_1 = \tau_1$ and $\Gamma_2 = \tau_2$. In this basis, Γ_χ is given by

$$\Gamma_\chi = \begin{pmatrix} 1 & 0 \\ 0 & -1 \end{pmatrix} , \tag{A10}$$

and the $2^n \times 2^n$ generators Σ_{ij} are

$$\Sigma_{ij} = \begin{pmatrix} \sigma_{ij} & 0 \\ 0 & -\sigma_{ij} \end{pmatrix} . \tag{A11}$$

It is clear that the $2^n \times 2^n$ matrix Σ_{ij} is reduced to two irreducible $2^{n-1} \times 2^{n-1}$ matrices σ_{ij} and $-\sigma_{ij}$.

3. Representation of SO(10)

The SO(10) Γ matrices are written

$$\Gamma_i = \begin{pmatrix}
 & & & & & & & & & & & 0 & & & -\tau_i & \tau_i \\
 & & & & & & & & & & & & & -\tau_i & & \\
 & & & & & & & & & & & & \tau_i & & & \\
 & & & & & & & & & & \tau_i & -\tau_i & & & 0 & \\
 & & & & & & & & -\tau_i & \tau_i & & & & & & \\
 & & & & & & 0 & & -\tau_i & & & & & & & \\
 & & & & & & \tau_i & & & & & & & & & \\
 & & & & & -\tau_i & & & & & & 0 & & & & \\
 & & & & \tau_i & & & & & & & & & & & \\
 & & & -\tau_i & & & & & & & & & & & & \\
 & & \tau_i & & & & & & & & 0 & & & & & \\
 & -\tau_i & & & & & & & & & & & & & & \\
 \tau_i & & & & & & & & & & & & & & &
\end{pmatrix}, \quad i = 1-3,$$

$$\Gamma_4 = \begin{pmatrix}
 & & & & & & 0 & & & i\tau_1^{(4)} \\
 & & & & & 0 & & & -i\tau_1^{(4)} & \\
 & & & & & & & -i\tau_1^{(4)} & & \\
 & & & & & i\tau_1^{(4)} & & & & \\
 & & & & -i\tau_1^{(4)} & & & & & \\
 & & & 0 & & & & & 0 & \\
 & & i\tau_1^{(4)} & & & & & & & \\
 & i\tau_1^{(4)} & & & & & 0 & & & \\
 -i\tau_1^{(4)} & & & & & & & & &
\end{pmatrix},$$

$$\Gamma_5 = \begin{pmatrix}
 & & & & & & 0 & & & i\tau_3^{(4)} \\
 & & & & & 0 & & & -i\tau_3^{(4)} & \\
 & & & & & & & -i\tau_3^{(4)} & & 0 \\
 & & & & & i\tau_3^{(4)} & & & & \\
 & & & & -i\tau_3^{(4)} & & & & & \\
 & & & 0 & & & & & 0 & \\
 & & i\tau_3^{(4)} & & & & & & & \\
 & i\tau_3^{(4)} & & & & & 0 & & & \\
 -i\tau_3^{(4)} & & & & & & & & &
\end{pmatrix},$$

$$\Gamma_6 = \begin{pmatrix}
 & & 0 & -\tau_1^{(8)} \\
 & 0 & & \\
 & \tau_1^{(8)} & & 0 \\
 0 & & \tau_1^{(8)} & \\
 & & & 0 \\
 -\tau_1^{(8)} & & 0 &
\end{pmatrix},$$

$$(\text{A}12)$$

$$\Gamma_7 = \begin{pmatrix} & & 0 & -\tau_3^{(8)} \\ & 0 & & \\ & & \tau_3^{(8)} & 0 \\ & 0 & \tau_3^{(8)} & \\ & & & 0 \\ -\tau_3^{(8)} & 0 & & \end{pmatrix} ,$$

$$\Gamma_8 = \begin{pmatrix} 0 & -i\tau_1^{(16)} \\ i\tau_1^{(16)} & 0 \end{pmatrix} ,$$

$$\Gamma_9 = \begin{pmatrix} 0 & -i\tau_3^{(16)} \\ i\tau_3^{(16)} & 0 \end{pmatrix} ,$$

$$\Gamma_{10} = \begin{pmatrix} 0 & \mathbf{1}^{(16)} \\ \mathbf{1}^{(16)} & 0 \end{pmatrix} ,$$

where $\tau_i^{(n)}$ is an $n \times n$ matrix extension of the Pauli matrix τ_i; hence $\tau_i^{(2)} = \tau_i$,

$$\tau_1^{(4)} = \begin{pmatrix} 0 & \mathbf{1}^{(2)} \\ \mathbf{1}^{(2)} & 0 \end{pmatrix} , \tau_2^{(4)} = \begin{pmatrix} 0 & -i\mathbf{1}^{(2)} \\ i\mathbf{1}^{(2)} & 0 \end{pmatrix} , \tau_3^{(4)} = \begin{pmatrix} \mathbf{1}^{(2)} & 0 \\ 0 & -\mathbf{1}^{(2)} \end{pmatrix} ,$$

and so on. From these Γ matrices we can easily construct 16×16 irreducible matrices, σ_{ij}. It is more convenient, however, to use a new σ_{ij} obtained from the unitary transformation,

$$\sigma_{ij} \to U^{-1}\sigma_{ij}U ,$$

$$U = \begin{pmatrix} \mathbf{1}^{(4)} & 0 & & \\ 0 & u & & 0 \\ & & \mathbf{1}^{(4)} & 0 \\ 0 & & 0 & u \end{pmatrix}$$

with

$$u = \begin{pmatrix} 0 & 1 & & \\ 1 & 0 & & 0 \\ & & 0 & 1 \\ 0 & & 1 & 0 \end{pmatrix} . \tag{A13}$$

Using the new basis, the **16**-dimensional spinor field $\xi_+(\mathbf{16})$ is

$$\xi_+(\mathbf{16}) = (u\ u\ u\ \nu\ \bar{u}\ \bar{u}\ \bar{u}\ \bar{\nu}\ d\ d\ d\ e\ \bar{d}\ \bar{d}\ \bar{d}\ \bar{e})_L^T . \tag{A14}$$

The gauge interactions for $\xi_+(\mathbf{16})$ are given by

$$\mathcal{L} = \bar{\psi}(\partial\!\!\!/ - \frac{ig}{2\sqrt{2}}\sigma_{jk}A\!\!\!/_{jk})\psi , \tag{A15}$$

where $\psi \equiv \xi_+(\mathbf{16})$ and A_{jk}^μ are 45-dimensional gauge fields (real field). The factor $1/2\sqrt{2}$ is inserted to normalise the coupling in agreement with the conventional definition. To write the Yukawa couplings to ψ fields, we must introduce a new spinor $\tilde{\psi}$ to represent the charge conjugate field ψ^*:

$$\tilde{\psi} \equiv \beta\psi^* , \qquad (A16)$$

with

$$\beta \equiv \Gamma_2\Gamma_4\Gamma_5\Gamma_8\Gamma_9 .$$

Since $\beta\sigma_{ij}^*\beta^{-1} = -\sigma_{ij}$, the thus-defined $\tilde{\psi}$ transforms as a spinor field of SO(10). The possible forms of the Yukawa interactions for ψ are then

$$\tilde{\psi}^\dagger\Gamma_\mu\psi\phi^\mu , \qquad \tilde{\psi}_{[}\Gamma_\mu\Gamma_\nu\Gamma_{\rho]}\psi\phi^{\mu\nu\rho} ,$$

$$\tilde{\psi}^\dagger{}_{[}\Gamma_\mu\Gamma_\nu\Gamma_\rho\Gamma_\sigma\Gamma_{\eta]}\psi\phi^{\mu\nu\rho\sigma\eta} \qquad , \text{ etc.} \qquad (A17)$$

Here, ϕ^μ is a vector, $\phi^{\mu\nu\rho}$ is an antisymmetric third-rank tensor, and $\phi^{\mu\nu\rho\sigma\eta}$ is an antisymmetric fifth-rank tensor, whose dimensions are $\mathbf{10}$, $\mathbf{120}$, and $\mathbf{126}$, respectively.

The Yukawa couplings of $\phi^\mu(\mathbf{10})$ which yield the fermion mass matrix are given explicitly by

$$\begin{aligned} \mathcal{L}_Y &= f\tilde{\psi}^\dagger\Gamma_\mu\phi_\mu\psi + \text{h.c.} \\ &= 2f(\bar{u}_R u_L + \bar{\nu}_R\nu_L)(\phi_9 - i\phi_{10}) \\ &\quad + 2f^\dagger(\bar{d}_L d_R + \bar{e}_L e_R)(\phi_9 - i\phi_{10}) + \dots . \end{aligned} \qquad (A18)$$

This is (9.120).

Representations in terms of SU(4)×SU(2)$_L$×SU(2)$_R$ subalgebra can be constructed by noting that the five Cartan generators are given by

$$\begin{aligned} \lambda_3 &= \frac{1}{2}(\sigma_{12} - \sigma_{34}) , \\ \lambda_8 &= -\frac{1}{2\sqrt{3}}(\sigma_{12} + \sigma_{34} + 2\sigma_{56}) , \\ \lambda_{15} &= \frac{1}{\sqrt{6}}(\sigma_{12} + \sigma_{34} - \sigma_{56}), \end{aligned} \qquad (A19)$$

for the SU(4) part,

$$\tau_{L3} = -\frac{1}{2}(\sigma_{78} + \sigma_{910}) , \qquad (A20)$$

for SU(2)$_L$, and

$$\tau_{R3} = -\frac{1}{2}(\sigma_{78} - \sigma_{910}) , \qquad (A21)$$

for SU(2)$_R$; λ_i is the SU(4) generalisation of Gell–Mann's λ matrices.

With a straightforward calculation, we can write the gauge interaction of (A15) explicitly in terms of $\mathrm{SU(3)}_c \times \mathrm{SU(2)}_L \times \mathrm{SU(2)}_R$ components. The interaction part reads

$$
\begin{aligned}
\mathcal{L}_{\mathrm{int}} = &- \bar{\psi}_{L,R}^{ia} \frac{ig}{2} [\lambda^\alpha]_{ab} \gamma_\mu \psi_{L,R}^{ib} G_\mu^\alpha \\[2mm]
&- \bar{\psi}_L^{ia} \frac{ig}{2} [\tau^\beta]_{ij} \gamma_\mu \psi_L^{ja} W_{L\mu}^\beta - \bar{\psi}_R^{ia} \frac{ig}{2} [\tau^\beta]_{ij} \gamma_\mu \psi_R^{ja} W_{R\mu}^\beta \\[2mm]
&+ \frac{q}{\sqrt{2}} [\bar{q}_L^{ia} \gamma_\mu (\ell_R^i)^c + \bar{\ell}_L^j \gamma_\mu (q_R^{ja})^c + \epsilon_{abc} \overline{(q_R^{jb})^c} \gamma_\mu q_L^{ic}] X_{\mu a}^{ij} \\[2mm]
&+ \text{h.c.} \,,
\end{aligned} \tag{A22}
$$

where **16** in (A15) is
$$
\psi_L = (\psi_L, \psi_R^c), \tag{A23}
$$
and
$$
\begin{aligned}
\psi_{L,R} &= (q, \ell)_{L,R} \\
q_{L,R} &= \begin{pmatrix} u_1 \; u_2 \; u_3 \\ d_1 \; d_2 \; d_3 \end{pmatrix}_{L,R} \\
\ell_{L,R} &= \begin{pmatrix} \nu \\ e \end{pmatrix}_{L,R} .
\end{aligned} \tag{A24}
$$

The indices α run $1-15$, and β run $1-3$; i, j take 1, 2, and a, b take $1-3$. The gauge fields are
$$
G^\alpha = (\mathbf{8} + \mathbf{3} + \mathbf{3}^* + \mathbf{1}) \tag{A25}
$$
of $\mathrm{SU(3)}_c$,
$$
W_{L,R} = \mathbf{3} \tag{A26}
$$
of $\mathrm{SU(2)}_{L,R}$, and
$$
X_a^{ij} = (\mathbf{3}, \mathbf{2}, \mathbf{2}) \tag{A27}
$$
of $\mathrm{SU(3)}_c \times \mathrm{SU(2)}_L \times \mathrm{SU(2)}_R$. Note that G and $W_{L,R}$ are real and X are complex fields.

The decomposition of the irreducible representations of SO(10) into those of subgroup components is given in [1403]. It is often convenient to construct representations on the basis of those of SU(5); see, e.g., [1489].

10 Magnetic Moment of the Neutrino

10.1 Neutrino Magnetic Moment
in the Weinberg–Salam Model

From the general argument (see Sect. 5.1), only the Dirac neutrino can have a magnetic moment. The transition moment, which is relevant to $\nu_i \to \nu_j + \gamma$, may exist for both Dirac and Majorana neutrinos. A straightforward calculation of the one-loop diagram [1012,1204] (see also [1490]) depicted in Fig. 8.15 gives for the Dirac neutrino,

$$T = -i\varepsilon^\mu q^\nu \bar{\nu}_j(p')\sigma_{\mu\nu}(A + B\gamma_5)\nu_i(p) \,, \tag{10.1}$$

where $q = p' - p$, and

$$A = -\frac{eG_F}{8\sqrt{2}\pi^2}(m_{\nu_i} + m_{\nu_j})\sum_\ell U_{j\alpha}^\dagger U_{\alpha i}F([m_{\ell_\alpha}/m_W]^2) \,, \tag{10.2}$$

$$B = -\frac{eG_F}{8\sqrt{2}\pi^2}(m_{\nu_i} - m_{\nu_j})\sum_\ell U_{j\alpha}^\dagger U_{\alpha i}F([m_{\ell_\alpha}/m_W]^2) \,, \tag{10.3}$$

with

$$F(x) = \frac{1}{(1-x)^2}\left[-\frac{3}{4}(2 - 5x + x^2) + \frac{3}{2}\frac{x^2\log x}{1-x}\right] \tag{10.4}$$

$$\simeq -\frac{3}{2} + \frac{3}{4}x \,, \quad (x \ll 1) \,. \tag{10.5}$$

Using the general expression (5.1),

$$T = -i\varepsilon^\mu \bar{\nu}(p')[F_2(q^2) - G_2(q^2)\gamma_5]\sigma_{\mu\nu}q^\nu \nu(p) \,, \tag{10.6}$$

the magnetic dipole moment is defined by

$$\mu = F_2(0) = A \,, \tag{10.7}$$

and similarly the electric dipole moment is

$$d = G_2(0) = B \ .\tag{10.8}$$

Comparing (10.6) to (10.1) with $i = j$, we obtain [1012,1010,1011]

$$\mu_{\nu_i} = \frac{3eG_F}{8\pi^2\sqrt{2}} m_{\nu_i} \left[1 - \frac{1}{2} \sum_{\ell=1}^{3} \left(\frac{m_\ell}{m_W} \right)^2 |U_{\ell i}|^2 \right] \ ,\tag{10.9}$$

where the second term is negligible. We note that the chirality flip, which induces the magnetic moment, arises only from the neutrino mass; for this reason (10.9) is a very small quantity,

$$\mu_{\nu_i} = 3.20 \times 10^{-19} \mu_{\mathrm{B}} \left(\frac{m_{\nu_i}}{1\,\mathrm{eV}} \right) \ ,\tag{10.10}$$

where $\mu_{\mathrm{B}} = e/2m_e$ is the Bohr magneton. The experiment using a ν_e beam measures $\mu_{\nu_e} = \sum_i \mu_{\nu_i} |\nu_{e_i}|^2$. The electric dipole moment always vanishes because of the factor $m_{\nu_i} - m_{\nu_j}$ in (10.3), even if U includes CP-violating phases.

For the transition moment $(i \neq j)$, the contribution from the first term of (10.5) vanishes in the summation over ℓ due to the orthogonality condition of U (GIM mechanism [129]); thus,

$$\mu_{\bar{\nu}_j \nu_i} = \frac{3eG_F}{32\sqrt{2}\pi^2} (m_{\nu_i} + m_{\nu_j}) \sum_{\alpha=1}^{3} U_{j\alpha}^{\dagger} U_{\alpha i} \left(\frac{m_{\ell\alpha}}{m_W} \right)^2 \ ,\tag{10.11}$$

$$d_{\bar{\nu}_j \nu_i} = \frac{3eG_F}{32\sqrt{2}\pi^2} (m_{\nu_i} - m_{\nu_j}) \sum_{\alpha=1}^{3} U_{j\alpha}^{\dagger} U_{\alpha i} \left(\frac{m_{\ell\alpha}}{m_W} \right)^2 \ .\tag{10.12}$$

Hence, the decay width of $\nu_i \to \nu_j + \gamma$ is given by [1093, 1491]

$$\Gamma(\nu_i \to \nu_j + \gamma) = \frac{m_{\nu_i}^3}{8\pi} \left(1 - \frac{m_{\nu_j}^2}{m_{\nu_i}^2} \right)^3 \left[|\mu_{\bar{\nu}_j \nu_i}|^2 + |d_{\bar{\nu}_j \nu_i}|^2 \right]\tag{10.13}$$

$$\simeq \frac{\alpha m_{\nu_i}^5}{128\pi^4} G_F^2 \frac{9}{16} \left(\frac{m_\tau}{m_W} \right)^4 |U_{j\tau}^{\dagger} U_{\tau i}|^2 \ .\tag{10.14}$$
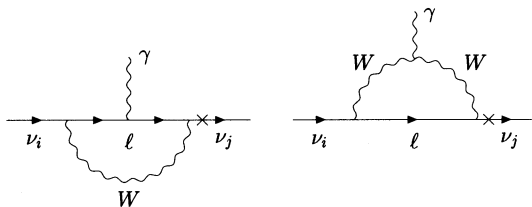
Fig. 10.1. Radiative corrections giving rise to a magnetic dipole moment of the Dirac neutrino within the Weinberg–Salam theory. The cross is a Dirac mass insertion.

Here we used the fact that $m_\tau \gg m_\mu, m_e$ and also assumed $m_{\nu_i} \gg m_{\nu_j}$. Numerically,

$$\Gamma(\nu_i \to \nu_j + \gamma) = (10^{29}\,\text{yr})^{-1} \left(\frac{m_{\nu_i}}{30\,\text{eV}}\right)^5 |U_{j\tau}^\dagger U_{\tau i}|^3 \,, \qquad (10.15)$$

i.e.,

$$\tau(\nu_i \to \nu_j + \gamma) \geq 4 \times 10^{29}\,\text{yr}(m_{\nu_i}/30\,\text{eV})^{-5} \,, \qquad (10.16)$$

where use is made of $|U_{j\tau}^\dagger U_{\tau i}|^2 \leq |\sin\theta\cos\theta|^2 \leq 1/4$ by unitarity. The transition moment is very small, typically $\mu \sim 10^{-22}\mu_\text{B}(m_\nu/1\text{eV})$, as a result of both chiral suppression and GIM cancellation.

The case for Majorana neutrinos. The Feynman diagrams for the Majorana neutrino are given in Fig. 10.2. We have both a charged lepton and an antilepton propagating in the internal loop. Correspondingly, the transition matrix is

$$T_{ji} = -i\varepsilon^\mu \bar{\nu}_j(p')\{[F_2(q^2)_{ji} - F_2(q^2)_{ij}] - [G_2(q^2)_{ji} - G_2(q^2)_{ij}]\gamma_5\}\sigma_{\mu\nu}q^\nu \nu_i(p)$$
$$= -i\varepsilon^\mu \bar{\nu}_j(p')[2i\,\text{Im}F_2(q^2)_{ji} - 2\,\text{Re}\,G_2(q^2)_{ji}\gamma_5]\sigma_{\mu\nu}q^\nu \nu_i(p) \,. \qquad (10.17)$$

The relative minus sign in each bracket comes from an exchange of the two fermions corresponding to arrows in the opposite direction. Equation (10.17) shows explicitly (e.g. [1490]) that

$$\mu_{\nu_i} = d_{\nu_i} = 0 \,. \qquad (10.18)$$

For the transition moment only one of the two terms of (10.17) is nonvanishing if the interaction respects CP invariance: the first term vanishes if the relative CP of ν_i and ν_j is even, and the second term vanishes if odd [1492,1204,1490,1493].

In the standard model we obtain from (10.2) and (10.3),

$$d_{\nu_i \nu_j} = 2\text{Re}\,G_2(0)_{ji}$$
$$= \frac{3eG_F}{16\pi^2\sqrt{2}}(m_{\nu_i} - m_{\nu_j})\sum_{\ell=1}^{3}\text{Re}\left[U_{j\alpha}^\dagger U_{\alpha i}\left(\frac{m_{\ell\alpha}}{m_W}\right)^2\right] \,, \qquad (10.19)$$
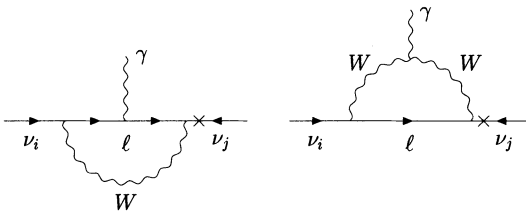
Fig. 10.2. Same as Fig. 8.15 for the Majorana neutrino. The cross is a Majorana mass insertion.

$$\mu_{\nu_i\nu_j} = 2i \text{ Im } F_2(0)$$

$$= \frac{3eG_F}{16\pi^2\sqrt{2}}(m_{\nu_i} + m_{\nu_j})\sum_{\ell=1}^{3} i \text{ Im } \left[U^{\dagger}_{j\alpha}U_{\alpha i}\left(\frac{m_{\ell\alpha}}{m_W}\right)^2\right], \quad (10.20)$$

allowing for violation of the CP invariance. The decay rate of $\nu_i \to \nu_j + \gamma$ is calculated by (10.13). If CP is conserved, $U^{\dagger}_{j\alpha}U_{\alpha i}$ is either real (when relative CP of ν_i and ν_j is even) or pure imaginary (when it is odd), and only one of (10.19) and (10.20) remains nonvanishing, respectively. The decay rate of $\nu_i \to \nu_j + \gamma$ for the Majorana neutrino is just twice that for the Dirac neutrino (10.14) [1204].

10.2 Neutrino Magnetic Moment in the Left–Right Symmetric Model

If there is a right-handed current that mixes with a left-handed current, chiral suppression does not work, and the magnetic moment is greatly enhanced.

Let us consider the $SU(2)_L \times SU(2)_R \times U(1)$ model with the interaction Lagrangian

$$\mathcal{L}_{\text{int}} = \frac{g_L}{\sqrt{2}}W^{\dagger}_{L\mu}(\bar{\nu}_{eL}\gamma_{\mu}e_L + \bar{\nu}_{\mu L}\gamma_{\mu}\mu_L + \bar{\nu}_{\tau L}\gamma_{\mu}\tau_L) + \text{h.c.}$$

$$+\frac{g_R}{\sqrt{2}}W^{\dagger}_{R\mu}(\bar{\nu}_{eR}\gamma_{\mu}e_R + \bar{\nu}_{\mu R}\gamma_{\mu}\mu_R + \bar{\nu}_{\tau R}\gamma_{\mu}\tau_R) + \text{h.c.} \quad (10.21)$$

The mass term is given by

$$\mathcal{L}_{\text{mass}} = (\bar{e}, \bar{\mu}, \bar{\tau})_R \begin{pmatrix} m_e & & 0 \\ & m_{\mu} & \\ 0 & & m_{\tau} \end{pmatrix} \begin{pmatrix} e \\ \mu \\ \tau \end{pmatrix}_L$$

$$+(\bar{\nu}_1, \bar{\nu}_2, \bar{\nu}_3)_R \begin{pmatrix} m_1 & & 0 \\ & m_2 & \\ 0 & & m_3 \end{pmatrix} \begin{pmatrix} \nu_1 \\ \nu_2 \\ \nu_3 \end{pmatrix}_L, \quad (10.22)$$

where the unitary transformations,

$$\nu_{iL} = U^{\dagger}_{i\alpha}\nu_{\alpha L},$$

$$\nu_{iR} = V^{\dagger}_{i\alpha}\nu_{\alpha R}, \quad (10.23)$$

are applied to the mass matrix for ν_e, ν_{μ}, and ν_{τ} to diagonalise the neutrino mass term. With (10.23) the interaction term (10.21) is written

$$\mathcal{L}_{\text{int}} = \frac{g_L}{\sqrt{2}}W^{\dagger}_{L\mu}\bar{\nu}_{iL}U^{\dagger}_{i\alpha}\gamma_{\mu}\ell_{\alpha L} + \text{h.c.} + \frac{g_R}{\sqrt{2}}W^{\dagger}_{R\mu}\bar{\nu}_{iR}V^{\dagger}_{i\alpha}\gamma_{\mu}\ell_{\alpha R} + \text{h.c.} \quad (10.24)$$

After symmetry breaking of both $\mathrm{SU}(2)_L$ and $\mathrm{SU}(2)_R$, we may write the mass term for the gauge bosons as

$$
\begin{aligned}
\mathcal{L}_{\mathrm{mass}} &= \frac{1}{2}(W_L^+ \ \ W_R^+) \begin{pmatrix} m_{W_L}^2 & \delta \\ \delta^* & m_{W_R}^2 \end{pmatrix} \begin{pmatrix} W_L^- \\ W_R^- \end{pmatrix} \\
&= \frac{1}{2}(W_1^+ \ \ W_2^+) \begin{pmatrix} m_{W_1}^2 & 0 \\ 0 & m_{W_2}^2 \end{pmatrix} \begin{pmatrix} W_1^- \\ W_2^- \end{pmatrix} ,
\end{aligned} \tag{10.25}
$$

where the second line is obtained by

$$
\begin{aligned}
W_1 &= W_L \cos\phi - W_R \sin\phi\, e^{i\psi} , \\
W_2 &= W_L \sin\phi\, e^{-i\psi} + W_R \cos\phi
\end{aligned} \tag{10.26}
$$

and

$$
\mathrm{tg}\, 2\phi = \frac{2|\delta|}{m_{W_R}^2 - m_{W_L}^2} . \tag{10.27}
$$

The off-diagonal element of mass matrix (10.25) can generally be complex, allowing for CP violation.

The diagrams giving radiative transitions are depicted in Fig. 10.3. Calculation of the magnetic moment [1494,1490] yields

$$
\begin{aligned}
\mu_{\nu_i} &= \frac{e g_L^2 m_{\nu_i}}{32\pi^2} \left[\frac{3}{2} \frac{\cos^2\phi}{m_{W_1}^2} \left(1 - \frac{1}{2} \sum_{\alpha=1}^{3} |U_{\alpha i}|^2 \mathcal{E}_\alpha^{(1)} \right) \right. \\
&\quad \left. + \frac{3}{2} \frac{\sin^2\phi}{m_{W_2}^2} \left(1 - \frac{1}{2} \sum_{\alpha=1}^{3} |U_{\alpha i}|^2 \mathcal{E}_\alpha^{(2)} \right) \right] \\
&\quad + \frac{e g_R^2 m_{\nu_i}}{32\pi^2} \left[\frac{3}{2} \frac{\sin^2\phi}{m_{W_1}^2} \left(1 - \frac{1}{2} \sum_{\alpha=1}^{3} |V_{\alpha i}|^2 \mathcal{E}_\alpha^{(1)} \right) \right. \\
&\quad \left. + \frac{3}{2} \frac{\cos^2\phi}{m_{W_2}^2} \left(1 - \frac{1}{2} \sum_{\alpha=1}^{3} |V_{\alpha i}|^2 \mathcal{E}_\alpha^{(2)} \right) \right] \\
&\quad + \frac{e g_L g_R}{32\pi^2} \sin\phi \cos\phi \sum_{\alpha=1}^{3} m_{\ell_\alpha} \mathrm{Re}(e^{-i\psi} V_{i\alpha}^\dagger U_{\alpha i}) \\
&\quad \times \sum_{k=1}^{2} (-1)^k \frac{4}{m_{W_k}^2} \left[-1 + \mathcal{E}_\alpha^{(k)} \left(\ln \frac{1}{\mathcal{E}_\alpha^k} - \frac{9}{8} \right) \right] ,
\end{aligned} \tag{10.28}
$$

where $\mathcal{E}_\alpha^k = m_{\ell_\alpha}^2 / m_{W_k}^2$. Note that the last term does not vanish, even if $m_{\nu_i} = 0$. This gives an example where the neutrino magnetic moment is not proportional to the neutrino mass.
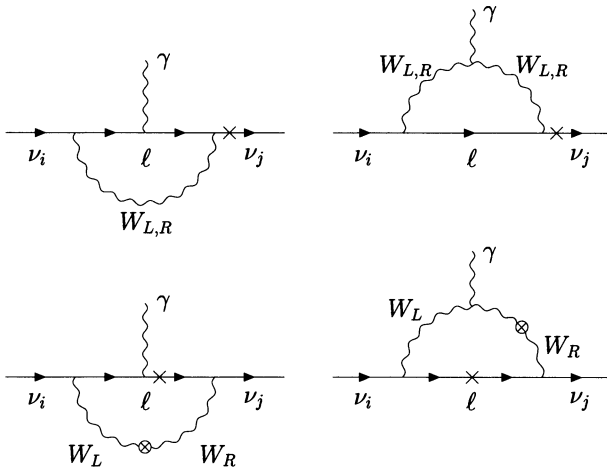
Fig. 10.3. Radiative corrections giving rise to a magnetic moment in the left–right symmetrical model. The circled cross shows W_L–W_R mixing.

The electric dipole moment is calculated to give

$$d_{\nu_i} = \frac{e g_L g_R}{8\pi^2} \sin\phi \cos\phi \sum_{\alpha=1}^{3} m_{\ell_\alpha} \mathrm{Im}(e^{i\psi} U_{i\alpha}^\dagger V_{\alpha i})$$

$$\times \sum_{k=1}^{2} (-1)^k \frac{1}{m_{W_k}^2} \left[-1 + \mathcal{E}_\alpha^{(k)} \left(\ln\frac{1}{\mathcal{E}_\alpha^{(k)}} - \frac{9}{8} \right) \right] , \qquad (10.29)$$

which is nonvanishing only if CP is violated, i.e., $\mathrm{Im}(e^{i\psi}...) \neq 0$.

The first four terms of (10.28) give only small contributions and are negligible. Assuming that $m_{W_2} \gg m_{W_1} \simeq m_W$ and $g_L = g_R = g$, we obtain

$$\mu_{\nu_i} \simeq -\frac{e g^2}{8\pi^2} \sin\phi \cos\phi \sum_\alpha m_{\ell_\alpha} \mathrm{Re}(e^{-i\psi} V_{i\alpha}^\dagger U_{\alpha i})$$

$$\times \frac{1}{m_W^2} \left[-1 + \frac{m_{\ell_\alpha}^2}{m_W^2} \left(\ln\frac{m_W^2}{m_{\ell_\alpha}^2} - \frac{9}{8} \right) \right] \qquad (10.30)$$

$$\simeq \frac{e G_F}{\sqrt{2}\pi^2} \sin\phi \cos\phi \sum m_{\ell_\alpha} \mathrm{Re}(e^{-i\psi} V_{i\alpha}^\dagger U_{\alpha i})$$

$$= \frac{\sqrt{2} G_F}{\pi^2} \sin\phi \cos\phi \, m_e \sum_\alpha m_{\ell_\alpha} \mathrm{Re}(e^{-i\psi} V_{i\alpha}^\dagger U_{i\alpha}^\dagger) \mu_{\mathrm{B}}$$

$$= \sin\phi \cos\phi [1.5 \times 10^{-9} \ \ \mathrm{Re}(e^{-i\psi} V_{i\tau}^\dagger U_{\tau i})$$

$$+ 0.9 \times 10^{-10} \ \ \mathrm{Re}(e^{-i\psi} V_{i\mu}^\dagger U_{\mu i})$$

$$+ 0.4 \times 10^{-12} \ \ \mathrm{Re}(e^{-i\psi} V_{ie}^\dagger U_{ei})] \mu_{\mathrm{B}} . \qquad (10.31)$$

The lepton mixing angle determines which term dominates. Note that if the magnetic moment is measured, e.g., for ν_μ, the intermediate charged lepton

state is the muon and the α-summation simplifies to $m_\mu e^{-i\psi}$; then $\mu_{\nu_\mu} = 0.9 \times 10^{-10} \cos\psi \sin\phi \cos\phi \, \mu_B$.

A constraint on W_L–W_R mixing is derived from the Michel parameter of μ decay [1495], which yields

$$|\sin\phi| \leq 0.05 \quad (90\% \text{ CL}) . \tag{10.32}$$

The end-point energy spectrum of e^+ in stopped polarised muon decay [1434] gives

$$|\sin\phi| \leq 0.035 \qquad \text{for } m_{W_R} \to \infty , \tag{10.33}$$

and

$$m_{W_R} \geq 475 \,\text{GeV} \qquad \text{for small } \phi . \tag{10.34}$$

A reanalysis in [1496] gives similar results. A study of longitudinal polarizations of e^+ in Fermi and Gamow–Teller nuclear β decays gives a constraint [1497],

$$\left(\frac{m_{W_L}}{m_{W_R}} \right)^2 |\sin\phi| < 1.2 \times 10^{-3}. \tag{10.35}$$

A stronger constraint on $|\sin\phi|$ is derived in the following way. If there is W_L–W_R mixing, the mass of W_L shifts by the amount

$$\delta m^2_{W_L} \simeq -\delta^2/m^2_{W_R}$$
$$= \sin^2\phi \, m^2_{W_R} . \tag{10.36}$$

By requiring that the Weinberg–Salam theory prediction for m_W not be disturbed by more than two standard deviations (100 MeV), we obtain, with the aid of the limit on W_R mass, $m_{W_R} > 720 \,\text{GeV}$ from Tevatron [1498],

$$|\sin\phi| \leq 0.005 . \tag{10.37}$$

If we use a limit $m_{W_R} \geq 1.6 \,\text{TeV}$ from $K^0 - \bar{K}^0$ mixing [1499] (which is somewhat model-dependent though), we obtain $|\sin\phi| \leq 0.0023$. Adopting the conservative (model-independent) limit of (10.37), we are led to

$$\mu_{\nu_e} \lesssim 2 \times 10^{-15} \cos\psi \, \mu_B . \tag{10.38}$$

For ν_μ and ν_τ, $\mu_{\nu_\mu} \lesssim 0.5 \times 10^{-12} \cos\psi \, \mu_B$ and $\mu_{\nu_\tau} \lesssim 0.8 \times 10^{-11} \cos\psi \, \mu_B$, respectively.

A stronger constraint is derived from cosmology. Successful primordial nucleosynthesis requires that the extra contribution to the cosmic energy density from the right-handed neutrinos ν_{iR} be small [1500], so that the effective number of species is less than 0.25 at the time of p/n freeze-out. All ν_{iR}'s should decouple from the thermal bath above the charm quark threshold, $T \sim 2 \,\text{GeV}$. From this, we obtain $|\sin\phi| \lesssim 10^{-5}$, which leads to $\mu_{\nu_e} \lesssim 1 \times 10^{-14} \mu_B$.

Transition moment.   The transition moment is calculated to give

$$
\mu_{\nu_j \nu_i} = \frac{3e(m_{\nu_i} + m_{\nu_j})}{256\pi^2} \sum_{\alpha=1}^{3} \left[-g_L^2 \left(\frac{\cos^2\phi}{m_{W_1}^2} \mathcal{E}_\alpha^{(1)} + \frac{\sin^2\phi}{m_{W_2}^2} \mathcal{E}_\alpha^{(2)} \right) U_{j\alpha}^\dagger U_{\alpha i} \right.
$$

$$
\left. - g_R^2 \left(\frac{\sin^2\phi}{m_{W_1}^2} \mathcal{E}_\alpha^{(1)} + \frac{\cos^2\phi}{m_{W_2}^2} \mathcal{E}_\alpha^{(2)} \right) V_{j\alpha}^\dagger V_{\alpha i} \right]
$$

$$
+ \frac{e g_L g_R}{16\pi^2} \sin\phi \cos\phi \sum_{\alpha=1}^{3} m_{\ell_\alpha} \left(e^{i\psi} U_{j\alpha}^\dagger V_{\alpha i} + e^{-i\psi} V_{j\alpha}^\dagger U_{\alpha i} \right)
$$

$$
\times \left\{ \sum_{k=1}^{2} \frac{(-1)^k}{m_{W_k}^2} \left[-1 + \mathcal{E}_\alpha^{(k)} \left(\ln\frac{1}{\mathcal{E}_\alpha^{(k)}} - \frac{9}{8} \right) \right] \right\} \tag{10.39}
$$

and

$$
d_{\nu_j \nu_i} = \frac{3e(m_{\nu_i} - m_{\nu_j})}{256\pi^2} \sum_{\alpha=1}^{3} \left[-g_L^2 \left(\frac{\cos^2\phi}{m_{W_1}^2} \mathcal{E}_\alpha^{(1)} + \frac{\sin^2\phi}{m_{W_2}^2} \mathcal{E}_\alpha^{(2)} \right) U_{j\alpha}^\dagger U_{\alpha i} \right.
$$

$$
\left. + g_R^2 \left(\frac{\sin^2\phi}{m_{W_1}^2} \mathcal{E}_\alpha^{(1)} + \frac{\cos^2\phi}{m_{W_2}^2} \mathcal{E}_\alpha^{(2)} \right) V_{j\alpha}^\dagger V_{\alpha i} \right]
$$

$$
+ \frac{e g_L g_R}{16\pi^2} \sin\phi \cos\phi \sum_{\alpha=1}^{3} m_{\ell_\alpha} \left[e^{i\psi} U_{j\alpha}^\dagger V_{\alpha i} - e^{-i\psi} V_{j\alpha} U_{\alpha i} \right]
$$

$$
\times \left\{ \sum_{k=1}^{2} \frac{(-1)^k}{m_{W_k}^2} \left[-1 + \mathcal{E}_\alpha^{(k)} \left(\ln\frac{1}{\mathcal{E}_\alpha^{(k)}} - \frac{9}{8} \right) \right] \right\} . \tag{10.40}
$$

For $m_\nu \ll m_\ell$, $m_{W_2} \gg m_{W_1} = m_W$, and $g_L = g_R(= g)$, (10.39) and (10.40) are

$$
\mu_{\nu_j \nu_i} \simeq \frac{eG_F}{2\sqrt{2}\pi^2} \sin\phi \cos\phi \ \ m_\tau (e^{i\psi} U_{j\tau}^\dagger V_{\tau i} + e^{-i\psi} V_{j\tau}^\dagger U_{\tau i}) \tag{10.41}
$$

and

$$
d_{\nu_j \nu_i} \simeq \frac{eG_F}{2\sqrt{2}\pi^2} \sin\phi \cos\phi \ \ m_\tau (e^{i\psi} U_{j\tau}^\dagger V_{\tau i} - e^{-i\psi} V_{j\tau}^\dagger U_{\tau i}) , \tag{10.42}
$$

where we retained only the contribution from the τ loop. The decay rate of $\nu_i \to \nu_j + \gamma$ calculated using (10.13) is

$$
\Gamma(\nu_i \to \nu_j + \gamma) = \frac{\alpha}{8\pi^4} G_F^2 \sin^2\phi \cos^2\phi \ \ m_\tau^2 m_{\nu_i}^3 \left(1 - \frac{m_{\nu_j}^2}{m_{\nu_i}^2} \right)^3
$$

$$
\times (|U_{j\tau}^\dagger V_{\tau i}|^2 + |V_{j\tau}^\dagger U_{\tau i}|^2) . \tag{10.43}
$$

Numerically,

$$\Gamma(\nu_i \to \nu_j + \gamma)$$
$$= (0.22 \times 10^{15}\,\text{s})^{-1} \sin^2\phi \cos^2\phi (|U_{j\tau}^\dagger V_{\tau i}|^2 + |V_{j\tau}^\dagger U_{\tau i}|^2)(m_{\nu_i}/10\text{eV})^3$$
$$\lesssim (0.9 \times 10^{19}\,\text{s})^{-1} (|U_{j\tau}^\dagger V_{\tau i}|^2 + |V_{j\tau}^\dagger U_{\tau i}|^2)(m_{\nu_i}/10\,\text{eV})^3\,, \tag{10.44}$$

using constraint (10.37). If $|V_{1,2\tau}^\dagger U_{\tau 3}|^2 \le 1/4$, ν_τ decay can be as fast as

$$\tau(\nu_3 \to \nu_{2,1} + \gamma) \gtrsim 1 \times 10^{12}\,\text{yr}(m_{\nu_3}/10\,\text{eV})^{-3}\,. \tag{10.45}$$

The absence of chirality suppression appears in the m_ν^3 dependence of (10.45), rather than m_ν^5 in (10.16). The transition amplitude does not receive GIM suppression in the left–right symmetric model. For a subelectronvolt neutrino mass, however, the lifetime of radiative decay is too long anyway to have phenomenological significance.

10.3 Model with a Charged Scalar Particle

Another case in which a chirality suppression is lifted for the neutrino magnetic moment is a model with a charged scalar particle [1501]. The scalar particle can be either an $SU(2)_L$ singlet or a doublet. Here we consider the former [1095, 1501]. The $SU(2)_L$ singlet scalar does not couple to quarks, so that we do not need to worry about the flavour-changing neutral current induced by a scalar particle in the hadron sector, which otherwise would give rise to a very strong constraint and exclude any extension such as the model considered here. The singlet scalar carries a unit electric charge.

The Yukawa coupling of the charged singlet scalar η^+ is given by

$$\mathcal{L}_{\text{int}} = g_{ij}\,\overline{\ell_L^{ci}}\,\ell_L^j\,\eta + f_{ij}\,\overline{\nu_R^{ci}}\,e_R^j\,\eta + \text{h.c.}\,, \tag{10.46}$$

where

$$g_{ij} = -g_{ji} \tag{10.47}$$

from $SU(2)_L$ symmetry and Fermi statistics (we ignore here the neutrino mass).[1]

Calculation of the diagram depicted in Fig. 10.4 yields

$$\mu_{\nu_i} = e\sum_{j=1}^{3} \frac{f_{ij}g_{ji}^\dagger + g_{ij}f_{ji}^\dagger}{32\pi^2} \frac{m_{\ell_j}}{m_\eta^2}\left(\ln\frac{m_\eta^2}{m_{\ell_j}^2} - 1\right)\,. \tag{10.48}$$

---

[1] This η is basically identical with h of Sect. 7.2. The difference is that η does not violate a lepton number at any vertices.
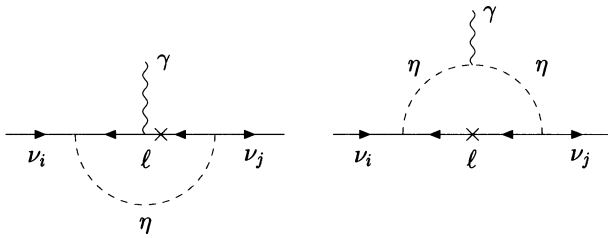
Fig. 10.4. Radiative corrections by a charged scalar particle η, giving rise to a magnetic moment of a neutrino.

If τ dominates in the intermediate state,

$$\mu_{\nu_i} = e\frac{f_{i3}g_{3i}^\dagger + g_{i3}f_{3i}^\dagger}{32\pi^2}\frac{m_\tau}{m_\eta^2}\left(\ln\frac{m_\eta^2}{m_\tau^2} - 1\right) . \qquad (10.49)$$

The η loop may also contribute to the neutrino mass (Fig. 10.5). This diagram, however, is logarithmically divergent, and it must be cancelled by a counter term; i.e., the mass of the neutrino is not calculable and is arbitrary.

The original motivation to consider such a model was whether it is possible to have a large magnetic moment for ν_e of the order of $\mu_{\nu_e} = (10^{-10} - 10^{-11})\mu_{\mathrm{B}}$ that would play an interesting role in the solar neutrino problem, as we discuss later in this chapter. Later considerations showed that the transition moment between ν_e and ν_μ (or ν_τ) is more relevant to the solar neutrino problem. The transition moment is given by

$$\mu_{\nu_i\nu_j} = e\sum_k \frac{f_{ik}g_{kj}^\dagger + g_{ik}f_{kj}^\dagger}{32\pi^2}\frac{m_{\ell_k}}{m_\eta^2}\left(\ln\frac{m_\eta^2}{m_{\ell_k}^2} - 1\right) . \qquad (10.50)$$

In order to give $\mu_{\nu_e\nu_\mu} = 10^{-11}\mu_{\mathrm{B}}$, we must have

$$e\frac{g_{13}f_{32}^\dagger + f_{13}g_{32}^\dagger}{2}\frac{1}{m_\eta^2}\left(\ln\frac{m_\eta^2}{m_\tau^2} - 1\right) \simeq 10^{-6}\,\mathrm{GeV}^{-2} , \qquad (10.51)$$

where $g_{13}f_{32}^\dagger$ is relevant to $\nu_{eL} \to \nu_{eR}$ and $f_{13}g_{32}^\dagger$ to $\nu_{eR} \to \nu_{eL}$. Therefore, what concerns us is the first term. We need

$$\frac{g_{13}f_{32}^\dagger}{m_\eta^2} \simeq 6 \times 10^{-7}\,\mathrm{GeV}^{-2} \qquad (10.52)$$
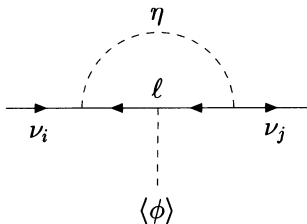
Fig. 10.5. Diagram for the neutrino mass induced by radiative corrections due to an η particle.

for $m_\eta \approx 100\,\text{GeV} - 1\,\text{TeV}$. The second term, if it is large, would induce $\mu \to e + \gamma$ decay that conflicts with experiment.

Constraints on nonstandard Yukawa couplings.   When one introduces a nonstandard scalar particle, one must be concerned with possible effects induced by this particle. Examples are

   (i) $e - \mu$ universality in τ decay. A constraint is directly derived from τ decay on the combination $g_{13}f_{32}^\dagger/m_\eta^2$, which appears in (10.51). The η exchange induces an extra contribution to $\tau \to e\bar{\nu}_\mu\nu_\tau$ as

$$\Gamma(\tau \to e\bar{\nu}_\mu\nu_\tau) \simeq \frac{1}{6144}\left|\frac{g_{13}f_{32}^\dagger}{m_\eta^2}\right|^2 m_\tau^5 \,, \tag{10.53}$$

which disturbs $e - \mu$ universality. The experiment $B_e/B_\mu = 0.998 \pm 0.011$ leads to

$$\frac{g_{13}f_{32}^\dagger}{m_\eta^2} \leq 0.8 \times 10^{-5}\,\text{GeV}^{-2} \,, \tag{10.54}$$

where the 2σ error is taken as a limit. A more stringent constraint is obtained on g_{13} from the η-exchange diagram of Fig. 10.6 since the first diagram interferes with W exchange; an effective G_τ^{eff} derived from τ decay modifies to [1502]

$$(G_\tau^{\text{eff}})^2 = G_F^2\left(1 + \frac{1}{4}\frac{|g_{13}|^2/m_\eta^2}{G_F/\sqrt{2}}\right) \,. \tag{10.55}$$

This also disturbs $e - \mu$ universality in τ decay. We expect

$$\frac{B_\mu}{B_e} = 1 - \frac{\sqrt{2}}{4G_F}\frac{|g_{13}|^2}{m_\eta^2} \,, \tag{10.56}$$

so that we obtain

$$\frac{|g_{13}|^2}{m_\eta^2} < 3 \times 10^{-7}\,\text{GeV}^{-2} \,, \tag{10.57}$$

allowing for the 2σ error. This constraint on g_{13} together with the requirement in (10.52) implies

$$\frac{|f_{23}|^2}{m_\eta^2} \geq 1 \times 10^{-6}\,\text{GeV}^{-2} \,. \tag{10.58}$$

   We now discuss constraints on other Yukawa couplings that do not appear in (10.52): g_{12}, g_{23}, and f_{ij}.

(a)

(b)
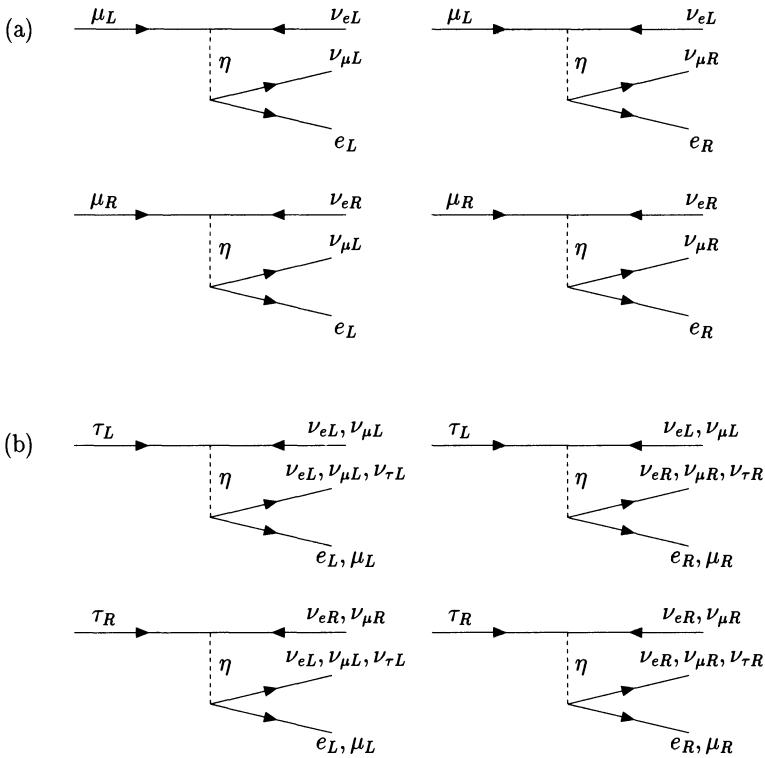
Fig. 10.6. (a) Anomalous muon decay induced by an η particle. (b) The same for τ decay.

(ii) Anomalous magnetic moment $(g-2)$ of leptons. A calculation of Fig. 10.7 gives radiative corrections to $(g-2)$ of leptons, as

$$\delta\mu_{\ell\alpha} = -\frac{em_{\ell\alpha}}{16\pi^2}\frac{1}{12m_\eta^2}[(gg^\dagger)_{\alpha\alpha} + (ff^\dagger)_{\alpha\alpha}] , \qquad (10.59)$$

or

$$\delta(g_\alpha - 2) = \frac{2\mu_{\ell\alpha}}{\mu_B} = -\frac{1}{48\pi^2}\frac{m_{\ell\alpha}^2}{m_\eta^2}[(gg^\dagger)_{\alpha\alpha} + (ff^\dagger)_{\alpha\alpha}] . \qquad (10.60)$$
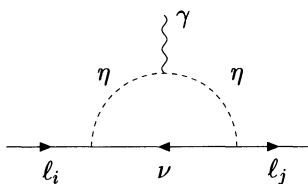
Fig. 10.7. Contribution to the lepton anomalous magnetic moment from radiative corrections involving the η particle.

From $\delta(g_e - 2)/2 < 2.9 \times 10^{-10}$, we obtain

$$\frac{(g^\dagger g)_{11}}{m_\eta^2}, \quad \frac{(ff^\dagger)_{11}}{m_\eta^2} < 2.7 \times 10^{-1}\,\mathrm{GeV}^{-2} . \tag{10.61}$$

For the muon, we have $\delta(g_\mu - 2)/2 \lesssim 4 \times 10^{-9}$,[2] which leads to

$$\frac{(g^\dagger g)_{22}}{m_\eta^2}, \quad \frac{(ff^\dagger)_{22}}{m_\eta^2} < 3 \times 10^{-4}\,\mathrm{GeV}^{-2} . \tag{10.62}$$

(iii) Charged-current interaction universality. The η exchange induces an anomalous μ decay (Fig. 10.6). The first diagram interferes with W exchange, and the effective G_F is given by (10.55) where g_{13} is replaced by g_{12} [1502]. From the unitarity test (3.110), we get

$$\frac{|g_{12}|^2}{m_\eta^2} < 1.6 \times 10^{-7}\,\mathrm{GeV}^{-2} . \tag{10.63}$$

(iv) $\mu \to e + \gamma$. The η induces a flavour-changing neutral current in the lepton sector. In particular, the diagram shown in Fig. 10.8 causes $\mu \to e\gamma$
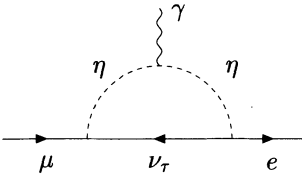
Fig. 10.8. Diagram that induces $\mu \to e\gamma$.

with the amplitude

$$T(\mu \to e\gamma) = \frac{e}{32\pi^2} \frac{m_e + m_\mu}{12m_\eta^2} [(gg^\dagger)_{12} + (ff^\dagger)_{12}] . \tag{10.64}$$

The empirical limit (8.10) yields

$$\frac{(g^\dagger g)_{12}}{m_\eta^2} \simeq \frac{g_{13}g_{32}}{m_\eta^2} < 3\times10^{-8}\,\mathrm{GeV}^{-2} , \quad \frac{(f^\dagger f)_{12}}{m_\eta^2} < 3\times10^{-8}\,\mathrm{GeV}^{-2} . \tag{10.65}$$

---

[2] A recent muon precession experiment gives a finite value of $4.3 \pm 0.16 \times 10^{-10}$ for this difference [1503]. However, the precision of the estimate of hadronic contributions is suspect. Dicus et al. [1504] took this $g_\mu - 2$ anomaly positively, and attempted to account for it using the η model.

The first constraint means that

$$\frac{g_{32}}{g_{13}} < 0.3 \left(\frac{g_{13}^2/m_\eta^2}{10^{-7}\,\mathrm{GeV}^2} \right)^{-1}.$$
(10.66)

We can satisfy (10.52) without having too large a disparity among g_{ij}:

$$\left|\frac{g_{12}}{g_{13}}\right| \leq 1 \,, \quad \left|\frac{g_{23}}{g_{13}}\right| < 0.3 \,,$$
(10.67)

for $g_{13}^2/m_\eta^2 \sim 10^{-7}\,\mathrm{GeV}^{-2}$. For f_{ij}, the constraint from τ decay is rather weak as η exchange induced by these couplings does not interfere with W exchange, but a strong limit is obtained from the absence of $\mu \to e + \gamma$, which requires disparity among the couplings as

$$\left|\frac{(f^\dagger f)_{12}}{(f_{23})^2}\right| < 0.03 \,,$$
(10.68)

for $|f_{23}|^2/m_\eta^2 \sim 1 \times 10^{-6}\,\mathrm{GeV}^{-2}$, which is the lower limit of inequality (10.58).

Constraints from primordial nucleosynthesis are strong. The process $\nu_{Le} + \tau \to \nu_{R\mu} + \tau$ produces $\nu_{R\mu}$ via the η exchange, where the same combination of Yukawa couplings appears as that for the ν_e–ν_μ transition moment. Since a nonnegligible number of τ particles existed until the universe cooled to a few hundred MeV, the Yukawa coupling required by (10.52) means that $\nu_{R\mu}$ decouples only at ≈ 300 MeV. This nearly saturates the allowance of the relativistic degree of freedom for successful nucleosynthesis. The two other right-handed neutrinos, ν_{Re}, $\nu_{R\tau}$, should have decoupled above the charm and tau threshold in order not to increase the relativistic degree of freedom excessively. This leads to strong limits on the Yukawa couplings relevant to right-handed neutrinos. To satisfy the upper limit (10.58), we need disparities,

$$\left|\frac{f_{1i}}{f_{23}}\right|, \quad \left|\frac{f_{3i}}{f_{23}}\right| < 10^{-4}.$$
(10.69)

Empirical large mixing between $\nu_{L\mu}$ and $\nu_{L\tau}$ implies that such strong disparities would be hard to realise. Hence, this constraint renders a large magnetic moment with a scalar-particle radiative correction unattractive. The maximum magnetic moment we can have without imposing a large disparity in f_{ij} and g_{ij} is $\mu \simeq 3 \times 10^{-16}\mu_\mathrm{B}$.

Transition moment.   The decay rate for $\nu_i \to \nu_j + \gamma$ is given by (10.13) with $d_{\nu_i \nu_j} = \mu_{\nu_i \nu_j}$. For $\mu_{\nu_\mu \nu_e} \simeq 10^{-11}\mu_\mathrm{B}$, we expect

$$\tau(\nu_\mu \to \nu_e + \gamma) \gtrsim 0.2 \times 10^{14}\,\mathrm{yr}\,(1\,\mathrm{eV}/m_{\nu_\mu})^3 \,,$$
(10.70)

assuming that $m_{\nu_\mu} \gg m_{\nu_e}$.

η-induced neutrino oscillation in matter. The η particle may induce neutrino oscillation in matter, even when neutrinos are massless [1505]. As discussed in Sect. 8.6, neutrinos acquire an effective mass in matter as a result of interaction with electrons. MSW neutrino conversion, which takes place if the induced mass compensates for the intrinsic neutrino mass, does not take place in the $m_\nu = 0$ limit. The η exchange, however, induces an off-diagonal effective mass, and the balance between W and η exchanges causes neutrino conversion, even if the neutrino is massless [212, 1506].

Consider only the left-handed neutrinos, and assume that they are massless. Through the first term of (10.46), neutrinos acquire effective masses in matter via the diagram shown in Fig. 10.9. The effective Hamiltonian is given by

$$
H = n_e \begin{pmatrix} \sqrt{2}G_F & 0 & 0 \\ 0 & \dfrac{g_{12}^2}{4m_\eta^2} & \dfrac{-g_{12}g_{13}}{4m_\eta^2} \\ 0 & -\dfrac{g_{12}g_{13}}{4m_\eta^2} & \dfrac{g_{13}^2}{4m_\eta^2} \end{pmatrix} , \tag{10.71}
$$

where the neutral-current interaction from Z^0 exchange is omitted because it contributes to all neutrino species in the same way. With (10.71) the mixing angle ψ between ν_μ and ν_τ is given by

$$
\tan 2\psi = \frac{2g_{12}g_{13}}{g_{12}^2 - g_{13}^2} . \tag{10.72}
$$

Thus, the maximal mixing $\psi = \pi/4$ occurs if $g_{12} = g_{13}$, even if they are small. The oscillation length is given by

$$
L_{\mathrm{osc}} = \frac{2\pi}{(g_{12}^2 + g_{13}^2)n_e/4m_\eta^2} , \tag{10.73}
$$

which is independent of neutrino energy.

For the atmospheric ν_μ flux propagating through Earth, L_{osc} is

$$
L_{\mathrm{osc}} \simeq 37 R_\oplus G_6^{-1}[1 + (g_{13}^2/g_{12}^2)]^{-1} , \tag{10.74}
$$

where $G_6 \simeq g_{12}^2/m_\eta^2 \times 10^6$ and $R_\oplus$ is the radius of Earth. The decrease of the up-going muon neutrino flux is given by [1505]

$$
P(\nu_\mu \to \nu_\tau) = \frac{1}{2} \sin^2 2\psi[1 - \cos(4\pi R_\oplus/L_{\mathrm{osc}})] . \tag{10.75}
$$
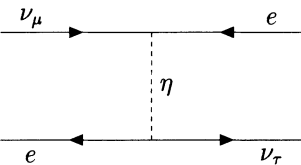
Fig. 10.9. $\nu_\mu - \nu_\tau$ exchange interaction induced by an η particle.

Using the present experimental constraints on g_{12}^2/m_η^2 and g_{13}^2/m_η^2, the decrease is, at most, 10% for the allowed parameters of g_{ij}. The feature characteristic of this effect is that $P(\nu_\mu \to \nu_\tau)$ is energy-independent. The intrinsic mass difference between ν_μ and ν_τ suppresses this effect.

10.4 Variants of the Scalar Model

In the model described in the previous section, the η-loop radiative correction for the neutrino mass is logarithmically divergent and, hence, a counter term must be introduced to cancel the divergence. Although this model is logically consistent, the neutrino mass is completely arbitrary, and the model does not give any insight into the smallness of the neutrino mass.

This point becomes a serious problem if the neutrino is of the Majorana type because both mass and transition moment are given by nonrenormalisable higher dimensional operators, and therefore the mass correction is finite and calculable; the η radiative correction that gives a large transition moment inevitably gives too large a neutrino mass. Consider a Feynman diagram that gives the leading contribution to the transition moment (Fig. 10.10). It gives a transition moment of the order of $e\frac{g}{16\pi^2}\langle H\rangle^2/M^3$, where g is a combination of Yukawa couplings that appear in the diagram and M is the mass of scalar particles. To give a transition moment of the order of $10^{-11}\mu_B$, we should have $M \sim 100$ GeV for $g \simeq O(10^{-4})$. The Feynman diagram obtained by removing the external photon line gives a radiative correction to the neutrino mass, which is $\sim \frac{g}{16\pi^2}\langle H\rangle^2/M \sim O(100)$ keV. In other words, if we take the ratio of m_ν to μ_ν,

$$\frac{m_\nu}{\mu_\nu} \sim \frac{M^2}{e} , \qquad (10.76)$$

the unknown factor g cancels, and the requirement that $m_\nu \leq 0.1$ eV and $\mu_\nu \simeq 10^{-11}\mu_B$ means $M^2 \leq (0.1\,\text{GeV})^2$.

This argument shows that some suppression mechanism that operates only for the neutrino mass is needed. A number of extensions of the η model have been considered for this purpose, and we shall briefly review a few attempts (though not necessarily successful).
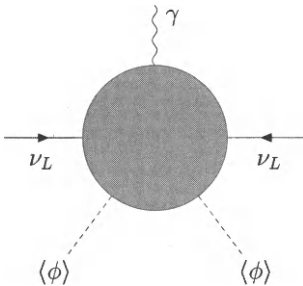
Fig. 10.10. Diagram that gives a leading contribution to the transition moment for Majorana neutrinos.

10.4.1 Voloshin's Symmetry

The most general mass term for neutrinos is written

$$\mathcal{L} = -\frac{1}{2} m_{ij} \overline{\psi_L^{ic}} \psi_L^j + \text{h.c.} , \qquad (10.77)$$

where ψ is a Weyl spinor and indices $i, j = 1, ..., N$ with N the number of neutrino species. We assume that all spinors are $SU(2)_L$ doublets. Due to the Fermi statistics, we should have

$$m_{ij} = m_{ji} . \qquad (10.78)$$

The interaction with the magnetic moment is written

$$\mathcal{L}_{\text{mag}} = \mu_{ij} \overline{\psi_L^{ic}} \sigma_{\mu\nu} \psi_L^j F^{\mu\nu} , \qquad (10.79)$$

with antisymmetric μ_{ij},

$$\mu_{ij} = -\mu_{ji} . \qquad (10.80)$$

If we take two neutrino spinors ψ_L^1 and ψ_L^2 and assume that they form a doublet of some SU(2) symmetry, the mass term transforms as a triplet, and the magnetic moment as a singlet. Thus, insofar as this SU(2) (referred to as $SU(2)_\nu$) is exact symmetry, the mass term is forbidden, while the magnetic moment is nonvanishing [1507].

This $SU(2)_\nu$ symmetry requires that ψ_L^1 and ψ_L^2 belong to the same representation of the standard-model gauge group, i.e., doublets of $SU(2)_L$, and the neutrinos are necessarily Majorana-type fermions. The most natural candidate of this $SU(2)_\nu$ may be horizontal (family) $SU(2)_F$ symmetry, where the electron and muon families form a doublet [1508].

The problem in the models with family symmetry is whether one can keep $SU(2)_\nu$ breaking sufficiently small by fine-tuning the parameters in the Higgs potential, whereas breaking of family SU(2) symmetry is of $O(1)$ for the charged leptons. Once $SU(2)_\nu$ is broken, a large neutrino mass is induced. As an example, let us take the scalar η model extended to form a doublet of $SU(2)_F$. $SU(2)_F$ breaking is characterised by $\delta m_\eta^2 = m_{\eta_1}^2 - m_{\eta_2}^2$, where the $\eta_{1,2}$ denote two components of the horizontal doublet η. The neutrino mass is then written as [1507, 1509]

$$m_{\nu_e} \sim \frac{1}{e} \mu_{\nu_e} \frac{\delta m_\eta^2}{\ln(m_\eta^2/m_\mu^2)} . \qquad (10.81)$$

This vanishes in the limit of $\delta m_\eta^2 = 0$. If we require $m_{\nu_e} < 0.1\,\text{eV}$ and $\mu_{\nu_e} > 10^{-11} \mu_{\text{B}}$, we must have

$$\frac{\delta m_\eta^2}{m_\eta^2} < 3 \times 10^{-5} , \qquad (10.82)$$

a high degree of degeneracy between η_1 and η_2 masses. To understand large difference between m_e and m_μ in this model, one must assume that electron and muon masses are zero in the $SU(2)_F$ limit and that muon mass is generated in the first order of $SU(2)_F$ breaking. The model can, in principle, be fine-tuned in the Higgs potential, but there arises unwanted approximate global symmetry related to the phase rotation of the η field [1508]; the associated pseudo-Nambu–Goldstone boson has a mass less that $1\,\text{GeV}$, which is excluded by experiment.

Other examples include a model with discrete Abelian [1510] or non-Abelian symmetry [1511]. All models proposed so far, however, need similar fine-tuning to give a large magnetic moment of $\mu_{\nu_e} = 10^{-10} - 10^{-11}\mu_B$ while keeping the neutrino mass sufficiently small.

The models that were viable in the past met difficulty after the discovery of the neutrino mass from atmospheric neutrino experiments.

10.4.2 Helicity Suppression Mechanism

Let us suppose that the Feynman diagram in Fig. 10.11a gives a dominant contribution to the magnetic moment [1512]. The "blob" represents an effective vertex that converts a spin-zero boson h^- into a weak boson by emitting a photon. To generate a transition moment, a chirality flip is needed, which is provided by h's Yukawa coupling to the lepton.

On the other hand, the mass term is generated by the diagram in Fig. 10.11b. The "blob" here converts a spin-zero field into a vector field, which takes place only when the vector boson is longitudinally polarised. Now, the longitudinal component of the weak boson W^+ is an unphysical Higgs whose Yukawa coupling to fermions (f) always involves m_f/m_W. This factor suppresses the neutrino mass term. Furthermore, since both vertices on the fermion line of Fig. 10.11b flip chirality, another lepton mass insertion is necessary to obtain a net chirality flip of the mass term. Hence, the suppression factor in the mass diagram amounts to m_f^2/m_W^2.

A concrete model (based on the Zee model discussed in Sect. 7.2) is given by Barr et al. [1512], who found that

$$\mu_{ij} \sim 10^{-2}\frac{e}{(16\pi^2)^2}\frac{\kappa_{ij}\langle H\rangle^2}{M^3}, \tag{10.83}$$

while the mass is suppressed as

$$m_{ij} \sim 10^{-2}\frac{1}{(16\pi^2)^2}\frac{\kappa_{ij}(m_{\ell i}^2 - m_{\ell j}^2)\langle H\rangle^2}{M^3}. \tag{10.84}$$

Here $\kappa_{ij} = -\kappa_{ji}$ is the antisymmetric Yukawa coupling of h given in (6.57).

At this level, it appears possible to obtain a large magnetic moment, $\mu \simeq (10^{-10} - 10^{-11})\mu_B$, while keeping the off-diagonal neutrino mass of $m_{\nu_e\nu_\mu}$ of the order of $0.1\,\text{eV}$. For example, $\kappa_{ij} \simeq 1$ and $M \simeq 100\,\text{GeV}$ yield $\mu \simeq$

$10^{-11}\mu_B$, and at the same time, give $m_{\nu_e\nu_\mu} \simeq 0.1$ eV. The tree-level diagram of the heavy h exchange, however, induces the extra contribution to $\mu \to \nu_\mu e \bar\nu_e$ which interferes with main decay amplitude, as discussed in the previous section. This contribution largely exceeds the empirical limit by $O(10^2)$. The model is thus already excluded.

Furthermore, in this model, another one-loop diagram of Fig. 6.4 contributes to the mass term as shown in Sect. 7.2; this contribution is not necessarily suppressed. One must impose some extra discrete symmetry to remove this diagram to make the scenario viable.

We conclude that no reasonable model has been found with a scalar particle to enhance the transition moment of Majorana neutrinos to the order of $\mu \simeq (10^{-10} - 10^{-11})\mu_B$ consistent with other phenomenology.
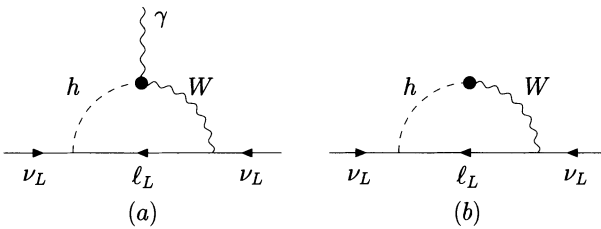
Fig. 10.11. (a) A variant η model giving a magnetic moment to the neutrino. (b) Diagram that induces neutrino mass.

10.5 Astrophysical Significance
of the Neutrino Magnetic Moment

In the standard model the magnetic moment of neutrinos is a very small quantity due to chirality suppression. There is a gap of many orders of magnitude between the standard-model prediction, (10.10), and the empirical limit $\mu_{\nu_e} < 10^{-10} - 10^{-9}\mu_B$ from laboratory experiments or $\mu_{\nu_i} < 10^{-11}\mu_B$ from astrophysics. If the magnetic moment were found to have a value larger than (10.10), this should indicate the presence of interactions that violate chirality conservation beyond the standard model. In this section we review the problems where a large magnetic moment could be astrophysically relevant.

10.5.1 Solar Neutrino Problem

An interesting indication of a large magnetic moment was given by the solar-neutrino experiment. In 1986 Davis reported [1513] that the solar-neutrino capture rate at the Homestake ^{37}Cl detector varies with time and it anticorrelates with solar activity characterised by sunspot numbers for solar cycle 21 (see also [1514] for an earlier suggestion). It was later shown that this anticorrelation persisted to the next solar cycle (solar cycle 22, starting from autumn

1986) [1515]. While it was a matter of debate that the observed anticorrelation was due merely to a statistical fluke (for statistical tests, see [1516]), the effect clearly visible in their figures was intriguing, in particular, since it would be difficult to imagine any astrophysical mechanisms that correlate the neutrino flux produced in the core of the Sun with an outer layer phenomenon, such as solar activity. Voloshin, Vysotsky, and Okun [1517] proposed a fascinating solution by which this anticorrelation could be explained if the neutrino had a magnetic moment as large as

$$\mu_{\nu_e} \sim 1 \times 10^{-10} \mu_{\mathrm{B}} \ , \qquad (10.85)$$

just below the limit set by laboratory experiments. The mechanism is that a left-handed neutrino (Dirac neutrino) precesses into a right-handed neutrino under the influence of the magnetic field expected in the convective layer of the Sun [1518]. For a relativistic neutrino the probability of the $\nu_L \to \nu_R$ flip is given by

$$P(\nu_L \to \nu_R) = \sin^2(\mu B L \sin \phi) \ , \qquad (10.86)$$

where ϕ is the angle between the direction of the neutrino beam and the magnetic field ($\phi \sim 90°$ for solar neutrinos). The solar magnetic field is expected to be stronger when the Sun is more active. If $\mu B L \sim \pi/2$ for the solar maximum, complete suppression of neutrino captures is anticipated in the ^{37}Cl detector since the right-handed neutrino is sterile to the detector. For $L \sim 0.3 R_{\odot}$ (the length of the convective layer) and $B_{\mathrm{max}} \sim 2\,\mathrm{kGauss}$, (10.85) gives $\mu B L \sim 1.2$, about the desired condition. This was the only explanation known to explain the anticorrelation, if it exists at all. This has motivated studies of the neutrino magnetic moment for both solar neutrino phenomenology and particle physics model building.
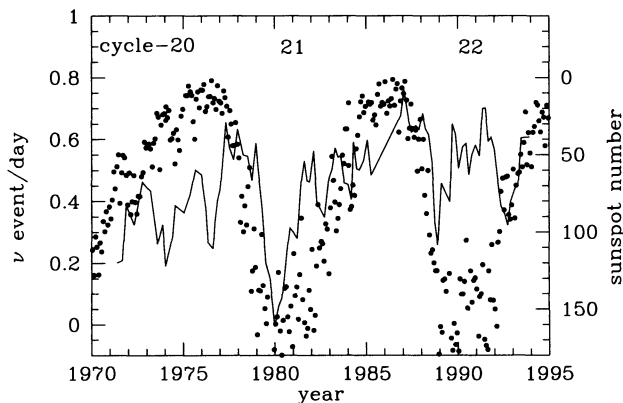
Fig. 10.12. Five-point running average of the solar neutrino capture rate (day^{-1}) on ^{37}Cl in the Homestake experiment (*solid curve*). Sunspot numbers are shown by *solid circles*.

Unfortunately, after the solar maximum of 1989, this anticorrelation was obscured; see Fig. 10.12 which is constructed from the data published by Cleveland et al. [721] by taking a five-point running average, as done by Davis [1513]. Another negative piece of evidence comes from Kamiokande (1987–1995) [722] and Super-Kamiokande (1996–2001) [1519] which do not see a time variation of more than 20%. Nevertheless, the possibility is still interesting that the magnetic moment or transition moment would take part in the reduction of solar neutrino flux, irrespective of whether or not the solar neutrino flux varies, and many studies have been done in this direction.

The first point to be considered is that there is a mechanism to suppress the spin precession. This was already noticed by Voloshin et al. [1517]. In a realistic situation, ν_L receives a refractive effect in matter from interactions via the neutral current, whereas ν_R does not. This causes an energy gap between ν_L and ν_R, i.e., the Hamiltonian for neutrino propagation is

$$H = \begin{pmatrix} \sqrt{2}G_F(n_e - \frac{1}{2}n_n) & \mu_\nu B \\ \mu_\nu B & 0 \end{pmatrix} . \tag{10.87}$$

Here, the (1,1) component is $V(\nu_e, e) + V(\nu_e, p) + V(\nu_e, n) = \sqrt{2}G_F(n_e - n_n/2)$ $\simeq 5.5 \times 10^{-15}$ eV$(\rho/0.1\,\text{g cm}^{-3})$ [see (3.239, 3.240); $n_e = n_p$ is assumed] and the off-diagonal components are $\mu_\nu B = 5.8 \times 10^{-16}$ eV$(\mu_\nu/10^{-10}\mu_\text{B})(B/1\,\text{kGauss})$. For a typical density in the convective layer of the Sun, $\rho = 0.2\,\text{g cm}^{-3}$ at $0.7R_\odot$ and $0.02\,\text{g cm}^{-3}$ at $0.9R_\odot$, the precession by the off-diagonal element is suppressed unless $\mu_\nu BL \gtrsim 10$. A calculation [1520] shows that one needs $\mu BL \sim 3 \times (\pi/2)$ to bring the flux suppressed to the level of one-fourth of the standard solar-model value, assuming a large magnetic field between $r = 0.8R_\odot$ and $0.9R_\odot$. This means that $B_\text{max} \sim 10\,\text{kGauss}$ is necessary. The value of (10.85) is already one order of magnitude larger than the limit from stellar cooling (2.111). If $\mu \sim 10^{-11}\mu_\text{B}$, one needs $B_\text{max} \sim 100\,\text{kGauss}$, which is the maximum value we can imagine for the magnetic field in the interior of the Sun.

Lim and Marciano [1521] (see also [1522]) showed that this problem is circumvented if the $\nu_L \to \nu_R$ flip takes place between ν_e and ν_μ (or ν_τ) when the mass gap between ν_{Le} and $\nu_{R\mu}$ vanishes by the matter effect at a specific position in the Sun. Consider the case of two Dirac neutrinos, and write them as

$$\psi = \begin{pmatrix} \nu_{eL} \\ \nu_{\mu L} \\ \nu_{eR} \\ \nu_{\mu R} \end{pmatrix} . \tag{10.88}$$

The evolution equation is given by

$$i\frac{d}{dt}\psi = \mathcal{H}\psi , \tag{10.89}$$

where

$$
\mathcal{H} = \begin{pmatrix}
-\frac{\delta m^2}{4E}\cos 2\theta + V_e, & \frac{\delta m^2}{4E}\sin 2\theta , & \mu_{ee}B, & \mu_{e\mu}B \\
\frac{\delta m^2}{4E}\sin 2\theta , & \frac{\delta m^2}{4E}\cos 2\theta + V_\mu , & \mu_{\mu e}B, & \mu_{\mu\mu}B \\
\mu_{ee}^* B, & \mu_{\mu e}^* B, & -\frac{\delta m^2}{4E}, & 0 \\
\mu_{\mu\mu}^* B, & \mu_{\mu\mu}^* B, & 0, & \frac{\delta m^2}{4E},
\end{pmatrix} . \tag{10.90}
$$

Here, $\delta m^2 = m_{\nu_\mu}^2 - m_{\nu_e}^2$, and V_e and V_μ are the potentials felt by the left-handed ν_e and ν_μ, which are given by $V_e = \sqrt{2}G_F(n_e - \frac{1}{2}n_n)$ and $V_\mu = -\frac{1}{\sqrt{2}}G_F n_n$; θ is the intrinsic neutrino mixing angle. From expression (10.90) we find that a $\nu_{eL} - \nu_{\mu R}$ resonance occurs when

$$
V_e = \frac{\delta m^2}{4E}(1 + \cos 2\theta) , \tag{10.91}
$$

or

$$
\left(n_e - \frac{1}{2}n_n\right)_{\text{res}} = \frac{\delta m^2 \cos^2 \theta}{2\sqrt{2}G_F E} . \tag{10.92}
$$

This is similar to the condition for MSW resonance (8.107). The analysis becomes very simple in the limit of $\theta=0$ and $\mu_{ee} = \mu_{\mu\mu} = 0$. The 4×4 matrix of (10.90) reduces to two blocks of 2×2 matrices, and the block that involves ν_{eL} represents the $\nu_{eL} \to \nu_{\mu R}$ transition, which is not suppressed by matter effects [1521, 1522].

The neutrino may also be of the Majorana type. The spin precession then takes place between ν_{eL} and $\nu_{\mu R}^c$ or $\nu_{\tau R}^c$. For

$$
\psi = \begin{pmatrix} \nu_{eL} \\ \nu_{\mu L}^c \end{pmatrix} , \tag{10.93}
$$

the Hamiltonian is

$$
\mathcal{H} = \begin{pmatrix}
-\frac{\delta m^2}{4E}\cos 2\theta + V_e, & \mu_{e\mu}B \\
\mu_{\mu e}^* B, & \frac{\delta m^2}{4E}\cos 2\theta + \overline{V}_\mu ,
\end{pmatrix} , \tag{10.94}
$$

where $\overline{V}_\mu = -V_\mu$.

One may proceed with an analysis in a way similar to the MSW effect, but information about the profile of the magnetic field inside the Sun is missing.[3] Nevertheless, one may consider the following scenario for the effect on solar

---

[3] The generation of a magnetic field in the Sun is a well-known unsolved problem. The basic idea is to assume a dynamo, with which amplification of the magnetic field takes place while the poloidal field is wound up by differential rotation

neutrinos. The magnetic field is supposed to be very small in the radiative zone ($R < 0.71 R_\odot$) since the solar dynamo does not work, e.g., [1531]. The magnetic field would have its maximum (the maximum estimate is about 100 kGauss [1529]) at the bottom of the convective layer and decrease gradually outwards. On the other hand, the position where the neutrino mass gap vanishes is a function of neutrino energy. For low-energy neutrinos this takes place where the matter density is high, and for high-energy neutrinos, where the density is low. If δm_{12}^2 takes the value for which this cancellation takes place for intermediate energy solar neutrinos (^{7}Be, pep, CNO neutrinos) just at around the bottom of the convective layer, cancellation for pp neutrinos occurs in the high density radiative region. Therefore, no magnetic effect is expected on pp neutrinos. The maximum magnetic effect is expected for ^{8}B neutrinos. The energy gap vanishes well outside the envelope, where the density is low and the effect of mass difference is negligible; we expect the conversion of the left-handed neutrinos into the right-handed ones to be maximal: $P_{\nu_{eL} \to \nu_{\mu R}} \sim 1/2$, leading to 50% suppression of ^{8}B neutrino reactions in experiments. For this scenario to happen, the authors of [1532] assume that $\delta m_{12}^2 \sim 10^{-8}$ eV^2 and $B_{\max} \gtrsim 100$ kGauss for $\mu_{e\mu} \simeq 10^{-11} \mu_B$.

If the time variation of the magnetic field that correlates with solar activity is a surface phenomenon, time variation of the neutrino flux should be observed for the highest energy neutrinos. This predicts a more conspicuous time variation in the Kamiokande experiment, which does not see such effects. Therefore, the original motivation to consider spin precession is lost. It only serves to provide a mechanism to suppress the neutrino flux of intermediate and high energies.[4]

10.5.2 Neutrino Radiative Decay and Cosmology

We expected interesting physical effects from neutrino radiative decay in cosmology. The number of relic neutrinos is so huge that the energy stored in

---

to produce a toroidal field (due to $\mathbf{B} \cdot \nabla \omega$ term; called the ω effect), which then erupts to form bipolar magnetic fields by a twisting motion, called the 'α effect' due to $\alpha \mathbf{j} = \nabla \times \alpha \mathbf{B}$ (the $\alpha\omega$ dynamo) [1523]. It had been considered that this mechanism takes place in the bulk of the convective zone [1524], but magnetic buoyancy quickly removes the magnetic flux from the convective zone [1525]. Moreover, concrete models do not agree with observations of the solar surface [1526]. A recently accepted idea is that a dynamo operates in a thin layer at the bottom of the convective zone or underneath it (the convective overshoot region) [1527], where vertical shear $d\Omega/dr$ is inferred from helioseismological data [1528]. With this model a strong magnetic field of the order of 60–160 kGauss is inferred at the bottom of the convective zone [1529]. The magnetic field observed on the surface of the Sun and other stars is $\lesssim 1$–5 kGauss [1530].

[4] There are a few attempts to reconcile the time variation seen in the Homestake detector with its absence at the Kamiokande by assuming a large magnetic moment of neutrinos [1533] or a large η coupling to electrons [1534]. Neither possibility fits low energy phenomenology any longer, however.

massive neutrinos is enormous compared with any astrophysically produced energies in a later epoch. Hence, photonic decay of a tiny fraction of neutrinos would result in significant astrophysical consequences. For this reason, a lot of studies were done of cosmological effects of radiatively decaying neutrinos, when the possibility was still open for neutrinos of mass larger than ≈ 10 eV. The arguments for this subject are now obsolete, as we know that neutrino masses are no more than a few eV and mass differences are even smaller. We present the arguments, however, not as a historical record, but as proto-types of the argument to show how weakly interacting massive particles that undergo radiative decays would cause cosmological effects.

In Fig. 10.13 we show a summary of cosmological (and astrophysical) constraints in the τ_ν–m_ν plane. Constraints are derived from the following considerations: (1) If neutrinos decay with a lifetime $\gtrsim 10^5$ yr, the photons
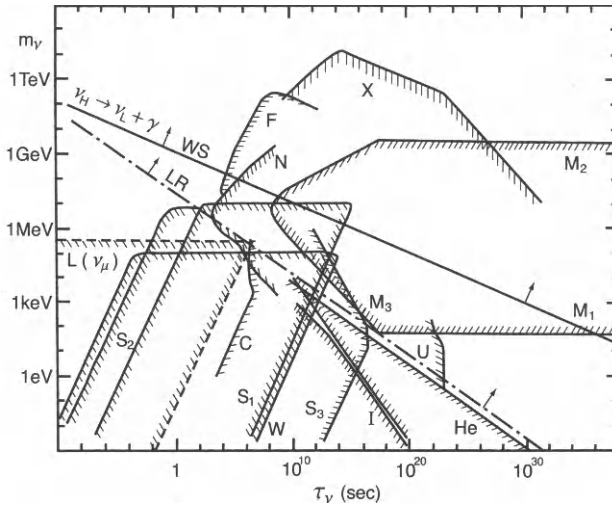
Fig. 10.13. Constraints on radiatively decaying neutrinos. $M_{1,2}$: limit from cosmological mass density [255, 1085, 1087]. This limit applies to any unstable (or stable) neutrinos; X: limit from diffuse X-(γ-) ray radiation [1010]; U: limit from UV radiation [1093,1087,1010,1535–1538]; C: constraint against distortion of the cosmic microwave background radiation [1010, 1093, 1536, 1539]; I: allowed window for U due to interstellar infrared emission [1536]; N: constraint from nucleosynthesis [1093, 1540]; F: limit from photofission of light elements [1541]; S_1: limit from diffuse X rays from supernovae [1542]; S_2: limit from supernova energetics [1542]; S_3: limit from the absence of γ rays from SN1987A [1543]; W: limit from diffuse X rays from white dwarfs [1544]; He: limit against excessive cooling of He star (corresponding to $\mu_\nu = 10^{-11}\mu_B$) [742,1027,740]. L stands for the laboratory limit from a search for $\nu_\mu \rightarrow \nu_e + \gamma$ [1545] (the limit applies only to ν_μ). The two oblique lines represent maximally allowed decay rates in the Weinberg–Salam model [(10.16)] (WS) and in the left–right symmetric model [(10.45)] (LR).

produced in the decay remain unthermalised for there are no free electrons in the universe and yield a diffuse UV, X ray, or γ ray background radiation, depending on neutrino mass [1093,1087,1010,1535–1537] (the recent update is due to the EGRET observation of γ rays [1538]). The observed background radiation sets a limit on lifetime that should be longer than $\approx 10^{23}$ s (denoted by 'U' and 'X' in Fig. 10.13). (2) If the lifetime is 10^5 s $< \tau_\nu < 10^5$ yr, the emitted photons will be thermalised by Compton scattering, while the total number of photons of cosmic microwave background (CMB) is unchanged; hence, they would distort the CMB spectrum [1093,1010,1536,1539], whereas the empirical limit is very strong, $\Delta E/E_{\mathrm{CMB}} < 5 \times 10^{-5}$ [829] (see Sect. 4.6.2, bottom). This constraint is denoted by 'C'. (3) If the lifetime is shorter, high-energy photons are consumed to increase the CMB temperature. If this occurred after the Big-Bang nucleosynthesis ($\sim 10^2$ s), it would disturb the agreement of the nucleosynthesis calculation of n_B/n_γ with the observed elemental abundance. This constraint is indicated by 'N' [1093,1540]. (4) Photons emitted during the nucleosynthesis epoch also disturb element synthesis by fission of nuclei produced ('F') [1541]. If the decay takes place before nucleosynthesis, it is harmless. Additionally, the constraints from the mass density of the Universe, as derived in (5.44), (5.59) and (5.61) are indicated by 'M'.

We have more constraints from astrophysical considerations: (5) Neutrinos are emitted copiously from supernovae and white dwarfs, much more than emission of photons. Therefore, if these neutrinos were to decay with a lifetime shorter than the age of the universe, they would substantially increase the diffuse background photons ('S_1', 'W') [1544, 1542], and (6) if more than 1% of the neutrinos emitted from stellar collapse were to decay before they reached the envelope of the progenitor star, they would drastically alter the energetics of type II supernovae ('S_2') [1542]. (7) Constraints are also available from the absence of excess γ rays emitted from SN1987A ('S_3') [1543]. (8) The constraint against excess cooling of helium stars, as discussed in Sect. 5.1.3, gives a limit displayed as 'He' in the figure.

Neutrinos with a very short lifetime are not constrained by astrophysics or cosmology, but for ν_μ such a case is excluded by laboratory experiments searching for $\nu_\mu \rightarrow \nu + \gamma$ ($\tau/m_{\nu_\mu} > 15.4$ s $\cdot$ eV^{-1} at the 90% CL) [1545].

The limits on neutrino decay lifetime expected from (10.16) (standard model) and (10.45) (left–right symmetric model) are indicated in Fig. 10.13. The line corresponding to (10.45) is practically the fastest radiative decay for which we can make a particle physics model consistent with other laboratory experiments.

10.5.3 Neutrino Magnetic Moment and the Early Universe

We have discussed that ν_L flips into ν_R via scattering off charged particles, if the neutrino has a magnetic (transition) moment (Sect. 5.1.3). The nucle-

osynthesis constraint that effective relativistic degree of freedom at the n/p freeze-out be smaller than 0.25 led to $\mu_\nu < 0.6 \times 10^{-10}\mu_B$.

An interesting result can be derived if the primordial magnetic field would have existed in the early universe (see [1546] for a review).[5] The magnetic field also flips ν_L into ν_R and increases the effective relativistic degree of freedom in the early universe. If the cosmic magnetic field decreases following the canonical power law, $B \propto a^{-2}$ as the universe expands, the nucleosynthesis constraint leads to

$$\mu_\nu < 10^{-15}\mu_B (B_0/10^{-10}\,\mathrm{Gauss})^{-1}, \tag{10.95}$$

where B_0 is the intergalactic magnetic field today [532]. If the primordial magnetic field has the strength to yield $B_0 \approx 10^{-9}$ Gauss today, the constraint on the magnetic moment is $10^{-16}\mu_B$.

---

[5] A primordial magnetic field has often been suggested to provide a seed field for a galactic dynamo. Astrophysically, a more easily acceptable idea for the seed field is that it arises from mass loss of evolved stars.

11 Baryon Asymmetry in the Universe and Neutrinos

11.1 Introduction

The number of baryons in the universe is of an order of magnitude just enough to form galaxies. Human beings would not have existed if there were too many or too few, say, beyond two orders of magnitude either way. In the modern view, the origin of baryons in the universe is ascribed to the action of baryon number (B) violating elementary processes in some early epoch of the universe, rather than is given as an initial condition. Sakharov pointed out that universe's baryon asymmetry may be explained if three conditions cooperate: (i) there is a fundamental process that violates baryon number, (ii) C and CP invariance is violated at the same time, and (iii) there is a deviation from thermal equilibrium acting on the B violating process [1547].

After the advent of grand unification, Ignatiev et al. and Yoshimura found that the first condition, which is not met in the standard theory, is naturally satisfied in addition to C and CP violation [1548, 1549]. The nonequilibrium condition can be satisfied by the delayed decay of heavy particles that are decoupled from thermal equilibrium [1550].[1] The most commonly accepted scenario for this mechanism was to use decays of heavy coloured Higgs bosons [1551]. Asymmetrical pair decays $H^c \rightarrow (\bar{q}\ell, qq)$ and $\overline{H}^c \rightarrow (q\bar{\ell}, \bar{q}\bar{q})$ can produce baryon number of a desired order of magnitude, if CP violation in the Yukawa coupling is of order unity. (For a review, see [1552].)

It was then recognised that standard electroweak theory contains baryon number nonconservation. The conservation of the baryon current is broken by quantum corrections through triangle anomaly, as noted by 'tHooft [259]. The presence of anomaly implies the presence of infinitely many vacua which are classified by a topological property. These vacua are connected by non-perturbative effects via instantons. This tunneling causes baryon number nonconservation. It was thought, however, that this is not a realistic possibility because the process is suppressed by the factor $\exp(-16\pi/g^2)$, which is extremely small. Kuzmin, Rubakov, and Shaposhnikov (KRS) [260, 1553] noted that this suppression does not work at a temperature close to the electroweak phase transition. At high temperature, the Boltzmann barrier

---

[1] The first attempts, where the scattering process $qq \rightarrow \bar{q}\ell$ was considered, however, dismissed the third condition. This was corrected in the later work [1550].

becomes smaller (or vanishing), and the transition that connects different vacua easily takes place. The solution corresponding to this transition is called 'sphalerons.' This process also violates lepton number L, whereas the combination $B - L$ is strictly conserved.

This means that baryon asymmetry that has existed before the electroweak phase transition epoch, such as that generated by GUT, may well be all erased by the action of the KRS effect, unless baryon number is generated with $\Delta B \neq \Delta L$. This erasure applies to baryons generated from SU(5) GUT but also to those from GUTs with SO(10) or higher symmetries. On the other hand, this process opens the new possibility of generating baryon asymmetry without resorting to a GUT scenario.

The first idea is obviously to use this KRS mechanism itself to generate baryon number [1554]. The problem is that, while the KRS mechanism is very efficient for erasing preexisting baryon asymmetry, it is a nontrivial task to find a process to generate it. One possibility is to use the boundary effect of bubbles which could form at the electroweak phase transition. The prerequisite of this scenario is that the electroweak phase transition must be strongly first order. This requires that the Higgs mass be significantly smaller than 80 GeV. The empirical lower limit on the electroweak Higgs mass $m_{\mathrm{H}} > 114$ GeV [320], however, implies that the phase transition cannot be of first order. The remaining possibility of making the transition first order is in the SUSY extension in which the stop mass could be smaller than the top-quark mass. There is another problem that the effect of CP violation expected in the standard model is far too small to produce the desired amount of baryon asymmetry. In SUSY models the possibility remains that one may appeal to complex phases of gaugino couplings to cause large CP violation. With the proviso mentioned here, the production of baryon number at the electroweak phase transition still remains a viable possibility.

The necessity of $B - L$ violation in baryogenesis inspires us to resort to lepton number production in the decay of heavy Majorana neutrinos that violate $B - L$ at a temperature above the electroweak phase transition [261]. Since Majorana neutrino decay violates lepton number, one can satisfy Sakharov's conditions for lepton number in the same way as for baryon number production in the GUT scenario. The difference compared with the GUT scenario is that lepton-number production does not require too large a mass for Majorana neutrinos; so this may take place at a relatively low temperature. Unification of weak and strong interactions is unnecessary. The generated lepton number turns into baryon number under the action of the KRS mechanism. The heavy Majorana mass controls the light neutrino mass, so Sakharov's condition translates to a condition on light neutrino properties.

Another mechanism is proposed within SUSY theories by Affleck and Dine [1555]. In SUSY theories there are many flat directions in the potential that contains scalar quarks and scalar leptons. After SUSY breaking these flat directions acquire soft SUSY-breaking masses of the order of TeV. Since these

masses vanished in the very early universe, expectation values of scalar fields may take large values, of the order of the Planck scale. These scalar fields commence coherent oscillations in the 'flat direction,' when the expansion rate of the universe becomes comparable to their masses. If some baryon-number violating nonrenormalizable operators exist, they induce baryon number creation. This would, in principle, be a viable scenario if the baryons produced are diluted by a factor of 10^{10} by some later entropy production. Recent studies, however, revealed that whether this mechanism actually works is more subtle than was thought. The problem is that nonlinear oscillation of the scalar field excites nontopological soliton modes and these semistable solitons are harmful to cosmology. A way out seems still possible, but it requires a tricky scenario to produce baryon number. Lepton-number production is easier with an Affleck–Dine type scenario, but a strong constraint is placed on the neutrino mass.

11.2 Sphaleron-Induced Baryon-Number Violation

11.2.1 Instanton-Induced Baryon-Number Nonconservation

Baryon- and lepton-number currents are defined by (2.121) and (2.122). It is easy to see that these currents are conserved:

$$\partial_\mu j_{\mathrm{B}}^\mu = 0 \ , \qquad \partial_\mu j_{\mathrm{L}}^\mu = 0 \ . \tag{11.1}$$

Thus, the charges,

$$B = \int d^3x \ j_{\mathrm{B}}^0 \tag{11.2a}$$

and

$$L = \int d^3x \ j_{\mathrm{L}}^0 \ , \tag{11.2b}$$

are also conserved at the classical level.

As discussed in Sect. 2.4, these conservation laws are violated by U(1) anomaly [259]. In the presence of anomaly, (11.1) is modified to

$$\partial_\mu j_{\mathrm{B}}^\mu = \frac{N_f}{32\pi^2} g^2 F_{\mu\nu}^a \widetilde{F}_{\mu\nu}^a \ ,$$
$$\partial_\mu j_{\mathrm{L}}^\mu = \frac{N_f}{32\pi^2} g^2 F_{\mu\nu}^a \widetilde{F}_{\mu\nu}^a \ , \tag{11.3}$$

where

$$F^a_{\mu\nu} = \partial_\mu W^a_\nu - \partial_\nu W^a_\mu + g\epsilon^{abc} W^b_\mu W^c_\nu \ ,$$
$$\widetilde{F}^a_{\mu\nu} = \epsilon_{\mu\nu\lambda\sigma} F^{a\lambda\sigma} \ , \tag{11.4}$$

and N_f is the number of generations. W^a_μ in (11.4) is the SU(2) gauge field $(a = 1\text{--}3)$. Equation (11.3) means that

$$\partial_\mu(j^\mu_B - j^\mu_L) = 0 \tag{11.5}$$

and

$$\partial_\mu(j^\mu_B + j^\mu_L) = \frac{N_f}{16\pi^2} g^2 F^a_{\mu\nu} \widetilde{F}^a_{\mu\nu} \ . \tag{11.6}$$

The Euclidean integral of (11.6) over d^4x gives a change of $B + L$ between $\tau = -\infty$ and $\tau = +\infty$ (here $\tau = it$), as

$$\int d^4x \, \partial_\mu \, j^\mu_{B+L} = \int d^3x \, j^0_{B+L} \Big|_{\tau=+\infty} - \int d^3x \, j^0_{B+L} \Big|_{\tau=-\infty}$$

$$= (B+L)\Big|_{\tau=+\infty} - (B+L)\Big|_{\tau=-\infty}$$

$$= \Delta(B+L) \ . \tag{11.7}$$

On the other hand, the right-hand side of (11.6) is

$$\int d^4x \partial_\mu j^\mu_{B+L} = 2N_f \frac{g^2}{32\pi^2} \int d^4x F^a_{\mu\nu} \widetilde{F}^{a\mu\nu}$$

$$= 2N_f n \ , \tag{11.8}$$

where n is an integer, called the winding number. Therefore,

$$\Delta(B+L) = 2N_f n \ . \tag{11.9}$$

The change in $B + L$ is caused by a tunneling effect due to instantons [259, 1556]; the tunneling rate is

$$\Gamma \sim |e^{-S(\text{instanton})}|^2$$

$$= e^{-16\pi^2/g^2} \ . \tag{11.10}$$

This value is very small (10^{-170}) and this process had not been considered physically relevant. This is true at zero temperature, but the situation is different at high temperatures, as we shall see below. Note that $B - L$ is strictly conserved by the virtue of (11.5).

11.2.2 B Violation in Minkowski Space-Time

We consider the SU(2) model, omitting the U(1) part which does not play an essential role in the argument. We take the Lagrangian

$$\mathcal{L} = -\frac{1}{4}F^a_{\mu\nu} \, F^{a\mu\nu} + |D_\mu\phi|^2 - V(\phi) \, , \qquad (11.11)$$

where

$$D_\mu\phi = (\partial_\mu - \frac{ig}{2}\tau^a \, W^a_\mu)\phi \, , \qquad (11.12)$$

and

$$V(\phi) = \lambda\left(\phi^\dagger\phi - \frac{1}{2}v^2\right)^2 \, , \qquad \lambda > 0 \, , \qquad (11.13)$$

with ϕ an SU(2) doublet. By adopting the gauge for which $W^a_0 = 0$, (11.11) is written

$$\mathcal{L} = \frac{1}{2}(\dot{W}^a_i)^2 - \frac{1}{4}F^a_{ij} \, F^a_{ij} + |\dot{\phi}|^2 - |D_i\phi|^2 - V(\phi) \, . \qquad (11.14)$$

Using canonical variables,

$$\pi_{Wi} = \frac{\delta\mathcal{L}}{\delta\dot{W}_i} = \dot{W}_i \, ,$$

$$\pi_\phi = \dot{\phi}^* \, , \qquad \pi_{\phi^*} = \dot{\phi} \, , \qquad (11.15)$$

the Hamiltonian density is given by

$$\begin{aligned}
\mathcal{H} &= \pi_{W_i}\dot{W}_i + \pi_\phi\dot{\phi} + \pi_{\phi^*}\dot{\phi}^* - \mathcal{L} \\
&= \frac{1}{2}(\dot{W}_i)^2 + |\dot{\phi}|^2 + \frac{1}{4}F^a_{ij} \, F^a_{ij} + |D_i\phi|^2 + V(\phi) \, .
\end{aligned} \qquad (11.16)$$

The vacuum solution is given by

$$\begin{aligned}
\dot{W}^a_i &= 0, & \dot{\phi} &= 0, \\
F_{ij} &= 0, & D_i\phi &= 0, & V(\phi) &= 0 \, .
\end{aligned} \qquad (11.17)$$

$F_{ij} = 0$ means that $W^a_i(\mathbf{x})$ is given by a pure gauge function, i.e., the solution is

$$\widehat{W}_i(\mathbf{x}) \equiv W^a_i\tau^a = -\frac{2i}{g}\partial_i g(\mathbf{x}) \cdot g^{-1}(\mathbf{x}) \, ,$$

$$\phi(\mathbf{x}) = \frac{v}{\sqrt{2}}g(\mathbf{x})\begin{pmatrix} 0 \\ 1 \end{pmatrix} \, , \qquad (11.18)$$
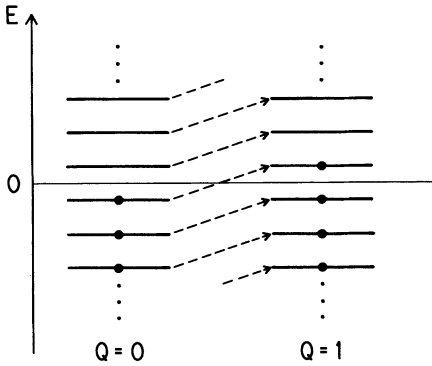
Fig. 11.1. Fermion energy levels for two states with different topological numbers, showing that the state with $Q = 1$ has unit baryon number.

where $g(\mathbf{x})$ is an element of the SU(2) group and represents a mapping from the three-dimensional sphere S^3 to SU(2). Because

$$\pi_3(\mathrm{SU}(2)) = Z, \tag{11.19}$$

the function $g(\mathbf{x})$ is classified by a topological number [1557,1556]: the vacuum is classified into topologically distinct classes, labeled by the Chern–Simons charge,

$$Q = \frac{1}{24\pi^2} \int d^3x \; \epsilon^{ijk} Tr(\partial_i g \cdot g^{-1} \partial_j g \cdot g^{-1} \partial_k g \cdot g^{-1}), \tag{11.20}$$

which takes an integer.

   In the presence of fermions the zero-energy level changes when Q changes; this causes baryon-number violation [1558]. Let us suppose that all levels with $E < 0$ ($k = -1, -2, ...$) are filled (Dirac sea) for $Q = 0$. This may be defined as a $B = 0$ state. The change into $Q = 1$ causes the zero-energy level to come between $k = -1$ and $k = -2$ in the original level scheme. This means that the state with $Q = 1$ has $B = 1$ (see Fig. 11.1).

   In reality, we can see from (11.9) that the change in topology by one unit ($\Delta Q = n = 1$) causes a change in $2N_f$ in $B + L$, while conserving $B - L$. The level crossing is associated with the creation of $3N_f$ quarks and N_f leptons, i.e., the selection rule is $\Delta B = \Delta L = N_f \Delta Q$.

11.2.3 Sphalerons

Klinkhammer and Manton [1559] found a static, classical, saddle-point solution that connects the $Q = 0$ state with the $Q = 1$ state. The field equations derived from (11.14) are

$$(D_i F_{ij})^a = \frac{i}{2} g[\phi^\dagger \tau^a (D_j \phi) - (D_j \phi)^\dagger \tau^a \phi],$$

$$D_i^2 \phi = 2\lambda \left(\phi^\dagger \phi - \frac{1}{2} v^2 \right) \phi. \tag{11.21}$$

The solution was found under the assumption that W_i^a and ϕ take the form

$$W_i^a = \frac{2i}{g} f(r) \left(i\varepsilon_{iaj} x_j \frac{1}{r^2} \right) ,$$

$$\phi = \frac{v}{\sqrt{2}} h(r) \, i\frac{\boldsymbol{\tau}\mathbf{x}}{r} \begin{pmatrix} 0 \\ 1 \end{pmatrix} . \tag{11.22}$$

The behaviour of W and ϕ is displayed as a function of r in Fig. 11.2. This
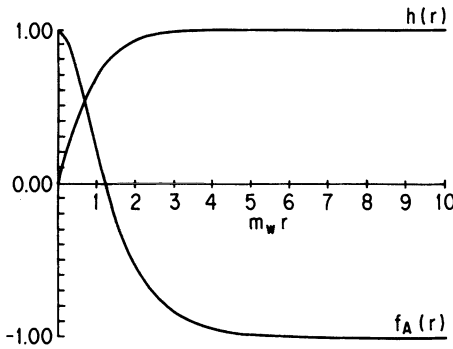
Fig. 11.2. The functions $f_A(r)$ and $h(r)$ for the sphaleron.

solution is called a 'sphaleron.' With (11.16) the mass of the sphaleron is calculated as

$$M_{\mathrm{sph}} = c \, m_W \frac{8\pi}{g^2} , \tag{11.23}$$

with c varying from 1.6 (for $\lambda \simeq 0$) to 2.7 (for $\lambda \to \infty$). The solution has a topological charge of $1/2$.

At a finite temperature the transition from the $Q = 0$ to $Q = 1$ state takes place across the potential barrier by thermal fluctuations with a factor $\exp(-M_{\mathrm{sph}}/T)$. The sphaleron corresponds to the solution representing the top of the barrier.[2] The transition crossing over this barrier is not suppressed at a high temperature $T \gtrsim M_W$ [260].

11.2.4 The Rate of the B-Violating Process

The transition probability can be calculated with the aid of Langer's theory [1560] for the transition between two degenerate ground states. The transition rate (in the entire volume) is given by

$$\Gamma = [NV]T \, e^{-\Delta F/T} \, e^{-M_{\mathrm{sph}}/T} , \tag{11.24}$$

---

[2] $\sigma\phi\alpha\lambda\varepsilon\rho\sigma\varsigma$ means 'ready to fall.'

where ΔF is the free-energy contribution from excitations around the sphaleron solution, $\Delta F =$ (free energy at sphaleron) − (free energy at vacuum), NV is the product of the volume and the normalisation factor arising from the zero mode in the sphaleron background, and is given by

$$NV = \Pi_A \left(\frac{N_A T}{2\pi} \right)^{1/2} \Omega_A . \tag{11.25}$$

Here, Ω_A is the volume for the zero mode (e.g., $\Omega_A = V$ for the translational mode, $8\pi^2$ for the rotational mode), and N_A is the adopted normalisation for the wave function of the zero mode, $\langle \phi_A | \phi_A \rangle = N_A$. Affleck extended this to quantum theory and obtained [1561]

$$\Gamma = \frac{\omega_-}{\pi T} \, \text{Im} \, \mathcal{F}_{\text{sp}} , \tag{11.26}$$

where ω_- is the energy (imaginary) of the unstable mode around the sphaleron and $\text{Im}\mathcal{F}_{\text{sp}}$ is the imaginary part of the free energy of the sphaleron contribution,

$$\text{Im} \, \mathcal{F}_{\text{sp}} = \frac{NV}{4\beta \sin \left(\frac{1}{2}\omega_-/T \right)} e^{-\Delta F/T} \, e^{-M_{\text{sph}}/T} . \tag{11.27}$$

Applying this formula to our case yields [1562]

$$\Gamma = \frac{T\omega_-}{m_W(T)} \left(\frac{\alpha_w}{4\pi} \right)^4 (NV) \left[\frac{2m_W(T)}{\alpha_w T} \right]^7 \kappa e^{-M_{\text{sph}}(T)/T} , \tag{11.28}$$

where $\alpha_W = g^2/4\pi$,

$$(NV) = (NV)_{\text{trans}} \cdot (NV)_{\text{rot}} \approx 5 \times 10^4 T^3 V , \tag{11.29}$$

and $\kappa \sim O(1)$ is the determinant of the nonzero modes near the sphaleron [1563]; ω_- is a known quantity.

The most important part in (11.28) is the Boltzmann factor where $M_{\text{sph}}(T)$ and $m_W(T)$ are T-dependent. A numerical evaluation shows that at a temperature T of 100 GeV $\lesssim T \lesssim T_c$ (T_c is the temperature for the electroweak phase transition, above which $m_W(T) = 0$), Γ becomes faster than the expansion rate $\dot{a}/a$ of the universe, i.e., this baryon-violating process comes to equilibrium.

For $T > T_c$ it is not obvious what takes places since the sphaleron configuration does not exist and the semiclassical treatment fails. On the other hand, there is no apparent reason for $B + L$ violation to be suppressed. In fact, it has been shown that $B + L$ violation takes place at a high temperature with the rate (per unit volume) proportional to $\gamma = \alpha_W^4 T$ [1564]. This dependence is understood roughly as follows. The change of baryon number per unit time per unit volume is given by $\gamma \sim (\Gamma/V)(1/n_F)$, where V is the volume and n_F is the density of fermions which is proportional to $\sim T^3$. Γ/V is

evaluated by the integral, but roughly speaking, $\Gamma \sim \alpha_W T$, and V is of the order of the Compton wave length cubed of the effective W boson mass at high temperature $M_W \sim \alpha_W T$, i.e., $V^{-1} \sim (\alpha_W T)^3$; one then finds $\Gamma/V \simeq \kappa(\alpha_W T)^4$. Arnold et al. [1565] pointed out, however, that the rate of $B + L$ violation is suppressed by damping effects in the plasma and the $B + L$ violating processes become slower by an extra factor of α_W than the rate based on the scaling argument. Namely, $\Gamma/V \simeq \kappa\alpha_W^5 T^4$.

Computer simulations on the lattice [1566, 1567] confirmed this result. The transition rate is given approximately by

$$\frac{\Gamma}{V} \simeq (25 \pm 2)\alpha_W^5 T^4 . \tag{11.30}$$

(Numerically, this is not inconsistent with earlier results of $\alpha_W^4 T^4$ [1568, 1569].) From (11.30) we find that

$$\gamma \sim 2 \times 10^2 \times \alpha_W^5 T . \tag{11.31}$$

This is larger than the expansion rate of the universe (4.178), $\gamma_{\exp} \equiv \dot{a}/a \simeq 17T^2/m_{\mathrm{pl}}$, for

$$T \lesssim \frac{200}{17}\alpha_W^5 m_{\mathrm{pl}} \simeq 1.4 \times 10^{12}\ \mathrm{GeV}, \tag{11.32}$$

using $\alpha_W \simeq 1/40$.

The result described here does not conflict with the conclusion by Gross et al. [1454], who claimed that the instanton effect is suppressed at finite temperatures. What causes the effect here is classical thermal fluctuations, not quantum tunneling described by instantons.

The important conclusion is that neither baryon number nor lepton number is conserved under the action of sphalerons. The only conserved quantity is $B - L$. Starting from an arbitrary initial state, what is left after the action of sphalerons can be seen in the following way. When the sphaleron action is in equilibrium, we have a relation among particles i with chemical potentials μ_i, such that

$$N_{\mathrm{f}}(\mu_{u_L} + 2\mu_{d_L}) + \sum_{i=1}^{N_f} \mu_{\nu_L^i} = 0 . \tag{11.33}$$

In addition, above the critical temperature of the electroweak phase transition, the sum of electromagnetic charge (Q) and that of the third component of weak isospin (T_3) must vanish, i.e.,

$$Q = 2N_f(\mu_{u_L} + \mu_{u_R}) - N_f(\mu_{d_L} + \mu_{d_R})$$
$$- \sum_i (\mu_{\ell_L^i} + \mu_{\ell_R^i}) - 4\mu_W - 2N_{\mathrm{H}}\mu_{\mathrm{H}^-} = 0 , \tag{11.34}$$

$$T_3 = \frac{3}{2}N_f(\mu_{u_L} - \mu_{d_L}) + \frac{1}{2}\sum_i(\mu_{\nu_L^i} - \mu_{\ell_L^i})$$
$$- 4\mu_W - N_H(\mu_{H^0} - \mu_{H^-}) = 0 . \tag{11.35}$$

The equilibrium relations also demand that

$$\mu_{H^-} = \mu_{H^0} + \mu_W ,$$
$$\mu_{d_L} = \mu_{u_L} + \mu_W ,$$
$$\mu_{\ell_L^i} = \mu_{\nu_L^i} + \mu_W ,$$
$$\mu_{u_R} = -\mu_{H^0} + \mu_{u_L} ,$$
$$\mu_{d_R} = \mu_{H^0} + \mu_{d_L} ,$$
$$\mu_{\ell_R^i} = \mu_{H^0} + \mu_{\ell_L^i} . \tag{11.36}$$

From (11.33)–(11.36) we obtain [1564, 1570]

$$\Delta B_f = \frac{8N_f + 4N_H}{22N_f + 13N_H}\Delta(B - L)_i , \tag{11.37}$$

where $\Delta(B-L)_i$ is the initial value of $B-L$, ΔB_f is the final baryon number, and N_H is the number of Higgs doublets. This means that if $\Delta(B - L) = 0$ initially, no baryons remain after the action of sphalerons; for instance, since SU(5) GUT baryogenesis respects $B - L$, the generated baryon number is all erased by the sphaleron effect above the electroweak energy scale.[3]

See [1573] for a general review of sphaleron-induced baryon number non-conservation.

11.2.5 Constraints on $B - L$ Violating Interactions

If some interactions that violate $B - L$ come into thermal equilibrium at the temperature where sphaleron action is effective, the combined effects erase all preexisting baryon- and lepton-number excess in the universe. The presence of baryon asymmetry today requires that such erasure should not have taken place. This requirement leads to constraints on $B - L$ violating interactions [1574].

The simplest example is given by the dimension-five operator discussed in Sect. 6.6,

$$L = \frac{1}{2M}\ell_L\ell_L\phi\phi , \tag{11.38}$$

---

[3] It is argued that a small amount of baryon number excess survives sphaleron-induced processes even if $\Delta(B - L) = 0$, if one takes account of the charged lepton mass [1571]. This effect, however, is very small ($< 10^{-6}$), and is negligible in any case. See also [1572].

which violates L by two units. The interaction (11.38) causes $\ell_L + \phi \rightarrow \bar{\ell}_L + \phi^\dagger$ scattering with the cross section

$$\sigma(\ell_L + \phi \rightarrow \bar{\ell}_L + \phi^\dagger) \simeq \frac{1}{\pi}\left(\frac{1}{2M}\right)^2, \qquad (11.39)$$

where masses of the particles are neglected. The rate of this lepton-number-violating process is

$$\Gamma_{\Delta L \neq 0} \simeq \langle \sigma n_\phi \rangle$$
$$\simeq 0.12 \times \frac{1}{4\pi}\frac{T^3}{M^2}, \qquad (11.40)$$

where $n_\phi = [\zeta(3)/\pi^2]T^3$ is the number density of ϕ particles at temperature $T \gg m_\phi$. The condition under which this process does not come into thermal equilibrium at temperature T_1 is

$$\Gamma_{\Delta L \neq 0}(T_1) < \gamma_{\exp} \simeq 17 T_1^2/m_{\rm pl}, \qquad (11.41)$$

which leads to

$$M > 0.8 \times 10^{14} \left(\frac{T_1}{10^{12}\,{\rm GeV}}\right)^{1/2}\,{\rm GeV}. \qquad (11.42)$$

In [1574] T_1 was conservatively taken as the electroweak energy scale. The authors of [1570, 1575, 1576] extended it to 10^{12} GeV [see (11.32)], the temperature below which the $B + L$ violating transition becomes faster than the expansion rate $\gamma_{\exp}$ of the universe.

Since the neutrino mass is given by $m_\nu = \langle\phi\rangle^2/M$, (11.42) leads to a constraint on m_ν as [1574,1570,1575,1576]

$$m_\nu < 0.8\,{\rm eV}\left(\frac{10^{12}\,{\rm GeV}}{T_1}\right)^{1/2}. \qquad (11.43)$$

If no mechanisms generate baryon asymmetry below $T \simeq 10^{12}$ GeV, T_1 is taken as 10^{12} GeV and (11.43) strongly constrains neutrino mass. Alternatively, some $B - L$ violation process would give rise to a $B - L$ number excess, once the out-of-equilibrium condition happens to be satisfied. Then, T_1 must be taken as that temperature, and the constraint becomes weaker.[4] If baryon

---

[4] Some other reasons to truncate T_1 on a smaller energy scale are also discussed. For instance, the authors of [1577] argued in the context of SUSY theories that chiral gaugino charges inhibit erasure of baryon/lepton asymmetry above the effective SUSY-breaking scale $\approx 10^8$ GeV.

asymmetry is generated at the electroweak transition, the constraint reduces to $m_\nu < 50\,\text{keV}$ which is the original limit given in [1574]. In Sect. 11.5 we discuss the Affleck–Dine scenario, in which a very large amount $(n_B/n_\gamma \approx 1)$ of baryon number is supplied to the thermal bath at a temperature 100–0.1 TeV. With this scenario the constraint disappears if the baryon number supply happens at $T \lesssim 1\,\text{TeV}$ because erasure by a factor of $\Gamma t \approx 10^{10}$ would just bring the baryon number to the empirically desired value[5]. (If $T < 1\,\text{TeV}$, the erasure is not sufficient and we must invoke some other mechanism for further dilution of baryon number.)

The argument can be extended to the case that involves any $B - L$ violating operators [1575]. Consider the interaction via a nonrenormalisable effective operator of dimension $D = 4 + n$,

$$\mathcal{L}_D = \frac{O_D}{M^n} . \tag{11.44}$$

The rate of interactions induced by (11.44) is

$$\Gamma_D(T) \sim \frac{T^{2n+1}}{M^{2n}} . \tag{11.45}$$

If we impose

$$\Gamma_D(T) \lesssim \gamma_{\exp}(T) \tag{11.46}$$

to avoid thermal equilibrium of the $B - L$ violating process, we have the condition that

$$M^{2n} \gtrsim 0.06 m_{\text{pl}} T^{2n-1} . \tag{11.47}$$

If we set $T \approx 10^{12}\,\text{GeV}$ again, we obtain

$$M \gtrsim 10^{9/n} T^{1-1/2n} \approx 10^{12+3/n}\,\text{GeV} . \tag{11.48}$$

If we apply this constraint to the $\Delta B = 2$ interaction that causes $n - \bar{n}$ oscillation $(D = 9)$ [1580],

$$M \gtrsim 10^{12.6}\,\text{GeV} . \tag{11.49}$$

The null results of n–$\bar{n}$ oscillation, $\tau_{n\bar{n}} \gtrsim 8.6 \times 10^7$ s (at a 90% confidence level) from a free neutron experiment [1581], or $> 1.2 \times 10^8$ s from bound neutrons

---

[5] In this case isocurvature (isothermal) baryon fluctuations [1578], which are usually difficult to realise, may be generated [1579]. The desire was to understand cosmic structure formation without the aid of dark matter. However, no models were constructed that are consistent with CMB observations.

of ^{16}O and ^{56}Fe in nucleon decay experiments, with the aid of a calculation of the nuclear suppression factor [1582], give

$$(M)_{\Delta B=2} \gtrsim 2 \times 10^6 \text{ GeV} . \tag{11.50}$$

This means that if $n - \bar{n}$ oscillation were observed at the level of the present experimental limit, condition (11.47) requires that the temperature of baryogenesis T satisfies

$$T \lesssim 10^{5.0} \text{ GeV} . \tag{11.51}$$

11.2.6 Electroweak Baryogenesis

It would be most attractive if baryon number could be produced naturally during the electroweak phase transition without introducing any additional mechanisms [1554, 1583]. For this to happen, this transition must be first order to fulfill the out-of-equilibrium condition. One promising possibility is to resort to bubble formation during the strong first-order phase transition [1584].

Consider quarks that go through the wall (Higgs fields) of bubbles. Under C and CP violation in the Yukawa coupling, a left-handed quark and its charge conjugate have different transmission and reflection probabilities through the wall. This causes, say, a number of q_L larger than that of q_L^c in front of the wall, and the opposite behind the wall. This apparent disparity in baryon number is compensated for by the opposite disparity of right-handed quarks, so that there is no net baryon asymmetry at this stage. The action of sphalerons changes this situation. In the epoch of bubble nucleation, the low-temperature phase is realised inside the bubble, while the high-temperature phase persists outside the wall. The sphaleron that acts on left-handed quarks outside the wall erases baryon asymmetry in left-handed quarks, whereas that of right-handed quarks remains intact. This creates net baryon asymmetry. If the system were in a static state, this asymmetry is further erased by the combined action of the helicity flip of q_L to q_R caused by the Higgs interaction and the sphaleron effect. If, however, the wall expands and passes through the domain sufficiently fast, compared to the rate of the helicity flip, the baryon number created outside the wall is frozen at that value because sphaleron action does not work inside the bubble.

For this scenario to work, the electroweak phase transition must be of strong first order [1554, 1583]. This requires that the mass of the Higgs scalar be smaller than a critical value [1584, 1585]. The most reliable result on the critical mass obtained so far is that from a lattice simulation for four-dimensional theory, which shows that the electroweak phase transition turns into second order above the Higgs mass $m_\phi = 73.3 \pm 6.4$ GeV [1586] (see also [1587] for earlier work). This result nearly agrees with the value obtained by perturbative calculations, including two-loop [1588, 1589], although

perturbation theory breaks down for a Higgs mass larger than m_W because of infrared singularities.[6] This critical value is compared with the empirical limit on the Higgs mass obtained at LEP ($m_\phi > 114\,\text{GeV}$) [320]. Therefore, it is unlikely that the electroweak phase transition is of first order within the standard model.

Addition of an extra scalar particle may somewhat relax this constraint [1590]. The most interesting case is seen in the supersymmetric extension of the standard model, where we have two Higgs particles (see Sect. 9.3.2). It has been pointed out by perturbative calculations [1591] that the electroweak phase transition could be of first order if the stop mass is smaller than the top mass, so that the Coleman–Weinberg effective potential is dominated by bosonic contributions. The constraint derived on the lighter Higgs mass is $m_\phi < 100 - 115\,\text{GeV}$ for the phase transition to be of first order.[7] There may be a narrow window consistent with the current empirical limit on the Higgs mass in the minimal supersymmetric standard model, $m_h > 91\,\text{GeV}$ [320].

One more important condition is whether CP violation is sufficiently large to produce the required asymmetry. It has been known that CP violation caused by the Kobayashi–Maskawa matrix is too small because it appears only in higher order (g^{12}) loop diagrams where all three generations contribute though Higgs couplings. A typical value of CP asymmetry is 10^{-20}, far too small to explain the empirical value by a huge factor of 10^{-10} [1554, 1594].[8] This means that CP violation observed in kaon or B meson physics is *irrelevant* to that responsible for baryon asymmetry (unless it fails to fit KM phenomenology). We need a CP asymmetry factor at least of the order of 10^{-8}. It has been pointed out that there is a possibility of enhancing CP violation in the supersymmetric extension using the phase in gaugino couplings. Some authors argued that the maximum size of baryon asymmetry in such a model is consistent with the required value [1592]. For detailed calculations, see [1595]. Provided that all necessary conditions discussed here are satisfied, one still needs a dynamical calculation for the nucleation and evolution of bubbles, in order to verify the scenario.

---

[6] One-loop results receive an $O(100\%)$ correction from two-loop contributions, and the perturbation is invalidated beyond two loop due to infrared singularities. For this reason, the validity of the perturbative results is not clear.

[7] Quiros obtained $m_\phi < 115\,\text{GeV}$ [1592] from an effective potential analysis, and Csikor et al [1593] obtained $m_\phi < 103 \pm 4\,\text{GeV}$ from a 4-D numerical simulation of an effective theory that contains particles appearing in the minimal supersymmetric standard model.

[8] If standard theory would give a first-order phase transition and everything we discussed works at 100% efficiency, the expected baryon asymmetry is $\alpha_W^6 (m_t m_b/m_W^2)^4 \, (m_s m_c/m_W^2)^2 \times(\text{entropy dilution}) \sim 10^{-22} * 10^{-2}$.

11.3 Baryon-Number Production with GUT

In the original scenario of GUT baryogenesis, one attempted to use the heavy gauge bosons X and Y (leptoquarks) [1596], which decay while they decouple from equilibrium. This is called the delayed decay scenario. It was soon realised that this gauge-boson decay does not produce the required baryon asymmetry for the reason that the X and Y boson masses predicted are too low to satisfy the out-of-equilibrium condition (in non-SUSY GUT).[9] The alternative scenario was to use decays of coloured Higgs particles [1551]. If more than two Higgs particles exist, sufficiently large baryon asymmetry can be generated (provided that the KRS effect is switched off).

The essence of the scenario is as follows. Consider SU(5) GUT and suppose two colour-triplet Higgs multiplets $H_c^{(1)}$ and $H_c^{(2)}$ that belong to representation **5** of SU(5). The Yukawa couplings to quarks and leptons are given by

$$\mathcal{L}_{\text{Yukawa}} = h_{ij}^{(k)} f(\mathbf{10}_i) f(\mathbf{10}_i) H^{(k)} + f_{ij}^{(k)} f(\mathbf{5}^*{}_i) f(\mathbf{10}_j) H^{(k)\dagger} \,. \qquad (11.52)$$

The baryon number arises from a disparity between the baryon-number non-conserving decays

$$H_c^{(i)} \to \ell q, \qquad H_c^{(i)} \to \bar{q}\bar{q} \,, \qquad (11.53)$$

and their conjugates,

$$\bar{H}_c^{(i)} \to \bar{\ell}\bar{q}, \qquad \bar{H}_c^{(i)} \to qq \,, \qquad (11.54)$$

where ℓ denotes ℓ_L or e_R and q denotes q_L, d_R, or u_R. The net baryon number produced by pair decay of H_c and $\overline{H}_c$ is given by

$$\epsilon = \frac{\frac{1}{3}\Gamma(H_c \to \ell q) - \frac{2}{3}\Gamma(H_c \to \bar{q}\bar{q})}{\Gamma(H_c \to \ell q) + \Gamma(H_c \to \bar{q}\bar{q})} + \frac{-\frac{1}{3}\Gamma(\overline{H}_c \to \bar{\ell}\bar{q}) + \frac{2}{3}\Gamma(\overline{H}_c \to qq)}{\Gamma(\overline{H}_c \to \bar{\ell}\bar{q}) + \Gamma(\overline{H}_c \to qq)} \,. \qquad (11.55)$$

In order to generate baryon asymmetry, the baryon-number production must take place out of equilibrium. This is realised by the decay that takes place while these particles decouple from equilibrium [1551, 1597], i.e., when the temperature of the universe cools below the mass of decaying particles so that inverse decay is blocked by the Boltzmann factor [1550]. We note, however, that baryon-number generation is *not a direct result of an imbalance* between decay and inverse decay; if the decay of H_c generates $\epsilon > 0$, its inverse

---

[9] In SUSY we have a large enough X and Y boson mass. The lowest order diagram that produces baryon asymmetry needs two coloured Higgs in the loop diagram. The Higgs mass receives a strong constraint from the absence of proton decay; thus baryon asymmetry is too small for the allowed Higgs mass.

decay also generates $\epsilon > 0$ as a result of CPT invariance, as stressed by Dolgov [1598].[10] Under equilibrium, however, the 'produced baryon number' is erased by a nonresonant scattering process that is required by unitarity. When inverse decay is blocked, this balance is violated, and nonzero baryon number results from nonzero ϵ.

The out-of-equilibrium condition is written roughly as

$$\Gamma_{\mathrm{H}}/\gamma_{\mathrm{exp}} \lesssim 1 \,, \tag{11.56}$$

which is satisfied when $T \approx m_{\mathrm{H_c}}$. Here $\Gamma \approx \alpha_{\mathrm{H}} m_{\mathrm{H_c}}$ is the decay rate ($\alpha_{\mathrm{H}} = h^2/4\pi$), and γ_{exp} is given by (4.178) with $g_* \simeq 53$. This condition reads approximately

$$m_{H_c} > \alpha_{\mathrm{H}} \times 7 \times 10^{17}\,\mathrm{GeV} \,. \tag{11.57}$$

A more accurate estimate should resort to numerical integration of the Boltzmann equation for the baryon-number density and the Higgs-particle density. Fry et al. [1599] solved it and gave a fitting formula to the integration for the ratio of the final baryon number to the specific entropy,

$$\frac{k n_{\mathrm{B}}}{s} \simeq 0.5 \times 10^{-2} \epsilon \frac{1}{1 + (3K)^{1.2}} \tag{11.58}$$

for Higgs decays, where

$$K \equiv \frac{1}{2} \frac{\Gamma}{\gamma_{\mathrm{exp}}} \bigg|_{T=m_{H_c}} \tag{11.59}$$

$$\simeq 3.5 \times 10^{17}\,\mathrm{GeV}\,\alpha_H \frac{1}{m_{\mathrm{H_c}}} \left(\frac{53}{g_*}\right)^{1/2} \,. \tag{11.60}$$

Yet to be done is a calculation of ϵ. In the presence of CP violation, the Yukawa couplings have complex phases, but this does not give a disparity between the pair branching ratios: (11.52) alone does not cause the required disparity in partial widths. Let us write the decay amplitude $A = \sum_i g_i F_i(s)$ where g_i and $F_i(s)$ are the effective coupling constant and the amplitude for decay into channel i. The disparity of the pair decay modes in channel i is then proportional to

$$\left|\sum_i g_i F_i(s)\right|^2 - \left|\sum_i g_i^* F_i(s)\right|^2 = i \sum_i \mathrm{Im}(g_i g_i^*) \mathrm{disc}[F_i(s) F_i^*(s)], \quad (11.61)$$

_____

[10] This is a point often misunderstood.

where

$$\text{disc}[G(s)] \equiv G(s + i\epsilon) - G(s - i\epsilon) \tag{11.62}$$

is the discontinuity (imaginary part) of the scattering amplitude and s is the energy (Mandelstam) variable. The required disparity arises only when Yukawa couplings are complex and scattering amplitudes have a nonvanishing dispersive part, i.e., it arises from the interference between a tree and a one-loop rescattered diagram. Figure 11.3 is the simplest diagram. A computation for the decay of $H_c^{(1)}$ [1551, 1600] gives

$$
\begin{aligned}
\epsilon^{(1)} = \frac{1}{8\pi} &[\text{tr}(h^{(1)\dagger}h^{(1)}) + \text{tr}(f^{(1)\dagger}f^{(1)})]^{-1} \\
&\times \text{Im tr}(f^{(1)\dagger}f^{(2)}h^{(1)\dagger}h^{(2)}) \\
&\times \left[F\left(m^2_{H_c^{(2)}}/m^2_{H_c^{(1)}}\right) + G\left(m^2_{H_c^{(2)}}/m^2_{H_c^{(1)}}\right) \right]
\end{aligned}
\tag{11.63}
$$

(similarly for $H_c^{(2)}$). Here, $F(x)$ and $G(x)$ are

$$F(x) \simeq 1 - x\ln\left(\frac{1+x}{x}\right) , \tag{11.64}$$

$$G(x) = \frac{1}{x-1} , \tag{11.65}$$

which represent contributions from vertex and self-energy corrections, respectively.

To estimate the order of magnitude, we take the largest values of $h^{(i)}$ to be $O(1)$ and those of $f^{(i)}$ to be $O(0.1)$ (in parallel with the Yukawa couplings for the t and b quarks $|h_{33}^{(i)}| \simeq 1$ and $|f_{33}^{(i)}| \simeq 0.1$). We then obtain

$$\epsilon^{(1)} \simeq \frac{1}{8\pi} \eta_1 \times 10^{-2}[F(x) + G(x)] , \tag{11.66}$$

where $\eta_1 = \sin\varphi$ with $\varphi = \arg[\text{tr}(f^{(1)\dagger}f^{(2)}h^{(1)\dagger}h^{(2)})]$, the factor representing CP violation, and $x = m^2_{H_c^{(2)}}/m^2_{H_c^{(1)}}$. Adding the contribution from $H_c^{(2)}$
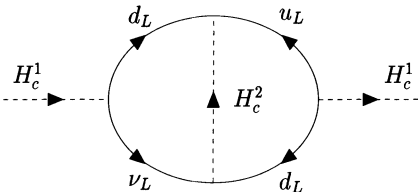
Fig. 11.3. The simplest diagram giving rise to baryon-number generation is coloured Higgs decay in the SU(5) model. The decay rate is given by the discontinuity (imaginary part) of this diagram.

decay, we obtain

$$\epsilon = \epsilon^{(1)} + \epsilon^{(2)} \approx \frac{1}{8\pi}\eta_1 \times 10^{-2} \left[F(x) - F(1/x) + G(x) - G(1/x)\right] , \quad (11.67)$$

where we set $\eta_2 \approx \eta_1$. If $m_{H_c} \simeq 10^{14}\,\text{GeV}$ and $x \simeq 0.5$, we obtain

$$\frac{kn_{\text{B}}}{s} = 0.5 \times 10^{-2} \times \frac{\epsilon}{1 + (3K)^{1.2}} \simeq -2 \times 10^{-9}\eta_1 . \qquad (11.68)$$

The empirical baryon abundance $kn_{\text{B}}/s \simeq (6-9) \times 10^{-11}$ is explained for $\eta_1 \simeq -(0.03\text{--}0.05)$.

The crucial problem with this scenario is that the processes (11.53) and (11.54) conserve $B - L$. So, the baryon number generated from this scenario is all erased by the KRS effect. This is not only a characteristic of SU(5) GUT, but also of any GUTs with higher symmetry since they always have U(1)$_{B-L}$ symmetry as discussed in Sect. 9.3.3.

In the presence of heavy Majorana neutrinos and the Majorana interaction, however, we can save the scenario, so that it leads to baryon-number production with the following modifications [1601]. With SU(5) GUT, this is an ad hoc (but necessary in view of the presence of massive neutrinos) assumption, but in SO(10) this is naturally included. We add to (11.52) the term that contains **1** for ν_R,

$$\Delta\mathcal{L}_{\text{Yukawa}} = +g_{ij}^{(k)} f(\mathbf{1}_i) f(\mathbf{5^*}_j) H^{(k)}. \qquad (11.69)$$

We assume that all heavy Majorana neutrinos, $N_i \equiv \nu_{iR} + \nu_{iR}^c$, are heavier than the colour-triplet Higgs particles, but they are not heavy enough to satisfy the out-of-equilibrium condition. We have seen that decays of coloured Higgs and its conjugate produce baryon and lepton numbers, while $B - L$ is conserved. For a temperature window $10^{12}\,\text{GeV} \le T \le m_{H_c}$, the KRS effect does not work, whereas the heavy Majorana neutrinos N_i's induce lepton-number-violating interactions

$$\frac{1}{2M_i}\ell_i\phi\ell_i\phi , \qquad (11.70)$$

where M_i is the effective mass of N_i in the basis that these interactions are flavour-diagonal. If the process induced by this interaction is in thermal equilibrium, lepton number is no longer conserved, and all L asymmetry ΔL_i generated from the colour-triplet Higgs decay is erased by the scattering process $\ell_i + \phi \to \bar{\ell}_i + \phi^\dagger$. On the other hand, the baryon number produced remains intact and thus satisfies $B - L \ne 0$. When the temperature drops to $T \le 10^{12}\,\text{GeV}$, KRS baryon-number violation takes place, and the ΔB_i produced is converted partially into L asymmetry, but baryon asymmetry remains in the amount of

$$\Delta B_f = 0.35\Delta B_i , \qquad (11.71)$$

if the Majorana interaction has already decoupled from equilibrium by $T = 10^{12}$ GeV. This condition leads to a constraint,

$$m_{\nu_i} < 0.8\text{eV} , \tag{11.72}$$

for $i = 1, 2, 3$ by the argument similar to that presented in Sect. 11.2.5.

In this argument we assumed that $\ell_i + \phi \to \bar{\ell}_i + \phi^\dagger$ is sufficiently faster than the expansion rate above $T = 10^{12}$ GeV. This gives the condition

$$M_i \lesssim 10^{15} \left(\frac{T}{10^{14}\,\text{GeV}} \right)^{1/2} \text{GeV} . \tag{11.73}$$

By setting $T = g_i M_i$ and writing the mass of the right-handed neutrino $M_{R_i} = g_i M_i$ with the Yukawa coupling $g_i \leq 1$, we find that $M_{R_i} < 10^{16}$ GeV is the condition that right-handed neutrinos are in thermal equilibrium. Now, taking $T \simeq m_{\text{H}_c} \leq 10^{15}$ GeV, we obtain a constraint on the neutrino mass as

$$m_{\nu_i} \gtrsim 2 \times 10^{-2}\,\text{eV} , \tag{11.74}$$

for at least one species of neutrinos. The two conditions (11.72) and (11.74) are both satisfied in nature.

When right-handed neutrinos are lighter than coloured Higgs particles, the scenario we describe in the following section produces baryon asymmetry.

11.4 Leptogenesis from Heavy Majorana Neutrinos

There is a simple model for generating $B - L$ asymmetry [261]. We add three families of right-handed Majorana neutrinos ν_R^i ($i = 1$–3) to the standard model. The Lagrangian, which includes ν_R^i, is

$$\mathcal{L}_{N_R} = \overline{\nu^i}_R \not{\partial} \nu_R^i + \frac{M_i}{2} \overline{\nu^{ic}}_R \nu_R^i + h_{ij} \overline{\nu^i}_R \ell_L^j \phi^\dagger + \text{h.c.} \tag{11.75}$$

We take a basis in which the Yukawa coupling $f_{ij} \bar{e}_R^i \ell_L^j \phi$ is diagonal ($f_{ij} = f_i \delta_{ij}$) and assume that the Yukawa coupling h_{ij} involves a CP-violating phase.

The heavy Majorana neutrino, $N \equiv \nu_R + \nu_R^c$, has two decay channels,

$$N \to \ell_L + \bar{\phi} , $$
$$\to \bar{\ell}_L + \phi . \tag{11.76}$$

If CP is violated, a difference emerges between the branching ratios for the two decay channels through the interference term between the tree diagram and the one-loop diagram of N decay (Fig. 11.4). This leads to net lepton-number (equivalently $B - L$) generation. For simplicity, we assume that
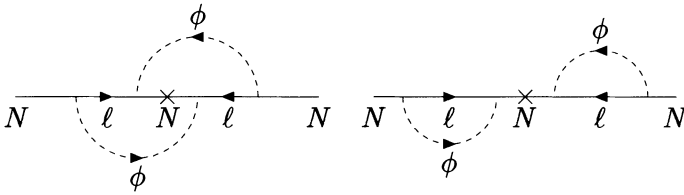
Fig. 11.4. Diagrams leading to lepton-number generation in heavy Majorana neutrino decay. The decay rate is given by the discontinuity (imaginary part) of the diagrams.

$M_1 < M_2 < M_3$ and that the baryon-number generation is predominantly due to the decay of the lightest particle N^1. The magnitude of lepton-number production by the decay of one N^1 is calculated as [261, 1602][11]

$$\epsilon = \frac{\Gamma(N^1 \to \ell_L + \bar{\phi}) - \Gamma(N^1 \to \bar{\ell}_L + \phi)}{\Gamma(N^1 \to \ell_L + \bar{\phi}) + \Gamma(N^1 \to \bar{\ell}_L + \phi)} \tag{11.77}$$

$$\simeq \left(\frac{1}{4\pi}\right) \frac{1}{(hh^\dagger)_{11}} \sum_{j=2,3} \mathrm{Im}(hh^\dagger)^2_{1,j} \left[I(M_j^2/M_1^2) + J(M_j^2/M_1^2)\right] \tag{11.78}$$

with

$$I(x) = x^{1/2}\{1 + (1 + x)\ln[x/(1 + x)]\} \tag{11.79}$$

and

$$J(x) = \frac{x^{1/2}}{1 - x} \, . \tag{11.80}$$

Here $I(x)$ and $J(x)$ denote contributions from the one-loop vertex and self-energy corrections, respectively.

If we assume that h_{33} is the largest entry of h_{ij} and $M_3 \gg M_1$, we obtain

$$\epsilon \simeq \left(\frac{3}{8\pi}\right) |h_{33}|^2 \left(\frac{M_1}{M_3}\right) \delta \, , \tag{11.81}$$

where $\delta = -\sin\varphi'$ with $\varphi' = \arg[(hh^\dagger)^2_{13}]$. We remark that this phase is different from the CP-violating phase appearing in neutrino oscillation (see Sect. 8.11). Using the seesaw formula

$$m_{\nu_3} \simeq \frac{|h_{33}\langle\phi\rangle|^2}{M_3}, \tag{11.82}$$

---

[11] Reference [261] forgot to add the self-energy contribution.

we get

$$\epsilon \simeq \left(\frac{3}{8\pi}\right)\frac{m_{\nu_3}M_1}{\langle\phi\rangle^2}\delta \tag{11.83}$$

$$\simeq 1 \times 10^{-6} \times \left(\frac{M_1}{10^{10}\,\text{GeV}}\right)\delta \ , \tag{11.84}$$

for $m_{\nu_3} \simeq 0.05\,\text{eV}$ and $\langle\phi\rangle \simeq 250\,\text{GeV}$.

The argument is now parallel to the baryon asymmetry generation discussed in Sect. 11.3. The out-of-equilibrium condition is satisfied by the delayed decay scenario. The final lepton excess is given by (11.58)

$$\frac{kn_L}{s} \simeq 0.5 \times 10^{-2}\epsilon\frac{1}{1+(3K)^{-1.2}} \ , \tag{11.85}$$

where K is defined by (11.59) with appropriate changes. An explicit calculation of the Boltzmann equation was carried out and the result confirmed (11.85) [1603–1605]. Assuming that the out-of-equilibrium condition is satisfied, i.e. $K \simeq 1$, we obtain from (11.84)

$$\frac{kn_L}{s} \simeq \delta \times 10^{-9} \times \left(\frac{M_1}{10^{10}\,\text{GeV}}\right). \tag{11.86}$$

This lepton excess is immediately converted into a baryon excess by the KRS effect,

$$n_{\text{B}} = -\frac{28}{79}n_{\text{L}} \ , \tag{11.87}$$

from (11.37) for $N_{\text{f}} = 3$ and $N_{\text{H}} = 1$. If we assume maximal CP violation $\delta=1$, baryon asymmetry in the present universe is predicted as

$$\frac{kn_{\text{B}}}{s} \simeq 3 \times 10^{-10}\delta\left(\frac{M_1}{10^{10}\,\text{GeV}}\right) . \tag{11.88}$$

The observation $kn_{\text{B}}/s \simeq (0.6 - 0.9) \times 10^{-10}$ implies $M_1 \simeq 10^{9-10}$ GeV for $\delta \simeq 0.1 - 1$. This agrees with the numerical integration by Buchmuller and Plumacher [1605].

The argument assumes out-of-equilibrium for decay of the heavy Majorana neutrino N^1. Let us examine what this condition requires. The decay rate of N^1 is given by

$$\Gamma \simeq \frac{1}{8\pi}\sum_{k=1,2,3} h_{1k}h_{k1}^{\dagger}M_1 \ . \tag{11.89}$$

The condition $\Gamma \leq \gamma_{\text{exp}}$ at temperature $T \simeq M_1$ leads to

$$\tilde{\mu}_{\nu_1} \equiv \frac{1}{M_1}\sum_{k=1,2,3} h_{1k}h_{k1}^{\dagger}|\langle\phi\rangle|^2 \lesssim 2 \times 10^{-3}\,\text{eV} \ . \tag{11.90}$$

Note that this form does not appear in the neutrino mass matrix.[12] The limit
(11.90) is consistent with experiment, unless three neutrinos have degenerate
masses. We also note that CP violation that apears in neutrino oscillation has
no direct connexion with CP violation that is relevant to leptogenesis. For
example, leptogenesis may take place even if neutrino oscillation conserves
CP.

In the above argument, we assumed implicitly the equilibrium abundance
of the right-handed neutrino in the early universe. This is clearly satisfied if
there are gauge interactions that act for right-handed neutrinos. If such gauge
interactions do not exist and Lagrangian (11.75) is the only interaction for
the right-handed neutrino, we must check whether right-handed neutrinos are
produced by leptons and Higgs scalars in sufficient abundance. A calculation
by Buchmuller and Plumacher [1605] is shown in Fig. 11.5, where n_B/s is
plotted as a function of $\tilde{\mu}_1$ for $\delta = 1$. The increase in n_B/s for small $\tilde{\mu}_1$ is
due to the increasing production of right-handed neutrinos for a larger Higgs
coupling, and the decrease towards a larger $\tilde{\mu}_1$ represents the suppression
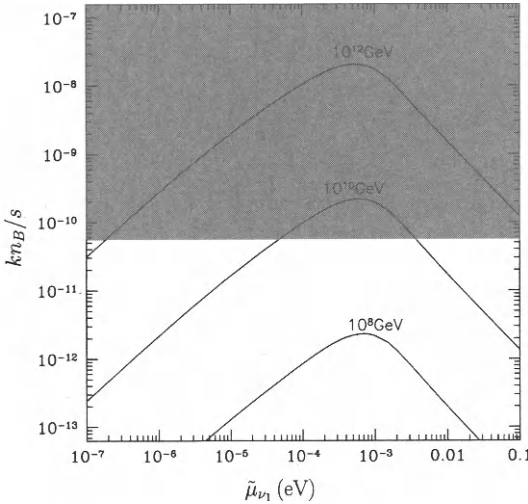
Fig. 11.5. Baryon abundance represented in units of kn_B/s as a function of 'neutrino mass' $\tilde{\mu}_1$ for an assumed right-handed neutrino mass $M = 10^8$, 10^9, and 10^{10} GeV and for $\delta = 1$ [1605]. The allowed region ($\delta \leq 1$) is shown by shading.

---

[12] The expression that enters $\tilde{\mu}_{\nu_1}$ is

$$\tilde{\mu}_{\nu_1} = \left(h_{11} \frac{1}{M_1} h_{11}^{\dagger} + h_{21} \frac{1}{M_2} h_{12}^{\dagger} + h_{31} \frac{1}{M_3} h_{13}^{\dagger} \right) \langle \phi \rangle^2,$$

whereas the terms that appear in the left-handed neutrino mass are

$$m_{\nu_3} = \left(h_{31} \frac{1}{M_1} h_{13} + h_{32} \frac{1}{M_2} h_{23} + h_{33} \frac{1}{M_3} h_{33} \right) \langle \phi \rangle^2.$$

Therefore baryon excess cannot be directly represented by a combination of left-handed neutrino masses.

by the K factor in (11.85). Each curve reaches a maximum at around $\tilde{\mu}_1 \sim 0.6 \times 10^{-3}$, and n_B/s at the maximum is close to the value of (11.88), which indicates that the abundance of right-handed neutrinos from the lepton Higgs interaction via the Yukawa coupling reaches the equilibrium value before out-of-equilibrium decay begins. The figure demonstrates that we have an allowed region where we expect the observed baryon abundance for an appropriate $(\delta < 1)$ value if $M \gtrsim 10^9$ GeV.

The extension to supersymmetric models is straightforward and makes no changes in the conclusion [1605]. In some specific supersymmetric models where symmetry breaking is induced by the supergravity effect, the leptogenesis temperature $T \simeq 10^{9-10}$ GeV would have a marginal conflict with cosmological limits from over-production of gravitinos [1606];[13] the allowed window would be small.

The model of leptogenesis is embedded in many unified models that lead to massive neutrinos, and leptogenesis is studied in many aspects [1608]; see [1609] for a review. Some authors [1610] considered the extension in which heavy Majorana neutrinos are replaced by heavy $SU(2)_L$ triplet scalar particles (see Sect. 6.7 in this connexion). To violate CP invariance, however, two triplet scalar particles are needed, so that the relation to the low energy phenomenology is lost in this model.

Leptogenesis from ν_R oscillation. Akhmedov et al. [1611] proposed a mechanism that generates lepton asymmetry from CP-violating oscillation of medium heavy right-handed neutrinos. They considered the situation that one species of right-handed neutrinos (say, ν_{R3} and $\bar{\nu}_{R3}$) is produced copiously (relative to others) out of equilibrium in charged lepton–quark scattering via Higgs exchanges, and they oscillate into other ν_{Ri} and $\bar{\nu}_{Ri}$ with probabilities $P(\nu_{R3} \nrightarrow \nu_{R3}) \neq P(\bar{\nu}_{R3} \nrightarrow \bar{\nu}_{R3})$. The remaining ν_{R3} and $\bar{\nu}_{R3}$ interact with quarks or leptons to go back to charged leptons and quarks, but the difference between ν_R and $\bar{\nu}_R$ creates lepton asymmetry. (It is assumed that interactions of ν_{R1} and ν_{R2} with matter are sufficiently weak and they go back to charged leptons only after sphaleron actions are ineffective.) It is also crucial that the oscillation time competes with the expansion time.

Since the top quark has the largest Yukawa coupling, the production of ν_{R3} from $t_R\ell_L \to q_L\nu_R$, $\bar{q}_L\ell_L \to \bar{t}_R\nu_R$ ($\bar{q} = \bar{t},\bar{b}$), and $t_R\bar{q}_L \to \bar{\ell}_L\nu_R$ takes place at the rate

$$\Gamma \simeq \frac{9h_t^2}{64\pi^3}h_3^2T, \tag{11.91}$$

where $h_t \simeq 1$ and h_3 is the Yukawa coupling for $\nu_{R3}\ell_{L3}$. ν_R oscillation takes place when the oscillation timescale $\delta M^2/2T$ becomes comparable to γ_{exp},

---

[13] This problem is circumvented if the right-handed neutrino is produced in the reheating processes of inflation [1607].

i.e., $T_{\rm osc} \sim (\delta M^2 m_{\rm pl}/17)^{1/3}$, where we suppose $\delta M^2 \sim M_1^2 \sim M_2^2 \sim M_3^2$ ($\sim M^2$). In a later epoch ($T < T_{\rm osc}$), oscillation becomes too fast, and asymmetry creation is suppressed by averaging. The ν_{R3} number produced relative to lepton density (n_ℓ) in the epoch $T \sim T_{\rm osc}$ is $\approx \Gamma\gamma_{exp}^{-1}$. The fraction of right-handed neutrinos converted to left-handed leptons is also $\approx \Gamma\gamma_{exp}^{-1}$. Thus, lepton asymmetry produced in the first epoch of oscillation is $\Delta n_L/n_\ell \sim (\Gamma\gamma_{exp}^{-1})^2$ for maximal CP violation. Using (11.87), we obtain

$$\frac{kn_{\rm B}}{s} \sim 0.2 \times 10^{-2} (\Delta n_L/n_\ell)^2 \sim 0.2 \times 10^{-2} \left[\frac{9h_t^2 h_3^2}{64\pi^3} \left(\frac{m_{\rm pl}}{17M} \right)^{2/3} \right]^2 . \quad (11.92)$$

Constraints are derived on M from left over baryon asymmetry (Sect. 11.2.5) and the condition that ν_R decays before the epoch of primordial nucleosynthesis:

$$1\,{\rm GeV} < M \ll 100\,{\rm GeV}. \quad (11.93)$$

This means that the epoch of leptogenesis $T \sim 10^6 - 10^7$ GeV. Using $m_{\nu 3} \simeq h_3^2 \langle \phi \rangle^2 / M$, we obtain $M \simeq 10^{15} h_3^2$ GeV for $m_{\nu 3} \simeq 5 \times 10^{-2}$ eV, and $M \ll 100$ GeV means $h_3^2 \ll 10^{-13}$. With this result, (11.92) reads

$$\frac{kn_{\rm B}}{s} \sim 3 \times 10^{-4} (h_3^2)^{2/3} \ll 5 \times 10^{-13} . \quad (11.94)$$

This seems too small to explain the observations, but it is a surprise that such a somewhat 'tricky' scenario produces a rather large baryon asymmetry.

11.5 Affleck–Dine Baryogenesis and Its Variants

In supersymmetric models some combinations of scalar fields do not enter the potential, and thus constitute 'flat directions' of the scalar potential. An example is

$$\phi = \left(\epsilon_{\alpha\beta\gamma} \tilde{u}_{R\alpha}^c \tilde{d}_{R\beta}^c \tilde{d}_{R\gamma}^c \right)^{1/3} , \quad (11.95)$$

where $\tilde{u}_R$ and $\tilde{d}_R$ are the scalar partners of the right-handed u and d quarks and α, β, and γ refer to colour indices. This combination, being colour singlet and electroweak charge singlet, does not enter the potential. This ϕ carries baryon number $-1/3$. It may have a large (of the order of the Planck scale) nonzero expectation value in the very early universe since the potential is flat. If the potential in this direction is lifted by some effective operators in a later epoch, say, by SUSY breaking, baryon number will be created during

coherent oscillation of the ϕ field, which is referred to as the Affleck–Dine (AD) field [1555].

The elements that determine the amount of baryon asymmetry are the initial amplitude of the AD field and the size of nonrenormalizable operators that violate the baryon number, which give the AD field a phase rotation. Assume that there are no scales other than the electroweak scale and the SUSY-breaking scale up to the Planck scale. We expect that the initial amplitude of the AD field is naturally about the Planck scale $m_{\rm pl}$. As in (11.95) we take a flat direction $\phi_{\rm AD}$ (the AD field) composed of scalar antiquark fields, which carry baryon number $-1/3$. When SUSY is broken, the AD field acquires the effective potential,

$$
V = m_{\rm SUSY}^2 \left(a_{11}\phi_{\rm AD}^\dagger \phi_{\rm AD} + a_{30}\frac{\phi_{\rm AD}^3}{m_{\rm pl}} + a_{03}\frac{\phi_{\rm AD}^{\dagger 3}}{m_{\rm Pl}} + a_{22}\frac{\phi_{\rm AD}^{\dagger,2}\phi_{\rm AD}^2}{m_{\rm pl}^2} + ... \right) ,
$$
(11.96)

where $m_{\rm SUSY}$ is the SUSY-breaking scale of the order of $\sim 1\,\mathrm{TeV}$ and $m_\phi = a_{11}^{1/2} m_{\rm SUSY}$ is the mass of the AD field. The terms that involve $m_{\rm pl}$ on the right-hand side represent the nonrenormalizable interactions that turn on upon SUSY breaking. These are the terms that give rise to baryon-number generation.

The evolution of the $\phi_{\rm AD}$ field is described by

$$
\ddot{\phi}_{\rm AD} + 3H\dot{\phi}_{\rm AD} + \frac{\partial V}{\partial \phi_{\rm AD}^\dagger} = 0,
$$
(11.97)

where $H = \gamma_{exp}$. When H decreases to the order of $\phi_{\rm AD}$ mass at $T \sim \sqrt{m_\phi M_{\rm pl}}$, the AD field starts coherent oscillation, and the interaction of higher order terms creates baryon number. Let us now calculate baryon asymmetry. Since the $\phi_{\rm AD}$ field carries baryon charge $-1/3$, the baryon number density $n_{\rm B}$ is written

$$
n_{\rm B} = -\frac{1}{6}i\left(\dot{\phi}_{\rm AD}^\dagger \phi_{\rm AD} - \phi_{\rm AD}^\dagger \dot{\phi}_{\rm AD} \right).
$$
(11.98)

Using (11.97), the evolution of $n_{\rm B}$ is

$$
\dot{n}_{\rm B} + 3Hn_{\rm B} = -\frac{1}{3}m_{\rm SUSY}^2 \mathrm{Im}\left(3a_{03}\frac{\phi_{\rm AD}^{\dagger 3}}{m_{\rm pl}} + 2a_{22}\frac{\phi_{\rm AD}^{\dagger 2}\phi_{\rm AD}^2}{m_{\rm pl}^2} + ... \right).
$$
(11.99)

Motion of $\phi_{\rm AD}$ in the phase direction, which is initiated by the relative phase between a_n and the initial amplitude of $\phi_{\rm AD}^0$, generates baryon number. Baryon number is predominantly generated just after AD field oscillation begins at time $t_{\rm osc} \simeq 1/H_{\rm osc} \simeq m_\phi^{-1}$ because the amplitude $\phi_{\rm AD}$ is maximum

in that epoch and damps as $\phi_{\mathrm{AD}} \sim t^{-1}$ during oscillation due to the expansion viscosity. Thus, we obtain baryon asymmetry

$$n_{\mathrm{B}} \approx \frac{\delta_{\mathrm{eff}}}{3} \frac{m_{\mathrm{SUSY}}^2}{m_\phi} |\phi_{\mathrm{AD}}^0|^2 \,, \tag{11.100}$$

where $\delta_{\mathrm{eff}} \approx \sin[\arg(a_{03}) - 3\arg(\phi_{\mathrm{AD}})]$ is the effective CP-violating phase, and $|\phi_{\mathrm{AD}}^0| \simeq m_{\mathrm{pl}}$ and $a_n \simeq O(1)$ are assumed. The energy density ρ of the universe is dominated by the ϕ_{AD} field, $\rho_\phi \sim m_{\mathrm{pl}}^2 m_\phi^2$, and thus the ratio n_{B}/ρ_ϕ is constant until ϕ_{AD} decays into light particles. Decay of the AD field produces specific entropy s of radiations such that $\rho_\phi/s = 3T_\phi/4$, where T_ϕ is the reheating temperature after the AD field decays. We thus find

$$\frac{n_{\mathrm{B}}}{s} = \left(\frac{\rho_\phi}{s}\right)\left(\frac{n_{\mathrm{B}}}{\rho_\phi}\right) \simeq \frac{3T_\phi}{4} \frac{\delta_{\mathrm{eff}}}{3} \frac{m_{\mathrm{SUSY}}^2}{m_\phi^3}. \tag{11.101}$$

Since $m_{\mathrm{SUSY}} \approx m_\phi$ and $T_\phi \approx m_\phi$, we obtain $O(1)$ baryon asymmetry unless δ_{eff} is extremely small. Therefore, we must invoke some mechanism that creates huge entropy to dilute the baryon density to the empirical value by a factor of 10^{-10}. The baryon number produced is thermalised in a hot plasma into real baryons at a relatively low temperature $T_\phi \approx 0.1$–1 TeV.

Another problem of the AD scenario concerns the initial condition. Though we have assumed ad hoc that ϕ_{AD} takes a Planck scale value, this is not trivial. If we would prepare an initial condition with inflation models, the large inflaton vacuum energy violates SUSY, which induces for the AD field a SUSY-breaking mass term of the order of the expansion rate of the universe. The induced mass term is usually positive, which rapidly drives the AD field towards the origin during inflation, invalidating the Affleck–Dine mechanism [1612, 1613]. To avoid this problem, we may assume that the AD field has a nonminimal coupling with the inflation field so that the induced mass-square is negative, which allows the AD field to develop a large expectation value [1613].

There is yet another problem recently noted [1614, 1615]. Due to nonlinear modes, coherent oscillation in the flat direction creates nontopological solitons called Q-balls [1616, 1617],[14] and Q-balls carry a dominant amount of baryon numbers created in the Affleck–Dine mechanism. These Q-balls are semistable and decay into light particles in a late epoch, which causes a cosmological overdensity problem. See [1614, 1615] for details.

Affleck and Dine constructed a model within renormalisable classes of the potential, assuming that there are no scales other than electroweak and SUSY-breaking scales. In general, we may have a nonrenormalisable potential

---

[14] Solitons of field theories are classified into topological and nontopological solitons. The stability of nontopological solitons is ensured by the energy conservation law [1618].

that respects supersymmetry, which is suppressed by a factor of $m_{\rm pl}^{-n}$ below the Planck scale [1619]. Furthermore, the effective potential of the form ϕ^{n+4}/M^n ($M < m_{\rm pl}$) may be induced from renormalisable interactions if there is an additional scale, such as a GUT scale. These potentials reduce the range of the flat potential and restrict the initial value of $\phi_{\rm AD}$ to be smaller than the Planck scale. This would reduce the baryon number created, as desired. It turns out, however, that all dimension-five superpotentials (which is the lowest dimensional operator) preserve $B - L$, (except for one that gives rise to lepton production, which we shall discuss in what follows). This means that baryon number generated by such a mechanism is erased by the KRS effect.

Affleck–Dine leptogenesis.   The flat-direction scalar field that is relevant to leptogenesis is [1620]

$$\phi_i = (2\phi_u \tilde{\ell}_i)^{1/2} \,, \tag{11.102}$$

where ϕ_u is the Higgs field that gives the u quark a mass and $\tilde{\ell}_i$ is the charged scalar-lepton of generation i. If there is a Majorana interaction with a right-handed neutrino mass of M_{Ri}, the theory induces a dimension-five operator in superpotential in this direction,

$$W = h_i^2 \frac{1}{2M_{Ri}} \left(L_i H_u \right)^2 \,, \tag{11.103}$$

where $H_u = \phi_u + \tilde{\phi}_u \theta$ and $L_i = \tilde{\ell}_i + \ell_i \theta$ are two relevant superfields and h_i is the Yukawa coupling of right-handed neutrinos. From the superpotential of (11.103), we find $h_i^2/M_{Ri} = m_{\nu_i}/\langle \phi_u \rangle^2$. The potential corresponding to (11.103) is

$$V_F = \frac{h_i^2}{4M_{Ri}^2} |\phi|^6 \,. \tag{11.104}$$

With this potential lepton number is produced when the flat-direction AD field ϕ starts coherent oscillation at $H \approx m_\phi$ upon SUSY breaking. Before SUSY breaking, the value of the AD field is determined by the balance of (11.104) and the expansion rate. It gradually decreases until SUSY is broken and ϕ acquires a mass. After SUSY breaking,

$$\delta V = m_\phi^2 |\phi|^2 + \frac{m_{\rm SUSY}}{8M_R} h^2 \left(a_m \phi^4 + \text{h.c.} \right) \,, \tag{11.105}$$

where the second term is induced because of the presence of (11.103) (we drop subscript i). When the mass sets in and AD field oscillation starts, the amplitude of the AD field has the value of $\sqrt{m_\phi M_R/h^2}$, which we take as the initial condition. We take $m_\phi \approx m_{\rm SUSY} \approx 1$ TeV and $|a_m| \approx 1$.

The calculation of lepton-number production is parallel to that given for the original AD mechanism, with the replacements $V \rightarrow V_{\text{total}} = V_F + \delta V$ in (11.97) and a factor $1/2$ in place of $-1/6$ in (11.98). The right-hand side of (11.99) is now $(h^2 m_{\text{SUSY}}/2M_R)\text{Im}(a_m \phi_0^4 + ...)$, so that the resulting lepton asymmetry is

$$n_L \simeq \frac{h^2 m_{\text{SUSY}}}{2M_R}\text{Im}(a_m \phi_0^4 + \text{h.c.})t \bigg|_{H=H_{\text{osc}}} \approx \delta_{\text{eff}} m_\phi^2 \frac{M_R}{h^2} , \quad (11.106)$$

where $\delta_{\text{eff}} \approx \sin[(4 \arg \phi_0 + \arg a_m)]$ represents a factor from effective CP-violating phases, and we put $m_\phi \approx m_{\text{SUSY}}$, $\phi|_{H=H_{\text{osc}}} \simeq \sqrt{m_\phi M_R/h^2}$, and $t_{\text{osc}} \simeq 1/m_\phi$.

If oscillation of the AD field starts in the radiation-dominated universe, the AD field decays most likely in the radiation-dominated epoch since the density of the AD field $m_\phi^3 M_R$ is small. The temperature T when AD oscillation starts is $T \approx \sqrt{m_\phi m_{\text{pl}}}$, and entropy $s \approx T^3$, so that we obtain

$$\frac{n_L}{s} = \delta_{\text{eff}} \left(\frac{m_\phi}{m_{\text{pl}}}\right)^{1/2} \frac{M_R}{h^2 m_{\text{pl}}} . \quad (11.107)$$

About one-third of this lepton number is converted into baryon number by the KRS effect. For $m_\phi \sim 1\,\text{TeV}$ and $\delta_{\text{eff}} \sim 1$, we get $n_{\text{B}}/s \sim 0.3 \times 10^{-8}(h^{-2}M_R/m_{\text{pl}})$. We obtain the correct baryon abundance for $M_R/h^2 m_{\text{pl}} \sim 0.01$, which means $m_\nu \sim 10^{-3}$ eV.

This argument, however, ignores the thermal effect [1613, 1621, 1622]. For the case that concerns us, $\phi_u \rightarrow u_R^i + \bar{u}_L^i$ is in thermal equilibrium. It is likely that at least first-generation quarks give the ϕ field a thermal mass of the order of $f_1^2 T^2$, where f_i is the usual Yukawa coupling of ith generation quarks and leptons, i.e., the effective mass of the ϕ field reads

$$m_{\text{eff}}(\phi) = m_\phi^2 + f_i^2 T^2. \quad (11.108)$$

For the condition we consider, the second term dominates (as clear from the expression below), and oscillation of the ϕ field begins at $\dot{a}/a = T^2/m_{\text{pl}} \sim f_i T$, i.e., $T_{\text{osc}} \sim f_i m_{\text{pl}}$, $H_{\text{osc}} \sim f_i^2 m_{\text{pl}}$, and $|\phi_{\text{osc}}| \sim (H_{\text{osc}} M_R/h^2)^{1/2}$. We have then, $n_{\text{B}} \simeq f_i^2 m_\phi (M_R/h^2)m_{\text{pl}}$. Since $s \simeq T_{\text{osc}}^3$, we obtain

$$\frac{n_B}{s} = 0.3\frac{1}{f_i}\frac{m_\phi}{m_{\text{pl}}}\frac{M_R}{h^2 m_{\text{pl}}} . \quad (11.109)$$

The condition that ith generation quarks contribute to thermal mass is $f_i|\phi_{\text{osc}}| < T_{\text{osc}}$. Consider the case that only first-generation quarks contribute to thermal mass. The condition is

$$\frac{1}{f_2^2} < \frac{1}{h^2}\frac{M_R}{m_{\text{pl}}} < \frac{1}{f_1^2} . \quad (11.110)$$

This means $10^4 < (1/h^2)M_R/m_{\rm pl} < 10^8$, and hence $n_{\rm B}/s = 0.3 \times (10^{-8} - 10^{-4})$. A realistic value of $n_{\rm B}/s$ is obtained when $M_R/h^2 \approx 10^4 \times m_{\rm pl}$, which is the condition that second-generation quarks do not give thermal mass to the ϕ field. This requires

$$m_{\nu_1} \approx 10^{-9}\,{\rm eV} \ . \tag{11.111}$$

A similar condition is obtained even when second-generation quarks contribute to thermal mass. Virtually the same result is obtained in an inflationary universe [1623]. See [1609] for a review.

11.6 Summary

We have discussed four classes of baryogenesis scenarios. The present status of research may be summarised as follows (see Table 11.1).

(i) Electroweak baryogenesis: This is conceptually the simplest scenario. With non-SUSY models, however, this case is excluded because the empirical lower limit of the Higgs particle indicates that the electroweak phase transition is of the second order. Furthermore, there is no known mechanism to enhance the effect of CP violation. With SUSY models, the possibility is not yet excluded that phase transition is of marginally first order. It is, however, not obvious whether this first-order transition, if any, is strong enough to provide the necessary nucleation of bubbles. There is a mechanism to enhance CP violation to the necessary order using gaugino phases. Dynamical calculations are needed to see whether this mechanism really works. Overall, the possibility seems marginal, but not yet excluded.

(ii) GUT models may generate baryon asymmetry with the proviso that Majorana interactions are present. A significant modification, however, is needed from the original scenario which does not require Majorana interactions. The model requires the right-handed Majorana neutrino mass to be larger than the coloured Higgs mass.

Table 11.1. Status of models of baryogenesis.

Mechanism	SUSY?	Status/requirement
Electroweak	non-SUSY	excluded
	SUSY	marginal
original GUT	non-SUSY/SUSY	does not work
GUT with Majorana int	non-SUSY/SUSY	valid if $10^{-2}{\rm eV} < m_{\nu_3} < 1$ eV
ν_R decay leptogenesis	non-SUSY/SUSY	valid if $\tilde{\mu}_{\nu_1} < 10^{-3}$ eV
AD baryogenesis	SUSY	need large entropy production
		Q-ball problem (?)
AD leptogenesis	SUSY	$m_{\nu_1} \approx 10^{-9}$ eV

(iii) Baryogenesis via leptogenesis from delayed decays of heavy Majorana neutrinos: It is a viable scenario. Two scenarios (ii) or (iii) depend on neutrino masses.

(iv) Coherent oscillation of the scalar field with a baryon-number-violating potential. It seems difficult to make a reasonable model to give an empirical baryon number with the original Affleck–Dine scenario or its modifications. It seems, however, still possible to make a model via leptogenesis with the Affleck–Dine mechanism. A very light neutrino mass is needed for successful prediction of empirical baryon asymmetry, however.

It is interesting to note that successful models can be more easily constructed with the aid of Majorana neutrinos in all cases.

Note Added in Proof

While the manuscript was in production, we have noticed two very important pieces of experimental work concerning the solar neutrino problem.

One is a direct measurement of the neutral-current-induced reaction of ^{8}B solar neutrinos at the Sudbury Neutrino Observatory (SNO). In its first report [235] the SNO group already inferred the neutral-current-induced reaction rate of $\nu + e$ elastic scattering by subtracting the charged-current-induced reaction rate, which was estimated from the measurements of the $\nu_e + d \to e^- + p + p$ reaction. This provided a confirmation of the neutrino oscillation hypothesis at a statistical significance of 3.3σ (Sect. 8.8). In the latest report of the SNO [1624] a direct measurement of the neutral-current-induced reaction, $\nu + d \to \nu + p + n$, was carried out by observing 6.25 MeV γ rays from neutron capture on deuterium. The resulting flux $\phi_\nu(\mathrm{NC}) = 5.09_{-0.43}^{+0.44}(\mathrm{stat.})_{-0.43}^{+0.46}(\mathrm{syst.}) \times 10^6$ cm^{-2}s^{-1} is almost exactly the value predicted by the standard solar model of BP2000: $\left(5.05_{-0.81}^{+1.01}\right) \times 10^6$ cm^{-2}s^{-1}. This is a dramatic demonstration that the neutrino flux inferred from the charged-current reaction rate, $\phi_\nu(\mathrm{CC}) = 1.76_{-0.05}^{+0.06}(\mathrm{stat.})_{-0.09}^{+0.09}(\mathrm{syst.}) \times 10^6$ cm^{-2}s^{-1}, is strongly affected by neutrino oscillation. Figure A.1 shows the electron-neutrino and μ/τ-neutrino fluxes from the Sun obtained from charged- and neutral-current induced reactions on deuterium and from electron scattering: $\phi_{\nu_e} = \phi_\nu(\mathrm{CC})$ and $\phi_{\nu_\mu \nu_\tau} = \phi_\nu(\mathrm{NC}) - \phi_\nu(\mathrm{CC})$. The three estimates converge to a consistent region.

The SNO data of day and night neutrino spectra [1625], together with existing data from other experiments, are used to constrain neutrino mixing parameters. The result selects LMA as the best favoured solution, whereas LOW is marginally allowed only when the error range is extended to 99.73% CL. The SMA is completely ruled out. The maximal mixing is rejected at $\gtrsim 99.97\%$ [1625]. The same conclusion is obtained by independent analyses, although the detailed contours in parameter space and the statistical significance levels somewhat vary depending upon authors [1626]. The parameters of LMA are approximately $\Delta m^2 = (3-18) \times 10^{-5}$ eV^2 and tg$^2\theta = 0.32-0.67$.

The other important advancement is the confirmation of the disappearance of reactor electron antineutrinos at the KamLAND detector, which actively authenticates the LMA solution [1627]. The average distance of 180 km between the power reactors and the Kamioka observatory makes the detector
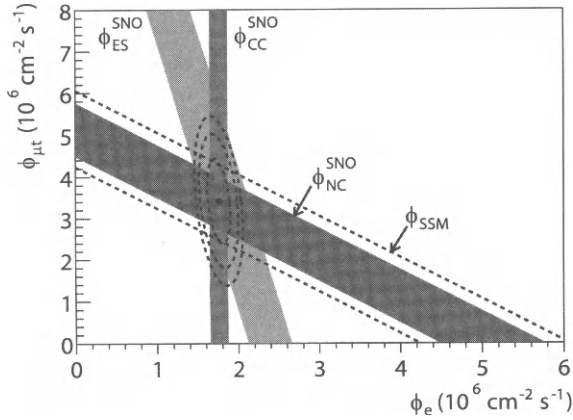
Fig. A.1. Solar neutrino fluxes of μ (and τ) neutrinos versus electron neutrinos observed on Earth. The three bands are estimates from charged- and neutral-current reactions on deuterium (CC and NC, respectively) and from electron scattering (ES) measured at SNO. The region indicated by dotted lines is the prediction of BP2000 standard solar model. After [1624]
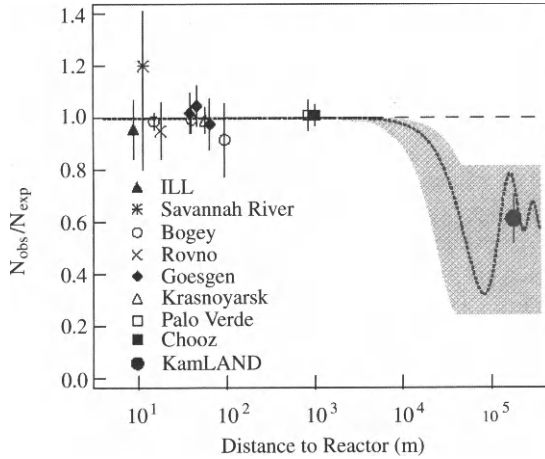
Fig. A.2. Fraction of the measured reactor antineutrino fluxes to those expected with the no-oscillation hypothesis plotted as a function of the reactor–detector distance. The rightmost point is the KamLAND measurement, and the other data points stand for available experiments to date. The expectation for the LMA solution of the solar neutrino problem is shown by shading. After [1627]

just sensitive to neutrino oscillation if the $\nu_e - \nu_{\mu\tau}$ mixing parameters fall in the LMA region. The KamLAND result indicates that the $\bar{\nu}_e$ flux is reduced to 0.611 ± 0.085(stat.)± 0.041(syst.) times the no-oscillation expectation, where the largest entry of the systematic error comes from the uncertainty in the estimate of the detector fiducial volume. Figure A.2 shows a summary of the fraction of the measured antineutrino flux versus expected with the no-oscillation hypothesis as a function of the reactor–detector distance and the rightmost point stands for the KamLAND measurement (the expectation for the LMA solution is shown by shading). The analysis indicates the mass difference squared $\Delta m^2 = \left(6.9{}^{+2}_{-1}\right) \times 10^{-5}$ eV^2, which is located in the middle of the LMA. There is one more solution, though less favoured, which is $\Delta m^2 \simeq 1.5 \times 10^{-4}$ eV^2 allowed at 95% CL. This region is also included in the LMA. The mixing angle is not well determined, but the mass difference squared is sharply determined. Most importantly, this result rejects all solar neutrino solutions other than the LMA by actively observing the signature characteristic of the LMA (see Table 8.3).

The KamLAND experiment also begins to see geophysical neutrino signals, although the group, for the time being, quotes only the upper limit, which corresponds to 110 TW of the terrestrial heat (see Sect. 4.7).

References

1. W. Pauli, Letter to L. Meitner and her colleagues dated 4 December 1930 (letter open to the participants of the conference in Tübingen) (1930), recorded in W. Pauli, *Wissenschaftlicher Briefwechsel mit Bohr, Einstein, Heisenberg u.a.*, Band II (Springer, Berlin, 1985) p. 39. A reference to 'neutrino' is seen in a letter from Heisenberg to Pauli on 1 December 1930: "Zu Deinen Neutronen möchte ich noch bemerken: ...".
2. J. Chadwick, Verh. d. deutschen phys. Ges. **16**, 383 (1914).
3. O. von Baeyer, O. Hahn, Phys. Zs. **11**, 488 (1910). Earlier measurements were done by O. Hahn, L. Meitner, Phys. Zs **9**, 321 (1908); **9**, 697 (1908), but their assumption used to estimate the energy turned out to be incorrect.
4. O. von Baeyer, O. Hahn, L. Meitner, Phys. Zs. **12**, 273 (1911).
5. E. Rutherford, H. Robinson, Phil. Mag. **26**, 717 (1913).
6. C.D. Ellis, Proc. R. Soc. London A **99**, 261 (1921).
7. E. Rutherford, Phil. Mag. **28**, 305 (1914).
8. L. Meitner, Z. Phys. **9**, 145 (1922); **11**, 35 (1922).
9. C.D. Ellis, Proc. R. Soc. London A **101**, 1 (1922); J. Chadwick, C.D. Ellis, Proc. Camb. Phil. Soc. **21**, 274 (1922).
10. C.D. Ellis, W.A. Wooster, Proc. R. Soc. London A **117**, 109 (1927); L. Meitner, W. Orthmann, Z. Phys. **60**, 143 (1930). Meitner was first sceptical about the meaning of the experiment of Ellis and Wooster as to whether γ rays might be missed (Letter from Pauli to Bohr dated 25 April 1929, W. Pauli, Wissenschaftlicher Briefwechsel, op. cit. p. 495), but eventually she was convinced by herself.
11. N. Bohr, in *Convegno di Fisica Nucleare* (R. Accad. d'Italia, Roma 1932), p. 119; J. Chem. Soc. 1932, 349 (Faraday Lectures); earlier reference is seen in a letter from Pauli to Bohr dated 5 March 1929, "... Willst Du den armen Energiesatz noch weiter maltraitieren?" (W. Pauli, Wissenschaftlicher Briefwechsel, op. cit. p. 493).
12. R. de L. Kronig, Naturw. **16**, 335 (1928); W. Heitler, G. Herzberg, Naturw. **17**, 673 (1929); F. Rasetti, Z. Phys. **61**, 598 (1930).
13. W. Pauli, Phys. Rev. **38**, 579 (1931) [Title only].
14. W. Pauli, in *Aufsätze und Vorträge über Physik und Erkenntnistheorie* (F. Vieweg und Sohn, Braunschweig 1961) S. 156.
15. L.M. Brown, Phys. Today, Sept. 1978 issue, p. 23.
16. J. Chadwick, Proc. R. Soc. London (A) **136**, 692 (1932).
17. W. Heisenberg, Z. Phys. **77**, 1 (1932); D. Iwanenko, Nature **129**, 798 (1932).
18. F. Rasetti, in E. Fermi, *Note e Memorie*, ed. by E. Amaldi et al. vol. I. (Academia Naz. dei Lincei, Roma 1962), p. 538.

19. W. Pauli, in *Discussion du Rapport de M. Heisenberg "La Structure du Noyau"* in *Structure et Propriétés des Noyaux Atomiques, Rapports et Discussions du Septième Conseil de Physique*, Brussels, October 1933, ed. by Institut International de Physique Solvay (Gauthier-Villars, Paris 1934), p. 324.

20. E. Fermi, Ricerca Scient. 4(2), 491 (1933); Z. Phys. **88**, 161 (1934); Nuovo Cimento **11**, 1 (1934); the second paper is a German translation of the third one.

21. S. Weinberg, *The Quantum Theory of Fields*, Vol. I (Cambridge University Press, Cambridge 1995).

22. e.g., H.A. Bethe, R.F. Bacher, Rev. Mod. Phys. **8**, 82 (1936).

23. F. Perrin, in *Structure et Propriétés des Noyaux Atomiques, Rapports et Discussions du Septième Conseil de Physique, idem* p. 327; Compt. Rendus **197**, 1625 (1933).

24. G. Gamow, E. Teller, Phys. Rev. **49**, 895 (1936).

25. M. Fierz, Z. Phys. **104**, 553 (1937).

26. E.J. Konopinski, G.E. Uhlenbeck, Phys. Rev. **48**, 7 (1935).

27. B.W. Sargent, Proc. R. Soc. London (A) **139**, 659 (1933).

28. E.J. Konopinski, G.E. Uhlenbeck, Phys. Rev. **60**, 308 (1941).

29. E. Feenberg, K.C. Hammack, Phys. Rev. **75**, 1877 (1949); L.W. Nordheim, Phys. Rev. **75**, 1894 (1949); M.G. Mayer, S.A. Moszkowski, L.W. Nordheim, Rev. Mod. Phys. **23**, 315 (1951).

30. O. Haxel, J.H.D. Jensen, H.E. Suess, Phys. Rev **75**, 1766 (1949). M.G. Mayer, Phys. Rev. **75**, 1969 (1949); M.G. Mayer, J.H.D. Jensen, *Elementary Theory of Nuclear Shell Structure* (Wiley, New York 1955).

31. E.J. Konopinski, L.M. Langer, Ann. Rev. Nucl. Sci. **2**, 261 (1953).

32. B. Stech, J.H.D. Jensen, Z. Phys. **141**, 175 (1955).

33. B.M. Rustad, S.L. Ruby, Phys. Rev. **89**, 880 (1953); J.S. Allen, W.K. Jentschke, Phys. Rev. **89**, 902 (1953).

34. E.J. Konopinski, H.M. Mahmoud, Phys. Rev. **92**, 1045 (1953).

35. L. Michel, Proc. Phys. Soc. A **63**, 514 (1950) Phys. Rev. **86**, 814 (1952).

36. R. Sagane, W.L. Gardner, H.W. Hubbard, Phys. Rev. **82**, 557 (1951); A. Lagarrigue, C. Peyrou, J. Phys. Radium **12**, 848 (1951).

37. T.D. Lee, C.N. Yang, Phys. Rev. **102**, 290 (1956).

38. T.D. Lee, C.N. Yang, Phys. Rev. **104**, 254 (1956).

39. R.T. Cox, C.G. McIlwraith, B. Kurrelmeyer, Proc. Nat. Acad. Sci. USA **14**, 544 (1928); C.T. Case, Phys. Rev. **36**, 1060 (1930).

40. E. Amaldi, in *Colloque International sur l'Histoire de la Physique des Particules* (Paris, 1982), J. de Physique, Colloque C-8, suppl. no. 12 (Les Edition de Physique, Les Ulis 1982), p. C8-261.

41. R. Budde et al., Phys. Rev. **103**, 1827 (1956).

42. C.S. Wu, E. Ambler, R.W. Hayward, D.D. Hoppes, R.P. Hudson, Phys. Rev. **105**, 1413 (1957).

43. E. Ambler, M.A. Grace, H. Halban, N. Kurti, H. Durand, C.E. Johnson, H.R. Lemmer, Phil. Mag. **44**, 216 (1953).

44. R.L. Garwin, M. Lederman, M. Weinrich, Phys. Rev. **105**, 1415 (1957); J.L. Friedman, V.L. Telegdi, Phys. Rev. **105**, 1681 (1957).

45. A. Salam, Nuovo Cimento Serie X **5**, 299 (1957); L.D. Landau, Zh. Eksp. Teor. Fiz. **32**, 407 (1957); Nucl. Phys. **3**, 127 (1957); T.D. Lee, C.N. Yang, Phys. Rev. **105**, 1671 (1957).

46. H. Weyl, Z. Phys. **56**, 330 (1929).

47. W. Pauli, *Handbuch d. Phys.*, ed. by A. Smekal, **24/1**, 83 (1933) [especially p. 226].

48. W.B. Herrmannsfeldt, D.R. Maxson, P. Stähelin, J.S. Allen, Phys. Rev. **107**, 641(L) (1957).

49. H. Frauenfelder et al., Phys. Rev. **106**, 386 (1957); L.A. Page, M. Heinberg, Phys. Rev. **106**, 1220 (1957).

50. E. Ambler, R.W. Hayward, D.D. Hoppes, R.P. Hudson, C.S. Wu, Phys. Rev. **106**, 1361 (1957); H. Postma, W.J. Huiskamp, A.R. Miedema, M.J. Steenland, H.A. Tolhoek, C.J. Gorter, Physica **23**, 259 (1957).

51. M. Goldhaber, L. Grodzins, A.W. Sunyar, Phys. Rev. **109**, 1015(L) (1958).

52. E.C.G. Sudarshan, R.E. Marshak, in *Proc. Padua Conf. on Mesons and Recently Discovered Particles* (1957); Phys. Rev. **109**, 1860(L) (1958).

53. R.P. Feynman, M. Gell-Mann, Phys. Rev. **109**, 193 (1958).

54. J.J. Sakurai, Nuovo Cimento, Serie X **7**, 649 (1958).

55. S.S. Gershtein, Ya.B. Zel'dovich, Zh. Eksp. Teor. Fiz. **29**, 698 (1955).

56. H.L. Anderson, C.M.G. Lattes, Nuovo Cimento, Serie X **6**, 1356 (1957).

57. T.D. Lee, C.S. Wu, Ann. Rev. Nucl. Sci. **15**, 381 (1965).

58. M.T. Burgy, V.E. Krohn, T.B. Novey, G.R. Ringo, V.L. Telegdi, Phys. Rev. **110**, 1214 (1958).

59. M. Gell-Mann, Phys. Rev. **111**, 362 (1958).

60. B.W. Ridley, Nucl. Phys. **25**, 483 (1961); C.H. Johnson, F. Pleasonton, T.A. Carlson, Phys. Rev. **132**, 1149 (1963); J.B. Vise, B.M. Rustad, Phys. Rev. **132**, 2573 (1963).

61. T. Fazzini, G. Fidecaro, A.W. Merrison, H. Paul, A.V. Tollestrup, Phys. Rev. Lett. **1**, 247 (1958); G. Impeduglia et al., Phys. Rev. Lett. **1**, 249 (1958); H.L. Anderson, T. Fujii, R.H. Miller, L. Tan, Phys. Rev. Lett. **2**, 53 (1959).

62. A.F. Dunaitsev, V.I. Petrushkin, Yu.D. Prokoshkin, V.I. Rykalin, Phys. Lett. **1**, 138 (1962); P. Depommier, J. Heintze, C. Rubbia, V. Soergel, Phys. Lett. **5**, 61 (1963).

63. Y.K. Lee, L.W. Mo, C.S. Wu, Phys. Rev. Lett. **10**, 253 (1963).

64. J.D. Fox, C.F. Moore, D. Robson, Phys. Rev. Lett. **12**, 198 (1964).

65. M. Gell-Mann, Caltech report CTSL-20 (1961); Phys. Rev. **125**, 1067 (1962); Y. Ne'eman, Nucl. Phys. **26**, 222 (1961).

66. M. Gell-Mann, Phys. Lett. **8**, 214 (1964); G. Zweig, CERN Geneva - TH. 401 and CERN-TH-412 (1964).

67. M. Gell-Mann, M. Lévy, Nuovo Cimento Serie X **16**, 705 (1960); in this paper credit for the PCAC relation is given to R.P. Feynman.

68. Y. Nambu, Phys. Rev. Lett. **4**, 380 (1960); J. Bernstein, S. Fubini, M. Gell-Mann, W. Thirring, Nuovo Cimento **17**, 757 (1960); K.-C. Chou, Zh. Eksp. Teor. Fiz **39**, 703 (1960) [JETP **12**, 492 (1961)].

69. M. Gell-Mann, Physics **1**, 63 (1964).

70. S.L. Adler, R.F. Dashen, *Current Algebras and Applications to Particle Physics*, (W.A. Benjamin, New York 1968).

71. H. Bethe, R. Peierls, Nature **133**, 532 (1934).

72. M. Fierz, Helv. Phys. Acta **9**, 245 (1936).

73. S. Tomonaga, H. Tamaki, Sci. Papers Inst. Phys.-Chem. Res. (Tokyo) **33**, 288 (1937).

74. H.A. Bethe, Proc. Cam. Phil. Soc. **31**, 108 (1935).

75. M.E. Nahmias, Proc. Cam. Phil. Soc. **31**, 99 (1935); see also J. Chadwick, D.E. Lea, Proc. Cam. Phil. Soc. **30**, 59 (1934).

76. H.R. Crane, Phys. Rev. **55**, 501 (1939).

77. E. Fermi, declassified report CP-383 (November 26, 1942), reprinted in E. Fermi, *Note e Memorie*, op. cit. Vol. II, p. 263 ; Proc. Am. Phil. Soc. **90**, 20 (1946).

78. K. Way, E.P. Wigner, Phys. Rev. **73**, 1318 (1948).

79. H.R. Crane, Rev. Mod. Phys. **20**, 278 (1948).

80. B. Pontecorvo, Chalk River Laboratory report, PD-205 (1946).

81. L.W. Alvarez, UCRL report 328 (1949).

82. E. Fermi, *Nuclear Physics* (University of Chicago Press, Chicago 1950).

83. W. Pauli, Letter to O. Klein dated 8 January 1931, in *Wissenschaftlicher Briefwechsel*, *idem*, Band II (Springer, Berlin 1985) S. 51.

84. A.I. Leipunski, Proc. Cam. Phil. Soc. **32**, 301 (1936).

85. H.R. Crane, J. Halpern, Phys. Rev. **53**, 789 (1938).

86. J.C. Jacobsen, O. Kofoed-Hansen, Det. Kgl. Danske Viedensk. Selskab. Mat.-Fys. Medd. **23**, Nr. 12, 1 (1945); C.W. Sherwin, Phys. Rev. **73**, 216 (1948).

87. G.W. Rodeback, J.S. Allen, Phys. Rev. **86**, 446 (1952).

88. I. Broser, H. Kallmann, Z. f. Naturf. **2a**, 439; 642 (1947).

89. G.T. Reynolds, F.B. Harrison, G. Salvini, Phys. Rev. **78**, 488 (1950); H. Kallmann, Phys. Rev. **78**, 621 (1950); M Ageno, M. Chiozzotto, R. Querzoli, Phys. Rev. **79**, 720 (1950); F.N. Hayes et al., Science **116**, 140 (1952).

90. C.L. Cowan, Jr., F. Reines, F.B. Harrison, E.C. Anderson, F.N. Hayes, Phys. Rev. **90**, 493 (1953).

91. F. Reines, C.L. Cowan, Jr., Phys. Rev. **92**, 830 (1953).

92. F. Reines, C.L. Cowan, Jr., Nature **178**, 446 (1956); C.L. Cowan, Jr. et al., Science **124**, 103 (1956).

93. F. Reines, C.L. Cowan, Jr., Phys. Rev. **113**, 273 (1959).

94. R. Davis, Jr., Phys. Rev. **97**, 766 (1955).

95. R. Davis, Jr., Bull. Am. Phys. Soc. II **4**, 217 (1959).

96. H.P. Holmgren, R. Johnston, Bull. Am. Phys. Soc. II, **3**, 26 (1958).

97. A.G.W. Cameron, Bull. Am. Phys. Soc. II, **3**, 227 (1958); Ann. Rev. Nucl. Sci. **8**, 299 (1958); W.A. Fowler, Astrophys. J. **127**, 551 (1968).

98. B. Pontecorvo, Zh. Eksp. Teor. Fiz. **37**, 1751 (1959) [Sov. Phys. JETP **10**, 1236 (1960)].

99. M. Schwartz, Phys. Rev. Lett. **4**, 306 (1960).

100. G. Danby, J.-M. Gaillard, K. Goulianos, L.M. Lederman, N. Mistry, M. Schwartz, J. Steinberger, Phys. Rev. Lett. **9**, 36 (1962).

101. S. Fukui, S. Miyamoto, Nuovo Cimento **11**, 113 (1959); see also Reports INS-TCA 10 and 11 (University of Tokyo, INS, 1957); the spark chamber was developed from flash chambers invented by M. Conversi, A. Gozzini, Nuovo Cimento Serie X **2**, 189 (1955).

102. For the development of spark chambers, see conference proceedings in Rev. Sci. Instr. **32**, 479 (1961).

103. H. Yukawa, Proc. Phys. Math. Soc. Japan **17**, 48 (1935).

104. S.H. Neddermeyer, C.D. Anderson, Phys. Rev. **51**, 884 (1937); J.C. Street, E.C. Stevenson, Phys. Rev. **51**, 1005 (1937); Y. Nishina, M. Takeuchi, T. Ichimiya, Phys. Rev. **52**, 1198 (1937); see also P. Kunze, Z. Phys. **83**, 1 (1933); J.F. Carlson, J.R. Oppenheimer, Phys. Rev. **51**, 220 (1936); Which

work is taken as the discovery of the μ meson is a subtle problem; see an annotation by C. Peyrou, in *Colloque International sur l'Histoire de la Physique des Particules*, op. cit.

105. W. Bothe, W. Kolhörster, Z. Phys. **56**, 751 (1929).

106. H. Yukawa, Proc. Phys. Math. Soc. Japan **19**, 712 (1937).

107. W. Heitler, Proc. R. Soc. London A**166**, 529 (1938); L.W. Nordheim, Phys. Rev. **55**, 506 (1939).

108. Y. Tanikawa (1942), cited in Sakata and Inoue, the following paper; S. Sakata, T. Inoue, Nihon Sugaku-Butsuri-Gakwaishi **16**, 232 (1942) [in Japanese]. [English publication was delayed by the war circumstances: S. Sakata, T. Inoue, Prog. Theor. Phys. **1**, 143 (1946); Y. Tanikawa, Prog. Theor. Phys. **2**, 220 (1947).]

109. M. Conversi, E. Pancini, O. Piccioni, Phys. Rev. **71**, 209 (1947).

110. S. Tomonaga, G. Araki, Phys. Rev. **58**, 90 (1940); E. Fermi, E. Teller, V. Weisskopf, Phys. Rev. **71**, 314 (1947).

111. C.M.G. Lattes, H. Muirhead, G.P.S. Occhialini, C.F. Powell, Nature **159**, 694 (1947); see also D.H. Perkins, Nature **159**, 126 (1947); G.P.S. Occhialini, C.F. Powell, Nature **159**, 186 (1947).

112. E.P. Hincks, B. Pontecorvo, Phys. Rev. **75**, 698 (1949); J. Steinberger, Phys. Rev. **75**, 1136 (1949); R.B. Leighton, C.D. Anderson, A.J. Seriff, Phys. Rev. **75**, 1432 (1949).

113. R.E. Marshak, H.A. Bethe, Phys. Rev. **72**, 506 (1947).

114. B. Pontecorvo, Phys. Rev. **72**, 246 (1947).

115. C.N. Yang, J. Tiomno, Phys. Rev. **79**, 495 (1950).

116. E.R. Caianiello, Nuovo Cimento Serie IX **8**, 534 (1951).

117. B. Pontecorvo, in *Colloque International sur l'Histoire de la Physique des Particules*, op. cit. p. C8-221; J. Tiomno, G. Puppi, remarks on a talk of F. Reines, in *Colloque International sur l'Histoire de la Physique des Particules*, op. cit., p. C8-255.

118. E.P. Hincks, B. Pontecorvo, Phys. Rev. **73**, 257 (1948); O. Piccioni, Phys. Rev. **74**, 1754 (1948).

119. K. Nishijima, Phys. Rev. **108**, 907 (1957).

120. J. Schwinger, Ann. Phys. (NY) **2**, 407 (1957).

121. Y. Katayama, K. Matumoto, S. Tanaka, E. Yamada, Prog. Theor. Phys. **28**, 675 (1962).

122. Z. Maki, M. Nakagawa, S. Sakata, Prog. Theor. Phys. **28**, 870 (1962).

123. S. Sakata, Prog. Theor. Phys. **16**, 686 (1956).

124. A. Gamba, R.E. Marshak, S. Okubo, Proc. Nat. Acad. Sci. USA **45**, 881 (1959).

125. Y. Yamaguchi, Suppl. Prog. Theor. Phys. **11**, 1 (1959).

126. N. Cabibbo, Phys. Rev. Lett. **10**, 531 (1963).

127. P. Tarjanne, V.L. Teplitz, Phys. Rev. Lett. **11**, 447 (1963).

128. Z. Maki, Prog. Theor. Phys. **31**, 331; 333 (1964); Y. Hara, Phys. Rev. **134**, B701 (1964); B.J. Bjørken, S.L. Glashow, Phys. Lett. **11**, 255 (1964).

129. S.L. Glashow, J. Iliopoulos, L. Maiani, Phys. Rev. D**2**, 1285 (1970).

130. M.K. Gaillard, B.W. Lee, Phys. Rev. D**10**, 897 (1974); errors are corrected in M.K. Gaillard, B.W. Lee, R.E. Schrock, Phys. Rev. D**13**, 2674 (1976); see also M.K. Gaillard, B.W. Lee, J.L. Rosner, Rev. Mod. Phys. **47**, 277 (1975).

131. K. Niu, E. Mikumo, Y. Maeda, Prog. Theor. Phys. **46**, 1644 (1971).

132. M. Kobayashi, T. Maskawa, Prog. Theor. Phys. **49**, 652 (1972); also private communication (1974).

133. J.J. Aubert et al., Phys. Rev. Lett. **33**, 1404 (1974).

134. J.-E. Augustin et al., Phys. Rev. Lett. **33**, 1406 (1974).

135. G. Goldhaber et al., Phys. Rev. Lett. **37**, 255 (1976).

136. M.L. Perl et al., Phys. Rev. Lett. **35**, 1489 (1975).

137. L.M. Lederman, in *Proc. 1977 Eur. Conf. Particle Phys.*, Budapest, 1977 ed. by L. Jenik, I. Montvay (Central Research Institute for Physics, Budapest 1977), Vol. 1, p. 303; S.W. Herb et al., Phys. Rev. Lett. **39**, 252 (1977).

138. K. Kodama et al., Phys. Lett. B**504**, 218 (2001).

139. H. Fritzsch, M. Gell-Mann, in *Proc. 16th Int. Conf. High Energy Phys.*, Fermilab, 1972 (Fermilab, Batavia 1972), Vol. 2, p. 135; H. Fritzsch, M. Gell-Mann, H. Leutwyler, Phys. Lett. **47**B, 365 (1973).

140. O.W. Greenberg, Phys. Rev. Lett. **13**, 598 (1964); M.Y. Han, Y. Nambu, Phys. Rev. **139**, B1006 (1965).

141. N.N. Bogolyubov, B.V. Struminsky, A.N. Tavkhelidze, Dubna report JINR D-1968 (1965).

142. Y. Miyamoto, Prog. Theor. Phys. Suppl. Extra Number p. 187 (1965).

143. D.J. Gross, F. Wilczek, Phys. Rev. Lett. **30**, 1343 (1973); H.D. Politzer, Phys. Rev. Lett. **30**, 1346 (1973).

144. S. Weinberg, Phys. Rev. Lett. **31**, 494 (1973).

145. H. Georgi, H.D. Politzer, Phys. Rev. D**9**, 416 (1974); D.J. Gross, F. Wilczek, Phys. Rev. D**9**, 980 (1974).

146. G. Miller et al., Phys. Rev. D**5**, 528 (1972); H.L. Anderson et al., Phys. Rev. Lett. **38**, 1450 (1977); J.I. Friedman, H.W. Kendall, Ann. Rev. Nucl. Sci. **22**, 203 (1972).

147. J.D. Bjorken, Phys. Rev. **163**, 1767 (1967).

148. R.P. Feynman, Phys. Rev. Lett. **23**, 1415 (1969).

149. G. Hanson et al., Phys. Rev. Lett. **35**, 1609 (1975).

150. E. Eichten et al., Phys. Rev. Lett. **34**, 369 (1975); Erra. **36**, 1276 (1976).

151. K.G. Wilson, Phys. Rev. D**10**, 2445 (1974); A.M. Polyakov, Phys. Lett. **59**B, 82 (1975).

152. M. Creutz, Phys. Rev. Lett. **43**, 553 (1979).

153. T.D. Lee, C.N. Yang, Phys. Rev. Lett. **4**, 307 (1960).

154. Y. Yamaguchi, Prog. Theor. Phys. **23**, 1117 (1960); N. Cabibbo, R. Gatto, Nuovo Cimento Serie X **15**, 304 (1960).

155. M. Veltman, Physica **29**, 161 (1963); J.S. Bell, M. Veltman, Phys. Lett. **5**, 94 (1963).

156. S. van der Meer, CERN report 61-7 (1961); M. Giesch, S. van der Meer, G. Pluym, K.M. Vahlbruch, *Proc. Int. Conf. Elementary Particles*, Siena, Vol. 1, p. 536 (1963).

157. e.g., M.M. Block et al., Phys. Lett. **12**, 281 (1964); J.K. Bienlein et al., Phys. Lett. **13**, 80 (1964); G. Bernardini et al., Phys. Lett. **13**, 86 (1964); see *Proc. Int. Conf. on Fundamental Aspects of Weak Interactions*, BNL, 1963 (Brookhaven National Laboratory, Upton), pp. 89–190.

158. C.V. Achar et al., Phys. Lett. **18**, 196 (1965); ibid. **19**, 78 (1965).

159. F. Reines et al., Phys. Rev. Lett. **15**, 429 (1965).

160. J.D. Bjorken, E.A. Paschos, Phys. Rev. D**1**, 3151 (1970); R.P. Feynman *Photon Hadron Interactions* (W.A. Benjamin, Reading, Massachusetts 1972).

161. R.C. Lamb, R.A. Lundy, T.B. Novey, D.D. Yavanovitch, M.L. Good, R. Hartung, M.W. Peters, A. Subramanian, Phys. Rev. Lett. **15**, 800 (1965); R. Burns, G. Danby, E. Hyman, L.M. Lederman, W. Lee, J. Rettberg, J. Sunderland, Phys. Rev. Lett. **15**, 830 (1965).
162. G. Arnison et al., Phys. Lett. **122**B, 103 (1983); **126**B, 398 (1983).
163. M. Banner et al., Phys. Lett. **122**B, 476 (1983).
164. O. Klein, in *Proc. Conf. "Les Nouvelles Theorische la Physique"*, Warsaw (Paris, 1939), p. 81.
165. W. Heisenberg, Ann. d. Phys. 5. Folge, **32**, 20 (1938).
166. J. Schwinger, Ann. Phys. (NY) **2**, 407 (1957).
167. J. Leite Lopes, Nucl. Phys. **8**, 234 (1958).
168. S.L. Glashow, Nucl. Phys. **22**, 579 (1961).
169. C.N. Yang, R.L. Mills, Phys. Rev. **96**, 191 (1954).
170. R. Utiyama, Phys. Rev. **101**, 1597 (1956).
171. A. Salam, J. Ward, Phys. Lett. **13**, 168 (1964).
172. F. Englert, R. Brout, Phys. Rev. Lett. **13**, 321 (1964); P.W. Higgs, Phys. Rev. Lett. **13**, 508 (1964); G.S. Guralnik, C.R. Hagen, T.W.B. Kibble, Phys. Rev. Lett. **13**, 585 (1964); T.W.B. Kibble, Phys. Rev. **155**, 1554 (1967).
173. Y. Nambu, Phys. Rev. Lett. **4**, 380 (1960); Y. Nambu, G. Jona-Lasinio, Phys. Rev. **122**, 345 (1961); J. Goldstone, Nuovo Cimento Serie X **19**, 154 (1961).
174. For an experimental attempt, see M. Aglietta et al., Astropart. Phys. **1**, 1 (1992).
175. S. Weinberg, Phys. Rev. Lett. **19**, 1264 (1967).
176. A. Salam, in *Elementary Particle Theory, Proc. 8th Nobel Symp.*, Aspenäsgården, 1968, ed. by N. Svartholm (Almqvist and Wiksell, Stockholm, 1968) p. 367.
177. R.P. Feynman, Acta Phys. Polonica **24**, 697 (1963).
178. L.D. Faddeev, V.N. Popov, Phys. Lett. **25**B, 29 (1967).
179. B.S. De Witt, Phys. Rev. **162**, 1195; 1239 (1967).
180. G. 't Hooft, Nucl. Phys. B**35**, 167 (1971).
181. S. Weinberg, Phys. Rev. D**5**, 1412 (1972).
182. C. Bouchiat, J. Iliopoulos, Ph. Meyer, Phys. Lett. **38**B, 519 (1972).
183. For earlier discussions of neutral currents, G. Gamow, E. Teller, Phys. Rev. **51**, 288 (1937); N. Kemmer, Phys. Rev. **52**, 906 (1937); G. Wentzel, Helv. Phys. Acta. **10**, 108 (1937); J. Leite Lopes [167].
184. F.J. Hasert et al., Phys. Lett. **46**B, 121; 138 (1973).
185. C.Y. Prescott et al., Phys. Lett. **77**B, 347 (1978).
186. S. Weinberg, Rev. Mod. Phys. **46**, 255 (1974); in *Proc. 19th Int. Conf. High Energy Phys.*, Tokyo, 1978, ed. by S. Homma, M. Kawaguchi, H. Miyazawa (Physical Society of Japan, Tokyo 1979) p. 907.
187. E. Majorana, Nuovo Cimento **14**, 171 (1937).
188. J.H. Christenson, J.W. Cronin, V.L. Fitch, R. Turlay, Phys. Rev. Lett. **13**, 138 (1964).
189. F.N.D. Kurie, J.R. Richardson, H.C. Paxton, Phys. Rev. **49**, 368 (1936).
190. E.M. Lyman, Phys. Rev. **55**, 234(A) (1939).
191. R.O. Haxby, W.E. Shoupp, W.E. Stephens, W.H. Wells, Phys. Rev. **58**, 1035 (1940).
192. E.J. Konopinski, Phys. Rev. **72**, 518(L) (1947).
193. S.C. Curran, J. Angus, A.L. Cockcroft, Nature **162**, 302 (1948); Phil. Mag. **40**, 53 (1949).

194. G.C. Hanna, B. Pontecorvo, Phys. Rev. **75**, 983 (1949).

195. D.R. Hamilton, W.P. Alford, L. Gross, Phys. Rev. **83**, 215 (1951).

196. L.M. Langer, R.J.D. Moffat, Phys. Rev. **88**, 689 (1952).

197. K.-E. Bergkvist, Nucl. Phys. **B39**, 317; 371 (1972).

198. V.A. Lubimov et al., Phys. Lett. **94**B, 266 (1980).

199. M. Goeppert-Mayer, Phys. Rev. **48**, 512 (1935).

200. W.H. Furry, Phys. Rev. **56**, 1184 (1939).

201. H. Primakoff, S.P. Rosen, Rep. Prog. Phys. **22**, 121 (1959); Proc. Phys. Soc. London **78**, 464 (1961).

202. B. Pontecorvo, Phys. Lett. **26B**, 630 (1968).

203. B. Pontecorvo, Zh. Eksp. Teor. Fiz. **33**, 549 (1957) [Sov. Phys. JETP **6**, 429 (1958)]; Zh. Eksp. Teor. Fiz. **34**, 247 (1958) [Sov. Phys. JETP **7**, 172 (1958)].

204. M. Gell-Mann, A. Pais, Phys. Rev. **97**, 1387 (1955).

205. V. Gribov, B. Pontecorvo, Phys. Lett. **28B**, 493 (1969).

206. J.N. Bahcall, S.C. Frautschi, Phys. Lett. **29**B, 623 (1969).

207. R. Davis, Jr., D.S. Harmer, K.C. Hoffman, Phys. Rev. Lett. **20**, 1205 (1968); see also R. Davis, Jr., Phys. Rev. Lett. **12**, 303 (1964) for the result of a pilot experiment and a proposal for a larger detector.

208. S.M. Bilenky, B. Pontecorvo, Phys. Rept. **41**, 225 (1978).

209. J.N. Bahcall, R. Davis, Jr., in *Essays in Nuclear Astrophysics*, ed. C.A. Barnes, D.D. Clayton, D. Schramm (Cambridge University Press, Cambridge 1982) p. 243.

210. J.N. Bahcall, *Neutrino Astrophysics* (Cambridge University Press, Cambridge 1989).

211. S.P. Mikheyev, A.Yu. Smirnov, Yad. Fiz. **42**, 1441 (1985) [Sov. J. Nucl. Phys. **42**, 913 (1985)]; Nuovo Cimento **9**C, 17 (1986).

212. L. Wolfenstein, Phys. Rev. **D17**, 2369 (1978).

213. H.A. Bethe, Phys. Rev. Lett. **56**, 1305 (1986).

214. G. Battistoni et al., Phys. Lett. **133**B, 454 (1984) [NUSEX].

215. H.S. Park et al., Phys. Rev. Lett. **54**, 22 (1985) [IMB].

216. K. Arisaka et al., J. Phys. Soc. Jpn. **54**, 3213 (1985) [Kamiokande].

217. J. Bartelt et al., Phys. Rev. **D36**, 1990 (1987) [Soudan].

218. Ch. Berger et al., Nucl. Phys. **B313**, 509 (1989) [Frejus].

219. J.C. Pati, A. Salam, Phys. Rev. Lett. **31**, 1240 (1973); Phys. Rev. **D8**, 1240 (1973).

220. H. Georgi, S.L. Glashow, Phys. Rev. Lett. **32**, 438 (1974).

221. H. Georgi, H.R. Quinn, S. Weinberg, Phys. Rev. Lett. **33**, 451 (1974).

222. M.A. Markov, in *Proc. 1960 Annual Int. Conf. High Energy Phys. Rochester*, 1960, ed. by E.C.G. Sudarshan, J.H. Tinlot, A.C. Melissinos (Rochester University, New York 1960) p. 578.

223. T.J. Haines et al., Phys. Rev. Lett. **57**, 1986 (1986) [IMB].

224. K.S. Hirata et al., Phys. Lett. **B205**, 416 (1988) [Kamiokande].

225. D. Casper et al., Phys. Rev. Lett. **66**, 2561 (1991); R. Becker-Szendy et al., Phys. Rev. **D46**, 3720 (1992) [IMB].

226. Y. Fukuda et al., Phys. Lett. **B335**, 237 (1994) [Kamiokande].

227. Y. Fukuda et al., Phys. Rev. Lett. **81**, 1562 (1998); Phys. Lett. **B436**, 33 (1998) [Super-Kaimokande].

228. K.S. Hirata et al., Phys. Rev. Lett. **63**, 16 (1989) [Kamiokande].

229. F. Reines, W.R. Kropp, Phys. Rev. Lett. **12**, 457 (1964).

230. V.A. Kuzmin, Zh. Eksp. Teor. Fiz. **49**, 1532 (1965) [Sov. Phys. JETP **22**, 1051 (1966)].

231. A.I. Abazov et al., Phys. Rev. Lett. **67**, 3332 (1991) [SAGE].

232. P. Anselmann et al., Phys. Lett. B**285**, 376 (1992) [Gallex].

233. A.W. Sunyar, M. Goldharber, Phys. Rev. **120**, 871 (1960).

234. H.H. Chen, Phys, Rev. Lett. **55**, 1534 (1985); University of California Irvine Neutrino Group Report No. 120 (1984).

235. Q.R. Ahmad et al., Phys. Rev. Lett. **87**, 071301 (2001) [SNO].

236. S. Weinberg, in *Proc. First Workshop on Grand Unification*, ed. by P.H. Frampton, S.L. Glashow, A. Yildiz (Math. Sci. Press, 1980) p. 347; in *Proc. 23rd Int. Conf. High Energy Phys.*, Berkeley 1986, ed. by S.C. Loken (World Scientific, Singapore 1987), Vol. I, p. 271.

237. T. Yanagida, in *Proc. Workshop on the Unified Theory and Baryon Number in the Universe*, ed. by O. Sawada, A. Sugamoto (KEK report 79-18, 1979), p. 95; M. Gell-Mann, P. Ramond, R. Slansky, in *Supergravity*, ed. by P. van Nieuwenhuizen, D.Z. Freedman (North Holland, Amsterdam 1979), p. 315.

238. N. Arkani-Hamed, S. Dimopoulos, G. Dvali, J. March-Russell, Phys. Rev. D**65**, 024032 (2002); Y. Grossman, M. Neubert, Phys. Lett. B**474**, 361 (2000).

239. G. Gamow, M. Schönberg, Phys. Rev. **59**, 539 (1941).

240. B. Pontecorvo, Zh. Eksp. Teor. Fiz. **36**, 1615 (1959) [Sov. Phys. JETP **9**, 1148 (1959)].

241. G.M. Gandelman, V.S. Pinaev, Zh. Eksp. Teor. Fiz. **37**, 1072 (1959) [Sov. Phys. JETP **10**, 764 (1960)].

242. H.-Y. Chiu, P. Morrison, Phys. Rev. Lett. **5**, 573 (1960).

243. R.B. Stothers, Phys. Rev. Lett. **24**, 538 (1970).

244. F. Reines, H.S. Gurr, H.W. Sobel, Phys. Rev. Lett. **37**, 315 (1976).

245. A.D. Dolgov, Ya.B. Zel'dovich, Rev. Mod. Phys. **53**, 1 (1981).

246. E.W. Kolb, M.S. Turner, *The Early Universe* (Addison-Wesley, Redwood 1990).

247. R.A. Alpher, H. Bethe, G. Gamow, Phys. Rev. **73**, 803 (1948).

248. C. Hayashi, Prog. Theor. Phys. **5**, 224 (1950).

249. R.A. Alpher, J.W. Follin, Jr., R.C. Herman, Phys. Rev. **92**, 1347 (1953).

250. F. Hoyle, R.J. Tayler, Nature **203**, 1108 (1964).

251. P.J.E. Peebles, Astrophys. J. **146**, 542 (1966).

252. S.S. Gershtein, Ya.B. Zel'dovich, Pis'ma Zh. Eksp. Teor. Fiz. **4**, 174 (1966) [JETP Lett. **4**, 120 (1966).].

253. G. Marx, A.S. Szalay, in *Neutrino 72*, Vol. 1 (Technoinform, Budapest, 1972), p. 191.

254. R. Cowsik, J. McClelland, Astrophys. J. **180**, 7 (1973).

255. R. Cowsik, J. McClelland, Phys. Rev. Lett. **29**, 669 (1972).

256. A.S. Szalay, G. Marx, Astron. Astrophys. **49**, 437 (1976); G.S. Bisnovaty-Kogan, I.D. Novikov, Astron. Zh. **57**, 899 (1980); J.R. Bond, G. Efstathiou, J. Silk, Phys. Rev. Lett. **45**, 1980 (1980); J.R. Bond, A.S. Szalay, Astrophys. J. **274**, 443 (1983); H. Sato, F. Takahara, Prog. Theor. Phys. **64**, 2029 (1980).

257. P.J.E. Peebles, Astrophys. J. **263**, L1 (1982).

258. M. Rees, *Perspectives in Astrophysical Cosmology* (Cambridge University Press, Cambridge 1995).

259. G. 't Hooft, Phys. Rev. Lett. **37**, 8 (1976); Phys. Rev. D**14**, 3432 (1976).

260. V.A. Kuzmin, V.A. Rubakov, M.E. Shaposhnikov, Phys. Lett. **155**B, 36 (1985).
261. M. Fukugita, T. Yanagida, Phys. Lett. B**174**, 45 (1986).
262. J. Tiomno, Nuovo Cimento Serie X **1**, 226 (1955).
263. B. Touschek, Z. Phys. **125**, 108 (1949).
264. E.S. Abers, B.W. Lee, Phys. Rept. **9**, 1 (1973).
265. J.C. Taylor, *Gauge Theories of Weak Interactions* (Cambridge University Press, Cambridge 1976).
266. S. Weinberg, *The Quantum Theory of Fields*, Vol. II (Cambridge University Press, Cambridge 1996).
267. K. Fujikawa, B.W. Lee, A.I. Sanda, Phys. Rev. D**6**, 2923 (1972).
268. T.D. Lee, C.N. Yang, Phys. Rev. **128**, 885 (1962).
269. B.W. Lee, J. Zinn-Justin, Phys. Rev. D**5**, 3121; 3137 (1972); G. 't Hooft, M. Veltman, Nucl. Phys. B**50**, 318 (1972); C. Becchi, A. Rouet, R. Stora, Commun. Math. Phys. **42**, 127 (1975).
270. A.A. Slavnov, Teor. Math. Fiz. **10**, 153 (1972) [Theor. Math. Phys. **10**, 99 (1972)]; J.C. Taylor, Nucl. Phys. B**33**, 436 (1972).
271. G. 't Hooft in [180]; F. Abe et al., Phys. Rev. Lett. **74**, 2626 (1995).
272. J.S. Bell, R. Jackiw, Nuovo Cimento **60**A, 47 (1969); S.L. Adler, Phys. Rev. **177**, 2426 (1969); the triangle diagram was first calculated by H. Fukuda, Y. Miyamoto, Prog. Theor. Phys. **4**, 347 (1949); see also J. Steinberger, Phys. Rev. **76**, 1180 (1949).
273. For a conceptually simple derivation, see K. Fujikawa, Phys. Rev. Lett. **42**, 1195 (1979).
274. P.J. Mohr, B.N. Taylor, Rev. Mod. Phys. **72**, 351 (2000) [CODATA].
275. Particle Data Group (D.E. Groom et al.), Eur. Phys. J. C**15**, 1 (2000) [RPP2000].
276. T.D. Lee, Phys. Rev. **128**, 899 (1962).
277. A. Sirlin, Nucl. Phys. **71**, 29 (1974).
278. P. Abreu et al., Eur. Phys, J. C**12**, 225 (2000) [DELPHI]; R. Barate et al., Eur. Phys, J. C**14**, 1 (2000) [ALEPH]; M. Acciarri et al., Eur. Phys. J. C**16**, 1 (2000) [L3].
279. B. Abbott et al., Phys. Rev. Lett. **84**, 222 (2000) [D0]; F. Abe et al., Phys. Rev. D**52**, 2624 (1995) [CDF].
280. P. Abreu et al., Phys. Lett. B**462**, 410 (1999) [DELPHI]; G. Abbiendi et al., Phys. Lett. B**453**, 148 (1999) [OPAL]; M. Acciarri et al., Phys. Lett. B**454**, 386 (1999) [L3]; R. Barate et al., Phys. Lett. B**453**, 121 (1999) [ALEPH].
281. H. Abramowicz, Phys. Rev. Lett. **57**, 298 (1986); A. Blondel et al., Z. Phys. C**45**, 361 (1990) [CDHS].
282. J.V. Allaby et al., Phys. Lett. B**177**, 446 (1986); Z. Phys. C**36**, 611 (1987) [CHARM].
283. C.G. Arroyo et al., Phys. Rev. Lett. **72**, 3452 (1994); K.S. McFarland et al., Eur. Phys. J. C**1**, 509 (1998) [CCFR].
284. A. Sirlin, Phys. Lett. B**232**, 123 (1989); S. Fanchiotti, A. Sirlin, Phys. Rev. D**41**, 319 (1990).
285. W.J. Marciano, J.L. Rosner, Phys. Rev. Lett. **65**, 2963 (1990).
286. A. Sirlin, Phys. Rev. D**22**, 971 (1980); D**29**, 89 (1984).
287. K.-I. Aoki, Z. Hioki, R. Kawabe, M. Konuma, T. Muta, Prog. Theor. Phys. Suppl. **73**, 1 (1982).

288. W.F.L. Hollik, Fortsch. Phys. **38**, 165 (1990).

289. E.C.G. Stueckelberg, A. Petermann, Helv. Phys. Acta **26**, 499 (1953); M. Gell-Mann, F.E. Low, Phys. Rev. **95**, 1300 (1954); N.N. Bogoliubov, D.V. Shirkov, *Introduction to the Theory of Quantized Fields* (Wiley-Interscience, New York 1959), Chap. 8.

290. K. Symanzik, Commun. Math. Phys. **18**, 227 (1970); C.G. Callan, Phys. Rev. **D2**, 1541 (1970).

291. S. Fanchiotti, B. Kniehl, A. Sirlin, Phys. Rev. **D48**, 307 (1993).

292. J. Erler, Phys. Rev. **D59**, 054008 (1999).

293. G. Degrassi, S. Fanchiotti, A. Sirlin, Nucl. Phys. **B351**, 49 (1991).

294. M. Veltman, Nucl. Phys. **B123**, 89 (1977).

295. G. 't Hooft, M. Veltman, Nucl. Phys. **B44**, 189 (1972).

296. P. Langacker, in *Electroweak Physics Beyond the Standard Model*, ed. by J.W.F. Valle, J. Velasco (World Scientific, Singapore 1991), p. 75; Phys. Rev. Lett. **63**, 1920 (1989); P. Langacker, M. Luo, Phys. Rev. **D44**, 817 (1991).

297. J. Ellis, G.L. Fogli, Phys. Lett. **B249**, 543 (1990).

298. Particle Data Group (L. Montanet et al.), Phys. Rev. **D50**, 1173 (1994) [RPP94].

299. F. Abe et al., Phys. Rev. Lett. **74**, 2626 (1995) [CDF].

300. B. Abbott et al., Phys. Rev. **D58**, 052001 (1998) [D0]; F. Abe et al., Phys. Rev. Lett. **82**, 271 (1999) [CDF].

301. J. Erler, P. Langacker, in Eur. Phys. J **C15** (2000), p. 95.

302. L.F. Abbott, R.M. Barnett, Phys. Rev. **D18**, 3214 (1978); J.E. Kim, P. Langacker, M. Levine, H.H. Williams, Rev. Mod. Phys. **53**, 211 (1981).

303. U. Amaldi et al., Phys. Rev. **D36**, 1385 (1987); G.L. Fogli, D. Haidt, Z. Phys. **C40**, 379 (1988); G. Costa et al., Nucl. Phys. **B297**, 244 (1988); J. Ellis, G.L. Fogli, Phys. Lett. **B232**, 139 (1989).

304. M. Veltman, Acta Phys. Polon. **B8**, 475 (1977).

305. B.W. Lee, C. Quigg, H.B. Thacker, Phys. Rev. **D16**, 1519 (1977).

306. L.D. Landau, A. Abrikosov, L. Halatnikov, Nuovo Cimento, Serie X, Suppl. **3**, 80 (1956).

307. M. Aizenman, Phys. Rev. Lett. **47**, 1 (1981); J. Fröhlich, Nucl. Phys. **B200** [FS4], 281 (1982).

308. L. Maiani, G. Parisi, R. Petronzio, Nucl. Phys. **B136**, 115 (1978).

309. R. Dashen, H. Neuberger, Phys. Rev. Lett. **50**, 1897 (1983).

310. J. Kuti, L. Lin, Y. Shen, Phys. Rev. Lett. **61**, 678 (1988); A. Hasenfratz et al., Phys. Lett. **B199**, 531 (1987); Nucl. Phys. **B317**, 81 (1989); G. Bhanot, K. Bitar, U.M. Heller, H. Neuberger, Nucl. Phys. **B353**, 551 (1991); U.M. Heller, M. Klomfass, H. Neuberger, P. Vranas, Nucl. Phys. **B405**, 555 (1993); See the argument in H. Neuberger, Nucl. Phys. B (Proc. Suppl) **17**, 17 (1990).

311. S. Coleman, E. Weinberg, Phys. Rev. **D7**, 1888 (1973).

312. S. Weinberg, Phys. Rev. Lett. **36**, 294 (1976); A.D. Linde, Phys. Lett. **70B**, 306 (1977).

313. I.V. Krive, A.D. Linde, Nucl. Phys. **B117**, 265 (1976); N.V. Krasnikov, Yad. Fiz. **28**, 549 (1978); P.Q. Hung, Phys. Rev. Lett. **42**, 873 (1979); H.D. Politzer, S. Wolfram, Phys. Lett. **B82**, 242 (1979).

314. M.J. Duncan, R. Philippe, M. Sher, Phys. Lett. **B153**, 165 (1983); M. Linder, Z. Phys. **C31**, 295 (1986); M. Sher, Phys. Rept. **179**, 273 (1989); C. Ford, D.R.T. Jones, P.W. Stephenson, M.B. Einhorn, Nucl. Phys. **B395**, 17 (1993).

315. N. Cabibbo, L. Maiani, G. Parisi, R. Petronzio, Nucl. Phys. B**158**, 295 (1979).

316. G. Altarelli, G. Isidori, Phys. Lett. B**337**, 141 (1994).

317. B. Pendleton, G.G. Ross, Phys. Lett. **98**B, 291 (1981); M. Harada, Y. Kikukawa, T. Kugo, H. Nakano, Prog. Theor. Phys. **92**, 1161 (1994).

318. I. Hinchliffe, in *Review of Particle Properties*, C. Caso et al., Eur. Phys. J. C**3**, 1 (1998), p. 244f.

319. D. Decamp et al., Phys. Lett. B**236**, 233 (1990); B**245**, 289 (1990); B**246**, 306 (1990).

320. ALEPH, DELPHI, L3, and OPAL Collaboration, hep-ex/0107029.

321. ALEPH, DELPHI, L3, and OPAL Collaboration, hep-ex/0107030.

322. M. Acciarri et al., Phys. Lett. B**495**, 18 (2000) [L3]; R. Barate et al., Phys. Lett. B**495**, 1 (2000) [ALEPH].

323. J. Ellis, G.L. Fogli, E. Lisi, Phys. Lett. B**389**, 321 (1996); A. Gurtu, Phys. Lett. B**385**, 415 (1996); G. Degrassi, P. Gambino, A. Sirlin, Phys. Lett. B**394**, 188 (1997); S. Dittmaier, D. Schildknecht, Phys. Lett. B**391**, 420 (1997); K. Hagiwara, D. Haidt, S. Matsumoto, Eur. Phys. J. C**2**, 95 (1998); G. D'Agostini, G. Degrassi, Eur. Phys. J. C**10**, 663 (1999).

324. S. Weinberg, Phys. Rev. D**19**, 1277 (1979); L. Susskind, Phys. Rev. D**20**, 2619 (1979).

325. S. Dimopoulos, L. Susskind, Nucl. Phys. B**155**, 237 (1979); E. Eichten, K. Lane, Phys. Lett. **90**B, 125 (1980).

326. M.E. Peskin, T. Takeuchi, Phys. Rev. D**46**, 381 (1992); see also PDG [275].

327. L. Maiani, Gif-sur-Yvette Summer School on Particle Physics, 11th Gif-sur-Yvette, France, 1979 (Inst. Nat. Phys. Nucl. Phys. Part., Paris, 1979); M. Veltman, Acta Phys. Pol. B**12**, 437 (1981); E. Witten, Nucl. Phys. B**188**, 513 (1981).

328. Y. Okada, M. Yamaguchi, T. Yanagida, Prog. Theor. Phys. **85**, 1 (1991); J. Ellis, G. Ridolfi, F. Zwirner, Phys. Lett. B**257**, 83 (1991); H.E. Haber, R. Hempfling, Phys. Rev. Lett. **66**, 1815 (1991).

329. D.L. Pursey, Physica, **18**, 1017 (1952).

330. T. Kinoshita, A. Sirlin, Phys. Rev. **113**, 1652 (1959).

331. G. Källen, *Springer Tracts in Modern Physics*, **46**, 67 (1968).

332. T. van Ritbergen, R.G. Stuart, Phys. Rev. Lett. **82**, 488 (1999).

333. D. Wilkinson and B.E.F. Macefield, Nucl. Phys. A **158**, 110 (1970).

334. R.E. Marshak, Riazuddin, C.P. Ryan, *Theory of Weak Interactions in Particle Physics* (Wiley-Interscience, New York 1969).

335. L.B. Okun, *Weak Interactions of Elementary Particles*, (Pergamon Press, Oxford 1966).

336. E.S. Abers, R.E. Norton, D.A. Dicus, Phys. Rev. Lett. **18**, 676 (1967); E.S. Abers, D.A. Dicus, R.E. Norton, H.R. Quinn, Phys. Rev. **167**, 1461 (1968).

337. T. Kinoshita, Phys. Rev. Lett. **2**, 477 (1959).

338. D.I. Britton et al., Phys. Rev. Lett. **68**, 3000 (1992); G. Czapek et al., Phys. Rev. Lett. **70**, 17 (1993).

339. S. Aoki et al., Phys. Rev. D**62**, 094501 (2000) [cp-pacs]; V. Giménez, L. Giusti, F. Rapuano, M. Talevi, Nucl. Phys. B**531**, 429 (1998). The pion decay constant has been routinely calculated in many lattice QCD simulations. The examples listed here are only those that use fully non-perturbative methods including renormalisation factors.

340. For reviews, C. Bernard, Nucl. Phys. B (Proc. Suppl.) **94**, 159 (2001); S. Hashimoto, Nucl. Phys. B (Proc. Suppl.) **83**, 3 (2000).

341. M. Ademollo, R. Gatto, Phys. Lett. **10**, 339 (1964).

342. H. Leutwyler, M. Roos, Z. Phys. C**25**, 91 (1984).

343. M. Morita, *Beta Decay and Muon Capture* (W.A. Benjamin, Reading, Massachusetts 1973).

344. R.J. Blin-Stoyle, *Fundamental Interactions and the Nucleus* (North-Holland, Amsterdam 1973).

345. H. Behrens, J. Jänecke, *Numerical Tables for Beta-Decay and Electron Capture* (Springer, Berlin 1969).

346. S.M. Berman, Phys. Rev. **112**, 267 (1958); T. Kinoshita, A. Sirlin, in [330]; G. Källén, Nucl. Phys. B**1**, 225 (1967). Berman pointed out that earlier calculations contained errors in the treatment of the infrared divergence.

347. A. Sirlin, Phys. Rev. **164**, 1767 (1967).

348. A. Sirlin, in [277]; W.J. Marciano, A. Sirlin, Phys. Rev. Lett. **56**, 22 (1986).

349. I.S. Towner, Nucl. Phys. A**540**, 478 (1992).

350. W. Jaus, G. Rasche, Phys. Rev. D**41**, 166 (1990).

351. D.H. Wilkinson, Nucl. Phys. A**377**, 474 (1982); see also V. Linke, H.J. Rothe, Z. Phys. **212**, 190 (1968); M.M. Nieto, Rev. Mod. Phys. **40**, 140 (1968).

352. V.M. Shekhter, Zh. Eksp. Teor. Fiz. **35**, 458 (1958) [Sov. Phys. JETP **8**, 316 (1959)].

353. W.J. Marciano, Ann. Rev. Nucl. Part. Sci. **41**, 469 (1991).

354. H. Yukawa, S. Sakata, Proc. Phys.-Math. Soc. Jpn., **17**, 467 (1935).

355. L.W. Alvarez, Phys. Rev. **54**, 486 (1938).

356. R.B. Firestone, V.S. Shirley, *Table of Isotopes*, 8th ed. (Wiley, New York 1996); see also C.M. Lederer, V.S. Shirley, *Table of Isotopes*, 7th ed. (Wiley, New York 1978).

357. M. Siegbahn, *Spektroskopie der Röntgenstrahlen* (J. Springer, Berlin 1931).

358. J.A. Bearden, A.F. Burr, Rev. Mod. Phys. **39**, 125 (1967); see also J.A. Bearden, Rev. Mod. Phys. **39**, 78 (1967).

359. A.H. Wapstra, G.J. Nijgh, R. van Lieshout, *Nuclear Spectroscopy Tables* (North-Holland, Amsterdam 1959).

360. I.S. Towner, J.C. Hardy, nucl-th/9809087 (Talk at WEIN98).

361. A. Sirlin, Phys. Rev. D**35**, 3423 (1987). This reference gives the formula that has been used conventionally. The correct result was obtained by T. Kinishita and A. Sirlin, Phys. Rev. **113**, 1652 (1959), whereas earlier results by the same authors contain errors; see Berman [346].

362. W. Jaus, G. Rasche, Phys. Rev. D**35**, 3420 (1987).

363. J.C. Hardy et al., Nucl. Phys. A**509**, 429 (1990); I.S. Towner, J.C. Hardy, Nucl. Phys. A**205**, 33 (1973).

364. W.E. Ormand, B.A. Brown, Phys. Rev. C**52**, 2455 (1995); see also P. Navrátil, B.R. Barrett, W.E. Ormand, Phys. Rev. C**56**, 2542 (1997).

365. F.C. Barker, Nucl. Phys. A**579**, 62 (1994); **537**, 134 (1992).

366. M.G. Mayer, J.H.D. Jensen, ref. [30]; R.D. Lawson, *Theory of the Nuclear Shell Model* (Oxford University Press, Oxford 1980).

367. I. Talmi, Rev. Mod. Phys. **34**, 704 (1962).

368. S. Cohen, D. Kurath, Nucl. Phys. **73**, 1 (1965).

369. B.H. Wildenthal, Prog. Part. Nucl. Phys. **11**, 5 (1984); B.A. Brown, B.H. Wildenthal, At. Data Nucl. Data Tables **33**, 347 (1985).

370. E. Caurier, A.P. Zuker, A. Poves, G. Martínez-Pinedo, Phys. Rev. C**50**, 225 (1994).

371. D.H. Wilkinson, Nucl. Phys. A**225**, 365 (1974).

372. W.-T. Chou, E.K. Warburton, B.A. Brown, Phys. Rev. C**47**, 163 (1993).

373. B.A. Brown, B.H. Wildenthal, Phys. Rev. C**28**, 2397 (1983); in [369].

374. H.J. Rose, O. Häusser, E.K. Warburton, Rev. Mod. Phys. **40**, 591 (1968).

375. I.S. Towner, Phys. Rep. **155**, 263 (1987).

376. A. Arima, K. Shimizu, W. Bentz, H. Hyuga, Adv. Nucl. Phys. **18**, 1 (1987).

377. B.A. Brown, Phys. Rev. Lett. **69**, 1034 (1992).

378. R.G. Sachs, *Nuclear Theory* (Addison Wesley, Reading, Massachusetts 1953); M. Chemtob, M. Rho, Nucl. Phys. A**163**, 1 (1971); D.O. Riska, G.E. Brown, Phys. Lett. **38**B, 193 (1972); K. Kubodera, J. Delorme, M. Rho, Phys. Rev. Lett. **40**, 755 (1978); E. Ivanov, E. Truhlik, Nucl. Phys. A**316**, 437 (1979).

379. I.S. Towner, F.C. Khanna, Nucl. Phys. A**399**, 334 (1983).

380. E.G. Adelberger, A. García, P.V. Magnus, D.P. Wells, Phys. Rev. Lett. **67**, 3658 (1991).

381. J.F. Donoghue, B.R. Holstein, S.W. Klimt, Phys. Rev. D**35**, 934 (1987); see also R.E. Shrock, L.-L. Wang, Phys. Rev. Lett. **41**, 1692 (1978); M. Bourquin et al., Z. Phys. C**21**, 27 (1983).

382. R. Flores-Mendieta, A. García, G. Sánchez-Colón, Phys. Rev. D**54**, 6855 (1996).

383. N. Isgur, D. Scora, B. Grinstein, M.B. Wise, Phys. Rev. D**39**, 799 (1989).

384. J.P. Alexander et al., Phys. Rev. Lett. **77**, 5000 (1996) [CLEO].

385. H. Abramowicz et al., Z. Phys. C**15**, 19 (1982) [CDHS].

386. S.A. Rabinowitz et al., Phys. Rev. Lett. **70**, 134 (1993) [CCFR].

387. P. Abreu et al., Phys. Lett. B**439**, 209 (1998) [DELPHI].

388. N. Isgur, M.B. Wise, Phys. Lett. B**232**, 113 (1989).

389. M. Feindt, in *Proc. Int. Europhysics Conf. High Energy Phys.*, Jerusalem, 1997 (Springer, Berlin 1999), p. 90.

390. A.P. Heinson, in *Proc. 2nd Int. Conf. on B Phys. and CP Violation*, Honolulu, 1997 ed. by T.E. Browder, F.A. Harris, S. Pakvasa (World Scientific, Singapore 1998), p. 369.

391. L.-L. Chau, W.-K. Keung, Phys. Rev. Lett. **53**, 1802 (1984); see also L. Maiani, Phys. Lett. **62**B, 183 (1976).

392. C. Jarlskog, Phys. Rev. Lett. **55**, 1039 (1985).

393. I. Dunietz, O.W. Greenberg, D.-d. Wu, Phys. Rev. Lett. **55**, 2935 (1985).

394. G.C. Branco, L. Lavoura and J.P. Silva, *CP Violation* (Clarendon Press, Oxford, 1999).

395. L. Wolfenstein, Phys. Rev. Lett. **51**, 1945 (1983).

396. E. Ma, J. Okada, Phys. Rev. Lett. **41**, 287 (1978).

397. G. 't Hooft, Phys. Lett. **37**B, 195 (1971).

398. C.E. Ortiz et al., Phys. Rev. Lett. **85**, 2909 (2000); for earlier work, see J.N. Bahcall et al., Phys. Rev. C**54**, 411 (1996); J.N. Bahcall, B.R. Holstein, Phys. Rev. C**33**, 2121 (1986).

399. M. Ram, Phys. Rev. **155**, 1539 (1967).

400. P. Salomonson, Y. Ueda, Phys. Rev. D**11**, 2606 (1975).

401. M. Green, M. Veltman, Nucl. Phys. B**169**, 137 (1980).

402. K.-I. Aoki et al., Prog. Theor. Phys. **65**, 1001 (1981); K.-I. Aoki, Z. Hioki, Prog. Theor. Phys. **66**, 2234 (1981).

403. S. Sarantakos, A. Sirlin, W.J. Marciano, Nucl. Phys. B**217**, 84 (1983).

404. J.N. Bahcall, M. Kamionkowski, A. Sirlin, Phys. Rev. D**51**, 6146 (1995).

405. T. Kinoshita, J. Math. Phys. **3**, 650 (1962); T.D. Lee, M. Nauenberg, Phys. Rev. **133**, B1549 (1964).

406. P. Vogel, Phys. Rev. D**29**, 1918 (1984).

407. S.A. Fayans, Yad. Fiz. **42**, 929 (1985) [Sov. J. Nucl. Phys. **42**, 590 (1985)].

408. M. Igarashi, S. Nakamura, Prog. Theor. Phys. **40**, 576 (1968).

409. C.H. Llewellyn-Smith, Phys. Rep. **3**, 261 (1972).

410. B. Bartoli, F. Felicetti, V. Silvestrini, Riv. Nuovo Cimento **2**, 241 (1972); M. Gourdin, Phys. Rept. **11**, 29 (1974).

411. N.J. Baker et al., Phys. Rev. D**23**, 2499 (1981); K.L. Miller et al., Phys. Rev. D**26**, 537 (1982); T. Kitagaki et al., Phys. Rev. D**42**, 1331 (1990); earlier results are compiled in Baker et al., op. cit.

412. L.A. Ahrens et al., Phys. Rev. D**35**, 785 (1987); for earier experiments, W. Lee et al., Phys. Rev. Lett. **37**, 186 (1976); D. Cline et al., Phys. Rev. Lett. **37**, 252 (1976); J. Horskotte et al., Phys. Rev. D**25**, 2743 (1982) and references therein.

413. S. Nakamura, T. Sato, V. Gudkov, K. Kubodera, Phys. Rev. C**63**, 034617 (2001).

414. M. Fukugita, Y. Kohyama, K. Kubodera, Phys. Lett. B**212**, 139 (1988).

415. W.C. Haxton, Phys. Rev. D**36**, 2283 (1987).

416. T. Kuramoto, M. Fukugita, Y. Kohyama, K. Kubodera, Nucl. Phys. A**512**, 711 (1990).

417. J. Toivanen et al., Nucl. Phys. A**694**, 395 (2001).

418. J.N. Bahcall, C.A. Barnes, Phys. Lett. **12**, 48 (1964).

419. J.C. Hardy, R.I. Verrall, Phys. Rev. Lett. **13**, 764 (1964); P.L. Reeder, A.M. Poskanzer, R.A. Esterlund, Phys. Rev. Lett. **13**, 767 (1964).

420. R.G. Sextro, R.A. Gough, J. Cerny, Nucl. Phys. A**234**, 130 (1974).

421. A. García et al., Phys. Rev. Lett. **67**, 3654 (1991).

422. T.W. Donnelly, J.D. Walecka, Ann. Rev. Nucl. Sci. **25**, 329 (1975).

423. T.W. Donnelly, Phys. Lett. **43**B, 93 (1973).

424. R.S. Raghavan, S. Pakvasa, B.A. Brown, Phys. Rev. Lett., **57**, 1801 (1986); R.S. Raghavan, S. Pakvasa, Phys. Rev. D**37**, 849 (1988).

425. C.D. Goodman et al., Phys. Rev. Lett. **44**, 1755 (1980); F. Petrovich, W.G. Love, R.J. McCarthy, Phys. Rev. C**21**, 1718 (1980).

426. T.N. Taddeucci et al., Nucl. Phys. A**469**, 125 (1987).

427. J.W. Watson et al., Phys. Rev. Lett. **55**, 1369 (1985).

428. N. Hata, W. Haxton, Phys. Lett. B**353**, 422 (1995); W.C. Haxton, Phys. Lett. B**431**, 110 (1998).

429. S.M. Austin et al., Phys. Rev. Lett. **73**, 30 (1994).

430. H. Ejiri et al., Phys. Lett. B**433**, 257 (1998).

431. J.N. Bahcall, Rev. Mod. Phys. **50**, 881 (1978).

432. J.N. Bahcall, Phys. Rev. Lett. **23**, 251 (1969).

433. J.N. Bahcall, Phys. Rev. Lett. **12**, 300 (1964).

434. W. Trinder et al., Phys. Lett. B**349**, 267 (1995).

435. J. Rapaport et al., Phys. Rev. Lett. **47**, 1518 (1981).

436. D. Wells, Bull. Am. Phys. Soc. Serie II, **37**, 1296 (1992); M.B. Aufderheide et al., Phys. Rev. C**46**, 2251 (1992).

437. E.G. Adelberger, W.C. Haxton, Phys. Rev. C**36**, 879 (1987).

438. M.B. Aufderheide, S.D. Bloom, D.A. Resler, C.D. Goodman, Phys. Rev. C49, 678 (1994).

439. J.N. Bahcall, R.K. Ulrich, Rev. Mod. Phys. 60, 297 (1988).

440. T.W. Donnelly, W.C. Haxton, Nucl. Phys. A287, 506 (1977).

441. G. Audi, A.H. Wapstra, cited in [445].

442. J.N. Bahcall, M.H. Pinsonneault, S. Basu, Astrophys. J. 555, 990 (2001).

443. W. Hampel, L.P. Remsberg, Phys. Rev. C31, 666 (1985).

444. D. Krofcheck et al., Phys. Rev. Lett., 55, 1051 (1985).

445. J.N. Bahcall, Phys. Rev. C56, 3391 (1997).

446. G.J. Mathews et al., S.D. Bloom, G.M. Fuller, J.N. Bahcall, Phys. Rev. C32, 796 (1985).

447. K. Grotz, H.V. Klapdor, J. Metzinger, Astron. Astrophys. 154, L1 (1986).

448. P. Anselmann et al., Phys. Lett. B342, 440 (1995); W. Hampel et al., Phys. Lett. B388, 384 (1996).

449. J.N. Abdurashitov et al., Phys. Rev. Lett. 77, 4708 (1996); Phys. Rev. C59, 2246 (1999).

450. S.S. Gershteïn, N. van Hieu, R.A. Éramzhyan, Zh. Eksp. Teor. Fiz. 43, 1554 (1962) [Sov. Phys. JETP 16, 1097 (1963)].

451. H.C. Lee, Nucl. Phys. A294, 473 (1978).

452. J. Bernabéu, P. Pascual, Nucl. Phys. A324, 365 (1979).

453. T.W. Donnelly, R.D. Peccei, Phys. Rep. 50, 1 (1979).

454. J. Arafune, M. Fukugita, Y. Kohyama, K. Kubodera, Phys. Lett. B217, 186 (1989).

455. M. Pourkaviani, S.L. Mintz, J. Phys. G16, 569 (1990).

456. J.S. O'Connell, T.W. Donnelly, J.D. Walecka, Phys. Rev. C6, 719 (1972).

457. H. Überall, B.A. Lamers, J.B. Langworthy, F.J. Kelly, Phys. Rev. C6, 1911 (1972).

458. B.T. Chertok et al., Phys. Rev. C8, 23 (1973).

459. E.A.J.M. Offermann et al., Phys. Rev. C44, 1096 (1991).

460. B.A. Bodmann et al., Phys. Lett. B339, 215 (1994).

461. S. Nozawa, Y. Kohyama, K. Kubodera, Prog. Theor. Phys. 70, 892 (1983).

462. S.L. Mintz, M. Pourkaviani, Phys. Rev. C40, 2458 (1989).

463. J. Engel, E. Kolbe, K. Langanke, P. Vogel, Phys. Rev. C54, 2740 (1996).

464. R.C. Allen et al., Phys. Rev. Lett. 64, 1871 (1990); D.A. Krakauer et al., Phys. Rev. C45, 2450 (1992).

465. E. Kolbe, K. Langanke, S. Krewald, Phys. Rev. C49, 1122 (1994).

466. N. Auerbach, N. Van Giai, O.K. Vorov, Phys. Rev. C56, R2368 (1997).

467. A.C. Hayes, I.S. Towner, Phys. Rev. C61, 044603 (2001).

468. B. Bodmann et al., Phys. Lett. B267, 321 (1991); 280, 198 (1992); in Neutrino 92, Granada, 1992, ed. by A. Morales, Nucl. Phys. B (Proc. Suppl.) 31, 301 (1993) [KARMEN].

469. B. Armbruster et al., Phys. Lett. B423, 15 (1998) [KARMEN].

470. C. Athanassopoulos et al., Phys. Rev. C55, 2078; C56 2806 (1997).

471. M. Buballa, S. Drożdż, S. Krewald, J. Speth, Ann. Phys. 208, 346 (1991).

472. P. Vogel, in 5th International WEIN Symposium: A Conference on Physics beyond the Standard Model, Santa Fe 1998 (World Scientific, Singapore 1999), p. 204.

473. K. Kubodera, S. Nozawa, Int. J. Mod. Phys. E3, 101 (1994).

474. J.B. Langworthy, B.A. Lamers, H. Überall, Nucl. Phys. A280, 351 (1977).

475. F.J. Kelly, H. Überall, Phys. Rev. Lett. **16**, 145 (1966).

476. S.D. Ellis, J.N. Bahcall, Nucl. Phys. **A114**, 636 (1968).

477. A. Ali, C.A. Dominguez, Phys. Rev. **D12**, 3673 (1975).

478. S. Nozawa, Y. Kohyama, T. Kaneta, K. Kubodera, J. Phys. Soc. Jpn., **55**, 2636 (1986); J.N. Bahcall, K. Kubodera, S. Nozawa, Phys. Rev. **D38**, 1030 (1988).

479. H.A. Bethe and R. Peierls, Proc. R. Soc. London, **A149**, 176 (1935).

480. N. Tatara, Y. Kohyama, K. Kubodera, Phys. Rev. **C42**, 1694 (1990); M. Doi, K. Kubodera, Phys. Rev. **C45**, 1988 (1992). Their unpublished calculations are summarised in [473].

481. J.D. Walecka, in *Meson Physics*, Vol. 2, eds. V.W. Hughes, C.S. Wu (Academic Press, New York 1975), p. 113.

482. S. Ying, W.C. Haxton, E.M. Henley, Phys. Rev. **C40**, 3211 (1989).

483. S. Ying, W.C. Haxton, E.M. Henley, Phys. Rev. **C45**, 1982 (1992).

484. M. Butler, J.-W. Chen, Nucl. Phys. **A675**, 575 (2000); M. Butler, J.-W. Chen, X. Kong, Phys. Rev. **C63**, 035501 (2001)

485. R.V. Reid, Jr., Ann. Phys. (N.Y.) **50**, 411 (1968); M. Lacombe et al., Phys. Rev. **C21**, 861 (1980) [Paris potential]; R.B. Wiringa, V.G.J. Stoks, R. Schiavilla, Phys. Rev. **C51**, 38 (1995) [Argonne potential]; V.G.J. Stoks, R.A.M. Klomp, C.P.F. Terheggen, J.J. de Swart, Phys. Rev. **C49**, 2950 (1994) [Reid93 potential, Nijmegen potential].

486. J. Carlson, D.O. Riska, R. Schiavilla, R.B. Wiringa, Phys. Rev. **C44**, 619 (1991).

487. S.P. Riley et al., Phys. Rev. **C59**, 1780 (1999); see also S.E. Willis et al., Phys. Rev. Lett. **44**, 522 (1980).

488. I.S. Towner, Phys. Rev. **C58**, 1288 (1998).

489. J.S. Bell, C.H. Llewellyn Smith, Nucl. Phys. **B28**, 317 (1971).

490. R.A. Smith, E.J. Moniz, Nucl. Phys. **B43**, 605 (1972).

491. E.V. Bugaev, G.S. Bisnovatyi-Kogan, M.A. Rudzsky, Z.F. Seidov, Nucl. Phys. **A324**, 350 (1979).

492. T.K. Gaisser, J.S. O'Connell, Phys. Rev. **D34**, 822 (1986).

493. M. Nakahata et al., J. Phys. Soc. Jpn. **55**, 3786 (1986); T. Kajita, in *Physics and Astrohysics of Neutrinos*, ed. by M. Fukugita, A. Suzuki (Springer Verlag, Tokyo 1994), p. 559.

494. S.K. Singh, E. Oset, Phys. Rev. **C48**, 1246 (1993).

495. M. Fukugita, Y. Kohyama, K. Kubodera, T. Kuramoto, Astrophys. J. **337**, L59 (1989).

496. E. Kolbe, K. Langanke, F.-K. Thielemann, P. Vogel, Phys. Rev. **C52**, 3437 (1995).

497. S.L. Mintz, M. Pourkaviani, Nucl. Phys. **A594**, 346 (1995).

498. S.M. Berman, M. Veltman, Nuovo Cimento Serie X **38**, 993 (1965).

499. C.H. Albright, L.S. Liu, Phys. Rev. **140**, B748 (1965).

500. S.L. Adler, Ann. Phys. **50**, 189 (1968).

501. G.L. Fogli, G. Nardulli, Nucl. Phys. **B160**, 116 (1979).

502. P. Allen et al., Nucl. Phys. **B176**, 269 (1980) [BEBC]; B. Conforto, in *Proc. Topical Conf. on Neutrino Phys.*, ed. by G. Michette, P.B. Renton, Oxford (1978), p. 90.

503. J. Bell et al., Phys. Rev. Lett. **41**, 1008; 1012 (1978) [FNAL]; B. Roe, in *Proc. Topical Conf. on Neutrino Phys.*, ed. by A.G. Michette, P.B. Renton, Oxford (1978), p. 94.

504. S.J. Barish et al., Phys. Rev. Lett. **36**, 179 (1976); Phys. Rev. D**19**, 2521 (1979) [ANL]; G. Levman, *in Proc. Topical Conf. on Neutrino Phys.*, ed. by A.G. Michette, P.B. Renton, Oxford (1978), p. 58.

505. W. Lerche et al., Phys. Lett. **78**B, 510 (1978) [GGM]; M. Pohl, in *Proc. Topical Conf. on Neutrino Phys.* ed. by A.G. Michette, P.B. Renton, Oxford (1978), p. 78.

506. A.J. Dufner, Y.S. Tsai, Phys. Rev. **168**, 1801 (1968).

507. R.C.E. Devenish, D.H. Lyth, Nucl. Phys. B**93**, 109 (1975).

508. D. Rein, L.M. Sehgal, Ann. Phys. **113**, 79 (1981).

509. G.L. Fogli, G. Nardulli, Nucl. Phys. B**165**, 162 (1980).

510. S.L. Adler, S. Nussinov, E.A. Paschos, Phys. Rev. D**9**, 2125 (1974).

511. R.P. Feynman, *Photon-Hadron Interactions* (W.A. Benjamin, Reading, Massachusetts 1972).

512. G. Altarelli, G. Parisi, Nucl. Phys. B**126**, 298 (1977); see also V.N. Gribov, L.N. Lipatov, Yad. Fiz. **15**, 781 (1972) [Sov. J. Nucl. Phys. **15**, 438 (1972)].

513. H.L. Lai et al., Phys. Rev. D**51**, 4763 (1995) [CTEQ3]; J. Botts et al., Phys. Lett. B**304**, 159 (1993) [CTEQ1]; E. Eichten, I. Hinchliffe, K. Lane, C. Quigg, Rev. Mod. Phys. **56**, 579 (1984); **58**, 1065 (1986) (E).

514. M. Glück, E. Reya, A. Vogt, Z. Phys. C**53**, 127 (1992)

515. J.F. Owens, W.K. Tung, Ann. Rev. Nucl. Part. Sci. **42**, 291 (1992).

516. A.D. Martin, W.J. Stirling, R.G. Roberts, Phys. Lett. B**354**, 155 (1995); Phys. Rev. D**47**, 867 (1993).

517. in *Review of Particle Physics* Eur. Phys. J. C**15**. 1 (2000), p. 230.

518. W.J. Marciano, A. Sirlin, Phys. Rev. D**22**, 2695 (1980), R.G. Stuart, Z. Phys. C**34**, 445 (1987); experimentalists often use a computer code prepared in D.Yu. Bardin, O.M. Fedorenko, Sov. J. Nucl. Phys. **30**, 418 (1979).

519. H. Georgi, H.D. Politzer, Phys. Rev. D**14**, 1829 (1976); R.M. Barnett, Phys. Rev. D**14**, 70 (1976).

520. E.g., M. Diemoz, F. Ferroni, E. Longo, G. Martinelli, in *Neutrino Physics*, ed. by K. Winter (Cambridge University Press, Cambridge, 1991), p. 496

521. C. Quigg, M.H. Reno, T.P. Walker, Phys. Rev. Lett. **57**, 774 (1986); D.W. McKay, J.P. Ralston, Phys. Lett. B**167**, 103 (1986); A.V. Butkevich et al., Z. Phys. C**39**, 241 (1988).

522. M. Derrick et al., Phys. Lett. B**316**, 412 (1993); Z. Phys. C**65**, 379(1995) [ZEUS]; I. Abt et al., Nucl. Phys. B**407**, 515 (1993); T. Ahmed et al., Nucl. Phys. B**439**, 471(1995).

523. G.M. Frichter, D.W. McKay, J.P. Ralston, Phys. Rev. Lett. **74**, 1508 (1995).

524. R. Gandhi, C. Quigg, M.H. Reno, I. Sarcevic, Astroparticle Phys. **5**, 81 (1996).

525. D.Z. Freedman, Phys. Rev. D**9**, 1389 (1974); see H.A. Bethe, in *Proc. Int. School of Phys., 'Enrico Fermi'*, Course 91, Varenna 1984 (North Holland, Amsterdam 1986) p. 181, for a review of stellar collapse theory.

526. A. Drukier, L. Stodolsky, Phys. Rev. D**30**, 2295 (1984).

527. M.W. Goodman, E. Witten, Phys. Rev. D**31**, 3059 (1985).

528. P.G. Roll et al., Ann. Phys. (NY) **26**, 442 (1964).

529. R. Opher, Astron. Astrophys. **37**, 135 (1974); L. Stodolsky, Phys. Rev. Lett. **34**, 110 (1974).

530. N. Cabibbo, L. Maiani, Phys. Lett. **114**B, 115 (1982); P. Langacker, J.P. Leveille, J. Sheiman, Phys. Rev. D**27**, 1228 (1983).

531. P.F. Smith, J.D. Lewis, Phys. Lett. **127**B, 185 (1983).
532. M. Fukugita, D. Nötzold, G. Raffelt, J. Silk, Phys. Rev. Lett. **60**, 879 (1988).
533. D. Nötzold, G. Raffelt, Nucl. Phys. B**307**, 924 (1988).
534. F.J. Botella, C.-S. Lim, W.J. Marciano, Phys. Rev. D**35**, 896 (1987).
535. K. Enqvist, K. Kainulainen, J. Maalampi, Nucl. Phys. B**349**, 754 (1991).
536. S.L. Glashow, S. Weinberg, Phys. Rev. D**15**, 1958 (1977).
537. A.J. Buras, in *Probing the Standard Model of Particle Interactions*, ed. by F. David, R. Gupta (Elsevier, Amsterdam 1999), hep-ph/9806471.
538. T. Inami, C.S. Lim, Prog. Theor. Phys. **65**, 297 (1981).
539. S. Aoki et al., Phys. Rev. Lett. **80**, 5271 (1998) [JLQCD]; G. Kilcup, R. Gupta, S.R. Sharpe, Phys. Rev. D**57**, 1654 (1998); A. Ali Khan et al., Phys. Rev. D**64**, 114506 (2001) [CP-PACS]; see also M.B. Gavela et al., Nucl. Phys. B**306**, 677 (1988); C.W. Bernard, A. Soni, Nucl. Phys. Proc. Suppl. **17**, 495 (1990); G.W. Kilcup et al., Phys. Rev. Lett. **64**, 25 (1990); N. Ishizuka et al., Phys. Rev. Lett. **71**, 24 (1993).
540. J. Bijnens, J.-M. Gérard, G. Klein, Phys. Lett. B**257**, 191 (1991).
541. O. Hahn, F. Strassmann, Naturw. **27**, 11 (1939); L. Meitner, O.R. Frisch, Nature **143**, 239 (1939); see also O. Hahn, L. Meitner, F. Strassmann, Naturw. **26**, 475 (1938).
542. M.F. James, J. Nucl. Energy **23**, 517 (1969); see also Y. Declais et al. Phys. Lett. B **338**, 383 (1994) for newer data.
543. A. Suzuki, Nucl. Phys. B (Proc. Suppl.) **77**, 171 (1999).
544. G. Zacek et al., Phys. Rev. D**34**, 2621 (1986).
545. P. Vogel, G.K. Schenter, F.M. Mann, R.E. Schenter, Phys. Rev. C**24**, 1543 (1981); B.R. Davis, Jr., P. Vogel, F.M. Mann, R.E. Schenter, Phys. Rev. C**19**, 2259 (1979).
546. K. Schreckenbach, G. Golvin, W. Gelletly, F. von Feilitzsch, Phys. Lett. B**160**, 325 (1985); for an earlier experiment, R.E. Carter, F. Reines, J.J. Wagner, M.E. Wyman, Phys. Rev. **113**, 280 (1959).
547. A.A. Hahn et al., Phys. Lett. B**218**, 365 (1989).
548. B. Achkar et al., Phys. Lett. B**374**, 243 (1996).
549. N. Bohr, Phys. Rev. **55**, 418 (1939); N. Bohr, J.A. Wheeler, Phys. Rev. **56**, 426 (1939).
550. R.A. Lundy et al., Phys. Rev. Lett. **14**, 504 (1965); D. Dekkers et al., Phys. Rev. **137**, B962 (1965); J.V. Allaby et al., CERN Yellow Report 70-12 (1970); T. Eichten et al., Nucl. Phys. B**44**, 333 (1972); W.F. Baker et al., Phys. Lett. **51**B, 303 (1974); D.S. Barton et al., Phys. Rev. D**27**, 2580 (1983).
551. L.A. Ahrens et al., Phys. Rev. D**34**, 75 (1986) (BNL WBB); R. Blair et al., in *Neutrino 81*, Maui, 1981, ed. R.J. Cence, E. Ma, A. Roberts (University of Hawaii, Honolulu, 1981) Vol. 1, p. 311 (Fermilab NBB).
552. J.R. Sanford, C.L. Wang, BNL report 11299; 11479 (1967); C.L. Wang, Phys. Rev. Lett. **25**, 1068 (1970).
553. A. Liland, H. Pilkuhn, Phys. Lett. **29**B, 663 (1969).
554. S.J. Barish et al., Phys. Rev. D**16**, 3103 (1977).
555. M. Giesch et al., Nucl. Instr. Meth. **20**, 58 (1963).
556. C.A. Ramm, in Proc. *Int. Conf. Fundamental Aspects of Weak Interactions*, BNL report 837(C-39, 1963) p. 91.
557. C. Visser, NUBEAM, A Neutrino-Beam Simulator, Hydra Applications Library (CERN, 1979).

558. T. Maruyama, Ph D Thesis, Tohoku university report RCνS-01-02 (Tohoku University, 2000); K. Kaneyuki, personal communication.

559. M.A. Markov, I.M. Zheleznykh, Nucl. Phys. **27**, 385 (1961); G.T. Zatsepin, V.A. Kuzmin, Zh. Eksp. Teor. Fiz. **41**, 1818 (1961) [Sov. Phys. JETP **14**, 1294 (1962)]; L.V. Volkova, G.T. Zatsepin, Izv. Akad. Nauk SSSR ser Phys. **29**, 1740 (1965) [Eng. trans. **29**, 1570 (1965)].

560. R. Cowsik, Y. Pal, S.N. Tandon, Proc. Ind. Acad. Sci. **63**, 217 (1966); J.L. Osborn, S.S. Said, A.W. Wolfendale, Proc. Phys. Soc. London **86**, 93 (1965).

561. A.C. Tam, E.C.M. Young, *Proc. 11th Int. Cosmic Ray Conf.*, Budapest (1969) Vol.4, p. 307; L.V. Volkova, G.T. Zatsepin, Yad. Fiz. **14**, 211 (1971) [Sov. J. Nucl. Phys. **14**, 117 (1972)]. A. Dar, Phys. Rev. Lett. **51**, 227 (1983); T.K. Gaisser, T. Stanev, S.A. Bludman, H. Lee, Phys. Rev. Lett. **51**, 223 (1983).

562. K. Mitsui, H. Komori, Y. Minorikawa, Nuovo Cimento C9, 995 (1986).

563. T.K. Gaisser, T. Stanev, G. Barr, Phys. Rev. D**38**, 85 (1988); G. Barr, T.K. Gaisser, T. Stanev, Phys. Rev. D**39**, 3532 (1989).

564. V. Agrawal, T.K. Gaisser, P. Lipari, T. Stanev, Phys. Rev. D**53**, 1314 (1996).

565. M. Honda, K. Kasahara, K. Hidaka, S. Midorikawa, Phys. Lett. B**248**, 193 (1990); M. Honda, T. Kajita, K. Kasahara, S. Midorikawa, Phys. Rev. D**52**, 4985 (1995).

566. E.V. Bugaev, V.A. Naumov, Phys. Lett. B**232**, 391 (1989); see also E.V. Bugaev, V.A. Naumov, Izv. Akad. Nauk SSSR Ser. Fiz. **50**, 2239 (1986); Yad. Fiz. **45**, 1380 (1987) [Sov. J. Nucl. Phys. **45**, 857 (1987)].

567. A.V. Butkevich, L.G. Dedenko, I.M. Zheleznykh, Yad. Fiz. **50**, 142 (1989) [Sov. J. Nucl. Phys. **50**, 90 (1989)]; see also L.G. Dedenko, Izv. Akad. Nauk SSSR Ser. Fiz. **29**, 1722 (1965); A.V. Butkevich et al., Izv. Akad. Nauk SSSR Ser. Fiz. **46**, 2428 (1982).

568. H. Lee, Y.S. Koh, Nuovo Cimento **105**B, 883 (1990).

569. M. Kawasaki, S. Mizuta, Phys. Rev. D**43**, 2900 (1991).

570. L.V. Volkova, Yad Fiz. **31**, 1510 (1980) [Sov. J. Nucl. Phys. **31**, 784 (1980)].

571. Y. Tserkovnyak, R. Komar, C. Nally, C. Waltham, hep-ph/9907450.

572. G. Battistoni et al., Astroparticle Phys. **12**, 315 (2000); P. Lipari, Astroparticle Phys. **14**, 153 (2000).

573. T.K. Gaisser et al., Phys. Rev. D**54**, 5578 (1996).

574. M. Honda, in *Physics and Astrophysics of Neutrinos*, op. cit. (see [493]) p. 606.

575. J.F. Ormes, W.R. Webber, *Proc. Int. Conf. Cosmic Rays*, London (1965), Spec 13, p. 349; M.J. Ryan, J.F. Ormes, V.K. Balasubrahmanyan, Phys. Rev. Lett. **28**, 985 (1972).

576. W.R. Webber, R.L. Golden, S.A. Stephens, in *Proc. 20th Int. Conf. Cosmic Rays*, ed. V.A. Kozyarivsky et al., (Moscow 1987), Vol. 1, p. 325.

577. E.S. Seo et al., Astrophys, J. **378**, 763 (1991) [LEAP].

578. R. Bellotti et al., Phys. Rev. D**60**, 052002 (1999) [MASS].

579. M. Boezio et al., Astrophys. J. **518**, 457 (1999) [CAPRICE].

580. W. Menn et al., Astrophys. J. **533**, 281 (2000) [IMAX].

581. T. Sanuki et al., Astrophys. J. **545**, 1135 (2000) [BESS].

582. J. Alcaraz et al., Phys. Lett. B**490**, 27 (2000) [AMS].

583. M. Amenomori et al., Phys. Rev. D**62**, 112002 (2000).

584. M. Ichimura et al., Phys. Rev. D**48**, 1949 (1993).

585. V.I. Zatsepin et al., in *Proc. 23rd Int. Cosmic Ray Conf.*, Calgary, 1993, Vol. 2, p. 13.
586. K. Asakimori et al., Astrophys. J. **502**, 278 (1998) [JACEE].
587. J. Alcaraz et al., Phys. Lett. B**494**, 193 (2000) [AMS].
588. J.J. Engelmann et al., Astron. Astrophys. **233**, 96 (1990).
589. M. Simon et al., Astrophys. J. **239**, 712 (1980)
590. E.N. Parker, *Interplanetary Dynamical Processes* (Interscience, New York 1963), p. 161.
591. L.J. Gleeson, W.I. Axford, Astrophys. J. **149**, L115 (1967); Astrophys. J. **154**, 1011 (1968).
592. J.R. Jokipii, P.J. Coleman Jr., J. Geophys. Res. **73**, 5495 (1968).
593. K. Nagashima, S. Sakakibara, K. Murakami, I. Moroshita, Nuovo Cimento C**12**, 173 (1989).
594. C. Störmer, Astrophysics **1**, 237 (1930); *The Polar Aurora* (Oxford Clarendon Press, London 1955).
595. D.R. Barraclough et al., J. Geomag. Geoelectr. **37**, 1157 (1985).
596. D.J. Cooke, Phys. Rev. Lett. **51**, 320 (1983).
597. L.I. Dorman, V.S. Smirnov, M.I. Tyasto, *Cosmic Rays in the Magnetic Field of the Earth* (Nauk, Moscow 1973, in Russian).
598. W.E. Forsythe, *Smithonian Physical Tables* (Smithsonian Institution Press, Washington, D.C. 1969).
599. S. Hayakawa, *Cosmic Ray Physics: Nuclear and Astrophysical Aspects* (Wiley-Interscience, New York, 1969); the problem may be handled by GEANT of CERN computer programme library (PHYS001).
600. R.P. Kokoulin and A.A. Petrukhin, in *Proc. 11th Int. Conf. Cosmic Rays*, Budapest 1969, Acta Phys. **29** Suppl. Vol. 4, 277 (1970).
601. L.B. Bezrukov, E.V. Bugaev, Yad. Fiz. **33**, 1195 (1981) [Sov. J. Nucl. Phys. **33**, 635 (1981)]; W. Lohmann, R. Kopp, R. Voss, CERN Yellow Report 85-03 (1985); S. Klimushin, E. Bugaev and I. Sokalski, in *Proc. 27th Int. Cosmic Ray Conf.*, Hamburg 2001, op. cit. Vol. 3, 1009 (2001).
602. M. Honda, T. Kajita, K. Kasahara, S. Midorikawa, Phys. Rev. D**64**, 053011 (2001).
603. L.V. Volkova, in *Cosmic Gamma Rays, Neutrinos and Relativistic Astrophysics*, ed. by M.M. Shapiro, J.P. Wefel (Kluwer, Dordrecht 1989), p. 139; see also S.M. Barr, T.K. Gaisser, P. Lipari, S. Tilav, Phys. Lett. B**214**, 147 (1988).
604. K. Kasahara, S. Torii, T. Yada, in *Proc. 16th Int. Cosmic Ray Conf.*, Kyoto 1979, ed. by S. Miyake (University of Tokyo, Tokyo 1979), Vol. 13, p. 70.
605. K. Hänssgen, J. Ranft, Comput. Phys. Commun. **39**, 37 (1986).
606. B. Nilsson-Almqvist, E. Stenlund, Comput. Phys. Commun. **43**, 387 (1987).
607. T.K. Gaisser, R.J. Protheroe, T. Stanev, in *Proc. 18th Int. Cosmic Ray Conf.*, Bangalore 1983, ed. by N. Durgaprasad et al., Vol. 5, (Tata Institute, Bombay 1983) p. 174.
608. A.N. Kalinovsky, N.V. Mokhov, Yu.P. Nikitin, *Transport of High Energy Particles Through Matter* (Energoatomizdat, Moscow 1985); L.R. Kimel, N.V. Mokhov, University Bulletin, Physics (Tomsk University) **10**, 17 (1974).
609. A. Ferrari, P. R. Sala, ATLAS, Trieste Internal Note ATL-PHYS-97-113 (1997)

610. M. Honda, T. Kajita, K. Kasahara, S. Midorikawa, in *Proc. Int. Cosmic Ray Conf. 2001*, Hamburg, ed. by K.-H. Kampert, G. Heinzelmann, C. Spiering (Copernicus Gesellschaft, Katlenburg-Lindau 2001), Vol. 3, p. 1162 (2001).

611. S. Roesler, R. Engel, J. Ranft, hep-ph/0012252 (SLAC-PUB-8740); in *Proc. Int. Cosmic Ray Conf. 2001*, Hamburg (op. cit.), Vol. 2, p. 439 (2001).

612. S. Chandrasekhar, *An Introduction to the Study of Stellar Structure* (University of Chicago Press, Chicago 1939).

613. M. Schwarzschild, *Structure and Evolution of the Stars* (Princeton University Press, Princeton 1958).

614. C. Hayashi, R. Hōshi, D. Sugimoto, Prog. Theor. Phys. Suppl. **22**, 1 (1962).

615. D.D. Clayton, *Principles of Stellar Evolution and Nucleosynthesis* (McGraw-Hill, New York 1968).

616. J.P. Cox, R.T. Giuli, *Principles of Stellar Structure* (Gordon and Breach, New York 1968).

617. R. Kippenhahn, A. Weigert, *Stellar Structure and Evolution* (Springer, Berlin 1990).

618. S.L. Shapiro, S.A. Teukolsky, *Black Holes, White Dwarfs and Neutron Stars* (Wiley, New York 1983).

619. H.A. Kramers, Phil. Mag. **46**, 836 (1923).

620. C.W. Allen, *Astrophysical Quantities*, 3rd ed. (Athlone Press, London 1973).

621. R. Emden, *Gaskugeln* (B.G. Teubner, Leipzig 1907); see [612].

622. R. Atkinson, F.G. Houtermans, Z. Phys. **54**, 656 (1929).

623. G. Gamow, E. Teller, Phys. Rev. **53**, 608 (1938).

624. J.N. Bahcall, Astrophys. J. **143**, 259 (1966).

625. E. Schatzman, J. Phys. Radium **9**, 46 (1948).

626. E.E. Salpeter, Austr. J. Phys. **7**, 373 (1954).

627. E.E. Salpeter, H.M. van Horn, Astrophys. J. **155**, 183 (1969); H.C. Graboske, H.E. De Witt, A.S. Grossman, M.S. Cooper, Astrophys. J. **181**, 457 (1973); H.E. Mitler, Astrophys. J. **211**, 513 (1977).

628. C. Carraro, A. Schäfer, S.E. Coonin, Astrophys. J. **331**, 565 (1988); H. Dzitko, S. Turck-Chièze, P. Delbourgo-Salvator, C. Lagrange, Astrophys. J. **447**, 428 (1995).

629. A.V. Gruzinov, J.N. Bahcall, Astrophys. J. **504**, 996 (1998).

630. N.J. Shaviv, G. Shaviv, Astrophys. J. **468**, 433 (1996).

631. M. Brüggen, D.O. Gough, Astrophys. J. **488**, 867 (1997).

632. C.F. von Weizsäcker, Phys. Zs. **38**, 176 (1937).

633. H.A. Bethe, C.L. Critchfield, Phys. Rev. **54**, 248; 862 (1938).

634. E.E. Salpeter, Phys. Rev. **88**, 547 (1952).

635. E. Frieman, L. Motz, Phys. Rev. **83**, 202 (1951).

636. J.N. Bahcall, R.M. May, Astrophys. J. **155**, 501 (1969).

637. M. Kamionkowski, J.N. Bahcall, Astrophys. J. **420**, 884 (1994).

638. J.N. Bahcall, Phys. Rev. **128**, 1297 (1962); Phys. Rev. D**49**, 3923 (1994).

639. I. Iben, Jr., K. Kalata, J. Schwartz, Astrophys. J. **150**, 1001 (1967).

640. E.G. Adelberger et al., Rev. Mod. Phys. **70**, 1265 (1998).

641. P.D. Parker, J.N. Bahcall, W.A. Fowler, Astrophys. J. **139**, 602 (1964).

642. C.F. von Weizsäcker, Phys. Zs. **39**, 633 (1938).

643. H.A. Bethe, Phys. Rev. **55**, 434 (1939).

644. J.N. Bahcall, M.H. Pinsonneault, S. Basu, Astrophys. J. **555**, 990 (2001) [BP2000]; J.N. Bahcall, S. Basu, M.H. Pinsonneault, Phys. Lett. B**433**, 1 (1998) [BP98].

645. W.A. Fowler, Rev. Mod. Phys. **56**, 149
646. W.A. Fowler, G.R. Caughlan, B.A. Zimmerman, Ann. Rev. Astron. Astro-phys. **5**, 525 (1967); **13**, 69 (1975); M.J. Harris, W.A. Fowler, G.R. Caughlan, B.A. Zimmerman, *ibid* **21**, 165 (1983); G.R. Caughlan, W.A. Fowler, Atomic Data and Nuclear Data Tables, **40**, 283 (1988).
647. A. Dar, G. Shaviv, Astrophys. J. **468**, 933 (1996).
648. C. Angulo et al., Nucl. Phys. A**656**, 3 (1999).
649. M. Junker et al., Phys. Rev. C**57**, 2700 (1998) [LUNA].
650. V.S. Vasilevskii, I. Yu Rybkin, Sov. J. Nucl. Phys. **50**, 411 (1989); S. Typel, G. Bluge, K. Langanke, W.A. Fowler, Z. Phys. A**339**, 249 (1991); P. De-scouvemont, Phys. Rev. C**50**, 2635 (1994); A. Csótó, Phys. Rev. C**49**, 3035 (1994).
651. R.F. Christy, I. Duck, Nucl. Phys. **24**, 89 (1961); T.A. Tombrello, G.C. Phillips, Phys. Rev. **122**, 224 (1961); T.A. Tombrello, P.D. Parker, Phys. Rev. **131**, 2582 (1963).
652. R.W. Kavanagh, T.A. Tombrello, J.M. Mosher, D.R. Goosman, Bull Am. Phys. Soc. **14**, 1209 (1969)
653. P.D. Parker, Phys. Rev. **150**, 851 (1966); Astrophys. J. **153**, L85 (1968).
654. B.W. Filippone, A.J. Elwyn, C.N. Davids, D.D. Koetke, Phys. Rev. C**28**, 2222 (1983).
655. F.J. Vaughn, R.A. Chalmers, D. Kohler, L.F. Chase, Jr., Phys. Rev. C**2**, 1657 (1970).
656. F. Hammache et al., Phys. Rev. Lett. **80**, 928 (1998).
657. A. Azhari et al., Phys. Rev. C**60**, 055803 (1999).
658. M. Haas et al., Phys. Lett. B**462**, 237 (1999).
659. T. Kikuchi et al., Phys. Lett. B**391**, 261 (1997); see also T. Motobayashi et al., Phys. Rev. Lett. **73**, 2680 (1994).
660. N. Iwasa et al., Phys. Rev. Lett. **83**, 2910 (1999).
661. R.G.H. Robertson, Phys. Rev. C**7**, 543 (1973); F.C. Barker, Aust. J. Phys. **33**, 177 (1980).
662. R. Schiavilla, R.B. Wiringa, V.R. Randharipande, J. Carlson, Phys. Rev. C**45**, 2628 (1992).
663. L.E. Marcucci et al., Phys. Rev. Lett. **84**, 5959 (2000); see also idem Phys. Rev. C**63**, 015801 (2001).
664. L. Heyney, M.S. Vardya, P. Bodenheimer, Astrophys. J. **142**, 841 (1965).
665. W.F. Huebner, in *Physics of the Sun*, ed. by P.A. Sturrock et al. (Reidel, Dordrecht 1986), vol. I, p. 33.
666. C.A. Iglesias, F.J. Rogers, Astrophys. J. **464**, 943 (1996); http://www-phys.llnl.gov/Research/OPAL/index.htm; earlier version is given in ibid, **371**, L73; **371**, 408 (1991).
667. For classical literature used for long, H.N. Russell, Astrophys. J. **70**, 11 (1929); L. Goldberg, E.A. Müller and L.H. Aller, Astrophys. J. Suppl. **5**, 1 (1960).
668. N. Grevesse, A. Noels, in *Origin and Evolution of the Elements*, ed. by N. Pantzos et al. (Cambridge University Press, Cambridge 1993), p. 15; the latest compilation is given in N. Grevesse, A.J. Sauval, in *Origin of Elements in the Solar System: Implications of Post-1957 Observations*, ed. by O. Manuel (Kluwer, Dordrecht 2000), p. 261; see also E. Anders, N. Grevesse, Geochim. Cosmochim. Acta **53**, 197 (1989).

669. W.R. van Schmus, J.A. Wood, Geochim. Cosmochim. Acta **31**, 747 (1967).

670. S. Basu, H.M. Antia, Mon. Not. R. astr. Soc. **287**, 189 (1997).

671. H. Holweger, M. Kock, A. Bard, Astron. Astrophys. **296**, 233 (1995).

672. D.E. Blackwell, A.E. Lynas-Gray, G. Smith, Astron. Astrophys. **296**, 217 (1995).

673. A. McWilliam, Ann. Rev. Astron. Astrophys. **35**, 503 (1997).

674. F.J. Rogers, F.J. Swenson, C.A. Iglesias, Astrophys. J. **456**, 902 (1996) [OPAL]; O.R. Pols, C.A. Tout, P.P. Eggleton, Z. Han, Mon. Not. R. astr. Soc. **274**, 964 (1995); D.B. Guenther, P. Demarque, Y.-C. Kim, M.H. Pinsonneault, Astrophys. J. **387**, 372 (1992); for earlier work, see, P.P. Eggleton, J. Faulkner, B.P. Flannery, Astron. Astrophys. **23**, 325 (1973); D. Mihalas, W. Däppen, D.G. Hummer, Astrophys. J. **331**, 815 (1988).

675. J.N. Bahcall, M.H. Pinsonneault (with G.J. Wasserburg), Rev. Mod. Phys. **67**, 781 (1995).

676. C. Fröhlich, J. Lean, 1998, Geophys. Res. Lett. **25**, 4377 (1998); D. Crommelynck, A. Fichot, V. Domingo, R. Lee, III, Geophys. Res. Lett. **23**, 2293 (1996); the mean value quoted here is due to [644].

677. P.D. Noerdlinger, Astron. Astrophys. **57**, 407 (1977).

678. A.N. Cox, Jr., A. Guzik, R.B. Kidman, Astrophys. J. **342**, 1187 (1989).

679. J.N. Bahcall, A. Loeb, Astrophys. J. **360**, 267 (1990).

680. A. Kovetz, G. Shaviv, Astrophys. J. **426**, 787 (1994).

681. S. Turcotte et al., Astrophys. J. **504**, 539 (1998).

682. J.N. Bahcall, W.A. Fowler, I. Iben, R.L. Sears, Astrophys. J. **137**, 344 (1963); see also R.L. Sears, Astrophys. J. **140**, 477 (1964); P. Pochoda, H. Reeves, Planet. Space Sci, **12**, 119 (1964).

683. J.N. Bahcall, N.A. Bahcall, G. Shaviv, Phys. Rev. Lett. **20**, 1209 (1968).

684. S. Turck-Chièze, S. Cahen, M. Cassé, C. Doom 1988, Astrophys. J. **335**, 415 (1988); S. Turck-Chièze, I. Lopez, Astrophys. J. **408**, 347 (1993).

685. D.B. Guenther, A. Jaffe, P. Demarque, Astrophys. J. **345**, 1022 (1989).

686. I.-J. Sackman, A.I. Boothroyd, W.A. Fowler, Astrophys. J. **360**, 727 (1990).

687. C.R. Proffitt, Astrophys. J. **425**, 849 (1994).

688. O. Richard, S. Vauclair, C. Charbonnel, W.A. Dziembowski, Astron. Astrophys. **312**, 1000 (1996).

689. F. Ciacio, S. Degl'Innocenti, B. Ricci, Astron. Astrophys. Suppl. **123**, 449 (1997).

690. D.B. Guenther, P. Demarque, Astrophys. J. **484**, 937 (1997).

691. J.N. Bahcall, M.H. Pinsonneault, Rev. Mod. Phys. **64**, 885 (1992).

692. R.B. Leighton, R.W. Noyes, G.W. Simon, Astrophys. J. **135**, 474 (1962).

693. R.K. Ulrich, Astrophys. J. **162**, 993 (1970); see also J. Leibacher, R.F. Stein, Astrophys. Lett. **7**, 191 (1971).

694. C.L. Pekeris, Astrophys. J. **88**, 189 (1939); T.G. Cowling, Mon. Not. R. astr. Soc. **101**, 367 (1941).

695. F.-L. Deubner, Astron. Astrophys. **44**, 371 (1975).

696. C.L. Wolff, Astrophys. J. **177**, L87 (1972); H. Ando, Y. Osaki, Publ. Astr. Soc. Japan **27**, 581 (1975); R.K. Ulrich, E.J. Rhodes, Jr., Astrophys. J. **218**, 521 (1977).

697. A. Claverie et al., Nature **282**, 591 (1979).

698. G. Grec, E. Fossat, M.A. Pomeranz, Nature **288**, 541 (1980).

699. P. Ledoux, Th. Walraven, *Handb. d. Phys.* **51**, 353 (1958); J. Christensen-Dalsgaard, D. Gough, J. Toomre, Science **229**, 923 (1985); W. Unno, Y. Osaki, H. Ando, H. Shibahashi *Non-Radial Oscillation of Stars*, 2nd ed. (University of Tokyo Press, Tokyo 1979; 2nd edn, 1989); D. Gough, J. Toomre, Ann. Rev. Astron. Astrophys. **29**, 627 (1991);

700. M. Tassoul, Astrophys. J. Suppl. **43**, 469 (1980); see also Yu.V. Vandakurov, Astr. Zh. **44**, 786 (1967).

701. K.G. Libbrecht, M.F. Woodward, J.M. Kaufman, Astrophys. J. Suppl. **74**, 1129 (1990); Y. Elsworth et al., Mon. Not. R. astr. Soc. **251**, P7 (1991); J.W. Harvey et al., Science **272**, 1284 (1996) (GONG: Global Oscillation Network Group); W.I. Chaplin et al., Solar Phys. **168**, 1 (1996) (BiSON: Birmingham Solar Oscillation Network); S. Tomczyk et al., Mon. Not. R. astr. Soc. **292**, 243 (1997) (LOWL: Low degree with degree denoted by L); S. Turck-Chièze et al., Solar Phys. **175**, 247 (1997) (GOLF: Global Oscillation at Low Frequencies); E.J. Rhodes et al., Solar Phys. **175**, 287 (1997) (MDI: Michelson Doppler Imager); S. Thiery et al., Astron. Astrophys. **355**, 743 (2000) (GOLF).

702. Y. Elsworth et al., Nature **347**, 536 (1990).

703. J.N. Bahcall, M.H. Pinsonneault, S. Basu, J. Christensen-Dalsgaard, Phys. Rev. Lett. **78**, 171 (1997).

704. J. Christensen-Dalsgaard et al., Nature **315**, 378 (1985); J. Christensen-Dalsgaard, J. Schou, M.J. Thompson, Mon. Not. R. astr. Soc. **242**, 353 (1990).

705. H. Shibahashi, T. Sekii, in Proc. Symp. *Seismology of the Sun and Sun-Like Stars*, Tenerife, 1988 (ESA SP-286) ed. E.J. Rolfe (ESA, Paris 1988) p. 471; T. Sekii, H. Shibahashi, *ibid.* p. 521; Publ. Astron. Soc. Jpn. **41**, 311 (1989).

706. S.V. Vorontsov, in *Seismology of the Sun and Sun-Like Stars*, op. cit., p. 475 (1988).

707. R.L. Parker, Ann. Rev. Earth Planet. Sci. **5**, 35 (1977); W. Menke, *Geophysical Data Analysis: Discrete Inverse Theory* (Academic, Orland 1984); A. Deepak, *Inversion Methods in Atmospheric Remote Sounding* (Academic Press, New York 1977)

708. S. Basu et al., Mon. Not. R. astr. Soc. **292**, 243 (1997); S. Basu, Mon. Not. R. astr. Soc. **298**, 719 (1998)

709. A.S. Brun, S. Turck-Chièze, P. Morel, Astrophys. J. **506**, 913 (1998); S. Turck-Chièze, in Neutrino 2000, Nucl. Phys. B. (Proc. Suppl.) **91**, 73 (2001).

710. A.S. Brun, S. Turck-Chièze, J.P. Zahn, Astrophys. J. **525**, 1032 (1999).

711. J.N. Bahcall, R.K. Ulrich, Rev. Mod. Phys. **60**, 297 (1988).

712. J.N. Bahcall, A. Ulmer, Phys. Rev. D**53**, 4202 (1996).

713. D. Ezer, A.G.W. Cameron, Can. J. Phys. **45**, 3429 (1967); the table is taken from D. Sugimoto, *Uchū-Butsurigwaku* (Space Physics) [in Japanese], ed. C. Hayashi, S. Hayakawa (Iwanami, Tokyo 1978), p. 185.

714. D. Schönberner, T. Blöcker, F. Herwig, T. Driebe, cited in *Allen's Astrophysical Quantities*, 4th ed., ed. by A.N. Cox (Springer, New York 1999), p. 395.

715. R. Davis, Jr., in Proceedings cited in [716].

716. E.G. Friedlander (Ed.), *Proceedings: Informal Conference on Status and Future of Solar Neutrino Research*, Brookhaven National Laboratory, New York

1978 (BNL, Upton 1978), Vol. I and II; M.L. Cherry, K. Lande, W.A. Fowler (Eds.), *Solar Neutrinos and Neutrino Astronomy*, Homestake 1984, AIP Conference Proceedings No. 126 (American Inst. Physics, New York 1985).

717. K.S. Hirata et al., Phys. Rev. Lett. **63**, 16 (1989); **65**, 1297 (1990) [Kamiokande].

718. K. Arisaka et al., J. Phys. Soc. Japan **54**, 3213 (1985) [Kamiokande]; see H. Ikeda et al., in *Proc. 17th Int. Conf. Cosmic Rays*, Paris 1981 (1982), Vol. 7, p. 185 for the proposal.

719. J.N. Bahcall, in *Neutrino 90, Proc. 14th Int. Conf. on Neutrino Phys. and Astrophys.*, CERN, 1990, ed. by J. Panman, K. Winter, Nucl. Phys. B (Proc. Suppl.) **19**, 94 (1991); M. Fukugita, T. Yanagida, Mod. Phys. Lett. A**6**, 645 (1991); J.N. Bahcall, H.A. Bethe, Phys. Rev. Lett. **65**, 2233 (1990); Phys. Rev. D**47**, 1298 (1993); S. Bludman, N. Hata, P. Langacker, Phys. Rev. D**49**, 3622 (1994).

720. D.N. Abdurashitov et al., Phys. Lett. B**328**, 234 (1994) [SAGE].

721. B.T. Cleveland et al., Astrophys. J. **496**, 505 (1998).

722. Y. Fukuda et al., Phys. Rev. Lett. **77**, 1683 (1996) [Kamiokande].

723. S. Fukuda et al., Phys. Rev. Lett, **86**, 5651 (2001) [Super-Kamiokande].

724. M. Altmann et al., Phys. Lett. B**490**, 16 (2000) [GALLEX/GNO].

725. J.N. Abdurashitov et al., astro-ph/0204245 (2002); Phys. Rev. C**60**, 055801 (1999) [SAGE].

726. H.-Y. Chiu, R.C. Stabler, Phys. Rev. **122**, 1317 (1961); V.I. Ritus, Zh. Eksp. Teor. Fiz. **41**, 1285 (1961) [JETP **14**, 915 (1962)].

727. H.-Y. Chiu, R.C. Stabler, ref. [726]; H.Y. Chiu, Phys. Rev. **123**, 1040 (1961).

728. J.B. Adams, M.A. Ruderman, C.-H. Woo, Phys. Rev. **129**, 1383 (1963); C.L. Inman, M.A. Ruderman, Astrophys. J. **140**, 1025 (1964). These references give results too large by a factor of 4 for decay of the transverse mode. This error was corrected by M.H. Zaidi, Nuovo Cimento A**40**, 502 (1965).

729. G.G. Festa, M.A. Ruderman, Phys. Rev. **180**, 1227 (1969).

730. G. Beaudet, V. Petrosian, E.E. Salpeter, Astrophys. J. **150**, 979 (1967).

731. D.A. Dicus, Phys. Rev. D**6**, 941 (1972) [The cross section formula for the photoneutrino production contains an error in the factor]; D.A. Dicus, E.W. Kolb, D.N. Schramm, D.L. Tubbs, Astrophys. J. **210**, 481 (1976); P.J. Schinder et al., Astrophys. J. **313**, 531 (1987); N. Itoh, Y. Kohyama, Astrophys. J. **275**, 858 (1983); N. Itoh et al., Astrophys. J. **339**, 354 (1989); E. Braaten, Phys. Rev. Lett. **66**, 1655 (1991); E. Braaten, D. Segel, Phys. Rev. D**48**, 1478 (1993); M. Haft, G. Raffelt, A. Weiss, Astrophys. J. **425**, 222 (1994).

732. N. Itoh, H. Hayashi, A. Nishikawa, Y. Kohyama, Astrophys. J. Suppl. **102**, 411.

733. H.-Y. Chiu, E.E. Salpeter, Phys. Rev. Lett. **12**, 413 (1964).

734. E.G. Flowers, P.G. Sutherland, J.R. Bond, Phys. Rev. D**12**, 315 (1975); S. Hannestad, G. Raffelt, Astrophys. J. **507**, 339 (1998).

735. H. Suzuki, in *Frontiers of Neutrino Astrophysics*, Takayama, 1992 ed. Y. Suzuki, K. Nakamura (Universal Academy Press, Tokyo 1993), p. 219; T.A. Thompson, A. Burrows, J.E. Horvath, Phys. Rev. C**62**, 035802 (2000).

736. P. Schröder, R. Smith, K. Apps, Astron. Geophys. **42**, 6.26 (2001).

737. I. Iben, Jr., Ann. Rev. Astron. Astrophys. **5**, 571 (1967); **12**, 215 (1974); I. Iben, Jr., A. Renzini, Phys. Rep. **105**, 329 (1984); P. Bouvier, A. Maeder

(Eds.), *Advanced Stages in Stellar Evolution* (Geneva, 1977); A. Maeder, A. Renzini (Eds.), *Observational Tests of the Stellar Evolution Theory*, Proc. IAU Symp. 105 (Reidel, Dordrecht 1984).

738. B. Paczyński, Acta Astron. **20**, 47 (1970).

739. A.V. Sweigart, P.G. Gross, Astrophys. J. Suppl. **32**, 367 (1976); **36**, 405 (1978).

740. G.G. Raffelt, Phys. Rev. Lett. **64**, 2856 (1990).

741. D.J. Faulkner, R.D. Cannon, Astrophys. J. **180**, 435 (1973).

742. M. Fukugita, S. Yazaki, Phys. Rev. **D36**, 3817 (1987).

743. G.G. Raffelt, *Stars as Laboratories for Fundamental Physics* (University of Chicago Press, Chicago 1996); Ann. Rev. Nucl. Part. Sci. **49**, 163 (1999).

744. F. Hoyle, W.A. Fowler, Astrophys. J. **132**, 565 (1960); W.D. Arnett, Astrophys. Space Sci. **5**, 180 (1969); I. Iben, Tutkov, Astrophys. J. Suppl. **54**, 335 (1984); for reviews, S.E. Woosley, T.A. Weaver, Ann. Rev. Astron. Astrophys. **24**, 205 (1986); K. Nomoto, M. Hashimoto, Astrophys. Space Sci. **131**, 395 (1987); W. Hillebrandt, J.C. Niemeyer, Ann. Rev. Astron. Astrophys. **38**, 191 (2000).

745. T.A. Weaver, G.B. Zimmerman, S.E. Wooseley, Astrophys. J. **225**, 1021 (1978)

746. E.M. Burbidge, G.R. Burbidge, W.A. Fowler, F. Hoyle, Rev. Mod. Phys. **29**, 547 (1957).

747. A.G.W. Cameron, Publ. Astron. Soc. Pacific **69**, 201 (1957).

748. R.B. Stothers, Astrophys. J. **155**, 935 (1969); R.B. Stothers, C.-W. Chin, Astrophys. J. **158**, 1039 (1969).

749. R.H. Fowler, Mon. Not. R. astr. Soc. **87**, 114 (1926).

750. S. Chandrasekhar, Astrophys. J. **74**, 81 (1931); see also idem Phil. Mag. **11**, 592 (1931).

751. L. Mestel, Mon. Not. Roy. astr. Soc. **112**, 583 (1952).

752. S.C. Villa, Astrophys. J. **146**, 437 (1966); **149**, 613 (1967).

753. W. Baade, F. Zwicky, Proc. Nat. Acad. Sci. USA **20**, 254 (1934).

754. C. Chiosi, G. Bertelli, A. Bressan, Ann. Rev. Astron. Astrophys. **30**, 235 (1992).

755. K. Nomoto, Astrophys. J. **277**, 791 (1984).

756. B.G. Marsden (Ed.), IAU Circular 4316 (1987): communication of the discovery of I. Shelton by W. Kunkel, B. Madore, followed by communications by F.M. Bateson, R.H. McNaught, B. Warner.

757. K. Hirata et al., Phys. Rev. Lett. **58**, 1490 (1987).

758. R.M. Bionta et al., Phys. Rev. Lett. **58**, 1494 (1987).

759. J. Arafune, M. Fukugita, Phys. Rev. Lett. **59**, 367 (1987); K. Sato, H. Suzuki, Phys. Rev. Lett. **58**, 2722 (1987); J.N. Bahcall, T. Piran, W.H. Press, D.N. Spergel, Nature **327**, 682 (1987); A. Burrows, J.M. Lattimer, Astrophys. J. **318**, L63 (1987); S.W. Bruenn, Phys. Rev. Lett. **59**, 938 (1987); S.H. Kahana, J. Cooperstein, E. Baron, Phys. Lett. **B196**, 259.

760. M. Koshiba, Phys. Rep. **220**, 211 (1992).

761. J. Middleditch et al., New Astronomy **5**, 243 (2000).

762. S.A. Colgate, R.H. White, Astrophys. J. **143**, 626 (1966).

763. W.D. Arnett, Can. J. Phys. **44**, 2553 (1966); **45**, 1621 (1967).

764. H.A. Bethe, Rev. Mod. Phys. **62**, 801 (1990); H.A. Bethe, G. Brown, Sci. Am. **252**, Nr. 5, 40 (1985).

765. D. Arnett, *Supernovae and Nucleosynthesis* (Princeton University Press, Princeton 1996).

766. A.S. Burrows, in *Supernovae*, ed. by A.G. Petschek (Springer, Berlin 1990), p. 143.

767. H. Suzuki, in *Physics and Astrophysics of Neutrinos*, ed. by M. Fukugita, A. Suzuki (Springer Verlag, Tokyo 1994), p. 763.

768. H.A. Bethe, J.H. Applegate, G.E. Brown, Astrophys. J. **241**, 343 (1980).

769. T.J. Mazurek, Nature **252**, 287 (1974); K. Sato, Prog. Theor. Phys. **53**, 595 (1975).

770. P. Goldreich, S.V. Weber, Astrophys. J. **238**, 991 (1980).

771. H.A. Bethe, G.E. Brown, J.H. Applegate, J.M. Lattimer, Nucl. Phys. **A324**, 487 (1979).

772. S.A. Colgate, M.H. Johnson, Phys. Rev. Lett. **5**, 235 (1960).

773. A. Burrows, T.J. Mazurek, Astrophys. J. **259**, 330 (1982); H.A. Bethe, A. Yahil, G.E. Brown, Astrophys. J. **262**, L7 (1982).

774. A. Burrows, T.J. Mazurek, Nature **301**, 315 (1983); A. Burrows, J.M. Lattimer, Astrophys. J. **307**, 178 (1986).

775. S.E. Woosley, R.D. Hoffman, Astrophys. J. **395**, 202 (1992); B.S. Meyer et al., Astrophys. J. **399**, 656 (1992); K. Takahashi, J. Witti, H.-Th. Janka, Astron. Astrophys. **286**, 857 (1994); R.D. Hoffman, S.E. Woosley, Y.-Z. Qian, Astrophys. J. **482**, 951 (1997); B.S. Meyer, G.C. McLaughlin, G.M. Fuller, Phys. Rev. **C58**, 3696 (1998).

776. R.W. Lindquist, Ann. Phys. **37**, 487 (1966); E. Baron et al., Astrophys. J. **339**, 978 (1989).

777. R.D. Arnett, Astrophys. J. **218**, 815 (1977); R.L. Bowers, J.R. Wilson, Astrophys. J. Suppl. **50**, 115 (1982); S.W. Bruenn, Astrophys. J. Suppl. **58**, 771 (1985); E.S. Myra et al., Astrophys. J. **318**, 744 (1987); H. Suzuki [767].

778. H.-T. Janka, W. Hillebrandt, Astron. Astrophys. Suppl. **78**, 375 (1989).

779. A. Mezzacappa, S.W. Bruenn, Astrophys. J. **405**, 637; 669; (1993); S. Yamada, Astrophys. J. **475**, 720 (1997).

780. A. Burrows et al., Astrophys. J. **539**, 865 (2000).

781. J.I. Castor, Astrophys. J. **178**, 779 (1972).

782. O.E.B. Messer, A. Mezzacappa, S.W. Bruenn, M.W. Guidry, Astrophys. J. **507**, 353 (1998).

783. S. Yamada, H.-T. Janka, H. Suzuki, Astron. Astrophys. **344**, 533 (1999).

784. T. Totani, K. Sato, H.E. Dalhed, J.R. Wilson, Astrophys. J. **496**, 216 (1998).

785. A. Burrows et al., Astrophys. J. **539**, 865 (2000).

786. H.-T. Janka, W. Hillebrandt, Astron. Astrophys. **224**, 49 (1989).

787. P.M. Giovanoni, D.C. Ellison, S.W. Bruenn, Astrophys. J. **342**, 416 (1989).

788. H. Suzuki, personal communication (2001).

789. E. Baron et al., Nucl. Phys. **A440**, 744 (1985); J. Cooperstein, E. Baron, in *Supernovae*, ed. by A.G. Petschek (Springer, New York 1990) p. 213.

790. G.E. Brown, Phys. Rept. **163**, 1; 167 (1988).

791. J.R. Wilson, in *Numerical Astrophysics*, ed. by J.M. Centrella, J.M. LeBlanc, R.L. Bowers (Jones and Bartlett, Boston 1984), p. 422; J.R. Wilson, R.W. Mayle, S.E. Woosley, T.A. Weaver, Ann. N. Y. Acad. Sci. **470**, 267 (1986); R.W. Mayle, in *Supernova, op. cit.* p. 267.

792. H.A. Bethe, J.R. Wilson, Astrophys. J. **295**, 14 (1985).

793. S.W. Bruenn, Astrophys. J. **341**, 385 (1989).

794. E.S. Myra, S.A. Bludman, Astrophys. J. **340**, 384 (1989).

795. N.K. Glendenning, Phys. Rev. Lett. **57**, 1120 (1986).

796. J.R. Wilson, R.W. Mayle, Phys. Rep. **163**, 63 (1988); **227**, 97 (1993).

797. A. Burrows, B.A. Fryxell, Astrophys. J. **418**, L33 (1993); A. Burrows, J. Hayes, B.A. Fryxell, Astrophys. J. **450**, 830 (1995); M. Herant et al., Astrophys. J. **435**, 339 (1994); W. Keil, H.-Th. Janka, E. Müller, Astrophys. J. **473**, L111 (1996); S.W. Bruenn, A. Mezzacappa, Astrophys. J. **433**, L45 (1994); A. Mezzacappa et al., Astrophys. J. **493**, 848 (1998).

798. D.S. Miller, J.R. Wilson, R.W. Mayle, Astrophys. J. **415**, 278 (1993); M. Herant et al., [797] A. Burrows, J. Hayes, B.A. Fryxell, [797]; H.-T. Janka, E. Müller, Astron. Astrophys. **306**, 167 (1996); A. Mezzacappa et al., Astrophys. J. **495**, 911 (1998).

799. A. Mezzacappa, astro-ph/0010577 (2000); M. Liebendörfer et al., Phys. Rev. D**63**, 103004 (2001) (in their version 1 paper a successful explosion was reported, but in version 2 it failed); H.-Th. Janka, Astron. Astrophys. **368**, 527 (2001); M. Rampp, H.-Th. Janka, Astrophys. J. **539**, L33 (2000); S.W. Bruenn, K.R. De Nisco, A. Mezzacappa, Astrophys. J. **560**, 326 (2001).

800. L.M. Krauss, Nature **329**, 689 (1987); A. Burrows, Astrophys. J. **334**, 891 (1988).

801. J.N. Bahcall, R.A. Wolf, Phys. Rev. **140**B, 1452 (1965).

802. S. Tsuruta, A.G.W. Cameron, Nature **207**, 364 (1965).

803. B.L. Friman, O.V. Maxwell, Astrophys, J. **232**, 541 (1979).

804. O.V. Maxwell, Astrophys, J. **231**, 201 (1979)

805. G. Baym, C. Pethick, Ann. Rev. Astron. Astrophys. **17**, 415 (1979); S. Tsuruta, Phys. Rep. **292**, 1 (1998).

806. F.R. Stephenson, D.A. Green, *Historical Supernovae and their Remnants*, (Clarendon Press, Oxford, 2002).

807. D.A. Green, Publ. Astron. Soc. Pacific **103**, 207 (1991).

808. G.A. Tammann, Astron. Astrophys. **8**, 458 (1970); Ann. N. Y. Acad. Sci. **302**, 61 (1977); J.G. Hills, Astrophys. J. **221**, 973 (1978).

809. A.G. Lyne et al., Mon. Not. R. astr. Soc. **295**, 743 (1998); K.T.S. Brazier, S. Johnston, Mon. Not. R. astr. Soc. **305**, 671 (1999); see for earlier works, R. Narayan, Astrophys. J. **319**, 162 (1987); J.H. Taylor, R.N. Manchester, Astrophys. J. **215**, 885 (1977); a catalogue of quasars is given by J.H. Taylor, R.N. Manchester, A.G. Lyne, Astrophys. J. Suppl. **88**, 529 (1993).

810. S. van den Bergh, R.D. McClure, Astrophys. J. **425**, 205 (1994); this estimate is based on R. Evans, S. van den Bergh, R.D. McClure, Astrophys. J. **345**, 752 (1989).

811. G.A. Tammann, W. Löffler, A. Schröder, Astrophys. J. Suppl. **92**, 487 (1994).

812. E. Cappellaro et al., Astron. Astrophys. **322**, 431 (1997).

813. A. Sandage, *The Hubble Atlas of Galaxies* (Carnegie Institute of Washington, Washington, D.C. 1961).

814. P. Madau, M. Della Valle, N. Panagia, Mon. Not. R. astr. Soc. **297**, L17 (1998).

815. G.S. Bisnovatyi-Kogan, Z.F. Seidov, Sov. Astron. **26**, 132 (1982).

816. L.M. Krauss, S.L. Glashow, D.N. Schramm, Nature **310**, 191 (1984).

817. A. Dar, Phys. Rev. Lett. **55**, 1422 (1985); S.E. Woosley, J.R. Wilson, R. Mayle, Astrophys. J. **302**, 19 (1986).

818. T. Totani, K. Sato, Y. Yoshii, Astrophys. J. **460**, 303 (1996); R.A. Malaney, Astroparticle Phys. **7**, 125 (1997); D.H. Hartmann, S.E. Woosley, Astroparticle Phys. **7**, 137 (1997).

819. M. Kaplinghat, G. Steigman, T.P. Walker, Phys. Rev. D**62**, 043001 (2000).

820. (UV) P. Madau et al., Mon. Not. R. astr. Soc. **283**, 1388 (1996); S.J. Lilly, O. Le Févre, F. Hammer and D. Crampton, Astrophys. J. **460**, L1 (1996); A.J. Connolly et al., Astrophys. J. **486**, L11 (1997); C.C. Steidel et al., Astrophys. J. **519**, 1 (1999); M.A. Treyer et al., Mon. Not. R. astr. Soc. **300**, 303 (1998); M. Sullivan et al. Mon. Not. R. astr. Soc. **312**, 442 (2000):
    (Hα) J. Gallego, J. Zamorano, A. Aragón-Salamanca, M. Rego, Astrophys. J, 455, L1 (1995); K. Glazebrook et al., Mon. Not. R. astr. Soc. **306**, 843 (1999); L. Tresse, S.J. Maddox, O. Le Fèvre, J.-G. Cuby, Mon. Not. R. astr. Soc. **337**, 369 (2002):
    (Far IR) H. Flores et al., Astrophys. J **517**, 148 (1999):
    (Radio) D.B. Haarsma, R.B. Partridge, R.A. Windhorst, E.A. Richards, Astrophys. J., **544**, 641 (2000); S. Serjeant, C. Gruppioni, S. Oliver, Mon. Not. R. astr. Soc. **330**, 621 (2002);
    (Model) Y.C. Pei, S.M. Fall, Astrophys. J. **454**, 69 (1995).

821. M. Fukugita, M. Kawasaki, astro-ph/0204376 (2002).

822. W. Zhang et al., Phys. Rev. Lett. **61**, 385 (1988) [KAMIOKANDE].

823. K.S. Hirata, Ph.D. thesis, ICRR report 239-91-8 (University of Tokyo, Tokyo 1991); cited in K. Nakamura et al. [915].

824. Y. Totsuka, personal communication (2001).

825. S. Weinberg, *Gravitation and Cosmology: Principles and Applications of the General Theory of Gravity* (Wiley, New York 1972).

826. P.J.E. Peebles, *Physical Cosmology* (Princeton University Press, Princeton 1971); *Principles of Physical Cosmology* (Princeton University Press, Princeton 1993).

827. G. Gamow, Phys. Rev. **70**, 572 (1946).

828. Ya.B. Zel'dovich, L.B. Okun', S.B. Pikel'ner, Usp. Fiz. Nauk **87**, 113 (1965) [Sov. Phys. Uspekhi **8**, 702 (1966)].

829. D.J. Fixsen et al., Astrophys. J. **473**, 576 (1996).

830. A.D. Dolgov, M. Fukugita, Phys. Rev. D**46**, 5378 (1992); JETP Lett. **56**, 123 (1992); S. Dodelson, M.S. Turner, Phys. Rev. D**46**, 3372 (1992); S. Hannestad, J. Madsen, Phys. Rev. D**52**, 1764 (1995); A.D. Dolgov, S.H. Hansen, D.V. Semikoz, Nucl. Phys. B**503**, 426 (1997); N.Y. Gnedin, O.L. Gnedin, Astrophys. J. **509**, 11 (1998).

831. R.A. Alpher, J.W. Follin, Jr., R.C. Herman, Phys. Rev. **92**, 1347 (1953); Pioneering work made following [827] is: R.A. Alpher, H. Bethe, G. Gamow, [247].

832. P.J.E. Peebles, Astrophys. J. **146**, 542 (1966).

833. A.A. Penzias, R.W. Wilson, Astrophys. J. **142**, 419 (1965).

834. J. Bernstein, L.S. Brown, G. Feinberg, Rev. Mod. Phys. **61**, 25 (1989).

835. R.V. Wagoner, W.A. Fowler, F. Hoyle, Astrophys. J. **148**, 3 (1967); H. Sato, Prog. Theor. Phys. **38**, 1083 (1967).

836. F. Hoyle, R.J. Tayler, Nature **203**, 1108 (1964).

837. R.I. Epstein, J.M. Lattimer, D.N. Schramm, Nature **263**, 198 (1976).

838. J. Yang, D.N. Schramm, G. Steigman, R.T. Rood, Astrophys. J. **227**, 697 (1979); J. Yang et al., Astrophys. J. **281**, 493 (1984); C.J. Copi, D.N. Schramm, M.S. Turner, Science **267**, 192 (1995).

839. A.M. Boesgaard, G. Steigman, Ann. Rev. Astron. Astrophys. **23**, 319 (1985).
840. R.V. Wagoner, Astrophys. J. **179**, 343 (1973); L. Kawano, Fermilab report FERMILAB-Pub-88/34-A (1988).
841. K.A. Olive, G. Steigman, E.D. Skillman, Astrophys. J. **483**, 788 (1997).
842. B.E.J. Pagel, E.A. Simonson, R.J. Terlevich, M.G. Edmunds, Mon. Not. R. astr. Soc, **255**, 325 (1992); see also J. Lequeux et al., Astron. Astrophys. **80**, 155 (1979).
843. Y.I. Izotov, T.X. Thuan, Astrophys. J. **500**, 188 (1998).
844. L. Searle, W.L.W. Sargent, Astrophys. J. **173**, 25 (1972); M. Peimbert, S. Torres-Peimbert, Astrophys. J. **193**, 327 (1974); D. Kunth, W.L.W. Sargent, Astrophys. J. **273**, 81 (1983).
845. D. Tytler, J.M. O'Meara, N. Suzuki, D. Lubin, Phys. Scr. T**85**, 12 (2000) for a summary of their earlier results; newer data are given in J.M. O'Meara et al., Astrophys. J. **552**, 718 (2001); D. Kirkman et al., astro-ph/0103305; see also S. D'Odorico et al., astro-ph/0102162 (2001).
846. A. Songaila, L.L. Cowie, C.J. Hogan, M. Rugers, Nature **368**, 599 (1994); R.F. Carswell et al., Mon. Not. R. astr. Soc. **268**, L1 (1994); J.K. Webb et al., Nature **388**, 250 (1997); D. Tytler et al., Astron. J. **117**, 63 (1999).
847. M. Tosi, in *From Stars to Galaxies*, ASP Conference Series **98** (Astron. Soc. Pacific, San Francisco 1996), p. 299; M. Tosi, G. Steigman, F. Matteucci, C. Chiappini, Astrophys. J. **498**, 226 (1998).
848. K.A. Olive, G. Steigman, T.P. Walker, Phys. Rep. **333**, 389 (2000).
849. K.A. Olive, in *Review of Particle Physics*, ed. by D.E. Groom, Eur. Phys. J. **15**, 133 (2000).
850. P. de Bernardis, Nature **404**, 955 (2000) [Boomerang]; S. Hanany et al. Astrophys. J. **545**, L5 (2000) [MAXIMA].
851. W. Hu, Nature **404**, 939 (2000).
852. C.B. Netterfield, Astrophys. J. **571**, 604 (2002) [Boomerang].
853. V.F. Shvartsman, Zh. Eksp. Teor. Fiz. Pisma **9**, 315 (1969) [JETP Lett. **9**, 184 (1969)]; G. Steigman, D.N. Schramm, J.E. Gunn, Phys. Lett. **66B**, 202 (1977).
854. K.A. Olive, D.N. Schramm, G. Steigman, Nucl. Phys. B**180**[FS2], 497 (1981).
855. P.J.E. Peebles, Astrophys. J. **153**, 1 (1968).
856. Ya.B. Zeldovich, R.A. Sunyaev, Astrophys. Space Sci. **4**, 301 (1969).
857. P.J.E. Peebles, *Large Scale Structure of the Universe* (Princeton University Press, Princeton 1983).
858. A.R. Liddle, D.H. Lyth, *Cosmological Inflation and Large-Scale Structure* (Cambridge University Press, Cambridge 2000).
859. A.H. Guth, Phys. Rev. D**23**, 347 (1981).
860. A. Albrecht, P.J. Steinhardt, Phys. Rev. Lett. **48**, 1220 (1982); A.D. Linde, Phys. Lett. **108**B, 389 (1982).
861. A.D. Linde, *Particle Physics and Inflationary Cosmology* (Harwood, New York 1990).
862. S.W. Hawking, Phys. Lett. **115**B, 295 (1982); A.A. Starobinsky, Phys. Lett. **117**B, 175 (1982); A.H. Guth, S.-Y. Pi, Phys. Rev. Lett. 49, 1110 (1982).
863. E. Lifshitz, J. Phys. U.S.S.R. **10**, 116 (1946).
864. J.R. Bond, quoted in J.R. Primack, G.R. Blumenthal, in *Formation and Evolution in the Universe*, ed. by J. Audouze, J. Tran Thanh Van (Reidel, Dordrecht 1983), p. 163.

865. J.M. Bardeen, J.R. Bond, N. Kaiser, A.S. Szalay, Astrophys. J. **304**, 15 (1986).

866. M. Davis, Jr., G. Efstathiou, C.S. Frenk, S.D.M. White, Astrophys. J. **292**, 371 (1985); D.J. Eisenstein, W. Hu, Astrophys. J. **511**, 5 (1999).

867. E.R. Harrison, Phys. Rev. D1, 2726 (1970); P.J.E. Peebles, J.T. Yu, Astrophys. J. **162**, 815 (1970); Ya.B. Zeldovich, Mon. Not. R. astr. Soc. **160**, 1p (1972).

868. D.J. Baumgart, J.N. Fry, Astrophys. J. **375**, 25 (1991); M.S. Vogeley, C. Park, M.J. Geller, J.P. Huchra, Astrophys. J. **391**, L5 (1992) [CfA2]; K.B. Fisher et al., Astrophys. J. **402**, 42 (1992) [IRAS]; J.A. Peacock, S.J. Dodds, Mon. Not. R. astr. Soc. **267**, 1020 (1994); H.A. Feldman, N. Kaiser, J.A. Peacock, Astrophys. J. **426**, 23 (1994) [QDOT]; S.J. Maddox, G. Efstathiou, W.J. Sutherland, Mon. Not. R. astr. Soc. **283**, 1227 (1996) [APM]; H. Lin et al., Astrophys. J. **471**, 617 (1996) [LCRS]; W.J. Percival et al., Mon. Not. R. astr. Soc. **327**, 1297 (2001) [2dF]; S. Dodelson et al., Astrophys. J. **572**, 140 (2002) [SDSS]; M. Tegmark, A.J.S. Hamilton, Y. Xu, Mon. Not. R. astr. Soc. **335**, 887 (2002).

869. J.P. Henry, K.A. Arnaud, Astrophys. J. **372**, 410 (1991); S.D.M. White, G. Efstathiou, C.S. Frenk, Mon. Not. R. astr. Soc. **262**, 1023 (1993); V.R. Eke, S. Cole, C.S. Frenk, Mon. Not. R. astr. Soc. **282**, 263 (1996); P.T.P. Viana, A.R. Liddle, Mon. Not. R. astr. Soc. **281**, 323 (1996); N.A. Bahcall, X. Fan, R. Cen, Astrophys. J. **485**, L53 (1997); T. Kitayama, Y. Suto, Astrophys. J. **490**, 557 (1997); U.-L. Pen, Astrophys. J. **498**, 60 (1998).

870. P.J.E. Peebles, J.T. Yu, in [867]; R.A. Sunyaev, Ya.B. Zeldovich, Astrophys. Sp. Sci. **7**, 3 (1970).

871. J.R. Bond, G. Efstathiou, Mon. Not. R. astr. Soc. **226**, 655 (1987).

872. J.R. Bond, A.H. Jaffe, Phil. Trans. R. Soc. London, **357**, 57 (1999); W. Hu, N. Sugiyama, J. Silk, Nature **386**, 37 (1997).

873. U. Seljak, M. Zaldarriaga, Astrophys. J. **469**, 437 (1996). This describes a computer code package CMBFAST, which is widely used to calculate C_ℓ.

874. R.K. Sachs, A.M. Wolfe, Astrophys. J. **147**, 73 (1967).

875. C.L. Bennett et al., Astrophys. J. **464**, L1 (1996).

876. F. Bunn, M. White, Astrophys. J. **480**, 6 (1997).

877. G.F. Smoot et al., Astrophys. J. **396**, L1 (1992).

878. E.L. Wright et al., Astrophys. J. **396**, L13 (1992).

879. G. Efstathiou, J.R. Bond, S.D.M. White, Mon. Not. R. astr. Soc. **258**, 1p (1992).

880. A.T. Lee et al., Astrophys. J. **561**, L1 (2001); R. Stompor, Astrophys. J. **561**, L7 (2001) [MAXIMA].

881. A.E. Lange et al., Phys. Rev. D63, 042001 (2001); A. Jaffe et al., Phys. Rev. Lett. **86**, 3475 (2001); A. Balbi et al., Astrophys. J. **545**, L1 (2000); M. Tegmark, M. Zaldarriaga, Phys. Rev. Lett. **85**, 2240 (2000); W. Hu, M. Fukugita, M. Zaldarriaga, M. Tegmark, Astrophys. J. **549**, 669 (2001); S.L. Bridle et al., astro-ph/0006170.

882. M. Tegmark, M. Zaldarriaga, astro-ph/0207047

883. L. van Waerbeke et al., Astron. Astrophys. **358**, 30 (2000); **374**, 757; N. Kaiser, G. Wilson and G. Luppino, astro-ph/0003338 (2000); D. Bacon, A. Refregier, R. Ellis, Mon. Not. R. astr. Soc. **318**, 625 (2000); D.M. Wittman

et al., Nature **405**, 143 (2000); H. Hoekstra, Y.K.C. Yee, M.D. Gladders, astro-ph/0204295.

884. R.A.C. Croft et al. Astrophys. J. **581**, 20 (2002); N.Y. Gnedin, A.J.S. Hamilton, Mon. Not. R. astr. Soc. **334**, 107 (2002).

885. M.J. Rees, J.P. Ostriker, Mon. Not. R. astr. Soc. **179**, 541 (1977); J. Silk, Astrophys. J. **211**, 638 (1977); G.R. Blumenthal, S.M. Faber, J.R. Primack, M.J. Rees, Nature **311**, 517 (1984).

886. X. Fan et al., Astron. J. **122**, 2833 (2001) [SDSS].

887. M. Fukugita, in *Review of Particle Physics*, ed. by D.E. Groom, Eur. Phys. J. **15**, 136; in *Structure Formation in the Universe* (NATO ASI, Cambridge), ed. by R.G. Crittenden, N.G. Turok (Kluwer, Dordrecht 2001), p. 93.

888. W.L. Freedman et al., Astrophys. J. **553**, 47 (2001).

889. M. Fukugita, F. Takahara, K. Yamashita, Y. Yoshii, Astrophys. J. **361**, L1 (1990).

890. S.M. Carroll, W.H. Press, E.L. Turner, Ann. Rev. Astron. Astrophys. **30**, 499 (1992); J.P. Ostriker, P.J. Steinhardt, Nature **377**, 600 (1995); M. Fukugita, in *Critical Dialogues in Cosmology in Celebration of the 250th Anniversary of Princeton University*, ed. by N. Turok (World Scientific, Singapore 1997), p. 204.

891. A.G. Riess et al., Astron. J. **116**, 1009 (1998); S. Perlmutter et al., Astrophys. J. **517**, 565 (1999).

892. G. Efstathiou, W.J. Sutherland, S.J. Maddox, Nature **348**, 705 (1990).

893. M. Fukugita, C.J. Hogan, P.J.E. Peebles, Astrophys. J. **503**, 518 (1998).

894. S.M. Faber, J.S. Gallagher, Ann. Rev. Astron. Astrophys. **17**, 135 (1979).

895. J. Binney, S. Tremaine, *Galactic Dynamics* (Princeton University Press, Princeton 1987), Chap. 10.

896. F. Zwicky, Helv. Phys. Acta **6**, 110 (1933); S. Smith, Astrophys. J. **83**, 23 (1936); M. Schwarzschild, Astron. J. **59**, 273 (1954).

897. D. Fabricant, P. Gorenstein, Astrophys. J. **267**, 535 (1983); W. Forman, C. Jones, Ann. Rev. Astron. Astrophys. **20**, 547 (1982).

898. G. Fahlman, N. Kaiser, G. Squires, D. Woods, Astrophys. J. **437**, 56 (1994); J.A. Tyson, P. Fischer, Astrophys. J. **446**, L55 (1995); G. Squires et al., Astrophys. J. **469**, 73 (1996); I. Smail et al., Astrophys. J. **479**, 70 (1997); for a review, see Y. Mellier, Ann. Rev. Astron. Astrophys. **37**, 127 (1999); the method is formulated in N. Kaiser, G. Squires, Astrophys. J. **404**, 441 (1993).

899. D. Lynden-Bell, R.D. Cannon, P.J. Godwin, Mon. Not. R. astr. Soc. **204**, 87P (1983).

900. D.N.C. Lin, D. Lynden-Bell, Mon. Not. R. astr. Soc. **198**, 707 (1982).

901. F.D. Kahn, L. Woltjer, Astrophys. J. **130**, 705 (1959); J.E. Gunn, Commun. Astrophys. **6**, 7 (1975).

902. D. Zaritsky, R. Smith, C. Frenk, S.D.M. White, Astrophys. J. **478**, 39 (1997).

903. T.A. McKay, astro-ph/0108013 (2001).

904. V.C. Rubin, W.K. Ford, Jr., Astrophys. J. **159**, 379 (1970); V.C. Rubin, N. Thonnard, W.K. Ford, Jr., M.S. Roberts, Astron. J. **81**, 719 (1976); D.H. Rogstad, G.S. Shostak, Astrophys. J. **176**, 315 (1972).

905. S.M. Kent, Astron. J. **91**, 1301 (1986); **93**, 816 (1987).

906. J.P. Ostriker, P.J.E. Peebles, A. Yahil, Astrophys. J. **193**, L1 (1974).

907. M. Aaronson, C. P. O'Dea, W.A. Dert, T.J. Balonek, Astrophys. J. **266**, L1 (1983); M. Aaronson, E.W. Olszewski, Astron. J. **94**, 657 (1987).

908. J. Verhoogen, *Energetics of the Earth* (National Academy of Science, Washington D.C. 1980).
909. G. Eder, Nucl. Phys. **78**, 657 (1966).
910. G. Marx, I. Lux, Acta. Phys. Hungarica **28**, 63 (1970).
911. C. Avilez, G. Marx, B. Fuentes, Phys. Rev. D**23**, 1116 (1981).
912. M. Kobayashi, Y. Fukao, Geophys. Res. Lett. **18**, 633 (1991).
913. R.S. Raghavan et al., Phys. Rev. Lett. **80**, 635 (1998).
914. S. Hart, A. Zindler, Chem. Geol. **57**, 247 (1986).
915. K. Nakamura, T. Kajita, M. Nakahata, A. Suzuki, in *Physics and Astrophyscs of Neutrinos*, ed. by M. Fukugita, A. Suzuki (Springer, Tokyo 1994), p. 249; A. Suzuki, ibid p. 388 for a historical account.
916. H. Ishino, Ph.D. thesis (University of Tokyo 1999) [Super-Kamiokande].
917. J. Boger et al., Nucl. Instr. Meth. A**449**, 172 (2000); A.B. McDonald, in *Neutrino 2000, Proc. 19th Int. Conf. on Neutrino Phys. and Astrophys.*, Sudbury, June 2000, ed by J. Law, R.W. Ollerhead, J.J. Simpson, Nucl. Phys. B (Proc. Suppl.) **91**, 21 (2001).
918. R.M. Bionta et al., Phys. Rev. Lett. **51**, 27 (1983).
919. C. Arpesella et al., BOREXINO at Gran Sasso ed. by G. Bellini, M. Campanella, D. Giugni (INFN-Milano/AT&T Bell-NJ, 1991); G. Ranucci et al., in *Neutrino 2000, Proc. 19th Int. Conf. Neutrino Phys. Astrophys.*, Sadbury, June 2000, ed. by J. Law, R.W. Ollerhead, J.J. Simpson, Nucl. Phys. B (Proc. Suppl.) **91**, 58 (2001).
920. T. Kirsten, in *Inside the Sun*, Proceedings of IAU Colloquia, No. 121 (Versailles, France), ed. by G. Berthomieu, M. Cribier (Kluwer, Dordrecht 1990), p. 187; W. Hampel, Phil. Trans. R. Soc. London A **343**, 3 (1994).
921. C. Athanassopoulos et al., Phys. Rev. Lett. **75**, 2650 (1995) [LSND].
922. G. Drexlin et al., Nucl. Instr. Meth. A**289**, 490 (1990); H. Gemmeke, G. Drexlin, *Upgrade of KARMEN Neutrino-Calorimeter*, http://www-ik1.fzk.de/www/karmen/karmen_e.html [KARMEN].
923. M. Apollonio et al., Phys. Lett. B**420**, 397 (1998) [CHOOZ].
924. F. Boehm et al., Phys. Rev. D**62**, 072002 (2000); the final report is given in Phys. Rev. D**64**, 112001 (2000) [Palo Verde].
925. P.A. Cerenkov, Comptes Rendus Acad. Sci. URSS **8**, 451 (1934); I. Franck, I. Tamm, Comptes Rendus Acad. Sci. URSS **14**, 109 (1937).
926. A. Morel, L. Prieur, Limnology and Oceanography **22**, 709 (1977).
927. Hamamatsu Photonics Co. Ltd., *Photomultiplier Tubes and Related Products* (product catalogue).
928. H. Kume et al., Nucl. Instr. Meth. **205**, 443 (1983).
929. S. Kasuga et al., Phys. Lett. B**374**, 238 (1996) [Kamiokande].
930. M. Nakahata et al., Nucl. Instr. Meth. A**421**, 113 (1999) [Super-Kamiokande].
931. M. Nakahata, personal communication.
932. H. Bethe, Z. Phys. **76**, 293 (1932).
933. F. Bloch, Z. Phys. **81**, 363 (1933).
934. S.M. Seltzer, M.J. Berger, Int. J. Radiat. Isotopes **33**, 1189 (1982).
935. N. Bohr, Danske Videnskab. Selskab. Math.-fys. Meddelelser **18**, 1 (1948).
936. E. Fermi, *Nuclear Physics* (University of Chicago Press, Chicago 1949), p. 27f.
937. H. Bethe, in *Handb. d. Physik*, Band 24/I (J. Springer, Berlin 1933), p. 273 (the formula is given in p. 523).

938. E. Fermi, Phys. Rev. **57**, 485 (1940); G.C. Wick, Nuovo Cimento Serie IX **1**, 302 (1943); R.M. Sternheimer, Phys. Rev. **88**, 851 (1952); R.M. Sternheimer, M.J. Berger, S.M. Seltzer, At. Data Nucl. Data Tables **30**, 261 (1984).

939. F.D. Brooks, Nucl. Instrum. Methods **162**, 477 (1979); J.B. Birks, *The Theory and Practice of Scintillation Counting* (Pergamon Press, London 1964); E. Schram, R. Lombaert, *Organic Scintillation Detectors* (Elsevier, Amsterdam 1963).

940. H. Ishikawa, *Measurement Method for Liquid Scintillation* (Nanzando, Tokyo 1977) [in Japanese].

941. T. Hagner et al., Astroparticle Phys. **14**, 33 (2000).

942. T. Hagner et al., in *Proc. 2nd Int. Workshop Low Energy Solar Neutrino Detection*, Tokyo 2000, ed. by Y. Suzuki, M. Nakahata, S. Moriyama (World Scientific, Singapore 2001), p. 152.

943. G. Alimonti et al., Nucl. Instrum. Methods A**440**, 360 (2000) [BOREXINO].

944. E. Andres et al., Astroparticle Phys. **13**, 1 (2000) [AMANDA].

945. K. Kobayakawa, Nuovo Cimento **47**, 156 (1967).

946. S. Higashi et al., Nuovo Cimento Serie X **43**A, 334 (1966).

947. J. Babson et al., Phys. Rev. D**42**, 3613 (1990) [DUMAND].

948. I.A. Belolaptikov et al., Astroparticle Phys. **7**, 263 (1997); V.A. Balkanov et al., astro-ph/9903342.

949. e.g., O.C. Allkofer, D.P. Bhattacharyya, Phys. Rev. D**34**, 1368 (1986); V.A. Naumov, S.I. Sinegovsky, E.V. Bugaev, Phys. At. Nucl. **57**, 412 (1994) [Yad. Fiz. **57**, 439 (1994)].

950. A.W. Wolfendale (Ed.), *Cosmic Rays at Ground Level* (Institute of Physics, London 1973).

951. Y. Takeuchi et al., Phys. Lett. B**452**, 418 (1999).

952. G. Alimonti et al., Astroparticle Phys. **8**, 141 (1998) [BOREXINO].

953. A. Suzuki, K. Inoue, personal communication (2002) [KamLAND].

954. G. Alimonti et al., Phys. Lett. B**422**, 349 (1998) [BOREXINO].

955. M. Cribier et al., Gallex report 1997.

956. L.W. Alvarez, Lawrence Radiation Laboratory Physics Note 767 (1973).

957. R.S. Raghavan, in Proceedings of Informal Conference on Status and Future of Solar Neutrino Research, BNL, 1978, BNL report 50879, ed. by G. Friedlander (1978), Vol. 2, p. 270.

958. W.C. Haxton, Phys. Rev. C**38**, 2474 (1988).

959. M. Cribier et al., Nucl. Instr. Meth. **378**, 233 (1996).

960. R.D. Scott, Nature **264**, 729 (1976); G.S. Hurst et al., Phys. Rev. Lett. **53**, 1116 (1984); in *Solar Neutrinos and Neutrino Astronomy*, Homestake, 1984, ed. by M.L. Cherry, K. Lande, W.A. Fowler (AIP Conf. Proc. No. 126, 1985) p. 152.

961. W.C. Haxton, Phys. Rev. Lett. **60**, 768 (1988).

962. J.N. Bahcall, Phys. Rev. Lett. **23**, 251 (1969).

963. G.A. Cowan, W.C. Haxton, Science **216**, 51 (1982).

964. D.Z. Freedman, D.N. Schramm, D.L. Tubbs, Ann. Rev. Nucl. Part. Sci. **27**, 167 (1977); M.S. Freedmann, Nucl. Instr. Meth. A**271**, 267 (1988); M.S. Freedman et al., Science **193**, 1117 (1976).

965. V.V. Kuzminov, A.A. Pomansky, V.L. Chihladze, Nucl. Instr. Meth. A**271**, 257 (1988).

966. K. Wolfsberg et al., in *Solar Neutrinos and Neutrino Astronomy*, Homestake, 1984, ed. by M.L. Cherry, K. Lande, W.A. Fowler (AIP Conf. Proc. No. 126, 1985) p. 196.

967. J.N. Bahcall, Phys. Rev. D**38**, 2006 (1988).

968. W. Henning et al., in *Solar Neutrinos and Neutrino Astronomy*, Homestake, 1984, ed. by M.L. Cherry, K. Lande, W.A. Fowler (AIP Conf. Proc. No. 126, 1985) p. 203.

969. R.S. Raghavan, Phys. Rev. Lett. **37**, 259 (1976).

970. L. Pfeiffer et al., Phys. Rev. C**19**, 1035 (1979); A.K. Drukier, R. Nest, Nucl. Instr. Meth. A**239**, 605 (1985); Y. Suzuki et al., Nucl. Instr. Meth. A**275**, 142 (1989); A**293**, 615 (1990); M. Avenier, Nucl. Phys. (Proc. Suppl.) **28A**, 496 (1992); J.C. Lund et al., Nucl. Instr. Meth. A**272**, 885 (1988); N.E. Booth, Appl. Phys. Lett. **50**, 293 (1987); A. de Bellefon et al., Saclay report DPHPE 89-17 (1989); for a review, Y. Suzuki, K. Inoue, in *Physics and Astrophysics of Neutrinos*, ed. M. Fukugita, A. Suzuki (Springer, Tokyo 1994) p. 694.

971. C. Rubbia, CERN EP report 77-8 (1977); C. Rubbia et al., INFN report INFN/AE-85-7 (1985); J.N. Bahcall, M. Baldo-Ceolin, D.B. Cline, C. Rubbia, Phys. Lett. **178**B, 324 (1986); F. Arneodo et al. Nucl. Instr. Meth. A**455**, 376 (2000); in particular S. Bonetti et al. Nucl. Instr. Meth. A**286**, 135 (1990) for technical aspects.

972. R.S. Raghavan, Phys. Rev. Lett. **78**, 3618 (1997).

973. H. Ejiri et al., Phys. Rev. Lett. **85**, 2917 (2000).

974. A. Drukier, L. Stodolsky, Phys. Rev. D**30**, 2295 (1984).

975. B. Cabrera, L.M. Krauss, F. Wilczek, Phys. Rev. Lett. **55**, 25 (1985).

976. S.H. Moseley, J.C. Mather, D. McCammon, J. Appl. Phys. **56**, 1257 (1984); D. McCammon et al., J. Appl. Phys. **56**, 1263 (1984).

977. R.E. Lanou, H.J. Maris, G.M. Seidel, Phys. Rev. Lett. **58**, 2498 (1987).

978. J. Adams et al. Phys. Lett. B**341**, 431 (1995); Nucl. Instr. Meth. B**444**, 51 (2000); R.E. Lanou in *Proc. 2nd Int. Workshop Low Energy Solar Neutrino Detection*, ed. by Y. Suzuki, M. Nakahata, S. Moriyama (World Scientific, Singapore 2001), p. 70.

979. G, Steigman, C.L. Sarazin, H. Quintana, J. Faulkner, Astron. J. **83**, 1050 (1978).

980. W.H. Press, D.N. Spergel, Astrophys. J. **296**, 679 (1985); L.M. Kraus, K. Freese, D.N. Spergel, W.H. Press, Astrophys. J. **290**, 1001 (1985).

981. J. Silk, K. Olive, M. Srednicki, Phys. Rev. Lett. **55**, 257 (1985).

982. T. Damour, L.M. Krauss, Phys. Rev. Lett. **81**, 5726 (1998).

983. L.M. Krauss, M. Srednicki, F. Wilczek, Phys. Rev. D**33**, 2079 (1986).

984. T.K. Gaisser, G. Steigman, S. Tilav, Phys. Rev. D**34**, 2206 (1986).

985. M. Srednicki, K.A. Olive, J. Silk, Nucl. Phys. B**279**, 804 (1987).

986. J.S. Hagelin, K.W. Ng, K.A. Olive, Phys. Lett. B**180**, 375 (1987); M. Kamionkowski, Phys. Rev. D**44**, 3021 (1991); A. Bottino et al., Phys. Lett. B**265**, 57 (1991); R. Gandhi et al., Phys. Rev. D**49**, 3691 (1994); L. Bergström, J. Edsjö, P. Gondolo, Phys. Rev. D**55**, 1765 (1997); L. Bergström et al., JHEP 9908, 010 (1999).

987. J.M. LoSecco et al., Phys. Lett. B**188**, 388 (1987) [IMB].

988. M. Mori et al., Phys. Lett. B289, 463 (1992); Phys. Rev. D**48**, 5505 (1993) [Kamiokande].

989. M.M. Boliev et al., in *TAUP'95*, Nucl. Phys. B (Proc. Suppl.) **48**, 83 (1996).

990. M. Ambrosio et al., Phys. Rev. D**60**, 082002 (1999) [MACRO].

991. S. Desai, in *Sources and Detection of Dark Matter and Dark Energy in the Universe*, Marina del Rey, 2000, ed. by D. Cline (Springer, Berlin 2001) p. 428 [Super-Kamiokande].

992. G. Vacanti et al., Astrophys. J. **377**, 467 (1991); T. Tanimori et al., Astrophys. J. **492**, L33 (1998).

993. T. Yoshikoshi et al., Astrophys. J. **487**, L65 (1997).

994. S.A. Dazeley, J.R. Patterson, G.P. Rowell, P.G. Edwards, Astroparticle Phys. **15**, 313 (2001).

995. P. Goret et al., Astron. Astrophys. **270**, 401 (1993); T. Tanimori et al., Astrophys. J. **497**, L25 (1998).

996. M. Punch et al., Nature **358**, 477 (1992).

997. J. Quinn et al., Astrophys. J. **456**, L83 (1996); S.M. Bradbury et al., Astron. Astrophys. **320**, L5 (1997).

998. V.L. Ginzburg, *Theoretical Physics and Astrophysics* (Pergamon Press, Oxford 1979).

999. V.S. Berezinskiy, G.T. Zatsepin, Sov. J. Nucl. Phys. **11**, 111 (1970); F.W. Stecker, Astrophys. Space Sci. **20**, 47 (1973); V.S. Berezinsky, C. Castagnoli, P. Galeotti, Nuovo Cimento **8C**, 185 (1985).

1000. P. Askebjer et al., Science **267**, 1147 (1995).

1001. F. Stecker, C. Done, M.H. Salamon, P. Sommers, Phys. Rev. Lett. **69**, 2738 (1992); L. Nellen, K. Mannheim, P.L. Biermann, Phys. Rev. D**47**, 5270 (1993); K. Mannheim, Astroparticle Phys. **3**, 295 (1995); F. Halzen, E. Zas, Astrophys. J. **488**, 669 (1997); W. Bednarek, R.J. Protheroe, Phys. Rev. Lett. **79**, 2616 (1997); T.K. Gaisser, R.J. Protheroe, T. Stanev, Astrophys. J. **492**, 219 (1998); S. Colafrancesco, P. Blasi, Astroparticle Phys. **9**, 227 (1998); E. Waxman, J. Bahcall, Phys. Rev. D**59**, 023002 (1998); V.S. Berezinsky, V.I. Dokuchaev, Astroparticle Phys. **15**, 87 (2001); D. Guetta, M. Spada, E. Waxman, Astrophys. J. **559**, 101 (2001).

1002. T.K. Gaisser, F. Halzen, T. Stanev, Phys. Rep. **258**, 173 (1995); J.G. Learned, K. Mannheim, Ann. Rev. Nucl. Part. Sci. **50**, 679 (2000).

1003. J. Bernstein, M. Ruderman, G. Feinberg, Phys. Rev. **132**, 1227 (1963).

1004. N.G. Deshpande, Oregon preprint OITS-107 (1979); C.Q. Geng, R.E. Marshak, Phys. Rev. D**39**, 693 (1989); R. Foot, G.C. Joshi, H. Lew, R.R. Volkas, Mod. Phys. Lett. A**5**, 95 (1990); K.S. Babu, R.N. Mohapatra, Phys. Rev. Lett. **63**, 938 (1989).

1005. K.S. Babu, R.N. Mohapatra, Phys. Rev. D**42**, 3866 (1990).

1006. L. Davis, Jr., A.S. Goldhaber, M.M. Nieto, Phys. Rev. Lett. **35**, 1402 (1975).

1007. H.F. Dylla, J.G. King, Phys. Rev. A**7**, 1224 (1973); see also J.C. Zorn, G.E. Chamberlain, V.W. Hughes, Phys. Rev. **129**, 2566 (1963).

1008. J. Baumann, R. Gähler, J. Kalus, W. Mampe, Phys. Rev. D**37**, 3107 (1988); R. Gähler, J. Kalus, W. Mampe, Phys. Rev. D**25**, 2887 (1982).

1009. G. Barbiellini, G. Cocconi, Nature **329**, 21 (1987).

1010. J.E. Gunn, B.W. Lee, I. Lerche, D.N. Schramm, G. Steigman, Astrophys. J. **223**, 1015 (1978).

1011. K. Fujikawa, R.E. Shrock, Phys. Rev. Lett. **45**, 963 (1980).

1012. W.J. Marciano, A.I. Sanda, Phys. Lett. **67**B, 303 (1977); B.W. Lee, R.E. Shrock, Phys. Rev. D**16**. 1444 (1977).

1013. C.L. Cowan, Jr., F. Reines, Phys. Rev. **107**, 528 (1957).

1014. A.V. Derbin, Yad. Fiz. **57**, 236 (1994) [Part. At. Nucl. **57**, 222 (1994)].
1015. A.V. Derbin, L.A. Popeko, A.V. Chemyi, G.A. Shishkina, Pisma Zh. Eksp. Teor. Fiz. **43**, 164 (1986); G.S. Vidyakin et al., Pisma Zh. Eksp. Teor. Fiz. **55**, 212 (1992); L.A. Popeko et al., Pisma Zh. Eksp. Teor. Fiz. **57**, 755 (1993).
1016. A.V. Kyuldjiev, Nucl. Phys. B**243**, 387 (1984).
1017. D.A. Krakauer et al., Phys. Lett. B**252**, 177 (1990).
1018. J. Dorenbosch et al., Z. Phys. C**41**, 567 (1989).
1019. L.A. Ahrens et al., Phys. Rev. D**41**, 3297 (1990).
1020. H. Grotch, R.W. Robinett, Z. Phys. C**39**, 553 (1988).
1021. P. Abreu et al. (Delphi collaboration), Z. Phys. C**74**, 577 (1997).
1022. M. Acciarri et al. (L3 collaboration), Phys. Lett. B**412**, 201 (1997).
1023. A.M. Cooper-Sarker et al., Phys. Lett. B**280**, 153 (1992).
1024. G.V. Domogatskiĭ, D.K. Nadezhin, Yad. Fiz. **12**, 1233 (1970); [Sov. J. Nucl. Phys. **12**, 678 (1971)].
1025. P. Sutherland et al., Phys. Rev. D**13**, 2700 (1976).
1026. M.A.B. Bég, W.J. Marciano, M. Ruderman, Phys. Rev. D**17**, 1395 (1978).
1027. S.I. Blinnikov, Moscow preprint ITEP-88-19 (1988).
1028. J.M. Lattimer, J. Cooperstein, Phys. Rev. Lett. **61**, 23 (1988); R. Barbieri, R.N. Mohapatra, Phys. Rev. Lett. **61**, 27 (1988); D. Nötzold, Phys. Rev. D**38**, 1658 (1988).
1029. N. Iwamoto, L. Qin, M. Fukugita, S. Tsuruta, Phys. Rev. D**51**, 348 (1995).
1030. J. Morgan, Phys. Lett. B**102**, 247 (1981); Mon. Not. R. astr. Soc. **195**, 173 (1981)
1031. P. Elmfors, K. Enqvist, G. Raffelt, G. Sigl, Nucl. Phys. B**503**, 3 (1997).
1032. W.A. Bardeen, R. Gastmans, B. Lautrup, Nucl. Phys. B**46**, 319 (1972); A.D. Dolgov, Ya.B. Zeldovich, ref. [245]; G. Auriemma, Y. Srivastava, A. Widom, Phys. Lett. B**195**, 254 (1987); J.L. Lucio, A. Rosado, A. Zepeda, Phys. Rev. D**31**, 1091 (1985); for an early discussion of form factors see J. Bernstein, T.D. Lee, Phys. Rev. Lett. **11**, 512 (1963).
1033. G. Degrassi, A. Sirlin, W.J. Marciano, Phys. Rev. D**39**, 287 (1989).
1034. J, Schwinger, Phys. Rev. **75**, 651 (1949).
1035. M. Fukugita, K. Kubodera, Z. Phys. C**9**, 365 (1981).
1036. J. Law, Phys. Lett. **102**B, 371 (1981).
1037. O. Fackler et al., Phys. Rev. Lett. **55**, 1388 (1985).
1038. R.L. Martin, J.S. Cohen, Phys. Lett. **110**A, 95 (1985).
1039. H. Ågren, V. Carravetta, Phys. Rev. A**38**, 2707 (1988).
1040. S. Jonsell, H. Monkhovst, Phys. Rev. Lett. **76**, 4476 (1996).
1041. W. Kolos et al., Phys. Rev. A**37**, 2297 (1988).
1042. I.G. Kaplan, V.N. Smutny, G.V. Smelov, Phys. Lett. **112**B, 417 (1982); **161**B, 389 (1985); Zh. Eksp. Teor. Fiz. **84**, 833 (1983) [Sov. Phys. JETP **57**, 483 (1983)]; I.G. Kaplan, G.V. Smelov, V.N. Smutnyi, Dokl. Akad. Nauk. SSSR **279**, 1110 (1984) [Sov. Phys. Doklady **29**, 1023 (1984)].
1043. J. Arafune, T. Watanabe, Phys. Rev. C**34**, 336 (1986); J. Arafune, N. Koga, K. Morokuma, T. Watanabe, J. Phys. Soc. Jpn. **55**, 3806; 3813 (1986).
1044. T.A. Claxton, S. Schafroth, P.F. Meier, Phys. Rev. A**45**, 6209 (1992).
1045. H. Kawakami et al., Phys. Lett. B**256**, 105 (1991).
1046. E.F. Tretyakov, Izv. Akad. Nauk. USSR, Ser. Fiz. **39**, 583 (1975).
1047. V.V. Vladimirskii, E.K. Tarasov, Yu.V. Trebuhkovskii, Pribory i Tekhnika Eksperimenta **1**, 13 (1956).

1048. V.M. Lobashev, P.E. Spivak, Nucl. Instr. Meth. **A240**, 305 (1985); A. Picard et al., Nucl. Instr. Meth. **B63**, 345 (1992).

1049. T. Ohshima, H. Kawakami, in *Physics and Astrophysics of Neutrinos*, ed. by M. Fukugita, A. Suzuki (Springer, Tokyo 1994), p. 448; W. Kündig, E. Holzschuh, M. Fritschi, H. Stüssi, in *Neutrino Physics*, ed. by K. Winter (Cambridge University Press, Cambridge 1991) p. 144; K.D. Sevier, *Low Energy Electron Spectroscopy* (Wiley-Interscience, New York 1971) for precision electron spectroscopy.

1050. S. Boris et al., Phys. Lett. **B159**, 217 (1985); Phys. Rev. Lett. **58**, 2019 (1987).

1051. J.F. Wilkerson et al., Phys. Rev. Lett. **58**, 2023 (1987).

1052. E. Holzschuh, M. Fritschi, W. Kündig, Phys. Lett. **B287**, 381 (1992).

1053. R.G.H. Robertson et al., Phys. Rev. Lett. **67**, 957 (1991).

1054. Ch. Weinheimer et al., Phys. Lett. **B300**, 210 (1993).

1055. W. Stoeffl, D.J. Decman, Phys. Rev. Lett. **75**, 3237 (1995).

1056. V.M. Lobashev et al., Phys. Lett. **B460**, 227 (1999).

1057. Ch. Weinheimer et al., Phys. Lett. **B460**, 219 (1999); **464**, 352 (1999) (E).

1058. A. de Rújula, Nucl. Phys. **B188**, 414 (1981); see also A. de Rújula, M. Lusignoli, Nucl. Phys. **B219**, 277 (1983).

1059. IBEC was first studied by E.C.G. Stueckelberg [Nature **137**, 1070 (1936); Helv. Phys. Acta. **9**, 533 (1936)] and C. Møller [Phys. Zeits d. Sowjetunion **11**, 9 (1937)]. It was first observed by H. Bradt et al. [Helv. Phys. Acta **19**, 222 (1946)]. The theory was further developed by R.J. Glauber, P.C. Martin, Phys. Rev. **104**, 158 (1956); P.C. Martin, R.J. Glauber **109**, 1307 (1958), A. de Rújula (in ref. [1058]) and others. For a review, see W. Bambynek et al., Rev. Mod. Phys. **49**, 77 (1977).

1060. C.L. Bennett et al., Phys. Lett. **107**B, 19 (1981).

1061. J.U. Andersen et al., Phys. Lett. **113**B, 72 (1982).

1062. S. Yasumi et al., Phys. Lett. **B334**, 229 (1994).

1063. P.T. Springer, C.L. Bennett, P.A. Baisden, Phys. Rev. **A35**, 679 (1987).

1064. M. Jung et al., Phys. Rev. Lett. **69**, 2164 (1992).

1065. K. Assamagan et al., **D53**, 6065 (1996).

1066. B. Jeckelmann, P.F.A. Goudsmit, H.J. Leisi, Phys. Lett. **B335**, 326 (1994); see also B. Jeckelmann et al., Nucl. Phys. **A457**, 709 (1986).

1067. R. Abela et al., Phys. Lett. **146**B, 431 (1984).

1068. B. Jeckelmann et al., Phys. Rev. Lett. **56**, 1444 (1986).

1069. H.B. Anderhub et al., Phys. Lett. **114**B, 76 (1982).

1070. R. Barate et al. (Aleph Collaboration), Eur. Phys. J. **C2**, 395 (1998).

1071. H. Albrecht et al. (ARGUS Collabration), Phys. Lett. **B202**, 149 (1988) [$m_{\nu_\tau} < 31$ MeV]; D. Cinabro et al. (CLEO Collabration), Phys. Rev. Lett. **70**, 3700 (1993) [$m_{\nu_\tau} < 32.6$ MeV].

1072. G. Alexander et al. (OPAL Collaboration), Z. Phys. **C72**, 231 (1996).

1073. S. Tremaine, J.E. Gunn, Phys. Rev. Lett. **42**, 407 (1979).

1074. Ya.B. Zeldovich, Astron. Astrophys. **5**, 84 (1970).

1075. Y.P. Jing, H.J. Mo, G. Börner, L.Z. Fang, Astrophys. J. **416**, 1 (1993); A. Klypin, J. Holtzman, J. Primack, E. Regős, Astrophys. J. **416**, 1 (1993).

1076. W. Hu, D.J. Eisenstein, M. Tegmark, Phys. Rev. Lett. **80**, 5255 (1998).

1077. G.F. Smoot et al., in [877]; C.L. Bennett et al., Astrophys. J. **464**, L1 (1996).

1078. S.D.M. White, G. Efstatiou, C.S. Frenk, Mon. Not. R. astr. Soc. **262**, 1023 (1993).

1079. R. Valdarnini, T. Kahniashvili, B. Novosyadlyj, Astron. Astrophys. **336**, 11 (1998).
1080. R.A.C. Croft, W. Hu, R. Davé, Phys. Rev. Lett. **83**, 1092 (1999).
1081. M. Fukugita, G.-C. Liu, N. Sugiyama, Phys. Rev. Lett. **84**, 1082 (2000).
1082. W. Hu, M. Fukugita, M. Zaldarriaga, M. Tegmark, in [881].
1083. Ø. Elgarøy et al., Phys. Rev. Lett. **89**, 061301 (2002) [2dF].
1084. J. Arafune, M. Fukugita; K. Sato, H. Suzuki; [759]; J.N. Bahcall, S.L. Glashow, Nature (London) **326**, 476 (1987); W.D. Arnett, J.L. Rosner, Phys. Rev. Lett. **58**, 1906 (1987); E.W. Kolb, A.J. Stebbins, M.S. Turner, Phys. Rev. D**35**, 3598 (1987); A. Burrows, J.M. Lattimer [759]; K. Hikasa, M. Kobayashi, M. Yoshimura, Prog. Theor. Phys. **78**, 180 (1987); S.H. Kahana, J. Cooperstein, E. Baron [759].
1085. P. Hut, Phys. Lett. **69**B, 85 (1977); B.W. Lee, S. Weinberg, Phys. Rev. Lett. **39**, 165 (1977);
1086. R. Scherrer, M.S. Turner, Phys. Rev. D**33**, 1585 (1986); J. Bernstein, L. Brown, G. Feinberg, Phys. Rev. D**32**, 3261 (1985).
1087. D.A. Dicus, E.W. Kolb, V.L. Teplitz, Phys. Rev. Lett. **39**, 168 (1977); Astrophys. J. **221**, 327 (1978).
1088. M.I. Vysotskii, A.D. Dolgov, Ya.B. Zeldovich, Zh. Eksp. Teor. Fiz., Pisma Red. **26**, 200 (1977) [JETP Lett. **26**, 188 (1977)].
1089. L.M. Krauss, Phys. Lett. **128**B, 37 (1983).
1090. J. Ellis et al., Nucl. Phys. B**238**, 453 (1984).
1091. G. Jungman, M. Kamionkowski, K. Griest, Phys. Rep. **267**, 195 (1996) for a review.
1092. e.g., J. Ellis, A. Ferstl, K.A. Olive, Phys. Lett. B**481**, 304 (2000); Phys. Rev. D**63**, 065016 (2001); R. Arnowitt, B. Dutta, hep-ph/0211042, to be published in *10th Int. Conf. Supersymmetry and Unifications of Fundamental Interactions (SUSY02)*, Hamburg, 2002; M. Drees et al., Phys. Rev. D**63**, 035008 (2001).
1093. K. Sato, M. Kobayashi, Prog. Theor. Phys. **58**, 1775 (1977).
1094. G.B. Gelmini, M. Roncadelli, Phys. Lett. **99**B, 411 (1981).
1095. A. Zee, Phys. Lett. **93**B, 389 (1980).
1096. J.A. McLennan, Jr., Phys. Rev. **106**, 821 (1957).
1097. Ya.B. Zel'dovich, Dokl. Akad. Nauk. SSSR **86**, 505 (1952); E.J. Konopinski, H.M. Mahmoud, in ref. [34].
1098. L. Wolfenstein, Phys. Lett. **107**B, 77 (1981).
1099. M. Magg, Ch. Wetterich, Phys. Lett. **94**B, 61 (1980); J. Schechter, J.W.F. Valle, Phys. Rev. D**22**, 2227 (1980).
1100. H.M. Georgi, S.L. Glashow, S. Nussinov, Nucl. Phys. B**193**, 297 (1981).
1101. K. Choi, C.W. Kim, W.P. Lam, A. Santamaria, Carnegie-Melon preprint CMU-HEP 89-22 (1989); K. Choi, A. Santamaria, Phys. Lett. B**267**, 504 (1991).
1102. C. Jarlskog, M. Matsuda, S. Skadhauge, M. Tanimoto, Phys. Lett. B**449**, 240 (1999).
1103. R.N. Mohapatra, J.W.F. Valle, Phys. Rev. D**34**, 1642 (1986).
1104. P. Horava, E. Witten, Nucl. Phys. B**460**, 506 (1996); P. Horava, Phys. Rev. D**54**, 7561 (1996); E. Witten, Nucl. Phys. B**471**, 135 (1996).
1105. N. Arkani-Hamed, S. Dimopoulos, G. Dvali, Phys. Lett. B**429**, 263 (1998).
1106. K.M. Case, Phys. Rev. **107**, 307 (1957); see also P.D. Mannheim, Int. J. Theor. Phys. **23**, 643 (1984).

1107. J. Serpe, Physica **18**, 295 (1952).
1108. W. Pauli, Nuovo Cimento Serie X **6**, 204 (1957).
1109. F. Gürsey, Nuovo Cimento Serie X **7**, 411 (1958).
1110. L.A. Radicati, B. Touschek, Nuovo Cimento Serie X **5**, 1693 (1957).
1111. C. Ryan, S. Okubo, Nuovo Cimento Serie X, Suppl. **2**, 234 (1964).
1112. H. Jehle, Phys. Rev. **75**, 1609(L) (1949).
1113. H. Goldberg, Phys. Rev. Lett. **50**, 1419 (1983).
1114. e.g., H. Primakoff, S.P. Rosen, in [201]; Ann. Rev. Nucl. Part. Sci. **31**, 145 (1981).
1115. M. Doi, T. Kotani, H. Nishiura, K. Okuda, E. Takasugi, Phys. Lett. **103**B, 219 (1981).
1116. W.C. Haxton, G.J. Stephenson, Jr., Prog. Part. Nucl. Phys. **12**, 409 (1984).
1117. M. Doi, T. Kotani, E. Takasugi, Prog. Theor. Phys. Suppl. **83**, 1 (1985).
1118. J.D. Vergados, Phys. Rep. **133**, 1 (1986).
1119. T. Tomoda, Rep. Prog. Phys. **54**, 53 (1991).
1120. M. Moe, P. Vogel, Ann. Rev. Nucl. Part. Sci. **44**, 247 (1994).
1121. J. Suhonen, O. Civitarese, Phys. Rept. **300**, 123 (1998).
1122. A. Molina, P. Pascual, Nuovo Cimento **41**A, 756 (1977).
1123. J.D. Vergados, Phys. Rev. C**24**, 640 (1981).
1124. T. Tomoda, Phys. Lett. B**474**, 245 (2000).
1125. W.C. Haxton, G.J. Stephenson, Jr., D. Strottman, Phys. Rev. D**25**, 2360 (1982); M. Doi, T. Kotani, H. Nishiura, E. Takasugi, Prog. Theor. Phys. **70**, 1353 (1984); see [345] for numerical tables of relativistic corrections.
1126. E.J. Konopinski, *The Theory of Beta Radioactivity* (Clarendon Press, Oxford 1966).
1127. A. Balysh et al., Phys. Rev. Lett. **77**, 5186 (1996).
1128. K. You et al., Phys. Lett. B**265**, 53 (1991).
1129. M. Günther et al., Phys. Rev. D**55**, 54 (1997).
1130. L. Baudis et al., Phys. Rev. Lett. **83**, 41 (1999).
1131. F.T. Avignone III et al., Phys. Lett. B**256**, 559 (1991).
1132. H.S. Miley et al., Phys. Rev. Lett. **65**, 3092 (1990).
1133. A.A. Vasenko, Mod. Phys. Lett. A**5**, 1299 (1990).
1134. S.R. Elliott et al., Phys. Rev. C**46**, 1535 (1992); see also S.R. Elliott, A.A. Hahn, M.K. Moe, Phys. Rev. Lett. **59**, 2020 (1987).
1135. R. Arnold et al., Nucl. Phys. A**658**, 299 (1999).
1136. M. Alston-Garnjost et al., Phys. Rev. C**55**, 474 (1997).
1137. H. Ejiri et al., Nucl. Phys. A**611**, 85 (1996).
1138. A. De Silva, M.K. Moe, M.A. Nelson, M.A. Vient, Phys. Rev. C**56**, 2451 (1997).
1139. D. Dassié et al., Phys. Rev. D**51**, 2090 (1995).
1140. A.S. Barabash et al., Phys. Lett. B**345**, 408 (1995).
1141. R. Arnold et al., Z. Phys. Rev. C**72**, 239 (1996).
1142. A.Sh. Georgadze et al., Yad. Fiz. **58**, 1170 (1995) [Phys. At. Nucl. **58**, 1093 (1995)].
1143. H. Ejiri et al., J. Phys. Soc. Jpn. **64**, 339 (1995).
1144. T. Bernatowicz, et al., Phys. Rev. C**47**, 806 (1993).
1145. A. Alessandrello et al., Nucl. Phys. B (Proc. Suppl.) **48**, 238 (1996).
1146. T. Kirsten et al., in *Nuclear Beta Decays and Neutrino*, Osaka, 1986, ed. by T. Kotani, H. Ejiri, E. Takasugi (World Scientific, Singapore 1986) p. 81; T. Kirsten, H. Richter, E. Jessberger, Phys. Rev. Lett. **50**, 474 (1983); Z. Phys. C**16**, 189 (1983).

1147. N. Takaoka, Y. Motomura, K. Nagao, Phys. Rev. C**53**, 1557 (1996).

1148. R. Luescher et al., Phys. Lett. B**434**, 407 (1998).

1149. V.A. Artemev et al., Pisma Zh. Eksp. Teor. Fiz. **58**, 256 (1993) [JETP Lett. **58**, 262 (1993)].

1150. M. Kobayashi, S. Kobayashi, Nucl. Phys. A**586**, 457 (1995).

1151. A.L. Turkevich, T.E. Economou, G.A. Cowan, Phys. Rev. Lett. **67**, 3211 (1991).

1152. A.S. Barabash et al., Z. Phys. A**357**, 351 (1997).

1153. L. Zhao, B.A. Brown, W.A. Richter, Phys. Rev. C**42**, 1120 (1990).

1154. T. Tsuboi, K. Muto, H. Horie, Phys. Lett. **143**B, 293 (1984).

1155. E. Caurier, A. Poves, A.P. Zuker, Phys. Lett. B**252**, 13 (1990); E. Caurier, A.P. Zucker, A. Poves, G. Martínez-Pinedo, in [370].

1156. K. Ogawa, H. Horie, in *Nuclear Weak Process and Nuclear Structure*, ed. by M. Morita et al. (World Scientific, Singapore 1989) p. 308.

1157. J.D. Vergados, Phys. Rev. C**13**, 865 (1976).

1158. A.H. Huffman, Phys. Rev. C**2**, 742 (1970).

1159. L. Zamick, N. Auerbach, Phys. Rev. C**26**, 2185 (1982).

1160. J. Krumlinde, P. Möller, Nucl. Phys. A**417**, 419 (1984).

1161. K. Grotz, H.V. Klapdor, J. Metzinger, J. Phys. G**9**, L169 (1983); K. Grotz, H.V. Klapdor, Phys. Lett. **153**B, 1 (1985).

1162. K. Grotz, H.V. Klapdor, in [1161]; Phys. Lett. **157**B, 242 (1985); Nucl. Phys. A**460**, 395 (1986).

1163. P. Vogel, P. Fisher, Phys. Rev. C**32**, 1362 (1985).

1164. T. Tomoda, A. Faessler, K.W. Schmid, F. Grümmer, Phys. Lett. **157**B, 4 (1985); Nucl. Phys. A**452**, 591 (1986).

1165. O. Civitarese, A. Faessler, T. Tomoda, Phys. Lett. B**194**, 11 (1987); T. Tomoda, A. Faessler, Phys. Lett. B**199**, 475 (1987).

1166. P.B. Radha et al., Phys. Rev. Lett. **76**, 2642 (1996).

1167. G.H. Lang, C.W. Johnson, S.E. Koonin, W.E. Ormand, Phys. Rev. C**48**, 1518 (1993); see also W. von der Linden, Phys. Rep. **220**, 53 (1992).

1168. E. Caurier, F. Nowacki, A. Poves, J. Retamosa, Phys. Rev. Lett. **77**, 1954 (1996).

1169. J. Retamosa, E. Caurier, F. Nowacki, Phys. Rev. C**51**, 371 (1995).

1170. J. Engel, P. Vogel, M.R. Zirnbauer, Phys. Rev. C**37**, 731 (1988).

1171. J. Engel, P. Vogel, X. Ji, S. Pittel, Phys. Lett. B**225**, 5 (1989).

1172. A. Staudt, K. Muto, H.V. Klapdor-Kleingrothaus, Europhys. Lett. **13**, 31 (1990); K. Muto, E. Bender, H.V. Klapdor, Z. Phys. A**324**, 177; 187 (1989).

1173. J.G. Hirsch, O. Castaños, P.O. Hess, Nucl. Phys. A**582**, 124 (1995); O. Castaños, J.G. Hirsch, O. Civitarese, P.O. Hess, Nucl. Phys. A**571**, 276 (1994).

1174. A. Arima et al., Phys. Lett. B**30**, 517 (1969).

1175. F. Šimkovic et al., Phys. Lett. B**393**, 267 (1997).

1176. S. Stoica, H.V. Klapdor-Kleingrothaus, Phys. Rev. C**63**, 064304 (2001).

1177. A.A. Raduta, A. Faessler, S. Stoica, W.A. Kaminski, Phys. Lett. B**254**, 7 (1991).

1178. M. Baranger, Phys. Rev. **120**, 957 (1960).

1179. J.A. Halbleib, Sr., R.A. Sorensen, Nucl. Phys. A**98**, 542 (1967).

1180. A. Griffiths, P. Vogel, Phys. Rev. C**46**, 181 (1992).

1181. P. Vogel, M.R. Zirnbauer, Phys. Rev. Lett. **57**, 3148 (1986).

1182. For earlier attempts, E. Fireman, Phys. Rev. **74**, 1238(A) (1948); **75**, 323(L) (1949); J.S. Lawson, Jr., Phys. Rev. **81**, 299(A) (1951); M.I. Kalkstein, W.F. Libby, Phys. Rev. **85**, 368(L) (1952).

1183. E. Fiorini et al., Phys. Lett. B**25**, 602 (1967)

1184. D.O. Caldwell et al., Phys. Rev. Lett. **59**, 419 (1987).

1185. J.J. Simpson et al., Phys. Rev. Lett. **53**, 141 (1984).

1186. M.G. Inghram, J.H. Reynolds, Phys. Rev. **76**, 1265(L) (1949); **78**, 822(L) (1950).

1187. N. Takaoka, K. Ogata, Z. Naturforsch. **21a**, 84 (1966).

1188. T. Kirsten, W. Gentner, O. Müller, Z. Naturforsch. **22a**, 1783 (1967); T. Kirsten, W. Gentner, O.A. Schaeffer, Z. Phys. **202**, 273 (1967).

1189. O.K. Manuel, in *Nuclear Beta Decays and Neutrino*, Osaka, 1986, ed. by T. Kotani, H. Ejiri, E. Takasugi (World Scientific, Singapore 1986) p. 71; E.W. Hennecke, O.K. Manuel, D.D. Sabu, Phys. Rev. C**11**, 1378 (1975); E.W. Hennecke, Phys. Rev. C**17**, 1168 (1978).

1190. K. Marti, S.V.S. Murty, Phys. Lett. **163**B, 71 (1985).

1191. A. Kawashima, K. Takahashi, A. Masuda, Phys. Rev. C**47**, R2452 (1993).

1192. A. Halprin, S.T. Petcov, S.P. Rosen, Phys. Lett. **125**B, 335 (1983).

1193. H. Primakoff, S.P. Rosen, Phys. Rev. **184**, 1925 (1969).

1194. J.D. Vergados, Phys. Rev. D**25**, 914 (1982).

1195. J.D. Vergados, Nucl. Phys. B**218**, 109 (1983); M. Doi, T. Kotani, Prog. Theor. Phys. **87**, 1207 (1992).

1196. C.P. Enz, Nuovo Cimento Serie X **6**, 250 (1957).

1197. R.N. Mohapatra, G. Senjanović, Phys. Rev. D**23**, 165 (1981).

1198. M. Doi, T. Kotani, H. Nishiura, E. Takasugi, Prog. Theor. Phys. **69**, 602 (1983).

1199. R.N. Mohapatra, Phys. Rev. D**34**, 909 (1986).

1200. Z.G. Berezhiani, A.Yu. Smirnov, J.W.F. Valle, Phys. Lett. **291**, 99 (1992).

1201. G.K. Leontaris, K. Tamvakis, J.D. Vergados, Phys. Lett. **171**B, 412 (1986); J.D. Vergados, Phys. Lett. B**184**, 55 (1987); R.N. Mohapatra, Phys. Rev. D**34**, 3457 (1986).

1202. T.P. Cheng, L.-F. Li, Phys. Rev. Lett. **38**, 381 (1977); Phys. Rev. D**16**, 1425 (1977)*; B.W. Lee, S. Pakvasa, R.E. Shrock, H. Sugawara, Phys. Rev. Lett. **38**, 937 (1977)*; H. Terazawa, Prog. Theor. Phys. **57**, 1808 (1977); B.W. Lee, R.E. Shrock, Phys. Rev. D**16**, 1444 (1977)*; J.D. Bjorken, K. Lane, S. Weinberg, Phys. Rev. D**16**, 1474 (1977); S.T. Petkov, Yad. Phys. **25**, 641 (1977)* [Sov. J. Nucl. Phys. **25**, 340 (1977)]. (* also presents a calculation of $\mu \to eee$.)

1203. C.N. Yang, J. Tiomno, Phys. Rev. **79**, 495 (1950).

1204. P.B. Pal, L. Wolfenstein, Phys. Rev. D**25**, 766 (1982).

1205. J. Schechter, J.W.F. Valle, Phys. Rev. D**22**, 2227 (1980).

1206. S.M. Bilenky, J. Hošek, S.T. Petcov, Phys. Lett. **94**B, 495 (1980).

1207. M. Doi et al., Phys. Lett. **102**B, 323 (1981).

1208. J. Schechter, J.W.F. Valle, Phys. Rev. D**23**, 1666 (1981).

1209. M. Fukugita, T. Yanagida, in *Physics and Astrophysics of Neutrinos*, ed. by M. Fukugita, A. Suzuki (Springer-Verlag, Tokyo 1994), p. 1.

1210. S. Eliezer, A.R. Swift, Nucl. Phys. B**105**, 45 (1976).

1211. S. Nussinov, Phys. Lett. **63**B, 201 (1976).

1212. B. Kayser, Phys. Rev. D**24**, 110 (1981).

1213. C. Giunti, C.W. Kim, U.W. Lee, Phys. Rev. D**44**, 3635 (1991).

1214. Y. Grossman, H.J. Lipkin, Phys. Rev. D**55** 2760 (1997).

1215. L. Stodolsky, Phys. Rev. D**58**, 036006 (1998).

1216. R.G. Winter, Lett. Nuovo Cimento **30**, 101 (1981).

1217. J.N. Bahcall, Phys. Rev. Lett. **71**, 2369 (1993).

1218. T. Yanagida, M. Yoshimura, Prog. Theor. Phys. **64**, 1870 (L) (1980).

1219. V. Barger, P. Langacker, J.P. Leveille, S. Pakvasa, Phys. Rev. Lett. **45**, 692 (1980).

1220. F. Reines, Ann. Rev. Nucl. Sci. **10**, 1 (1969); M.A. Markov, in *Proc. 1960 Annual Int. Conf. High Energy Phys. at Rochester*, 1960, ed. by E.C.G. Sudarshan, J.H. Tinlot, A.C. Melissinos (Rochester University, New York 1960) p. 578; M.A. Markov, I.M. Zheleznykh, Nucl. Phys. **27**, 385 (1961).

1221. G.T. Zatsepin, V.A. Kuzmin, J. Exptl. Theor. Phys. (USSR) **41**, 1818 (1961) [Sov. Phys. JETP **14**, 1294 (1962)].

1222. P.H. Frampton, S.L. Glashow, Phys. Rev. D**25**, 1982 (1982).

1223. D.S. Ayres et al., Phys. Rev. D**29**, 902 (1984); G.V. Dass, K.V.L. Sarma, Phys. Rev. D**30**, 80 (1984).

1224. B. Pontecorvo, Zh. Eksp. Teor. Fiz. **53**, 1717 (1967) [Sov. Phys. JETP **26**, 984 (1967)].

1225. Earlier studies include: J.N. Bahcall, S.C. Frautschi, Phys. Lett. **29**B, 623 (1969); S.M. Bilenky, B. Pontecorvo, Phys. Lett. **61**B, 248 (1976); H. Fritzsch, P. Minkowski, Phys. Lett. **62**B, 72 (1976); S. Nussinov [1211]; R. Ehrlich, Phys. Rev. D**18**, 2323; see S.M. Bilenky, B. Pontecorvo, Phys. Rep. **41**C, 225 (1978) for a review of earlier attempts.

1226. F. Reines, in *Proc. Int. Conf. on Neutrino Phys.*, Aachen (1976) ed. by H. Helmut, H. Reithler, P. Zerwas (Vieweg 1977); V. Barger, K. Whisnant, R.J.N. Phillips, Phys. Rev. D**22**, 1636 (1980); experimental feasibilities were considered by A.K. Mann, H. Primakoff, Phys. Rev. D**15**, 655 (1977).

1227. J. Blietschau et al. (CERN Gargamelle Collaboraton), Nucl. Phys. B**133**, 205 (1978).

1228. F. Reines, H.W. Sobel, E. Pasierb, Phys. Rev. Lett. **45**, 1307 (1980).

1229. F. Boehm et al., Phys. Lett. **97**B, 310 (1980).

1230. H. Deden et al., Phys. Lett. **98**B, 310 (1981); N. Armenise et al. Phys. Lett. **100**B, 182 (1981); O. Erriquez et al., Phys. Lett. **102**B, 73 (1981); P. Nemethy et al., Phys. Rev. D**23**, 262 (1981); N.J. Baker et al., Phys. Rev. Lett. **47**, 1576 (1981); N. Ushida et al., Phys. Rev. Lett. **47**, 1694 (1981).

1231. R. Barbieri, D.V. Nanopoulos, G. Morchio, F. Strocchi, Phys. Lett. **90**B, 91 (1980).

1232. V. Barger, K. Whisnant, R.J.N. Phillips, Phys. Rev. D**24**, 538 (1981).

1233. S.L. Glashow, L.M. Kraus, Phys. Lett. B**190**, 199 (1987).

1234. V. Barger, R.J.N. Phillips, K. Whisnant, Phys. Rev. Lett. **65**, 3084 (1990); **69**, 3135 (1992).

1235. A. Acker, S. Pakvasa, J. Pantaleone, Phys. Rev. D**43**, R1754 (1991).

1236. Z.G. Berezhiani, A. Rossi, Phys. Rev. D**51**, 5229 (1995); E. Calabresu, N. Ferrari, G. Fiorentini, M. Lissia, Astroparticle Phys. **4**, 159 (1995); P.I. Krastev, S.T. Petcov, Nucl. Phys. B**449**, 605 (1995); J.N. Bahcall, P.I. Krastev, A.Yu. Smirnov, Phys. Rev. D**58**, 096016 (1998).

1237. A. Romosan et al., Phys. Rev. Lett. **78**, 2912 (1997); L. Borodovsky et al., Phys. Rev. Lett. **68**, 274 (1992); B. Blumenfeld et al., Phys. Rev. Lett. **62**,

2237 (1989); L.S. Durkin et al., Phys. Rev. Lett. **61**, 1811 (1988); C. Angelini et al., Phys. Lett. B**179**, 307 (1986); L.A. Ahrens et al., Phys. Rev. D**31**, 2732 (1985).

1238. F. Bergsma et al., Phys. Lett. **142**B, 103 (1984); F. Dydak et al., Phys. Lett. **134**B, 281 (1984) [CDHSW]; I.E. Stockdale et al., Z. Phys. C**27**, 53 (1985) [CCFR].

1239. N. Ushida et al., Phys. Rev. Lett. **57**, 2897 (1986); M. Gruwé et al., Phys. Lett. B**309**, 463 (1993) [CHARM II]; K.S. McFarland et al., Phys. Rev. Lett. **75**, 3993 (1995) [CCFR].

1240. P. Astier et al., Nucl. Phys. B**611**, 3 (2001); Phys. Lett. B**483**, 387 (2000) [NOMAD]; E. Eskut et al., Phys. Lett. B**497**, 8 (2001) [CHORUS].

1241. A. Aguilar et al., Phys. Rev. D**64**, 112007 (2001); C. Athanassopoulos et al., Phys. Rev. Lett. **75**, 2650 (1995) [LSND].

1242. J.E. Hill, Phys. Rev. Lett. **75**, 2654 (1995).

1243. K. Eitel, Nucl. Phys. B (Proc. Suppl.) **91**, 191 (2001) [KARMEN].

1244. B. Achkar et al., Nucl. Phys. B**434**, 503 (1995) [Bugey].

1245. M. Apollonio et al., [923]; B**466**, 415 (1999) [CHOOZ].

1246. H. Murayama, personal communication; see also idem in RPP2000 [275], p. 360.

1247. H. Noumi et al., Nucl. Instr. Meth. A**398**, 399 (1997) [K2K].

1248. S.H. Ahn et al., Phys. Lett. B**511**, 178 (2001) [K2K].

1249. M.F. Crouch et al., Phys. Rev. D**18**, 2239 (1978).

1250. F. Reines, in *Proc. Int. Cosmic Ray Conf.*, Kyoto 1978, Vol. 14, p. 60 (Institute for Cosmic Ray Research, Tokyo 1978).

1251. K.S. Hirata et al., Phys. Lett. B**280**, 146 (1992) [Kamiokande].

1252. Z. Koba, H.B. Nielsen, P. Olesen, Phys. Lett. **38**B, 25 (1972).

1253. S.J. Barish et al., Phys. Rev. D**19**, 2521 (1979).

1254. T. Kajita, personal communication (2001).

1255. R. Becker-Szendy et al., Phys. Rev. Lett. **69**, 1010 (1992) [IMB].

1256. M.M. Boliev et al., in *Proc. Int. Workshop on Neutrino Telescope*, Venezia, ed. by M. Baldo-Ceolin (INFN, Padova), p. 235.

1257. M. Aglietta, Europhys. Lett. **8**, 611 (1989) [Nusex].

1258. Ch. Berger et al., Phys. Lett. B**245**, 305 (1990) [Frejus].

1259. Y. Fukuda et al., Phys. Lett. B**388**, 397 (1996) [Kamiokande].

1260. J. Kameda, in *Proc. Int. Cosmic Ray Conf.*, Hamburg 2001, op. cit. (see [610]) Vol. 3, p. 1057 [Super-Kamiokande].

1261. Y. Fukuda et al., Phys. Rev. Lett. **82**, 2644 (1999) [Super-Kamiokande].

1262. Y. Fukuda et al., Phys. Lett. B**467**, 185 (1999) [Super-Kamiokande].

1263. S. Fukuda et al., Phys. Rev. Lett. **85**, 3999 (2000) [Super-Kamiokande].

1264. MACRO collaboration, Phys. Lett. B**434**, 451 (1998); hep-ex/0001044 (2000); F. Ronga, *Proc. 30th Int. Conf. High Energy Phys.*, Osaka 2000, ed. by C.S. Lim, T. Yamanaka (World Scientific, Singapore 2001), Vol. 2, p. 910.

1265. E. Peterson, in *Proc. 30th Int. Conf. High Energy Phys.*, op. cit. Vol. 2, p. 907.

1266. S. Hatakeyama et al., Phys. Rev. Lett. **81**, 2016 (1998) [Kamiokande].

1267. K. Daum et al., Z. Phys. C**66**, 417 (1995).

1268. R. Clark et al., Phys. Rev. Lett. **79**, 345 (1997).

1269. W.W.M. Allison et al., Phys. Lett. B**449**, 137 (1999); see also, idem Phys. Lett. B**391**, 491 (1997).

1270. Y. Fukuda et al., Phys. Lett. B**433**, 9 (1998) [Super-Kamiokande].
1271. T. Kajita, Y. Totsuka, Rev. Mod. Phys. **73**, 85 (2001).
1272. S. Fukuda, Phys. Rev. Lett. **86**, 5656 (2001).
1273. G.L. Fogli, E. Lisi, D. Montanino, A. Palazzo, Phys. Rev. D**64**, 093007 (2001).
1274. J.N. Bahcall, M.C. Gonzalez-Garcia, C. Pena-Garay, JHEP **0108**, 014 (2001); see also J.N. Bahcall, P.I. Krastev, A.Yu. Smirnov, JHEP **0105**, 015 (2001).
1275. Y. Fukuda et al., Phys. Rev. Lett. **82**, 2430 (1999).
1276. H. Murayama, in RPP2000, Eur. Phys. J. C**15**, 360 (2000).
1277. V. Barger, K. Whisnant, S. Pakvasa, R.J.N. Phillips, Phys. Rev. D**22**, 2718 (1980).
1278. P.D. Mannheim, Phys. Rev. D**37**, 1935 (1988).
1279. S.P. Mikheev and A.Yu. Smirnov, Zh. Eksp. Teor. Fiz. **92**, 404 (1987) [Sov. Phys. JETP **65**, 230 (1987)].
1280. A. Friedland, Phys. Rev. D**64**, 013008 (2001).
1281. S.J. Parke, Phys. Rev. Lett. **57**, 1275 (1986).
1282. W.C. Haxton, Phys. Rev. Lett. **57**, 1271 (1986).
1283. L. Landau, Phys. Sowjetunion **2**, 46 (1932); C. Zener, Proc. R. Soc. London A**137**, 696 (1932); E.C.G. Stueckelberg, Helv. Phys. Acta **5**, 369 (1932).
1284. T.K. Kuo, J. Pantaleone, Phys. Rev. Lett. **57**, 1805 (1986).
1285. S.P. Mikheev, A.Yu. Smirnov, Usp. Fiz. Nauk **153**, 3 (1987) [Sov. Phys. Usp. **30**, 759 (1987)].
1286. T.K. Kuo, J. Pantaleone, Rev. Mod. Phys. **61**, 937 (1989).
1287. E.T. Whittaker, G.N. Watson, *Modern Analysis* (Cambridge University Press, Cambridge 1927).
1288. S. Toshev, Phys. Lett. B**196**, 170 (1987); T. Kaneko, Prog. Theor. Phys. **78**, 532 (1987); S.T. Petcov, Phys. Lett. B**200**, 373 (1988); B**214**, 139 (1988).
1289. P.I. Krastev, S.T. Petcov, Phys. Lett. B**207**, 64 (1988).
1290. T.K. Kuo, J. Pantaleone, Phys. Rev. D**39**, 1930 (1989).
1291. O.V. Bychuk, V.P. Spiridonov, Mod. Phys. Lett. A**5**, 1007 (1990).
1292. S.P. Rosen, J.M. Gelb, Phys. Rev. D**34**, 969 (1986).
1293. V. Barger, R.J.N. Phillips, K. Whisnant, Phys. Rev. D**34**, 980 (1986); J. Bouchez et al., Z. Phys. C**32**, 499 (1986); E.W. Kolb, M.S. Turner, T.P. Walker, Phys. Lett. B**175**, 478 (1986); S.J. Parke, T.P. Walker, Phys. Rev. Lett. **57**, 2322 (1986); W.C. Haxton, Phys. Rev. D**35**, 2352 (1987); J.N. Bahcall, J.M. Gelb, S.P. Rosen, Phys. Rev. D**35**, 2976 (1987); A. Dar, A. Mann, Y. Melina, D. Zajfman, Phys. Rev. D**35**, 3607 (1987); P.I. Krastev, S.T. Petcov, Phys. Lett. B**207**, 64 (1988); J.N. Bahcall, W.C. Haxton, Phys. Rev. D**40**, 931 (1989); K.S. Hirata et al., Phys. Rev. Lett. **65**, 1301 (1990); P.I. Krastev, S.P. Mikheev, A.Yu. Smirnov, Inst. Nucl. Research (Moscow) preprint, P-695 (1991).
1294. Analyses with three neutrinos were carried out by H.W. Zaglauer, K.H. Schwarzer, Phys. Lett. B**198**, 556 (1987); C.W. Kim, W.K. Sze, Phys. Rev. D**35**, 1404 (1987); T.K. Kuo, J. Pantaleone, Phys. Rev. D**35**, 3432 (1987); S.T. Petcov, Phys. Lett. B**214**, 259 (1988); S.P. Mikheyev, A.Yu. Smirnov, Phys. Lett. B**200**, 560 (1988).
1295. More modern analyses are given in P. Anselmann, Phys. Lett. B**285**, 390 (1992); X. Shi, D.N. Schramm, J.N. Bahcall, Phys. Rev. Lett. **69**, 717 (1992); P.I. Krastev, S.T. Petcov, Phys. Lett. B**299**, 99 (1993); S.A. Bludman, N. Hata, D.C. Kennedy, P.G. Langacker, Phys. Rev. D**47**, 2220 (1993);

M. White, L. Krauss, E. Gates, Phys. Rev. Lett. **70**, 375 (1993); Phys. Rev. D**51**, 2631 (1995); N. Hata, P. Langacker, Phys. Rev. D**50**, 632 (1994); D**52**, 420 (1995); G.L. Fogli, E. Lisi, D. Montanino, Phys. Rev. D**49**, 3626 (1994); G.L. Fogli, E. Lisi, Astroparticle Phys. **3**, 185 (1995); E. Calabresu et al. ref. [1236]; P.I. Krastev, S.T. Petcov, ref. [1236]; J.N. Bahcall, P.I. Krastev, A.Yu. Smirnov, ref. [1236].

1296. J.N. Bahcall, P.I. Krastev, A.Yu. Smirnov, ref. [1236].

1297. S.P. Mikheyev, A.Yu. Smirnov, in '*86 Massive Neutrinos in Astrophysics and in Particle Physics, Proc. of the 6th Moriond Workshop*, Tignes 1986, ed. by O. Fackler, J. Tran Thanh Van (Editions Frontières, Gif-sur-Yvette 1986) p. 355; J. Bouchez et al. [1293]; A. Dar, A. Mann, Nature (London) **325**, 790 (1987); A.J. Baltz, J. Weneser, Phys. Rev. D**35**, 528 (1987); M. Cribier, W. Hampel, J. Rich, D. Vignaud, Phys. Lett. B**182**, 89 (1986); M.L. Cherry, K. Lande, Phys. Rev. D**36**, 3571 (1987); S. Hiroi, H. Sakuma, T. Yanagida, M. Yoshimura, Phys. Lett. B**198**, 403 (1987): Prog. Theor. Phys. **78**, 1428 (1987); A.J. Baltz, J. Weneser, Phys. Rev. D**37**, 3364 (1988). G.L. Fogli, E. Lisi, D. Montanino, ref. [1295]; H. Hata, P. Langacker, ref. [1295]; J.N. Bahcall, P.I. Krastev, Phys. Rev. D**56**, 2839 (1997); M. Maris, S.T. Petcov, Phys. Rev. D**56**, 7444 (1997);

1298. F.D. Stacey, *Physics of the Earth* (Wiley, New York 1969); A.M. Dziewonski, F. Gilbert, Quart. J. R. astr. Soc. **35**, 401 (1973); K.E. Bullen, *The Earth's Density* (Chapman and Hall, London 1975); A.M. Dziewonski, D.L. Anderson, Phys. Earth Planet. Interior **25**, 207 (1981) (PERM).

1299. Y. Suzuki, personnal communication (2000).

1300. J.N. Bahcall, P.I. Krastev, ref. [1297].

1301. S.T. Petcov, Phys. Lett. B**434**, 321 (1998).

1302. Y. Fukuda et al., Phys. Rev. Lett. **82**, 2430 (1999).

1303. A. Friedland, Phys. Rev. Lett. **85**, 936 (2000); G.L. Fogli, E. Lisi, D. Montanino, A. Palazzo, Phys. Rev. D**62**, 113004 (2000).

1304. T.P. Walker, D.N. Schramm, Phys. Lett. B**195**, 331 (1987).

1305. L. Wolfenstein, Phys. Lett. B**194**, 197 (1987).

1306. P.O. Lagage, M. Cribier, J. Rich, D. Vignaud, Phys. Lett. B**193**, 127 (1987).

1307. A.Yu. Smirnov, D.N. Spergel, J.N. Bahcall, Phys. Rev. D**49**, 1389 (1994).

1308. J. Arafune, M. Fukugita, T. Yanagida, M. Yoshimura, Phys. Rev. Lett. **59**, 1864 (1987).

1309. B. Jegerlehner, F. Neubig, G. Raffelt, Phys. Rev. D**54**, 1194 (1996).

1310. C. Lunardini, A.Yu. Smirnov, Phys. Rev. D**63**, 073009 (2001).

1311. J. Arafune, M. Fukugita, in ref. [759]; J. Arafune, M. Fukugita, T. Yanagida, M. Yoshimura, [1308]; H. Minakata, H. Nunokawa, K. Shiraishi, H. Suzuki, Mod. Phys. Lett. A**2**, 827 (1987); S.P. Mikheyev, A.Yu. Smirnov, Pisma Zh. Eksp. Teor. Fiz. **46**, 11 (1987) [JETP Lett. **46**, 10 (1987)]; D. Nötzold, Phys. Lett. B**196**, 315 (1987); T.K. Kuo, J. Pantaleone, Phys. Rev. D**37**, 298 (1988).

1312. S.P. Mikheyev, A.Yu. Smirnov, ref. [1297].

1313. P. Langacker, S. T. Petcov. G. Steigman, S. Toshev, Nucl. Phys. B**282**, 589 (1987).

1314. K. Enqvist, K. Kainulainen, J. Maalampi, Nucl. Phys. B**349**, 754 (1991).

1315. K. Kainulainen, Phys. Lett. B**244**, 191 (1990).

1316. K. Enqvist, K. Kainulainen, M. Thomson, Nucl. Phys. B**373**, 498 (1992).

1317. A.D. Dolgov, S.H. Hansen, Astroparticle Phys. **16**, 339 (2002).

1318. Y. Hosotani, Nucl. Phys. B**191**, 411 (1981).

1319. M. Fukugita, M. Tanimoto, Phys. Lett. B**515**, 30 (2001).

1320. E. Ma, P. Roy, Phys. Rev. D**52**, R4780 (1995); R. Foot, R.R. Volkas, Phys. Rev. D**52**, 6595 (1995); E.J. Chun, A.S. Joshipura, A.Yu. Smirnov, Phys. Lett. B**357**, 608 (1995).

1321. N. Okada, O. Yasuda, Int. J. Mod. Phys. A**12**, 3669 (1997).

1322. S.M. Bilenky, C. Giunti, W. Grimus, Eur. Phys. J. C**1**, 247 (1998).

1323. V. Barger, S. Pakvasa, T.J. Weiler, K. Whisnant, Phys. Rev. D**58**, 093016 (1998).

1324. V. Barger et al., Phys. Lett. B**489**, 345 (2000).

1325. O.L.G. Peres, A.Yu. Smirnov, Nucl. Phys. B**599**, 3 (2001).

1326. B. Richter, hep-ph/0008222.

1327. V. Barger et al., hep-ph/0103052; see also M. Freund, P. Huber, M. Lindner, Nucl. Phys. B**615**, 331 (2001).

1328. Super-Kamiokande group, personal communication.

1329. Y. Itow et al., hep-ex/0106019; MINOS Technical Design Report NuMI-L-337 (1998); Fermilab FN 692 (2000).

1330. J. Arafune, M. Koike, J. Sato, Phys. Rev. D**56**, 3093 (1997).

1331. P. Lipari, Phys. Rev. D**61**, 113004 (2000); V. Barger et al., Phys. Rev. D**63**, 113011 (2001).

1332. N. Cabibbo, Phys. Lett. **72B**, 333 (1978).

1333. S.M. Bilenky, S.T. Petcov, Rev. Mod. Phys. **59**, 671 (1987).

1334. S. Pakvasa, in *Proc. 20th Int. Conf. High Energy Phys.*, Madison, Wisconsin, 1980, ed. by L. Durand, L.G. Pondrom (American Institute of Physics 1981) Part **2**, 1165 (1980); V. Barger, K. Whisnant, R.J.N. Phillips, Phys. Rev. Lett. **45**, 2084 (1980); S.M. Bilenky, F. Nidermaler, Yad. Fiz. **34**, 1091 (1981) [Sov. J. Nucl. Phys. **34**, 606 (1981)].

1335. M. Tanimoto, Phys. Rev. D**55**, 322 (1997).

1336. J. Arafune, J. Sato, Phys. Rev. D**55**, 1653 (1997).

1337. H. Minakata, H. Nunokawa, Phys. Rev. D**57**, 4403 (1998).

1338. M. Koike, J. Sato, Phys. Rev. D**61**, 073012 (2000); J. Sato, in *Proc. KEK Int. Workshop High Intensity Muon Source*, Tsukuba 1999, ed. by Y. Kuno, T. Yokoi (World Scientific, Singapore 2001), p. 299.

1339. T.K. Kuo, J. Pantaleone, Phys. Lett. B**198**, 406 (1987).

1340. V. Barger, S. Geer, R. Raja, K. Whisnant, Phys. Rev. D**62**, 073002 (2000).

1341. H.-Y. Chen, Phys. Rev. D**34**, 2794 (1986).

1342. H. Georgi, H.R. Quinn, S. Weinberg, Phys. Rev. Lett. **33**, 451 (1974).

1343. H. Georgi, in *Particles and Fields*, AIP Proc. ed. by C.E. Carlson (AIP, New York 1975), p. 575.

1344. H. Fritzsch, P. Minkowski, Ann. Phys. (NY) **93**, 193 (1975).

1345. S. Dimopoulos, S. Raby, F. Wilczek, Phys. Rev. D**24**, 1681 (1981).

1346. S. Coleman, J. Mandula, Phys. Rev. **159**, 1251 (1967).

1347. J. Wess, B. Zumino, Nucl. Phys. B**70**, 39 (1974); D.V. Volkov, V.P. Akulov, Phys. Lett. **46B**, 109 (1973).

1348. J. Wess, B. Zumino, Phys. Lett. B**49**, 52 (1974).

1349. A. Salam, J. Strathdee, Phys. Rev. D**11**, 1521 (1975).

1350. J.R. Ellis, T.K. Gaisser, G. Steigman, Nucl. Phys. B**177**, 427 (1981).

1351. N. Sakai, T. Yanagida, Nucl. Phys. B**197**, 533 (1982); S. Weinberg, Phys. Rev. D**26**, 287 (1982).

1352. F. Wilczek, A. Zee, Phys. Rev. D**25**, 553 (1982); A. Zee, *1981 INS Symp. on Quark and Lepton Phys.* (Inst. Nucl. Study, Univ. of Tokyo, Tokyo 1981), p. 224.

1353. C.D. Froggatt, H.B. Nielsen, Nucl. Phys. B**147**, 277 (1979).

1354. E. Cremmer, B. Julia, Phys. Lett. **80**B, 48 (1978); Nucl. Phys. B**159**, 141 (1979).

1355. C.G. Callan, Jr., R.F. Dashen, D.J. Gross, Phys. Lett. B**63**, 334 (1976); R. Jackiw, C. Rebbi, Phys. Rev. Lett. **37**, 172 (1976).

1356. A.A. Belavin, A.M. Polyakov, A.S. Schwartz, Yu.S. Tyupkin, Phys. Lett. **59**B, 85 (1975).

1357. E. Witten, Nucl. Phys. B**156**, 269 (1979); G. Veneziano, Nucl. Phys. B**159**, 213 (1979).

1358. M. Fukugita, Y. Kuramashi, M. Okawa, A. Ukawa, Phys. Rev. D**51**, 3952 (1995); Y. Kuramashi et al., Phys. Rev. Lett. **72**, 3448 (1994).

1359. R.D. Peccei, H.R. Quinn, Phys. Rev. Lett. **38**, 1440 (1977); Phys. Rev. D**16**, 1791 (1977).

1360. S. Weinberg, Phys. Rev. Lett. **40**, 223 (1978); F. Wilczek, Phys. Rev. Lett. **40**, 279 (1978).

1361. R.D. Peccei, in *CP Violation*, ed. by C. Jarlskog (World Scientific, Singapore 1989).

1362. S. Coleman, Nucl. Phys. B**307**, 867 (1988).

1363. S. Aoki et al., Phys. Rev. D**62**, 014506 (2000); M.B. Gavela et al., Nucl. Phys. B**312**, 269 (1989) carried out a similar calculation, resulting in a matrix element which does not agree with Aoki et al.'s. This is, however, ascribed to the latter authors' neglect of a term in the form factor; see Aoki et al. for discussion.

1364. S.J. Brodsky, J. Ellis, J.S. Hagelin, C.T. Sachrajda, Nucl. Phys. B**238**, 561 (1984) and references therein; the largest α is given by this literature and the smallest by J. Donoghue, E. Golowich, Phys. Rev. D**26**, 3092 (1982); for lattice QCD calculation of $\langle 0|O|p \rangle$, Y. Hara et al., Phys. Rev. D**34**, 3399 (1986); K.C. Bowler et al., Nucl. Phys. B**296**, 431 (1988).

1365. A.J. Buras, J.R. Ellis, M.K. Gaillard, D.V. Nanopoulos, Nucl. Phys. B**135**, 66 (1978).

1366. T.J. Goldman, D.A. Ross, Phys. Lett. **84**B, 208 (1979); Nucl. Phys. B**171**, 273 (1980).

1367. For example W.J. Marciano, in *Proceedings of Eighth Workshop on Grand Unification*, ed. by C. Wali (World Scientific, Singapore 1987) p. 185.

1368. For example, Y. Totsuka, in *Proc. 1985 Int. Symp. Lepton Photon Interaction High Energies*, Kyoto 1985, ed. by M. Konuma, K. Takahashi (Yukawa Hall, Kyoto 1986), p. 120.

1369. R. Becker-Szendy et al., Phys. Rev. D**42**, 2974 (1990). M Shiozawa et al., Phys. Rev. Lett. **81**, 3319 (1998).

1370. J. Ellis, S. Kelly, D.V. Nanopoulos, Phys. Lett. B**260**, 131 (1991); U. Amaldi, W. de Boer, H. Fürstenau, Phys. Lett. B**260**, 447 (1991); P. Langacher, M.X. Luo, ref. [296]; W.J. Marciano, ref. [353]; U. Amaldi et al., Phys. Lett. B**281**, 374 (1992).

1371. M. Tanimoto, personal communication

1372. A. Ali Khan et al., Phys. Rev. Lett. **85**, 4674 (2000) [CP-PACS].

1373. S. Weinberg, *Festschrift* to I.I. Rabi, Proc. N. Y. Acad. Sci. **38**, 185 (1977).

1374. H. Fusaoka, Y. Koide, Phys. Rev. D**57**, 3986 (1998).

1375. A.M. Polyakov, JETP Lett. **20**, 194 (1974); G. 't Hooft, Nucl. Phys. B**79**, 276 (1974).

1376. Ya.B. Zeldovich, M.Yu. Khlopov, Phys. Lett. **79**B, 239 (1978); J.P. Preskill, Phys. Rev. Lett. **43**, 1365 (1979).

1377. A.H. Guth, S.-H. Tye, Phys. Rev. Lett. **44**, 631 (1980). Erratum: Phys. Rev. Lett. **44**, 963; M.B. Einhorn, K. Sato, Nucl. Phys. B**180**, 385 (1981).

1378. J. Wess, J. Bagger, *Supersymmetry and Supergravity* (Princeton University Press, Princeton 1983).

1379. S. Weinberg, *The Quantum Theory of Fields III, Supersymmetry* (Cambridge University Press, Cambridge 2000).

1380. P. Fayet, Phys. Lett. **84**B, 416 (1979).

1381. S. Dimopoulos, H. Georgi, Nucl. Phys. B**193**, 150 (1981); N. Sakai, Z. Phys. C**11**, 153 (1981).

1382. M.T. Grisaru, W. Siegel, M. Rocek, Nucl. Phys. B**159**, 429 (1979).

1383. H.P. Nilles, Phys. Rept. **110**, 1 (1984).

1384. M.B. Einhorn, D.R.T. Jones, Nucl. Phys. B**196**, 475 (1982).

1385. S. Dimopoulos, S. Raby, F. Wilczek, Phys. Lett. **112**B, 133 (1982); J. Ellis, D.V. Nanopoulos, S. Rudaz, Nucl. Phys. B**202**, 43 (1982).

1386. J. Hisano, H. Murayama, T. Yanagida, Nucl. Phys. B**402**, 46 (1993).

1387. P. Nath, A.H. Chamseddine, R. Arnowitt, Phys. Rev. D**32**, 2348 (1985).

1388. T. Goto, T. Nihei, Phys. Rev. D**59**, 115009 (1999).

1389. V. Lucas, S. Raby, Phys. Rev. D**55**, 6986 (1997).

1390. Y. Hayato et al., Phys. Rev. Lett. **83**, 1529 (1999) [Super-Kamiokande].

1391. K.S. Hirata et al., Phys. Lett. B**220**, 308 (1989) [Kamiokande].

1392. J. Hisano, H. Murayama, T. Yanagida, Phys. Rev. Lett. **69**, 1014 (1992).

1393. H. Murayama, A. Pierce, Phys. Rev. D**65**, 055009 (2002).

1394. T.W.B. Kibble, J. Phys. A**9**, 1387 (1976).

1395. A. Vilenkin, Phys. Rep. **121**, 263 (1985).

1396. T.W.B. Kibble, Phys. Rep. **67**, 183 (1980).

1397. A. Albrecht, N. Turok, Phys. Rev. Lett. **54**, 1868 (1985); D.B. Bennett, F.R. Bouchet, Phys. Rev. Lett. **60**, 257 (1988); B. Allen, E.P.S. Shellard, Phys. Rev. Lett. **64**, 119 (1990).

1398. A. Stebbins, AP. J. **327**, 584 (1988); N. Turok, U.-L. Pen, U. Seljak, Phys. Rev. D**58**, 023506 (1998); C.R. Contaldi, M. Hindmarsh, J. Megneijo, Phys. Rev. Lett. **82**, 679 (1999).

1399. D.P. Bennett, F.R. Bouchet, Phys. Rev. Lett. **63**, 1334 (1989); B. Allen, E.P.S. Shellard, Phys. Rev. D**45**, 1898 (1992).

1400. J.C. Pati, A. Salam, Phys. Rev. D**10**, 275 (1974); R.N. Mohapatra, J.C. Pati, Phys. Rev. D**11**, 2558 (1975); G. Senjanovic, R.N. Mohapatra, Phys. Rev. D**12**, 1502 (1975).

1401. R.N. Mohapatra, G. Senjanovic, Phys. Rev. Lett. **44**, 912 (1980); Phys. Rev. D**23**, 165 (1981).

1402. H. Georgi, S.L. Glashow, Phys. Rev. D**6**, 429 (1972); D.J. Gross, R. Jackiw, Phys. Rev. D**6**, 477 (1972).

1403. R. Slansky, Phys. Rep. **79**, 1 (1981).

1404. M.S. Chanowitz, J.R. Ellis, M.K. Gaillard, Nucl. Phys. B**128**, 506 (1977).

1405. G. Branco, A. Masiero, Phys. Lett. B**97**, 95 (1980); T. Yanagida, M. Yoshimura, Phys. Lett. B**97**, 99 (1980).

1406. S.F. Tuan, Mod. Phys. Lett. A**7**, 641 (1992).

1407. J.A. Harvey, D.B. Reiss, P. Ramond, Nucl. Phys. B**199**, 223 (1982).

1408. H. Georgi, C. Jarlskog, Phys. Lett. **86**B, 297 (1979).

1409. A. Smirnov, Phys. Rev. D**48**, 3264 (1993); M. Tanimoto, Phys. Lett. B**345**, 477 (1995).

1410. B. Stech, Phys. Lett. B**465**, 219 (1999).

1411. K.S. Babu, S.M. Barr, Phys. Lett. B**381**, 202 (1996); C.H. Albright, K.S. Babu, S.M. Barr, Phys. Rev. Lett. **81**, 1167 (1998); K. Oda, E. Takasugi, M. Tanaka, M. Yoshimura, Phys. Rev. D**59**, 055001 (1999); T. Blazek, S. Raby, K. Tobe, Phys. Rev. D**60**, 113001 (1999); K.S. Babu, B. Dutta, R.N. Mohapatra, Phys. Lett. B**458**, 93 (1999); K.S. Babu, J.C. Pati, F. Wilczek, Nucl. Phys. B**566**, 33 (2000); R. Dermisek, S. Raby, Phys. Rev. D**62**, 015007 (2000).

1412. K.S. Babu, J.C. Pati, F. Wilczek, in [1411].

1413. E. Witten, Phys. Lett. **91**B, 81 (1980).

1414. Y. Nomura, T. Yanagida, Phys. Rev. D**59**, 017303 (1998); M. Bando, T. Kugo, K. Yoshioka, Phys. Lett. B**483**, 163 (2000); M. Bando, N. Maekawa, Prog. Theor. Phys. **106**, 1255 (2001).

1415. S. Rajpoot, Phys. Rev. D**22**, 2244 (1980).

1416. H. Georgi, D.V. Nanopoulos, Nucl. Phys. B**159**, 16 (1979); Q. Shafi, M. Sondermann, C. Wetterich, Phys. Lett. **92**B, 304 (1980); T.G. Rizzo, G. Senjanovic, Phys. Rev. Lett. **46**, 1315 (1981).

1417. W.E. Caswell, J. Milutinović, G. Senjanović, Phys. Rev. D**26**, 161 (1982); R.W. Robinett, J.L. Rosner, Phys. Rev. D**25**, 3036 (1982).

1418. Y. Tosa, G.C. Branco, R.E. Marshak, Phys. Rev. D**28**, 1713 (1983).

1419. M. Machacek, Nucl. Phys. B**159**, 37 (1979).

1420. V.V. Dixit, M. Sher, Phys. Rev. D**40**, 3765 (1989).

1421. M.K. Parida, P.K. Patra, Phys. Rev. Lett. **66**, 858 (1991).

1422. D. Chang, R.N. Mohapatra, M.K. Parida, Phys. Rev. Lett. **52**, 1072.

1423. R.N. Mohapatra, M.K. Parida, Phys. Rev. D**47**, 264 (1993).

1424. M. Fukugita, T. Yanagida, in [719].

1425. N.G. Deshpande, E. Keith, P.B. Pal, Phys. Rev. D**46**, 2261 (1992); N.T. Shaban, W.J. Stirling, Phys. Lett. B**291**, 281 (1992); M.K. Parida, P.K. Patra, C.C. Hazra, Phys. Rev. D**43**, 2351 (1991); G.M. Asatryan, S.G. Matinyan, Yad. Fiz. **55**, 479 (1992) [Sov. J. Nucl. Phys. **55**, 265 (1992)].

1426. D. Chang et al., Phys. Rev. D**31**, 1718 (1985).

1427. T. Yanagida, Phys. Rev. D**20**, 2986 (1979).

1428. T. Maehara, T. Yanagida, Prog. Theor. Phys. **61**, 1434 (1979); R.N. Cahn, H. Harari, Nucl. Phys. B**176**, 135 (1980).

1429. Y. Chikashige, R.N. Mohapatra, R.D. Peccei, Phys. Rev. Lett. **45**, 1926 (1980).

1430. Y. Chikashige, R.N. Mohapatra, R.D. Peccei, Phys. Lett. **98**B, 265 (1981).

1431. D.B. Reiss, Phys. Lett. B**115**, 217 (1982).

1432. F. Wilczek, Phys. Rev. Lett. **49**, 1549 (1982); G.B. Gelmini, S. Nussinov, T. Yanagida, Nucl. Phys. B**219**, 31 (1983).

1433. M. Fukugita, T. Yanagida, Phys. Rev. Lett. **66**, 2705 (1991).

1434. A. Jodidio et al., Phys. Rev. D**34**, 1967 (1986).

1435. S. Adler et al., Phys. Rev. Lett. **79**, 2204 (1997).

1436. M. Fukugita, T. Yanagida, Phys. Rev. Lett. **55**, 2645 (1985).

1437. J. Feng, T. Moroi, H. Murayama, E. Schnapka, Phys. Rev. D**57**, 5875 (1998).

1438. S.L. Glashow, Phys. Lett. B**256**, 255 (1991).

1439. K.F. Smith et al., Phys. Lett. B**234**, 191 (1990).

1440. V. Baluni, Phys. Rev. D**19**, 2227 (1979); R.J. Crewther, P. Di Vecchia, G. Veneziano, E. Witten, Phys. Lett. **88**B, 123 (1979).

1441. For example, see R.D. Peccei, in *Proc. Grand Unified Theories and Related Topics*, Kyoto, 1981, ed. by M. Konuma, T. Maskawa (World Scientific, Singapore 1981) p. 347.

1442. J.E. Kim, Phys. Rev. Lett. **43**, 103 (1979).

1443. A.P. Zhitnitskiĭ, Yad. Fiz. **31**, 497 (1980) [Sov. J. Nucl. Phys. **31**, 260 (1980)].

1444. M. Dine, W. Fischler, M. Srednicki, Phys. Lett. **104**B, 199 (1981).

1445. M.A. Shifman, A.I. Vainshtein, V.I. Zakharov, Nucl. Phys. B**166**, 493 (1980).

1446. C. Vafa, E. Witten, Phys. Rev. Lett. **53**, 535 (1984); Nucl. Phys. B**234**, 173 (1984).

1447. R.N. Mohapatra, G. Senjanović, Z. Phys. C**17**, 53 (1983).

1448. R. Holman, G. Lazarides, Q. Shafi, Phys. Rev. D**27**, 995 (1983).

1449. P. Langacker, R.D. Peccei, T. Yanagida, Mod. Phys. Lett. A**1**, 541 (1986).

1450. D.A. Dicus, E.W. Kolb, V.L. Teplitz, R.V. Wagoner, Phys. Rev. D**18**, 1829 (1978); see also M.I. Vysotskii, Ya.B. Zeldovich, M.Yu. Khlopov, V.M. Chechetkin, Pis'ma Zh. Eksp. Teor. Fiz. **27**, 533 (1978) [JETP Lett. **27**, 502 (1978)]; the argument for the constraint on exotic scalar particle emission from stars was first made by K. Sato, H. Sato, Prog. Theor. Phys. **54**, 1564 (1975).

1451. M. Fukugita, S. Watamura, M. Yoshimura, Phys. Rev. Lett. **48**, 1522 (1982); Phys. Rev. D**26**, 1840 (1982); D.S.P. Dearborn, D.N. Schramm, G. Steigman, Phys. Rev. Lett. **56**, 26 (1986); G.G. Raffelt, Phys. Rev. D**33**, 897 (1986); D**41**, 1324 (1990); constraints from neutron star cooling were discussed in N. Iwamoto, Phys. Rev. Lett. **53**, 1198 (1984); G.G. Raffelt, D. Dearborn, Phys. Rev. D**36**, 2211 (1987); D**37**, 549 (1988); G.G. Raffelt, A. Weiss, Phys. Rev. D**51**, 1495 (1995).

1452. R. Mayle et al., Phys. Lett. B**203**, 188 (1988); B**219**, 515 (1989); W. Keil et al., Phys. Rev. D**56**, 2419 (1997); A. Burrows, M.S. Turner, R.P. Brinkmann, Phys. Rev. D**39**, 1020 (1989); see G.G. Raffelt, in ref. [743] and therein.

1453. J. Preskill, M.B. Wise, F. Wilczek, Phys. Lett. **120**B, 127 (1983); L.F. Abbott, P. Sikivie, Phys. Lett. **120**B, 133 (1983); M. Dine, W. Fishler, Phys. Lett. **120**B, 137 (1983).

1454. D.J. Gross, R.D. Pisarski, L.G. Yaffe, Rev. Mod. Phys. **53**, 43 (1981).

1455. M. Fukugita, M. Yoshimura, Phys. Lett. **127**B, 181 (1983); M. Turner, Phys. Rev. D**33**, 889 (1986).

1456. R.L. Davis, Phys. Lett. B**180**, 225 (1986); R.A. Battye, E.P.S. Shellard, Phys. Rev. Lett. **73**, 2954 (1994); D. Harari, P. Sikivie, Phys. Lett. B**195**, 361 (1987).

1457. P. Sikivie, Phys. Rev. Lett. **51**, 1415 (1983).

1458. S. de Panfillis et al. Phys. Rev. Lett. **59**, 839 (1987); W.U. Wuensch et al., Phys. Rev. D**40**, 3153 (1989); C. Hagmann et al., Phys. Rev. D**42**, 1297 (1990); Phys. Rev. Lett. **80**, 2043 (1998); D. Kinion, K. van Bibber, in *Proc. 30th Int. Conf. High Energy Phys.*, Osaka 2000, op. cit. Vol. 2,

p. 1007; S. Matsuki, K. Yamamoto, Phys. Lett. B**263**, 523 (1991); I. Ogawa, S. Matsuki, K. Yamamoto, Phys. Rev. D**53**, R1740 (1996); K. Yamamoto et al. hep-ph/0101200; see N.J.T. Smith, in *Proc. 30th Int. Conf. High Energy Phys.*, op. cit. Vol. 1, p. 287 for a review of the current status.

1459. P. Sikivie, Phys. Rev. Lett. **48**, 1156 (1982).

1460. G. Lazarides, Q. Shafi, Phys. Lett. **115**B, 21 (1982).

1461. S.M. Barr, D.B. Reiss, A. Zee, Phys. Lett. **116**B, 227 (1982).

1462. J. Sato, T. Yanagida, Nucl. Phys. B (Proc. Suppl.) **77**, 293 (1999); P. Rammond, Nucl. Phys. B (Proc. Suppl.) **77**, 3 (1999).

1463. F. Vissani, JHEP **9811**, 025 (1998).

1464. J.K. Elwood, N. Irges, P. Ramond, Phys. Rev. Lett. **81**, 5064 (1998); N. Irges, S. Lavignac, P. Ramond, Phys. Rev. D**58**, 035003 (1998); G. Altarelli, F. Feruglio, JHEP 9811:021 (1998); Y. Nir, Y. Shadmi, JHEP **9905**, 023 (1999); S. Lola, G.G. Ross, Nucl. Phys. B**553**, 81 (1999); Q. Shafi, Z. Tavartkiladze, Phys. Lett. B**482**, 145 (2000); P.H. Frampton, A. Rasin, Phys. Lett. B**478**, 424 (2000); G. Altarelli, F. Feruglio, I. Masima, JHEP **0011**, 040 (2000).

1465. N. Haba, Phys. Rev. D**59**, 035011 (1998); A. Aranda, C.D. Carone, R.F. Lebed, Phys. Rev. D**62**, 016009 (2000); A. Aranda, C.D. Carone, P. Meade, Phys. Rev. D**65**, 013011 (2002).

1466. L. Hall, H. Murayama, N. Weiner, Phys. Rev. Lett. **84**, 2572 (2000); N. Haba, H. Murayama, Phys. Rev. D**63**, 053010 (2001).

1467. H.B. Nielsen, Y. Takanishi, Nucl. Phys. B**604**, 405 (2001).

1468. R. Barbieri, G. Dvali, L.J. Hall, Phys. Lett. B**377**, 76 (1996); R. Barbieri, P. Creminelli, A. Romanino, Nucl. Phys. B**559**, 17 (1999); C.D. Carone, L.J. Hall, Phys. Rev. D**56**, 4198 (1997); C.D. Carone, M. Sher, Phys. Lett. B**420**, 83 (1998); G. Eyal, Phys. Lett. B**441**, 191 (1998); E. Ma, Phys. Lett. B**456**, 48 (1999); C. Wetterich, Phys. Lett. B**451**, 397 (1999); R. Barbieri, L.J. Hall, G.L. Kane, G.G. Ross, hep-ph/9901228; Y.L. Wu, Int. J. Mod. Phys. A**14**, 4313 (1999); T. Bluzek, S. Raby, K. Tobe, Phys. Rev. D**62**, 055001 (2000); R.G. Roberts, A. Romanino, G.G. Ross, L. Velasco-Sevilla, Nucl. Phys. B**615**, 358 (2001).

1469. H. Harari, H. Haut, J. Weyers, Phys. Lett. B**78**, 459 (1978).

1470. Y. Koide, Phys. Rev. D**28**, 252 (1983); D**39**, 1391 (1989); see also Y. Koide, Phys. Rev. Lett. **47**, 1241 (1981).

1471. M. Fukugita, M. Tanimoto, T. Yanagida, Phys. Rev. D**57**, 4429 (1998); H. Fritzsch, Z.Z. Xing, Phys. Lett. B**440**, 313 (1998).

1472. V. Barger, S. Pakvasa, T.J. Weiler, K. Whisnant, Phys. Lett. B**437**, 107 (1998).

1473. M. Tanimoto, Phys. Rev. D**59**, 017304 (1999); R.N. Mohapatra, S. Nussinov, Phys. Lett. B**441**, 299 (1998); S.K. Kang, C.S. Kim, Phys. Rev. D**59**, 091302 (1999).

1474. H. Fritzsch, Z.Z. Xing, Phys. Lett. B**372**, 265 (1996).

1475. H. Fritzsch, Phys. Lett. **70**B, 436 (1977); **73**B, 317 (1978); Nucl. Phys. B**155**, 189 (1979).

1476. M. Shin, Phys. Lett. B**145**, 285 (1984); H. Harari, Y. Nir, Phys. Lett. B**195**, 586 (1987); C.H. Albright, M. Lindner, Phys. Lett. B**213**, 347 (1988); C.H. Albright, Phys. Lett. B**227**, 171 (1989); K.S. Babu, Q. Shafi, Phys. Lett. B**294**, 235 (1992).

1477. S. Dimopoulos, L.J. Hall, S. Raby, Phys. Rev. Lett. **68**, 1984 (1992); V. Barger, M.S. Berger, T. Han, M. Zralek, Phys. Rev. Lett. **68**, 3394 (1992).

574   References

1478. M. Fukugita, M. Tanimoto, T. Yanagida, Prog. Theor. Phys. **89**, 263 (1993);
M. Tanimoto, Phys. Lett. B**345**, 477 (1995).
1479. M. Jezabek, Y. Sumino, Phys. Lett. B**440**, 327 (1998); G. Altarelli, F. Feruglio, Phys. Lett. B**439**, 112 (1998).
1480. G. Altarelli, F. Feruglio, Phys. Lett. B**451**, 388 (1999); hep-ph/9905536.
1481. M. Bando, T. Kugo, K. Yoshioka, Phys. Rev. Lett. **80**, 3004 (1998).
1482. F. Vissani, hep-ph/9708483; H. Georgi, S.L. Glashow, Phys. Rev. D**61**, 097301 (2000); S. Lola, J.D. Vergados, Prog. Part. Nucl. Phys. **40**, 71 (1998); G. Altarelli, F. Feruglio, I. Masina, Phys. Lett. B**472**, 382 (2000); E. Akhmedov, G.C. Branco, M.N. Rebelo, Phys. Lett. B**478**, 215 (2000); R.N. Mohapatra, Phys. Rev. D**64**, 091301 (2001); M. Jezabek, Nucl. Phys. Proc. Suppl. **100**, 276 (2001); Q. Shafi, Z. Tavartkiladze, hep-ph/0101350; K. Choi, E.J. Chun, K. Hwang, W.Y. Song, Phys. Rev. D**64**, 113013 (2001); P. Frampton, S.L. Glashow, T. Yanagida, Phys. Lett. B**548**, 119 (2002).
1483. P.H. Frampton, S.L. Glashow, D. Marfatia, Phys. Lett. B**536**, 79 (2002).
1484. A. Kageyama, S. Kaneko, N. Shimoyama, M. Tanimoto, hep-ph/0204291.
1485. L. Wolfenstein, Nucl. Phys. B**175**, 93 (1980).
1486. A.Yu. Smirnov, Z. Tao, Nucl. Phys. B**426**, 415 (1994); A.Yu. Smirnov, M. Tanimoto, Phys. Rev. D**55**, 1665 (1997).
1487. P.H. Frampton, S.L. Glashow, Phys. Lett. B**461**, 95 (1999).
1488. K.S. Babu, Phys. Lett. B**203**, 132 (1988).
1489. R.N. Mohapatra, B. Sakita, Phys. Rev. D**21**, 1062 (1980); F. Wilczek, A. Zee, in ref. [1352].
1490. R.E. Shrock, Nucl. Phys. B**206**, 359 (1982).
1491. S.T. Petcov, Yad. Fiz. **25**, 641 (1977) [Sov. J. Nucl. Phys. **25**, 340 (1977)]; T. Goldman, G.J. Stephenson Jr., Phys. Rev. D**16**, 2256 (1977).
1492. J. Schechter, J.W.F. Valle, Phys. Rev. D**24**, 1883 (1981).
1493. B. Kayser, Phys. Rev. D**26**, 1662 (1982).
1494. J.E. Kim, Phys. Rev. D**14**, 3000 (1976); M.A. Bég, W.J. Marciano, M. Ruderman, Phys. Rev. D**17**, 1395 (1978).
1495. D.P. Stoker et al., Phys. Rev. Lett. **54**, 1887 (1985).
1496. G. Barenboim et al., Phys. Rev. D**55**, 4213 (1997).
1497. V.A. Wichers, T.R. Hageman, J. van Klinken, H.W. Wilschut, D. Atkinson, Phys. Rev. Lett. **58**, 1821 (1987).
1498. S. Abachi et al., Phys. Rev. Lett. **76**, 3271 (1996).
1499. G. Beall, M. Bander, A. Soni, Phys. Rev. Lett. **48**, 848 (1982).
1500. K.A. Olive, D.N. Schramm, G. Steigman, Nucl. Phys. B**180**, 497 (1981).
1501. M. Fukugita, T. Yanagida, Phys. Rev. Lett. **58**, 1807 (1987).
1502. A. Zee, Phys. Lett. **161**B, 141 (1985).
1503. H.N. Brown et al., Phys. Rev. Lett. **86**, 2227 (2001).
1504. D.A. Dicus, H.-J. He, J. N. Ng, Phys. Rev. Lett. **87**, 111803 (2001).
1505. M. Fukugita, T. Yanagida, Phys. Lett. B**206**, 93 (1988).
1506. J.W.F. Valle, Phys. Lett. B**199**, 432 (1987).
1507. M.B. Voloshin, Yad. Fiz. **48**, 804 (1988) [Sov. J. Nucl. Phys. **48**, 512 (1988)].
1508. M. Leurer, N. Marcus, Phys. Lett. B**237**, 81 (1990); K.S. Babu, R.N. Mohapatra, Phys. Rev. Lett. **63**, 228 (1989); Phys. Rev. D**42**, 3778 (1990).
1509. R. Barbieri, R.N. Mohapatra, Phys. Lett. B**218**, 225 (1989); J. Liu, Phys. Lett. B**225**, 148 (1989).
1510. H. Georgi, L. Randall, Phys. Lett. B**244**, 196 (1990).

1511. K.S. Babu, R.N. Mohapatra, Phys. Rev. Lett. **64**, 1705 (1990); G. Ecker, W. Grimus, H. Neufeld, Phys. Lett. B**232**, 217 (1990); D. Chang, W.Y. Keung, G. Senjanović, Phys. Rev. D**42**, 1599 (1990); D. Chang, W.Y. Keung, S. Lipovaca and G. Senjanović, Phys. Rev. Lett. **67**, 953 (1991).

1512. S.M. Barr, E.M. Freire, A. Zee, Phys. Rev. Lett. **65**, 2626 (1990).

1513. R. Davies, in *7th Workshop on Grand Unification/ICOBAN'86*, Toyama, Japan, ed. by J. Arafune (World Scientific, Singapore 1987).

1514. G.A. Bazilevskaya, Yu.I. Stozhkov, T.N. Charakhchyan, Pis'ma Zh. Eksp. Teor. Fiz. **35**, 273 (1982) [JETP Lett. **35**, 341 (1982)]; G.A. Bazilevskaya et al., Yad. Fiz. **39**, 856 (1984) [Soviet J. Nucl. Phys. **39**, 543 (1984)].

1515. R. Davis, Jr., in *Frontiers of Neutrino Astrophysics*, Takayama 1992, ed. by Y. Suzuki, K. Nakamura (Universal Academy Press, Tokyo 1993), p. 47.

1516. J.N. Bahcall, G.B. Field, W.H. Press, Astrophys. J. **320**, L69 (1987); J.N. Bahcall, W.H. Press, Astrophys. J. **370**, 730 (1991); B.W. Filippone, P. Vogel, Phys. Lett. B**246**, 546 (1990); H. Nunokawa, H. Minakata, Int. J. Mod. Phys. A**6**, 2347 (1991); J.W. Bieber, D. Seckel, T. Stanev, G. Steigman, Nature **348**, 407 (1990).

1517. M.B. Voloshin, M.I. Vysotskiĭ, Yad. Fiz. **44**, 845 (1986) [Sov. J. Nucl. Phys. **44**, 544 (1986)]; L.B. Okun, Yad. Fiz. **44**, 847 (1986) [Sov. J. Nucl. Phys. **44**, 546 (1986)]; M.B. Voloshin, M.I. Vysotskiĭ, L.B. Okun, Yad. Fiz. **44**, 677 (1986) [Sov. J. Nucl. Phys. **44**, 440 (1986)]; Zh. Eksp. Teor. Fiz. **91**, 754 (1986) [Sov. Phys. JETP **64**, 446 (1986)].

1518. A. Cisneros, Astrophys. Space Sci. **10**, 87 (1971).

1519. Super-Kamiokande collaboration, private communication.

1520. R. Barbieri, G. Fiorentini, Nucl. Phys. B**304**, 909 (1988).

1521. C.S. Lim, W.J. Marciano, Phys. Rev. D**37**, 1368 (1988).

1522. E.Kh. Akhmedov, Phys. Lett. B**213**, 64 (1988).

1523. E.N. Parker, Astrophys. J. **122**, 293 (1955); H.W. Babcock, Astrophys. J. **133**, 572 (1961); R.B. Leighton, Astrophys. J. **140**, 1547 (1964).

1524. H.K. Moffat, *Magnetic Field Generation in Electrically Conducting Fluids* (Cambridge University Press, Cambridge 1978); E.N. Parker, *Cosmic Magnetic Field* (Clarendon Press, Oxford 1979).

1525. E.N. Parker, Astrophys. J. **198**, 205 (1975).

1526. P.A. Gilman et al., Astrophys. J. Suppl. **53**, 243 (1983); G.A. Glatzmaier, Astrophys. J. **291**, 300 (1985).

1527. E.A. Spiegel, N.O. Weiss, Nature **287**, 616 (1980); P.A. Gilman, C.A. Morrow, E.E. DeLuca, Astrophys. J. **338**, 528; A.R. Choudhuri, Astrophys. J. **355**, 733; E.N. Parker, Astrophys. J. **408**, 707 (1993).

1528. E. Schatzman, in *Solar Interior and Atmosphere*, ed. by A.N. Cox, W.C. Livingston, M.S. Matthews (University of Arizona Press, Tucson 1991), p. 192; K.G. Libbrecht, C.A. Morrow, idem p. 479.

1529. S. D'Silva, R.A. Choudhuri, Astron. Astrophys. **272**, 621 (1993); E.N. Parker, in *Solar Magnetic Fields*, ed. by M. Schüssler, W. Schmidt (Cambridge University Press, Cambridge 1994).

1530. G.W. Preston, Astrophys. J. **164**, 309 (1971).

1531. N. Boruta, Astrophys. J. **458**, 832 (1996).

1532. J. Pulido, E.Kh. Akhmedov, Astroparticle Phys. **13**, 227 (2000); J. Derkaoui, Y. Tayalati, Astroparticle Phys. **14**, 351 (2001); A.A. Bykov, V.Yu. Popov, T.I. Rashba, V.B. Semikoz, hep-ph/0002174; E.Kh. Akhmedov, J. Pulido,

Phys. Lett. B**485**, 178 (2000); O.G. Miranda et al., Nucl. Phys. B**595**, 360 (2001).

1533. A. Suzuki, M. Mori, K. Numata, Y. Oyama, Phys. Rev. D**43**, 3557 (1991).

1534. M. Fukugita, T. Yanagida, Phys. Rev. Lett. **65**, 1975 (1990).

1535. A. De Rujúla, S. Glashow, Phys. Rev. Lett. **45**, 942 (1980).

1536. J. Silk, A. Stebbins, Astrophys. J. **269**, 1 (1983); M. Kawasaki, K. Sato, Phys. Lett. **169**B, 280 (1986).

1537. J. Maalampi, K. Mursula, M. Roos, Phys. Rev. Lett. **56**, 1031 (1986); J. Murthy, R.C. Henry, Phys. Rev. Lett. **58**, 1581 (1987).

1538. P. Sreekumar et al., Astrophys. J. **494**, 523 (1998) [EGRET].

1539. M. Fukugita, M. Kawasaki, Astrophys. J. **353**, 384 (1990).

1540. D.A. Dicus, E.W. Kolb, V.L. Teplitz, R.V. Wagoner, Phys. Rev. D**17**, 1529 (1978); S. Miyama, K. Sato, Prog. Theor. Phys. **60**, 1703 (1978); E.W. Kolb, R.J. Scherrer, Phys. Rev. D**25**, 1481 (1982).

1541. D. Lindley, Astrophys. J. **294**, 1 (1985); M. Kawasaki, N. Terasawa, K. Sato, Phys. Lett. B**178**, 71 (1986); see also D. Lindley, Mon. Not. R. astr. Soc. **188**, 15p (1979) (fission was first considered by this last paper, but it ignored the photon–photon process).

1542. S.W. Falk, D.N. Schramm, Phys. Lett. **79**B, 511 (1978).

1543. F. von Feilitzsch, L. Oberauer, Phys. Lett. B**200**, 580 (1988); E.L. Chupp, W.T. Vestrand, C. Reppin, Phys. Rev. Lett. **62**, 505 (1989); E.W. Kolb, M.S. Turner, Phys. Rev. Lett. **62**, 509 (1989).

1544. R. Cowsik, Phys. Rev. Lett. **39**, 784 (1977).

1545. D.A. Krakauer et al., Phys. Rev. D**44**, R6 (1991); J.S. Frank et al., Phys. Rev. D**24**, 2001 (1981).

1546. E. Asseo, H. Sol, Phys. Rept. **148**, 307 (1987); see also, P. Coles, Comment Astrophys. **16**, 45 (1992) for the cosmological implication of the primordial magnetic field.

1547. A.D. Sakharov, Pis'ma Zh. Eksp. Teor. Fiz. **5**, 32 (1967) [JETP Lett. **5**, 24 (1967)].

1548. A.Yu. Ignatiev, N.V. Krasnikov, V.A. Kuzmin, A.N. Tavkhelidze, in *Neutrino 77, Proc. Int. Conf. on Neutrino Phys. and Neutrino Astrophys.*, Baksan Valley 1977, ed. by M.A. Markov et al. (Nauka, Moscow 1978) Vol. II, p. 293; Phys. Lett. **76**B, 436 (1978).

1549. M. Yoshimura, Phys. Rev. Lett. **41**, 281 (1978).

1550. D. Toussaint, S.B. Treiman, F. Wilczek, A. Zee, Phys. Rev. D**19**, 1036 (1979); S. Weinberg, Phys. Rev. Lett. **42**, 850 (1979); M. Yoshimura, Phys. Lett. **88**B, 294 (1979).

1551. S.M. Barr, G. Segre, H.A. Weldon, Phys. Rev. D**20**, 2494 (1979); D.V. Nanopoulos, S. Weinberg, Phys. Rev. D**20**, 2484 (1979); A. Yildiz, P. Cox, Phys. Rev. D**21**, 906 (1980).

1552. A.D. Dolgov, Ya. B. Zel'dovich, Rev. Mod. Phys. **53**, 1 (1981); M. Yoshimura, in *Grand Unified Theories and Related Topics*, ed. M. Konuma, T. Maskawa (World Scientific, Singapore 1981), p. 235; E.W. Kolb, M.S. Turner, Ann. Rev. Nucl. Part. Sci. **33**, 645 (1983); E. Kolb, M. Turner, *The Early Universe* (Addison-Wesley, Reading, Massachusetts 1990); A.D. Dolgov, Phys. Rep. **222**, 309 (1992).

1553. See also S. Dimopoulos, L. Susskind, Phys. Rev. D**18**, 4500 (1978).

1554. M.E. Shaposhnikov, Nucl. Phys. B**287**, 757 (1987); B**299**, 797 (1988); for a review see, A.G. Cohen, D.B. Kaplan, A.E. Nelson, Ann. Rev. Nucl. Part. Sci. **43**, 27 (1983).

1555. I. Affleck, M. Dine, Nucl. Phys. B**249**, 361 (1985).

1556. For a review, S. Coleman, in *The Whys of Subnuclear Physics*, Erice 1977, ed. by A. Zichichi (Plenum Press, New York 1979) p. 805.

1557. J. Arafune, P.G.O. Freund, C. Goebel, J. Math. Phys. **16**, 433 (1975).

1558. N.H. Christ, Phys. Rev. D**21**, 1591 (1980).

1559. F.R. Klinkhamer, N.S. Manton, Phys. Rev. D**30**, 2212 (1984); see also N.S. Manton, Phys. Rev. D**28**, 2019 (1983).

1560. J.S. Langer, Ann. Phys. (NY) **54**, 258 (1969).

1561. I. Affleck, Phys. Rev. Lett. **46**, 388 (1981).

1562. P. Arnold, L. McLerran, Phys. Rev. D**36**, 581 (1987); A. Ringwald, Phys. Lett. B**201**, 510 (1988); D.Yu. Grigoriev, V.A. Rubakov, Nucl. Phys. B**299**, 67 (1988); S.Yu. Khlebnikov, M.E. Shaposhnikov, Nucl. Phys. B**308**, 885 (1988).

1563. T. Akiba, H. Kikuchi, T. Yanagida, Phys. Rev. D**40**, 588 (1989).

1564. S.Yu. Khlebnikov, M.E. Shaposhnikov, Nucl. Phys. B**308**, 885 (1988); see also P. Arnold, L. McLerran, Phys. Rev. D**36**, 581 (1987); the latter authors gave an α_W dependence different from that of the former authors at high temperature.

1565. P. Arnold, D. Son, L.G. Yaffe, Phys. Rev. D**55**, 6264 (1997).

1566. D. Bödeker, G.D. Moore, K. Rummukainen, Phys. Rev. D**61**, 056003 (2000); G.D. Moore, hep-ph/0009161.

1567. G.D. Moore, N. Turok, Phys. Rev. D**56**, 6533 (1997); J. Ambjørn, A. Krasnitz, Nucl. Phys. B**506**, 387 (1997)

1568. D.Yu. Grigoriev, V.A. Rubakov, M.E. Shaposhnikov, Phys. Lett. B**216**, 172 (1989); Nucl. Phys. B**326**, 737 (1989).

1569. J. Ambjørn, T. Askgaard, H. Porter, M.E. Shaposhnikov, Nucl. Phys. B**353**, 346 (1991); J. Ambjørn, A. Krasnitz, Phys. Lett. B**362**, 97 (1995).

1570. J.A. Harvey, M.S. Turner, Phys. Rev. D**42**, 3344 (1990); B.A. Campbell, S. Davidson, J. Ellis, K.A. Olive, Phys. Lett. B**297**, 118 (1992).

1571. V.A. Kuzmin, V.A. Rubakov, M.E. Shaposhnikov, Phys. Lett. B**191**, 171 (1987); H. Dreiner, G.G. Ross, Nucl. Phys. B**410**, 188 (1993).

1572. J.M. Cline, K. Kainulainen, K.A. Olive, Phys. Rev. D**49**, 6394 (1994).

1573. M. Shaposhnikov, in *Lattice 91, Proc. Int. Symp. Lattice Field Theory*, Tsukuba, 1991, ed. by M. Fukugita et al., Nucl. Phys. B (Proc. Suppl.) **26**, 78 (1992).

1574. M. Fukugita, T. Yanagida, Phys. Rev. D**42**, 1285 (1990).

1575. B.A. Campbell, S. Davidson, J.R. Ellis, K.A. Olive, Phys. Lett. B**256**, 457 (1991); Astroparticle Phys. **1**, 77 (1992).

1576. W. Fischler, G.F. Giudice, R.G. Leigh, S. Paban, Phys. Lett. B**258**, 45 (1991); A.E. Nelson, S.M. Barr, Phys. Lett. B**246**, 141 (1990).

1577. L.E. Ibáñez, F. Quevedo, Phys. Lett. B**283**, 261 (1992).

1578. A.G. Doroshkevich, Ya.B. Zeldovich, R.A. Sunyaev, Sov. Astron. **22**, 523 (1978); P.J.E. Peebles, Nature **327**, 210 (1987).

1579. M. Fukugita, V.A. Rubakov, Phys. Rev. Lett. **56**, 988 (1986).

1580. V.A. Kuzmin, Pis'ma Zh. Eksp. Teor. Fiz. **12**, 335 (1970) [JETP Lett **12**, 228 (1970)]; R.N. Mohapatra, R.E. Marshak, Phys. Rev. Lett. **44**, 1316 (1980).

1581. M. Baldo-Ceolin et al., Phys. Lett. B**236**, 95 (1990).

1582. M. Takita et al., Phys. Rev. D**34**, 902 (1986); C. Berger et al., Phys. Lett. B**240**, 237 (1990); see C.B. Dover, A. Gal, J.M. Richard, Phys. Rev. D**27**, 1090 (1983) for a nuclear physic for the binding effect.

1583. J. Ambjørn, M.L. Laursen, M.E. Shaposhnikov, Nucl. Phys. B**316**, 483 (1989); L. McLerran, Phys. Rev. Lett. **62**, 1075 (1989); N. Turok, J. Zadrozny, Phys. Rev. Lett. **65**, 2331 (1990); L. McLerran, M. Shaposhnikov, N. Turok, M. Voloshin, Phys. Lett. B**256**, 451 (1991); M. Dine, P. Huet, R. Singleton, Jr., Nucl. Phys. B**375**, 625 (1992).

1584. A.G. Cohen, D.B. Kaplan, A.E. Nelson, Nucl. Phys. B**349**, 727 (1991); A.E. Nelson, D.B. Kaplan, A.G. Cohen, Nucl. Phys. B**373**, 453 (1992).

1585. A.D. Linde, Phys. Lett. B**70**, 306 (1977); A.M. Guth, E.J. Weinberg, Phys. Rev. Lett. **45**, 1131 (1980); P.J. Steinhart, Nucl. Phys. B**179**, 492 (1981).

1586. Y. Aoki, F. Csikor, Z. Fodor, A. Ukawa, Phys. Rev. D**60**, 013001 (1999).

1587. K. Kajantie et. al., Phys. Rev. Lett. **77**, 2887 (1996).

1588. M. Dine, R.G. Leigh, P. Huet, A. Linde, D. Linde, Phys. Rev. D**46**, 550 (1992).

1589. W. Buchmuller, O. Philipsen, Nucl. Phys. B**443**, 47 (1995); J.R. Espinosa, Nucl. Phys. B**475**, 273 (1996); J.M. Cline, G.D. Moore, Phys. Rev. Lett. **81**, 3315 (1998).

1590. A.I. Bochkarev, S.V. Kuzmin, M.E. Shaposhnikov, Phys. Lett. B**244**, 275 (1990); J.R. Espinosa, M. Quiros, F. Zwirner, Phys. Lett. B**307**, 106 (1993).

1591. M. Carena, M. Quiros, C.E.M. Wagner, Phys. Lett. B**380**, 81 (1996); Nucl. Phys. B**524**, 3 (1998).

1592. M. Quiros, Nucl. Phys. Proc. Suppl. **101**, 401 (2001).

1593. F. Csikor et al., Phys. Rev. Lett. **85**, 932 (2000).

1594. G.R. Farrar, M.E. Shaposhinikov, Phys. Rev. Lett. **70**, 2833 (1993); **71**, 210 (1993) (E).

1595. M. Joyce, K. Kainulainen, JHEP **7**, 18 (2000); M. Carena et al., Nucl. Phys. B**599**, 158 (2001).

1596. T. Yanagida, M. Yoshimura, Nucl. Phys. B**168**, 534 (1980).

1597. E.W. Kolb, S. Wolfram, Nucl. Phys. B**172**, 224 (1980); J. Fry, K.A. Olive, M.S. Turner, Phys. Rev. D**22**, 2977 (1980).

1598. A.D. Dolgov, Yad. Fiz. **32**, 1606 (1980) [Sov. J. Nucl. Phys. **32**, 831 (1980)].

1599. J.N. Fry, K.A. Olive, M.S. Turner, Phys. Rev. Lett. **45**, 2074 (1980); Phys. Rev. D**22**, 2977 (1980).

1600. A.Yu. Ignat'ev, V.A. Kuz'min, M.E. Shaposhnikov, Pisma Zh. Eksp. Teor. Fiz. **30**, 726 (1979) [JETP Lett. **30**, 688 (1979)]; F.J. Botella, J. Roldan, Phys. Rev. D**44**, 966 (1991); J. Liu, G. Segrè, Phys. Rev. D**48**, 4609 (1993).

1601. M. Fukugita, T. Yanagida, Phys. Rev. Lett. **89**, 131602 (2002)

1602. M. Flanz, E.A. Paschos, U. Sarkar, Phys. Lett. B**345**, 248 (1995); B**384**, 487 (1996) (E); L. Covi, E. Roulet, F. Vissani, Phys. Lett. B**384**, 169 (1996); A. Pilaftsis, Phys. Rev. D**56**, 5431 (1997); W. Buchmuller, M. Plumacher, Phys. Lett. B**431**, 354 (1998).

1603. M.A. Luty, Phys. Rev. D**45**, 455 (1992).

1604. M. Plumacher, Z. Phys. C**74**, 549 (1997); Nucl. Phys. B**530**, 207 (1998).

1605. W. Buchmuller, M. Plumacher, Phys. Rept. **320**, 329 (1999); hep-ph/0007176; A.S. Joshipura, E.A. Paschos, W. Radejohann, Nucl. Phys. B**611**, 227 (2001).

1606. J. Ellis, G.B. Gelmini, J.L. Lopez, D.V. Nanopoulos, S. Sarkar, Nucl. Phys. B**373**, 399 (1992); M. Kawasaki, T. Moroi, Progr. Theor. Phys. **93**, 879 (1995); E. Holtmann, M. Kawasaki, K. Kohri, T. Mori, Phys. Rev. D**60**, 023506 (1999).

1607. G.F. Giudice, M. Peloso, A. Riotto, I. Tkachev, JHEP **9908**, 014 (1999); T. Asaka, K. Hamaguchi, M. Kawasaki, T. Yanagida, Phys. Lett. B**464**, 12 (1999); Phys. Rev. D**61**, 083512 (2000); G. Lazarides, N.D. Vlachos, Phys. Lett. B**459**, 482 (1999); G. Lazarides, Springer Tracts Mod. Phys. **163**, 227 (2000).

1608. W. Buchmuller, T. Yanagida, Phys. Lett. B**445**, 399 (1999); J. Ellis, S. Lola, D.V. Nanopoulos, Phys. Lett. B**452**, 87 (1999); H. Goldberg, Phys. Lett. B**474**, 389 (2000); M.S. Berger, B. Brahmachari, Phys. Rev. D**60**, 073009 (1999); K. Kang, S.K. Kang, U. Sarkar, Phys. Lett. B**486**, 391 (2000); R. Barbieri, P. Creminelli, A. Strumia, N. Tetradis, Nucl. Phys. B**575**, 61 (2000); E.J. Chun, S.K. Kang, Phys. Rev. D**63**, 097902 (2001); D. Falcone, F. Tramontano, Phys. Rev. D**63**, 073007 (2001); H.B. Nielsen, Y. Takanishi, Phys. Lett. B**507**, 241 (2001); M. Hirsch, S.F. King, Phys. Rev. D**64**, 113005 (2001); W. Buchmuller, D. Wyler, Phys. Lett. B**521**, 291 (2001).

1609. W. Buchmuller, hep-ph/0107153

1610. P.J. O'Donnell, U. Sarkar, Phys. Rev. D**49**, 2118 (1994); E. Ma, U. Sarkar, Phys. Rev. Lett. **80**, 5716 (1998).

1611. E.Kh. Akhmedov, V.A. Rubakov, A.Yu. Smirnov, Phys. Rev. Lett. **81**, 1359 (1998).

1612. M.K. Gaillard, H. Murayama, K.A. Olive, Phys. Lett. B**355**, 71 (1995).

1613. M. Dine, L. Randall, S. Thomas, Nucl. Phys. B**458**, 291 (1996).

1614. K. Enqvist, J. McDonald, Phys. Lett. B**425**, 309 (1998); Nucl. Phys. B**538**, 321 (1999).

1615. J. McDonald, JHEP **0103**, 022 (2001).

1616. A. Kusenko, M. Shaposhnikov, Phys. Lett. B**418**, 46 (1998).

1617. S. Kasuya, M. Kawasaki, Phys. Rev. D**61**, 041301 (2000); Phys. Rev. D**62**, 023512 (2000).

1618. S. Coleman, Nucl. Phys. B**262**, 263 (1985); for a review, see T.D. Lee, Y. Pang, Phys. Rep. **221**, 251 (1992) and references therein.

1619. T. Gherghetta, C. Kolda, S.P. Martin, Nucl. Phys. B**468**, 37 (1996).

1620. H. Murayama, T. Yanagida, Phys. Lett. B**322**, 349 (1994).

1621. R. Allahverdi, B.A. Campbell, J. Ellis, Nucl. Phys. B**579**, 355 (2000).

1622. A. Anisimov, M. Dine, Nucl. Phys. B**619**, 729 (2001).

1623. T. Asaka, M. Fujii, K. Hamaguchi, T. Yanagida, Phys. Rev. D**62**, 123514 (2000); M. Fujii, K. Hamaguchi, T. Yanagida, Phys. Rev. D**64**, 123526 (2001).

1624. Q. R. Ahmad et al. Phys. Rev. Lett. **89**, 011301 (2002) [SNO]

1625. Q. R. Ahmad et al. Phys. Rev. Lett. **89**, 011302 (2002) [SNO]

1626. V. Barger, D. Marfatia, K. Whisnant, B. P. Wood, Phys. Lett. B **537**, 179 (2002); A. Bandyopadhyay, S. Choubey, S. Goswami, D. P. Roy, Phys. Lett. B **540**, 14 (2002); J. N. Bahcall, C. M. Gonzalez-Garcia and C. Peña-Garay, JHEP **7**, 54 (2002); P. C. de Holanda, A. Yu. Smirnov, hep-ph/0205241; A Strumia, C. Cattadori, N. Ferrari, F. Vissani, Phys. Lett. B **541**, 327 (2002); G. L. Fogli et al., Phys. Rev. D **66**, 053010 (2002).

1627. K. Eguchi et al., Phys. Rev. Lett. **90**, 021802 (2003) [KamLAND].

Index